

Rohana Hassan · Marina Yusoff
Zulhabri Ismail · Norliyati Mohd Amin
Mohd Arshad Fadzil *Editors*

InCIEC 2013

Proceedings of the International
Civil and Infrastructure Engineering
Conference 2013

InCIEC 2013

Rohana Hassan · Marina Yusoff
Zulhabri Ismail · Norliiyati Mohd Amin
Mohd Arshad Fadzil
Editors

InCIEC 2013

Proceedings of the International Civil
and Infrastructure Engineering
Conference 2013

Editors

Rohana Hassan
Marina Yusoff
Norliyati Mohd Amin
Mohd Arshad Fadzil
Institute for Infrastructure Engineering
and Sustainable Management (IIESM)
Universiti Teknologi MARA
Shah Alam, Selangor
Malaysia

Zulhabri Ismail
Architecture, Planning and Surveying
Universiti Teknologi MARA
Shah Alam, Selangor
Malaysia

ISBN 978-981-4585-01-9 ISBN 978-981-4585-02-6 (eBook)
DOI 10.1007/978-981-4585-02-6
Springer Singapore Heidelberg New York Dordrecht London

Library of Congress Control Number: 2013956334

© Springer Science+Business Media Singapore 2014

This work is subject to copyright. All rights are reserved by the Publisher, whether the whole or part of the material is concerned, specifically the rights of translation, reprinting, reuse of illustrations, recitation, broadcasting, reproduction on microfilms or in any other physical way, and transmission or information storage and retrieval, electronic adaptation, computer software, or by similar or dissimilar methodology now known or hereafter developed. Exempted from this legal reservation are brief excerpts in connection with reviews or scholarly analysis or material supplied specifically for the purpose of being entered and executed on a computer system, for exclusive use by the purchaser of the work. Duplication of this publication or parts thereof is permitted only under the provisions of the Copyright Law of the Publisher's location, in its current version, and permission for use must always be obtained from Springer. Permissions for use may be obtained through RightsLink at the Copyright Clearance Center. Violations are liable to prosecution under the respective Copyright Law. The use of general descriptive names, registered names, trademarks, service marks, etc. in this publication does not imply, even in the absence of a specific statement, that such names are exempt from the relevant protective laws and regulations and therefore free for general use.

While the advice and information in this book are believed to be true and accurate at the date of publication, neither the authors nor the editors nor the publisher can accept any legal responsibility for any errors or omissions that may be made. The publisher makes no warranty, express or implied, with respect to the material contained herein.

Printed on acid-free paper

Springer is part of Springer Science+Business Media (www.springer.com)

Welcome Message

The Institute for Infrastructure Engineering and Sustainable Management (IIESM), Universiti Teknologi MARA (UiTM) has over the years been instrumental in providing a platform for several collaboration research programmes and publications involving all Civil Engineering disciplines. IIESM has so far focused on research with the aim to solve infrastructure and environmental engineering problems in a more sustainable way.

IIESM in collaboration with Universitas Gadjah Mada, Indonesia; Mahatma Gandhi University, India; and BRE Centre for Innovative Construction Materials, UK are organizing a 3-day “International Civil and Infrastructure Engineering Conference 2013, (InCIEC 2013)”. The conference is supported by IEEE Malaysia IE/IA Joint Chapter dated from 22 to 24 September 2013, in Kuching, Sarawak, Malaysia.

It is hoped that *InCIEC 2013* will be a useful platform for researchers to present their findings in areas that are multidisciplinary and related to Civil Engineering issues emphasising on concrete waste and earthquake engineering, flood management and intelligence development, fluvial and river engineering dynamics, geotechnical engineering, innovative construction materials and structures, bioremediation and engineering, nano-materials for engineering and timber engineering. Besides, this conference is also a platform for researchers to establish new interfaces, compare the findings; benchmark their work; exchange views and widen the scope and range of their research activities. The conference is also looking forward to new peers in diverse areas of expertise.

On behalf of the organising committee we take this opportunity to express our gratitude to all reviewers and participants for their support to ensure the success of this event. We also would like to thank all the authors, session chairpersons and delegates for the great support and contribution given. Last but not least, a special thank you goes to the organising committee, which has been working hard towards the success of this event. Without their cooperation, hard work and dedication, this event would simply not be possible.

We wish all participants and presenters a very pleasurable stay in Kuching, and do enjoy the conference.

Rohana Hassan
General Chair
InCIEC 2013

Advisory Committee

Zakiah Ahmad
Institute for Infrastructure Engineering
and Sustainable Management (IIESM),
Universiti Teknologi MARA, Malaysia

Sabu Thomas
Mahatma Ghandi University, India

Pete Walker
BRE Centre for Innovative Construction Materials
UK

Mustafa Kamal Hamzah
IEEE Malaysia IE/IA Joint Chapter

Azmi Ibrahim
Faculty of Civil Engineering
Universiti Teknologi MARA, Malaysia

Agus Kurniawan
Universitas Gadjah Mada, Indonesia

Abu Bakar Abdul Majeed
Research Management Institute (RMI)
Universiti Teknologi MARA, Malaysia

About IIESM



The Institute for Infrastructure Engineering and Sustainable Management (IIESM) was officially approved by the Universiti Teknologi MARA, Malaysia as an Institute on 7 January 2009. The formation of this Institute would further expedite research and publication activities at the university. IIESM focuses on research in all civil engineering disciplines that enlighten a broader scope in research and engineering education. Our aim is to solve infrastructure and environmental engineering problems in a more sustainable way and introduce new state-of-the-art technology.

It is a merger of ten (10) research excellence centres which are:

1. Timber Engineering Research Centre (TEReC)
2. Concrete Waste Engineering and Earthquake Research Centre (CWE²C)
3. Flood Management and Intelligence Development Centre (FloodMind)
4. Fluvial and River Engineering Dynamics Centre (FRiEnD)
5. Geotechnical Forensic Research Centre (GEOFORENSIC)
6. Innovative Construction Materials and Structures Centre (ICMSC)
7. Bioremediation Research Centre (mybioREC)
8. Geotechnical Engineering and Georisk Management Centre (myGERMEC)
9. Synergistic Innovative Management Research Centre (SIMReC)
10. Transportation Systems, Infrastructure and Intelligent Transport Research Centre (TransIIT)

Vision

To establish the institute as a premier entity to provide leadership in the scholarship of research and consultancy.

Mission

To be the excellence centre and an engine of growth for new knowledge to solve future problems.

Institute for Infrastructure Engineering and Sustainable Management (IIESM)
Level 3, Block 1, Engineering Complex,
Universiti Teknologi MARA, 40450 Shah Alam, Selangor, Malaysia
Phone: +60-3-55442780; +60-3-55211910
Fax: +60-35521-1911
E-mail: iiesm.fka@gmail.com
Website: <http://iiesm.uitm.edu.my>

Venue



Pullman Kuching is the newest addition to the 5-stars international brand in the city. Located in the heart of Kuching on top of the hill at Jalan Mathies, Pullman Kuching offers an astonishing panoramic view of the city and the Sarawak River. The hotel is adjacent to a two-storey city-lifestyle shopping centre “Hills Shopping Mall” and within walking distance of the commercial centre and city attractions. Pullman Kuching features 389 spacious, contemporary rooms and offers easy access to renowned Borneo national parks. The hotel is ideal for business guests, offering an abundance of conferencing space, state-of-the-art facilities and technology, plus a range of trendy restaurants and bars, and a high-end spa.

A few paths away from the Kuching Waterfront Promenade, guests can easily venture on foot to discover the city's diverse selection of shops, restaurants, temples and bazaars. Nearby attractions include Sarawak Cultural Village, Damai Beach, Bako National Park and Semenggoh Wildlife Centre to mingle around with the orangutans of Borneo.

Nestled in the Golden Triangle of Kuching, Pullman Kuching is just 11 km away from Kuching International Airport and is only a 20-min drive. Taxis are readily available.



Address: 1A Jalan Mathies, Sarawak
93100 Kuching, Malaysia
Tel. +60-82-222888
Fax. +60-82-222999
Email: H6332@accor.com
GPS: N 1° 33' 21.38" E 110° 21 4.04"

Organising Committee

International Advisory/Liason

Sabu Thomas
Mahatma Ghandi University, India.

Agus Kurniawan
Universitas Gadjah Mada, Indonesia.

Pete Walker
BRE Centre for Innovative
Construction Materials, UK.

Advisor

Mustafar Kamal Hamzah, IEEE Malaysia IE/IA Joint Chapter.
Zakiah Ahmad, Universiti Teknologi MARA, Malaysia.
Azmi Ibrahim, Universiti Teknologi MARA, Malaysia.
Abu Bakar Abdul Majeed, Universiti Teknologi MARA, Malaysia.

General Chair

Rohana Hassan, Universiti Teknologi MARA, Malaysia.

General Co-Chair

Marina Yusoff, Universiti Teknologi MARA, Malaysia.

Technical Programme Chair

Zulhabri Ismail, Universiti Teknologi MARA, Malaysia.

Publication Chair

Mohd Fadzil Arshad, Universiti Teknologi MARA, Malaysia.

Finance Chair

Anizahyati Alisibramulisi, Universiti Teknologi MARA, Malaysia.

Secretariat and Information Chair

Norliyati Mohd Amin, Universiti Teknologi MARA, Malaysia.

Website Chair

Marina Yusoff, Universiti Teknologi MARA, Malaysia.

Reviewers

Abbas Nemati	Member of Scientific Board, Iran
Abdelatif Hassini	University of Oran, Es senia, Algeria
Abdul Kadir Othman	Universiti Teknologi MARA
Abdul Talib Din	Universiti Teknikal Malaysia Melaka
Abdullah Alrabghi	Cranfield University, UK
Addisson Salazar	Universidad Politécnica de Valencia, Spain
Aditi Sharma	MBM Engineering College Jodhpur, India
Adnan Derahman	Universiti Teknologi MARA, Pahang
Adnan Enshassi	Islamic University of Gaza, Palestine
Afidah Abu Bakar	Universiti Teknologi MARA
Ahmad Alabqari Ma' Radzi	Universiti Tun Hussein Onn Malaysia
Ahmad Kamil Arshad	Universiti Teknologi MARA
Ahmad Rezaee jordehi	Universiti Putra Malaysia
Ahmad Saiful Azlin Puteh Salin	UiTM Perak and Accounting Research Institute
Ahmad Sana	Sultan Qaboos University, Oman
Ahmed El Oualkadi	Abdelmalek Essaadi University, Morocco
Ahmed Mohammed	University of Mosul, Iraq
Aidah Jumahat	Universiti Teknologi MARA
Ajay Bhushan	Mahamaya Technical University Noida, India
Akitoshi Matsuda	Panasonic, Japan
Alessandro Carrega	University of Genoa, Italy
Alessandro Testa	Institute for High Performance Computing and Networking, Italy
Ali Elrashidi	University of Bridgeport, USA
Ali Rafiei	University of Technology Sydney, Australia
Amelia Carolina Sparavigna	Politecnico di Torino, Italy
Amnorzahira Amir	Universiti Teknologi MARA
Amran Awang	Universiti Teknologi MARA, Perlis
Andrei Shin	Samsung SDS Co., Ltd., Korea
Andrew Thomson	University of Bath, UK
Angel Pretelin-Ricardez	Instituto Politecnico Nacional/UPIITA/México
Angkoon Phinyomark	Joseph Fourier University, France
Anil Kumar	World Institute of Technology Sohna, Gurgaon, India

Anizahyati Alisibramulisi	IIESM, Universiti Teknologi MARA
Arun Nambiar	California State University, USA
Ashkan Masoomi	Islamic Azad University, Ahram Branch, Iran
Ashutosh Dubey	Trinity Institute of Technology and Research Bhopal, India
Atabak Mohsen Nejad	PN University of Tehran, Central Organization, Iran
Azinoor Azida Abu Bakar	Universiti Teknologi MARA
Azizul Mohamad	Universiti Malaysia Perlis
Azlinda Saadon	Infrastructure University of Kuala Lumpur
Barjoyai Bardai	UNIRAZAK
Beatriz Sainz	University of Valladolid, Spain
Biju Issac	Teesside University, Middlesbrough, UK
Bilal Beydoun	Lebanese University, Lebanon
Bo Han	Aalborg University, Denmark
BoonKar Yap	Universiti Tenaga Nasional
Bushra Abbasi	Iran University of Science and Technology, Iran
Carolina Piñeiro-Pontevedra	University of Vigo, Spain
Che Maznah Mat Isa	Universiti Teknologi MARA
Che Zulzikrami Azner Abidin	Universiti Malaysia Perlis
Chi-Un Lei	The University of Hong Kong, Hong Kong
Christina Vargis	Universiti Teknologi MARA
Christophe Soares	University Fernando Pessoa, Portugal
Chung-Liang Chang	National Pingtung University of Science and Technology, Taiwan
Dabo Hammad	Universiti Teknologi Petronas
Daniel Brandon	University of Bath, UK
Deepak Petkar	Shivaji University Kolhapur, India
Dinesh Sathyamoorthy	Science and Technology Research Institute for Defence (STRIDE), Malaysia
Eduard Babulak	Sungkyunkwan University, Korea
Egon Ostrosi	UTBM, France
Emilio Jiménez Macías	University of La Rioja, Spain
Ervin Alvarez-Sánchez	Universidad Veracruzana, Mexico
Fadzli M Nazri	Universiti Sains Malaysia
Fauzilah Ismail	Universiti Teknologi MARA
Fengyou Sun	Shanghai Normal University, China
Francisco Torrens	Universitat de Valencia, Spain
Fuyi Tan	Universiti Sains Malaysia
Giovanni Palmerini	Università di Roma La Sapienza, Italy
Gökhan Erdemir	Michigan State University, USA
Gopalakrishnan	Indian Institute of Management Kozhikode, India
Narayanamurthy	
Gregorio Romero	Universidad Politecnica de Madrid, Spain
Gustavo Quintana-Carapia	Instituto Tecnológico de Toluca, Mexico

Hamid Darabi	Stevens Institute of Technology, USA
Hamidah Mohd Saman	Universiti Teknologi MARA
Hannaneh Rashidi-Bajgan	Payame Noor University, Iran
Haryati Awang	Universiti Teknologi MARA
Hassan Ahmed	Arab Academy for Science, Technology and Maritime Transport, Egypt
Henry Yuk-tung Ngan	The University of Sheffield, UK
Houman Ebrahimpour	Shahid Bahonar University of Kerman, Iran
Hui Liu	University of Rostock, Germany
Hwee-San Lim	Universiti Sains Malaysia
Illa Kolani	BUPT, China
Imran Ansari	King Abdullah University of Science and Technology, Saudi Arabia
Indika Perera	University of St. Andrews, UK
Irma Noorazurah Mohamad	Universiti Teknologi MARA
Ivson dos Anjos	UFPA-Federal University of Para�ba, Brazil
Jaekwang Kim	Sungkyunkwan University, Korea
Jaime Calvo-Gallego	University of Salamanca, Spain
Jamaluddin Mahmud	Universiti Teknologi MARA
James Rodway	University of Alberta, Canada
Jee Siong	Multimedia University, Malaysia
Jezaan Md Diah	Universiti Teknologi MARA
Joachim Wiest	CELLASYS GmbH, Germany
Juraidah Ahmad	Universiti Teknologi MARA
Karl Jones	Liverpool John Moores University, UK
Kazuyuki Kojima	Saitama University, Japan
Konstantin Melnikov	Laser and Information Technologies Co, Ltd., Belarus
Kullawat Chaowanawatee	Prince of Songkla University, Thailand
Lance Fiondella	University of Massachusetts, USA
Lau Tze Liang	Universiti Sains Malaysia
Lloyd Ling	University Technology Malaysia/Stanford U—GSB
Luming Zhao	Jiangsu Normal University, China
Mahmood Anwar	Universiti Teknologi Malaysia
Maria Grazia D’Elia	University of Salerno, Italy
Marina Yusoff	Universiti Teknologi MARA
Mariya Aleksandrova	Technical University of Sofia, Bulgaria
Mas Irfan Hidayat	Universiti Teknologi PETRONAS
Masria Mustafa	Universiti Teknologi MARA
Matthias Vodel	Chemnitz University of Technology, Germany
Mazidah Mukri	Universiti Teknologi MARA
Md Jan Nordin	Universiti Kebangsaan Malaysia
Mehmet Celenk	Ohio University, USA
Melany Ciampi	Safety, Health and Environment Research Organization, Brazil

Mohamed Hafez	Universiti Teknologi MARA
Mohamed Omar	Nottingham University Business School Malaysia
Mohammad Zia Ur Rahman	K L University, India
Mohammed Al-Saadi	Universiti Malaya
Mohd Azlan Mohd Ishak	Universiti Teknologi MARA
Mohd Fadzil Arshad	Universiti Teknologi MARA
Mohd Faizal Md Jaafar	Universiti Malaysia Pahang
Mohd Fozi Ali	Universiti Teknologi MARA
Mohd Hafiz Md Ali	Universiti Teknologi MARA
Mohd Shahrieel Mohd Aras	Universiti Teknikal Malaysia Melaka
Mohd-Nordin Mohd Mustaqim	IIESM, Universiti Teknologi MARA
Muhammad Akram Adnan	Universiti Teknologi MARA
Muhammad Naufal Mansor	Universiti Malaysia Perlis
Muhd Norhasri Muhd Sidek	Universiti Teknologi MARA
Neal Holcroft	University of Bath, UK
Nitish Gupta	Tata Consultancy Services, India
Noorsuhada Md Nor	Universiti Teknologi MARA
Noorzalinee Ghazali	Universiti Teknologi MARA
Norliyati Mohd Amin	Universiti Teknologi MARA
Norshariza Mohamad Bhkari	Universiti Teknologi MARA
Nur Mustaffa	Universiti Teknologi MARA
Nurbaiah Mohammad Noh	Universiti Teknologi MARA
Nuryazmeen Farhan Haron	Universiti Teknologi MARA
Óscar Oviedo-Trespalcios	Universidad del Norte, Colombia
Pablo Corral	Miguel Hernández University, Spain
Paik San H'ng	Universiti Putra Malaysia
Pascal Damien	Université Saint-Esprit de Kaslik (USEK), Lebanon
Paulus Sheetekela	MIPT SU, Russia
Peter Walker	University of Bath, UK
Qutaiba Ali	University of Mosul, Iraq
Ripu Sinha	EDUCOSM Technical Campus, India
Robert Dixon	Tomsk State University of Control Systems and Radioelectronics, Russia
Robert Szabolcsi	Óbuda University, Hungary
Rohana Hassan	IIESM, Universiti Teknologi MARA
Rosaura Palma-Orozco	Instituto Politécnico Nacional, Mexico
Rosli Abu Bakar	Universiti Malaysia Pahang
Runer Marson	Brazilian Army Research Institute Physical Fitness, Brazil
Santoso Wibowo	CQUniversity Melbourne, Australia
Satoru Okamoto	Shimane University, Japan
Sergey Biryuchinskiy	St.-Pb. State University of Film and Television, Russia
Seyed Mahdi Mazhari	University of Tehran, Iran

Shahida Begum	Universiti Tenaga Nasional, Malaysia
Shiou Ong	Universiti Teknologi PETRONAS
Siavash Fathollahi Dehkordi	Iran University of Science and Technology, Iran
Sim-Hui Tee	Multimedia University, Malaysia
Siotai Cheong	Tsinghua University, China
Siti Hashim	Malaysian Nuclear Agency, Malaysia
Siti Mariam Sumari	Universiti Teknologi MARA
Siti Nurulhuda Mohd Imran	Universiti Teknologi MARA
Sivarit Sultornsanee	University of the Thai Chamber of Commerce, Thailand
Suélia Rodrigues Fleury Rosa	University of Brasilia (UnB), Brazil
Sulaiman Abdulkareem	University of Ilorin, Nigeria
Sulzakimin Mohamed	Universiti Tun Hussein Onn, Malaysia
Syed Burhanuddin Hilmi Syed Mohamad	Universiti Tun Hussein Onn, Malaysia
Syed Hussain	Taif University, Saudi Arabia
T. Manjunath	Principal and Head of the Institution, India
Tachun Lin	Cameron University, USA
Tahir Ahmed	Universiti Teknologi Petronas
Tamer Nassef	Misr University for Science and Technology, Egypt
Tang Howe Eng	Universiti Teknologi MARA
Tehmina Ayub	Universiti Teknologi Petronas
Thevaneyan David	Universiti Teknologi MARA
Tomoko Saiki	Saiki Patent, Japan
Umesh Deshannavar	K. L. E. Society's College of Engineering and Technology, Belgaum, Karnataka, India
Waaail Al-waely	Al-Mustafa University College, Iraq
Wan Inn Goh	Universiti Tun Hussein Onn, Malaysia
Wardati Hashim	Universiti Teknologi MARA
Wei-Koon Lee	Universiti Teknologi MARA
Xiaohang Li	Purdue University, USA
Ye Cheng	MathWorks, USA
Yingqiong Gu	University of Notre Dame, USA
Yu Kuang	University of Nevada, Las Vegas, USA
Yutthana Tirawanichakul	Prince of Songkla University, Hatyai, Songkhla, Thailand
Zanariah Abd Rahman	Universiti Teknologi MARA
Zeeshan Ahmed	University of Wuerzburg Germany
Zuhaida Mohd Zaki	Universiti Teknologi MARA
Zul Hilmi Saidin	Universiti Teknologi MARA
Zulkifli Mohd. Rosli	Universiti Teknikal Malaysia Melaka

Contents

Part I Timber Engineering

Finite Element Model of Mortise and Tenon Joint Fastened with Wood Dowel Using Kempas Species	3
Haslin Idayu Amaruddin, Rohana Hassan, Norliyati Mohd Amin and Nor Jihan Abd Malek	
Strength Assessment of Malaysian Timbers in Structural Size	15
Mohd Jamil Abdul Wahab, Mohd Zamin Jumaat and Mohamad Omar Mohamad Khaidzir	
Dowel-Bearing Strength Properties of Two Tropical Hardwoods.	27
Rohana Hassan, Azmi Ibrahim, Zakiah Ahmad and Marina Yusoff	
Stiffness Modelling of Non-metallic Timber Connections with Pultruded Dowels	37
Daniël Brandon, Andrew Thomson, Martin Ansell, Julie Bregulla, Richard Harris and Peter Walker	
Mechanical Properties of Cement Composites Incorporating Oil Palm Stem Fiber	51
Dianah Mazlan and A. S. M. Abdul Awal	
Factor of Safety for Dowelled-Double Shear Kempas and Kapur Connections.	61
Rohana Hassan, Azmi Ibrahim, Zakiah Ahmad and Mohd. Nizam Shakimon	
Evaluation of Dowel-Bearing Strength for Wood Dowel Using ‘Spring Theory’	75
Rohana Hassan, Shaharin Hamid, Nity Azidah Mohammad Amini and Tengku Anita Raja Hussin	

Ultrasonic Wave Non-Destructive Method for Predicting the Modulus of Elasticity of Timber.	85
M. B. F. M. Puaad, Z. Ahmad and H. Muhamad Azlan	
Ultimate Strength of Kekatong Glued Laminated Timber Railway Sleepers	97
Norshariza Mohamad Bhkari, Zakiah Ahmad, Afidah Abu Bakar and Paridah Md Tahir	
Experimental Study to Single Shear Kapur Connection and Comparisons with European Yield Model	107
Mazlina Mohamad, Rohana Hassan and Khairul Effendy Ab Mutalib	
Particle Swarm Optimization for Single Shear Timber Joint Simulation	117
Marina Yusoff, Shahril Mohd Shalji and Rohana Hassan	
 Part II Concrete Waste and Earthquake Engineering	
Estimation of Ground Motion in Kuala Lumpur Due to Sumatra Subduction Earthquake	129
Tze Che Van and Tze Liang Lau	
Strength of Quarry Dust Modular Bricks and Wallethes Under Compression.	141
Atikah Fatma Md Daud and Zakiah Ahmad	
A New Lateral Load Pattern Study Based on a Different Limit States	153
Fadzli Mohamed Nazri and Bee Fang Ku	
Alkaline Activators Concentration Effect to Strength of Waste Paper Sludge Ash-Based Geopolymer Mortar.	169
A. R. M. Ridzuan, A. A. Khairulniza, M. A. Fadzil, J. Nurliza, M. A. M. Fauzi and W. M. F. W. Yusoff	
Seismic Performance of Laminated Rubber Bearing Bridges Subjected to High Intensity Earthquake Time-History Loading.	177
Wan Noor Azhar Wan Sulaiman and Norliyati Mohd Amin	
Chemical Characterization of Used Cooking Oil Foaming Agent as Admixture in Foamed Concrete.	191
M. M. A. Hafiz, A. R. M. Ridzuan, M. A. Fadzil and J. Nurliza	

Effect of Input Variable for Neural Network Architecture in Predicting Building Damage Subjected to Earthquake 201
 Rozaina Ismail, Azmi Ibrahim and Azlan Adnan

Potential Use of Industrial By-products for Developing High Strength Concrete Under Normal Curing Conditions. 215
 Dhawal Desai and Prakash Nanthagopalan

Seismic Analysis of Reinforced Concrete Structures in Low to Moderate Earthquake Zones of Peninsular Malaysia 225
 Jeffrey Chiang and Meng Siang Wong

A Review of Magnetorheological Elastomers: Characterization Properties for Seismic Protection 237
 Rozaina Ismail, Azmi Ibrahim and Hanizah Ab. Hamid

Fresh Properties of Self-Compacting Concrete Incorporating Palm Oil Clinker. 249
 Jegathish Kanadasan and Hashim Abdul Razak

Part III Flood Management and Intelligence Development

Flood Economy Appraisal: An Overview of the Malaysian Scenario 263
 Wei-Koon Lee and Irma Noorazurah Mohamad

Neural Network Approach to Coastal High and Low Water Level Prediction 275
 Wei-Koon Lee and Tuan Asmaa Binti Tuan Resdi

Comparative Study of Flood Frequency Analysis on Selected Rivers in Myanmar 287
 Ni Lar Win and Khin Maung Win

Part IV Fluvial and River Engineering Dynamics

Determination of Baseflow Index for Bernam River at Tanjung Malim 303
 Fauzi Bin Baharudin, Asma Nabilla Iskak and Amirudean Shafiee

Water Sensitive Urban Design in Existing Urban Settings: Case Study of Dry Detention Pond in Kuching City	315
Darrien Yau Seng Mah, Afdal Haziq bin Mohamad Salehe and Frederik Josep Putuhena	
Enhancing Water Resources and Coastal Engineering Curricula Using Visual Basic Programs in MS-Excel	323
Ahmad Sana	
Regression Analysis for Dimensionless Discharge Ratios Prediction. . .	331
Issam A. Al Khatib	
Potential of Estuary Transverse Flow Salinity Intrusion Due to Extreme Estuarine Flooding	343
Farhan Haron Nuryazmeen, Tahir Wardah and Irma Noorazurah Mohamad	
 Part V Transportation Systems, Infrastructure and Intelligent Transport	
Assessing Pedestrians' Perspective on the Walkability of Pedestrian Environment Under Mixed-Use Development	355
Noor Iza Bahari, Ahmad Kamil Arshad and Zahrullaili Yahya	
An Analysis of User Satisfaction on Public Transport Terminal Based on Users Survey	369
Nornikmah Mohammad Noor, Ahmad Kamil Arshad, Ismacahyadi Bagus Mohd Jais and Masria Mustafa	
Evaluation of Pedestrian Level of Service for Tehran Crosswalks; Case Study of Nabovat Square in East of Tehran.	377
Seyed Abdolhadi Daneshpour, Mohadeseh Mahmoudi and Bushra Abbasi	
Physical Properties of Modified Asphalt Binder with Nanopolyacrylate.	389
E. Shaffie, J. Ahmad, A. K. Arshad, D. Kamarun, F. Kamaruddin and M. A. Shafiee	
How Much Money Can Be Saved? Impact of Driving Style on Bus Fuel Consumption	399
M. Rohani and R. Buhari	

Neglecting Helmet Usage in Rural Area: Behavioral Causal Factors According to Different Age Groups 413
 Nur Sabahiah and Abdul Sukor

Pedestrian Egress Behavior During Classroom Evacuation: A Simulation Approach 423
 Masria Mustafa, Zanariah Abd Rahman,
 Mohamad Noor Faiz Mohamad Najid and Yasmin Ashaari

Part VI Geotechnical Engineering

Groundwater Level Detection by Using a Two-Dimensional Electrical Resistivity Imaging. 437
 A. Derahman, H. Awang and N. M. Osman

PFA-Cement Mixture for Sand Column Parameter Stabilization. 449
 S. Shakri, M. A. Hafez and S. Norbaya

Dynamic Soil Stiffness Between WAK, SASW and SCPT Tests. 461
 Norazzlina M. Sa'don, Michael John Pender
 and Abdul Razak Abdul Karim

The Influence of Cyclic Load to the Properties of Weathered Granite 477
 N. A. M. Salim, Z. Mohamed and M. N. Berhan

Empirical Correlation of P-wave Velocity to the Density of Weathered Granite 489
 Mohd Mustaqim Mohd-Nordin and Zainab Mohamed

Strength of Soft Soil Stabilized Using Lime-POFA Mixtures. 501
 Norazlan Khalid, Mazidah Mukri, Faizah Kamarudin,
 Norbaya Sidek and Mohd Fadzil Arshad

Plasticity Index of Soft Soil Modified with Fly Ash and Oil Palm Shell Activated Carbon 511
 Siti Nur Aida Mario and Rudy Tawie

Rock Mass Classification System Used for Pahang-Selangor Raw Water Transfer Tunnel 519
 Romziah Azit and Mohd Ashraf Mohamad Ismail

Electrokinetic Remediation to Remove Heavy Metal from Contaminated Soils Using Purging Solution	531
Sabariah Arbai, Zainab Mohamed, Kamaruzzaman Mohamed and AzinoorAzida Abu Bakar	
 Part VII Innovative Construction Materials and Structures	
Ultimate Load Carrying Capacity of Precast Lightweight Foamed Concrete Sandwich Panel (PLFP) with Double Shear Truss Connectors Under Axial Eccentric Loading	541
N. Mohamad, W. I. Goh, R. Abdullah, Ismail Ahmad, S. Samsuddin and M. H. A. Rahman	
Strain Behaviour of Exposed Steel Reinforcement Bars Using FBG Sensor	557
M. S. Hamidah, M. J. Faizal Mohd, M. S. Norhasri Muhd, I. Noorli and S. Vasagavijayan	
Mechanical Properties of High-Strength Concrete Reinforced with PVA and Basalt Fibres	567
Tehmina Ayub, Nasir Shafiq, Muhd. Fadhil Nuruddin and Sadaqat Ullah Khan	
Compressive Strength and Density of Unfired Lightweight Coal Ash Brick	577
Mohamad Ezad Hafez Mohd Pahraraji, Hamidah Mohd Saman, Mohamad Nidzam Rahmat and Kartini Kamaruddin	
Fibre Reinforced Modulus of Elasticity and Compressive Strength of Foamed Concrete	589
R. Suzila, M. S. Hamidah, A. Anizahyati and M. R. Ahmad Ruslan	
Behavior of Reinforced Masonry Column Under Axial Loading Using Sand Quarry Dust Modular Unit	597
Zulhazmee Bakri, Zakiah Ahmad and Atikah Fatma Md Daud	
Charpy's Impact Test on Co-cured In-line Joint Unidirectional Kenaf Fibre Reinforced Plastic Composite	611
Safarina Haslimawaty Hamdan, Anwar Zainal Abidin and Zakiah Ahmad	

Active Fatigue Crack Detection and Classification of Reinforced Concrete Beams Using Acoustic Emission. 625
 Noorsuhada Md Nor, Azmi Ibrahim, Norazura Muhamad Bunnori, Hamidah Mohd Saman, Soffian Noor Mat Saliah and Shahiron Shahidan

Flexural Behavior of Reinforced Concrete (RC) Beams with Externally Bonded (EB) Carbon Fiber Reinforced Polymer (CFRP) Sheets. 637
 M. N. Nurbaiah, A. H. Hanizah and I. Nor Farhana

Heat of Sorption and Moisture Buffering Properties of Building Insulation Materials 649
 Neal Holcroft and Andy Shea

Performance Based Design of Self-Compacting Concrete Incorporating Class F Fly Ash. 663
 Juli Asni Lamide and Roslli Noor Mohamed

Mechanical Properties of Modular Cement Block Reinforced with Treated Oil Palm Trunk Fiber. 675
 Mazlina Mohamad and Zakiah Ahmad

Tensile and Interlaminar Shear Strength of Unidirectional Kenaf Fibre Reinforced Polymer with Overlapping Joint 689
 Safarina Haslimawaty Hamdan, Anwar Zainal Abidin and Zakiah Ahmad

Compressive Strength of Laminated Rubber Bearing Due to Different Temperature Exposure 701
 Norliyati Mohd Amin, Anizahyati Alisibramulisi and Norhayati Kadir

Effect of Superplasticizers on Workability of Fly Ash Based Geopolymer 713
 Behzad Nematollahi and Jay Sanjayan

The Effect of Steel Fibre on Flexural Strength of Fibre Reinforced Concrete at High Temperature 721
 Clotilda Petrus, Ruqayyah Ismail, Fariz Aswan Ahmad Zakwa, Nur Ashikin Marzuki, Nor Hafida Hashim and Khairil Imran Fadillah

Compressive Behavior of Steel Fiber Reinforced Concrete After Exposed to High Temperatures 731
 Ruqayyah Ismail, Fariz Aswan Ahmad Zakwan, Clotilda Petrus, Nur Ashikin Marzuki, Nor Hafida Hashim and Muhammad Fahmi Mustafa

Part VIII Bioremediation and Engineering

An Assessment of Water Demand in Malaysia Using Water Evaluation and Planning System	743
M. F. Ali, A. Saadon, N. F. Abd Rahman and K. Khalid	
Water Quality Measures Using QUAL2E: A Study on RoL Project at Upper Klang River	757
M. F. Ali, M. H. Ahmad, K. Khalid and N. F. Abd Rahman	
Performance of Aquatic Macrophytes on Removal and Accumulation of Sulfate and Potassium from Domestic Wastewater	769
Zul Hilmi Saidin, Ramlah Mohd Tajuddin, Dzaraini Kamarun and Norazah Abdul Rahman	
Greywater Reclamation Using Recycled Vertical Subsurface-Flow Constructed Wetland (RVFCW) for Non Potable Usage	783
Azianabiha A. Halip @ Khalid, Siti Nurulhuda Mohd Imran and Shahrul Azwan Shakrani	
Effect of Water Pressure to Water Loss in Water Distribution Network.	795
Irma Noorazurah Mohamad, Nur Syahiza Zainuddin, Azianabiha A. Halip @ Khalid and Mohamad Radhwan Abd Karim	
Monitoring and Preserving Water Quality Using GIS Tools and Statistical Approach	805
Mohd Adhar Abd Samad and Mohd Khairy Kamarudin	
The Effectiveness of <i>Pseudomonas putida</i> Atcc 49128 as Biodegradable Agent in Biodiesel Soil Contamination	817
N. M. Sunar, Q. A. Emparan, A. T. A. Karim, S. F. M. Noor, M. Maslan, F. Mustafa and N. Khaled	
The Quality of Kenaf Retting Water After Retting Using <i>Bacillus cereus</i> for Fiber Extraction	825
Mohd Nazrin Othman, Ramlah Mohd Tajuddin, Zakiah Ahmad and Mohd Fozi Ali	

Part IX Synergistic Innovative Management

Sustainable Considerations in the Operation of Onsite Construction Equipments and Vehicles: A Malaysian Perspective 837
 M. Waris, Mohd. Faris Khamidi and Arazi Idrus

Factors Contributing to Building Maintenance Performance of Heritage Buildings. 851
 Syed Burhanuddin Hilmi Syed Mohamad, Zainal Abidin Akasah and Mohammad Ashraf Abdul Rahman

Strength, Weakness, Opportunity and Threat Attributes of Malaysian Construction Firms in International Market 861
 Che Maznah Mat Isa, Hamidah Mohd Saman, Siti Rashidah Mohd Nasir and Aini Jaapar

Application of Automation Technology in Malaysian Construction Industry 871
 Siti Rashidah Mohd Nasir, Che Maznah Mat Isa and Kamilah Ali

Part X Nano-Materials for Engineering

Alteration of Nano Metakaolin for Ultra High Performance Concrete. 887
 A. Mohd Fadzil, M. S. Muhd Norhasri, M. S. Hamidah, M. R. Zaidi and J. Mohd Faizal

Hybrid Nanoparticle-Based XLPE/SiO₂/TiO₂ and XLPE/SiO₂ Nanocomposites: Nanoscale Hybrid Assembling, Mechanics and Thermal properties. 895
 Josmin P. Jose, Zakiah Ahmad and Sabu Thomas

About the Author 903

Author Index 905

Part I
Timber Engineering

Finite Element Model of Mortise and Tenon Joint Fastened with Wood Dowel Using Kempas Species

Haslin Idayu Amaruddin, Rohana Hassan, Norliyati Mohd Amin
and Nor Jihan Abd Malek

Abstract Finite element method (FEM) was used to model the behavior of mortise and tenon joint with wood dowel subjected to pull-out loads. The stress-state in the dowel was observed and the type of failure was indentified according to European Yield Model (EYM). The experimental results from Rohana [6] were used to validate a three-dimensional finite element model of mortise and tenon joint. In this study, linear-elastic orthotropic material was adopted to represent the Kempas wood behavior in FEM. The analysis was conducted by introducing tensile loads on the top of tenon to see the behavior of the dowel. The EYM mode of failures and load–displacement curves were then being compared between FEM results and experimental results obtained by Rohana [6].

Keywords Finite element method · Mortise and tenon · Wood dowel · EYM · Linear-elastic · Orthotropic material

1 Introduction

Mortise and tenon is the most common type of traditional timber joint used in timber structures. This type of joint has been used for hundreds of years and is recognized to be strong enough to support structural members. Mortise and tenon is a method of jointing two pieces of members by slotting a stud or tenon that is formed at the end of a member into a rectangular hole in the other member called mortise. The joint is reinforced using dowel to give ductile behavior to the joint.

H. I. Amaruddin
Faculty of Civil Engineering, Universiti Teknologi MARA, Pahang Bandar Pusat Jengka,
Pahang, Malaysia

R. Hassan (✉) · N. Mohd Amin · N. J. Abd Malek
Institute for Infrastructure Engineering and Sustainable Management (IIESM), Faculty of
Civil Engineering, Universiti Teknologi MARA, Shah Alam, Selangor, Malaysia
e-mail: rohan742@salam.uitm.edu.my

The durability of timber structure is much depending on the strength of the joint connection. Failure at any joint of the timber structure will affect the performance of the whole structure [1]. This research is focusing on mortise and tenon joint fastened with wood dowel using Kempas species of Malaysian timber. The method used in the study is Finite element method (FEM) or sometimes called finite element analysis (FEA).

There are not many papers reported on mortise and tenon joint in their studies. Among those papers, most of them are using their local timber as their research material. Shanks [2] investigated this type of traditional joint using oak timber. Kang et al. [3] reported using Chinese traditional timber. On the other hand, there are very limited researches studies on tropical timber. Rohana et al. had studied the performance of mortise and tenon joint with Kempas and Kapur species by experimental works [4–6]. However, laboratory works are time consuming and expensive. FEM is essential to minimize the time and cost consume by a project. Nevertheless, there is no FEM studies on wood connection using Malaysian timber was published. The problem in modeling the timber using FEM is to define the orthotropic material properties of the wood. Thus material testing is necessary as the mechanical properties of tropical timber are not available. In this study, the FEA of the mortise and tenon joint will be compared to the work done by Rohana [6] to see the significant of the results.

The main aim of the study was to observe the competent of FEM analysis to model the behavior of timber joint that is comparable to the existing experimental data obtained by Rohana [6] using LUSAS. To attain this aim, the specific objectives are set to model orthotropic behavior of timber made of kempas species, to simulate the stress state along the dowel subjected to pull out loads and to identify the European Yield Model mode of failure that represent the timber behavior.

This study was carried out to investigate the performance of mortise and tenon joint using finite element analysis (FEA). Several parameters were highlighted as the limitation of this research. This research only focused on mortise and tenon joint fastened with wood dowel. The entire joint including mortise, tenon and the dowel was using wood from kempas species. The analysis of mortise and tenon joint under pull-out loading was carried out using LUSAS software. The finite element model of the wood is orthotropic linear-elastic. The behavior of the timber joint was simulated to indentify the load–displacement curve of the joint and the stress state along the dowel to be compared to experimental results.

2 Application of Timber Structures

The introduction of engineered timber materials as well as the researches on timber materials in the past few years had improved the modern design of timber structures. Some countries have utilized timber structures in their construction to help preventing pollutions. Stadthaus in Hoxton, London is one of the applications of modern timber design. Stadthaus is a nine-storey residential apartment. This

building had been designed using cross laminated solid timber system (CLT) that was introduced by KLH UK Ltd. The construction of Stadthaus applied the combination of reinforced concrete and solid timber [7].

In Malaysia, Malaysian Timber Industry Board (MTIB) has taken a step forward by introducing the first glulam building using Malaysian timber. The building is called Glulam Gallery and is located in Tampoi, Johor. The glulam timber was made of Resak and Keruing of Malaysian timber. The connections were using glued-in rods, bolted and welded to brackets and steel plates. The aim of MTIB is to promote the utilizing of timber structures in Malaysia construction industries [8]. Construction of hotels and resorts in Malaysia seems to favour the use of timber. This is because timber structures have aesthetic values and they symbolize the Malaysian traditions. Sunset Valley, Langkawi was constructed as a tribute to Malaysian wood. The owner of this resort is a Dutch couple Andre and Ria. They decided to build this resort to show their passion on wood [9]. Terrapuri and Tanjung Jara Resort in Terengganu are also utilizing wood as their main construction materials.

Masjid kayu or its name Masjid Ulul Albab Seberang Jertih Terengganu is one of the unique mosques in Malaysia. It was completed in August 2011. The mosque was made of Cengal, Nyatoh and Balau wood. It was built by implementing Malay traditional wood craft. The foundation of the mosque was constructed using in situ reinforced concrete while the other parts of the building were using totally Malaysian wood. The connections between members were mortise and tenon joint system without any single nail [10].

3 Properties of Kempas Species

Kempas or its scientific name *koompassia malaccensis* normally grows in the lowland and in swampy area and classified as medium heavy hardwood (MHW). It has a density in the range of 770–1,120 kg m⁻³ air drying. MS 544 classified Kempas in strength group S.G 2 together with dedaru, merbatu and mertas for designs purpose [11]. Kempas is medium durable and it requires treatment before use. When treated, Kempas is suitable for heavy constructional works [12]. The information on kempas mechanical properties is also available in wood handbook [13]. The summary on mechanical properties of Kempas from three different sources is shown in Table 1.

4 Previous Studies on Fem of Joint

FEM is widely used in many researches to simulate stress–strain state of a complex model under specific conditions. This method is also competent to model joint behavior under unusual loading. It is also able to model the effect on the behavior of the joint while changing the parameters.

Table 1 Summary of kempas properties

Kempas properties	Moisture content (%)	Density (kg/m ³)	Specific gravity	MOE (MPa)	MOR (MPa)
Gan et al. [12]	–	945	–	18,600	122
MS 544, 2001	19	910	0.74	17,700	–
Wood handbook [13]	12	–	0.71	18,500	122

Geramitcioski and Vilos [14] studied the problem associated with the contact between end-plate connections of a steel structure using numerical approach. The researchers used FEM to obtain moment-rotation diagram of the end-plate connection. In the end, the researchers found that FEM simulation gave better solution for maximum loading of the end plate compared to EUROCODE 3. In addition, Anizahyati [15] used FEM to study on corrugated web beam to column connection with extended end-plate welded to beam. The aim was to investigate moment-rotation response of the joint and compared it with the experimental results. She found that the stiffness from the FEM was identical to the experimental value.

On the other hand, Sabuwala et al. [16] simulated the behavior of beam to column connection under blasting loads. The research was carried out using reinforced and unreinforced connection for both experimental and finite element analysis. The results obtained were then compared. They found that reinforced connection performed better under blast loading and the FEM was successful.

Finite element method of analysis had successfully proven the modeling of timber connection. Many studies had been conducted to analyze timber to timber connection using FEM. Xu et al. [17] conducted a study on timber connections with glued-in rods as dowel. The model developed was based on FEM of contact and non-linear behavior of material. They suggested that the gap between the connected timbers has a small effect on the ultimate moment capacity.

Guan and Inoue [18] utilized FEM to model failure mechanism of reinforced timber fasteners. They used bamboo plywood and carbon fiber as the local reinforcement. They successfully simulate the failure mechanism. The correlation between failures mode from FEM and experimental tests are identical.

In addition, Racher and Bocquet [19] developed finite element modeling to investigate non-linear behavior of wood beneath the fasteners and embedding properties of the wood. They concluded that shear strength and friction coefficient could affect the plastic behavior of timber beneath fastener. Villar et al. [20] modeled roof trusses with traditional joint using FEM. The purpose of the modeling was to perform detailed analysis of the strain–stress state of the joint. They concluded that friction on the contacting area is important as it affects the performance of the joint.

Dowelled timber connection under fire was investigated by Laplanche et al. [21]. They used 3D-FEM to represent the thermo-mechanical analysis of the connection. They found that the strength and stiffness reduction of dowel subjected to tensile force parallel to grain is depending on the length of exposure.

Daudeville and Yasumura [22] in their paper analyzed the failures of bolted wood joint. In the FEM, the wood was considered as transverse isotropic materials. The behavior of the wood in radial and tangential was considered as the mean value of the mechanical properties in these two directions. Linear-elastic was adopted. In this study the dowel was considered as fit without any friction. They found that the wood fracture was similar to experiment results. Franke and Quenneville [23] simulated the timber behavior in FEM to study the behavior of dowel under tension load perpendicular to the grain. They found that the FEM model of the cracks growth was similar to the laboratory test.

Chen et al. [24] studied on the effect of parameters such as the end distance, the material properties of the wood and the characteristic of joint element to the behavior dowel type timber joints subjected to tensile and compression loads. The study used plane stress analysis in 2D CASTEM FEM application. Three nodes elements, THR13 were used to model the timber and JO12 elements to model the contact between the dowel and the holes. From the FEM results, they observed that the compressive and tensile stresses were inversely proportionate to the length of end distance.

Shanks [2] used FEM to validate his experimental work. He investigated the stress-state of timber dowel, mortise and tenon subjected to pull out of tenon. He also observed the effect of variation in joint parameter to the stiffness. He found that the FEM had been successfully predicted the connection stiffness and changes of connection behavior due to the changes in parameters.

Johnn et al. [25] conducted a research on the effects off varied angle of timber frames on the performance of mortise and tenon connection subjected to tensile load. The yields mode of failures of the dowel, mortise and tenon members were observed. The researcher found that mortise splitting, tenon tear out, dowel bending and dowel shear were the obtained mode of failure. The type of dowel failures is given in Fig. 1 where I_s is crushing of mortise members, I_m is crushing of tenon, III_s is the rupture and bend of dowel with a plastic hinge at the centre of tenon and IV is crushing of both mortise and tenon members with two plastic hinge formed in the dowel. The researchers concluded that the mode of failure governed the ductility of a connection. The connection ductility decreased for small angle as compared to 90 degrees angle.

On the other hand, Rohana did a study on mortise and tenon joint with dowel fastener. The aim was to observe the behavior of the joint under shear, bending and tensile. The researcher compared the performance of mortise and tenon joint with steel, GFRP and wood dowel. The mode of failures of the joint followed EYM for double shear as stipulated in NDS [26]. The mode of failure for double shear connection has four types (Type I_m , I_s , III_s , IV). It was obtained that wood dowel failed under mode IV [6].

The results obtained from Rohana [6] were used as the basis of this research. This research studied the performance of mortise and tenon joint with wood dowel using FEM and validate the FEM findings with Rohana work. The finite element model in this study adopted the maximum yield loads in the experimental as the loading of the modeling. The modeling followed the tensile test conducted in the

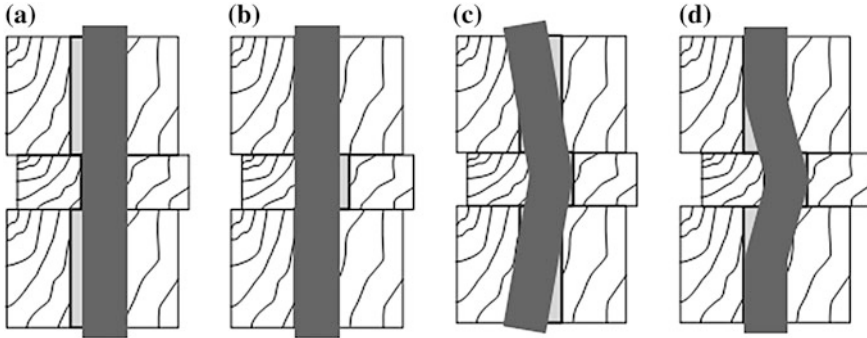


Fig. 1 Dowel mode of failures. **a** I_s, **b** I_m, **c** III_s, **d** IV [25]

laboratory. The point of consideration in load displacement comparison was taken at the tenon top similar to the laboratory test.

5 Research Methodology

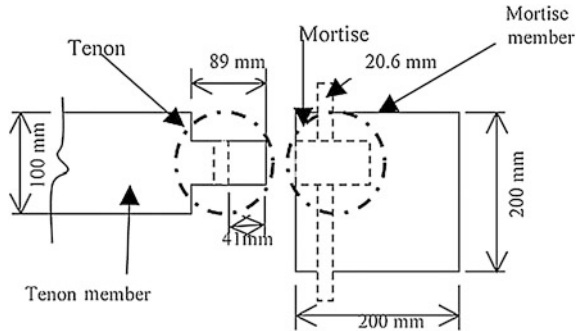
This study was divided into three phases. The first phase was the identification of wood mechanical properties such as the young modulus, shear modulus, Poisson's ratio, and mass density. The second stage was the development of the finite element model of the mortise and tenon joint. Several numbers of models were formed to obtain the most suitable meshing elements types and material properties. The third part of the study was the analysis process of the mortise and tenon joint model. The stress states and the failure behaviors of the dowel and the members were investigated.

The joint dimensions were briefly described in the subsequent topic which adopted the actual tensile test in the laboratory. To reduce computing time, only part where the tenon fit into the mortise was drawn and it was further simplified by introducing symmetry plane. The dimension of the mortise and tenon joint is shown in Fig. 2. The column size is 200×200 mm with a rectangular mortise hole of $41 \times 100 \times 150$ mm. While the beam was 100×150 mm with $41 \times 89 \times 150$ mm tenon at the end. The wood dowel diameter was 20.6 mm. To simplify the modeling process, a part where the tenon fit into the mortise hole was modeled instead of the actual size of the tested mortise and tenon joint.

5.1 Finite Element Model Using LUSAS

LUSAS is one of the application software based in United Kingdom's that uses finite element method in its analysis. The FEM is used to generate accurate approximate solutions for all linear and non-linear stress, dynamic and thermal

Fig. 2 Plan view of mortise and tenon joint [4]



problem. The LUSAS 14.7 (academic version) was used in this study. As this version is for academic use, limitation on number of nodes and some functions applied. Therefore, this study is bounded to those limitations.

Similar to Shanks [2], linear elastic orthotropic material was adopted to represent the joint in tensile because the connection was modeled in the elastic range only. However, elasto-plastic material behavior may closely represent the timber behavior as timber may have some ductility before failure. Shanks [2] also had proven that modeling nonlinear material behavior will increase the computing time for modeling and analysis but would give a small difference on the global response. Therefore, the timber behavior was assumed to be linear under pull out loading with brittle failure. The loading was the yield load taken from experimental test conducted in the laboratory by Rohana [6] since only the elastic part was modeled.

The shape of the dowel was assumed square to simplify the modeling process. Rod dowel may require higher order meshing elements thus required more nodes. The available LUSAS software in the Faculty of Civil Engineering, Universiti Teknologi MARA has its limitation in numbers of nodes of the whole model. Exceeding the limit will lead to fatal errors. Increasing number of nodes requires longer time to analyze. Fit dowel was assumed in this study since the available FEM application did not support contact element.

Solid model was used to imitate the actual timber joint. Bottom lines of the model were created for the half of the joint model. The lines were then being swept in the y direction to form surfaces. Volume geometry was defined by sweeping the surfaces in the z-axis. The volume that represented the hole was deleted.

Defining suitable element meshing is an important part in finite element modeling. A 3D solid continuum element was chosen and the model was meshed using 8 nodes, hexahedral element with three degree of freedoms on each node was known as 'HX8M'. Xu et al. [12] and Gonzalez et al. [1] also used similar mesh in their model. Regular mesh type was chosen. Automatic mesh tool is the best to be used to generate the mesh by specifying the element size. The total elements created for the dowel were 1,743 while for mortise and tenon members were 6,171 elements.

Table 2 Finite element model for orthotropic material properties

Property	Kempas	
E_L (N/mm ²)	E_x	17,700
E_R (N/mm ²)	E_y	2,885
E_T (N/mm ²)	E_z	1,274
G_{LR} (N/mm ²)	G_{xy}	1,522
G_{LT} (N/mm ²)	G_{xz}	1,431
G_{RT} (N/mm ²)	G_{yz}	152
ν_{LR}	ν_{xy}	0.369
ν_{LT}	ν_{xz}	0.618
ν_{RT}	ν_{yz}	0.428
Mass density (tonne)		0.93×10^{-9}

Solid orthotropic material properties were set to all members. The mechanical properties of kempas species was given by MS 544 [11] as in Table 2. In finite element modeling, nine mechanical properties must be identified for solid orthotropic material. The ratio of young modulus in the three orthotropic axis, $E_x:E_y:E_z$ were taken as 1:6:14 as specified in Wood handbook [13] for white oak wood while the shear modulus, G_{xy} was taken as proportion of 1:12 to the young modulus in the longitudinal direction, E_x . The Poisson's ratio in this study was assumed to be similar to Poisson's ratio of white oak given in Wood handbook which has equivalent specific gravity.

Therefore, the E_y is equal to 0.163 E_x and gives E_y as 2,885 Mpa. The E_x is taken as 17,700 Mpa from MS 544 [11]. The value of E_z is equal to 0.072 E_x and gives E_z as 1,274 Mpa. While the value of shear modulus (G) was also computed from the given ratio which was G_{xy} is equal to 0.086 E_x and gives G_{xy} as 2,885 Mpa. The shear moduli in xz and yz planes were calculated with the relation suggested by Sangree and Schafer. The relationship between the shear modulus in the three planes was given as $G_{xy}:G_{xz}:G_{yz}$ in the ratio of 10:9.4:1 [27].

Boundary conditions were applied to the model. The mortise member was fixed in all directions where the faces continuous in the full joint. Half model was created due to symmetry axis in yz plane. Thus symmetry boundary condition was assigned to the surfaces. For the tenon, the translation in x and z direction was zero.

The pull-out loading was applied to the tenon top surface similar to the experimental laboratory test. The loading applied as incremental of concentrated load where the total load had been set to 8 KN. Non-linear analyses was performed to see the behavior of the stress state by introducing load factors. The loading was then increased to 30 KN to observe the wood dowel behavior under higher loading.

6 Finite Element Method Output

In the finite element modeling, the mortise and tenon joint was modeled in 3D to closely represent the actual mortise and tenon joint in the laboratory. The finite element results were displayed in color contour as presented in Fig. 3. The stress

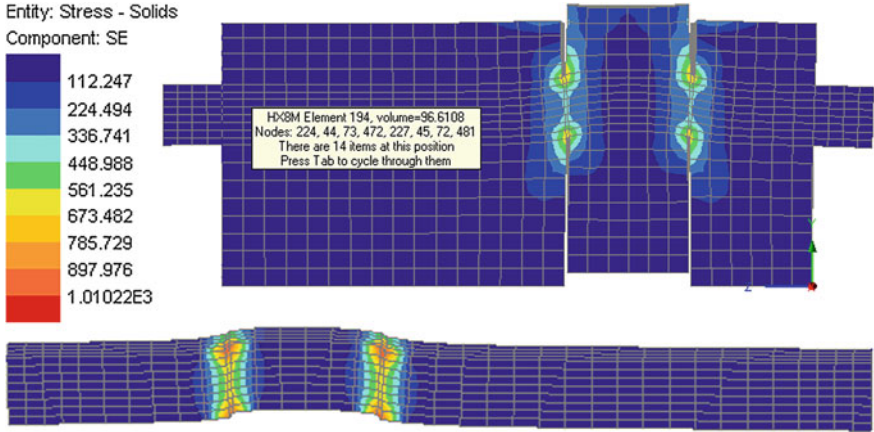


Fig. 3 Stress concentration in the joint

Fig. 4 Total failure of wood dowel in laboratory test (top), deformed shape of dowel in FEM at higher tensile load (bottom)



state of the dowel at any point can be determined by comparing the color contour with the key plot. The red color represents the higher stress location. The stress was mostly concentrated at the bearing area. The maximum stress at dowel was $1,434 \text{ N/mm}^2$. As the loading increased, the dowel started to bend to form two plastic hinges at the edge between the tenon surface and the mortise surface. These areas were experiencing higher stress.

The deformed mesh illustrated the dowel behavior under tensile. The deformed shape of the dowel was in mode IV of EYM mode of failure which was similar to wood dowels failure behavior obtained in the laboratory. There were two plastic hinges with associated wood crushing formed as the loads increased during the analysis. Higher stress was observed at the plastic hinge. The deformed dowel shows in Fig. 4.

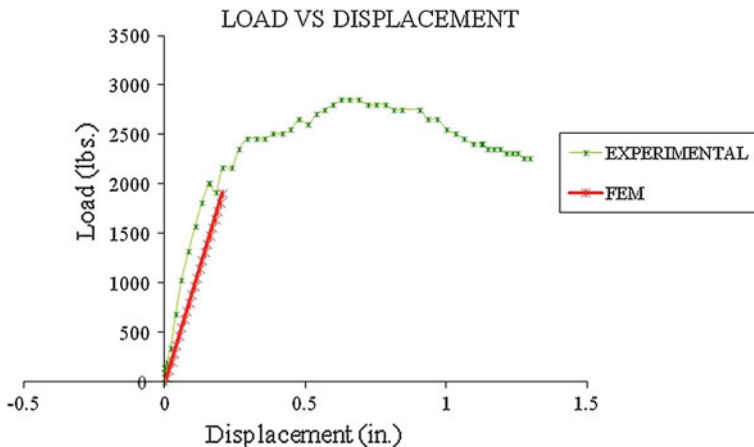


Fig. 5 Comparison of Load displacement *curve* from laboratory test and FEM [6]

A point on the wood dowel which experienced the most stress was taken as the reference point. The point was located on the plastic hinge area of the dowel. Stress–strain curve was plotted at the reference point. The shape of the curve is linear. This is because the finite element model was assumed to behave linear elastically. This might not be true in the laboratory test. The wood dowel had some ductility against tensile before total damage occurred as shown in the load–deformation curve obtained in the laboratory by Rohana [6] in Fig. 5. The FEM graph was plotted on the graph obtained in the laboratory to compare the shape of Load–displacement curve. The shape obtained was identical to the laboratory results where the stiffness was taken as yield at proportionate value. However, the graph shows that FEM underestimate the stiffness of the connection.

The obtained stiffness was low might be due to several factors. The material properties in the modelling were the approximated values taken form MS 544 and wood handbook. The assumed materials properties did not represent the actual wood tested in the laboratory. Meanwhile, the fit dowel assumed in the modelling might also affect the obtained results since a fit dowel is imposible to get in the laboratory. In the modelling, a square dowel was adopted in stead of circle dowel as it may also influence the results.

The stiffness from finite element model is 1.6 kN/mm which is low as compared to the experimental value of 3.6 KN/mm obtained by Rohana [6]. The maximum displacement is 5.1 mm with maximum loading of 8.5 kN. The yield load in the laboratory test was 8.1 kN. Therefore, the results obtained from the FEM were acceptable. Figure 5 shows the comprison of load–displacement curve from experiment and FEM.

7 Conclusion and Recommendation

The results from this study enhance the understanding of performance of mortise and tenon fastened with wood dowel. The behavior of the joints was studied by utilizing finite element model (FEM). The results from the finite element model had been compared with the experimental results obtained by Rohana [6]. A similar shape of load–displacement curve was found between the FEM results and the experimental results.

However, FEM underestimate the stiffness of the connection. Therefore, further improvement can be done for future studies. It is recommended that researchers must conduct laboratory works to find out the mechanical properties of the tested wood rather than relying on published data. Advanced FEM software is suggested to cater for limitation on modeling higher order meshing types and joints element.

Finite element model had shown that it is capable of predicting the behavior of mortise and tenon joint under tensile loads. Therefore, it is very useful to use FEM in research to reduce cost and time and also as a method to validate the findings in the experimental works.

Acknowledgments The authors would like to thank the Ministry of Higher Education (MOHE), Malaysia for funding this research through ERGS grant provided by Research Management Institute (RMI), Universiti Teknologi MARA.

References

1. J.L. Gonzalez Fueyo, M. Dominguez, J.A. Cabezas, M.P. Rubio, Design connections with metal dowel-type fasteners in double shear. *Mater. Struct.* **42**, 385–397 (2009)
2. J.D. Shank, Developing rational design guidelines for traditional joints in oak frame construction. PhD. thesis, University of Bath, UK, 2005
3. M. Kang, N. Yang, Q. Cha, Studies on static performance of mortise and tenon joint in traditional column and tie construction timber structure. *IEEE Conf. Publ.* **2011**, 6197–6200 (2011)
4. H. Rohana, I. Azmi, A. Zakiah, Shear and bending performance of mortise and tenon connection fastened with dowel. *J. Trop. For. Sci.* **22**(4), 425–432 (2010)
5. H. Rohana, I. Azmi and A. Zakiah, Shear capacity of dowelled mortise and tenon in tropical timber. *IOP conference series: Materials science and engineering*, vol. 17(1), pp. 012012, 2011
6. H. Rohana, Structural performance of GRFP dowelled mortise and tenon connections made of selected tropical species. PhD. thesis. Faculty of Civil Engineering, Universiti Teknologi Mara (UiTM), Shah Alam, Selangor Malaysia, 2011
7. M. Wells, Tall timber buildings: application of solid timber construction in multi-storey buildings. *CTBUH J.* **1**, 24–26
8. O. Azlina. Galeri Glulam Tampil Teknologi Terkini. *Sinar harian Edisi Johor* (2012). <http://www.sinarharian.com.my/edisi/johor/>
9. F. Motesbitsa, Sunset valley—tribute to Malaysian timber, timber Malaysia, Malaysian Timber Council, vol. 15(5), Sept–Oct 2009
10. M. Azman, Masjid Tanpa Paku. *Rona, Berita Minggu*, 19 Feb 2012

11. Malaysian Standard, MS 544: Part 2: 2001 Code of practice for structural use of timber. Department of Standards Malaysia, SIRIM
12. K.S. Gan, T. Choo, S.C. Lim, Timber notes—medium hardwoods I (Kapur, Kasai, Kelat, Keledang, Kempas). *Timber Technol. Bull., FRIM.* **11** (1999)
13. Wood Handbook (2010), *Wood as engineering material*. Centennial Edition. (Forest Product Laboratory. United States Department of Agriculture Forest Service, 2010), pp. 5-1–5-46
14. T. Geramitcioski, I. Vilos, Numerical modelling of the contact problem on the end-plate connections of the steel structures. *Appl. Technol. Innov.* **4**(1), 1–11 (2011)
15. A. Anizahyati, Analysis of corrugated web beam to column extended end plate connection using LUSAS software. Master science thesis. Faculty of Civil Engineering, Universiti Teknologi Malaysia, Johor, Malaysia, 2006
16. T. Sabuwala, D. Linzell, T. Krauthammer, Finite element analysis of steel beam to column connections subjected to blast loads. *Int. J. Impact Eng.* **31**, 861–876 (2005)
17. B.H. Xu, A. Bouchair, P. Racher, Analytical study and finite element modelling of timber connections with glued-in rods in bending. *Constr. Build. Mater.* **34**, 337–345 (2012)
18. Z. Guan, and M. Inoue, Modelling of failure mechanism of locally reinforced timber fastener. 10th world conference on timber engineering (WCTE), Miyazaki, Japan, 2–5 June 2008
19. P. Racher, J.F. Bocquet, Non-linear analysis of dowelled timber connections: a new approach for embedding modelling. *Electron. J. Struct. Eng.* **5**, 1–9 (2005)
20. J.R. Villar, M. Guaita, P. Vidal, R. Arguelles Bustillo, Numerical simulation of framed joints in sawn-timber roof trusses. *Span. J. Agric. Res.* **6**(4), 508–520 (2008)
21. K. Laplanche, D. Dhima, and P. Racher, Thermo-mechanical analysis of timber connection under fire using 3D finite element model. 9th World conference on timber engineering (WCTE), Portland, OR, USA, 6–10 Aug 2006
22. L. Daudeville, M. Yasumura, Failure analysis of timber bolted joints by fracture mechanics. *Mater. Struct. J.* **29**, 418–425 (1996)
23. B. Franke, P. Quenneville, Numerical modelling of failure behavior of dowel connections in wood. *J. Eng. Mech.* **137**(3), 186–195 (2011)
24. C.J. Chen, T.L. Lee, D.S. Jeng, Finite element modelling for the mechanical behaviour of dowel-type timber joints. *Comput. Struct. J.* **81**, 2731–2738 (2003)
25. P.J. Johnn, S.F. Fernando, R.W. Carson, R.T. Paul, Tensile strength of varied-angle mortise and tenon connections in timber frames. *J. Struct. Eng.* **138**(5), 634–636 (2012)
26. NDS, National design specification for wood construction American forest and paper association (AFPA), Washington D.C, 2005
27. R.H. Sangree, B.W. Schafer, Field experiments and numerical models for the condition assessment of historic timber bridges: case study. *J. Bridge Eng.* **13**(6), 595–601 (2008)

Strength Assessment of Malaysian Timbers in Structural Size

Mohd Jamil Abdul Wahab, Mohd Zamin Jumaat
and Mohamad Omar Mohamad Khaidzir

Abstract In Malaysian timber engineering practice, mechanical tests on timbers were conducted based on small clear timber specimens. Throughout the world, the practice of structural size timber assessment has been long-established. Stress values obtained from structural size timber are more accurate for allocating value in structural design. Preliminary testing works have been initiated to establish the mechanical properties of Malaysian timbers in structural form. Some commercial timbers were tested using structural size bending method. Results indicated that bending strength of structural size specimen is lower compared to small planks.

Keywords Bending · Modulus · Strength · Elasticity · Tropical

1 Introduction

The formal mechanical testing of Malaysian timbers started circa 1920s. Original documents of the experimental results date back to year 1929 still exist and are being kept in Timber Engineering Laboratory of Forest Research Institute Malaysia (FRIM). The method of testing was similar to BS 373:1957 and ASTM D143–52 [1]. The timbers were tested based on small clear specimen method in green and fully air-dried condition. Lee et al. [2] have compiled the mechanical test results of some commercial Malaysian timbers in Timber Trade Leaflet No. 34. However, several properties have not been estimated and some have been

M. J. A. Wahab (✉) · M. O. M. Khaidzir
Timber Engineering Laboratory, Forest Research Institute Malaysia, FRIM, Kepong,
Malaysia
e-mail: mohdjamil@frim.gov.my

M. Z. Jumaat
Department of Civil Engineering, University of Malaya, Kuala Lumpur, Malaysia

inadequately estimated, partly because the assessments were based on a small quantity of material and partly because there is variation in mechanical properties even in the same log. So far, in Malaysian timber engineering practice, mechanical tests on timber were conducted based on small clear timber specimens.

These data are the basis for strength groups (SG) of Malaysian timbers which refer to as SG1 to SG7. Besides, the values became the foundation of Malaysian Standard Code of Practice on Structural Use of Timber [3]. From a scientist point of view, stresses obtained from small clear specimen's method may have been technically convenient for the determination of timber's mechanical properties. However, the method cannot provide accurate values for structural engineering applications due to the great variations in biological materials. Structural engineers and designers need accurate and reliable values concerning the structural performance of timber in its' definite size.

Practically, timbers of structural sizes are very seldom free from defects. In fact, the load may be applied for an indefinite period instead of a few minutes. Unlike homogeneous materials, the result of timber defects on strength has been fairly established and recognized in the basic testing rules. Fully as significant as the presence of the defects are their size, number, and location in the piece [4]. Defects will have their greatest effect at points of maximum stress.

Stress values obtained from structural size timber are more accurate for allocating value in structural design since the risk of stress ratio is eliminated. Besides, the values will reflect more on the actual strength of the timber in use. Throughout the world, the practice of structural size timber assessment has been long-established. The formal stress grading system in the United States started since 1902 with tests on both small and structural size timbers [5]. The arrangement for structural timber test varies in different parts of the world. In Australia and North America, the measurement of deflection is at the middle point between supports, often referred as global measurement. Whereas in Europe, the measurement is over a gauge length between two loading points, usually referred as local measurement [6]. Although there are several dissimilarities on the testing set up, but the test pieces are in structural sizes.

Small specimen methods for mechanical testing of timber have resulted with incomparable values, hence totally unjustifiable conclusions. Local and global timber practitioners start inquiring on what are the stresses of Malaysian timbers in their structural form. The following sections of this paper will discuss on the stresses of some commercial timber tested in structural size.

2 Research Methodology

The assessment focuses on the determination of bending strength and modulus of elasticity in structural size timber planks. Evaluation of stresses is made by comparing the results with small specimen values. Timber samples were selected from several commercial timber groups. Each sample was cut into standard

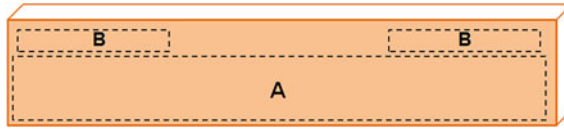


Fig. 1 Cutting pattern and nominal dimension of test specimens; A structural size specimen (50 × 150 × 3,050 mm) and B small clear specimen of 2 inches standard (50 × 50 × 762 mm)

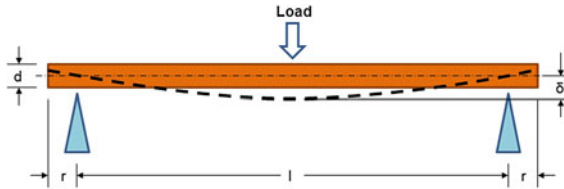


Fig. 2 Small clear timber specimen bending test arrangement; l bending span (711 mm), r overhang (25 mm), d specimen thickness (50 mm) and δ bending deflection (mm)

dimensions for structural size specimen and small clear specimen. Figure 1 illustrates the cutting pattern of the specimens.

2.1 Small Clear Specimen Method

Load was applied at the middle of the plank. The test arrangement is shown in Fig. 2. This particular configuration is referred as ‘three-point bending’ or ‘centre-point bending’. The bending strength is presented as bending modulus of rupture (MOR) which is the corresponding stress in the timber at a point of failure. The MOR in three-point bending was calculated based on the equation below

$$MOR = \frac{3P_{max}l}{2bd^2} \quad (1)$$

where P_{max} is the maximum applied load (N), l is the bending span (mm), b is the width of the specimen (mm) and d is the depth of the specimen (mm).

Load–deflection graphs were recorded automatically through Trapezium 2 software. Loads corresponding to increments of deflection were recorded. The modulus of elasticity (MOE) in three-point bending was calculated using the following equation

$$MOE = \frac{\Delta Pl^3}{4\Delta\delta bd^3} \quad (2)$$

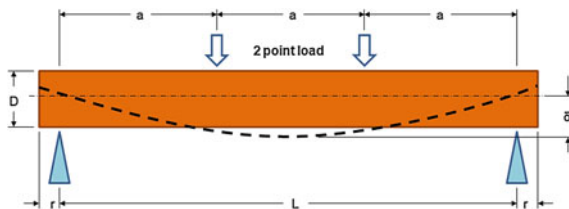


Fig. 3 Arrangement for structural size bending test; L bending span ($18 \times D$ mm), r overhang ($\geq D/2$ mm), D specimen thickness (mm), a distance between a loading point and the nearest support ($L/3$ mm) and δ bending deflection (mm)

where ΔP is the increment of load below the limit of proportionality (N), l is the bending span (mm), $\Delta \delta$ is the increment of deflection corresponding the load (mm), b is the width of the specimen (mm) and d is the depth of the specimen (mm).

2.2 Structural Size Timber Method

Test configuration for specimen in structural sizes is referred to as ‘four-point bending’. Arrangement for four-point bending test is illustrated in Fig. 3. The test piece was symmetrically loaded at two points over a span of 18 times the thickness (D). The test piece was simply supported on each side with an overhang of not less than half the thickness of the specimen. The distance between the two loading points was equal to the distance between one loading point and the nearest support. Small steel plates were inserted between the piece and the loading points to minimize the local indentation. Load was applied at constant loading-head movement adjusted so that the maximum load is reached within 5 ± 2 min.

Before testing, a critical section was determined in each piece of timber. The critical section was positioned at the centre of the mid span, between the inner load points. The tension edge of the piece was selected at random. The corresponding MOE in four-point bending was calculated from the following equation

$$MOE_{structural} = \frac{\Delta F(L^3 - 3La^2 + 2a^3)}{4\Delta\delta BD^3} \quad (3)$$

where L is the bending span (mm), a is the distance between a loading point and the nearest support (mm), B is the width of the plank (mm), D is the thickness of the plank (mm), ΔF is the increment of load (N) and $\Delta \delta$ is the increment of deformation corresponding to ΔF (mm).

Structural size bending strength was determined by bending the timber specimens to failure. The MOR in four-point bending was calculated from the following equation

$$MOR_{structural} = \frac{F_{max}a}{2W} \quad (4)$$

where F_{max} is the maximum load (N), a is the distance between an inner load point and the nearest support (mm) and W is the section modulus (mm^3).

3 Results and Discussion

3.1 Stress Analyses

To date, four sample groups of Malaysian hardwood were tested. However, due to limited project funding and timber availability, the number of specimens was not the same. The analysis is more likely to demonstrate the effect of plank's dimension on the strength and stiffness. Readers should bear in mind that the current strength and stiffness values of Malaysian timbers are based on small plank assessments, thus the results will explain the actuality in mechanical properties of structural timber. Test pieces from each sample were tested for both structural size and small planks. Initially, a sample of 33 planks of mixed hardwoods was tested in three different sizes each. The results are shown in Table 1. The moisture content (MC) of the test pieces was also calculated.

Generally, the bending strength of structural size planks is lower compared to the smaller one. The difference is apparent even between small planks of 2 cm and 2 in. Smaller plank resulted with less influence of defects, such as knots and cross grain. At the same time, it was impractical to totally avoid defect from structural size plank. Defective planks were previously proven to affect the strength of timber. On the other hand, the MOE value is higher for larger planks. However the differences are less significant than the MOR values.

To determine whether the result is the same regardless of density, three specific groups of timber were evaluated. Penaga, kulim and sesendok are timbers in SG1, SG3 and SG7 respectively. Samples of 40 penaga, 90 kulim and 33 sesendok were tested for small and structural size method. Table 2 shows the respective average results of MOR and MOE. For each sample, the results indicated that MOR of structural size specimen is lower compared to small planks. However, the differences were uneven and did not compare well for a fixed ratio. The distributions of structural data are scattered. Then again, structural size MOE values are higher compared to small planks. Thus these patterns are similar for all timber despite the consequences of the SG. The MOR and MOE comparisons of the three timber groups between two different plank sizes are shown in Figs. 4, 5 and 6.

Defects and wood grain deviation reduce the strength distinctly. For tropical timber, the deviation is difficult to distinguish. In actual visual grading practice, even the grain angle is not easy to be determined [7]. In fact, a clear and straight-grained plank may be expected to demonstrate slight variability in mechanical

Table 1 Average MOR and MOE values of mixed hardwood planks of three different sizes

Structural size (50 × 100 × 2,030 mm)	Small clear (50 × 50 × 760 mm)		Small clear (20 × 20 × 300 mm)		MC at test (%)
	MOR (MPa)	MOE (MPa)	MOR (MPa)	MOE (MPa)	
78.1 (20.8) ^a	16,074 (2,730)	14,198 (3,014)	117.1 (30.5)	14,677 (3,226)	20–30

^a Standard deviation values (in brackets)

Table 2 Average MOR and MOE values of penaga, kulim and sesendok

Timber name	Structural size (50 × 150 × 3,000 mm)		Small clear (50 × 50 × 760 mm)		Average MC at test (%)
	MOR (MPa)	MOE (MPa)	MOR (MPa)	MOE (MPa)	
	Penaga	108 (14.9)	18,331 (1,625)	144 (14.9)	
Kulim	75 (11.8)	13,736 (1,821)	94 (14.8)	12,805 (2,105)	21.0
Sesendok	43 (9.5)	8,454 (1,525)	53 (6.8)	6,925 (1,274)	18.0

^a Standard deviation values (in brackets)

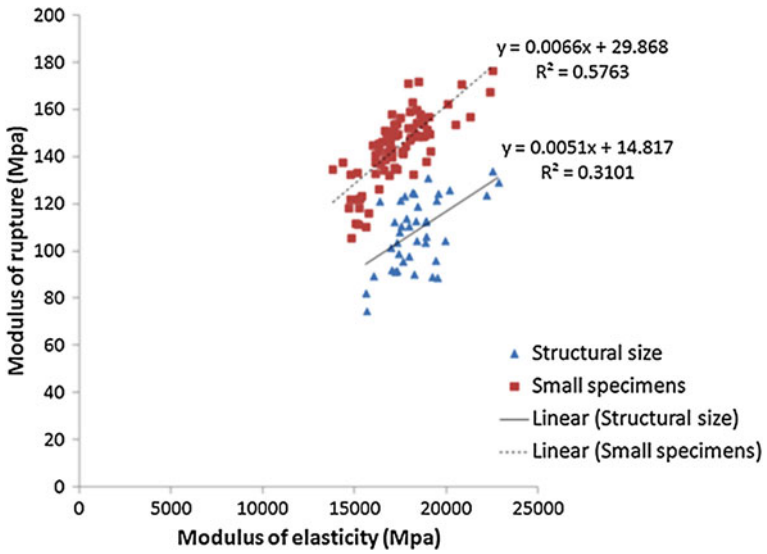


Fig. 4 Distribution of MOR and MOE results of penaga timber between structural and small planks

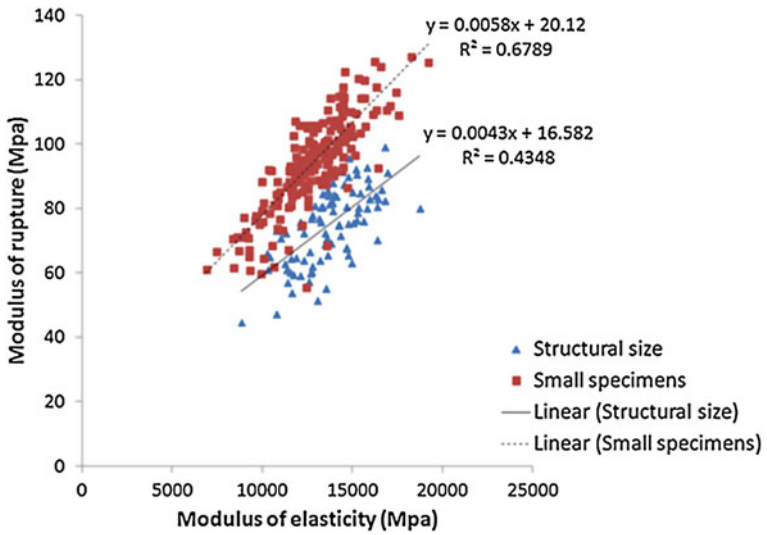


Fig. 5 Distribution of MOR and MOE results of kulim timber between structural and small planks

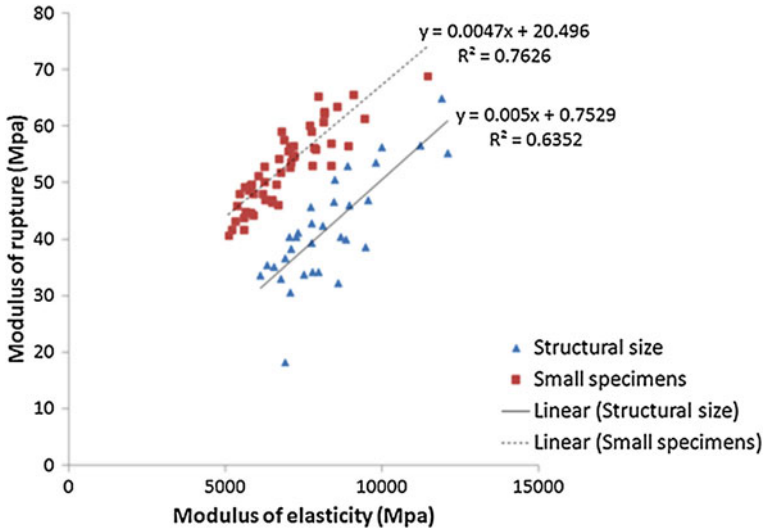


Fig. 6 Distribution of MOR and MOE results of sesendok timber between structural and small planks

Fig. 7 The crossed-gain failure of structural size test piece was noticeable



properties along the length [8]. Ironically, even when all factors known to influence the strength of timber have been considered, the strength value will still differ 10–15 % than another [9] (Fig. 7).

A number of factors have to be considered in testing large size timbers. Defects will have their greatest effect when at points of maximum stress. In a beam tested under centre loading, the maximum stress in bending occurs at the centre. Defects would have their maximum effect at the centre of the length on the bottom face and also on the lower edges of the vertical faces of the beam. If the defects were located toward the neutral axis and toward the ends, their effect would diminish.

Under third-point load, defects would have the maximum effect in the lower surface and edges anywhere between the loads.

The bearings at the load points require special attention in order to prevent indentation or premature compression failure both along and across the grain. This is taken care of by distributing the load through bearing plates and curved blocks. Another major source of error in edgewise large size bending will be linked to the initial twist of the timber piece. Twisted plank resulted in buckling during test. However, it was observed that buckling error can be eliminated by placing thin plate in gap between twisted plank and support. Vertical roller supports on both side of the test piece will improve the assistance.

It is, certainly, well known that the MC in timber has a tremendous effect on the strength of timber pieces. Above 25 % MC, the strength of timber does not alter, but as timber dries its strength increases. The exact MC below which there is an increase of strength is known as the “fibre saturation point” and it is not the same for every species [9]. In structural sizes, however, the development of defects tends to offset any increase in fibre strength that may take place as a result of a reduction in MC. Furthermore, tropical hardwood timbers, even after air seasoning for 1–2 years, are only partially dry. The outer shell may be somewhat near an air-dried condition, but the moisture content increases from this point to a practically green condition at the centre. This unequal distribution of moisture content causes a progressive failure and appears to be one of the large factors that prevent so called air-dried timbers from showing any higher strength than green timbers. After many years of seasoning, structural timbers will assume a more nearly uniform moisture content throughout, and, with the exception of additional weakening due to defects, would be expected to increase in strength.

In other words, it is highly essential that none of the details, such as average moisture content, moisture distribution, and size, number, and location of defects, be overlooked or slighted in any way if results of any significant value are to be obtained. Careful analysis should also be made of the data to see that none of the factors that affect the strength of structural timbers have been overlooked or misinterpreted.

3.2 Recent Research and Development

One very important and pertinent issue in the marketplace is the extension of the CE mark to cover timber destined for structural use. The letters “CE” are the abbreviation of French phrase “Conformité Européene” which literally means “European Conformity”. CE-marking is a manufacturer’s declaration that the product complies with the essential requirements of health, safety and environmental protection legislation. All timbers for any structural use in Europe (EU-25 plus Iceland, Liechtenstein, Norway and Switzerland), regardless of origin, had to be marked CE as referred in the European standard EN 14081 and classified according to mechanical criterion in structural form. Unfortunately, the assessment

of this strength prerequisite has not been carried out for most tropical species, including Malaysian timber species.

A national committee on strength grouping of timber has been discussing concerning the drawbacks for the execution of structural size assessment. The laboratories involve should be concerned on the capacity of staff and facility available. Testing structural size heavy hardwoods timbers anticipates the laboratory to be equipped with a principal testing machine not less than 300 kN of loading capacity. Generally, staff responsible for conducting the tests should possess a high level of understanding of the theory and procedure of the structural size test indicated by their qualification and experience. The governmental organizations such as Malaysian Timber Industrial Board (MTIB) and Malaysian Timber Council (MTC) should be aware of the high expenses needed to procure the samples required to execute the test. Millions of Ringgit has to be invested to fund the testing of over hundred of marketable timber species in large sizes. With more than 3,000 species of Malaysian timbers, it is almost impossible to conduct the structural size test for each species. Eventually the amount of tested planks plus remnants which are not reusable for structural application is just like creating extra damages to the timber businesses. Not to overlook the risk of unavailable timber species owing to the statistics of what is still available in the forests. Above and beyond, the time frame to accomplish the assessment would be unpredictable.

It appeared that in structural form timber does not perform as well as it turns out in small specimens. Nevertheless, these deceptive values have been referred for timber construction practice for decades went before. Thus preliminary testing works have been initiated to establish the relationship between small timber specimen and structural size properties that leads to the more precise mechanical strength values. A compliment should be given to University of Malaya for funding the groundwork project in structural size testing of Malaysian timbers which started at the end of 2009. Current project on structural size timber testing of Malaysian timber is being sponsored by Ministry of Science and Technology of Malaysian Government.

Strength and stiffness values of timber planks of different dimensions should be measured with extra concern compared to homogeneous materials. Solely use of strength values obtained from small plank test for classification and design of timber structures is not practically ideal. From these considerations it appears that for a better mechanical criterion of timber planks, testing method that measures as closely as possible in-service performance is required. Although the intended values may not be very accurate due to the characteristic of biological material, but is nonetheless necessary to be performed.

4 Conclusion

In general, the experimental results indicated that bending strength of larger plank is lower compared to the smaller one. In term of modulus of elasticity, larger plank is generally exhibits higher value compared to small plank. For academic

comparison, test method using small specimens still remains valid in characterising the mechanical properties of timber. However, by itself, the test specimen is not representative of actual plank being used in the construction practice. Unfortunately, this method became the basis for the structural stresses of Malaysian timbers for many years. Tests on timber of structural size give more precise and reliable values concerning the actual service condition of timber in construction. However, the drawback of cost and duration of time needed to execute large plank assessment of Malaysian timbers is extremely immeasurable.

Acknowledgments We are indebted to Che Muhammad Farid and Syarmiza Anuar for assisting in the mechanical testing work. The research was financed by the Institute of Research Management and Monitoring, University of Malaya and currently funded by Ministry of Science, Technology and Innovation Malaysia for the structural size timber assessment in Forest Research Institute Malaysia.

References

1. C. Engku Abdul Rahman, Basic and grade stresses for some Malaysian timbers. *Malayan Forester* **34**, 131–134 (1971)
2. H. Lee Yew, C. Engku Abdul Rahman, P. Chu Yue, The strength properties of some Malaysian timbers. Timber Trade Leaflet No. 34. Forest Department: Kuala Lumpur (1993)
3. MS 544, Code of practice for structural use of timber: Part 2—Permissible stress design of solid timber, Department of Standard Malaysia (First revision) (2001)
4. B. Madsen, H. Andrew Buchanan, Size effects in timber explained by a modified weakest link theory. *Can. J Civil Eng.* **13**(2), 218–232 (1986)
5. W.L. Galligan, D.W. Green, Structural lumber: an overview of research needs. *Am. Soc. Civil Eng* 3–27 (1984)
6. L. Bostrom, Determination of the modulus of elasticity in bending of structural timber—comparison of two methods. *Eur. J. Wood Wood Prod.* **57**(2), 145–149 (1999)
7. R. Geert, J.W. Van de Kuilen, Comparison of methods of strength classification of tropical hardwood timber, in *Proceedings of the Eleventh World Conference on Timber Engineering*, 20–24 June 2010, Riva Del Garda
8. D.S. Gromala, Determination of modulus of rigidity by ASTM D-198 flexural methods. *J. Test. Eval.* **13**(5), 352–355 (1985)
9. A.V. Thomas, Some notes on timber testing. *Malayan Forester* **1**, 56–59 (1931)

Dowel-Bearing Strength Properties of Two Tropical Hardwoods

Rohana Hassan, Azmi Ibrahim, Zakiah Ahmad and Marina Yusoff

Abstract Bearing strength of wood is one of the properties that are use to estimate the lateral connection of wood design strength based on the European Yield Model (EYM), National Design Specification [NDS 2005 in National design specification for wood construction american forest and paper association (AFPA), Washington D.C, 2005] theory. This study investigated the characterisation of load to grain directions and two dowel sizes in two high-density Malaysian hardwood species; Kempas (*koompassia Malaccensis*) and Kapur (*Dryobalanop* spp.). Experimental work as stipulated in ASTM 5764-9a [American Standard Testing Method (ASTM) D 5764-95a in], Standard test method for evaluating dowel-bearing strength of wood and wood-based products, 2007] was adopted. Result shows that according to the species, the lower strength group of species attributes to higher bearing strength of wood. It was also found that the bearing strength of parallel to the grain is higher than the perpendicular to the grain. In terms of dowel diameter, the bearing strength perpendicular and parallel to the grain decreased slightly as the dowel diameter increased regardless of the timber species. The EYM equations were found viable and sufficient in predicting the dowel-bearing strength of bigger dowel diameter for Kempas but not for the smaller dowel diameter. Contradict to Kempas species; the EYM equations were viable for the smaller dowel diameter and not for the bigger dowel diameter for Kapur. Thus, in the case of the insufficient predictions, three modified equations based on EYM, were proposed according to the specific gravity, density, species, dowel diameter and loading directions respectively.

R. Hassan (✉) · Z. Ahmad · M. Yusoff
Institute for Infrastructure Engineering and Sustainable Management (IIESM),
Universiti Teknologi MARA, Shah Alam, Malaysia
e-mail: rohan742@salam.uitm.edu.my

A. Ibrahim
Faculty of Civil Engineering, Universiti Teknologi MARA,
Shah Alam, Malaysia

Keywords Kempas (*Koompassia malaccensis*) • Kapur (*Dryobalanop* spp.) • European yield model (EYM) equations

1 Introduction

Currently, very limited studies about Malaysian tropical timber are published and reported especially on the experimental work using structural size timber and jointing system. Few papers are found discussed on bending and shear behavior of mortise and tenon connection [3–5], however these publications are still lacking of dowel-bearing strength information. The dowel-bearing behaviour is defines as the load-deformation behaviour of wood or wood-based products laterally loaded by a fastener where the fastener does not bend during loading [2]. Dowel-bearing strength is one of the properties of wood that affects the design value capacity (Z) of a nails, bolt or lag bolt. Few research literatures termed this property as embedment strength. Bearing strength is an important parameter to determine EYM.

ASTM is based on full-hole or the half-hole test. According to Awaludin et al. [6], in half-hole test method; the dowel uniformly loaded along its length, producing a uniform stress distribution through the projected bearing area. All ends of dowels are free to rotate, bearing stress under the dowel is considered to be uniformly distributed and the dowels fit tightly as possible in the hole.

Bearing strength tests in this study were performed in accordance with (ASTM)—D5764-9a [2] that is using half-hole test method. This method allows full exposure of the specimens during testing, thus detail observations on the specimens during the test such as appearance of cracks or any failure pattern shall be observed. This failure pattern cannot be observed if the full-hole test is use.

2 Literature Review

Many previous researches relate the dowel-bearing strength to the fastener or the wood characteristics. The fastener's characteristics are such as dowel diameter and dowel type (nails, bolts or screws) [7]. Dowel-bearing strength in relations to the wood characteristic are such as moisture content [8, 9] grain directions [10], density [11, 12]; specific gravity [13] and wood species [10]. Dowel-bearing strength was also being studied for the engineered wood materials such as glue laminated [14, 15] laminated veneer lumber [16] and plastic wood composite [17]. Embedment strength for parallel and perpendicular to the grain loading has been related to the bolt diameter and specific gravity by Wilkinson [13] using empirical

equation (Eqs. 1 and 2). These equations were derived based on the 5 % offset load rather than capacity and is applied in the current NDS 2005 [1] after a few modifications.

$$F_{e//} = 11,200G \quad (1)$$

$$F_{e\perp} = 6,100G^{1.45}d^{-0.5} \quad (2)$$

where $F_{e\perp}$ is the bearing strength in the perpendicular grain direction in psi unit, $F_{e//}$ is the bearing strength in parallel grain direction in psi unit, d fastener diameter in inch and G is specific gravity based on oven-dry weight.

Though the bearing strength can be easily evaluated from the empirical equations given by the previous studies and current standards, however, this bearing strength were developed from softwood species [6, 10–12]. As claimed by Awaludin [6], the calculated bearing strength might be questionable because the equations were developed mainly from the test data of softwood species. Thus further investigations of bearing strength for the tropical species is very much needed in order to specifically verify the applicability of the existing standards to the use of tropical species.

Existing data of dowel-bearing strength tested on tropical timber is very much limited. Pioneers in determining the bearing strength of wood base in Malaysia was started by Mohd Zamin Jumaat and his group of researchers in 2006 and 2008 [11, 12]. Their intention was to compile data of local timber since no study were previously conducted locally which emphasize in this area. Five other Malaysian species from different joint group according to MS 544 were tested. The species are Balau (*Shorea* spp.) (group J1), Kempas (*Koompassia malaccensis*) (group J2), Mempening (*Quercus* spp.) (group J3), Mengkulang (*Heritiera* spp.) (group J4) and Pulai (*Alstonia* spp.) (group J5). All specimens were compressed in parallel to grain direction with 0.31, 0.39 and 0.47 in. diameter dowel.

From the study, it was concluded that density is a major factor that influence the bearing strength characteristics. Bearing strength was also found almost constant regardless of dowel diameter except for the timber with greater densities. The bearing strength decreased slightly as the dowel diameter increased. This study were also found similar to Hilson et al. [18], Rammer [10] and Sawata and Yasumura [19]. Another record on bearing strength of Balau species with a limited number of tests were published by Awaludin et al. [6]. Only Awaludin et al. [6] tested on the bearing strength of hardwood species compressed on different angle which include the parallel and the perpendicular to the grain. They commented that the average bearing strength parallel to the grain was 7.25 % lower than the prediction given in EC 5, 2008. The bearing strength perpendicular to the grain evaluated based on bearing load at initial cracking was substantially different from any predictions given by previous studies or design standard.

3 Tests Methods

All bearing strength specimens were prepared from the cut of the mortise and tenon joints after the full scale joints were tested. The specimens were cut in the form of parallel and perpendicular to the grain. The method approached in this study to determine the bearing strength of wood embedded with steel is according to the ASTM-D5764-95a [2].

The dowel-bearing strength tests were performed on Kempas and Kapur wood block using steel dowels in accordance to ASTM D5764-95a [2], "Standard test method for evaluating dowel-bearing strength of wood and wood based composites". Wooden block specimens were prepared in the sizes of 1.61 by 3.74 by 4.92 in. Twenty replicates were prepared for 0.18 and 0.49 in. dowel diameter. In order to prepare the half-hole, two wooden blocks were clamped together with sufficient pressure to maintain contact between faces (Fig. 1a). Lead hole was then drilled in between the two pieces with hole larger than the dowel diameter. Clamps were then removed and the dowel was then inserted in the half hole. Both pieces were used for testing (Fig. 1b). The pre-boring holes were bored in tight-fitting to the dowels sizes according to the same way as would in the practice. The half-hole wooden block specimen is illustrated in Fig. 1c.

The testing assembly consisted of a rectangular wooden block with half-hole placed on the flat base on Universal Testing Machine (UTM) and a load head made of steel plate that pressed the dowel into the specimen. A picture of the dowel-bearing test setup is shown in Fig. 2.

The tests were run on a UTM hydraulic testing machine with a 224,808.9 lbs capacity load cell. A constant displacement rate of 0.04 in./min was used, and the tests were run until the load head touches the block or when the displacement remains constant. The resistance load was recorded from the load cell, and displacements were acquired from the external Linear Variable Differential Transformer (LVDT).

4 Results and Discussions

Bearing strength capacity was limited to the investigation of the load to the grain directions (perpendicular and parallel to the grain), timber species and dowel diameter. All specimens were in the particular range and group of specific gravity and moisture contents to replicate the actual timber properties. Bearing strength capacities were determine from 5 % offset load. The ultimate load was also taken for further comparison and analysis of the bearing strength behavior. The ultimate load is when the load head touched the block specimens or the load of each bearing stress before the block split or cracks. At this point the dowel material is considered bearing in full.

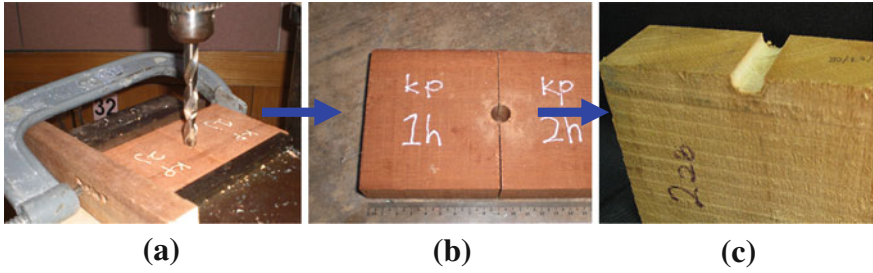


Fig. 1 Preparation of half-hole wooden block specimen for bearing test: (a) drilling of specimens, (b) two pieces of specimens and (c) specimen block ready for test

Fig. 2 Half-hole test configuration according to ASTM—D5764

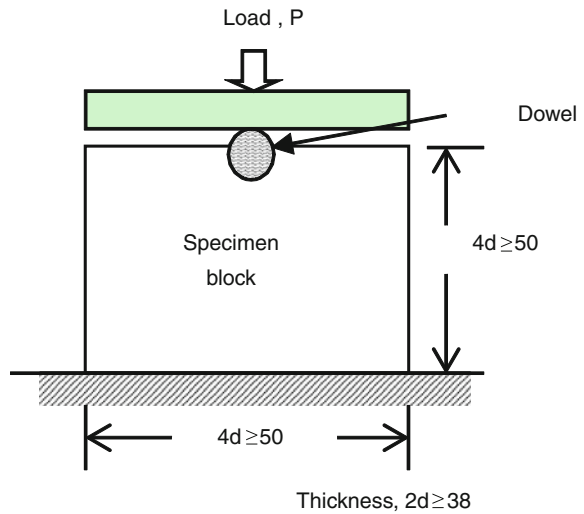


Figure 3 depicted that the bearing strength parallel to grain shown a linear increase up to the yielding of wood and was continuously increase its strength and displacement up to fracture. This also means that the steel dowel deforming the base material in the vicinity of the hole equally initially, reach its ultimate load capacity until further crushing on hole or cracks of block specimens and its stiffness degraded. However, the displacement of the parallel to grain to reach its ultimate was only about 0.2 in. whereas in perpendicular to grain, the displacement was extended up to 0.5 in. to reach its ultimate. It was also depicted that the bearing strength of parallel to grain was higher than the perpendicular to grain.

Figure 4 shows the relations of the dowel-bearing strength of Kempas and Kapur in perpendicular and parallel to grain direction for both 0.81 and 0.49 in. diameter dowel. It was obvious that all the mean values decreased when the dowel diameter increased. However, the bearing strength parallel to the grain decreased slightly as the dowel diameter increased regardless of the timber species. Whilst

Fig. 3 Bearing strength-displacement curve of perpendicular and parallel dowel bearing strength of Kempas

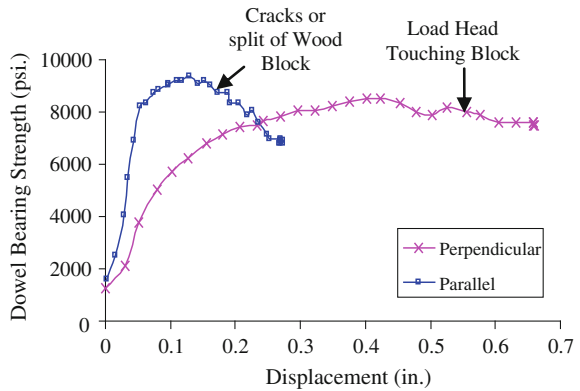
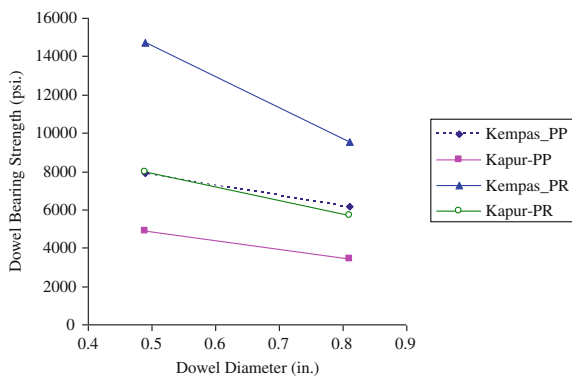


Fig. 4 Relations between dowel-bearing strength of Kempas and Kapur in perpendicular and parallel-grain direction for 0.81 and 0.49 in. diameter dowel



bearing strength of Kempas species substantially decreased as the dowel diameter increased. This characteristic shows that the harder of the base materials, the higher differences occurs in the bearing strength of wood on the effects of dowel diameter. This finding was found similar to Whale et al [20], Whale and Smith [21], Rammer [22], Miller [23] and Chui et al. [24]; which commented that the dowel diameter does influence the bearing strength of wood. This result also supports Gattesco [25] statement that the bearing strength is considerably influenced by the loading direction (perpendicular or parallel to the grain) and also the failure behavior during testing.

4.1 Theoretical Analysis

Results of experimental were also compared to the theoretical analysis in relations of specific gravity, density and dowel diameter. These equations are the NDS 2005 [1, Eqs. 3.11 and 3.12]. From the experimental tests, the mean value of density for

Table 1 Experimental versus theoretical bearing strength

Species	Descriptions	Bearing strength, F_c (psi)			
		0.81 in.		0.49 in.	
		Perpendicular	Parallel	Perpendicular	Parallel
Kempas	Experimental	6,185.28	9,520.96	7887.92	14726.11
	EYM (NDS 2005)	5,907.85	10192.00	7600.49	10192.00
Kapur	Experimental	3438.56	5706.32	4896.96	7959.28
	EYM (NDS 2005)	3874.59	7616.00	4981.61	7616.00

Kempas is 908 lbs/in³ lb and Kapur is 771 lbs/in³ lb whereas the specific gravity for Kempas species is 0.91 and for Kapur 0.68. These mean values are applied in the subsequent theoretical calculations. Details of the bearing strength comparisons between the experimental and theoretical are shown in Table 1.

Comparison of the theoretical analysis to the experimental was made according to species since there are significant differences between the bearing strength values of Kempas and Kapur species.

In comparison to NDS 2005 [1] for Kempas species, the bearing strength theoretical equation proved to be viable in predicting the experimental values of both perpendicular to grain (under predicted 4.49 %) and parallel to grain (over predicted 7.05 %) for 0.81 diameter dowel. NDS 2005 [1] has also accurately predicted the bearing strength perpendicular to grain (under estimated only by 3.64 %) for Kempas with 0.49 diameter dowel. However the NDS 2005 [1] has not accurately predicted parallel to grain (under estimated by 30.79 %) of Kempas species. This result also shows that bearing strength values between experimental and theoretical for the parallel to grain is very much different. From Sect. 3.2 in Chap. 5 discussions, it does show that the dowel-bearing strength is affected by the dowel diameter. The NDS 2005 [1] theoretical under estimates values is possibly due the effect of dowel diameter which has not been encountered in the parallel to grain theoretical equation. The accuracy of the theoretical equations in parallel to grain may also be affected by the density of the timber species since the density of Kempas (between 1.09 and 1.59 lbs/in³) and Kapur (0.82–1.16 lbs/in³) is high compared to the common European species (0.50–1.0 lbs/in³; [26]).

For Kapur species; the NDS 2005 [1] bearing strength theoretical equation was found not accurately predicted the experimental values of both perpendicular to grain (over predicted by 12.68 %) and parallel to grain (over predicted by 33.47 %) for 0.81 diameter dowel. However, for 0.49 diameter dowel, the NDS 2005 [1] has successfully predicted the bearing strength perpendicular to grain (over estimated only by 1.73 %) and parallel to grain (under estimated only by 4.31 %) of Kapur species. This shows that, NDS 2005 [1] is viable in predicting the Kempas species (strength group 2) with larger dowel diameter and for Kapur species (strength group 4) with smaller dowel diameter in both perpendicular and parallel to grain.

4.2 Modified NDS 2005: Bearing Strength Equation

Since the EYM equations for Kempas were found sufficient for 0.81 in. diameter dowel, therefore the modified formula for bearing strength of Kempas is only for 0.49 in. diameter. The suggested formula with 0 % differences to the experimental works in relations to the specific gravity from this study is proposed as Eq. 3.

$$Fe_{//} = 16182.54G \quad (3)$$

For Kapur species, since the NDS 2005 [1] has successfully predicted the smaller diameter (0.49 in. diameter) dowel, therefore the modifications are only for the bigger diameter (0.81 in. diameter) dowel. The modified NDS 2005 [1] for perpendicular and parallel to the grain for the 0.81 in. diameter dowel are the Eqs. 4 and 5.

$$Fe_{\perp} = 5398.23G^{1.45}d^{-0.5} \quad (4)$$

$$Fe_{//} = 8391.65G \quad (5)$$

5 Conclusions

Dowel-bearing strength of wood for Kempas and Kapur were investigated. Significant different between the bearing strength of Kempas and Kapur species were noticed. According to species, the lower strength group of species attributes to higher bearing strength of wood. It was also noticed that the bearing strength of parallel to grain was higher than the perpendicular to grain. In terms of dowel diameter, the bearing strength perpendicular and parallel to the grain decreased slightly as the dowel diameter increased regardless of the timber species. The EYM equations were found viable and sufficient in predicting the dowel-bearing strength of bigger dowel diameter for Kempas but not for the smaller dowel diameter. Contradict to Kempas species; the EYM equations were viable for the smaller dowel diameter and not for the bigger dowel diameter for Kapur. Thus, in the case of the insufficient predictions, three modified equations based on EYM, NDS 2005 [1] were proposed according to the specific gravity, density, species, dowel diameter and loading directions respectively.

Acknowledgments The authors would like to thank the Ministry of Higher Education, (MOHE) Malaysia for funding the project through ERGS 600-RMI/ERGS 5/3 (25/2012) from Universiti Teknologi MARA.

References

1. NDS 2005, National Design specification for wood construction american forest and paper association (AFPA), Washington, DC, 2005
2. American Standard Testing Method (ASTM) D 5764-95a, Standard Test method for evaluating dowel-bearing strength of wood and wood-based products, 2007
3. H. Rohana, I. Azmi, A. Zakiah, Shear and bending performance of mortise and tenon connection fastened with dowel. *J. Trop. For. Sci.* **22**(4), 425–432 (2010)
4. H. Rohana, I. Azmi, A. Zakiah, Bending behaviour of dowelled mortise and tenon joints in Kempas. *Sci. Res. J.* **5**(1), 1–11 (2008). (ISSN 165-7009)
5. H. Rohana, I. Azmi, A. Zakiah, Shear capacity of dowelled mortise and tenon joint in tropical timber. *J. Inst. Phys. IOP Conf. Ser. Mater. Sci. Eng.* **17**(1), 1–11 (2010)
6. A. Awaludin, W. Smittakorn, T. Hirai, Bearing properties of *Shorea obtusa* beneath a laterally loaded bolt. *J Wood Sci.* **53**(3), 204–210 (2007)
7. T.E. McLain, S. Thangjitham, Bolted wood-joint yield model. *ASCE J. Struct. Eng.* **109**(8), 1820–1835 (1993)
8. D.R. Rammer, S.G. Winistofer, Effect of moisture content on nail bearing strength. *Wood Fiber Sci. J. Soc. Wood Sci. Technol. (USA)* **33**(1), 126–139 (2001)
9. N. Sauvat, O. Pop, S. Merakeb, F. Dubois, Effect of moisture content variation on short term dowel-bearing strength. Paper presented at the 10th World conference on timber engineering (WCTE), Miyazaki, Japan, 2008
10. D.R. Rammer, Parallel-to-grain dowel-bearing strength of two guatemalan hardwoods. *For. Prod. J.* **49**(6), 77–87 (1999)
11. M.Z. Jumaat, A.A. Bakar, F.M. Razali, A.H.A. Rahim, J. Othman, in *The Determination of the Embedment Strength of Malaysian Hardwood*, Proceedings of the 9th World Conference on Timber Engineering. WCTE, Portland or USA, 6–10 Aug 2006 (126p)
12. M.Z. Jumaat, F. M. Razali, A.H.A. Rahim, in *Development of Limit State Design Method for Malaysian Bolted Timber Joints*. The 10th World Conference on Timber Engineering, WCTE 8, Miyazaki, Japan, 2–5 June 2008, pp. 1–176
13. T.L. Wilkinson, Dowel-bearing strength (Laboratory Report Research Paper No. FPL-RP-505): Forest Products Laboratory, One Gifford Pinchot Drive, WI 53705-2398, 1991
14. J.R. Church, B.W. Tew, Characterization of bearing strength factors in pegged timber connections. *J. Struct Eng.* **123**(3), 326–332 (1997)
15. M. Harada, T. Hayashi, M. Karube, K. Komatsu, in *Dowel-Bearing Properties of Glued Laminated Timber with a Drift Pin*. Proceeding of the 6th World Conference in Timber Engineering (WCTE), Whistler resort, British Columbia, Canada. 31 July–3 Aug 2000
16. K. Hwang, K. Komatsu, Bearing properties of engineered wood products I: effects of dowel diameter and loading direction. *Jpn. Wood Res. Soc.* **48**, 295–301 (2002)
17. D.A. Balma, Evaluation of bolted connections in wood plastic composites. Master science thesis, Washington State University, Washington, 1999
18. B.O. Hilson, L.R.J. Whale, D.J. Pope, I. Smith, Characteristic properties of nailed and bolted joints under short-term lateral load, part 3—analysis and interpretation of embedment test data in terms of density related trends. *J. Inst. Wood Sci.* **11**(2), 65–71 (1987)
19. K. Sawata, M. Yasamura, Determination of embedding strength of wood for dowel type fasteners. *J. Wood Sci.* **48**, 138–146 (2002)
20. L.R.J. Whale, I. Smith, Mechanical timber joints. Research Rep. No. 18/86, Timber Research and Development Association, High Wycombe, U.K, 1987
21. L.R.J. Whale, I. Smith, A method for measuring the embedding characteristics of wood and wood based materials. *Mater. Struct.* **22**, 403–410 (1989)
22. D.R. Rammer, Parallel-to-grain dowel-bearing strength of two guatemalan hardwoods. *For. Prod. J.* **49**(6), 77–87 (1999)
23. J.F. Miller Capacity of wood dowelged mortise and tenon joints. M.Sc. thesis, Department of Civil and Architectural Engineering, University of Wyoming, Laramie Wyoming, 2004

24. Y.H. Chui, I. Smith, Z. Chen, Influence of fastener size on lateral strength of steel-to-wood screw joints. *For. Prod. J.* **56**(7/8), 49 (2006)
25. N. Gattesco, Strength and local deformability of wood beneath bolted connectors. *ASCE J. Struct. Eng.* **124**(2), 195–202 (1998)
26. J.D. Shanks, Developing rational design guidelines for traditional joints in oak frame construction. Ph.D. thesis, University of Bath, 2005

Stiffness Modelling of Non-metallic Timber Connections with Pultruded Dowels

Daniël Brandon, Andrew Thomson, Martin Ansell, Julie Bregulla, Richard Harris and Peter Walker

Abstract Previous studies have shown that double shear timber connections with glass fibre reinforced polymer dowels are a viable alternative to metallic timber connections. Different models have been proposed for predicting the load capacity of the connection. A model which accurately predicts stiffness for connections of this type is, however, not yet published. This paper discusses a two dimensional linear finite element model that predicts the slip modulus of non-metallic timber connections made with pultruded dowels. The model is compared to experimental results and it is concluded that the two dimensional model is accurate.

Keywords Non-metallic · Timber connection · Densified veneer wood · GFRP · Pultruded rod

1 Introduction

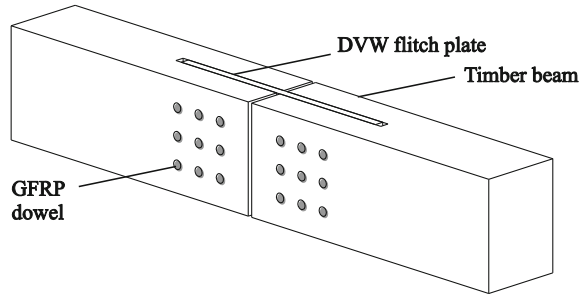
Recent studies [1–4] showed that double shear timber connections with glass fibre reinforced polymer (GFRP) dowels are a viable alternative for metallic connections. The advantages of this non-metallic connection type lie in the potential for reduced thermal bridging, reduced weight, enhanced fire resistance and enhanced corrosion resistance.

D. Brandon (✉) · A. Thomson · R. Harris · P. Walker
Department of Civil Engineering and Architecture, BRE CICM, Bath, UK
e-mail: d.brandon@bath.ac.uk

M. Ansell
Department of Mechanical Engineering, BRE CICM, Bath, UK

J. Bregulla
BRE Construction, BRE Ltd, Watford, UK

Fig. 1 Example of a non-metallic timber connection with GFRP dowels



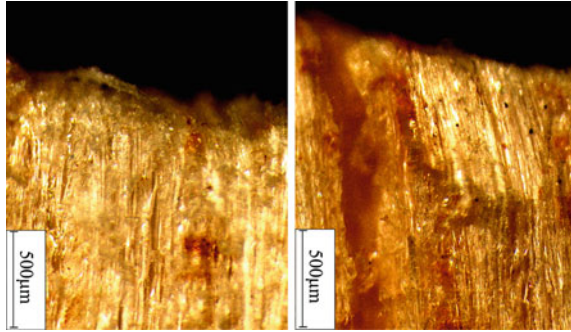
In the most recent study, densified veneer wood (DVW) was introduced as a flitch plate material in the connection [1]. DVW consists of cross layered beech veneer which is compressed at high temperatures and has more isotropic, stronger and stiffer material properties than timber. The connection is exemplified in Fig. 1.

The study presented in this paper is part of an on-going study to visco-elastic creep and fire performance of the non-metallic connection. A structural time independent model at room temperature will in the on-going study be used as a basis for the temperature and time dependent models. However, a model that accurately predicts the stiffness of the connection has not yet been published. This paper presents a model that predicts this stiffness. The model consists of beams and springs similar to models presented in [5, 6]. These models use beam elements and bi-linear springs and are suitable for describing the behaviour of metallic connections. In contrast to metal dowels, fibre reinforced dowels show large shear deformations [1] and a model predicting the slip modulus of the non-metallic connection should include this shear deformation. Experimental results from tests by Thomson [1, 2] are used to validate the model.

2 Background

Finite element models able to predict the embedment of dowels in timber have been published in different forms. Three dimensional models are very hard to make accurate, because the embedded timber cracks and its fibres buckle at low loads as can be seen in Fig. 2. The figure shows optical microscope images of the fibres before a load is applied (left) and after a load of 0.4 times the embedment strength is applied (right). Not including fibre buckling generally leads to an overestimation of the stiffness. One solution of this problem was proposed by Hong and Barrett [7]. The authors implemented a volume of material around the dowel that has reduced material properties. These properties were determined with embedment tests. The value of the three dimensional model, however, becomes questionable when the properties are obtained from a one dimensional foundation modulus. Another solution was offered by Xu et al. [8]. They implemented a modified yield criterion to take account of the tensile splitting and shear failure of

Fig. 2 Timber fibres under the dowel before (*left*) and after (*right*) loading



the timber around the dowel. Results of this model showed good agreement with experimental results. Implementing a user defined yield criterion in finite element software, however, requires a high level of expertise.

Two dimensional models using plane elements in which the dowel geometry is a circle e.g. [9], cannot take account of the thickness of a timber connection. The deformations of the dowel are then neglected. These models also face the same problems as the three dimensional models.

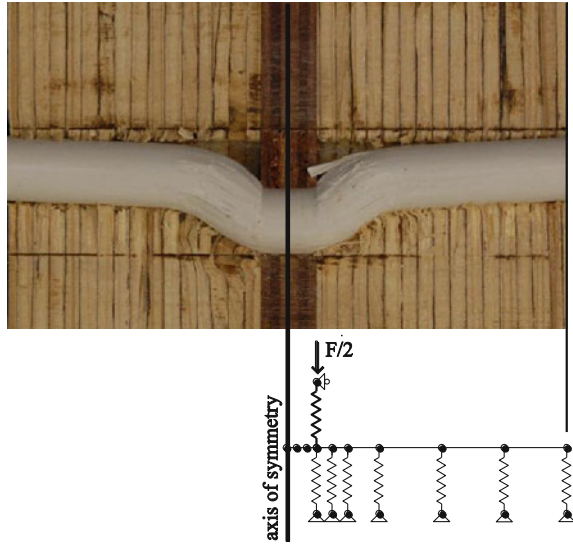
Published two dimensional finite element models using only one dimensional elements consist of beams and bi-linear springs, representing the dowel and timber respectively [5, 6]. These models are developed to describe the behaviour of timber connections with metallic fasteners. To describe the behaviour of the GFRP dowels, shear deformation becomes a significant factor. The non-linearity of the springs, however, becomes less important since the GFRP dowel will not yield as much as a steel dowel.

3 Two Dimensional Linear Analysis

The difficulties of modelling local fracture of embedded timber in connections in three dimensional finite element analysis, can be avoided with a two dimensional model that simplifies the timber embedment. The timber material is then simply modelled as a spring with a stiffness equal to the embedment stiffness. Suitable standard embedment tests are described in ASTM D5764 [10] and EN383 [11]. Both will obtain similar results as Santos et al. [12] showed with a large number of tests that no significant difference could be found in the foundation moduli obtained with both tests. The two dimensional finite element analysis should also include the embedment of the DVW and the flexural and shear deformation of the GFRP dowel.

The model is shown in Fig. 3 and consists of springs representing the DVW (shown with thicker lines), springs representing the timber and beams representing the GFRP dowel. The stiffness of the springs is equal to the embedment stiffness of

Fig. 3 Section of tested connection (*above*) and corresponding two dimensional model (*below*)



the material. This material is either timber or DVW. The element mesh of the beams is finer near the shear plane since the beam rotations are the highest in that location.

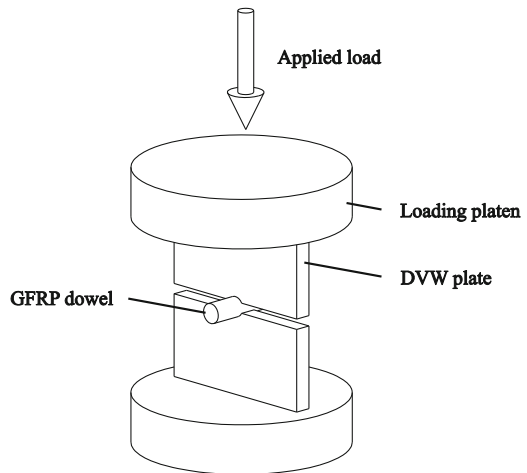
3.1 Material Properties

The material properties to be implemented were measured experimentally. The timber embedment tests were performed according to ASTM D5764 [10] with Douglas fir glulam. This test was chosen over the one described in EN383 [11] because of the ease of loading. The average moisture content of the timber was 13.1 % and the average dry density was 533 kg/m^3 . Test results of these embedment tests are shown in Table 1.

The test shown in Fig. 4 was used to determine the DVW embedment including the embedment of the GFRP. The test setup was presented earlier by Church and Tew [13]. A 12 mm GFRP rod with a length of 50 mm was compressed in between two DVW plates. These plates had dimensions of 100 by 50 by 10 mm. The DVW used in this research was made of cross wise layered beech veneer and had a density of approximately $1,300 \text{ kg/m}^3$. Leijten [14] presented a linear relationship between the density and the embedment stiffness of DVW. This relationship can be used to adjust the GFRP-DVW embedment stiffness, in case DVW of other densities is used. The pultruded GFRP rods used in this study consist of S-glass fibres with a polyester resin. In the tested system, two DVW plates were embedded with a GFRP dowel. The GFRP-DVW bearing stiffness corresponding to only one DVW plate was therefore twice the measured stiffness.

Table 1 Experimental results of material property tests

	Test results			
	No. of tests	Mean	Units	COV (%)
Embedment stiffness parallel to the grain	5	125×10^1	N/mm ²	13.4
Embedment stiffness perpendicular to the grain	5	321	N/mm ²	12.1
GFRP-DVW embedment stiffness	5	400×10^1	N/mm ²	11.0
GFRP shear modulus	4	274×10^1	N/mm ²	8.4
GFRP shear strength	4	33.7	N/mm ²	4.3

Fig. 4 Setup of DVW-GFRP embedment test

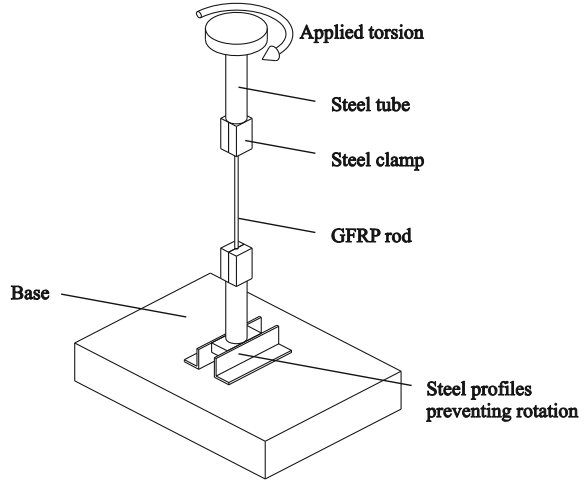
From five tests, the resulting mean embedment stiffness of the total system was 2.00 kN/mm^2 and the stiffness corresponding to one DVW plate is therefore 4.00 kN/mm^2 (Table 1).

The shear modulus and shear strength of the GFRP rod are measured with torsion tests. The setup is shown in Fig. 5. The torque and the rotation can be obtained with this test. With these data the shear modulus and the shear strength are determined [15]. Since the steel clamps are not infinitely stiff, the effective tested length of the dowel is equal to the distance between the clamps plus an additional clamping length. This additional length is determined by testing rods of two different lengths.

3.2 Analysis

The present model is made using Matlab v7.11.0, but can be made with other computational software. A global stiffness matrix $[K]$ is built up with element stiffness matrices of springs and beams. Different beam theories are considered and

Fig. 5 Setup of GFRP torsion test



compared. The general relationship between the displacement vector d and the force vector F is:

$$[K]\{d\} = \{F\}. \quad (1)$$

3.3 Spring Elements

Linear spring elements are used. The stiffness matrix for the spring elements can be found in general finite element text books [16]:

$$K_S = \begin{bmatrix} K & -K \\ -K & K \end{bmatrix} \quad (2)$$

where K is the stiffness of the spring. This element has two nodes with one degree of freedom (axial translation), hence the 2 by 2 matrix.

3.4 Bernoulli Beam Element

The classic beam theory or the Bernoulli beam theory is generally known by engineers. This theory assumes that plane cross sections of a beam stay plane and perpendicular to the midline of the beam, as can be seen in Fig. 6a. It can thus be said that the slope of the midline is equal to the rotation of the cross section:

$$dw/dx = \varphi \quad (3)$$

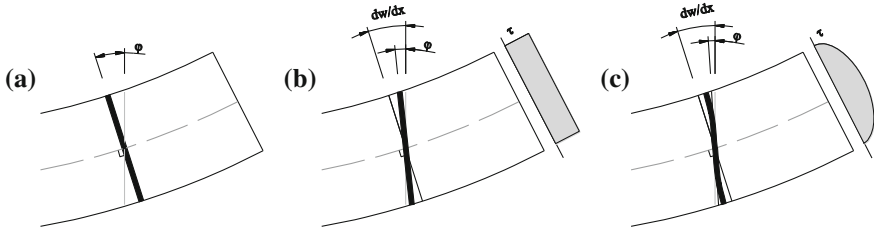


Fig. 6 Beam theories. **a** Euler-Bernoulli beam theory. **b** Timoshenko beam theory. **c** Higher order beam theory

The element stiffness matrix of this theory can among other methods be derived from beam equations by using the direct stiffness approach and can be found in the general literature [17]. The beam element has two nodes with two degrees of freedom: rotation and lateral translation.

3.5 Timoshenko Beam Element

In the Timoshenko beam theory it is assumed that plane cross sections remain plane, but not necessarily perpendicular to the midline. The rotation of the plane around the midline is caused by a shear stress which is constant over the height of the beam (Fig. 6b). The shear stresses in a beam are however known to be zero at the top and bottom of the beam. Many studies have been published on the calculation of a shear correction factor (k) that compensates for this assumption. The calculation of this factor is, however, not straightforward and more than one possible value for the shear correction factor can be found. In the Timoshenko beam theory, the slope of the midline minus the rotation caused by shear strain (γ) is equal to the rotation of the cross section [18]:

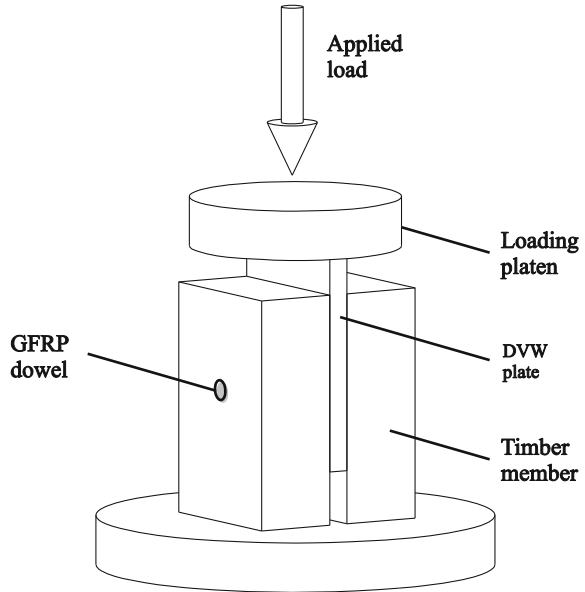
$$dw/dx - \gamma/k = \varphi \quad (4)$$

The element stiffness matrix of this theory can be derived from the beam equations [18] using the direct stiffness approach.

3.6 Higher Order Beam Element

The cross section of a beam under shear load does in reality not remain plane, because the shear stresses on top and bottom of the beam are zero. At the top and the bottom of the beams the shear strain (γ) is zero as well, meaning that that the cross section remains perpendicular to the top and bottom of the beam. The shear stresses of the cross section are highest in the middle and the section therefore

Fig. 7 GFRP-DVW connection test setup



rotates more at that location (Fig. 6c). Higher order beam theories describe this warping of the section.

Different higher order beam theories have been published that show only small variations in results [19, 20]. Ghugal and Shimpi [21] review many of these beam theories. The stiffness matrix derived by Eisenberger [22] from the equilibrium equations given by Heyliger and Reddy [19] has been used in this study. Eisenberger's element stiffness matrix has three degrees of freedom per node. Next to the lateral displacement and the rotation, nodes in this stiffness matrix contain a third degree of freedom describing the rotation of the section at the midline.

4 Experimental Work

A series of simple connection tests have been carried out with different dowel sizes (Fig. 7). The dowel diameters were 16, 12 and 8 mm respectively. Five tests were performed for each dowel size. The tested connections all had a side member thickness of 48 mm.

Thomson [1, 2] tested double shear connections with GFRP dowels and a DVW flitch plate. The materials used for these connection tests are similar to the materials used in this study. He performed tests parallel and perpendicular to grain, from which the setups are shown in Fig. 8. Different edge and end distances of the dowels were assessed and tests with one to three dowels were performed. Results taken from these tests are compared with the finite element model.

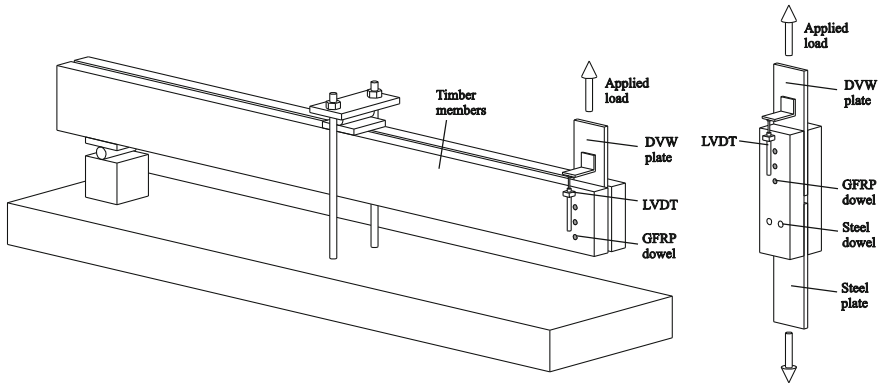
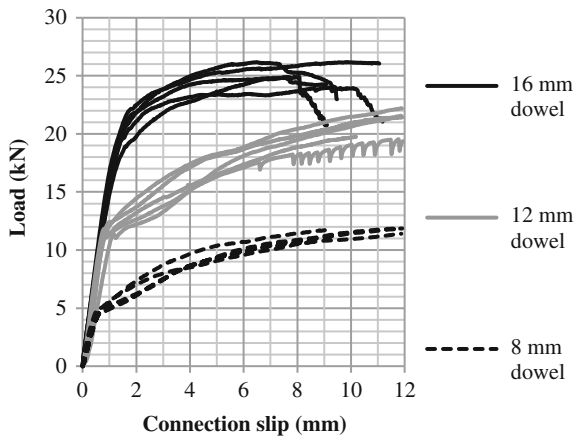


Fig. 8 Test setup perpendicular (*left*) and parallel (*right*) to grain [1, 2]

Fig. 9 GFRP-DVW connection test results



5 Results and Discussion

Figure 9 shows the load slip curves obtained from the GFRP-DVW connection tests shown in Fig. 7. It can be seen that the dowel diameter has a significant influence on the load capacity of the connection, and a less significant influence on the initial stiffness of the connection. This can be explained by the fact that an increase of dowel size does not lead to the same relative increase of the embedment stiffness. It can also be seen that the first part of the curve is approximately linear regardless of the dowel size. This indicates that this part can be modelled linearly. The linear part ends sharply indicating that the first failure mechanism takes place at that point. It also can be noticed that this point appears at a consistent load for every tested dowel size.

Figures 10 and 11 show the predicted dowel deflections at a load of 1 kN for connections loaded perpendicular to grain and parallel to grain respectively. The

Fig. 10 Perpendicular to grain dowel deflection of symmetrical half (1 kN load)

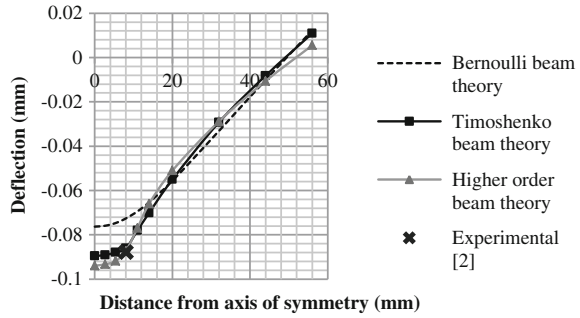
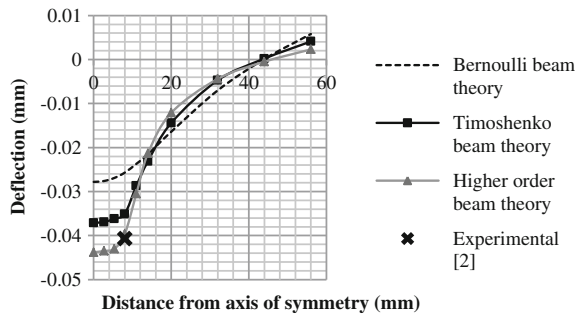


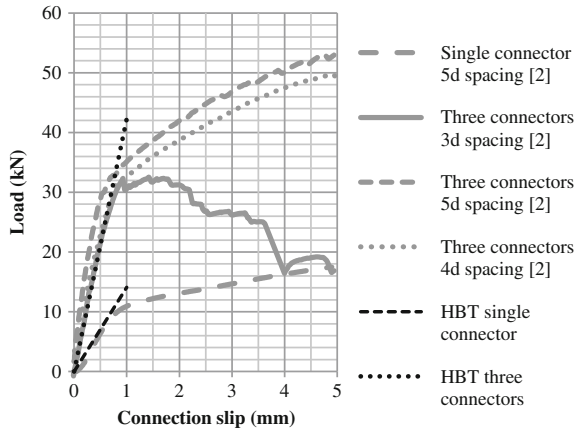
Fig. 11 Load slip curves



results corresponding to the Timoshenko beam elements are determined using a shear correction factor equal to 0.88. The experimentally gained average deflection of the dowel in the shear plane is gained by excluding the estimated embedment of the DVW from Thomson’s [1, 2] test results. For this, the average deflection of all tested dowels (30 dowels loaded perpendicular to grain and 95 dowels parallel to grain) are determined. Hereby, it is assumed that all connectors in one connection carry the same load. This will give only a slight underestimation of the average stiffness, since the maximum number of dowels per tested connection is three. In Figs. 10 and 11 it can be seen that the dowel deflections described by the Bernoulli beam theory, do not coincide well with the experimental results, indicating that the shear deformations play a significant role in the connection behaviour. It can also be seen that the dowel deflections described by the Timoshenko beam theory and the higher order beam theory both coincide well with the experimental results for predictions perpendicular to the grain. The prediction for parallel to grain deflection, however, is better with the higher order beam theory.

Thomson [1] concluded from his tests (Fig. 8) that the formation of partial shear plug in the timber was the first visible failure in parallel to grain loaded specimens. He concluded that this failure must have been caused by large deformations of the dowel, which are due to shear failure. In the load slip curves of Fig. 12 the moment of shear failure in the dowel can be located at the transition

Fig. 12 Parallel to grain dowel deflection of symmetrical half (1 kN load)



between the linear first part and the semi-ductile second part of the curve. The small variation in load of these points indicates a high consistency in material properties. The figure shows the results of Thomson [1, 2] as typical load–displacement plots for each tested group. The predictions given with the model using the higher order beam theory (HBT) are also shown in Fig. 12.

6 Conclusion

A two dimensional finite element analysis predicting the stiffness and strength of non-metallic timber connections with GFRP dowels and a DVW flitch plate was performed. The model consists of linear springs that represent the timber and beams that represent the GFRP dowels. Properties of these springs and beams were gained experimentally. Different beam theories were implemented in the analysis and compared. The analysis was validated by comparing results to experimental results presented by Thomson [1, 2].

Results presented in this paper are findings of an on-going research project. The goal of the project is to predict the creep behaviour and the fire performance of GFRP-DVW connections. The most important findings can be summarized as follows:

- The connection shows strong linear behaviour until the first failure mechanism occurs.
- This behaviour can be adequately modelled with a linear finite element model.
- The classic (Bernoulli) beam theory is not suitable for predicting the load-slip behaviour of the connection, because it lacks the ability to account for shear deformation.
- The higher order beam element published by Eisenberger [22] gave the most accurate results in both perpendicular and parallel to grain analysis.

- Both the Timoshenko beam and the higher beam gave accurate predictions.
- By comparing the experimental results with the results of the model it can be concluded that despite the simplicity of the model the model accurately predicts the connection stiffness.

Acknowledgments The authors would like to thank Tom Reynolds for sharing his expertise on timber embedment and Tim Holsgrove for providing advice on torsion testing. The authors would also like to thank the BRE Trust for supporting the project.

References

1. A. Thomson, *The Structural Performance of Non-metallic Timber Connections*, PhD thesis, Architecture and Civil Engineering, University of Bath, 2010
2. A. Thomson, R. Harris, M. Ansell, P. Walker, Experimental performance of non-metallic mechanically fastened timber connections. *Struct. Eng.* **88**(17), 25–32 (2010)
3. R.D. Drake, *The Advancement of Structural Connection Techniques for Timber Buildings*, PhD Thesis, University of Bath
4. M. Pedersen, *Dowel Type Timber Connections*, PhD thesis, Department of Civil Engineering, Danmarks Teknise Universitet, 2002
5. K. Sawata, M. Yasumura, Estimation of yield and ultimate strengths of bolted timber joints by nonlinear analysis and yield theory. *J. Wood Sci.* **49**(5), 383–391 (2003)
6. N. Nishiyama, N. Ando, Analysis of load-slip characteristics of nailed wood joints: application of a two-dimensional geometric nonlinear analysis. *J. Wood Sci.* **49**(6), 505–512 (2003)
7. J. Hong, D. Barrett, Three-dimensional finite-element modeling of nailed connections in wood. *J. Struct. Eng.* **136**(6), 715–722 (2010)
8. B.-H. Xu, A. Bouchaïr, M. Taazount, P. Racher, Numerical simulation of embedding strength of glued laminated timber for dowel-type fasteners. *J. Wood Sci.* **59**: 17–23 (2013)
9. L. Daudeville, L. Davenne, M. Yasumura, Prediction of the load carrying capacity of bolted timber joints. *Wood Sci. Technol.* **33**(1), 15–29 (1999)
10. ASME, ASTM D5764, Standard test method for evaluating dowel-bearing strength of wood and wood-based products, 2002
11. European Commission, *EN383 timber structures, test methods: determination of embedding strength and foundation values for dowel type fasteners* (European standard, Brussels, 2004)
12. C.L. Santos, A.M.P. De Jesus, J.J.L. Morais, J.L.P.C. Lousada, A comparison between the EN 383 and ASTM D5764 test methods for dowel-bearing strength assessment of wood: experimental and numerical investigations. *Strain* **46**(2), 159–174 (2010)
13. J. Church, B. Tew, Characterization of bearing strength factors in pegged timber connections. *J. Struct. Eng.* **123**(3), 326–332 (1997)
14. A.J.M. Leijten, *Densified Veneer Wood Reinforced Timber Connections with Expanded Tube Fasteners*, PhD thesis, Delft University Press, 1998
15. J.M. Gere, *Mechanics of Materials with Infotrac* (Thomson/Brooks/Cole, Stamford, 2004)
16. E. Oñate, *Structural Analysis With The Finite Element Method. Linear Statics: vol. 1: Basis and Solids* (Springer, Berlin, 2009)
17. C.M. Wang, J.N., Reddy, K.H. Lee, *Shear Deformable Beams and Plates. Materials and Mechanical 2000* (Elsevier Science Ltd, Amsterdam, 2000), pp. 1–312
18. S. Timoshenko, D.H. Young, *Elements of Strength of Materials*. 4edn, 1962

19. P.R. Heyliger, J.N. Reddy, A higher order beam finite element for bending and vibration problems. *J. Sound Vib.* **126**(2), 309–326 (1988)
20. M. Levinson, A new rectangular beam theory. *J. Sound Vib.* **74**(1), 81–87 (1981)
21. Y.M. Ghugal, R.P. Shimpi, A review of refined shear deformation theories for isotropic and anisotropic laminated beams. *J. Reinf. Plast. Compos.* **20**(3), 255–272 (2001)
22. M. Eisenberger, An exact high order beam element. *Comput. Struct.* **81**(3), 147–152 (2003)

Mechanical Properties of Cement Composites Incorporating Oil Palm Stem Fiber

Dianah Mazlan and A. S. M. Abdul Awal

Abstract With the increasing building activities in both developed and developing countries, there has been a growing concern to convert the agricultural and industrial waste to a construction material. Researches since decades ago have shown that the addition of fibers into the cement matrix enhanced the physical and mechanical behavior of mortar and concrete. This paper discusses the properties and usage of oil palm stem fiber as discrete reinforcing material in cement matrix. Cement mortar mixes containing 1–4 % fiber were made to investigate workability, water absorption and strength of the matrix. Test specimen comprising of cube, cylinder and beam were cast and tested for compressive, tensile and flexural strength respectively following ASTM standards. Laboratory test results reveal that the workability of cement mortar decreases with the increase of oil palm stem fiber. The water absorption capacity on the other hand was found to increase with the increasing amount of fiber content. Regarding strength, the compressive strength has been found to increase up to certain limit of 3 % fiber content, beyond which the strength decreased gradually. The tensile and flexural strength of the mortar matrix, however, showed a positive response in terms of fiber content. Results obtained and the observations made in the study suggest that oil palm stem fiber can effectively be used in producing lightweight construction materials.

Keywords Fiber reinforced composites · Oil palm stem fiber · Compressive · Tensile and flexural · Strength

D. Mazlan · A. S. M. Abdul Awal (✉)
UTM-Construction Research Centre, Faculty of Civil Engineering,
Universiti Teknologi Malaysia, 81310 Skudai, Johor Bahru, Malaysia
e-mail: abdulawal@utm.my

1 Introduction

Extensive research and development work in understanding and application of fiber concrete materials are still taking place all over the world. These activities include, amongst other things, the development of new, stronger fibers, better fiber reinforced composites and new substitutes for products which have some disadvantages. The idea of reinforcing relatively brittle materials with fibers has been known and practiced since ancient times. Mud huts constructed from baked clay reinforced with straw, and masonry mortar reinforced with animal hair, are primitive examples of the use of fiber reinforced materials in construction that date well back into history [1].

Natural fibers, as a substitute for human made fibers in composites component, have gained interest in last decade. During this century other fibers such as jute, sisal, coconut, ramie, banana, flax, hemp etc. have been used in cement-based products because of their better stiffness per unit weight and lower impact on environment [2]. Among the most promising of such materials are cellulose fibers. These are produced mechanically or chemically, either from wood or other vegetable fiber sources. The dimensions of individual fibers vary considerably from type to type and depend on the origin of the fiber source and method of preparation [3].

The oil palm is a tall-stemmed tree which belongs to palm family *Palmes*. The countries in the equatorial belt that cultivates oil palm are Benin Republic, Colombia, Ecuador, Nigeria, Zaire, Malaysia and Indonesia of which Malaysia is the largest producer of palm oil and palm oil products. It has been estimated that the total solid waste generated by this industry in some 200 palm oil mills in the country has amounted to about 10 million tons a year [4, 5].

Oil palm trees are usually felled after the age of 25 years, either due to their decreasing yield or because they have grown too tall which makes harvesting very difficult. For the disposal of oil palm stems, they are normally left to rot or are burnt in the field. However, freshly felled stems with their high moisture content cannot be easily burnt in the field. Leaving the stems in the field without further processing will physically hinder the process of planting new crops as the stem can take about 5 years to decompose completely [6].

As a normal practice, oil palm fibers are used for fuel combustion for generation of steam boiler for oil production process. Due to abundances, some of the fibers are discarded and thrown away. However, this by-product has been found to have a good potential in cement based composites [7]. Considering the availability and the potential benefits of the palm stem, research works have been initiated at the Universiti Teknologi Malaysia in exploring the full benefits of this waste material in construction. This paper highlights some fresh and hardened properties of cement mortar incorporating oil palm stem fiber as reinforcing material.

2 Materials and Test Method

2.1 Collection and Preparation of Oil Palm Stem Fiber

The oil palm stem has some sort of unique arrangement of fiber unlike other type of tree trunk. This makes the oil palm stem been chosen as a new reinforcing material. The processes of oil palm stem extraction begin after the oil palm tree is cut into a small piece of log. The process continues where every fiber strands in oil palm stem is extracted out and cut into desired length to around 20–30 mm. However, natural fiber cannot be used directly because of poor compatibility between fiber and matrix and due to high moisture sorption [8]. Chemical treatments are, therefore, considered in modifying the surface properties of fibers.

In this study the fibers were soaked in hot salty water for about 15 min to remove all kinds of dirt and to prevent any microbial deterioration thereby improving the quality of fibers. Finally, the fibers were oven dried for 24 h at a temperature of about 45 °C as to make sure that there is no water in the fiber. Figure 1 shows the treated and cut oil palm stem fibers that are ready to be mixed with mortar. It is generally understood that the bond between a mortar and fiber with rough surface will be stronger than that of the smooth surface. Interestingly, the existence of rough surface of palm fiber as illustrated in Fig. 2 would be a contributing factor in the development of bond strength of mortar matrix.

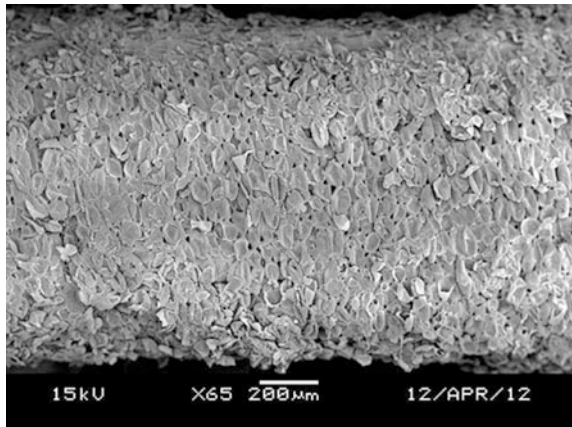
2.2 Preparation of Mortar and Test Details

The mortar mix was designed and prepared following ASTM C1329-05 [9] which is type N strength mortar. The proportion of cement:sand:water used in this study is 1:2.75:0.6. The fiber content used in this study ranged from 1 to 4 % by weight of cement. A total of 75 cubes, 45 cylindrical and 45 prismatic specimens were cast and tested at the age of 3, 7, 28 and 90 days. Flow table test, following ASTM C1437-07 [10] standard was carried out to measure the workability of mortar. In order to investigate water absorption of specimens, the test was conducted following ASTM C1403-06 [11]. For compressive strength of mortar, uniaxial compression test was carried out on 50 mm cube specimen following ASTM C109/C109M-11a [12]. The splitting tensile test was performed on the standard test cylinders measuring 50 × 100 mm conforming ASTM C496/C496M-04 [13]. The flexural strength test was, however, conducted on 40 × 40 × 160 mm beams under third-point loading following the ASTM C348-08 [14]. All specimens were cured by wrapping the samples by polyethylene sheets in order to prevent loss of moisture from the specimens.

Fig. 1 Cut and treated oil palm stem fiber



Fig. 2 SEM of oil palm stem fiber showing rough surface



3 Result and Discussion

3.1 Workability of Mortar Matrix

In this study flow table test was used to determine the workability of mortar. The flow values of mortar mixes having various amounts of fibers are illustrated in Table 1. Data presented in the figure reveals that workability in terms of flow gradually decreased with the increase in fiber content. This is to note that all the values ranged between 6 and 12 %, which are within the limiting values (4–11 %) for mortar with good flow level, as stipulated in ASTM1437-07. According to Rehsi [15], the fresh mortar matrix shows a certain amount of stiffening and reduction in workability when chopped fibers are added to it. The fiber may interlock and form balls if too long fiber is used. Unlike metallic fibers, the length of the chopped natural fibers added does not influence the additional water

Table 1 Effect of fiber content on workability of mortar

Fiber percentage (%)	Flow table (mm)	Flow level (%)
0	114	11.76
1	113	10.78
2	111	8.84
3	110	8.17
4	108	6.21

Table 2 Physical properties of cement mortar with various fiber content

Fiber content, by weight of cement (%)	Density (kg/m ³)	Water absorption (%)
0	2,160	6.97
1	2,139	9.83
2	2,117	10.25
3	2,097	12.19
4	2,078	13.54

requirement to any significant extent. Water-soluble constituent in the fibers cause retardation in the setting and hydration of the cement. Consequently, the strength of the fiber reinforced mortar is likely to affect.

3.2 Properties of Hardened Mortar Matrix

3.2.1 Density and Water Absorption

In Table 2, it can be seen that higher the fiber content in the mortar mix higher was the water absorption rate of the specimens. The specimens having high fiber-cement ratio showed higher percentage of moisture content and water absorption than those of low fiber-cement ratios due to the high fiber content. As shown in Table 2, the density and water absorption of control specimen i.e. with 0 % fiber were 2,160 kg/m³ and 6.97 % respectively. The corresponding values, for example, for the specimens with 3 % fiber were 2097 kg/m³ and 12.19 %. The water absorption rate of the specimens are higher not only because of the water absorption of natural fiber itself, but also due to the fact that the water-cement ratio employed in the mix ratio was slightly higher which created more void than usual. Moreover, it can be noticed that the inclusion of oil palm stem fiber in the mortar mixes decreased the hardened density due to the lower specific gravity of fiber that ultimately reduce the overall density of mortar, as summarized in Table 2.

Fig. 3 Compressive strength of mortar containing oil palm stem fiber

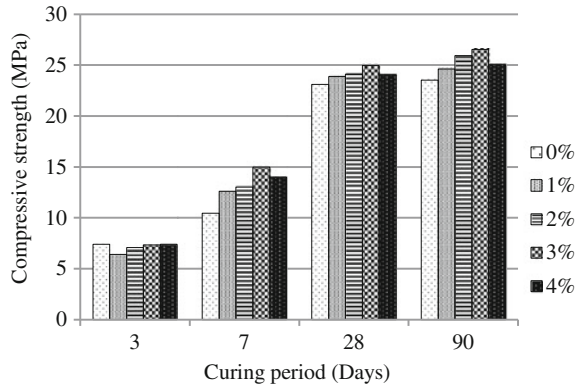
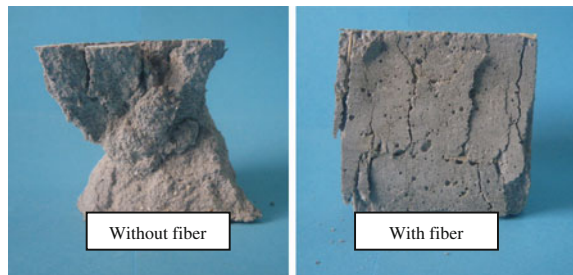


Fig. 4 Failure mode of mortar cube specimens under compressive load

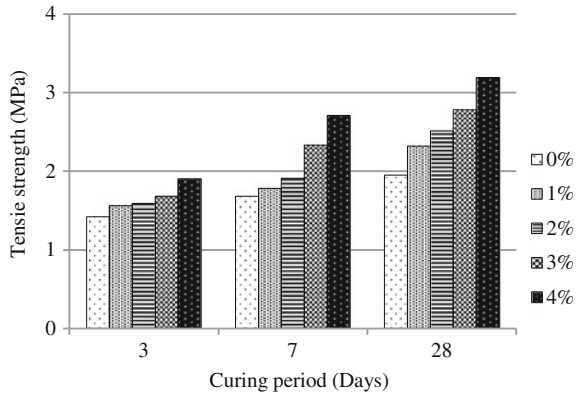


3.2.2 Compressive Strength

Figure 3 summarizes the compressive strength data of mortar at the age of 3, 7, 28 and 90 days. Obviously, longer the curing period higher was the compressive strength development in all mixes. Strength data shown in the figure, however, reveal that mortar specimens containing oil palm fiber were relatively weaker at early ages. With time, an increase in the development of strength has been noticed particularly for the mortar specimens with up to 3 % fiber. A similar observation has been made by Awal et al. [16] who found that the strength of fiber reinforced mortar increase linearly with the increase in fiber volume up to a certain limit.

Although the compressive strength of fiber reinforced mortar was much affected by the presence of fiber, the failure mode, however, exhibited a considerable change from fragile to a ductile state. Due to bridging effect of the fiber, the cube specimens did not crush into pieces rather held their integrity up to the end of the test. At typical failure mode of the 50 mm cube specimen under compressive strength test is illustrated in Fig. 4.

Fig. 5 Splitting tensile strength of mortar containing oil palm stem fiber



3.2.3 Splitting Tensile Strength

The tensile strength of mortar containing oil palm stem fiber was carried out at the age of 3, 7 and 28 days. It has been found that like compressive strength, the tensile strength of mortar specimens increased with increasing amount of fiber. Figure 5 shows that at all age the splitting tensile strength of mortar containing oil palm stem fiber was higher than that of control mixture. However, unlike in compression, there has been a sharp development of strength in tension with the increase in the fiber content of the specimens. The increase of strength may be due to uniformly distribution of fibers throughout the cement matrix. Ismail and Hashim [17] demonstrated that, with uniformly distribution of fiber the stress is said to be transferred in complex way that it fails after higher loading is applied.

It is interesting to note that like other fibers, the oil palm stem fibers appeared to control the cracking of mortar and alter the post cracking behavior. The oil palm stem fibers seem to provide a load redistribution mechanism after initial cracking. The fiber can also be considered as an absorber that absorbs stress when loading is applied on the sample. Unlike in normal mortar, it was difficult to separate the fractured specimens because of the bridging effect that kept the two mortar parts together as shown in Fig. 6.

3.2.4 Flexural Strength

Figure 7 illustrates the flexural behavior of mortar containing oil palm stem fiber in three different ages of 3, 7 and 28 days. The higher the percentage of oil palm stem fiber added, better was the performance of flexural strength. Although the flexural strength kept increasing with the increase of fiber content, the development of strength was prominent for to up a certain limit of 3 % fiber content. The addition of 4 % fiber in the mortar matrix was not found effective because it tends

Fig. 6 A typical fractured specimen under tensile load showing the oil palm fibers acting as bridging agent

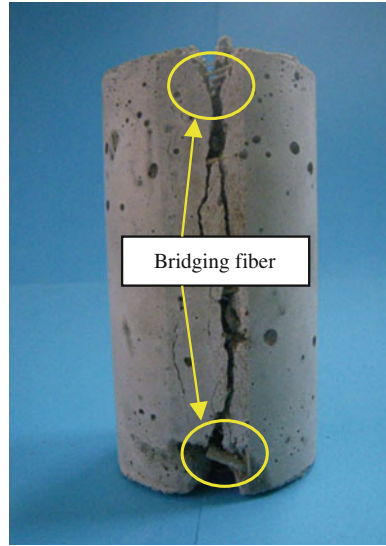
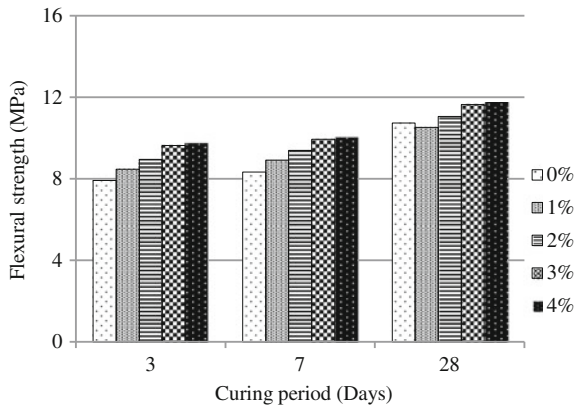


Fig. 7 Flexural strength of mortar containing oil palm stem fiber



to give lower value of flexural strength due to excess amount of fiber that contributes to weaker bonding between the particles resulting in a weaker mortar matrix.

An important aspect that can be outlined from the experimental results is the ductility and tenacity of mortar containing oil palm stem fiber. This phenomenon could be due to the higher deformability and energy absorption of the mortar during the failure. Wang and Belarbi [18] typified the flexural behavior of normal mortar failure to be more brittle and explosive in nature. Unlike in normal mortar, the beams containing oil palm stem fiber failed in ductile ways which the load dropped more smoothly and gently.

4 Conclusion

The experimental works carried out in this research draw some conclusions. These are:

- The inclusion of oil palm stem fiber affected the workability of mortar. It has been found that the workability of mortar mixes decreased with the increase of fiber content.
- Palm oil stem fiber has been found to improve the overall strength of mortar to a certain limit. This improvement has been shown to be prominent in case of splitting tensile and flexural strength as compared to that of compressive strength. Generally, higher the l/d ratio and fiber content, higher was the strength development.
- The results obtained and the observations made in the preliminary study suggest that the palm stem fiber has good potential as a reinforcing material. Long-term research work including deformation behavior and durability aspects, however, has been put forward for future study to obtain better understanding of this material in mortar and concrete mixes.

References

1. C.D. Johnston, Fiber reinforced cement and concrete, in *Advances in Concrete Technology*, 2nd edn., ed. by V.M. Malhotra (Canada Centre for Mineral and Energy Technology, Canada, 1994), pp. 603–674
2. H.K. Gram, Durability of natural fibres in concrete, in *Concrete Technology and Design*, vol. 5, ed. by R.N. Swamy (1988), pp. 173–207
3. Z. Fördös, Natural or modified cellulose fibres as reinforcement in cement composites, in *Concrete Technology and Design*, vol. 5, ed. by R.N. Swamy (1988), pp. 143–172
4. M. Rashid, M. Rozainee, Particulate emissions from a palm oil mill plant—a case study. *Jurnal Teknologi, Universiti Teknologi Malaysia* **22**, 19–24 (1993)
5. A.S.M.A. Awal, I.A. Shehu, Evaluation of heat of hydration of concrete containing high volume palm oil fuel ash. *Fuel* **105**, 728–731 (2013)
6. S.C. Lim, K.S. Gan, Characteristic and utilization of oil palm stem, timber technology bulletin, Forest Research Institute Malaysia, No. 35, 2005
7. Z. Ahmad, H.M. Saman, T.M. Tahir, Oil palm trunk fiber as a bio-waste resource for concrete reinforcement. *Int. J. Mech. Mater. Eng. (IJMME)* **5**(2), 199–207 (2010)
8. S. Kalia, B.S. Kaith, I. Kaur, *Pretreatments of natural fibers and their application as reinforcing material in polymer composites—a review*, Wiley International Science and Society of Plastic Engineering (2009)
9. ASTM C1329, Standard specification for mortar cement (2005)
10. ASTM 1437, Standard test method for flow of hydraulic cement mortar (2007)
11. ASTM C1403, Standard test method for rate of water absorption of masonry mortars (2006)
12. ASTM C109/C109M, Standard test method for compressive strength of hydraulic cement mortars (using 50 mm cube specimens) (2011)
13. ASTM C469/C469, Standard test method of splitting tensile strength of cylindrical concrete specimen (2011)
14. ASTM C348, Standard test method of flexural strength of hydraulic cement mortar (2008)

15. S.S Rehsi, Use of natural fiber concrete in India, in *Concrete Technology and Design*, vol. 5, ed. by R.N. Swamy (1988), pp. 243–255
16. A.S.M.A. Awal, D. Mazlan, M.L Mansur, Utilization of soft drink can as reinforcement in concrete, in *Proceedings of 3rd International Conference of EACEF* (European Asian Civil Engineering Forum), Universitas Atma Jaya Yogyakarta, Indonesia, pp. B15–B20 (2011)
17. M.A. Ismail, H. Hashim, Palm oil fiber concrete, in *The 3rd ACF International Conference* (2008) pp. 403–416
18. H. Wang, A. Belarbi, Flexural behavior of fiber reinforced concrete beams reinforced with FRP rebars. *ACI Struct. J.* **SP230-51**, 895–914 (2005)

Factor of Safety for Dowelled-Double Shear Kempas and Kapur Connections

Rohana Hassan, Azmi Ibrahim, Zakiah Ahmad
and Mohd. Nizam Shakimon

Abstract Load-carrying capacity, strength and stiffness properties are critical properties in determining the factor of safety for structural timber joint designs. The capability of joint in form of double shear is the guided method and based guidelines information in analyzing other modern and traditional joints design. The dowelled timber-to-timber strength capacity were used in this study to determine the performance and capability of the EYM theoretical equations to predict the load-carrying of mortise and tenon joints when it is dowelled with steel, GFRP or wood dowel. When the factor of safety is taken as the average of both species, the higher safety factor values is presented. The safety factor for joints dowelled with steel, GFRP and wood with references to the 5 % offset load is 2.7, 2.8 and 1.8 and ultimate values to the predicted values is 2.8, 2.9 and 2.5 respectively. As a conclusion, even though the safety factors is confirmed acceptable and the EYM is evidently suitable for predicting the GFRP and steel dowelled joints but not that accurate to predict the wood dowelled joint. In the case of wood dowels, though EYM are adequate to soundly predict the failure mode of the joints with wood dowel to an acceptable accuracy, modifications to the EYM equations are evidently necessary to predict the load-carrying capacity with a sufficient margin of safety for the design purposes.

Keywords Factor of safety · Kempas · Kapur · European yield model

R. Hassan (✉) · Z. Ahmad
Institute for Infrastructure Engineering and Sustainable Management (IIESM), UiTM,
40450 Shah Alam, Selangor D.E, Malaysia
e-mail: rohan742@salam.uitm.edu.my

A. Ibrahim · Mohd. Nizam Shakimon
Faculty of Civil Engineering, UiTM, 40450 Shah Alam, Selangor D.E, Malaysia

1 Introduction

Factor of safety in a timber connection is a value used to consider and allow for a safety factor during design. In engineering terms, a factor of safety is the ratio of the ultimate stress during working to the actual or allowable applied stress in service. The actual applied stress has to be much smaller than the ultimate stress to have a sufficient safety factor [1].

The value of the ultimate stress comes from the ultimate load to which a member is subjected to an actual working load that it can withstand. This result may be gathered from experimental or physical tests. The applied stress is the maximum allowable stress that the member is allowed to carry in terms of design capacity during the services of the member. This value may be gathered from the analytical models taking the actual values as the guidance.

According to Sarkar [1], the factor of safety depends on many other factors such as the homogeneity of the materials used and the accuracy with which stresses in members can be evaluated. Sarkar [1] also suggested that for most engineering structures, a factor of safety between 2 and 6 is suitable. While Madsen [2] mentioned that the design capacities of joints with laterally loaded nails designed by North American engineers are based on working stress using a factor of safety of 1.3 for members loaded in bending, tensile and compression.

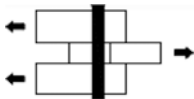
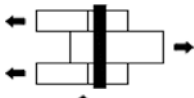


2 Literature Review

2.1 Factor of Safety

For wood dowelled mortise and tenon joints loaded in tensile, a factor of safety of 3.0 from an average of 3 numbers of specimens in a group is recommended by Kessel and Augustin [3]. The factor of safety recommended by Kessel and Augustin [3] was based on the ratio of ultimate strength from the experimental to the predicted/allowable load carrying capacity values. Schmidt and Daniels [4] recommended a factor of safety of 2.0 for mortise and tenon joints using the 5 % exclusion value of the 5 % offset strength.

Miller [5] determined the factor of safety for mortise and tenon joints loaded in shear using a ratio of a correlation equation produced at yield load introduced from his study to the existing EYM, NDS 2005 [6] formulas (Table 1). The factor of safety produced by Miller [5] for the wood dowelled mortise and tenon joints loaded in shear is 2.2. where;

Table 1 EYM for double shear timber-to-timber equations according to NDS, 2005

Failure mode	Characteristic load-carrying capacity, Z	Failure mode
	$\frac{Dl_m F_{em}}{4K_\theta}$	I _m
	$\frac{2Dl_s F_{es}}{4K_\theta}$	I _s
	$\frac{2k_3 D l_s F_{em}}{3.2(2+R_e)K_\theta}$	III _s
	$\frac{2D^2}{3.2K_\theta} \sqrt{\frac{2F_{em}F_{yb}}{3(1+R_e)}}$	IV

$$k_1 = \frac{\sqrt{R_e + 2R_e^2(1 + R_t + R_t^2) + R_1^2 R_e^3 - R_e(1 + R_t)}}{(1 + R_e)}$$

$$k_2 = -1 + \sqrt{2(1 + R_e) + \frac{2F_{yb}(1 + 2R_e)D^2}{3f_{em}l_m^2}}$$

$$k_3 = -1 + \sqrt{\frac{2(1 + R_e)}{R_e} + \frac{2f_{yb}(2 + R_e)D^2}{3F_{em}l_s^2}}$$

$$R_e = \frac{F_{em}}{F_{es}}$$

$$R_t = \frac{l_m}{l_s}$$

F_{em} dowel-bearing strength of the main member, psi.

F_{es} dowel-bearing strength of the side member, psi.

Z reference design value for fastener in double shear (Z taken as the smallest value from four yield limit equation) lbf.

$$K_\theta = 1 + \frac{\theta}{360}$$

D fastener diameter, in.

l_m thickness of the timber middle member, in.

l_s smaller of the thickness of the timber side member or the penetration depth, in.

F_{em} dowel-bearing strength of main (centre) member, psi.

$$\begin{cases} F_{e//} & \text{for load parallel to the grain} \\ F_{e\perp} & \text{for load perpendicular to the grain} \\ F_{e\theta} & \text{for load at angle to the grain } \theta \\ & \text{(see Hankinson formula)} \end{cases}$$

F_{es} dowel-bearing strength of side member, psi.

$$\begin{cases} F_{e//} & \text{for load parallel to the grain} \\ F_{e\perp} & \text{for load perpendicular to the grain} \\ F_{e\theta} & \text{for load at angle to the grain } \theta \\ & \text{(see Hankinson formula)} \end{cases}$$

F_{yb} bending yield strength of fastener, psi.

where;

- Yield Mode I = Wood crushing in either the main member or side members. Dowel stiffness is greater than wood strength.
- Yield Mode II = Wood crushing of both main and side member. Dowel stiffness is greater than wood strength.
- Yield Mode III_m = Dowel yield in bending at one plastic hinge point per shear plane and associated wood crushing of main member.
- Yield Mode III_s = Dowel yield in bending at one plastic hinge point per shear plane and associated wood crushing of side members.
- Yield Mode IV = Dowel yield in bending at two plastic hinge points per shear plane and associated wood crushing.

2.2 GFRP as a Dowel Material

Steel is a common material as a dowel fastener used in strengthening or fastening the structural timber member compared to wood dowel and glass fibre reinforced polymer (GFRP). Nowadays, GFRP has also being used and studied for structural purposes. Its used as a dowel replacement for timber connection has been reported by few researchers such as Pedersen [7], Drake [8] and Thomson [9]. From the previos finding, it was found that the strength of these connections are governed by GFRP shear failure. Their studies has also relates to the EYM theory and found that EYM is not suitable to accurately predict the capacity of timber connections with GFRP dowels since the EYM does not take shear failure into account. In the

present paper, direct applications of the EYM has been used in calculation. It is based on the basis theory of the EYM which the shear failure of the dowels was not taken into consideration in adopting the EYM theory.

This study has used the concept of factor of safety in relations to the allowable design strength to 5 % offset load and the ultimate load as a comparison to prove the reliability of the EYM in predicting the joint connected with GFRP dowel. The similar method was also determined for joint connected with wood dowel for comparison purposes.

3 Methodology

3.1 Double Shear Strength Properties

In this study, the double shear strength tests were done to determine the load carrying capacity of the double shear joint function to determine the factor of safety for the connections. The timber joints were fastened with steel, GFRP and wood dowel.

3.2 Sample Preparations

The specimens for the double shear were prepared in accordance with the ASTM D 5652-95 (reapproved 2007) [10]. Thirty (30) total numbers of double shear joints were prepared. The timber species for the base material (i.e. main and side) were of Kempas and Kapur species. For Kempas joints, 5 joints were fastened with steel, 6 joints fastened with GFRP dowel and 5 joints fastened with wood dowels (made of Kempas species). Whilst for Kapur joints, 5 joints were fastened with steel, 5 joints fastened with GFRP dowels and 4 fastened with wood dowels (made of Kapur species). Each timber specimen used was assured as clear from any defect and essentially clear and straight-grained. The double shear joint were formed using 3 pieces of timber block denoted as A, B and C and arranged as shown in Fig. 1.

The side members (block A and C) were cut three times wider than the main member (block B). Prior to the testing, a joint was drilled at each ends of the 3 pieces of specimens (member A, B and C) for the end grip-hole. The 3 pieces were then clamped together with sufficient pressure to maintain contact between faces. Lead hole was then drilled in between the three pieces with hole slightly larger than the dowel diameter. This size of hole is drilled base on the available on shelve hand- driller diameter closer to the size of dowel. All dowel diameters were as closed as possible to the available on shelve 0.81 in diameter of GFRP. A gap within 0.08 in was allowed between the dowel and the pre-drill hole based on the common construction practice.

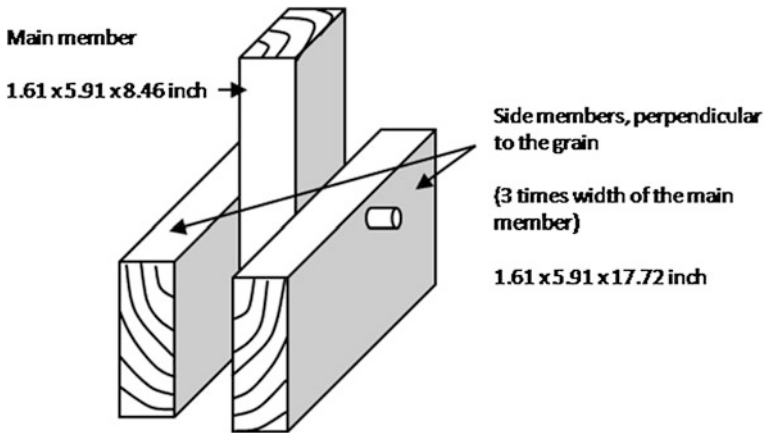
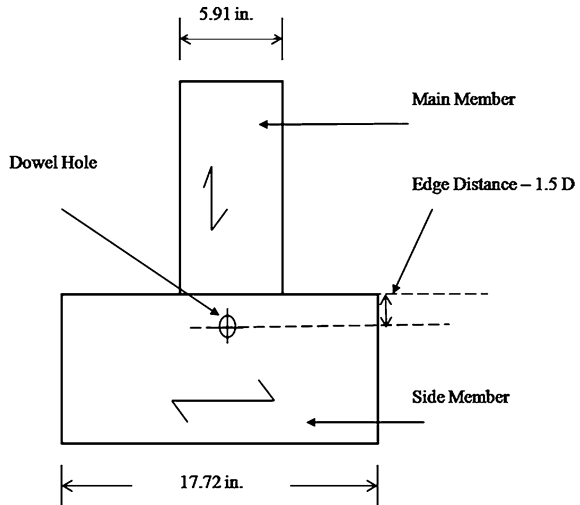


Fig. 1 Specifications of the main and side members for perpendicular to the grain specimens

Fig. 2 End distance of side member in perpendicular grain direction at a minimum distance-1.5D [9]



Clamps were then removed and the dowel was then inserted in the hole. The middle member was then clamped at the testing machine using the u-shape steel blocks followed by the clamping of the side members at both ends also by the u-shape steel blocks. The middle of the side members was filled with a wood block to avoid the side movement of members during testing. The fixed parameters of this connection are the sizes of the main and side members of the double shear joint and the dowel diameters.

The dimensions of middle specimens are 1.61 in. \times 5.91 in. \times 8.46 in. and side members 1.61 in. \times 5.91 in. \times 17.72 in. Three types of dowels were prepared from

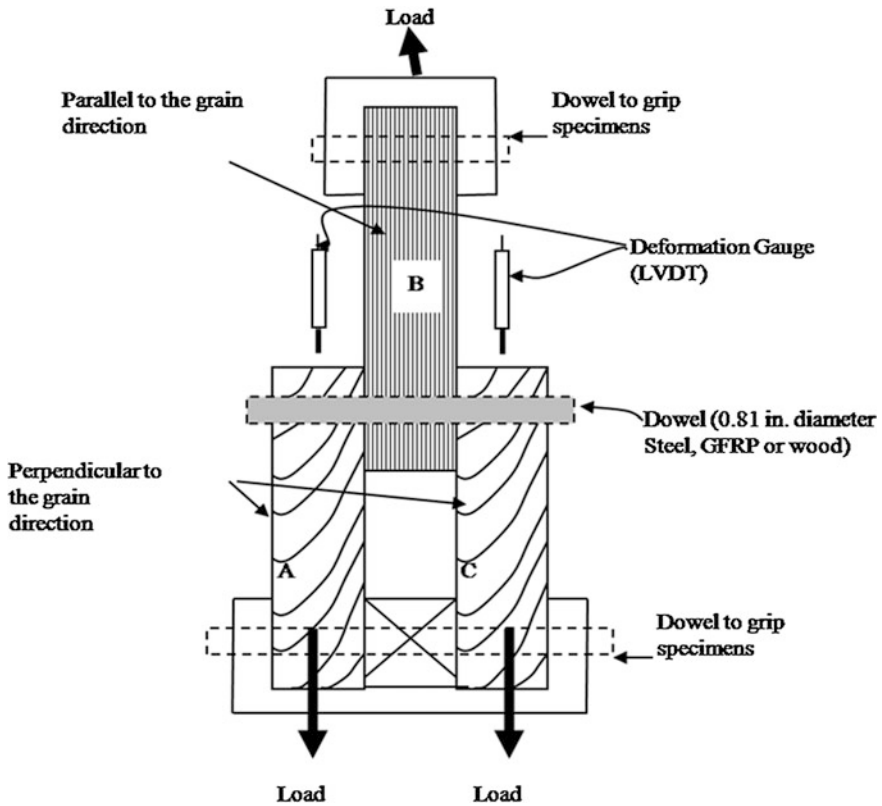


Fig. 3 Configuration of double shear connections loaded in tensile

steel, GFRP and wood were cut into the same 4.96 in. length. Fig. 2 depicts the geometry of the specimens and the minimum end distance applied in this study.

All air-dry test specimens were stored at 20 ± 3 °C and 65 ± 2 % relative humidity prior to testing. Materials for moisture content, density and specific gravity were cut after the test and were prepared accordingly.

3.3 Test Method

These test methods in ASTM D 5652-95 (reapproved 2007) [10] cover procedures for evaluating the strength and stiffness of single-bolted connections in wood or wood based products when subjected to static loading. The experiment for the joint dowelled with GFRP and wood were referred to the same standard as the double shear test standard for steel as the standard for GFRP and wood is not yet available. The joint were consists of three members dowelled with one dowel either steel, GFRP or wood dowel (Fig. 3).

Two Linear Variable Displacement Transducers (LVDTs) were mounted at both side members. Load was applied to each joint using a hand operated hydraulic pump and were gripped at the bottom of the specimens. The applied loading was captured using a load cell and all data logged to a computer. Since these studies were conducted to investigate the validity of the model at yield and the performance outcomes from the different dowel material, all connections were run up to total failure. The total failure is when the double shear connections are totally disconnected either caused by the failure in dowel, side member or main member failure. Testing were loaded and continued until a fracture occurred that was accompanied by a substantial non-recoverable drop-off in load. Ultimate shear strength and yield load were then recorded. The rate of the test were varies according to the type of dowels, since the failure rates of these material is different. The rate applied for this study is 0.01 inch/min when dowelled with steel or GFRP and 0.03 inch/min when dowelled using wood. All tests reached their maximum loading within 5 and 20 min as required by ASTM D 5652-95 standards [10].

4 Result and Discussion

Table 2 summarised the experimental and load carrying capacity, Z and the failure modes. Based on results in Table 2, the minimum Z values were accepted as the estimated failure load-carrying capacity for the joint. For joints made of Kempas species, it was found that the minimum estimated load-carrying capacity of double shear members strengthened with steel and GFRP computed from NDS 2005 [6] is similar; that is with 3,115.71 lbf. capacity in failure mode I_m .

Wood dowel estimated a lower strength value that is 2,426.70 lbf. with failure load corresponding to mode III_s . It was found that the theoretical values have under predicted the experimental for steel dowelled joints by 30.83 %, GFRP dowelled joints by 39.52 % and wood dowelled joints by 11.29 %. However, the gap between the predictions and the experimental is as expected since this value is meant for the safety factor. A more detailed analysis and discussion of the factor of safety of the double shear joints is covered in the later sections. For the joints manufactured with Kapur species, the similar behavior and pattern of failure to the joints made of Kempas was noticed. However joint manufactured with Kapur shows a lower strength capacity compared to the Kempas joints. It was found that the minimum estimated load-carrying capacity of the double shear members strengthened with steel and GFRP computed from NDS 2005 [6] is identical; that is with 1,867.38 lbf. capacity and corresponds to failure mode I_s . Wood dowel estimated a lower strength value that is 1,543.35 lbf. with failure load corresponds to mode III_s .

However, it is exhibited that EYM equations have successfully predicted all failure mode for Kapur species regardless of the dowel types. Nevertheless, the theoretical values have under predicted the experimental strength for steel dowelled joints by 59.52 %, GFRP dowelled joints by 57.86 % and wood dowelled

Table 2 Summary of experimental and theoretical

Species	Type of dowel	Experimental (actual load carrying capacity)		Theoretical [Z values for different failure mode (lbf.)]						Theoretical minimum Z values
		Average strength (lbf.)	Mode	Mode I _m	Mode I _s	Mode III _s	Mode IV	Z _r (lbf.)	Mode	
Kempas	Steel	4,504.72	I _s	3,115.71	3,238.59	4,793.28	6,775.51	3,115.71	I _m	
	GFRP	5,151.87	I _s	3,115.71	3,238.59	3,329.68	4,511.77	3,115.71	I _m	
Kapur	Wood	2,735.47	III _s	3,115.71	3,238.59	2,426.70	2,751.46	2,426.70	III _s	
	Steel	4,447.17	I _s	1,867.38	1,800.42	3,654.11	5,124.72	1,800.42	I _s	
	GFRP	4,272.49	I _s	1,867.38	1,800.42	2,422.81	3,412.52	1,800.42	I _s	
Wood	2,041.26	III _s	1,867.38	1,800.42	1,543.35	1,938.81	1,543.35	III _s		

^a Bolded figures are the minimum theoretical Z values

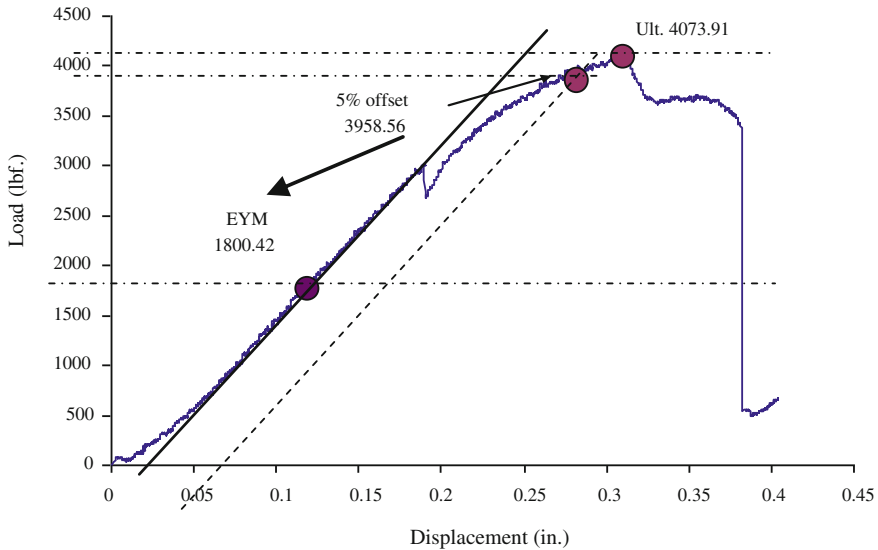


Fig. 4 An example of deviation between the 5 % offset to the analytical values

joints by 24.39 %. Further discussion of the gap between the predicted and the experimental are also discussed in the subsequent sections.

Both experimental failure mode for joint with steel or GFRP dowel were found to have failed in side members which fall under I_s category for both species. While in theoretical, both failure modes for joints fastened with steel or GFRP dowel failed in the same I_m region for Kempas. Though the prediction of Kempas species was not similar to the experimental, the failure mode of the joints with GFRP dowel were considered validated by the joint with steel. This is due to the failure mode of GFRP dowelled joints being similar to the steel dowelled joints and EYM is purposely developed for joints fastened with steel fasteners. The theoretical failure mode in NDS, 2005 [6] has successfully predicted the wood dowelled joints actual failure as it corresponds to a similar mode III_s to the experimental.

4.1 Factor of Safety for Double Shear Joints

The safety factors calculated from both the 5 % offset load and ultimate strength values are discussed in this study for the purposes of comparison. An example of the safety factor in ratio of 5 % offset and ultimate load to the EYM estimated values are shown in Fig. 4. Details of the results are shown in Table 3.

The 5 % offset load was determined by drawing a straight line to the initial linear portion of the load-deformation curve. The line was then offset by a deformation equal to 5 % offset of the dowel diameter (0.041 in.) which gives a

Table 3 Summary of safety factor (FoS) for kempas and kapur in the ratio of experimental strength values to the predicted EYM values

Species	Type of dowels	5 % offset load (lbf.)	Ultimate load (lbf.)	Predicted load (lbf.) (EYM)	FoS (5 % offset load to predicted)	FoS (ultimate load to predicted)
Kempas	Steel	4,504.72	4,758.75	3,115.71	1.45	1.53
	GFRP	5,151.87	5,236.92	3,115.71	1.65	1.68
	Wood	2,735.47	3,587.50	2,426.70	1.13	1.48
Kapur	Steel	4,447.17	4,580.30	1,800.42	2.47	2.54
	GFRP	4,272.49	4,555.10	1,800.42	2.37	2.53
	Wood	2,041.26	3,048.05	1,543.35	1.32	1.97

Table 4 Average values of factor of safety for combination of kempas and kapur species

Types of dowel	5 % offset load (lbf.)	Ultimate load (lbf.)	Predicted load (lbf.) (EYM)	FoS (5 % offset load to predicted)	FoS (ultimate load to predicted)
Steel	6,728.31	7,048.90	4,015.92	2.7	2.8
GFRP	7,288.12	7,514.47	4,015.92	2.8	2.9
Wood	3,756.10	5,111.53	3,198.38	1.8	2.5

displacement value of 0.061 in. from the initial linear portion as shown in Fig. 4. The load was then selected at which the offset line intersects the load-deformation curve. The factor of safety based on 5 % offset and ultimate load is both discussed in this study. Both factor of safety for Kempas species is found to be higher than Kapur species. Based on the factor of safety from the 5 % offset load, it can be seen that for joint made of Kempas species, the load-carrying capacity ratio of the 5 % offset load to the estimated for steel, GFRP and wood is 1.45, 1.65 and 1.13 respectively.

Though Kapur is a hardwood species, its density and strength is very much lower than Kempas. Nevertheless, the factor of safety for wood dowelled is only 1.32. Based on the factor of safety from ultimate load, for joint made of Kempas species, the load-carrying capacity deviation ratio of the experimental ultimate load to the estimated is 1.53 for joint strengthened with steel dowel, 1.68 for joint with GFRP dowel and 1.48 for the joint connected with wood dowel. On the other hand, the safety factor found in the joints connected with GFRP is validated by having a bigger value then the factor of safety for steel. The result of joint strengthened with steel dowel subsequently validates the current EYM accuracy to estimates timber joint strengthened with GFRP and wood dowel.

For Kapur species, the factor of safety is 2.54 for joint strengthened with steel dowel, 2.53 for joint with GFRP dowel and only 1.97 for the joint connected with wood dowel. It can be seen that the safety factor for the strength group 4 species is higher compared to the strength group 2 species. Therefore, it can be seen that the

result of Kapur joints strengthened with steel dowel also subsequently validates the current EYM accuracy to estimates of timber joints strengthened with GFRP and wood dowel.

The safety factor in the combination of Kempas and Kapur based on the types of dowels is according to the Table 4.

When the factor of safety is taken as the average of both species, the higher safety factor values is presented. The safety factor for joints dowelled with steel, GFRP and wood with references to the 5 % offset load is 2.7, 2.8 and 1.8 and ultimate values to the predicted values is 2.8, 2.9 and 2.5 respectively.

5 Conclusions

From the experimental work and the concept used in predicting the factor of safety applied in this study, the safety factors is shown viable. The EYM is found suitable to predict the GFRP dowelled joints but not that accurate to predict the wood dowelled joint. It is shown that the detailed treatment of the design of steel dowelled timber joints in EYM is equally applicable to GFRP dowelled timber joints matching even the failure modes therein. In the case of wood dowels, though EYM are adequate to soundly predict the failure mode of the joints with wood dowel to an acceptable accuracy, modifications to the EYM equations are evidently necessary to predict the load-carrying capacity with a sufficient margin of safety.

Acknowledgments The authors would like to thank the Ministry of Higher Education, (MOHE) Malaysia for funding the project through RIF 600 RMI/DANA/5/3/RIF (74/2012) Universiti Teknologi MARA.

References

1. B.K. Sarkar, *Strength of materials* (Tata McGraw-Hill Publications, Newyork, 2003)
2. B. Madsen, (1992). Structural Behaviour of Timber, Timber Engineering Ltd. North Vancouver. ASBN 0-9696162-0-1. p. 437
3. M.H. Kessel, R. Augustin, Load Behaviour of Connections with Oak Pegs, Translation by Schmidt, R., Timber Framing. J. Timber Framers, Guild North America, No. 39, pp. 8–11 (1996)
4. R.J. Schmidt, E.D. Daniels, Design considerations for mortise and tenon connections. Report for Timber Framers Guild, Becket, MA (1999)
5. J.F. Miller, Capacity of wood dowelled mortise and tenon joints. Master science thesis, Department of Civil and Architectural Engineering, University of Wyoming, Laramie Wyoming (2004)
6. NDS, National Design Specification for Wood Construction American Forest and Paper Association (AFPA) Washington D.C. (2005)
7. M.U. Pedersen, Dowel type timber connections- strength modelling. PhD Thesis, Department of Civil Engineering, Danmarks Tekniske Universitet, Denmark (2002)

8. R. Drake, The advancement of structural connection techniques for timber buildings. PhD Thesis University of Bath (2003)
9. A. Thomson, R. Harris, P. Walker, M. Ansell, Development of non-metallic timber connections for contemporary applications. CD *Proceeding of 11th World Conference on Timber Engineering* (WCTE). 20–24 June 2010. Trentino, Italy
10. American Society for Testing and Materials. Standard Test Method for Bolted Connections in Wood and Wood-Based Products. ASTM D 5652—95 (Reapproved 2007). ASTM, Philadelphia, Pa

Evaluation of Dowel-Bearing Strength for Wood Dowel Using ‘Spring Theory’

Rohana Hassan, Shaharin Hamid, Nity Azidah Mohammad Amini and Tengku Anita Raja Hussin

Abstract Dowel-bearing strength of wood base material is one of the important parameter to design the load carrying capacity of a timber joint. The information about the dowel-bearing strength using steel is available in National Design Standard (NDS, National Design Specification for Wood Construction American Forest and Paper Association (AFPA) Washington DC, 2005). However none of these standards include dowel-bearing strength compressed using wood dowel. Very limited studies were published in determining the dowel-bearing strength of wood base material compressed with wood dowel. The ‘Spring Theory’ proposed by Schmidt and Daniels (Design Considerations for Mortise and Tenon Connections. Report for Timber Framers Guild. Becket. MA, 1999) was found reliable to be applied for European timber species. However, the capability of this theory in determining the dowel-bearing strength of wood based compressed with wood dowel has not be investigated for tropical timber. Therefore this study is aimed to investigate the capability of the ‘Spring Theory’ for 12.7 mm wood dowel. ‘Spring Theory’ is about the combination result of wood dowel compressed with steel block (WDCSB) and wood block compressed with the steel dowel (WBCSD). It was found that ‘Spring Theory’ value of Kempas is 34.81 Mpa. The value of the proportional, 5 % offset and maximum load of Kempas is 11.74, 18.12 and 50.64 kN respectively. The ‘Spring Theory’ was found capable and valid in determining the wood dowel of Kempas compressed with 12.7 mm wood dowel.

R. Hassan (✉)

Institute for Infrastructure Engineering and Sustainable Management (IIESM), UiTM, 40450 Shah Alam, Selangor D.E., Malaysia
e-mail: rohan742@salam.uitm.edu.my

S. Hamid

Faculty of Civil Engineering, UiTM, 40450 Shah Alam, Selangor D.E., Malaysia

N. A. M. Amini · T. A. R. Hussin

Postgraduate Students, Faculty of Civil Engineering, UiTM, 40450 Shah Alam, Selangor D.E., Malaysia

Keywords Dowel-bearing strength · Malaysian timber · ‘Spring theory’ · Steel block · Wood dowel

1 Introduction

There are few properties need to be measured to determine connection capability. One of them is dowel-bearing strength. Dowel-bearing strength of wood base material is one of the important parameter to design the load carrying capacity of a timber joint. The information about the dowel-bearing strength using steel is available in National Design Standard (NDS) [1]. Dowel-bearing strength of few hardwood species has been studied by Jumaat et al. [2], Rammer [3] and Awaludin et al. [4]. However, the standard and the studies did not reported on dowel-bearing strength compressed using wood dowel and only limited to the dowel-bearing of wood compressed with steel dowel.

Since very limited studies were also published in determining the dowel-bearing strength of wood base material compressed with wood dowel, therefore the ‘Spring Theory’ proposed by Schmidt and Daniels [5] is relevant to use. The theory has been developed by Schmidt and Daniels [5] for soft wood function to reduce the numbers of test for the dowel-bearing strength compressed with wood dowel. ‘Spring Theory’ is about the combination result of wood dowel compressed with steel block (WDCSB) and wood block compressed with steel dowel (WBCSD).

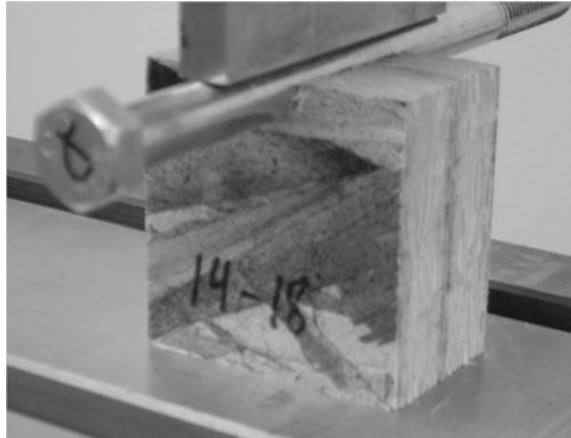
Since there are limitations to this timber design fundamental property, therefore the main objective of this study is to evaluate the dowel-bearing strength of Kempas species, one of the tropical wood species using the ‘Spring Theory’ that has been proposed for European wood. The results will finally be used to verify the capability of the ‘Spring Theory’ in predicting the dowel-bearing strength of Kempas.

2 Literature Review

2.1 Dowel-Bearing Strength of Wood

Dowel-bearing strength is the property of connection members that imparts resistance to embedding of a dowel. Whale and Smith [6] relates this property to species density and dowel diameter for bolts and nails. Whale and Smith [6] defined bearing strength as the maximum test load. A lower load level for bearing strength has been proposed for connection design provisions in the United States. One of the example of determining the dowel-bearing strength using compressed by steel dowel is as reported by Cates [7]. Cates [7] determined the half-hole dowel-bearing test that was performed using the procedures in ASTM D5764-97a, 2007 [8]. The specimens was tested by applying a compressive load on a bolt

Fig. 1 Dowel-bearing specimen test setup [7]



resting in the half-hole of the dowel-bearing specimen (Fig. 1). The 5 % offset were then determined from the test (Fig. 2).

2.2 Dowel-Bearing Strength Using ‘Spring Theory’

Schmidt and Daniels [5] reported that the peg or wood bearing was performed to determine the bearing strength for the peg population selected for the full-size joint test. They stated that the tests were performed using a 1.5" wide steel saddle (Fig. 3), which replaced the wood base material. The testing was performed using an Instron model 1332 testing machine and Labview data acquisition software. The pegs were tested at a load rate of 0.024 in/min.

The ‘Spring Theory’ curve procedures are:

1. In order to obtain a new curve with uniform increments of displacement, the dowel curve of WDCSB from the physical test should be filtered (smoothed).
2. To obtain a new curve with uniform increments of displacement, the dowel curve of WBCSD from the physical test should be also filtered (smoothed).
3. Material combination shall be resulted from the addition of the load-displacement average curve from WDCSB and from WBCSD.
4. The 5 % offset shall then be determined from the combination of load-displacement graph.

3 Research Methods

The dowel-bearing methodology was set up according to the similar method as proposed by Schmidt and Daniels [5]. Figure 4 show the visual representation of the dowel-bearing ‘Spring Theory’ purposed by Schmidt and Daniels [5].

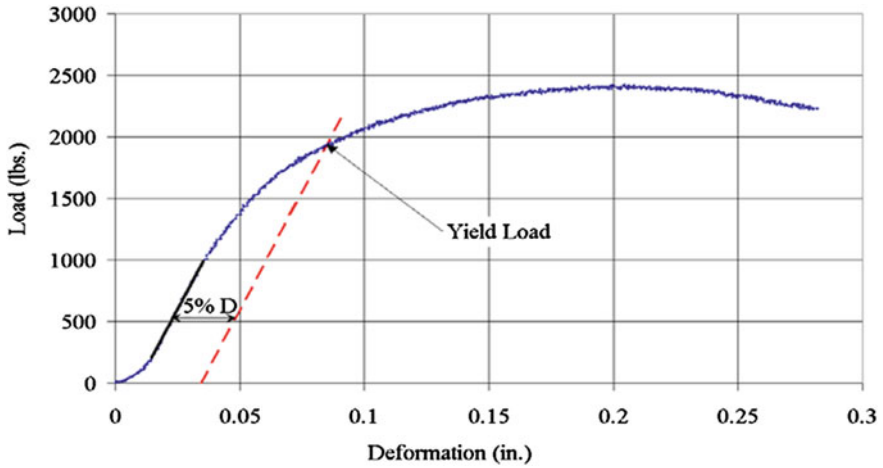


Fig. 2 Determining the yield load from a load versus displacement curve [7]

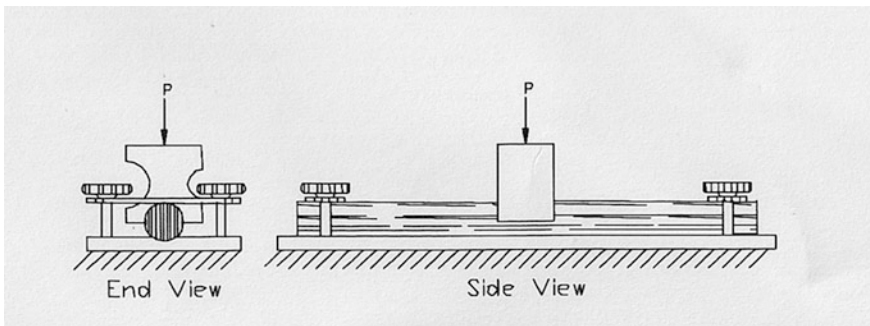


Fig. 3 Peg bearing test fixture [5]

3.1 Material Preparation and Set Up of the WDCSB

Ten (10) specimens were prepared for the average results. The specimens were cut in the position of parallel to the grain. The 12.7 mm with the length of 323 mm wood dowels were prepared from the same species and same batch of wood from the WDCSB tests. After the WDCSB test, the same dowels were measured for their moisture content and density. The yield points were then measured for the proportional; 5 % offset and the maximum values. The configuration of the WDCSB is as shown in Fig. 5.

The load rate to reach it failure for this study was 0.024 in/min in approximately four (4) to seven (7) minutes. The testing consist of a steel block with half-hole placed on the flat base on Universal Testing Machine (UTM) and steel plate with

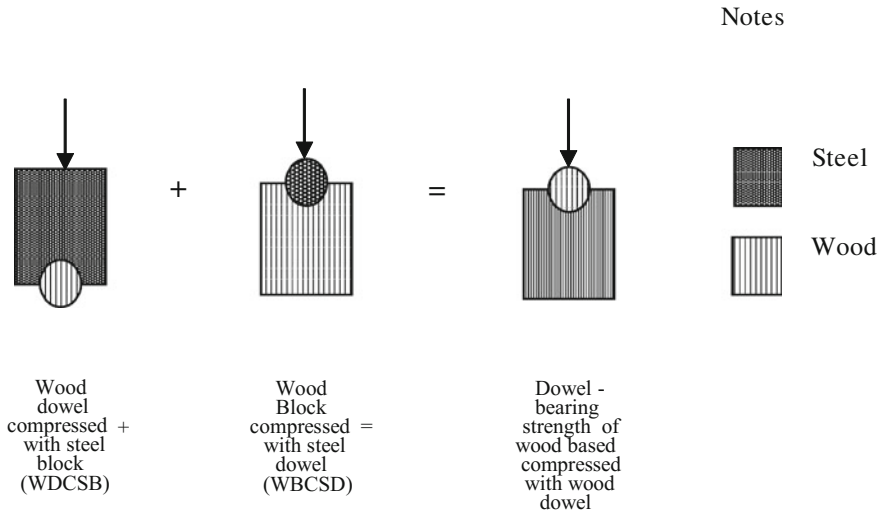
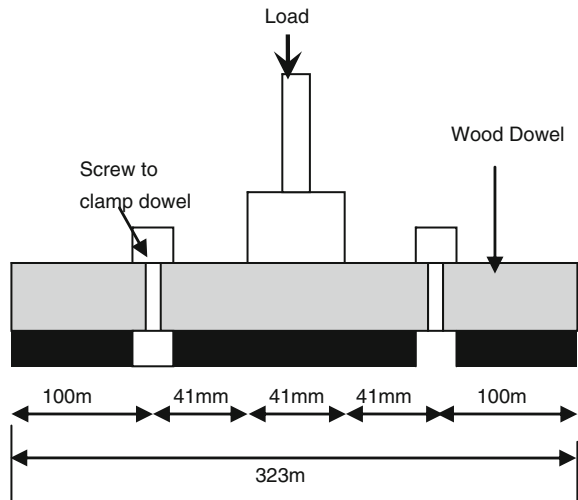


Fig. 4 Dowel bearing spring theory [5]

Fig. 5 Configuration and the geometry of the wood dowel



the load head pressed the dowel into the specimen. Figures 6 and 7 show the dowel-bearing test setup until the end of the test.

The dowel-bearing strength (F_e) was then evaluated by Eq. 1.

$$F_e = \frac{P_{0.05}}{Dt} \tag{1}$$

Fig. 6 WDCSB test set up

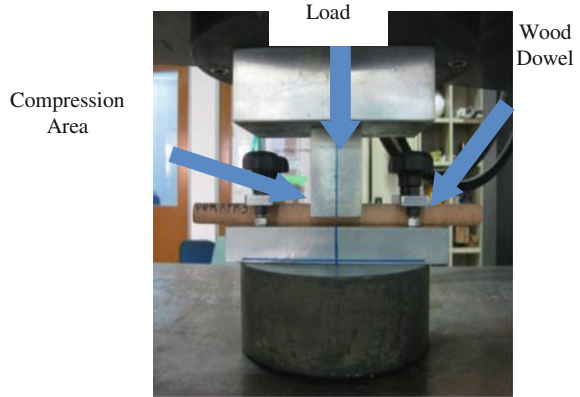
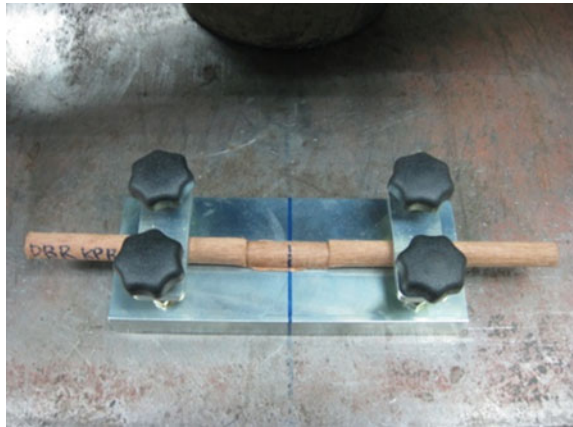


Fig. 7 Wood dowel after test



where;

F_e is the dowel-bearing strength, kN/mm

D is the dowel diameter, mm

$P_{0.05}$ is the 5 % offset yield load from the load displacement curve, kN

t is the length of contact between the dowel and the base material, mm

4 Results

4.1 Wood Block Compressed with Steel Dowel

The average result of ten (10) specimens of WBCSD shows that the proportional, 5 % offset, maximum load and bearing strength value of steel dowel is 17.74 kN,

Table 1 Compilation of WBCSD bearing strength

Sample code	Prop. value Load (kN)	5 % offset		Maximum		Bearing strength (Mpa)
		Load (kN)	Displacement (mm)	Load (kN)	Displacement (mm)	
ST1	18.31	28.62	3.84	54.2	11.15	54.96
ST2	18.05	24.03	2.67	48.92	10.42	46.15
ST3	20.67	34.61	3.82	60.5	10.2	66.47
ST4	16.09	22.76	2.97	45.89	10.08	43.71
ST5	18.18	28.11	2.72	50.94	9.97	53.99
ST6	15.39	27.97	3.3	50.99	10.08	53.72
ST7	19.57	29.72	2.04	52.19	9.75	57.08
ST8	16.49	27.37	2.75	54.54	10.1	52.56
ST9	17.67	25.66	3.45	47.45	11.81	49.28
ST10	16.97	28.67	2.88	59.17	10.82	55.06
Average	17.74	27.75	3.04	52.48	10.44	53.30

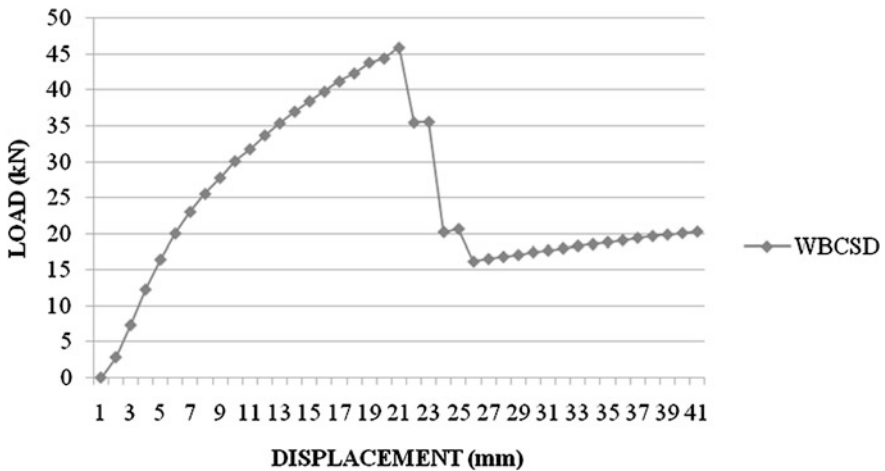


Fig. 8 Typical plot for WBCSD

27.75 kN/mm, 52.48 kN and 53.30 MPa respectively (Table 1). Figure 8 shows the typical plot for WBCSD.

4.2 Wood Dowel Compressed with Steel Block

The average result of ten (10) specimens of WDCSB shows that the proportional value, 5 % offset, maximum load and bearing strength of Kempas is 5.74 kN, 8.50 kN/mm, 48.80 kN and 16.32 MPa respectively (Table 2). Figure 9 shows the

Table 2 Compilation of WDCSB bearing strength

Sample code	Prop. value Load (kN)	5 % offset		Maximum		Bearing strength (Mpa)
		Load (kN)	Displacement (mm)	Load (kN)	Displacement (mm)	
KPS 1	6.29	9.36	1.77	65.86	5.21	17.98
KPS 2	5.39	7.90	1.42	40.36	5.17	15.17
KPS 3	4.69	6.88	1.43	55.02	5.73	13.21
KPS 4	4.92	8.18	1.34	47.27	5.29	15.71
KPS 5	5.43	7.44	1.50	38.44	5.28	14.29
KPS 6	5.55	8.77	1.47	40.03	5.24	16.84
KPS 7	6.29	8.48	1.39	39.45	5.48	16.29
KPS 8	6.36	10.01	1.84	69.54	5.49	19.22
KPS 9	5.49	7.99	1.78	30.89	5.53	15.34
KPS 10	6.94	9.95	1.46	61.13	5.19	19.11
Average	5.74	8.50	1.54	48.80	5.36	16.32

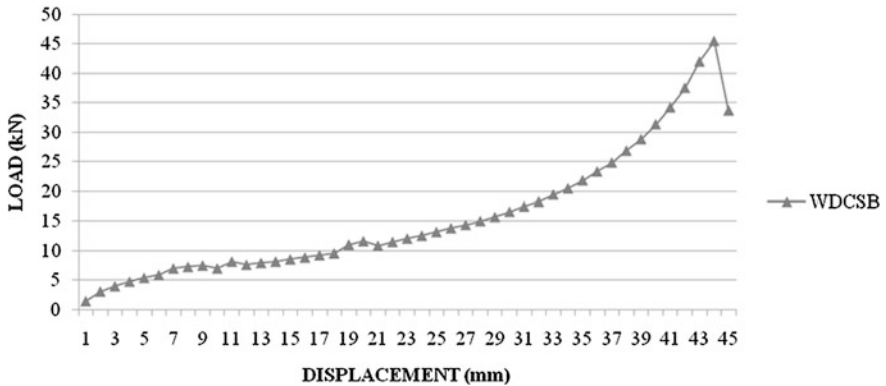


Fig. 9 Typical plot for WDCSB

typical plot for WDCSB. It shows the average curve of WDCSB. The patterns of typical plot for WDCSB curve increasing smoothly until about 45 kN load and about 44 mm displacement. Loads were increasing until the maximum capacity.

4.3 Dowel-Bearing of Wood Base Using ‘Spring Theory’ (WBCSD + WDCSB)

Table 3 shows the average result for ten (10) specimens. It was found that the proportional, 5 % offset, maximum load and ‘Spring Theory’ value of Kempas is 11.74, 18.12, 50.64 kN and 34.81 MPa respectively. Figure 10 shows the results

Table 3 Compilation of ‘spring theory’ (WBCSD + WDCSB)

Sample code	Prop. value Load (kN)	5 % offset		Maximum		Spring theory (Mpa)
		Load (kN)	Displacement (mm)	Load (kN)	Displacement (mm)	
Sc1	12.30	18.99	2.81	60.03	8.18	36.47
Sc 2	11.72	15.97	2.05	44.64	7.80	30.66
Sc 3	12.68	20.75	2.63	57.76	7.97	39.84
Sc 4	10.51	15.47	2.16	46.58	7.69	29.71
Sc 5	11.81	17.78	2.11	44.69	7.63	34.14
Sc 6	10.47	18.37	2.39	45.51	7.66	35.28
Sc 7	12.93	19.10	1.72	45.82	7.62	36.68
Sc8	11.43	18.69	2.30	62.04	7.80	35.89
Sc 9	11.58	16.83	2.62	39.17	8.67	32.31
Sc10	11.96	19.31	2.17	60.15	8.01	37.08
Average	11.74	18.12	2.29	50.64	7.90	34.81

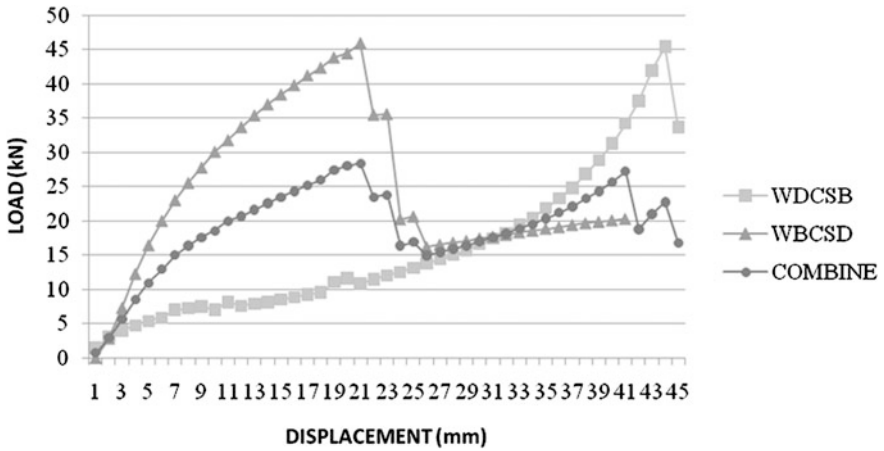


Fig. 10 Typical plot for WBCSD + WDCSB

for combination of WDCSB + WBCSD. It shows that the combined curve take placed between the WDCSB and WBCSD curves. It was found that the load is increasing until 29 kN and about 20 mm displacement. Figure 5 shows that the finding from this study is similar to the Schmidt and Daniels [5] and the ‘Spring Theory’ is valid to determine the dowel-bearing strength of Kempas compressed with 12.7 mm dowel wood dowel.

5 Conclusion

From the experimental and analysis of this study, it can be concluded that the dowel-bearing strength for WBCSD and WDCSB is 53.30 MPa and 16.32 MPa respectively. It also shows that the 'Spring Theory' is valid to determine the dowel-bearing strength of Kempas compressed with 12.7 mm wood dowel.

Acknowledgments The author would like to thank UiTM for funding the research through RAGS 600-RMI/RAGS 5/3 (51/2012) from Research Management Institute, Universiti Teknologi MARA.

References

1. NDS, *National Design Specification for Wood Construction*. (American Forest and Paper Association (AFPA), Washington DC, 2005)
2. M.Z. Jumaat, A.B. Bakar, F.A.M. Razali, A.H. Rahim, J. Othman, in WCTE: "*The Determination of the Embedment Strength of Malaysian Hardwood*". Proceedings of the 9th World Conference on Timber Engineering, (Portland, or, USA, 6–10 August 2006), p. 126
3. D.R. Rammer, Parallel-to-grain dowel-bearing strength of two guatemalan hardwoods. *For. Prod. J.* **49**(6), 77–87 (1999)
4. A. Awaludin, W. Smittakorn, T. Hirai, Bearing properties of *Shorea obtusa* beneath a laterally loaded bolt. *J. Wood Sci.* **53**(3), 204–210 (2007)
5. R.J. Schmidt, E.D. Daniels, *Design Considerations for Mortise and Tenon Connections*. Report for Timber Framers Guild. Becket, MA, (1999)
6. L.R.J. Whale, I. Smith, *Mechanical Timber Joints*, Research Rep. No. 18/86, Timber Research and Development Association, (High Wycombe, UK, 1987)
7. P.J. Cates, Dowel bearing strength and bolted connection behavior of oriented strand lumber. Master thesis, Department of Civil and Environment Engineering, Washington State University, 2002
8. American Standard Testing Method (ASTM) D 5764-97a, *Standard Test Method for Evaluating Dowel-Bearing Strength of Wood and Wood-Based Products*, (Washington DC, 2007)

Ultrasonic Wave Non-Destructive Method for Predicting the Modulus of Elasticity of Timber

M. B. F. M. Puaad, Z. Ahmad and H. Muhamad Azlan

Abstract Non-Destructive Testing (NDT) is a method proposed in the material studies to determine the physical and mechanical properties of a material without altering its end-use capabilities. This paper reports the investigation made the bending strength properties of timber beams using ultrasonic wave non-destructive test method and static destructive test. Timber beams from eight selected Malaysian timber of different strength grouping; Resak (SG4), Kapur (SG4), Merpauh (SG4), Bintangor (SG5), White Meranti (SG5), Jelutong (SG6), Sesendok (SG7) and Kelampayan (SG7) were used. The results from static and non destructive tests were statistically correlated and compared taking into account the density of the timber. The mean value for the modulus of elasticity established from the NDT tests were found to be higher than the corresponding value established from static tests.

Keywords NDT · Static bending · Modulus of elasticity · Modulus of rupture · Timber

1 Introduction

The applications of the ultrasonic and vibration methods have been used in the visual grading of the wood elements and structures [1]. The application of NDT has also been used in the evaluation of the occurrence and severity of defects in the material under conservation project [2], with the aim of comparing the residual

M. B. F. M. Puaad (✉)

Faculty of Civil Engineering, Universiti Teknologi MARA, 40500 Shah Alam, Malaysia
e-mail: bazli94949@yahoo.com

Z. Ahmad · H. Muhamad Azlan

Institute of Infrastructure Engineering and Sustainable Management (IIESM), Universiti Teknologi MARA, 40500 Shah Alam, Malaysia

section with the variations of density, usually associated with the loss of mass. These NDT methods present several advantages such as their practical utilization, transport and efficiency. Besides that, NDT methods which have no damage and undesirable effects on the samples, could estimate elastic properties with high accuracy in a short time [3].

Yang et al. [4] evaluated the mechanical properties of Douglas-fir and Japanese Cedar lumber by two different methods of nondestructive techniques namely ultrasonic wave technique and transverse vibration test and found that the transverse vibration test is a better nondestructive method of evaluating sawn lumber. Ross et al. [5] evaluated the correlations between stress wave MOE of the timber and bending and tensile strength of derived standard-size lumber and found that the correlations were low. Ross et al. [6] examined the relationship between log NDT measurement and the quality of lumber obtained from balsam fir and eastern spruce logs. They observed useful relationships, with the relationship being exceptionally strong for eastern spruce logs. Green and Ross [7] found similar results using the same technique with Douglas-fir, western hemlock, and southern pine logs. Gerhards [8] observed changes in the shape of a wave front in lumber containing knots and cross grain by measuring the change in wave speed in the vicinity of such defects.

Extensive research has been conducted on the use of stress wave technique (either ultrasonic or vibration methods) for assessing the mechanical properties of wood composites [9, 10].

The success of wood and wood products relates not only to the pleasant visual appearance of the wood material, but also to its favorable elastic and strength properties. Of these, the ability to resist bending stresses is often characterized as the most important, bending being the most common stress appearing in different kinds of wood products [11, 12].

Presently the destructive methods are used alone or at the same time with others NDT methods or techniques. The effectiveness (in terms of results) could be increased if some laboratorial tests were used to study the variability of the mechanical characteristics of the wooden elements using these techniques [13].

Since the NDT currently only able to predict the modulus of elasticity, then the main scope of the present work reported the static modulus of elasticity for small clear specimens and large size specimens in laboratory with a predefined set-up for mechanical testing and correlation of these properties with NDT techniques were analyzed.

2 Materials

A total of 240 pieces of timber beams from seven (7) selected Malaysian Tropical timber species from different strength groupings (SG) namely Resak (SG4), Kapur (SG4), Merpauh (SG4), Bintangor (SG5), White Meranti (SG5), Jelutong (SG6) Sesendok (SG7) and Kelampayan (SG7) with dimensions of 20 mm

Fig. 1 Test setup for NDT ultrasonic wave test



(thickness) × 20 mm (width) × 280 mm (length) were used for this study. These samples were selected from pool of visually graded timber in accordance with MS 1714 [14] by certified grader. Only timbers in select grade were chosen. The moisture content for each sample was measured using moisture meter as being between 12 and 18 % before testing.

3 Methodology

3.1 NDT

During the tests the ultrasonic test equipment UPV-E49 was used, with cylinder-shaped transducers as seen in Fig. 1. Two piezoelectric transducers were placed in two opposite faces of same specimen; a transmitter and receiver. This is considered as direct method parallel to the grain. The stress wave propagation time reading was recorded. The procedures were repeated and the average values were computed. The elastic properties of timber were estimated by the measurement of stress wave propagation time in these directions, assuming a continuous and homogeneous material.

For prismatic, homogeneous and isotropic elements, the modulus of elasticity was measured using Eq. (1);

$$E = \rho \cdot v^2 \tag{1}$$

where, E represents the dynamic modulus of elasticity (N/mm^2); v is the propagation velocity of the longitudinal stress waves (m/s) and ρ is the density of the specimens (kg/m^3). This technique is based on the fact that the speed of sound and attenuation depend on the strength and stiffness of wood.

3.2 Static Bending Test

Two (2) configurations of test set-up were prepared. For small clear specimens, the bending tests were set-up based on one point load test with the span to depth ratio used is 14 in accordance with ASTM D143 as shown in Figs. 2 and 3.

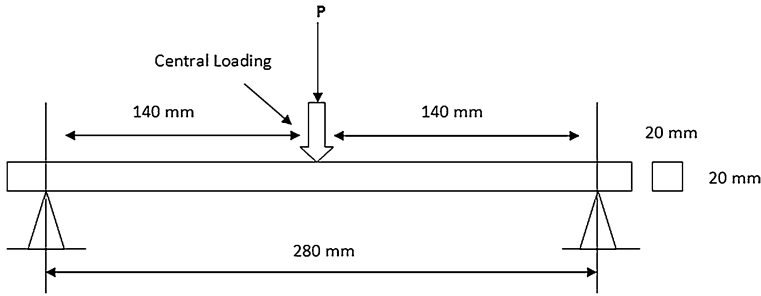


Fig. 2 Schematic diagram of bending test set-up for small clear specimen

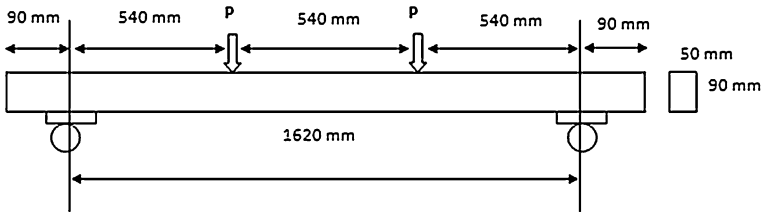


Fig. 3 Schematic diagram for bending test setup of large size specimens

The bending modulus of elasticity (MOE) of the beam evaluated were calculated using the following equations:

$$MOE = \frac{L^3 m}{4bh^3} \tag{2}$$

where,

b = width of the specimen (m)

m = slope of load-displacement graph

The static bending tests were conducted using Instron 3383 testing instrument equipped with 100 kN load cell. The specification of the test specimen is in accordance with BS 373: 1957 [15], Test methods for small clear specimens of timber. The test set-up is shown in Figs. 2 and 3. The load was applied at a rate of 0.11 mm/s.

As for large size specimens, a two point load tests were prepared where the distance between the two loading points, and the distance between the right and left fulcrums, were the same. The span to depth ratio used is 18 in accordance with ASTM D198 for large size specimens as shown in Fig. 3.

1. Modulus of Elasticity, MOE

$$MOE = \frac{P^l a(3L^2 - 4a^2)}{4bh^2 \Delta'}, \text{ GPa} \tag{3}$$

where,

b = Width of the specimen (mm)

h = Depth of the specimen (mm)

P' = Load at the proportional limit (N)

Δ' = Deflection at the proportional limit (N)

L = Length of the span (mm)

A = Half shear span (mm)

The test was carried out on 2,500 kN Universal Testing Machine (UTM). The physical measurements and moisture content for each specimen had been taken and recorded before testing while mode of failure were observed and recorded during the testing. Load as applied at a constant rate of 0.06 mm/s to achieve the ultimate load in about 10 min but not less than 5 min or more than 20 min.

4 Results and Discussions

4.1 Modulus of Elasticity for Small Clear Specimens and Large Size Specimens

As the aim of this study is to compare the MOE values obtained from static bending and NDT method, therefore only MOE values were reported here even though from bending tests, modulus of rupture can be obtained.

In general, for small clear specimens, there is no significant different in the MOE values found in this study and the value published in MS 544 Part 2 as shown in Table 1 except for the MOE for Bintangor which is 20 % lower than MOE stated in MS 544 Part 2 for small clear specimens.

An analysis of variance (ANOVA) at 0.05 % probability was performed to determine if there was significant difference in the mean MOE values among species for small clear specimens and large size specimens. Results from statistical analysis were tabulated in Table 1.

Based on ANOVA, the results show that there are significant differences in the MOE values (p value <0.005) among species for small clear specimens and large size specimens as shown in Tables 2 and 3 respectively.

From Table 2, it can be seen that the MOE values for small clear specimens are still in the same order as strength groupings. However, from this study it was found that there is no significant difference in the MOE values for Jelutong with the MOE value for Kelampayan even though they are from different strength groupings, SG6 and SG7 respectively. Similar trend was found for the MOE values for both Jelutong and Kelampayan from structural size specimens. Meanwhile, the MOE values for Merpauh, Resak and Kapur for small size specimens, there is no significant difference in the MOE values for Merpauh and Resak but there is significant difference with Kapur even though they are in the same strength

Table 1 Summary statistics of MOE for small clear specimens and large size specimens

Species	Strength group	Moisture content (%)	Density kg/m ³	MOE (MS 544 Part 2) GPa	MOE for small clear specimens		MOE for structural size specimens	
					MOE (GPa)	COV	MOE (GPa)	COV
Kapur	SG4	12.87	776	13.70	12.56	18.68	26.57	17.30
Merpauh	SG4	11.47	875	15.50	16.71	9.96	27.16	8.09
Resak	SG4	11.51	915	14.60	16.30	10.82	33.00	11.35
Bintangor	SG5	12.89	725	14.00	11.39	16.88	29.89	15.17
White Meranti	SG5	12.01	594	11.2	10.17	11.89	22.89	18.94
Jelutong	SG6	11.56	487	7.90	7.01	20.46	12.62	18.68
Kelempayan	SG7	11.71	547	7.60	6.97	21.58	15.00	22.73
Sesendok	SG7	11.67	483	8.60	7.33	17.29	15.36	21.74

Table 2 Duncan multiple comparison for MOE among timber species

Timber species	Subset for alpha = 0.05				
	1	2	3	4	5
Merpauh	16.7 ^a				
Resak	16.3 ^a				
Kapur		12.6 ^b			
Bintangor			11.4 ^c		
White Meranti				10.2 ^d	
Sesendok					7.3 ^e
Jelutong					7.0 ^e
Kelempayan					7.0 ^e

Note Means in the same column with the same superscript (either a, b, c, d, e) are not significantly different at *P*-value ≤0.05

groupings. But these values will provide the upper and lower bound of the MOE interval for the strength grouping SG4.

A contrast trend was found for the large size specimens whereby there are significant differences in the MOE values for Merpauh, Resak and Kapur but there is no significant difference in the MOE for Merpauh and Kapur as seen in Table 3. Besides that, the order of the MOE values also have changed; Resak > Merpauh > Kapur. The appealing difference was on the MOE values for Bintangor (SG5) since the MOE values was found to be higher than the MOE for Merpauh (SG4). From these data, it can be assumed that the strength groupings have changed.

When comparison was made on the MOE values between small clear specimens and large size specimens, the MOE for structural specimen are higher than both MOE produced by the tested small clear specimen and tabulated MOE values in MS 544: Part 2.

Table 3 Duncan multiple comparison for MOE among timber species

Timber species	Subset for alpha = 0.05					
	1	2	3	4	5	6
Resak	33.0 ^a					
Bintangor		29.9 ^b				
Merpauh			27.1 ^c			
Kapur			26.6 ^c			
White				22.9 ^d		
Meranti						
Sesendok					15.6 ^e	
Kelempayan						15.0 ^f
Jelutong						12.6 ^f

Note Means in the same column with same superscript (either a, b, c, d, e, f) are not significantly different at P -value ≤ 0.05

Parker [16] noted that current design practice for structural timber member is based on the elastic theory, which postulates that deformations are directly proportional to stresses. In other word, if an applied force (as measured by its resulting unit stress) produced certain deformation, twice the force and twice amount of deformation. These results further enhance the need to revise the mechanical properties of tropical timber based on structural size specimens. From this investigation, it can be said that the strength grouping of small clear specimen can be different from the large size specimen. Hence thorough investigation on the strength grouping of large size specimen should be done in order to safely design the timber structures.

4.2 MOE Dynamic Versus MOE Static

The stress wave’s velocity can be directly related to the elastic properties of timber and the propagation velocity of the longitudinal stress waves in an elastic media depends essentially on the stiffness and the density of the media itself [17].

Tables 4 and 5 show the summary of MOE results based on NDTs and static bending tests for small clear specimens and large size specimens respectively. It can be seen that generally the MOEs (both for NDT and static) increases as the density increases and the strength classes also increases which validate that the stiffness of the timber depends on the density, the higher the density the stiffer the materials are. When comparisons were made on the MOEs from NDT test and static bending tests, it can be seen that for large size specimens, MOE from static bending test denoted as MOE_B is higher than the MOE from NDT test which is denoted as MOE_D . This means that results of NDT generally underestimate the actual stiffness of the material. It is the other way round for small clear specimen where the MOE from static bending test and denoted as MOE_S is much smaller

Table 4 Summary of MOE_N for small clear specimens

Species	Strength grouping	MOE NDT		MOE Static ¹		Δ % ^a	Density (kg/m ³)
		MOE _N (GPa)	COV (%)	MOE _S (GPa)	COV (%)		
Kapur	4	19.1	16.45	12.56	18.68	52.07	770
Merpauh	4	26.6	9.74	16.71	9.96	59.19	853
Resak	4	23.7	16.67	16.30	10.82	45.40	914
Bintangor	5	18.3	19.91	11.39	16.88	60.67	650
White Meranti	5	16.2	13.27	10.17	11.89	59.29	571
Jelutong	6	10.2	14.38	7.01	20.46	45.51	431
Kelempayan	7	9.7	15.89	6.97	21.58	39.17	425
Sesendok	7	11.9	9.94	7.33	17.29	62.35	468

Note ^a Mean different in percentage between the MOE_N and MOE_S

Table 5 Summary of MOEs for large size specimens

Species	Strength grouping	MOE NDT		MOE static		Δ % ^a	Density (kg/m ³)
		MOE _D (GPa)	COV (%)	MOE _B (GPa)	COV (%)		
Kapur	4	21.0	14.43	26.57	17.30	-20.96	776
Merpauh	4	20.7	11.21	27.16	8.09	-23.78	875
Resak	4	24.5	20.86	33.00	8.09	-25.76	915
Bintangor	5	22.7	9.54	29.89	15.17	-24.05	725
White Meranti	5	16.1	18.04	22.89	18.95	-29.66	594
Jelutong	6	9.2	18.09	12.62	18.69	-27.10	487
Kelempayan	7	6.5	28.51	15.00	22.73	-56.67	547
Sesendok	7	9.5	20.31	15.36	21.74	-38.15	483

Note ^a Mean different in percentage between the MOE_D and MOE_B

than the MOE from NDT test and denoted as MOE_N, which mean that the NDT result is overestimate the actual stiffness.

The coefficient of variation of MOE_N for small clear specimen is in the range of 8–17 % except for Bintangor with a percentage of 19.9 %.

This indicates that the properties of solid timber used in this experiment are uniform except for Bintangor. The MOE of Kelempayan for structural size specimen is the lowest which is related to high in COV values. It was also found that the difference in the MOE_D and MOE_B is the highest (57 %).

As for Bintangor in small clear specimen, difference in the MOE_N and MOE_S is the highest, -61 % among other species. This may be due to the presence of defect that affect the wave to transmitted where Bintangor containing the internal defects which is causes horizontal shear characteristic meanwhile Kelempayan was found to contain a lot of knots. According to Lin et al. [18], the defect characteristics are the most-important factors affecting the properties of timber and

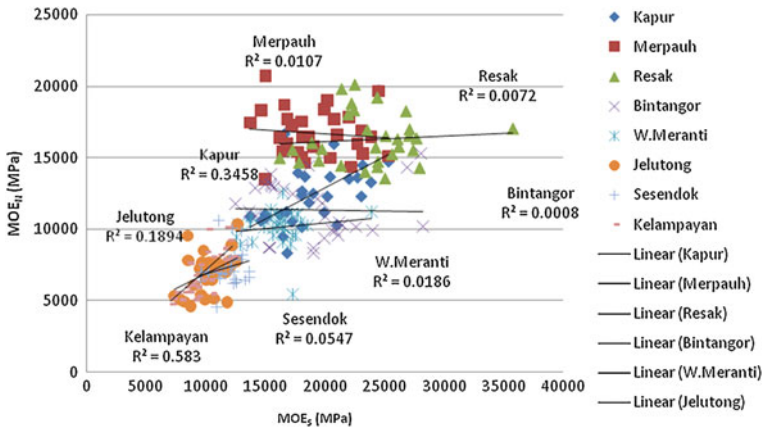


Fig. 4 MOE NDT (MOE_N) versus static bending MOE (MOE_S) for individual species for small clear specimen

the removal of defects should contribute to a larger strength in the sawn timber. This may be due to the presence of defect that affect the wave to transmitted where the full scale specimen for Kelempayan containing a lot of knots and Bintangor containing the internal defects which is causes horizontal shear characteristics.

5 Correlation Between MOE_N and MOE_S

As further treatment for the gathered data, statistical regression analyses between MOE_N and MOE_S were made. The closer data are grouped around the regression line and the lower the variability, the more successful a NDT parameter is at predicting performance. The regression analysis yields the so-called ‘coefficient of correlation’, R . Its square is called ‘coefficient of determination’, R^2 . The value of R^2 indicates the portion of the total variation of the predicted variable that is explained by the predictor see (Fig. 3) for each species. Correlation coefficients can range from -1 to 1 . A correlation coefficient nearing 1 suggests a strong positive relationship. A correlation coefficient of zero reveals that no relationship exists, positive or negative.

Figure 4 shows the relationship between MOE_N and MOE_S for individual species for small clear specimens and reveals that there are modest correlation have been found for Kapur ($R = 0.4$), Jelutong ($R = 0.2$) and Kelempayan ($R = 0.6$). However there are no correlations for the rest of the species. This can be seen from the R values which are very low, near to 0 .

Finally, it is interesting to compare MOE_{NDT} and MOE_{STATIC} for small clear specimens when all the data were combined as shown in Fig. 5. Similar relationship was also performed for structural size specimens. The results reveal a

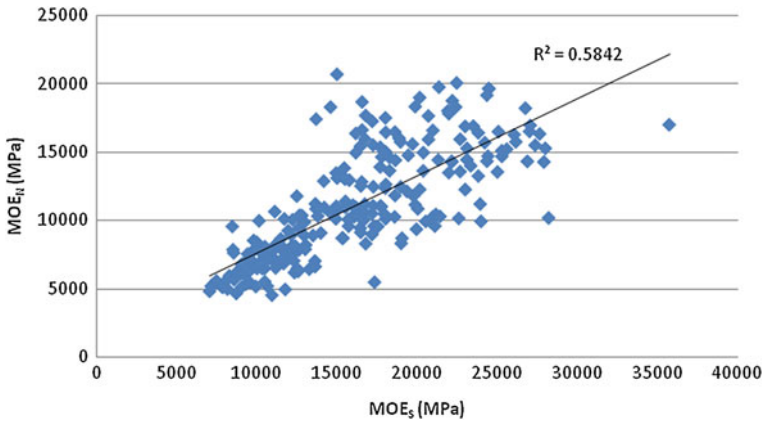


Fig. 5 MOE_{NDT} versus MOE_{STATIC} for all species for small clear specimens

good positive correlation between MOE_{NDT} and MOE_{STATIC} ($R \sim 0.6$). These results indicate that reasonably useful relationships exist among the transverse vibration properties of the timber and corresponding stiffness properties of the specimens.

6 Conclusions

Experimental bending tests and nondestructive tests were performed on small clear and large size timber specimens from selected Malaysian tropical timbers in strength groupings SG4 to SG7. A thorough examination of the tests has enabled the following conclusions to be drawn.

- In general, for small clear specimens, there is no significant different in the modulus of elasticity (MOE) values found in this study and the value published in MS 544 Part 2 except for the MOE for Bintangor which is 20 % lower than MOE stated in MS 544 Part 2.
- There are significant differences in the MOE values among species for small clear specimens and large size specimens. MOE for structural specimen are higher than both MOE produced by the tested small clear specimen and tabulated MOE values in MS 544: Part 2.
- For clear specimens, in MS 544 Part 2, Merpauh, Resak and Kapur are in the same groupings (SG4) but in this study, the MOE of Kapur was significant different from Merpauh and Resak. But these values will provide the upper and lower bound of the MOE interval for the strength grouping SG4.
- A contrast trend was found for the large size specimens whereby there are significant differences in the MOE values for Merpauh, Resak and Kapur but there is no significant difference in the MOE for Merpauh and Kapur. The order

of the MOE values also have changed; Resak > Merpauh > Kapur. The appealing difference was on the MOE values for Bintagor (SG5) since the MOE values was found to be higher than the MOE for Merpauh (SG4). From these data, it can be assumed that the strength groupings have changed.

- The MOEs (both for NDT and static) increases as the density increases and the strength classes also increases which validate that the stiffness of the timber depends on the density, the higher the density the stiffer the materials are.
- For large size specimens, MOE from static bending test is higher than the MOE from NDT. This means that results of NDT generally underestimate the actual stiffness of the material.
- For small clear specimen, the MOE from static bending test is much smaller than the MOE from NDT test, which mean that the NDT result overestimate the actual stiffness.
- Although correlation of the MOE between NDT and static bending test are relatively poor, but the result from the minimal percentage of difference between MOE_N and MOE_S reveal the possibility of producing result from the application of non-destructive technique in future are possible.

Acknowledgments We wish to thank the technicians of Faculty of Civil Engineering and Faculty of Mechanical Engineering, Universiti Teknologi Mara for their assistance and support. The work reported here was financially supported by Research Acculturation Grant Scheme, Ministry of Higher Education, Malaysia (600-RMI/RAGS 5/3 (53/2012)) and Universiti Teknologi Mara.

References

1. A.O. Feio, J.S. Machado, P.B. Lourenco, Compressive behavior and NDT correlations for chestnut wood (*Castanea sativa* Mill), in *Proceedings of International Seminar on structural analysis of historical constructions*, Padova, Apr 2004
2. R. Grolacher, Non-destructive testing of wood: an in situ method for determination of density. *Holz as Roh- undWerkstoff* **45**, 273–278 (1987)
3. M.M. Jalili, A.S. Pirayeshfar, S.Y. Mousavi, Non-destructive acoustic test (NDAT) to determine elastic modulus of polymeric composites. In EWGAE, Vienna, 8th to 10th Apr 2010
4. T.S. Yang, S.Y. Wang, C.J. Lin, M.J. Tsai, Evaluation of the mechanical properties of Douglas-fir and Japanese cedar lumber and its structural glulam by nondestructive techniques. *Constr. Build. Mater.* **22**, 487–493 (2008)
5. R.J. Ross, E.A. Geske, J.F. Murphy, Transverse vibration nondestructive testing using a personal computer. Research Paper FPL-RP-502. USDA Forest Service, Forest Product. Lab., Madison, WI. 17 (1991)
6. R.J. Ross, J.I. Zerbe, X. Wan, D.W. Green, R.P. Pellerin, Stress wave nondestructive evaluation of Douglas-fir peeler cores. *For. Prod. J.* **55**(3), 90–94 (2005)
7. D.W. Green, R.J. Ross, Linking log quality with product performance, in *Proceedings of IUFRO All Division 5 Interernational Conference IUFRO Secretariat*, Vienna, Austria (1997)
8. C.C. Gerhards, Effect of cross grain on stress waves in lumber. Research Paper FPL-RP-368. Madion, WI: US department of Agriculture, Forest Service, ForestProducts Laboratory (1981)

9. L. Bostrom, P. Hoyffmeyer, K. Solli, Tensile properties of machine strength graded timber for glued laminated timber, in *Proceedings of Pacific timber Engineering Conference*, New Zealand, pp. 215–222 (1991)
10. G.B. Fagan, J. Bodig, Computer simulation as a nondestructive evaluation tool, in *Proceedings of 5th nondestructive testing of wood symposium*, Pullman, WA, 9–11 (1985)
11. J. Bodig, B.A. Jayne, *Mechanics of Wood and Wood Composites* (Van Nostrand Reinhold, New York, 1982), pp. 712–723
12. B. Madsen, *Structural Behaviour of Timber* (Timber Engineering Ltd, Canada, 1992), pp. 405–413
13. L. Uzielli, Evaluation of timber elements bearing capacity. *L'Edilizia* **12**, 753–762 (1922)
14. MS 1714: 2003, Specification for visual strength grading of tropical hardwood timber (2003)
15. BS 373: 1957, Standard Test Methods for Small Clear Specimens of Timber (1957)
16. H. Parker, *Simplified Design of Wood Structure*, 5th edn. (Wiley, New York, 1994)
17. J.L. Sandoz, Grading of construction timber by ultrasound. *Wood Sci. Technol.* **2**, 95–108 (1989)
18. C.J. Lin, T.H. Yang, D.Z. Dong-Zhi Zhang, S.Y. Wang, F.C. Lin, Changes in the dynamic modulus of elasticity and bending properties of railroad ties after 20 years of service in Taiwan. *Build. Environ.*, Taiwan **42**, 1250–1256 (2005)

Ultimate Strength of Kekatong Glued Laminated Timber Railway Sleepers

Norshariza Mohamad Bhkari, Zakiah Ahmad, Afidah Abu Bakar
and Paridah Md Tahir

Abstract Pre-stressed concrete (PSC) sleepers are the main components of railway track systems in Malaysia. However, there are sections in the track system which PSC sleepers cannot be utilized, where timber sleepers are still needed. Due to limited supply of large sections timber logs and high cost in high grade timber, an alternative for this timber product is needed. Thus, this study is conducted to determine the ultimate strength of the alternative timber product which is glued laminated (glulam) timber railway sleepers from selected Malaysian tropical heavy hardwood timber species namely Kekatong. The static bending test at rail seats was carried out in order to achieve the objective and the test is accordance to AREMA Manual. The values of modulus of rupture (MOR) and modulus of elasticity (MOE) for two numbers of glulam timber sleepers were evaluated and compared with the MOR and MOE values of two numbers of solid timber sleeper. Then the properties are verified with the minimum performance requirement in AREMA Manual. The results showed the glulam Kekatong timber railway sleepers met the requirement set by AREMA with the static yield load surpassed the Keretapi Tanah Melayu Berhad (KTMB) specific design load.

N. M. Bhkari (✉)

Faculty of Civil Engineering, Universiti Teknologi MARA, 40450 Shah Alam,
Selangor, Malaysia

e-mail: norsharizamb@gmail.com

Z. Ahmad

Institute Infrastructure Engineering and Sustainable Management (IIESM), 40450,
Shah Alam, Selangor, Malaysia

A. A. Bakar

Faculty of Civil Engineering, Universiti Teknologi MARA, 40450 Shah Alam,
Selangor, Malaysia

P. M. Tahir

Institute of Tropical Forestry and Forest Product (INTROP), Putra Infoport, Universiti Putra
Malaysia, 43400 Serdang, Selangor, Malaysia

Keywords Glulam · Modulus of rupture · Modulus of elasticity · Rail seat · Timber sleeper

1 Introduction

Railway sleepers are one of the most important components in railway track system. Sleepers act as a beam that rest underneath the rails to support the track loading. Its functions are to transmit and distribute the oncoming loads to the ballast [1], give firm and even support to the rails and act as an elastic medium between the rails and the ballast [2]. Commercially, there are three types of material used for sleepers which are solid timber, pre-stressed concrete (PSC) and steel. Although solid timber sleepers is the oldest material used in railway track, the capability in terms of workability, adaptability, installation, replacement, cost and damping/shock absorbing is superior compared to PSC and steel sleepers [3]. These advantages make solid timber sleepers come as preferred material by the railway transportation companies at specific locations.

Hardwood timber is widely used as reported by [4], there are more than 2.5 billion timber sleepers installed throughout the world. In Malaysia, until August 2010, the number of timber sleepers was reduced and only 26.4 % (approximately of 750 thousand timber sleepers) from the total track length are remained. Most of them are replaced by concrete sleepers since limited resources of the required grade of hardwood timber namely grade SG1 and SG2, naturally durable timbers, depleting supply in large diameter logs, the increase in price and the life span of timber sleeper is lesser due to deterioration when using non-durable timbers and not properly treated. Although the use of timber sleepers is getting less, however timber sleepers are still in demand since there are certain location of railway track that PSC sleepers cannot be used such as at station and yard area, bridges and at the soil area contributing pumping to locomotives [5].

Therefore, there is a need to find an alternative to solid timbers sleepers and this has spurred the use of composite timber products such as glued laminated timber or glulam. Glulam is a timber product manufactured by gluing together individual pieces under controlled manufacturing conditions [6, 7]. Glulam has used in many building structures and bridges [8–10] but as railway sleepers, is limited and mainly based on softwood timber [11, 12]. Utilisation of railway sleepers using hardwood timber is still unknown. Thus, this study was aimed at developing glued laminated timber railway sleepers using selected Malaysian tropical hardwood namely, Kekatong (*Cynometra spp.*) that could meet the railway industry performance specifications. In order to achieve the objective, determination on ultimate strength of basic mechanical properties which are modulus of rupture (MOR) and modulus of elasticity (MOE) were evaluated at the rail seat.

2 Materials and Methods

2.1 Materials

The timber species used were Kekatong (*Cynometra spp.*) with density averaging 880–1,155 kg/m³ at 19 % moisture content [13]. The species is selected based on the availability and required species grade by Keretapi Tanah Melayu Berhad (KTMB). Since the selected samples are costly, only two numbers of solid Kekatong with sized 127×254×2000 mm were cut and the two numbers of glulam Kekatong sleepers with sized 127×254×2000 mm were manufactured in accordance with MS758:2001 by a glulam factory in Johor Bahru. The test materials for glulam were taken from the normal and controlled production process. Each glulam beam had six laminations with a range of lamella thickness of 15–24 mm. According to [14], these timbers are naturally durable, untreated and suitable for the outdoor exposure. Phenol-resorcinol formaldehyde (PRF) adhesive was used as a glued material for these beams which gave them a bond of exterior grade. Results for Kekatong solid and glulam timber sleepers were compared.

2.2 Static Bending Test at Rail Seat

The three-point static bending test was conducted in order to obtain the ultimate strength of Kekatong solid and glulam timber sleepers. The strength data will be used as a preliminary data for the next study on sleeper performance tests that required by AREMA Manual [15]. The static bending test is carried out at the rail seat of sleepers under positive moment for both sides as shown in Fig. 1. Figure 2 showed the test set-up including the elastomeric supports accordance to AREMA Manual. Since there is no specific standard available for timber railway sleepers, AREMA Manual was chosen as a guide for this study and some modification due to testing was been made in order to suite the requirement in the referred standard.

Three 100 mm transducers were placed at supports and mid-span. The transducer at mid-span was measured central displacement and the other two transducers were monitoring the unwanted misalignments. The strain gauges are installed at mid-span and, top and bottom of sleeper since the zone are critical for tension and compression during testing. All transducers and strain gauges were connected to the data logger for recording the displacement and strain data. The test was performed under a displacement control at a constant rate of 0.02 mm/sec. The rate was decided based on series of loading rate tests in the preliminary works. The load was applied until the tested sleepers totally failed. Structural cracks were inspected on all sleepers and values for displacement and loads were recorded.

The MOR values are calculated using (1). However, for the MOE value, the data are calculated based on linear relationship of stress and strain graph obtained

Fig. 1 Static bending test at rail seats

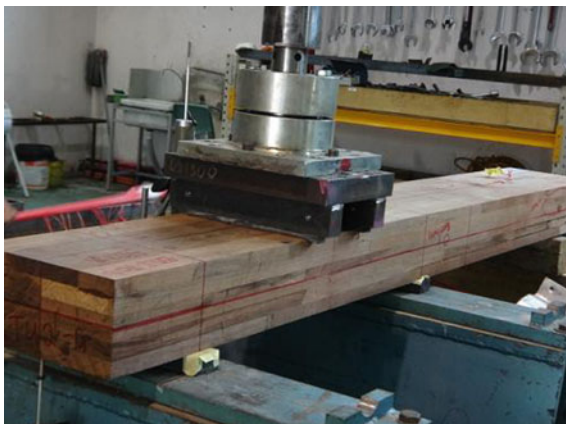
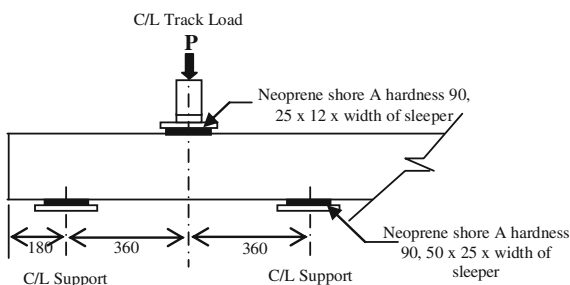


Fig. 2 Test arrangement at one of rail seat



through the laboratory data and (2) and (3) from basic structural mechanics were derived. The strain values are obtained from strain gauges data.

$$MOR = \frac{3P_{ult}L}{2bh^2} \tag{1}$$

$$M = \frac{PL}{4} \tag{2}$$

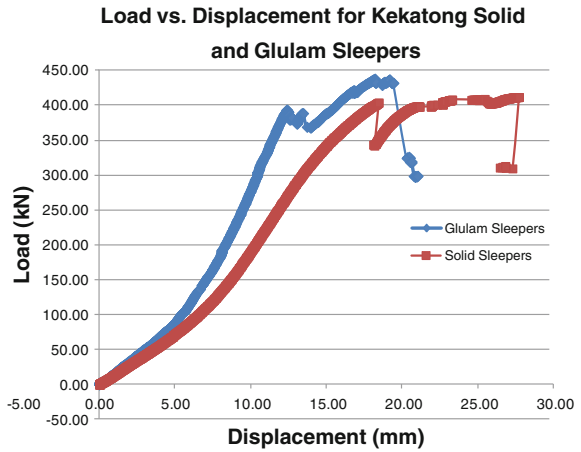
$$\sigma = \frac{My}{I} \tag{3}$$

where P_{ult} is the ultimate load borne by sleepers loaded to failure (N); b is the width of sleepers (mm); h is the depth of sleepers (mm); L is the span (mm); σ is stress value (N/mm²); y is distance to centre of gravity (mm); I is moment of inertia of the cross section (mm⁴).

2.3 Moisture Content Test

A moisture content test was conducted for 25 mm thick samples, cut through the full cross section using the oven-dry method as stipulated in [16].

Fig. 3 Load-displacement of Kekatong solid and glulam timber sleepers at one of tested rail seat



3 Results and Discussion

The ultimate strength and basic mechanical properties, MOR and MOE of Kekatong solid and glulam timber railway sleepers were analyzed and discussed in this section. The comparison between solid and glulam timber was made and the value was evaluated with AREMA requirement.

3.1 Load Versus Displacement for Solid and Glulam Timber Sleepers

Figure 3 shows a relationship between load and displacement at rail seat under positive moment for Kekatong solid and glulam timber sleepers. The graph was chosen as representative from four other graphs which, the graph had closed value with the calculated average value. Thus, the behaviour of load versus displacement is compared. The average ultimate load (P_{ult}) for Kekatong glulam sleepers is 431.04 kN with maximum deflection of 15.92 mm while the average ultimate load (P_{ult}) for Kekatong solid timber is 406.63 kN with 20.60 mm maximum deflection. It is 6 % higher on average ultimate load for Kekatong glulam timber sleepers compared to Kekatong solid timber sleepers.

Regarding to the displacement value and the area under the graph, the Kekatong solid timber sleepers shown that the test sample is stiffer compared to glulam timber sleepers. Physically, glulam timber sleeper is manufactured by gluing timber pieces. The length of lamella is varies depend on the available timber off-cut. Each lamella is jointed by finger joint using the appropriate glue. From the observation made during the laboratory testing, the failure of glulam normally starts at finger joint in tension side. This is gave an effect on the low stiffness of

Table 1 test results and requirement test values

Type of sleepers		P_{ult} (kN)	P_y (kN)	Δ_{max} (mm)	MOR (N/ mm^2)	MOE (N/ mm^2)	Density (kg/m^3)	Moisture content (%)
Glulam	<i>Average</i>	431.04	235.21	15.92	111.87	30,890.35	1620.36	9.98
Kekatong	<i>S.D.</i>	33.40	189.99	2.38	7.03	7,583.35	82.80	0.90
AREMA requirement [15]		–	–	–	66.9	11,700.00	–	19-28
Solid Kekatong	<i>Average</i>	406.63	246.51	20.60	115.71	18,533.72	1793.58	16.53
	<i>S.D.</i>	82.90	56.36	4.10	23.65	3,227.99	108.56	0.67
Requirement [17]		–	–	–	59.5	5,811.03	–	22 ^a

^a MOR and MOE values based on the stated MC

glulam timber sleepers compared to solid timber sleepers where the strength of fibres for solid timber acts as in one timber log. In order to increase the stiffness of glulam timber sleepers, the manufacturing process need to be controlled especially at the weakest point, the finger joint.

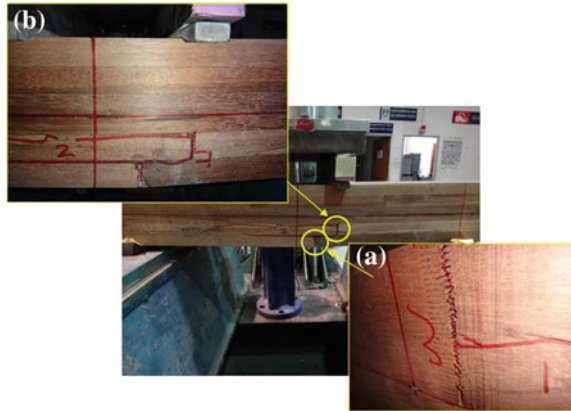
Table 1 gives the average values of P_y , yield load at first crack. Glulam and solid timber sleepers showed the P_y values are 235.21 and 246.51 kN respectively. It achieved about 45 % higher for glulam timber sleeper and 30 % higher for solid timber sleeper to reach the ultimate load after the first crack occurred. Both values at first crack are higher compared to the KTMB specified design load of 200 kN.

3.2 MOR and MOE for Solid and Glulam Timber Sleepers

Table 1 gives a summary of the average basic strength properties, MOR and MOE results for the Kekatong solid and glulam timber sleepers. Glulam timber sleepers are categorized under engineered wood product (EWP) ties or sleepers in AREMA Manual [15]. This standard gives the minimum performance requirements for components of engineered composite sleepers used in the railway track system. However, for solid timber sleepers, the strength requirements are referred to [17] as recommended by AREMA Manual.

The MOR value for glulam Kekatong is 111.87 N/mm² which the required value from AREMA Manual [15] is 66.9 N/mm². The value is 67 % higher compared to the required value. For solid Kekatong timber sleepers, the MOR value is 115.71 N/mm² which met the requirement of 59.5 N/mm² [17]. The results showed the MOR values for glulam Kekatong timber sleeper is slightly lower than that solid Kekatong timber sleeper, which the differences is less than 4 %. The MOR value for glulam timber sleeper is expected at least at par with the value of solid timber sleeper. To acquire the higher value of MOR for glulam

Fig. 4 Glulam Kekatong timber railway sleepers showing, **a** failure started at finger joint in lamella near the tension zone; **b** cracks propagated toward to the nearest finger joint in second lamellas and cracks continued toward the compression zone



timber sleepers, the glulam manufactured need to be controlled especially at finger joints.

The MOE value for glulam and solid Kekatong timber sleeper is higher compared to the required values. The MOE for glulam timber sleeper is $30,890.35 \text{ N/mm}^2$ and solid timber sleeper is $18,533.72 \text{ N/mm}^2$. From the results, the glulam timber sleepers showed the higher elasticity value compared to solid timber sleepers. Both, glulam and solid timber sleepers, the MOR and MOE values are complied with the minimum performance requirement [15] and [17]. The moisture content in the test specimen is lower than the required value.

3.3 Crack Morphology

Generally in solid timber, the failure occurs at ultimate load and the test specimens break apart into two separate pieces in a brittle manner. In glulam beam, the timber material is more ductile compared to solid timber in which the beam remains intact as one piece even after the maximum load has been reached and continues to carry a significant amount of load in the post-maximum load stage. The lamination in glulam serves as crack arrester in the tension mode.

From observation, there are a few different types of failure mode, between bending and shearing, occurred during the static bending test at the rail seats for glulam and solid Kekatong timber sleepers as shown in Figs. 4 and 5. In general, the failure types for solid timber sleepers are simple tension types [18]. This type of failure indicates that a particular timber has high density which is 966.52 kg/m^3 . As stated in [14], this timber species are grouped in strength group 2 (SG2).

For glulam Kekatong timber sleeper, the crack initiated at finger joint in the tension zone as shown in Fig. 4. The cracks slowly propagated until it reached the

Fig. 5 Solid Kekatong timber railway sleepers showing, **a** failure started near the tension zone and cracks propagated toward the compression zone; **b** failure at bottom view of solid timber sleepers



second weaker zone (finger joint) at second lamellas. Then, the cracks continued towards the compression zone.

The failure modes of solid timber sleepers start at tension zone as shown in Fig. 5. The cracks occurred along the longitudinal grain of the timber sleepers. The cracks pattern indicates that the solid timber sleeper failed by shearing off between fibres [19]. Some of test specimen for solid timber sleepers showed the failure occurred under tangential cracks. The combination of these failure showed the timber is anisotropic materials.

4 Results and Discussion

From the laboratory works showed that the average ultimate load for glulam timber sleepers obtained from static bending test at rail seats is higher compared to solid timber sleepers. The static yield load (P_y) for both glulam and solid timber sleepers are higher from the KTMB specified design load. In bending properties, MOR and MOE, the glulam and solid timber sleepers are met the requirement specified in AREMA Manual and [17]. However, the moisture content for glulam and solid timber sleepers is lower than required.

With the results obtained, glulam Kekatong timber railway sleeper has a potential to replace an existing solid Kekatong timber sleepers. The manufacturing of glulam timber railway sleepers is required in good quality by controlling and monitoring the process of seasoning, clamping and curing. The cracks pattern and the strength performance obtained from this study will help authors for further investigations.

Acknowledgments The provision of glulam and solid timber railway sleepers by Woodsfields Timber Industry (M) Sdn. Bhd. and supported documents by Keretapi Tanah Melayu Berhad (KTMB) are gratefully acknowledged. We wish to thank the technicians of Civil Engineering Faculty for their assistance and support.

References

1. J.S. Mundrey, *Railway track engineering*, 4th edn. (Tata Mc Graw Hill Education Private Limited, New Delhi, 2010)
2. KTMB, *KTMB Permanent Way Manual*, (2005)
3. A. Manalo, Behaviour of fibre composite sandwich structures: A case study on railway sleeper application, Doctoral dissertation, (2011)
4. Anon, History and development of the wooden sleeper, Ets Rothlisberger, unpublished
5. A. Razak, KTMB personal communication, 15 Feb 2012
6. Malaysian Timber Industry Board, *Glulam: Freedom of shape and design*, 2nd edn. (MTIB Brochure, Kuala Lumpur, 2011)
7. Anon, Handbook 1–Timber structures, educational materials for designing and testing of timber structures (TEMTIS), (2008)
8. G. Castro, F. Paganini, Mixed glued laminated timber of poplar and *Eucalyptus grandis* clones. *Holz als Roh-und Werkstoff* **61**, 291–298 (2003)
9. W.H.W. Mohamad, M.A. Razlan, Z. Ahmad, Bending strength properties of glued laminated timber from selected Malaysian hardwood timber. *Int. J. Civ. Environ. Eng.* **11**, 7–12 (2011)
10. A.S. Uppal, G.T. Fry, W.G. Byers, Fatigue strength of solid sawn timber railroad bridge stringers, unpublished, (2001)
11. E.V.M. Carrasco, L.B. Passos, J.N.R. Mantilla, Structural behaviour evaluation of Brazilian glulam wood sleepers when submitted to static load. *J. Constr. Build. Mater.* **26**, 334–343 (2012)
12. Anon, Design concepts glulam in railroad construction, APA EWS, unpublished, (1999)
13. Anon, 100 Malaysian timbers 2010 edition, Malaysian Timber Industry Board, (2010)
14. Malaysian Standard, Code of practice for structural use of timber: Part 2: Permissible stress design of solid timber, MS544: Part 2, (2001)
15. The American Railway Engineering and Maintenance-of-Way Association (AREMA), *Manual for railway engineering*, USA: American Railway Engineering and Maintenance-of-Way Association, (2012)
16. Malaysian Standard, Solid timber-Determination of moisture content (First edition, 2006), pp. MS837
17. P. Chow, J.R. Albert, D.D. David, K. Laine, J. Choros, S. Kalay, Proposed strength properties tests for wood crossties. *Articles in Crossties*, pp. 22–24, Jan–Feb (1995)
18. J. Bodig, B.A. Jayne, *Mechanics of wood and wood composites*, Van Nostrand Reinhold Company Inc, New York (1982)
19. S.H. Hamzah, K. Din, Appraisal of used wooden railway sleeper. *Journal of Engineering Science and Technology*, 3:224–233(2008)

Experimental Study to Single Shear Kapur Connection and Comparisons with European Yield Model

Mazlina Mohamad, Rohana Hassan and Khairul Effendy Ab Mutalib

Abstract Timber has long been regard as a common material used in construction since it is renewable and environmental friendly. However, very few publications in determining the load-carrying capacity of the tropical species with regards to the wood dowel connections are published. Since the existing theory in predicting single shear strength was developed mostly from the European and softwood timber, therefore this study is comparing the experimental to the load-carrying capacity calculated from the European Yield Model (EYM). This study determined the comparison of experimental to the theoretical on the influence of different end distance on single shear dowelled connections for Kapur species. Kapur is one of the tropical hardwood species and commonly used for construction purposes. The experimental 5 % offset and ultimate load-carrying capacity for the single shear strengths of 2.5D and 5D have been determined and compared to the value calculated theoretically using the EYM. Results show that the 5 % offset yield and ultimate strength capacity of 2.5D is 23 % and 20 % lower compared to the 5D respectively. The experimental 5 % offset yield of the 2.5D and 5D has also shown to be 75.52 and 81.06 % respectively higher than the theoretical. However, the experimental failure mode of the connections was found supported the theoretical expected failure mode. The dowels found to yield in bending at two plastic hinge points per shear plane and associated wood crushing. The EYM has successfully predicted the failure mode behavior however does not accurately predict the load carrying capacity of the single shear strength of the selected timber species.

Keywords Single shear · Kapur species · End distance · Failure mode · European yield model

M. Mohamad (✉) · K. E. A. Mutalib
Faculty of Civil Engineering, Universiti Teknologi MARA, Shah Alam, Selangor, Malaysia
e-mail: mazlina9090@salam.uitm.edu.my

R. Hassan
Institute for Infrastructure Engineering and Sustainable Management, Universiti Teknologi MARA, Shah Alam, Selangor, Malaysia

1 Introduction

Timber has long been regarded as the best material used in construction since it is renewable and environmental friendly. Even though Malaysia has been regarded as a country with higher sources of timber but timber industry in Malaysia is still far behind from other countries such as Europe, United States, and Australia. Currently, timber is rarely used as a building material. Therefore, research on Malaysia timber connection must be carried out to enhance the growth of timber industry.

In heavy construction, joints may require ingenuity and the use of specialized connectors, such as nail-plates, bolts, shear-plates, split rings, coach screws or glued-in threaded rods. The application of these requires some knowledge in design and construction skills. The shrinkage and swelling characteristics of timber in response to drying and wetting, the possibility of fungal decay in the presence of moisture and the need to protect metallic fasteners from fire or corrosion, call for special construction detailing. To eliminate this corrosion problem, therefore the dowels used in this study were made of wood dowel.

It is also historically proven that the use of wood dowel may also stand for nearly 100 years from the successfulness of the standing historical building such as Old Royal Palace in Perak, now acting as the museum building, originally built as a palace in 1926. Similar to the local mosque, Masjid Kg. Laut in Kelantan which is still in use was built in 1930s.

Currently, the existing standard about Malaysian timber is the Malaysian Standard MS 544, 2001 [1]. However, the MS 544, 2001 still has its limits. There are only some connections for timber design provided. The design with mechanical fasteners, nails, bolt and nuts are available however the basic load of the wood dowels according to the end distance capacity has not been clearly classified.

This research is based on the analysis on the effect of end distance for the single shear connections. Only one selected wood dowel diameter using Kapur species were tested. The wood dowels were made of Kapur species, similar to the tested members. The experimental results were compared to the theoretical European Yield Model (EYM) based on National Design Specification (NDS) 2005 [2]. The calculations on the theoretical were done based on the published data compiled by Rohana [3]. Rohana [3] has studied on the double shear Kapur connections fastened using wood and steel dowel and found that the flexural capacity performance of the wood dowel was found much better compared to the stiffness of steel dowel [3]. In order to determine the theoretical EYM in this study, the value of bearing strength (F_{em} and F_{es}) and the dowel yield (F_{yb}) of 12.7 mm Kapur is taken from her publication [3].

The main objective of this study is to determine and compare the ultimate shear strength of different end distance between 2.5D and 5D, where D is the diameter of the dowel used to strengthen the connection. This study is also to determine on the accuracy of the EYM in predicting the single shear strength of tropical hardwood connections since that the EYM has been developed mostly based on the European and softwood timber. In order to determine the reliability and accuracy of the

EYM to the tropical hardwood connections, therefore the theoretical calculations and failure modes of the connections using the European Yield Model (EYM), NDS 2005 [2] were also compared to the experimental results.

2 Materials and Method

2.1 Timber Properties

The connection members tested in this study were made of Kapur species. The scientific name for Kapur is *Dryobalanops* spp. It is included in family of Myrtaceae. In Malaysia, Kapur also known as Keladan and Kelansau. Kapur species is the large hardwood which is up to 45 m high with the diameter ranges from 800 to 100 cm. It can also be identified by its color where its sap is yellowish brown and its heartwood is reddish brown. Kapur timber species grain variable from straight to interlocked or spiral. Its texture coarse but even with the absence of growth rings [4].

2.2 European Yield Model

The European Yield Model (EYM) in the (NDS), 2005 [2] predicts yield strength for the connection based on the dowel bearing strength and fastener bending yield strength. The EYM incorporates connection geometry, dowel yield stress, and dowel bearing strength to predict the yield load for a connection [5]. The yield strength of the connection is defined from a load-deformation curve obtained from a connection test. The load deformation curves may vary according to the connection shape, length of fastener to diameter ratio, l/d , and on the applied load, whether it is parallel or perpendicular to grain. The yield point has been defined as the intersection of the load deformation curve with a straight line parallel to the initial portion of the load-deformation curve and offset a distance of 5 % of the fastener diameter from the origin of the load deformation curve. The types of failure modes are shown in Fig. 1. The failures of the dowels are according to the one plastic hinge at the single shear plane and are categorised accordingly in the EYM.







Where;

$$k_1 = \frac{\sqrt{R_e + 2R_e^2(1 + R_t + R_t^2) + R_1^2R_e^3} - R_e(1 + R_t)}{(1 + R_e)}$$

$$k_2 = -1 + \sqrt{2(1 + R_e) + \frac{2F_{yb}(1 + 2R_e)D^2}{3f_{em}l_m^2}}$$

$$k_3 = -1 + \sqrt{\frac{2(1 + R_e)}{R_e} + \frac{2F_{yb}(2 + R_e)D^2}{3F_{em}l_s^2}}$$

Fig. 1 European Yield Model (EYM) according to NDS 2005 [2]

Failure Mode	Characteristic load-carrying capacity, EYM	Failure Mode
	$\frac{Dl_m F_{em}}{4K_\theta}$	I _m
	$\frac{Dl_s F_{em}}{4K_\theta}$	I _s
	$\frac{k_1 D l_s F_{es}}{3.6 K_\theta}$	II
	$\frac{k_2 D l_s F_{em}}{3.2(1+2R_c)K_\theta}$	III _m
	$\frac{k_3 D l_s F_{em}}{3.2(2+R_c)K_\theta}$	III _s
	$\frac{D^2}{3.2K_\theta} \sqrt{\frac{2F_{em}F_{yb}}{3(1+R_c)}}$	IV

$$R_t = \frac{l_m}{l_s}, R_e = \frac{F_{em}}{F_{es}} \quad \text{and} \quad K_\theta = 1 + \frac{\theta}{360}$$

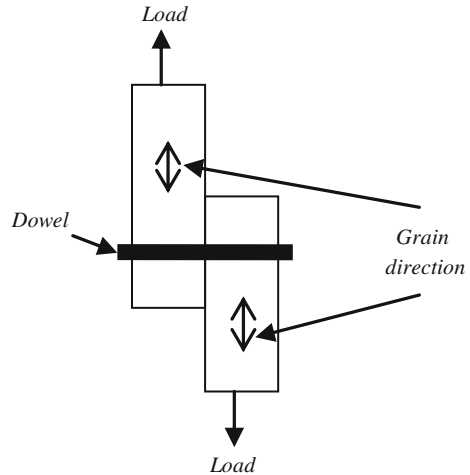
- F_{em} dowel-bearing strength of the main member, mPa = 54.88 mPa [2]
- F_{es} dowel-bearing strength of the side member, mPa. = 54.88 mPa [3]
- Z reference design value for fastener in single shear (Z taken as the smallest value from the six yield limit equation) kN
- D fastener diameter = 12.7 mm
- l_m thickness of the timber middle member = 41 mm
- l_s smaller of the thickness of the timber side member or the penetration depth = 41 mm
- F_{yb} bending yield strength of fastener = 90.06 mPa

Θ is the maximum angle of load to the grain ($0 \leq \theta \leq 90^\circ$) for any member in connection. Dowel-bearing strength of either the main member or the side member and at an angle of load to grain is given by the Hankinson formula (Eq. 1):

$$F_{e\theta} = \frac{F_{e//}F_{e\perp}}{F_{e//} \sin^2 \theta + F_{e\perp} \cos^2 \theta} \tag{1}$$

- Yield Mode I = Wood crushing in either the main member or side members. Dowel stiffness is greater than wood strength.
- Yield Mode II = Wood crushing of both main and side member. Dowel stiffness is greater than wood strength.
- Yield Mode III_m = Dowel yield in bending at one plastic hinge point per shear plane and associated wood crushing of main member.

Fig. 2 Single shear connection



- Yield Mode III_s = Dowel yield in bending at one plastic hinge point per shear plane and associated wood crushing of side members.
- Yield Mode IV = Dowel yield in bending at two plastic hinge points per shear plane and associated wood crushing.

2.3 Single Shear and End Distance

Single shear is the most common type of joint for timber structures (Fig. 2). Two members are held together through the combination of lateral and withdrawal resistance provided by dowel-type fastener. Single shear strength is the strength of a material or component against the type of yield or structural failure where the material or component fails in shear. Shear occur when timber beam are subjected to transverse loading [6]. The end distances set in this study were referred to the Fig. 3 (minimum spacing, edge and end distances for screws) [2].

2.4 Five Percent (5 %) Offset

The yield load as given by the EYM can be defined as any load on the load deformation curve. However, the onset of yielding in timber is not well defined point on the load deflection curve. As in EC 5, 2008 [7], the ultimate load is taken as the value of reference. The 5 % offset yield was introduced and become the basic description of strength in a single connection [8]. The 5 % offset yield is defined as the point where the load deflection curve is intersected by a line parallel to the linear region, but offset 5 % of the dowel diameter as shown in Fig. 4.

Fig. 3 Spacing, edge and end distance [2]

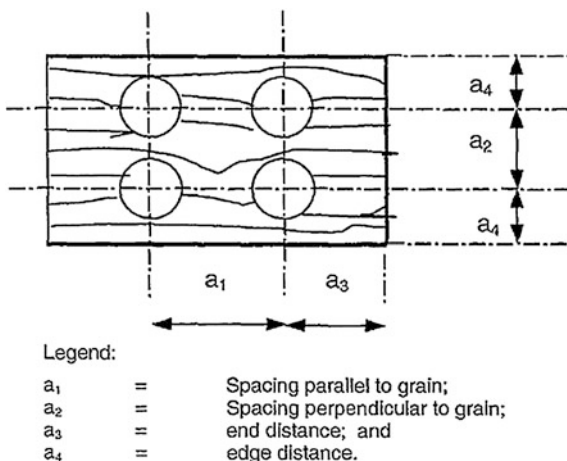
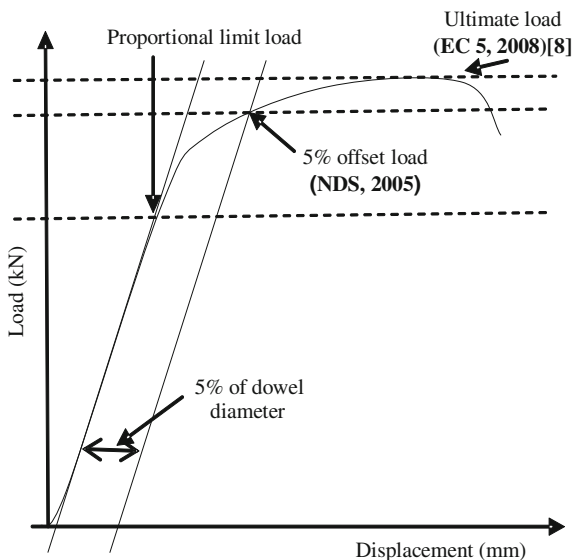


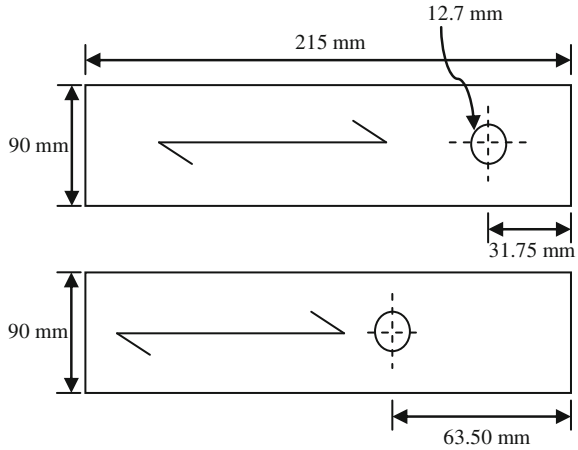
Fig. 4 Illustration of the 5 % diameter offset method and the ultimate load from load–displacement curve [3]



2.5 Sample Preparation

In this study, the specimens were prepared using Kapur species for both the main structure and also the dowels. The size of the specimens is $215 \times 90 \times 41$ and 12.7 mm for the dowel diameter (D). Four samples have been prepared for each end distance. Figure 5 shows the geometrical configuration of end distance and differences between both end distances values.

Fig. 5 Geometrical configuration of 2.5D and 5D end distances



2.6 Methodology: Single Shear Strength Test

The single shear test was done using Universal Testing Machine (UTM) to determine the load carrying capacity and deformation that the connection can support. Figure 6 shows the typical setup of the test. The tensile test was done by gripping the top and bottom segment of the specimens and pulled downward.

3 Results and Discussions

The observations on the load carrying capacity of the connections were based on the experimental and theoretical comparison between the 2.5D and 5D respectively.

3.1 Ultimate Shear Strength and Yield Load

Figure 7 shows the typical result between deformation and load for 2.5D and 5D end distances. Table 1 shows the 5 % offset load and the ultimate load for 2.5D and 5D respectively.

It also shows that experimentally, the 5 % offset and ultimate load of 2.5D is 23 and 20 % lower than the results of 5D. This results shows that end distance significantly contributed to the single shear connections.



Fig. 6 Typical single shear test setup

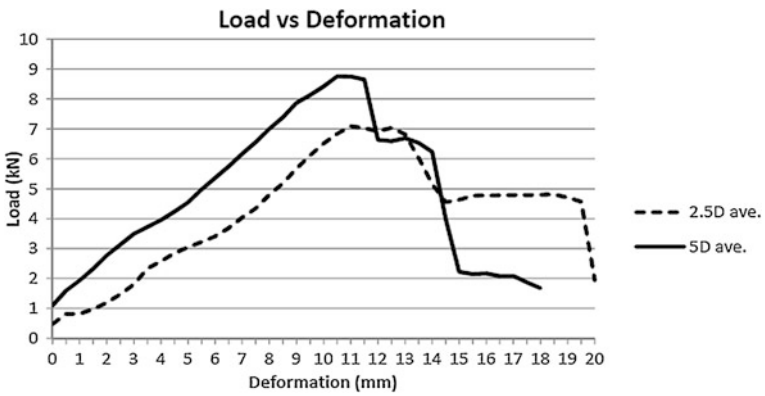


Fig. 7 Load versus deformation for shear test 2.5D versus 5D end distance

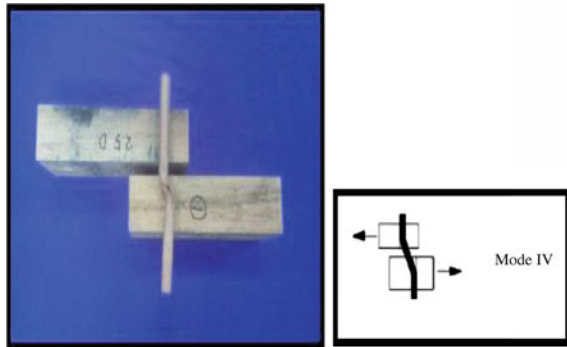
3.2 Failure Mode

A typical failure mode of sample 2.5D and 5D is shown in Fig. 8. Based on EYM, the both dowels failed in Mode IV. It shows that the bending capacity of the dowel is lower compared to the bearing capacity of the member. Mode IV failure also

Table 1 5 % Offset and ultimate load

No.	2.5D		5D	
	5 % offset load (kN)	Ultimate load (kN)	5 % offset load (kN)	Ultimate load (kN)
1	7.80	8.32	8.90	9.35
2	5.50	6.40	9.70	10.03
3	7.78	7.78	10.10	10.10
4	8.00	8.20	8.92	8.92
Mean	7.27	7.68	9.40	9.60

Fig. 8 Failure mode of sample 2.5D



shows that the dowel yield in bending at two plastic hinge points per shear plane and associated wood crushing.

3.3 Experimental Versus Theoretical (EYM)

The comparison of experimental to the theoretical is only made for the results at 5 % offset yield strength since the theory of EYM is based on the 5 % offset yield (Table 2). The 5 % offset yield average value is taken as the comparison.

Since that the EYM theoretical does not includes parameters of end distance in the equations, therefore only one value of the theoretical is referred to. The comparison also shows that the 2.5D and 5D from the experimental is 75.52 and 81.06 % respectively higher than the theoretical. It can be concluded that the EYM, NDS 2005 has under estimate the single shear connections for the tropical hardwood. It does shows that more study need to be done in order to modify the EYM, NDS 2005 [2] which was developed mostly based on the European and softwood timber to be reliable and accurately predict the single shear connections for the tropical hardwood connections.

Table 2 Theoretical and 5 % offset yield value

Mode	Theoretical (EYM) (kN)	5 % offset load (kN)	
		2.5D	5D
I _m	7.84		
I _s	7.84		
II	23.54		
III _m	2.85		
III _s	2.85		
IV	1.78	7.27	9.40

4 Conclusion

Results show that there are significant different of the 2.5D and the 5D. It was found that the 5 % offset yield and ultimate strength capacity of 2.5D is 23 and 20 % lower compared to the 5D respectively. The experimental 5 % offset yield of the 2.5D and 5D has also shown to be 75.52 and 81.06 % respectively higher than the theoretical. However, the experimental failure mode of the connections was found supported the theoretical expected failure mode. The dowels found to yield in bending at two plastic hinge points per shear plane and associated wood crushing. The EYM has successfully predicted the failure mode behavior however does not accurately predict the load carrying capacity of the single shear strength of the Kapur species.

Acknowledgments The authors would like to thank the Ministry of Science, Technology and Environment, Malaysia for funding the project through ERGS, UiTM.

References

1. MS 544: Part 2: 2001. Malaysian standard code of practice for structural use of timber. Department of Standards Malaysia. SIRIM
2. NDS, National design specification for wood construction american forest and paper association (AFPA), Washington, DC (2005)
3. H. Rohana, Structural performance of mortise and tenon joint strengthened with glass fibre reinforced polymer for selected tropical species. PhD thesis. Faculty of Civil Engineering, Universiti Teknologi MARA, Shah Alam, Selangor, Malaysia (2011)
4. J.K. Timber, Impex Private Limited Malaysian Kapur Wood, http://jktimber.tradeindia.com/Exporters_Suppliers/Exporter21700.377108/Malaysian_Kapur-Wood.html, (2011)
5. N. Harding, A.H.R. Fowkes, Bolted timber joints. in Proceedings of the Pacific Timber Engineering Conference. vol. 3, pp. 872–883 (1984)
6. Educational material for Designing and Testing Timber Structure—TEMTIS, *Handbook 1—Timber Structure*, Leonardo da Vinci Pilot Projects (2008)
7. Eurocode 5. Design of Timber Structures. (BS EN 1995-1-1-2004 +A1:2008)
8. Trada (2002) Fasteners for structural timber wood information, Buckinghamshire

Particle Swarm Optimization for Single Shear Timber Joint Simulation

Marina Yusoff, Shahril Mohd Shalji and Rohana Hassan

Abstract This paper presents a new paradigm that is possible to aid the traditional experimental analysis in timber joints research. Laboratory experiment has incurred a lot of cost and times to find optimize end distance of a timber joint. Particle swarm optimization (PSO) is applied and tested focusing on a single shear timber joints. The determination of fitness function is based on the findings from the previous datasets of the traditional laboratory experiments. The dataset includes the timber species of Kapur that emphasizes on 2D and 3.5D in diameter of end distance. Several PSO parameters were tested to find the maximum load carrying capacity of timber joint for different end distances. The findings show that PSO can give a feasible solution for a single shear strength timber joint performance. It demonstrates that the PSO has a potential to be used as a timber joint simulations that would be beneficial to timber joint researchers in predicting the load carrying capacity of a joint and contributes in reducing time and cost.

Keywords End distance • Fitness function • Kapur • Particle swarm optimization • Single shear • Timber joints connections

1 Introduction

Timber is one of the oldest and best-known structural materials, and one of the few renewable natural resources. It also is a desirable material for construction, building house or making furniture because it requires less energy to produce a

M. Yusoff (✉) · S. M. Shalji
Faculty of Computer and Mathematical Sciences, Universiti Teknologi MARA,
40450 Shah Alam, Selangor, Malaysia
e-mail: marinay@tmsk.uitm.edu.my

R. Hassan
Institute for Infrastructure Engineering and Sustainability Management, Faculty of Civil
Engineering, Universiti Teknologi MARA, 40450 Shah Alam, Selangor, Malaysia

usable end product than the other materials [1]. There are various species of timber in Malaysia such as Balau, Merbau, Kapur and Meranti. Timber species in Malaysia is grouped according to their strength and has been classified as strength group 1 to strength group 7 in MS 544: part 2: 2001 [2]. Strength group 1 is the strongest and as the strength group increased, the weaker the strength of the species. The timber species selected for this study is Kapur. Kapur species is categorised as medium hardwood and classified as strength group 4. This species is also considered as one of the easiest of supply and commonly use structural members. Nowadays, a cost for a timber is rising and it takes a long time to renew. Timber has been used as a structural material such as beam, column and roof trusses which brings to the use of fasteners and connections.

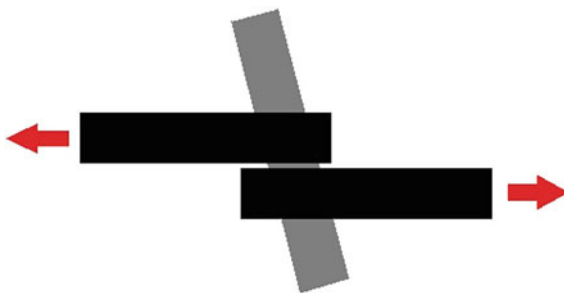
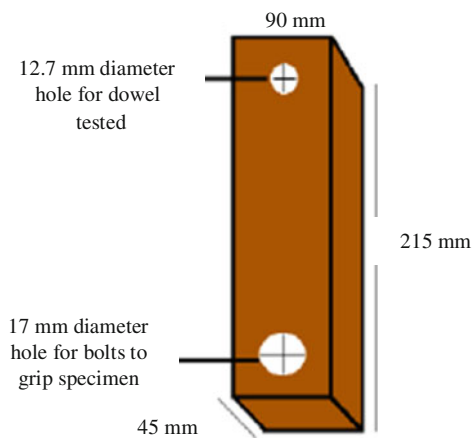
The competitiveness of a timber structure, relative to other building materials, may be determined by the efficiency of the connections. In most cases the fastening of timber to timber requires little skill or knowledge of design. Very limited publications about the tropical timber connections were found. The connection as reported are such as the shear and bending performance of structural, mortise and tenon connections for tropical timber [3–5].

Lacking of specific information for Malaysian timber in designing the load carrying capacity of joints and the influence of different end distance has led to this study. End distance is one of the major factors in designing the load carrying capacity of the timber connection. However, the actual load carrying capacity can only be determined using experimental work which incurred cost and time. This study emphasized in finding a simulation method in replacing the experimental laboratory testing method to determine and compare the ultimate shear strength of different end distance. Results of maximum load carrying capacity of single shear strength for Kapur joint compiled from previous laboratory work done by Abu Bakar [6] and Mat Nawi [7] has been taken for simulation. A lot of manual experiments are required to find the appropriate best end distance of a timber joint. Thus, this project aims of developing a system that can give feasible end distance of a timber joint without performing the manual experiment. With automated system, it will omit the cost and time as incurred in the experimental process.

The remainder of this article is organised as follows. [Section 2](#) explains some related works. The PSO is discussed in [Sect. 3](#). Experimental setup is introduced in [Sect. 4](#). Computational results are analysed in [Sect. 5](#); finally, [Sect. 6](#) concludes the paper and presents certain avenues for future research.

2 Single Shear Strength

Shear strength is defined as the maximum load typically applied normal to a fastener' axis that can be supported prior to fracture. In other common term, the load is applied laterally to the fasteners. There are two typical shear strengths; single and double shear strength. [Figures 1 and 2](#) show the single and the double shear strength [8]. Single shear is when load is applied in one plane that would

Fig. 1 Single shear joint**Fig. 2** Double shear joint**Fig. 3** The geometry of the timber specimen

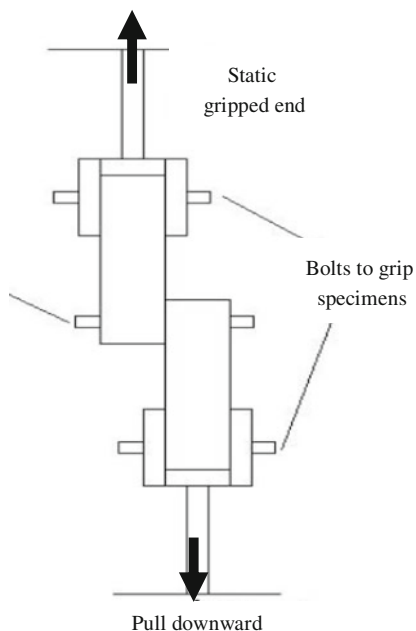


Fig. 4 The set up of the experimental pull-out test

result in the fastener being cut into two pieces meanwhile double shear is load applied in two planes that would result in three fastener pieces.

Method of single shear strength joint is an experiment to determine the maximum load carrying capacity of the joint. These joint can be fastened using the mechanical fasteners such as dowels, bolts and nuts and nails. The length of the centre of the mechanical fasteners to the end of the timber member is known as end distance. The end distance used in this study is at the length of 2 times the diameter ($2D$) and 3.5 times the diameter of dowels ($3.5D$). The diameter, D of the dowel is 12.7 mm (Fig. 3). The experimental set up is as shown in Fig. 4.

The performance of the two different end distances were also identified [6, 7] and compares the failure modes connection of different end distance based on European Yield Model (EYM) in National Design Specification, (NDS) 2005 [8]. This experiment use Kapur timber as a dowel. It also uses a different diameter of end distance to determine and compare the shear strength of Kapur timber. Figure 5 shows the example of result of $2D$ and $3.5D$ for load/deformation.

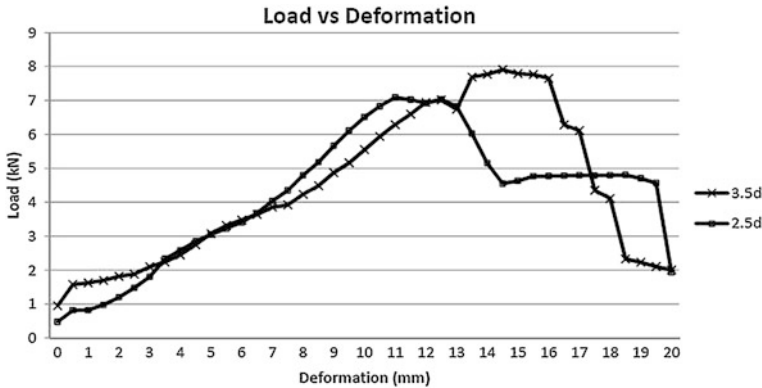


Fig. 5 Average 2D versus 3.5D end distance

3 Solution Using Particle Swarm Optimization

3.1 Computational Solutions

This section highlights the steps involved in a proposed computational solution. The first step is on the data conversion. The data of manual experiment were converted into graph in excel. This is to compare current experiment result with this project result. The graph is then converted into polynomial. Equation from this conversion is used for fitness identification.

The next step is the application of Particle swarm optimization (PSO). The determination of fitness function is based on the findings from the previous datasets of the traditional laboratory experiments. It was then tested on dataset includes the timber species of Kapur that emphasizes on 2D and 3.5D in diameter of end distance. Several PSO parameters were tested to find the maximum load carrying capacity of timber joint for different end distances.

3.2 Particle Swarm Optimization Implementation

PSO is an optimization approach proposed by Kennedy and Eberhart in 1995 inspired by social behavior of organisms such as a school of fishes and bird flocking [9, 10]. Each fish or bird is illustrated as a particle. Each particle moves stochastically in a search space for feasible solution. Each particle has its own velocity and position. PSO provides a mechanism that can process particle velocity and position in multi-dimensional space. Optimum feasible solution can be achieved by updating both velocity and position. The fitness values comprise of global (*Gbest*) and personal best (*Pbest*) derived from the simulated behavior of a

group of particles. $Pbest$ is the best solution offered by each particle at local search area while the $Gbest$ is the best solution on global scale.

PSO can be used to solve continuous and discrete problems [10, 11]. Canonical PSO algorithm has been used to solve continuous problems. Algorithm 1 shows PSO algorithm designed by [12].

Algorithm 1: PSO algorithm

```

1: Begin
2:   Initialize number of particles and populations
3:   Declare  $W$ ,  $C_1$  and  $C_2$ 
4:   Initialize  $V_{initialize(min)}$  and  $V_{initialize(max)}$ 
5:   Initialize  $D_{min}$  and  $D_{max}$ 
6:   Calculate  $Pbest$  and  $Gbest$  value for each particle
7:   Do
8:     For each particle
9:       Calculate new velocity value,  $V_{(new)}$ 
10:      Calculate new position,  $D_{(new)}$ 
11:      Calculate  $Pbest_{(new)}$ 
12:      Calculate  $Gbest_{(new)}$ 
13:   While (stopping condition is reached)
14: End

```

The algorithm starts with the initialization of the population of particles or swarm size, followed by the initialization of inertia weight (W) and acceleration constants (C_1 and C_2). Step 4 and 5 initialize the minimum value ($V_{initialize(min)}$) and maximum value of velocity ($V_{initialize(max)}$) and minimum position (D_{min}) and maximum value of position (D_{max}), respectively. Next is the calculation of $Pbest$ and $Gbest$ value for each particle. Step 9 calculates the new velocity value for each particle using Eq. 1. Step 10 updates the new position, $D_{(new)}$ using Eq. 2. Finally, $Pbest_{(new)}$ and $Gbest_{(new)}$ are determined based on the fitness value set for the problem. Iteration starts from step 7 until step 13 to update the current velocity and position of each particle. This iteration will be done until it satisfies the stopping condition.

$$V_{id(new)} = W * V_{id} + C_1 * r_1 (Pbest_{(id)} - X_{id}) + C_2 * r_2 * (Gbest_{(id)} - X_{id}) \quad (1)$$

$$X_{id(new)} = X_{id} + V_{id(new)} \quad (2)$$

where:

$V_{id(new)}$	new velocity of the i th particle in d th dimension
V_{id}	current velocity of the i th particle in d th dimension
X_{id}	current position of the i th particle in d th dimension
$X_{id(new)}$	new position of the i th particle in d th dimension
W	inertia weight

C_1 and C_2	acceleration coefficient
r_1 and r_2	random function in the range of [0,1]
$Pbest_{(id)}$	position of the personal best of the i th particle in d th dimension
$Gbest_{(id)}$	position of the global best derived from all particles in the swarm.

PSO has the capability to explore regions in the specified search space and exploit the search to refine feasible solutions. These search strategies are influenced by the following parameters; acceleration constants (C_1 and C_2) and inertia weight [13, 14] that has been applied in the PSO algorithm.

Cognitive component, $C_1 * r_1 * (Pbest_{(id)} - X_{id})$ is a combination of acceleration coefficient (C_1), random function, and the difference between the old position and personal best position in the local search area. This component reflects the performance of the individual particle i , from the past performance [13].

Social component, $C_2 * r_2 * (Gbest_{(id)} - X_{id})$ consists of acceleration coefficient (C_2), random function, and the difference between the old global position and the global best position after every iteration. This component reflects the performance of the particle i from the past performance that are obtained from all particles in the global search space. Both of these components have stochastic flavor with the contribution of $C_1 * r_1$ and $C_2 * r_2$ [13, 15]. As far as velocity update is concerned, the new velocity relies on these components and the inertia weight to ensure the velocity remains in the same direction as the previous velocity. Thus, the setting of these parameters is important to optimize the search space.

4 Experimental Setup

This section discusses the experimentation preparation. The data of manual experiment were converted into graph in excel. The purpose of converting data into coordinate graph is to compare current experiment result with this project result.

To find an equation, the graph is converted into polynomial. The Fig. 6 shows the conversion from the data obtained from laboratory experiment to polynomial for the 2D.

The fitness equation that used in this PSO is based on diameter of end distance in timber joint experiment. Table 1 shows fitness function for 2D and 3.5D. Table 2 is the parameter setting for the PSO parameters.

5 Results and Findings

This section discusses the results from the computational experiment of the PSO implementation. Table 3 demonstrates results for 2D using different numbers of iterations. The results show that the maximum end distance obtained at 5th iteration with 8.778. However, 10th and 15th iterations give low end distance value.

Fig. 6 Polynomial graph for 2D

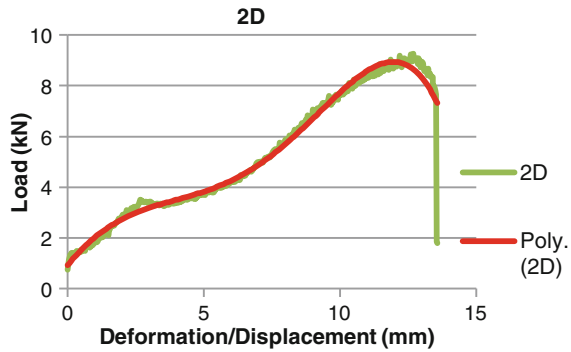


Table 1 Fitness function

End distance diameter	Fitness function
2D	$y = -0.0001x^5 + 0.0017x^4 + 0.0142x^3 - 0.2484x^2 + 1.3387x + 0.9129$
3.5D	$y = 0.0000029394x^6 - 0.0001720764x^5 + 0.0034772430x^4 - 0.0311259334x^3 + 0.1556688226x^2 - 0.0507105690x + 1.7557687041$

Table 2 Parameter setup

Parameter	Value
Inertia weight	0.0 – 1.0
C_1	2.0
C_2	2.0
Initial $V_{initialize(min)}$	-1
Initial $V_{initialize(max)}$	1
Number of particles in a swarm (population)	30
Stopping condition	Iteration equal to 10

Table 3 Result for 2D using velocity of -1 to 1

Velocity	Iteration	X	Y	Maximum end distance (mm)
-1 to 1	5	12.518	8.778	8.778
-1 to 1	10	10.870	8.494	8.494
-1 to 1	15	9.537	7.251	7.251

A few tuning processes were performed to find the most optimal solutions. For 2D, the velocity parameter was adjusted between ranges -3 to 3 and it provides better solution with the maximum of 8.839 end distance at 5th iterations as shown in Table 4.

Table 5 shows the results of 3.5D using velocity value between -1 and 1. The result also shows the maximum value for the end distance is at 5th iteration. The result seems similar to 2D by using the same parameter settings. The tuning process

Table 4 Result for 2D using velocity of -3 to 3

Velocity	Iteration	X	Y	Maximum end distance (mm)
-3 to 3	5	12.4059	8.83882	8.83882
-3 to 3	10	10.3491	8.05963	8.05963
-3 to 3	15	9.30713	7.01025	7.01025

Table 5 Result for 3.5D using velocity of -1 to 1

Velocity	Iteration	X	Y	Maximum end distance (mm)
-1 to 1	5	16.3331	10.0853	10.085
-1 to 1	10	16.2508	10.0844	10.084
-1 to 1	15	16.3579	10.0851	10.085

Table 6 Result for 2D using velocity of -4 to 4

Velocity	Iteration	X	Y	Maximum end distance (mm)
-4 to 4	5	16.2697	10.0848	10.085
-4 to 4	10	16.3333	10.0853	10.085
-4 to 4	15	16.3568	10.0851	10.085

is done with the minimum velocity of -3 and maximum velocity of 3 . For 2D, the velocity parameter was adjusted between ranges -3 to 3 and ranges of -4 and 4 , it provides similar results compared to velocity ranges between -1 and 1 . Table 6 provides consistent results with the maximum of 10.085 mm of the end distance.

The results show that the employment of PSO to find the maximum end distances for single shear strength is possible. The maximum end distance obtained is within the range that of obtained from the lab experiments. At only 5th iteration and swarm size of 30 , PSO offers good performance for the single shear timber joint connection.

6 Conclusion

The PSO implementation to find possible end distance in a single shear timber joints demonstrates the capability of PSO in solving the optimization problem. The results of 3.5D using velocity value between -1 and 1 show the maximum value for the end distance is at 5th iteration. The result seems similar to 2D by using the same parameter settings. For 2D, the velocity parameter was adjusted between ranges -3 to 3 and ranges of -4 and 4 , it provides similar results compared to velocity ranges between -1 and 1 . For the particular single shear timber joints, PSO able to obtain the end distance value that accommodates the range provided from the laboratory experiment. The ability of PSO to provide solutions would help the timber researcher in reducing time and cost of material for lab experiment.

However, testing on PSO should consider different types timber, joints, and composites may provide a better computational simulation results.

Acknowledgments Special thanks to RIF grants 600-RMI/DANA5/3/RIF (555/2012) from Research Management Institute, Universiti Teknologi MARA.

References

1. D.W. Green, Strength and stiffness. Wood, 1–5 (2001)
2. MS 544: Part 2, Malaysian Standard. Code of Practice for Structural use of Timber. Department of Standards Malaysia. SIRIM (2001)
3. H. Rohana, I. Azmi, A. Zakiah, Shear and bending performance of mortise and tenon connection fastened with dowel. *J. Trop. For. Sci.* **22**(4), 425–432 (2010)
4. H. Rohana, I. Azmi, A. Zakiah, Bending behaviour of dowelled mortise and tenon joints in kempas. *Sci. Res. J.* **5**(1), 1–11 (2008). ISSN 165-7009
5. H. Rohana, I. Azmi, A. Zakiah, Shear capacity of dowelled mortise and tenon joint in tropical timber. *J. Inst. Phys. Lop Conf. Ser.: Mat. Sci. Eng.* **17**(1), 1–11 (2010)
6. M. H. Abu Bakar, *Single shear strength of kapur in influence of end distance: 2.5D versus 3.5D*. Unpublished project report (Faculty of Civil Engineering, Universiti Teknologi MARA, 2012)
7. N. W. Mat Nawi, *Single shear strength of kapur in influence of end distance: 2D versus 2.5D*. Unpublished project report (Faculty of Civil Engineering, Universiti Teknologi MARA, 2012)
8. NDS, *National Design Specification for Wood Construction* (American Forest and Paper Association (AFPA), Washington D.C., 2005)
9. J. Kennedy, R. Eberhart, *Particle Swarm Optimization*, (1995)
10. J. Kennedy, *The Particle Swarm: Social Adaptation of Knowledge*, (1997) pp. 303–308
11. M. Yusoff, J. Ariffin, A. Mohamed, *Solving Vehicle Assignment Problem Using Evolutionary Computation*. in *Advances Swarm Intelligence*, vol 1 (Springer, Berlin, 2010), pp. 523–532
12. M. Yusoff, J. Ariffin, A. Mohamed, Discrete particle swarm optimization with a search decomposition and random selection for the shortest path problem. *J. Comput. Inf. Syst. Ind. Manag. Appl.* **4**, 578–588 (2012)
13. J. Venter, J. Sobieszczanski-Sobieski, Parallel particle swarm optimization algorithm accelerated by asynchronous evaluations. *J. Aerosp. Comput. Inf. Commun.* **3**(3), 123–137 (2006)
14. A.P. Engelbrecht, *Computational Intelligence: An Introduction* (Wiley, New York, 2007)
15. Y. Shi, Yuhui, R.C. Eberhart, Empirical study of particle swarm optimization. *Evolutionary Computation, CEC 99. Proceedings of the 1999 IEEE Congress on*, vol 3 (1999)

Part II
Concrete Waste and Earthquake
Engineering

Estimation of Ground Motion in Kuala Lumpur Due to Sumatra Subduction Earthquake

Tze Che Van and Tze Liang Lau

Abstract Kuala Lumpur has undesirable subsurface features and yet is the most important and densely populated city in Peninsular Malaysia. Due to this, it should be covered and protected from seismic impact possibilities. An attenuation model that can best estimates ground motion is essential prior to conducting seismic hazard assessment. With the scarcity of historical data, an attenuation model is difficult to be developed for Peninsular Malaysia. The present research focuses on subjecting five existing attenuation models, particularly for subduction earthquakes, to comparison with the actual ground motion records in Kuala Lumpur. Seismic records of Sumatra subduction earthquakes with the moment magnitude from 5.7 to 9.1 spanning in a distance range of 395–834 km were obtained from Malaysian Meteorology Department and other catalogues. Results are presented in graphs and root mean squared error (RMSE) between estimated PGA and actual records was also computed for each attenuation model. The result shows that Adnan et al. (Selection and development of appropriate attenuation relationship for Peninsular Malaysia, Kuala Lumpur, 2004) provides the smallest RMSE of differences between predicted PGA and actual PGA on soil sites in Kuala Lumpur for interface mechanism and on both rock and soil sites for intraslab mechanism of subduction earthquakes while Zhao et al. (Attenuation relations of strong ground motion in Japan using site classification based on predominant period 96(3):898–913, 2006) gives best prediction to PGA on rock site for interface subduction earthquakes.

Keywords Attenuation models • Sumatra subduction zone • Distant earthquake • Seismic • Ground motion estimation • Peak ground acceleration

T. C. Van (✉) • T. L. Lau
School of Civil Engineering, Universiti Sains Malaysia (USM), Pulau Pinang, Malaysia
e-mail: cathvan_911@hotmail.com

T. L. Lau
e-mail: celau@eng.usm.my

1 Introduction

Kuala Lumpur is filled with modern structure and high rise building in almost every corner. Ensuring the safety of this capital of Malaysia is very important to protect residents and commercial activities importance. Peninsular Malaysia is located at the tectonically stable Sunda plate. Although there is no large earthquake originated within Malaysia, this country is often disturbed by tremors propagated from the most renowned seismically active Sumatra subduction zone and Sumatra fault despite its distance of more than 350 km from the zone. With increasing incidences of tremors felt from earthquakes originated from Sumatra, many start to worry if Peninsular Malaysia, including Kuala Lumpur, is still safe from seismic activities. The subsurface of Kuala Lumpur consists of limestone bedrock. The overlying soil deposits comprises of alluvium or/and mine tailings as Kuala Lumpur was once a popular area for tin mining industries [1]. The thick soil over the limestone bedrocks, which has a common depth of around 50 m, makes undesirable features for structural foundations. Kuala Lumpur, which has thick soil layer and long distance from epicenters of Sumatra earthquakes, has the similar geological and geographical features as in the case of Mexico City earthquake in 1985.

Although there is no major damage of structure and casualties experienced due to tremors felt in Kuala Lumpur, the occurrence of moderate level ground motions can be disastrous to structure with no seismic resistant design. According to prediction by Megawati et al. [2], subduction earthquake from Sumatra with a moment magnitude larger than 7.8 could yield catastrophic ground motion in Singapore and Kuala Lumpur, even at a distance of 700 km. Probabilistic seismic hazard assessment has to be carried out for Kuala Lumpur, knowing its importance as the main centre of the country. Prior to the seismic risk assessment, selection of a reliable ground motion attenuation model is yet another challenging task.

An attenuation model is a simple mathematical model that relates ground motion parameters (i.e. spectral acceleration, velocity and displacement) to earthquake source parameters (i.e. magnitude, source-to-site distance and mechanism) and local conditions [3]. Empirical method is the most reliable method to develop an attenuation model. However, due to limitation of well-documented historical ground motion information recorded in Malaysia, it is not possible to formulate a new model using that method as it requires regression analysis of abundant available data. Conventionally, subjecting a number of existing attenuation models which has the similarity in geology, seismo-tectonic features or source-to-site distance to comparison has been carried out in Malaysia.

A study on formulating distant attenuation model for subduction earthquake and shallow crustal earthquake has been carried out [4]. For comparative purposes, these models are plotted and compared with only a few existing attenuation models, which are considered not comprehensive enough to show any aspect of differences and errors of the formulated model for Peninsular Malaysia. Four distant attenuation models developed for Malaysia and Singapore were also

subjected into comparison and selection for design response study [5]. Reference [6] compared four models established for stable tectonic regions with actual ground motion data in Peninsular Malaysia. However, tectonic mechanism is not considered in the study.

None of the studies mentioned above clearly present a comprehensive and detailed method in processing ground motion data to suit those selected existing attenuation models. Since then, a greater amount of new data has been recorded with more stations distributed within Peninsular Malaysia. Although studies on attenuation models have already been carried out in Malaysia, different data sets utilized could lead to obtaining big differences in results [7]. Thus, despite the incomprehensive method used in the previous studies, a revision to the current adopted attenuation model is required.

This study is mainly to determine the most suitable attenuation models for subduction earthquakes for Kuala Lumpur by comparing peak ground acceleration (PGA).

2 Sumatra Subduction Zone and its Impact to Peninsular Malaysia

Sumatra subduction zone is the extension of the convergent belt from Himalayan to south of Java and Sunda Islands, passing through front southward of Myanmar, Andaman, Nicobar Islands and Sumatra. It accommodates the northward motion of the Australian plate into Eurasia. With the subducting rate of 40–50 mm per year, this zone mostly produces shallow to intermediate thrust faulting earthquake [8]. Shallow earthquake can be more disastrous as waves propagate near the ground surface with less energy dissipation. This subduction zone had produced the two giant historical earthquakes: 1833 event and 2004 event with moment magnitude of 9 and 9.1 respectively.

Despite the distance of more than 400 km from Sumatra subduction earthquake sources, tremors can still be felt in Peninsular Malaysia. In 4 June 2000, the Bengkulu earthquake with Mw7.8 was reported to cause minor crack in building walls and fear among public especially in high rise building in Johor Bahru and also Klang Valley [9]. Tremors from two consecutive earthquakes from northern Sumatra of Indonesia in 14 June 2011 with Mw5.5 and Mw5.6 shocked public in Malacca, Selangor, Perak and Penang. And not to mention, the Mw9.1 megathrust earthquake generated from northern Sumatra on 26 December 2004 which triggers tsunami that took 68 lives, causing 6 missing and over 8,000 displaced in western coastal of Peninsular Malaysia [10]. Other than events mentioned above, there were a lot of subduction earthquake events that can be felt in Peninsular Malaysia.

3 Data Collection and Compilation

Seismic data used in this study were obtained from Malaysian Meteorology Department (MMD). These seismic data were recorded by a total of 13 stations located within Kuala Lumpur. Among those stations, 6 stations are set on soft soil (Fig. 1). To fill in missing data and avoid inaccurate details, catalogues from other seismological centers such as United States Geological Survey (USGS) database, International Seismological Centre (ISC) database and National Earthquake Information Center (NEIC) database have also been referred. However, only data from December 2004 to June 2012 were included in this study due to the availability of time histories provided by MMD. Among 76 earthquake events, there are 29 distant earthquakes originated from Sumatra subduction and fault zone recorded by seismic station in Kuala Lumpur.

3.1 Source Mechanisms

Global CMT project moment tensor solution and NEIC moment tensor solution were used to interpret and distinguish tectonic mechanism for each event. As a result, 15 events ranging from moment magnitude (M_w) 5.7–9.1 with 69 ground motion data are subduction earthquakes originated from Sumatra subduction zone. Those events were further classified into two types of source mechanisms: interface earthquakes and intraslab earthquakes. Interface earthquake occurs at a depth less than 50 km on shallow dipping planes. It is associated with thrust faulting of subducting oceanic plate which is in contact with the overriding continental crust. Classified as shallow earthquakes, interface earthquakes are capable in producing megathrust earthquakes up to magnitude 9. Intraslab earthquake, on the other hand, have steep dipping planes. Producing earthquakes with magnitude not larger than 8, intraslab earthquake typically occurs along normal faults where the subducting plate experiences stress and physical changes as it is pulled deeper into the asthenosphere (Fig. 1).

However, thrust mechanism is also assumed to be intraslab event if the event occurs at depth greater than 50 km as it is below the crustal contact zone. By using rake angle, fault motion and focal depth from catalogues and moment tensors, 13 events were identified as interface earthquakes while only 2 events are intraslab earthquakes.

3.2 Peak Ground Acceleration

The Peak Ground Acceleration (PGA) value utilized in this study is the geometrical mean of two horizontal components of ground motion acceleration at a site

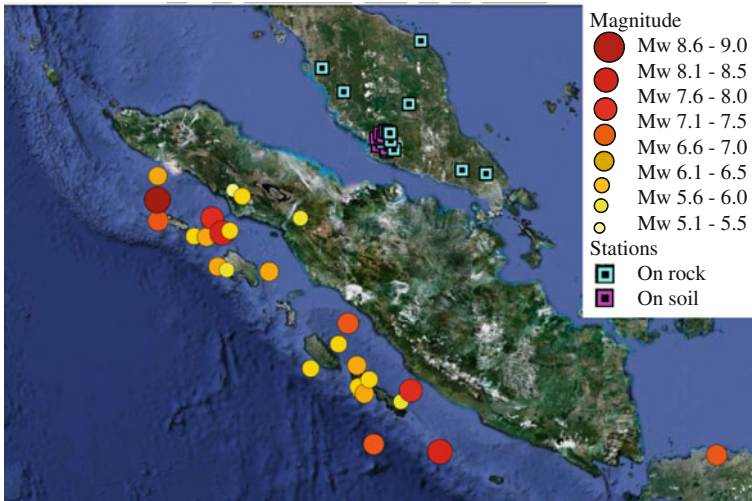


Fig. 1 Location of Sumatra subduction earthquake events from December 2004 to June 2012 and location of seismic stations within Peninsular Malaysia

ranging from 0.000045 to 0.002220 g. Out of 69 PGA records, 42 records were from rock sites and the rest were measured from soil sites.

3.3 Source-to-site Distance

Source-to-site distance is yet another important parameter in this study. Different attenuation models utilized different types of distance terms. Whilst distance to rupture plane (r_{rup}) and hypocentral distance (r_{hypo}) are also used in some models, distance used in this study was standardized as epicentral distance (r_{epi}) to ease comparison among attenuation models adopted. Moreover, the differences among r_{rup} , r_{hypo} and r_{epi} are insignificant compare to the long distance from source to site. The definition of r_{epi} used in this study is the horizontal distance between epicenter of an earthquake and the site of recording instrument.

4 Selection of Attenuation Models

Only subduction earthquake attenuation models derived by using empirical method are selected and compared in this study. All selected models were derived by regression analysis using different sets of ground motion records. Selected attenuation models with magnitude and distance used in development of each model are tabulated in Table 1. It is noticeable that the distance ranges for some of

Table 1 Summary of selected attenuation models

Attenuation model	Moment magnitude range	Distance range (km)	Site
Youngs et al. [11]	5.0–8.2	10–500	Mixed
Atkinson and Boore [12]	5.0–8.3	50–300	Rock and soil
Adnan et al. [4]	5.0–8.5	2–1122	Rock
Zhao et al. [13]	5.0–6.0	10–300	Rock and soil
Lin and Lee [14]	4.1–8.1	20–600	Rock and soil

the models were too small to cover the recorded long source-to-site distance from Sumatra subduction sources to seismic stations in Kuala Lumpur except Adnan et al. [4]. Nevertheless, these models may still provide the best match predictions to actual ground motions.

Different source mechanisms produce different level of motion. Thrust faulting at shallower surfaces generates the strongest motion compare to normal faulting from deeper ground. Thus, considering interface and intraslab mechanism separately is crucial in selection of attenuation model. In this study, all selected models weighed source mechanism as an essential aspect except Adnan et al. [4]. Being the only model developed for Peninsular Malaysia, Adnan et al. [4] model is included in the present study regardless to the exclusion of source mechanisms in the model. In addition, its consideration of farther source-to-site distance makes it a model worth to be compared with other models in this study.

Atkinson and Boore [12], Youngs et al. [11] and Adnan et al. [4] were developed for subduction zones at a global scale, which means seismic data were obtained from worldwide. On the other hand, Zhao et al. [13] and Lin and Lee [14] were derived by utilizing mainly local data from Japan and Taiwan respectively. An erratum for Atkinson and Boore [12] has been published in 2008 [15]. Therefore, the model adopted in this study has been corrected as suggested in the later paper.

5 Results and Discussions

The actual ground motion records were grouped according to moment magnitude with 1.0 interval starting from Mw6.0 to Mw9.0 for plotting. To provide better representation of actual conditions, focal depth varies for each group. Focal depth used for each group is the average of focal depth of events in respective groups. Each attenuation model has its own consideration for types of source mechanisms and site conditions. Thus, these data were also categorized into two site conditions namely, rock and soil sites.

Figure 2 shows the comparison of PGA estimated by attenuation models with actual records taken from rock site for interface subduction earthquake events. Most of the models predict larger PGA at higher moment magnitude. Lin and Lee [14] and Youngs et al. [11] predict PGA which differs significantly from the

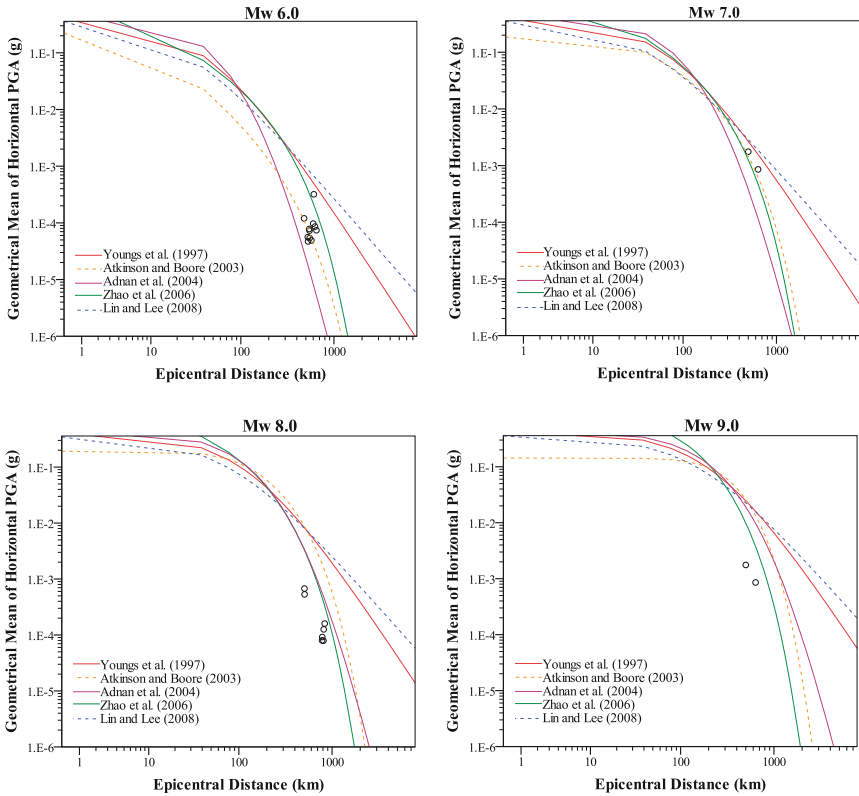


Fig. 2 Comparison of attenuation curves and recorded PGA on rock sites for interface subduction earthquakes with moment magnitude of 6.0, 7.0, 8.0 and 9.0 respectively

observed data. Atkinson and Boore [12] gives higher estimation as moment magnitude increases. Adnan et al. [4] also tends to saturate at higher magnitudes. It can be seen that Zhao et al. [13] produces curves fitter to the four magnitudes of data compare to the rest, despite the distance limitation.

On the other hand, graphs plotted in Fig. 3 exhibit comparison of PGA estimated by models with actual records taken from soil site for interface earthquake events. Zhao et al. [13] estimates PGA close to actual PGA from sites at lower magnitude. However, as magnitude increases, prediction from Zhao et al. [13] tends to deviate further from actual PGA. Adnan et al. [4] provides estimation with more consistency yet closest to actual PGA taken from soil site. Generally, Youngs et al. [11] and Lin and Lee [14] curves tend to attenuate slower and provide higher PGA value compare to recorded data.

The two intraslab earthquake events were binned into Mw7.0. With only 1 magnitude, only two graphs were produced for comparison purpose as shown in Fig. 4. From the graphs, Adnan et al. [4] curve attenuates faster than the rest and

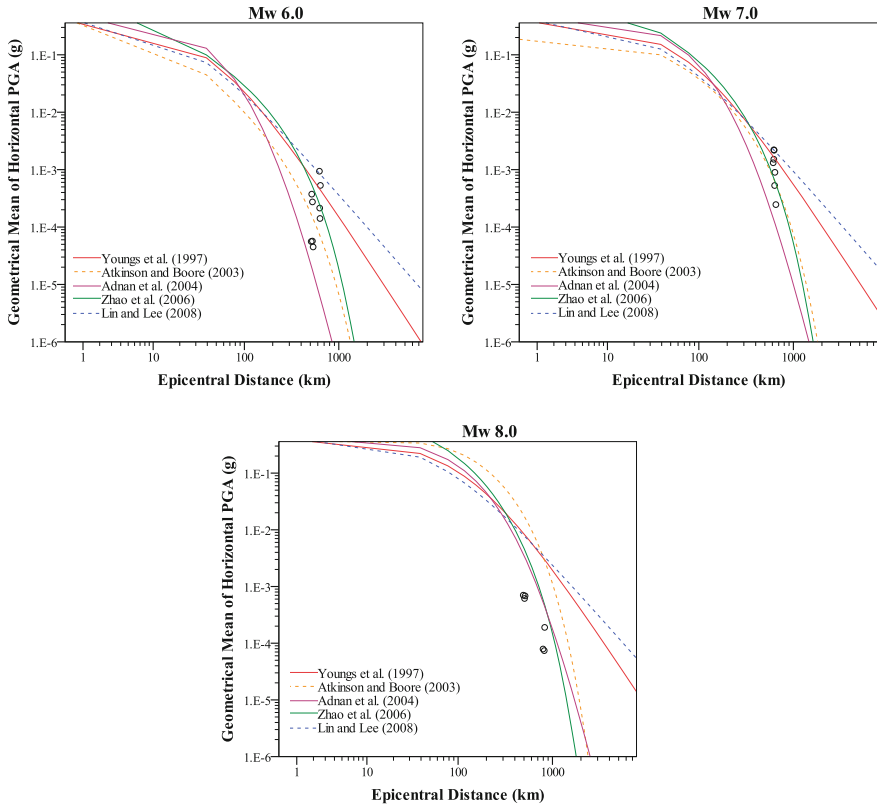


Fig. 3 Comparison of attenuation curves and recorded PGA on soil sites for interface subduction earthquakes with moment magnitude of 6.0, 7.0 and 8.0 respectively

gives the closest estimation of PGA. This is followed up by Zhao et al. [13], which provides the second best estimation of PGA for intraslab events. As there were only a few intraslab events, comparison between curves for each model for different moment magnitude could not be acquired.

In addition, root mean squared error (RMSE), which is also known as the standard error of the estimate, was also calculated to quantify the goodness of fit for predicted and actual value (Table 2). In other words, the smaller the RMSE value obtained, the better the estimation to the actual records. The RMSE is calculated after the data has been normalized into the range from 0 to 10. Among all, Adnan et al. [4] model provides the lowest RMSE for all types of source mechanisms and site conditions that were being considered in this study except for interface earthquakes on rock sites. The lowest RMSE on rock site for interface earthquakes is provided by Zhao et al. [13].

The locally-derived Lin and Lee [14], which predicts higher PGA compare to observed data from Kuala Lumpur, is only suitable for Taiwan and Greece regions

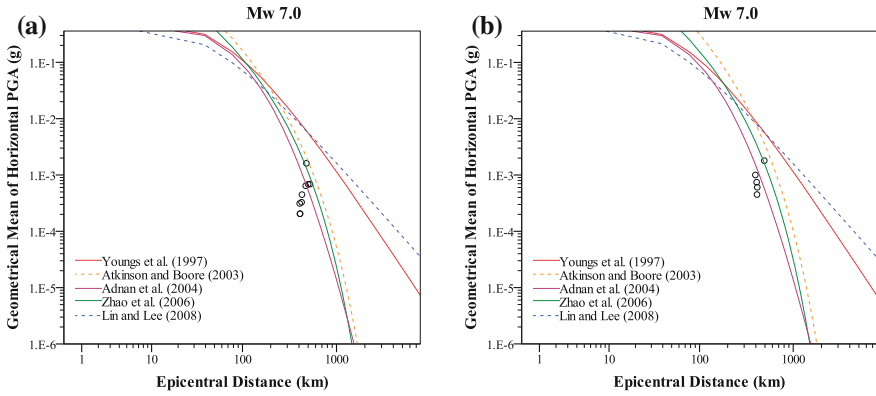


Fig. 4 Comparison of attenuation curves and recorded PGA for intraslab subduction earthquakes with moment magnitude 7.0 on (a) rock and (b) soil sites respectively

Table 2 Summary of root mean squared errors (RMSE)

Attenuation model	Moment magnitude (Mw)	Interface		Intraslab	
		Rock site	Soil site	Rock site	Soil site
Youngs et al. [11]	6	0.28	0.20	–	–
	7	0.71	0.23	4.58	3.33
	8	1.98	2.44	–	–
	9	8.64	–	–	–
	Mean RMSE	2.90	0.96	4.58	3.33
Atkinson and Boore [12]	6	0.06	0.21	–	–
	7	0.31	0.33	1.88	2.60
	8	1.73	4.67	–	–
	9	8.67	–	–	–
	Mean RMSE	2.69	1.74	1.88	2.60
Adnan et al. [4]	6	0.06	0.22	–	–
	7	0.34	0.72	0.59	0.18
	8	0.48	0.63	–	–
	9	5.29	–	–	–
	Mean RMSE	1.54	0.52	0.59	0.18
Zhao et al. [13]	6	0.13	0.19	–	–
	7	0.33	0.53	0.73	0.83
	8	0.61	1.20	–	–
	9	2.32	–	–	–
	Mean RMSE	0.85	0.64	0.73	0.83
Lin and Lee [14]	6	0.36	0.34	–	–
	7	0.85	0.40	4.33	3.05
	8	2.08	2.45	–	–
	9	8.26	–	–	–
	Mean RMSE	2.89	1.06	4.33	3.05

but not elsewhere [16]. Thus, the finding in this paper supports the results obtained in previous study [16]. Global-based Atkinson and Boore [12] and Youngs et al. [11] are unable to provide good estimations. This might be due to the worldwide data used in deriving those models that are too random and not specific for a certain region. Zhao et al. [13] gives closer prediction among all models in the present paper excluding Adnan et al. [4]. This might be due to the abundance of Japanese data (over 4,500 records) adopted in deriving the model which is more specific and similar in geological and geographical features to Sumatra subduction zone. Being the only attenuation model developed for Peninsular Malaysia, Adnan et al. [4] yields the lowest RMSE compare to other models considered in this paper except for interface events from rock sites.

6 Conclusions

Based on the results obtained, Adnan et al. [4] model provides the best fitting curve in estimating PGA on soil sites for interface mechanism and rock and soil sites for intraslab mechanism of subduction earthquakes compare to other selected models in the present study. On the other hand, Zhao et al. [13] yields the best estimation for PGA on rock sites for interface mechanism. In the future, this study will be extended to other attenuation models and further research on developing an attenuation model for Peninsular Malaysia should be carried out when recorded data are sufficient.

Acknowledgments The authors wish to express their sincere gratitude to Universiti Sains Malaysia for funding this research via a RU Grant (1001/PAWAM/814179). Special thanks also extended to Malaysian Meteorological Department for providing seismological data required for the analysis.

References

1. B.B. Tan, K.A. Al-Suba, K.A. Barat, X. Li, Y. Yin, K. Zhang et al., Urban geology of Kuala Lumpur and Ipoh, Malaysia. *J. Struct. Geol.* **27**(2005), 1781 (1778)
2. K. Megawati, T.C. Pan, K. Koketsu, Response spectral attenuation relationships for Sumatran-subduction earthquakes and the seismic hazard implications to Singapore and Kuala Lumpur. *Soil Dyn. Earthq. Eng.* **25**(1), 11–25 (2005)
3. W.K. Campbell, Prediction of strong ground motion using the hybrid empirical method and its use in the development of ground-motion (attenuation) relations in eastern North America. *Bull. Seismol. Soc. Am.* **93**(3), 1012–1033 (2003)
4. A. Adnan, H. Hendriyawan, I. Masyhur, Selection and development of appropriate attenuation relationship for Peninsular Malaysia. *Proceeding Malaysian Science and Technology Congress*, Kuala Lumpur, (2004)
5. H. Husen, T.A. Majid, F.M. Nazri, M.R. Arshad, A. Faisal, Development of design response spectra based on various attenuation relationships at specific location. In *International Conference on Construction and Building Technology (ICCBT08)*, (2008)

6. A. Adnan, Z.S. Shaerliza, S. Sumio, G. Hiroyuki, An investigation of the attenuation characteristics of distant ground motions in Peninsular Malaysia by comparing values of recorded with estimated PGA and PGV. *Malays. J. Civ. Eng.* **2**(1), 38–52 (2010)
7. N.A. Abrahamson, K.M. Shedlock, Overview. *Seism. Res. Lett.* **68**, 9–23 (1997)
8. R. McCaffrey, The tectonic framework of the Sumatran subduction zone. *Annu. Rev. Earth Planet. Sci.* **37**, 345–366 (2009)
9. M.R.C. Abas, Earthquake monitoring in Malaysia. *Seismic Risk Seminar 2001, Malaysia* 2001
10. OCHA-Geneva, OCHA situation report no. 18 earthquake and Tsunami Indonesia, Maldives, Sri Lanka. Ref: OCHA/GVA-2005/0010, January 2005, p. 9
11. R.R. Youngs, S-J. Chiou, W.J. Silva, J.R. Humphrey, Strong ground motion attenuation relationships for subduction zone earthquakes. *Seismol. Res. Lett.* **68**(1), 58–73 (1997)
12. G.M. Atkinson, D.M. Boore, Empirical ground-motion relations for subduction-zone earthquakes and their application to Cascadia and other regions. *Bull. Seismol. Soc. Am.* **93**(4), 1703–1729 (2003)
13. J.X. Zhao, Z. Jian, A. Akihiro, O. Yuki, O. Taishi, T. Toshimasa et al., Attenuation relations of strong ground motion in Japan using site classification based on predominant period. *Bull. Seismol. Soc. Am.* **96**(3), 898–913 (2006)
14. P.S. Lin, C.T. Lee, Ground-motion attenuation relationships for subduction-zone earthquakes in northeastern Taiwan. *Bull. Seismol. Soc. Am.* **98**(1), 220–240 (2008)
15. G.M. Atkinson, M.B. David, Erratum to empirical ground-motion relations for subduction zone earthquakes and their application to Cascadia and other regions. *Bull. Seismol. Soc. Am.* **98**(5), 2567–2569 (2008)
16. C. Beauval, F. Cotton, N. Abrahamson, N. Theodulidis, E. Delavaud, Rodriguez, et al., *Regional differences in subduction ground motions*. World Conference on Earthquake Engineering (Lisbonne, Portugal, 2012), p. 10

Strength of Quarry Dust Modular Bricks and Wallettes Under Compression

Atikah Fatma Md Daud and Zakiah Ahmad

Abstract The compressive strength of masonry can be verified using two methods namely the unit strength method and the prism test method. The characteristics of masonry are influenced by the properties of bricks and mortar. This paper reports the investigation made on the compressive strength of bricks manufactured using quarry dust as sand replacement. Two types of bricks were prepared; hollow and solid modular bricks with size of 190 mm (H) × 100 mm (L) × 100 mm (T) which is a little bit bigger than the normal brick size. The compressive strength of the bricks have been evaluated using individual unit and mortar strength, prism and wallettes. The effects of different joint thickness on the compressive strength were also evaluated. The strength of solid modular block with thicker mortar joint was found to be higher the strength of hollow block. Based on the strength, both bricks passed the minimum requirement of brick for government project.

Keywords Bricks · Mortar · Compressive strength

1 Introduction

River sand has been the most popular choice for the fine aggregate component of concrete in the past, but overuse of the material has led to environment concern, the depleting of securable river sand deposits and a concomitant price increase in the material. Due to this situation, some developing countries are facing a shortage in the supply of natural sand. Therefore a lot of studies have been carried out to

A. F. Md Daud (✉)

Department of Civil Engineering, Politeknik Sultan Salahuddin Abdul Aziz Shah,
Shah Alam, Selangor, Malaysia
e-mail: fatikah5488@gmail.com

Z. Ahmad

Institute of Infrastructure Engineering and Sustainable Management (IIESM), Faculty of
Civil Engineering, Universiti Teknologi MARA, Shah Alam, Selangor, Malaysia

replace natural sand such as fly ash, slag, limestone etc. [1, 2]. Malaysia is one of the countries that are facing the same problems as other developing countries. Quarry dust is a waste product after the extraction and processing of rocks to form fine particles less than 6 mm. Quite a number of researchers have investigated the potential of using quarry waste and its effect on the strength, workability and durability of concrete [3].

Abdullah [4] investigated the mechanical properties of bricks produced using quarry dust as sand replacement at different mix proportions of cement: sand: quarry dust namely 1:10:0 (M1), 1:7.5:2.5 (M2), 1:5:5 (M3), 1:2.5:7.5 (M4) and 1:0:10 (M5) as well as 1:1:5 (control). The results showed that the bricks containing 100 % quarry dust (1:0:10 (M5)) gave the highest strength and the lowest water absorption compared to other ratios. That study showed that bricks with quarry dust as sand replacement has great potential for construction. This paper reports the investigation made on quarry dust brick masonry prisms and wallettes under axial compression with different thickness of mortars on the surface of solid and hollow bricks.

In order to have a strong masonry unit, there must be good bond between the bricks and the mortar and the strength of the joints depend on the strength of the mortar, types of mortar, thickness of the mortar etc.

A good bond between the units and the binding material is essential and determines how the masonry transfers and resists stresses due to various applied loads [5]. Under compression, the brick masonry will failed in different form of failure characteristics. A number of failure theories have been proposed for brick masonry in compression [6–9]. The theories make an assumption that the bond between brick and mortar remains intact at the time of failure of the brick or mortar. But studies have also shown that the masonry failure is generally accompanied by bond failure in situations where very low brick–mortar bond strength is used [10, 11].

Sarangapani et al. [11] showed the relationship between the bond strength and compressive strength by keeping the mortar strength constant. They observed an increased compressive strength when the bond strength of the masonry increased. Meanwhile, study by Venkatarama and Vyas [5] showed that masonry compressive strength is not sensitive to bond strength variations when the masonry unit is stiffer than the mortar. During the compression of masonry prisms constructed with bricks that are stiffer than the mortar, the mortar in the bed joint has a tendency to expand laterally more than the bricks due to its lesser stiffness. Due to the confinement of brick–mortar interface, the shear stresses at that interface resulted in an internal state of stress which initiates vertical splitting cracks in bricks that lead to failure of the prisms [12, 13]. The stresses developed are generally attributed to the mechanical inter-locking of cement hydration products into the surface pores of the bricks [14].

Gumeste et al. [15] reported that the crushing of weakest brick in a wallette specimen often determines the masonry strength rather than the interaction between brick and mortar and may mask the influence of the mortar strength on the masonry strength. He also concluded that the failure of masonry specimens using

weak mortar is primarily due to loss of bond between mortar and brick units and in the case of stronger mortars failure is due to splitting of bricks.

As the performance of the bricks depends on the materials used and the performance of the walling depends on the properties of bricks and also mortar therefore this research investigated the compressive strength of hollow masonry manufactured using quarry dust as sand replacement as individual unit and also as wallet unit.

2 Materials

2.1 Brick

The bricks were supplied by Syarikat Kilang Papan Mohamad Yusuf dan Anak-anak as shown in Fig. 1. The brick size is 390 mm (L) × 19 mm (H) × 100 mm (W).

The bricks were manufactured using cement, sand and quarry dust with mix ratio of 1:5:5 (cement:sand:quarry dust).

2.2 Mortar

The mortar was prepared using a ready-to-use material named EMACO R1 and was used to replace the ordinary mortar mix. This is a fast curing mortar. EMACO R1 contains special cements, well graded sands and selected polymers to improve physical and application properties. The mortar was prepared by adding the water to the EMACO R1. Mixing water needed is 0.2 L for 1 kg of EMACO R1. This mortar was used in order to expedite the work. However the mortar has also been used by construction industry.

3 Test Methods

Before the construction of the wallethe specimens, the properties of the materials that is going to be used, had to be known. The knowledge of the properties of the mortar and brick would assist in the next analysis. Compressive strength of brick.

The compressive strength of individual brick was determined in accordance with BS 3921:1985. Five (5) randomly picked bricks were first immersed in water for 24 h. After pat dried, the dimensions of the bricks were measured and then placed in compression machine.

To ensure a uniform bearing for the brick specimen, the specimen will be placed between 3 mm thick plywood sheets to take up irregularities. The brick was loaded at a rate of 3.0 kN/s.

Fig. 1 Brick with quarry dust



3.1 Compressive Strength of Mortars

The compressive strength of mortar was performed in accordance with BS4551:1980 of size $50 \times 50 \times 50 \text{ mm}^3$. Six (6) cubes were prepared and tested after 7 and 28 days.

3.2 Compressive Strength of Masonry

3.2.1 Construction of Prism and Wallettes

Masonry wallettes and prisms were constructed in accordance with EN 1052-1:1999 [16]. The prisms were constructed from 5 layers of bricks as shown in Fig. 2a and the wallettes were fabricated using stretcher bond formation as shown in Fig. 2b and each type were bonded with two (2) different thickness of mortar namely 10 and 15 mm in order to determine the effect of mortar thickness on the bond strength. The codes allow the height to thickness ratio of the test prisms to range 2.0–5.0 and the height to thickness ratio for the prisms and wallettes for 10 and 15 mm mortar are 4.5 and 4.3 respectively. A total of 12 wallettes specimens were constructed.

3.2.2 Compressive Strength Test

The compression test of the wallette specimens were tested based on BS5628-1:2005. Lateral variable displacement transducers (L.V.D.Ts) were set-up on each wallette as shown in Fig. 3 at three points on each wallette, one near mid-span, and the other two were located at one-third of the height from top and bottom respectively. Strain gauges of 67 mm gauge length were also attached. As for prism test, no LVDT's were attached to the specimen because strain was not measured (see Fig. 4).

Fig. 2 Prisms; (a) 5-brick prism and (b) Stretcher bond walette specimen

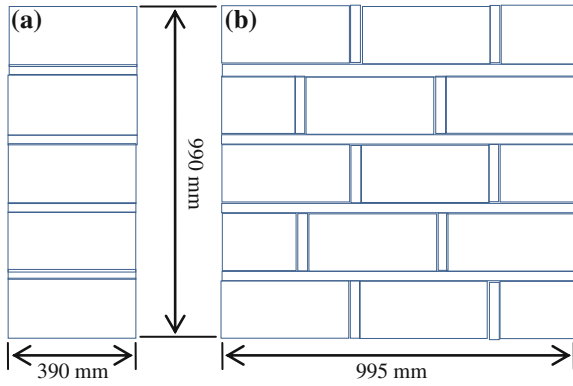


Fig. 3 Experimental set-up for testing of walette



Fig. 4 Experimental set-up for testing of 5-brick prism



4 Results and Discussions

4.1 Compressive Strength of Brick and Mortar

The compressive strength of individual brick or mortar was determined using Eq. (1).

$$F_c = \frac{P_c}{A} \quad (1)$$

where F_c is the compressive strength in MPa; P_c is the maximum load at fracture in Newtons; and A is the cross-sectional area in millimetres.

The compressive strength of mortar and the bricks (solid and hollow bricks) are shown in Table 1.

From Table 1, it can be seen that the compressive strength of the hollow modular block using quarry dust is 3.46 N/mm^2 whilst for solid modular block the

Table 1 Compressive strength

Item	Compressive strength (MPa)
Mortar	23.3 (for 7 days) and 33.8 (for 28 days)
Solid brick	6.46
Hollow brick	3.46

compressive strength is 6.46 N/mm^2 . According to EN771-1-6, a minimum mean value of compressive strength of masonry unit is 1.8 MPa to be used for masonry walls. In Malaysia, for any bricks to be used as construction materials, the minimum permissible average compressive strength specified by Public Works Department is 5.2 MPa for bricks and 2.8 MPa for hollow blocks per 10 samples taken at random from the Contractor's stock pile of 1,000 or part thereof [18]. Hence both types of quarry dust bricks passed the building requirement. These results also show that modular block unit is weaker than the mortar and it will give effect to the prism and wallette tests.

4.2 Compressive Strength of Masonry

Quality and consistency of workmanship has an enormous effect on the strength of masonry [17]. Therefore to ensure consistency in the construction of the samples, all wallettes and mortar batches were carefully controlled.

4.2.1 Characteristics of 5-Brick Prism

Figure 5 shows the compressive strength of prisms for solid brick. As expected that solid brick can resist more compressive load compared to hollow block. The compressive strength of solid brick is 70 and 154 % higher than hollow brick. This is due to the hollow section has not been filled with grout hence less mortar is actually bonding the surface of the bricks.

Failure of the masonry in compression was generally due to crushing and splitting of the bricks (Fig. 6) which later induced movement in the mortar as the load increased which supported the Gumeste et al. [15] findings where masonry with stronger mortars failure is due to splitting of bricks.

The compressive strength of masonry determined by the prism method is lower than the compressive strength determined using the unit strength method. The compressive strength of solid brick is 13 % higher than the compressive strength of prism for solid bricks for 15 mm thickness mortar. Meanwhile, the compressive strength of hollow brick is 55 % higher than the compressive strength of prism with hollow bricks with 15 mm mortar thickness.

This is due to the masonry prism failed in compression prior to reaching the load capacity of individual units. The restrain the unit places on the lateral

Fig. 5 Compressive strength of wallettes for different mortar thickness

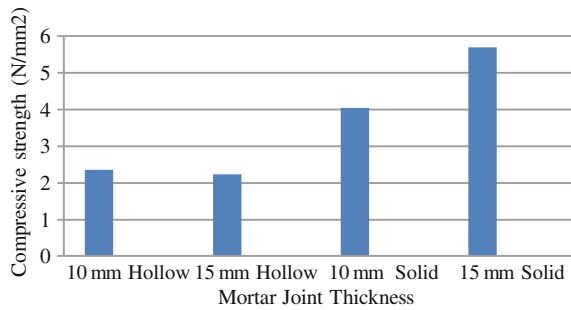


Fig. 6 Failure of solid 5-brick prism



expansion of the mortar joint induces lateral tensile stresses in the unit. Thus the boundary restraints on the unit in the prism will never be as great as they are on individual units when placed in compression between steel bearing plates.

As mentioned earlier the compressive strength of masonry is affected by the compressive strength of units, the type of mortar used, workmanship and curing and these variables are largely reflected in the results of prism test. Therefore, prism test results are more representative of actual in-place performance of the masonry than are tests of component masonry materials. The unit method of masonry does not provide quality control on workmanship and curing as does the prism method.

Fig. 7 Stress versus displacement graph for wallettes with different thickness of mortar

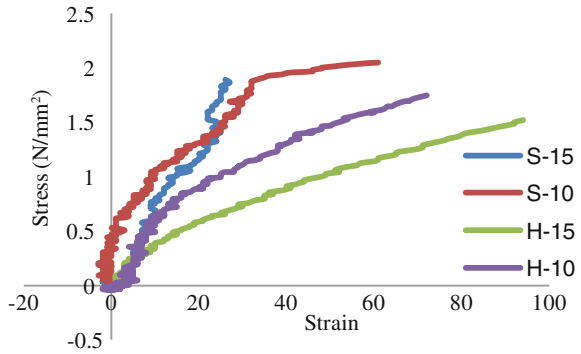
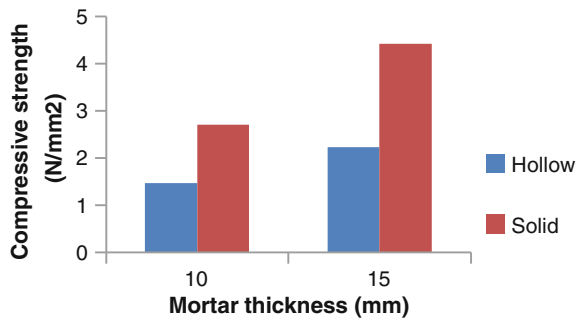


Fig. 8 Compressive strength of wallettes for different mortar thickness



4.2.2 Characteristic of Wallette

In Fig. 7 the stress versus strain of wallettes for different thickness of mortar shows almost similar behaviour for all samples even though the thicknesses of mortar joints are different.

Almost all specimens the collapse occurred when the specimens reached maximum load but with different vertical shortening. Wallettes with hollow bricks collapse at lower maximum load but higher vertical displacement which reflected ductile behaviour.

The results of the compressive strength testing of masonry using wallettes with different mortar thickness are presented in Fig. 8. Once again it can be seen that the compressive strength of wallettes with solid brick can resist more compressive load compared to hollow block. As the mortar thickness increases, the compressive strength also increases. The compressive strength of wallettes with solid brick and 15 mm mortar thickness is 97.8 % higher than wallettes with 10 mm mortar thickness.

The failure mode of wallette with 15 mm mortar was found to have higher degree of failure compared to 10 mm mortar joint thickness. Wider and longer vertical cracks can be seen (Fig. 8) on wallette with 15 mm mortar. Similar crack patterns were also observed on the wallette with 10 mm mortar thickness (Fig. 9).

Fig. 9 Crack observed in the wallette test; (a) 15 mm mortar thickness and (b) 10 mm mortar thickness



These vertical cracks mainly occurred in the bricks and not along the mortar line. These further masked the effect of mortar strength on masonry strength. The vertical stress gets concentrated at perpendicular direction and leads to splitting of the brick. Such behaviour has also been reported by Matthana [10].

The compressive strength of prisms with 15 mm mortar thickness is higher than compressive strength of wallettes by 29 %. However, compressive strength of prism is lower than the compressive strength of masonry unit by 13 %. For hollow bricks, there is no significant different in the compressive strength of prism and wallette with 15 mm thick mortar but this compressive strength is lower than the compressive strength of brick unit by 55 %.

At this point of time, the use of wallette for strength determination is hence more reliable. It may be necessary to test larger number of wallettes with different types of bond to arrive at reliable strength results. This study can be further enhanced by testing the brick–mortar bond strength.

5 Conclusion

The compressive strength properties of masonry bricks made from quarry dust as sand replacement were investigated. The following conclusions were derived:

- (a) The compressive strength of solid masonry unit is higher than hollow modular block. The thicker the mortar joint, the higher the compressive load.
- (b) The compressive strength of the masonry unit passed the minimum permissible average compressive strength specified by Public Works Department is 5.2 MPa for bricks and 2.8 MPa for hollow blocks. Hence the use of hollow bricks will allow for material saving as compared to solid bricks.
- (c) As the compressive strength of mortar used is higher than the compressive strength of bricks, the failure of the masonry in compression was generally due to crushing and splitting of the bricks.
- (d) The compressive strength of prisms with solid bricks for 15 mm mortar thickness is higher than compressive strength of wallettes by 29 %. However, compressive strength of prism is lower than the compressive strength of masonry unit by 13 %.

- (e) There is no significant different in the compressive strength of prism and wallette for hollow bricks with 15 mm thick mortar but this compressive strength is lower than the compressive strength of hollow brick unit by 55 %.

Acknowledgments We wish to thank Kilang Papan Mohd Yusuf dan Anak-anak (KPMY) for the provision of quarry dust bricks.

References

1. D.S. Rajendra Prasad, S. Suresh, G.S. Shashidar, Eco-friendly concrete mix design with industrial wastes by perceptive of constituents chemistry (2012), <http://www.eco-web.com/edi/120807.html>
2. S.T. Ramesh, R. Gandhimati, P.V. Nidheesh, S. Rajakumar, S. Prateekumar, Use of furnace slag and welding slag as replacement for sand in concrete. *Int. J. Energy Environ. Eng.* **4**(3), 1–6 (2013)
3. R.R. Ilangovana, N. Mahendrana, K. Nagamanib, Strength and durability properties of concrete containing quarry rock dust as fine aggregate. *ARPJ. J. Eng. Appl. Sci.* **3**(5), 20–26 (2008)
4. M.J. Abdullah, Compressive strength properties of brick using quarry dust. Unpublished Masters Thesis, Faculty of Civil Engineering, Universiti Teknologi Mara, Malaysia, 2012
5. B.V.V. Reddy, C.V.U. Vyas, Influence of shear bond strength on the compressive strength and stress-strain characteristics of masonry. *Mater. Struct.* **41**, 1697–1712 (2008)
6. H.K. Hilsdorf, An investigation into the failure mechanism of brick masonry loaded in axial compression. *Designing engineering, and constructing with masonry products*, Gulf, Houston, 1996, pp. 34–41, ed. by F. B. Johnson
7. C.L. Khoo, A.W. Hendry, A failure criterion for brickwork in axial compression. *Proceeding of 3rd International Brick Masonry Conference*, 1973, pp 139–145, ed. by L. Foertig, K. Gobel
8. W.S. McNary, D.P. Abrams, Mechanics of masonry in compression. *J. Struct. Eng.* **111**(4), 857–870 (1985)
9. R.H. Atkinson, J.L. Noland, D.P. Abrams, *A deformation theory for stack bonded masonry prisms in compression*. Proceedings of 7th International Brick Masonry Conference (Melbourne University, Melbourne, 1982), pp. 565–576
10. M.H.S. Matthana, Strength of brick masonry and masonry walls with openings. PhD thesis, Department of Civil Engineering, Indian Institute of Science, Bangalore, India, 1996
11. G. Sarangapani, B.V. Ventakarama Reddy, K.S. Jagadish, Brick–mortar bond and masonry compressive strength. *J. Mater. Civil Eng. (ASCE)* **17**(2), 229–237 (2005)
12. B. Kaushik Hermant, C. Rai Durgest, K. Jain Sudir, Stress-strain characteristics of clay brick masonry under uniaxial compression. *J. Mater. Civil Eng. (ASCE)* **19**(9), 728–739 (2007)
13. W.S. McNary, D.P. Abrams, Mechanics of masonry in compression. *J. Struct. Eng.* **111**(4), 857–870 (1985)
14. A.J. Francis, C.B. Horman, L.E. Jerrems, The effect of joint thickness and other factors on compressive strength of brickwork. In *Proceedings of 2nd international brick masonry conference, Stoke-on-Trent* (1971), pp. 31–37
15. K.S. Gumeste, B.V. Venkatarama Reddy, Strength and elasticity of brick masonry prisms and wallettes under compression. *Mater. Struct.* **29**, 241–253 (2006)
16. EN 1052-1 (1999) Method of test masonry. Part 1—Determination of compressive strength
17. D. Ewing Bryan, J. Kowalsky Mervyn, Compressive behavior of unconfined and confined clay brick masonry. *J. Struct. Eng. (ASCE)* **30**(4), 650–661 (2004)
18. MS 27:1971: Malaysian standard: Specification of precast concrete block

A New Lateral Load Pattern Study Based on a Different Limit States

Fadzli Mohamed Nazri and Bee Fang Ku

Abstract The main objective of this study is to overview the effect of different type lateral load patterns on the moment-resisting steel frames (MRSF) by push-over analysis. In this study, a number of different load patterns ($k = 0.5$, $k = 0$, $k = 0.5$, $k = 1$ and $k = 1.5$) were used since this characteristic has a major influence on the ensuing analysis in order to determine the capacity demands of the structure. Seismic analyses on models designed (2-, 4- and 6- storeys MRSF) based on Eurocode 8 with different lateral load patterns are carried out using SAP2000 software. Maximum base shear force and drift (%) that based on Vision 2000 and FEMA-356 are determined to evaluate the seismic performance of the MRSF. From the result, for every lateral load pattern, the maximum base shear force has a significant decrement in higher number of storeys MRSF with a uniform cross-section beams and columns due to larger structural weight. Performance is very close for uniform distribution ($k = 0$) and parabolic distribution ($k = 0.5$). Similarly inverted triangle distribution ($k = 1.0$) and another type of inverse parabolic distribution ($k = 1.5$) performance appears to be same. As a comparison of drift from the analysis with limit states that stated on Vision-2000 and FEMA-356, using FEMA-356 to evaluate the performance level is more suitable is has higher drift limit value for every stage and every lateral load pattern. In the graphs according to FEMA-356, it can be noticed that all the collapse points are located near the point which has maximum base shear value for all the lateral load pattern cases. In order to get more accurate results, further studies need to be done by using different material constructed the frames, using irregular shape of frames, or higher proposed storeys.

Keywords Drift • Eurocode 8 • FEMA-356 • Limit state • Pushover • Vision 2000

F. M. Nazri (✉) • B. F. Ku
School of Civil Engineering, Universiti Sains Malaysia, Pulau Pinang, Malaysia
e-mail: cefmn@eng.usm.my

1 Introduction

Study of seismic behaviour and relative structural performance of the building become intensively vital. Seismic performance of a building when subjected to earthquake force is depending on its structural response characteristics.

Buildings sited outside the seismic zones such as those in Malaysia are not designed for seismic loads. These buildings are designed according to BS 5950, which does not have any seismic provisions. Due to recent seismic faults in West Coast and Peninsular Malaysia, there is an urgent need to study the seismic performance of existing buildings in Malaysia. To design buildings with seismic resistance, Eurocode 8 (EC8) can be used as a designer guide serve to provide the general provisions and requirements for earthquake-resistant design and construction of buildings and other civil engineering works in seismic regions.

Therefore, a designer has certain control on the amount of the total (global) structural damage experienced by the structure based on an appropriate selection of stiffness, strength, and ductility (detailing) requirements in the conceptual seismic design stages of a project. Nevertheless, a designer has limited control over the distribution of damage, which is mainly caused by load redistribution effects characteristic of inelastic structural responses. The lateral load patterns in Eurocode 8 [1] and Equivalent Lateral Force (ELF) procedure is used to design lateral-load resisting systems for regular structures.

In Eurocode 8, there are two types of lateral load patterns that have been suggested, these are the triangular and the uniform one. It is known that these types of lateral load pattern are not reliable in capturing the dynamic behaviour [2]. This is because it is difficult to determine the force profile (up the structure) caused by a particular ground motion, i.e. every single earthquake record produces different behaviour. From this difficulty, in this study it will introduce a new lateral load pattern that probably manages to predict an appropriate demand capacity as compare with lateral load pattern that suggested by Eurocode 8. From the finding, the drift for each type of lateral load pattern will then compare with the limit states from the Vision-2000 [3] and FEMA-356 [4].

2 Nonlinear Analysis

2.1 Pushover Analysis

The nonlinear static procedure, colloquially known as “pushover analysis,” has become a standard method for estimating seismic deformation demands in building structures as well as their local and global capacities. As such, it has become a popular tool among practicing engineers for the evaluation of the safety of structures against an earthquake-induced collapse. This procedure is generally considered to be more realistic in gauging the vulnerability of buildings during

earthquakes than the linear procedures commonly contained in current codes. This procedure is recommended for structures in which “higher mode effects” are not significant. If these higher mode effects are significant, then the procedure needs to be supplemented with a linear dynamic analysis [5].

Based on Krawinkler [6], the nonlinear static analysis (pushover analysis) is a partial and relatively simple intermediate solution to the complex problem of predicting force and deformation demands imposed on structures and their elements by severe ground motion. The important terms are static and analysis. Static implies that a static method is being employed to represent a dynamic phenomenon; a representation that may be adequate in many cases but is doomed to fail sometimes. The analysis implies that a system's evolution has been created already and the pushover is employed to evaluate the solution and modify it as needed.

This study deals with the development of lateral load patterns for the conceptual seismic design of moment-resisting frame structures. The proposed lateral load patterns are based on inelastic behavior and are a fundamental component of a proposed seismic design methodology to limit the extent of structural damage in the system and distribute this damage uniformly along the height. These load patterns are expected to provide a uniform distribution of story ductility ratios when compared to the distributions obtained with moment-resisting frames designed based on the code compliant design lateral load patterns.

The implementation of the aforementioned methodology would not only distribute damage along the height of the frame, but also help avoid undesirable dynamic responses that occur once structural damage is concentrated in one or in a few stories, e.g., story drift amplifications caused by P-delta effects [7].

2.2 Lateral Load Patterns

In pushover analysis, the first step is to suppose a certain lateral load pattern, and then performs a static analysis of the structural model under this pattern. Several lateral load patterns have been suggested:

1. Inverted triangle distribution (modal pattern);
2. Uniform distribution;
3. Load distribution based on linear elastic dynamic analysis or response spectrum analysis of the building [8];
4. The adaptive distribution, which is varied as the inter story resistance changes in each load step [9];
5. Distribution proportional to the product of the mass and fundamental mode shape, which is used initially until the first yielding takes place, then the lateral forces are determined based on the product of the current floor displacement and mass at each step [10];
6. A distribution based on mode shapes derived from secant stiffness at each load step [11].

Fig. 1 Proposed lateral load patterns used in this study

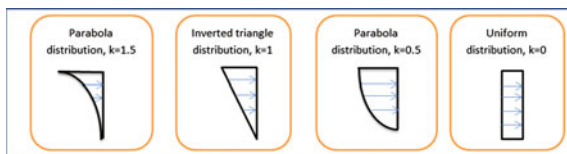


Figure 1 is the proposed lateral load patterns used in this study. They are parabolic distribution ($k = 1.5$), inverted triangle distribution ($k = 1.0$), another type of parabolic distribution ($k = 0.5$) and uniform distribution ($k = 0$).

The seismic action effects shall be determined by applying, to the two planer models, horizontal forces F_i to all stories. The seismic forces F_i , distributed along the height, are evaluated as follows:

$$F_i = F_b \frac{z_i^k m_i}{\sum_{i=1}^n z_i^k m_i} \quad (1)$$

where,

- n is the number of stories, and
- m_i and z_i are the i th floor mass and height measured from the foundation level, respectively
- k is an exponent related to the effective fundamental period of the structure.

3 Moment-Resisting Steel Frame (MRSF) Structure

3.1 General

Moment-resisting steel frames were widely regarded as an excellent lateral resisting system for building in seismic regions. In particular, moment resisting beam-to-column connections in welded steel moment frames (WSMF) were considered to be able to withstand large inelastic deformations without developing significant strength degradation or instabilities and that should damage occur, it would be limited to ductile yielding of beams and beam-column connections [12]. Resisting steel frames are highly regarded for their seismic per. Moment-resisting steel frames are highly regarded for their seismic performance. They have demonstrated great ductility in research, and they behaved well in past earthquakes. Research has historically focused on a strong-column weak-beam (SCWB) steel frame, since they have greater ductility than weak-column strong-beam (WCSB) frames; however, it is sometimes uneconomical or impractical to obtain SCWB behavior at every joint. Consequently, the UBC [13] and the NEHRP [14], permits the use of WCSB joints under specific conditions. Also, design philosophy of steel frames has changed over the years, and some of the conditions that led to favorable

field performance during past earthquakes may no longer be valid. Modern steel structures are often lighter and more flexible than older structures, and design requirements are continually changing [15].

Moment-resisting steel frames have been extensively used in regions of high seismicity for low-rise and midrise buildings because of their high ductility. In low-rise structures when all outer and inner frames are designed as lateral load resistant, the strong column weak beam (SCWB) principle leads to overdesign in columns when the beam design is governed by gravity loads. To achieve a more economical design, perimeter frame systems are used, especially in the United States. The perimeter frame approach, however, suffers from low redundancy and lack of redistribution capacity, making the whole structure potentially more vulnerable to global collapse. The overdesign in columns of space frame systems can be reduced by utilizing semi-rigid/partial-strength connections where columns are designed to be stronger than the connections. In doing so, the same SCWB design philosophy of protecting the columns against inelastic behavior is achieved because the connections are the main energy-dissipating elements of the system. The benefit of using such an approach is the significant reduction in column overdesign and the elimination of the potential for brittle fracture in fully welded connections through the use of field-bolted semi-rigid connections only. Therefore, using energy dissipative semi-rigid/partial-strength connections in the design of low-rise steel space frame systems in high seismic zones is an alternative to the perimeter frame design, and its potential advantages need to be further explored [16].

3.2 Frames Description

A total of 12 MRSF examined in the study. The frame plan view illustrated in Fig. 2 was adopted for all structures. The 2-, 4- and 6-storey MRSF with 3 bay model was considered in this study as shown pictorially in Table 1. This generic frame model has a constant storey height of 3.3 and 6 m of bay width.

4 Result

This study involves modeling, seismic analysis and redesign of beams and columns of moment-resisting steel frames (MRSF) based on Eurocode 8 for earthquake resistance purposes. Seismic analyses on models designed with different lateral load patterns are carried out using SAP2000 software. Maximum base shear force (F_b) and drift (%) are determined to evaluate the seismic performance of the moment-resisting frames. The limit state can be determined based on Vision-2000 [3] and FEMA-356 [4].

Fig. 2 Capacity curve of 2 storeys moment-resisting steel frame

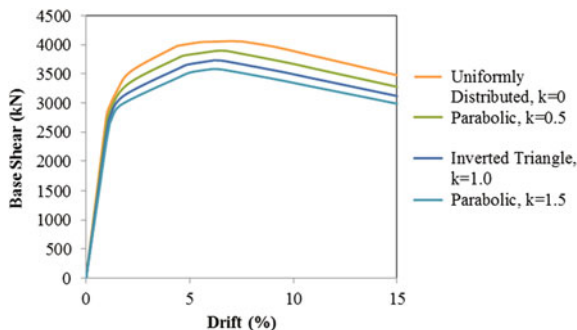
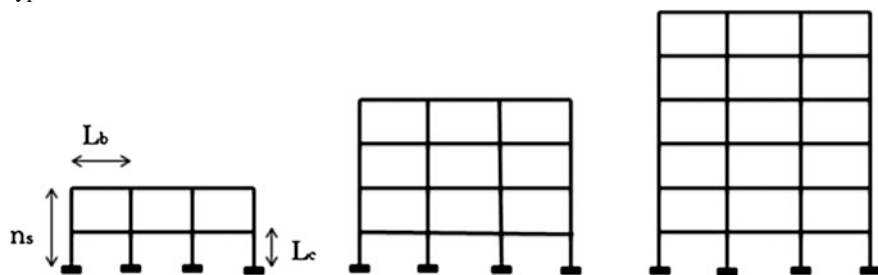


Table 1 Summary of building models will be used in this study

Type of frames



	2- storey			4- storey		6- storey	
Frame	n_s	n_b	L_b (m)	L_c (m)	Beam section (UB)	Column section (UC)	T_1 (s)
1	2	3	6	3.3	533 × 210 × 101	356 × 368 × 202	0.35
2	4	3	6	3.3	533 × 210 × 101	356 × 368 × 202	0.59
3	6	3	6	3.3	533 × 210 × 101	356 × 406 × 235	0.80

- n_s number of storey
- n_b number of bays
- L_b length of beam
- L_c length of column
- UB universal beam
- UC universal column
- T_1 period of the structure

4.1 Base Shear Force (F_b)

Base shear force (F_b) is the resultant lateral force occurs due to seismic ground motion at the base of a structure. The calculation of base shear force (F_b) depend on the soil condition at site, the level of ductility and the total weight of the structure, the fundamental period of vibration of the structure as well as the lateral load patterns.

Fig. 3 Capacity curve of 4 storeys moment-resisting steel frame

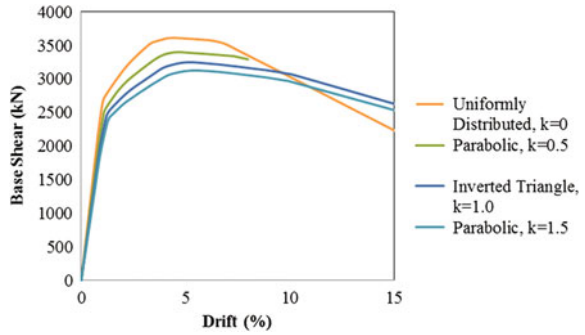
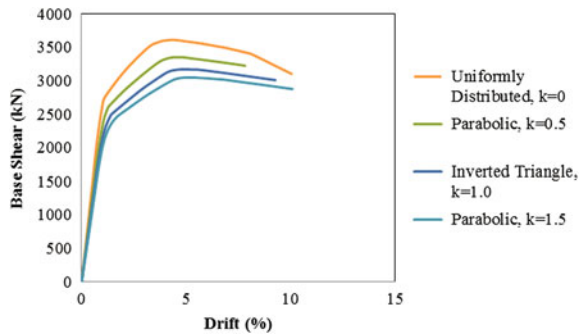


Fig. 4 Capacity curve of 6 storeys moment-resisting steel frame



Figures 2, 3 and 4 showed the capacity curve of the different storeys MRSF under different lateral load patterns.

From the figure above, it can be observed that the base shear force of MRSF under uniform distribution ($k = 0$) is the highest value, followed by parabolic distribution ($k = 0.5$), inverted triangle distribution ($k = 1.0$) and another type of parabolic distribution ($k = 1.5$). This is mainly due to smaller masses of the structural system. For every lateral load pattern, the base shear force has a significant decrement in higher number of storeys MRSF with same cross-section beams and columns due to larger structural weight.

4.2 Drift (%)

Lateral deflection is the predicted movement of a structure under lateral loads; and story drift is defined as the difference in lateral deflection between two adjacent stories. During an earthquake, large lateral forces can be imposed on structures; EC8 requires that the designer assess the effects of this deformation on both structural (such as beams and columns) and nonstructural elements (such as the windows and cladding). Without proper consideration during the design process,

large deflections and drifts can have adverse effects on structural elements, non-structural elements, and adjacent structures.

Assuming that the drift provisions in the EC8 can indeed be followed, the benefits of successfully implementing the provisions can be substantial. If properly designed, structural framing elements and connections not part of the lateral force resisting system should remain largely intact and be able to provide vertical support for the structure even at large deflections. This eliminates non-ductile failure of vertical load resisting system, such as that seen by some parking garages during the Northridge Earthquake in 1994. Non-structural exterior elements will remain largely undamaged by earthquake ground motion. This will help prevent falling hazard and will limit water intrusion after an earthquake. Finally, if the drift provisions in current codes are followed, buildings should generally not pound together, which should reduce the threat to the vertical stability of columns from impact from adjacent structures' non-co-planar floor diaphragms and should eliminate localized pounding damage at co-planar diaphragm locations.

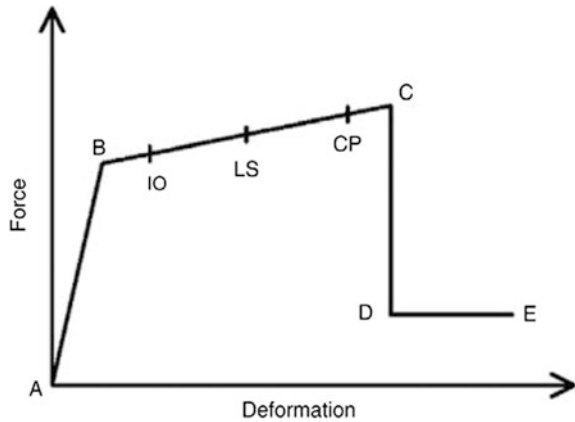
For every lateral load pattern, the drift at the collapse point has a significant decrement in higher number of storeys MRSF with same cross-section beams and columns due to larger structural weight. For 2 storeys MRSF, it can be noticed that the drift of MRSF under uniform distribution ($k = 0$) is the highest value, followed by parabolic distribution ($k = 0.5$), inverted triangle distribution ($k = 1.0$) and another type of parabolic distribution ($k = 1.5$). However, for 4- and 6- storeys MRSF, it can be noticed that the drift of MRSF under parabolic distribution ($k = 1.5$) is the highest value, followed by inverted triangle distribution ($k = 1.0$), another type of parabolic distribution ($k = 0.5$), and uniform distribution ($k = 0$).

4.3 Comparison of the Seismic Performance

Seismic performance of a structure is described by designating the maximum allowable damage state for an identified seismic hazard. ATC-40 [17] describes standard performance levels for structural and non-structural systems and several commonly used combinations of structural and nonstructural levels as (a) Operational, (b) Immediate occupancy, (c) Damage control, (d) Life safety, (e) Structural stability and (f) Not considered.

The performance level of a building is determined based up on its function and importance. Structures like hospital buildings, telecommunication centers, transportation facilities etc. are expected to have a performance level of operational or immediate occupancy for an identified seismic hazard that can occur for the structure. Meanwhile a residential building must have a performance level of damage control or life safety. Temporary structures or unimportant buildings or structures came under the performance level of structural stability or sometimes are not considered. The force deformation relationship as well as the performance levels of a structure as well as a structural element is given in Fig. 5.

Fig. 5 Force-deformation relationship of a typical plastic hinge [4]



According to FEMA-356 [4], for drift with 0.7 % transient and negligible permanent, the structural performance level is type S-1 immediate occupancy. FEMA-356 [4] also suggests 2.5 % for life safety and 5 % for near collapse.

One critical component of this approach is the definition of these performance limit states. It has been suggested that structural deformation, typically inter-storey drift, be employed as a relatively easy marker for the level of damage in the structural system. Vision-2000 [3] suggests permissible drifts of 0.2 % for fully operational, 0.5 % for operational, 1.5 % for life safety and 2.5 % for near collapse. There are questions as to whether drift is well correlated with damage in all cases.

In this study, the results of drift are compared according to Vision-2000 [3] and FEMA-365 [4]. This comparison is separated for different lateral load patterns (Figs. 6, 7, 8, 9, 10, 11, 12 and 13).

From the figures above, it can be observed that Vision-2000 has lower drift (%) for every stage compared to FEMA-356. With lower drift (%), there is lower base shear value. This is due to the safety factor used in Vision-2000 is higher and then the limit drift has lower value. Hence, if the designer uses this value of base shear to design the building, the value is considered low compared to FEMA-356. Consequence of this, the building designed may be not safe enough especially for higher number of storeys.

Using FEMA-356 to evaluate the performance level is more suitable. In the graphs according to FEMA-356, it can be noticed that all the collapse points are located near the point which has maximum base shear value for all the lateral load pattern cases. In order to get more accurate results, further studies need to be done by using different material constructed the frames, using irregular shape of frames, or higher proposed storeys.

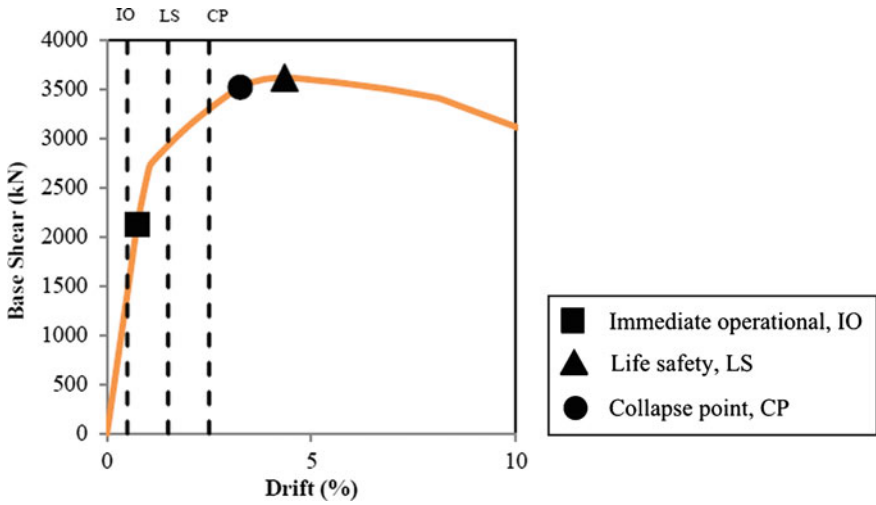


Fig. 6 Graph shows the performance level of 6 storeys MRSF under uniform distribution ($k = 0$) according to vision-2000

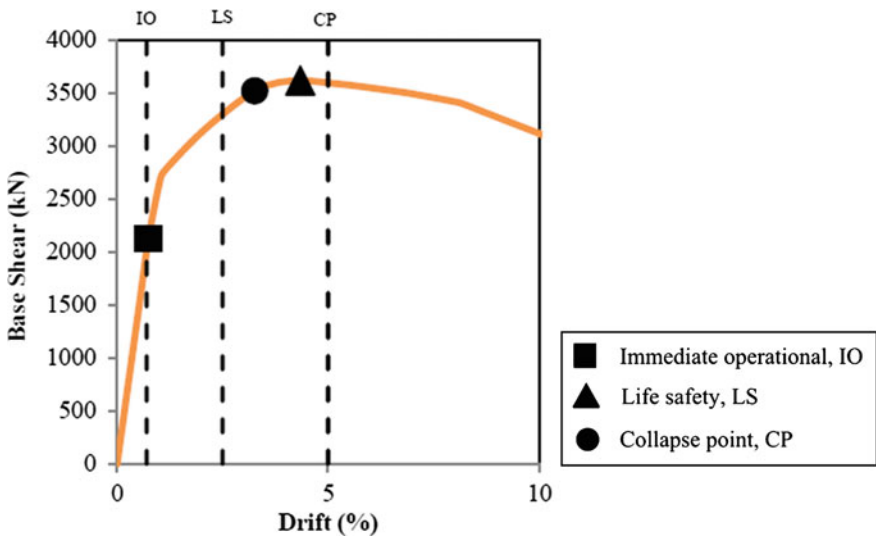


Fig. 7 Graph shows the performance level of 6 storeys MRSF under uniform distribution ($k = 0$) according to FEMA-356

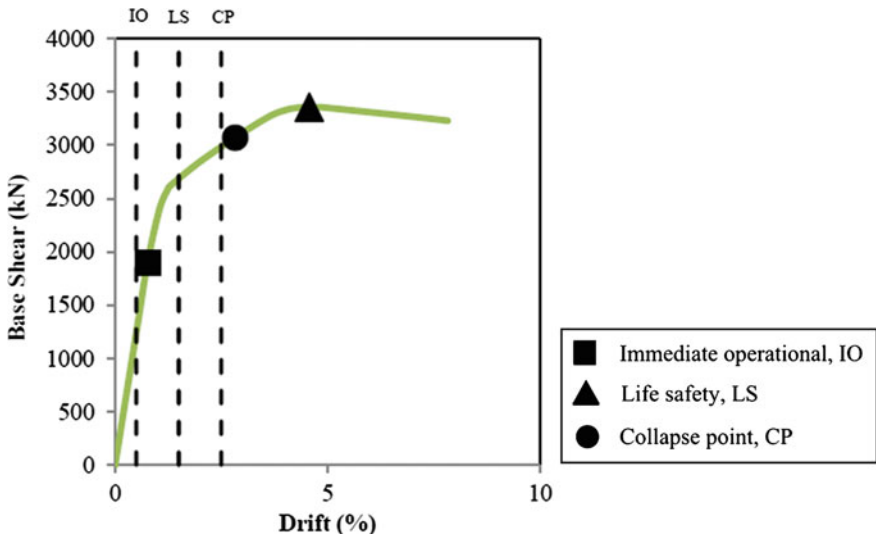


Fig. 8 Graph shows the performance level of 6 storeys MRSF under parabolic distribution ($k = 0.5$) according to vision-2000

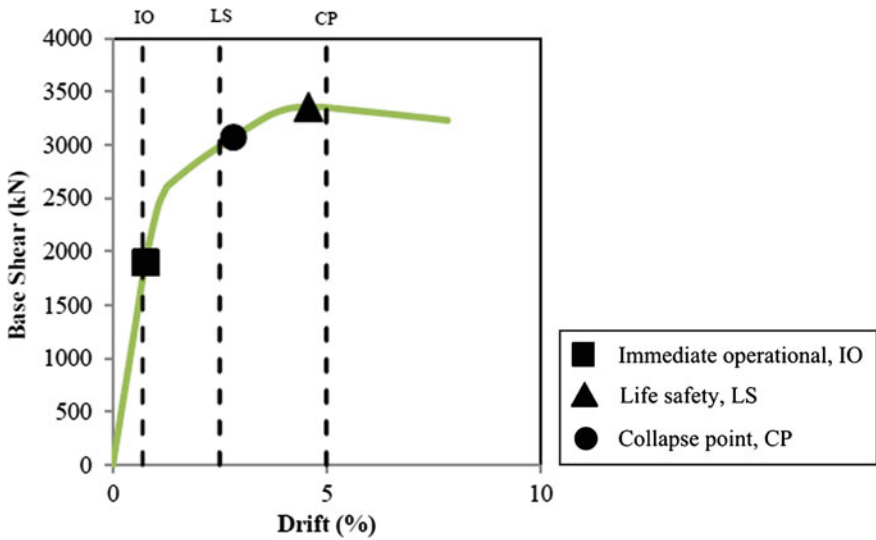


Fig. 9 Graph shows the performance level of 6 storeys MRSF under parabolic distribution ($k = 0.5$) according to FEMA-356

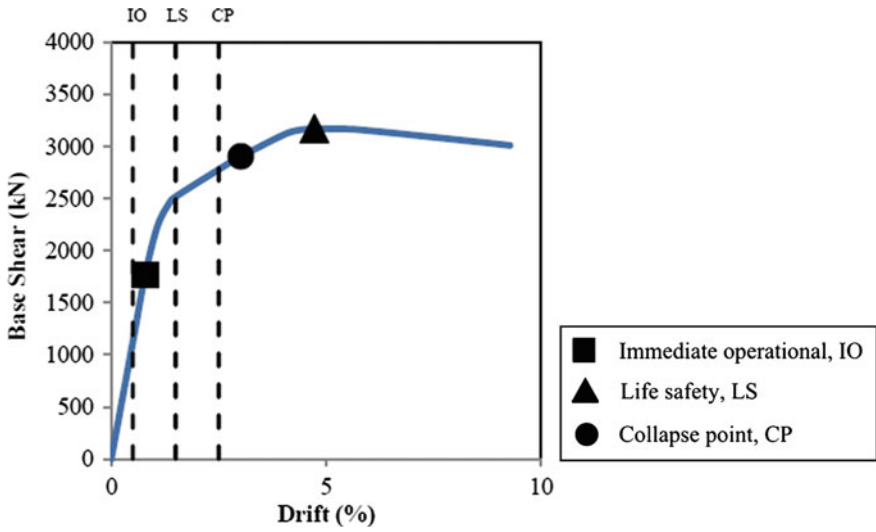


Fig. 10 Graph shows the performance level of 6 storeys MRSF under inverted triangle distribution ($k = 1.0$) according to vision-2000

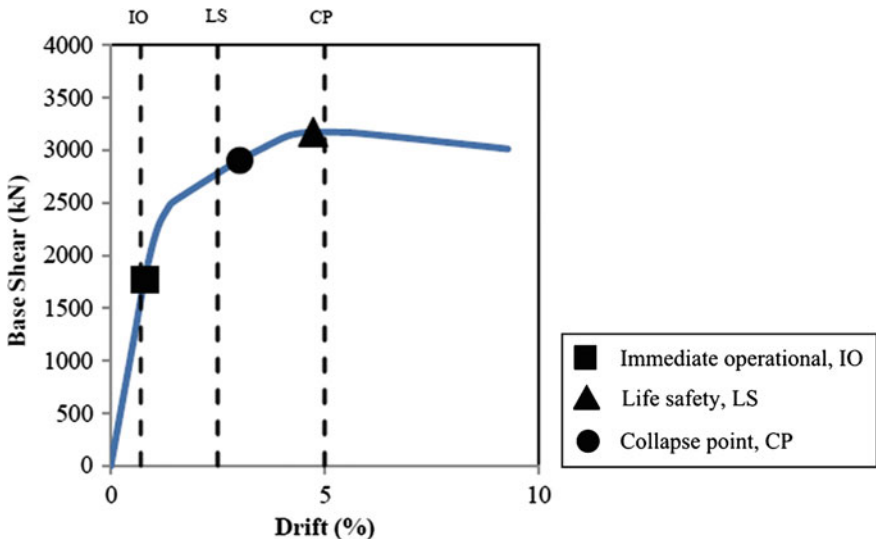


Fig. 11 Graph shows the performance level of 6 storeys MRSF under inverted triangle distribution ($k = 1.0$) according to FEMA-356

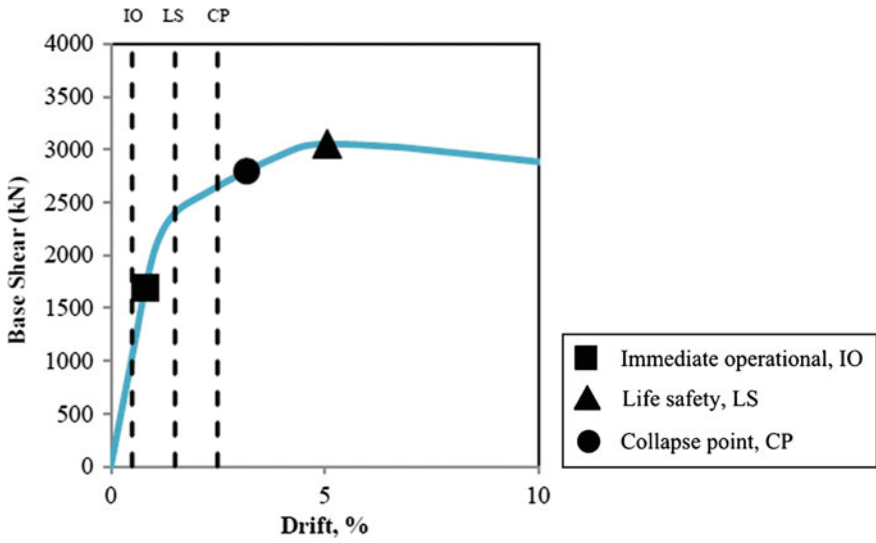


Fig. 12 Graph shows the performance level of 6 storeys MRSF under another type of parabolic distribution ($k = 1.5$) according to vision-2000

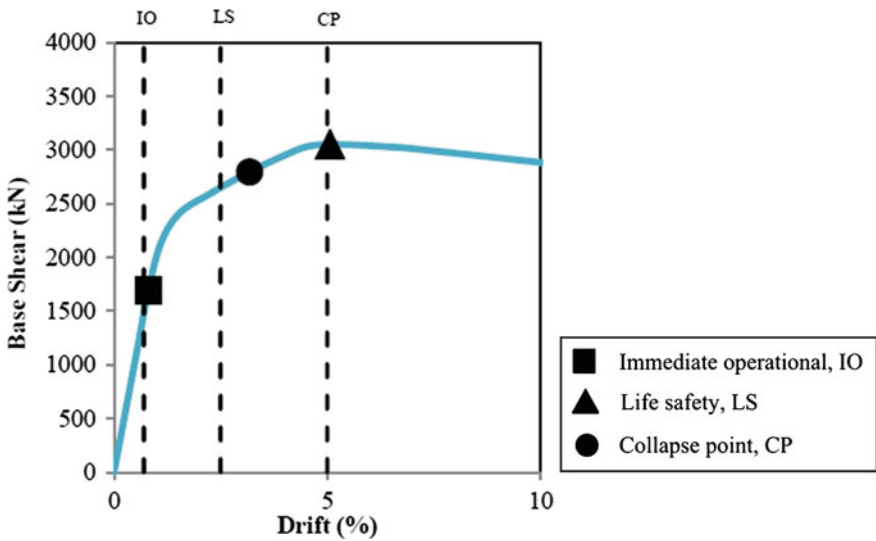


Fig. 13 Graph shows the performance level of 6 storeys MRSF under another type of parabolic distribution ($k = 1.5$) according to FEMA-356

5 Conclusion

This study evaluates the 2-, 4-, and 6- storeys MRSF under different lateral load patterns and compares its structural performance according to Vision-2000 [3] and FEMA-356 [4]. The following conclusions can be made from this research:

- (1) Lateral load patterns have been influenced the structural response such as base shear and drift.
- (2) For all the four type loadings the performance points are very close.
- (3) Performance is very close for uniform distribution ($k = 0$) and parabolic distribution ($k = 0.5$). Similarly inverted triangle distribution ($k = 1.0$) and another type of parabolic distribution ($k = 1.5$) performance appears to be same. This is due to the close similarity between the load patterns.
- (4) MRSF with uniform distribution is overestimated the base shear value. Parabolic distribution ($k = 0.5$) can be considered in design work.
- (5) Different lateral load pattern shows only slight change in performance point in regular MRSF. The case may vary for irregular buildings.
- (6) To select the exact lateral load pattern, performances of MRSF in different configuration have to be studied and should be compared with nonlinear time-history analysis.

There are many aspects that still required further study in this research. Following recommendations can be considered for further research study:

- (1) To study performances of MRSF under different lateral load patterns and compare with nonlinear time history analysis.
- (2) To study the effect of different material used for the moment-resisting frames such as concrete and timber.
- (3) To further study on higher storeys instead of 2-, 4- and 6- storeys MRSF.
- (4) To perform the similar study with different cross section of beams and columns for each floor.
- (5) To perform the similar study with irregular shape of steel frame.

Acknowledgments This research was supported by Universiti Sains Malaysia under a Short Term Grant (60312025).

References

1. BSI, Eurocode 8: Design of structures for earthquake resistant (2004)
2. R. Medina, Story shear strength patterns for the performance-based seismic design of regular frames. *ISET J. Earthq. Technol.* **41**(1), 101–125 (2004)
3. Vision-2000, Conceptual Framework for Performance Based Seismic Engineering of Buildings. Sacramento, CA, USA, Structural Engineers Association of California (SEAOC) (1995)

4. FEMA-356, Prestandard and Commentary for the Seismic Rehabilitation of Buildings (2000)
5. Villaverde, R., M. Asce, and P.E., Methods to Assess the Seismic Collapse Capacity of Building Structures: State of the Art (2008)
6. H. Krawinkler, Challenges and progress in performance-based earthquake engineering (1999)
7. K. Park, Lateral load patterns for the conceptual seismic design of moment-resisting frame structures (2007)
8. A.S. Moghadam, W.K. Tso, *Pushover Analysis For Asymmetric And Set-Back Multi-Story Buildings* (2000)
9. J.M. Bracci, S.K. Kunnath, A.M. Reinhorn, Seismic performance and retrofit evaluation of reinforced concrete structures. *J. Struct. Eng. ASCE* **123**(1), 3–10 (1997)
10. P. Fajfar, M. Fischinger, in *Proceedings 9th World Conference of Earthquake Engineering*, Tokyo. A method for nonlinear seismic analysis of regular building (1988)
11. M.O. Eberhard, M.A. Sozwn, Behavior-based method to determine design shear in earthquake-resistant walls. *J. Struct. Div.* **119**(2), 619–640 (1993)
12. D. Lignos, E. Miranda, Estimation of seismic performance of existing steel moment resisting frame buildings by using continuous models, in *Improving the Seismic Performance of Existing Buildings and Other Structures*, p. 916–925 (2009)
13. UBC, Uniform Building Code (1997)
14. NEHRP, National Earthquake Hazards Reduction Program (2003)
15. C. Roeder, S. Schneider, J. Carpenter, Seismic behavior of moment-resisting steel frames: Analytical study. *J. Struct. Eng.* **119**(6), 1866–1884 (1993)
16. D.N. Aksoylar, A. Elnashai, H. Mahmoud, Seismic performance of semirigid moment-resisting frames under far and near field records. *J. Struct. Eng.* **138**(2), 157–169 (2012)
17. ATC-40, Seismic evaluation and retrofit of concrete buildings. (Redwood City, CA, USA), Appl. Technol. Council. 1–2 (1996)

Alkaline Activators Concentration Effect to Strength of Waste Paper Sludge Ash-Based Geopolymer Mortar

A. R. M. Ridzuan, A. A. Khairulniza, M. A. Fadzil, J. Nurliza,
M. A. M. Fauzi and W. M. F. W. Yusoff

Abstract The purpose of this study is to determine the effect of concentration of sodium hydroxide solution on the strength of Waste Paper Sludge Ash (WPSA)-based geopolymer mortar. Initially, the WPSA samples were been analyzed using X-ray Fluorescence (XRF) to determine the chemical composition. From the XRF analysis, the by-product WPSA manufactured from Malaysian Newsprint Industry (MNI), located at Mentakab Pahang, Malaysia containing higher amount of calcium, silica and alumina. Alkaline solution are from soluble sodium-based used in geopolymerization are combination of Sodium Hydroxide (NaOH) and Sodium Silicate (Na_2SiO_3). The specimens were carried out on size $50 \times 50 \times 50$ mm cube and fresh mortar were been cured at an oven temperature and ambient temperature. The compressive strength tests were conducted after aging the specimen at 3, 7, 14, and 28 days. The results revealed that as the concentration of NaOH increased, the compressive strength of geopolymer mortar increases. However, the optimum NaOH concentration of WPSA geopolymer mortar is at 12 M. More than 12 M concentrations of NaOH were produced high porosity and decreasing the strength. The range of Na_2SiO_3 to NaOH solution ratio by mass to produce high strength geopolymer mortar is 2.5. Moreover, curing of fresh WPSA geopolymer mortar is performed mostly at an oven temperature compared to ambient temperature due to heat being a reaction accelerator.

Keywords Waste paper sludge ash (WPSA) · Geopolymer mortar · Strength · Alkaline activator

A. R. M. Ridzuan (✉) · A. A. Khairulniza · M. A. Fadzil · J. Nurliza ·
M. A. M. Fauzi · W. M. F. W. Yusoff
Institute for Infrastructure Engineering and Sustainable Management, Faculty of Civil
Engineering, Universiti Teknologi MARA, 40450 Shah Alam, Selangor, Malaysia
e-mail: ruslanridzuan@yahoo.co.uk

1 Introduction

The production of Ordinary Portland Cement (OPC) releases large amount of carbon dioxide (CO_2) to the atmosphere that significantly contributes to global greenhouse gas emissions. One ton of CO_2 gas is released into the atmosphere for every ton of OPC produced. Currently, the world annual OPC production is about 7–8 % of the global loading of carbon dioxide into the atmosphere [1, 2].

By the year of 2010, the global cement consumption is to reach 2 billion tons, meaning that approximately 2 billion tons of CO_2 been released into the atmosphere. Therefore, world need an alternative binder to produce more environmentally friendly. An alternative binder is to target reduction in CO_2 emissions from cement for example in this present study used Waste Paper Sludge Ash (WPSA) to replace cement. The use of WPSA may reduce the total energy demand for producing cement, lower the emissions of greenhouse gasses into the atmosphere from the concrete industry, and recycle the WPSA that otherwise only disposed in landfill. In this view, the utilization of WPSA can make valuable contribution to the reduction of environmental impact from concrete industry.

In 1978, Joseph Davidovits [3] developed a binder called geopolymer. Geopolymer is a result of geopolymerisation process of silicon and aluminium from the source materials with alkaline solutions. In geopolymerisation, alkaline activator plays an important role. The most suitable alkaline solution used in geopolymerisation is a combination of sodium hydroxide or potassium hydroxide and sodium silicate or potassium silicate [4–7]. The choice of the alkaline solution mainly depends upon the reactivity and the cost of the alkaline solutions. Previous studies [5, 8–10] indicate that sodium silicate solution in combination with sodium hydroxide is an effective alkaline activator. Palomo et al. [5], in their study on fly ash based geopolymers has reported that the type of alkaline activator was the significant factor affecting the mechanical strength of geopolymers. They found that the combination of sodium silicate and sodium hydroxide produced the highest compressive strength.

Concentration of sodium hydroxide (NaOH) is the most important factor for geopolymer synthesis [11]. The solubility of aluminosilicate increases with increase in hydroxide concentration [12]. The use of higher concentration of NaOH yield higher compressive strength of geopolymer concrete [10].

Most of the previous studies on the engineering properties of geopolymer concrete or mortar are utilized fly ash based geopolymer. Very limited studies available on the properties of geopolymer mortar produced using WPSA based binder of geopolymer mortar. Hardjito et al. [13], Hardjito and Rangan [14] conducted study on the effects of sodium hydroxide concentration on the compressive strength of fly ash based geopolymer mortar reported that alkaline concentration was proportionate to the compressive strength of geopolymer mortar. They have claimed that higher concentration of sodium hydroxide solution result in a higher compressive strength of geopolymer mortar.

2 Materials and Experimental Details

2.1 Materials

In this study, high calcium WPSA from Malaysian Newsprint Industry (MNI) in Mentakab, Pahang, Malaysia, was used as the source material. The WPSA particles are spherical, and grey in color. The chemical composition of WPSA as determined by X-Ray Fluorescence (XRF) analysis, given in Table 1. Figure 1 shows the paper making process flow from MNI.

A combination of sodium hydroxide (NaOH) and sodium silicate (Na_2SiO_3) solution was used as the alkaline activators in this research. Distilled water was used to dissolve NaOH pellets to prevent any effect of unknown contaminants. The mass of the NaOH dissolved in distilled water varies according to the required concentration of solution. The range of NaOH concentration used in this research was between 8 and 14 M.

2.2 Mix Design, Preparation and Curing of Mortar Specimens

The mix proportions of high calcium WPSA geopolymer mortar in this study were changed at Alkaline Activator Ratio (Sodium Silicate with Sodium Hydroxide) and molarities of Sodium Hydroxide. WPSA was used 100% as a binder for this mortar. The Alkaline Activator Ratio of sodium silicate to sodium hydroxide solution ($\text{Na}_2\text{SiO}_3/\text{NaOH}$) by mass was 2.5 for all mixture proportions. The different molarities of Sodium Hydroxide to waste paper sludge ash are 8, 12 and 14 M. All mix design by weight. Mix Design: Sand—1,382 kg/m^3 , WPSA—503 kg/m^3 , Alkaline Activators—255 kg/m^3 and Water—adjustable. The total specimens that the present study were used are 108 cubes mortar. The high calcium WPSA geopolymer mortar was processed in about 12 batches because it depended on curing method and molarities of NaOH. Compressive strength testing was conducted based on BSEN 12390-4:2000 Testing hardened concrete: Compressive strength—Specification for testing machines.

3 Result and Discussion

Figure 2 showed the strength effect of alkaline activator with ratio 2.5 at different molarities/concentration of NaOH. The finding proved that salient parameters affect the low compressive strength of geopolymer mortar is high CaO content in WPSA. High CaO content occurred in WPSA is due to utilization of lime in the

Table 1 Chemical composition of WPSA as determine by XRF

Formula	WPSA (%)
LOI	12.6
CaO	53.1
SiO ₂	19.3
Al ₂ O ₃	9.03
MgO	2.31
Fe ₂ O ₃	1.25
SO ₃	0.53

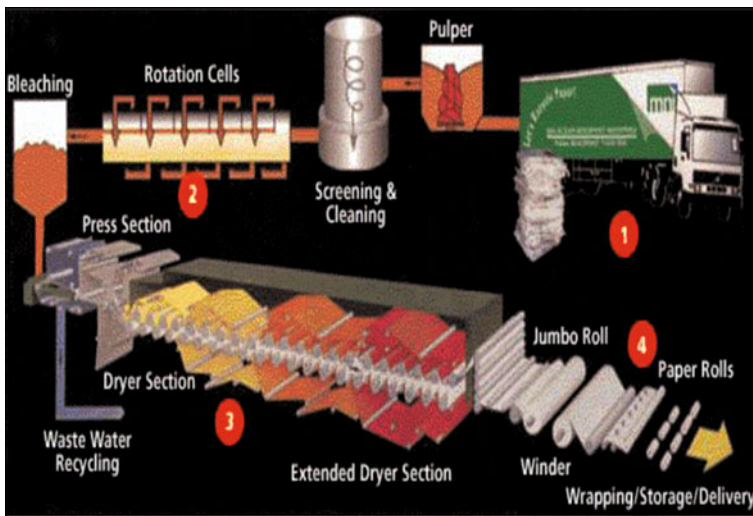


Fig. 1 Paper making process flow from MNI

whiteness, brightness, opacity, gloss, and smoothness process during production of paper. Graph show that 12 M NaOH is optimum molarities of WPSA geopolymer mortar compares to 8 and 14 M which is it gain highest strength up to 7.0 N/mm² at 28 days after oven curing. It was observed that an increase in compressive strength from 8 to 12 M but decreased from 12 to 14 M for all days of testing.

In normal geopolymer concrete as showed by Alonso and Palomo [15], it was evident that an activator with a 12 M of NaOH concentration led to better performances than 14 M of NaOH concentration due to an excess of OH⁻ concentration in the system involved a strength decrease of the alkali. This finding also been proven by Fadhil Nuruddin [16].

Based on Fig. 2, the compressive strength of concrete specimens increases as sodium hydroxide concentration in the aqueous phase increases from 8 to 12 M, however, it decreases with the further increase in sodium hydroxide concentration. It is accepted that an increase in alkali concentration enhanced geopolymerization

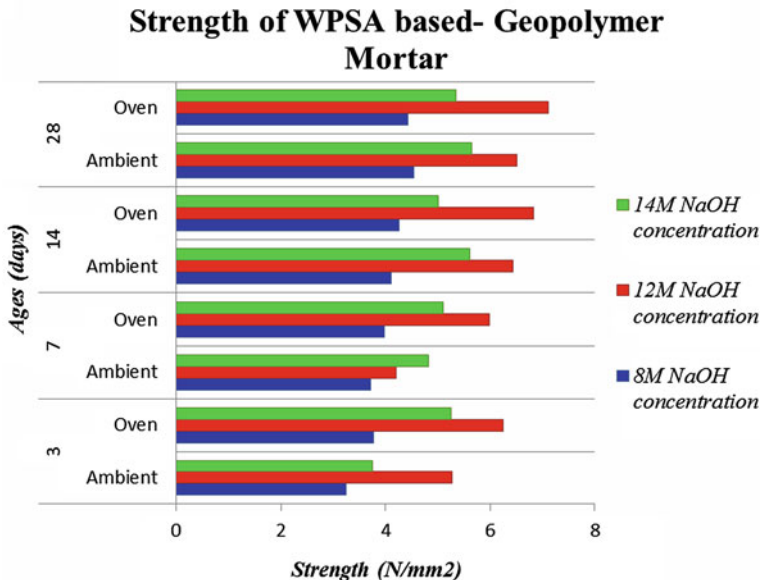


Fig. 2 Compressive strength of WPSA based geopolymer mortar with alkaline activators ratio 2.5

process resulting to an increase in the compressive strength of geopolymer. However, excess hydroxide ion concentration caused aluminosilicate gel precipitation at the very early stages, and subsequent geopolymerization was hindered, resulting in lower strength of geopolymer [17].

4 Conclusion

A higher concentration of sodium hydroxide in the aqueous phase proved to have positive effect on geopolymerization process and this is revealed by the improved compressive strength. However, an increase in the sodium hydroxide concentrations beyond 12 M caused negative effect on the geopolymerization resulting in lower the compressive strength. Based on the test results and subsequent discussions, the following broad conclusions can be drawn:

- Industrial by-products like WPSA can be advantageously used in producing geopolymer composites.
- In general, strength of WPSA geopolymer mortar increases with increase in alkaline activator ratio 12 M is optimum molarities of NaOH of WPSA geopolymer mortar.

- WPSA based geopolymer mortar can emerge as an eco-friendly and sustainable construction material and up to 7.0 N/mm^2 strength it can be used for the manufacture of compressed blocks/pavers.
- Based on Eurocode 6, minimum recommended compressive strength for material used as block or brick in unreinforced masonry is 5 MPa.

Acknowledgments Gratitude to the Ministry of High Education (MOHE) in providing the FRGS grant which initiated this project and to University Teknologi MARA (UiTM), and the Research Management Institute (RMI) with various facilities that helps in fulfilling towards completion of this research.

References

1. P.K. Mehta, Concrete technology for sustainable development. *Concrete Int.* **21**, 47–52 (1999)
2. V. M. Malhotra, High-performance high volume fly ash concrete. *Concrete Int.* **24**, 1–5 (2002)
3. J. Davidovits, Chemistry of geopolymeric systems, terminology, in *Proceeding of Geopolymer International Conference*, Saint-Quentin, France (1999)
4. B.V. Rangan, Fly ash-based geopolymer concrete. Research Report GC 4, Faculty of Engineering, Curtin University of Technology, Perth, Australia (2008)
5. A. Palomo, M.W. Grutzeck, M.T. Blanco, Alkali-activated fly ashes—A cement for the future. *Cem. Concr. Res.* **29**(8), 1323–1329 (1999)
6. H. Xu, J.S.J. van Deventer, Geopolymerisation of multiple minerals. *Miner. Eng.* **15**(12), 1131–1139 (2002)
7. V.F.F. Barbosa, K.J.D. MacKenzie, C. Thaumaturgo, Synthesis and characterization of materials based on inorganic polymers of alumina and silica: Sodium polysialate polymers. *Int. J. Inorg. Mater.* **2**(4), 309–317 (2000)
8. H. Xu, J.S.J. Van Deventer, The geopolymerisation of aluminosilicate minerals. *Int. J. Miner. Process.* **59**(3), 247–266 (2000)
9. A. Fernandez-Jimenez, A. Palomo, M. Criado, Microstructure development of alkali-activated fly ash cement: A descriptive model. *Cem. Concr. Res.* **35**(6), 1204–1209 (2005)
10. D. Hardjito, S.E. Wallah, D.M.J. Sumajouw, B.V. Rangan, On the development of fly ash-based geopolymer concrete. *ACI Mater. J.* **101**(6), 467–472 (2004)
11. F. Puertas, S. Martinez-Ramirez, S. Alonso, T. Vazquez, Alkali activated fly as/slag cements: Strength behaviour and hydration products. *Cem. Concr. Res.* **30**(10), 1625–1632 (2000)
12. H.A. Gasteiger, W.J. Frederick, R.C. Streisel, Solubility of aluminosilicates in alkaline solutions and a thermodynamic equilibrium model. *Ind. Eng. Chem. Res.* **31**(4), 1183–1190 (1992)
13. D. Hardjito, C.C. Cheak, I.C.H. Lee, Strength and setting times of low calcium fly ash-based geopolymer mortar. *Mod. Appl. Sci.* **2**(4), 3–11 (2008)
14. D. Hardjito, B.V. Rangan, Development and properties of low calcium fly ash based geopolymer concrete. Research Report GC 1, Faculty of Engineering, Curtin University of Technology, Perth, Australia (2005)
15. S. Alonso, A. Palomo, Alkaline activation of metakaolin and calcium hydroxide mixtures: Influence of temperature, activator concentration and solid ratio. *Material Letters* **47**(1–2), 55–62 (2001)

16. M.F. Nuruddin, S. Demie, M.F. Ahmed, N. Shafiq, Effect of superplasticizer and NaOH molarity on workability, compressive strength and microstructure properties of self-compacting geopolymer concrete, world academy of science. Eng. Technol. 74 (2011)
17. A.M. Mustafa Al Bakri, H. Kamarudin, M. Bnhussain, I. Khairul NizarI, A.R. Rafiza, Y. Zarina, Microstructure of different NaOH molarity of fly ash based green polymeric cement. J. Eng. Technol. Res. 3(2), 44–49 (2011)

Seismic Performance of Laminated Rubber Bearing Bridges Subjected to High Intensity Earthquake Time-History Loading

Wan Noor Azhar Wan Sulaiman and Norliyati Mohd Amin

Abstract Malaysia needs to be more aware of the seismic effect on the infrastructure facilities especially on the bridge structure located in the dense population which is prone to the earthquake especially in Peninsular Malaysia. If the bridges fail in the event of earthquake, the rescue and relief effort will be halted. The most common strategy to enable the bridge sustain under the seismic loading is by using base isolator. Base isolator will reduce the reaction of the seismic force to the bridge. At present, the studies of the numerical modeling using 3D solid element are minimal. In this paper, the Finite Element Analysis using 3D solid element was chosen because it increases the accuracy of analysis result. In order to obtain the details response of the laminated rubber bearing (LRB), transient analysis was done under Kobe earthquake excitation. Structural damage in the form of permanent deformation is unavoidable. The failure of the laminated rubber bearing will made the superstructure's weight disable to provide a reasonable balance between shear force transmitted to the pier and displacement of the bridge deck. It was also found that the high value of displacement occurred at the elastomer in the laminated rubber bearing under Kobe earthquake excitation.

1 Introduction

Malaysia is bordered by Sumatra and Philippines, which are the seismic sources zone. Malaysia has felt tremors several times due to the earthquake event originated from both countries especially in Peninsular Malaysia region.

W. N. A. W. Sulaiman (✉)

Faculty of Civil Engineering, University Technology MARA, Shah Alam, Selangor, Malaysia

e-mail: 2011386711@isiswa.uitm.edu.my

N. M. Amin

Institute for Infrastructure Engineering and Sustainable Management IIESM, University Technology MARA, Shah Alam, Selangor, Malaysia

e-mail: norli830@salam.uitm.edu.my

The earthquake event is originated from the intersection areas of Eurasian plate and Indo-Australian plate near Sumatra. Relatively, Malaysia is far away from seismic Sumatra zone but it is recorded that the nearest earthquake epicenter from Malaysia is approximately 350 km. The distance of the epicenter is almost same with the Mexico City earthquake in 1985 which it caused seriously damaged to the Mexico City. The 8.1 magnitude of the quake struck the Mexico City. The effects of the quake were particularly devastating because the city sits atop a combination of dirt and sand. These combinations are much less stable than bedrock and quite volatile during an earthquake occurred. Almost Klang Valley areas also sit atop of filling area which comprised of sand. Due to the above fact, Malaysia needs to be more aware to the seismic effect on the infrastructure facilities especially bridge structure at the location of high population. The bridge acts as an important link in transportation network. If the bridges fail due to the earthquake event, the relief and rehabilitation work will cripple. There are many cases the failure of bridges around the world such as Santa Clara River Bridge pounding damage in 1994 Northridge earthquake, Nishinomiya-ko Bridge due to the Hyogo-Ken Nanbu earthquake in 1995 and the Kobe earthquake in 1995 lead to destructive damage to the highway bridge.

2 Overview

Dynamic analysis is the main analysis in order to know the behavior of the structural subjected to earthquake excitation. Earthquake is classified as the non-periodical loading because the loading in irregular condition. The loading vary with time induced from ground motion. Ground motion is represented by the time history or seismograph in terms of acceleration, velocity and displacement for a specific location during an earthquake. Time history can be plotted in three dimension x , y and z . From the analysis, it can provide several informations that significant for design. For example, value of forces, moment and displacement will be obtained from the structural analysis. There are several methods in the dynamic analysis that suitable for the bridge structure under earthquake excitation. However, the time-history method was used in this study by using the actual earthquake time-history. The time-history method is a numerical step-by-step integration of equations of motion. It is usually required for critical or important or geometrically complex bridges.

Based on Powel [1], the selection of the analysis method is depending on the effective design decision. The selection must be suitable with complexity of bridge structure besides the local condition of the site. Therefore, for this study, time-history method of analysis is considered. This is because this study involving investigation of bridge element response in x , y and z direction subjected to Kobe earthquake time-history loading.

3 Transient Analysis

Since this study is related to the time-history analysis, it involved a method of analysis so called transient dynamic analysis. A transient dynamic analysis is a technique which is used to determine the time history dynamic response of a structure to arbitrary forces varying in time. On the right hand side of Eq. (1) any function for the load vector may be specified, i.e. $\mathbf{p}(t) = \mathbf{p}(t)$. This type of analysis yields the displacement, strain, stress and force time history response of a structure to any combination of transient or harmonic loads. To obtain a solution for the equation of motion (1) time integration has to be performed.

$$m\ddot{u}_t + c\dot{u} + ku = -mu_g \quad (1)$$

where k is the spring constant; \ddot{u}_t is the acceleration; \dot{u} is the velocity; u is the displacement; u_g is the ground acceleration; c is the damping ratio and m is the mass of dynamic system.

They can be broadly classified into implicit and explicit methods. Considering the stability of these two types of integration methods we notice that implicit methods are usually unconditionally stable which means that different time step sizes can be chosen without any limitations originating from the method itself.

Explicit methods on the other hand are only stable if the time step size is smaller than a critical one which typically depends on the largest natural frequency of the structure. Due to the small time step necessary for stability reasons explicit methods are typically used for short-duration transient problems in structural dynamics [2].

Based on the facts, implicit method has been used whereby there is no limitation to choose different time steps size for load vector input. The reason is because the load vectors input for this study represent the earthquake excitation with uncertainty different time step size.

Newmark's Method is used as numerical evaluation of dynamic response. This method is developed by N. M. Newmark in 1959. The method involved a family of time-stepping methods based on the following equations:

$$\dot{u}_{i+1} = \dot{u}_i + [(1 - \gamma)\Delta t]\ddot{u}_i + (\gamma\Delta t)\ddot{u}_{i+1} \quad (2)$$

$$u_{i+1} = u_i + [\Delta t]\dot{u}_i + \left[(0.5 - \beta)(\Delta t)^2 \right] \ddot{u}_i + \beta(\Delta t)^2 \ddot{u}_{i+1} \quad (3)$$

The parameter of β and γ define the variation of acceleration over a time step and determine the stability and accuracy characteristics of the method. Typical selection for γ is $1/2$ and $1/6 \leq \beta \leq 1/4$ is satisfactory from all points of view including that of accuracy. These two equations are combined with Eq. (1) at the end of the time step. It provide the basis for computing u_{i+1} , \dot{u}_{i+1} , \ddot{u}_{i+1} at time $i + 1$.

This method is very useful in order to determine the deformation response of the bridge structural element in x , y and z direction subjected to Kobe earthquake

Fig. 1 Girder falling in Lauhan bridge [4]



time-history loading. Newmark's Method is known as implicit method as the current time i is used at the end of the time step.

4 Earthquake Damage to Bridge

As bridge element is the vital link in transportation system, earthquake damage to bridge caused severe consequence. Therefore, understanding of the causes of damage is very important in order to overcome the damages through analysis and design consideration. Three general types of damages normally occur to the bridge due to the earthquake:

- a. Displacement in all direction (transverse, longitudinal and vertical)
- b. Exceeded reaction forces at connection system, and
- c. Inelastic structural response to the bridge components.

The most destructive of the bridge damages is the bridge deck collapse from the pier. Superstructures are designed to support service gravity load and lateral load for earthquake excitation. The superstructure is supported by bearing and pier. Superstructure consists of post stress beam and slab. The combination between those elements is called bridge deck. The bridge deck collapse or unseating from the pier and abutment is because of the relative displacement between bridge deck and pier. Figure 1 shows the example of how the bridge deck collapse.

The movement of the superstructure leads to failure of the bearing. When the bearing fails the superstructure tend to rotate and collapse. This can be seen as in Fig. 2 Nishinomiya-ko bridge bearing failure in the 1995 HyogoKen Nanbu earthquake.

Some bridges, the bearing is used to sustain with the force in one or two directions. At the same time it allows the movement in one or two direction. Therefore, when the bearing failed in an earthquake as in Fig. 3 it caused the

Fig. 2 Nishinomiya-ko bridge bearing failure in the 1995 HyogoKen Nanbu earthquake [5]



Fig. 3 The rubber bearing pad is dislocated [4]



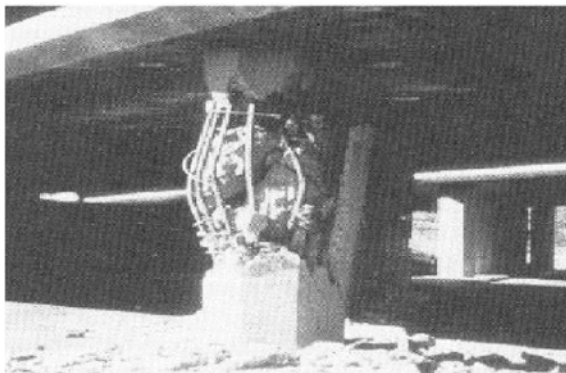
distribution of internal force between superstructure and substructure in unbalance condition.

The reinforcement ratio of stirrup is not enough, and the buckling of the main steel will result in the crushing of core concrete, then the pier could not be able support the upper loads from the bridge deck. This condition can be seen in Fig. 4.

5 Bridge Model

The existing bridge has been selected in order to investigate the capability of LRB that has been used in bridge subject to earthquake loading. The Kajang-Seremban Highway bridge is selected for this study to represent bridge model to conduct a linear dynamic time history. The bridge used Laminated Rubber Bearing which is

Fig. 4 Pier failure of viaduct in Northridge Earthquake [4]



aligned with this study to investigate the displacement of the LRB subjected to the Malaysia earthquake time-history loading. The bridge is selected also due to the availability of structural drawing and mechanical properties of structural elements.

The details of the bridge structural elements as in Fig. 5. The bridge is simply supported bridge using post stress beam. The abutment type is seat abutment. It is single span with length of 44,000 mm. However, the abutment is formed with column and crosshead beam. The Laminated Rubber Bearing is used with dimension 400×400 mm. The width of the deck is 15,300 mm where by it can be considered as R5 road geometry class. All the design consideration is based on BS 5400:2006.

The entire structural model is based on the existing bridge. The materials properties of the bridge as in Tables 1 and 2.

Kobe Time History loading was used in this study because the magnitude of quake is 7.0 M and availability of the earthquake data. The form of earthquake loads depends on the type of analyses. In this study, one synthetic sample of time history in x, y and z axis has been used. The data will be applied for the time-history analysis using Ansys software for this study. The time—history data is in acceleration versus time as in Fig. 6. The data is obtained from the Pacific Earthquake Engineering Research Centre (PEER).

6 Finite Element Analysis

The seismic analysis of Kajang—Seremban Highway is implemented by using Finite Element software in three dimensional modelling. All the structural members are used 3D solid element types hexahedral elements as in Fig. 6. The total Hexahedral elements that have been applied in the model are 67,000 elements (Fig. 7).

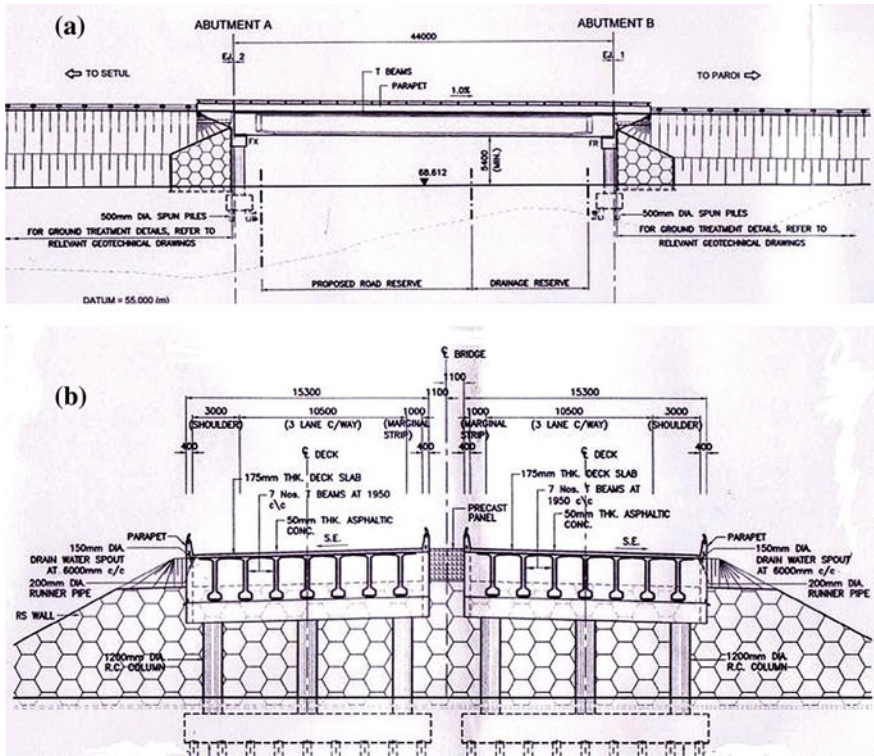


Fig. 5 The details of the bridge structural elements. a Elevation view. b Section view

Table 1 Material properties of each element in bridge model

Types of material	Young's modulus (kN/mm ²)	Poisson's ratio	Density (kg/m ³)
Post stress concrete	34	0.15	7,874
Rubber	0.01	0.4999	910
Reinforced concrete	31	0.15	2,400

All the elements in the model are using linear elastic properties. The bridge superstructure including the post stress beam and concrete deck were presented using linear elastic elements. Nominal properties were used for both post stress beam and concrete deck with the post stress beam having a modulus of elasticity of 34 kN/mm² and concrete deck having a modulus equal to 31 kN/mm².

Substructure elements were included in the computational models. Included in the substructure models were the abutment, column, crosshead beam and footing. Modulus of elasticity that has been assigned to the substructure elements is 31 kN/mm². The piles are not considered in this analysis. Fixed support is assigned at the bottom of footing. Soil—structure interaction was not considered at the behind of abutment since this study limited to the linear analysis.

Table 2 Laminated rubber bearing properties

Types	Dimension $L \times B \times t$ (mm)	Compressive stiffness (kN/mm)	Shear stiffness (kN/ mm)	Natural rubber thickness		Steel plate		Shape factor, S
				Inner slab t_1 (mm)	Outer slab t_0 (mm)	Nos	Thickness t_s (mm)	
Laminated rubber bearing	$400 \times 400 \times 50$	67	0.9	12	6	3	2	6.07

Fig. 6 Time-history Kobe earthquake

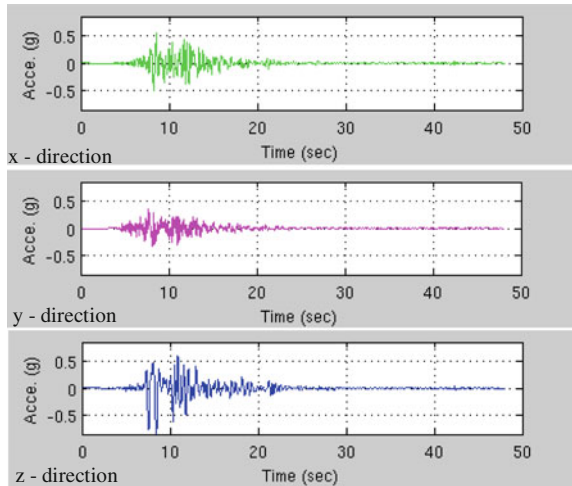
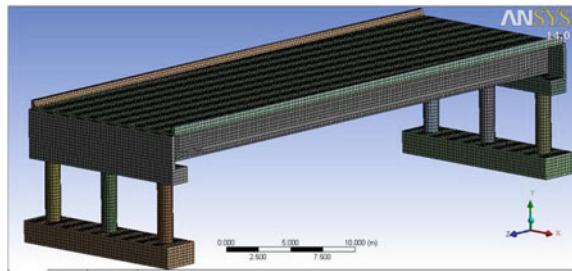


Fig. 7 Finite element modelling



Laminated Rubber Bearing also was modelled using solid element. The elastomer is modelled by using modulus of elasticity of 0.01 kN/mm^2 . While steel shims inside the elastomer using a modulus equal to 210 kN/mm^2 .

Figure 8 shown the numbers of degree of freedom is increased at the laminated rubber bearing in order to obtain the approximate result of the deformation under seismic loading.

Full transient analysis has been done in this study to define the behaviour of bearing under specified time history earthquake loading. However, modal analysis still needed in order to find the Rayleigh Damping for the bridge model. The purpose to conduct modal analysis is to obtain the natural frequency of the bridge and the mode shape. These two data are useful to find the value of Rayleigh Damping. Since the value of damping ratio is difference between of the other system or bridge therefore damping could be idealised as proportional to the stiffness of the structure. It is assumed that a portion of the energy is lost due to the deformation of the structure.

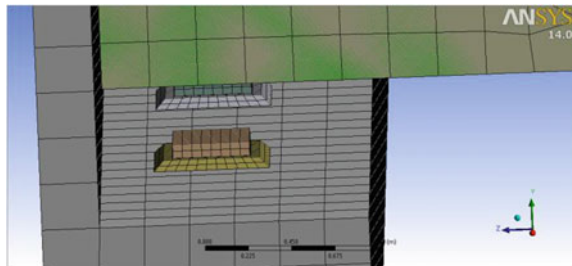
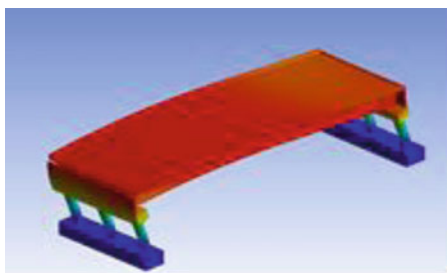


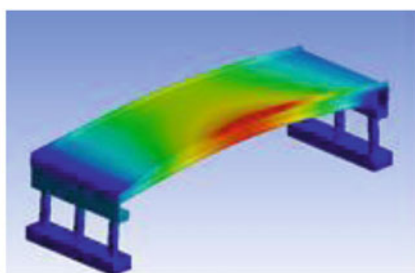
Fig. 8 Increasing discretisation of elements at the laminated rubber bearing

Table 3 Modes and frequency of the bridge

Modes	Frequency (Hz)
1	7.5756
2	8.1896
3	9.1494
4	12.153
5	16.176
6	16.344



Mode Shape 1



Mode Shape 2

Fig. 9 Mode 1 and 2

Damping is accounted for the model using 1.3 % [3]. Modal analysis was done by using Ansys software. The frequency and mode shape gave result as in Table 3. The analysis considered six modes. The shapes of the modes are as in Figs. 9, 10 and 11.

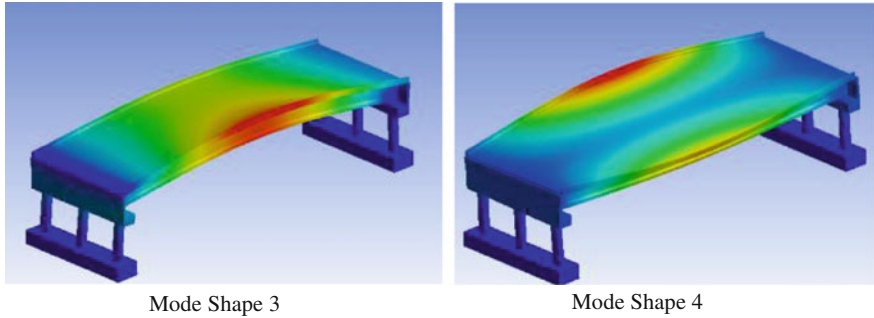


Fig. 10 Mode 3 and 4

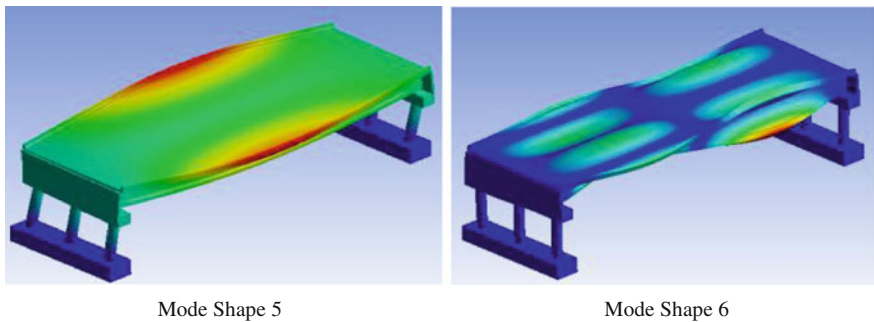


Fig. 11 Mode 5 and 6

7 Displacement Response

From the time-history analysis, displacement response of the bridge has been simulated. The graph displacement responses versus time were generated. Response of the bridge structural element can be observed from the graph based on the time-history earthquake excitation. It was found that the displacement response under Kobe is bigger since the bridge is not applied seismic design. The displacement response (in mm unit) of the laminated rubber bearing can be seen through the graph as in Fig. 12. The displacement in z direction gave the biggest value.

The maximum horizontal displacement is 381.29 mm under Kobe earthquake excitation. The Table 4 show the result has been obtained. The existing of LRB is designed to sustain with limit of displacement 34.92 mm in z direction. Based on the result, the LRB could not be able to sustain under the earthquake excitation (Fig. 13).

Laminated Rubber Bearing deformed to the maximum level under Kobe earthquake excitation. The deformation occurred due to the overturning of the structure.

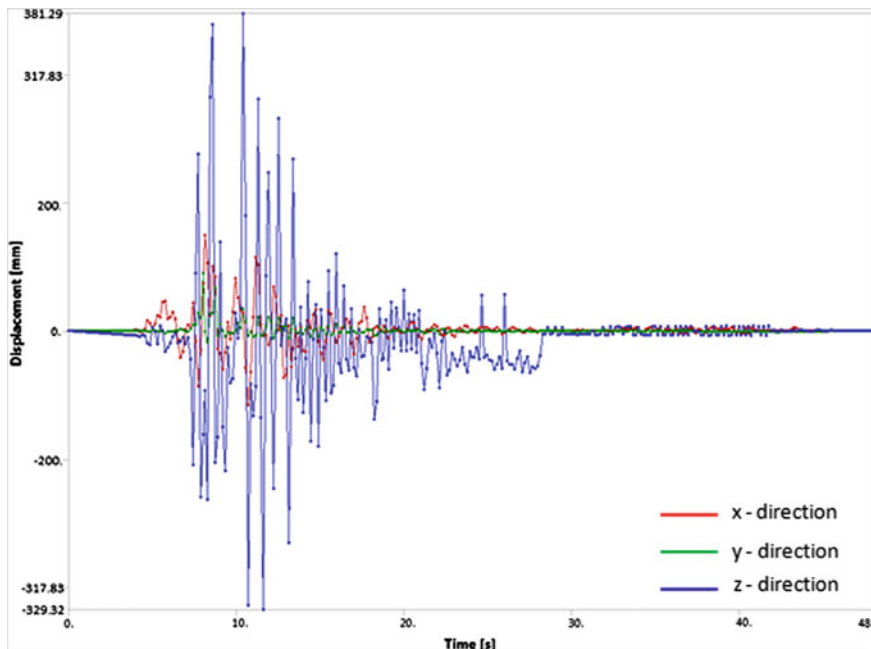


Fig. 12 Displacement responses of laminated rubber bearing subjected to Kobe earthquake time-history loading

Table 4 The result for the maximum displacement of the LRB in x, y and z direction subjected to Kobe earthquake loading intensity

Earthquake loading	Laminated rubber bearing displacement response (x-axis) (mm)	Laminated rubber bearing displacement response (y-axis) (mm)	Laminated rubber bearing displacement response (z-axis) (mm)
Kobe	189.46	101.23	381.29

It was also accompanied by the lateral shear exist between the steel plate and elastomer. Since the shear deformation is high it induce top of LRB to move upward by larger displacement. The LRB totally failed as the designed displacement value is only 1.59 mm in y-direction. The failure of the laminated rubber bearing will made the superstructure’s weight disable to provide a reasonable balance between shear force transmitted to the pier and displacement of the bridge deck. As a result the superstructure is dislocated or pounding from the abutment as in Fig. 1.

The Von Mises stresses is adopted to define the behaviour at pier. Time step at 10.4 s generates the high value of stress response. Based on Fig. 14, high stress occurred at the bottom of the pier. That was occurred when the laminated rubber bearing disable to provide a reasonable balance between shear forces transmitted to the pier and displacement of the bridge deck.

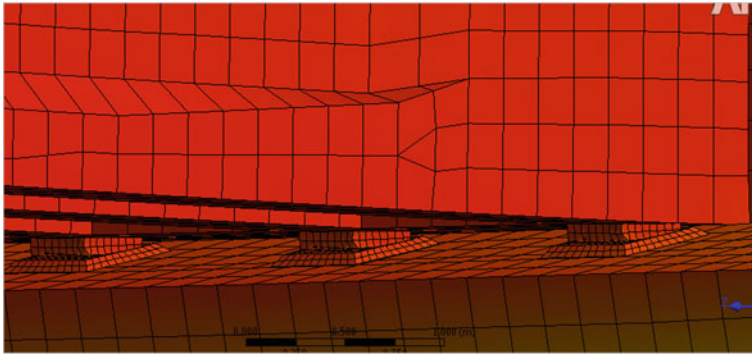


Fig. 13 The laminated rubber bearing deformed under Kobe earthquake excitation

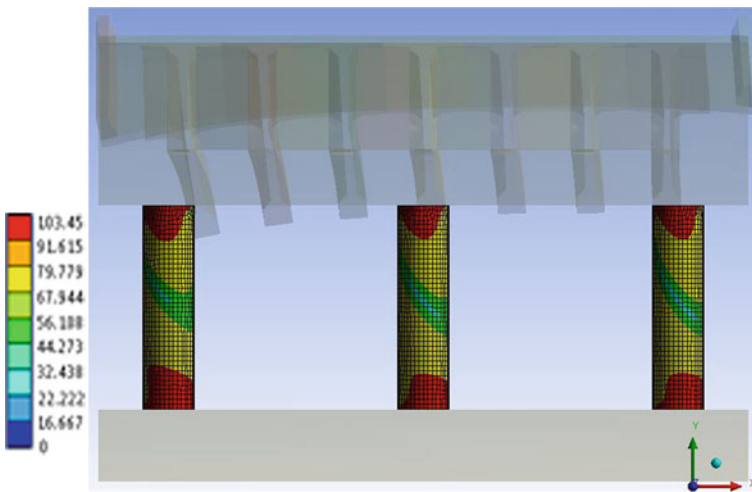


Fig. 14 Von Mises stress response (MPa) at pier subjected to Kobe earthquake at time step 10.4 s

8 Conclusion

A details study on rubber bearing is needed in earthquake engineering and bridge study to define the behaviour of bearing under ground motion. All direction of rubber bearing displacement can be studied by using 3D solid elements. A time-history analysis using Newmark's Method is very useful in order to obtain the response of rubber bearing and the whole structure for a specified time history of excitation.

From the analysis, several conclusions can be made regarding to the displacement behaviour of the rubber bearing such as listed below:

- a. The selected bridge can sustain under earthquake up to time step at 7.2 s.
- b. The maximum displacement of the laminated rubber bearing occurred at time step 10.4 s.
- c. The high stress of pier occurred at time step 10.4 s.
- d. The displacement of rubber bearing can be studied at specified time history earthquake loading through time history analysis.

Acknowledgments The authors wish to acknowledge the support of the University of Technology MARA (UiTM) and Faculty of Mechanical (UiTM). This work was done under the Exploratory Research Grant Scheme (ERGS), Ministry Higher Education Malaysia (MOHE). McMaster University.

References

1. G.H. Powell, Concept and principles for the application of nonlinear structural analysis in bridge design. Report No. UCB/SEMM-97/08, Department of Civil Engineering, University of California, Berkeley, 1997
2. E. Wang, T. Nelson, *Structural Dynamic Capabilities of Ansys* (CADFEM GmBH, Germany, 2002)
3. T. Katayama, A review of theoretical and experimental investigation of damping in structures. UNICIV Report No. 1–4, University of New South Wales, Sydney, Australia, 1965
4. W. Zhang, L. Yang, Analysis and inspiration on typical damage characteristic of bridges. *Appl. Mech. Mater.* **147**, 315–319 (2012)
5. W.F. Chen, L. Dan, *Bridge Engineering Seismic Design*, (CRC Press, Boca Raton, 2003)

Chemical Characterization of Used Cooking Oil Foaming Agent as Admixture in Foamed Concrete

M. M. A. Hafiz, A. R. M. Ridzuan, M. A. Fadzil and J. Nurliza

Abstract In order to reduce waste materials to be disposed, the new created used cooking oil foaming agent is created. This formulated is categorized as foaming agent admixture for foamed concrete applications. The sample had been collected at nearest restaurants located in Seksyen 7, Shah Alam, Selangor. To become foaming agent it must pass through specific process of formulation. Then, for chemical analysis is intention to characterize and screening chemical compounds of waste cooking oil. For this purposes, FTIR and EDAX which chemical instrumentations are been used. Chemical functional groups analysis for liquid foaming agent is done by FTIR. EDAX analysis specifically for solid material of foamed concrete. From the results FTIR analysis shown lipid groups are the major chemical functional groups. Meanwhile from EDAX analysis results, was shown the Calcium is the highest elements for both used cooking oil foamed and synthetic foamed concrete.

Keywords Used cooking oil · Foaming agent · Characterization · Analysis · Foamed concrete

1 Introduction

In line with Malaysia has abundant supply of palm oil, and now it is a good time to take part to deal with this renewable resource. By utilization of used cooking oil will help to reduce the waste disposal problems and also to avoid environmental pollutions [1]. Due to the environmental issues, here an intention to create new foaming agent admixture in order to utilize the waste from food industries.

M. M. A. Hafiz (✉) · A. R. M. Ridzuan · M. A. Fadzil · J. Nurliza
Institute of Infrastructure Engineering and Sustainable Management (IIESM), Faculty of Civil Engineering, Universiti Teknologi MARA, 40450 Shah Alam, Selangor, Malaysia
e-mail: mohdhafizmdali@gmail.com

The admixture applications are wide but it depends on what purposes to be added in concrete. Admixtures are will mix into concrete that contribute for unique characteristic on the concrete properties, behavior of concrete during fresh and harden and also have potential to affect the durability and mechanical of the concrete. Other than that, admixture is one of others added materials that to enhance the properties of the concrete which where to increase the workability, enhance rheological and adsorption of cement paste [2].

In this particular research will discover the characterization of formulated used cooking oil foaming agent for it major components and compare with other foaming agent such as protein and synthetic. For characterization, it might involve in chemical functional group analysis by fourier transform infra red FTIR instrumentation. Whereas for element identification will involve with energy dispersive x-ray EDAX which for analyzing the lightweight foamed concrete from new formulated used cooking oil with synthetic foamed concrete.

2 Materials and Method

2.1 Sample Collection and Filtration

Waste from used cooking oil was collected from nearest restaurant at Shah Alam, Selangor. These restaurants have involved in food preparation for every day and was produced a lot of used cooking oil. The food preparations in these particular restaurants were practically use palm oil mostly purposes for food frying. The impurities and oxides compounds present in used cooking oil also differ due to the different materials usages and high temperatures were applied during the food preparations.

First stage of this study is to characterize the chemical composition of used cooking oil by comparing it with palm oil, protein and synthetic foaming agents. The purpose of characterization the chemical elements are to compare and ensure for better understanding toward chemical functional groups among foaming agent and it elements present when in the concrete formed. For characterizing of chemical functional groups, analytical instrumentation is very helpful. Fourier Transform Infrared FTIR is required to perform this kind of analysis. Usually, samples strictly to be treated before it to be analyzed. Meanwhile the EDAX analysis has begin use for all foamed concrete that were used the same types foaming agents for FTIR analysis. All sample need to be coated with gold before it begin analyze by EDAX.

2.2 Formulation Used Cooking Oil Foaming Agent

For formulation process, the used cooking oil is required to be treated by filtration process. This steps is aim to remove the coarse solid materials and small debris

resulted from the food preparation. The initial steps of process is used cooking oil sample is keep in 30 L plastic drum at room temperature until ± 48 h. At the same time, the settlement process took part and function to allow the separation between suspended solid with used cooking oil by gravity. Next is where the filtration process to be proceed after the settlement process done at first step. This treatment process is involved with double stages of filtration. All the treated sample of used cooking oil will be stored into plastic drum. The formulation is started from treatment of used cooking oil until at final stage where the chemical formulation involved. The final formulation is achieved when the formulation will be able to become foam structure which so called foamability.

2.3 Chemical Characterization

The chemical screening is for characterization of the samples. Fourier Transform Infra Red spectroscopy FTIR is the instrument to analysis the functional group contain in the samples [3]. The observation done by FTIR was based on the wavelength value cm^{-1} and elucidation process based on the standard correlation chart [4]. The FTIR analysis is classified as non destructive which the sample been introduced can be collected and could be reuse for others purposes. For solid samples of these foamed concrete is begin analyze by EDAX which it based on the weight percent value of x-ray dispersive energy.

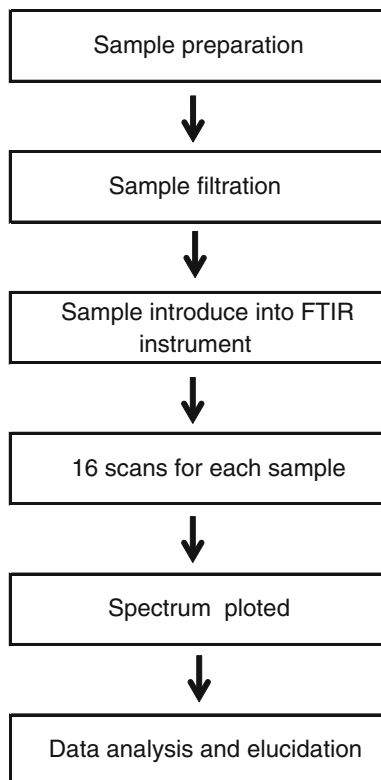
2.4 FTIR Analysis

The FTIR instrumentation is very useful and versatile for chemical functional groups characterization. This instrument easy to handle but the sample required pass through the sample preparation. The step by step of sample preparation is show in Fig. 1. The sample preparation intention to ensure only treated sample will be introduced into the instrument.

2.5 EDAX Analysis

Solid sample from foamed concrete will be introduced into the Field Emission Scanning Electron Microscopy FESEM-EDAX instrument then based on the morphology images the EDAX analysis is begin start by selecting the possible spot point on the sample through image captured by the FESEM.

Fig. 1 The sample preparation before the sample introducing into the FTIR instrumentation



3 Results

3.1 Chemical Functional Groups FTIR Analysis

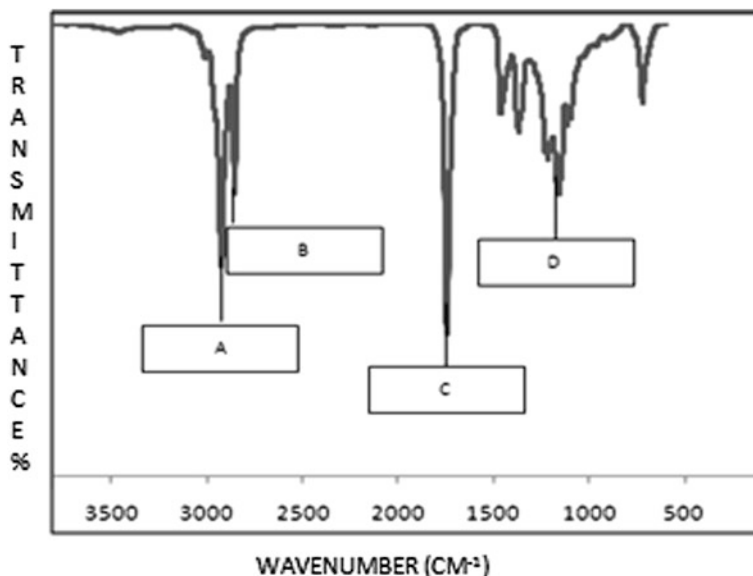
The each sample of used cooking oil, palm oil, protein and synthetic foaming agent has been characterize by using FTIR. This chemical instrumentation capable to analyze the sample then spectrum shown the possible functional groups of each sample by observing the peak spectrum produced. All the spectrums has been interpreted based on the frequency cm^{-1} (wavelength) and the possible functional groups have been stated based on the correlation chart [4].

Table 1 shown the functional groups of chemical compounds in used cooking oil based on the spectrum produced at Fig. 2.

Spectrums has been shown at Fig. 2 is representing the treated used cooking oil where the impurities and all solid materials has been discarded since the treatment took part before it will be introduced for FTIR analysis. This process is to ensure only proper and pure sample will be continued for the analysis. If the samples are not pure and well treated, it may alter and give negative end results. Due to these

Table 1 Functional groups of chemical compounds in used cooking oil

Label	Peak observe	Frequency (cm^{-1})
A	CH_2 —antisymmetric stretch of methylene group of membrane phospholipids	2928–2930
B	CH_3 stretch	2830–2750
C	$\text{C}=\text{O}$	1750–1736
D	$\text{C}-\text{C}$ stretch proline	850–750

**Fig. 2** The FTIR spectrum of used cooking oil

reason, each sample need to pass through the sample preparation that been mentioned on Fig. 1.

The analysis shown the spectrum for treated used cooking oil and four selected peaks has been elucidated. The wavenumber cm^{-1} range of this particular sample is between 500 and 3000. As refer to Table 1, about four functional groups were detected. The peaks is observed at 2928–2930 is CH_2 , the rest are CH_3 , $\text{C}=\text{O}$ and $\text{C}-\text{C}$ which are has been detected in the range between of 2830 and 750 respectively. After FTIR analysis, the possible elements present are stated in Table 1.

AS referred to the Fig. 3, the spectrum is produced is differ with the Fig. 2. Even the basis compounds of both samples are the same source. However, due to frying and food preparation may have change the properties of palm oil become used cooking oil. From the observation, the broad peak in Fig. 2 is O–H has been detected at wavenumber cm^{-1} 3400–3350. This broad spectrum present in palm oil but not in used cooking oil spectrum in Fig. 2. Based on the elucidation result

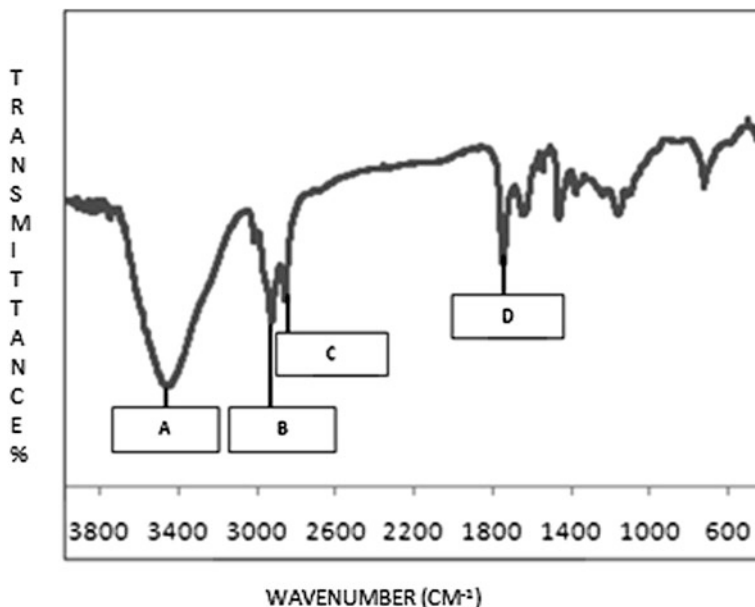


Fig. 3 The FTIR spectrum of palm oil

Table 2 The analysis of functional groups of palm oil

Label	Peak observe	Frequency (cm^{-1})
A	O-H broad peak	3400–3350
B	C-H, lipids	3000–2980
C	C-H ₃ , lipids protein	2875–2800
D	C=O, lipids (ester)	1720–1750

Table 3 The frequency cm^{-3} (wavelength) of protein foaming agent

Label	Peak observe	Frequency (cm^{-1})
A	N-H stretch	3250–3200
B	C=O, lipids	1720–1745
C	Amide III, proteins	1330–1200
D	-CO-O-C	1170–1070

on Table 2 the sample is obviously has contain mainly lipids compounds. It is clearly stated from wavenumber cm^{-1} 3000 to 1750 containing the functional group of C-H, C-H₃, C=O and all have been classified as lipid groups.

Table 3 shown the frequency cm^{-3} (wavelength) of protein foaming agent and the peak observes have been stated for each Wavenumber cm^{-1} .

Figure 4 shown the spectrum for protein foaming agent is begin appeared start at 1000 until to the highest at about 3250–3200 wavenumber cm^{-1} which where

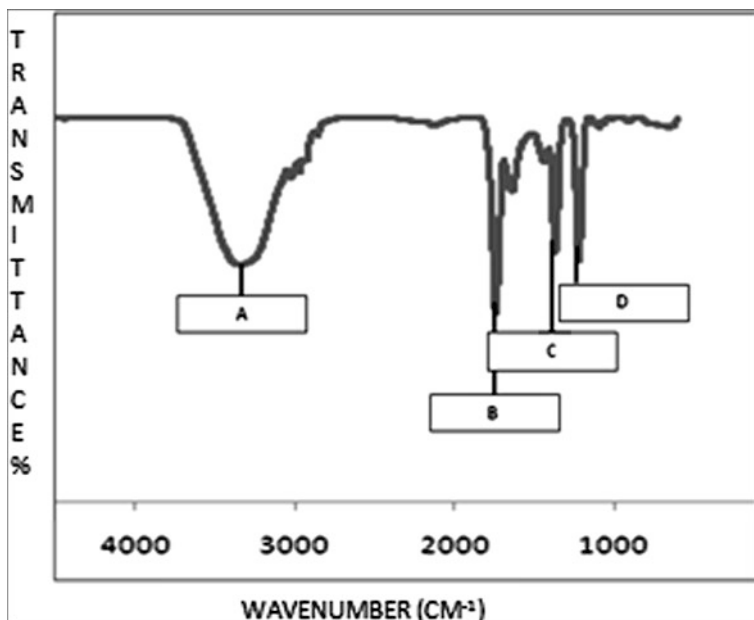


Fig. 4 The IR spectrum of protein foaming agent

Table 4 The elucidation of spectrums from the FTIR analysis of synthetic foaming agent

Label	Peak observe	Frequency (cm^{-1})
A	N-H stretch	3250–3200
B	C-H, lipids	3050–3000
C	C=O, lipids (esters)	1745–1720
D	Amide III, proteins	1200–1330

the broad spectrum at is produced. The broad spectrum is revealed as N–H stretch. Whereas other peaks that been observed in the Table 3 are C=O, Amide and CO–O–C at wavenumber cm^{-1} between 1720 and 1070. From the results of peak observed, varieties of functional groups have been detected and each peak located and appear at difference range of wavenumber cm^{-1} (Table 4, Fig. 5).

The spectrum of synthetic foaming agent is shown in the range of wavenumber cm^{-1} between 3250 until 1330. Based on the elucidation of the spectrum from the Fig. 6 has shown the broad spectrum was detected at the wavenumber cm^{-1} 3250–3200 is N–H stretch. Followed with others functional which at the peak 3050–3000 wavenumber cm^{-1} is C–H. For the rest functional groups are C=O and Amide which has been detected at different wavenumber cm^{-1} between 1745 and 1330.

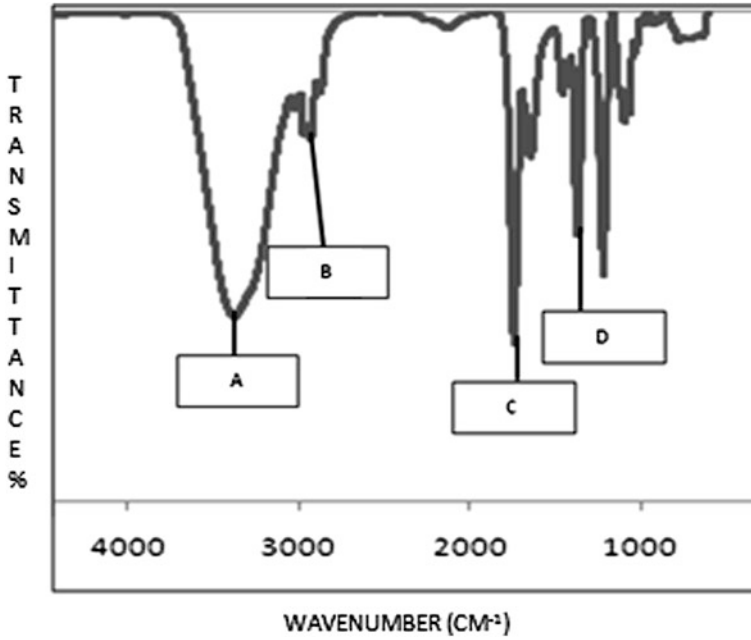


Fig. 5 The IR spectrum of synthetic foaming agent

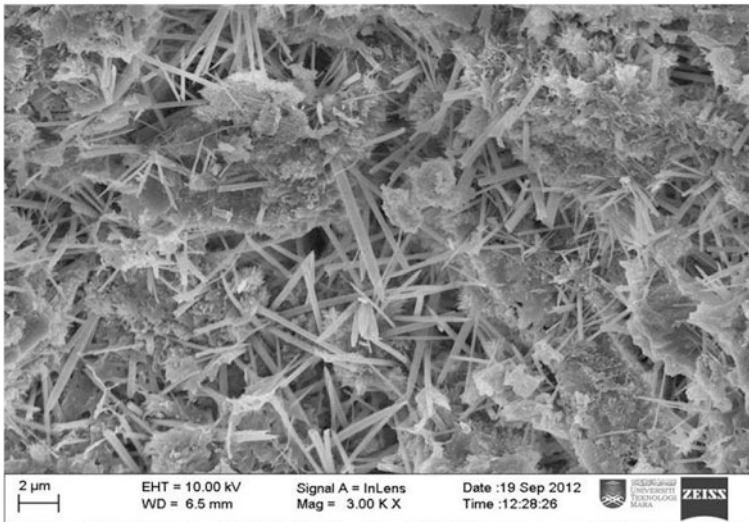


Fig. 6 The example of image of used cooking oil foamed concrete produced from FESEM-EDAX analysis

Table 5 The elements in foamed concrete containing used cooking oil foaming agent

Element	Weight (%)	Atomic (%)
O K	26.62	46.00
Al K	1.63	1.67
Si K	9.64	9.49
Ca K	62.12	42.85
Totals	100.00	100.00

Table 6 The elements present in the foamed concrete when synthetic foaming agent is used

Element	Weight (%)	Atomic (%)
O K	28.01	51.04
Si K	3.94	4.09
Ca K	56.10	40.80
Rb L	11.95	4.08
Totals	100.00	100.00

3.2 EDAX Analysis

Solid sample of foamed concrete was analysis by EDAX. This analysis intentionally to trace the elements present in foamed concrete where the foaming agents of used cooking oil and both synthetic and protein types. This chemical element trace will be showed their result in weight percentage. An example image had been captured by FESEM is shown in Fig. 6. The elements present in foamed concrete that used different foaming agents were shown in Tables 5 and 6.

This EDAX analysis had showed for both used cooking oil and synthetic foaming agent were used as admixture in foamed concrete. Based on Table 5 of EDAX result, Calcium Ca was the highest percentage (62.12 %) and Aluminium Al is the lowest percentage (1.63 %) have been detected for foamed concrete containing used cooking oil foaming agent. Table 6 was showed all the elements present in foamed concrete containing synthetic foaming agent. From the result, the highest percentage element is Calcium Ca (56.10 %) and the lowest percentage is Silica (3.94 %). These foamed concrete were compared among used cooking oil foamed concrete and synthetic foamed concrete but not for protein foamed concrete because of the limitation of scope of study. Both foamed concrete were curing until 90 days at air ambient condition. Since same binder was used for both foamed concrete which ordinary Portland cement OPC Calcium Ca is the highest percentage for both foamed concrete.

4 Conclusion

Reflect to the result from the FTIR for liquid foaming agent have shown all the major chemical functional groups for all foaming agents is derived from the lipids groups. Whereas based on elemental analysis from EDAX shown Calcium Ca is the major element present in used cooking oil and synthetic foamed concrete.

Acknowledgments The authors would like to express greatest appreciation and gratitude to the Institute of Infrastructure Engineering and Sustainable Management (IIESM) Faculty of Civil Engineering, Universiti Teknologi MARA (UITM) 40450 Shah Alam, Selangor, Malaysia and to Elanz Design Build Sdn. Bhd.

References

1. M. Paolini, R. Khurana, Admixture for recycling of waste concrete. *Cement Concr. Compos.* **20**, 221–229 (1998)
2. M. Collepardi, Admixtures used to enhance placing characteristics of concrete. *Cement Concr. Compos.* **20**, 103–112 (1998)
3. F.J. Holler, D.A. Skoog, S.R. Crouch, *Principles of Instrumentation Analysis* (Thomson Brooks/Cole, Stamford, 2007), pp. 455–468
4. D.L. Pavia, G.M. Lampman, G.S. Kriz, *Introduction to Spectroscopy* (Thomson Learning, Stamford, 2001) Appendix A-1

Effect of Input Variable for Neural Network Architecture in Predicting Building Damage Subjected to Earthquake

Rozaina Ismail, Azmi Ibrahim and Azlan Adnan

Abstract The artificial intelligent methodology is applied to building inspection system in this paper. Inspection results from Applied Technology Council (ATC) procedures are used as an indicator to the building damage level. Backpropagation algorithm with one hidden layer is used to develop the neural network and Borland C++ is used as the programming language. The choice of input variables is a fundamental. The neural network performance is analysed by removed the input one by one from the network. The mean square error (MSE) value is equal to 0.027 when all inputs are applied to the network. The lowest MSE is 0.025 when the length is excluded from the network. Lower MSE value indicates lower error among others. Even though the lowest MSE is presented when the length is excluded from the network, but the different was too small which is 0.002. Thus, the length is still applied in network. From the application of Artificial Neural Network (ANN), building samples gave the lowest value of MSE equal to 0.027 when 15 hidden neurons applied and the highest linear correlation coefficient was obtained when r is equal to 0.839 in testing phase and 0.762 in validation phase. Out of 112 samples in the testing phase, 104 samples were predicted accurately for degree of damage rating for the building which represents 93 % from the total data used. In the validation phase, 39 out of 52 samples were predicted accurately with 75 % accuracy. The results of this study indicate that the ANNs provide an efficient means of damage forecasting and would be useful by the owners of the building to predict building conditions under seismic load.

Keywords Seismic zonation • Earthquake evaluation of buildings • Artificial neural network (ANN) • Applied Technology Council (ATC) procedures

R. Ismail (✉) · A. Ibrahim · A. Adnan
Faculty of Civil Engineering, Universiti Teknologi MARA (UiTM), Selangor, Malaysia
e-mail: rozaina_fka_uitm@yahoo.com

1 Introduction

The performance of buildings during earthquake is unknown in Malaysia. The most existing building owners and regulators must ensure that their buildings are safely operated and present no risk to the public in case of an earthquake. The adequacy and safety level of buildings must be determined. The existing preliminary evaluation by ATC-21 based on a sidewalk survey of a building and data collection form which an inspector completes based on visual. A seismic risk analysis addressed to earthquake emergency management and protection strategies planning, requires vulnerability and damage evaluation performed at territorial scale [1].

2 Artificial Neural Network

Over the last few decades, there has been much research directed at predicting the future and making better decisions. Artificial neural networks (ANNs) allows model of complex systems to be built without requiring the explicit formulation of the possible relationships that may exist between variables. Data-driven modeling employing artificial intelligence and machine learning methods are finding increasing relevance and importance in various engineering process. The goal of data-driven modeling is to build a system that can adapt and learn from practical data. Artificial neural networks, coupled with an appropriate learning algorithm, can be used to learn complex relationships from a set of associated input-output vectors.

The ANN has been widely applied in forecasting selected natural phenomena in recent years. An Artificial Neural Network (ANN) is an information processing paradigm that is inspired by the way biological nervous systems, such as the brain, process information. The key element of this paradigm is the novel structure of the information processing system. It is composed of a large number of highly interconnected processing elements (neurons) working in unison to solve specific problems. ANNs, like people, learn by example. An ANN is configured for a specific application, such as pattern recognition or data classification, through a learning process. Learning in biological systems involves adjustments to the synaptic connections that exist between the neurons. This is true of ANNs as well [2].

Ramhormozian et al. [3] having a quick but reliable insight into the likelihood of damage to bridges immediately after an earthquake by using neural network. The use of ANN shows that the proposed intelligent monitoring system could provide prediction of up to 92 % rate of accuracy and activate the alert. Implementation of the system in building monitoring would allow for rapid, intelligent and accurate prediction of the building damage index due to earthquake [4]. Artificial neural network (ANN) is developed to predict bridge condition rating based on different intensity of seismic zonation. The study showed that the ANN has a potential to be used to predict the condition rating based on different seismic Intensity with prediction values are up to 90 % correct [5].

3 Artificial Neural Network Applied in this Study

Neural networks are applicable in virtually every situation in which a relationship between the predictor variables (independents, inputs) and predicted variables (dependents, outputs) exists, even when that relationship is very complex and not easy to articulate in the usual terms of “correlations” or “differences between groups”. Artificial neural networks (ANN) are among the newest signal-processing technologies in the engineer’s toolbox. The field is highly interdisciplinary, but our approach will restrict the view to the engineering perspective. In engineering, neural networks serve two important functions: as pattern classifiers and as non-linear adaptive filters. The neural network system used in this study is developed using C++ language. There are four main phases involved in the ANN applied in this study (refer Fig. 1).

In the Phase 1, the data preprocessing should be completed before the implementation of network. The *Neural Networks* package offers several algorithms to build models using data. Before applying any of the built-in functions for training, it is important to check that the data is “reasonable”. Naturally, you cannot expect to obtain good models from poor or insufficient data. Unfortunately, there is no standard procedure that can be used to test the quality of the data. Depending on the problem, there might be special features in the data that may be used in testing data quality.

After achieving the reliability level, the ANNs are ready for the implementation. In the implementation phase, there are two step involved; (1) Network Training and (2) Network Testing. One of the advantages of an ANN is that it does not require sophisticated knowledge from the end user to implement it. Then the next phase followed by the adaption of new experience. Network adaption is one of the important characteristics of the neural network. This phase also called as a network validation phase. The adaption phase represents updating the neural network knowledge with new experiences. Finally, the finding and result of the ANN application is discussed.

4 Preprocessing Data for Neural Network

4.1 Analysing Data for Seismic Zone

The data used in this study is limited to the data gathered during site survey phase. These include the data from building inventories, visual inspection report, and Finite Element Modeling. There are seven parameters applied to the ANN model which includes the parameter based on the seismic intensity at the building site. Peak ground acceleration, PGA value used is based on 2 % probability of accidence in 50 years (return period equal to 2,500 years). The PGA value for each building sample is determined using the macrozonation map shown in Fig. 2.

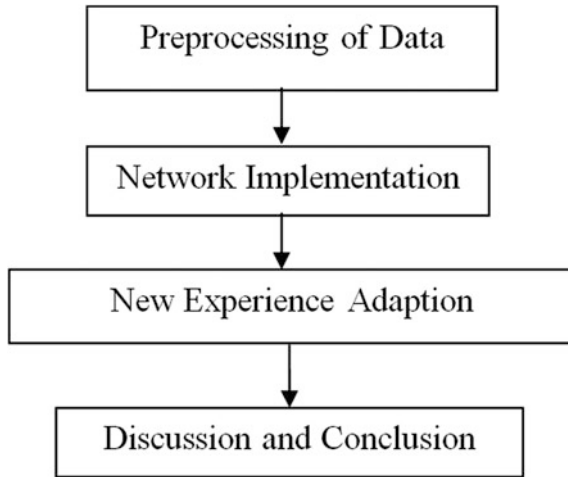


Fig. 1 Phase involved in the application of ANN

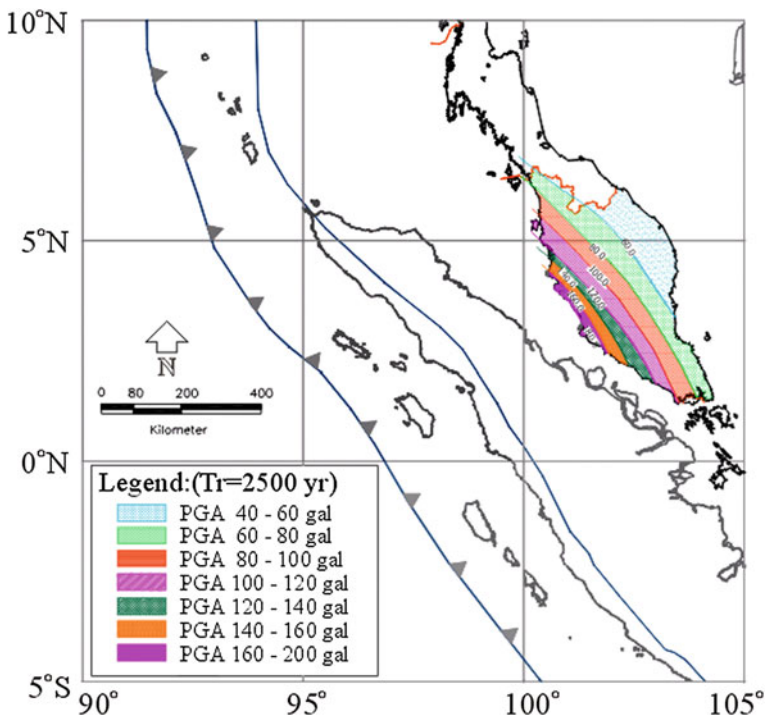


Fig. 2 Macrozonation map at 2 % PE in 50 years on rock site conditions for the Peninsular Malaysia (TR = 2,500 year) [6]

Table 1 Seismic zonation

Zone	Seismic intensity, PGA (gal)
1	31–50
2	51–70
3	71–90
4	91–110
5	111–130
6	131–150

Table 2 Classification of age range

Class	Age range
1	Year \leq 10
2	10 < Year \leq 20
3	20 < Year \leq 30
4	30 < Year \leq 40
5	40 < Year \leq 50
6	50 < Year \leq 60

Table 3 Classification of height range

Class	Height (H), range (m)
1	H \leq 10
2	10 < H \leq 20
3	20 < H \leq 30
4	30 < H \leq 40
5	40 < H \leq 50
6	50 < H \leq 60
7	60 < H \leq 70
8	70 < H \leq 80

The parameters are classified into specific groups to characterize their types and variety. Each group will be represented by a particular code to be used in the ANN development. Tables 1, 2, 3, 4 and 5 shows the classification made to the parameters. Referring to the map, PGA values for Peninsular Malaysia ranges from 40 to 200 gal, whereas for Johor state it ranges from 60 to 140 gal. For programming purposes, the PGA values are classified in ten groups starting from 0 to 200 gal with an interval of 20 gal.

Buildings can be classified according to different aspects such as their function, form of superstructure, as well as material and method used in construction, natural period of the buildings is used to classified building class in this study. Building samples used in this study are limited to concrete building only.

Table 4 Classification of natural period range

Class	Natural period (T), range (sec)
1	$T_n \leq 0.5$
2	$0.5 < T_n \leq 1.0$
3	$1.0 < T_n \leq 1.5$
4	$1.5 < T_n \leq 2.0$
5	$2.0 < T_n \leq 2.5$

Table 5 Classification of length range

Class	Length (L), range (m)
1	$L \leq 10$
2	$10 < L \leq 20$
3	$20 < L \leq 30$
4	$30 < L \leq 40$
5	$40 < L \leq 50$
6	$50 < L \leq 60$
7	$60 < L \leq 70$
8	$70 < L \leq 80$

5 Network Implementation

5.1 Network Training

In this study, the backpropagation (BP) algorithm using the generalized delta rule (GDR) for gradient calculation has been popularized as a method of training ANNs. This method has the advantage of being readily adaptable to highly parallel hardware architectures. The reason is due to the existence of a bias function instead of internal threshold (T_{1j} , T_{2j} , and T_{3k}). These values of T_{1j} , T_{2j} , and T_{3k} are not changed or updated as network training progress. In GDR, the values of $T_{1j} = 0$, $T_{2j} = T_{3k} = 1$ is provided. The GDR algorithm is more efficient than the other algorithm since the momentum parameter is coupled with a bias function. Hence, these values remain unchanged throughout the entire ANN network training [7].

Supervised training with error-correction learning procedure is exploited in this study to achieve the objective of predicting the performance of building on damage level using ANN, i.e., both inputs and outputs are known. The damage level ratings are given to the neural network during the network training, and the network can adjust the weights accordingly. A total of 27 buildings with 108 samples are used in the network training phase.

Also we know that different types of ANNs can represent different functions for the final hypothesis, so I would like to pick the network representation that requires the most amount of computational effort while giving the most accurate approximation for the final hypothesis. Alih [8] used the early stopping criteria in her study. Shrestha et al. [9] also used the early stopping criteria in the training process in the application of ANN for simulation of flood flow in a river system. Up to 250,000

training epochs (where each epoch consisted of all the training samples) could be run on the training data, used to implement early stopping and avoid overfitting the data. Overfitting here means the ANN is too complex so it reacts on noise in the data. In this study, the network training of a neural network is terminated based on early stopping conditions when training epoch reaches 250,000.

5.2 Network Testing

In this study, linear correlation coefficient (r) is applied to see the performance of trained network. Chen et al. [10] applied this procedure in his study for Truncated Data. One of the most important tasks in building a mathematical model of a process for prediction purposes is the selection of relevant input variables. In order to obtain a good set of representative variables we have to assume that we effectively can measure or observe all variables that we need, and that the data is not contaminated by outliers. There is no systematic way which can be followed, but some statistical methods like auto-correlation, partial-auto-correlation, and cross-correlation have been used successfully.

6 New Experience Adaption (Network Validation)

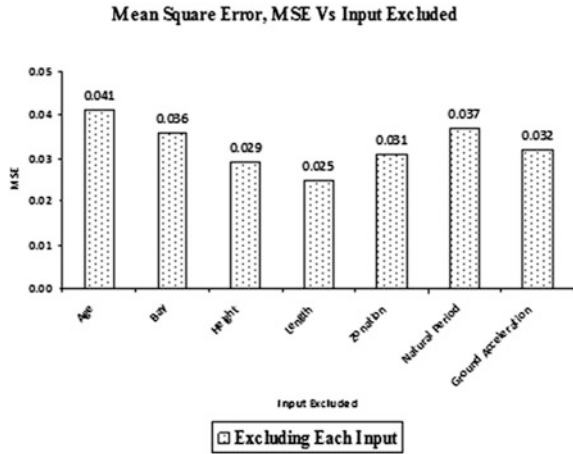
The network validation is conducted to verify the network reliability. Validating a network is achieved by presenting testing sets to the network. These sets should be new sets that the network has never been exposed to before. Network output using these sets is compare with the desired output to calculate the accuracy rate (i.e., reliability). If the accuracy rate is low, then the network is not properly trained and other training sets should be generated to retrain the network; otherwise, the network is considered to be reliable and ready for implementation [11]. The network testing is executed further in the network validation. The validation samples are taken from the 14 buildings with 56 sets of new data that have never been applied in the network training and testing. The prediction values are compared with the actual values to determine their differences between network training and testing.

7 Effect of Neural Network Structure

7.1 Effect of Input Variables

The selection of input variables to ANN is necessary to avoid “overfitting” data. The input in the layer also affects the performance pf the BPN. There are seven input parameters used as shown in Fig. 3. These include building age, number of bay,

Fig. 3 Mean square error for different input parameter



overall height, overall length, seismic zone, natural period and ground acceleration. The neural network performance can be analysed by removed the input one by one from the network. For example, when natural period is removed from the input layer and the performance of ANN is decreased, this shows the natural period gives significant effect to the network and this parameter should be applied in the system.

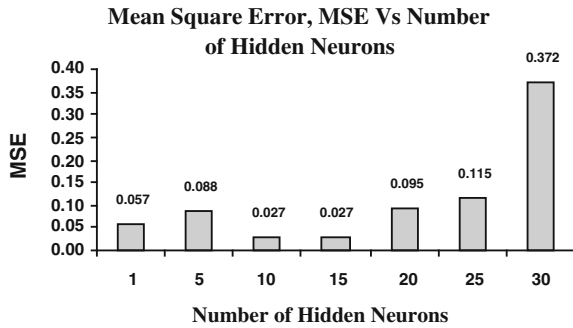
The selections of input variables are based on two factors; (1) the mean square error (MSE), and (2) the linear correlation coefficient, r . The MSE are used in the network training phase. The performance of the network was measured by the mean square error (MSE). The mean-square error criterion is used to simultaneously select the optimum rules. This optimization is performed over all one-to-one [12]. MSE value refers to the total errors between actual output and output given by the ANN.

7.2 Effect of Hidden Neurons

The comparative performance of the neural network structures with a different number of hidden layers is conducted. There are 15 number of neurons are applied in the network. Figure 4 presents the values of MSE when different numbers of hidden neurons are applied to the network. MSE value refers to the total errors between actual output and output given by the ANN. The results show that 10 and 15 number of hidden layers has the best performance, whereas the lower MSE value given which indicates better prediction for the ANN.

The effective number of hidden neurons applied to the network also can be seen by analysed through the linear correlation coefficient. Linear correlation with the higher value represents strong relationship between actual output and the output given by the ANN. In testing phase, the ANN performance is analysed through

Fig. 4 Mean square error for different number of hidden neurons



linear correlation coefficient and compared to the ANN performance with MSE. The linear correlations for degree of damage for building are higher in the middle of the histogram where 10, 15, and 20 hidden neurons are applied to the network. 15 hidden neurons provide the highest r for the degree of damage rating for both network testing and validation phase.

From the result, it shows that the analysis of MSE and linear correlation coefficients produced the same result for each phase. Therefore, 15 hidden neurons are chosen to be applied in the ANN system which is more stable in producing good performance at each phase.

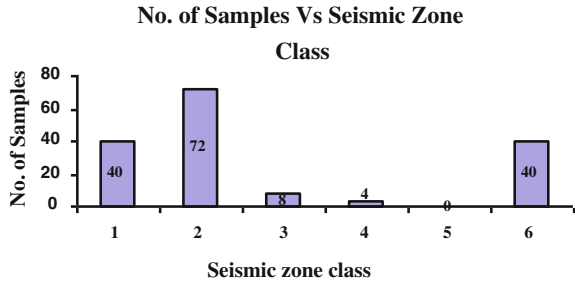
8 Result and Discussions

As mentioned earlier, data involved in developing the neural network needs to be analyzed first. This analysis consists of three stages;

8.1 Data Characteristic

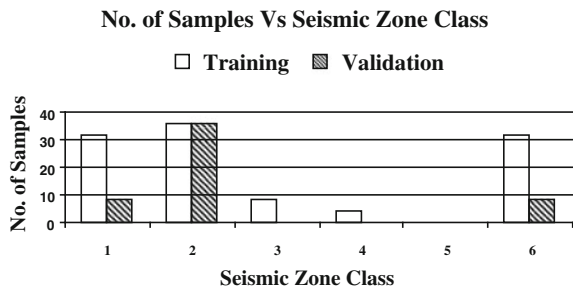
Characteristic of each data used in developing the neural network needs to be defined due to the random process applied to extract the data. The distributions of each inputs and outputs are defined through histograms and the relationships between these two variables are determined using linear correlation coefficient, r . Figure 5 shows the distribution of seismic zone at building sites. There are six zones involved with peak ground acceleration ranges from 31 to 150 gal. The distributions are quite even between the bridge samples. Zone class 2 shows the highest readings with 72 building samples, followed by class 1 and 6 both with 40 samples respectively. Zone 5 has the least samples with no building.

Fig. 5 Distribution of seismic zonation on building site



Zone	Seismic Intensity, PGA (gal)
1	31-50
2	51-70
3	71-90
4	91-110
5	111-130
6	131-150

Fig. 6 Distribution of training and validation data



8.2 Data Classification

After the characteristics of parameters are determined, the data then is being classified. There are two classifications involved; (1) network training and testing phase, (2) new experience adaption phase or called network validation phase. Up to 41 samples of concrete moment resistance frame buildings are used in this study. There are 27 samples used in the network training and testing phase and 14 samples are used for the network validation phase. The validation samples are cannot be used in the network training and testing phase before. This is to make sure that we are using the new data set to validate the output.

Figure 6 shows the distribution of seismic zonation for training and validation phase. Training and validation data are represented in all categories. Since the data distributions are uniform, the differences between training and validation data set are uniform as well. Seismic zone class 2 with PGA between 51–70 gal, has the highest number of samples in both phases.

Fig. 7 Actual rating and predicted rating by ANN during network testing phase for degree of damage rating

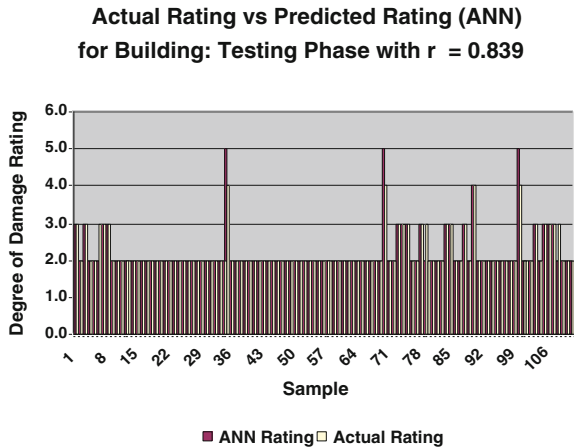
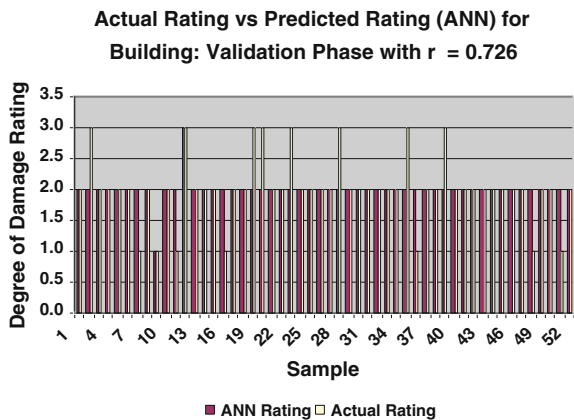


Fig. 8 Actual rating and predicted rating by ANN during network validation phase for degree of damage rating



8.3 Result Discussion for Building’s Damage Prediction

In this section, result from the application of ANN in each rating prediction is discussed. In this stage, the final ANN structure is used in which all seven input parameters and 15 hidden neurons are applied to the network. Mean square error between the actual output and output given by the ANN are discussed to evaluate the training phase. Linear correlation coefficient between the actual output and output given by the ANN is analyzed.

Figures 7 and 8 show the comparisons between the actual rating and rating given by the ANN in network testing and validation phase. It can be observed that the highest linear correlation coefficient is obtained when r equals to 0.839 in network testing phase and 0.762 in network validation phase.

The linear correlation coefficients indicate the strength of relationship between the actual rating and the rating given by ANN. Thus, the high values of r obtained shows the results given by the ANN are strong. This shows the network is able to produce accurate output using the weights it has generated. Up to 112 samples in the network testing phase, 104 samples are predicted 93 % accurately for degree of damage rating for the building. In the network validation phase, 39 out of 52 samples are predicted accurately with 75 % accuracy. The degree of damage rating range represent in the testing phase is 1–5 rating, while the network validation phase only rating with 1 and 3 degree of damage rating range involved.

9 Conclusions

The result form this study showed that out of 112 samples in the testing phase, 104 samples were predicted accurately for degree of damage rating for the building that represents 93 % from the total data used. In the validation phase, 39 out of 52 samples were predicted accurately with 75 % accuracy. From the application of ANN, the lowest value of MSE is 0.027 when 15 hidden neurons were applied in this study and the highest linear correlation coefficient is equal to 0.839 in testing phase and 0.762 in validation phase. The result obtained in the network testing and network validation phase, it can be seen that the ANN predictions are very much affected by the data applied to the network.

Acknowledgments A special thank you goes to project RAGS funder, Ministry of Education (MOE) and support from Research Management Institute (RMI), Universiti Teknologi MARA (UiTM).

References

1. S. Giovinazzi, The vulnerability assessment and the damage scenario in seismic risk analysis. Ph.D. Thesis, Technical University Carolo-Wilhelmina at Braunschweig, Braunschweig, Germany and University of Florence, Florence, Italy, 2005
2. C. Stergiou, D. Siganos, Neural networks, in Report of An Introduction to Artificial Neural Networks (1999)
3. S. Ramhormozian, P. Omenzetter, R. Orense, Artificial neural networks approach to predict principal ground motion parameters for quick post-earthquake damage assessment of bridges, in NZSEE Conference (2013)
4. M. Mardiyono, R. Suryanita, A. Adnan, Intelligent monitoring system on prediction of building damage index using neural-network, *TELKOMNIKA* **10**(1), 155–164 (2012)
5. A. Adnan, S.C. Alih, R. Ismail, The application of artificial neural network in predicting bridge condition based on seismic zonation, in The 14th World Conference on Earthquake Engineering, 2008, Beijing, China (2008)
6. A. Adnan, H. Hendriyawan, A. Marto, M. Irsyam, Development of seismic hazard map for peninsular malaysia, in Proceedings on Malaysian Science and Technology Congress. PWTC Kuala Lumpur, Malaysia, 1–26 Sept 2006

7. J. Leonard, M.A. Kramer, *Improvement of the backpropagation algorithm for training neural networks* (Elsevier, Oxford, Royaume-Uni, 1977)
8. S.C. Alih, The application of artificial neural network in nondestructive testing for concrete bridge inspection rating system. Master Degree Thesis, University of Technology Malaysia, 2007
9. R.R. Shrestha, S. Theobald, F. Nestmann, Simulation of flood in a river system using artificial neural network. *Hydrol. Earth Syst. Sci.* **9**(4), 313–321 (2005)
10. C.H. Chen, W.Y. Tsai, W.H. Chao, The product-moment correlation coefficient and linear regression for truncated data. *J. Am. Stat. Assoc.* **91** (1996)
11. M.A. Abdullah, A.A. Ali, Artificial neural network approach for pavement maintenance. *J. Comput. Civ. Eng.* 249–255 (1998)
12. G. Redinbo, Optimum mean-square error use of convolutional codes. *IEEE Trans. Inf. Theor.* **31**(1), 18–33 (1985)

Potential Use of Industrial By-products for Developing High Strength Concrete Under Normal Curing Conditions

Dhawal Desai and Prakash Nanthagopalan

Abstract In the last decade, there has been a substantial increase in the use of high strength concrete (HSC) due to extensive construction of high rise buildings owing to restricted space and increased demand for living space in urban areas. For achieving high strength and durable concrete, it is essential to have minimum void content by packing the ingredients of the concrete densely. There have been lot of research studies performed on HSC, however, there are possibilities to improve the properties of HSC and economy by using conceptual mixture design and using industrial by-products (mineral admixtures). The present study focused on the development of high strength concrete using particle packing concept and properties such as flowability and compressive strength were assessed for different binder combinations [Micro Silica (MS): Ultrafine Fly Ash (UFA)]. For the mixture designing purpose, modified Andreassen model of particle packing was used. The water/binder (w/b) ratio of 0.20 was used. From the results, it is observed that a maximum slump of 780 mm and maximum 56 day compressive strength of 130.7 MPa using normal water curing was achieved.

Keywords High strength concrete • Industrial by-products • Particle packing • Ultrafine materials • Flowability

1 Introduction

High strength concrete, by definition according to ACI, is the concrete with compressive strength more than 60 MPa. It is currently used in tall structures, pre-cast spans of super bridges and also helps in size reduction of structural elements to

D. Desai (✉)

Undergraduate Student, Department of Civil Engineering, IIT Bombay, Mumbai, India

P. Nanthagopalan

Assistant Professor, Department of Civil Engineering, IIT Bombay, Mumbai, India

increase utilizable space. To achieve this strength, apart from high cement content, very low w/c ratio (less than 0.25) and High Range Water Reducers (HRWR), fine particles such as micro silica and ultrafine fly ash [1, 2] are essential for the reduction of voids, in turn leads to good packing density of particles. This packing of fine particles leaves less space for voids to be filled with water, which thus reduces the water demand and increases the strength of the concrete [3–7]. HSC is more durable because the low water-to-cementitious materials ratio results in very low porosity [8]. Earlier works by Long [9] shows that HSC has cement content higher than 400 kg/m^3 . Further, observations from the literature [1, 9–12] suggest that ultrafine materials improve the fresh and hardened properties of concrete (compressive strength of 180 MPa) by both chemical reaction and physical action (to increase particle packing). Researchers [1, 2, 10] have shown that to achieve excellent strength and slump flow, the following factors needs to be considered: usage of high cement content with low w/c ratio, usage of ultrafine materials, usage of high range water reducers for low w/c ratio, limit the maximum size of coarse aggregate to 10 mm. After summarizing results from tests on different types of concrete, Richard and Cheyrezy came to the conclusion that the crack size is [13] proportional to the maximum aggregate size [14]. During the development of high strength self-compacting concrete, Kwan [13] found that addition of condensed silica fume (CSF) (with a mean particle size of about $0.1 \mu\text{m}$) at a water/cement ratio less than 0.28 increases the workability of concrete. Although there is large increase in surface area by the addition of CSF, the increase in workability may be explained by the gap filling ability of CSF particles (due to their high fineness) which fill the gaps between cement particles and frees water from the gaps to lubricate the mix. The authors have measured the packing density of blended cementitious materials and showed that the packing density could be significantly increased by the addition of CSF. They have also showed that there would be considerable increase in the flowability of the cement paste by addition of CSF at a water/cementitious ratio of 0.2. Researches have also shown that addition of micro silica enhances the mechanical properties of the paste by filling voids, thus enhancing rheology and producing secondary hydrates [15].

It was shown by Obla et al. [16] that water demand of the cementitious system would be reduced by using ultra-fine fly ash (with a mean particle size of about $3 \mu\text{m}$) with cement in the mix. This happens most probably due to the increase in packing density.

Self-compacting concrete of grade as high as 100 MPa was produced by Kwan and Ng [17] by using a mixture of different types of cementitious materials to maximise the packing density of the mix.

2 Research Significance

Considering the rate of growth in construction activities going on around the world, it is evitable that the demand for high strength concrete will take a boost in coming years for the construction of high rise buildings, bridges and highways. This has

created a need to study its performance and behaviour under varying composition of materials. On the other hand, there are serious availability and sustainability issues with the raw materials. In this regards, it is deemed essential to use industrial by-products for the sustainable production of concrete. The objective of this research is to study variation in workability and compressive strength of high strength concrete on changing proportions of Densified Micro Silica (DMS) and UFA. Previous studies [10, 18] have been carried out in this field but the current research considers particle packing concept and also uses less amount of cement replacement materials to reduce the cost of concrete. Therefore, in the present study CSF and UFA were optimised based on particle packing models to get the maximum packing density and the optimised combinations were used for performing the fresh (slump flow) and hardened properties (compressive strength) of concrete.

3 Materials Used

Ordinary Portland cement of 53 grade conforming to IS 12269-2004 [19] was used. The chemical test results of cement are shown in Table 1. Two industrial by-products viz. Densified Micro Silica (DMS) conforming to ASTM C1240-12 [20] and Ultrafine Fly Ash (class F) conforming to IS 3812-1999 [21] were also used. The particle size distribution of cement, MS and UFA was determined using laser diffractometer and the results are shown in Fig. 1. The maximum size of coarse aggregate was limited to 10 mm. Natural river sand was used as fine aggregate for the investigation. Both, coarse and fine aggregates conforms to IS 383-1997 [22]. The specific gravity of coarse aggregates and fine aggregates was determined according to [23]. Poly Carboxylic Ether based superplasticizer with solid content of 31.75 % conforming to IS 9103-2004 [24] was used. The physical properties of materials are shown in Table 2.

From the literature [25], it is observed that the mean size of DMS will be less than 1 μm , however, the results indicates that the mean size of DMS is obtained as 11.76 μm . This could attribute to the difficulty in dispersion of the Densified Micro Silica.

4 Experimental Methodology

4.1 *Optimisation of Material Compositions for Achieving Maximum Particle Packing*

It is understood from the literature that high cement content with very low water/binder ratio is essential for achieving high strength concrete. Therefore, a binder content of 1,000 kg/m^3 of concrete was selected out of which 800 kg/m^3 was cement.

Table 1 Chemical test results of the cement

Property	Value
Lime saturation factor	0.94
Ratio of % alumina to iron oxide	1.47
Insoluble residue (% by mass)	0.96
Magnesia (% by mass)	1.45
Sulphuric anhydride (% by mass)	2.40
Total loss on ignition (%)	1.40
Chloride content (% by mass)	0.049

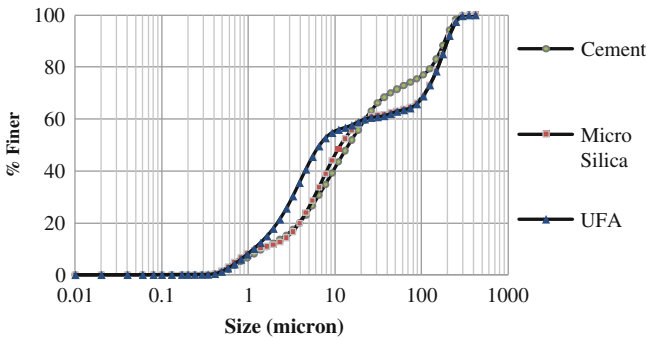


Fig. 1 Particle size distribution of cement, DMS and UFA

Table 2 Physical properties of materials

Property	Cement	DMS	UFA	4.75 mm	10 mm
Specific gravity	3.15	2.25	2.30	2.35	2.97
Mean diameter	14.43 μm	11.76 μm	6.72 μm	652 μm	7,689 μm

The remaining 200 kg/m^3 of fine materials were a combination of industrial by-products, DMS and UFA. The proportions of DMS, UFA, fine and coarse aggregates were optimised based on particle packing concept using modified Andreassen model. A software ‘EMMA Mix Analyzer’ (Freeware software [26]) developed based on Andreassen model was used as a tool for optimising the proportions. Figure 2 represents a sample screenshot of a packing density curve of the resulting concrete. The curve (red colour) indicates the theoretical maximum packing density curve for the given materials with minimum and maximum size available using Andreassen model while the curve with blue colour represents the packing density curve for a selected combination of materials used in this study. The combinations of the materials have to be changed such that the deviation of the blue curve from the red curve is minimised to ensure good packing density of the mixture.

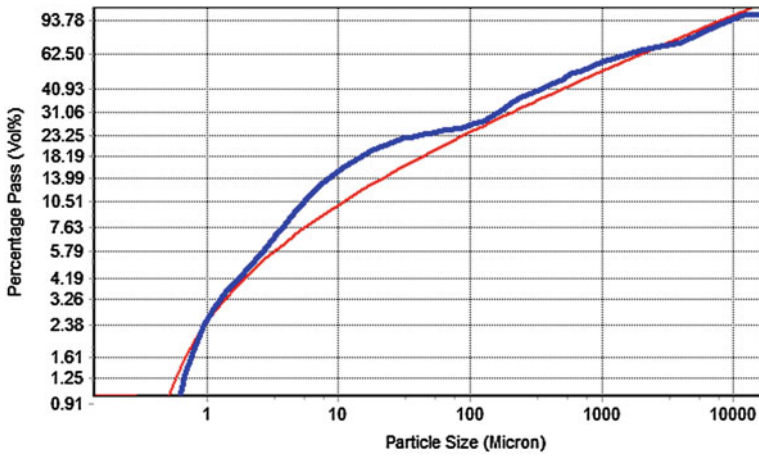


Fig. 2 Showing packing density curves for Andreassen model (*red*) and that of the concrete designed (*blue*)

Table 3 Ratio of DMS with UFA in different samples

Sample ID	DA	DB	DC
DMS:UFA (by volume)	1:3	2:2	3:1

Table 4 Proportions for concrete mixes (kg/m^3)

Sample	Cement	MS	UFA	4.75 mm	10 mm	Water	SP
DA	800	49	151	500	671	200	13
DB	800	99	101	600	543	200	13
DC	800	149	51	600	540	200	13

Many combinations were investigated for packing density out of which three ratios by volume of DMS and UFA were chosen based on the higher packing density. The combinations are given in Table 3.

A water/binder ratio of 0.20 was chosen and superplasticizer (SP) amount was fixed to 1.3 %. Except DMS and UFA combinations, every other materials and its proportions are kept constant to understand the properties of concrete due to ultrafine materials.

The details of the mixture proportions of materials used in this study is given in Table 4.

4.2 Mixing Procedure

All the dry ingredients were mixed in a Pan mixture (speed 25 rpm) for 3 min to ensure homogeneous mixture. Then 80 % of the total water content was added and mixed for 2 min. Further, superplasticizer was uniformly mixed with the

remaining amount of water and then added into the mixture and subsequently mixed for 6 min. This procedure was adopted based on the previous experience with high strength production in our laboratory [27]. As the maximum size of the aggregates is 10 mm, cubes of size $100 \times 100 \times 100$ mm were used for casting and demoulded after 24 h and cured in water at room temperature till testing.

5 Results and Discussion

The slump flow test was performed for all the mixtures by using the standard slump cone test [28]. The compressive strength test on cubes was performed at 7, 28 and 56 days as per IS 516-2002 [29].

5.1 Slump Test Results

Table 5 shows slump test results. Mixes DA and DB show excellent flowability thus behaving as self-compacting concrete. As the DMS amount increases from DA to DC, the surface area increased leading to decrease in the flowability of the mixtures and it complies with the findings by Kwan [13] and Obla et al. [16].

The workability in DC is exceptionally lower than DA and DB, due to the presence of high content of micro silica.

5.2 Effect of DMS and UFA Content on Compressive Strength

The results of the compressive strength test are shown in Table 6. Compressive strength tests were performed at 56 days also to assess the pozzolanic effect of the mineral admixtures added to the concrete. The mix DA gains up to 95 MPa in 56 days especially post 28 days, the percentage gain is high due to the presence of high amount of UFA (150 kg/m^3). The Mix DB having equal amount ($\sim 100 \text{ kg/m}^3$) of DMS and UFA produces the highest strength (123 MPa) coupled with high early strength and post 28 days strength also. This dual benefit of high early strength and post 28 day strength could be attributed to the presence of DMS (for early strength) and UFA (for 28 days strength gain). The strength in DB is highest because of high silica content in concrete by DMS and an optimum amount of UFA contributing to better particle packing. The mix DC has gained up to a strength of 95 MPa at 28 days due to the presence of higher amount of DMS. Further, it can be observed that the percentage gain in compressive strength from 7 to 28 days is maximum in DC. It can be inferred from Table 6 that, the average 28 day

Table 5 Slump test results

Sample	DA	DB	DC
Slump flow (mm)	780	650	240 ^a

^a Slump (mm)

Table 6 Compressive test result

Sample	Cube number	7 day, MPa	Avg. 7 day, MPa	Cube number	28 day, MPa	Avg. 28 day, MPa	Cube number	56 day, MPa	Avg. 56 day, MPa
DA	1	64.42		1	73.51		1	93.6	
	2	68.78	68.48	2	75.96	77.02	2	95.3	95.23
	3	72.26		3	81.58		3	96.8	
DB	1	69.33		1	75.2		1	115.2	
	2	74.46	73.04	2	78.33	77.39	2	124.4	123.43
	3	75.34		3	78.65		3	130.7	
DC	1	67.89		1	94.3		1	104.1	
	2	74.39	72.25	2	96.2	95.76	2	106.4	105.93
	3	74.46		3	96.8		3	107.3	

compressive strength increases from sample DA to DB to DC due to increase in silica content in concrete coming from DMS. This is because in concrete with low w/c, the capillary pores disappear and the Interfacial Transition Zone (ITZ) is filled up with C–S–H hydrates produced by the pozzolanic reaction of silica fume [30].

6 Conclusion

The results presented in this study show that varying compositions of ultra-fine materials can considerably and substantially influence the concrete properties. The study also shows that compressive strength and slump flow can be optimised by optimising the fine content in the ternary mixture. The optimum content of the industrial by-products, DMS and UFA, is nearly 10 %, for both, by weight of the total binder content which results in maximum particle packing to give a maximum average compressive strength of 123 MPa and a slump flow of nearly 650 mm. DMS supports early strength gain and UFA supports post 28 days strength gain due to the pozzolanic action. Prolonged mixing period was necessary to get a homogenised mixture and to increase the workability of the mixtures because of high binder content.

Another industrial by-product, ultrafine slag is being used to study its influence on concrete properties along with MS and UFA. Further studies will be carried out to understand durability and shrinkage properties on changing proportions of ultra-fine materials, for all combination of materials. Possibility of achieving early high strengths by using steam curing will be also explored.

Acknowledgments The authors would like to acknowledge Ambuja Cements Ltd., ELKEM and BASF Construction Chemicals for their support in terms of providing materials for this research.

References

1. C. Wang, C. Yang, F. Liu, C. Wan, X. Pu, Preparation of ultra-high performance concrete with common technology and materials. *Cem. Concr. Compos.* **34**, 538–544 (2012)
2. F. de Larrard, Ultrafine particles for the making of very high strength concretes. *Cem. Concr. Res.* **19**, 161–172 (1989)
3. S.A.A.M. Fennis, J.C. Walraven, J.A. den Uijl, Compaction-interaction packing model: regarding the effect of fillers in concrete mixture design. *Mater. Struct.* **46**, 463–478 (2013)
4. F. de Larrard, *Concrete Mixture Proportioning: A Scientific Approach* (E & FN Spon, London, 1999)
5. R.K. Dhir, M.J. McCarthy, K.A. Paine, Engineering property and structural design relationships for new and developing concretes. *Mater. Struct.* **38**(275), 1–9 (2005)
6. A. Kronlöf, Filler effect of inert mineral powder in concrete. Dissertation, VTT Technical research centre of Finland, 1997
7. H.H.C. Wong, A.K.H. Kwan, Packing density of cementitious materials: measurement and modelling. *Mag. Concr. Res.* **60**(3), 165–175 (2008)
8. N. Roux, C. Andrade, M.A. Sanjuan, Experimental study of durability of reactive powder concretes. *J. Mater. Civ. Eng.* **8**(1), 1–6 (1996)
9. T.P. Long, High strength concrete at high temperature: an overview (2008), available from <http://fire.nist.gov/bfrlpubs/build02/pdf/b02171.pdf>. Accessed 20 Jan 2012
10. G. Longa, X. Wanga, Y. Xie, Very-high performance concrete with ultrafine powders. *Cem. Concr. Res.* **32**, 601–605 (2002)
11. P.K. Mehta, Advancements in concrete technology. *ACI Concr. Int.* **21**(6), 69–76 (1999)
12. P.C. Aitcin, A. Neville, High performance concrete demystified. *Concr. Int.* **15**, 21–26 (1993)
13. A.K.H. Kwan, Use of condensed silica fume for making high strength, self-consolidating concrete. *Can. J. Civ. Eng.* **27**(4), 620–627 (2000)
14. P. Richard, M. Cheyrezy, Composition of reactive powder concretes. *Cem. Concr. Res.* **25**(7), 1501–1511 (1995)
15. S. Allena, C. M. Newton, Ultra-high strength concrete mixtures using local materials, in *Concrete Sustainability Conference* (2010)
16. K.H. Obla, R.L. Hill, M.D.A. Thomas, S.G. Shashiprakash, O. Perebatova, Properties of concrete containing ultra-fine fly ash. *ACI Mater. J.* **100**(5), 426–433 (2003)
17. A.K.H. Kwan, I.Y.T. Ng, Grade 80-100 self-consolidating concrete for Hong Kong. *HKIE Trans.* **11**(2), 1–7 (2004)
18. R. Deeb, A. Ghanbari, B.L. Karihaloo, Development of self-compacting high and ultra-high performance concretes with and without steel fibres. *Cem. Concr. Compos.* **34**, 185–190 (2012)
19. IS 12269-2004, Specification for 53 grade Ordinary Portland Cement, Bureau of Indian Standards, New Delhi
20. ASTM C1240-12, Standard specification for Silica Fume used in cementitious mixtures, American Society for Testing and Materials
21. IS 3812-1999, Specification for Fly Ash for use as pozzolana and admixture, Bureau of Indian Standards, New Delhi
22. IS 383-1997, Specification for Coarse and Fine aggregate from natural sources for concrete, Bureau of Indian Standards, New Delhi
23. IS 2386-1997, Indian code for methods of test for aggregates for concrete, Bureau of Indian Standards, New Delhi
24. IS 9103-2004, Concrete admixtures—specification, Bureau of Indian Standards, New Delhi

25. FHWA-IF-05-016, Silica Fume user's manual, Federal Highway Administration, US Department of Transportation, April 2005
26. Website: <http://www.elkem.com/en/silicon-materials/support/software-emma/>
27. D. Desai, P. Nanthagopalan, Experimental investigations on the influence of industrial by products on highly flowable high strength concrete, in 1st International Conference on Advanced Nanocomposite for Construction Materials (ICNC 2013), Kottayam, India, 12–14 March 2013
28. IS 1199:1959 (Reaffirmed 1999), Indian code for method of tests for concrete, Bureau of Indian Standards, New Delhi
29. IS 516-2002, Indian code for method of tests for concrete, Bureau of Indian Standards, New Delhi
30. M. Courtial, M.-N. de Noirfontaine, F. Dunstetter, M. Signes-Frehel, P. Mounanga, K. Cherkaoui, A. Khelidj, Effect of polycarboxylate and crushed quartz in UHPC: microstructural investigation. *Constr. Build. Mater.* **44**, 699–705 (2013)

Seismic Analysis of Reinforced Concrete Structures in Low to Moderate Earthquake Zones of Peninsular Malaysia

Jeffrey Chiang and Meng Siang Wong

Abstract It is fortunate that Peninsular Malaysia is relatively free from direct earthquake effect, except for far field seismic effect from Sumatra 350 km away, on its western seaboard side. Hence, the majority of local reinforced concrete structures are not designed to resist earthquakes specifically. There is no provisions in the British Standards used, i.e. BS 8110:1987 for seismic design considerations. In May 2010, when UK has withdrawn BS 8110 among other structural codes, it has adopted Eurocodes as the mainstay of concrete design standards, including Eurocode 8 for earthquake-resistance design of structures. It has specific rules as a design provisions for concrete buildings. The Institution of Engineers Malaysia has embarked on a study and development of a design standard for earthquake design for reinforced concrete building structures, which is still on-going. The intention is to address the fears and concerns of Malaysian public in the light of swaying highrise buildings and light damages to some reinforced concrete structures, due to strong intensity earthquakes felt from the 2004 Aceh, 2005 Nias and 2009 Padang earthquakes in Sumatra. Of more immediate concern is local earthquake in the vicinity of Bukit Tinggi fault-line, currently inactive, lying a mere 30 km away from city centre of Kuala Lumpur. This paper gave an insight into how the Eurocode 8 [1] (BSI, BS EN 1998-1:2004: Eurocode 8: Design of Structures for Earthquake Resistance—Part 1: General Rules, Seismic Actions and Rules for Buildings, p. 230, 2004) can be applied for Malaysian practices in analysing reinforced concrete building structures. A sample seismic analysis is carried out comparing the outcome using Eurocode 8 and UBC-97 [2] (International Code Council, Uniform Building Code, International Conference of Building Official, p. 442, 1997), based on a local earthquake scenario. Reference is also made to the Component Attenuation Model developed by Australian researchers, which has

J. Chiang (✉)

Professor, INTI International University, Nilai, Negeri Sembilan, Malaysia
e-mail: jeffrey.chiang@newinti.edu.my

M. S. Wong

Research Assistant, Universiti Tunku Abdul Rahman, Kuala Lumpur, Malaysia

been touted as accurate and reliable in formulating expected peak ground accelerations in Peninsular Malaysia. This will be a useful input into analysing reinforced concrete structures in a relatively low to moderate earthquake zone.

Keywords Seismic · Earthquake · Concrete · Structures · Component · Attenuation

1 Introduction

The Component Attenuation Model (CAM) provides a systematic way of combining generic information from global models with local information. CAM is suitable for regions lacking in instrumented earthquake data where a representative response spectrum attenuation model cannot be developed from measured strong motion accelerogram data by conventional regression analysis such as the case in Malaysia. Lam et al. [3] have recognised the potential of the seismological model for a worldwide application and transformed the Atkinson version of the model developed for the Central and North America (CENA) region from the original Fourier spectrum format into the engineering response spectrum format [3–5]. CAM provides attenuation relationships for three response parameters which can be used to construct response spectrum in either the response spectral acceleration (RSA), response spectral velocity (RSV) or response spectral displacement (RSD) formats [4]. This analytical approach is also known as Capacity Spectrum Method.

2 Background Information

2.1 General

The reduction in wave amplitude with distance from a source of a given magnitude due to geometric spreading, absorption, scattering, and critical reflections are defined as an attenuation function. A lot of attenuation functions have been introduced and yet it is hard to determine which and when to use the appropriate attenuation function for the specific location or site. This might be due to the inhomogeneous characteristic of soil and bedrock properties across the whole world.

2.2 Derivation of CAM by Nelson et al. [6]

The Component Attenuation Model (CAM) can be used to determine the peak response spectral parameters. These peak response values can be used to construct acceleration, velocity and displacement response spectra that are important in the

Table 1 Coefficients of the source function [6]

Parameter type	Δ^*	a_1	a_2	a_3	C
SD_{\max}	12 mm	0.2	0.8	2.3	0.003
SV_{\max}	93.5 mm/s	0.35	0.65	1.8	0.005
SA_{\max}	7.3 m/s ² or 0.74 g	0.40	0.60	1.5	0.015

seismic design of building. CAM is expressed as the product of a source factor, a geometrical attenuation factor, a whole path anelastic attenuation factor, a mid-crust amplification factor and an upper crust modification factor [6]. The Component Attenuation Model (CAM) is formulated as follow [6] (Table 1):

$$\Delta = \alpha(M)G(R, D)\beta(R, Q)\gamma(\text{crustal type}) \quad (1)$$

where

Δ Response spectral parameter (displacement, velocity and displacement) of interest (SD_{\max} , SV_{\max} , SA_{\max})

$\alpha(M)$ Source function, which may be described as

$$0.78\Delta^*[a_1 + a_2(M-5)^{a_3}] \quad (2)$$

M Moment magnitude

a_1, a_2 Coefficients obtained by curve fitting and polynomial functions to the stochastically

a_3 Simulated results for earthquake at a site-source distance of 30 km.

$G(R, D)$ Geometrical attenuation factor which accounts for the effects of the crustal wave guide, which depends on range of site-source distance, as shown below:

$$G(R, D) = \frac{30}{R} \quad (R < 1.5 D) \quad (3)$$

$$G = \frac{30}{1.5 D} \quad (1.5 D \leq R \leq 2.5 D) \quad (4)$$

$$G = \left(\frac{30}{1.5 D}\right) \sqrt{\frac{2.5 D}{R}} \quad (R > 2.5 D) \quad (5)$$

where

R Site-source distance

D Crustal thickness (measured between the surface of the earth and the Moho-discontinuity).

$\beta(R, Q)$ An elastic whole path attenuation factor which accounts for energy dissipation along the wave travel path (which is extremely important for modeling the seismic hazard at long distances from the source)

$$\beta(R, Q) = \left(\frac{30}{R}\right)^{CR} \quad (6)$$

γ Models both the mid-crust amplification and the combined effects of upper crust amplification and attenuation where they exist. They are crustal type.

$$\gamma(\text{crustal type}) = C_m C_u \quad (7)$$

where

$C_m = C_u = 1$ for “Hard Rock” and $C_m = 1.3$ and $C_u = 1.15$ for “Rock”.

Inter-relationship between the velocity, acceleration and displacement response spectrum ($SV(T)$, $SA(T)$ and $SD(T)$ respectively):

$$SV(T) = \frac{SA_{max}T}{2\pi} \quad (T < T_1) \quad (8)$$

$$SV(T) = SV_{max} \quad (T_1 < T < T_2) \quad (9)$$

$$SA(T) = SA_{max} \quad (T < T_1) \quad (10)$$

$$SA(T) = \frac{SV_{max}2\pi}{T} \quad (T_1 < T) \quad (11)$$

$$SD(T) = \frac{SV_{max}T}{2\pi} \quad (T < T_2) \quad (12)$$

$$SD(T) = SD_{max} \quad (T_2 < T) \quad (13)$$

where T_1 and T_2 are the corner periods of the response spectra used.

$$T_1 = 0.1 + 0.1(M - 5) \quad (14)$$

$$T_2 = 0.5 + 0.5(M - 5) \quad (15)$$

Note: The corner period T_1 controls the maximum response spectral acceleration, with SA_{max} increasing with decreasing values of T_1 .

On the other hand, the corner period T_2 controls the maximum response spectral displacement (SD_{max}) which is proportionate with T_2 .

$$\text{Peak Ground Velocity} = \frac{SV_{max}}{2} \quad (16)$$

$$\text{Peak Ground Acceleration} = \frac{SA_{max}}{3} \quad (17)$$

3 Methodology for Seismic Displacement Demand

3.1 Application of CAM Model in Determining the Seismic Displacement Demand

The Component Attenuation Model is an innovative framework by which the velocity and displacement demand on Single Degree of Freedom (SDOF) systems are expressed as product of component factors representing conditions of the source, path, local and site. CAM takes advantage of the theoretical constraints of the earthquake magnitude (seismic moment) on the displacement demand (in high period range). There are also less variabilities in the estimation of the peak velocity demand (in the median period range) than acceleration demand (in the low period range) [7].

The focus of CAM on velocity and displacement (as opposed to acceleration) is also consistent with the objective of the assessment which is for protecting lives and lowering the risks of building collapses [7].

3.2 Estimation of Peak Velocity Demand, V_{max}

$$V_{max} = \alpha_v \cdot G \cdot \beta_v \cdot \gamma \cdot S \quad (18)$$

where V_{max} is given in unit mm/s, and the other corresponding terms are given as,

$$\alpha_v = 70 \left\{ 0.35 + 0.65(M - 5)^{1.8} \right\} \quad (19)$$

$$G = \frac{30}{R} \quad (R \text{ in km for } R < 50 \text{ km}) \quad (20)$$

$$\beta_v = \left(\frac{30}{R} \right)^{0.005R} \quad (R \text{ in km for } R < 50 \text{ km}) \quad (21)$$

Note that the following terms apply.

M Moment magnitude

R Site source distance

γ Crustal factor (value is typically in the range 1.0–2.0)

S The site factor (value is in the order of 1.5–2.0 for average site).

3.3 Estimation of Peak Displacement Demand, D_{max}

$$D_{max} = \alpha_D \cdot G \cdot \beta_D \cdot \gamma \cdot S \quad (22)$$

where D_{\max} is given in unit mm, and the other corresponding terms are given as,

$$\alpha_D = \alpha_v \left(\frac{T_2}{2\pi} \right) \text{ for } M \leq 8 \quad (23)$$

or

$$\alpha_D = 10^{M-5} \text{ for } M \leq 6.5 \quad (24)$$

$$G = \frac{30}{R} \text{ R in km for } R < 50 \text{ km} \quad (25)$$

$$\beta = \left(\frac{30}{R} \right)^{0.003R} \text{ R in km for } R < 50 \text{ km} \quad (26)$$

$$T_2 = 0.5 + \left(\frac{M-5}{2} \right) \text{ for } M \leq 8 \quad (27)$$

Note that the following terms apply.

M Moment magnitude

γ Crustal factor (value is typically in the range 1.0–1.6)

S The site factor (value is in the order of 1.5–2.0 for average site).

4 Analysis and Results

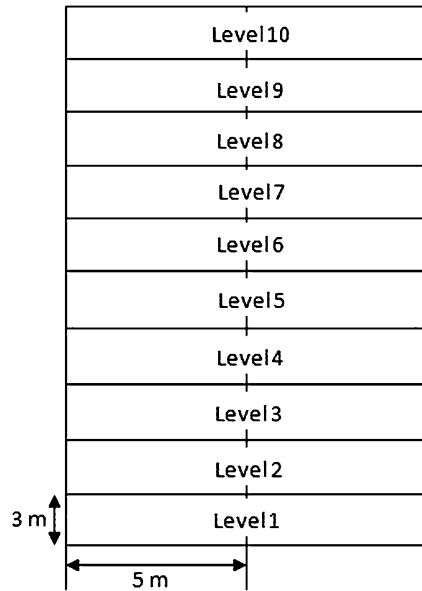
4.1 Seismic Analysis

In this seismic analysis subsection, it includes the application of CAM model in determining seismic peak ground acceleration and related parameters, and also the base shear calculation using UBC-97 and Eurocode 8. A sample model of a simple structure and assumptions made are shown in Fig. 1.

Assumptions made

- | | |
|--|--|
| • Concrete density: 25 kN/m ³ | • 10 storey RC structure consists of 2 bays |
| • Usage: residential apartment | • System type: moment resisting frame and braced frame |
| • Site soil property: stiff clay | • RC column: 500 × 500 × 3 m |
| • RC beam: 300 × 300 × 5 m | • Slab thickness: 300 mm |
| • Earthquake magnitude: M5.5 | • Site-source distance: 30 km |
| • Length of rupture: 40 km | |
-

Fig. 1 A simple model of a 10-storey RC structure for seismic analysis



4.2 Base Shear Calculation

In this subsection, UBC-97 [2] and Eurocode 8 [1] will be used to determine the base shear of the structure. The steps for both UBC-97 and Eurocode 8 are almost the same except for the base shear formula and horizontal force distribution. The results are presented in Table 2. Note that base shear formula in UBC-97 and Eurocode 8 refers to:

$$V = \frac{2.5C_dIW}{R_c}$$

where $R_c = 5.5$ [2]

$$F_b = s_d(T_1)m\lambda$$

[1].

The proportion of base shear to building self-weight is shown below for the two codes applied:

$$UBC97 : \frac{\text{Base shear, } V}{\text{Building Weight, } W} = \frac{854}{7,500} \times 100\% = 11.39\%$$

$$EC8 : \frac{\text{Base shear, } V}{\text{Building Weight, } W} = \frac{6,910}{7,500} \times 100\% = 92.13\%$$

Table 2 Results for forces and shear at each floor of the model building [8]

Base shear Floor	UBC-97		Eurocode 8	
	$V = 854 \text{ kN}$		$F_B = 6,910 \text{ kN}$	
	Force at floor X (kN)	Shear at floor X (kN)	Force at floor i (kN)	Shear at floor i (kN)
F1	14.5	854.0	125.6	6,910
F2	29.0	839.5	251.3	6,784.4
F3	43.5	810.5	376.9	6,533.1
F4	58.0	767.0	502.5	6,156.2
F5	72.5	709.0	628.2	5,653.6
F6	87.1	636.5	753.8	5,025.5
F7	101.6	549.4	879.5	4,271.6
F8	116.1	447.8	1,005.1	3,392.2
F9	130.6	331.7	1,130.7	2,387.1
F10	145.1	201.1	1,256.4	1,256.4
		= (145.1 + 56)		

4.3 Seismic Displacement Demand: Applying CAM Model

Given: $M = 5.5$, $R = 30 \text{ km}$, $D = 15 \text{ km}$

Calculation of values for V_{max} and PGV for average sites:

$$V_{max} = \alpha_v \cdot G \cdot \beta_v \cdot \gamma_v \cdot S$$

where,

$$\begin{aligned} V_{max}(\text{average site}) &= (37.566 \text{ mm/s})(1.33)(1.0)(1.69)(1.5) \\ &= 126.656 \text{ mm/s*} \end{aligned}$$

$$\begin{aligned} V_{max}(\text{rock site}) &= (37.566 \text{ mm/s})(1.33)(1.0)(1.69) \\ &= 84.437 \text{ mm/s} \end{aligned}$$

$$PGV(\text{rock site}) = \frac{84.437}{1.8} = 46.91 \text{ mm/s}$$

$$PGV(\text{average site}) = 46.91 \times 1.4 = 65.67 \text{ mm/s}$$

Calculation of values for D_{max} for average sites (Figs. 2, 3):

$$D_{max} = \alpha_D \cdot G \cdot \beta_D \cdot \gamma_D \cdot S$$

where,

$$D_{max} = (4.484)(1)(1.33)(1.69)(1.5) = 15.118 \text{ mm}$$

Fig. 2 Displacement response spectrum

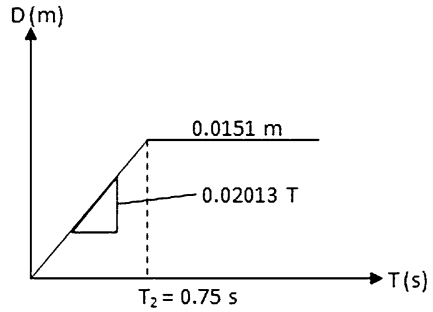
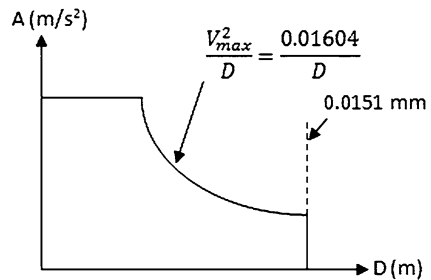


Fig. 3 Acceleration-displacement response spectrum (ADRS)



4.4 Seismic Displacement Demand: Analytical Static Method

Calculation of building displacement

Given the following information:

Height of column, $h_c = 3 m$

Span of beam, $L_g = 5 m$

Modulus of elasticity of concrete, $E_c = 37.4 \times 10^6 kN/m^2$

Mass per floor, $m = 75 tons/floor$

Column dimension: $500 \times 500 \times 3,000 mm$

Beam dimension: $300 \times 500 \times 5,000 mm$.

Assumptions made for determining base shear for EC8:

Moment magnitude, $M \leq 5.5$ (type 2 elastic response spectra)

Ground type D

Peak Ground Acceleration (PGA) = $0.04 g$

$T = 0.937 s$

$S = 1.8, T_B = 0.10 s, T_C = 0.30 s, T_D = 1.2 s,$

$\eta = 1$ (5 % viscous damping).

Table 3 Determined effective parameters [8]

Determined parameters	UBC-97	Eurocode 8
Effective displacement Δ_{eff} (mm)	118.1	930.3
Effective mass M_{eff} (t)	592.6	596.8
Effective stiffness K_{eff} (kN/m)	7,233	7,427
Effective period, T_1 (s)	1.80	1.78
Effective period, T_2 (s)	14.4	11.6
Acceleration a (m/s^2)	0.133	0.132
Overall displacement Δ (m)	0.94	0.12

4.5 Results and Discussion

From Table 2, it can be seen that the base shear calculated using Eurocode 8 shows a higher value which is 6,475 kN whereas for UBC-97, it is 854 kN given the same conditions and assumptions made. The differences in base shear occurred due to the different factors taking into account in the formulation used in both UBC-97 and Eurocode 8.

Eurocode 8 provides two types of response spectrum which are applicable to earthquake magnitude less than 5.5 or greater than earthquake magnitude 5.5 which are considered to be applicable to Malaysia. Using UBC-97, the calculated base shear shows a lower value than Eurocode 8. This is due to the reducing factor used in UBC-97 which takes into account the resistant type of structure which is higher than Eurocode 8 which uses a correction factor of 0.85 that accounts for the fact that buildings with at least three storeys and translational degrees of freedom in each horizontal direction, the effective modal mass of the 1st (fundamental) mode is smaller, on average by 15 %, than the total building mass.

The results also show that for both the UBC-97 and Eurocode 8, the base floor of a building has the highest shear force. As for the horizontal distribution of force, the highest floor of the building will experience the highest force. This is mainly due to the effect of inertial force at the free end of the top floor, upon exertion of base shear from seismic action at the foundation level.

From Tables 4a and 4b, it can be observed that the highest inter-storey drifts occurred at second level of the building and the highest deflection would occur at the highest floor of the building for both cases of UBC-97 and Eurocode 8. However, the calculated deflections using Eurocode 8 is much higher than those from UBC-97, which is nearly up to eight times at each level. After multiplying the calculated factor from Table 3 to the horizontal forces and deflection in Tables 4a and 4b, the response of the building is then obtained. It can be seen that the response of building calculated using Eurocode 8 has a lower displacement with higher horizontal force at each level of the building compared to UBC-97.

Table 4a Response of building to earthquake (UBC-97) [8]

Floor	UBC-97			
	Before scaling		500 × 500 mm (factor = 0.94)	
	Force (kN)	Deflection (& inter-story drift) (mm)	Force (kN)	Deflection (mm)
10	201.1	152.89 (5.5)	136.394	143.72
9	331.7	147.43 (9.1)	122.764	138.58
8	447.8	138.42 (12.2)	109.134	130.12
7	549.4	126.26 (16.1)	95.504	118.69
6	636.5	110.12 (17.3)	81.874	103.52
5	709.0	92.84 (19.3)	68.15	87.27
4	767.0	73.59 (20.8)	54.52	69.17
3	810.5	52.76 (22.0)	40.89	49.59
2	839.5	30.75 (22.8)	27.26	28.91
1	854.0	7.96 (8.0)	13.63	7.48

Table 4b Response of building to earthquake (EC 8) [8]

Floor	Eurocode 8			
	Before scaling		500 × 500 mm (factor = 0.1193)	
	Force (kN)	Deflection (& inter-story drift) (mm)	Force (kN)	Deflection (mm)
10	1,256.4	1,190.9 (34.1)	149.900	142.092
9	2,387.1	1,156.8 (64.9)	134.910	138.019
8	3,392.2	1,091.9 (92.2)	119.920	130.280
7	4,271.6	999.8 (116.1)	104.930	119.283
6	5,025.5	883.7 (136.6)	89.940	105.436
5	5,653.6	747.1 (153.6)	74.950	89.144
4	6,156.2	593.5 (167.3)	59.960	70.816
3	6,533.1	426.3 (177.5)	44.970	50.858
2	6,784.4	248.8 (184.3)	29.980	29.679
1	6,910	64.4 (64.1)	14.990	7.685

Note The scaling factor is dependent on the shear force. Since both code provides different value of base shear, therefore two different scaling factors are used

4.6 Comment and Conclusion

The CAM model as shown in Sect. 3.1 will help to ease the task of structural engineers in the design of structures that could resist earthquake. By plotting the Force–Displacement graph with the Acceleration–Displacement Response Spectrum, the response of the structure can be determined during an earthquake event and thus the capacity of the structure can be determined. However, the CAM model used in this paper is generated based on Australia site conditions. This paper aims to provide some indications of the applicability and demonstrate the ease of using CAM model which may be suitable for Malaysia. Seismological modelling for Malaysia should be undertaken with CAM model as the basis.

The calculation of base shear and deflection based on Eurocode 8 shows a higher value compared to UBC-97. After multiplying the horizontal force and deflection with scaling factor, the response of building calculated using Eurocode 8 shows almost equal displacement with higher horizontal force at each level of the building compared to UBC-97. For the analytical static method in determining the seismic displacement demand as shown in Sect. 3.3, there is a minor section where the PGA and PGV used are referred to the Australian Standard which is used to construct the response spectrum. This should be modified to suit the conditions in Malaysia in order to obtain more accurate results.

Acknowledgments The authors would like to acknowledge The Institution of Engineers Malaysia for providing the platform to undertake detailed study into earthquake issues, under the IEM Technical Committee on Earthquake, which is drafting the Malaysian Standards for earthquake design in building structures. The authors also appreciate the support of Universiti Tunku Abdul Rahman and INTI International University in allowing active collaboration in undertaking joint research and submitting this technical paper as collaborative work by the authors.

References

1. BSI, *BS EN 1998-1:2004: Eurocode 8: Design of Structures for Earthquake Resistance—Part 1: General Rules, Seismic Actions and Rules for Buildings* (2004), p. 230
2. International Code Council, *Uniform Building Code*, International Conference of Building Officials (1997), p. 442
3. N.T.K. Lam, J.L. Wilson, G.L. Hutchison, Generation of synthetic earthquake accelerograms using seismological modelling: a review. *J. Earthquake Eng.* **4**(3), 321–354 (2000)
4. N.T.K. Lam, J.L. Wilson, A.M. Chandler, G.L. Hutchison, Response spectral relationships for rock sites derived from the component attenuation model. *Earthquake Eng. Struct. Dynamics* **29**(10), 1457–1490 (2000)
5. N.T.K. Lam, J.L. Wilson, A.M. Chandler, G.L. Hutchison, Response spectrum modelling for rock sites in low and moderate seismicity regions combining velocity, displacement and acceleration predictions. *Earthquake Eng. Struct. Dynamics* **29**, 1491–1525 (2000)
6. N.T.K. Lam, J.L. Wilson, A.M. Chandler, G.L. Hutchison, *Introduction to the Component Attenuation Model and Applications in Australia* (Department of Civil and Environmental Engineering, 2000), pp. 137–146
7. N.T.K. Lam, H.H. Tsang, *Two Day Course on “Earthquake Ground Motions and Responses of Reinforced Concrete Building”*. Course Notes, The Institution of Engineers Malaysia (IEM), 22–23 June 2010, p. 269
8. M.S. Wong, Reviewing seismic design consideration in Malaysia RC building due to local seismic effects. Chapter 6–9, BEng(Hons) thesis, Univ TAR, 2010, pp. 70–141

A Review of Magnetorheological Elastomers: Characterization Properties for Seismic Protection

Rozaina Ismail, Azmi Ibrahim and Hanizah Ab. Hamid

Abstract Magnetorheological (MR) materials are belong to the group of smart materials that can be significantly altered in a controlled under the influence of an external stimulant which by changing their viscoelastic properties due to stress, pH level, moisture content, electric fields or in the case of MREs, magnetic fields. The MREs are interesting materials especially for the active stiffness and vibration control of structural systems. As a controllable stiffness element, MREs can offer innovative engineering solutions to various engineering challenges. Recently, they are being considered as new enabling components in active control systems, such as adaptive tuned vibration absorber and improving seismic protection base-isolated structures. The characteristic response will be influenced by many factors including; the elastomer matrix, the size, distribution, composition and percentage volume of the ferromagnetic particles, and whether the ferromagnetic particles are aligned in chains or randomly dispersed. A review is presented in this paper of the characteristic properties of magnetorheological elastomers and how these properties are affected by varying magnetic fields and the indicated compositional parameters. Besides describing the fundamental behavior of MREs, various applications of MREs for seismic protection are discussed and compared.

Keywords Magnetorheological (MR) elastomer · Properties · Seismic

1 Introduction

Traditional dynamic absorber has limited its application and vibration absorption capacity for its narrow working frequency bandwidth. MRE is a kind of smart material whose modulus can be controlled by applied magnetic field. The idea of

R. Ismail (✉) · A. Ibrahim · H. Ab. Hamid
Faculty of Civil Engineering, Universiti Teknologi MARA (UiTM), Selangor, Malaysia
e-mail: rozaina_fka_uitm@yahoo.com

using MR fluids, foam and elastomer devices for vibration mitigation applications was first proposed by Carlson and Jolly [1]. Magnetorheological Elastomer (MRE) is composed of tiny ferrous particles in chains and an elastomer such as synthetic and natural rubbers. When liquid state rubber combined with ferrous particles is exposed to a steady magnetic field, the ferrous particles will form chain-like structures arranged along the magnetic field during the curing process [2]. Klingenberg [3] discuss the applications and challenges of MR fluid. MR fluids have a wide array of applications, including variable dampers [4–6], visco damper [7], and vibration damper [8], and Venkateswara Rao et al. [9] studied the functional behavior of isotropic magnetorheological gels but MR fluids have distinct shortcomings. Liquid leakage can result in environmental contamination. Also, particle residue can degrade the performance of MR devices. MR elastomers, the solid analogs of MR fluids, may be a good solution to overcome the disadvantages of MR fluids. MRelastomers are the solid-type analogue of the well-known MR fluids, in which the fluid component is replaced with rubber-like solid materials such as silicon rubber, natural rubber, polyurethane sealant and polybutadiene as well as their blends.

The MR elastomer' elastic modulus or stiffness varies with the magnitude of the applied magnetic field by aligning iron particles as shown in Fig. 1 [10].

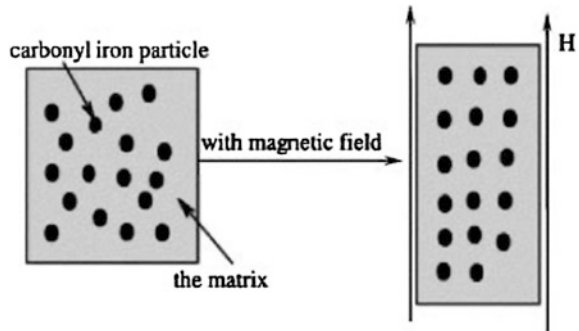
2 Properties of Magnetorheological Elastomers

Kallio [11] studied the influence of the alignment of the magnetic particles on the composite properties with and without applied magnetic fields. It was found that the stiffness and damping properties of both isotropic and aligned MREs can be modified by applying external magnetic field. In isotropic MREs the stiffness and damping increase in the magnetic field if the filler volume fraction exceeds 15 %. The damping also increases with the increasing volume fraction of iron and it has a maximum value at 27 vol. % when measured with applied magnetic field. The damping and stiffness properties of aligned MREs depend on the mutual directions of load, magnetic field and the particle alignment in the composite. It was also found that by optimizing the particle density and alignment, either the stiffness or the damping of MREs can be increased by applying the magnetic field.

Structurally, field responsive elastomers can be thought of as solid analogs of field responsive fluids. Like many field responsive fluids, field responsive elastomers are composed of polarizable particles dispersed in a polymer medium and the physical phenomena responsible for the field sensitivity of these elastomers is very similar. Indeed the 'strength' of field responsive fluids is characterized by their field dependent yield stress while the strength of field responsive elastomers is typically characterized by their field dependent modulus [1].

Jung et al. [12] studied a dynamic model of an MR elastomer which obtained based on characteristic test results of MR elastomers in shear mode. The results

Fig. 1 Schematic representation of MR elastomers [10]



further suggest that the feasibility of using MR elastomers as variable stiffness elements for enhancing the performance of conventional base-isolation systems.

Iacobescu et al. [13] investigated the Magnetorheological Elastomer Surface Properties by Atomic Force Microscopy. Collette et al. [14] considered two systems based on a magnetorheological elastomer (MRE): a MRE isolator under a frequency varying harmonic excitation and a MRE Dynamic Vibration Absorber (DVA) mounted on a frequency-varying structure under a random excitation. It is shown that the commandability of the elastomer improves the isolation performances in the first case, and decreases the stress level in the structure in the second case.

Magnetorheological (MR) rubber materials are the solid analog of magnetorheological fluids; hence, their rheological properties can be controlled by an applied magnetic field. If the particles embedded in the matrix are carbonyl iron, they have to be aligned by a magnetic field before the curing of the rubber, in order to achieve a substantial MR effect. Besides the achieved level of dispersion, the rheological properties of the matrix material do not influence the MR effect [15].

The mechanical properties of the MR materials change when subjected to an external magnetic field. The MREs are interesting candidates especially for the active stiffness and vibration control of structural systems [11]. The damping and stiffness properties of the MREs depend significantly on the mutual directions of load, magnetic field and the particle alignment in the composite. The measured curves (Figs. 2, 3) show that the dynamic stiffness decreases near the resonance.

3 Characteristic of MRE

Ying et al. [16] presented study focuses on the nonlinear dynamic characteristics of MRE. The MRE was fabricated and specimens were tested to show nonlinear mechanical properties and dynamic behaviors. It has been obtained that: (1) The applied magnetic fields can induce the nonlinear relation between forces and deformations; (2) The dynamic behaviors at low frequency can be modeled by

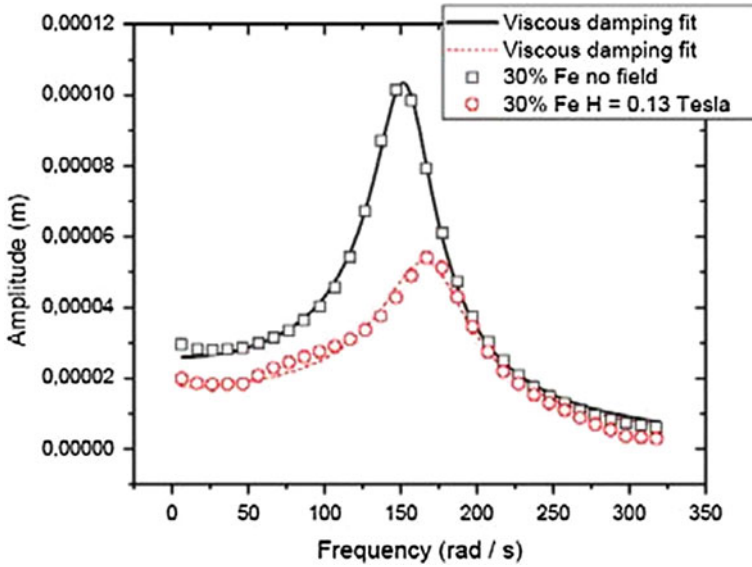


Fig. 2 DMA frequency scan results for an isotropic MRE with 30 vol. % of iron. The results are shown with fitted viscoelastic model and they were measured without the magnetic field and with the field strength H of 0.13 Tesla [11]

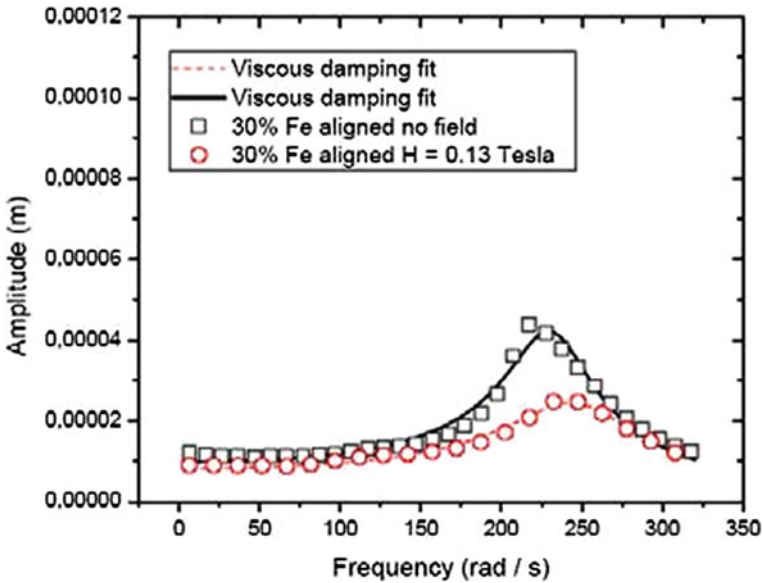


Fig. 3 DMA frequency scan results of an aligned MRE with 30 vol. % of iron as measured in Direction 1. The results are shown with fitted viscoelastic model, and they were measured without the magnetic field (*upper curve*) and with the field strength H of 0.13 Tesla (*lower curve*) [11]

Fig. 4 Equivalent stiffness versus fields (*dot* for test; *line* for modeling) [16]

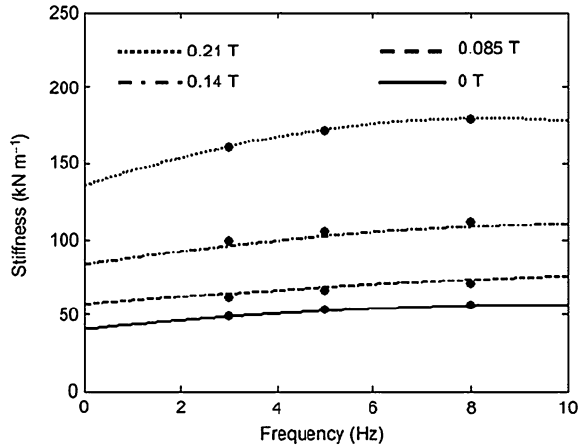
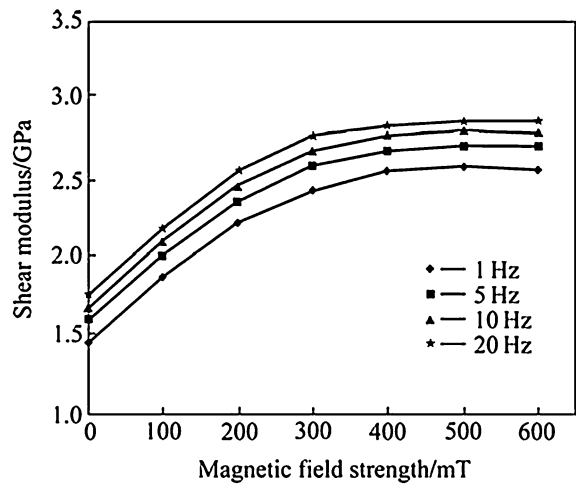


Fig. 5 Shear modulus with different magnetic fields and excited frequencies [17]



combining the nonlinear elasticity and linear damping; (3) The equivalent stiffness and loss factor depend linearly on the frequency in certain interval and depend nonlinearly on the magnetic field for small deformation. Figure 4 illustrates the increase of the equivalent stiffness with the frequency and magnetic field intensity.

Jung et al. [12] studied the dynamic characterization of magneto-rheological elastomers in shear mode. Dong et al. [17] proposed a new adaptive variable stiffness absorber. On the basis of the measured mechanical characteristics, the MRE absorber was developed and its working characteristics were also tested under various input currents and excited frequencies. The experimental results are shown in Fig. 5. From Fig. 5, it can be found that the shear modulus increases as the excited magnetic field increases. As a result, the damping characteristic was assumed as a constant in this study.

4 Magnetorheological Elastomers for Seismic Protection

The objective of seismic isolation systems is to decouple the building structure from the damaging components of the earthquake input motion, i.e. to prevent the superstructure of the building from absorbing the earthquake energy. The entire superstructure must be supported on discrete isolators whose dynamic characteristics are chosen to uncouple the ground motion. Some isolators are also designed to add substantial damping. Displacement and yielding are concentrated at the level of the isolation devices, and the superstructure behaves very much like a rigid body. Some of the commonly used isolation systems by Sajal [18].

Behrooz et al. [19] focused on control of a scaled building structure using a new semi-active Variable Stiffness and Damping Isolator (VSDI) and demonstrate the feasibility of using VSDIs a 1:16 scaled, three-story building is constructed and installed on a shake table and its base is supported by four prototype VSDIs. The VSDIs can be regulated in real time by varying the applied magnetic field through a controller. A phenomenological model is proposed and implemented on VSDI devices. The scaled El Centro earthquake excitation is applied to the system, and the vibration mode is controlled by a Lyapunov-based control strategy.

In traditional seismic design approach, strength of the structure is suitably adjusted to resist the earthquake forces. In base isolation technique approach, the structure is essentially decoupled from earthquake ground motions by providing separate isolation devices between the base of the structure and its foundation. The main purpose of the base isolation device is to attenuate the horizontal acceleration transmitted to the superstructure. All the base isolation systems have certain features in common. They have flexibility and energy absorbing capacity. The main concept of base isolation is to shift the fundamental period of the structure out of the range of dominant earthquake energy frequencies and increasing the energy absorbing capability. The concept is explained in Fig. 6 [20].

Elastomers with field responsive rheology hold promise in enabling simple variable stiffness devices. Although there are few applications appearing in the literature for controllable elastomers, there are countless applications for systems that employ a variable stiffness [1]. Among these are Adaptive Tuned Vibration Absorber based on Magnetorheological Elastomer [2], seat vibration control [21], and smart base isolation system using real-time hybrid simulation [22].

Doo et al. [23] conducted feasibility study of MRE under several historical earthquake excitation. The result show that the application of MRE was recusing the responses of the structure due to seismic excitations considered in the study.

Table 1 summarizes the maximum values of the structural responses for the four different test cases by Eem et al. [10]. In the table, the values in parenthesis represent the improvement of the smart base isolation system compared to the passive-type base isolation system. They show that the maximum structural responses for the smart base isolation are much smaller than those of the passive isolation system. The experimental results confirm the feasibility of smart base isolation for improving the seismic performance based-isolated structure.

Fig. 6 Concepts of base isolation and dampers [20]

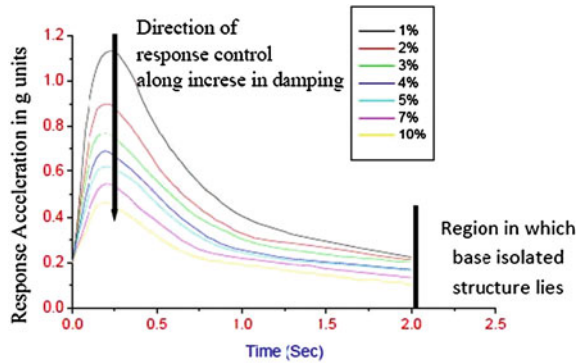


Figure 7 shows the scaled single-story shear building structure sits atop MR elastomer-based isolation systems. The results show that the proposed MR elastomer base-isolation system with the fuzzy logic control algorithm outperforms the conventional passive-type base isolation system in reducing the responses of the building structure for the seismic excitations considered in his study.

4.1 Modeling of MRE

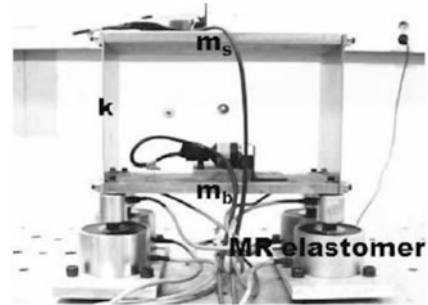
Shen et al. [24] modeled the MRE with new methods for fabricating magnetorheological (MR) elastomers are introduced. The experimental results show that the modulus of polyurethane MR elastomers can increase by 28 % under a strong magnetic field. Comparatively, the rubber MR elastomer has low modulus change ability. The analytical results of the model are in agreement with experimental data.

Li et al. [25] addressed the challenge facing current base isolation design/practice by proposing a new type of seismic isolator for the base isolation system, namely an adaptive seismic isolator. The novel adaptive seismic isolator utilizes magnetorheological elastomer (MRE) for its field-sensitive material property. The configuration of the novel MRE seismic isolator, as shown in Fig. 8, incorporates the laminated structural design of a traditional laminated rubber bearing. It consists of multilayer thin MRE sheets bonded onto multilayer thin steel plates. The laminated structure is essential for the seismic isolator used in civil engineering applications. The laminated structure allows high flexibility in the horizontal direction by the shearing deformation of MRE sheets, which can also be varied instantly under an applied magnetic field.

Eem et al. [22] study the seismic performance evaluation of an MR elastomer-based smart base isolation system using real-time hybrid simulation. According to the preliminary characterization test results, the horizontal stiffness of the sample

Table 1 Maximum structure responses (improvement) [10]

Test cases	Base drift	Structure drift	Acc. at base floor	Acc. at top floor
Fixed-base (Exc. freq. = 12.4 Hz)	–	16.42 mm	–	73.5 m/s ²
Base-isolation (Exc. freq. 12.4 Hz)	2.91 mm	1.07 mm	1.02 m/s ²	4.75 m/s ²
Bate-isolation (Exc. freq. = 7.5 Hz)	2.21 mm	1.92 mm	3.76 m/s ²	7.58 m/s ²
Smart base-isolation (Exc. freq. = 7.5 Hz)	0.76 mm (65.61 %)	0.81 mm (57.81 %)	1.39 m/s ² (63.03 %)	2.31 m/s ² (69.53 %)

Fig. 7 Experimental structure (smart base-isolation system) [10]

is varied by 30 %. Figure 9a, b show schematic diagrams of the proposed isolator and its prototype, respectively.

Choi et al. [26] presented the study of MRE for response reduction of the seismically excited base-isolated building, which is an eight story base isolated non-linear building similar to existing buildings in Los Angeles, California. The simple strategy of the semiactive fuzzy control algorithm for linear elastomeric isolated or nonlinear friction isolated building structure is presented in Fig. 10. The results of the numerical simulations show that the proposed control systems could be beneficial in reducing seismic responses of base isolated structures.

4.2 Experimental of MRE

A novel adaptive seismic isolator was developed by Li et al. [27] as the key element to form smart seismic isolation system. The novel isolator contains unique laminated structure of steel and MR elastomer layers, which enable its large-scale civil engineering applications, and a solenoid to provide sufficient and uniform magnetic field for energizing the field-dependent property of MR elastomers. With the controllable shear modulus/damping of the MR elastomer, the developed adaptive seismic isolator possesses a controllable lateral stiffness while

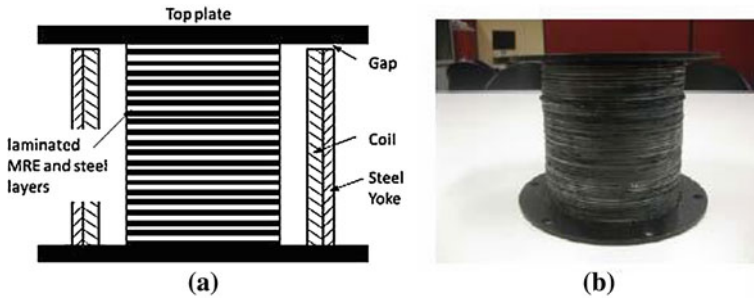


Fig. 8 **a** Cross section of the MRE seismic isolator, and **b** the laminated MRE and steel structure [25]

maintaining adequate vertical loading capacity. Experimental results show that the first prototypical MRE seismic isolator can provide stiffness increase up to 37.49 %, while the second prototypical MRE seismic isolator provides amazing increase of lateral stiffness up to 1,630 %. Such range of increase of the controllable stiffness of the seismic isolator makes it highly practical for developing new adaptive base isolation system utilizing either semi-active or smart passive controls.

The detailed experimental setup by Li et al. [25] is shown in Fig. 11. In order to evaluate and characterize the novel MRE seismic isolator, a series of pseudo-dynamic and dynamic tests were conducted. Experimental results show that the proposed adaptive seismic isolator can successfully alter the lateral stiffness and damping force in real time up to 37 and 45 % respectively.

The smart base isolation system based on the MR elastomer-based isolator is taken into consideration in the experimental part. Figure 12 shows the setup of the experimental part. As shown in the Fig. 12, a shaking table system is used to provide the input excitation to the MR elastomer-based isolator. The results show that the proposed smart base isolation system outperforms the passive base isolation system in reducing the responses of the structure for the excitations considered in this study [22].

A magnetorheological elastomer (MRE) was manufactured and tested, and a MRE sandwich beam was also fabricated from a MRE between two thin aluminum layers. An experimental test rig was set up to investigate the vibration response of the MRE sandwich beam under a non-homogeneous magnetic field. The experimental results show that the first natural frequency of the MRE sandwich beam decreased as the magnetic field applied to the beam was moved from the clamped end of the beam to the free end of the beam. It is also noted that the MRE sandwich beam had the capability to left shift the first natural frequency when the magnetic field was increased in the activated regions [28].

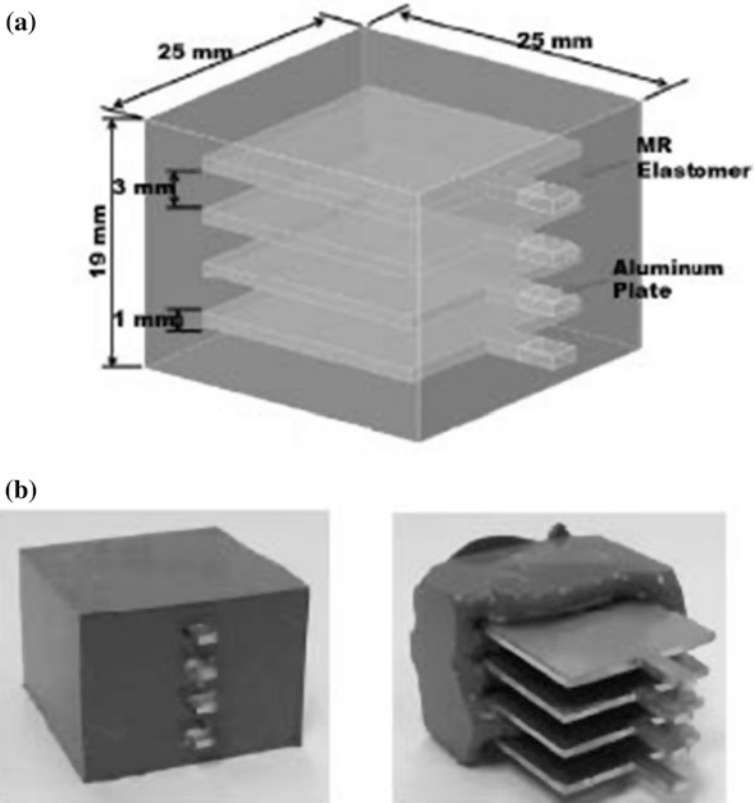
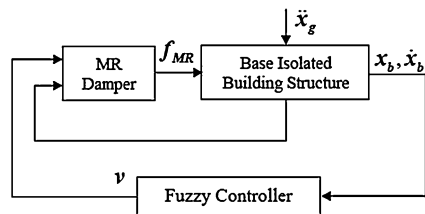


Fig. 9 Laminated MR elastomer-based isolator. **a** Schematic diagram of the isolator. **b** Prototype of the isolator [22]

Fig. 10 Control diagram of the semiactive control system of base isolated building [26]



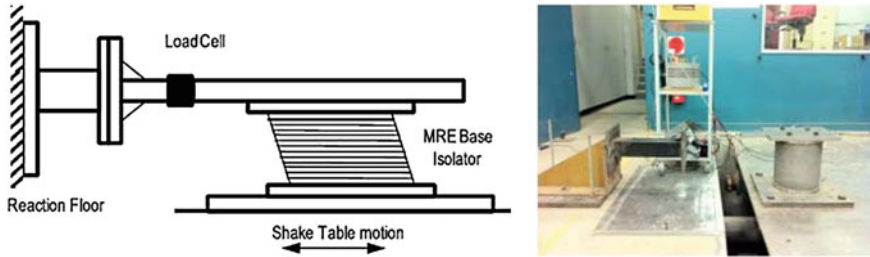


Fig. 11 Sketch of the experimental setup and the test photo [25]

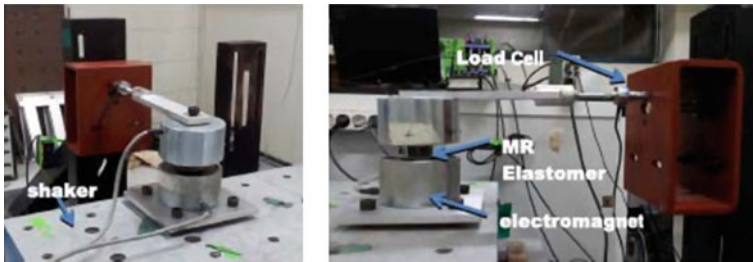


Fig. 12 Experimental setup [22]

5 Conclusions

This paper presents a review of all relevant papers known to the authors describing properties, characteristic, modeling, and experiment of magnetorheological elastomer due to seismic protection. These types MRE allow changes on the dynamic stiffness of the structure. Such response is desired as new technologies.

Acknowledgments The authors would like to acknowledge that this research has been carried out as part of a project RAGS funded by Ministry of Education (MOE) and support from Research Management Institute (RMI), Universiti Teknologi MARA (UiTM).

References

1. J.D. Carlson, M.R. Jolly, MR Fluid, foam and elastomer devices. *Mechatronics* **10**, 555–569 (2000)
2. H.X. Deng, X.L. Gong, Adaptive tuned vibration absorber based on magnetorheological elastomer. *J. Intell. Mater. Syst. Struct.* **18**, 1205–1210 (2007)
3. D.J. Klingenberg, Magnetorheology: applications and challenges. *AIChE J.* **47**(2), 246–249 (2001)
4. J. Heinonen, *Preliminary Study of Modelling Dynamic Properties of Magnetorheological Fluid Damper* (VTT publications, 2006), 36p

5. W.H. Li, X.Y. Wang, X.Z. Zhang, Y. Zhou, Development and analysis of a variable stiffness damper using an MR bladder. *Smart Mater. Struct.* **18**, 074007 (8 pp) (2009)
6. S. Nagarajaiah, Nonlinear, seismic response spectra of smart sliding isolated structures with independently variable MR dampers and variable stiffness SAIVS system. *Struct. Eng. Mech.* **24**(3), 375–393 (2006)
7. J.H. Ding, Theoretical and experimental study on structural repressed system using viscous fluid dampers. Ph. D. dissertation, Harbin Institute of Technology, 2001
8. I. Bica, Advances in magnetorheological suspension: production and properties. *J. Ind. Eng. Chem.* **12**(4), 501–515 (2006)
9. P. Venkateswara Rao, S. Maniprakash, S.M. Srinivasan, A.R. Srinivasa, Functional behavior of isotropic magnetorheological gels. *Smart Mater. Struct.* **19**, 085019 (9 pp) (2010)
10. S.H. Eem, H.J. Jung, J.H. Koo, Application of MR elastomers for improving seismic protection of seismic protection of base-isolated structure. *IEEE Trans. Magn.* **47**(10) (2011)
11. M. Kallio, The elastic and damping properties of magnetorheological elastomers, vol. 565 (VTT publications, 2005), 149 p
12. H.J. Jung, S.J. Lee, D.D. Jang, I.H. Kim, J.H. Koo, F. Khan, Dynamic characterization of magneto-rheological elastomers in shear mode. *IEEE Trans. Magn.* **40**, 3930–3933 (2009)
13. G.E. Iacobescu, M. Balasoiu, I. Bica, Investigation of magnetorheological elastomer surface properties by atomic force microscopy. *J. Supercond. Novel Magn.* (2012)
14. C. Collette, G. Kroll, G. Saive, V. Guillemier, M. Avraam, A. Preumont, Isolation and damping properties of magnetorheologic elastomers. *J. Phys.: Conf. Ser.* **149**, 012091 (2009)
15. M. Lokander, B. Stenberg, Performance of isotropic magnetorheological rubber materials. *Polym. Test.* **22**, 245–251 (2003)
16. Z.G. Ying, Y.Q. Ni, M. Sajjadi, Nonlinear dynamic characteristics of magneto-rheological visco-elastomers. *Sci China Tech Sci* **56**, 878–883 (2013)
17. X. Dong, M. Yu, C. Liao, W. Chen, A new variable stiffness absorber based on magneto-rheological elastomer. *Trans. Nonferrous Met. Soc. China* **19**, s611–s615 (2009)
18. K.D. Sajal, Seismic base isolation—an overview. *Curr. Sci.* **87**(10) (2004)
19. M. Behrooz, X. Wang, F. Gordaninejad, Control of structures featuring a new MRE isolator system, in *Proceedings of SPIE 8341, Active and Passive Smart Structures and Integrated Systems* (2012)
20. S.J. Patil, G.R. Reddy, State of art review—base isolation systems for structures. *Int. J. Emerg. Technol. Adv. Eng.* (2012)
21. W. Li, X. Zhang, H. Du, Development and simulation evaluation of a magnetorheological elastomer isolator for seat vibration control. *J. Intell. Mater. Syst. Struct.* (2012)
22. S.H. Eem, H.J. Jung, J.H. Koo, Seismic performance evaluation of an MR elastomer-based smart base isolation system using real-time hybrid simulation. *Smart Mater. Struct.* **22**, 055003, 10 pp (2013)
23. J.D. Doo, M. Usman, S.S. Hoon, M.Y. Jong, J.H. Jo, Feasibility study of mr elastomer-based base isolation system. (2008), unpublished
24. Y. Shen, M.F. Golnaraghi, G.R. Heppler, Experimental research and modeling of magnetorheological elastomers. *J. Intell. Mater. Syst. Struct.* **15** (2004)
25. Y. Li, J. Li, W. Li, B. Samali, Development and characterization of a magnetorheological elastomer based adaptive seismic isolator. *Smart Mater. Struct.* **22**, 035005, 12 pp (2013)
26. K.-M. Choi, H.-J. Jung, I.-W. Lee, Fuzzy control strategy for seismic response reduction of smart base isolated benchmark building, in *17th ASCE Engineering Mechanics Conference* (2004)
27. J. Li, Y. Li, W. Li, B. Samali, Development of adaptive seismic isolators for ultimate seismic protection of civil structures. *Sensors and Smart Structures Technologies for Civil, Mechanical, and Aerospace Systems*, San Diego, California, USA, 2013, pp. 1–12
28. G. Hu, M. Guo, W. Li, H. Du, G. Alici, Experimental investigation of the vibration characteristics of a magnetorheological elastomer sandwich beam under non-homogeneous small magnetic fields. *Smart Mater. Struct.* **20**(12), 1–7 (2011)

Fresh Properties of Self-Compacting Concrete Incorporating Palm Oil Clinker

Jegathish Kanadasan and Hashim Abdul Razak

Abstract Self-compacting concrete (SCC) has diversified the utilization of concrete in the construction industry due to its capability to consolidate on its own without the need of any external mechanical vibration. This property allows for complex architectural design as well as reduction in the construction time. Palm oil clinker (POC) is a waste material from the palm oil processing plants. The consumption of this waste by products in concrete could help to revive the sustainability of aggregates which is currently depleting. Particle packing (PP) concept is introduced in evaluating the proportion of aggregates and void over a given volume. Based on these values, the mix design is developed for POC SCC. Evaluations of fresh and hardened properties of POC SCC indicate the suitability of POC to be utilized in the construction industry.

Keywords Palm oil clinker • Self-compacting concrete • Particle packing

1 Introduction

Self-compacting concrete (SCC) has wide-ranging structural applications in the construction industry due to its potential to consolidate on its own without vibration and produce quality structures. These properties coupled with enhanced behavior of the concrete itself in terms of mechanical and durability features has increased the popularity of SCC in construction and building. Agricultural industry in Malaysia has been one of the backbone of the country for the past few decades.

J. Kanadasan (✉) · H. A. Razak
StrucHMRS Group, Department of Civil Engineering, University of Malaya,
Kuala Lumpur, Malaysia
e-mail: jegathish@siswa.um.edu.my

Fig. 1 A large chunk of palm oil clinker collected from the palm oil mill



Conversion of useful consumer goods from this industry generates considerably high volume of waste. A proper waste management is required to ensure these materials do not give rise to environmental problems. Palm oil clinker (POC) is a waste by-product originating from the incineration process of oil palm shells and fibers. They are generally irregular in shape, porous and with good lightweight characteristics.

Particle packing (PP) study gives an insight on the interaction between POC aggregates and natural aggregates at different replacement levels. The void volume and corresponding PP were incorporated into a series of mix design development process to obtain the final mix proportion. In this research, focus was given on understanding the POC replacement as aggregates besides incorporation POC powder. POC powder is utilized as binder material to enhance the SCC properties. POC powder was used in the mix design process to supplement the required paste volume generated from the PP analysis. This powder material could also act as a viscosity modifying agent to alter the paste configuration. POC powder was purposely chosen to ensure the maximum usage of palm oil waste products in SCC.

2 Materials

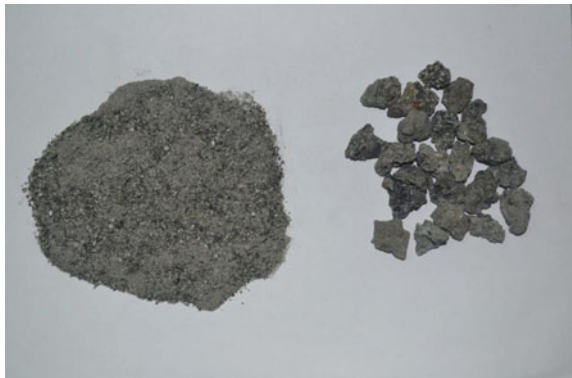
2.1 Aggregates

Figure 1 shows a large chunk of POC which was obtained from the palm oil mill. Figure 2 shows the highly porous nature of POC, while Fig. 3 shows the coarse and fine POC which are utilized in SCC. For coarse aggregates, both gravel and coarse POC were obtained in sizes ranging from 5 to 14 mm. While for sand and fine POC, they were collected below 5 mm. Table 1 shows the physical properties of all aggregates used in this research.

Fig. 2 Porous characteristics of palm oil clinker



Fig. 3 POC fine and POC coarse after crushing stage



2.2 Cementitious and Binder Materials

Ordinary Portland cement (Type I) was used throughout the study. POC powder was obtained by ball mill grinding process of POC. The chemical properties of cement and POC Powder used in this research are tabulated in Table 2.

2.3 Admixtures

A polycarboxylate based superplasticizer (SP) was utilized in this research. The density of the SP was 1.08 kg/L. The amount of solids within the SP was 40 %.

Table 1 Physical properties of aggregates

Properties	Aggregate			
	Fine POC	Coarse POC	Sand	Gravel
Aggregate size (mm)	<5	5–14	<5	5–14
Specific gravity	2.15	1.73	2.66	2.63
Moisture content (%)	0.5 ± 0.25	1 ± 0.5	0.08	0.28
Water absorption (%)	10 ± 5	3 ± 2	0.39	0.58
Aggregate crushing value (%)	–	56.44	–	17.93
Aggregates crushing value 10 % fines	–	16.99	–	–

Table 2 Chemical composition of binders

Chemical properties		
Oxides	Cement	POC powder
CaO	64.00	6.37
SiO ₂	20.29	59.90
SO ₃	2.61	0.39
Fe ₂ O ₃	2.94	6.93
Al ₂ O ₃	5.37	3.89
MgO	3.13	3.30
P ₂ O ₅	0.07	3.47
K ₂ O	0.17	15.10
TiO ₂	0.12	0.29
Mn ₂ O ₃	0.12	–
Na ₂ O	0.24	–
Others	0.94	0.36
Loss on ignition	1.40	1.89
<i>Bogue compound composition of cement</i>		–
<i>Compound</i>		
C ₃ S	58.62	
C ₂ S	13.95	
C ₃ A	9.26	
C ₄ AF	8.95	
<i>Physical properties</i>		
Specific gravity	3.15	2.59

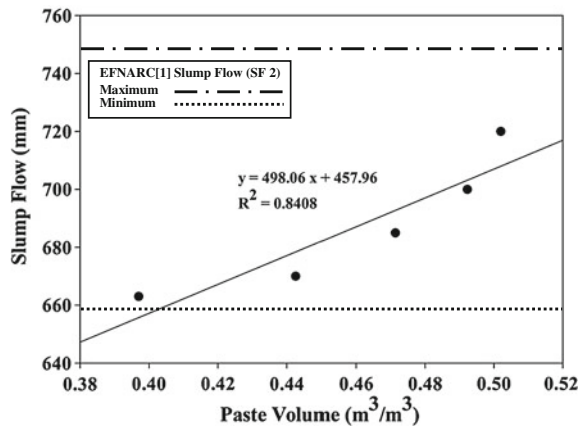
3 Research Programme

Table 3 shows the mix proportion for POC SCC. For all the mixes, the fresh SCC properties such as slump flow, T₅₀₀, V-funnel and L-box were evaluated according to EFNARC [1] specification. Besides that, the SCC mixes were also tested for mechanical properties in terms of density reduction, ultrasonic pulse velocity (UPV), compressive strength and electrical resistivity at an early age of one day. The fresh and hardened properties were correlated to establish a relationship between them.

Table 3 Mix proportion

Components	POC substitution (%)				
	0	25	50	75	100
POC coarse	–	94	178	256	332
POC fine	–	175	331	477	623
Gravel	619	428	270	130	–
Sand	938	649	410	197	–
Cement	550	550	550	550	550
POC powder	84	150	192	226	237
Water	190	210	223	232	236
S.P. (%)	1.00	0.75	0.50	0.40	0.35
W/B	0.30	0.30	0.30	0.30	0.30

Fig. 4 Relationship between paste volume and slump flow



4 Results and Discussion

4.1 Slump Flow

Figure 4 shows the effect of paste volume on the slump flow. In addition, Fig. 5 depicts the relationship between slump flow, POC substitution ratio and paste volume. For POC 100, the immense amount of voids between the POC aggregates elevates the paste volume required for SCC. This indirectly provides an extra amount of paste that will be required to establish lubrication between POC particles. Compared to POC 0 which has the highest value of PP, the need for an additional paste volume is reduced due to lesser availability of pores within the aggregate skeleton. Due to that, a smaller slump flow diameter is obtained compared to all the other mixes. All the mixes fall into SF2 class which is between 660 and 750 mm. The higher rolling capability of the aggregates which has been coated and introduced with extra amount of lubrication contributes to this situation.

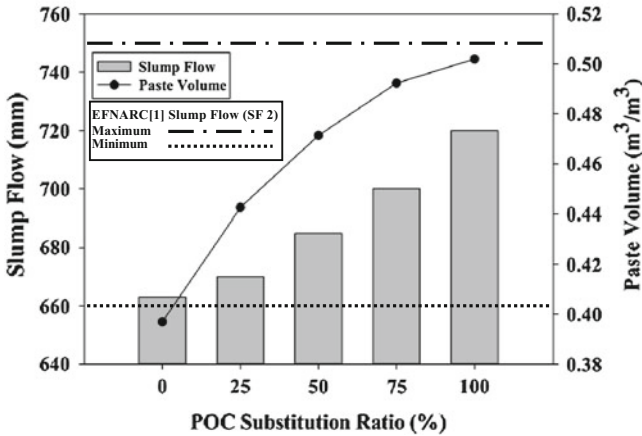
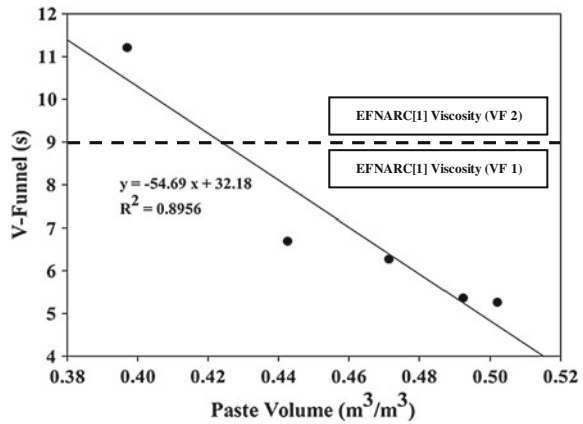


Fig. 5 Relationship between slump flow, POC substitution ratio, paste volume

Fig. 6 Relationship between paste volume and V-funnel



4.2 V-Funnel and T_{500}

Figure 6 shows the effect of paste volume on the V-funnel flow time. On the other hand, Fig. 7 illustrates the relationship between V-funnel flow time, POC substitution ratio and paste volume. The viscosity of the mix directly influences the flow time. Generally, a reducing flow time trend can be observed from the graph as the amount of POC increases in SCC. POC 100 with an elevated paste volume helps to induce a good passing ability and flow ability criteria due to lower viscosity of the mix. An increase in the viscosity of the POC 0 mix was observed due to the greater friction between the aggregates and the available paste.

Mix POC 0 can be classified into class VF2 while all the other remaining mixes will be in VF1. Figure 8 shows the effect of paste volume on the T_{500} time. While

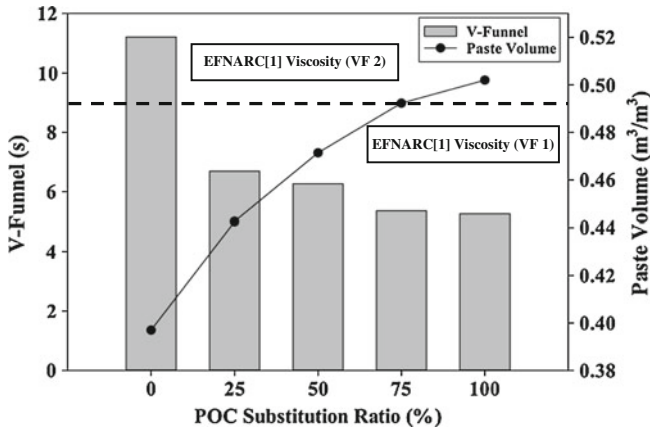
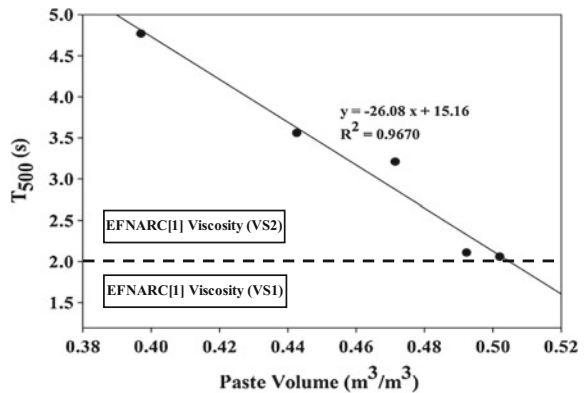


Fig. 7 Relationship between V-funnel, POC substitution ratio, paste volume

Fig. 8 Relationship between paste volume and T_{500}



the relationship between T_{500} time, POC substitution ratio and paste volume are depicted in Fig. 9. The viscosity of the mix plays an important role in T_{500} determination. As the POC replacement ratio increases, the T_{500} time reduces which can be explained by the increase in paste volume.

4.3 L-Box

For all the POC SCC mixes, the L-box passing height was 1.0 satisfying PA2 range. This was greatly influenced by the introduction of correction lubrication factor (CLF) which provides extra paste volume to enhance the lubrication between the aggregates. Besides that, the fine to total aggregates ratios (F/A) of 0.6 which was employed throughout the study indicate improved rolling and passing capability of the aggregates.

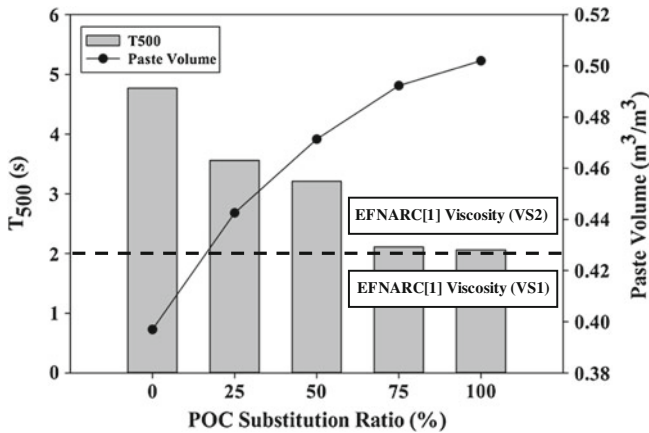


Fig. 9 Relationship between T_{500} , POC substitution ratio and paste volume

4.4 Density

POC which are lightweight in nature reduces the overall weight of the concrete structure. Figure 10 illustrates the relationship between POC substitution level, density of the hardened POC and concrete weight reduction. It is clear that with full replacement of POC, a lower density of POC which is very close to $2,000 \text{ kg/m}^3$ can be achieved and can be classified as lightweight concrete. POC 75 can be also considered as lightweight concrete since it is also very close to the boundary of lightweight concrete region ($2,050\text{--}2,100 \text{ kg/m}^3$). Almost 16 % of concrete weight reduction was observed with the complete replacement of POC over natural aggregates.

4.5 Ultrasonic Pulse Velocity

Figure 11 shows the effect of paste volume on the UPV readings. The aggregate packing level of SCC plays a vital role in exhibiting the pulse movement rate. A higher packing level of natural aggregates represented by POC 0 shows highest UPV reading compared to all other mixes. A decreasing trend in terms of UPV readings can be observed with an increasing POC replacement ratio. The porous state of POC aggregates as well as huge amount of voids between the POC aggregates due to its shape plays an important role to produce a lower pulse transfer. In general, POC 100 which represents complete substitution of POC can be classified as in the satisfactory region.

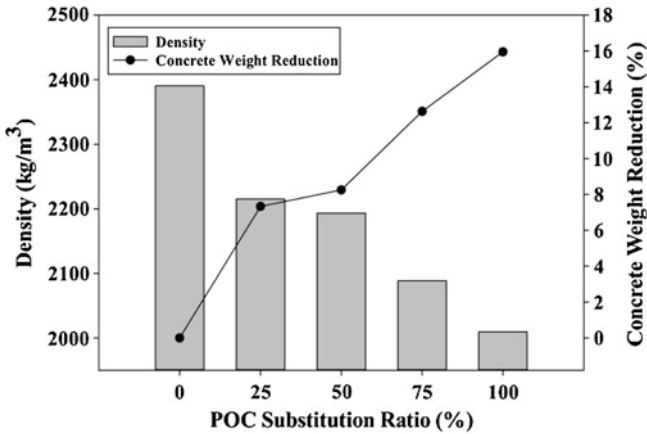
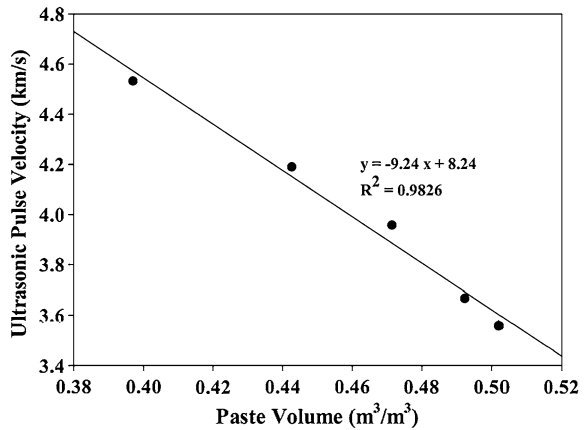


Fig. 10 Relationship between density, POC substitution ratio and concrete weight reduction

Fig. 11 Relationship between paste volume and ultrasonic pulse velocity



4.6 Compressive Strength

Figure 12 shows the relationship between paste volume and compressive strength. The lightweight nature of POC 100 affects the compressive strength greatly. This situation can be explained and supported by the lower aggregate crushing value (ACV) which was found for the POC aggregates. Although sufficient amount of paste provided, again the strength of the overall concrete is majorly bounded by the aggregates capability to take up the given load. In addition, a lower ACV 10 % fines indicates a very low load bearing capacity of POC aggregates under certain fixed load.

Figure 13 shows the changes in UPV readings with compressive strength. The paste volume which indirectly depicts the PP values indicates that higher packing degree of the concrete structure produces higher UPV readings.

Fig. 12 Relationship between paste volume and compressive strength

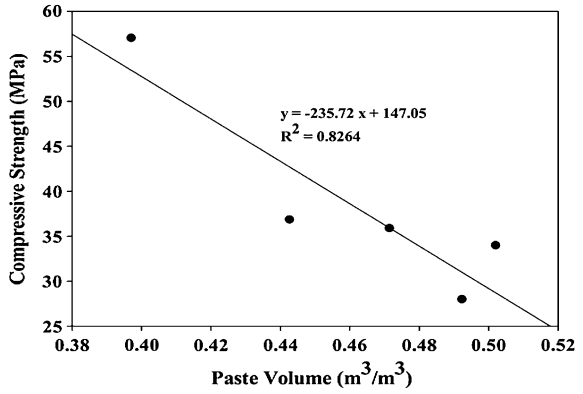


Fig. 13 Relationship between ultrasonic pulse velocity and compressive strength

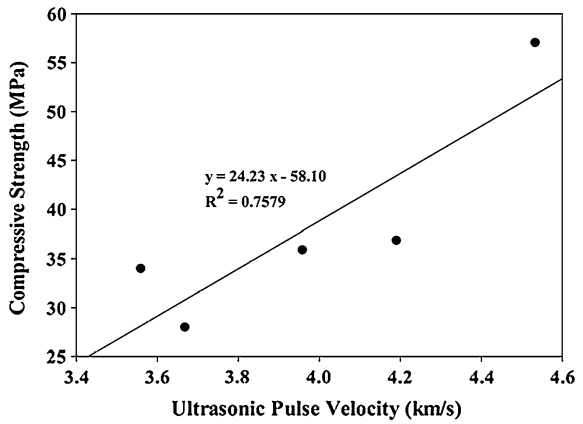
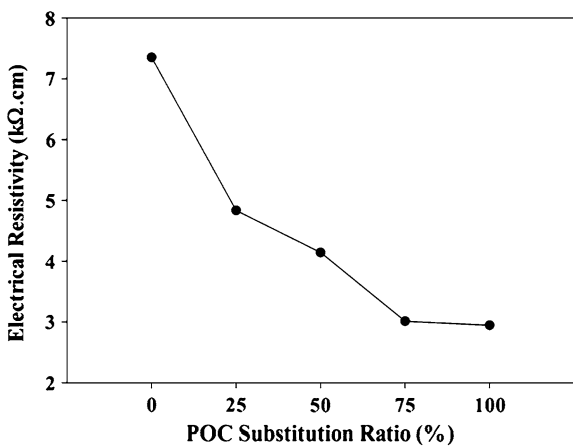


Fig. 14 Relationship between POC substitution ratio and electrical resistivity



4.7 *Electrical Resistivity*

Figure 14 shows the effect of POC replacement on the electrical resistivity readings. The increase in POC replacement ratio generally reduces the resistivity results. However, the differences between them are considerably low and are expected to increase over time. This test provides a good indication on the corrosion rate.

5 Conclusion

The fresh properties of POC SCC satisfied the EFNARC [1] requirements. Introduction of mix design based on PP and paste volume induces significant achievement of optimized concrete structure with elevated fresh and hardened properties performance. Sustainability of the aggregates can be preserved with the utilization of POC aggregates in SCC besides reducing the environmental pollution problems.

Acknowledgments The authors would like to sincerely appreciate and thank University Malaya for supporting this research work through grant UM.C/625/1/HIR/105 and PV079/2012A. Thanks are also due to staffs and members of the Concrete Technology laboratory, University of Malaya for their support and immense help provided throughout the research.

Reference

1. EFNARC, The European Guidelines for Self-Compacting Concrete: Specification, Production and Use, 2005, p. 68

Part III
Flood Management and Intelligence
Development

Flood Economy Appraisal: An Overview of the Malaysian Scenario

Wei-Koon Lee and Irma Noorazurah Mohamad

Abstract Flood is the most devastating natural disaster in Malaysia. Its increased frequency and magnitude has caused to the country substantial financial losses as well as other intangible damage. In this paper, the challenges of flood damage appraisal and the importance of reliable cost-benefit analysis is discussed. In addition, flood financing options are also reviewed to evaluate the overall scenario of flood economy in the country. It is concluded that we need a methodological approach to produce consistent and reliable flood economy estimate for critical decision-making.

Keywords Cost-benefit analysis • Economy impact • Project financing • Flood damage losses • Flood control

1 Introduction

Malaysia is a blessed country that is exempted from many natural disasters. Although we have experienced the ripple effect of tsunamis as a result of the Indonesian earthquake during the last decade, our exposure to natural disasters remains moderate, if not low, with the exception of the chronic issue of flood.

According to the statistical compilation of PreventionWeb, a project under the United Nation Office for Disaster Risk Reduction (UNISDR), there was a total of 58 events of natural disaster in Malaysia for the period between year 1980 to 2010,

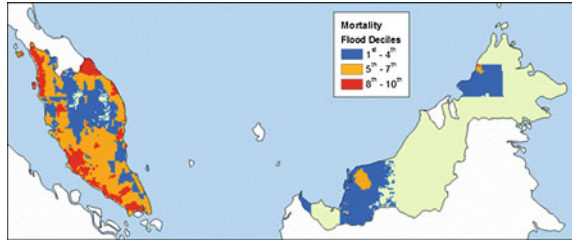
W.-K. Lee (✉)

FloodMIND, Institute of Infrastructure Engineering and Sustainability Management (IIESM), Univeriti Teknologi MARA (UiTM), Shah Alam, Malaysia
e-mail: Leewei994@salam.uitm.edu.my

I. N. Mohamad

Faculty of Civil Engineering, Univeriti Teknologi MARA (UiTM), Shah Alam, Malaysia

Fig. 1 Malaysian flood mortality. *Source* CHRR



claiming a total of 1,239 lives of the 640,000 people affected [1]. Of all the different categories of natural disasters considered, flood accounted for over half the registered events. Floods contribute to 8 out of the 10 disaster events with the highest human exposure, and affect over 85 % of all the disaster-stricken people. Floods are thus the primary hazard affecting Malaysia, in particular the west coast of the Peninsular [2].

Even though flood is not amongst the most lethal (see e.g. Fig. 1 on flood mortality distribution), its economy damage is immense. The 2007 flood alone which affected vast areas in the state of Johor caused an estimated loss of USD 605 million (in US Dollar), the highest of all disaster events in the 3 decades. During the same period, the total flood losses amounted to USD 1 billion, which is more than half the total economy loss due to natural disasters [1].

Based on the analysis of Global Risk Data Platform published by United Nation Environmental Programme (UNEP) [3], Fig. 2 shows the global flood vulnerability, where Malaysia has an estimated annual human exposure of 25,000 and the total casualty approaches 10. Figure 3 shows that Malaysian economic losses due to flood is estimated at close to USD 60 million per year [3]. The scenario is not utterly grave but calls for political will and provision of funding in order for preventive measures or scheme to be implemented. More specifically, the cost-benefit analysis, and analysis of the pros and cons of various mode of financing options are essential for the government, whether at the federal or state level, to make an informed decision.

In this paper, the approach on flood damage assessment and the concept of cost-benefit analysis are reviewed. The need of a national methodology of flood economy appraisal is emphasized and discussed. Specific focus is given to urban flash flood where the human exposure and the potential economy damage is the highest and the most critical.

2 Flood Scenario in Malaysia

Malaysia has an equatorial climate with high temperatures and relative humidity. According to Drainage and Irrigation Department (DID) Malaysia, the annual average rainfall in Peninsular Malaysia, Sabah and Sarawak are 2,420, 2,630 and

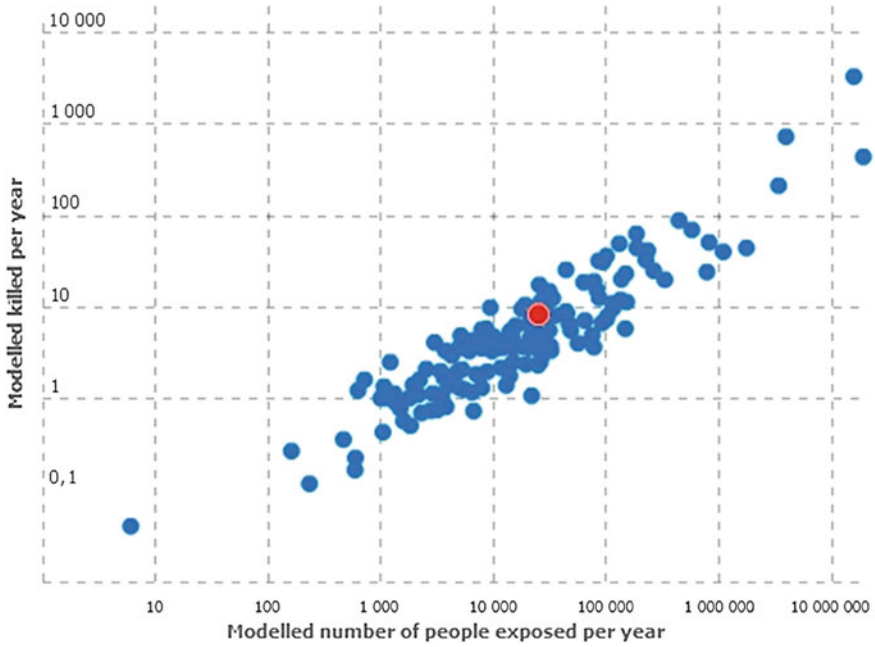


Fig. 2 Global flood vulnerability, with the highlighted point showing Malaysia. Source UNEP

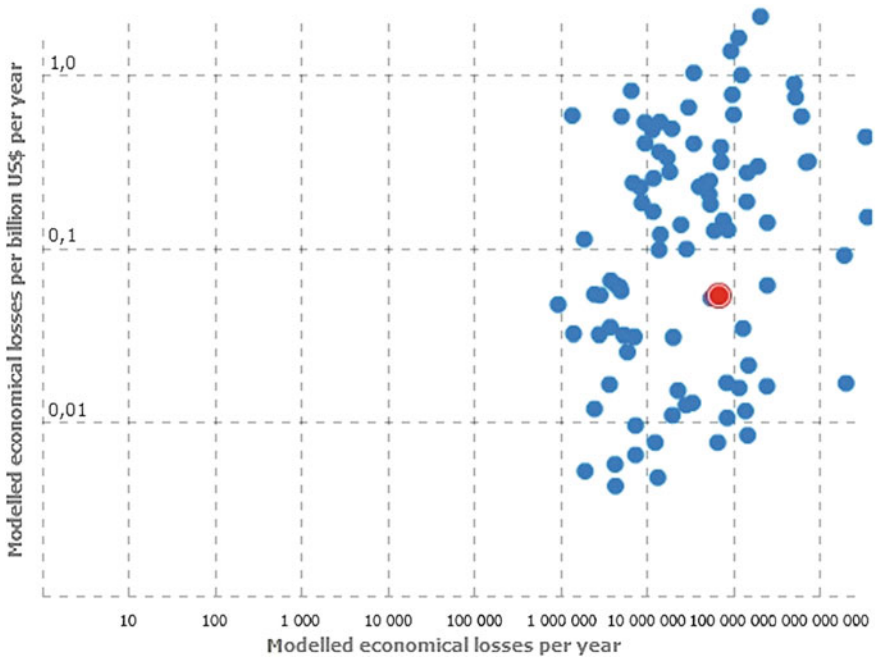


Fig. 3 Global flood economic risk index (ERI), with the highlighted point showing Malaysia. Source UNEP

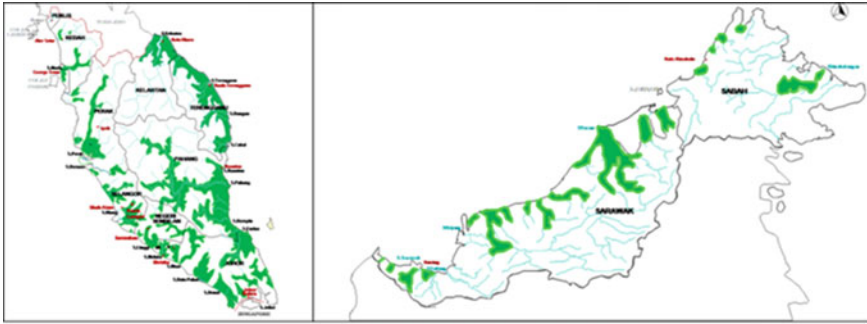


Fig. 4 Flood-prone areas in Malaysia. *Source DID*

3,830 mm respectively. Heavier precipitation is typically recorded in the east coast of Peninsular Malaysia and the coastal regions of Sabah and Sarawak. The northeast (November–February) and southwest (April–September) monsoons bring most of the rainfall, with the former being more severe. It is not surprising to record as much as 600 mm in 24 h in extreme cases [4]. Overall, it is estimated that 9 % or 29,800 km² of the country are flood-prone (see Fig. 4) involving 4 million people [5]. This includes places such as Rantau Panjang, Kota Baru, Dungun, Pekan, Segamat, Kota Tinggi, Alor Setar, Perlis, and Penang.

The urbanized west coast of Peninsular Malaysia is susceptible to flood mainly from the month of September to November during the inter-monsoonal period when convectional thunderstorms are prevalent [4]. These storms bring short but very intense rainfall as highlighted above which can overload the drainage systems within short time-period, causing localized flash flood. The Director-General of the Meteorological Department, Che Gayah Ismail, has mentioned that a ‘heavy rain’ as low as 30 mm may trigger flash flood in certain low-lying areas in the Klang Valley, namely places such as Gombak, Jinjang, Sri Hartamas, Setapak, Cheras, and Sungai Besi [6].

Table 1 shows the major flash flood events in various part of Malaysia. Records show that the occurrence of flash flood is closely related to urbanized catchment where drainage infrastructure fails to keep up with the changing land use. On the basis of increased population density as a result of urban migration and population growth, flood hazards in urban settlements is expected to escalate both in terms of human exposure and economy damage [7].

The occurrences of extreme flood event are increasingly become more frequent, with over 10 incidents of flood exceeding 100-year annual recurrence interval between the 10-year period from 2003 to 2012 [9]. Furthermore, the maximum annual rainfall intensity has also increased substantially. For example, the 1, 3 and 6 h rain for the period 2000–2007 are 17, 29 and 31 % higher respectively, compared to the period 1970–1980. This corresponds to high rainfall intensities of 112, 133 and 145 mm/h respectively, a definite threat to the ageing and poorly-maintained drainage system in the country [9]. Recently, failed drainage system

Table 1 Major flash flood in Malaysia [8]

Date	Place
Jan 1971	Kuala Lumpur
10 Jun 2003	Kuala Lumpur
6 Dec 1999	Shah Alam
26 Feb 2006	Shah Alam
2 Mar 2006	Shah Alam
19 Dec 2006	Muar, Johor Bahru, Skudai, Segamat
10 Jan 2007	Muar, Johor Bahru, Skudai, Segamat
10 Jun 2007	Kuala Lumpur
Dec 2007	East coast Peninsular
Nov 2010	Kedah and Perlis

near the Damansara-Puchong Expressway has been touted as the main culprit leading to the rapid rising water near the popular IOI Mall commercial centre in Puchong [10].

The impact of rising river runoff can be compounded by high coastal water level. For instance, the major flood in Klang in March 2012 which inundated two-third of the city is associated with the backwater effect of astronomical tide. The same incidence is reported to have recurred the same year in the month of October [6]. It is estimated that there are some 300,000 people who live within 1 km of Malaysian coastline, and 600,000 within the 2 km band [2]. Considering the projected sea level rise (SLR), extreme flood due to the coupled effect of coastal high water and river runoff spells disaster to the coastal community, such as Klang, Teluk Intan and Pulau Pinang.

For the period between the year 1984–2010, it is estimated that SLR in Malaysia ranges between 0.2 and 4.4 mm annually depending on location [9]. Although this is well below global average, Malaysia cannot be indifferent considering the fact that Malaysia has long coastline of over 4,600 km which makes us highly vulnerable to coastal high water. The irony of SLR is that the threat is certain but not imminent. While it is happening and is expected to pose increasing threat to the coast fronts, the lack of the evidence of its direct impact continues to elude the attention of the authorities. It is crucial that hydrologists give more due attention to the increased frequency of flooding in coastal cities—to demarcate the contributing factor of rainfall-induced runoff and coastal high water level, the latter being a possible manifestation of SLR instead of the seasonal tidal extreme.

3 Flood Damage Assessment

Flood losses can be broadly categorized into tangible or intangible losses [11]. Both categories can be further subdivided into losses owing to direct and indirect contact with flood (see Table 2). Tangible losses can be assessed in a straightforward manner in terms of the actual cost incurred to repair or replace the losses

Table 2 Categories of flood losses [11]

	Direct losses	Indirect losses
Tangible losses	E.g. building and contents, infrastructures, vehicles, crops, livestock, personal belongings and assets etc	E.g. costs of rescue operation, aid, medical and lawsuit expenses, disruption to transport, business, commerce, employment etc
Intangible losses	E.g. lives, injuries, damages to historical and ecological heritage etc	E.g. stress, anxiety, trauma disruption to lives, loss of community, loss of societal resources etc

sustained, direct cost of humanitarian operation (including rescue and medical administration) and provision (including shelters and sustenance), and the projected loss of revenue due to sustained disruption to businesses, employment and transportation. In addition, administrative and legal expenses also need to be accounted for. This mammoth task of quantifying, to the required degree of accuracy, the complete cost factor of the disaster, calls for careful considerations of every relevant aspect without undue omission in order to produce an all-encompassing estimate.

Notwithstanding the complex and demanding tasks above, the world being a global village in this age of connectivity and information explosion means an economy study of the above nature can be performed relatively easily by a scientist in a remote country, extracting basic data available online, and applying a standard methodology to produce an estimate which conjures a global big picture (see e.g. [2]). However, these works are typically produced at such miserable coarse scale, giving no attention at all to the actual context such that its direct application for localized decision-making is greatly restricted. Malaysia should not be dependent on crude estimates like this for our national planning, or specifically, flood planning in the present discussion.

Insurance companies have established methodological way of approximating flood losses (see e.g. [12]). However, due to the fact that flood insurance is still not popular for households in Malaysia, it is not possible to gauge the total losses in a flood event through insurance pay out. Individual claim amount is only indicative of damages in identical residential buildings in the vicinity but not representative of other premises due to the variability of floor area and flood depth, and not to mention, household contents which differs considerably. The same argument applies to all commercial, industrial, institutional buildings.

It is worth noting that insurance company depends as much on third-party or direct damage assessment in order to determine the compensation and premium amount. Hence, independent appraisal of flood damage remains an important source in flood economy study. Besides, for planning purposes, the more relevant data is the total damage to the entire community, the town, city, state or country, as a function of the inundation depth, area and duration, instead of individual household losses.

Owing to the inherent difficulties of a comprehensive damage appraisal, [13] proposed a two-tier approach, namely a rapid assessment method (RAM) and a

detailed assessment method (DAM). The former is a first level approximation which requires only basic information, whereas the latter requires extensive data collection and may be adopted for critical flood region. However, [13] carried out exemplary detailed assessment following the methodology developed in Australia, which has limited applicability in the Malaysian context. It was acknowledged that we need to derive our very own damage curve and damage functions to ensure an accurate reflection of Malaysian flood losses.

In general, flood damage estimates tend to be inaccurate for smaller events with error up to a factor of 2 but greatly improved for higher levels of aggregations [14]. It is thus important to obtain flood loss data from diverse, reliable and preferably direct sources for verification. In order to check for consistency, estimates produced for similar or recurring events may be compared. The ultimate aim is to produce flood damage estimate that is suitable for the purpose of planning and critical decision-making.

While tangible losses can be appropriately assessed in monetary terms, the value of intangible losses cannot be easily determined. Casualties, injuries, human exposure, and the duration of flooding thus continue to be important indicators of the extent of intangible losses. Any damages to buildings, resources or heritage of value to the society or country (Table 2) will require separate appraisal to realize the actual cost incurred.

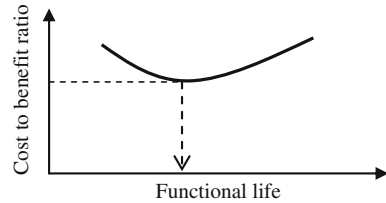
The information on damage costs, when properly archived, provides invaluable insight into the long term cumulative cost incurred by similar events and will no doubt facilitate the decision-making concerning flood-related projects. The authority will thus be on good ground to either approve or delay the capital expenditure. In either case, the stakeholders can be assured of a well-thought and well-justified decision, even if it is a 'do nothing' or 'business as usual' decision [15].

4 Cost-Benefit Analysis

Essentially, the cost of flood damage is the potential benefits that can be derived from a proposed flood control solution. This, together with the realistic cost of the proposed solution must both be appropriately translated into monetary term, taking into consideration the present and future value equivalent of these estimates in order to provide the equal basis for comparative study.

Where it is deemed necessary to implement flood control, or flood mitigation measures, engineers and engineering economists need to begin with the groundwork of assessing the real need and exploring the most economical solution. Theoretically, a project with a functional life of 20 years, for example, should not cost more than the anticipated cumulative loss over the same time period. The ratio of cost to benefit should be maintained below unity, and the lowest value adopted in the determination of the optimum functional life (see Fig. 5). Additional benefits associated with a flood mitigation or flood control project is non-other the stimulating impact on domestic economy especially the construction sector and

Fig. 5 Cost-benefit analysis to determine optimum functional life



increased employment opportunities [16]. There is no doubt, however, that these justifications can be easily overruled due to political reasoning, leading to decision that favours the government on its goodwill to the people but translate to unnecessary financial burden to the country.

Subsequent to the major flood event in Klang in March 2012, the Selangor state government has allocated RM 5.2 million (in Ringgit Malaysia) for short-term flood mitigation, knowingly that a larger sum would be needed to solve the plight and may have to be solicited from the federal government [17]. Meanwhile, the federal government needs to weight between the disparate need across different states of varying woes.

The fundamental issue then lies in the question of which investment yields the most benefit for the country. This in fact, is example of an indirect cost, i.e. the potential gain if the allocation had been used for another purpose which also directly benefits the people in a different way. In this case, the decision will have to be made based on the evaluation of urgency and importance of the respective option, where both monetary and non-monetary return will have to be appropriately assessed.

Take for example the capital city Kuala Lumpur (KL), where the Stormwater Management and Road Tunnel (SMART) was constructed at a whopping cost of RM 1.8 billion (over USD 500 million) in order to alleviate the flash flood plight of the finance and commercial centre of the country [18]. The cost is equivalent to almost 10 times the anticipated national annual loss due to flood events, and is more than half the historical flood cost for the period between the year 1980–2010. This has not yet included the cost of construction of the detention ponds, neither the operating and maintenance costs. As expected, the project functions to prevent the occurrences of flash flood in a number of intense rainfall events [19]. Nonetheless, it also has not been able to eliminate a number of flash flood events due to extreme weather, and has thus aroused great dissatisfaction amongst KL folks [20]. Hence, it is natural to ask whether such a massive investment is able to deliver tangible benefits that out weight its price over the facility lifespan in the locality within its spatial extent of influence. Can Malaysian taxpayer, the urban dwellers of KL city, and the government be assured that the scheme is worth the money spent?

Meanwhile, the residents of Kota Tinggi continue to live in worry of another flood that would submerge the entire town and following the devastation flood in 2006 and 2007 which inundated the nearby housing area for as long as 2 weeks [21]. It was estimated that a flood mitigation project for Kota Tinggi would cost RM 2.2 billion and take up to 15 years to complete [22]—a massive investment

that the government is reluctant to commit for the historical district. It is reported that up to 10 projects totaling RM 67 million were executed under the 9th Malaysia Plan which included de-silting, construction of flood walls, as well as river widening and deepening [23].

For the year 2012, RM 1 billion was allocated under the government Flood Mitigation Plan, of which Kota Tinggi was not amongst the benefactor [16]. It is evident that decision makers need to weight between a total curative solution which costs a bomb, or a partial preventive solution which costs a fraction of the former. Hence, it is vital that a clear 'intention dimension' be established in lieu of a vague idea of 'solving the problem'. Well defined scenarios will no doubt greatly facilitate accurate and realistic costing of potential direct and indirect benefits.

One related problem in the implementation of flood control project is delayed completion, which results in cost escalate, reduced capacity or non-functionality. As of the end of year 2011, 20 ongoing flood mitigation projects in Malaysia were allegedly to have not been fully completed due to funding issue [22, 23]. It may thus be concluded that decision driven by political motives and the inclination to jump into ambitious mega-scale project that promises to solve the problem once-an-for-all at a much higher premium should be avoided unless appropriately justified. This by no means disregards the well-being of the community but to put things under objective examination. It is worth noting that capital investment aside, operation and maintenance cost are important components that ought to be included in the cost analysis to accurately reflect the total anticipated financial commitment of the solution [15].

In brief, cost-benefit analysis is a well-established method for decision-making but its relevance and applicability depends largely on the availability of reliable data in monetary terms and stakeholders' participations.

5 Financing Options

Table 3 shows the national expenditure on flood mitigations which escalated through every 5-year Malaysia Plan. It is estimated that the cost for future river improvement and flood mitigation works will continue to soar and remain daunting for a developing country like Malaysia.

Following our experience of contracting public work to private contractors through built-operate and transfer scheme since 1980s, Malaysian government continues to favour such arrangement as a viable mean of improving the public facilities. In the 2012 national budget announcement, flood-related projects are categorized under the Special Stimulus Package to be financed primarily through Private Financing Initiative (PFI) [16]. The main shortcoming of this approach, however, is the inherent need for the private sector to recoup the investment. Hence the project must incorporate scope which is revenue-generating such as dual-function infrastructure (e.g. SMART tunnel in KL, expressway-cum-floodway, flood control cum water supply reservoir etc.). In the absence of a profitable

Table 3 Flood mitigation expenditure in Malaysia (*Source* DID, Malaysia)

Period	RM	Remark
1971–1975	14 million	2nd Malaysia plan
1976–1980	56 million	3rd Malaysia plan
1981–1985	141 million	4th Malaysia plan
1986–1990	155 million	5th Malaysia plan
1991–1995	431 million	6th Malaysia plan
1996–2000	845 million	7th Malaysia plan
2001–2005	1.8 billion	8th Malaysia plan
2006–2010	4 billion ^a	9th Malaysia plan
2011–2015	5 billion ^a	10th Malaysia plan

^a Data is based on allocated amount

by-function, the main source of funding falls back to the state or the federal government. International funding remains a fall reaching option considering the overall financial strength of the country.

Another viable option is to make it compulsory for property development to incorporate the design and construction of flood prevention measures, particularly those located in the vicinity of flood-prone area. As discussed, the densely populated urbanized area is the most vulnerable to destructive flash flood. In addition to adequate drainage design, provision of pervious ground surface to promote infiltration, e.g. porous parking area, swales, green areas, detention pond, underground storage, rainwater harvesting etc. plays significant role in reducing urban surface runoff [24]. Other state-of-the-art technology or innovations include green roof etc. This option allows the cost of flood mitigation to be transferred to developers, and partially shared by property buyers, as a premium to an urban address. Similar concepts can also be implemented in older developments through tax incentives to individuals and businesses.

Along the same line, large conglomerates should be encouraged to invest and contribute towards the upkeep of main water ways or rivers through adoption programs which also involve the general public. Example includes the WATER (Working Actively Through Education and Rehabilitation) Project by Guinness Anchor Berhad (GAB), Malaysia since 2007 [25]. The initiatives will ease the burden of local council in water way and river maintenance, as well as educate the general public. With increased awareness, projects alike not only reduce the problem of pollution, but also interference and intrusion upon major water ways and rivers that might reduce their discharge capacity.

6 Conclusions

The economy impact of flood is evident and acute for a developing country like Malaysia. Our exposure to flood risk is increasing, both in terms of frequency, area and population affected. Critical decision-making related to flood disaster must be

supported by a thorough cost-benefit analysis which takes into consideration all relevant factors that accurately reflect the national and local scenario. There is thus a need to establish a comprehensive and all-encompassing methodology for reliable appraisal of flood economy. It will be an invaluable tool to both the federal and state governments to objectively assess and thus allocate appropriate resources for the betterment of people's livelihood.

Acknowledgments The author acknowledges the Flood Control Research Center (FCRC), UiTM for the support on the present work, and Prof. Daniel Gunaratnam (Washington DC) for the stimulating discussions on the subject matter.

References

1. PreventionWeb, Malaysia—disaster statistic. Data source: EM-DAT: the OFDA/CRED international disaster database, Universiti Catholique de Louvain, Brussels, Belgium, data version: v11.08. Website: <http://www.preventionweb.net/english/countries/statistics/?cid=105>. Accessed 18 Apr 2013
2. Center for hazards and risk research at Columbia University (CHRR), Malaysia natural disaster profile. Website: <http://www.ldeo.columbia.edu/chrr/research/profiles/malaysia.html>. Accessed 22 Apr 2013
3. UNEP/UNISDR, Global risk data platform. Website: <http://preview.grid.unep.ch/>. Accessed 20 Apr 2013
4. Drainage and Irrigation Department, Managing flood problem. Online publication, Malaysia, 12 Nov 2011
5. Drainage and Irrigation Department, Flood phenomenon. Online publication, Malaysia, 12 Nov 2011
6. The Star, Klang Valley folk on rain and flash flood alert. Website: <http://thestar.com.my/news/story.asp?sec=nation&file=/2012/10/18/nation/12186169>, 18 Oct 2012
7. B. Jongman, P.J. Ward, J.C.J.H. Aerts, Global exposure to river and coastal flooding: Long term trends and changes. *Glob. Env. Change* **22**, 823–835 (2012)
8. Wikipedia, Floods in Malaysia. Website: http://en.wikipedia.org/wiki/Floods_in_Malaysia. Accessed 7 May 2013
9. M. F. Mohamad, Key challenges in urban flood management: Knowledge, experience and policy in Malaysian perspective. Regional workshop on climate change and urban flooding management. UNESCAP (2013)
10. The Star, IOI mall flash floods due to underground drainage malfunction. Website: <http://thestar.com.my/news/story.asp?file=/2013/2/19/nation/20130219220943&sec=nation>, 19 Feb 2013
11. Emergency Management Australia, in Disaster Loss Assessment Guidelines. Australian Emergency Manuals Series, Part III, Emergency Management Practice. vol. 3 (Guide 11. State of Queensland and Commonwealth of Australia, 2002)
12. The National Flood Insurance Program, The cost of flooding. Website: http://www.floodsmart.gov/floodsmart/pages/flooding_flood_risks/the_cost_of_flooding.jsp. Accessed 9 May 2013
13. KTA Tenaga Sdn. Bhd., Flood damage assessment of 26 April 2001 flooding affecting the Klang valley and the preparation of generalised procedures and guidelines for assessment of flood damages (Final report). Drainage and Irrigation Department, Malaysia (2003)
14. R.A. Pielke Jr, M.W. Downton, J.Z. Barnard Miller, Flood damage in the United States 1926–2000: A reanalysis of national weather service estimates. Env. Societal Impacts Group. National Center for Atmospheric Research

15. D.-N. Lamothe, G. Neveu, B. Görlach, E. Interwies, Evaluation of the impact of floods and associated protection policies (Final report). Contract No. 07.0501/2004/389669, European Commission DG Environment (2005)
16. N.A. Razak, Ucapan Belanjawan 2012. Berita Harian. Website: http://www.bharian.com.my/bharian/articles/UcapanBelanjawan2012/belanjawan/belanjawan2012/article_html, 7 Oct 2011
17. Selangor Times, Flash flood alert in Klang. Website: <http://www.selangortimes.com/index.php?section=news&permalink=20121012104126-flash-flood-alert-in-klang>, 12 Oct 2012
18. Wikipedia. SMART tunnel. Website: http://en.wikipedia.org/wiki/SMART_Tunnel. Accessed 17 May 2013
19. M.F.K. Ariffin, Stormwater management and road tunnel: SMART doing better than expected. Letters to the editor, new straits times. Website: <http://www.nst.com.my/opinion/letters-to-the-editor/stormwater-management-and-road-tunnel-smart-doing-better-than-expected-1.164493>, 31 Oct 2012
20. K. Pragalath, Flash floods: Where is SMART? FMT news. Website: <https://www.freemalaysiatoday.com/category/nation/2012/03/09/flash-floods-where-is-smart/>, 9 Mar 2012
21. Z. Musa, 2006–2007 floods still linger on the minds of Kota Tinggi folk. The star. Website: <http://thestar.com.my/metro/story.asp?file=/2013/3/15/southeast/12834461&sec=southeast>, 15 Mar 2013
22. P. Aruna, 20 flood mitigation projects but none fully completed. AsiaOne News/Asia News Network. Website: <http://www.asiaone.com/News/AsiaOne%2BNews/Malaysia/Story/A1Story20111110-309674.html>, 10 Nov 2011
23. The Star, All 23 flood mitigation projects nationwide progressing as scheduled. Website: <http://thestar.com.my/news/story.asp?file=/2011/11/17/focus/9918770&sec=focus>, 17 Nov 2011
24. Drainage and Irrigation Department, Urban stormwater management manual for Malaysia (Manual Saliran Mesra Alam Malaysia), 2nd edn. Malaysia (2012)
25. A. Koay, Volunteers help to keep Sungai Way clean. The star. Website: <http://thestar.com.my/lifestyle/story.asp?file=/2013/4/1/lifefocus/12828241&sec=lifefocus>, 1 Apr 2013

Neural Network Approach to Coastal High and Low Water Level Prediction

Wei-Koon Lee and Tuan Asmaa Binti Tuan Resdi

Abstract This paper presents a model of coastal high and low water prediction using feed forward back-propagation (FFBP) network and generalized regression neural network (GRNN). High and low water level prediction is very important to planning and development of nearshore activities and applications. We show that using 30-day hourly data and 5 main constituents as the input, good results are obtained in the training stage for both models. However, simulations for one-month and one-year period show that the network models are incapable of reproducing the high and low water accurately. The results for one-month simulation do provide some level of effective prediction but for one-year simulation has much larger errors.

Keywords Coastal high and low water levels · Tidal forecasting · FFBP · GRNN

1 Introduction

The daily tidal fluctuations in the coastal area occur because of the gravitational influences and the relative positions between the Earth, the moon and the sun, coupled with the effect of Earth's rotation. Conventionally, tidal forecast is produced from harmonic analysis which requires large amount of observation data. Typically, the minimum length of tidal observation required is one year, and this goes up to 18 years if a complete analysis is targeted. In the absence of long term observation data, it has been shown that artificial neural network (ANN) can be

W.-K. Lee (✉)

FloodMIND, IIESM, UiTM, Shah Alam, Malaysia

e-mail: Leewei994@salam.uitm.edu.my

T. A. B. T. Resdi

Faculty of Civil Engineering, UiTM, Shah Alam, Malaysia

used to predict tidal fluctuation efficiently [1–5]. Artificial Neural Network is very suitable in this study because tidal is known as one of the nonlinear relationship. It is difficult to solve this problem if used others methods.

In Malaysia, tidal tables produced by National Hydrographic Centre (NHC) and Department of Survey and Mapping (JUPEM) provide reasonable coverage to show the typical tidal characteristics along our long coastline. Nonetheless, they are not representative of the actual tidal variations in specific locations where the shoreline features and bathymetry may differ substantially from the nearest available gauging stations. Satisfactory tidal forecast has been reported using back-propagation neural network with as few as 30-day hourly data in any location of interest [6, 7].

It is worth noting that in long-term forecast, the hourly tidal fluctuation is of little interest. More importantly is the extreme high and low water levels which are crucial for coastal planning and development. Hence, in order to produce reliable reference for the construction of coastal and nearshore structures and facilities, research effort should be directed towards predicting the occurrences of the extremities.

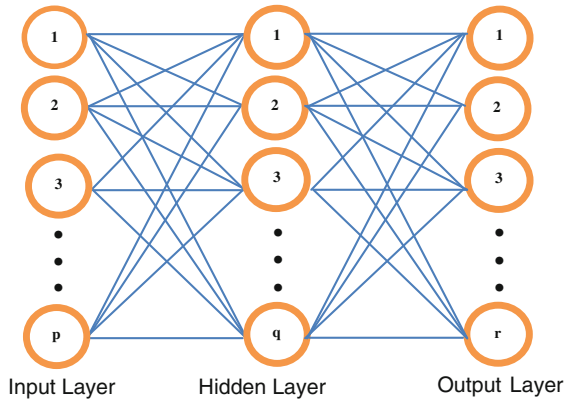
In this paper, we investigate the possibility of using ANN to predict long term coastal high and low water levels for Bintulu station (Stn No. 74005) located in Bintulu Port (03°15' 44"N, 133° 58' 20"E) which is part of JUPEM's Tidal Observation Network (TON). Hourly tidal data is obtained for the period 1994–2004, where the local tidal characteristic is classified as mixed, and predominantly diurnal. Section 2 describes the feed forward back-propagation (FFBP) network and the generalized regression neural network (GRNN) used in the present study; Sect. 3 describes the network architecture design and network training; Sect. 4 presents the results obtained. Conclusions and recommendations are made in Sect. 5.

2 Literature Review

Artificial neural network is commonly used in problems of exclusive and nonlinear relationship. It is a parallel computing system that imitates the biological neural network of the brain by interconnecting many artificial neurons. The key strength of an artificial neural network is its ability to learn and generalize, thus providing solutions to complex problems which normally is difficult to manage by traditional ways of approximation.

A feed forward neural network is an artificial neural network where connections between the units do not form a directed cycle. On the other hand, FFBP is a representative learning model where the network repeatedly adjusts the weights and biases in the network so as to minimize the error function. Figure 1 shows the typical structure of a FFBP network which can be described in the form of $I_p H_q O_r$, where I is the input layer, H is the hidden layer, and O is the output layer respectively, and p , q , r are the number of neuron in the respective layer. FFBP

Fig. 1 Typical structure of a feed-forward back-propagation neural network (FFBP)



algorithm is very sensitive to the selected initial weight values. It is also may provide performances significantly differing from each other. Another problem faced when the application of FFBP is the local minima issue [9]. A local minimum problem is occurs because of the algorithm. It is always changes the weights to cause the error to fall. The simple error can be rise and it is will not decrease further [10].

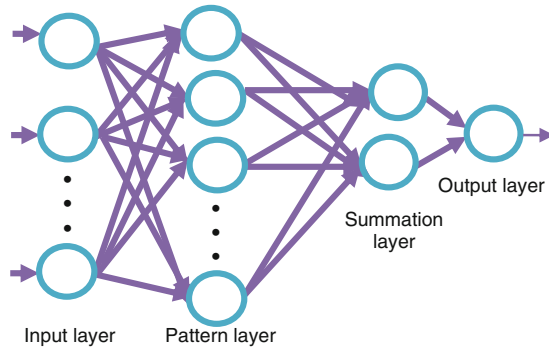
The generalized regression neural network is a variant of the radial basis ANNs and is often used for function approximation and the estimation of continuous variables [8]. The advantages of GRNN are fast learning and convergence to the optimal regression surface as the number of sample becomes very large. Successful implementation depends heavily on the spread factor to obtain a smooth approximation. In the training procedure, GRNN does not frequently encountered local minima problem as in FFBP applications and it also does not generate physically unreasonable estimates (Fig. 2).

3 Model Development

In the design of network architecture, a number of factors to be considered include the number of hidden layers, number of neurons in each layer, and learning factor for the FFBP model, and spread factor for the GRNN model. In the present study, the neural network models are designed using MATLAB Neural Network Toolbox. Following [6, 7], the trained network performance is evaluated using the normalized root mean square error, RMS and the correlation coefficient, R:

$$RMS = \sqrt{\frac{\sum_{j=1}^M (Y_j - O_j)^2}{\sum_{j=1}^M O_j^2}} \tag{1}$$

Fig. 2 The structure of general regression neural network (GRNN)



$$R = \frac{\sum_{j=1}^M (Y_j - \bar{Y})(O_j - \bar{O})}{\sqrt{\sum_{j=1}^M (Y_j - \bar{Y})^2 (O_j - \bar{O})^2}} \tag{2}$$

where M is the total number of sample, Y_j and O_j are the value of the observations, \bar{Y} and \bar{O} are the arithmetic mean.

Our attempt is to produce equally good forecast using 30-day data as reported in [6, 7]. Taking the hourly observations for Bintulu station, our first step is to derive the high and low water profile for the period 1–30 January 1994. Figure 3 shows the 65 data points (as opposed to the total hourly data points of 720) identified which envelopes the high and low water during the period. At least two spring tide and two neap tide conditions are successfully captured. The diurnal tidal effect is filtered where only the higher high and the lower low water levels are extracted. Since the 65 data points are no longer distributed in equal time interval, their respective actual time of occurrence is also saved with reference to 1 January 1900, 00:00 am to compensate for the astronomical arguments and Greenwich phase lag.

The number of main constituents used in the input layer directly affects the accuracy of tidal forecasting. Preliminary investigation shows that increasing the number of constituents does not necessarily yield better results. Hence, a total of 5 harmonic constituents (i.e. input layer = I_{10}) are applied, namely the M_2 , K_1 , S_2 , O_1 and N_2 components [6, 7]. The observed tide is the sum of a number of harmonic constituents, each of whose periods corresponds with the period of some component of the relative astronomical motions between Earth, Sun and Moon. There are 390 harmonic constituents are known. Meanwhile, the output layer is a single variable giving the water level as a function of the time duration specified (i.e. output layer = O_1).

For the FFBP model, the initial trials examine the training performance as a function of the number of layer and the number of neuron in the layers. Network training is performed using Levenberg–Marquardt optimization technique which approaches second order training speed and eliminates the need to tune learning rate and momentum coefficient. Levenberg–Marquardt Optimization is a standard

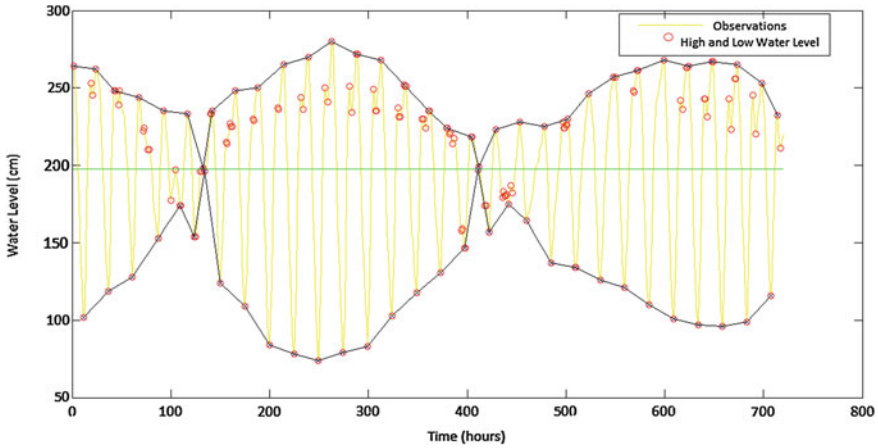


Fig. 3 The high and low water envelope for Bintulu (Stn. No. 74005) for the period 1/1/1994–33/1/1994

Fig. 4 The effect of number of neuron on normalized root mean square error

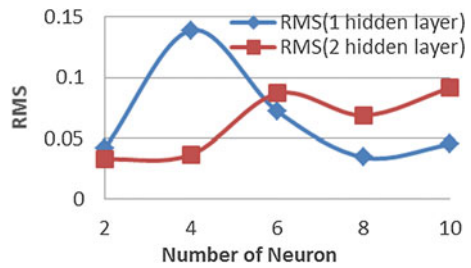
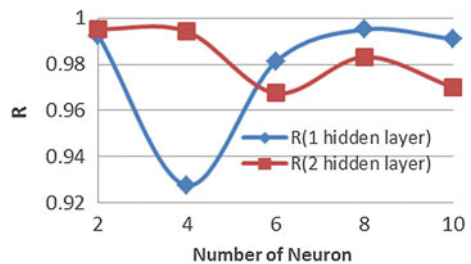


Fig. 5 The effect of number of neuron on correlation coefficient



virtual in nonlinear optimization. Levenberg–Marquardt algorithm is selected to train the network which is based on the numerical optimization technique [10]. The results are plotted in Figs. 4 and 5. It may be summarized that the case of two hidden layer with 2 neurons (i.e. $H_{2,2}$), and the case of one hidden layers with 8 neurons (i.e. H_8) give the most promising results. Figure 6a, b shows the high and low water levels are reproduced satisfactorily. The $I_{10}H_{2,2}O_1$ model gives $RMS = 0.0328$, and $R = 0.9953$; the $I_{10}H_8O_1$ model gives $RMS = 0.0345$, and

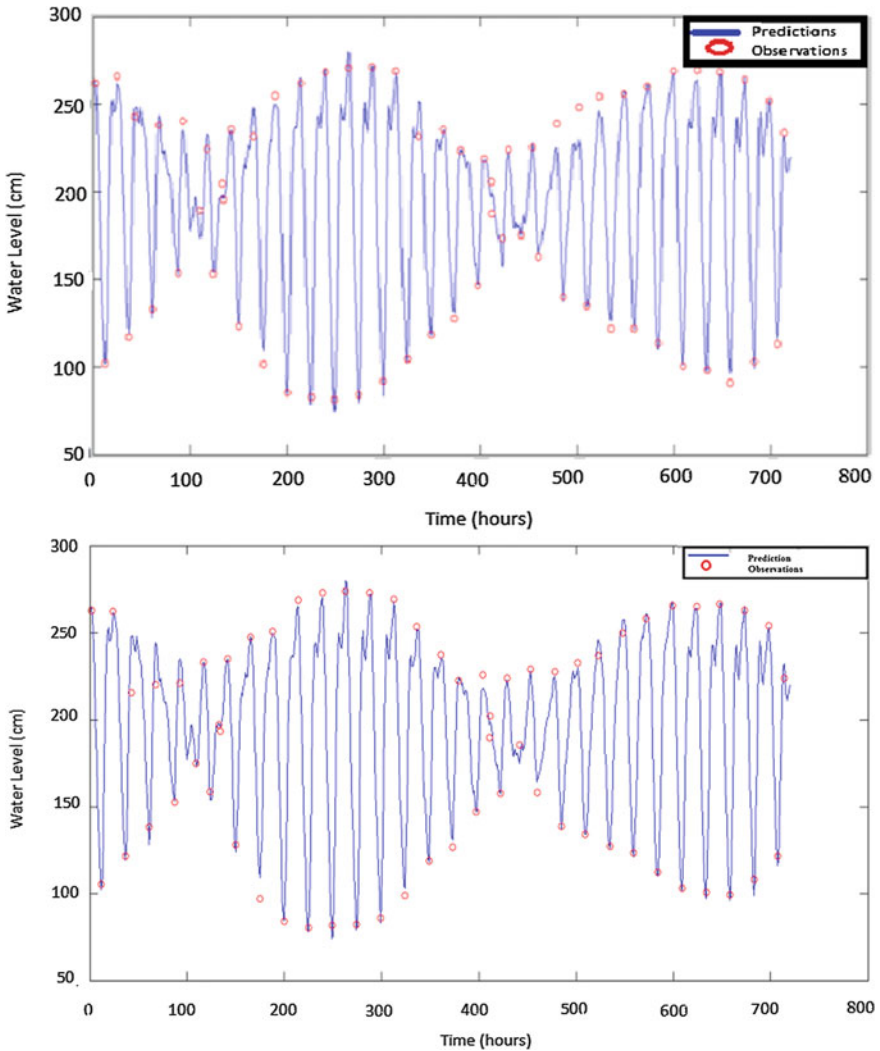


Fig. 6 30-day high and low water level training using FFBP model. **a** Two hidden layers with 2 neurons. **b** One hidden layer with 8 neurons

$R = 0.9951$. Based on visual inspection, both models produce good fit of the spring high and low water levels. Nevertheless, the high and low water profile produced by the $I_{10}H_8O_1$ model is flawed, specifically, in the region of the first neap high water. Based on the value of RMS, the best result is $I_{10}H_{2.2}O_1$ (RMS = 0.0328), but when based on the Fig. 6a, b, the best result is $I_{10}H_8O_1$ (RMS = 0.0345). This occurs because of the different of number of neuron and layer.

For the GRNN model, the number of input units (first layer) equal to the number of parameters. This layer is fully connected to the second layer (pattern).

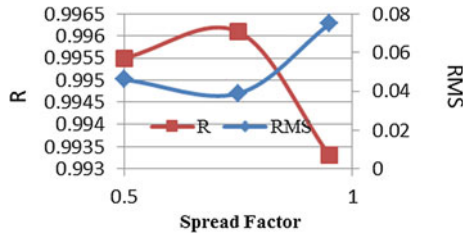


Fig. 7 The effect of spread factor on normalized root mean square error (*RMS*) and correlation coefficient (*R*)

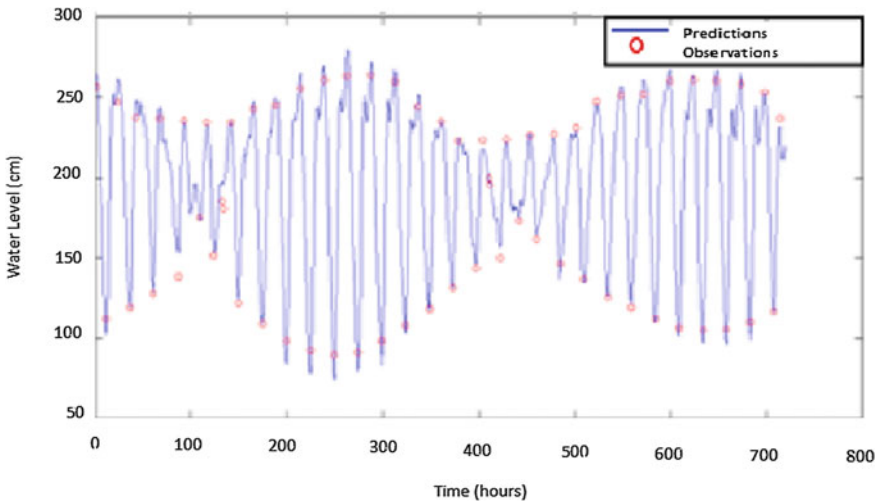


Fig. 8 30-day high and low water level training using GRNN model

Each unit represents a training pattern. Its output is a measure of the distance of the input from the stored patterns. The pattern unit outputs are passed on to the summation units. Figure 7 shows the trial results of the spread factor, where the optimum value chosen is 0.75. Comparing Fig. 6a, b with Fig. 8, we note that the training result given by GRNN is inferior to that produced by the FFBP models. The higher RMS may be attributed to the poor match in capturing the first spring tide high and low water.

4 Network Simulations

In this section, we use the network models developed in the preceding section to simulate the hourly tidal water level fluctuation in Bintulu (Stn. No. 74005). Figure 9a, b shows the one-month tidal simulations using the FFBP network model

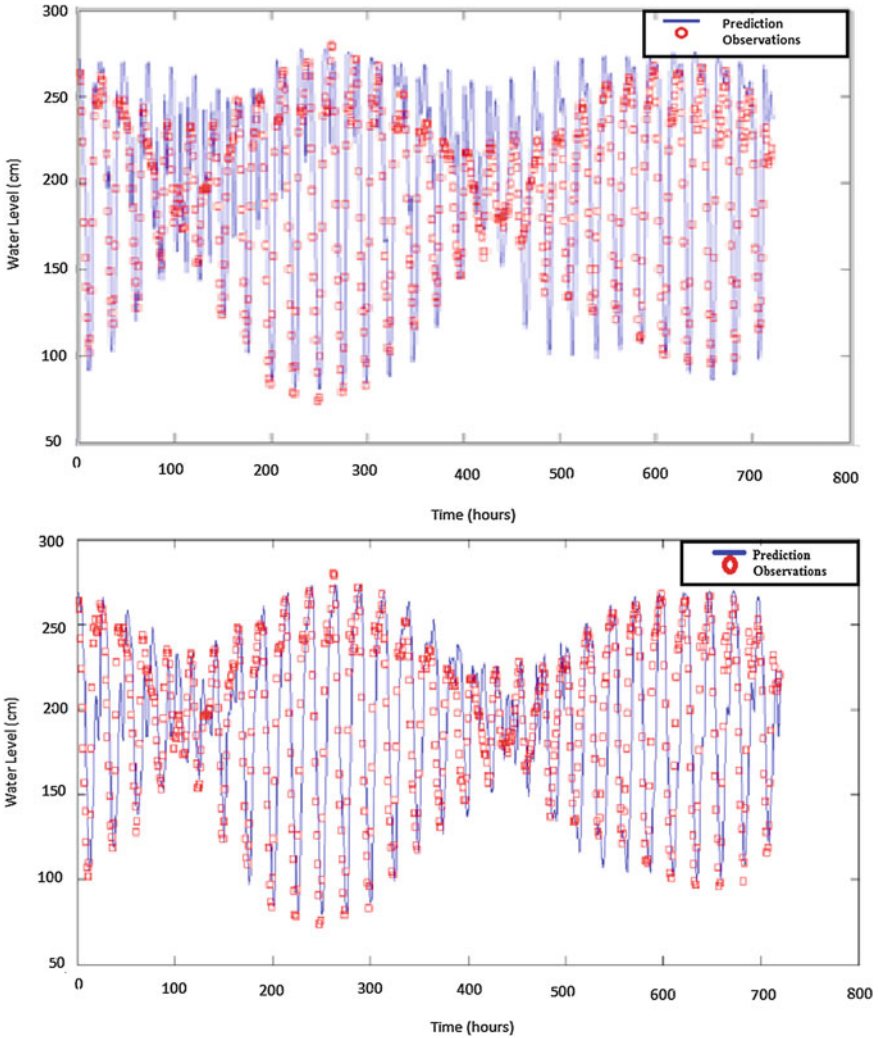


Fig. 9 One-month tidal forecast using FFBP. **a** Two hidden layers with 2 neurons. **b** One hidden layer with 8 neurons

with network architecture of $I_{10}H_{2,2}O_1$ and $I_{10}H_8O_1$ respectively. Although good agreement is obtained for the spring high and low water levels, the neap tide condition is poorly reproduced. The neap tide condition is poorly reproduced because the result and analysis is not achieved with the observation data. As a consequence, the correlation coefficients are only slightly above 0.8, and the root mean square errors are around 0.15.

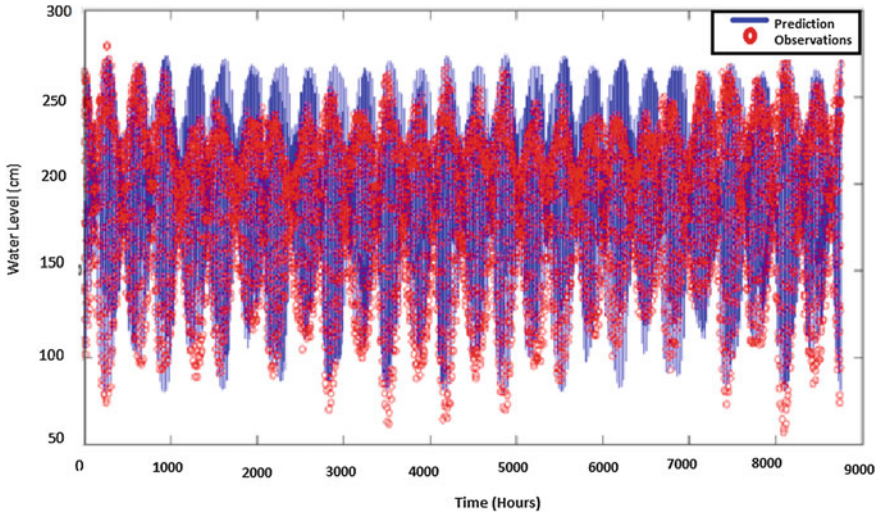


Fig. 10 One-year tidal forecast using FFBP ($I_{10}H_8O_1$)

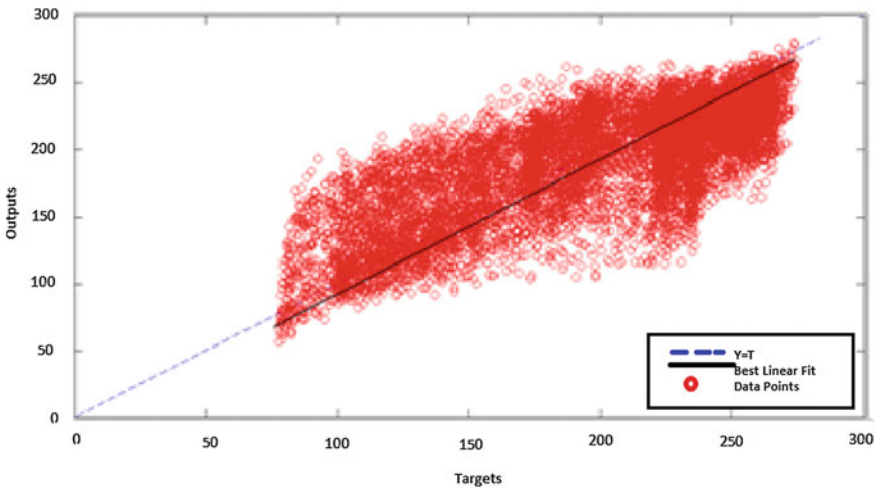


Fig. 11 Regression analysis for one-year tidal prediction using FFBP ($I_{10}H_8O_1$)

We further verify the outcome of one-year tidal simulation using the $I_{10}H_8O_1$ model (Fig. 10). The results deteriorate further to $RMS = 0.1784$, and $R = 0.7156$, with considerable scatter in the regression plot (Fig. 11).

Next, we performed the same tests on the GRNN model with spread factor of 0.75. Figure 12a shows that similar to the FFBP model, the one-month prediction

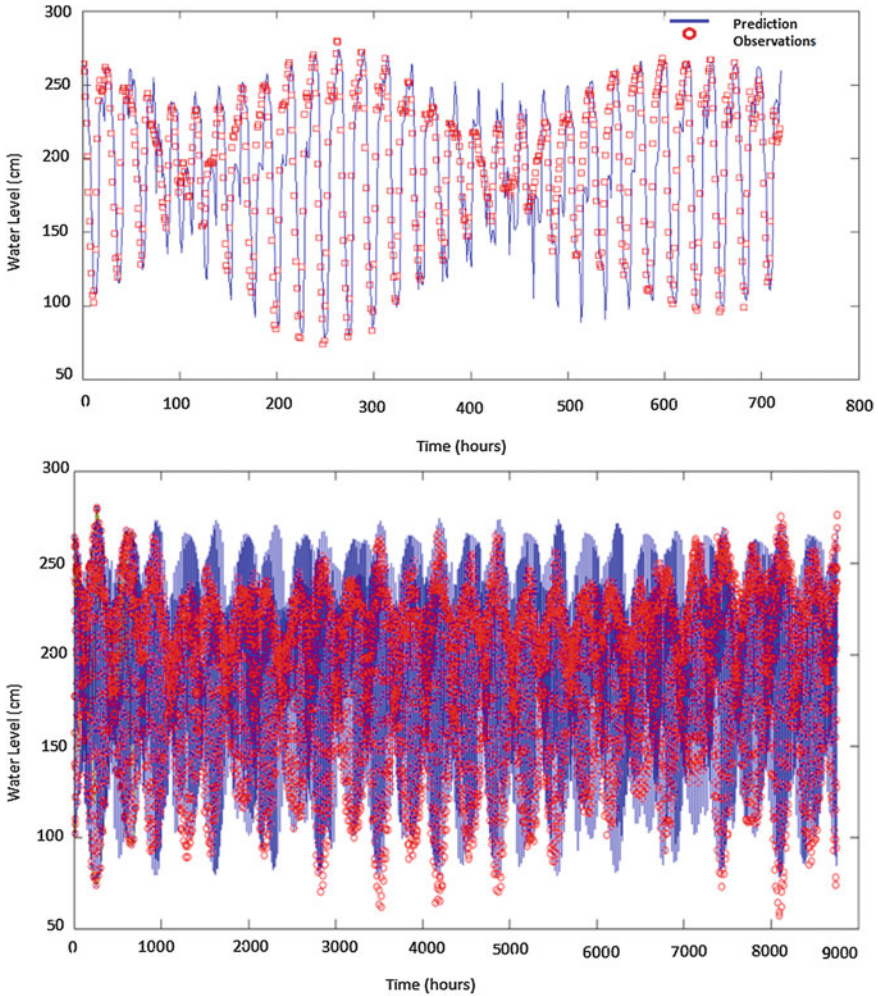


Fig. 12 Tidal forecast using GRNN. **a** One month. **b** One year

reproduces the spring highs and lows, but not the neap highs and lows. Figures 11a, b and 12a show that the prediction and observation data is not accurate and more scatter. The value of RMS ($=0.1488$) and R ($=0.8434$) are only marginally better than the two FFBP models. The result of the one-year prediction (Fig. 12b) is similar to the FFBP models, with even larger scatter in the regression plot (Fig. 13).

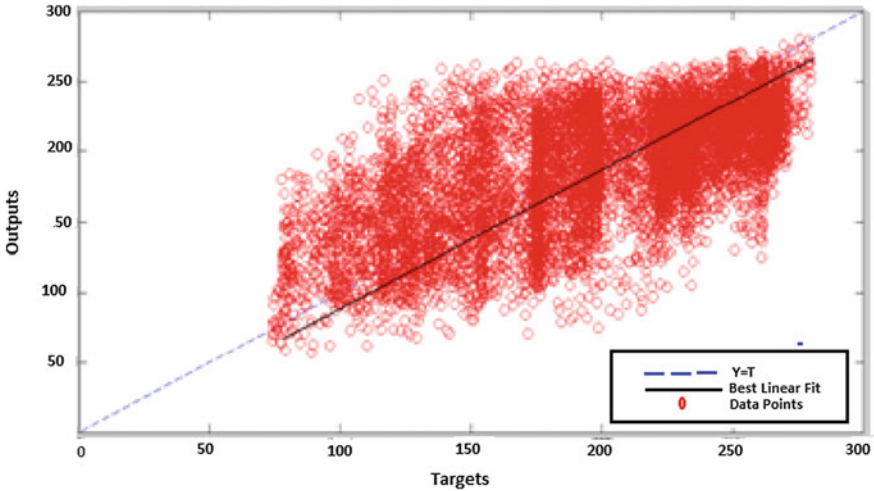


Fig. 13 Regression analysis for one-year tidal prediction using GRNN

5 Conclusions

FFBP and GRNN models are developed and trained using the tidal observations at Bintulu station in JUPEM’s TON. Considering only the 5 main tidal constituents and using only 30-day hourly data, the tidal high and low water profile is derived and used to train the network structure to determine the best network architecture. We selected two FFBP models ($I_{10}H_{2,2}O_1$ and $I_{10}H_8O_1$) and one GRNN models (spread factor = 0.75) which shows promising training results for the purpose of tidal predictions. Simulations show that all the 3 models are able to reproduce the one-month spring high and low water levels but not the neap high and low water levels. Results deteriorate further when used for one-year simulations with considerable scatter observed in the regression plots.

It may thus be concluded that the present network models considered fail to produce reliable long term high and low water levels for coastal applications. We note however that owing to the diverse network options and parameters available, the potential of applying ANN for the present purpose remains open. Further investigation and exploration is needed in order to identify the right model that can capitalize on short term high and low water observations to predict the long term extremes for coastal planning purposes.

Acknowledgments We thank JUPEM for the data provided in the present study.

References

1. C.P. Tsai, T.L. Lee, Back-propagation neural network in tidal level forecasting. *J. Waterwa. Port. Coast. Eng.* **12**(4), 195–202 (1999)
2. T.L. Lee, D.S. Jeng, Application of artificial neural networks in tide-forecasting. *Ocean Eng.* **29**, 1003–1022 (2002)
3. T.L. Lee, C.P. Tsai, D.S. Jeng, R.J. Shieh, Neural network for the prediction and supplement of tidal record in Taichung. Taiwan. *Adv. Eng. Software.* **33**, 329–338 (2002)
4. T.S. Lee, Back-propagation neural network for long-term tidal predictions. *Ocean Eng.* **31**, 225–238 (2004)
5. T.S. Lee, Neural network prediction of a storm surge. *Ocean Eng.* **33**, 483–494 (2006)
6. W.K. Lee, Long term tidal forecasting and hindcasting using QuickTIDE tidal simulation package. *J. Inst. Eng. Malaysia* **68**(2), 59–64 (2007)
7. Lee, W.K., Long term tidal forecasting using back-propagation neural network. *Proceedings of Malaysian Science Technology Congress (MSTC)*, 19–21 November 2012, COSTAM
8. D.F. Specht, A general regression neural network. *IEEE Trans. Neural Networks* **2**(6), 568–576 (1991)
9. V.M. Patel, J. Jignesh, Rainfall-runoff modelling using artificial neural network (a literature review). *National conference on recent trends in engineering and technology*, May 2011
10. S. Solanki, H.B. Jethva, A review on back-propagation algorithms for feedforward networks. *Int. Res. Anal.* **2**(1), 73–75 (2013)

Comparative Study of Flood Frequency Analysis on Selected Rivers in Myanmar

Ni Lar Win and Khin Maung Win

Abstract A number of probability distributions are used to estimate flood discharges with various return periods of extreme hydrologic events. Among others, Log-Normal, Gumbel, Pearson Type III and Log-Pearson Type-III distributions are used in this study. The parameters of these distributions are estimated from the given data by the method of moments. The objectives of this study are: to carry out the flood frequency analysis using the different distributions to selected rivers in Myanmar, namely the Chindwin and Yenwe Rivers and to identify the most appropriate probability distribution for the basins under study. Log-Pearson Type III distribution can be recommended for both Chindwin and Yenwe basins among other distributions under study. The estimated flood values can be used in the engineering design of hydraulic structures such as dams, bridges, culverts, levees and other structures located along rivers and streams and for the effective management of flood plains.

Keywords Flood frequency analysis · Probability distribution · Chindwin and Yenwe rivers

1 Introduction

Estimation of the magnitude and frequency of occurrence of extreme hydrologic events, such as severe storms, floods, and droughts are important in water resources planning and management. Frequency analysis of hydrologic data is one

N. L. Win (✉) · K. M. Win

Faculty of Science, Technology, Engineering and Mathematics, INTI International University, Putra Nilai, Malaysia
e-mail: larwin.ni@newinti.edu.my

K. M. Win

e-mail: maungwin.khin@newinti.edu.my

of the widely used methods of estimating the return period associated with a flood of a given magnitude through the use of probability distributions [1–8].

A number of probability distributions are used to fit the probability of occurrence of flood series. Details of these distributions are available in the literature including [9–11] among others. Selection of the most appropriate distribution for annual maximum series has been paid attention worldwide. Log-Pearson Type III distribution is the recommended technique for flood frequency analysis by the U.S. Water Advisory Committee on Water Data, USGS [3]. It is used to estimate the flood discharges for the streams in Iowa, USA [4]. The Generalized Extreme Value distribution is the standard method for UK as reported in [2] and it is adopted in regional flood frequency analysis in Northern Iceland [5] and Nile equatorial basins [6]. Gumbel distribution is used in Nyanyadzi river in Zimbabwe [7]. A World Meteorological Organization survey of 54 agencies in 28 countries reveals that Log-Normal distribution with 3 parameters is not a standard in any country, Generalized Extreme Value is a standard in one country, and Log-Pearson Type III is a standard in seven countries [8].

Numerous goodness-of-fit procedures exist for comparing the fit of alternative probability distributions to streamflow sequences. Since the introduction of L-moments, numerous investigators have recommended them to assess the goodness-of-fit of various probability distributions to regional samples of streamflow [8, 12, 13] and others. Vogel and Wilson [8] constructed L-moments diagrams for annual maximum streamflow at more than 1,455 rivers in the United States and concluded that the Generalized Extreme Value, three-parameter Log-Normal and the Log-Pearson Type III distributions provide good approximations to the distribution of annual maximum flood series. Since Log-Pearson Type III has been selected as the base method in the U.S., they suggested the agencies and countries to reevaluate their standards with respect to the choice of a suitable model for flood frequency analysis. Stedinger and Griffis [14] also recommended that the regional skew map given in [3] be updated to use the additional 30 years of data now available, to appropriately adjust for low outliers identified in the samples used to estimate the regional skew, and to use new and powerful statistical estimation procedures developed to use such data set.

The objectives of the study are hence twofold: (1) to carry out the flood frequency analysis using Log-Normal, Gumbel (Extreme Value Type I), Pearson Type III and Log-Pearson Type III which are commonly used frequency distributions to selected rivers in Myanmar, namely the Chindwin and Yenwe rivers and (2) to identify the most appropriate probability distribution for the basins under study. The estimated flood values can be used in the engineering design of hydraulic structures such as dams, bridges, culverts, levees and other structures located along rivers and streams and for the effective management of flood plains.

Table 1 Location of gauging stations under study

No.	Name of the river	Gauging station	Location	Data period	Area (km ²)
1	Chindwin	Hkamti	N26°00' E94°42'	1972–1995	27,420
2	Chindwin	Htamathi	N25°50' E95°17'	1971–1995	39,410
3	Chindwin	Homalin	N24°52' E94°54'	1968–1995	43,124
4	Yenwe	Myochau-ng	N17°57' E96°44'	1968–1995	790

2 Data Used in This Study

In this study, two rivers namely Chindwin and Yenwe rivers in Myanmar are selected. The Chindwin river has floods several times in a year from the onset of rainy season to the end of the monsoon. Annual maximum discharges are collected at Hkamti, Htamathi and Homalin stations for Chindwin river. Average annual rainfall at Hkamti, Htamathi and Homalin stations are 3,847, 3,262 and 2,314 mm respectively. The mean monthly temperature varies from 28 °C in May to 18 °C in January.

Myochaung station for Yenwe river which is a tributary of Sittoung is also selected in this study. It lies in a tropical monsoon area with an average annual rainfall of about 2,000 mm. The mean monthly temperature varies from 31 °C in April to 25 °C in January. The location and area of these stations are shown in Table 1. Series of annual maximum discharge of each basin is plotted in Fig. 1.

It can be seen from Fig. 1 that the variation of the flood values from the mean in Chindwin is small compared to the variation in Yenwe basin. Statistical characteristic of each series is given in Table 2. Annual maximum series of Chindwin basins have negative skews while Yenwe has a positive skew.

3 Methodology

3.1 Testing for Outliers

Reference [9] recommends that adjustments be made for the outliers of the data. If the station skew is greater than +0.4, tests for high outliers are considered first and if the station skew is less than -0.4, tests for low outliers are considered first. Where the skew is between ±0.4, tests for both high and low outliers should be applied before eliminating any outliers from the data set. The following equation is used to detect high outliers:

$$y_H = \bar{y} + K_N s \quad (1)$$

Fig. 1 Annual maximum discharge series of Chindwin and Yenwe basins

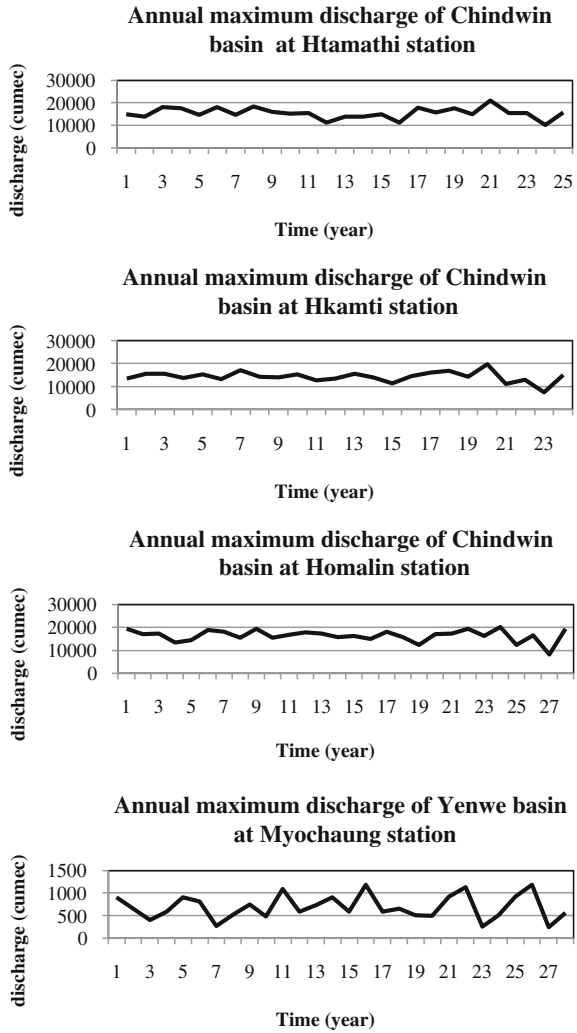


Table 2 Statistical characteristics of each basin

No.	Gauging station	Mean (m ³ /s)	Standard deviation (m ³ /s)	Coefficient of variation	Skewness coefficient
1	Hkamti	14,254	2342.0	0.16	-0.6
2	Htamathi	15,476	2407.9	0.16	-0.17
3	Homalin	16,485	2593.0	0.16	-1.25
4	Myochaung	692	274.0	0.40	0.19

where

- y_H high outlier threshold in log units
- \bar{y} mean logarithm of variate
- s standard deviation of y 's
- K_N 10 % significance level K values.

The following equation is used to detect low outliers:

$$y_L = \bar{y} - K_N s \tag{2}$$

where y_L = low outlier threshold in log units and other terms are as defined earlier.

3.2 Frequency Analysis Using Frequency Factors

Chow [9] proposed the frequency factor equation shown in (3) which is applicable to many probability distributions used in hydrologic frequency analysis.

$$x_T = \mu + K_T \sigma \tag{3}$$

which may be approximated by

$$x_T = \bar{x} + K_T s \tag{4}$$

where

- x_T value of the variate x of a random hydrologic series with a return period T ,
- \bar{x} mean of the variate,
- s standard deviation of the variate,
- K_T frequency factor which depends upon the return period T and assumed frequency distribution

In the event that the variable analyzed is $y = \log x$, then the same method is applied to the statistics for the logarithms of the data using

$$y_T = \bar{y} + K_T s \tag{5}$$

and the required value of x_T is found by taking the antilog of y_T .

Table 3 summarizes the probability density function, the range of the variable, and equations for estimating the distribution's parameters from sample moments for each distribution [9]. The theoretical K_T relationships for the selected probability distributions: Log-Normal, Pearson Type III, Log-Pearson Type III and Gumbel distributions extracted from [9] are given below.

Table 3 Probability distributions for fitting hydrologic data

Distribution	Probability density function	Equations for parameters
Log-normal	$f(x) = \frac{1}{x\sigma\sqrt{2\pi}} \exp\left(-\frac{(y-\mu_y)^2}{2\sigma_y^2}\right)$ where $y = \log x, x > 0$	$\mu_y = \bar{y}$ $\sigma_y = S_y$
Extreme value type I (Gumbel)	$f(x) = \frac{1}{x} \exp\left[-\frac{x-u}{\alpha} - \exp\left(-\frac{x-u}{\alpha}\right)\right]$ $-\infty < x < \infty$	$\alpha = \frac{\sqrt{6}S_x}{\pi}$ $u = \bar{x} - 0.5772\alpha$
Pearson type III	$f(x) = \frac{\lambda^\beta (x-\varepsilon)^{\beta-1} e^{-\lambda(x-\varepsilon)}}{\Gamma(\beta)}$ $x \geq \varepsilon$	$\lambda = \frac{S_y}{\sqrt{\beta}}$ $\beta = \left(\frac{2}{C_s}\right)^2$ $\varepsilon = \bar{x} - S_x - \sqrt{\beta}$
Log-Pearson type III	$f(x) = \frac{\lambda^\beta (y-\varepsilon)^{\beta-1} e^{-\lambda(y-\varepsilon)}}{x\Gamma(\beta)}$ where $y = \log x$ $\log x \geq \varepsilon$	$\lambda = \frac{S_y}{\sqrt{\beta}}$ $\beta = \left(\frac{2}{C_s(y)}\right)^2$ $\varepsilon = \bar{y} - S_y - \sqrt{\beta}$

1. Gumbel distribution

The frequency factor K_T for different return period T is given in (6).

$$K_T = -\frac{\sqrt{6}}{\pi} \left\{ 0.5772 + \ln \left[\ln \left(\frac{T}{T-1} \right) \right] \right\} \tag{6}$$

2. Log-Pearson Type III distribution

The frequency factor depends on the return period T and the coefficient of skewness C_s . When $C_s = 0$, the frequency factor is equal to the standard normal variable z. The value of z corresponding to an exceedence probability of p ($p = 1/T$) can be calculated by finding the value of an immediate variable w:

$$w = \left[\ln \left(\frac{1}{p^2} \right) \right]^{1/2} \quad (0 < p < 0.5) \tag{7}$$

then calculating z using the approximation

$$z = w - \left[\frac{(2.515517 + 0.802853w + 0.010328w^2)}{(1 + 1.432788w + 0.189269w^2 + 0.001308w^3)} \right] \tag{8}$$

$$K_T = z + (z^2 - 1)k + \frac{1}{3}(z^3 - 6z)k^2 - (z^2 - 1)k^3 + zk^4 + \frac{1}{3}k^5 \tag{9}$$

where $k = C_s/6$, and $C_s =$ coefficient of skewness of logarithms of the series.

3. Pearson Type III distribution

For this distribution, the same equation in Log-Pearson Type III applies except that C_s is skewness of the original series (without taking the logarithmic values).

4. Log-Normal distribution

For this distribution, the same equation in Log-Pearson Type III applies using $C_s = 0$.

3.3 Statistical Analysis

Goodness of fit between the observed events and the fitted distribution is tested by the two most commonly used tests: Chi square and Kolmogorov–Smirnov (K–S) [15].

1. Chi square test

The statistic is calculated by

$$\chi^2 = \sum_{j=1}^k \frac{(O_j - E_j)^2}{E_j} \quad (10)$$

where O_j is the observed number of events in the j th class interval and E_j is the number of events that would be expected from the theoretical distribution.

2. Kolmogorov–Smirnov (K–S) test

The statistic D_n is evaluated by observing the deviation of the sample distribution function $P(x)$ from the completely specified continuous hypothetical distribution function $P_0(x)$, such that

$$D_n = \text{Max}|P(x) - P_0(x)| \quad (11)$$

The test requires that the computed value D_n from the sample distribution be less than the tabulated value of D_n at the required significance levels of 0.05 and 0.1.

3.4 Reliability of Analysis

The reliability of the results of frequency analysis depends on how well the assumed probability model applies to a given set of hydrologic data. This can be done by calculating confidence limits which are upper and lower boundary values of the confidence interval. For estimating the event magnitude for return period T , the upper limit $U_{T,\alpha}$ and lower limit $L_{T,\alpha}$ may be specified by adjustment of the frequency factor equation given in [9]:

$$U_{T,\alpha} = \bar{x} + sK_{T,\alpha}^U \quad (12)$$

$$L_{T,\alpha} = \bar{x} + sK_{T,\alpha}^L \quad (13)$$

where α is a significance level and is obtained by $\alpha = \frac{1-\beta}{2}$, $\beta =$ confidence interval.

$K_{T,\alpha}^U$ and $K_{T,\alpha}^L$ are upper and lower confidence factors, which can be determined for normally distributed data using the noncentral t distribution. Approximate values for these factors are given by the following equations:

$$K_{T,\alpha}^U = \frac{K_T + \sqrt{K_T^2 - ab}}{a} \quad (14)$$

$$K_{T,\alpha}^L = \frac{K_T - \sqrt{K_T^2 - ab}}{a} \quad (15)$$

in which $a = 1 - \frac{Z_\alpha^2}{2(n-1)}$ and $b = K_T^2 - \frac{Z_\alpha^2}{n}$.

The quantity Z_α is the standard normal variable with exceedence probability α .

4 Results

4.1 Flood Discharges

Annual maximum discharge series of Chindwin River at Hkamti, Htamathi and Homalin stations and Yenwe at Myochaung station are checked whether outliers exist in the data series before using them. Based on the skewness coefficient of the data series used, outliers are calculated and given in Table 4. K_N value based on the number of data in the series is obtained from the table for outlier test in [3].

It is observed that the annual maximum discharges in the year 1994 are smaller than the low outliers for Chindwin at all stations. However, useful historical information is not available to adjust for low outliers and therefore they are retained in the series. There is no high outlier observed in all series.

Flood discharges with recurrence intervals of 2, 5, 10, 20, 50 and 100 years are calculated using four probability distributions: Log-normal, Gumbel, Pearson Type III and Log Pearson type III distributions. The results are given in Tables 5, 6, 7, 8 that show large differences in results obtained by the different methods, particularly at the larger return periods. It can be seen that Gumbel distribution gives the highest estimated flood discharges for Chindwin and Log-Normal distribution gives the highest for Yenwe. The estimated discharges for high return period (50 and 100 years) using Log-Normal and Gumbel distributions yield about 10–20 % higher than the flood values estimated by Pearson Type III and Log-Pearson Type III distributions for all basins under study.

Table 4 Outliers (cumec) for Chindwin and Yenwe basins

River	Gauging station	No. of data	K_N	Low outlier	High outlier
Chindwin	Hkamti	24	2.467	8,922	22,105
Chindwin	Htamathi	25	2.486	10,197	22,920
Chindwin	Homalin	28	2.534	10,220	25,831
Yenwe	Myochaung	28	2.534	211.21	1,920

Table 5 Flood discharges X_T (cumec) obtained by different distributions for Chindwin at Hkamti station

Return period (years)	Log-normal	Gumbel	Pearson type III	Log-Pearson type III
2	14,043	13,902	14,485	14,724
5	16,394	16,346	16,258	16,285
10	17,776	17,963	17,065	16,811
20	19,005	19,515	17,671	17,110
50	20,489	21,520	18,294	17,324
100	21,542	23,029	18,674	17,408

Table 6 Flood discharges X_T (cumec) obtained by different distributions for Chindwin at Htamathi station

Return period (years)	Log-normal	Gumbel	Pearson type III	Log-pearson type III
2	15,287	15,111	15,544	15,587
5	17,534	17,582	17,520	17,572
10	18,837	19,216	18,516	18,522
20	19,987	20,785	19,320	19,253
50	21,364	22,813	20,204	20,012
100	22,334	24,338	20,782	20,479

Table 7 Flood discharges X_T (cumec) obtained by different distributions for Chindwin at Homalin station

Return period (years)	Log-normal	Gumbel	Pearson type III	Log-Pearson type III
2	16,248	16,091	17,002	17,163
5	18,952	18,751	18,654	18,696
10	20,542	20,512	19,270	19,114
20	21,954	22,202	19,670	19,306
50	23,660	24,385	20,015	19,401
100	24,870	26,028	20,192	19,420

4.2 Statistical Analysis

The two most commonly used tests of goodness of fit namely Chi square and Kolmogorov–Smirnov tests are applied to check the fit of probability distributions used in this study. Tables 9 and 10 list the values of Chi square statistics (χ^2) and Kolmogorov–Smirnov (D_n) respectively.

Table 8 Flood discharges X_T (cumec) obtained by different distributions for Yenwe at Myo-chaung station

Return period (years)	Log-normal	Gumbel	Pearson type III	Log-Pearson type III
2	636.8	650.6	681.0	667.6
5	918.7	931.7	918.8	924.3
10	1112.9	1117.8	1049.8	1069.2
20	1303.8	1296.3	1161.3	1191.6
50	1558.0	1527.0	1290.6	1330.0
100	1754.4	1700.6	1379.1	1421.1

Table 9 Comparison of Chi square statistics for different distributions for the basins under study

Basin	Log-normal	Gumbel	Pearson type III	Log-Pearson type III
Hkamti	4.75	5.86	4.96	5.56
Htamathi	6.03	3.98	4.71	3.51
Homalin	3.01	3.01	3.48	5.91
Yenwe	2.5	2.81	4.17	1.84

Table 10 Comparison of Kolmogorov–Smirnov statistics for different distributions for the basins under study

Basin	Log-normal	Gumbel	Pearson type III	Log-Pearson type III
Hkamti	0.13	0.13	0.091	0.18
Htamathi	0.11	0.11	0.10	0.14
Homalin	0.12	0.14	0.14	0.21
Yenwe	0.11	0.06	0.10	0.11

It can be observed from the Chi square values of four distributions for all basins given in Table 9 that the values are less than the critical value at 95 % confidence level. From Table 10, it can be seen that all the computed values of D_n are less than the critical value at 95 % confidence level. From both statistical tests, no distinction among all distributions can be made for the basins under study. All distributions are acceptable to fit to the annual maximum series of Chindwin and Yenwe basins at 95 % confidence interval.

If the goodness of fit is the criterion used to select a specified distribution, then the distribution with three parameters will usually provide a much better fit than two parameters [16]. In this study, Log-Pearson Type III is selected as the recommended distribution since it includes the skew coefficient as a variable and therefore is more flexible than the Log-Normal which has a skew of zero of the logarithms. Log-Normal is considered as the special case of Log-Pearson Type III distribution. Another reason is that Pearson Type III is capable of fitting frequency relations that may, for hydrologic reasons, be highly skewed [1].

4.3 Reliability Analysis

Reliability analysis for the basins under study is performed using log-Pearson Type III distribution. The confidence limits with 90 % confidence interval are calculated and shown in Tables 11 and 12.

Graphical presentations of estimated flood discharges using all probability distributions under study together with the confidence limits using Log-Pearson Type III for each basin are shown in Fig. 2.

It can be seen from Fig. 2 that the confidence interval is quite wide especially in Yenwe basin since the sample size of each series is small in this study.

5 Conclusions

Based on the analysis of statistical tests, Gumbel, Pearson Type III and Log-Pearson Type III and Log-Normal distributions are suitable to estimate flood discharges for Chindwin and Yenwe basins.

Log-Pearson Type III distribution can be recommended for Chindwin and Yenwe basins since it includes the skew variable and therefore is more flexible than other distributions.

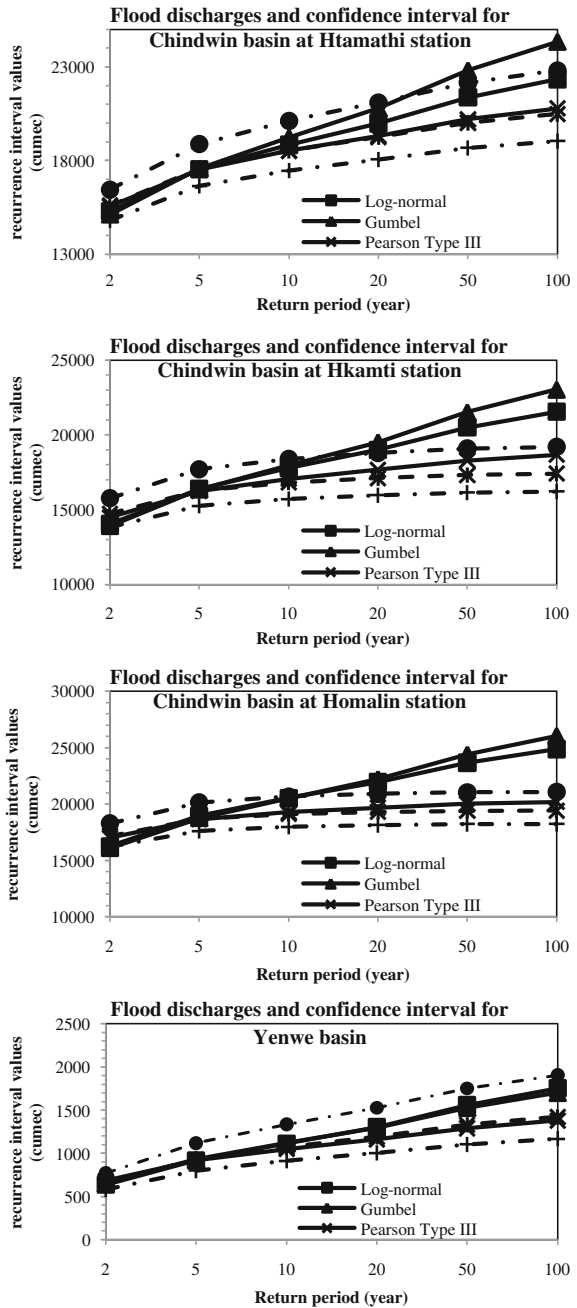
Table 11 Confidence limits (cumec) for Chindwin at Hkamti and Htamathi stations

Basin	Chindwin at Hkamti		Chindwin at Htamathi	
	Upper limit	Lower limit	Upper limit	Lower limit
2	15755.7	13840.6	16444.4	14809.3
5	17703.1	15261.3	18867.0	16639.6
10	18393.6	15713.8	20115.7	17450.6
20	18793.5	15967.1	21103.9	18055.3
50	19082.1	16146.3	22151.7	18670.2
100	19196.0	16216.0	22805.6	19042.8

Table 12 Confidence limits (cumec) for Chindwin Basin at Homalin and Yenwe Basin

Basin	Chindwin at Homalin		Yenwe	
	Upper limit	Lower limit	Upper limit	Lower limit
2	18273.3	16214.5	770.0	582.1
5	20141.2	17612.7	1117.9	798.9
10	20672.2	17979	1334.7	911.2
20	20917.8	18144.7	1526.8	1002.3
50	21041.2	18227.2	1752.3	1102.1
100	21065.8	18243.7	1905.6	1166.5

Fig. 2 Flood discharges and confidence interval vs return period for Chindwin and Yenwe basins



A study on frequency analysis for other gauging stations of Chindwin basin as well as the other river basins needs to be performed to develop the regional frequency analysis. Future research can be carried out by using other parameter estimator such as L moments in frequency analysis for the river basins in Myanmar.

Acknowledgments Thanks are due to staff officers from Hydrology section, Irrigation Department and Meteorology and Hydrology Department, Myanmar for their friendly collaboration in data gathering.

References

1. M.A. Benson, Uniform flood-frequency estimating methods for federal agencies. *Water Resour. Res.* **4**(5), 891–908 (1968)
2. European Cooperation in Science and Technology, *Review of applied-statistical methods for flood-frequency analysis in Europe*, Centre for Ecology and hydrology, Natural Environmental Research Council, (2012)
3. Interagency Advisory Committee on Water Data, Guidelines for determining flood flow frequency: Hydrology Subcommittee Bulletin #17B, available from Office of Water data Coordination, U.S. Department of the Interior Geological Survey, Reston, VA, 1982
4. D.A. Eash, Techniques for estimating flood-frequency discharges for the streams in IOWA, US Geological Survey, Water-Resources Investigation Reports 00-4233, IOWA Department of Transportation and the IOWA Highway Research Board (Project HR-395A), 2001
5. P. Crochet, Evaluation of two delineation methods for regional flood frequency analysis in Northern Iceland, Report, Icelandic Meteorological Office, (2012)
6. A.O. Opere, S. Mkhandi, P. Willems, At site flood frequency analysis for the Nile equatorial basins. From http://www.unesco.org/fileadmin/MULTIMEDIA/FIELD/Cario/pdf/AT_SITE_FLOOD-FREQUENCY_ANALYSIS.pdf
7. N. Mujere, Flood frequency analysis using the Gumbel distribution. *Int. J. Comput. Sci. Eng.* **3**(7), 2774–2778 (2011)
8. R.M. Vogel, I. Wilson, Probability distribution of annual maximum, mean, and minimum streamflows in the United States. *J. Hydrologic Eng.* **1**, 69–76 (1996)
9. V.T. Chow, D.R. Maidment, L.W. Mays, *Applied Hydrology* (McGraw-Hill Inc, New York, 1988)
10. K.C. Patra, *Hydrology and Water Resources Engineering*, 2nd edn. (Alpha Science International Ltd, Oxford, 2008)
11. K. Subramanya, *Engineering Hydrology*, 3rd edn. (Tata McGraw Hill Publishing Company Limited, New Delhi, 2009)
12. O.S. Selaman, S. Said, F.J. Putuhena, Flood frequency analysis for Sarawak using Weibull, Gringorten and L-moments formula. *J. Inst. Eng. Malaysia* **68**(1), 43–52 (2007)
13. U.N. Ahmad, A. Shabri, Z.A. Zakaria, Flood frequency analysis of annual maximum stream flows using L-Moments and TL-Moments. *Appl. Math. Sci.* **5**(5), 243–253 (2011)
14. J.R. Stedinger, V.W. Griffis, Flood frequency analysis in the United States: Time to update. *J. Hydrologic Eng. ASCE* **13**, 199–204 (2008)
15. A. Hayter, *Probability and Statics for Engineers and Scientists*, Thomson Higher Education, 3rd edn. (2007)
16. R.M. Vogel, D.E. McMartin, Probability plot goodness-of-fit and skewness estimation, procedure for the Pearson type 3 distribution. *Water Resour. Res.* **27**(12), 3149–3158 (1991)

Part IV
Fluvial and River Engineering Dynamics

Determination of Baseflow Index for Bernam River at Tanjung Malim

Fauzi Bin Baharudin, Asma Nabilla Iskak and Amirudean Shafiee

Abstract Baseflow is the portion of streamflow that comes from “the sum of deep subsurface flow and delayed shallow subsurface flow”. Baseflow separation is often used to determine the portion of a streamflow hydrograph occurs from baseflow, and the portion occurs from overland flow. Many methods for baseflow separation exist, but for this study only the Lyne and Hollick filter method is used. The location for this study is Sungai Bernam at Tanjung Malim. In this study, the type of data used is daily streamflow data. The data collected are obtained from DID. Next, the data will be analyzed based on different durations; which are for a month, for a year and for 5 years. The results show that there is no fixed pattern for the value of baseflow index (BFI). All the values range between 0.6 and 0.8 and this vary over space and time based on regional climate, topography, landscape and geological characteristics.

Keywords Streamflow · Baseflow · BFI · Lyne and hollick filter method

1 Introduction

Assessment of water resources kept in different storages and moving along different pathways in a catchment are important for its optimal use and protection, and also for the prediction of floods and low flows. Moreover, understanding of the runoff generation processes is essential for assessing the impacts of climate and land use changes on the hydrological response of a catchment. Baseflow is the portion of streamflow that comes from “the sum of deep subsurface flow and delayed shallow subsurface flow”. Baseflow separation is often used to determine

F. B. Baharudin (✉) · A. N. Iskak · A. Shafiee
Faculty of Civil Engineering, Universiti Teknologi MARA, Shah Alam, Selangor, Malaysia
e-mail: fauzi1956@salam.uitm.edu.my

the portion of a streamflow hydrograph occurs from baseflow, and the portion occurs from overland flow [1].

The scope of this study is to determine the baseflow index by using the Lyne and Hollick baseflow separation method. Before the study can be done, there is some fundamental and basic knowledge that need to be understood. The Baseflow Index (BFI) is used as a measure of the baseflow characteristics of catchments. It also indicates the influence of soil and geology on river flow and useful in the water quality assessment and low flow conditions. It will provide a systematic way of assessing the proportion of baseflow in the total runoff of a catchment. Based on regional climate, topography, landscape, and geological characteristics, baseflow availability will vary over space and time [2].

Generally, in order to separate the baseflow from the streamflow, there are four types of methods that can be used. The methods are graphical baseflow separation, filtering algorithms, analytical approach and recession analysis. These methods are well established and have been utilized by many researchers [3].

2 Problem Statement

As stated earlier, baseflow availability will vary over space and time based on regional climate, topography, landscape, and geological characteristics. In order to determine the baseflow index of a river in Selangor, the Bernam River was selected. The method that will be used in this study is the Lyne and Hollick filter method. This study can further enhance the understanding on the application of this method and to determine the suitability of this method for Malaysia which is a tropical country. At the same time, Malaysia still lacks in term of the study on baseflow index of a river. Hence, this study was carried out.

3 Objectives

This study is conducted to enhance the understanding in the baseflow index of a river in Selangor. Additionally, the specific objectives for this study are; (1) to estimate the baseflow by hydrograph separation through Lyne and Hollick filter method and (2) to determine the baseflow index (BFI) for Sungai Bernam at Tanjung Malim.

4 Scope of Study

This study is carried out in order to determine the baseflow index of a river in Selangor. There are few considerations or conditions that are required to be followed in this research. The conditions required are:

- (a) Location: Sungai Bernam at Tanjung Malim.
- (b) Type of data: stream flow data (m³/s)
- (c) Final outcome: Baseflow value, hydrograph separation and baseflow index (BFI) value.
- (d) Method used: Lyne and Hollick method.
- (e) Equation used to calculate baseflow value [4]:

$$b_k = a \cdot b_{k-1} + \frac{1 - a}{2}(y_k + y_{k-1}) \tag{1}$$

where

- b_k baseflow value for k th day
- α filter parameter (0.925)
- b_{k-1} baseflow value for $k - 1$ day
- y_k streamflow at k th day
- y_{k-1} streamflow at $k - 1$ day

With the value of $b_k \leq y_k$.

- (f) Hydrograph separation: streamflow and baseflow versus days.
- (g) Baseflow index (BFI) value:

$$BFI = \frac{\text{average for baseflow}}{\text{average for streamflow}} \tag{2}$$

5 Significance of Study

This study is to determine the applicability of Lyne and Hollick method of baseflow index for certain regions. This research can give a better understanding on the use of Lyne and Hollick method, because people are used to more advanced methods of baseflow index determination [5]. Results from this study will be able to assist researchers in this country to further develop or have a better understanding of river baseflow by using this method.

6 Methodology

This study was carried out at Bernam River at Tanjung Malim. The river is located in Hulu Selangor district. This river forms the boundary between Selangor and Perak as shown in Fig. 1. Bernam River flows from Mount Liang Timur in the east on the Titiwangsa Mountains to the Straits of Malacca in the west. The peak of Mount Liang Timur itself marks the point where Pahang, Perak and Selangor meet.



Fig. 1 Location of the station (3615412)

Based on Department of Irrigation and Drainage (DID) records, the discharge and river stage station is: 3615412—Sg Bernam at Tanjung Malim as shown in Fig. 1. The catchment area for the study area is 186 km².

6.1 Data Collection

The data was obtained from the Department of Irrigation and Drainage (DID). Type of data that was obtained is streamflow data. This data was taken for 24 h periods beginning at midnight for each day, for every month, for 12 consecutive years. The data that was obtained for this study is the annual stream flow data from year 2000 until present (November 2011).

7 Result and Analysis

This section analyzed the streamflow data that was obtained from DID. In order to obtain the value of baseflow index (BFI), the Eq. 1 was used. Several hydrographs were produced and compared. The entire charts in this section (Figs. 2, 3, 4, 5, 6, 7)

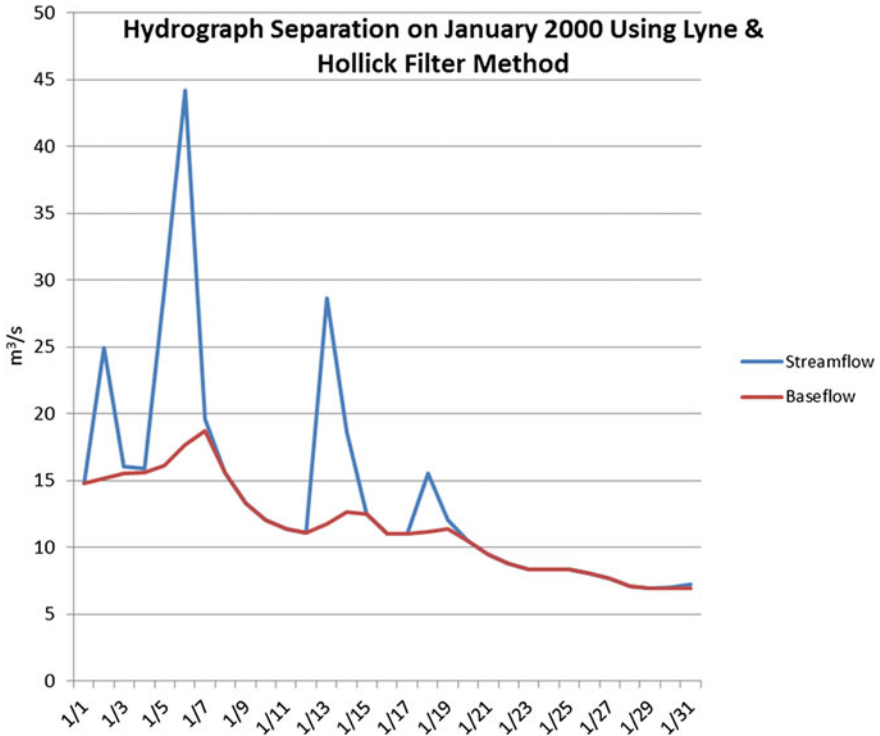


Fig. 2 The hydrograph separation for January 2000

were plotted using streamflow data and baseflow data that were calculated. The hydrograph separation in this section is the streamflow and baseflow data versus day for a month, year and years. Blue lines represent streamflow data and red lines represent baseflow data. Figures 2, 3, 4, 5, 6 and 7 also shows that the values of baseflow data are always lower than stream flow data.

7.1 Hydrograph for January and February 2000

Figure 2 shows the hydrograph separation for January 2000. It consists of 1st January 2000 until 31st January 2000. By using Eq. 1, each value for baseflow was calculated and plotted. From the graph, the highest values of streamflow occurring were on 6 January 2000 (44.2 m³/s), followed by 28.68 m³/s (13 January 2000), 24.97 m³/s (2 January 2000) and 15.53 m³/s at 18 January 2000. At the same time

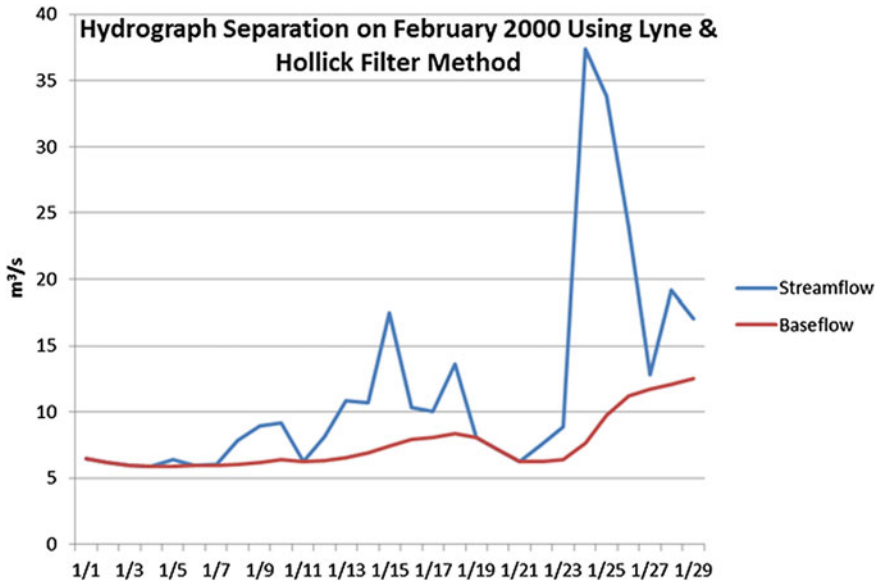


Fig. 3 The hydrograph separation for February 2000

the highest baseflow value occurred on 7 January 2000 (18.74 m³/s). After that, the baseflow index was determined by using average of the baseflow over stream flow. The BFI value for January 2000 is 0.817.

Figure 3 shows the hydrograph separation for February 2000. It started from 1 February 2000 to 28 February 2000. Based on the graph, there were several peaks of streamflow value occurring which were on 24 February 2000 (37.42 m³/s), 28 February 2000 (19.19 m³/s) and 15 February 2000 (17.51 m³/s). Next, the highest baseflow value for February 2000 was on 29 February 2000 (12.06 m³/s). After getting all the value and the average, the BFI value obtained is 0.643.

7.2 Hydrograph for Year 2000 and 2001

Figure 4 shows the hydrograph separation for 12 months in year 2000. The data values were from 1 January 2000 until 31 December 2000. The collected streamflow data for few months was calculated in order to obtain the baseflow value data. Based on the graph, it shows a few peak stream flow values. The highest streamflow value for year 2000 were on 23 December 2000 (80.92 m³/s), followed by 67.48 m³/s (3 August 2000) and 58.38 m³/s (20 November 2000).

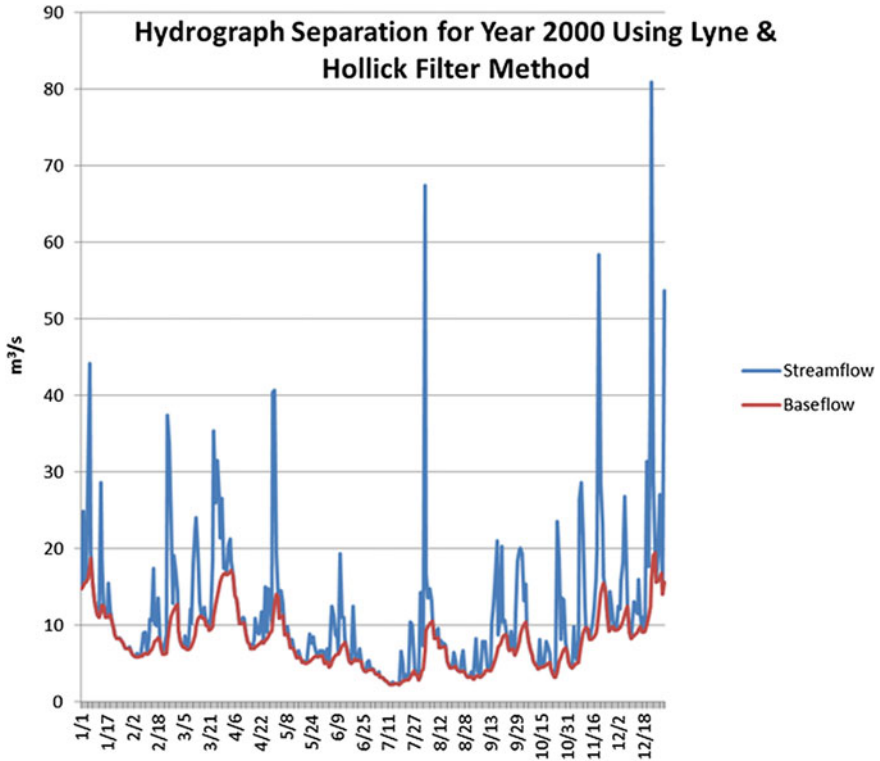


Fig. 4 The hydrograph separation for year 2000

Then, the highest baseflow value for year 2000 was 19.46 m³/s (25 December 2000) and the BFI value calculated is 0.687.

Figure 5 shows the hydrograph separation for year 2001. As per Fig. 5, the data taken was from 1 January 2001 until 31 December 2001. From the graph, the peak streamflow values can be seen at almost every month. But, the highest value was on 26 April 2001 (41.2 m³/s), followed by 22.48 m³/s (7 May 2001) and 21.44 m³/s (9 November 2001). Next, the highest baseflow value was on 1 January 2001 (18.33 m³/s). After getting the baseflow data, the BFI value was obtained which is 0.822.

7.3 Hydrograph for Year 2000–2004 and Year 2005–2009

Figure 6 shows the hydrograph separation for five years. The years consist of year 2000 until 2004. Each year consists of 12 months data which are from 1 January

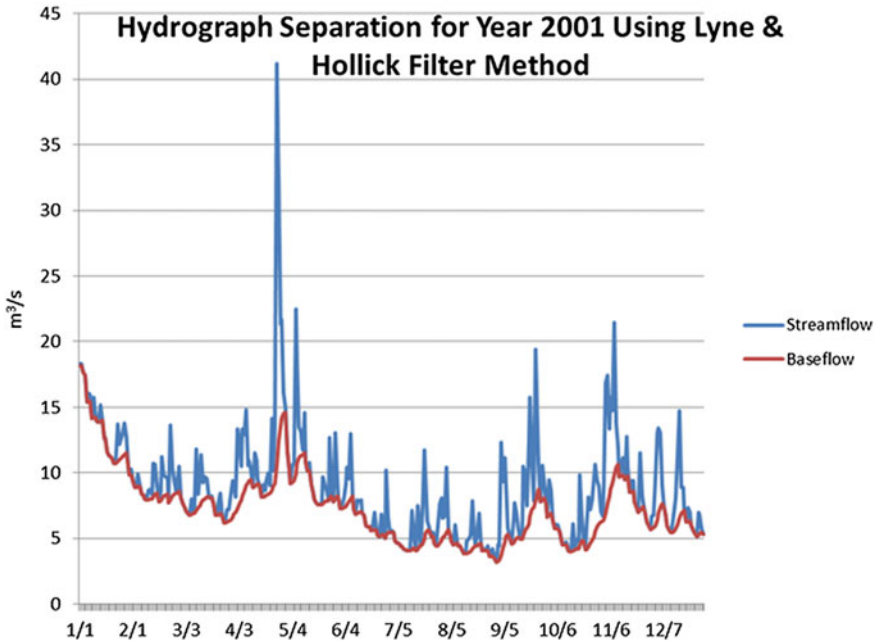


Fig. 5 The hydrograph separation for year 2001

until 31 December. The highest streamflow values for 2000–2004 occurred are on 23 December 2000 ($80.92 \text{ m}^3/\text{s}$) followed by $75.84 \text{ m}^3/\text{s}$ (6 May 2004) and $67.48 \text{ m}^3/\text{s}$ (3 August 2000). Then, the highest baseflow occurred are on 13 November 2004 ($20.23 \text{ m}^3/\text{s}$). The average of baseflow and streamflow data was divided in order to obtain the BFI value, which is 0.729.

Figure 7 shows the hydrograph separation using Lyne & Hollick filtering method for years 2005 until 2009. The data obtained was from 1 January until 31 December for five years. Based on the figure, it shows different streamflow values throughout the years. Based on that, the highest streamflow occurring were on 9 April 2006 ($145.27 \text{ m}^3/\text{s}$) followed by $102.18 \text{ m}^3/\text{s}$ (27 April 2006) and $79.63 \text{ m}^3/\text{s}$ (3 May 2006). Next, the highest baseflow value for year 2005–2009 was $26.78 \text{ m}^3/\text{s}$ (11 September 2006). Then, the plotted data was used in getting the BFI value. The BFI value for five years (2005–2009) is 0.675.

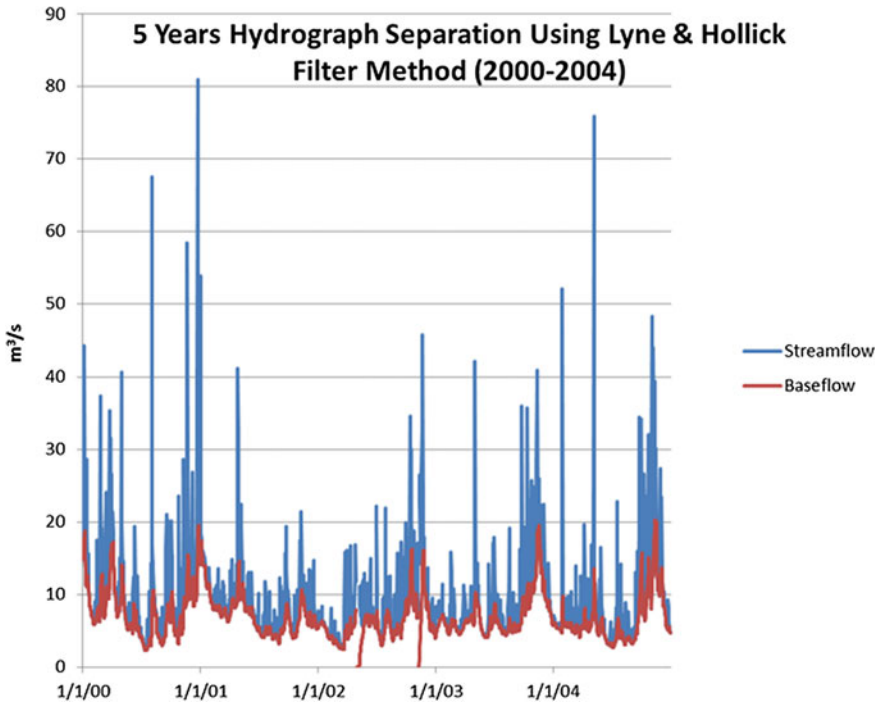


Fig. 6 The hydrograph separation for 5 years (2000–2004)

7.4 The Comparison of BFI Value Between Hydrographs

Table 1 shows the values of BFI for different durations. The value shows that there is no fixed pattern for the value of BFI. First, the BFI value for January 2000 is 0.817 and for February 2000 is 0.643. Second, the BFI value for year 2000 is 0.687 and year 2001 is 0.822. Next, the value for years 2000–2004 is 0.729 and for years 2005–2009 is 0.675. Lastly, the BFI value for years 2000–2009 is 0.703.

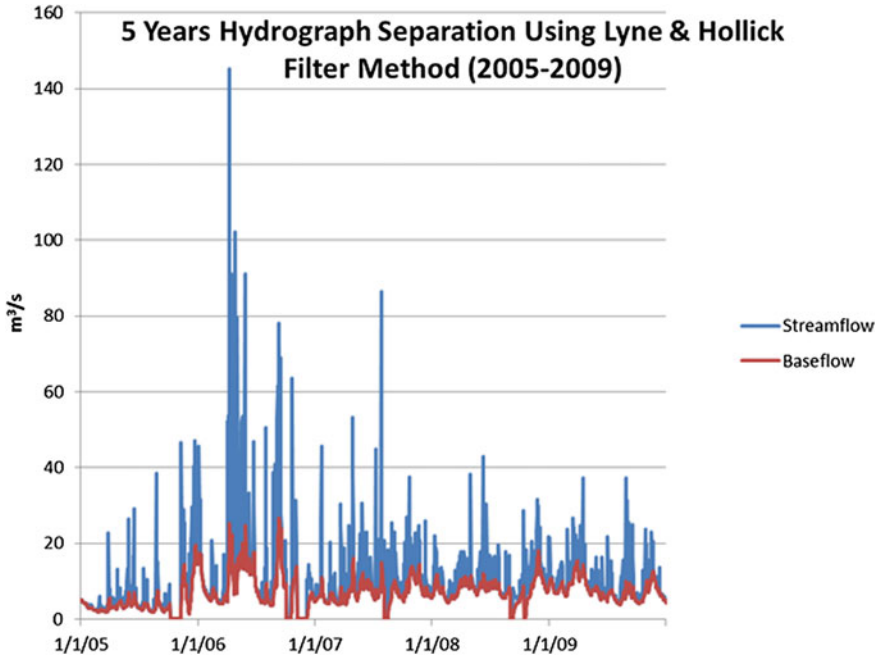


Fig. 7 The hydrograph separation for 5 years (2005–2009)

Table 1 Comparison and percentages values for different duration

	Duration	BFI value	Percentages of streamflow are estimated to be baseflow (%)
For a month	January 2000	0.817	81.7
	February 2000	0.643	64.4
For a year	Year 2000	0.687	68.7
	Year 2001	0.822	82.2
For 5 years	Years 2000–2004	0.729	72.9
	Years 2005–2009	0.675	67.5
For 10 years	Years 2000–2009	0.703	70.3

8 Conclusion

The hydrograph separation is a mathematical process used to determine the baseflow. This hydrograph separation used the streamflow monitoring information as input and partitions the observed flow into rapidly and slowly varying components, i.e., surface runoff and baseflow, respectively.

The BFI is the average rate of baseflow relative to the average rate of total stream flow. It has no unit and the increasing values indicate an increasing

contribution of baseflow to stream flow. Based on the objective stated, the value of baseflow was shown on the hydrograph separation.

In order to get the hydrograph separation, the value of baseflow should less than or equal to streamflow (baseflow \leq stream flow). Then, the baseflow indexes (BFI) for the river in Selangor can be calculated.

Table 1 shows that on January 2000, BFI value indicates that 81.7 % of streamflow are estimated to be baseflow. Next, on February 2000 there is 64.4 % of stream flow is estimated to be baseflow. Then, for the year 2000 and 2001 there is 68.7 % and 82.2 % of streamflow are estimated to be baseflow respectively. Besides, for the years 2000–2004 and years 2005–2009 produced 72.9 % and 67.5 % of streamflow which are estimated to be baseflow respectively. As for the year 2000–2009, the percentage of stream flow estimated to be baseflow is 70.3 %.

Malaysia is a tropical country that has different types of seasons throughout the year. Supposedly, there is some pattern on the rainfall events for certain months. This pattern should lead to expected shape and peak for the hydrograph separation. From the basic knowledge on the monsoon season in Malaysia, the hydrograph separation that is produced should have peak values from October to January (Northeast Monsoon) and May to September (Southwest Monsoon) with a larger peak in October/December. Unfortunately, the hydrograph separations obtained are not restricted to this pattern. This situation probably happens because of climatic changes in Malaysia.

Climatic change can happen due to global warming and greenhouse gas emissions. Hence, leading to El nino and La nina. During El Niño period, warmer water in the central and eastern Pacific supplies the atmosphere immediately above it with additional heat and moisture. It favours strong rising motion and thus lowers the atmospheric surface pressure in the rising motion area. The raising moist air condenses to form large areas of thunderstorm clouds and heavy rainfall in the area. In the western part of the Pacific including the Malaysian region, atmospheric pressure increases, resulting in relatively drier weather. On the other hand, La nina is an extreme weather phenomenon usually characterized by cooling of ocean temperature and surface waters in the Pacific eventually leading to heavier rainfalls and floods.

Next, the streamflow is also affected by the watershed condition. At the same time, watersheds are affected by the different physical and climatic differences. A watershed is the area of land where all of the water that is under it or drains off of it goes into the same place. John Wesley Powell, scientist geographer defines it best when he said that a watershed is:

that area of land, a bounded hydrologic system, within which all living things are inextricably linked by their common water course and where, as humans settled, simple logic demanded that they become part of a community.

The physical appearance of watershed refers to topography, type of soil and vegetation cover. As for Bernam river basin, the steep land or topography will produce greater runoff hence, affecting the streamflow value. Next, this river basin consists of tropical hill rainforest. The trees, grassland and different size of

vegetation can produce and control the runoff values which are affecting the stream flow.

In conclusion, the values of baseflow and baseflow index (BFI) can be quantified and represented well using Lyne & Hollick method, and the values may vary over space and time based on the regional climate, topography, landscape, and geological characteristics.

Acknowledgments The authors sincerely thank all parties namely Faculty of Civil Engineering UiTM, RMI and DID which have contributed precious inputs and supports. This study is funded by RAGS grant (600-RMI/RAGS 5/3 (198/2012)).

References

1. K. Eckhardt, How to construct recursive digital filters for baseflow separation. *Hydrol. Process.* **19**, 507–515 (2005)
2. C. Santhi et al., Regional estimation of base flow for the conterminous United States by hydrologic landscape regions. *J. Hydrol.* **351**, 139–153 (2008)
3. A.L. Gonzales et al., Comparison of different base flow separation methods in a lowland catchment. *Hydrol. Earth Syst. Sci. Discuss.* **6**, 3483–3515 (2009)
4. K. Eckhardt, Technical note: analytical sensitivity analysis of a two parameter recursive digital baseflow separation filter. *Hydrol. Earth Syst. Sci. Discuss.* **8**, 9469–9480 (2011)
5. K. Eckhardt, A comparison of baseflow indices, which were calculated with seven different baseflow separation methods. *J. Hydrol.* **352**, 168–173 (2008)

Water Sensitive Urban Design in Existing Urban Settings: Case Study of Dry Detention Pond in Kuching City

Darrien Yau Seng Mah, Afdal Haziq bin Mohamad Salehe and Frederik Josep Putuhena

Abstract This paper is intended to investigate the potential of dry detention pond in long-established urban settlements in Kuching City. Such pond is inserted to a typical terrace housing estate by means of computer modelling using SWMM software. The initial outputs of model are to identify occurrence of positive altered runoff patterns. Such modelling results provide a tool quantitatively to measure the probable use of the proposed measures to improve the existing urban drainage system.

Keywords Drainage · Hydrology · Infiltration · On-site detention · Rainfall · Runoff · Storm water · SWMM · Water cycle

1 Introduction

One of the components of water cycle is the process of infiltration, where rain water seeps into soil layers. Before any development is undertaken, land area acts as a rainforest catchment to absorb most of the rain water into ground water table. Cuttings of trees as well as land clearings for construction of infrastructures to meet the needs of the people such as roads, buildings, airports and shopping complexes have resulting in low permeability of the surface terrain, thus increasing the surface runoff. This source of running water causes problem like flash flood, erosion and so on.

The above-mentioned volumes of running water can be alleviated through Water Sensitive Urban Design (WSUD) approach. It is an effort to incorporate natural processes to urban water cycle in hoping to restore as much as possible a

D. Y. S. Mah (✉) · A. H. b. M. Salehe · F. J. Putuhena
Department of Civil Engineering, Faculty of Engineering, Universiti Malaysia Sarawak (UNIMAS), Kota Samarahan, Sarawak, Malaysia
e-mail: ysmah@feng.unimas.my

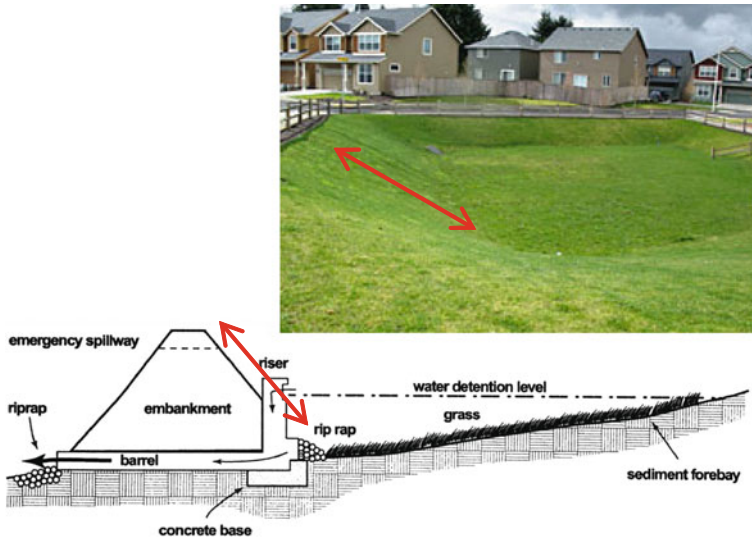


Fig. 1 Dry detention pond with embankment [5]

balanced water cycle [1–3]. In the current practices, natural infiltration process is hindered, for concrete drains contain the rain water within its compounded channel walls for rapid disposal. It discontinues the natural infiltration process particularly in urbanized landscapes.

In Malaysia, the Department of Irrigation and Drainage (DID) enforces the use of *Manual Saliran Mesra Alam* (MSMA) in urban drainage system. However, the State of Sarawak, due to her independent governance from the Federal Government, is not practicing MSMA at the moment. Seeing the advantages of WSUD approach, it is now gradually introduced in the Sarawakian scenes. MSMA lists out some designs of water infrastructures with WSUD-orientation [4]. In this paper, the authors focus on dry detention pond.

2 Dry Detention Pond

In order to re-introduce a healthy urban water cycle, infiltration process should be incorporated in a storm water drainage system. It is easier to include WSUD components in new projects, starting from the planning stages. On the other hand, it is quite difficult to change the existing drainage system, especially in a well-established residential area. Having a WSUD component that can be integrated into a rigid concrete drainage system would be the most welcome to reduce any disturbances to the residents.

Fig. 2 Dry detention pond with slow flow drain [6]



Fig. 3 Dry detention pond combined with wet pond [7]



As such, a detention system of WSUD approach is attempted here, in the form of a dry detention pond, to be fitted to an existing concrete drainage system in any typical terrace housing estate. The dry detention pond is intended as an agent that provides temporary storage of runoff, at the same time, allowing infiltration of rain water side by side a conventional drainage system.

There are many types of dry detention pond exist nowadays. Each type may come with different designs, but most serve the same purpose. Below are a few examples of dry detention pond.

Dry detention pond in Fig. 1 utilizes the slopes of the landforms. The pond is designed to detain some water during precipitation. There will be a visible water pond for a short period of time and later on gradually decreases as water infiltrates into the ground. There is one outlet for allowing excess water to flow out to the nearby waterways, if the water exceeds the holding capacity of the pond.

Figure 2 shows another form of dry detention pond. For this design, a series of slow flow drain is provided to dissipate the thrusting energy of storm water when it enters the facilities from the urban settlements.

Fig. 4 Dry detention pond in the Engineering Campus of USM (Penang) [8]. **a** Before storm event—as football field. **b** After storm event—as temporary water pond



Dry detention ponds are often used in combination with wet ponds, as in Fig. 3. Such application allows extended detention of storm water to improve water quality because it can minimize downstream erosion and control of pollutant as more suspended solids can be removed.

From the three examples illustrated above, it can be said that dry detention pond has ecological and aesthetic values, as it is “green” and merges with landforms. It assists to enhance water quality by filtering the storm water before discharging to waterways. It also functions as flood control by permitting natural infiltration to occur so that the volume of surface runoff is reduced. However, the dry detention ponds in all three examples are large in size that such designs require proper planning at the early stage of a township development.

Nevertheless, there are examples of smaller-scaled dry detention ponds as depicted in Figs. 4 and 5. The example in the campus of Universiti Sains Malaysia (USM), the dry detention pond is retrofitted to an existing football field [8]. Take the example in Taiping, the dry detention pond is small because of its location in the town center [9]. As such, dry detention ponds are flexible to be fitted into existing urban settings with limited land spaces.

Fig. 5 Dry detention pond in Klinik Kesihatan Taiping (Perak) [9]



Fig. 6 Study area—Casa Mabella, Kuching [10]

3 Case Study

It is a fact that empty lands are limited in existing urban settings. Under the Malaysian housing requirements, at least 10 % of total area of a housing project should be reserved as public open space. Therefore, such land can be adopted for dry detention pond in an existing housing estate. One typical housing estate, Casa Mabella in the suburb Tabuan Laru, about 5 km away from the Kuching City is taken as study area.

The estate is established for over 20 years beside a small tributary of Stutong River. The existing concrete drains of the housing estate flow into the river. It can be observed in Fig. 6, there is a community park with paved footway for exercise at the right-hand side of the air photo. This piece of land can be easily converted to dry detention pond, without removing a single tree and maintaining its current features. However, for demonstration here, a smaller area (inset of the figure) is taken for

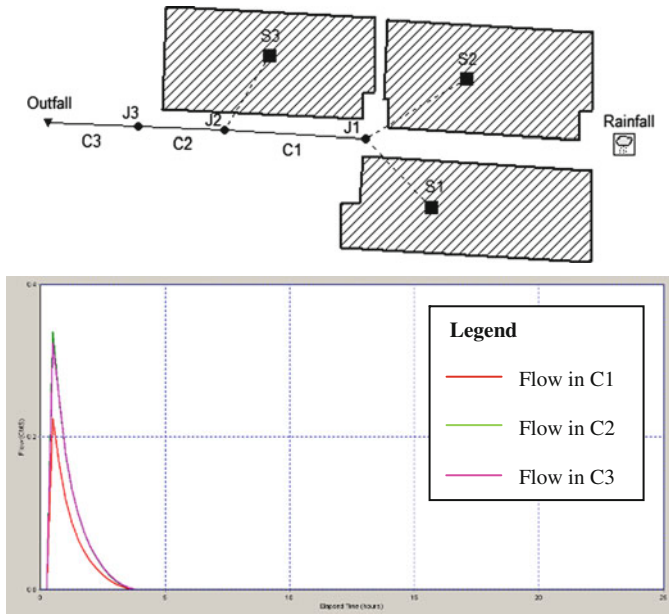


Fig. 7 Scenario 1: with conventional concrete drain only

study using computer software. The method is to introduce a dry detention pond as what-if scenarios virtually in Storm Water Management Model (SWMM) environment to inspect the potentials of such application.

Storm water drainage system is manmade system to intercept components of water cycle in urban catchment. From rainfall to runoff, from runoff to infiltration, these hydrological processes can be represented mathematically. Thus, a computer model is capable to imitate these processes. SWMM simulates the dynamic rainfall-runoff processes, in which runoff component of SWMM operates on a collection of sub-catchment areas on which rainfall and runoff is generated. The routing component of SWMM transports the runoff through a conveyance system until it reaches an outfall [11].

4 Results and Discussion

Two scenarios are presented here. Scenario 1 is basically a representation of the existing rectangular concrete drain (0.45 × 0.60 m). In Fig. 7, a 15-min storm event with an intensity of 20-year ARI befalls the sub-catchments of S1, S2 and S3. The design rainfall is estimated at 43 mm. Runoff generated from these roof catchments is drained through the nodes of J1, J2 and J3 and conduits of C1, C2 and C3. The storm water is discharged in Outfall.

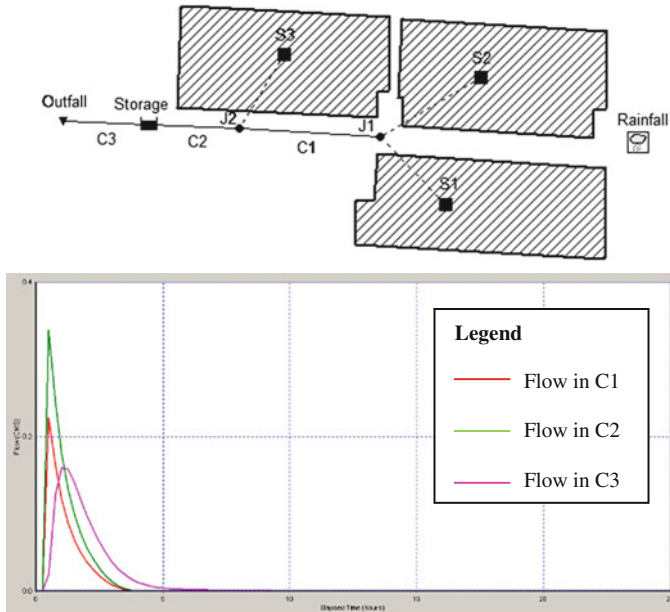


Fig. 8 Scenario 2: with addition of dry detention pond

Results are presented in the time series of flows in the conduits. C1 has a peak flow of $0.22 \text{ m}^3/\text{s}$ for receiving runoff from catchments S1 and S2. C2 has a peak flow of $0.34 \text{ m}^3/\text{s}$. When reaching C3, the peak diminishes a bit to $0.32 \text{ m}^3/\text{s}$. The storm surge is fully disposed of its excess water to waterways within 3 h.

The modeling set up in Scenario 1 is repeated in Scenario 2, except J3 is replaced by a dry detention pond. In this case, a pond of 944 m^2 wide and 0.3 m deep is represented as storage unit. Storm water travelling from C1 and C2 is modeled to enter the dry detention pond first. When the capacity of the pond is full, only then the storm water is allowed to flow to C3. Figure 8 shows that C1 and C2 remain its flows as in Scenario 1. However, peak flow in C3 is estimated to drop 47 % to $0.18 \text{ m}^3/\text{s}$. The storm water is expected to take time to spread in the pond before entering C3. It slows down the running water as the model predicts prolong full discharge to waterways in 5 h.

5 Concluding Remarks

This is an applied water engineering research by means of computer modeling to investigate a component of dry detention pond as a way of introducing WSUD approach to existing housing estate with rigid drainage.

Dry detention pond is capable of to fit into limited land space of urban areas. It is found to slow down surface runoff to receiving stream. This can reduce the risk of flash flood. It also introduces natural infiltration process in the urban housing estate.

Acknowledgments The authors express gratitude to opportunity, research, financial supports rendered by Universiti Malaysia Sarawak.

References

1. P.J. Coombes, J.R. Argue, G. Kuczera, Figtree place: a case study in water sensitive urban development (WSUD). *Urban Water* **1**(4), 335–343 (2000)
2. T.H.F. Wong, Water sensitive urban design—the journey thus far. *Aust. J. Water Res.* **3**(3), 213–222 (2006)
3. R.R. Brown, J.M. Clarke, *Transition to Water Sensitive Urban Design: The Story of Melbourne, Australia* (Facility for Advancing Water Biofiltration, Monash University, Australia, 2007)
4. Malaysian Department of Irrigation and Drainage (DID), *Urban Stormwater Management Manual for Malaysia* (2000)
5. <http://www.stormwaterpartners.com> (18 Jan 2013)
6. <http://sites.lafayette.edu> (18 Jan 2013)
7. <http://garnerscreekutility.org> (18 Jan 2013)
8. N.A. Zakaria, *Sustainable Urban Drainage System, Solutions to Flash Flood, River Pollution and Water Shortage* (Penerbit Universiti Sains Malaysia, Penang, 2007)
9. S.H. Lai, D.Y.S. Mah, Field investigation of dry pond for urban stormwater drainage. *Hydrol. Sci.* **57**(6), 1249–1255 (2012)
10. <http://wikimapia.org> (25 Jan 2013)
11. J. Gironás, L.A. Roesner, L.A. Rossman, J. Davis, A new applications manual for the storm water management model (SWMM). *Environ. Model. Softw.* **25**(6), 813–814 (2010)

Enhancing Water Resources and Coastal Engineering Curricula Using Visual Basic Programs in MS-Excel

Ahmad Sana

Abstract A large number of calculations in the water-related subjects like Fluid Mechanics, Hydrology, Hydraulics, Water Resources Engineering and Coastal Engineering involve iterations. In the past, because of limited computational facilities available to the professional community, approximate formulae were developed that are still in use. Utilization of Visual Basic for Applications (VBA) in MS-Excel can tremendously reduce the time incurred on iterations in the engineering practice and in turn reduce the dependence on approximate formulae. This study elaborates the enhancements in the curricula of Hydrology, Water Resources and Coastal Engineering at Sultan Qaboos University, Sultanate of Oman, by including short VBA programs. Typical examples of such program usage are calculations of friction factor, design of open channels, design of sanitary sewers, calculation of cumulative infiltration by Green-Ampt formula, and solution of wave dispersion relation. This improvement in the curricula would encourage the students to fully utilize the advanced features of MS-Excel, thus improving productivity in the fields of water resources and coastal engineering.

Keywords VBA • MS-Excel • Water resources engineering • Coastal engineering

1 Introduction

The commonly available software like MS-Excel is widely used in the engineering community in order to carry out simple calculations. This software, in fact, offer more features than usually utilized. In most of the situations, a spreadsheet software like MS-Excel can be utilized to carry out detailed analysis of engineering

A. Sana (✉)
Department of Civil and Architectural Engineering,
Sultan Qaboos University, Muscat, Sultanate of Oman
e-mail: sana@squ.edu.om

phenomena rather than importing data from other specific engineering software and creating tables and graphs only. In other professional fields like management and economics, the utilization of the worksheet involves more advanced features. Therefore, there is a need to educate the engineering students for more advanced features involving the use of VBA to fully utilize the capabilities of such software. Moreover, a seamless interface among various Microsoft software enables the user to use the worksheets in a more effective way. Generally the engineering students have a good background in computer programming facilitating the usage of VBA.

Here some of the ongoing activities regarding the use of VBA in MS-Excel in teaching the subjects of Fluid Mechanics, Water Resources Engineering, Hydrology and Coastal Engineering to undergraduate Civil Engineering students are described. The present study will be useful in order to improve the Civil Engineering curriculum in line with the ABET requirements pertaining to the use of modern techniques necessary for engineering practice.

2 User Versus Developer

The application of computers to carryout engineering design and analysis may be included in the existing engineering curricula by various means. In case of water-related courses (Fluid Mechanics, Hydraulics, Water resources engineering, Hydrology, Coastal engineering etc.) the use of computer becomes extremely important for practical applications. Reference [1] presented the use of an equation solver for hydraulic design teaching, [2, 3] have given examples on the use of worksheets for hydraulic systems analysis and design. The later have shown the use of Solver add-in in MS-Excel to analyze pipe networks. The use of spreadsheets in other civil engineering courses is also common; [4, 5] have shown examples of structural engineering and geotechnical engineering, respectively.

Many engineering situations require specifically developed technical software those are mostly commercial and therefore very expensive by virtue of the initial cost as well as that required for update from time to time. However, in most of the situations small scale programs coupled with the commonly available software may be effectively utilized for design and analysis. Such type of small programs are easy to use and update as per field requirements. Moreover, the students using commercial software are deprived of the understanding of fundamental principles underlying the solution of the practical problem thus becoming mere users of the software. Whereas more and more challenging engineering problems faced by contemporary engineering professionals require a strong background in the basic knowledge of engineering principles. An engineer with such a background is able to develop his own small scale applications using the available common software, conveniently avoiding the use of commercial software in many situations and has a better capability to tackle the present and future engineering problems. In other words, an engineering curriculum should be designed to educate the engineers to perform the role of developers whenever required not mere users of the software.

In addition, an engineer having background in developing computer applications may prove to be more efficient learner and user of the commercial software and therefore more valuable to an organization as compared to the one who does not have such skills.

3 Problems and Solutions

3.1 Calculation of Friction Factor

In order to calculate head loss in pipes the well known Darcy-Weisbach equation is used as shown below [6]:

$$h_L = f \frac{L V^2}{D 2g} \tag{1}$$

where, h_L = head loss, f = friction factor, L, D = length and diameter of the pipe, respectively, V = average velocity of flow and g = acceleration due to gravity. For turbulent flow, generally Colebrook equation is used to calculate the friction factor given as:

$$\frac{1}{\sqrt{f}} = -2 \log \left(\frac{e/D}{3.7} + \frac{2.51}{N_R \sqrt{f}} \right) \tag{2}$$

where, e = Nikuradse’s equivalent roughness height and N_R = Reynolds number. It is evident from (2) that trials have to be made in order to calculate the friction factor because it is implicitly expressed. For a single pipe, the trials can be easily done. However, in case of a pipe network analysis the head loss has to be determined for every pipe at every step. An automated solution procedure may result in considerable computational economy. Therefore, a VBA function can be developed as follows to solve (2) to obtain friction factor:

1. Static Function Log10(X)
2. Log10 = Log(X)/Log(10#)
3. End Function
4. Function darcyf(ReynoldsNum, RelRoughness)
5. ‘
6. ‘ Function darcyf
7. ‘ Recorded 2/28/2006 by Ahmed Sana
8. ‘ To calculate friction factor for Darcy-Weisbach
9. ‘ Equation using Colebrook Equation
10. ‘
11. darcyf0 = 0.01
12. 12 darcyf = 1 / (2 * Log10(RelRoughness / 3.7 + 2.51 / ReynoldsNum / (darcyf0) ^ (1/2))) ^ 2

13. If Abs(darcyf – darcyf0) > = 0.00001 Then
14. darcyf0 = darcyf
15. GoTo 12
16. End If
17. darcyf = Round(darcyf, 3)
18. End Function

Here the line numbers are shown for explanation only. In the program only those statements have to be numbered that have been referred somewhere (for example statement number 12 here). First three lines are used to define a logarithm to the base 10. This step can be avoided if Colebrook equation is derived in terms of the natural logarithm. Here, the equation is used in its original form. Line 4 to 18 pertains to the function darcyf which has two arguments as required by Colebrook equation, i.e. Reynolds number (ReynoldsNum) and relative roughness (RelRoughness) of the conduit. The method of successive substitution is used as might be used in manual calculations in lines 12–16 after initializing the value of the friction factor in line 11. Line 17 is used just to round off the value of friction factor to three decimal places. In order to calculate the friction factor darcyf (*Reynolds number, Relative roughness*) function has to be invoked like any other Excel function providing the values of its arguments in parentheses. In order to use this function the VBA program has to be in the same spreadsheet where the function is to be invoked, however, it can be stored as an add-in as well to be used in any spreadsheet.

This program was taught in the form of a tutorial to the undergraduate students in the subjects of Hydraulics and Water Resources Engineering. In order to elucidate the importance of this method, the students were asked to plot Moody's diagram using their own calculations. Obviously, without the use of a program, the calculations to plot Moody's diagram would require an extremely long time. Other useful examples of this methodology relevant to water resources engineering include the case of a conduit flowing partially full (sewer design), design of trapezoidal open channels, calculation of velocity of approach in a weir and design and analysis of culverts.

3.2 Calculation of Cumulative Infiltration

In water resources engineering and hydrology, Green-Ampt method is widely used in order to calculate infiltration in the soil. Considering the physical process of infiltration the following equation may be derived for cumulative infiltration, F [7]:

$$F(t) = Kt + \psi\Delta\theta \ln\left(1 + \frac{F(t)}{\psi\Delta\theta}\right) \quad (3)$$

where, K = hydraulic conductivity, t = time, ψ = suction head of the soil and $\Delta\theta$ is the change in moisture content of the soil due to infiltration. It may be noted that (3) can be solved by a simple successive substitution method. However, in many situations a large number of iterations are needed to reach the solution. For a few cases of computation Goal Seek tool may be used in MS Excel. But for a large number of field conditions a simple VBA program may prove to be very convenient. The undergraduate students in a Hydrology class at Sultan Qaboos University were asked to develop such a program. In order to elucidate the use of this program the following example was used.

Example: Use the Green-Ampt method to evaluate the infiltration rate and cumulative infiltration depth for a silty clay soil ($\psi = 29.22$ cm, $K = 0.05$ cm/h, effective porosity, $\theta_e = 0.423$) at 0.1 h increments up to 6 h from the beginning of infiltration. Assume initial effective saturation, $S_e = 20$ % and continuous ponding [7, p. 125].

Solution: From the known relationship between given soil properties and conditions $\Delta\theta$ can be calculated. Also, it is known that infiltration rate, $f = K(\psi\Delta\theta/F + 1)$. It is clear that in order to solve this problem, (3) has to be solved 60 times. The solution can be obtained using VBA program written for this purpose and is shown in Fig. 1.

3.3 Calculation of Wave Length

In the field of coastal engineering, the first quantity that one has to calculate is the wave length L based on the water depth d and period of oscillation T of the wave. The simplest formula for this purpose is derived as per small amplitude wave theory as [8]:

$$L = \frac{gT^2}{2\pi} \tanh\left(\frac{2\pi d}{L}\right) \quad (4)$$

where, g is the acceleration due to gravity. This equation is implicit by virtue of the wave length and therefore, requires iterations. There have been a number of efforts in the past to propose explicit approximate formulae to calculate the wave length that gives almost similar result as (4). A simple VBA program similar to the one used for (2) can be utilized to obtain the exact solution of (4) instantly.

Incorporating simple VBA programs in the undergraduate courses motivate those students who have interest and potential to develop their own software applications for engineering problems. One such example is an application based on small amplitude wave theory by one of the undergraduate students in the subject of Coastal Engineering at Sultan Qaboos University in Fall 2006 semester. This application was developed in Visual Basic and computes almost all the basic wave properties for given wave height, wave period and water depth. The main menu of this application is shown in Fig. 2.

Fig. 1 Cumulative infiltration and infiltration rate VBA program for Green-Ampt method

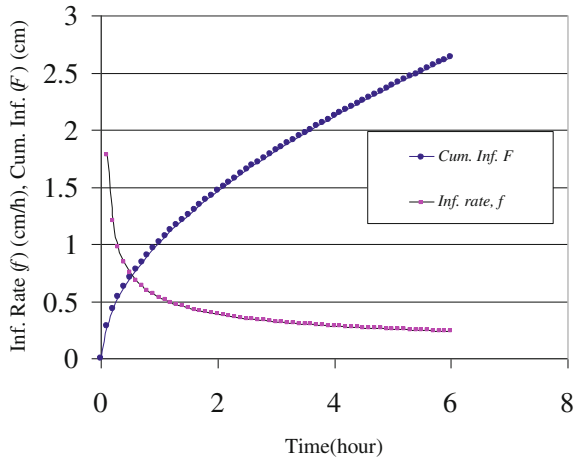
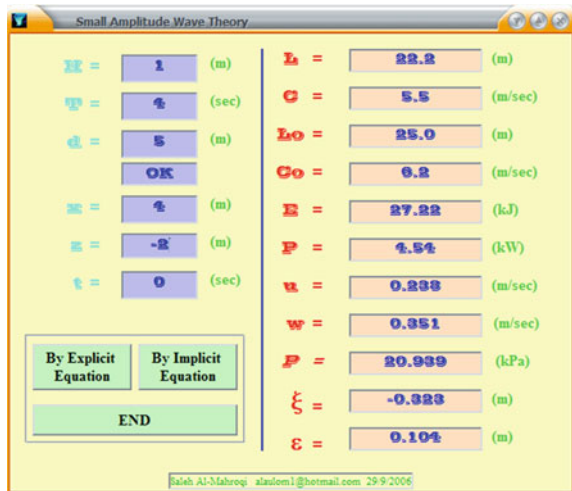


Fig. 2 Main menu of a Visual Basic application developed by an undergraduate student to calculate wave properties using small amplitude wave theory



The students can be motivated to use programming in solving the relevant problems by assigning small scale design projects. Such projects could be completed using manual calculations by handheld calculators, however, it may require considerable amount of time. On the other hand, the use of programming could significantly increase the computational efficiency.

3.4 Design of a Sewer Pipe

The sanitary sewers are designed to run partially full as per specifications almost everywhere. The sewer capacity at a certain location is based on the future

quantities of wastewater from domestic, commercial and industrial sources. These quantities are generally estimated using statistical techniques from the population projections.

For a partial flow in circular pipe, geometry of the cross-section and Manning’s formula can be used to derive an implicit equation for water surface angle ϕ as follows [6]:

$$\frac{(\phi - \sin \phi)^{5/3}}{\phi^{2/3}} = \frac{20.16nQ}{D^{8/3}S_0^{1/2}} \tag{5}$$

where, D is the pipe diameter, n , Manning’s roughness factor, Q , discharge and S_0 , slope of the sewer. In a typical design problem, the pipe diameter is assumed in the beginning and then checked for allowable maximum and minimum velocities, maximum depth of flow and the Sulfide generation potential. It is obvious that (5) has to be solved several times for each pipe in order to meet the design specifications. Such type of implicit equations may be solved using *Goal Seek* function in MS-Excel. However, a simple VBA program in MS-Excel would be extremely efficient in carrying out these computations. The program is listed as follows:

Function theta(dia, manningn, disch, slope)

```

‘ Calculate theta for partially full circular pipe
‘ using Mannings formula
‘ Enter the arguments in the alphabetical order
‘ e.g. diameter, mannings n, Q and slope
theta0 = 1#
rhs = 20.16 * manningn * disch / dia ^ (8 / 3) / slope ^ (1 / 2)
10 lhs = ((theta0 - Sin(theta0)) ^ (5 / 3)) / theta0 ^ (2 / 3)
If Abs(lhs - rhs) >= 0.01 Then
    theta0 = theta0 + 0.01
    GoTo 10
End If
theta = Round(theta0, 3)
‘ theta = lhs
End Function
    
```

4 Conclusions

MS-Excel is a widely used spreadsheet application among the engineering community. However, the advanced features of this software are sparingly used by most of the practicing engineers. The curricula of water resources related subjects and coastal engineering leading towards a bachelor’s degree in Civil Engineering may be enhanced using simple VBA programs in MS-Excel. A few examples of the efforts made at Sultan Qaboos University in this regard are presented here.

These improvements in the curricula are in line with the ABET requirements relevant to the use of modern techniques in engineering practice. In addition, such enhancements in the curricula may prove to be a source of motivation for potential engineering software developers.

This approach ensures that the engineering students utilize their fundamental knowledge in order to solve the problems in an efficient manner. The available technical software may also be included in the engineering curricula, however, it must be ensured that the students develop an insight to understand the technical background of the solution procedure.

References

1. T.K. Jewell, Teaching hydraulic design using equation solvers. *J. Hydraul. Eng.* **127**(12), 1013–1021 (2001)
2. P.T. Weiss, J.S. Gulliver, What do students need in hydraulic design projects? *J. Hydraul. Eng.* **127**(12), 984–991 (2001)
3. D.H. Huddleston, V.J. Alarcon, W. Chen, Water distribution network analysis using Excel. *J. Hydraul. Eng.* **130**(10), 1033–1035 (2004)
4. K.M. El-Sawy, A.M.I. Sweedan, Innovative use of computer tools in teaching structural engineering applications. *Australas. J. Eng. Educations* **16**(1), 35–54 (2010)
5. H. Canakci, Pile foundation design using Microsoft Excel. *Comput. Appl. Eng. Educ.* **15**(4), 355–366 (2007)
6. D.A. Chin, *Water Resources Engineering* (Prentice Hall, New Jersey, 2000), 750 pp
7. V.T. Chow, D.R. Maidment, L.W. Mays, *Applied Hydrology* (McGraw-Hill Inc., Singapore, 1988), p. 572
8. R.M. Sorensen, *Basic Coastal Engineering* (Kluwer Academic Publishers, The Netherlands, 1997), p. 301

Regression Analysis for Dimensionless Discharge Ratios Prediction

Issam A. Al Khatib

Abstract Experimental testing of 3 different dimensionless discharge ratios in an asymmetrical rectangular compound channel was conducted. The geometry effect of the cross section on the discharge ratios has been investigated. It was found that both the main channel width, B , and the step height, Z , affected these ratios. Numerical values of the regression coefficients for the resulting 27 single-variable models representing 3 types of dimensionless discharge ratios for each of the 9 cross-sections have been derived. Another set of multiple-variable regressions models has been derived using two additional dimensionless parameters which take into account the widths of the constructed asymmetric compound channel and the floodplain water depth. Although scaling of the experimental results requires further study for application to wide open channels, these findings may be useful in practical applications for narrow channels.

Keywords Hydraulics • Open channel • Compound cross section • Asymmetric • Regression analysis

1 Introduction

Accurate flow predictions in compound channels are necessary for solving many practical problems in river engineering. For example, flood prevention can be achieved by different measures such as dredging the main channel and lowering or smoothing the flood plains that depends on total discharge in compound channels [1–3]. Likewise, the local flow conditions determine the erosion and deposition rates of sediment in the main channel and flood plains. As a result, prediction of

I. A. Al Khatib (✉)

Institute of Environment and Water Studies, Birzeit University, Birzeit, Palestine
e-mail: ikhatib@birzeit.edu

the discharge capacity of compound channels is essential to imply in flood mitigation schemes [4, 5].

A review of the literature, though not exhaustive, reveals that the primary contributions have been those of the following authors [6–11].

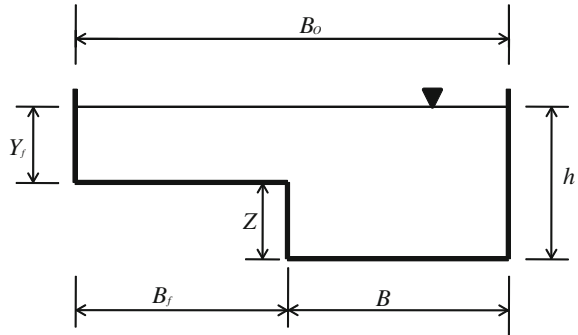
A compound channel consists typically of a main river channel and floodplains. Water is present for the majority of the time in the main channel, while the floodplains, although dry for most of the time, have a vital role to play during flood events. These floodplains generally extend laterally away from the main channel and increase the conveyance capacity during flood events [12, 13]. When water in the main channel flows in an out-of-bank condition and on to the adjoining flood plain, owing to the abrupt change of the shape of the cross section and heterogeneous boundary roughness, there are a bank of vertical vortices found in many experiments by different authors [14, 15], along the vertical interface between the main channel and the flood plain. There, flow structure and flow resistance become very complex and flow shows very strongly three-dimensional characteristics [16–18].

Experimental studies indicate that lateral momentum transfer occurs between main channels and flood plains and generally slows down the flow into the main channel while accelerating the flow into the flood plain [19–21]. The whole process resists the flow and lowers the discharge capacity of the compound channel. In order to obtain the discharge, it is essential to accurately estimate the flow velocities and discharge in each compartment [22].

In nature, the compound channel represents natural rivers where higher discharges will occasionally occur in them, and cause the channel to flow in an overbank condition, thereby increasing the flow width, depth and area. The channel cross-section is now different and incorporating the main river channel and the adjacent floodplains [23, 24]. However, it is still an open channel with a more complex roughness, geometry and planform. The floodplains are therefore an integral part of the whole river system. It should be recognized that for overbank flow, not only does the cross-section shape change significantly from its inbank shape, but also the streamwise pathways for flow may alter considerably [14]. In nature, there is a continuum of hydraulic processes coming into action above the bankfull level. There is also a significant increase in the complexity of the flow behavior once overbank flow starts. This is to say, once the river flows in out-of-bank manner as frequently occurs in flood flow conditions, then the discharge in the whole channel, the main river and its associated floodplains, is considerably more difficult to calculate than when the river is flowing wholly inbank [25–27].

The aim of this article was to understand the discharge distribution in channels with asymmetrical rectangular compound sections having different geometries and to utilize the regression analysis in the prediction and generalization of dimensionless discharge ratios.

Fig. 1 Cross-section of the asymmetric rectangular compound channel used in the experiments



2 Experimental Setup and Experiments

Nine different models having a rectangular asymmetric compound cross section and having three different step heights and three main channel widths were tested. A rectangular glass-walled laboratory flume of 11.5 m length, 0.30 m width, and 0.3 m depth with a bottom slope of 0.0025 was used in the experiments at the fluid mechanics laboratory, Mechanical Engineering Department, Birzeit University, Palestine. Discharge was measured volumetrically with a flow meter with 0.1 L accuracy. A point gauge was used along the centerline of the flume for head measurements. All depth measurements were done with respect to the bottom of the flume. A pitot tube of circular section with external diameter of 8 mm was used to measure the static and total pressures which were used for velocities at required points in the experiments conducted throughout this study.

Models were manufactured from Plexiglas and placed at about mid length of the laboratory flume. Figure 1 shows the cross section of the models with symbols designating important dimensions of the model elements. In this study model types tested are denoted by ($i = 10, 15, 20$; $j = 2, 4, 6$). Here B and Z are the width and step height of the main channel of the asymmetric compound cross section, respectively. The subscripts i and j designate the numerical values of B and Z in centimeter used in this study, respectively. It is worth mentioning that such dimensions were selected in order to have a wide range of dimensionless values of geometric parameters.

The required experiments first were conducted in the models of the smallest B ($=10$ cm) with varying Z values ($=2, 4$ and 6 cm) and then B was increased to 15 cm at the required amount of Z ($=2, 4$ and 6 cm), and finally for $B = 20$ cm with the same three values of Z . The length of the asymmetric compound channel was 2 m.

In order to determine the velocity distribution in the rectangular compound cross sections the channel cross section was divided by a number of successive lines normal to the direction of the flow. Then the total and static heads were measured at several points along these normal lines by the use of pitot (Preston)

tube. More points were taken close to the channel boundary. Towards the free surface, the distances between the points where the velocities measured were increased. The velocity area method was used to find the discharge for each zone of the cross section, which could then be summed to give the full cross-sectional discharge in all models.

3 Presentation and Discussion of Results

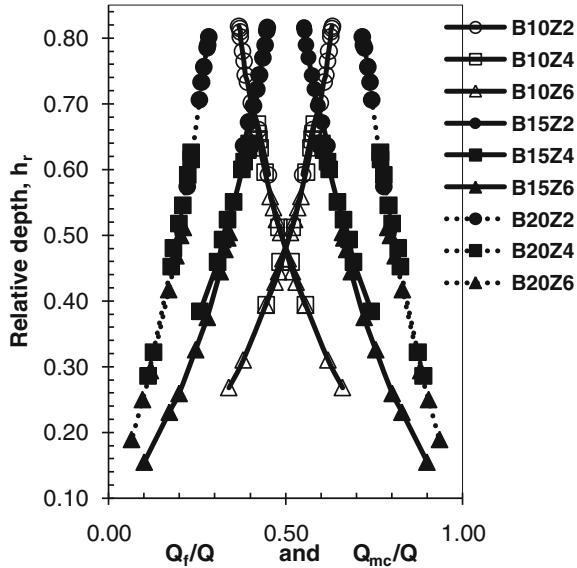
3.1 Variation of Discharge Ratios Q_{mc}/Q , Q_f/Q and Q_{mc}/Q_f with Relative Depth, h_r

For any model to be adequate, it must accurately describe not only the total cross-sectional discharge (Q), but also the main channel and floodplain discharges, Q_{mc} and Q_f , respectively.

Figure 2 shows the proportions of the discharges in the main channel and floodplain, Q_{mc}/Q (curves on the right hand side), Q_f/Q (curves on the left hand side), for six different models, B10Z2, B10Z6, B15Z2, B15Z6, B20Z2, B20Z6, respectively. They are related to the relative depth, h_r , because it reflects the geometry effect on the discharge distribution in the channels of compound cross section since h_r is defined as the floodplain to the main channel water depth ratio Y_f/h and also dimensionless quantity.

From Fig. 2, one can conclude that the Q_f/Q ratio increases as h_r increases while the Q_{mc}/Q ratio slightly decreases as h_r increases for each model tested. This situation confirms the transfer of momentum from the main channel to the floodplains. There is a point of intersection between the proportions of flow in the main channel and floodplain in the models B10Z4 and B10Z6. This means that at these two points of intersection, the discharges are equal in both the main channel and the floodplain. The corresponding h_r values for these two points of intersection are 0.486 for B10Z4 and 0.484 for B10Z6. For the other models there are no points of intersection. This means that the main channel discharge is always greater than that of the floodplain for any h_r value tested because of the increasing main channel width except for the models B10Z2, B10Z4 and B10Z6 where the main channel discharge is always less than that of the floodplain for all tested h_r values due to the large value of the floodplain width, B_f with respect to the main channel width, B . For the other models, there are no points of intersection. This means that the main channel discharge is always greater than that of the floodplain for any h_r value tested because of the increasing main channel width. However, from the general trends shown in the figures, it can be concluded that at higher h_r values than those tested, the curves of Q_f/Q_t and Q_{mc}/Q_t intersect each other. However, it should be kept in mind that as the main channel width increases, the slopes of h_r versus Q_f/Q_t and Q_{mc}/Q_t curves get steeper with the increasing h_r value. This

Fig. 2 Variation of the discharge ratios, Q_f/Q and Q_{mc}/Q with the relative depth, h_r , for all tested models



means that the Q_f/Q_t and Q_{mc}/Q_t curves for a given cross section may not practically intersect each other.

In addition, it can be stated that the effect of the main channel width on the discharge ratios is more than that of the step height, Z (Fig. 2). For a given h_r the value of Q_{mc}/Q increases as the main channel width increases. The situation is different for the variation of Q_f/Q with h_r ; the Q_f/Q value increases with decreasing main channel width for a given h_r . For models with a fixed main channel width, if the step height is increased or decreased, the Q_f/Q or Q_{mc}/Q values insignificantly change for small values of h_r . Above certain values of h_r , the h_r versus Q_{mc}/Q curves of a model of constant main channel width coincide with each other even if the step heights of models are different. The same conclusion can also be drawn for the curves of Q_f/Q versus h_r .

3.2 Generalization of the Discharge Dimensionless Ratios Q_f/Q , Q_{mc}/Q , Q_{mc}/Q_f with the Relative Depth

A generalized single variable regression model has been derived to predict the dimensionless discharge distribution values Q_f/Q , Q_{mc}/Q and Q_{mc}/Q_f as a function of the relative depth, h_r . The prediction model is in the form indicated by Eqs. (1, 2).

$$\left(\frac{Q_f}{Q}\right) = a_1 [h_r]^{b_1} \tag{1}$$

$$\left(\frac{Q_{mc}}{Q}\right) = a_2[h_r]^{b_2} \quad (2)$$

Table 1 provides the derived numerical values of the regression parameters (a_1 , b_1 ; a_2 , b_2) for a total of 18 different models representing three types of dimensionless discharge ratios for each of the 9 different asymmetric compound cross-section cases. The derivation of the generalized model provided in Eqs. (1) and (2) has been accomplished based on the optimization of the correlation coefficient (r), which has been maximized to very high values, which for a line of perfect would have a value of ± 1 . In addition, the average correlation coefficients are given in Table 1.

All of the obtained statistics indicate that the derived regression models are powerful and can effectively be used to estimate the dimensionless discharge ratios with a high degree of reliability for constructed asymmetric compound cross-sections based only on the relative depth. The model regression parameters (a_1 , b_1 ; a_2 , b_2) need to be estimated for any particular cross-section geometry since Table 1 indicates that these coefficients are different for each compound cross-section type.

The measured dimensionless discharge ratio (Q_{mc}/Q) and the predicted one by utilizing Eq. (2) are plotted for B10Z4 as shown in Fig. 3. As seen from this figure, the values of the measured and predicted dimensionless discharge ratio are very close to each other. Using the procedure described the dimensionless discharge ratios in an asymmetric rectangular compound cross section can be estimated with high accuracy with a maximum absolute error of 8.6 and 1.6 % for Q_f/Q and Q_{mc}/Q respectively, and the mean absolute error was 1.3 and 0.5 % respectively. These error percentages were obtained by introducing the measured and predicted dimensionless discharge ratios for a given h_r value in Eqs. (1) and (2) respectively.

3.3 Multiple-Variable Regression Prediction Models

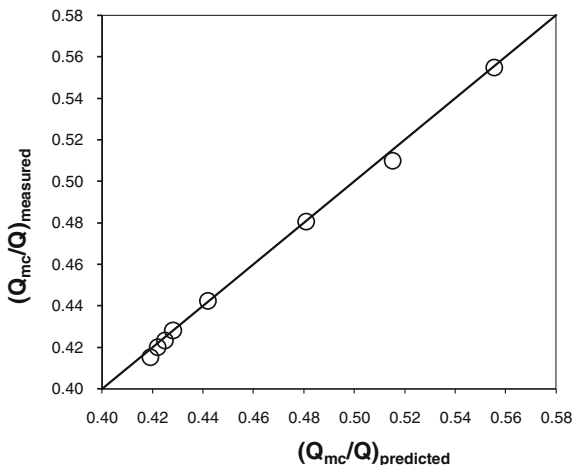
A generalized multiple-variable regression model has been derived to predict each of the 2 types of dimensionless discharge ratios as a function of 3 dimensionless parameters. The first dimensionless parameter is the relative depth (h_r) used as the main parameter in developing the single-variable regression models. The two additional dimensionless parameters are W and B_1 and take into consideration the channel the channel width dimensions (B_o , B_f and B) used in constructing the various asymmetric compound cross-section types in addition to h_r . The prediction model is also exponential in form as indicated by Eq. (2).

$$\ln(Q_i) = a_4 + b_4 h_r + b_5 W + \left(\frac{c_4}{B_1}\right) + c_5(WB_1) \quad (3)$$

Table 1 Values of the exponents, coefficients and correlation coefficients of the relationships given by Eqs. (1, 2)

Exponent, coefficient and r	Types of models										Average value of r
	B10Z2	B10Z4	B10Z6	B15Z2	B15Z4	B15Z6	B20Z2	B20Z4	B20Z6		
a_1	0.693	0.720	0.797	0.515	0.577	0.715	0.330	0.368	0.460	0.996	
b_1	0.439	0.511	0.637	0.652	0.830	1.005	0.723	0.948	1.148		
r	0.993	0.996	0.997	0.995	0.998	0.989	0.997	0.999	0.997		
a_2	0.321	0.333	0.343	0.500	0.502	0.550	0.680	0.703	0.708	0.996	
b_2	-0.641	-0.546	-0.505	-0.465	-0.413	-0.272	-0.244	-0.192	-0.173		
r	0.996	0.999	0.998	0.997	0.996	0.997	0.994	0.995	0.994		

Fig. 3 Measured versus predicted Q_{mc}/Q ratio for model B10Z4



where \ln = natural logarithm function, Q_i = dimensionless discharge ratio ($i = 1$ and 2). $Q_1 = \frac{Q_f}{Q}$; $Q_2 = \frac{Q_{mc}}{Q}$; $W = B_o/B$; $B_1 = h_f/B$; a_4 = regression constant, b_4 , b_5 , c_4 and c_5 = regression coefficients.

According to Eq. (3), a multiple-variable predictive model can be derived for each two types of dimensionless discharge ratios resulting in two different regression models. Therefore, the dimensionless discharge ratios as obtained from the 9 different compound cross-section types will be pooled together for the purpose of developing one multiple-variable regression model for each of the two dimensionless discharge ratios. Although the relationship between the dependent variable and the independent variables in Eq. (3) is a non-linear one, the equation is linear in terms of the coefficients, hence, the linear multiple-variable regression techniques can be applied which are mainly dependent on the minimization of the sum of squared errors.

Table 2 provides the derived regression parameters (a_4 , b_4 , b_5 , c_4 and c_5) for the 2 dimensionless discharge ratios. When deriving the generalized model provided in Eq. (3), optimization of 3 main regression statistics was done to arrive at the best possible estimated regression equation. The first main statistic is the model coefficient of determination (R^2), which has been maximized to very high values ranging from 0.971 to 0.982. These R^2 values are considered high but relatively smaller than those associated with the derived single-variable regression models. This can be attributed to using more variables in the multiple-variable regression models compared to the single-variable models and to the more homogeneity of the data used to develop the single-variable models as compared to the data used in the multiple variable models. The adjusted R^2 has ranged from 0.969 to 0.981 which means that 96.9 to 98.1 % of the variation in the dimensionless discharge ratio is explained by the variations in the three dimensionless parameters (W , B_1 and h_f). The second main statistic is the standard error (S_{Q_i}) associated with

Table 2 Regression coefficients and statistics for multiple-variable prediction models

Statistic	Q ₁	Q ₂
R ²	0.982	0.971
R ² _{adj}	0.981	0.969
S _{Q_i}	0.03724	0.09
CV _i (%)	2.6 %	4.8 %
a ₄	0.612	-2.55
b ₄	-0.656	-1.1013
b ₅	-0.297	0.601
c ₄	-0.006	-0.078
c ₅	-0.068	-0.168
t _{b4}	-15.437	9.822
t _{b5}	-20.282	16.879
t _{c4}	-2.255	-12.215
t _{c5}	-4.946	-4.991

the dependent variable (Q_i), which has been minimized to the lowest possible values as provided in Table 2. The third main statistic is the coefficients of variation (CV_i) wherein their values are acceptably small with values below 5 % (2.6 and 4.8 %). The fourth main statistic is the Student t-value associated with the independent variable coefficients (b₄, b₅, c₄ and c₅). The corresponding t-values have been maximized to reflect a confidence level exceeding 99.8 % which reflects a very high level of reliability in the predictive strength of the developed models.

4 Conclusions

In this study, a series of laboratory experiments was conducted to investigate the effect of the main channel width, B, and the step height, Z, of channels with asymmetric rectangular compound cross sections on different dimensionless discharge ratios as a function of the relative depth, h_r. It was found that both the main channel width, B, and the step height, Z, affected these ratios.

A generalized three different dimensionless discharge ratios for 9 different asymmetric rectangular compound cross-section types have been presented. The derived numerical values of the regression parameters (a₁, b₁; a₂, b₂) for a total of 18 different single variable prediction models, representing two types of dimensionless discharge ratios for each of the 9 different asymmetric compound cross-section cases, have been derived. All the obtained statistics have indicated that the derived prediction models are good, and can effectively be used to estimate the dimensionless discharge ratios with a high degree of reliability for the constructed asymmetric compound cross-sections based only on the relative depth.

The dimensionless discharge ratios for the nine different compound cross-section configurations were pooled together for the purpose of generating a

multiple-variable regression model for each mean flow type. The result is three distinct multiple-variable predictive models which are function of three dimensionless dependent parameters. The three dimensionless parameters include the channel relative depth and two other dimensionless parameters defined in terms of the channel widths dimensions. The four main statistics outlined earlier have indicated the high reliability and significance of the derived multi-variable predictive models. These findings may be useful in practical applications to narrow asymmetric compound channels with. To extend the results, further study with a large-scale model under different hydraulic conditions is required.

References

1. A. Bigil, H. Altun, Investigation of flow resistance in smooth open channels using artificial neural network. *Flow Meas. Instrum.* **19**, 404–408 (2008)
2. M. Sahu, K.K. Khatua, S.S. Mahapatra, A neural network approach for prediction of discharge in straight compound open channel flow. *Flow Meas. Instrum.* **22**, 438–446 (2011)
3. B.N.S. Ghimire, M.J. Reddy, Development of stage-discharge rating curve in river using genetic algorithms and model tree, in *International Workshop Advances In Statistical Hydrology*, Taormina, Italy, 23–25 May 2010
4. B.C. Van Prooijen, J.A. Battjes, W.S.J. Uijtewaal, Momentum exchange in straight uniform compound channel flow. *J. Hydraul. Eng., ASCE* **131**(3), 175–183 (2005)
5. K.C. Patra, Discharge assessment for two stage meandering and straight compound channels. *ISH J. Hydraul. Eng.* **II**(3), 125–140 (2005)
6. R.R. Wright, M.R. Carstens, Linear momentum flux to overbank sections. *J. Hydraulics Div.* **96**(9), 1781–1793 (1970)
7. H.G. Lyall, Measurement of flow distribution and secondary flow in ducts composed of two square interconnected sub-channels, in *Symposium on Internal Flows*, Paper 33, pp. E16–E23 (1971)
8. P. Prinos, S. Tavoularis, R. Townsend, Flow measurements in compound ducts, in *Proceedings of the International Conference on Computational Methods and Experimental Measurements*, Porto Caras, USA, pp. 189–197 (1986)
9. C.J. Lai, D.W. Knight, Distributions of streamwise velocity and boundary shear stress in compound ducts, in *Proceedings of the 3rd International Symposium on Refined Flow Modelling and Turbulence Measurements*, eds. by Y. Iwasa, N. Tamimi, A. Wada (IAHR, Tokyo Japan, 1988)
10. D.G. Rhodus, D.W. Knight, Distribution of shear force on the boundary of a smooth rectangular duct. *J. Hydraul. Eng., ASCE* **120**(7), 787–807 (1994)
11. D.W. Knight, J.D. Demetriou, Flood plain and main channel flow interaction. *J. Hydraul. Eng., ASCE* **109**(8), 1073–1092 (1983)
12. M. Omran, Modelling stage-discharge curves, velocity and boundary shear stress distribution in natural and artificial channels using a depth-averaged approach. PhD thesis, The University of Birmingham, England, UK (2005)
13. B. Unal, M. Mamak, G. Seckin, M. Cobaner, Comparison of an ANN approach with 1-D and 2-D methods for estimating discharge capacity of straight compound channels. *Adv. Eng. Softw.* **41**, 120–129 (2010)
14. D.W. Knight, K. Shiono, Turbulence measurements in a shear layer region of a compound channel. *J. Hydraul. Res., IAHR* **28**(2), 175–196 (1990)
15. W.R.C. Myers, Velocity and discharge in compound channels. *J. Hydraul. Eng.* **113**(6), 753–766 (1987)

16. D.W. Knight, Flow mechanics and sediment transport in compound channels. *Int. J. Sedim. Res.* **14**(2), 217–236 (1999)
17. P. Rameshwaran, P.S. Naden, Three-dimensional numerical simulation of compound channel flows. *J. Hydraul. Eng.* **129**(8), 645–652 (2003)
18. L.S. Hin, N. Bessaih, L.P. Ling, A.A. Ghani, N.A. Zakaria, M.Y. Seng, Discharge estimation for equatorial natural rivers with overbank flow, *International. J. River Basin Manage.* **6**(1), 13–21 (2008)
19. K.C. Patra, S.K. Kar, Flow interaction on meandering river with flood plains. *J. Hydraul. Eng.* **126**(8), 593–604 (2000)
20. K. Shiono, J.S. Al-Romaih, D.W. Knight, Stage-discharge assessment in compound meandering channels. *J. Hydraul. Eng.* **125**(1), 66–77 (1999)
21. D. Stephenson, P. Kolovopoulos, Effects of momentum transfers in compound channels. *J. Hydraul. Eng.* **116**(12), 1512–1522 (1990)
22. G.A. Seckin, Comparison of one dimensional method for estimating discharge capacity of straight compound channels. *Can. J. Civ. Eng.* **31**, 619–631 (2004)
23. M.R. Abidin, Modeling of compound channel for optimum river storage capacity, in *1st International Conference on Managing Rivers in the 21st Century: Issues & Challenges*, Penang, Malaysia, 21–23 Sept 2004, pp. 1–18
24. Z. Yang, W. Gao, W. Huai, Estimation of discharge in compound channels based on energy concept. *J. Hydraul. Res.* **1**(50), 105–113 (2012)
25. P. Ackers, Stage-discharge functions for two-stage channels: the impact of new research. *J. Inst. Water Environ. Manage.* **7**(1), 52–61 (1993)
26. P.R. Wormleaton, D.J. Merrett, An improved method of calculation for steady uniform flow in prismatic main channel/floodplain sections. *J. Hydraul. Eng.* **28**(2), 157–173 (1990)
27. P. Conway, J.J. O'Sullivan, M.F. Lambert, Stage-discharge prediction in straight compound channels using 3D numerical models, in *Proceedings of the Institution of Civil Engineers, Water Management*, vol. 166, no. 1, pp. 3–15 (2012)

Potential of Estuary Transverse Flow Salinity Intrusion Due to Extreme Estuarine Flooding

Farhan Haron Nuryazmeen, Tahir Wardah and Irma Noorazurah Mohamad

Abstract During normal flow conditions, the phenomenon of estuary salinity intrusion influences the changes along the estuary. The changes can be seen on the water quality along the estuary and river downstream. However, during the extreme estuarine flooding, the water quality condition will decrease, due to the influences of the transverse flow salinity intrusion. At the same time, it will reduce the productions of aquatic life. Besides, a significant impact will affect public and the surrounding area due to the extreme estuarine flooding leads to the estuary transverse flow salinity intrusion. This paper presents the potential and on-going research of estuary transverse flow salinity intrusion due to extreme estuarine flooding.

Keywords Estuarine flooding · Transverse flow · Salinity intrusion · Estuary

1 Introduction

Estuaries are places where seawater (saltwater) is measurably diluted by inflow freshwater (river). Distribution of salinity in the estuary changes gradually depending on various factors such as space, time, movement of tides in the estuarine system, fresh water discharge from river, difference in fluid density, shape of estuary, wind effect, and Coriolis effects.

Estuaries, which are rich in nutrients, act as a habitat to some aquatic lives. Estuaries also have economic importance such as fishery, recreation. Furthermore, estuaries have been the main focus of human as a route of communication and trade, especially for people in rural areas far from the coast. Recently, human-

F. H. Nuryazmeen (✉) · T. Wardah · I. N. Mohamad
Faculty of Civil Engineering, Universiti Teknologi MARA, Shah Alam, Selangor, Malaysia
e-mail: neemzay@yahoo.com

induced activities such as dredging of shipping lanes along the bottom estuarine, the disposal of industrial wastes into the water system and shoreline development influence estuarine dynamics which include mixing process. These activities might contribute to salinity changes and further adversely affect the estuarine ecosystem. The presence of resisting structures in the estuary or along its banks might also affect the salinity patterns.

Other than that, the pollution in the estuary and the surrounding area will become more serious during flood. Flood events can be defined as the changes of wet and dry conditions. It is a common condition in estuaries, and rivers or flooding due to dam breaks and also prolonged rainfall [1]. For example, the phenomenon of extreme flood events in Malaysia, specifically in Johor in 2006 and 2007 as well as in Pahang in 2001 and 2007, would give adverse effects to humans when they use contaminated water such as food poisoning, hepatitis A, and blue baby syndrome. Besides, it gave significant impact to animals, and plants as well. In addition, the salinity level in the areas also had decreased dramatically. When such phenomenon occurs, aquatic life along the estuaries and river area will be affected due to the decline of water quality level.

This paper explains briefly the pilot study of the potential of estuary transverse flow salinity intrusion due to extreme estuarine flooding. The aim of this research is to identify the effect of extreme estuarine flooding leads to salinity intrusion flow in transverse direction. Hence, it will affect the populations and the environments along the affected area.

2 Estuary Transverse Flow Salinity Intrusion and Extreme Estuarine Flooding

2.1 Estuary Transverse Flow Salinity Intrusion

The extreme estuarine flood events do not only influence the changes along the estuary (longitudinal or x-direction), but it also affects the land due to the transverse flow (horizontal or y-direction) (Fig. 1). The extreme estuarine flooding leads to transverse flow salinity intrusion affect the water quality and the environment. For example, the productions of aquatic life will decrease gradually. Humans, animals, and mangrove areas will be affected as well.

2.2 Extreme Estuarine Flooding

The phenomenon of extreme flood events had occurred in Johor in 2006 and 2007, and also in Pahang in 2001 and 2007. The extreme flood events had impacted the estuaries like Pulai River estuary in Johor, where the estuary salinity reduced significantly. When the estuary salinity declined, the dissolved oxygen (DO) level

Fig. 1 An example of transverse flow (*y-direction*) in estuary due to extreme flood event

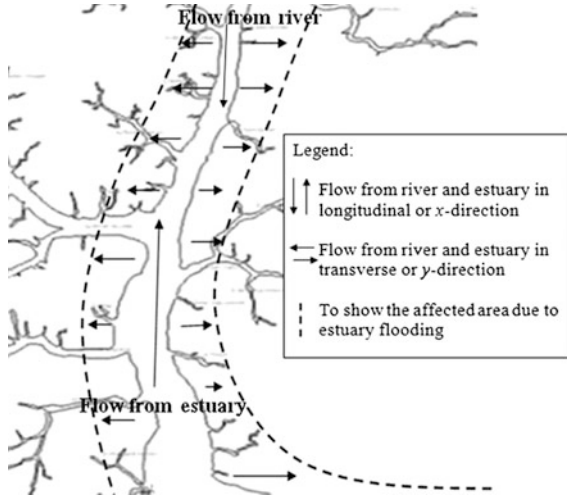


Fig. 2 The decline in mussels production on Johor Straits due to flood event (Source [3])



increased, and vice versa, as also reported in the study by Reynolds-Fleming and Luettich [2] at Neuse River estuary, North Carolina, USA. During the phenomenon, the economically important shellfish and aquaculture industry in Western Johor Strait suffered significantly from the storm-driven low salinity event [3]. In addition, the production of mussels in Johor Straits reduced due to high fresh water inflow (Fig. 2). The mussel production must meet a minimum quality requirement or standard in order to get a certificate for export purposes.

Fig. 3 Sungai Pahang along Pekan, Pahang was flooded in 2001 and 2007 during the northeast monsoon season



3 Potential Estuary Transverse Flow Salinity Intrusion due to Extreme Estuarine Flooding

In 2001 and 2007, during the northeast monsoon season, district of Pekan, Pahang was hit by severe flood waves. Houses near the estuary and coastal were destroyed by high tides and severe flooding due to prolonged rainfall (Fig. 3). However, the Sungai Pahang estuary along Pekan also flooded even though there was no rain because of siltations at the mouth of the river.

Other than that, salinity level in estuarine system also changes during flood. Salinity level declines dramatically during monsoon season, for examples, in 2001 and 2007. Figures 4 and 5 show the locations of water quality monitoring stations at Sungai Pahang estuary, and the graph of salinity level near Sungai Pahang estuary at eight river stations from 2001 until 2011 respectively. Figure 5 indicates salinity level changes dramatically in some monitoring stations and other stations changes gradually along the Sungai Pahang estuary between 2000 and 2011. Meanwhile, Fig. 6 shows hydrological stations in Pahang. The changes of salinity level along Sungai Pahang estuary specifically during extreme flood events in 2001 and 2007 due to prolonged rainfall in Pahang (Fig. 7). Other than that, fluctuation of water level (Fig. 8) and the high stream flow (Fig. 9) near Sungai Pahang basin lead to estuary transverse flow salinity intrusion from 2000 until 2012. Hence, it will impact to populations and the environment along the affected area due to water quality along the estuary and river deteriorate.

Fig. 6 Hydrological stations in Pahang (Source DID Malaysia)

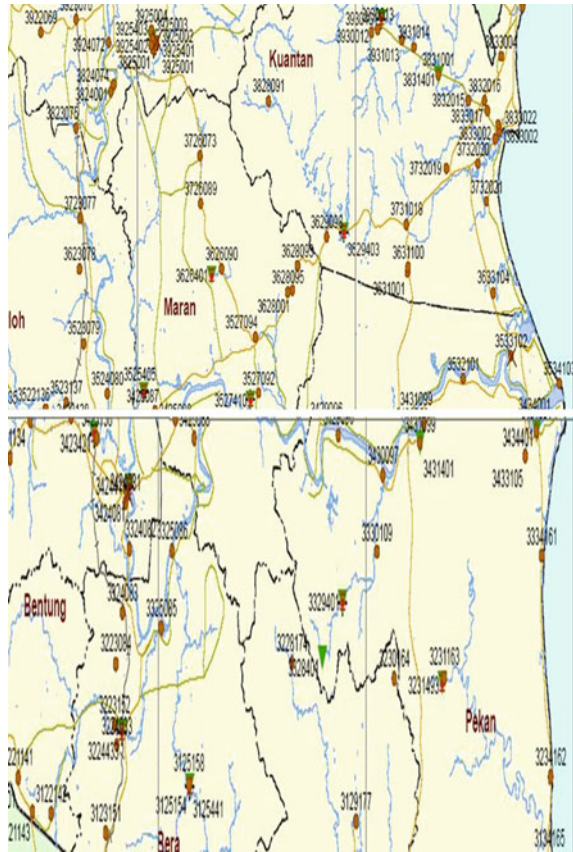


Fig. 7 Hydrograph near Sungai Pahang basin from 2000 until 2012 (Source DID Malaysia)

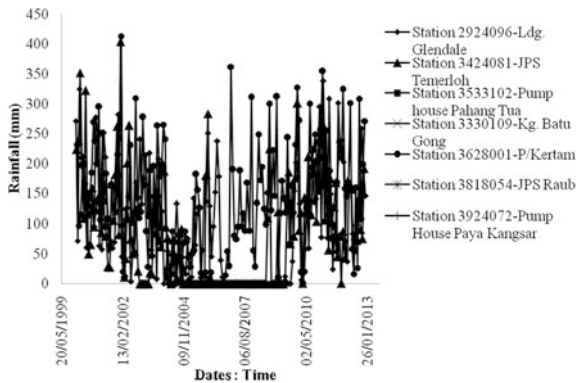


Fig. 8 Water level near Sungai Pahang basin from 2000 until 2012 (Source DID Malaysia)

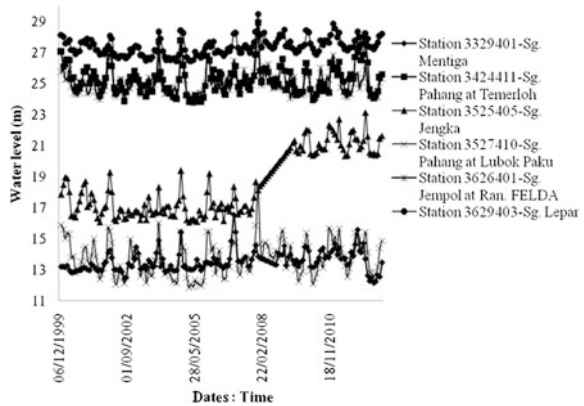
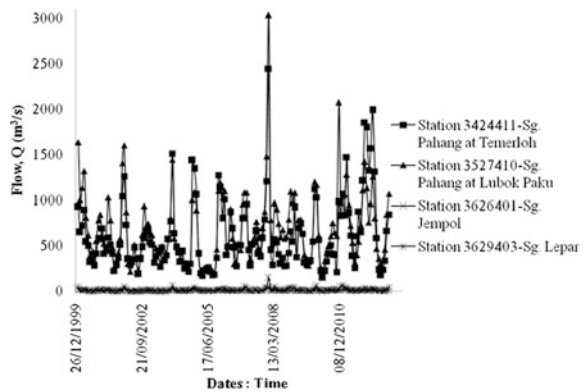


Fig. 9 Stream flow near Sungai Pahang basin from 2000 until 2012 (Source DID Malaysia)



4 On-Going Research

Many studies have been done to evaluate the estuarine characteristics such as changes in estuarine salinity [4–11], sediment from various aspects of the shear effect [12–19], influence of wind [20–24], tidal effects [25–29], and runoff effects [6, 7, 30], using numerical modelling. However, there is still lacking of numerical modelling and experimental studies to see the mixing process between saltwater and freshwater in estuary during normal flow and high flow in transverse flow.

Estuarine flooding and transverse flow salinity intrusion in estuarine system can be modelled using the Shallow Water Equations (SWEs). Most previous studies only develop 1-Dimensional (1D) [31, 32] or 2-Dimensional (2D) [18, 33–37] model using SWEs for several cases such as improving the grid-based, studying the general fluid density differences, and studying the sediment transport. Other than that, previous studies have built models using SWEs for solving problems such as wetting–drying fronts [34, 38, 39], dam breaks [39–41], one-layer flows [41, 42], two-layer flows [43, 44], and mud flow intrusions [42]. It is applied to the various conditions in many rivers, lakes, and the sea. However, these previous

studies do not investigate the problem of salinity intrusion in the estuary during flood. Therefore, the use of SWEs to develop shallow water modelling (SWM) is expected to reveal the flood hydrodynamics and salinity intrusion in the estuary and their impact on the water quality and the environment.

The SWEs are one of hyperbolic partial differential equations (PDEs) governing fluid flow in coastal regions, estuaries, rivers, and channels. The principles of conservation of mass and conservation of momentum have been used in deriving the Navier–Stokes equations. Vertical integration allows the vertical velocity to be removed from the SWEs because the value of the parameter in z-direction is much smaller than the value of the parameter in y-direction.

The SWEs consist of three independent variables, which are time, t , and two spatial coordinates, x and y (1, 2 and 3). The dependent variables are the fluid depth, h , and the fluid velocity, u and v . From the equations below (2, 3), g represents for acceleration of gravity. With the selection of the correct unit, mass conserved quantity, which is proportional to h , and momentum, which is proportional to uh and vh , the PDEs in case of no Coriolis, friction or viscous forces are:

$$\frac{\partial h}{\partial t} + \frac{\partial(uh)}{\partial x} + \frac{\partial(vh)}{\partial y} = 0. \quad (1)$$

$$\frac{\partial(uh)}{\partial t} + \frac{\partial(u^2h + \frac{1}{2}gh^2)}{\partial x} + \frac{\partial(uvh)}{\partial y} = 0. \quad (2)$$

$$\frac{\partial(vh)}{\partial t} + \frac{\partial(uvh)}{\partial x} + \frac{\partial(v^2h + \frac{1}{2}gh^2)}{\partial y} = 0. \quad (3)$$

5 Conclusion

In order to overcome the various problems caused by flood, flood management is one of the important tasks for the Government and other authorities. Other than that, to assess flood hazard, safety measure, and eradication, various accurate and efficient flood modelling tools are required. To identify the impact of transverse salinity intrusion due to extreme estuarine flooding on the water quality and the environment of the affected region, a shallow water modelling (SWM) for salinity intrusion in estuarine system will be developed. SWEs will be used in order to develop the flood and salinity intrusion model accurately and efficiently for the Government and private use in the future.

This research is part of the water quality aspects and flood risk management that needs to be done in order to maintain the water in good quality specifically in estuarine systems.

Acknowledgments This work was supported in part by the Ministry of Higher Education (MOHE) and Universiti Teknologi MARA (UiTM), Malaysia under Grant Research

Acculturation Grant Scheme (RAGS). The first author is a PhD candidate of Faculty of Civil Engineering, Universiti Teknologi MARA, Malaysia and this paper is part of her research.

References

1. J.M. Zokagoa, A. Soulaïmani, Modeling of wetting–drying transitions in free surface flows over complex topographies. *Comput. Methods Appl. Mech. Eng.* **199**, 2281–2304 (2010)
2. J.V. Reynolds-Fleming, R.A. Luettich Jr, Wind-driven lateral variability in a partially mixed estuary. *Estuar. Coast. Shelf Sci.* **60**(3), 395–407 (2004)
3. Berita Harian, Newspaper of Malaysia, 2007
4. W.C. Liu, M.H. Hsu, A.Y. Kuo, J.T. Kuo, The influence of river discharge on salinity intrusion in the Tanshui Estuary, Taiwan. *J. Coastal Res.* **17**(3), 544–552 (2001)
5. R.A. Locarnini, L.P. Atkinson, A. Valle-Levinson, Estimating the mean temperature and salinity of the Chesapeake Bay mouth. *Estuaries* **25**(1), 1–5 (2002)
6. M. Larson, R. Bellanca, L. Jönsson, C. Chen, P. Shi, A model of the 3D circulation, salinity distribution, and transport pattern in the Pearl River Estuary, China. *J. Coastal Res.* **21**(5), 896–908 (2005)
7. J. Cao, R. Li, and Y. Zhu, Study on Saltwater Intrusion in the Yangtze River Estuary by 3D Numerical Model, in *Education Technology and Training, 2008. and 2008 International Workshop on Geoscience and Remote Sensing. ETT and GRS 2008. International Workshop on*, vol. 2 (IEEE, New York, 2008), pp. 81–84
8. L.G. Fang, S.S. Chen, H.L. Li, and C.D. Gu, Monitoring water constituents and salinity variations of saltwater using EO-1 Hyperion satellite imagery in the Pearl River Estuary, China, in *IGARSS*, vol. 1 (IEEE, New York, 2008), pp. 438–441
9. M.L. Becker, R.A. Luettich Jr, M.A. Mallin, Hydrodynamic behavior of the Cape Fear River and estuarine system: a synthesis and observational investigation of discharge–salinity intrusion relationships. *Estuar. Coast. Shelf Sci.* **88**(3), 407–418 (2010)
10. J. Parsa, A. Etemad-Shahidi, An empirical model for salinity intrusion in alluvial estuaries. *Ocean Dyn.* **61**(10), 1619–1628 (2011)
11. J. Lee, A. Valle-Levinson, Influence of bathymetry on hydrography and circulation in the region between an estuary mouth and the adjacent continental shelf. *Cont. Shelf Res.* **41**, 77–91 (2012)
12. K.M.H. Huijts, H.M. Schuttelaars, H.E.D. Swart, and A. Valle-Levinson, Lateral entrainment of sediment in tidal estuaries: an idealized model study. *J. Geophys. Res.* **111**(C12), 1–14 (2006)
13. K.E.K. Abderrezzak, A. Paquier, E. Mignot, Modelling flash flood propagation in urban areas using a two-dimensional numerical model. *Nat. Hazards* **50**, 433–460 (2009)
14. S.N. Chen, L.P. Sanford, Lateral circulation driven by boundary mixing and the associated transport of sediments in idealized partially mixed estuaries. *Cont. Shelf Res.* **29**(1), 101–118 (2009)
15. S.N. Chen, L.P. Sanford, D.K. Ralston, Lateral circulation and sediment transport driven by axial winds in an idealized, partially mixed estuary. *J. Geophys. Res.* **114**, 1–18 (2009)
16. A.G.L. Borthwick, S.C. Leon, J. Jozsa, Adaptive quadtree model of shallow-flow hydrodynamics. *J. Hydraul. Res.* **39**(4), 413–424 (2010)
17. W. Wu, A. Sanchez, M. Zhang, An implicit 2-D depth averaged finite-volume model of flow and sediment transport in coastal waters, in *Coastal Engineering*, (2010), pp. 1–13
18. L.C. Rijn, Analytical and numerical analysis of tides and salinities in estuaries; part I: tidal wave propagation in convergent estuaries. *Ocean Dyn.* **61**(11), 1719–1741 (2011)
19. J. Murillo, B. Latorre, P. García-Navarro, A Riemann solver for unsteady computation of 2D shallow flows with variable density. *J. Comput. Phys.* **231**, 4775–4807 (2012)
20. C.D. Winant, Three-dimensional wind-driven flow in an elongated, rotating basin. *J. Phys. Oceanogr.* **34**, 462–476 (2004)

21. Q. Liang, A.G.L. Borthwick, P.H. Taylor, Chaotic mixing in a basin due to a sinusoidal wind field. *Int. J. Numer. Meth. Fluids* **47**, 871–877 (2005)
22. X. Guo, A. Valle-Levinson, Wind effects on the lateral structure of density-driven circulation in Chesapeake Bay. *Cont. Shelf Res.* **28**(17), 2450–2471 (2008)
23. D.A. Narváez, A. Valle-Levinson, Transverse structure of wind-driven flow at the entrance to an estuary: Nansemond River. *J. Geophys. Res.* **113**, 1–9 (2008)
24. S. Popinet, R.M. Gorman, G.J. Rickard, H.L. Tolman, A quadtree-adaptive spectral wave model. *Ocean Model.* **34**, 36–49 (2010)
25. R.J. Chant, Secondary circulation in a region of flow curvature: relationship with tidal forcing and river discharge. *J. Geophys. Res.* **107**, 1–11 (2002)
26. X. Guo, A. Valle-Levinson, Tidal effects on estuarine circulation and outflow plume in the Chesapeake Bay. *Cont. Shelf Res.* **27**(1), 20–42 (2007)
27. P. Cheng, A. Valle-Levinson, Influence of lateral advection on residual currents in microtidal estuaries. *J. Phys. Oceanogr.* **39**, 3177–3190 (2009)
28. J. Parsa, A.E. Shahidi, Prediction of tidal excursion length in estuaries due to the environmental changes. *Int. J. Environ. Sci. Technol.* **7**(4), 675–686 (2010)
29. I. Safak, A. Sheremet, A. Valle-Levinson, A.F. Waterhouse, Variation of overtides by wave enhanced bottom drag in a North Florida tidal inlet. *Cont. Shelf Res.* **30**(18), 1963–1970 (2010)
30. J.C. Warner, W.R. Geyer, J.A. Lerczak, Numerical modeling of an estuary: A comprehensive skill assessment. *J. Geophys. Res.* **110**, 1–13 (2005)
31. M. Castro, J. Macias, and C. Pares, A Q-scheme for a class of systems of coupled conservation laws with source term. Application to a two-layer 1-D shallow water system. *ESAIM: M2AN*, **35**(1), 107–127 (2001)
32. M.J. Castro, J.A. García-Rodríguez, J.M. González-Vida, J. Macias, C. Pares, M.E. Cázquez-Cendon, Numerical simulation of two-layer shallow water flows through channels with irregular geometry. *J. Comput. Phys.* **195**, 1–31 (2004)
33. K. Anastasiou, C.T. Chan, Solution of the 2D shallow water equations using the finite volume method on unstructured triangular meshes. *Int. J. Numer. Meth. Fluids* **24**(11), 1225–1245 (1997)
34. Q. Liang, A.G.L. Borthwick, Simple treatment of non-aligned boundaries in a Cartesian grid shallow flow model. *Int. J. Numer. Meth. Fluids* **56**, 2091–2110 (2008)
35. Q. Liang, G. Du, J.W. Hall, A.G.L. Borthwick, Flood inundation modeling with an adaptive quadtree grid shallow water equation solver. *J. Hydrol. Eng.* **134**(11), 1603–1610 (2008)
36. A. Kurganov, G. Petrova, Central-upwind schemes for two-layer shallow water equations. *SIAM J. Sci. Comput.* **31**(3), 1742–1773 (2009)
37. G. Kesserwani, Q. Liang, Dynamically adaptive grid based discontinuous Galerkin shallow water model. *Adv. Water Resour.* **37**, 23–39 (2012)
38. Q. Liang, A.G.L. Borthwick, Adaptive quadtree simulation of shallow flows with wet–dry fronts over complex topography. *Comput. Fluids* **38**(2), 221–234 (2009)
39. Q. Liang, Flood simulation using a well-balanced shallow flow model. *J. Hydrol. Eng.* **136**, 669–675 (2010)
40. Q. Liang, A.G.L. Borthwick, G. Stelling, Simulation of dam- and dyke-break hydrodynamics on dynamically adaptive quadtree grids. *Int. J. Numer. Meth. Fluids* **46**, 127–162 (2004)
41. M.J. Castro, A.M. Ferreira, J.A. García-Rodríguez, J.M. González-Vida, J. Macías, C. Parés, and M. Elena Vázquez-Cendón, The numerical treatment of wet/dry fronts in shallow flows: application to one-layer and two-layer systems. *Mathematical and Computer Modelling*, **42**(3–4), 419–439 (2005)
42. S.C. Chen, S.H. Peng, H. Capart, Two-layer shallow water computation of mud flow intrusions into quiescent water. *J. Hydraul. Res.* **45**, 13–25 (2007)
43. R. Abgrall, S. Karni, Two-layer shallow water system: A relaxation approach. *SIAM J. Sci. Comput.* **31**(3), 1603–1627 (2009)
44. B. Spinewine, V. Guinot, S. Soares-Frazão, Y. Zech, Solution properties and approximate Riemann solvers for two-layer shallow flow models. *Comput. Fluids* **44**(1), 202–220 (2011)

Part V
Transportation Systems, Infrastructure
and Intelligent Transport

Assessing Pedestrians' Perspective on the Walkability of Pedestrian Environment Under Mixed-Use Development

Noor Iza Bahari, Ahmad Kamil Arshad and Zahrullaili Yahya

Abstract Walkability is define as to which extent does the built environment support and encourage walking. Many challenges faced by local authorities in providing a highly walkable built environment to the pedestrian causing the facilities being abandoned by the users. In order to encourage walkability, the qualities of built environment must meet the pedestrians' expectation. On-street questionnaire survey was conducted on two different sidewalk segments within mixed-use development in Kuala Lumpur City Centre in order to assess the pedestrians' perception and expectation on sidewalk facilities. The respondents were asked to give rating on different sidewalk attributes and the results were analyzed using simplified weighted factor analysis. It was found that only the sidewalk width was given positive result for both sidewalks whereas different results were given for other sidewalk attributes. Besides that, even though safety while using the sidewalk was the most important factor that influence walking decision, the pedestrian felt that improvement should be made in term of sidewalk facilities rather than safety for both sidewalk. In conclusion, the pedestrians do not satisfied with almost all of the existing sidewalk attributes. Improvement should be made in term of sidewalk facilities in order to increased walkability in Malaysian city.

Keywords Pedestrian environment · Walkability · Pedestrian perception · Sidewalk facilities · Pedestrian travel behaviour

N. I. Bahari (✉) · A. K. Arshad · Z. Yahya
Department of Highway and Transportation Faculty of Civil Engineering, UiTM,
Shah Alam, Selangor, Malaysia
e-mail: izabahari@gmail.com

1 Introduction

Over the past decade, the world is shifting from auto-centric development towards providing a more walkable city due to the undeniable benefits of walking to human health, economic development, energy conservation to environmental friendly. Walkability linked to the quality of built environment and usually was define differently depending on what areas it covers and how it is being interpreted. Reference [1] define walkability as to what extend does the built environment support and encourages walking. He also added that a richly connected path network that provides access to various places, safe and comfortable street which can be used for varied age and degree of mobility will produce a highly walkable city that invites walking [1].

However, current Malaysian City is not a pedestrian-friendly city due to existence of major deficiencies in the pedestrian facilities. Only minimum facilities were provided for the pedestrian caused physical challenge to the elderly and person with disabilities. Inadequate pedestrian facilities will cause constant conflict to occur between pedestrians, traffic and roadside development [2]. This scenario were worsens when the sidewalk was used by unlicensed vendor or hawker for their business purposes [3].

The quality of walk path is an adequate predictor of walkability and the key to increased walkability which contribute towards pedestrianisation [3, 4]. Urban environment plays an important role towards pedestrian preference and decision to walk because pedestrian sees, hear, smell and felt the surrounding environment [5, 6]. The likelihood of walking are also affected by the quality of walk path and path context [1, 7]. In order to create a positive walking experience to the pedestrian, the walk path network must engage with their interest [8]. This means that aesthetic and amenities elements should be incorporated in the design because it is one of the aspects that can influence walking experience positively [1]. People tend to walk more frequently and further in high sidewalk qualities environment [3, 9–11].

The Malaysian Government is aware of the benefits contributed from areas with high pedestrian activity towards increasing the economic growth in Malaysia. Currently, a program to construct and upgrade the existing pedestrian network has been initiated between Dewan Bandaraya Kuala Lumpur, DBKL and private sector. This development consists of a total length of 4.5 km of covered and elevated pedestrian linkage in the city center to be completed by the year 2012 for short term plan and full pedestrian network across KL city with total of 45 km for long term plan and is expected to be completed by the year 2014 [12, 13].

Reference [14] state that planning and engineering question should be answered in proving facilities for the pedestrian. However, providing adequate pedestrian facilities are harder than expected especially in urban mixed-use development. This is because the pedestrians are not engineer and sometimes they do not understand the function of each sidewalk facilities from engineering perspective. Usually pedestrian perception was not incorporated in urban design world-wide [15]. Since the pedestrian facilities are designed for pedestrians, their perception should be

considered in order to ensure convenient pedestrian mobility [16]. Reference [17] emphasize that the concept of sensibility ergonomics which is define as the application of human sensitivity into engineering approach to a product should be apply in designing the sidewalk facilities so that pleasant and comfortable walking environment can be developed.

Reference [18] found that satisfaction of pedestrian is strongly associated with emotional perception rather than physical components. Reference [5] added that the pedestrian faces variety of sensation which will cause them to make a series of decision and judgments for navigating the environment once they are exposed to the public environment.

Different pedestrian perception may be experienced according to the same general design criteria with specific sidewalk design element and components under the various environments [3]. Therefore, the objective of this paper is to assess the walkability of the pedestrian environment under mixed-used development in Kuala Lumpur city from pedestrians' perspective. The objective is accomplished through pedestrian on-street questionnaire survey to assess on the pedestrian perception on the existing facilities and what expected improvement that they want to see towards the existing facilities. The results were analyzed using simplified weighted factor analysis.

2 Methodology

Pedestrians' perception and expectation towards the existing sidewalk facilities in the mixed land use area within Kuala Lumpur City Center was assessed through on-street questionnaire survey. A total of 60 respondents were chosen and divided equally into two in which 30 respondents were in being interview at Jalan Tuanku Abdul Rahman and another 30 respondents were in Central Market (Lebuh Ampang) area. Therefore, travel purpose of the pedestrian may be closely related shopping, leisure, work, school, access to public transportation and also heritage. The survey parameters considered in this study are sidewalk condition, personal safety, crossing, street furniture, adjacent traffic, aesthetic and amenities, overall travel experience, factors that influence walking decision and improvement needed. Commercial areas that have the same characteristics were selected in this study.

2.1 Study Area

Kuala Lumpur has the fastest population and economic growth among other metropolitan region within the country. The draft KL City Plan 2020 has identified commercial areas that are in line with the distribution of urban center the Kuala Lumpur Structure Plan 2020 known as City Center Commercial (CCC) which have the potential to support Kuala Lumpur's economic growth. These CCC are

Fig. 1 Study location 1 in Jalan Tuanku Abdul Rahman, Kuala Lumpur [14]



commercial zones that allow broad range of commercial activities to be conducted towards pioneering highest order of commercial activities [13].

Two study areas were selected within the CCC in Kuala Lumpur as shown in Figs. 1 and 2. These areas have the same mixed-use development characteristics with the same numbers of building of interest (13) as stated by KL Heritage center [14]. Both of these areas consist of business center, shopping complex, heritage interest area, public transport station and education center within walking distance. This area offers similar range of pedestrian activities from shopping, leisure, transit commute, and school. Therefore, the pedestrian perception while using the sidewalk facilities can be assessed.

2.2 On-Street Questionnaire Survey

Paper-based on-street questionnaire method was used in order to assess the pedestrian perception and expectation while using the sidewalk at the studied location during the working weekdays' peak hour. In this method, the interviewer waits at the end of the sidewalk and aim at the selected pedestrian that was walking from the beginning towards the end of the sidewalk. When the pedestrian reached the end, the pedestrian was invited and asked to participate in the questionnaire survey. If they agreed, they were interviewed. The Survey question comprises four sections in which Sect. 1 focused on the pedestrian personal information and their familiarity of the sidewalk. Section 2 assess on the pedestrian perception on the existing sidewalk

Fig. 2 Study location 2 in Market Square, Lebu Ampang area, Kuala Lumpur [14]



condition through the parameters as states earlier. In Sect. 3, the pedestrian were required to give their rating on their overall impression of travel experience. Lastly, the pedestrians were required to give their suggestion on how to improve the existing sidewalk facilities subjectively in Sect. 4. The key factors for improving pedestrian facilities were also identified through the results that are collected.

2.3 Data Analysis

The questionnaires survey was analyzed by combining factor analysis as in [16, 18] and conversion of semantic scale to numeric scale as in [9] to produced simplified weighted factor analysis. Weighted factor analysis is carried out by converting the data that were collected to weighted score. The weighted score were calculated through multiplying the numbers of respondent involved to the weighing factor. Table 1 shows the weighing factors and examples of “weighing scoring” for the data obtained. The average weighing score is calculated by dividing the total weighted score with the number of respondent involved in the survey. The positive (+ve) value indicates that the respondent is satisfied with the existing sidewalk while negative (–ve) value indicates that the respondent is not satisfied with the existing sidewalk. Whereas, values that are approaching zero (0) indicate that the sidewalk condition is acceptable.

Table 1 Weighted factor and calculation example for sidewalk condition and overall travel experience

Scale of agreement	Weighing factors	No. of respondents	Weighted score
Very satisfy	2	3	6
Satisfy	1	9	9
Acceptable	0	6	0
Unsatisfy	-1	4	-4
Very unsatisfy	-2	4	-8
Total			3

3 Result and Discussions

The location of the study areas are mixed-use development in Kuala Lumpur city. The study population consists of people who travelled for the purposed of shopping, leisure, work, school, access to public transportation and also heritage. The respondents' age groups were from 18 to above 50 years old. The age variation may be closely related to income, occupation, sex and other socioeconomic characteristics.

3.1 Pedestrian Perception on the Existing Sidewalk Facilities

Different results were seen for both sidewalks when the pedestrian perception was assessed for different sidewalk attributes as shown in Table 2. Jalan Tuanku Abdul Rahman received five out of fifteen positive responds with the highest value of 0.41667 were obtained for sidewalk width and location of the sidewalk and the sidewalk attributes of curvilinear were rated as acceptable (0.00000) by the pedestrians. Whereas Lebu Ampang only received positive value for the sidewalk width (0.09091) and acceptable value of 0 were obtained for the levelness of the sidewalk.

Overall, most of the pedestrian were not satisfied with the existing sidewalk attributes' condition. This is proven by the negative (-ve) values obtained for almost all of the sidewalk attributes with different highest negative value for both roads. The pedestrians group from Jalan Tuanku Abdul Rahman gives highest negative value (0.83333) for protection against weather.

On the other hand, pedestrian at Lebu Ampang were not satisfy the most in personal safety against adjacent traffic and facilities for the elderly and person with disabilities which received highest negative value of (0.81818). The same attributes which is facilities for elderly and person with disabilities also obtained second highest (-0.75000) at Jalan Tuanku Abdul Rahman. This proof that other groups of pedestrian are aware of the importance to provide facilities to this and

Table 2 Score result for pedes pedestrian perception on the sidewalk condition according sidewalk

No. Attribute	Jalan Tuanku Abdul Rahman		Lebuah Ampang		Average score	
	Total weighted score	Average weighted score	Total weighted score	Average weighted score	Total weighted score	Average weighted score
1 Presence of Sidewalk	4	0.33333	-5	-0.45455	-0.5	-0.06061
2 Location of sidewalks	5	0.41667	-6	-0.54545	-0.5	-0.06439
3 Continuity of sidewalks	2	0.16667	-6	-0.54545	-2.0	-0.18939
4 Sidewalk width	5	0.41667	1	0.09091	3.0	0.25379
5 Levelness and condition of sidewalk	-2	-0.16667	0	0.00000	-1.0	-0.08333
6 Obstructions	-2	-0.16667	-5	-0.45455	-3.5	-0.31061
7 Curvilinear curbs or curb cuts	0	0.00000	-5	-0.45455	-2.5	-0.22727
8 Condition of the walking surface	-3	-0.25000	-5	-0.45455	-4.0	-0.35227
9 Cleanliness of the sidewalk	-3	-0.25000	-8	-0.72727	-5.5	-0.48864
10 Protection from weather	-10	-0.83333	-5	-0.45455	-7.5	-0.64394
11 Facilities for person with disabilities/elderly	-9	-0.75000	-9	-0.81818	-9.0	-0.78409
12 Separation from traffic	-3	-0.25000	-5	-0.45455	-4.0	-0.35227
13 Personal safety while using the sidewalk	-1	-0.08333	-6	-0.54545	-3.5	-0.31439
14 Personal safety against the adjacent traffic/parked vehicle	-4	-0.33333	-9	-0.81818	-6.5	-0.57576
15 Maintenance of the sidewalk	-2	-0.16667	-3	-0.27273	-2.5	-0.21970
Total Average Score						-4.41288



Fig. 3 Pedestrian's view of the sidewalk facilities in Jalan Tuanku Abdul Rahman (Image from field survey by author)

Fig. 4 Pedestrian's view of the sidewalk facilities in Lebu Ampang (Image from field survey by author) [19]



lack in provision of the facilities will cause safety problem to this group of pedestrian. The condition of the sidewalk in Jalan Tuanku Abdul Rahman and Lebu Ampang are shown in Figs. 3 and 4 respectively.

3.2 Pedestrian Perception on the Overall Travel Experienced

Six parameters namely pathway or sidewalk, crossing, street furniture, personal safety, adjacent traffic, aesthetic and amenities were assessed in term of the pedestrian perception on the overall travel experienced.

The results obtained were shown in Table 3. Different pedestrian perceptions were received for both sidewalks again. Pedestrian in Jalan Tuanku Abdul Rahman give equally positive respond (0.16667) for most of the sidewalk attribute except for crossing and adjacent traffic that obtained negative value of -0.33333 and -0.25000 respectively.

On the other hand, pedestrians in Lebu Ampang rated as unsatisfied for their overall travel experience. The pedestrian give negative comment for all six of the sidewalk parameters. They also agreed that the street furniture (-0.81818) and also aesthetic and amenities attributes (-0.72727) were not provided or very minimum provision and the location is not appropriate causing obstruction to them as shown in Fig. 4.

3.3 Pedestrian Expectations

In order to assess on the pedestrian expectations, the pedestrians were asked on the key factor that influences their travel decision as presented in Fig. 5. Next, they were questioned on area of the improvement needed to improve the sidewalk facilities in order to encourage more people to walk as presented in Fig. 6. Figure 5 shows that all the respondents agreed that safety is the most important factor influencing pedestrian walking decision compared to other factors. As for other factors, the pedestrian gave different level of factor affecting walking decision according to their needs and purposes of using the sidewalk facilities for both sidewalks.

Surprising result was shown in Fig. 6 on the improvement needed for both Jalan Tuanku Abdul Rahman and Lebu Ampang. The pedestrians felt that even though safety were the highest factor that influence walking decision for both sidewalk areas, more improvement were needed in term of sidewalk facilities compare to safety for both sidewalks. This is because to them, safety depends on the pedestrian ability, awareness and limitation while using the sidewalk. The pedestrian felt that they are the one who is responsible for safety purpose and only minimum provision is needed for safety purpose such as street lamps at night, separation between traffic and sidewalk, law and enforcement for driver that parked their vehicle non-parking area within the sidewalk and motorcyclists that parked or ride their motorcycle on the pedestrian sidewalk.

However, the respondent from Lebu Ampang expected that improvement for safety purposes should be done which is shown in Fig. 6 where safety have the second highest value for area should be improved. In contrast, safety was the least area of improvement needed for respondent from Jalan Tuanku Abdul Rahman.

Table 3 Score result for pedestrian perception on the overall travel experienced according to sidewalk

No.	Attribute	Jalan Tuanku Abdul Rahman		Lebuh Ampang		Average score	
		Total weighted score	Average weighted score	Total weighted score	Average weighted score	Total weighted score	Average weighted score
1	Overall travel experience	2	0.16667	-3	-0.27273	-0.5	-0.05303
2	Pathway/sidewalk	2	0.16667	-3	-0.27273	-0.5	-0.05303
3	Crossing	-4	-0.33333	-6	-0.54545	-5	-0.43939
4	Street furniture	2	0.16667	-9	-0.81818	-3.5	-0.32576
5	Personal safety	0	0.00000	-6	-0.54545	-3	-0.27273
6	Adjacent traffic	-3	-0.25000	-7	-0.63636	-5	-0.44318
7	Aesthetics and amenities	1	0.08333	-8	-0.72727	-3.5	-0.32197
Total average score							-1.90909

Fig. 5 Factor that influence walking decision

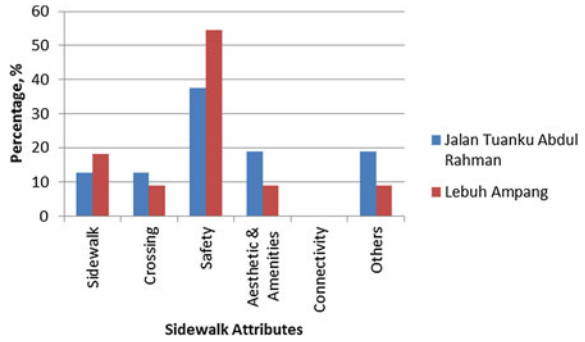
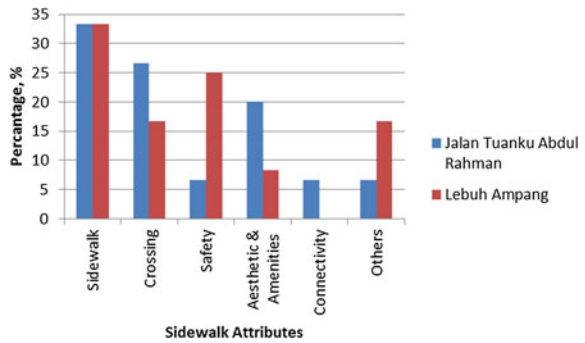


Fig. 6 Areas of improvement needed



Respondent from Jalan Tuanku Abdul Rahman expected to see more improvement in term of crossing and aesthetic and amenities to be done after sidewalk. Whereas both of the attributes as said above were the least areas of improvement needed for respondent in Lebu Ampang. Pedestrians in Lebu Ampang would like to see improvement in term of public transportation station for other areas.

4 Conclusion

The objective this paper is to assess the walkability of the pedestrian environment under mixed-used development in Kuala Lumpur city from pedestrians' perspective. The objective is fulfilled through assessing the pedestrian perception, preference and expectation towards various existing sidewalk facilities in Kuala Lumpur city by means of questionnaires survey. From the result, it was found that pedestrians who travelled at Jalan Tuanku Abdul Rahman were satisfied with their overall travel experience compared to pedestrian who used the facilities at Lebu Ampang. This is proven through the positive responses received on the current sidewalk facilities condition from them on the existing sidewalk facilities when they were asked to rate and give their opinion.

In contrast, the respondents from Lebu Ampang were not satisfied with their overall travel experienced which could be seen by the negative values given for most of the parameters that were assessed. Respondents from both sidewalk areas agreed that there were no or minimum provision on facilities for elderly and person with disabilities even though they are the groups of pedestrian that depends the most to the sidewalk facilities provided for their mobility.

In conclusion, most of the pedestrians were not satisfied with the existing sidewalk facilities provided to them. They suggest that improvements should be made especially in terms of sidewalk pedestrian crossing and sidewalk safety in order to increase the walkability in Kuala Lumpur city. Findings from this research are expected to help the transport planners and traffic engineers to understand the current walkability condition in Kuala Lumpur city from pedestrian perception and expectation towards existing sidewalk facilities.

Acknowledgments The author would like to express gratitude to all volunteers in completing the survey and express their comments in this research study. Last but not least, valuable comments from supervisor and referees for are very much appreciated. This research is supported by Ministry of Science, Technology and Innovation (MOSTI) under eScienceFund with reference number 100-RMI/SF 16/6/2 (29/2012) and Research Management Institute, Universiti Teknologi MARA.

References

1. M. Southworth, Designing the walkable city. *J. Urban Plan. Dev.* **131**(4), 246–257 (2005)
2. K.K. Laxman, R. Rastogi, S. Chandra, pedestrian flow characteristics in mixed traffic conditions. *J. Urban Plan. Dev.* **136**(1), 23–33 (2010)
3. K.R. Rahaman, J.M. Lourenco, J.M. Viegas, Perceptions of pedestrians and shopkeepers in european medium-sized cities: study of guimaraes. Portugal *J. Urban Plan. Dev.* **138**(1), 26–34 (2012)
4. F. Jaskiewicz, *Pedestrian level of service based on trip quality, transportation research circular E-C019* (TRB National Research Council, Washington, 2000)
5. J. Zacharias, Pedestrian behavior and perception in urban walking environment. *J. Plan. Lit.* **16**, 3–18 (2001)
6. S.L. Handy, Urban form and pedestrian choices. *Trans. Res. Rec.* **1552**, 135–144 (1996)
7. S. Lotfi, J. Koohsari, Neighborhood walkability in a city within a developing country. *J. Urban Plan. Dev.* **137**(4), 402–408 (2011)
8. M.Z. Shah, *Rating pedestrian facilities with P-index and the application of google map (F. o. B. Environment, Trans.)* (Universiti Teknologi Malaysia, Malaysia, 2010)
9. C.E. Kelly, M.R. Tight, F.C. Hodgson, M.W. Page, A comparison of three methods for assessing the walkability of the pedestrian environment. *J. Transp. Geogr.* **19**(6), 1500–1508 (2011)
10. K. Gardner, J. Tim, B. Keith, P. Tim, Developing a pedestrian strategy for London, *Transport policy and its implementation*, 1996
11. V.P. Sisiopiku, D. Akin, Pedestrian behaviors at and perceptions towards various pedestrian facilities: an examination based on observation and survey data. *Transp. Res. Part F: Traffic Psychol. Behav.* **6**(4), 249–274 (2003)
12. Kementerian Wilayah Persekutuan dan Kesejahteraan Bandar, (2011) KWPKB: greater Kuala Lumpur/Klang Valley. <http://app.kwpkb.gov.my/greaterklkv/entrypoint-project-pedestrian/>. Accessed 12 July 2012

13. Dewan Bandaraya Kuala Lumpur (2004) DBKL: Kuala Lumpur Structure Plan 2020. http://www.dbkl.gov.my/pskl2020/english/urban_design_and_landscape/index.htm. Accessed 11 July 2012
14. www.badanwarisan.org.my. Accessed 26 2013
15. M.S. Islam, K.R. Rahaman, S.J. Ahmed, Demands of participants or supply of opportunities: measuring accessibility of activity places based on time geographic approach. *J. Urban Plan. Dev.* **134**(4), 159–165 (2008)
16. N. Hidayat, K. Choocharukul, K. Kishi, Understanding pedestrian perceptions on sidewalk performance: a comparative study between Bangkok and Jakarta. *TRB Annual Meeting Report* 2011
17. B.J. Lee, T.Y. Jang, W. Wang, M. Namgung, Design criteria for an urban sidewalk landscape considering emotional perception. *J. Urban Plan. Dev.* **135**(4), 133–140 (2009)
18. W. Wang, P. Li, W. Wang, M. Namgung, Exploring determinants of Pedestrians' satisfaction with sidewalk environments: a case study in Korea. *J. Urban Plan. Dev.* **138**(2), 166–172 (2011)
19. N.I. Bahari, A.K. Arshad, and Z. Yahya, Assessing the pedestrians' perception of the sidewalk facilities based on pedestrian travel purpose, in *IEEE 9th International Colloquium on Signal Processing and its Applications (CSPA)* (2013), pp. 27–32

An Analysis of User Satisfaction on Public Transport Terminal Based on Users Survey

Nornikmah Mohammad Noor, Ahmad Kamil Arshad, Ismacahyadi Bagus Mohd Jais and Masria Mustafa

Abstract The main objective of this research is to do an analysis of the user satisfaction on the service provided by a public transport terminal by distributing the questionnaire. The survey had been carried out to the users of two public transport terminals which are Terminal One Seremban and Klang Sentral. These terminals had been recently upgraded with a variety of facilities but there were still complaints from the users about their deficiencies. The methods used were face to face interview and questionnaires distribution to the users of the terminals. The data obtained was analyzed by weighted parameter method to determine the satisfaction level. From this study, it had been determined that the most user consideration was safety and security and Cleanliness and comfort of the terminals as their top priority, followed amenities, information and lastly access and connection.

Keywords User satisfaction · Public transport terminals services · User survey

1 Introduction

User satisfaction is the main concern in any services provided. Therefore the evaluation of the significant that related to user satisfaction is a priority. User satisfaction is defined as the overall level of compliance with user expectations, measured as a percentage of really met expectations [1]. The Government of Malaysia has targeted that by 2012 Malaysia's public transport system become the mode of choice of urban commuters. In order to achieve the target, terminal's condition also play a very important role to attract the user to commute by public

N. M. Noor (✉) · A. K. Arshad · I. B. M. Jais · M. Mustafa
Faculty of Civil Engineering, Universiti Teknologi MARA, Shah Alam, Selangor, Malaysia
e-mail: nor_nkmh@yahoo.com.my

transport. Travel by public transit involves much more than moving about on buses and trains. It involved walking from one's origin to a bus stop or train station, waiting for the vehicles to arrive, boarding the vehicle, travelling in the vehicle, alighting from the vehicle, and then walking to one's final destination [2]. Hill et al. mentioned that user satisfaction represent a measure of company performance according to the customers need. This means by measuring the user satisfaction, the service quality can be measured. Customers express their points of view about the services by providing judgments on some services aspects by means of ad hoc experimental surveys, known in the literature as customer satisfaction survey [3].

The contribution of this paper is the analysis of the user satisfaction on the service provided by a public transport terminal by distributing the questionnaires.

2 Literature Review

Several studies on the user satisfaction have been carried out before. Castillo and Benitez [4] had studied about methodology for modeling and identifying users satisfaction issues in public transport systems based on users surveys. This paper presents a methodology to identify and quantify the relationship between the ratings given to the overall satisfaction and those given to specific aspects of the service or specific rating. Eboli and Mazzulla [5] had proposed the structural equation modeling for analyzing passengers' perceptions about railway services. In this work a tool for analyzing passengers' perception in terms of satisfaction with transit services is proposed. In addition, Eboli and Mazzulla [6] also had study about a methodology for evaluating transit service quality based on subjective and objective measures from the passenger's point of view. In this paper the methodology considering both passenger perceptions and transit agency performance measures involving the main aspect characterizing a transit service. Gromule [7] also had done the analysis of the quality of service of the Riga Coach Terminal from the viewpoint of travelers. The main attention for this research is analysis of the reason why travelers choose train rather than bus in some regional direction in Latvia. Iseki and Taylor [8], Eboli and Mazulla [9], Cantwell et al. [10], and Ismail et al. [11] also had done studies on user point of view. In these studies, different attributes on customer satisfaction were determined such as analysis of user perceptions of transit stops and stations, examining the factors that impact public transport commuting satisfaction, a new customer satisfaction index for evaluating transit service quality and transit manager's perspectives on evaluating performance. Therefore studies in user perception are required in order to recover user satisfaction for the services provided.

3 Methodology

3.1 Site Study

The site study was conducted to know the real conditions of the terminals. The existing services and facilities provided by the terminals were determined. The main objective of this study is to analyze user satisfaction on the existing terminals condition. In the survey questionnaire, questions on customer satisfaction were provided with responses using the scale of 1–5. The survey form was divided into three sections, which are A, B, and C. Section A covers customer information or respondent's demography such as gender, age, profession, monthly income, purpose of using terminal, how commute to the terminal, frequency of using terminal and how the terminal attract the customer. Section B is about the effectiveness and service quality of the terminal. The parameters cover the availability of the information, safety and security of the terminals, adequacy and maintenance of the amenities, cleanliness and comfort of the terminal atmosphere, access and connection to and from the terminal, and lastly the overall performance of the services provide at the terminal. Finally, Section C covers the customer point of view on factors that is important in service quality and any other comment or suggestion from them that they think necessary to improve the terminal services. Two terminals were considered in these studies which are Terminal One Seremban and Klang Sentral. Terminal One located at the centre of the Seremban town which has 1,400 parking bays and 70 bus bays with the 40,000 sq meters of space at the terminal. This terminal was attached with Terminal One Shopping Center. This is one of the reasons this terminals always pack with users. As shown in Fig. 1 the waiting area of Terminal One Seremban.

In addition, Klang Sentral is a new commercial hub in the northern part of the royal town of Klang in Selangor, Malaysia. It is situated about 9 km away from the Klang town centre. Klang Sentral is also the new controversial and highly-debated ultra-modern transport terminal for the local and intercity bus and taxi services in Klang. This terminal equipped with CCTV and Fully air-conditioned terminal, including waiting area, ticket counter and others. Figure 2 shows the waiting area of Klang Sentral.

These two terminals were considered due to more or less similar on its condition. The study was conducted both in weekdays and weekends during peak hour and off peak hour. Peak hours were determined of off office hour. Which means at 7–8 am, during lunch break 1–2 pm and starting at 5 until 7 pm. While off peak hours is any time during office hour and late at night. Target participant for this study is students and educated youth.

Fig. 1 Waiting area in terminal one Seremban



Fig. 2 Waiting area in Klang Sentral



3.2 Data Analysis

The data gathered from the questionnaire was analyzed by using weighted parameter method. The weighted factor (W) used was -2 , -1 , 0 , 1 and 2 . From the questionnaire for the scale 1 the weighted factor is -2 , scale 2 the weighted factor is -1 , scale 3 the weighted factor is 0 , the scale 4 the weighted factor is 1 and lastly for the scale 5 the weighted factor is 2 . The number of respondent score for the scale was multiplied to the weighted factor to determine the satisfaction value (SV). Then all the satisfaction was sum up to get the total satisfaction Value (TSV). It can be shown by the equation below:

$$SV = \text{No.of participant} \times W \quad (1)$$

No of participant represent the number of respondent respond to the scale while weighted score was the value mentioned above. The satisfaction value (SV) will

varies from negative value to positive value. The total satisfaction value (TSV) was the summation of satisfaction value of the same element. It can be simplify by the equation below:

$$TSV = \sum SV \quad (2)$$

The value of Satisfaction and total satisfaction will be varies from negative to positive values. By considering the zero value as the boundary condition, the satisfaction value will be analyzed. Negative value means the facilities still do not meet the satisfaction level they required. Zero values mean average or neutral level of satisfaction. Positive values show the user satisfied with the services provided. The higher value shows the greater their satisfaction on that element. While for the important elements should take into consideration based on user surveys can be obtained by calculating their vote on the elements. In the questionnaire had been included spaces where the users have to choose by their own which elements they want to be take into consideration.

4 Result and Discussion

After calculating the satisfaction of each of the elements in the questionnaires, the results obtained are as shown in Table 1. The first column represent the elements had been outlined in the questionnaires. Second column represent the category or the parameters been considered in this study. The third column is the code of the elements being analyzed in the questionnaires. The code was used so it is easier to analyze the satisfaction level. The satisfaction column represent the Total Satisfaction Column had been calculated by using the method mentioned in Methodology which considered both formula. For Element I1 the satisfaction value was 7 which show the information provided at the terminals really satisfied the user perceptions. While for element SS1 the satisfaction value is -6 . Negative sign represent the unsatisfied. Therefore the safety and security for both terminals was in very poor conditions. Average value for element CC shows that user still not satisfied with the cleanliness and comfort of the terminals. Klang Sentral was equipped with air-condition but the atmosphere still not comfortable for the user. Terminal do not have specific waiting are therefore it deserved to get negative value from user satisfaction. Access and connection (AC) for both terminals satisfied the users. It is easy to be there either by private vehicles or public vehicles. Both terminals provide local bus and taxis services to ease the user. As for user attendance, for elements UA2 get -2 values. It showed that users feel that the staffs do not be nice to them. Most of the users give the same comment about the staff behavior. Overall performance only gets 1 satisfaction value. This shows the terminals still in poor condition. More improvements need to be taking into measure to improve the satisfaction values.

Table 1 Satisfaction value

Question on the survey	Category	Code	Satisfaction
The information is available and easy to understand	Information	I1	7
The user feel safe and secure at any time	Safety and security	SS1	-6
The facilities provided adequate and fulfill the user needs	Amenities	A1	-1
The facilities are well maintained and always in good condition		A2	0
<i>Average</i>			-0.5
The terminal's coziness	Cleanliness and comfort	CC1	-3
The terminal's conservation and cleanliness		CC2	-10
The terminal's illumination		CC3	-11
This terminal provides adequate visual arrival of busses at the terminal		CC4	-7
The facilities provided always clean and well maintained		CC5	-4
<i>Average</i>			-7
The terminal is easy to access from user origin location	Access and connection	AC1	4
The terminal merge different mode of transit to ease the users		AC2	2
<i>Average</i>			3
Driver kindness	User attendance	UA1	2
Staff kindness		UA2	-2
<i>Average</i>			0
Are the user satisfied with the service quality of the terminal	Overall performance	OP	1

Table 2 Important element of public transport terminal services

Characteristic	Category	Percentage (%)
Important element of public transport terminal services	Information	8.7
	Safety and security	34.8
	Amenities	17.4
	Cleanliness and comfort	34.8
	Access and connection	4.3
	User attendance	0

Table 2 shows important element of public transport terminal services had been outlined by the users. Security and safety is their main consideration so do with the comfort and cleanliness. Each element gets 34.8% consideration by the user. Follows by the amenities (17.4%), information (8.7%) and access and connection (4.3%) safety and security always be the first consideration based on the previous

research. This element also the main reason the users choose to use the terminals. Based on face to face interview most of them admit they have to use the terminals but the terminals condition did not attract them at all.

5 Conclusions

In this paper, the user satisfaction on the services provided by Terminal One Seremban and Klang Sentral had been determined. The data was analyzed by using weighted parameter method to determine the user satisfaction level. The management of both this terminals should take certain steps to improve the existing services provided by the terminals to give the satisfaction to the users.

Based on the study done, the services provided by the terminals that did not satisfy the customer were the safety and security, and the cleanliness of the terminals. Its means the users concern more on their safety and comfort while being at the terminals. After all the deficiencies had been identified and appropriate actions had been implemented, the satisfaction of the customer towards the terminals can be increased.

Further study will be conducted at different terminals to compare the findings. Thus the Customer Satisfaction's Model is expected to be developed.

Acknowledgments Authors wishes to express our outmost gratitude to which it may be concern especially to Faculty of Civil Engineering, Universiti Teknologi MARA and Research Management Institute, University Teknologi Mara under Research Intensive Fund with reference no 600-RMI/DANA 5/3/RIF (75/2012). Not to forget the supervisor who always give guidance in order to finish up the paper and for those who help and support along the process of collecting data, analyzed the data and preparing this paper.

References

1. Y. Tyrinopoulos, C. Antoniou, Public transit user satisfaction: variability and policy implications. *Transp. Policy* **15**, 260–272 (2008)
2. Government Transformation Programme, Jabatan Perdana Menteri (2011)
3. N. Hill, G. Brierley, R. MacDougall, *How to Measure Customer Satisfaction* (Gower Publishing, Hampshire, 2003)
4. J.M. Del Castillo, F.G. Benitez, A methodology for modeling and identifying users satisfaction issues in public transport systems based on users surveys. *Procedia—Social Behav. Sci.* **54**, 1104–1114 (2012)
5. L. Eboli, G. Mazzulla, Structural equation modelling for analysing passengers' perceptions about railway services. *Procedia—Social Behav. Sci.* **54**, 96–106 (2012)
6. L. Eboli, G. Mazzulla, A methodology for evaluating transit service quality based on subjective and objective measures from the passenger's point of view. *Transp. Policy* **18**, 172–181 (2011)

7. V. Gromule, Analysis of the quality of service of the riga coach terminal from the viewpoint of travellers, in *Proceedings of the 8th International Conference Reliability and Statistics in Transportation and Communication*, 15–18 Oct 2008
8. B.D. Taylor, H. Iseki, Style versus service? an analysis of user perceptions of transit stops and stations. *J. Public. Transp.* **13**, 23–44 (2010)
9. L. Eboli, G. Mazulla, A new customer satisfaction index for evaluating transit service quality. *J. Public Transp.* **12**, 21–37 (2009)
10. B. Caulfield., M. Cantwell, M. O'Mahony, Examining the factors that impact public transport commuting satisfaction. *J. Public Transp.* **12**, 1–21 (2009)
11. M. Ismail, Z.M. Ali, N.R.M. Suradi, A.S. Ismail, Importance-performance analysis and customer satisfaction index for express bus services, in *World Congress on Nature & Biologically Inspired Computing (NaBIC 2009)*, 2009

Evaluation of Pedestrian Level of Service for Tehran Crosswalks; Case Study of Nabovat Square in East of Tehran

Seyed Abdolhadi Daneshpour, Mohadeseh Mahmoudi
and Bushra Abbasi

Abstract Walking, as the first mode of transportation, has an effective role in human life. Quality of walkways is also a major factor which encourages walking. The increase of vehicular traffic in recent decades turned the pedestrian safety of the conflicted zones, like crosswalks, to one of the main concerns of urban dwellers. In this research, pedestrian safety in Tehran is evaluated through determining the level of service of crosswalks. As a multifunctional public urban space, Nabovat square, which is located in the eastern part of Tehran, is selected as the case study of the research. This empirical study tends to determine the level of service of crosswalks around Nabovat Square using the models presented in Highway Capacity Manual 2000. Consequently, the risk which a pedestrian takes in order to pass the crosswalks is also determined. Most of the data was collected through direct observation of the area at different times of the day. Additionally, some statistical data such as traffic flow and width of crosswalks were collected from Tehran Comprehensive Transportation & Traffic Studies Company. Finally, the result of this study provides evidence which clarifies lack of safety in the crosswalks of Tehran. The evaluated result can be considered as one of the great concerns of Tehran's residents, therefore, recommended improvement measures have been included to enhance level of service of crosswalks, and some suggestions have been presented for further studies.

Keywords Nabovat Square · Level of service · Walkways' safety · Walkability

S. A. Daneshpour · B. Abbasi
School of Architecture and Environmental Design, Iran University of Science and
Technology, Tehran, Iran

M. Mahmoudi (✉)
Faculty of Built Environment, University of Malaya, Kuala Lumpur, Malaysia
e-mail: Mohadeseh.mah@gmail.com

1 Introduction

By the growth of mega cities from different perspectives such as size, distance, population and simultaneously increasing number of the motorized vehicles' in the cities during the last century, pedestrian movement gradually decreased. This issue has brought several concerns to the society from socio-economics and environmental aspects to health problems [1].

Therefore, most related professions have sought to improve the walking issue in today's modern life. Meanwhile, urban designer, urban planners and traffic engineers play one of the most significant roles in changing the built environment in a way to encourage and support pedestrian walking.

In the famous book of "Public Spaces, Public Life", three main criteria for having a walkable environment have been demonstrated as; protection, comfort, and enjoyment [2]. Protection against traffic and accidents, protection against crime and violence, and protection against unpleasant sense experiences are three major groups under the protection category. The activities which are categorized under the enjoyment scale are grouped as the possibilities for walking, standing, staying or sitting, possibilities to observe, possibilities for hearing or talking, and possibilities to play. Possibility of enjoying positive aspects of climate, aesthetic quality or positive sense-experiences, are groups which are categorized under the scale of comfort. The importance of qualities related to enjoyment and comfort may vary to pedestrians in choosing their path, but protection-feeling safe and secure-has the highest priority for pedestrian route choice, regardless of their destination [3].

Pedestrians are undoubtedly considered as the vulnerable users of the streets. In 2010, the fatalities involving pedestrians in London accounted for 46 % [4]. Also, in Iran pedestrian safety is one of the major concerns. Statistics show that 30 % of people who are killed in the accident are pedestrians [5]. This problem is one of the main barriers which discourage Tehran's residents to walk, rather than traveling by motorized vehicle [3]. For instance, lots of parents do not let their children to walk to school, even when it is not too far. They prefer to travel by car, just because of their concern about safety from vehicular traffic [6]. Therefore, in order to evaluate the pedestrian safety in Tehran, one of Tehran's urban spaces with high pedestrian flow, is selected as the case study of the research.

Tehran is composed of 22 districts with 686 km² urban area [7]. District 8 is called Narmak area and is one of the earliest planned residential areas of Tehran. Due to its special structure, Narmak is known as a sustainable district for its safe, accessible and livable environment [8]. Nabovat square is a multifunctional urban space which is considered as the regional center of this area [9]. Nabovat square is like a plaza that is surrounded by various commercial and administrative buildings as well as a religious center. This square, which is highly recognized for its walkability, is considered as the case study of this research. Figure 1 shows the situation of Nabavot square as a regional center of eastern Tehran in whole, and district 8 in particular. Also, Fig. 2 illustrates the location of this square in the plan

Fig. 1 Centers of spatial structure of Tehran master plan and the situation of Nabovat square in district 8 *source [9]*

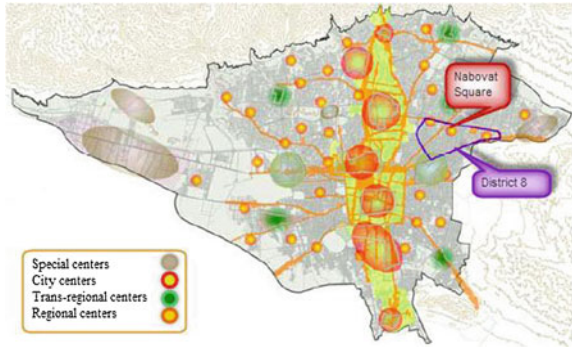


Fig. 2 Location of Nabovat square in district 8 plan *source [9]*



Fig. 3 Aerial view of Nabovat square



of district 8. Figure 3, then, presents the aerial view of this area and Nabovat roundabout with multi lines for vehicular transportation and the pedestrian crosswalk. Indeed Nabovat Square is a great sample of shared space that is accessible by rapid public or private transportation and pedestrians. Since this area works as a semi pedestrian mall, more than thousands of pedestrians pass the pavements every day. So, because of the importance of this square and high volume of its traffic, as well as large number of pedestrians passing the above mentioned area, the crosswalks of studied area are evaluated to determine whether pedestrians are protected against the traffic movement and accidents or not.

2 Pedestrian Level of Service

Level of Service is generally used to measure the quality of walkway accommodation in accordance to pedestrian travelling demands. The concept of Level of Service (LOS) was firstly used to describe the quality of stream and traffic in Highways; however, this notion is also used for other travelling modes in the current days. The first performance measure is the sidewalk capacity which was developed in the early 1970s [10]. Additionally, the only established method of quantifying sidewalk capacity and assessing the facilities provided for pedestrians, illustrated in Highway Capacity Manual [11]. In fact a guideline was made like what was provided for vehicular movement, by applying Level of Service concept. The research was done by Lautso and Murole and was one of the first studies on Level of Service that incorporated many significant factors with computation of Pedestrian Level of Service [12]. This study was also expanded by later researches.

Khisty considered the qualitative environmental factors for evaluation of pedestrian facilities so that the conditions of sidewalks are measured by the pedestrian Level of Service. Convenience, comfort, safety and security were some of the factors measured by using parameters such as speed of walkers, travel time, pedestrian's freedom to maneuver and traffic interruption [13]. Hence, the traffic volume can affect the pedestrian comfort, which means there will be restrictions in walking route and speed where the pedestrian traffic volume is high. Therefore, comfort level and consequently the pedestrian LOS will be low. On the other hand, where the pedestrian is not facing a high traffic volume, the comfort degree usually increases [14].

In Iran, the pedestrian Level of Service standards is categorized under six classes [15], as it is shown at Table 1.

Table 2 shows the suggested criteria for this classification. As it is visible in this table, the operational capacity of Iran's sidewalks is 68 p/min/m of effective width that is considered for Level of Service E, and the movement space for every person is 0.6 m².

It is also important to notify that LOS standards are applicable only to *effective width of walkways*, deducting the space close to walls or any obstruction in walkway space. Pedestrians usually keep away about 15 cm from walls, shop windows or Krebs, therefore, the effective width of walkways are used for analysis and applying the standards, rather than the whole sidewalk width [16]. The *effect of platoon flow* is the other notion that should be considered for this analysis. Formation of different groups of pedestrians is always seen in sidewalks and crosswalks. These groups are created around the corner of intersections while waiting for the red traffic light, and move all with each other when the traffic light turns green. This case may also happen near to public transport stations. To consider the effect of platoon flow in sidewalks, it is advised to add averagely 13 p/min/m to the volumes that are more than 1.65 p/min/m [17].

Table 1 The classification of level of service in Iran

LOS	Description
A	Pedestrians usually move in their favorite route, by their favorite speed, without changing their track for others (free flow). It is less likely for one to collide with other
B	There is enough space for pedestrians to choose their favorite speed of walking to pass each other. There is minor conflicts and speed restrictions
C	There is enough space for pedestrians to choose the usual speed of walking to pass each other in one-way flows. But the cross or reverse flows are difficult
D	Freedom of choosing their walking speed is limited. There is intermittent shuffling and significant conflict among pedestrians. They also need to change their speed frequently
E	Pedestrians are usually experiencing a shuffling walk. Passing, reverse and cross flows are very difficult. All pedestrian have problem walking by a normal speed and need to adjust their steps repeatedly. The movement is very slow, with intermittent stopping
F	Critical density strongly limits the walking speed and having contact with others is inevitable. The reverse or cross flows in these sidewalks are impossible. The flow looks more like queuing rather than a pedestrian movement

Source [15]

Table 2 The suggested criteria for pedestrian level of service in Iran

Level of service	Average area (m ² /p)	Traffic and speed		
		Average walking speed (m/min)	Pedestrian flow rate (p/min/m)	Ratio of volume to capacity
A	6	≥76	≤13	≤0.18
B	6–4	76–74	13–19	0.18–0.27
C	4–2.6	74–71	19–27	0.27–0.4
D	2.6–1.6	71–65	27–41	0.4–0.6
E	1.6–0.6	65–40	41–68	0.6–1
F	<0.6	<40	Varied	Varied

Source [15]

3 Research Method

Time–Space (TS) method is generally used to examine walkways quantitatively, and evaluate the adequacy of space where the peak-period demand of pedestrians is predicted. TS method is one of the first methods used to determine the level of service for sidewalks and signalized crosswalks [16]. This method shows the pedestrian level of activities in the space as well as the pedestrian safety. In the development of New York City, TS method was approved as a validated measure for street conditions and pedestrian traffic in sidewalks, crosswalks and corners [18]. This method is one of the first approaches, yet, it is not the only method of evaluation. In order to determine level of service of crosswalks, different methods are used based on existence of signal on the intersections and different patterns of pedestrian traffic. Since Nabovat Square crosswalks are unsignalized crosswalks, the analysis techniques are demonstrated as follows:

3.1 Evaluation of Unsignalized Crosswalk

The unsignalized pedestrian crossing is a conflict zone between the pedestrian flow and vehicular traffic which is not controlled by any signal or traffic light. Most crashes occur within this area of high risk. Considering this problem, Effective Critical Headway (ECH) is defined as minimum time headway needed by a pedestrian for a safe cross [19]. If the headway between vehicles arrival is more than the required time for passing, the pedestrian will pass through the crosswalk, otherwise he/she should wait to find the required time. In these situations, pedestrians usually judge themselves to determine whether the available headway is long enough to cross safely or not. In order to analyze the level of Service and safety of unsignalized intersection, Highway Capacity Manual 2,000 provided a model to compute the pedestrian delay time at the unsignalized intersection [20]. This model and its equations are presented as follows:

The effective critical headway for a pedestrian is computed using Eq. (1):

$$t_c = L / S_p + t_s \tag{1}$$

where

- t_c Effective critical headway for a pedestrian (s)
- S_p Average walking speed of a pedestrian (m/s)
- t_s Start up time and end clearance time of pedestrian (s)
- L Length of crosswalk (m)

In order to find out the group critical headway in the cases that platooning exists in the area, the pedestrian spatial distribution is going to be computed according to Eq. (2). Additionally, for computation of spatial distribution, the platoon size should be discovered by field observation, or is estimated by using Eq. (3)

$$N_p = \text{INT} [0.75(N_c - 1) / W_E] + 1 \tag{2}$$

where

- N_p Pedestrians' spatial distribution (p)
- N_c Total number of pedestrians in the crossing platoon (p)
- W_E Effective crosswalk width (m) 0.75 = the distance used by a pedestrian for avoiding interference with others while passing (the default effective width)

$$N_c = (v_p e^{v_p t_c} + v e^{-v t_c}) / (v_p + v) e^{(v_p - v) t_c} \tag{3}$$

where

- V_p Pedestrian flow rate (p/s)
- V Vehicular flow rate (veh/s)

$$t_G = t_c + 2(N_p - 1) \tag{4}$$

Table 3 Suggested criteria for determination of LOS in unsignalized crosswalks

Level of service	Average delay per pedestrian (S)	Likelihood of risk-taking behavior
A	<5	Low
B	<5–10	
C	<10–20	Moderate
D	<20–30	
E	<30–45	High
F	>45	Very high

Source [11]

where:

t_G Group critical headway (s)

Finally the delay of pedestrians are considered as the LOS measure, which is computed using Eq. (5). Table 3, also shows the classification of LOS based on the delay time of pedestrian at unsignalized intersection.

$$d_p = \frac{1}{v} (e^{vt_G} - vt_G - 1) \tag{5}$$

where:

d_p Average pedestrian delay time (s)

Consequently, level of service of crosswalks is determined based on delay time at Tables 4 and 5.

4 Result

Data collection was conducted through two phases for the crosswalks located in four sides of the Nabovat square—north, west, south, and east. Figure 4 shows locations of the studied crosswalks. At the first phase, the physical data like the length and width of crosswalks were collected through field measurement. The other statistical data which was mostly related to the pedestrian behaviour, like the speed of walking and pedestrian flow rate, was collected at the second phase through direct observation. The studied crosswalks were observed over two months, from September to October 2012, during eight times (once a week). Since the crosswalks are usually designed for the peak hours, the observation process includes two periods of peak hours in weekdays. This process takes place, each time, during a fifteen-minute period, within the normal and routine condition of crosswalks in their peak hours, from 7:00 am to 10:00 am in the morning and 4:00 pm to 7:00 pm in the evening.

However, except for the increase of pedestrian flow rate in evening, no other special difference was seen in pedestrian behaviour between morning and evening.

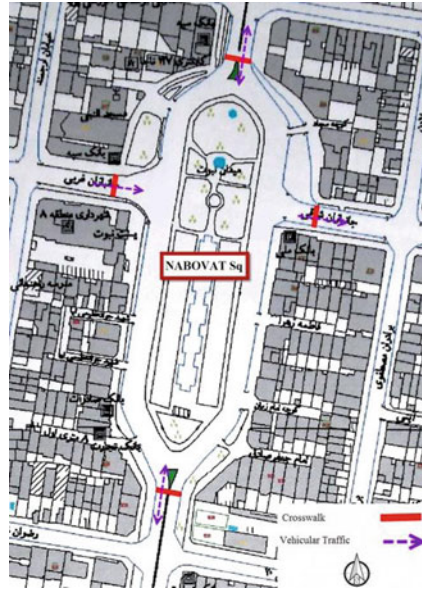


Fig. 4 Red line shows the location of crosswalks in Nabovat square



Fig. 5 Pedestrians passing the crosswalks around Nabovat square; a North crosswalk; b East crosswalk; c South crosswalk; d West crosswalk

Since it was not possible to use the surveillance camera, all the data collection and the observation process were done by the authors. Figure 5 illustrates nabovat's pedestrians passing the studied crosswalks.

Table 4 Level of service of crosswalks (data collected during peak hours in the morning)

Crosswalk	L (m)	W (m)	S _p (m/s)	V (veh/s)	V _p (p/s)	t _c (s)	N _c	N _p	t _G (s)	d _p (s)	LOS
North	7.45	3	1.2	0.44	0.04	9.21	5.55	2	11.21	301.77	F
West	12.6	3	1.2	0.57	0.09	13.50	303.15	76	163.50	5.2264E + 40	F
South	7.5	3	1.2	0.37	0.09	9.25	6.22	2	11.25	159.647032	F
East	11.9	3	1.2	0.31	0.08	12.92	11.89	3	16.92	591.64	F

Table 5 Level of service of crosswalks (data collected during peak hours in the evening)

Crosswalk	L (m)	W (m)	S _p (m/s)	V (veh/s)	V _p (p/s)	t _c (s)	N _c	N _p	t _G (s)	d _p (s)	LOS
North	7.45	3	1.2	0.49	0.16	9.21	22.22	6	19.21	24,969.2206	F
West	12.6	3	1.2	0.71	0.15	13.50	2,620.54	655	1,321.5	Very large number	F
South	7.5	3	1.2	0.73	0.18	9.25	166.47	42	91.25	1.1644E + 29	F
East	11.9	3	1.2	0.53	0.60	12.92	476.26	119	248.92	3.7252E + 57	F

By using the presented model for data analyzation, the effective critical headway for a pedestrian, pedestrians’ spatial distribution, group critical headway, and finally pedestrian delay, were computed for each studied crosswalk in the morning and the evening separately. The above mentioned step is taken after the data collection process is completed. The collected data and the result of the analysis have been illustrated in Tables 4 and 5.

Conducting this analysis shows the average delay of a pedestrian to pass these crosswalks safely and the level of service of crosswalks. As shown in the Tables 4 and 5, the average delays at all crosswalks in both morning and evening time are more than 45 s, especially at the evening which include high number of passing pedestrians. The highest evaluated delay times, like 24,969 s—in north crosswalk at evening time—include such long period of time that keep no patient for pedestrians to wait. Therefore, based on Table 3, level of service of all crosswalks are determined as F, and are certainly not estimated as a safe crossing space for pedestrians. As the result, serious conflict between vehicular traffic and crossing pedestrians are usually seen on the sidewalks.

5 Discussion and Conclusion

This study has investigated the safety of unsignalized crosswalks around nabovat square by determining their level of service. While the statistical analysis shows that pedestrians should take a high risk in crossing the studied areas, high number of people are still walking through this area daily and the area is well known for its

walkability in the city of Tehran. However, pedestrians who are averse to take unnecessary risks, face serious difficulties while passing these crosswalks. Since there are other areas in Tehran with similar conditions to nabovat square and its crosswalks, the findings of this study do provide clear evidences for unsafe crosswalks as one of the main concerns of pedestrians in this Capital City. Also, these results illustrate the reason for Tehran's high pedestrian fatalities, which needs to receive special attention, as well as cooperation of different experts and organizations. Urban designers, traffic engineers and Tehran municipality are all responsible for improving the level of service for crosswalks and enhance the pedestrian safety, and can only succeed through keen synergy.

In addition, some suggestions such as installing the signals at the intersections and wide overpasses with elevators for the elderly and disabled, specially at the west crosswalk, which accommodate the highest volume of pedestrian flow, are recommended. Also pedestrian priority to vehicular traffic, in crossing the streets, has significant effect on pedestrian safety. Performing operational measures, such as changing the paving and the furniture of streets near to the crosswalks around the square, will help to decrease the speed of vehicles and therefore, dedicate higher priority for pedestrians. Finally, further studies on interaction between pedestrian and vehicles are suggested for better understanding of pedestrian crossing behaviour in these conflicted zones.

Acknowledgments The authors would like to acknowledge the contribution of Tehran Comprehensive Transportation and Traffic Studies Company for assisting in data collection.

References

1. B.B. Brown, C.M. Werner, J.W. Amburgey, C. Szalay, Walkable route perceptions and physical features: converging evidence for en route walking experiences. *Environ. Behav.* **39**(1), 34–61 (2007)
2. J. Gehl, L. Gemzre, *Public spaces, public life*. Copenhagen: Danish architectural press and the royal Danish academy of fine arts. School of Architecture (1996)
3. L.W. Chau, H.N. Ismail, S. Hamidi, Effects of trip purpose on preferred walking environment and route choice of pedestrians in Narmak, Tehran. *CIDP Monograph, Universiti Teknologi Malaysia*, No. 6. Nov 2010
4. B. Li, A model of pedestrians' intended waiting times for street crossings at signalized intersections. *Transp. Res. Part B: Methodol.* **51**, 17–28 (2013)
5. Unknown. 30% of people who are killed in accident are pedestrian, *Asre Iran* (2013). Retrieved from <http://www.asriran.com/fa/news/254569/>
6. R. Shokoohi, N.R. Hanif, M.M. Dali, Children walking to and from school in Tehran: associations with neighbourhood safety, parental concerns and children's perceptions. *Procedia—Social Behav. Sci.* **38**, 315–323 (2012)
7. Tehran municipality: Tehran. Public and international relation department (2013). Retrieved from <http://en.tehran.ir/Default.aspx?tabid=104>
8. M.M. Azizi, Sustainable residential neighbourhood: the case study of Narmak neighbourhood, Tehran. *J. Honare-ha-ye Ziba* **27**, 35–46 (2006)

9. Tehran district 8 municipality: Detailed plan of Tehran district 8. (2006) Retrieved from <http://region8.tehran.ir/Default.aspx?tabid=157>
10. J.J. Fruin, *Pedestrian Planning and Design* (Metropolitan Association of Urban Designers and Environmental Planners Inc, New York, 1971)
11. TRB, National Research Council: Special report 209: Highway capacity manual. Washington, DC., (1994)
12. K. Lautso, P. Murole, A study of pedestrian traffic in Helsinki: methods and result. *Traffic Eng. control* **15**(9), 446–449 (1974)
13. C.J. Khisty, Evaluation of pedestrian facilities: beyond the level-of-service concept. *Transp. Res. Rec.: J. Transp. Res. Board* **1438**, 45–50 (1994)
14. T. Dandan, W. Wei, L.U. Jian, B. Yang, Research on methods of assessing pedestrian level of service for sidewalk. *J. Transp. Sys. Eng. Inf. Technol.* **7**(5), 74–79 (2007)
15. Research and Technical Criteria Office, *Pedestrian Facilities; Technical Basics*, vol. 1 (Planning and Budget organization Publications, Tehran, 1996)
16. J.J. Fruin, *Designing for pedestrians: A Level of Service Concept* (Prentice Hall, Englewood Cliffs, NJ, 1992)
17. B. Hosseini Yarandi, Examination of problems of pedestrian traffic and parking spaces in Nabovat square with providing the improvement measures. Tehran Municipality: Tehran Comprehensive Transportation and Traffic Studies Co. 2008
18. J.J. Fruin, B.T. Ketcham, P. Hecht, Validation of the time-space corner and crosswalk analysis method. *Transp. Res. Rec.: J. Transp. Res. Board* **1168**, 39–44 (1988)
19. B. Li, A model of pedestrians' intended waiting times for street crossings at signalized intersections. *Transp. Res. Part B: Methodol.* **51**, 17–28 (2013)
20. TRB, National Research Council: Highway capacity manual. Washington, DC. (2000)

Physical Properties of Modified Asphalt Binder with Nanopolyacrylate

E. Shaffie, J. Ahmad, A. K. Arshad, D. Kamarun, F. Kamaruddin
and M. A. Shafiee

Abstract Modification of asphalt binder using polymers has been increasingly used by our government to enhance the properties of bituminous mixes and to prolong the lifetime of roads in the face of increased traffic. This paper reports the procedure for determining the physical properties of asphalt binder using penetration grade binder of 80/100 with nanopolyacrylates (NPA). The asphalt binder was modified with different percentages of NPA (0, 2, 4, 6, 8 and 10 % by weight of asphalt binder) in order to determine the appropriate proportion of asphalt binder and NPA that can provide special potential in enhancing the properties and strength of the bituminous road to achieve the specifications required. Asphalt binder properties were evaluated in penetration, softening and penetration index. The results of this investigation indicated that the 6 % by weight of NPA in asphalt binder is the most effective proportion, having potential to improve physical properties of asphalt such as increasing softening point and decreasing the penetration and high penetration index. The results also demonstrate that the NPA binders outperformed conventional asphalt binder in term of engineering properties and it can be concluded that NPA polymer is feasible to be used as asphalt modifier and has potential for improvement in the field of pavement material and construction in future.

Keywords Modified binder · Nanopolyacrylate · Natural rubber · Physical properties

E. Shaffie (✉) · J. Ahmad · A. K. Arshad · F. Kamaruddin · M. A. Shafiee
Institute of Infrastructure Engineering and Sustainable Management (IIESM), Universiti
Teknologi MARA, 40450 Shah Alam, Malaysia
e-mail: eka@salam.uitm.edu.my

D. Kamarun
Faculty of Applied Science, Universiti Teknologi MARA, 40450 Shah Alam, Malaysia

1 Introduction

Conventional bituminous mixture has shown satisfactory results as binder for road construction for so many years. However, for the past few years, states experienced problems in severity and permanent deformation on the road pavement. This problem with permanent deformation, or rutting, was attributed to an increase in truck tire pressure, axle loads, and volume of traffic [1]. The situation is evident for the last three decades, that the pavement has been facing more demands than before resulting in the need for an enhancement in the properties of bituminous materials [2].

Due to this problem, many researchers have conducted bituminous modification to improve the physical properties as well as the rheological properties of the bitumen using modifier. Several additives and modifier such as natural rubber latex (NR), Styrene Butadiene Styrene Block Copolymer (SBS), Styrene Butadiene Rubber Latex (SBR), and Ethyl Vinyl Acetate (EVA) have been studied by previous researchers to improve the asphalt binder properties, but only few types are suitable and compatible with binder for modification [3]. A study conducted by Nrachai [4] found that the natural rubber latex is the best alternative for road making due to flexibility and stability improvement in asphalt pavement and extend service life of the road pavement. In another study, Isacsson and Lu [5] reported that SBS improves resistance to flow at high temperature without making the binder become stiffer at low temperature.

As the focuses are more on modification of asphalt using conventional polymer, there is lack of work on modification of asphalt using nanocomposite polymer. Recently, researchers showed their interests on asphalt binder's modification using nano composites materials. From literature review, several studies have been conducted using polymer nano composites which consist of a blend of one (or more) polymer(s) with various nanomaterials such as nanoclays, carbon nanotubes, etc. [6, 7]. Mojtaba studied the potential benefits of nano-SiO₂ powder and SBS in asphalt mixtures. This study concluded that the asphalt mixture modified by 5 % SBS plus 2 % nano-SiO₂ powder could be the optimum proportion which increases physical and mechanical properties of asphalt binder and mixtures [8]. Abdullah studied the potential of nanoclay and warm asphalt additives on the asphalt binder properties. It was found that the addition of nanoclay and warm mix asphalt additives (WAA) in asphalt binder can improve the physical properties of asphalt [9]. According to Ref. [10] the addition of nanoclay and carbon microfiber improves the stripping performance mixtures or decreases the potential of moisture damage. Sureshkumar [11] studied the influence of adding clay in polymer modified asphalts. Results show that the polymer modified asphalt influences the final rheological properties of asphalt binder due to clay which have compactibilizing effect on asphalt and polymer, thus lead to better dispersion of the polymer in the asphalt.

The addition of nanomaterials in asphalt pavement mixes has the potential to enhance further the mechanical properties of asphalt mixes and overcome the

shortcomings of using polymer in asphalt pavement mixes. However, the use of nanopolyacrylate (NPA) has not been explored in improving the properties of asphalt binder. Hence, in this study, a new asphalt binder based on nanosized polyacrylates was conducted. NPA modified asphalt binders were prepared by incorporating NPA into asphalt binder. The properties of the modified binders were evaluated using the conventional test methods such as penetration and softening point test. The application of NPA in modified asphalt binder is expected to improve engineering properties of asphalt binder.

2 Materials and Method

2.1 Aggregate and Asphalt Binder

Granite aggregates used in this study were obtained from Blacktop Quarry, Rawang located in Klang Valley. The aggregates were processed by washing, oven drying and sieving. All the aggregates were sieved to the appropriate size using sieving machine and then stored in individual bins according to the size of aggregates. The specific gravity of the coarse and fine aggregate was determined according to ASTM standard procedures. The asphalt binder used in this study was 80/100 penetration grade. The asphalt binder physical properties were tested and fulfilled the standard requirements.

2.2 Nanopolyacrylate Polymer

Nanopolyacrylate (NPA) used in this study was provided by the Nan Pao Resins Chemical CO., Taiwan. Polyacrylate, also commonly known as acrylics belongs to a group of polymer which could be referred as plastic. This polymer is commonly used for their transparency and its ability to resist breakage and elasticity. The nanopolyacrylate consist of 39–40 % polyacrylate resin with the average diameter of 50 nm. Table 1 shows the properties of the nanopolyacrylate.

2.3 Preparation of Nanopolyacrylate Modified Asphalt Binder

In this study, preparation of Nanopolyacrylate modified binder is developed by adding the base binder of 80/100 penetration grade with NPA. An initial study to investigate the essential amounts of polymers to be mixed with binder manually at various temperatures and mixing time was conducted. However, this technique

Table 1 Properties of nanopolyacrylate (NPA)

Property	Value
Diameter (nm)	± 50 nm
Appearance	Milky white
PH value	6.5–8.0
Viscosity	Less than 200 cps (LVT NO: 2/60 rpm, 25 °C)
Solid content	40 ± 1.5 %
Tg point	55 ± 1 °C

was not able to produce a homogeneous binder mix. Therefore, there is a need to evaluate the effect of possible changes in temperature and time of blending on the properties of the binder. Due to this reason, the binder samples were prepared at various blending velocity, mixing time and mixing temperatures and then tested for their physical properties.

The wet process mixing method was selected to prepare polymer modified binder in which the NPA is added to the base binder before introducing into the aggregates. The NPA binder was processed in the laboratory using a cylindrical flask equipped with a propeller. To determine the optimum proportion of polymer, three variables were considered in the preparation process; mixing time, mixing temperature and mixing velocity. The NPA was added to the base binder using four interaction blending velocity (500, 1,000, 1,500 and 2,000 rpm), two interaction blending time (30 and 60 min), two different blending temperature (140 and 160 °C) and five NPA percentages (0, 2, 4, 6, 8, and 10 % by weight of binder) respectively. For the preparation of a sample, 500 g of base asphalt binder was melted at 110 °C and poured into a 500 ml container. Then, the asphalt binder was heated in the oven at 150 °C until it liquefies. The NPA is then added slowly into the liquid asphalt binder and sheared using a high shear mixer with mechanical stirrer at different blending velocity and time. Figure 1 shows the equipment and sample preparation process. The polymer modified asphalt binder is then evaluated for further physical properties test to determine the effect of the possible changes in temperature, time and blending velocity.

3 Results and Discussion

3.1 Determination of Optimum Blending Velocity

To determine the optimum blending velocity, a trial blending mixture using 3 % of NPA was selected and mixed at 160 °C for 30 min. Four trial mixing speed between 500 and 2,000 rpm at an increment of 500 rpm were used. Trial mixing speed was terminated at 2,000 rpm due to the mixer motor capability. Physical properties (softening point, penetration and penetration index) of the modified binder were then conducted to determine the best blending velocity. Results in



Fig. 1 Mixing process of polymer modified asphalt binder

Table 2 shows that, the blending velocity has a significant effect on physical properties of the binder. The ductility value shows downward and upward trend throughout the test. When the blending velocity was increased beyond that speed, the penetration value started to decrease. However, the blending velocity does not have significant effect on the softening point and the value is almost constant throughout the test. Based on previous study [12] the blending velocity was selected based on the average PI value obtained. Monograph was used to determine the PI value based on penetration and softening point results. Therefore, the average of PI value of 0.85 was used to determine the appropriate blending velocity to be used. Figure 2 shows the appropriate blending velocity of 1,650 rpm which is selected as the appropriate blending velocity in this study.

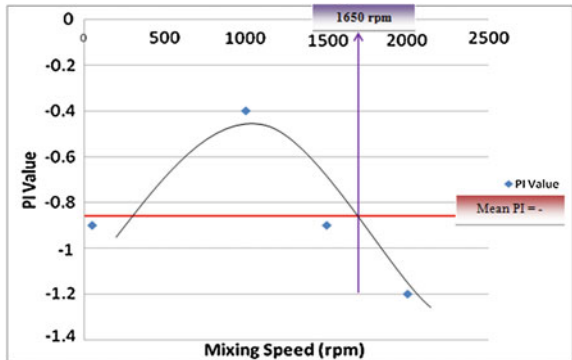
3.2 Determination of the Blending Time and Blending Temperature

Further evaluation to determine the blending time and blending temperature is obtained using the appropriate blending velocity of 1,650 rpm. The appropriate mixing variables for blending time and blending temperature was carried out at 160 °C/30 min, 160 °C/60 min, 140 °C/60 min, and 140 °C/30 min respectively. Physical properties (ductility, softening point, penetration and penetration index (PI)) of the binder were considered to determine the best blending time and temperature as shown in Fig. 3. Combination of blending temperature and blending time at 140 °C/60 min produced higher PI which indicates that the bitumen is more resistant to temperature susceptibility compared to the other three mixing time and mixing temperature combinations. Results also show that an

Table 2 Physical properties of modified asphalt binder using different blending velocity

Mixing speed (rpm)	Penetration (dmm)	Softening point (°C)	Ductility (cm)	PI value	Mean of PI
500	77	47	22.7	-0.9	-0.85
1,000	62	51	19.5	-0.4	-0.4
1,500	52	51	22.5	-0.9	-0.9
2,000	45	51	27.5	-1.2	-1.2

Fig. 2 Appropriate blending velocity



increase in blending time at 140 °C also increases the softening point from 54 to 57 and its penetration index (PI) value. A similar trend could be seen at 160 °C mix temperature whereby an increase in the blending time from 30 to 60 min also increases the softening point temperature from 50 to 60. A possible explanation for this phenomenon may be the dispersion of NPA in asphalt binder which shows that longer blending time is gave better dispersion of NPA in asphalt binder which also resulted in stiffer asphalt binder, hence increasing the softening point value [13]. Meanwhile, the blending time appears to not have any significant effect on the penetration value except for the blending time at 160 °C. Based on these results, the blending velocity of 1,650 rpm at blending temperature of 140 °C with blending time of 60 min were selected as mixing variables in this study.

3.3 Determination of Optimum Polymer Content

The final evaluation of this study is to determine the optimum proportion of NPA. The amount of polymer used in this study varies from 0 to 10 % by weight of asphalt binder with an increment of 2 % for each blend. The blending time of 1,650 rpm at blending temperature of 140 °C with blending time of 60 min were used as mixing variables. Further evaluation using physical properties testing [Penetration, softening point and penetration index (PI)] were conducted to determine the best proportion NPA content. Figure 4 shows the physical properties

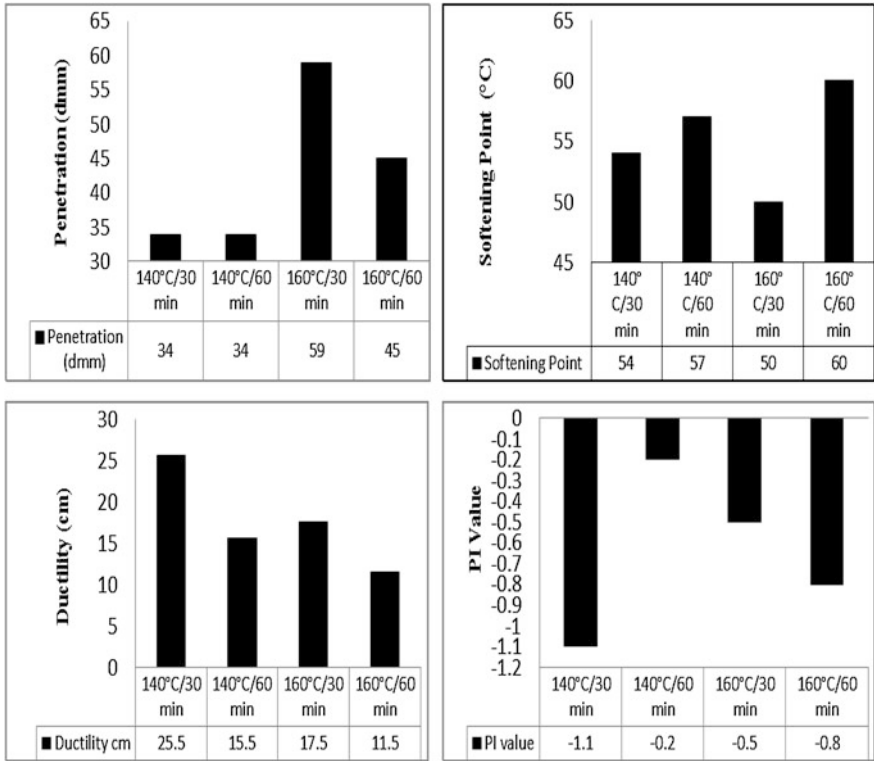


Fig. 3 Appropriate blending velocity

[softening point, penetration and penetration index (PI)] of the binder in determining the optimum proportion of NPA. Based on this figure, the penetration value of conventional binder (80/100 penetration grade) is 92 dmm. The result shows that, the penetration value decreased from 92 to 70 and 64 respectively with the addition of 2 and 4 % NPA, which shows the tendency of strength. The penetration value then increase as more NPA is added which resulted in lacked of homogeneity in the binder mixture. At 6 % NPA by weight, the penetration value shows a return point to the value of 64. After that, the addition of more NPA content (8 and 10 %) increased the penetration value from 64 to 65 and 66 respectively. Again, these penetration results have shown that, excess NPA content will affect the dispersion of NPA in asphalt and will cause the mixture to become softer which is indicated by the higher penetration value [13].

In terms of softening point, it can be seen that the softening point temperature increases with an increase in NPA content at the initial stage (2 and 4 %). After that, the softening point gradually decreased as more NPA is added. The maximum softening point temperature was achieved at 4 % NPA content. This phenomenon may have happened due to the condition of NPA. When mixing, NPA which

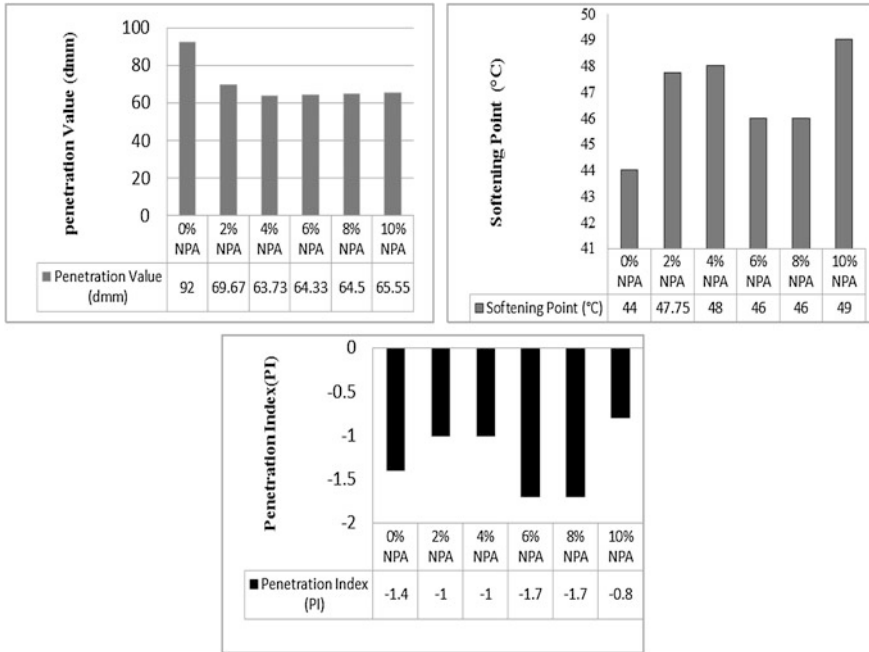


Fig. 4 Physical properties of asphalt binder at different NPA content

consists of a complex molecular chain in the asphalt tends to harden the mix which will cause difficulties to soften the mixture. However, at a high NPA content (6 and 8 %) the softening point temperature tends to decrease from 48 to 46. The lowering of the softening point temperature may be due to the excess NPA content. The excess NPA content will affect the dispersion of polyacrylate in the asphalt and cause the mixture to become softer [13].

This figure also shows the penetration index value of the modified binder. Penetration index indicates temperature susceptibility. The penetration index (PI) shows the sensitivity of asphalt to temperature change. Higher PI values indicate lower thermal susceptibility which is that the roads have sensitivity to temperature changing and can be indicated the trend on durability of the roads. According to [14] the value of PI ranges from around -3 for highly temperature susceptible bitumens to around $+7$ for highly blown low-temperature susceptible (high PI) bitumen. Generally, asphalt binder has negative PI value. Figure 4 shows the graph of PI results. Based on this result, it shows that adding more NPA polymer could increase PI value. It means NPA polymer helps reduce temperature susceptibility due to an increase in softening point and reduction in penetration value. This shows that adding more percentage of NPA will increase PI value at 2 and 4 %. The PI value showed a decrease after adding 6 and 8 % of NPA, however increased again when NPA is added to 10 %. This shows that excess of NPA affects the dispersion of polymer in asphalt causing the mixed asphalt with high

penetration value (asphalt would be softer.). The optimum content of NPA that should be added as modifier is 6 % by the weight of binder because at 6 % the penetration and softening point value shows a return point. This means that percentage of modifier has exceeded the limit and cause the modified binder become softer. At that particular point the percentage for optimum content of polyacrylate is selected. Therefore, based on these result, 6 % of NPA content was selected as the optimum amount of polymer that could be added to the conventional binder.

4 Conclusions

Based on the results obtained from this study, the following conclusions have been reached:

1. The optimum mixing speed, temperature and time for NPA is 1,650 rpm, 140 °C and 60 min.
2. The optimum percentage of the NPA selected is 6 % by weight of the binder.
3. The addition of the NPA to the binder will decrease the penetration value and increase the softening point of the bitumen.
4. The PI value of the bitumen increase as more NPA is added to the bitumen. The penetration and softening point have demonstrated the increased in stiffness (hardness) and improve the temperature susceptibility of the NPA polymer modified binders.
5. Based on the PI value, the presence of NPA polymer improves the temperature susceptibility of the asphalt. The asphalt mixtures containing asphalt binder with higher PI are more resistant to low temperature cracking as well as permanent deformation (rutting).

As a conclusion, the NPA is feasible to be used as asphalt modifier to enhance the properties of the binder in terms of temperature susceptibility and physical properties. The NPA also has potential for strength and durability improvement in the field of pavement material and construction compared to conventional asphalt binder.

Acknowledgments Special thanks to the Research Management Institute (RMI) of Universiti Teknologi MARA for providing the financial support under Excellent fund. The authors would like to thank the Faculty of Civil Engineering, Universiti Teknologi MARA Malaysia for providing the experimental facilities and to all technicians at Highway and Traffic Engineering Laboratory.

Sponsor by Research Management Institute (RMI), Universiti Teknologi Mara (UiTM).

References

1. E.R. Brown, S.A. Cross, A national study of rutting in hot mix asphalt (HMA) pavements. NCAT report No. 92–95, Auburn University, Auburn, AI, 1992
2. G.D. Airey, Rheological evaluation of ethylene vinyl acetate polymer modified bitumen. *J. Constr. Build. Mater.* **16**, 473–487 (2002)
3. G. Polacco, Rheological properties of asphalt/SBS/clay blends. *Eur. Polymer J.* **44**(11), 3512–3521 (2008)
4. T. Nrachai, P. Chayatan, L. Direk, The modification of asphalt with natural rubber latex. *Proc. East. Asia Soc. Transp. Stud.* **5**, 679–694 (2005)
5. U. Isacson, X. Lu, Testing and appraisal of polymer modified road bitumens, state of the art. *Mater. Struct.* **28**(1995), 139–159 (2000)
6. M. Alexander, P. Dubois, Polymer-layered silicate nanocomposites: Preparation, properties and uses of a new class of materials. *Master Sci. Eng.* **28**(1–2), 1–63 (2000)
7. R.K. Gupta, V. Pasanovic-Zujo, S.N. Bhattacharya, Shear and extensional rheology of EVA/layered silicate nanocomposites. *J. Nonnewton. Fluid Mech* **128**(2–3), 116–125 (2005)
8. G. Ojtaba, M.M. Seyed, T. Majid, J.K. Reza, Modification of stone matrix asphalt with nano-SiO₂. *J. Basic Appl. Sci. Res.* **2**(2), 1338–1344 (2012)
9. M.E. Abdullah, K.A. Zamhari, N. Nayan, M.R. Hainin, M. Hermadi, Physical properties and storage stability of asphalt binder modified with nanoclay and warm mix asphalt additives. *World J. Eng.* **9**(2), 155–160 (2012)
10. S.W. Goh, M. Akin, Z. You, X. Shi, Effect of deicing solutions on the tensile strength of micro- or nano-modified asphalt mixture. *Constr. Build. Mater.* **25**, 195–200 (2011)
11. M. Sureshkumar, S. Filippi, G. Polacco, I. Kazatchkov, J. Stastna, L. Zanzotto, Internal structure and linear viscoelastic properties of EVA/asphalt nanocomposites. *Eur. Polymer J.* **46**, 621–633 (2010)
12. G. Rusbintardjo, R. Hainin, Bitumen modification using oil palm fruit ash for stone mastic asphalt. Doctor of philosophy thesis, Faculty of Civil Engineering Universiti Teknologi Malaysia, 2011
13. V. Nopparat, P. Jaratsri, N. Nuchanat, Modification of asphalt cement by natural rubber for pavement construction. *Rubber Thai. J.* **1**, 32–39 (2012). (Journal home page: www.rubberthai.com)
14. J. Read, D. Whiteoak, *The Shell Bitumen Handbook*, 5th edn. (Thomas Telford Publishing, London, 2003), pp. 62–66, 136. (Thomas Telford Ltd, 1 Heron Quay, London E14 4JD)

How Much Money Can Be Saved? Impact of Driving Style on Bus Fuel Consumption

M. Rohani and R. Buhari

Abstract This paper presents the influences of driving style on bus fuel consumption. The study conducted was based on real data collected in Southampton UK using two research buses. This study has confirmed that the aggressive driving consumed significantly higher fuel consumption than economic and normal driving. It was estimated that, driving shifting from aggressive toward economic style can reduce approximately 16.86 l diesel fuel consumption and save about GBP 25.46 daily for a single bus.

Keywords Component · Formatting · Style · Styling

1 Introduction

There is no standard definition of eco-driving that existed in the literature. Available definitions of eco-driving suggested by a previous researchers tend to relate the driving behaviour with fuel economical. For example, ECOWILL [1] describes eco-driving as a smarter and fuel-efficient driving that represents a new driving culture. Eco-driving makes the best use of advanced vehicle technologies and improves road safety. Other researchers, Baltuti [2] describes the ‘eco’ in eco-driving as a driving style which takes ecologic and economic benefit considerations. The ecological and economical benefits are significantly reduced fuel consumption and green house effect.

Boriboonsomsin et al. [3] suggested the eco-driving as one of the conservation programs that can be very cost effective. Various advice such as shifting to a higher gear as soon possible, maintaining steady speeds, anticipating traffic flow,

M. Rohani (✉) · R. Buhari
Smart Driving Research Center, Faculty of Civil and Environmental Engineering,
Universiti Tun Hussein Onn Malaysia, Batu Pahat, Malaysia
e-mail: munzilah@uthm.edu.my

accelerating and decelerating smoothly, keeping the vehicle and keeping the vehicle in good maintenance through the eco-driving tips are aimed to minimise fuel consumption while driving [3].

Many eco-driving projects conducted to date concentrate on providing eco-driving advice, by mean of training to drivers. For example, CIVITAS [4], a bus company in Tallinn, provides eco-driving training for its drivers. The bus company looks an eco-driving as an element to address problems such as pollution, noise, emission and also to improve the company's passenger satisfaction in comfort and safety. In Australia, a pilot study conducted by Rose and Symmons [5] suggested that heavy duty bus driver who attended the full eco-driving training significantly use lower fuel consumption than the driver who did not attend the training.

Other methods applied for eco-driving monitoring is by the application of a special device. For example, Boriboonsomsin et al. [3] found that an on-board eco-driving device has made an improvement in driver behaviour. The use of the device is to make real-time instantaneous fuel consumption as a result from driving behaviour available to be seen by the driver. The fuel data guides the driver to a more economical driving. As a result average fuel economy improves 6 % on city streets and 1 % on highway.

Stagecoach is a bus company in the UK that invested multi-million pound sterling on eco-driving technology [6]. The investment includes the installation of GreenRoad system in 6,500 buses in Scotland, England and Wales. The scheme is targeted to reduce 4 % fuel consumption and accident rate. GreenRoad system used is an on-board system that provides driver with real-time feedback on their driving style. The information provided includes speed, braking, acceleration, lane-handling and turning. Further to the system, the Stagecoach also is one of the first UK bus companies that applies a new GreenRoad's new engine idling solution. This new system is able to monitor specific trips by identifying unnecessary idling based on agreed thresholds.

Foot-LITE is an ongoing UK-based project on eco-driving that provide both online and offline feedback for driver. The project is aimed to address an important parameter in vehicle driving such as engine speed, gear choice and throttle position [7]. In the system proposed, driving feedback will be delivered to the driver in order to promote the take up and retention of eco-driving efficient and safe driver behaviour. The system is also able to monitor driver's behaviour, road network conditions and vehicle metrics [7]. The advance system in Foot-LITE project analyse all gathered data via an on-board device. From the analysis driver will be provided all related information, advice and useful reminders.

Bus driver eco-driving substantially benefit to bus operational cost, environment and safety. Specifically, Vogel [8] list the advantages of eco-driving as follows;

- More cost-effective driving
- Less pollution
- Quicker journeys
- Greater road safety

- Less wear and tear on vehicle parts
- Longer life-span of tires
- More driving comfort

In Europe, eco-driving program has started to establish more seriously in 2001 [9]. The program is partly financed by the former European Energy Efficiency Programme (EEEP). It is co-ordinated by the Austrian Energy Agency (AEA). The project was targeted at specific groups of driver and successfully reduced 5–20 % fuel consumption in various countries such as German, and Switzerland.

2 Research Setting and Approach

2.1 Research Aim

The objective of this research is to compare the bus fuel consumption between different driving styles (economic, normal and aggressive). It is also estimate how much saving can be attained from driving style changes.

2.2 Research Approach

This study was conducted in urban driving environment in Southampton, UK areas. During the period of data collection, 54 UniLink bus drivers driving styles were monitored within the same route continuously during bus service operation hours. However, for the analysis purposes, the focus has been given only on instantaneous driving style 10 s after the driver leaving from stationary at selected bus stops, signalized intersections and roundabout. The selection of these 10 s data is based on the highest rate of acceleration and fuel consumption observed from the real data that strongly considered for research analysis.

2.3 Research Equipment and Data

Data used in this study was collected on-board using 2 research buses; a Mercedes-Benz Citaro and Scania Omnicity which were equipped with an automatic transmission of 6 and 5 gears respectively. The engines of the buses are also different. The Mercedes Citaro complies with Euro 4 emission standard while Scania Omnicity complies Euro 5 and EEV. Both buses were operated by UniLink, a bus company from Southampton, UK.

On-board device, a Portable Vehicle CANBus Systems (PVCS) was installed on research buses to collect real time data. The PVCS iLogCAN data logger developed by Squarell technology is designed with a Fleet Management System (FMS) interface to monitor a CANbus activity under actual on-road driving. This special device was used to capture bus location, speed, and the behaviour of the driver who controls the accelerator pedal as well as the instantaneous fuel consumption.

Seven study sites selected in this study are 3 bus stops, 3 signalised intersections and 1 roundabout. For all study sites the general characteristics of the site and data collected are summarised as follow:

- On each site, the road segment has one lane for both directions and is fairly flat with a minor grade.
- The traffic condition between sites in the same group is fairly similar.
- The bus stop type for each study site is 'bus stop marking on the carriageway', which is referred as 'bus cage'.
- Only behaviour from passing straight ahead at signalised intersection is included in the data analysis at such intersections (no right or left turn is counted).
- Only behaviour from passing through is included in the data analysis at such roundabout.

2.4 Clustering driving Style

Bus driver driving behaviours data were clustered into three driving styles; aggressive, normal and economic. In this study, the cluster analysis applied involved 4 steps of analysis

- Selection of variables,
- Determination of cluster hierarchy in the variables using hierarchical analysis
- Cluster analysis using K-mean method and
- Cluster validation using discriminant analysis

Further explanation of cluster analysis in this study is available from [10].

3 Results and Discussion

In this study, the correlation between fuel consumption and clustered driving style was assessed. Spearman Rho correlation analysis was conducted aim to explore the relationship between clustered driving style with average fuel consumption. Result from analysis for both Mercedes and Scania buses is shown in Table 1. The finding from this result indicated that, the driving style has a significant correlation with

Table 1 Spearman Rho correlation between average fuel consumption with clustered driving style

Bus		Clustered driving style
Mercedes Citaro	Average fuel consumption	0.472 ^a
	Clustered driving style	1.000
Scania OmniCity	Average fuel consumption	0.300
	Clustered driving style	1.000

^a Correlation is significant at 0.05 level (2-tailed)

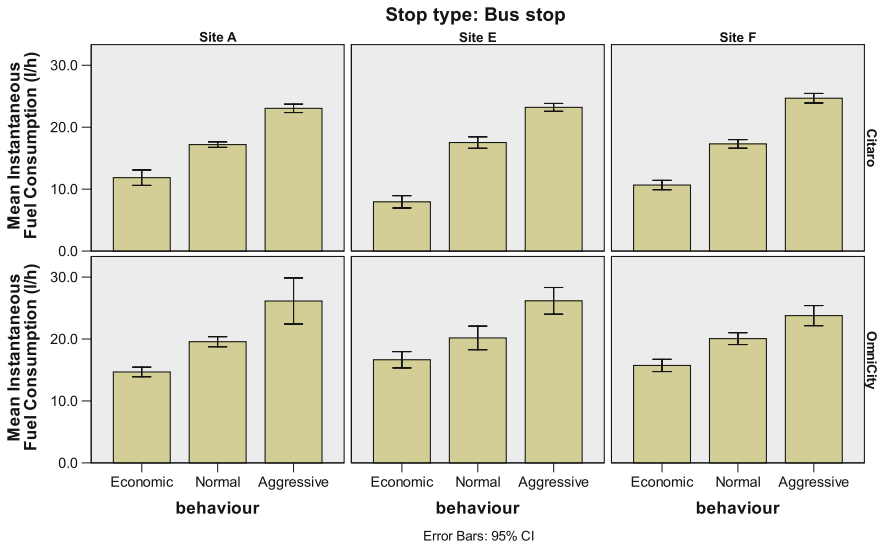


Fig. 1 Comparison of bus fuel consumption between economic, normal and aggressive driving at difference study sites (bus stop)

average fuel consumption. This also can be seen graphically from Figs. 1, 2 and 3 which demonstrated that the fuel consumption increase as the driving behavior change from economic to normal and aggressive respectively.

Further analysis for the research data was also conducted to test the significant different in fuel consumption from one behavior to another. To conduct this, a Mann–Whitney test was used. The result from Table 2 shows that, for both research buses, the aggressive bus driving at most of study sites consumed significant higher fuel consumption than that of normal and economic bus driving ($p < 0.016$). However, this result is not significant at Site D for Scania bus. Nevertheless the higher mean found in aggressive driving (see Fig. 3) indicated that the driver used slightly higher fuel consumption than the normal driver.

Regarding the how much the fuel cost can be saved from driving style change when leaving from bus stop, signaled intersection and roundabout, Table 3

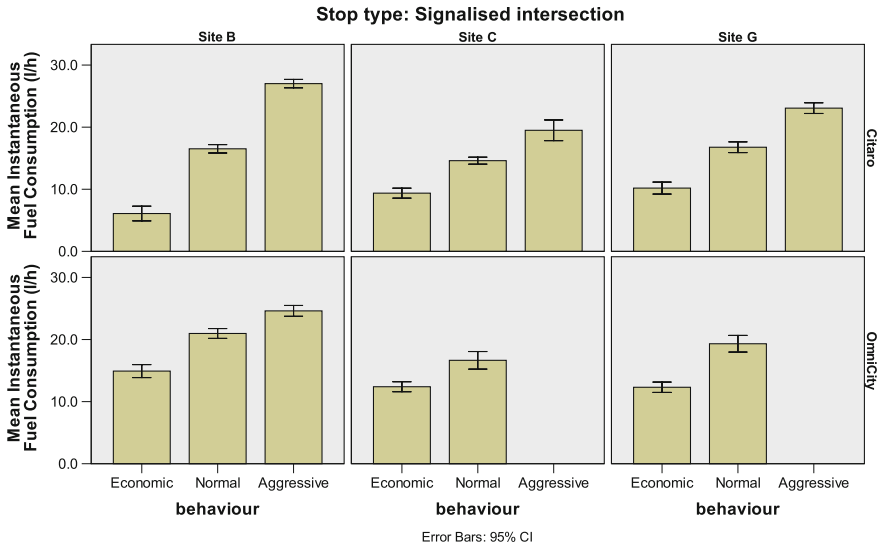


Fig. 2 Comparison of bus fuel consumption between economic, normal and aggressive driving style at different study sites (signalised intersection)

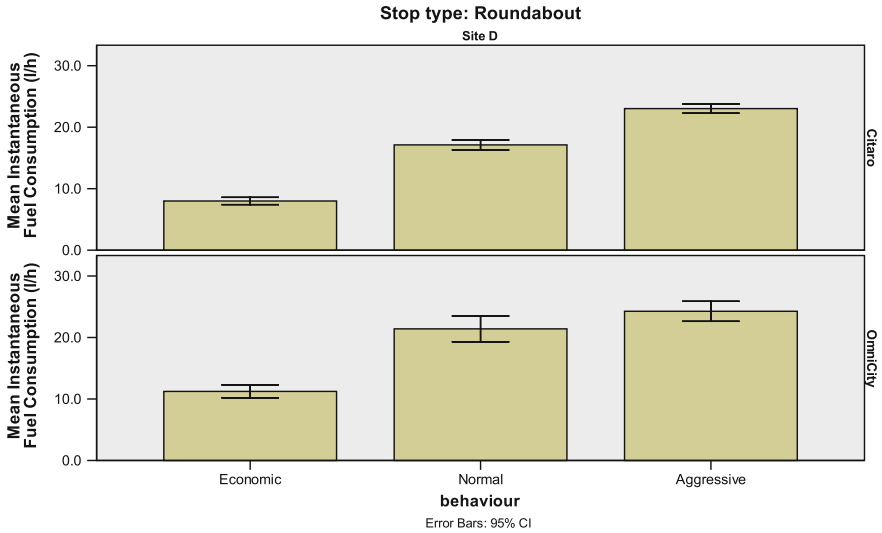


Fig. 3 Comparison of bus fuel consumption between economic, normal and aggressive driving style at roundabout

Table 2 Comparison test for instantaneous fuel consumption between aggressive, economic and normal driving

Clustered driving style	Stop type	Site	Bus	Sig. (2-tailed)
Economic versus normal driving	Bus stop	Site A	Citaro	0.0000001
			OmniCity	0.0000001
		Site E	Citaro	0.0000001
			OmniCity	0.002
		Site F	Citaro	0.0000001
			OmniCity	0.0000001
	Signalised intersection	Site B	Citaro	0.0000001
			OmniCity	0.0000003
		Site G	Citaro	0.0000001
			OmniCity	0.0000004
		Site C	Citaro	0.000001
			OmniCity	0.000001
Roundabout	Site D	Citaro	0.0000001	
		OmniCity	0.078	
Normal versus aggressive driving	Bus stop	Site A	Citaro	0.00000003
			OmniCity	0.0000001
		Site E	Citaro	0.00000001
			OmniCity	0.000004
		Site F	Citaro	0.000001
			OmniCity	0.001
	Signalised intersection	Site B	Citaro	0.000002
			OmniCity	0.00001
		Site G	Citaro	0.000005
			OmniCity	0.000001
		Site C	Citaro	0.0000001
			OmniCity	–
Roundabout	Site D	Citaro	0.0000003	
		OmniCity	0.000001	
Aggressive versus economic driving	Bus stop	Site A	Citaro	0.0000001
			OmniCity	0.0000001
		Site E	Citaro	0.0000001
			OmniCity	0.0000001
		Site F	Citaro	0.0000003
			OmniCity	0.0000001
	Signalised intersection	Site B	Citaro	0.0000001
			OmniCity	0.0000001
		Site G	Citaro	0.0000001
			OmniCity	0.0000002
		Site C	Citaro	0.0000005
			OmniCity	–
Roundabout	Site D	Citaro	0.0000001	
		OmniCity	0.0000001	

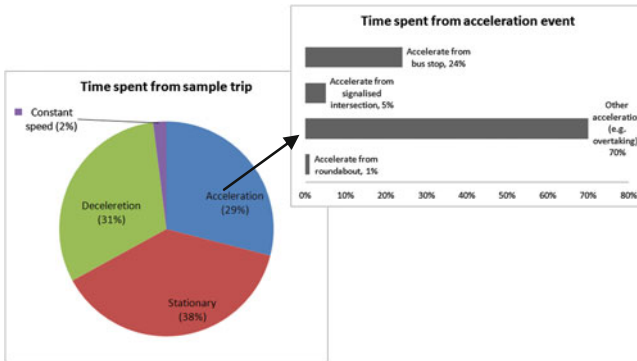


Fig. 4 Percentage of time spent on stationary, acceleration, deceleration and constant speed observed from normal driving and specific acceleration events behaviour

presents the calculation of the mean of instantaneous and percentage of fuel saving from driving style shifting from normal to economic, aggressive to normal and aggressive to economic. The estimation within all the study sites and research buses indicated that, the percentage of fuel saving from driving style shifting varied between 17 and 77 %. The analysis conducted also shows that driving shifting from normal to economic and aggressive to normal can promote fuel saving of up to 37 and 24 % respectively. The greatest fuel saving was observed to be from aggressive to economic (52 %) driving shift. This result is considerably accepted since fuel consumption is dependent on various factors such as road geometry, traffic condition and bus technology.

Saving benefit from driving style shift can be further estimated based on a daily and monthly trip basis. To estimate the bus fuel cost, a real driving profile from sampled data was taken (data was collected in Southampton, UK). The driver took 2 h 30 min to complete the journey from Southampton General Hospital (SGH) to Dock Gate 4 at Southampton city centre and getting back to SGH. Within the journey, the driver stopped 60 times at bus stops, 12 times at signalised intersections and 2 times at roundabouts. Assumption was made that the driver always adopted normal driving style at all stop types.

Figure 4 shows the percentage of each driving phase (acceleration, deceleration, stationary, and constant speed) observed from the data. Time spent within the bus trip at stationary, acceleration, deceleration and constant speed were 38, 29, 31 and 2 % respectively. Within the acceleration phase, 30 % of the times were spent to accelerate the bus away from bus stop, signalised intersection and roundabout (percentage was considered only the 10 s strong acceleration). The proportion of fuel consumption within the trip is shown in Fig. 5. The calculation of fuel consumption of the driving profile showed that, driver spent 74 % of the fuel consumption on acceleration, 13 % on deceleration, and 13 % on stationary and constant speed. It was also observed from the data that, driver used 16.99 l diesel

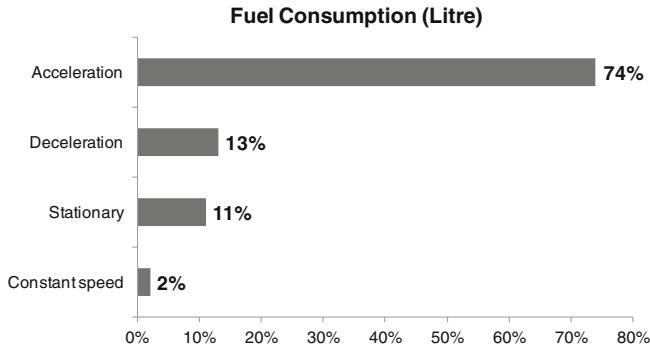


Fig. 5 Proportion of fuel Consumption of normal driving

to complete 1 trip duty. From this figure, percentage fuel spent on acceleration was calculated as 12.63 l (refer Fig. 5 and Table 3).

Tables 4, 5, 6, 7, 8 presents daily fuel consumption from sample data and the calculation of estimated fuel consumption and fuel cost for economic, normal and aggressive driving. For economic driving, it was estimated that fuel consumed from acceleration phase leaving bus stops, roundabouts and signalised intersections were 1.69, 0.04 and 0.29 l respectively. By assuming that the fuel consumption from other driving events were at the same rate, the result of total fuel consumption for the entire trip was observed to be lower than normal driving (19.85 L). Similarly, aggressive driving was estimated to consume 22.66 l diesels for the whole trip.

From the estimation of fuel consumption, the daily fuel usage can be calculated. Assume that the bus operated 6 trips daily; therefore the total fuel consumption for economic, normal and aggressive are 119.1, 128.04 and 135.96 l respectively.

The analysis conducted show that, fuel saving from driving shift benefit to reduce bus operational costs. For example, driving shift from aggressive towards economic, save 16.86 l diesel daily. If the diesel price is GBP 1.51 per litre, the bus company can save GBP 25.46. Across the fleet, if the company owned 10 buses, this can save GBP 256.6 daily or GBP 7,637.58 monthly.

Table 3 Mean of instantaneous fuel consumption and percentage of fuel consumption saving from driving style shifting at bus stop, signalised intersection and roundabout

Citaro	Stop type	Driving style				Percentage saving from driving style shifting			
		Economic		Normal		Aggressive		Normal to economic	Aggressive to economic
		Mean instantaneous fuel consumption (l/h)	Normal instantaneous fuel consumption (l/h)	Mean instantaneous fuel consumption (l/h)	Aggressive instantaneous fuel consumption (l/h)	Normal to normal	Aggressive to normal		
	Bus stop	11.852	17.191	23.045	31.06	25.40	48.57		
	Site A								
	Site E	7.949	17.522	23.203	54.63	24.48	65.74		
	Site F	10.660	17.303	24.681	38.39	29.89	56.81		
	Site	6.091	16.516	27.011	63.12	38.86	77.45		
	Signalised intersection								
	Site B								
	Site C	9.373	14.604	19.494	35.82	25.09	51.92		
	Site G	10.188	16.768	23.065	39.24	27.30	55.83		
	Roundabout								
	Site D	7.998	17.123	23.025	53.29	25.64	65.26		
	Site	14.683	19.564	26.140	24.95	25.16	43.83		
	Bus stop								
	Site A	16.652	20.178	26.166	17.47	22.88	36.36		
	Site F	15.735	20.065	23.777	21.58	15.61	33.82		
	Site	14.919	20.977	24.614	28.88	14.78	39.39		
	Signalised intersection								
	Site B	12.399	16.653		25.54	-	-		
	Site C	12.314	19.321		36.26	-	-		
	Site G	11.233	21.405	24.261	47.52	11.77	53.70		
	Roundabout								
	Site D								
	Average				36.983	23.90	52.39		

Table 4 Daily fuel consumption from sample data

Driving profile	Time spent from sample trip (s)	Percentage	Average fuel consumption (l/h)	Fuel consumption (l)	Fuel consumption (%)
Constant speed (A)	129.4	1.56	6.84	0.25	1.45
Acceleration	2,441.6	29.45	18.62	12.63	74.36
Deceleration (B)	2,564.8	30.93	3.17	2.26	13.30
Stationary (C)	3,155.7	38.06	2.11	1.85	10.89
Total fuel consumption				16.99	100
Total fuel consumption excluding fuel from acceleration, (A + B + C)				4.36	25.64

Table 5 Estimated fuel consumption for normal driving style

Acceleration from	Time spent from sample trip (s)	Percentage	Average fuel consumption (l/h)	Fuel consumption (l)	Total fuel consumption from trip (l)
Bus stop	600	26.53	17.34	2.89	16.98 + 4.36 = 21.34
Roundabout	20	0.88	17.12	0.10	
Signalised intersection	120	5.31	15.96	0.53	
Other points (e.g. overtaking)	1,521.6	67.28	–	9.11	

Table 6 Estimated fuel consumption for economic driving style

Acceleration from	Time spent from sample trip (s)	Percentage	Average fuel consumption (l/h)	Fuel consumption (l)	Total fuel consumption from trip
Bus stop	600	26.53	10.15	1.69	15.49 + 4.36 = 19.85
Roundabout	20	0.88	8	0.04	
Signalised intersection	120	5.31	8.6	0.29	
Other points (e.g. overtaking)	1,521.6	67.28		9.11	

Table 7 Estimated fuel consumption for aggressive driving style

Acceleration from	Time spent from sample trip (s)	Percentage	Average fuel consumption (l/h)	Fuel consumption (l)	Total fuel consumption from trip
Bus stop	600	26.53	23.64	3.94	$18.30 + 4.36 = 22.66$
Roundabout	20	0.88	23.03	0.13	
Signalised intersection	120	5.31	23.19	0.77	
Other points (e.g. overtaking)	1,521.6	67.28		9.11	

Table 8 Estimated daily fuel consumption and fuel cost

	Economic driving	Normal driving	Aggressive driving
Daily fuel consumption*	$19.85 \times 6 = 119.1$	$21.34 \times 6 = 128.04$	$22.66 \times 6 = 135.96$
Daily fuel cost**	$119.1 \times 1.51 = 179.84$	$128.04 \times 1.51 = 193.34$	$135.96 \times 1.51 = 205.30$

*Assume that, the bus operated 6 trips daily

**Assume that, 1 l diesel price is GBP 1.51

4 Conclusion

Research findings suggested that in general, driving style can affect bus fuel consumption and bus operation cost through fuel cost. Aggressive driving after leaving from bus stops, signalized intersection and roundabout were found to consumed extra 23.9 and 52.4 % fuel than the normal and economic style respectively.

The result of this study provides evidence and support previous report of benefit of eco driving on bus fuel consumption [5, 8]. By changing driving style from aggressive to economical style, bus operator can save 16.86 l daily. This amount is worth for GBP 25.46 daily or GBP 763.76 monthly for a single bus. The finding of this study is practically important to ease bus operation cost.

Acknowledgments The Author gratefully acknowledge the contribution of Prof. Mike McDonald and Dr. Tim Felstead from University of Southampton, Ministry of Malaysia Higher Education, Universiti Tun Hussein Onn Malaysia and UniLink.

References

1. ECOWILL, Ecodriving—the concept. Cited 2012 8 July 2012. Available from <http://www.ecodrive.org/en/home/2012>

2. J. Baltutis, Benefit of eco-driving. Low sulphur diesel awareness training and workshop 2010. Cited 2012 8 July 2012. Available from http://www.unep.org/transport/PDFs/Ecodriving/Ecodriving_pwpt.pdf
3. K. Boriboonsomsin, A Vu, M Barth, Eco-driving: Pilot evaluation of driving behaviour changes among U.S. drivers. College of Engineering, Center for Environment Research and Technology, p. 18, (2010)
4. A.M. Orntlich, Eco-driving training for bus drivers. Cited 2012 7 July 2012. Available from http://www.civitas-initiative.org/index.php?id=79&sel_menu=17&measure_id=463
5. G. Rose, M. Symmons, Testing ecodriver training in Australian conditions. in *31st Australian Transport Research Forum*, pp. 183–193 (2012)
6. R. Postlethwaite, Stagecoach multi-million-pound investment in eco-driving technology. Cited 2012 7 July 2012. Available from <http://greenroad.com/press-releases/stagecoach-multi-million-pound-investment-in-eco-driving-technology/2012>
7. R.G. Fairchild, R.G. Using On-board driver feedback systems to encourage safe, ecological and efficient driving: The foot-LITE project. in *The Society for the Study of Artificial Intelligence and Simulation of Behaviour Convention*. Scotland: Proceedings of the Persuasive Technology and Digital Behaviour Intervention Symposium (2009)
8. F.X. Vogel, Eco-driving: An everyday option for reducing petroleum dependence. Sustainable transportation for the 21st century. Cited 2012 7 July 2012. Available from http://www.movingahead2010.com/unite/images/stories/PPT/B1A-Vogel_Francis.pdf (2010)
9. Ecodrive.org, Improves road safety, fuel efficiency and combats climate change. Vienna, p. 12 (2012)
10. M. Rohani, Clustering driving behaviour based on simple K-mean analysis. in *International Review of Civil Engineering (I.R.E.C.E)*, 2, pp. 179–184 (2011)

Neglecting Helmet Usage in Rural Area: Behavioral Causal Factors According to Different Age Groups

Nur Sabahiah and Abdul Sukor

Abstract Helmet law is established to reduce the fatal head injury to motorcyclists when the motorcycle accident occurs. Despite its proven effectiveness, the rate of use of a helmet is actually still lower than what could be achieved by proper legislation and inexpensive enforcement especially in rural areas. This study is focused on the underlying behavioral factors related to different ages of motorcyclist neglecting helmet behavior. The data for this study were obtained by using self-reported questionnaire survey involving 459 motorcyclists in rural area. For analysis purposes, the respondents were divided into three age groups, which are 16–25 years old, 26–40 years old and above 40 years old. The relationship between psychological factors and the neglect of using helmet behavior was analyzed by using ordinal logistic regression. The findings showed that attitude was the strongest affecting factor for helmet use of all groups. The respondents aged 16–25 were affected by their perception of danger and what they perceived on others behavior. The respondents of 26–40 years were affected by perception towards others and the perception of being caught. For respondents aged 40 years and above their neglecting helmet behaviors were influenced by their accident and being ticketed experience.

Keywords Helmet safety · Motorcyclists' behavior · Attitude · Theory of planned behavior

N. Sabahiah (✉) · A. Sukor
School of Civil Engineering, Universiti Sains Malaysia, Engineering Campus, Nibong
Tebal, Penang, Malaysia
e-mail: cesabahiah@eng.usm.my

1 Introduction

Compliance towards helmet usage is an important factor that needed to be addressed in reducing the fatality rate of motorcyclists. Neglecting the helmet usage is regarded as risky behavior because it could lead to death or fatal injury if the motorcyclists involve in an accident. Previous study in Malaysia reported that more than 60 % of all documented fatal injuries to motorcyclists in Malaysia involved head injury cases [1]. Meanwhile, the statistical data from the Royal Malaysian Police (PDRM) in 2002 showed that the head injury was 87 % of the fatal injuries involving motorcyclists [2]. In addition, it is agreed that the use of helmet could reduce the risk of head injury up to 72 % [3].

Actually, helmet legislation in Malaysia started to be enforced in early 1970s. However, the helmet compliance was reported in many versions. According to Krisnan [4] and Radin Umar et al. [5] only 55 % of motorcyclists used helmets properly in 1995 during the absence of the policemen and 41 % in 1998, as reported in the Research Report for National Road Safety Council. Another study reported in [6] showed that 54.4 % of motorcyclists used helmet properly, 13.6 % tied the helmet loosely, 8.0 % did not tie the helmet and 24.0 % did not use the helmet in rural areas.

To increase the awareness on helmet usage in Malaysia, advertisements due to motorcycle campaign were carried out in the national television by the Ministry of Transport, Malaysia [7]. 94.4 % of road users claimed that their awareness on road safety has increased and 97.7 % agreed that the television was the main source for the awareness. In addition, outdoor billboard and newspaper advertisements featuring proper usage of helmets were also used to enhance the awareness [8]. However, the violation towards helmet law was still not resolved, especially in the rural area.

The location factor, between rural and urban locations, was found to be significant to affect the behavior of not using the helmet. Therefore extra effort is needed in order to increase the helmet usage [6]. Similar research was done in Vietnam found that the use of helmet depended on the road hierarchy used by the motorcyclists. The study indicated that the motorcyclists in Vietnam were likely to use the helmet when they used the national road rather than other provincial roads [9]. In Thailand, the usage rate in rural area was also very low compared to in the streets of urban areas [10].

In addition, to understand the factors that influence the motorcycle accident, age has been recognized as one of the risk factors. Chang and Yeh [11] and Crundall et al. [12] reported that the major contribution leading to the risky behaviors in young male motorcyclists is their lack of experience in riding motorcycles. However, Rutter et al. [13] previously reported contradictory results. They claimed that experience factor was not significantly with age. Instead, young motorcyclists tend to show risky behavior because they are young and not because of lack of experience and skills. Meanwhile, older motorcyclists were assumed to be matured and less involved in risky behaviors.

Besides of acknowledging the socio-demographic factors, it is important to investigate the motorcyclists' behavioral and psychological perspective in order to understand the underlying factors that contribute to the neglecting helmet behavior. According to Roger and Rothengatter [14] the application of psychology and behavioral understanding about road users is needed to deal with the complexity of human behavior. It is also supported by Chesam et al. [15] that the study of the behaviors of motorcyclists based on cognitive aspects could be an effective contribution to the policy and engineering practice.

The theory of Planned Behavior is an established behavioral theory that usually used in the studies that relate to risky behaviors [16]. This theory consists of three important elements, which are attitude, perceived behavioral control and subjective norm that lead to the intention of performing the behavior. The attitude was defined as the tendency to evaluate an entity with some degree of favor or disfavor, ordinarily expressed in cognitive, affective and behavioral responses [17].

Meanwhile, perceived behavioral control in the Theory of Planned Behavior can be measured by direct questions on the basis of belief about the ability to deal with specific situations. High level of perceived behavioral control could strengthen a person's intention to perform the behavior. Another component in the Theory of Planned Behavior which is a subjective norm is referred as belief about what important others expect the person to do and coupled with the person's motivation to comply with the expectation. The theory of Planned Behavior has distinguished the social influence to be focused more on the important others such as family and peers. However, descriptive normative element is also suggested to be added in the theory [18]. This is to observe on how the behavior of other peoples in the same the environment could give influence.

Another behavioral theory that is usually concerned with understanding the human behavior is the theory of risk perception [19]. The theory suggests that human actually has a preferred level of risk which they are willing to accept. In parallel, human also adjust their behavior to maintain that preferred level of risk. The perceived danger is believed to be linked with the perception of risk [20]. Persons with low perceived danger would have a higher tendency to engage in risky behaviors than those with lower perceived danger.

Perception of being caught is another factor that related to the violation behavior. In order to avoid the violation behavior, enforcement and rules are necessary because motorcyclists cannot be expected to learn about the negative consequences of behavior from their own experiences [21]. The effectiveness of enforcement is directly related to its perceived threat, which is mostly affected by the likelihood of being arrested.

To date, there are still many gaps in motorcycle safety research in Malaysia that focusing on motorcyclists' psychology and behavioral as causing factors. Therefore this study was aimed to investigate the underlying factors of not wearing a helmet by using the extended Theory of Planned behavior. In reporting this study, this paper is organized as follows: Sect. 2 describes the questionnaire and statistical method that implemented; Sect. 3 presents the results of the analysis of data; finally, Sect. 4 is devoted to discussion and conclusion from the found results.

2 Methodology

In this study, a self-report survey was carried out in typical rural areas in Muar, Johore from June to August 2009. The purpose of the survey was described in the front page of the questionnaire form and the motorcyclists were asked for their willingness to participate in the survey. Those who were willing to answer the questionnaire received souvenirs as a token of appreciation. After excluding the survey forms with missing answers, only 459 survey forms were suitable for further analysis, yielding an effective response rate of 93 %. Overall, the respondents with the age from 16 to 25 years old formed the majority of the sample (62 %). All respondents selected for this study were purposely focused on male.

The behavior of not using a helmet was chosen as the main motorcyclists' risky behavior investigated in this study. The respondents were asked to report their frequency of not using a helmet in the past month according to the 4-point Likert scale (Table 1).

Based on the psychological theories related to the risky behavior, the relevant questions for psychological determinants were constructed. The respondents were asked to answer the questions according to a 4-point Likert scale, ranging from 1 = *strongly agree* to 4 = *strongly disagree* (Table 2). In addition to psychological determinants, respondents' history of motorcycle accidents and experience of being ticketed due to the violation behavior were also investigated. For analysis purposes, the data were divided into three levels of age groups namely from 16 to 25 years old, 26 to 40 years old and more than 40 years old. This is to gain an in-depth understanding of not using helmet behavior according to different level of age groups.

Ordinal logistic regression was used as statistical method in this study because the independent variable (not using helmet) consists of ordinal response. Ordinal logistic regression is the extension of logistic regression for dichotomous outcomes. Thus, the equation for ordinal logistic regression is as follows:

$$\text{logit}(Y \leq i) = \ln \left(\frac{P(Y \leq i)}{1 - P(Y \leq i)} \right) = \alpha_i + \beta_1 x_1 + \beta_2 x_2 + \dots + \beta_m x_m \quad i = 1, \dots, k \quad (1)$$

P (Y) in this study is the probability that a motorcyclist involves in violating the use of helmet behavior, which is the function of a vector of independent variables X. The constant in the equation is α_i , and β_i is the coefficient of the m -th independent variable. In order to examine the psychological factors that contribute to the risky behaviors, logistic regression by using the forward stepwise method was applied. The analysis was done by using the SPSS Ordinal Regression procedure, or Polytomous Universal Model (PLUM), which is an extension of the general linear model to ordinal categorical data. For ordinal logistic regression result, a positive sign for the coefficient relates to the higher score for the dependent variable, while a negative sign of coefficient relates to the lower score of the Likert Scale.

Table 1 Question regarding not using helmet behavior

Behavior	Question	Answer scale
Not using a helmet	My frequency of riding without using helmet in the past month is	1. Never 2. Once 3. More than once 4. More than five times

Table 2 Statement regarding not using helmet behavior

Definition	Question and answer scale
<i>Attitude towards helmet</i>	Using helmet is not enjoyable for me
Respondents' likeliness of not using a helmet	Answer scale 1. Strongly agree 2. Agree 3. Disagree 4. Strongly disagree
<i>Perceived behavior control</i>	It is hard for me to use the helmet while riding the motorcycle
Respondents' perception of their ability whether it is hard or easy to use helmet while riding	Answer scale 1. Strongly agree 2. Agree 3. Disagree 4. Strongly disagree
<i>Perceived danger of not using helmet</i>	For me, riding without using a helmet is dangerous
The respondents feeling of being threatened while riding without using the helmet	Answer scale 1. Strongly agree 2. Agree 3. Disagree 4. Strongly disagree
<i>Fear of being caught</i>	I fear to be caught by the policemen when I ride a motorcycle without using the helmet
Respondents' fear of being caught by policemen while not using a helmet	Answer scale 1. Strongly agree 2. Agree 3. Disagree 4. Strongly disagree
<i>Perceived others' behavior</i>	In my opinion, the percentage of motorcyclists not using the helmet is
Respondents' perception on other human not using a helmet	Answer scale 1. 10–20 % 2. 30–40 % 3. 50 % 4. 60–70 % 5. 80–100 %

Table 3 Proportion of scores for self-reported data on not using helmet behavior

Age range	Distribution of scores (%)				Mean/SD
	Never	Once	More than once	More than 5 times	
16–25 years N = 248	47.20	16.70	19.70	16.40	2.05/1.15
26–40 years N = 111	68.30	9.90	14.90	6.90	1.60/0.98
>40 years N = 100	83.30	7.30	6.30	3.10	1.29/0.72

3 Result

Table 3 presents the proportion analyses for motorcyclists' self-reported data on not using helmet behavior. The mean values show that young respondents aged 16–25 years were more likely not to use the helmet, as compared to the elder motorcyclists. Only 47 % of young respondents claimed that they never neglect the use of helmet in the past month. Meanwhile, 83 % of elder respondents aged more than 40 years claimed that they never neglect the use of helmet in the past month, while 68 % of respondents aged between 26 and 40 years claimed that they never did so. This is in line with the other violation scores where young motorcyclists tended to involve in neglecting the use of helmet behavior compared to the elder motorcyclists.

Tables 4, 5 and 6 below show the psychological factors that influence the motorcyclists' behavior of neglecting the use of helmet according to their age distribution. Attitude and perception of others who neglected the use of helmet behavior significantly affected the respondents' behavior in all cases. This revealed that motorcyclists, regardless of age, would be likely to neglect the use of helmet if they did not prefer using the helmet while riding. In addition, the more they perceived that other motorcyclists tended to neglect using the helmet, the more they were likely to do the same action.

Table 4 shows the psychological determinants that influenced the behavior of not using a helmet for the motorcyclists aged 16–25 years. Other than the attitude and perception other human behavior, the tendency of not using a helmet for this group was also influenced by their less perception towards danger. This reveals that the young motorcyclists, who likely disagree that not using a helmet is a dangerous activity, would be likely to neglect the use of helmets.

Meanwhile, for the respondents aged 26–40 years, their behavior of not using the helmet were also influenced by the less perception of being caught (Table 5). This indicates that the more they perceived on the presence of policemen, the more likely they will comply with the use of helmet however, for the motorcyclists aged more than 40 years, the result in Table 6 shows that their experience of being involved in the accident was the strongest factor that avoids them from violating the use of helmets. This is followed by their attitude, where the respondents who

Table 4 Logistic regression results from not using a helmet (16–25 years)

Variable	Unstandardised coefficient	Standardized coefficient	t-stat	Sig
Attitude	−0.904	−0.504	−7.008***	0.000
Perceived others not using a helmet	1.011	0.462	7.777***	0.000
Perceived danger	0.404	0.037	2.711**	0.007

***p < 0.001; **p < 0.01; *p < 0.05; # p < 0.1

Table 5 Logistic regression results from not using a helmet (26–40 years)

Variable	Unstandardised coefficient	Standardized coefficient	t-stat	Sig
Attitude	−1.559	−0.870	−4.599***	0.000
Perceived others not using a helmet	0.738	0.337	2.436*	0.015
Perception of being caught	0.543	0.258	1.953#	0.051

***p < 0.001; **p < 0.01; *p < 0.05; # p < 0.1

Table 6 Logistic regression results from not using a helmet (more than 40 years)

Variable	Unstandardised coefficient	Standardized coefficient	t-stat	Sig
Own accident experience	−2.286	−0.910	−3.093#	0.082
Attitude	−1.610	−0.899	−2.489***	0.000
The experience of being ticketed	−1.833	−0.727	−3.309**	0.001

***p < 0.001; **p < 0.01; *p < 0.05; # p < 0.1

do not enjoy using the helmet would be likely to neglect the use of helmets. Besides that, the motorcyclists' experience of being ticketed due to the violation of traffic rules would be likely to cause them to comply with the use of helmets. Similar to other age groups, the respondents who perceived that many other motorcyclists involved in not using helmet behavior, they were more likely to engage with the neglect of using helmet behavior.

4 Discussion and Conclusion

The ignorance of helmet law has been considered as an important safety issue especially in the countries that have a high number of motorcyclists [22, 23]. This study aimed to investigate the underlying psychological factors that influenced the motorcyclists' tendency to not using helmets in rural area by comparing the respondents in three groups of age.

First of all, negative attitude towards helmet was found as the most important psychological determinant that instigated the occurrence of neglecting the use of helmet in this study. The attitude was found significant to affect the behavior of all age groups in this study. The effect of attitude towards risky behaviors were confirmed by previous studies [24, 25]. Furthermore, this study also found that the respondents aged 16–25 years had the less perception towards the danger that caused them to not use a helmet. This indicates that for any action to increase the level of helmet use compliance for young motorcyclists, it is needed to understand their level of risk taking behavior and factors that contribute to the risk taking action.

In contrast with the motorcyclists aged 26–40 years, the presence of policemen was found to influence their not using helmet behavior. However, in this study, the level of helmet use compliance for this group was more than 60 %. This finding indicates that to increase the helmet use compliance for the middle age group in the rural area, the enforcement by the presence of policemen is needed. Meanwhile, for the respondents aged more than 40 years, their experience of being involved in accident showed the strongest factor that influenced the use of helmet behavior. It is also supported by another factor namely the experience of being ticketed. This reveals that with age, the motorcyclists would be likely to obey the traffic rules might because of their experience on the accident or experience of being ticketed. In addition, it also shows that the motorcyclists aged 40 and above were already matured and more experience compares to the younger motorcyclists.

In addition, perceived behavior of others also influenced the helmet use in this study. The motorcyclists were tended to be affected by other motorcyclists' behavior on neglecting the use of helmets. This is accordance with previous studies by Yechiam [26], Rosebloom [27] and Fleiter et al. [28] that human tend to rely on the behaviors that displayed by others. Based on this finding, further study is recommended to consider the effect of implementing conformity strategy [29]. According to this strategy, to increase the awareness of using a helmet, motorcyclists should be convinced that many other motorcyclists actually tend to wear the helmet compare to small numbers of motorcyclists that choose to violate the law. They also should be encouraged to conform themselves into the group that complies with the helmet law. However based on the findings in this study the conformity strategy might not influence the motorcyclists with aged 40 and above. This is because this study revealed that if the older motorcyclists had an accident experienced or being ticketed by police, they would likely not involved with the neglecting helmet behavior.

In general, the present study gives some glimpse for road safety policy and practice. It is suggested that in order to tackle the helmet usage problem, it is needed to consider different approaches for different level of age. For example, the young motorcyclists are needed to be tackled through their risk perception. They need to be educated on how to reduce their risk taking behavior while riding on the road. It should be started through the driving/riding school curriculum all over the country. Meanwhile for the older motorcyclists, enforcement in the rural areas seems to be the best implementation that needs to be reinforced. It is believed that by strict continuous enforcement, the rate of using a helmet in rural areas will be increased.

As a conclusion, motorcycle safety cannot be tackled by only focusing on certain issues. The combination of policy, education, inputs from mass media, support from the community and also research that combining the engineering practice and behavioral studies is obviously needed. Therefore, it is hoped that this paper could fill in the gap of the road safety engineering practice especially in the motorcycle safety study.

References

1. T.Y. Pang, R.S. Radin Umar, A.A. Azhar, S. Harwant, A.W. Sharom, M. Abdul Halim, N. Zahari, O. Mohd Shafie, Fatal injuries in Malaysian motorcyclists. *Int. Med. Res. J.* **3**, 115–119 (1999)
2. Royal Malaysian Police, Statistical report road accident Malaysia -2002, Traffic Branch, Bukit Aman, Kuala Lumpur, 2004
3. B.C. Liu, R. Ivers, R. Norton, S. Boufous, S. Blows, S.K. Lo, Helmets for preventing injury in motorcycle riders. *Cochrane Database Syst. Rev.* (2009). Available from URL http://www.thecochranelibrary.com/userfiles/ccoch/file/Safety_on_the_road/CD004333.pdf (Cited 17 Mac 2011)
4. R. Krisnan, in *36th Annual Seminar, National Road Safety Council*, Malaysia, 1995
5. R. Radin Umar, M. Norghani, H. Hussain, H. Shakor, Short and long term plan of action on motorcycle safety program. Research report, 1, 1998
6. S. Kulanthayan, R. Umar, H. Hariza, M. Nasir, Modeling of compliance behavior of motorcyclists to proper usage of safety helmets in Malaysia. *Traffic Inj. Prev.* **2**, 239–246 (2001)
7. M.M.T. Nasir, S. Kulanthayan, A.H. Musa, H. Ahmad Hariza, R.S. Radin Umar, The effectiveness of motorcycle safety campaign: helmet use, conspicuous clothing and illegal racing. Research report 1/2003, Road Research Centre, Universiti Putra Malaysia, 2003
8. R.S.R. Umar, S. Kulanthayan, T.H. Law, A.H. Musa, M.T. Mohd Nasir, Helmet initiative programs in Malaysia. *Pertanika J. Sci. Technol. Suppl.* **13**, 29–40 (2005)
9. D. Hung, M. Stevenson, R. Ivers, Prevalence of helmet use among motorcycle riders in Vietnam. *Inj. Prev.* **12**, 409–413 (2006)
10. V. Kasantikul, J.V. Ouellet, T.A. Smith, Head and neck injuries in fatal motorcycle collision as determined by detailed autopsy, in *Proceedings of the 46th Association for the Advancement of Automotive Medicine Annual Conference*, 2002
11. H. Chang, T. Yeh, Risk factors to driver fatalities in single-vehicle crashes: comparisons between non-motorcycle drivers and motorcyclists. *J. Transp. Eng.* **132**, 227–236 (2006)
12. D. Crundall, P. Bibby, D. Clarke, P. Ward, C. Bartle, Car drivers' attitudes towards motorcyclists: a survey. *Accid. Anal. Prev.* **40**, 983–993 (2008)
13. D. Rutter, L. Quine, D. Chesham, Predicting safe riding behavior and accidents: demography, beliefs, and behavior in motorcycling safety. *Psychol. Health* **10**, 369–386 (1995)
14. J.A. Groeger, J.A. Rothengatter, Traffic psychology and behavior. *Transp. Res. Part F* **1**, 1–9 (1998)
15. D. Chesham, D. Rutter, L. Quine, Motorcycling safety research: a review of the social and behavioral literature. *Soc. Sci. Med.* **37**, 419–429 (1993)
16. I. Ajzen, The theory of planned behavior. *Organ. Behav. Hum. Decis. Process.* **50**, 179–211 (1991)
17. A.H. Eagly, S. Chaiken, *The Psychology of Attitudes*, Belmont (Wadsworth, USA, 1993)

18. R.B. Cialdini, M.R. Trost, Social influence: social norms, conformity, and compliance, in *The Handbook of Social Psychology*, ed. by D. Gilbert, S. Fiske, G. Lindzey (McGraw-Hill, New York, 1998), pp. 151–192
19. L. Sjoberg, The methodology of risk perception research. *Qual. Quant.* **34**, 407–418 (2000)
20. P. Slovic, B. Fishhoff, S. Lichtenstein, Behavioral decision theory perspectives on risk and safety. *Acta Psychol.* **56**, 183–203 (1984)
21. L. Aberg, Traffic rules and traffic safety. *Saf. Sci.* **29**, 205–215 (1998)
22. W. Swaddiwudhipong, C. Boonmak, P. Nguntra, P. Mahasakpan, Effect of motorcycle rider education on changes in risk behaviors and motorcycle related injuries in rural Thailand. *Trop. Med. Int. Health* **3**, 767–770 (1998)
23. M. Lin, S. Chang, L. Pai, P. Keyl, A longitudinal study of risk factors for motorcycle crashes among junior college students in Taiwan. *Accid. Anal. Prev.* **35**, 243–252 (2003)
24. P.D. Pelsmacker, W. Janssens, The effect of norms, attitudes and habits on speeding behavior: Scale development and model building and estimation. *Accid. Anal. Prev.* **39**, 6–15 (2007)
25. H.W. Warner, L. Aberg, Drivers' belief about exceeding the speed limits. *Transp. Res. Part F* **11**, 376–386 (2008)
26. E. Yechiam, M. Druyan, E. Ert, Observing others' behavior and risk taking in decisions from experience. *Judgment Decis. Mak. J.* **3**, 493–500 (2008)
27. T. Rosenbloom, Crossing at red light: behavior of individuals and groups. *Transp. Res. Part F* **12**, 389–394 (2009)
28. J.J.L. Fleiter, J. Alexia, B. Watson, How do other human influence your driving speed? Exploring the 'who' and the 'how' of social influences on speeding from a qualitative perspective. *Transp. Res. Part F: Traffic Psychol. Behav.* **13**, 49–62 (2010)
29. P.W. Schultz, J. Tabanico, T. Rendón, Normative beliefs as agents of influence: basic process and real-world applications, in *Attitudes and Attitude Change*, ed. by R. Prislin, W. Crano (Psychology Press, New York, 2008), pp. 385–409

Pedestrian Egress Behavior During Classroom Evacuation: A Simulation Approach

Masria Mustafa, Zanariah Abd Rahman,
Mohamad Noor Faiz Mohamad Najid and Yasmin Ashaari

Abstract Pedestrians evacuation is a multi-agent system which composed of pedestrians with interaction. Usually, special flow of pedestrians' evacuation occurs in emergency situation such as in case of fire. Interactions between pedestrians become more complicated, when all pedestrians moving towards a bottleneck area. The objective of this study was to examine the egress behavior of pedestrians during panic situation in a classroom environment. The results revealed that the pedestrians behave aggressively in order to evacuate themselves from the bottleneck area and different number of exit in the classroom gives different route choice during the evacuation process.

Keywords Evacuation · Bottleneck · Pedestrians simulation · SimWalk

1 Introduction

An increasing amount of literature is devoted to discuss about the pedestrians movement pattern in indoor or outdoor environment. A better understanding of human behavior is the key to plan to manage the pedestrians flow. In order to

M. Mustafa (✉) · Y. Ashaari
Lecturer, Faculty of Civil Engineering, Universiti Teknologi MARA,
40450 Shah Alam, Selangor, Malaysia
e-mail: masria@salam.uitm.edu.my

Z. A. Rahman
PhD Student, Faculty of Civil Engineering, Universiti Teknologi MARA,
40450 Shah Alam, Selangor, Malaysia

M. N. F. M. Najid
Undergraduate Student, Faculty of Civil Engineering, Universiti Teknologi MARA,
40450 Shah Alam, Selangor, Malaysia

determine the pedestrians' behavior some parameters should be measured such as walking speed, spatial use and person counts [1].

Panic refers to pedestrians' behavior during an emergency situation. Panic is defined by breakdown of ordered, cooperative behavior of individuals due to anxious reactions. Often, panic is characterized by attempted escape of many individuals from a real evacuation process, which may end up in interaction of people in a group [2]. An example of emergency situation is when a building is on fire and pedestrians compete to save themselves through the exit area. High density of pedestrians made the situation become worst which can contribute to pedestrians' accident. In some emergency cases, if the person is not sure the best thing to do at that time, there is a tendency of them to show a herding behavior. Herding behavior as in [3] is defined as "go with the flow" or "follow the other pedestrians".

The initial hypothesis for this study is pedestrians' behavior during a building evacuation which can be determined by analyzing their walking speed. There are different factors affecting the walking speeds of pedestrians as in [4], such as the personal characteristics of pedestrians like age, gender, weight, height and breadth.

The particular problem of pedestrians' behavior during classroom evacuation was found to be important. This study will benefit the users to evacuate the building especially for non-familiar users of the building where often with visiting purposes.

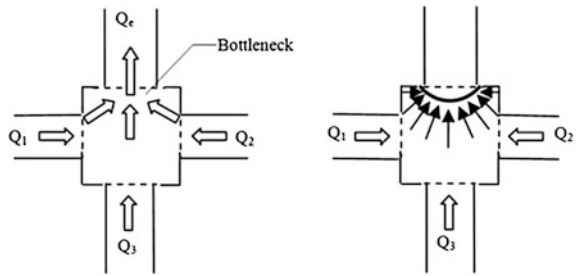
2 Emergencies and Evacuation

Evacuation planning involves constructing plans for rapid movement of people from an emergency affected area. However, these plans are actually constructed only to prepare for emergency, before more information is available about the actual threat. The same evacuation plans are to be used regardless of the origin of hazard and location of people, which might render them unsafe. However, recent new technology of pedestrians' simulation gives advantages to plan an evacuation with more complicated simulated scenarios with different characteristic.

The emergency evacuation processes are affected by many uncertain factors. The factors for real evacuation are traffic accidents, number of deaths from the hazard and number of injuries caused by the evacuation [5]. For trial evacuation, some people are spontaneously evacuated before being told to do so. However, some people refused to be evacuated because they have already know it is only a trial version. In addition, people stated that the alerting method, pedestrians' cooperation and well trained emergency responders contribute to the efficiency and effectiveness of the evacuation process.

In case of emergency, the movement of a pedestrian is more straightforward than in the general cases [3]. The movement of commuters in a railway station for example is more complicated because they choose the route to reach their destination which is usually guided by signboard or map. However, in case of a

Fig. 1 Bottleneck situation as in [6]



building evacuation, the aims and routes used are known and usually the same; i.e.: the exit way. That is why pedestrians’ movement in an emergency case is more straightforward than general cases.

In an emergency situation, pedestrians from any areas or angle who rushed to an exit way would block the pedestrians movement and increase pedestrians density. Therefore, a formation of an arch shape blockings at exit bottlenecks, which instantaneously causes a cease in evacuation flow will occur. When the arches break, the pedestrians will suddenly leave just like avalanche bunches. More seriously, this phenomenon can cause psychological panic that could lead to more dangerous situation. For example, a pedestrian stampede which is one of the most disastrous forms that often leading to fatalities as people are trampled [2]. Figure 1 shows the example of pedestrians’ movement in bottleneck situation where in an emergency situation, crowd route from any areas rushing to an exit would block the crowd movement and increase crowd density and then form an arch shape blockings at exit bottlenecks, which instantaneously causes a cease in evacuation flow. When the arches break, pedestrians will suddenly leave just like avalanche bunches. More seriously, this phenomenon can cause people psychological panic that could cause dangerous situation like a crowd stampede which is one of the most disastrous forms that often leading to fatalities as people are trampled [6].

A well-developed skill in assessing a complex traffic situation and being able to choose and execute an appropriate response are an essential key for a safe pedestrians’ behavior [7]. A model for pedestrians flow and pedestrian dynamics are based from a series of force which include will forces (the desire of the pedestrian to reach a place at a certain time), pedestrian collision avoidance forces, obstacle or wall avoidance forces, pedestrian contact forces and obstacle or wall contact forces. The forces are the results from internal and external forces. The forces are considered as follows:

1. Internal forces: will force, pedestrian collision, obstacle or wall avoidance forces.
2. External forces: pedestrian contact forces, obstacle or wall contact forces.

When the pedestrians’ motion is accurately predicted, it can be used to assess the possibility of safety hazard and operational performance at the event for example in the cinemas or conference center where many people are gathered [8].

Pedestrians' behavior was investigated during the emergency evacuation at Shuangjing Station in Beijing. The result from the evacuation capacity model shows that 8,942 people can be evacuated within 6 min under emergency. It was found that the critically affected elements during the emergency evacuation process were the characteristic of the evacuees, the evacuation facilities and the evacuation organization and management [9].

An evacuation of pedestrians in a transit terminal such as subway station was studied where an agent-based model was used for the evacuation process. The effective evacuation time considered the effect from the density of the occupant and the width of the exit door and automatic fare gates. It was found that the evacuation time becomes longer with the increasing of the occupants' densities and different occupant densities correspond to a different critical exit width. The automatic gates however played the roles of making the evacuation process more orderly [10].

In this study, the focus was on pedestrians' evacuation in case of fire in a building. Pedestrians' evacuation means the method and solution for the pedestrians to move from a danger area to a safer area. Whilst, it means that pedestrians must move using the correct route to ensure their safety.

3 Pedestrian Simulation Model

Modeling a wide range of pedestrians behavior is not simple and some model developed from discrete choice and social force can be used to describe how pedestrian deviate from their free flow behavior due to the presence of other pedestrian [11]. There are several types of Microscopic Pedestrian Simulation Model (MPSM) and to be exact are the Benefit Cost Cellular Model, Magnetic Force Model, Queuing Network Model, Cellular Automata Model and Social Force Model. Many simulation models have been designed and available in the market. Each simulation package has its characteristics and advantages. Some of the examples include AnyLogic, Arena, PanicSim, Exudox, Legion, ProModel, PedGo, Simul8 and KanbaraSim. The pedestrian simulation software has been used widely as a tool in managing the operational and strategies of pedestrians' movement. Social Force Model (SFM), for example has been widely used by simulation software where SimWalk software (developed by Savannah Simulation AG Switzerland) was used as a test bed of this study uses SFM as its fundamental equation to determine the path of the pedestrian [12].

The greatest advantage of the SFM which differentiate it from other MPSM model is the ability in representing the communication between pedestrian in more realistic way. For this distinction, most researchers considered SFM as the representative model for the environmental phenomena that are triggered by the interaction among pedestrians such as congestion. SimWalk is capable to design the pedestrians walking areas and simulating the movement of pedestrians through the shortest route in order to reach destination after evading all the obstacles [12].

There are two types of SimWalk which are SimWalk Pro and SimWalk Transport. SimWalk Pro is use to analyze the safety evaluation of stations, airports, sports stadium, building, etc. while SimWalk Transport is use more on to stimulate and analyze the passenger movements in trains, metro and bus station. Besides, SimWalk can also help to optimize timetable, passenger transfer times and connections. Furthermore, by using this software, we can measure the effectiveness of a transportation system such as density, personal count such as exits or self-defined in space, walking speeds, travel times, space, pedestrians' trails as well as Level of Service (LOS).

4 Methodology and Data Collection

Generally, pedestrian modeling is divided into two different scales which are microscopic models and macroscopic models. In microscopic models, each pedestrian is represented separately as an individual agent and his/her behavior is explored independently. While in macroscopic models, pedestrians are analyzed in groups where it is generally described by mass densities, flow and average velocity [13]. In this study, the simulation method using SimWalk software is categorized as microscopic model that have different types of pedestrians with individual properties such as route selection. Figure 2 shows the example of SimWalk configuration.

SimWalk can be define as a flexible pedestrian simulation software focusing on evacuation, transportation and urban application and it is decision support software for traffic engineers, transit planners, architects and urban planners [14]. The software use a flexible model which allow users to define the density, agent flow, the range of speed for pedestrians, the level of service (LOS), time step and speed loss.

Video recording is a method used for collecting data in this study. Portable Vision Based Traffic Analyser (PVBTA), Video Based Traffic Analysis (TRAIS) and Semi-Automatic Video Analyser (SAVA) software were used for data extraction. Video recording has become common and suitable equipment for empirical pedestrians study. Automatic evaluation of pedestrians' trajectories could be the advantage, but video recording also has its limitations where some recording software such as TRAIS requires user to specify the starting and finishing points of pedestrians manually and the position of the camera should be at suitable place. It is often imply small areas of recording and oblique camera positions. The pedestrians could be hidden in the video in a huge pedestrians' crowd [15].

Data were obtained from a video recording during a trial fire drill that has been conducted in a building at Faculty of Civil Engineering, Universiti Teknologi MARA (UiTM). The fire drill started with the fire alarm and whistle to notify the students in the class that there is an emergency case. They have to move quickly to

Fig. 2 Configuration in SimWalk

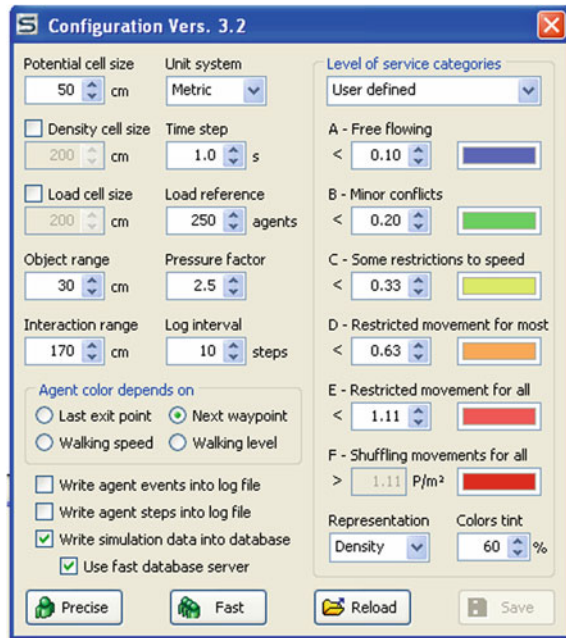
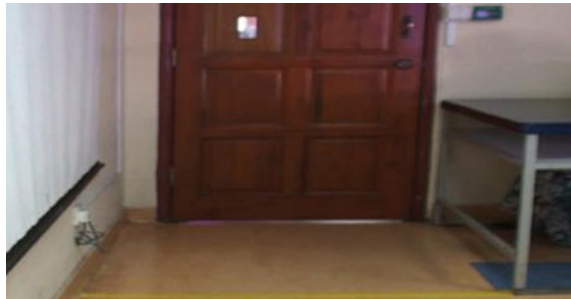


Fig. 3 Exit door in the classroom



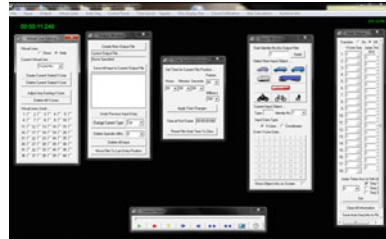
a safe area by using stairs. When all people have left the building and reached the safe area, the evacuation process is considered finished.

PVBTA device had been placed in one of the classroom located at Level 8, Faculty of Civil Engineering, during a fire drill session. Figure 3 shows the exit door in the classroom and the use of a wide lens of the PVBTA enabled the camera to view the entire walking area in the classroom. During the trial, there were 35 students in the class. TRIAS or Video Based Traffic Analysis in Fig. 4 was used to specify the parameter needs in recording the video using PVBTA. SAVA in Fig. 5 is the software that provides a basis for analyzing traffic film data. The basic functionality of the program includes being able to forward the film one frame at a time using the media player controls, arrow keys or the mouse wheel.

Fig. 4 TRIAS



Fig. 5 SAVA



There is a pedestrian application in SAVA which can be used to extract the pedestrian's speed and counting the pedestrians. It was used as the data extraction tools for the video recorded. TRIAS is used only for the video recording with the specific parameters and then SAVA will take place to extract the pedestrians' data of the speed and person counts. After the data was extracted from SAVA, SimWalk was used to validate and simulate the data where some output can be measured such as route selection, walking speed and density.

5 Results and Discussions

5.1 Route Selection

Figure 6 shows the differences between pedestrians' trail during real time (video recording) and simulation. Figure 6a shows pedestrians at the left side of the classroom chosed to use the left lane to go to the exit door. Same goes to the pedestrians at the right side of the classroom. They chosed the right lane to make a move towards the exit door. For pedestrians in the middle row, some used the right lane and some used the left lane to walk to the exit door. On the other hand, in SimWalk simulation (Fig. 6b), the different trail for the pedestrians at the middle row could be seen. All of them used the right side lane to evacuate themselves. That could cause congestion at the right lane and more time will be taken by the pedestrians to reach the exit door. The pedestrians cannot overtake each other because the space is not enough.

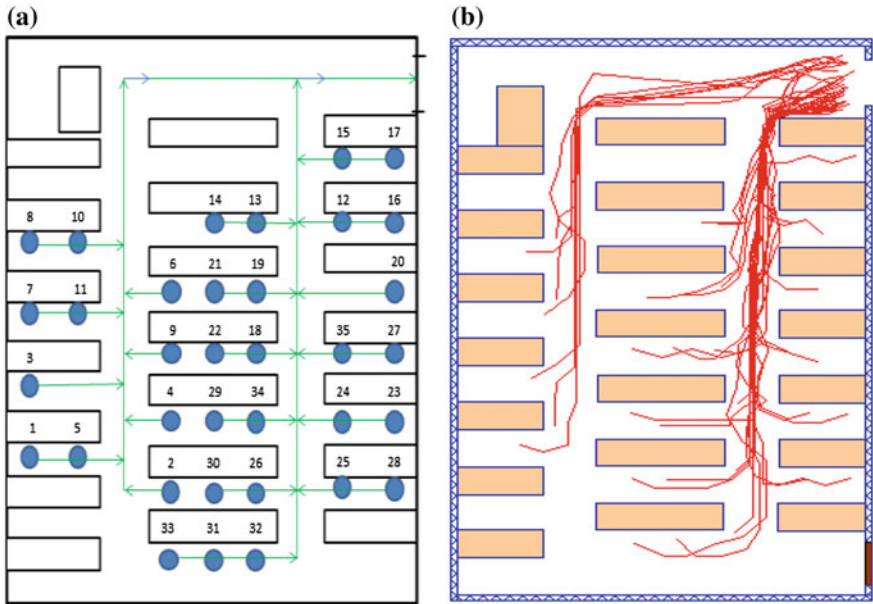


Fig. 6 Comparison of pedestrian's trail between a real (video recording) and b simulation

Figure 7 shows the pedestrians' trail in SimWalk software if only one door open and two doors open. There are many differences if we compare between these figures. Using only one door for evacuation, longer time was needed by the pedestrians to exit the classroom. The evacuation result when only one door was opened is 38s. When both doors are opened, 36s was needed by the pedestrians to leave the classroom.

Figure 7a also shows all pedestrians from the right row and the middle row used the right lane to go to the exit door while pedestrians at the left row of the classroom used the left lane to go to the exit door. The pedestrians from the two lanes will then meet at a point which was at the front lane. The pedestrians can choose to exit the classroom through the front or back door and make a better decision to choose their route to evacuate in a shorter time if any of the exits is congested.

5.2 Pedestrians' Density

Figure 8 shows the difference in maximum density between two situations in a classroom whether only one door open and both door open. Figure 8a (one door open) shows that there are four different colors covering the classroom area. Yellow color ($>1.72P/m^2$) shows a restricted movement for most pedestrians (LOS

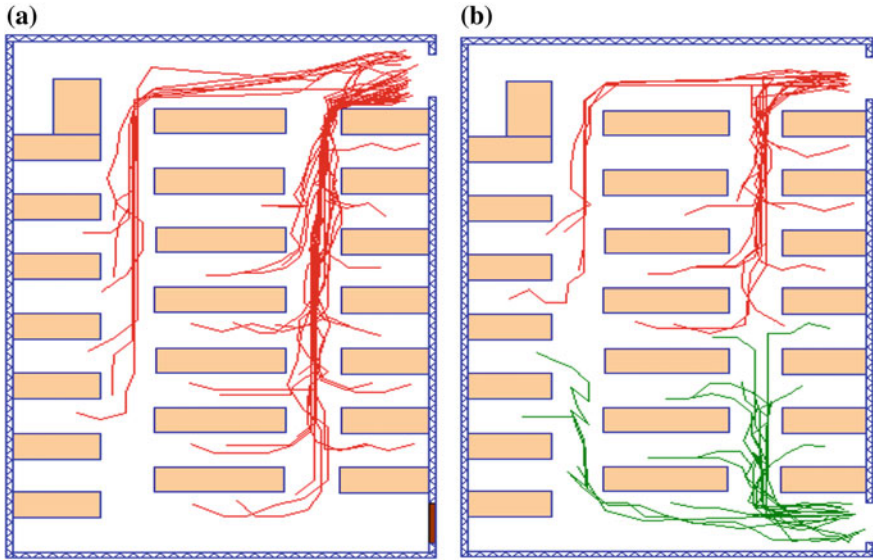


Fig. 7 Comparison of pedestrian's trail between **a** one door open and **b** two doors open in a classroom

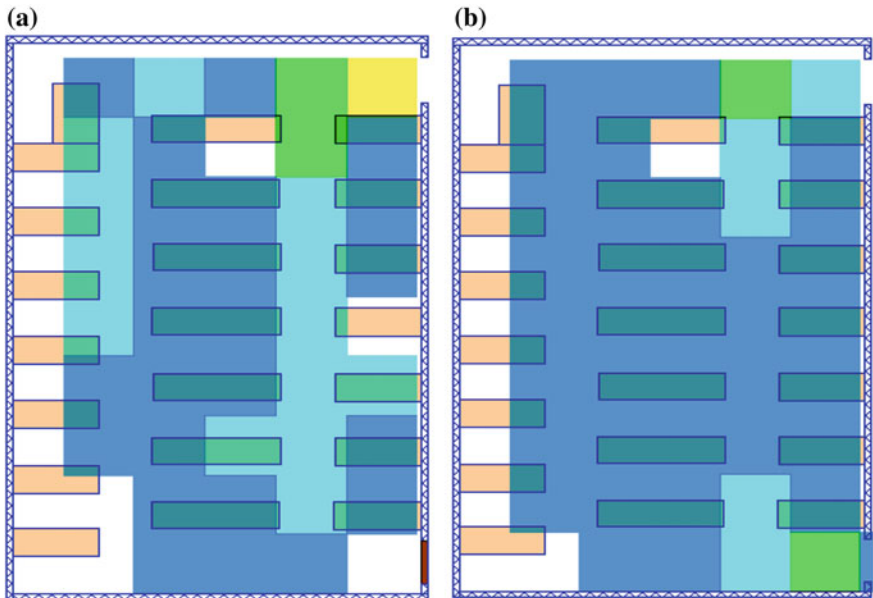
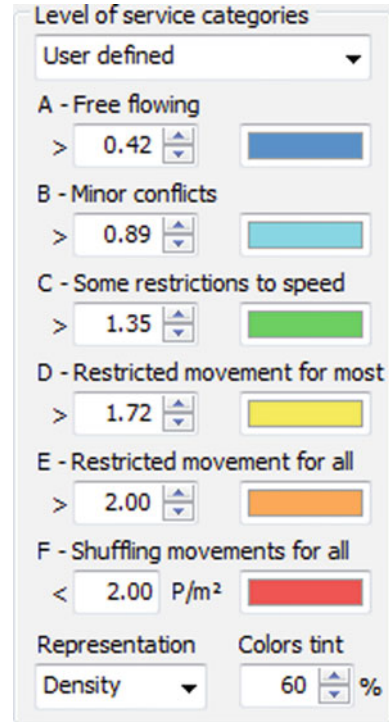


Fig. 8 Different maximum density between **a** one door open and **b** two doors open in a classroom

Fig. 9 Exit door in the classroom



D). In Fig. 8b, with both door open for exit, there is no restricted movement area. The blue color is the major color represented in both situations where it shows a free flow condition of pedestrian's movement (LOS A). Free flow movement can be found more frequently when two doors are open during the evacuation (Fig. 9).

5.3 Walking Speed

Figure 10 depicted the comparison of walking speed for each pedestrians between real (video recording) and simulation. It can be seen that in real evacuation, the speed has more variation as compared to the simulated one. In Fig. 10a, the highest speed of pedestrians is 0.92 m/s which is lower than the highest speed in Fig. 10b which is 1.23 m/s. The lowest speed of pedestrians in real (video recording) is 0.22 m/s as compared to 0.52 m/s as the lowest speed using simulation. Besides that, the average speed for real (video recording) is 0.40 and 0.63 m/s for simulation.

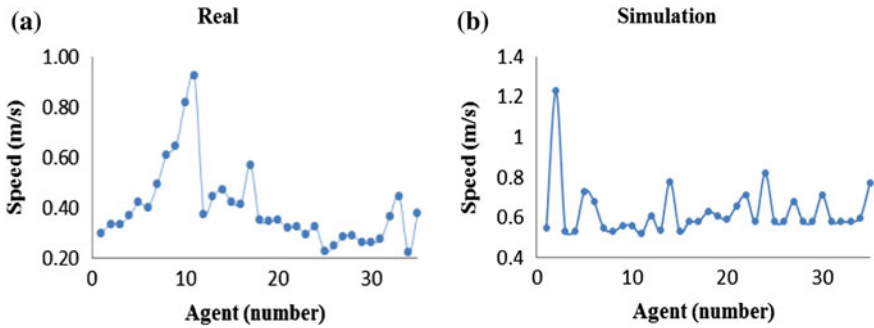


Fig. 10 Different of walking speed between a real (video recording) and b simulation

6 Conclusion and Recommendation

This study investigated the egress behavior during a classroom evacuation. The simulation approached used shows the variations in route selection when the people are on a panic situation. Door is the important function in any classroom that will be used as an exit way for the pedestrians to evacuate themselves. In this study, only one door was open when we observed the pedestrians using video recording. However, many scenarios can be created using simulation. It is recommended that both doors in every classroom are open to be used to ease and fasten the pedestrians’ evacuation process. The simulation results have verified that the time taken for all pedestrians to exit when only one door was open is longer than both doors were open. A better use of exits door consists of more differentiated path with less congestion and reduced evacuation times is advisable.

This study has utilized one of the applications of SimWalk which are the pedestrians’ trail and density in route selection during the evacuation process in classroom. In the future, studies involving realistic condition of pedestrians dynamic such as bottlenecks at the exit with variation dimension of door can be conducted.

Acknowledgments This study is funded by Universiti Teknologi MARA, Malaysia.

References

1. PED, in 6th International Conference on Pedestrian and Evacuation Dynamics, retrieved 30/11/12, from <http://www.ped2012.org/>
2. D. Helbing, A. Johansson, Pedestrian, Crowd and Evacuation Dynamics, in *Encyclopedia of Complexity and Systems Science*, pp. 6476–6495 (2009)
3. A. Schadschneider, W. Klingsch, H. Klüpfel, T. Kretz, C. Rogsch, A. Seyfried, Evacuation dynamics: empirical results, modeling and applications, in *Encyclopedia of Complexity and Systems Science*, pp. 3142–3176 (2008)

4. W. Daamen, S.P. Hoogendoorn, *Experimental Research of Pedestrian Walking Behavior*. Transportation Research Board annual meeting (National Academy Press, Washington DC, 2003), pp. 1–16
5. L.J. Dotson, J. Jones, D. Schneck, R. Sullivan, Identification and analysis of factors affecting emergency evacuations (2005), Nureg/CR-6864, vol. 1, retrieved 30/11/12, from <http://www.nrc.gov/reading-rm/doc-collections/nuregs/contract/cr6864/v1/>
6. L. Huang, D. Liu, Y. Zhang, Dynamics-based stranded-crowd model for evacuation in building bottlenecks. *Math. Probl. Eng.* **2013**, 7 p (2013) (Article ID 364791)
7. J. Oxley, B. Fildes, E. Ihsen, J. Charlton, R. Day, Differences in traffic judgements between young and old adult pedestrians. *Accid. Anal. Prev.* **29**(6), 839–847 (1997)
8. R. Lohner, On the modeling of pedestrian motion. *Appl. Math. Model.* **34**(2), 366–382 (2010)
9. H. Cheng, X. Yang, Emergency evacuation capacity of subways station. *Soc. Behav. Sci.* **43**, 339–348 (2012)
10. W. Lei, A. Li, R. Gao, X. Hao, B. Deng, Simulation of pedestrians' evacuation in a huge transit terminal subway station. *Phys. A: Stat. Mech. Appl.* **391**(22), 5355–5365 (2012)
11. M.C. Campanella, S.P. Hoogendoorn, W. Dameen, Calibrating walker models: variations of parameter due to traffic regimes, in *European Conference on Mathematical and Theoretical Biology* (2011)
12. Z. Zainuddin, K. Thinakaran, I.M. Abu-Sulyman, Simulating the Circumambulation of the Ka'aba using SimWalk. *Eur. J. Sci. Res.* **38**(3), 454–464 (2009)
13. A.S. Sahaleh, M. Bierlaire, B. Farooq, A. Danalet, F.S. Hänseler, Scenario Analysis of Pedestrian Flow in Public Spaces, in *Proceeding of the 12th Swiss Transport Research Conference (STRC)*, Monte Verità, Ascona, Switzerland, May 2012
14. P. Stucki, Obstacles in Pedestrian Simulations, Department of Computer Sciences, Master Thesis, ETH Zurich, 2003
15. A. Johansson, D. Helbing, H.Z. Al-Abideen, S. Al-Bosta, *From Crowd Dynamics to Crowd Safety: A Video Based Analysis* (World Scientific Publishing Company (WPSC), 2008)

Part VI
Geotechnical Engineering

Groundwater Level Detection by Using a Two-Dimensional Electrical Resistivity Imaging

A. Derahman, H. Awang and N. M. Osman

Abstract Groundwater level is one of the main factors that should be considered in slope stability analysis. Generally, surface water resulted from rain infiltrates to the ground will increase the groundwater table, thus can trigger slope failures. Many methods can be employed to explore and investigate the presence of water in the sloping areas. One of the conventional methods that are commonly used is observation well where piezometer is installed in the well. The purpose is to measure the level and hydraulic head of groundwater in aquifers. However, this kind of technique needs to be dealt with tedious works as drilling is to be carried out for standpipe installation. Even though this technique is technically easy to understand, it only can provide one single point water level data of the area unless there are a numbers of well to be drilled. This means that the observation well can only provide the information at a discrete point. In order to obtain continuous ground water level and other underground profile a technique that can provide the continuous sub-surface information should be carried out. This paper presents findings of a study of groundwater detection using a non-destructive method namely electrical resistivity imaging. The objective of the study is to determine how reliable the method can be used in detecting ground water level and to what extent it can provide the sub-surface information. A 2-D electrical resistivity imaging was carried out on two slope areas where a landslide was taken place at one of the areas. The groundwater level was also monitored using the observation well at very limited borehole points. The results of the 2-D electrical resistivity imaging and piezometer then were compared.

A. Derahman · N. M. Osman (✉)

Faculty of Civil Engineering, Universiti Teknologi MARA Pahang, 26400, Bandar Tun Abdul Razak, Jengka, Pahang, Malaysia
e-mail: nurmasyitah@pahang.uitm.edu.my

H. Awang

Faculty of Civil Engineering, Universiti Teknologi MARA Malaysia, 40000 Shah Alam, Selangor, Malaysia
e-mail: harya406@salam.uitm.edu.my

Keywords Groundwater · Two-dimensional electrical resistivity imaging · Slopes

1 Introduction

In tropical country like Malaysia, natural hazards such as slope failures are very common. One of the factors that contribute to this hazard is groundwater which plays an important role as an agent that triggers to the slope failures. The groundwater occurs in two distinct zones which are separated by the water table or also known as phreatic surface. The phreatic zone is subjected to the gravitational forces. It saturates the pore spaces in the soil below the water table. It also has an internal pore pressure that is greater than the atmospheric pressure and the water tends to flow laterally. The vadose water zones are located above the water table where the water percolates and moving downwards to link together with the phreatic water below the water table. Increasing of groundwater level beneath the slopes is assisted by infiltration of rain water as rains are very frequent in the tropical region. The effect of wetness on shear strength of soil is characterised based on a stress state variable known as suction. The suction effect is derived from the surface tension force on the water meniscus, which clings between soil particles [6] and generally its magnitude increases as moisture decreases. However, shear strength does not indefinitely increase with suction since it started to decrease beyond residual suction [3, 5, 9, 12]. The apparent shear strength reduction due to the surface water infiltration is actually governing the rain induced slope failure [10]. Therefore determination of groundwater level in any areas of concern is significant as a prevention measures.

There are many methods that can be carried out to investigate the presence of groundwater level. One of the common methods used is piezometer. This conventional method is widely used where a hole need to be drilled for observation well and also for the installation of the piezometer. This method requires more care during the installation work to ensure a proper installation is done. Besides, if the vibrating wire of piezometer is to be used, the electric units have a risk to damage due to lightning. Furthermore the power source needs to be maintained by replacing a new battery periodically. Even though this method is technically easy to understand, the information provided is limited to a single data point. Meaning that for an area it needs more than one point to represent enough information of the groundwater level as it may varies from one point to another. Due to these reasons, a method that can provide continuous information of groundwater levels, a non-tedious and a non-destructive works is highly recommended. Friedel et al. [4] investigated a case study of a slope endangered by rainfall-induced landslides using 3D resistivity tomography together with geotechnical assessment. They found that the combination of electrical resistivity survey and geotechnical survey able to help in optimizing the design of forthcoming monitoring experiment. Rosli et al. [11] used the resistivity technique for slope failure monitoring and they found

that the factor which cause landslide is the subsurface boulders and the saturated zone which result subsidence of the surface.

Even though many researches have been carried out in using resistivity method, but there is still no finding of reliability in detecting groundwater level using this non-destructive method at slope areas. In reflection to the above problem and the gaps in the previous researches, a study on detecting groundwater level using electrical resistivity imaging method was carried out at two locations of slope areas in the states of Johor and Perak. A landslide was taken place at one of the areas few years ago. The objectives of this study are to determine the groundwater level of the slopes using resistivity images and to compare the groundwater level between the values of piezometer and the image provided by resistivity method. Thus it is hope that this study will show how reliable electrical resistivity imaging can be used as a groundwater level detector and to what extent it can contribute information related to slope instability.

2 Materials and Methods

2.1 Site Locations

Two sites of Southern and Northern Peninsula Malaysia were selected for this study. The southern site is located in Senai, Johor and the northern is located at Slim River, Perak as shown in Fig. 1.

The site in Senai had experienced slope failure in 2007. This slope has a height of about 24 m and a width of 240 m. It was surrounded by palm trees plantation before the tragedy of the slope failure. Meanwhile the site in Slim River is a very steep slope which is higher than slope at Senai. It is also surrounded by palm trees plantation.

2.2 Borehole and Piezometer Test

Four boreholes were drilled where two boreholes were sunk at each site. From the boreholes record the soil profiles of the slopes were prepared to shows the each layer of the soils material. The soil profiles are to be used in analysis in order to predict the presence of groundwater level at the slopes area. Several data are needed such as coordinates of the boreholes point and reduced ground level for this process such as borehole name, total depth of boreholes, coordinates, water level, SPT 'N' values etc.

The application of the piezometer was used in measuring the groundwater levels and pressures in the boreholes. The piezometers were installed inside of the boreholes which is similar as the observation well. The electrical dip meter used to measure the head inside of the piezometer. Installation of piezometer is referred to



Fig. 1 Location of study sites at Senai, Johor and Slim River, Perak

Carter [2], where the equipment of piezometer consists of a porous pot connected to a vertical pipe which is installed in a borehole or driven into the ground. The installation of piezometer in boreholes usually uses Polyvinyl Chloride or also known as PVC pipes. This kind of materials is the ultimate in simplicity, reliability and cheapness where it is the most common types of piezometer in use. The piezometer tip is surrounded by a sand filter and it is usual to seal off test section with plugs of bentonite clay, which forms a water tight seal. Besides, the bentonite powder also used and mixed with water in a bucket so that it can be moulded into balls in the hands. Then the balls are thrown down into the borehole. Otherwise, the bentonite pellets may be poured down the hole. When the electrodes at the bottom of the dip meter touched the water surface, an electrical circuit is closed and a buzzer sounds inside the reel will activated, during that time, then record the reading of the water surface.

In Senai site, there are two piezometers that were installed at BH1 and BH2 namely as PSS4-1T and PSS4-1B respectively as in Fig. 2a. Also in Slim River site, there are two piezometers were installed at BH1 and BH2 namely as PSC2-1T and PSC2-1B, respectively in Fig. 2b.

2.3 Electrical Resistivity Imaging

The main equipment used in the electrical resistivity measurement is ABEM Terrameter SAS 4,000 with multi electrodes system. It consists of 41 stainless steel

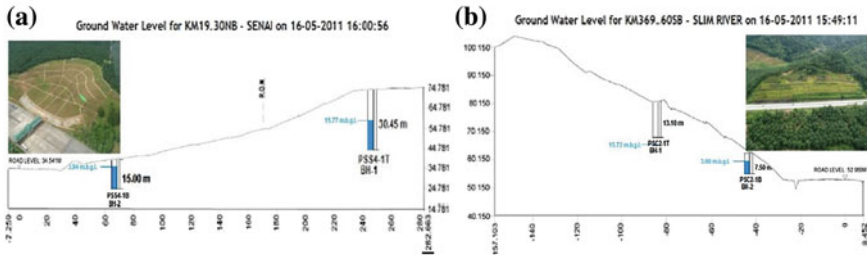


Fig. 2 a Locations of piezometer installation in Senai. b Locations of piezometer installation in Slim River

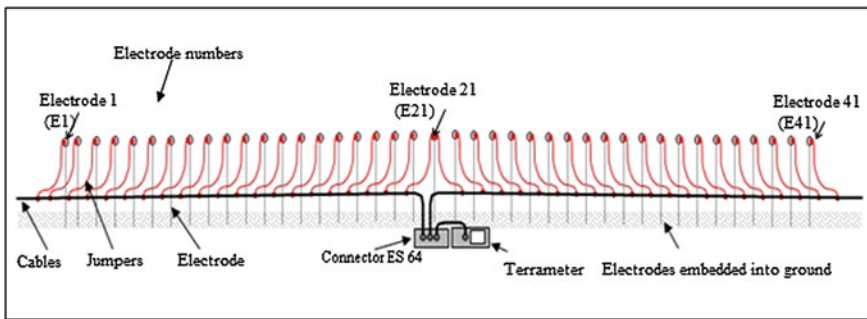


Fig. 3 Schematic layout of the resistivity line

electrodes that were pinned to the ground along a survey line. Two cables were laid and connected to each electrodes starting from electrode number one (E1) and end up with electrode number 41 (E41). Each of the cables has 21 take outs where E1 and E21 were connected to first and last take out of cable number one respectively. The first takeout of cable number two was also connected to E21 and the last takeout to E41. Both cable number one and cable number two were connected by electrode selector (ES64) at the centre of the survey line where the main unit of Terrameter SAS 4,000 was then connected to ES64. The schematic layout of the resistivity line is shown in Fig. 3. Spacing between the electrodes at Senai site is 5 m and at Slim River site is 2.5 m. These lines were located near to the boreholes locations which were at the top and bottom of the slopes. The location of resistivity lines at both sites is shown in Fig. 4.

Data collected by Terrameter were transferred to computer for data conversion and interpretation. A software named as RES2D Inversion was used to process and to convert the resistivity data into resistivity image. All methods of electrical resistivity imaging including field procedures and data conversation were referred to Instruction Manual for Terrameter SAS 4000 Version 8 [1] and Loke and Baker [8].

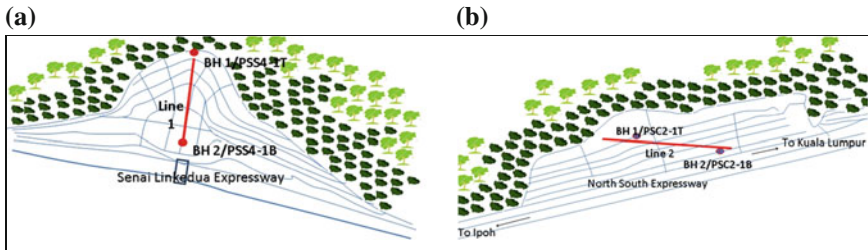


Fig. 4 a Locations of resistivity lines in Senai. b Locations of resistivity lines in and Slim River site

3 Result and Discussion

3.1 Boreholes Result

The borehole results for Senai site is shown in Tables 1 and 2 and for Slim River site the results is shown in Tables 3 and 4. BH-1 and BH-2 for Senai site shows there are three layers of soils which indicate the CLAY, GRAVEL and SILT. This type of soils is categorized in the associated group of fine grained, gravel and fill, respectively. BH-1 and BH-2 for Slim River site shows there are shows four layers of soil which indicate the SILT, SAND, GRAVEL and SANDSTONE where the soils is categorized in the associates groups as fill, sand, gravel and rock, respectively.

3.2 Piezometer Results

The results of groundwater level were collected from the piezometers that were installed at the both sites. The result of groundwater level at Senai site is shown in Table 5. The groundwater level reading was taken from PSS4-1T at the top and PSS4-1B at the bottom of the slope which is 15.77 and 3.94 m respectively below the ground level. As well as for groundwater level at Slim River site the reading of groundwater level is shown in Table 6. The groundwater level reading at this location was taken from PSC2-1T at the top and PSC2-1B at the bottom of the slopes which is 15.72 and 3.00 m respectively below the ground level.

3.3 Results of Electrical Resistivity Imaging

The results of electrical resistivity imaging were obtained in resistivity images and values. The results of resistivity images are displayed as scaled resistivity-depth pseudosections. In this study the blue colour region represents a lower resistivity

Table 1 BH-1 at Senai site

Depth (m)	Thickness (m)	Soil description	'N' value
0.00–1.50	1.50	Top soil: dark brownish yellow silty CLAY	–
1.50–3.00	1.50	Medium dense dark reddish brown silty sandy GRAVEL (laterite)	18
3.00–4.50	1.50	Stiff dark reddish orange clayey SILT	6
4.50–7.50	3.00	Stiff to medium stiff dark reddish orange clayey SILT	9
7.50–9.00	1.50	Stiff light yellow brown clayey SILT	13
9.00–10.50	1.50	Very stiff light yellowish brown sandy SILT	23
10.50–12.00	1.50	Stiff dark reddish yellow slightly sandy SILT	14
12.00–13.50	1.50	Very stiff dark reddish yellow clayey SILT	19
13.50–15.00	1.50	Very stiff dark reddish yellow mottled brown clayey SILT	17
15.00–18.00	3.00	Very stiff dark yellowish red mottled brown clayey SILT	17, 18
18.00–19.50	1.50	Stiff light yellowish brown clayey SILT	11
19.50–21.00	1.50	Very stiff dark yellowish brown clayey SILT	20
21.00–22.50	1.50	Stiff dark yellowish brown clayey SILT	14
22.50–24.00	1.50	Stiff dark reddish yellow clayey SILT	10
24.00–25.50	1.50	Stiff dark reddish yellow clayey SILT	12
25.50–27.00	1.50	Very stiff dark reddish brown slightly sandy SILT	20
27.00–28.50	1.50	Very stiff dark yellowish brown spotted white clayey SILT	22
28.50–30.00	1.50	Very stiff light red spotted white clayey SILT	17
30.00–30.45	1.50	Very stiff dark red spotted white clayey SILT	25

Table 2 BH-2 Senai site

Depth (m)	Thickness (m)	Soil description	'N' value
0.00–1.50	1.50	Top soil: dark reddish brown silty CLAY	–
1.50–3.00	1.50	Medium stiff light yellowish brown clayey SILT	5
3.00–6.00	3.00	Medium stiff light yellowish brown silty CLAY	7
6.00–7.50	1.50	Hard dark greenish grey gravelly SILT	50
7.50–9.00	1.50	Very dense dark greyish grey very silty sandy GRAVEL	50
9.00–10.50	1.50	Medium dense dark greenish grey very silty very sandy GRAVEL	20
10.50–13.50	3.00	Stiff dark greyish green slightly sandy CLAY	9, 18
13.50–15.00	1.50	Stiff dark yellowish orange silty CLAY	10
15.00–15.45	0.45	Stiff light brownish red silty CLAY	12

area, yellow or green colour region represents a medium resistivity area while the red or purple colour regions represent a relatively higher resistivity area. The images of the resistivity measurement for both site studies were correlated with the piezometer and borehole results. The resistivity values was correlated to the borehole and was interpreted as in Table 7. The resistivity value for Line 1 is 1.00–1,000 ohm m for Senai site as in Fig. 5. Meanwhile, the resistivity value for Line 2 is 10.00–12,000 ohm m for Slim River site as shown in Fig. 6.

Table 3 BH-1 Slim River site

Depth (m)	Thickness (m)	Soil description	'N' value
0.00–1.50	1.50	Top soil: brownish sandy SILT	–
1.50–3.00	1.50	Stiff light grey red slightly sandy SILT	15
3.00–4.50	1.50	Hard yellowish brown slightly gravelly SILT	50
4.50–6.00	1.50	Hard yellowish brown slight sandy SILT	50
6.00–7.50	1.50	Hard light grey clayey SILT	50
7.50–9.00	1.50	Hard yellowish gravelly SILT	50
9.00–10.50	1.50	Hard yellowish sandy SILT	50
10.50–11.60	1.10	Hard light grey sandy SILT	50
11.60–13.10	1.50	Weak rock light grey mottled red fractured moderately weathered medium strong rock SANDSTONE	–

Table 4 BH-2 Slim River site

Depth (m)	Thickness (m)	Soil description	'N' value
0.00–1.50	1.50	Wash bore	–
1.50–3.00	1.50	Hard brownish gravelly SILT	50
3.00–4.50	1.50	Hard brownish clayey SILT	50
4.50–6.00	1.50	Very dense brownish very silty very sandy GRAVEL	50
4.50–6.00	1.50	Very dense brownish very silty very sandy GRAVEL	50
6.00–7.50	1.50	Encounter rock light brown grey moderately weathered medium strong rock SANDSTONE	50

Table 5 Groundwater level (GWL) statistic from 15-05-2011 to 16-05-2011 at Senai site

Boreholes	Highest GWL (m.b.g.l)	Lowest GWL (m.b.g.l)
BH-1	15.77	15.77
BH-2	3.94	0.00

Table 6 Groundwater level (GWL) statistic from 15-05-2011 to 16-05-2011 at Slim River site

Boreholes	Highest GWL (m.b.g.l)	Lowest GWL (m.b.g.l)
BH-1	15.72	15.72
BH-2	3.00	0.00

The groundwater level for Senai which is 15.77 m below ground level for BH-1 is located at the top of the slope. However, the BH-2 indicated the groundwater level is 3.94 m below ground level. The piezometer reading shows that the groundwater level is matched and fell within the area of resistivity values that indicated the low resistivity and consist of higher water content. The results also shown that BH-2 was fallen at clayey material which is the typical resistivity

Table 7 Results of resistivity values at Senai site and Slim River site with soil profiles by referred the typical resistivity values

Types of soils and waters	Typical resistivity values of soil/rock materials (Ohm m)	Line 1 (Senai) Resistivity value (Ohm m)	Line 2 (Slim River) Resistivity value (Ohm m)
Clay	1–100	30–100 and 1–50	–
Alluvium (silt and gravel)	10–800	50–300	200–800
Groundwater (fresh)	10–100	10–100	10–100
Sand	200–3,000	–	1,000–3,000 and 1,500

Notes Typical resistivity values of soil/rock material, Loke [7]

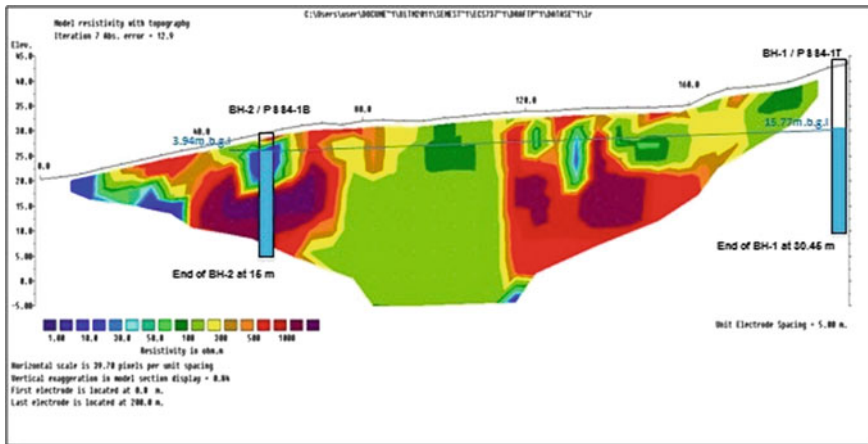


Fig. 5 Comparison between soil profiles and resistivity values at location 1 Senai

values is around 1–100 ohm m. It is shown that the groundwater level for Senai site was fell at the lower resistivity values which is around 1–800 ohm m, where the soil materials is consist of clayey and silt materials.

The groundwater level for Slim River site which is 15.72 m below ground level for BH-1 is located at the top of the slope. The BH-2 indicated the groundwater level is 3.0 m below ground level. The result also shown that BH-2 was fallen at silt material which is the resistivity values is 3,000 ohm m. It is shown that the figure indicated that the groundwater level for Slim River site fell at a medium resistivity values and near to the lower resistivity area where consist of water content.

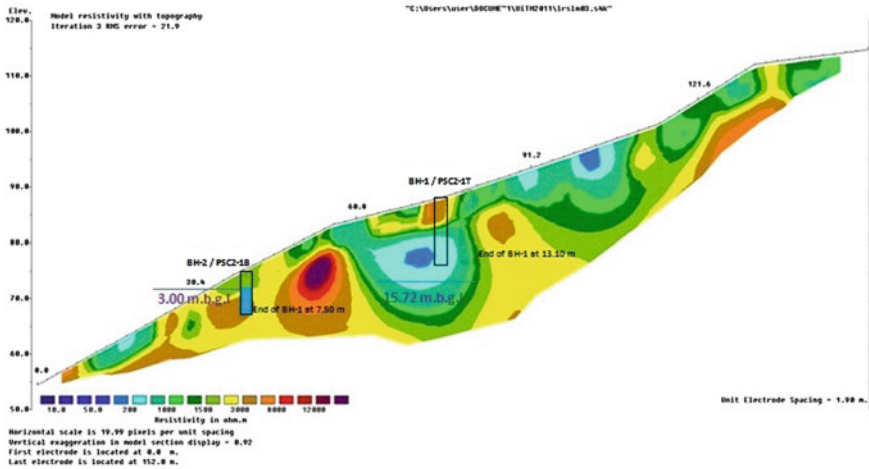


Fig. 6 Comparison between soil profiles and resistivity values at location 2 Slim River

4 Conclusions

The two-dimensional electrical resistivity imaging is carried out to predict the presence of groundwater level at slopes area. In order to study the resistivity images together with other destructive methods such as boreholes and piezometer the application on how to run the equipment’s were also discussed.

Therefore, it can be concluded that the two-dimensional electrical resistivity imaging is suitable as application in geotechnical engineering works, mining, hydrology, environmental, especially in slope engineering as it may help to provide some data to minimize chances of slopes failures and landslides tragedy. It was proven that the application of this survey is appropriate to measure the distribution of resistivity on the ground surface. With the results from the resistivity images the layers of the ground’s subsurface can be determined. It also can help to monitor the presence of the groundwater level at every soil layers. This is meets the objective of these studies.

Collectively, the results data from piezometer can also use to detect the groundwater level at the slope areas arise and results from resistivity survey were analyzed to ensure their similarity. This kind of resistivity survey is a good indirect predictor of water content and is an instrument that can measure the depth of slope profile. The cross section of the slope can also be made and visualize the distribution of the resistivity of the ground subsurface.

Finally, the result shows that a groundwater level by piezometer and resistivity images located at the area where a slope failure occurred matched to each other. It is also proven that the increasing groundwater level contributed to the slope failures. This finding meets the objective of the study where it is reliable to detect groundwater using electrical resistivity as a non-destructive method.

References

1. ABEM Terrameter SAS 1000/ SAS 4000 (2009), ABEM Instrument AB, Sweden. retrieved from http://www.abem.se/files/upload/manual_terrater.pdf
2. M. Carter, *Geotechnical Engineering Handbook* (University of Wales Institute of Science and Technology, Pentech Press, Plymouth, New York, 1983)
3. V. Escario, J. Juca, in *Strength and Deformation of Partly Saturated Soils*, 12th International Conference on Soil Mechanics and Foundation Engineering, vol. 3 (Rio de Janeiro, 1989), pp. 43–46
4. S. Friedel, A. Thielan, S.M. Springman, Investigation of a slope endangered by rainfall-induced landslides using 3D resistivity tomography and geotechnical testing. *J. Appl. Geophys.* **60**, 100–114 (2006)
5. J.K.M. Gan, D.G. Fredlund, Shear strength characteristics of two saprolitic soils. *Can. Geotech. J.* **33**, 595–609 (1996)
6. G.W.C. Kaye, T.H. Laby, *Tables of Chemical Constants*, 14th edn. (Longman, Harlow, 1973)
7. M.H. Loke, in *Time-Lapse Resistivity Imaging Inversio*. The Environmental and Engineering Society European Section, Hungary, 6–9 September 1999
8. M.H. Loke, R.D. Barker, Rapid least-squares inversion of apparent resistivity pseudosections using a quasi-Newton method. *Geophys. Prospect.* **44**, 131–152 (1996)
9. M.J. Noor, W.F. Anderson, in *A Comprehensive Shear Strength Model for Saturated and Unsaturated Soils*. Proceedings of the 4th International Conference on Unsaturated Soils, vol. 2 (ASCE Geotechnical Publication, USA, 2006), pp. 1992–2003
10. H. Rahardjo, D.G. Fredlund, in *Calculation Procedures for Slope Stability Analyses Involving Negative Pore-Water Pressures*, Proceeding International Conference Slope Stability Engineering, Development, Applications, (Isle of Wight, 1991)
11. S. Rosli, A.W.M. Hussien, M. Nawawi, A.A. Fouzan, M. Azar, in *Monitoring Slope Failure using 2-D Electrical Resistivity Imaging in Pahang, Malaysia*, International Conference on Environment 2008 (ICENV 2008), (School of Physics, University Sains Malaysia, Pulau Pinang, 2008)
12. D.G. Toll, B.H. Ong, H. Raharjo, in *Triaxial Testing of Unsaturated Samples of Undisturbed Residual Soil from Singapore*, Proceedings of the Conference on Unsaturated Soils for Asia, (Singapore, Balkeema, 2000), pp. 581–586

PFA-Cement Mixture for Sand Column Parameter Stabilization

S. Shakri, M. A. Hafez and S. Norbaya

Abstract Most of the waste materials produced by construction practice and factories are considered as waste products to be disposed. Disposal of these materials in landfills can inculcating ecological pollution and chemical effects on the environment. Rather than disposing and letting these waste materials unattended, finding a solution or method to recycle these waste materials are better, particularly for Fuel Ash. Therefore, this study was premeditated to investigate the effectiveness of using Pulverized Fuel Ash (PFA) in improving the geotechnical parameters. Shear Box Test and Unconfined Compression Test (UCT) were conducted on this study. Shear Box test was prepared by combining three materials; sand, cement and PFA and 7 days of curing time. The results show the average rate for the treated samples of shear strength increased in the range between 130 and 145 kPa, in parallel with the increase in percentage of sand and PFA. While for UCT test, the samples were prepared based on two different conditions: with and without lime to examine whether it would affect the strength of the cement (Sand-PFA) mixture or by using cement alone to see if it is enough to get the desired results. Samples were prepared by using various percentages of materials and 28 days of curing time. The results show the average rate of Unconfined Compression Strength (UCS) of samples are between 2 and 18 MPa which increases proportionally with increase in percentage of material. Based on data obtained from the experiments, it can be concluded that, the parameters of soil will be treated by increasing the percentage of material used. However, there are limitations on the addition of materials that are used because the graph will begin to show a decline if the percentage increase is added to the mixture exceeds the optimal dose.

Keywords Pulverized fuel ash · Pozzolanic · Ground improvement · Shear box · UCT · Chemical stabilization

S. Shakri (✉) · M. A. Hafez · S. Norbaya
Faculty of Civil Engineering, Universiti Teknologi MARA, 40450 Shah Alam,
Selangor, Malaysia
e-mail: shagamy2@yahoo.com

1 Introduction

Sustainable development is an important concept to be considered as a ground improvement method to replace the conventional construction practices, especially in terms of projects that impose massive impact on environment. Since 1980s, any solution introduced for ground improvement method must abide by extremities. Based on Environmental Impact Assessment (EIA), each of project undertaken should investigate the possible negative effects of a man-made structure on surrounding environment with regards to the biosphere elements. EIA might prohibit use of certain technologies and solutions to mitigate the probability of anticipated excessive noise, vibration, remolding the ground, ground water contamination and compromising available resources of material in vicinity of site. Therefore, the planning and the use of environmentally friendly methods is very important in construction practises. When considering the eco-friendly methods, materials to be used are also included in the judgment and it is a profitable bonus if the materials used are the materials from the waste disposal such as fly ashes.

In order to achieve this, one of the easiest scheme would be to salvage the way advances in reduction and saving resources is to replace the new material rather than conventional sources of construction materials. Prabakar and Dendorkar [1] reported that fly ash can be successfully used to improve the geotechnical parameters such as bearing capacity and shear strength. Guleria and Dutta [2] have been conducting research on the impact of tire chips mixed with lime, gypsum, and fly ash composites for quantification of unconfined compressive strength. Research has found that the use of the mixture can increase the potential for implementation of road sub-base medium with light traffic. Najim and Hall [3] have shown through their research, the use of pulverized fuel ash (PFA) can improve the bearing capacity and at the same time solve the problems of settlement under the road embankment clay. Most of the materials mentioned above are considered as waste products to be disposed. Disposal of these materials in landfills can deduce ecological pollution as inclusion chemistry and top of it, it becomes worst if the wastes are harmful to the environment and human health.

2 Ground Improvement and Process of Pozzolanic

Method of ground improvement has been practiced since many decades before, reported by McDowell [4] the ancient Egyptians and Mesopotamians had created and applied the stabilization methods for ground modification works to stabilize the earth roads works by increasing some of soil properties. In 1906, USA introduced the first experiment on stabilization work by studying the strength and weakness of admixing sand and clay [5], and in 1980 and 1982, the first experiment on case of deep soil stabilization was successfully reported and executed in

practice by using cement powder and method adopted and this method was known as DJM (Dry Jet Mixing) method [6].

Cement and lime are the common materials that have been used as a binder under chemical stabilization to stabilize and remediate soft soil. Based on previous study, between 1 and 3 % of lime and cement is needed for stabilization process and 2–10 % for cementation process [7], and according to [8] the amount of cement between 4.5 and 5.6 % and lime between 4.5 and 6.8 % of dry soil weight are recommended among these binders as appropriate mix design to increase the UCS of remediated column. However, this percentage ratio used can be less or more based on type of soil, water ratio, chemical effect due to the material used and method of preparation.

Chemical stabilization is referred to procedures, in which chemical additives are mixed with soil to enhance a number of geotechnical characteristics such as axial and shear strength, axial and radial strains, and permeability indexes. Different chemical procedures are involved in improvement of chemical stabilization techniques including surface ion exchange of clay particle or chemical reactions to strengthen the bonding of soil elements or filling the voids with expansive nature of admixed materials [9]. Pozzolanic reaction is a process that will increase the strength and durability of the soil. Actual impact will depend on several factors such as; characteristic of stabilizing agent, characteristic and condition of soil, mixing condition and curing condition. Following are the chemical reactions under pozzolanic reaction.



The higher the ratio of Al, Si and Ca, the pozzolanic process will be smooth and will stabilize the soil. In addition, pozzolanic reaction also reacts with the temperature where, high temperature and fast cooling greatly affects the best material to be installed as a stabilizer to give a round shape and the nature of the particles are amorphous.

3 Experimental Investigation

3.1 Material Used

Pulverized fuel ash (PFA), cement, lime, sand and natural soft soil were used for the experimental investigations. PFA is a solid waste from the combustion of coal with a high temperature (about 1,000 °C) in coal based power stations coal. For this study, the source of the PFA have been taken from Power-plant Stesen of Sultan Salahuddin Abdul Aziz at Kapar Selangor Malaysia. This stesen is one of the power plant under the purview of TNB Malaysia Bhd. Portland cement has

Table 1 Chemical composition of PFA, cement and lime

Component	PFA (%)	Cement (%)	Lime (PFA)
Silica (SiO ₂)	40–60	20.65	12.25
Alumina (Al ₃ O ₃)	20–30	5.87	7.78
Iron oxide (Fe ₂ O ₃)	4–10	2.52	3.82
Calcium oxide (CaO)	5–30	63.55	69.67
Magnesium oxide (MgO)	1–6	2.75	0.88
Sulphur trioxide (SO ₃)	0–2	1.63	2.77
Sodium oxide (Na ₂ O)	0–2	0.85	0.12
Potassium oxide (K ₂ O)	0–4	0.63	0.79
Loss on ignition (LOI)	0–3	1.54	1.95

Table 2 Properties of natural soft soil

Properties	Ratio
Moisture content, w_c (%)	58–60
Plastic limit, w_p (%)	30.83
Liquid limit, w_l (%)	50.52
Plastic index, I_p (%)	19.69
Parti cal density (Mg/m ³)	2.23

been used as a type of cement based on the availability of this product and according to [10] this type of cement has an ideal ratio of material properties needed for this study. Sand particles passing through 4.75 mm sieve were used to mixed with other materials. The moisture content of sand used are ranged between 5.28 and 6.7 % when it is in a natural state. The particle density of sand has been obtained and recorded as 2.45 Mg/m³. Thus, the soil classification of sand used is Well Graded SAND. For type of lime, natural hydraulic lime was used in this study. It has been chosen due to it clay contents in the range of 10–20 % and providing flexibility on mixture and pozzolanic reaction. Summary of the chemical composition of PFA, cement and lime have been presented in Table 1. While for natural soft soil, it has been prepared as second layer for shear box test. It has been used to study the effects between sample of mixture with natural of soil. Table 2 shows the properties of soft soil used in this study.

3.2 Preparation of Shear Box Test

Shear box or direct shear box tests were performed on various mixture of samples in general accordance with [11] standard test method for direct shear tests of soils under consolidated drained conditions. According to ASTM D 3080-90, the direct shear box test has several particle-size to box size requirements when preparing specimens for testing. It is recommended that the minimum specimen width should not be less than ten times the maximum particle-size diameter and the minimum

initial specimen thickness should not be less than six times the maximum particle diameter. Therefore, a 60×60 mm size of shear box test was used for this experiment. Samples were prepared differently by using various percentage of PFA, cement and sand. 40, 50, 60, 70 and 80 % of PFA were used while for cement 4, 8, 12 and 16 % were used. As for the sand, percentage is added to each mixture through make up of 100 % mixture of calculation, for example with 4 % of cement mixed with 40 % PFA bringing the total was 44 %, so over 56 % of the mixture is from sand. After the samples were prepared, it will be cured based on 7 days curing time period before be tested with natural soft soil collected from site.

3.3 Preparation of Unconfined Compression Test

Unconfined Compression Test (UCT) is used to measure the unconfined compressive strength of the sample. The test was performed on various mixture of samples in general accordance with [11]. The cylinder samples with 100 mm high and 50 mm diameter were prepared differently by using various percentage of PFA, cement, lime and sand. 40, 50, 60, 70 and 80 % of PFA were used while for cement, 4, 8, 12 and 16 % of ratio have been designed. Sample for cement-lime have been prepared for comparative purposes which the ratio of 15 and 20 % were prepared and mix with sand. Similar to shear box test, the percentage of sand is added to each mixture to make up 100 % of mixture for calculation. For example with 15 % of cement/cement-lime mixed with 30 % PFA bringing the total was 45 %, so over 55 % of the mixture is from sand. After the samples were prepared, it will be cured based on 28 days curing time period before be tested.

4 Result and Discussion

The raw data were obtained from the laboratory experiments have been analyzed and conclusion has been made by referring to the method and previous theories. Results obtained have been presented in the form of graph to make it easier to be understood (Figs. 1, 2, 3 and 4).

4.1 Friction Angle Characteristic

Figures 5, 6, 7 and 8 show the shear strength characteristics of the modified samples by cement and sand improved by PFA with using various configuration. Figure 5 shows the characteristics of shear strength based on 4 % of cement and mixed by various percentage of PFA and Sand. Result showed readings for shear strength will increase parallel with rising percentage of PFA where the highest

Fig. 1 Preparation of sample for shear box test



Fig. 2 Shear box test



Fig. 3 Process of curing sample

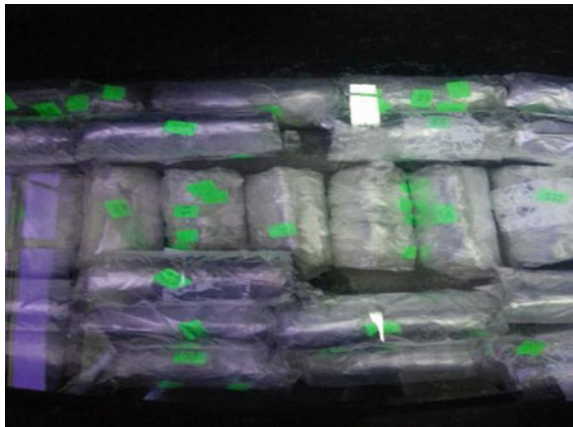
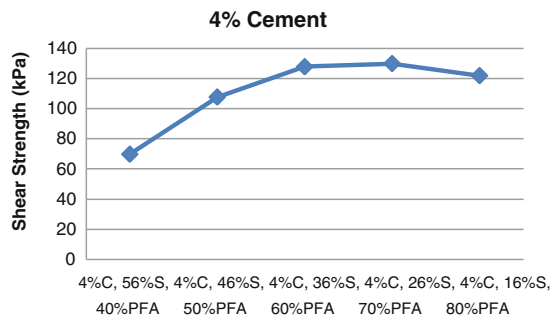


Fig. 4 Sample after curing process



Fig. 5 Shear strength of various configuration of sand and PFA with 4 % cement



value were recorded when PFA used was 70 %, shear strength was recorded at 129.89 kPa. However, as percentage of PFA continues to increase exceed 70 %, shear strength reduced to 121.89 kPa.

In Fig. 6, percentage of cement used is 8 % and the highest value for the shear strength was recorded at 141.73 kPa, which is the percent utilization of 50 % PFA. But however when percentage of PFA exceed 5 %, the values of shear strength decreased and recorded at 106.1 kPa when percentage of PFA is 80 %. As happen in Figs. 5, 6 and 7 graph showing equation in the form of graph movement parallel with the percentage of PFA used. In Fig. 7, percentage of cement used was 12 % and it recorded the highest of shear strength at 135.88 kPa which is percentage of PFA used was 60 % and when exceed to 60 %, shear strength reduced and recorded at 126.23 kPa where percentage used of PFA was 80 %. Figure 8 also shows the same results. The highest value of shear strength recorded at 131.26 kPa where the percentage use of PFA was 60 % and reduced to 123.27 kPa when percentage of PFA used was 80 %.

Figure 9 shows the overall results of the graph to the shear strength of the sample with cement consumption is from 4 to 8 % and the use of PFA in turn is from 40 to 80 %. Apparent by observation of the formation of the pattern graph shows the use of PFA has optimum level. The addition of PFA as one of material in increasing the strength of the sample is the right choice, but it has its limit level

Fig. 6 Shear strength of various configuration of sand and PFA with 8 % cement

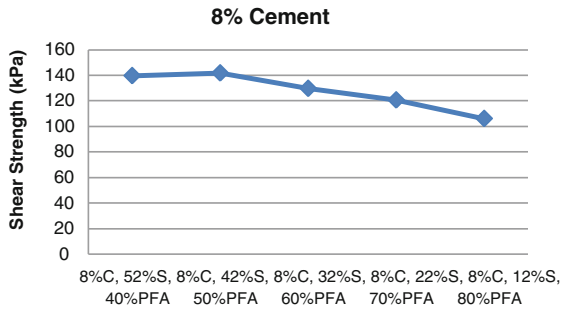


Fig. 7 Shear strength of various configuration of sand and PFA with 12 % cement

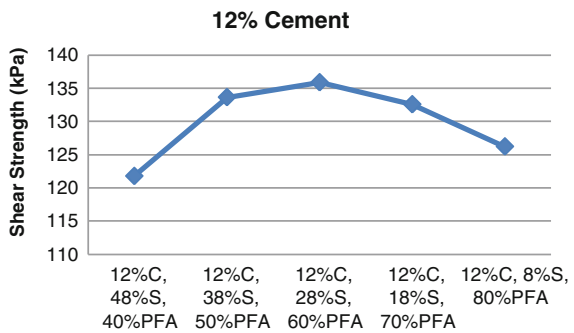
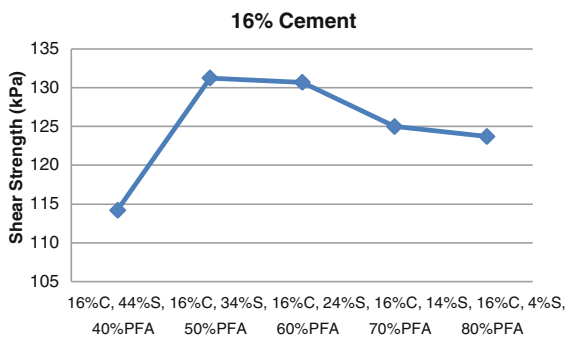


Fig. 8 Shear strength of various configuration of sand and PFA with 16 % cement



which if exceeded the limit, the decrease in shear strength of the sample will be recorded.

The same goes to the use of cement in which the use of high percentage of cement is not the right choice to increase the shear strength of the material because shear strength is related to friction of material where the whole mixture is important and optimal utilization percentage of each material is important to get the optimum shear strength.

Figure 10 shows the summary results of the highest shear strength of the cement consumption by 4, 8, 12 and 16 %. Through observation of the graph in

Fig. 9 Summary of graph of shear strength with various configuration of PFA and cement

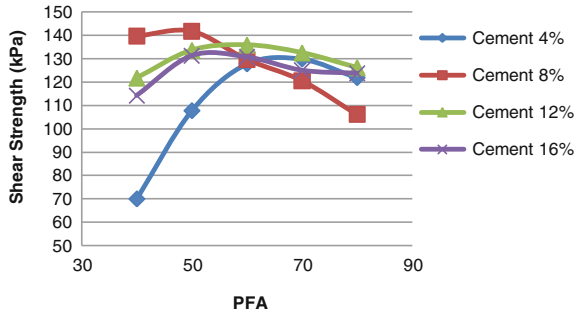


Fig. 10 Summary of the highest of shear strength recorded for different configuration of PFA and cement

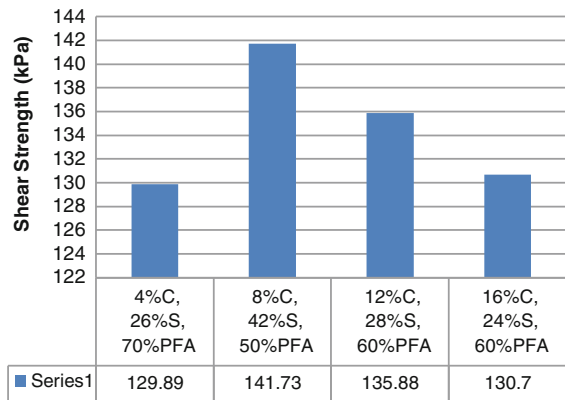


Fig. 10, the results show the percentage optimal use of PFA is between 50 and 60 % and the percentage of cement consumption is between 8 and 12 %.

4.2 Unconfined Compression Strength Characteristic

For most blended mixtures, the gain in strength beyond 28 days is not significant. Increasing the PFA content from 40 to 80 % further increases the uniaxial strength of the treated soil for a varied cement content of 4–16 %. When PFA is mixed with cement, the consequential increase in strength is quite striking, which reflects the self-hardening nature of cement. Figure 11 shows a pattern of formation graph of UCS of various configuration of PFA with 4, 8, 12 and 16 % cement. By observation of the graph in Fig. 11, can be expressed in the early stages of use percentage PFA is low between 40 and 50 %, cementing the specimen suffered less effective due to the increase in coarse nature, thus revealing the low early strength due to tensile cracking when uniaxial loading. This is attributed to the premature failure of these specimens due to splitting of ends and spalling of the surface

Fig. 11 UCS of various configuration of PFA with 4, 8, 12 and 16 % cement

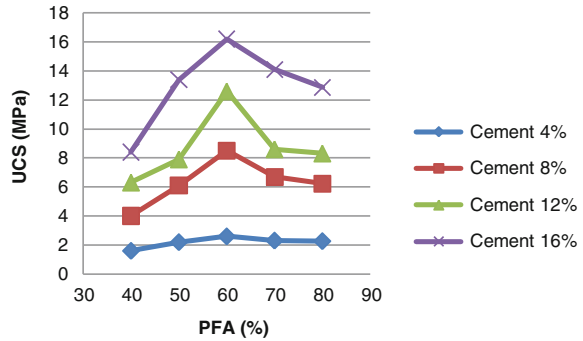
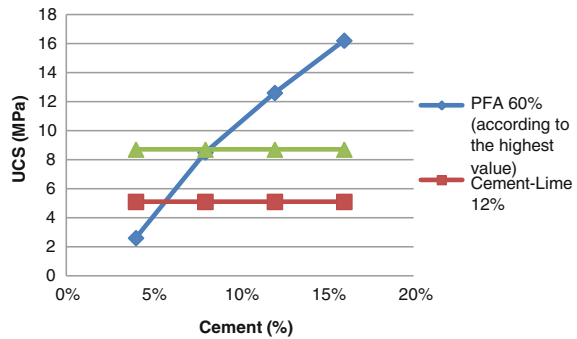


Fig. 12 Comparison of UCS of 60 % PFA used with 15 and 20 % lime-cement



probably caused by a reduction in overall effective stress cohesion; hence strength as a result of high sand-PFA content. The samples with sand-PFA lesser than 50 % developed higher shear failure and did not show premature tensile splitting and surface instability modes. In addition, after 28 days of curing, pozzolanic reactivity and cementation caused considerable improvement in their uniaxial compressive strength.

Through the graph in Fig. 11 also indicated that the pattern formation of graph is same as the graph to the formation of shear box test. Where there is an optimal level of PFA mixture within 60 %, where in the first period before the graph shows an increase in the strength of the material will then fall upon exceed the optimum level. However, the formation of cement graph is different from the formation of the PFA graph. Extension of the cement will have increased strength in parallel, Thus proves that cement is a material that is suitable for increasing the strength of the other materials. It can be concluded that no optimal level for cement due to increased percentage of cement used, but keep in mind one of the purposes of this experiment is to find the total cement consumption percentage appropriate to help raise the strength of the material and at the same time reduce the cost of substance use.

Through the graph in Fig. 12 shows the comparison of UCS with 60 % of PFA used with 15 and 20 % lime-cement. Through observation can be expressed increasing percentage of cement is one of the causes of the increasing strength of the

material. In the comparison between the use of PFA-cement and lime-cement, PFA-cement consumption is more relevant than lime-cement consumption. The graph shows the use of 7 % cement and 60 % PFA are sufficient to obtain the same strength through the use of 15 % lime-cement and better than the use of 12 % lime-cement. This happens because the pozzolanic bond formation in PFA-cement mixture is more accurate than the lime-cement and this is because PFA contains higher silica and alumina compared with lime. Indeed lime has a high calcium content compared with PFA, but when lime mixed with cement, pozzolanic bond becomes less accurate due to lack of silica and alumina content and has excessive calcium content as cement itself already has a high calcium content but lacks silica and alumina content and needs to be reminded pozzolanic process is the process by which the contents of calcium, silica and alumina are required evenly for the best bond. Unlike the bond for the PFA-cement mixture, although PFA contains low calcium content but higher silica and alumina, and cement even contains low silica and alumina but higher calcium and when these materials are mixed, the resulting strong bond through the contents of equal calcium, silica and alumina.

5 Conclusion and Recommendation

In this research, a series of shear box and unconfined compression tests were conducted to measure shear strength and strength (UCS) that a mixture of PFA-Cement-Sand medium, with different content of each material, can provide for further application especially the ones that are in the field of ground improvement techniques, i.e.; sand columns, DDM and embankments leveling. After the tests, it has been observed that, PFA which is a waste-by product of power plants, can be significantly associated with the increase of shear strength and UCS in this mixture, however there is a limitation for adding PFA since excessive amount of this material will generate an acidic environment which delays the formation of cementitious gels. Initial moisture content has also an important impact on the final shear strength and UCS, as if it is in the range of OMC, then the specimen was found to be higher in strength than those which were not.

Based on result from shear box test, it can be seen that the formation of graph is such as Mohr-circle form in which the graph is moving upward in conjunction with additional ingredients are added to produce an increase in the shear strength. But when it reaches the optimum level, it began to decline even if the percentage of material is further increased and this is due to the strength of the friction and angle of friction is no longer manipulated by the quantity of material, but other factors may be sought through further study. From the graph, it can be concluded, the quantity of sand is not the main factor though of course the strength of the friction force is coming from the sand but it also requires a well-balanced composition with the addition of other substances, especially PFA and cement that can be formulated is a substance that also plays a major role in increasing the friction force.

For UCT, after 28 days of curing, unconfined compression test of stabilized columns that contained 60 % PFA with 16 % cement gives the highest strength compared to PFA less than 60 % and exceed 60 %. Excessive sand-PFA content in stabilized columns could cause premature failure such as splitting of ends of the specimen and spalling of the surface. The discrepancy between soils with added cement and soils with added lime-cement is large.

However, the findings of the present experimental study are affected by various factors such as, effect of natural soil used for shear box test because it has been collected from site and impossible to be collected from an isotropic sample. Dimension of sample, where sample are prepared based on same mould however, during curing time it has been removed from mould and it is impossible to avoid the changes of size even 1 mm², curing time of preparation of sample etc. Thus, more tests with various material, sample, configuration etc. have to be conducted to make general conclusions.

Acknowledgments The author would like to express an acknowledgement University Technology Mara for the Excellent Fund Project.

References

1. J. Prabakar, N. Dendorkar, Influence of fly ash on strength behavior of typical soils. *Constr. Build. Mater.* **18**(4), 263–267 (2004)
2. S. Guleria, R. Dutta, Tension and compression behaviour of fly ash-lime-gypsum composite mixed with treated tyre chips. *Invent Impact: Civil Eng.* 15 (2011), Article ID 310742. doi:[10.5402/2011/310742](https://doi.org/10.5402/2011/310742)
3. K.B. Najim, M.R. Hall, Mechanical and dynamic properties of self-compacting crumb rubber modified concrete. *Constr. Build. Mater.* **27**(1), 521–530 (2012)
4. C. McDowell, Stabilization of soils with lime, lime-flyash, and other lime reactive materials. *Highw. Res. Board Bull.* 60–66 (1959)
5. Z. Kézdi, *Stabilized Earth Roads, Highway Research Board Bulletin* (Elsevier, New York, 1979)
6. Y. Emori, H. Kawasaki et al., Isolation and sequence analysis of cDNA clones for the small subunit of rabbit calcium-dependent protease. *J. Biol. Chem.* **261**(20), 9472–9476 (1986)
7. H.Y. Fang, *Introductory Geotechnical Engineering: An Environmental Perspective* (Routledge, London, 2006)
8. O. Azadegan, M.J. Yaghoubi et al., A laboratory study of the behavior of the lime/cement slurry and compacted un-reinforced piles. *Electron. J. Geotech. Eng.* **16**, 375–386 (2011)
9. M. Terashi, I. Juran, *Ground improvement—state of the art*, GeoEng, Melbourne, Australia 461–519 (2002)
10. ASTM C150 M, *Standard Specification for Portland Cement* (2001)
11. ASTM D3080, *Standard Tests Method ASTM International*, West Conshohocken, PA (1998)

Dynamic Soil Stiffness Between WAK, SASW and SCPT Tests

Norazzlina M. Sa'don, Michael John Pender
and Abdul Razak Abdul Karim

Abstract This paper describes an experimental investigation for determining the dynamic soil stiffness by applying the principles of WAK (wave-activated stiffness [K]) test analysis, spectral analysis of surface waves (SASW) method and seismic cone penetration test (SCPT). The WAK and SASW tests were performed by applying an impact load on a circular steel plate of 50 cm diameter in vertical direction. A sledgehammer equipped with a dynamic force transducer was used to produce the impact load. The force time signal from the dynamic loading (input) and acceleration time signals from vertical accelerometers (output) were recorded during the tests. The dynamic stiffness of soil was obtained by considering the soil to be vibrating as a single degree of freedom (SDOF) system. The SCPT was performed by measuring the travel times of body waves propagating between a seismic shear wave source at the ground surface activated at each level and an array of geophones. The dynamic soil stiffness obtained from WAK and SASW tests compared very well with the SCPT test.

Keywords WAK · SASW · Dynamic · Soil stiffness · Shear modulus

1 Introduction

In situ geophysical tests have become very important tools for the evaluation of dynamic soil properties and are specially well-suited for hard-to-sample soils. In particular, seismic tests supply good quality data regarding soil behaviour at very

N. M. Sa'don (✉) · A. R. A. Karim
Department of Civil Engineering, Universiti Malaysia Sarawak (UNIMAS),
Kota Samarahan, Sarawak, Malaysia
e-mail: msazzlin@feng.unimas.my

M. J. Pender
Department of Civil and Environmental Engineering, The University of Auckland,
Auckland, New Zealand

small strain level. According to Jardine et al. [1], most soils behave elastically at very small strains, giving rise to a constant stiffness and provide the upper bound (i.e. G_{max}) for stiffness measurement. Also, the theory of elasticity can be directly used to derive the ground stiffness by considering the propagation of elastic waves in an elastic medium. At large strains ($>0.1\%$), plastic behaviour dominates and the stiffness approaches a minimum value (G_{min}). The field seismic testing is one of the techniques used to determine the variation of shear-wave velocity (V_s) for small-strain stiffness profiles with depth at shearing strains less than 0.001% . In a code-based design, the average V_s over the top 30 m (V_{s30}) is used as the key variable for determination of the site response to dynamic excitation such as an earthquake or machine vibration [2]. Field seismic testing methods can be classified as *non-intrusive* if all the instrumentation is mounted on the surface and *intrusive* when boreholes or penetrometers is used to measure the shear wave velocity. The analysis of surface wave propagation in soils for characterization purposes has gained great popularity in the past decades because of the intrinsic advantages of such testing techniques. In particular the non-invasive nature of these methods makes them less costly and time effective when compared to borehole methods, such as cross-hole, down-hole tests or SCPT [3].

The following section provides a brief summary of preferred two non-intrusive and one intrusive method, which is of interest to this paper. The non-intrusive methods; wave activated stiffness (WAK) test and spectral analysis of surface wave (SASW) test and followed by an intrusive method of the seismic cone penetration test (SCPT). The first two methods were preferred due to fast, economic, and no boreholes required, while the latter provides an extremely rapid and reliable way of determining strength and modulus information in one sounding. Also, those techniques are capable of measuring in situ small strain dynamic stiffness of the soil. The test procedure and early development are described in substantial detail by Briaud and Lepert [4] for WAK test, SASW method by [5–8] and [9] for SCPT method. In this paper, evaluation and comparison of dynamic stiffness obtained from the WAK test analysis, spectral analysis of surface waves (SASW) method and cone penetration tests (SCPT) are presented and discussed.

2 Field Seismic Testing Methods

2.1 Wave-Activated Stiffness [K] Test

The WAK (wave-activated stiffness [K]) test, developed by Briaud and Lepert [4], is a dynamic load test performed by hitting a spread footing with sledgehammer in the vertical direction to measure the stiffness of the soil underlying the footing. The force–time signal from the hammer dynamic load cell (input) and the velocity–time signal from the geophones on the spread footing (output) are recorded during the impact. The stiffness of the soil is obtained by considering the

soil to be vibrating as a single degree of freedom (SDOF) system. The most important feature of this test for the design of foundation is that, although essentially a dynamic test, the excitation and the free-body response are of such low frequency that the output may be used to predict the static-output relationship and the transfer function will be independent of the magnitude of the input [10]. Moreover, Briaud and Lepert [4] showed that an analysis of the force and velocity signals using the fast Fourier transform provides a good estimate of the stiffness of the footing-soil assembly. The idea of WAK test comes from the non-destructive techniques (NDT) developed by Paquet [11] and Stokoe et al. [12] for foundation control and also finds its basis and background in the work of several leading researchers in soil dynamics [13].

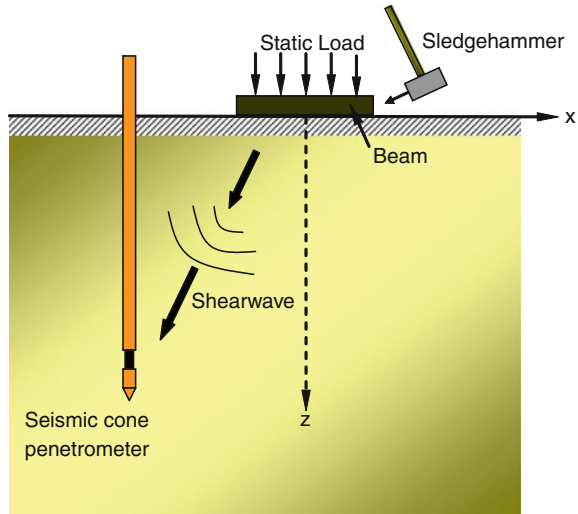
2.2 Spectral Analysis Surface Waves Test

The spectral analysis surface waves (SASW) method is a seismic technique used for in situ evaluation to determine shear wave velocity and shear modulus profiles of target sites. The method has been introduced by Nazarian and Stokoe [14] as an extension of a steady-state Rayleigh wave technique by Richart et al. [15]. The tests consists generally of three steps; (a) field testing, (b) evaluation of dispersion curve by phase unwrapping method to compute the variation of Rayleigh wave velocity with frequency, and (c) determination of shear wave velocity profile by inversion curve. In the SASW method, both the source and receivers are placed on the ground surface. Impulsive, harmonic or random-noise load was used to apply vertical excitation to generate Rayleigh waves. Propagation of the waves is monitored with the surface receivers located at known distances apart. The SASW method is based on dispersive characteristic of surface waves because it allows different materials to be sampled by using different wavelengths. Most of the surface wave energy exists within one wavelength of depth and in layered media; the propagation velocity of surface waves become dependent on the frequency or wavelength and different frequencies will propagate with different velocities. This velocity is termed phase velocity or apparent Rayleigh wave velocity [5].

2.3 Seismic Cone Penetration Test

The introduction of seismic measurements into the cone penetration test (CPT) procedures enables the specific determination of the dynamic shear modulus (G_{max}). In order to obtain the measurement of dynamic shear modulus, a small rugged velocity seismometer has been incorporated into the cone penetrometer. The seismometer is placed in the horizontal direction and oriented transverse to the signal source to detect the component of the shear wave arrivals [8]. The SCPT is a modification of the cone penetrometer tests used to determine the variation with

Fig. 1 Field's arrangements for seismic cone penetration test



depth of the shear wave velocity in down-hole testing arrangements [9]. A seismic source is generated at the surface near the insertion point of the cone to generate the shear waves. The travel times of the shear wave energy are measured at one or more locations above the cone tip as shown in Fig. 1. After testing at one depth, the cone is penetrated further into the soil, and the test is repeated. One of the important benefits of this method is that the seismic data can be combined with the cone resistance values to represent a clearer profile of both soil type, strength, stiffness and layering [16].

3 Field Investigations

3.1 Site Descriptions

The selected site is located in Albany, north of Auckland City, within an area being developed for residential purposes. The site consists of residual clay of yellowish in colour. The material at the site was referred as Auckland residual clay.

This material is a product of in situ weathering through which the Waitemata group sandstones and siltstones are transformed to produce a highly variable cohesive soil [17].

The physical properties of the Auckland residual soil is tabulated in Table 1.

Table 1 Index properties of Auckland residual clay

Liquid limit, w_{LL} (%)	61.5
Plastic limit, w_{PL} (%)	30.2
Plasticity index, I_p	31.3
Natural water content, w_N (%)	38.0
Undrained shear strength, s_u (kPa)	100.0

Fig. 2 Test set-up



Fig. 3 Field's test instrumentation set-up



3.2 Instrumentation and Test Procedure

A circular steel plate with 500 mm diameter and 25.4 mm thick were rigidly placed on a new flat ground surface as shown in Fig. 2. From the figure, it can be seen that a layer of plaster was laid between the steel plate and the ground surface to make sure that a good contact between soils and silts was established, and no energy losses should occur due to plastic shearing of the soil beneath the plate. A Dytran instrumented sledgehammer model 5803A was utilised to produce an impact loadings.

Fig. 4 Experimental set-up for WAK and SASW testing

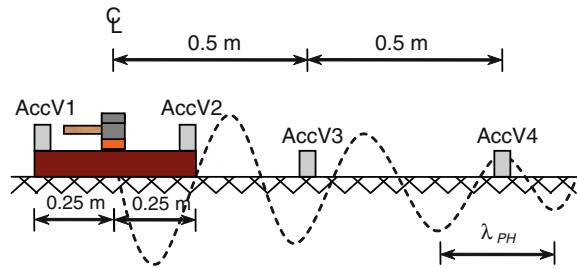


Figure 3 shows the 16 Bit data acquisition box connected to a computer for recording the output and input signals during the tests. MATLAB 2007 software was used to control the data acquisition operations. The sample rate used in all tests was 500 data per second. A total of four vertical accelerometers with ± 2 g sensitivities were used in the WAK and SASW tests for recording the acceleration produced by the instrumented sledgehammer. The accelerometers were chosen instead of geophones in these tests. This is because the geophones were not appropriate for detecting the change in stiffness due to the high accelerations generated by impulsive forces as recommended by Merrifield and Davies [10].

Two vertical accelerometers (AccV1 and AccV2) were screwed on top of the circular steel plate for soil stiffness determination (WAK tests). The remaining two accelerometers, labelled as AccV3 and AccV4, were securely placed on the ground at 50 and 100 cm, respectively from the centre of the steel plate to measure shear wave velocity produced by dynamic loading (SASW tests). By applying the experimental setup shown in Fig. 4, the WAK and SASW tests were implemented one after the other. The soil is assumed to be a linear, isotropic and homogeneous medium and measured at small strain levels. Thus, the wave propagating through the soil layer travel in the vertical direction (WAK) is similar to the wave travel in the horizontal direction (SASW).

For each geophysical test point, two impact tests with an average of four blows were performed. All tests were performed by hitting the centre of the circular steel plate using the sledgehammer equipped with a dynamic force transducer. A rubber tip was attached to the sledgehammer to focus the energy of the impact in the lower frequencies as suggested by Briaud and Lepert [4]. In all cases, the operator attempted to produce a similar magnitude of force, and the response was recorded for the duration of 120 s. Typical load signal obtained from the impact loading was illustrated in Fig. 5.

The SCPT given in Fig. 6 was conducted at two locations and was pushed down up to 4.0 m depth with one meter intervals. The test consists of measuring the travel times of body waves propagating between a seismic shear wave source at the ground surface activated at each level and an array of geophones. The tests were conducted to determine the shear wave velocity and shear modulus of the soil under small strain.

Fig. 5 Typical force signals produced by the impact loading

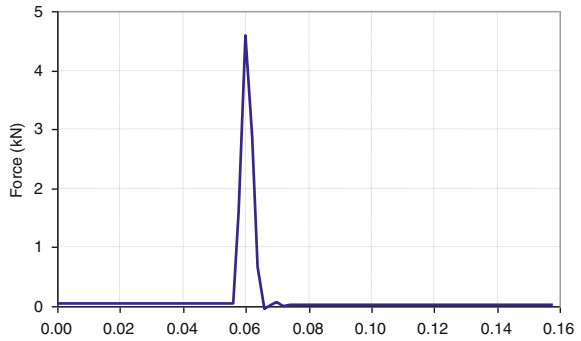


Fig. 6 Seismic cone penetration tests



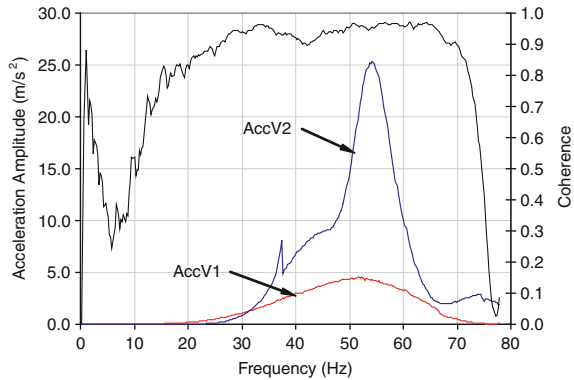
4 Results and Discussion

4.1 Wave-Activated Stiffness [K] Test

The force–time signal from the impact loading (input) and the acceleration-time signal obtained from the vertical accelerometers (output) were analysed. For WAK tests, only accelerometers attached on the steel plate were considered in the analysis. The coherence values between the input and output were initially determined as shown in Fig. 7.

These coherence values were used as an indicator of data quality in a given frequency range and only information corresponding to high values of such function are considered. The result shows that the output recorded was over 95 % at frequency ranging from 20 to 80 Hz. This indicates perfect correlation between the two signals and that the signals are not contaminated with random background noise. Thus, only the responses corresponding to 20 Hz and above were considered for further analyses. An average of four blows was used to produce the power

Fig. 7 Power spectrum readings from two accelerometers and coherence functions for impact loading



spectrum for both vertical accelerometers (AccV1 and AccV2) attached on the steel plate, as shown in Fig. 7.

Figure 8 illustrate the punching mode of vibrations that was determined in the range of 10–80 Hz. Punching modes was determined by averaging both the AccV1 and AccV2 signals. This punching mode is the mode of interest in determining the stiffness of the soil against the vertical motion (K_v). Therefore, the average of the signals from the two accelerometers was used to obtain the acceleration of the footing for all other tests. The peak frequencies indicate punching mode is presented in Fig. 8.

The vertical stiffness (K_v) of the soil was then calculated by using the equation given below:

$$K_v = 2\pi \left(\frac{\text{Frequency}}{\text{Velocity/Force}} \right) \tag{1}$$

while the shear modulus (G_s) and Young's modulus (E_s) of the residual clay were determined by using the equation for elastic stratum on rigid base of surface circular foundation as stated below:

$$G_s = \frac{K_v(1 - \nu_s)}{2R} \tag{2}$$

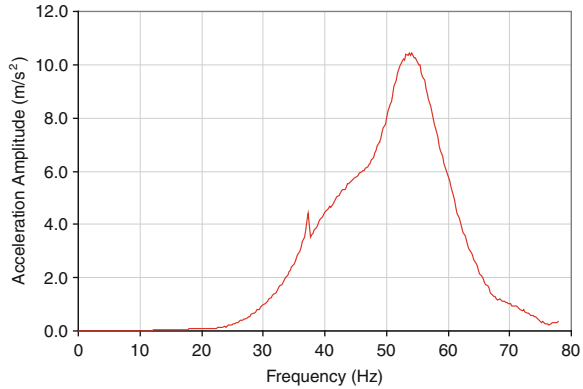
$$E_s = 2G_s(1 + \nu_s) \tag{3}$$

The shear wave velocity (V_s) which is related to the dynamic elastic constants of the soil is calculated by using Eq. (4):

$$V_s = \sqrt{G_s \rho_s} \tag{4}$$

where R = radius of circular plate; ν_s = Poisson ratio of 0.4 and $\rho_s = 1,700 \text{ kg/m}^3$ (ρ_s is the density of the soil taken from published literature for Auckland residual clay).

Fig. 8 Punching modes of impact loading



The vertical stiffness (K_v) and the shear modulus (G_s) of the soil determined from dynamic load were calculated and summarized in Table 2.

4.2 Spectral Analysis Surface Waves Test

The SASW tests were performed to determine the shear wave velocity and shear modulus of the Auckland residual clay. Only the two vertical accelerometers (V3 and V4) that were placed on the ground surface were used in the analysis of the SASW tests. The typical signal processing results based on the cross power spectrum and phase angle for SASW testing are presented in Figs. 9 and 10, respectively. The SASW analysis was modelled as a linear system, which the soil media are measured at small strain levels. According to Stokoe and Nazarian [5], the cross power spectrum is a good tool in determining the relative phase difference between two signals caused by time delays, propagation delays or varying paths between receivers. Also, the coherence function shows the frequency range at which most of energy is concentrated and indicates that the signals recorded are not contaminated with random background noise (i.e. high response-to-noise ratio). Thus, from the coherence function, only frequency ranges for which coherence was greater than 0.9 are considered and further analysed to determine the shear modulus and shear wave velocity.

By knowing the distance between the receivers (x) and the phase shift ($\Delta\theta$) for each frequency (f) determined from the cross power spectrum of the two signals, the phase velocity (V_{PH}), and wavelength (λ_{PH}), associated with a given frequency can be calculated by the following formulas:

$$\text{Phase velocity, } V_{PH} = \frac{360xf}{\Delta\theta} \tag{5}$$

Table 2 Auckland residual clay properties under small strain obtained from WAK test analysis

Test point	Shear modulus, G_s (MPa)	Shear waves velocity, V_s (m/s)	Max depth, $D_{max} = V_s/f$ (m)
WAK 1	48	167	2.4
WAK 2	33	139	2.6

Fig. 9 Coherence functions and the cross power spectrum recorded

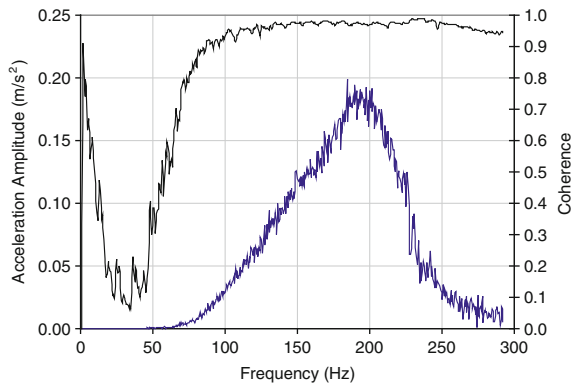
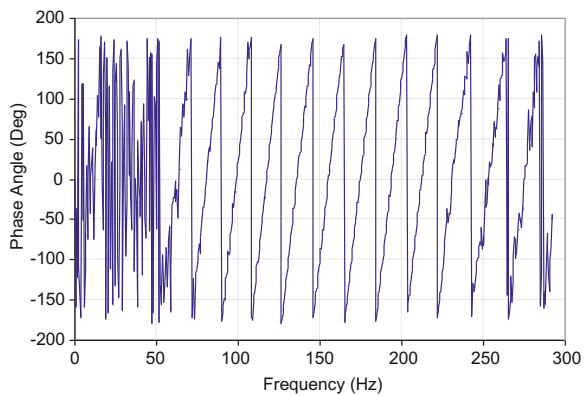


Fig. 10 Phase components of the cross power spectrum



$$\text{Wavelength, } \lambda_{PH} = \frac{V_{PH}}{f} \tag{6}$$

These calculations yield an experimental dispersion curve (V_{PH} vs. λ_{PH}) for the receiver spacing. Once all experimental dispersion curves for a set of receiver spacing are constructed, they are combined together and a composite experimental dispersion curve of a site is developed. The dispersion curve may be disturbed in the low frequency range because of the near field effect which occurs due to limitation of recording equipment and attenuation properties of soil media. To

Table 3 Filtering criteria for SASW test (adopted from [18])

Source	First receiver	Receiver spacing
Lysmer	$2.5\lambda < x$	–
Heisey et al. [19]	$x = \Delta x$	$0.333\lambda < \Delta x < 2\lambda$
Sanchez-Salinerro et al.	$x = \Delta x$	$2\lambda < \Delta x$
Roesset et al.	$\lambda < x < 2\lambda$	$0.5x < \Delta x < x$
Gucunski and Woods	–	$0.5\lambda < \Delta x < 4\lambda$
Tokimatsu et al.	$0.25\lambda < x + \Delta x/2$	$0.0625\lambda < \Delta x < \lambda$

Note x indicates near receiver distance from source; Δx is receiver spacing; and λ is wavelength

Table 4 Typical calculation for Rayleigh’s wave velocities for impact tests

f (Hz)	$\Delta\theta$ (deg)	λ (m)	$Z = \lambda/2$ (m)	$V_{PH} = V_R$ (m/s)	$V_s = 1.1 V_R$ (m/s)
121.9	151	1.192	0.397	145.33	159.8
122.4	155	1.154	0.366	141.30	155.4
139.0	177	1.017	0.339	141.37	155.5

Table 5 Auckland residual clay properties under small strain obtained from SASW test analysis

Test point	Shear modulus, G_s (MPa)	Shear waves velocity, V_s (m/s)	Max depth, $D_{max} = V_s/f$ (m)
SASW 1	49	171	2.5
SASW 2	42	157	2.4

overcome near field effect, a filtering criterion is commonly applied to the information extracted from a single testing setup.

Many filtering criteria were proposed as shown in Table 3 adopted from Ref. [18]. In this study, [19] criterion was chosen as it is widely used in SASW method.

Table 4 shows typical calculations for Rayleigh wave velocity V_R , which gives phase differences, $\Delta\theta$, against distance, x (0.5 m), at peak frequencies recorded. Reference [15] stated that in linear elastic homogeneous medium, Rayleigh wave velocity of propagation is dependent on frequency and its value is about 10 percent less than that of the shear waves velocity, V_s ($V_s \approx 1.1V_R$).

Thus, by employing an approximate straightforward inversion technique, the shear modulus of Auckland residual clay, G_s , was calculated from the shear wave velocity by using $G_s = V_s^2/\rho_s$. G_s is the shear modulus at a very small strain measured in a short period of time. The Young’s modulus, E_s was then determined using Eq. (3). The results obtained from SASW are tabulated in Table 5.

Also, the effective sampling depth for each wavelength is considered in this paper to be equal to a fraction of the wavelength obtained. It has been recommended by several authors that 1/2–1/3 of the wavelength is representative of the effective depth of sampling [5].

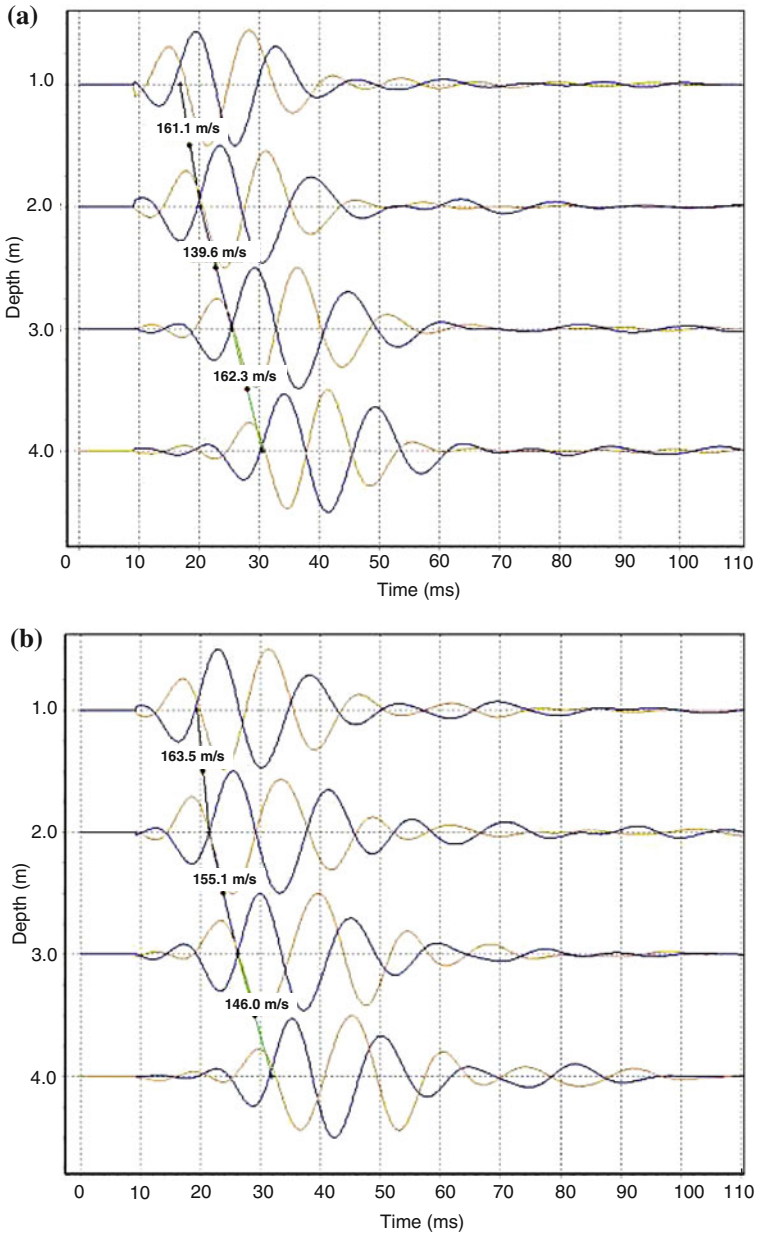


Fig. 11 Results from the SCPT data. a SCPT 1. b SCPT 2

Table 6 Auckland residual clay properties under small strain obtained from SCPT

Location	Shear wave velocity V_s (m/s)	Shear modulus G_s (MPa)	Depth D (m)
SCPT 1	161	44	1–2
	140	33	2–3
	162	45	3–4
SCPT 2	164	45	1–2
	155	41	2–3
	146	36	3–4

Table 7 Summary of dynamic soil properties under small strain for different tests

Location	Shear wave velocity V_s (m/s)	Shear modulus G_s (MPa)	Depth range D (m)
WAK	139–167	33–43	0.5–2.6
SASW	157–171	42–49	0.5–2.5
SCPT	140–164	33–45	1.0–4.0

4.3 Seismic Cone Penetration Test

Figure 11 illustrates the results for the SCPT recorded. The tests were conducted to determine the shear wave velocity and shear modulus of the soil under small strain. The shear wave velocity recorded from SCPT, and the calculated shear modulus was tabulated in Table 6.

5 Relationship Between WAK, SASW and SCPT

WAK, SASW and SCPT tests have been performed in Albany site. In the analysis, the soil is assumed to be a linear, isotropic and homogeneous medium, thus the wave propagating through the soil layer travel in the vertical direction is similar to the wave travel in the horizontal direction. From the results summarized in Table 7, the shear wave velocity and shear modulus of the soil determined from SCPT shows a good relationship with both WAK and SASW tests.

6 Conclusion

The non-invasive (WAK and SASW) and invasive (SCPT) seismic approach have shown a good agreement in evaluating the shear modulus and shear wave velocity of the soil. Further, the objectives of this paper to demonstrate the non-invasive method is fast, economic and no boreholes required were achieved.

Acknowledgments The authors would like to express gratitude to the Universiti Malaysia Sarawak (UNIMAS), for the financial support granted to the first author, CDL Investments for permission to use the land for the research and Perry Drilling for carrying out the extensive CPT and SCPT testing.

References

1. R.J. Jardine, D.M. Potts, A.B. Fourie, J.B. Burland, Studies of the influence of non-linear stress-strain characteristics in soil-structure interaction. *Geotechnique* **36**(3), 377–396 (1986)
2. K.H. Stokoe II, Field seismic testing in geotechnical earthquake engineering, in *Earthquake Geotechnical Engineering*, ed. by K.D. Pitilakis (Springer, Netherlands, 2007), pp. 151–157
3. S. Foti, R. Lancellotta, L. V. Socco, L. Sambuelli, Application of fk analysis of surface waves for geotechnical characterization. in *Fourth International Conference on Recent Advances in Geotechnical Earthquake Engineering and Soil Dynamics and Symposium in Honour of Professor W.D. Liam Finn*, San Diego, California (2001) Paper No: 1.14
4. J.-L. Briaud, P. Lepert, WAK test to find spread footing stiffness. *J. Geotech. Eng.* **116**(3), 415–431 (1990)
5. K. H. Stokoe II, S. Nazarian, Use of Rayleigh waves in liquefaction studies. Measurement and use of shear wave velocity for evaluating dynamic soil properties. in *Proceedings of a Geotechnical Engineering Division Session*, ASCE Convention, Denver, Colorado, May 1, pp. 1–17 (1985)
6. D. Yuan, S. Nazarian, Automated surface wave method: inversion technique. *J. Geotech. Eng.* **119**(7), 1112–1126 (1993)
7. N. Gucunski, R.D. Woods, Numerical simulation of the SASW test. *Soil Dyn. Earthq. Eng.* **11**, 213–227 (1992)
8. P.K. Robertson, R.G. Campanella, Seismic CPT to measure in situ shear wave velocity, in *Measurement and Use of Shear Wave Velocity for Evaluating Dynamic Soil Properties*, ed. by R.D. Woods (ASCE, Denver, 1985), pp. 34–48
9. R. G. Campanella, P.K. Robertson, D. Gillespie, in *Seismic cone penetration, Use of In-Situ Tests in Geotechnical Engineering*, ed. by S. P. Clemence. Proceedings, In-Situ 1986 (ASCE Geotechnical Special Publication No. 6, Balcksburg, 1986) pp. 116–130
10. C.M. Merrifield, M.C.R. Davies, A study of low-energy dynamic compaction: field trials and centrifuge modelling. *Geotechnique* **50**(6), 657–681 (2000)
11. J. Paquet, Study vibratory concrete piles; harmonic and transient response; application control. *Annals of the Institute of Technical Building and Public Works*, vol. 245, pp. 789–803 (1968) (in French)
12. K.H. Stokoe, L.D. Olson, L.D. Reese, *Integrity testing of drilled shaft*. in *Proceedings of International Association of Drilled Shaft Contractors, Geotechnical Engineering Faculty Workshop*, Fort Collins, Colo., July (1987)
13. J.-L. Briaud, M. Ballouz, LATWAK: impact test to obtain pile lateral static stiffness. *J. Geotech. Eng.* **122**(6), 437–443 (1996)
14. S. Nazarian, K.H. Stokoe II, *In Situ Shear Wave Velocities from Spectral Analysis of Surface Waves*. Proceedings of the Eighth World Conference on Earthquake Engineering, San Francisco, California, vol. III, 21–28 July 1984, pp. 31–38
15. F.E. Richart Jr, R.D. Wood, J.R. Hall Jr, *Vibration of Soils and Foundations* (Prentice-Hall, New Jersey, 1970)
16. K.H. Stokoe II, S.H. Joh, R.D. Woods, Some contributions of in situ geophysical measurements to solving geotechnical engineering problems. in *International Conference on Site Characterization (ISC-2)*, Porto, Portugal (2004)
17. N. M Sa'don, Full-scale static and dynamic lateral loading of a single pile. PhD Thesis, University of Auckland, NZ, 2012

18. V. Ganji, N. Gucunski, S. Nazarian, Automated inversion procedure for spectral analysis of surface waves. *J. Geotech. Geoenvironmental Eng.* **124**, 757–770 (1998)
19. J.S. Heisey, K.H. Stokoe II, A.H. Meyer, Moduli of pavement systems from spectral analysis of surface waves. *Research Record No. 852*, Transportation Research Board, pp. 22–31 (1982)

The Influence of Cyclic Load to the Properties of Weathered Granite

N. A. M. Salim, Z. Mohamed and M. N. Berhan

Abstract This paper briefly elaborates the influences of cyclic loading to the physical and dynamic properties of weathered granite. Petrological description of weathered rocks is also discusses as well as other important characteristics of rock which may affect the cyclic loads analysis. To find out the possible effect between weathered rock physical and dynamic properties with cyclic loading, weathered specimens are tested under same cyclical load condition of 1 Hz, stress ratio of 0.14 and using sinusoidal waveforms.

Keywords Weathered rock · Dynamic · Cyclic load · Rock properties

1 Introduction

Dealing with weathered rock is not easy and to classify them accordingly to its weathering degree needs to be adequately determined, especially when its associates with the determination of rock fatigue failure. Fatigue failure in rocks is said to be closely related to their petrological, physical and mechanical properties [1–3]. In order to understand holistically the behavior of weathered rock, the first step is to investigate the material microscopically, followed by the determination of rock properties; which have significant affects by its weathering condition. To assess weathering, a few methods can be adopted to classify rock material based on its weathering condition. Microscopically, thin section is prepared to evaluate

N. A. M. Salim (✉) · Z. Mohamed
Institute for Infrastructure Engineering and Sustainable Management (IIESM),
Faculty of Civil Engineering, Universiti Teknologi MARA, Shah Alam, Malaysia
e-mail: nurulain2@yahoo.com

M. N. Berhan
Institute for Infrastructure Engineering and Sustainable Management (IIESM),
Faculty of Mechanical Engineering, Universiti Teknologi MARA, Shah Alam, Malaysia

the existing rock mineral structure influenced by weathering. Grain size and mineral composition of rock specimen is examined under polarized microscope. While characterization based on rock properties is conducted using non-destructive test such as ultrasonic pulse velocity and Schmidt rebound hammer and the specimens were also classified based on its strength and porosity.

This paper elaborates the effect on weathered granite properties due to the increasing numbers of uniaxial cyclic compression loads on specimen. The experimental data obtained are analyzed to clarify the changes in velocity of brittle rocks in relation to their cyclic stress history. Relationship between the numbers of cycles with the dynamic properties of rock is also discussed. Results are described based on different weathering grades of granite namely grade II, grade III and grade IV. Throughout this paper, V_p is referred to as compressional wave velocity while V_s is shear wave velocity.

2 Experiment Procedure and Tests

2.1 Selecting Rock Specimen

Cylindrical specimen of height-to-diameter ratio (h/d) of 2 is used for all tests. Block samples were collected from Kuang Quarry, Sg. Buloh and specimens were prepared based on Ref. [4]. The weathering degree of each specimen is characterized by using Schmidt rebound number and the weathering classification of hand-sized specimen is referred to Ref. [5].

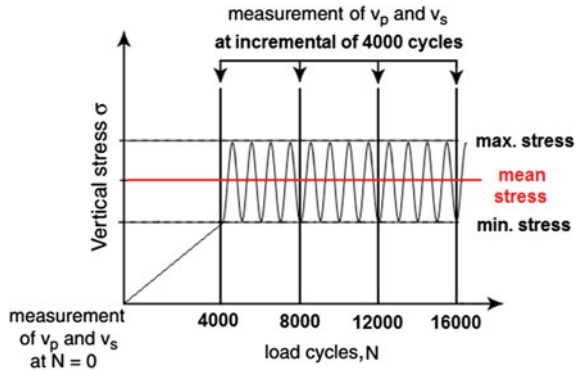
Cyclic loading test is conducted on grade II, III and IV granite specimen. The cyclic test is designed using constant sinusoidal wave and the maximum load for the test is at 70 % of the unconfined compressive strength (UCS). Maximum load applied on granite specimen is 79 MPa for grade II, 30 MPa for grade III and 10 MPa for grade IV. The stress ratio is kept constant at 0.14 for every test specimen. The specimen compressive wave velocity and shear wave velocity is recorded every 4,000 cycles of cyclic loading as illustrated in Fig. 1.

However, the effect on rock specimen by initial impact of machine piston is generally neglected in conducting this test.

2.2 Surface Characterization and Petrographic Description

Specimen core surface is described by its discoloration, staining and grain boundaries. The specimen surface images was captured using digital camera is set to macro mode; which enables sharper and close-up image. The description of the observation is explained in Table 1. The observation is meant to describe the dissimilarity of their physical appearances by specimen weathering grades.

Fig. 1 Measurement process for v_p and v_s



To supplement the analysis, a detailed petrographic study of thin-sections was undertaken to characterized rock by weathering grade.

Petrographical variations exhibited in granite specimens were evaluated with the aid of a polarizing optical microscope. Specimen is categorized as medium-grained which has 1–5 mm in size. The mineral composition is mainly quartz, feldspar, biotite mica and other accessory minerals. Petrographic analysis was done based on specimen weathering grade which is Grade II (R-num.: 45–47), Grade III (R-num.: 34–37) and Grade IV granite (R-num.: 16–18).

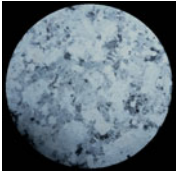
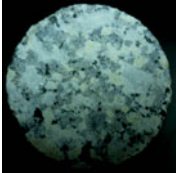
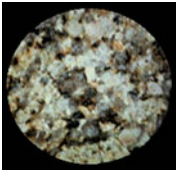
The analysis shows as weathering grade increases, some minerals becomes altered. The ongoing process of weathering may cause slight staining in grade II specimen. Although the minerals do not show any significant increase in the degree of alteration (Table 2a), slight sericitization of plagioclases is seen and microcracks is also display in Quartz grains.

With the development of weathering (Grades III), specimen is notably stained and the grain boundaries are intact to semi-intact. Besides, moderate sericitization of plagioclases is found in specimen (Table 2b). Moderately decomposed K-feldspars at times are shown in specimen. Slight to moderate chloritization of biotites is also common. Slight to moderate stained in grain boundaries is shown however the minerals are intact in general. Microcracks in Quartz are also seen in Grade III specimen as Quartz is a stable mineral and could not be altered.

As weathering intensifies (Grade IV), specimen considerably stained with loose grain boundaries (Table 2c). Highly altered plagioclases and biotites are common. Moderately to highly decomposed K-feldspars are also found in specimen.

The preparation of thin-section of specimen appearances in terms of staining, alteration of individual minerals, nature of grain boundaries and existing micro-crack portray a clear gradational weathering effect on the investigated rocks. Therefore, petrographic study is conducted to substantiate the weathering classification.

Table 1 Surface characteristic based on weathering grades

Specimen core	Surface characteristic	Weathering grade
	<ul style="list-style-type: none"> • Insignificant amount of staining on the surface • Intact grain boundaries 	II
	<ul style="list-style-type: none"> • Slight to moderate staining • Slightly decomposed • Intact grain boundaries 	III
	<ul style="list-style-type: none"> • Highly staining on the surface • Highly decomposed with loose grain 	IV

2.3 Physical and Mechanical Properties

A total of 30 representative specimens with different weathering grades are used to determine their physical and mechanical properties. To reduce specimen variables, those properties need to determine adequately prior cyclic loading test. The physical properties which measured in this study are rebound number, moisture content, porosity, dry density and also compressional wave velocity, V_p . While for mechanical properties are uniaxial compressive strength (UCS), static Young modulus, E_s and Poisson’s ratio. The mean values for the physical and mechanical properties are tabulated in Tables 3 and 4 respectively.

From Table 3, specimens were initially categorized by rebound number; where the mean rebound number, R for grade II specimen is 46, grade III is 36 and grade IV specimen is 17. Significant variation in properties can be observed in grade II, III and IV specimens. For physical properties, moisture content and porosity is found increase as the weathering grades increases. While for dry density and compressional wave velocity, V_p the value is decrease as the weathering grade increases.

As for mechanical properties, uniaxial compressive strength and the static young modulus, E_s were found increase with the increase in weathering grade. However, Poisson’s ratio is decreases with the increase in weathering grade.

Table 2 Photomicrograph of granite based on weathering grades

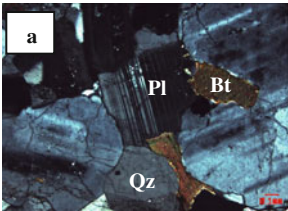
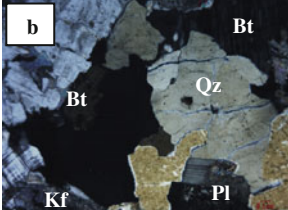
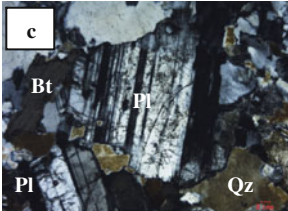
Photomicrograph	Description
	<p><i>Grade II</i></p> <ul style="list-style-type: none"> • Insignificant alteration in rock minerals • Minor crack with no alteration can be seen in Quartz
	<p><i>Grade III</i></p> <ul style="list-style-type: none"> • Slight alteration can be seen in plagioclase feldspar (Pl) and K-feldspar (Kf) • No alteration in Quartz (Qz) but minor crack can be seen • No obvious alteration in biotite (Bt)
	<p><i>Grade IV</i></p> <ul style="list-style-type: none"> • Higher alteration can be seen in plagioclase feldspar (Pl) • No alteration in Quartz (Qz) but minor crack can be seen • No obvious alteration in biotite (Bt)

Table 3 Physical properties of granite specimen

Weathering grade	Physical properties (Mean value)				
	Rebound No. (N)	Moisture content (%)	Porosity (%)	Dry density (kg/m ³)	Vp (m/s)
II	46	0.114	0.898	2,660	6,715
III	36	0.305	0.899	2,602	3,365
IV	17	0.964	0.900	2,505	2,092

Table 4 Mechanical properties of granite specimen

Mechanical properties (Mean value)		
UCS (MPa)	Static young modulus, Es (GPa)	Static Poisson ratio
112.903	34.525	0.330
42.297	21.251	0.334
13.628	5.361	0.345

Fig. 2 Free-free resonant column test and equipment set-up

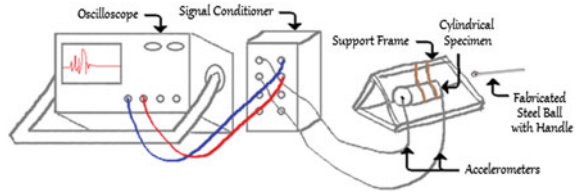


Table 5 Velocities and dynamic properties of grade II granite

Sample No.	GRSG2				GR22G2			
	Primary wave, V_y (m/s)	Shear wave, V_y (m/s)	Dynamic modulus, E	Dynamic Poisson's ratio, ν	Primary wave, V_p (m/s)	Shear wave, V (m/s)	Dynamic modulus, E	Dynamic Poisson's ratio, ν
0	7,536	2,246	70.31	0.451	7,429	3,019	67.23	0.431
4,000	7,424	3,074	70.51	0.397	8,000	2,988	66.67	0.419
8,000	6,933	3,098	70.51	0.375	8,667	2,973	66.67	0.433
12,000	6,881	3,083	68.81	0.355	8,000	2,988	66.67	0.419
16,000	6,118	3,057	66.87	0.324	7,879	2,978	66.12	0.417
20,000	5,778	3,033	64.37	0.310	7,429	2,992	66.12	0.403
24,000	–				6,500	3,039	66.12	0.360
28,000					6,118	3,072	66.12	0.331
32,000					5,943	3,092	66.12	0.314
36,000					5,778	3,115	66.12	0.295
40,000					5,714	3,125	66.12	0.287

2.4 Free-Free Resonant Column Method in Determining V_p and V_s

Measured compressional, shear wave velocities and signal amplitudes are sensitive to the changes in the rock's properties through damaged or disturbed region. Free-free resonance column (FFRC) method is adopted in this study to determine the effect of cyclic loading to the properties of weathered granite specimens. This method enables the determination of compressional wave velocity, V_p as well as shear wave velocity, V_s .

Rock specimens were mounted between accelerometers and hanging by a support frame as in Fig. 2. The compressional wave velocity, V_p of ultrasonic waves travelling certain distance of the specimens can be calculated by measuring the time between the sending and receiving waves. The waves are generated by hammering one side of specimen surface using fabricated steel ball. Dynamic properties such as E_D and Poisson's ratio are determined using Mathcad software; which also included the value of V_p as well as V_s .

At every increment of 4,000 cycles, V_p and V_s are recorded to observe the influence of cyclic loads to the specimens. The results are then summarized in Tables 5, 6 and 7 according to its weathering grade. The cyclic load tests are stopped

Table 6 Velocities and dynamic properties of grade III granite

Sample No.	GR161G3				GR42G3			
	Primary wave, V_F (m/s)	Shear wave, V_s (m/s)	Dynamic modulus, E	Dynamic Poisson's ratio, ν	Primary wave, V_F (m/s)	Shear wave, V_s (m/s)	Dynamic modulus, E	Dynamic Poisson's ratio, ν
0	5,579	2,609	47.64	0.460	5,786	2,591	48.04	0.450
4,000	7,571	2,499	46.24	0.439	6,972	2,581	47.80	0.421
8,000	6,628	2,588	48.58	0.410	6,972	2,555	47.76	0.422
12,000	6,625	2,615	49.53	0.410	6,152	2,554	47.33	0.396
16,000	5,888	2,619	48.58	0.409	6,152	2,526	47.31	0.399
20,000	4,818	2,735	48.58	0.408	5,810	2,570	47.13	0.378
24,000	4,818	2,746	46.24	0.377	5,976	2,561	46.78	0.393
28,000	4,609	2,864	50.01	0.186	5,810	2,570	46.63	0.378
32,000	4,417	2,813	47.17	0.159	5,504	2,589	46.63	0.358
36,000	4,417	2,861	46.24	0.179	5,229	2,613	46.63	0.334
40,000	–				4,754	2,681	46.63	0.267

when the difference in velocities is apparent and continue up to 40,000 cycles only. However, there are specimens which fail before reaching 40,000 cycles.

Initially, the compressional wave velocity, V_p and shear wave velocity, V_s of specimens are recorded prior subjected to any loads. The reason is to observe the possible effect contributed by cyclic loads onto specimens. At the first 4,000 cycles, results shows most of the specimens experienced the rise in V_p , while having reduction in V_s . The percentage of increments for V_p is found between 7.1 and 42.8 %. It is observed that, the percentage is increase as the weathering grade increases. While the reduction percentage for V_s is around 1.0–4.2 %. However, it is differ for GR8G2 specimen; where V_p is started to decrease (Fig. 3), while V_s is increasing for the first 4,000 cycles (Fig. 4). It is hard to explain theoretically since specimen is categorized as strong rock (Grade II) compared to other specimens. However, based on V_s at 4,000 cycles, the graph is dramatically increased, showing that the specimen started to suffer by cyclic loads; perhaps small cracks may have develop in rock by this condition. It is revealed that shear wave is more sensitive to small discontinuities as compared to compressional wave [6]. As cycles continue further, GR8G2 failed approximately at 20,000 cycles. Thus, the result verifies the previous statement.

As cycles continue to 8,000 cycles, the increments of V_p is observed while V_s is decreases. Normally as a rock being compressed, at the early stage of loading the flaws exhibited in rock specimen including cracks and voids are affectively closed; though in reality the cracks will not be completely close. As specimen being compressed and flaws is closed, specimen having lower reading in V_s in this stage. Once continues to 12,000 cycles, V_p beginning to decreases as cycles increases. As rock becoming weaker, V_s started to have lower reading.

Table 7 Velocities and dynamic properties of grade IV granite

Sample No.	GR29G4				GR24G4			
	Primary wave, V_F (m/s)	Shear wave, V_s (m/s)	Dynamic modulus, E,	Dynamic Poisson's ratio, ν	Primary-wave, V_F (m/s)	Shear wave, V_s (m/s)	Dynamic modulus, E	Dynamic Poisson's ratio, ν
0	2,287	1,554	12.79	0.465	2,551	1,371	13.47	0.450
4,000	3,710	1,271	11.99	0.434	4,456	1,334	11.68	0.451
8,000	3,586	1,246	11.51	0.431	5,305	1,300	11.23	0.468
12,000	3,470	1,262	11.75	0.424	4,285	1,295	11.00	0.450
16,000	3,470	1,276	11.99	0.422	3,979	1,313	11.23	0.439
20,000	3,470	1,262	11.75	0.424	3,841	1,288	10.71	0.437
24,000	3,362	1,293	11.95	0.413	3,594	1,293	10.78	0.426
28,000	3,362	1,282	11.72	0.409	3,375	1,299	10.78	0.413
32,000	3,260	1,254	11.25	0.413	3,276	1,288	10.56	0.409
36,000	3,164	1,243	11.02	0.409	3,276	1,273	10.33	0.411
40,000	2,988	1,236	10.80	0.397	3,183	1,247	9.919	0.409

Basically, results were based on the entire graph trend, although slight fluctuation can be seen in V_p and V_s reading between 8,000 and 40,000 cycles. Slight result fluctuation probably cause by surroundings interference such as noise and vibration from neighboring laboratory while conducting the test. As cycles continue, V_p shows a declining trend for all grade II, grade III and grade IV specimens; where specimens beginning to experience the effect caused by cyclic loadings. As V_p decreases, V_s kept increasing indicating small cracks start to open-up and develop.

2.5 Dynamic Properties Effect on Specimen Subjected to Cyclic Loads

From Mathcad application, dynamic properties are able to be determined. The relation between dynamic properties with cyclic loads is illustrated in Figs. 3 and 4. From the result, it shows that the value of dynamic modulus is decreased at the first 4,000 cycles, except for GR8G2. The result show a slight decrease compared to the dynamic modulus before subjected to cyclic loads; at this stage specimens should becomes more rigid as the loads being applied. However, the specimen shows different behaviour. This can be explained that dynamic modulus depends on stress, where dynamic modulus decreases at high stress and increases with stress at low [7]. Dynamic modulus may increase as V_p increases in static compression but in cyclic compression loads, due to high impact and stress, the result is vice versa.

Based on Fig. 5, dynamic modulus is slowly reducing as cycles continue. However, the rate of reduction is found minimal except for GR8G2. Its dynamic

Fig. 3 Relation between compressional waves velocity, V_p with number of cycle

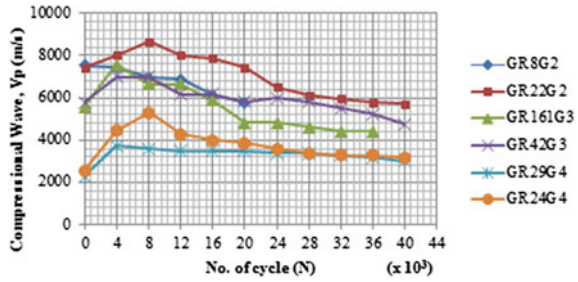


Fig. 4 Relation between shear waves velocity, V_s with number of cycle

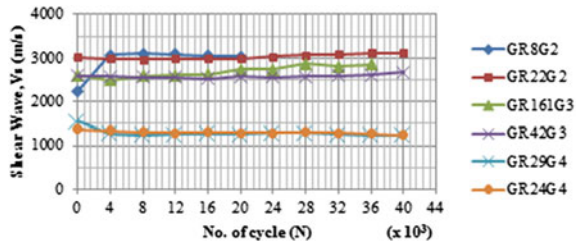
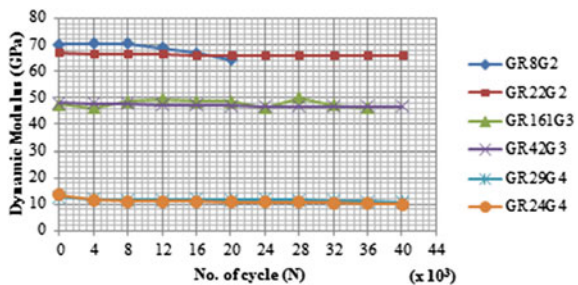


Fig. 5 Relation between dynamic modulus with number of cycle

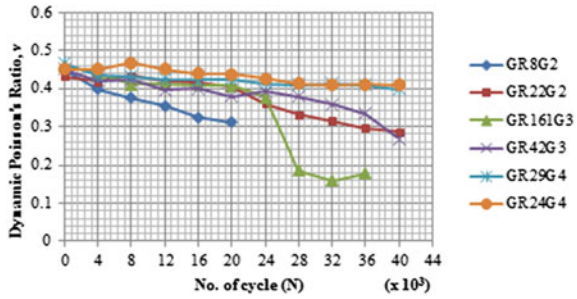


modulus is rapidly decreasing, showing the sign of losing rigidity at 8,000 cycles and apparently failing at 20,000 cycles. Rock losing its rigidity when cracks start to develop. Normally, young modulus is greatly influenced by crack densities [8].

On top of that, static young modulus is found lower than dynamic modulus. Mean value of dynamic modulus for grade II specimens is about 49.8 % higher, grade III is 55.58 % while for grade IV is 59.17 %. It is revealed that static method gives values of the modulus uniformly lower than by the dynamic method [9–11] and that the discrepancy is greatest in those rocks in which cracks, cavities and so forth.

On the other hand, Poisson’s ratio showing a declining trend for all specimens. However, the graph shows gradational decrease between 4,000 cycles to 20,000 cycles. As cycles continue, some specimen shows drastic dropped especially for GR161G3. This is probably due to the sudden increase in axial and radial strain exhibited in specimen between 24,000 and 28,000 cycles. As cycle further up to

Fig. 6 Relation between dynamic Poisson’s ratio with number of cycle



28,000 cycles, the strain slowly reducing the pace as seen in Fig. 6. It indicates that the specimen beginning to deform gently.

Between static Poisson’s ratio and dynamic Poisson’s ratio, it is found that the value in dynamic method is much higher. The percentage of increments is increase as weathering grade of specimen increase. The percentage increase is 25.71, 26.59 and 24.67 % for grade II, III and IV accordingly.

3 Discussion

It is well known that repeated—cyclic stress will effect the dynamic responses of rock since the stress will rearranged the rock microstructure and thus changing the dynamic properties of the rock. It seems that weathered granite specimens do affect by cyclic loading. The effect experienced by the specimens to V_p , V_s and dynamic properties value displayed similar trending. Though, the properties in dynamic method show some difference in contrast with static method. Static method gives modulus value consistently lower as compared to the dynamic method. However, the result is depending on weathering grades of specimen. For grade II granite, dynamic modulus has increased at 49.8 %, grade III is 55.58 % and grade IV is 59.17 %. As crack lengths decrease, the dynamic modulus increases. The percentage of increment is found increased as weathering grade increase.

While for Poisson’s ratio, the increment percentage for grade II specimen is 25.71 %, grade III is 26.59 % and finally grade IV is 24.67 %. Discrepancy of result is probably due to the amount of irreversible strain is higher in grade II specimen.

4 Conclusion

From the result, conclusion has been made as following:

1. Weathered granite specimens do affect by cyclic loading. Initial impacts of cycles (4,000–8,000 cycles) contribute to the rigidity of specimens and further

cycles (12,000–40,000 cycles) specimens beginning to suffer by the cyclic loads.

2. Static method gives modulus value uniformly lower as compared to the dynamic method. The increment percentage of dynamic modulus is found increased as weathering grade increases.
3. Discrepancy in Poisson's ratio result is caused by the amount of irreversible strain display in specimens.

Acknowledgments The authors are thankful to the Universiti Teknologi MARA (UITM) and Ministry of Higher Education (MoHE), Malaysia for providing scholarship and facilities to the authors to conduct this study.

References

1. N.T. Burdine, Rock failure under dynamic loading conditions. *Soc. Pet. Eng. J.* **3**, 1–8 (1963)
2. F. Homand-Etienne, S. Mora, R. Houpert, Strain and fatigue behaviour of rock, in *Proceeding 5th Congress of the International Society for Rock Mechanics*, vol. 1, Melbourne, 10–15 April 1983 (A. A. Balkema, Publ Rotterdam), pp. A129–A132
3. M.N. Bagde, V. Petros, Fatigue and dynamic energy behaviour of rock subjected to cyclical loading. *Int. J. Rock Mech. Min. Sci.* **46**, 200–209J (2009)
4. ISRM, E.T. Brown (ed.), *Rock Characterization, Testing and Monitoring-ISRM Suggested Methods* (Pergamon Press, Oxford, 1981)
5. E.W. Brand, H.B. Phillipson, Site investigation and geotechnical engineering practice in Hong Kong. *Geotech. Eng.* **15**, 97–153 (1984)
6. Y. Shen, A.F. Sheehan, K.G. Dueker, C. de Groot-Hedlin, F. Gilbert, Mantle discontinuity structure beneath the southern East Pacific Rise from P-to-S converted phases. *Science* **280**, 1232–1235 (1998)
7. B.V. Pashkov, E.I. Mashinski, Seismic velocities and attenuation in pressurized consolidated rocks. *Russ. Geol. Geophys.* **47**(2), 301–307
8. J.F. Labuz, L. Biolzi, Characteristic strength of quasi-brittle materials. *Int. J. Solid. Struct.* **35**(31–32), 4191–4204 (1998)
9. J.M. Ide, Comparison of statically and dynamically determined Young's modulus of rocks. *Proc. Natl. Acad. Sci.* **22**(2), 81–92 (1936)
10. A. Mockovčiaková, A. Pandula, Study of the relation between the static and dynamic moduli of rocks. *Metalurgija* **42**(1), 37–39 (2003)
11. M.M. Alam, M.L. Hjuler, Change of static and dynamic elastic properties due to CO₂ injection in North Sea Chalk, in *74th EAGE Conference & Exhibition Incorporating SPE EUROPEC 2012* Copenhagen, Denmark, 4–7 June 2012

Empirical Correlation of P-wave Velocity to the Density of Weathered Granite

Mohd Mustaqim Mohd-Nordin and Zainab Mohamed

Abstract Tropical rock weathering caused decomposition and disintegration of granite rock minerals thus reduces its physical and mechanical properties. The conventional method of characterization and classification of weathered granite becomes a discouraging task due to low sample recovery. A shift to non-destructive technique for characterization of weathered granite by using elastic wave velocity was studied. The deterioration of the quality of weathered granite was defined in terms of density as a tangible variable. An experimental testing to determine the elastic wave velocity by Free-Free Resonant Column (FFRC) test was introduced and carried out on weathered granite of Grade II, Grade III and Grade IV. The results were compared to the common PUNDIT technique for reliability test. The degree of accuracy of elastic wave velocity by the two test methods showed a good consistency. From the experimental study, an empirical correlation between elastic wave velocity to the density of tropically weathered granite is proposed.

Keywords Weathered granite • FFRC • PUNDIT • P-wave velocity

1 Introduction

The geotechnical rock mass characterization of weathered rock has been a daunting task due to low sample recovery. Thus an advance characterization technique to assess the in situ condition is explored through the non-destructive

M. M. Mohd-Nordin (✉)
Faculty of Civil Engineering, Universiti Teknologi MARA, 40450 Shah Alam,
Selangor, Malaysia
e-mail: mustaqimnordin@ppinang.uitm.edu.my

Z. Mohamed
Institute of Infrastructure Engineering and Sustainable Management (IIESM),
Universiti Teknologi MARA, 40450 Shah Alam, Selangor, Malaysia

technique such as Ground Penetrating Radar (GPR), Seismic Refraction Survey and Electrical Resistivity Survey. One of the techniques that can be used to characterize the weathered rock mass properties is through wave propagation technique. This non-destructive technique was easy to apply for both field and laboratory conditions [1].

According to Bell [2], the continuous process of weathering especially on the tropical rock mass is habitually caused by the physical disintegration, chemical decomposition affects and biological activities. The weathering process leads to a general weakening of a rock due to the alteration of minerals, the developments of voids and physical disintegration [1, 3]. Hence, the physical properties such the stiffness and the density consequently are reduced. The reduction of rock material shear strength due to weathering process significantly has precipitated to rock mass failure [4]. Thus, the deterioration of rock material due to the weathering process has also resulted to degradation for geomechanical properties of rock material representing the rock mass. In general, the weathering process causes a reduction in strength and an increase in deformability as the weathered rock relative to unweathered rock.

Numerous investigations had discovered the effect of various conditions of rock mass characteristic on P-wave velocity. Reference [5] was investigated the effect of fracture frequency and material hardness on the characteristic of P-wave velocity. Meanwhile, Refs. [6] and [7] were investigated the effect on various degree of saturation of rock on P-wave velocity by using Ultrasonic Non-destructive Digital Indicating Tester (PUNDIT) and Free-Free Resonant Column (FFRC) test respectively. References [8] and [9] were studied the influence of the fracture roughness on the P-wave velocity by using the ultrasonic transmission test.

As suggested by Arikan et al. [10], the P-wave velocity is one of the most suitable parameters as a quantitative estimation of weathering grades for engineering purposes. According to Oh et al. [7], the stiffness and density characteristics of rock material can be determined from the resonant test through the elastic wave properties such the P-wave velocity. Therefore, Sener et al. [11] concluded that the engineering properties of the weathered rock such granitic rocks can be accurately predicted by P-wave velocity characteristic.

Reference [12] pointed that the dynamic properties of the weathered rock material such as the P-wave velocity are highly influenced by the elastic modulus and the density of the rock material. Significantly, the change of weathering grade consequently influences the elastic modulus and density of rock material and thus characterized the P-wave velocity. In this study, the Free-Free Resonant Column (FFRC) test as a resonant method is used to determine the P-wave velocity [7, 12–14], thus correlate the result with respect to the weathering grades of granite. An analytical comparative measurement with the PUNDIT results significantly determined to validate the accuracy of P-wave velocity that obtained from the FFRC test.

2 Methodology

The dynamic properties such as the P-wave velocity of natural rock material can be obtained from the resonant approach. In this study, the P-wave velocity was determined and analyzed due to the effect of the weathering grades of granite by using the Free–Free Resonant Column (FFRC) test. The validation of the P-wave velocity results then were carried out from the Portable Ultrasonic Non-destructive Digital Indicating Tester (PUNDIT) test.

In the sampling of weathered granite rock materials, the sample of Grade II, Grade III and Grade IV (Fig. 1) were obtained and classified by using the Schmidt hammer rebound number or R value tested on block samples [2]. Accordingly, the R-value with range from less than 25, 25–45 and above 45 are classified as Grade IV, III and II respectively. The cylindrical samples with dimension of length to diameter ratio of 2:1 is prepared according to Brown [15], and weighted to determine the density of each sample with respect R-value. Then, both end surfaces of the sample was polished sufficiently smooth plane to archive a good coupling for the accelerometers or signal emitter and receiver.

In the experimental of FFRC, a cylindrical rock sample is suspended under a supported frame by using a string to create a free boundary condition around the sample. The mechanical impact from a steel ball is applied to generate a seismic response on the rock sample. The seismic signal is then captured by the accelerometers that attached at the both ends of the sample. Vacuum grease is applied to ensure a perfect attachment between the accelerometer and the surface of the rock sample.

The accelerometers are connected to the signal conditioner and an oscilloscope for capturing and analysis the P-wave propagation signal. The schematic diagram and the actual setup of FFRC test are shown in Fig. 2a, b respectively. The P-wave velocity was determined by applying (1), where L is the sample length and Δt is the travel time of the signal between both ends of the sample.

In the experimental of PUNDIT, P-wave velocity was measured by electrical excitation or pulse generation at rate of 5 pulses per second. The setting up of test consists of ultrasonic tester, emitter and receiver. The cylindrical sample of rock sample is positioned coupling between the emitter and the receiver horizontally (Fig. 3).

$$V_p = \frac{L}{\Delta t} \quad (1)$$

3 Results and Analysis

Table 1 is summarized the results of P-wave velocity (V_p) determined from the FFRC and PUNDIT test. The densities of the cylindrical weathered rock samples (determined by mass over volume) are also presented. The characteristics of



Fig. 1 Samples consist of three grades of weathered granite

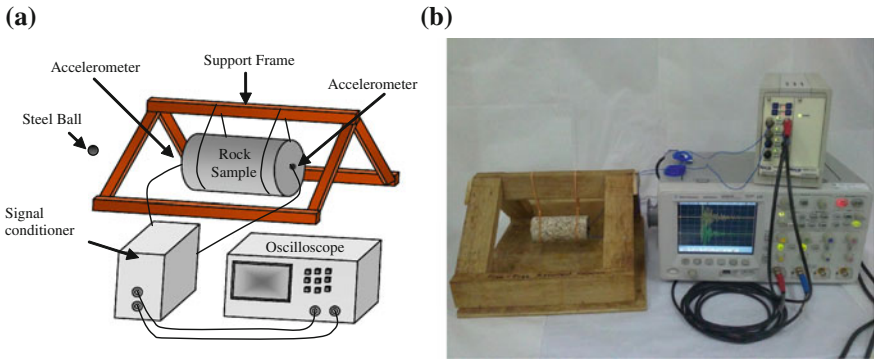


Fig. 2 a Schematic diagram. b Actual setup of experimental free-free resonant column (FFRC)

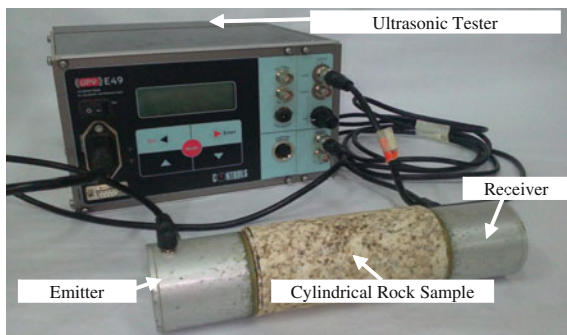


Fig. 3 Experimental setup of portable ultrasonic non-destructive digital indicating tester (PUNDIT) test

Table 1 Summary results of V_p from FFRC and PUNDIT test on Grade II, III and IV of weathered granite rock sample

Sample		Density, ρ (kg/m ³)	V_p (m/s)		
			FFRC	PUNDIT	
Grade II	IIa	2,607	3,448	2,846	
	IIb	2,627	6,318	5,389	
	IIc	2,626	6,775	4,705	
	IId	2,679	6,200	4,813	
	IIe	2,634	7,621	5,126	
	IIf	2,624	6,980	4,740	
	IIg	2,593	6,241	4,333	
	IIh	2,625	6,927	5,126	
	IIi	2,610	5,637	4,107	
	IIj	2,588	3,848	3,398	
	IIk	2,592	4,042	3,353	
	Grade III	IIIa	2,575	5,078	3,844
		IIIb	2,596	4,995	3,915
IIIc		2,600	4,280	3,353	
IIId		2,629	5,119	4,015	
IIIe		2,615	4,927	3,990	
IIIf		2,576	3,907	3,232	
IIIg		2,662	5,574	4,471	
IIIh		2,588	5,057	4,094	
IIIi		2,583	4,718	3,797	
IIIj		2,506	4,099	3,473	
IIIk		2,510	2,167	1,780	
IIIl		2,475	2,124	1,795	
IIIm		2,469	2,593	2,259	
Grade IV	IVa	2,580	4,268	3,561	
	IVb	2,469	2,966	2,541	
	IVc	2,536	2,837	2,263	
	IVd	2,526	3,143	2,632	
	IVe	2,577	3,985	2,443	
	IVf	2,582	4,069	3,060	
	IVg	2,548	3,390	2,777	
	IVh	2,539	2,797	2,410	
	IVi	2,461	1,953	1,746	
	IVj	2,402	1,898	1,587	
	IVj	2,401	1,968	1,827	

P-wave velocity on different grades of weathered granite were analyzed by plotting the P-wave velocity versus the density of rock samples. The direct relationship for each grade of weathering was analyzed by the linear regression. Accordingly, the degree of weathering has significantly influences the density of the rock material thus affects the material strength as well as its P-wave velocity as its dynamic response.

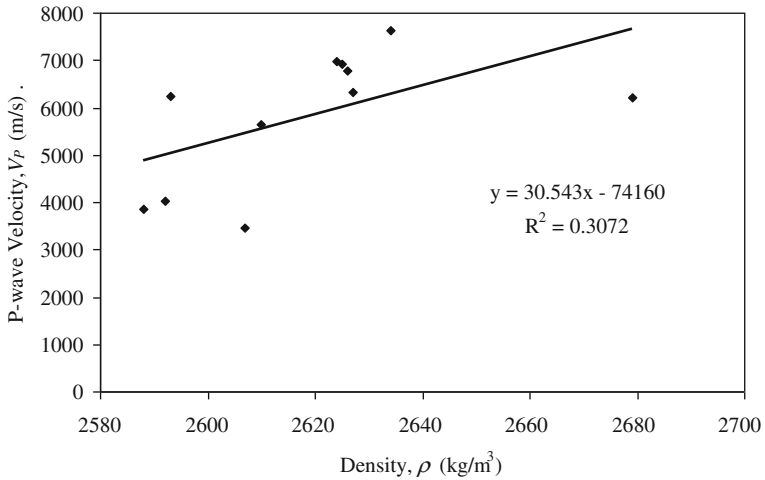


Fig. 4 P-wave velocity versus the density distribution for Grade II of granite

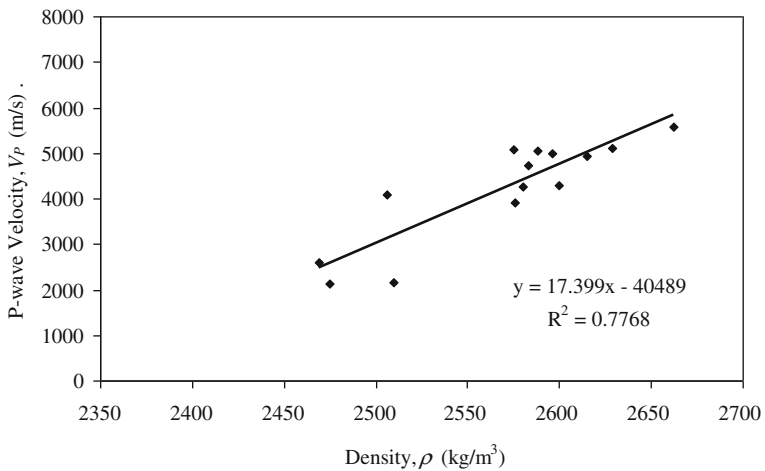


Fig. 5 P-wave velocity versus density distribution for Grade III of granite

As shown in Fig. 4, the relationship between the P-wave velocity and the density of weathered rock material from 11 samples of Grade II tested is graphically represented by linear regression and results the R^2 value equal to 0.3072, as in (2) Significantly, this low value of regression variation indicates the low dependent variable of dynamic response, which is P-wave velocity, to the rock material density. For the density between the range of 2,588 and 2,679 kg/m^3 , the maximum and minimum of P-wave velocity are 7,621 and 3,448 m/s respectively.

The relationship between P-wave velocity and the weathered rock material density as in (3) for Grade III of granite significantly shows the higher R^2 value

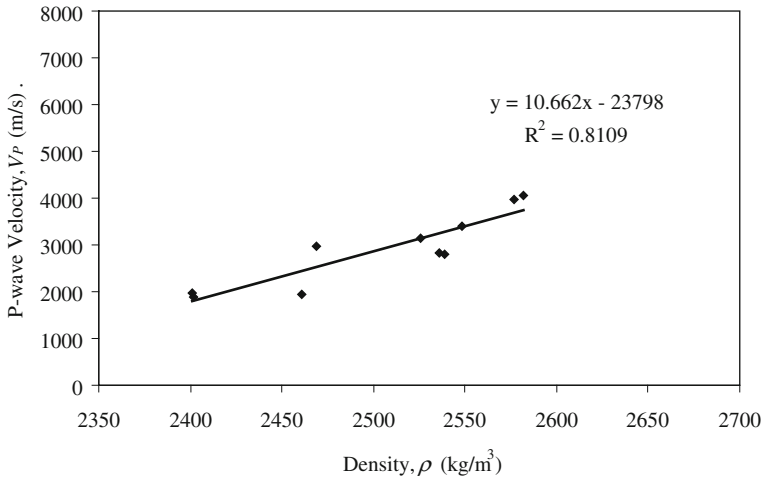


Fig. 6 P-wave velocity versus density distribution for Grade IV of granite

results from the linear regression by 0.7768. As shown in Fig. 5, the maximum and minimum of P-wave velocity are resulted from the density range between 2,469 and 2,662 kg/m³ are 5,574 and 2,124 m/s respectively. Similarly, a linear relationship is observed in Fig. 6 between P-wave velocity and weathered rock material density of Grade IV of weathered granite, as in (4). A stronger correlation is presented by R² value equal to 0.8109. From the density between the range of 2,401 and 2,582 kg/m³, the maximum and minimum of P-wave velocity are 4,069 and 1,898 m/s respectively.

Based on the regression variation of P-wave velocity to the grades of weathered granite, the relationship of P-wave velocity to the grade of weathering is higher for Grade IV, followed by Grade III and Grade II. The distribution results of P-wave velocity with respect to the density for Grade II of weathered granite show more dispersion compare to Grade III and Grade IV.

$$\text{Granite Grade II; } V_p = 30.543 \rho - 74160, R^2 = 0.3072 \tag{2}$$

$$\text{Granite Grade III; } V_p = 17.399 \rho - 40489, R^2 = 0.7768 \tag{3}$$

$$\text{Granite Grade IV; } V_p = 10.662 \rho - 23798, R^2 = 0.8109 \tag{4}$$

4 Discussion

The accuracy of P-wave velocity measured by the FFRC test for Grade II, III and IV of weathered granite is verified by the results from the conventional PUNDIT test. As shown in Fig. 7, the direct relationship by the linear regression between

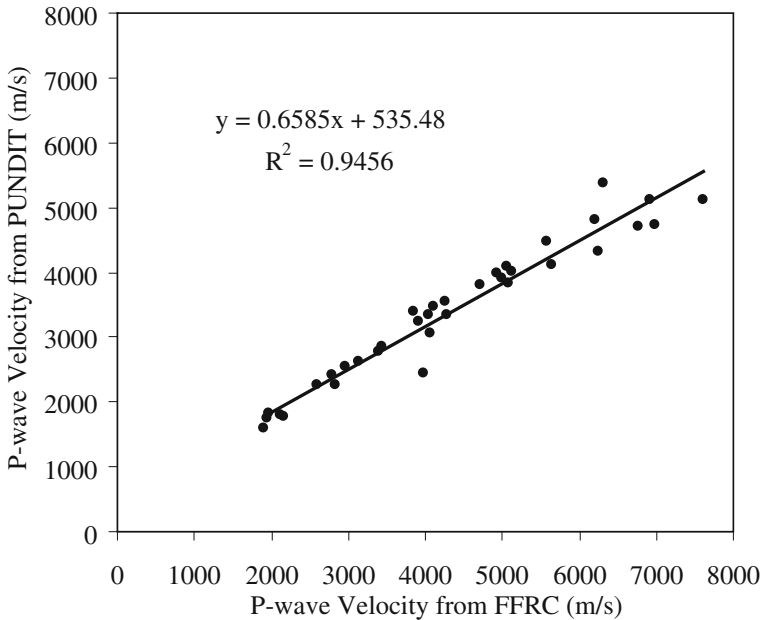


Fig. 7 Comparison of P-wave velocity between PUNDIT and FFRC

the P-wave velocity of PUNDIT and FFRC shows a strong correlation by R^2 value equal to 0.9456. Therefore, the P-wave velocity results from the FFRC test are considered verified to represent the P-wave properties of Grade II, III and IV of weathered granite sample material. Significantly, the difference between the FFRC and PUNDIT test is their mode of wave excitation. For FFRC test, the compression wave is generated by mechanical impact of steel ball, while in the PUNDIT test is generated by electrical pulse.

The characteristic of P-wave velocity from the effect of weathered rock sample density is presented in Fig. 8. Accordingly, the correlation variation between the P-wave velocity and the density for respective grade of weathered granite is modeled. From this graphical plot, the regression of exponential trend line was adopted that gives the best R^2 value equal to 0.7905. Hence, an empirical equation has been introduced as (2) to express the estimation of P-wave velocity, V_P from the density, ρ of the weathered granite.

From the trend characteristic of V_P with respect to the density of the weathered granite, the distribution results can be divided into three levels of V_P . For the Grade II of weathered granite, there is no sample recorded the V_P lower than 3,000 m/s. However, 36 % from the Grade II samples are recorded the V_P in the range between 3,000 and 6,000 m/s. While, the rest 64 % of the Grade II samples are recorded the V_P value above 6,000 m/s.

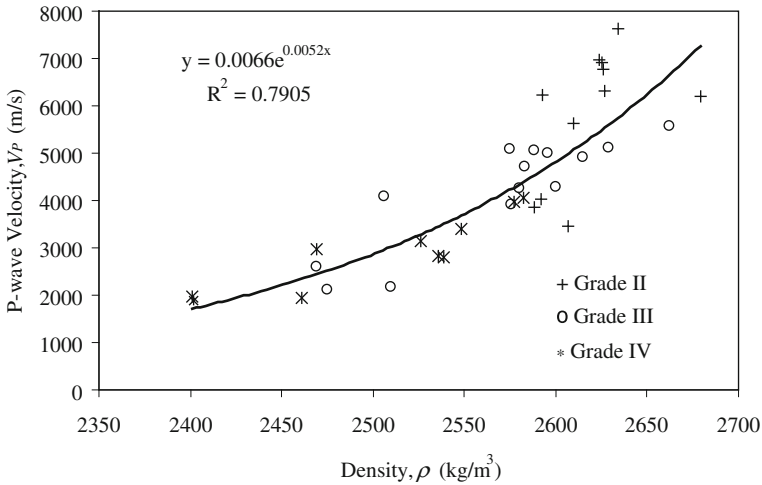


Fig. 8 Relationship between P-wave velocity and density for weathered granite rock mass

For weathered granite rock mass;

$$V_p = 0.0066e^{0.0052\rho}, R^2 = 0.7905 \tag{5}$$

For the Grade III samples, there are 21 % of the samples are recorded the V_p value lower than 3,000 m/s. Meanwhile, the rest of 79 % are recorded in the range between 3,000 and 6,000 m/s. However, none of the sample from the Grade III is recorded the V_p value above 6,000 m/s. The V_p distribution from the Grade IV samples shows that 60 % are recorded the V_p lower than 3,000 m/s. While, the rest of 40 % are recorded in range between 3,000 and 6,000 m/s. These trend characteristic of V_p distribution highlighted that the V_p for Grade II, III and IV generally can be ranged by greater than 6,000 m/s, between 3,000 and 6,000 m/s and lower than 3,000 m/s (Table 2).

The relationship of weathering grades to the density of weathered granite significantly introduced the trend characteristic to estimate the level of V_p from the density of weathered granite. As tabulated in Table 3, the distribution for density of weathered granite is divided into three levels of range. From the density of the Grade II samples that has the range greater than 2,500 kg/m³, about 27 % has recorded between 2,500 and 2,600 kg/m³. Meanwhile, the rest 73 % of the samples are at the range greater than 2,600 kg/m³.

Meanwhile, the Grade III samples have a wider range of material density. About 14 % of samples are ranged lower than 2,500 kg/m³, while most of the samples which approximately 79 % are in the range between 2,500 and 2,600 kg/m³. The balance of 7 % are recorded the density above 2,600 kg/m³. For the Grade IV of weathered granite, although the 60 % of the samples are in the range between 2,500 and 2,600 kg/m³, the rest of 40 % are recorded below 2,500 kg/m³ and no sample is recorded higher than 2,600 kg/m³.

Table 2 Distribution of P-wave velocity with respect to grades of weathering for granite

Grade of weathering	P-wave velocity, V_p (m/s)		
	$V_p < 3,000$ (%)	$3,000 < V_p < 6,000$ (%)	$V_p > 6,000$ (%)
Grade II	0	36	64
Grade III	21	79	0
Grade IV	60	40	0

Table 3 Distribution of density with respect to grades of weathering for granite

Grade of weathering	Density of weathered granite, ρ (kg/m ³)		
	$\rho < 2,500$ (%)	$2,500 < \rho < 2,600$	$\rho > 2,600$
Grade II	0	27	73
Grade III	14	79	7
Grade IV	40	60	0

Therefore, the correlation of V_p to Grade II, Grade III and Grade IV granite samples as achieved in term of empirical equation as above, respectively. However for weathered granite rock mass, the correlation of V_p to the weathered rock mass density has exponential relationship as per (5). Distribution for the density with respect to the grades of weathering significantly leads to a higher accuracy and better characterization and classification of weathered granite rock mass quality based on V_p value as compared to conventional method.

5 Conclusion

The P-wave velocity that determined from the FFRC test and validated to common PUNDIT test showed a good fit. From three weathering grades of granite tested, Grade IV by its density showed strong correlation with V_p despite the least percentage of sample recovery when compared to Grade III and Grade II. It is concluded that, the trend characteristic of V_p with respect to the density from three grades of weathering significantly introduced an empirical correlation to estimate the V_p by using a simple density parameter of weathered granite.

Acknowledgments The research was supported by the Fundamental Research Grant Scheme (600-RMI/ST/FRGS 5/3/Fst (27/2010)) from the Ministry of Higher Education of Malaysia. Laboratory facilities was supported by Institute for Infrastructure Engineering and Sustainable Management, Faculty of Civil Engineering, Universiti Teknologi MARA Malaysia.

References

1. S. Yagiz, P-wave velocity test for assessment of geotechnical properties of some rock materials. *Bull. Mater. Sci.* **34**(4), 947–953 (2010)
2. F.G. Bell, *Engineering in Rock Masses* (Butterworth-Heinemann, England, 1994). ISBN 0750619651
3. E. Arel, A. Tugrul, *Weathering and its Relation to Geomechanical Properties of Cavusbasi Granitic Rock in Northwestern Turkey* (Springer, Berlin, 2000), pp. 123–133
4. E. Hoek, *Practical Rock Engineering*. Evert Hoek Consulting Engineer Inc (2007)
5. S. Kahraman, A correlation between P-wave velocity, number of joints and Schmidt hammer rebound number. *Int. J. Rock Mech. Min. Sci.* **38**, 729–733 (2001)
6. S. Kahraman, The Correlations between the Saturated and Dry P-wave velocity of Rocks. *Ultrasonic* **46**, 341–348 (2007)
7. T.M. Oh, M.S. Cha, G.C. Cho, E.S. Hong, Stiffness and energy loss characteristics during saturating-drying processes in granite, in *Proceedings of the International Conference on Advanced Non-Destructive Evaluation (ANDE) II 2007*, Busan, Korea, pp. 678–683 (2007)
8. S. Nakagawa, K.T. Nihei, L.R. Myer, Shear-induced conversion of Seismic Waves across single fracture. *Int. J. Rock Mech. Min. Sci.* **37**, 203–218 (2000)
9. S. Kahraman, The effects of fracture roughness on P-wave velocity. *Eng. Geol.* **63**, 347–350 (2002)
10. F. Arıkan, R. Ulusay, N. Aydin, Characterization of weathered acidic volcanic rocks and a Weathering classification based on a rating system. *Bull. Eng. Geol. Environ.* **66**, 415–430 (2007)
11. C. Sener, T. Sule, C. Nurchan, Influence of weathering on the engineering properties of Harsit Granitic Rocks (NE Turkey). *Bull. Eng. Geol. Environ.* **67**, 97–104 (2008)
12. M.S. Cha, G.C. Cho, Compression wave velocity of cylindrical rock specimen: engineering modulus interpretation. *Jpn. J. Appl. Phys.* **46**(7B), 4497–4499 (2007)
13. ASTM C 215-08, Standard Test Method for Fundamental Transverse, Longitudinal, and Torsional Frequencies of Concrete Specimens
14. N. Ryden, Determining the asphalt mastercurve from free-free resonant testing on cylindrical samples, in *Proceedings of 7th International Symposium on Nondestructive Testing in Civil Engineering, held in Nantes, France*, ISBN: 978-2-7208-2542-5 (2009)
15. E.T. Brown (ed.), *Rock Characterization, Testing and Monitoring-ISRM Suggested Methods* (Pergamon Press, Oxford, 1981), p. 221

Strength of Soft Soil Stabilized Using Lime-POFA Mixtures

Norazlan Khalid, Mazidah Mukri, Faizah Kamarudin, Norbaya Sidek and Mohd Fadzil Arshad

Abstract This paper presents the study on the strength of Malaysian soft soil stabilized using mixing of lime and palm oil fly ash (Lime-POFA). Palm Oil Fly Ash (POFA) additives used in this study is a finely product from waste product from the process of burning palm oil fiber and described as a by-product of thermal power plants where palm oil fiber shell, and empty fruit bunches was burnt at temperatures ranging from 800 to 1,000 °C until it is in fly ash condition. According to ASTM C618, the POFA used in this study has been tested and classified as Class-F fly ash accordingly to ASTM C618 because POFA describe as siliceous and aluminous materials that possess little or no cementitious value. In that condition, POFA need to combines with small quantities of lime for pozzolanic reaction. The samples of soft soil classified as slightly sandy CLAY of intermediate plasticity has been used in this study. The optimum of 3 % hydrated lime used in this study as an active additive to the various percentage mixtures of POFA for the pozzolanic reaction. The first objective of this study is to determine the optimum proportion of POFA to be mixed with 3 % lime to stabilize the clay soil based on the compressive strength at 0, 14 and 28 days of curing periods. The second objective is to determine the strength development of clay soil stabilized at the optimum percentage of POFA mixed with 3 % lime at 0, 14 and 28 days of curing periods. This study involved in unconfined compression strength to determine the strength of stabilized clay soil. The development of compressive strength of soil stabilized using (Lime-POFA) were compared to the compressive strength of unstabilized soil. The result shows, the 6 % POFA mixed with 3 % Lime was the suitable proportion in term of strength and strength development and can be used as additives to stabilize clay soil.

Keywords Soil stabilization · Compressive strength · Lime · Palm oil fly ash

N. Khalid (✉) · M. Mukri · F. Kamarudin · N. Sidek · M. F. Arshad
Faculty of Civil Engineering, Universiti Teknologi MARA, Shah Alam, Malaysia
e-mail: aln_kh82@yahoo.com

1 Introduction

Soft soil considered as a problematic soil to the geotechnical engineer's and causes major problems at any construction such as subgrade problems due to the undesirable engineering properties. Commonly, soft soils are known to have low strength, high compressibility and the water contents are also known to be high at almost to its liquid limits. Moreover, soft soil has brought problems because the behavior is unpredictable. Soft soil has the shear strength of less than 25 kPa and it is a mineral combination of hydrous aluminium, silicates, quartz, feldspar, carbonate, oxides, hydroxides, and organic materials [3]. Soft soil usually found in coastal area or river area and the thickness is different depending on that area. The soft soil in Malaysia usually found in coastal area at west coast of Peninsular Malaysia. The thickness of soft clay soil strata in West Coast of Peninsular Malaysia is (5–35 m) and (3–20 m) thick at East Coast of Peninsular Malaysia [1].

The soil modification, stabilization, or both can be classified in group of soil improvement. Soil modification is an addition an active additives such as lime and cement to soil to change its index properties, while soil stabilization is the treatment of soils to improve the texture, increase strength, increase the CBR value and reduce shrink-swell characteristics such that they become totally suitable for construction for a long term. Both techniques introduced many years ago and the main purpose to render the soils capable of meeting the requirements of the specific engineering projects [9]. The techniques of soil stabilization and soil improvement using lime and/or cement are well established and were published by many researches [7]. The optimum lime content for stabilize the Malaysian cohesive soils was recorded between 3 and 6 % [8]. There's an alternative technologies which more sustainable, environmentally friendly and economical. Fly ash stabilization exhibit increased and enhanced both the unconfined compressive strength and the CBR values substantially as well as durability in terms of water resistance, swelling, shrinkage modulus of elasticity and has the potential to offer an alternative for soft subgrade improvement of highway construction [6, 11, 12]. Recently, it has been found that appropriate chemical stabilization can improve undesirable characteristics of such soil [10].

Fly ash is one of the wastes products from manufacturing industry. Generally, fly ash considered as pozzolana, which is not cementitious itself. It has an ability to combine with Ca-rich materials such as lime, cement, etc. to form cementitious ones; e.g. calcium silicate hydrate (CSH), calcium aluminate hydrate (CAH), calcite (CaCO_3), etc. among soil particles due to the hydration and long-term pozzolanic reaction [10]. Soft clay is pozzolanic in nature and require the presence of lime that released by the cement to initiate the pozzolanic reaction [13]. The mixture of 9 % cement and 3 % fly ash gives the best result of strength to stabilize the expensive soils [2]. Previous study shows palm oil fly ash has good pozzolanic properties as a cement substitute [3]. The fly ash stabilization increased both the unconfined compressive strength and the CBR values substantially and has the potential to offer an alternative for soft subgrade improvement of highway construction [12].

The aim of this study is to show the use of palm oil fly ash (POFA) as an additive to stabilize a soft soil. This is an experimental study to determine the concentration percentage POFA mixed with 3 % Lime as an additive based on compressive strength and the development of compressive strength at 0, 14 and 28 days of curing periods. The result shows that the 6 % POFA mixed with 3 % Lime was giving the highest strength and considered the suitable proportion to stabilize slightly sandy CLAY of high plasticity and can be used as additives to clay soil.

2 Materials

2.1 Soft Soil Sample

The soft soil samples are collected from Kampung Sijangkang, Selangor, Malaysia and collected in disturbed and undisturbed samples at 2 m from ground level was in grey colour. The samples were tightly sealed and wrapped with plastic after collecting to maintain the original moisture contents before transported, stored at room temperature and testing in the laboratory. The samples were tested for physical and engineering properties in natural state (considered as undisturbed samples) and remolded samples (considered as disturbed samples). The samples were tested for physical properties based on BS 1377: Part 2: 1990.

2.2 Palm Oil Fly Ash

Palm Oil Fly Ash (POFA) additives used in this study was from waste product from the process of burning palm oil fiber or oil palm fiber (OPF). POFA described as a by-product of thermal power plants where palm oil fiber (OPF), shell, and empty fruit bunches was burnt at temperatures ranging from 800 to 1,000 °C until it is in fly ash condition. Previous study shows POFA has good pozzolanic properties that were used as cement substitute [3]. This POFA obtained from Sg. Tengi Palm Oil Factory at Kuala Kubu Bharu, Selangor, Malaysia.

2.3 Lime

Lime was also used widely to stabilize weak fly ash to reduce settlement and to increase bearing capacity. Hydrated lime [$\text{Ca}(\text{OH})_2$] was used in this study act as an main active additive to the POFA for the pozzolanic reaction. Hydrated lime was available widely in Malaysia and was provided from Geotechnical Laboratory of Faculty of Civil Engineering UiTM Shah Alam. Fly ashes containing sufficient

Table 1 Details of sample

Specimens	Lime (%)	POFA (%)
Soil (Undisturbed)	–	–
Soil (Remolded)	–	–
Soil + 3Lime	3	2
Soil + 3Lime + 2POFA	3	4
Soil + 3Lime + 4POFA	3	6
Soil + 3Lime + 6POFA	3	8

lime content and reactive silica develop good strength on addition of water while fly ashes containing only reactive silica with insufficient lime content will improve their strength only with the addition of the hydrated lime.

2.4 Sample Preparation and Testing

This study involved two soil samples considered as control. The first undisturbed samples were prepared accordingly to natural state of water content and the second disturbed samples were remolded samples prepared based on optimum moisture content at maximum dry density. The additives consisted of 3 % lime as main activator mixed with various percentages of POFA (2, 4, 6 and 8 %) shown in Table 1. The soil was stabilized based on the dry unit weight of the clay soil.

The laboratory testing was conducted to determine the physical properties of clay soil and POFA such as particle size distribution, specific gravity, atterberg limit, moisture content, compaction characteristic and natural moisture content. All the entire testing based on BS 1377:1990. The mixtures are compacted at maximum dry density, optimum moisture content and molded into cylindrical specimens of 38 mm diameter and 76 mm high based on BS 1377-7:1990 [4] for unconfined compressive strength (UCS) test. The specimen samples wrapped and placed at room temperature condition to protect from loss of moisture content. The samples were cured for 0, 14 and 28 days before being tested. The curing time has a significant effect on unconfined compressive strength [13] and to allow the reaction between soil and additive Lime-POFA to take place, to form a homogeneous mixture, and to strengthen the clay soils particles.

3 Materials Properties

3.1 Clay Soil Properties

The sample of soil had been tested for physical properties and the result shown in Table 2. Based on the properties result of soil sample, it shows in the natural state

Table 2 The physical properties of clay soil sample

Properties	Values
Natural moisture content, w (%)	75
Specific gravity (Gs)	2.65
Plastic limit (%)	24.96
Liquid limit (%)	48.77
Plastic index (%)	23.81
Compaction characteristics	
Optimum moisture content (%)	20
Maximum dry density (%)	14
Particle size distribution	
Gravel (%)	0
Sand (%)	8.18
Fine/Silt (%)	80.60
Clay (%)	11.22
D ₆₀	0.036
D ₃₀	0.013
D ₁₀	0.001
Coefficient of uniformity (C _u)	27.95
Coefficient of curvature (C _c)	3.88
Classification	Slightly sandy CLAY of intermediate plasticity

Table 3 The chemical constituent of soft soil sample

Element	Concentration (%)
SiO ₂	63.02
Al ₂ O ₃	17.27
Fe ₂ O ₃	3.59
CaO	0.15
K ₂ O	2.05
Na ₂ O	0.21
MgO	1.03
SO ₃	0.67
L.O.I	–

the natural water content of soil much higher is about 75 % and the specific gravity of 2.65. The soils sample covered about 8.18 % sand size, 80.60 % of fine or silt size and 11.22 % clay size. The plastic limit and liquid limit are 24.96 and 48.77 % respectively. Meanwhile the plastic index is about 23.81 %. Based on the results properties, the soft soil samples classified as slightly sandy CLAY of intermediate plasticity.

The chemical constituent result for Sijangkang soft soil are presented in Table 3. It shows that, the soft soil samples having pozzolanic properties due to the percentage composition for major constituent components such as silicon dioxide (SiO₂), alumina oxide (Al₂O₃) and iron oxide (Fe₂O₃).

Table 4 The physical properties of palm oil fly ash (POFA)

Properties	Values
Specific gravity (Gs)	1.66
Particle size distribution	
Sand (%)	0.06
Fine/Silt (%)	99.94
Clay (%)	0
Classification (ASTM C618)	Class-F fly ash

Table 5 The chemical properties of palm oil fly ash (POFA)

Element	Concentration (%)
SiO ₂	69.01
Al ₂ O ₃	5.41
Fe ₂ O ₃	4.18
CaO	5.58
K ₂ O	8.76
Na ₂ O	0.14
MgO	3.07
SO ₃	0.06

3.2 Palm Oil Fly Ash Properties

The palm oil fly ash (POFA) had been tested for physical properties and the result shown in Table 4. The specific gravity POFA is about 1.66 and considered as light materials.

Table 5 shows the chemical composition result for palm oil fly ash (POFA). Based on ASTM C618 for classification of fly ash, the palm oil fly ash (POFA) classified as Class-F fly ash because the total combination percentage composition for major constituent components such as silicon dioxide (SiO₂), alumina oxide (Al₂O₃) and iron oxide (Fe₂O₃) more than 70 %. This class-F POFA describe as siliceous and aluminous materials that possess little or no cementitious value consist a little quantity of Calcium Carbonate or free lime (CaO) lower than 10 %. Furthermore the class-F POFA considered as non self-cementing ash because having pozzolanic properties and no or small quantities of self-cementing properties sources of calcium and magnesium ions.

3.3 Lime

The hydrated lime [Ca(OH)₂] were used as a an active additive to the POFA for the pozzolanic reaction to improve some engineering properties of the clays. The chemical properties of hydrated lime listed in Table 6.

Table 6 Properties of hydrated lime [5]

Element	Concentration (%)
SiO ₂	20.63
Al ₂ O ₃	5.87
Fe ₂ O ₃	2.52
CaO	63.55
K ₂ O	0.63
Na ₂ O	0.85
MgO	2.79
SO ₃	1.62
L.O.I	1.54

4 Results and Discussion

The laboratory testing was carried out to achieve the aim and objective of study. This part shows the result of this study.

4.1 The Compressive Strength of Clay Soil Stabilized with Lime-POFA Mixtures at 0, 14 and 28 days of Curing Periods

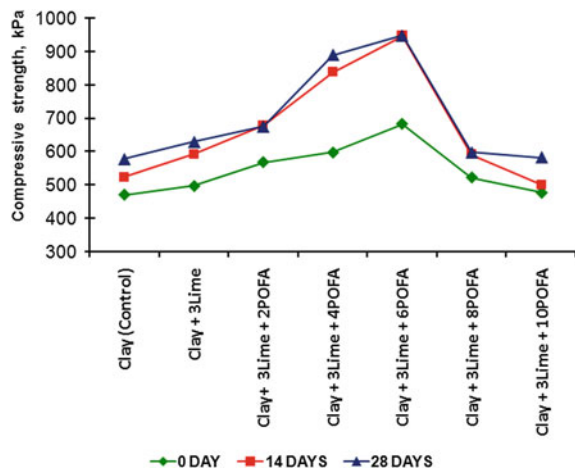
Table 7 presents the compressive strength of clay soil stabilized using mixtures of Lime-POFA at curing periods of 0, 14 and 28 days. The clays soil samples in natural state (undisturbed samples) shows the lowest in compressive strength compared to the control sample (remolded sample) and stabilized clays with mixtures of Lime-POFA. However, most stabilize soil samples shows increment in compressive strength at curing periods.

Meanwhile, Fig. 1 illustrated the pattern of compressive strength of clay soil stabilized with various mixtures of Lime-POFA at 0, 14 and 28 days of curing periods. It can be seen the compressive strength of clays soil stabilized with various mixtures of Lime-POFA shows the better results in terms of increments of compressive strength at curing periods compared to unstabilized clay soil sample (control) and clay stabilized with 3 % of lime. However, it can be seen the best combination of 3 % Lime mixed with 6 % POFA (3 % Lime + 6 % POFA) was giving the highest result of compressive strength to stabilize clay soil at all curing periods compared to unstabilized clay soil and other mixtures. This happened due to the highly active silica content of POFA and clay soil were react with lime for pozzolanic reaction to form calcium aluminium hydrate (CAH) and calcium silicate hydrate (CSH) to bind the soil particle and thus increasing the soil strength.

Table 7 The compressive strength result of clay soil stabilized with Lime-POFA mixtures at curing periods

Samples	Compressive strength (kPa)		
	0 day	14 days	28 days
CLAY (Undisturbed)	26.3	29.9	37
CLAY (Remolded)	470.5	522.5	578
Clay + 3 % Lime	497.5	592.5	629.3
Clay + 3 % Lime + 2 % POFA	567.1	678.7	675.2
Clay + 3 % Lime + 4 % POFA	597.3	838.4	889.4
Clay + 3 % Lime + 6 %POFA	682	947.6	949.1
Clay + 3 % Lime + 8 % POFA	521.1	591.3	597.5
Clay + 3 % Lime + 10 % POFA	477.2	499.4	582.1

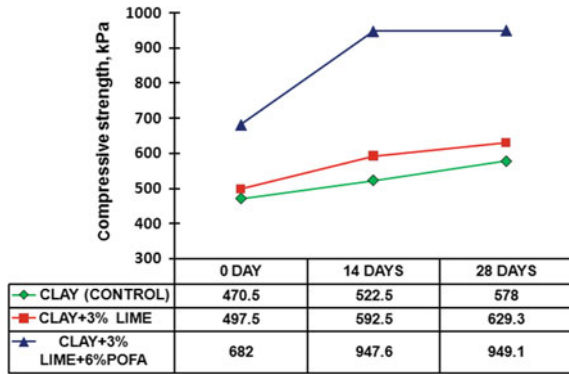
Fig. 1 Graph of clay soil stabilized various Lime-POFA mixtures versus compressive strength at 0, 14 and 28 days of curing periods



4.2 The Development of Compressive Strength of Clay Soil Stabilized with Optimum of Lime-POFA Mixtures

The unconfined compressive strength testing was performed on the clay soil stabilized at optimum mixtures about (3 % Lime + 6 % POFA) at curing periods of 0, 14 and 28 days. The results of development of compressive strength of clay soil stabilized with optimum mixtures of (3 % Lime + 6 % POFA) presented in Fig. 2 with respect to the curing periods at 0, 14 and 28 days. The result was compared to the unstabilized clay soil (control) and clay stabilized with 3 % Lime only. It was observed, the increment on compressive strength for clay soil stabilized with (3 % Lime) and (3 % Lime + 6 % POFA) respected to curing time compared to the unstabilized clay soil (control). However, the result shows that the compressive strength of clay soil stabilized with optimum mixtures of (3 % Lime + 6 % POFA) was giving the highest and best result compared to stabilize with 3 % of

Fig. 2 Graph of clay soil stabilized various Lime-POFA mixtures versus compressive strength at 0, 14 and 28 days of curing periods



lime only. It can be noticed that the strength of stabilized clay soil increased with curing periods from 0 up to 28 days. This stabilization process increase the strength might be beyond to 28 days of compressive strength result until the process is stable and fully stabilized. However, the result for clay stabilized with (3 % Lime + 6 % POFA) shows a constant strength at 14–28 days and might be fully stabilized. The curing time process in stabilization process has a significant effect on compressive strength [14] and indicates that the strength of clay soil stabilization is depending on the presence of Lime and/or POFA because the pozzolanic reaction and the cementation process.

5 Conclusion

Based on the study the following conclusion is made:

1. The Sijangkang soft soil can be classified as sandy CLAY of high plasticity soils. The suitable concentration percentage mixing of Lime-POFA was determined about 6 % POFA mix with 3 % Lime (3 % Lime-6 % POFA) to stabilize the sandy CLAY of high plasticity soils was giving the highest compressive strength. This Class-F POFA used in combination of mixing with 3 % Lime for pozzolanic reaction and the strength increase up to 947.6 kPa.
2. The clay soil stabilized using combination of 3 % Lime-6 % POFA mixtures considered effective to enhance clay soil strength for long periods and. It shows combination mixing of 3 % Lime-6 % POFA were increased the compressive strength of the clay soil until 28 days and this strength will get higher might be beyond to 28 days.
3. This will reduce the construction cost and solving disposal problems and towards the green The use of WPSA will reduced the construction cost, time and will solving the disposal of waste byproduct problems towards green environmentally.

Acknowledgments The author would like to express an acknowledgement to the Research Management Institute, UiTM Shah Alam for providing Excellent Fund (RIF) 600-RMI/DANA 5/3/RIF (115/2012) to complete this study and also to Faculty of Civil Engineering, UiTM Shah Alam, Malaysia, and for providing the facilities such as the geotechnical laboratory and advanced geotechnical laboratory to accomplish this study. The author also wishes to acknowledge cooperation given by laboratory technician and the undergraduate student from Faculty of Civil engineering, UiTM Shah Alam for this study.

References

1. A.I.M.B. Abdullah, P. Chandra, Engineering properties for coastal subsoils in peninsula Malaysia, in *Proceedings of the 9th South East Asia Geotechnical Conference*, vol. 1, Bangkok, Thailand (1987), pp. 127–138
2. O.O. Amu, A.B. Fajobi, S.O. Afekhuai, Stabilizing potential of cement and fly ash mixture on expensive soils. *J. Appl. Sci.* **5**(9), 1669–1673 (2005)
3. A.S.M. Awal, W. Hussin, The effectiveness of palm oil fuel ash in preventing expansion due to Alkali-silica reaction. *Cem. Concr. Compos.* **19**, 367–372 (1997)
4. British Standard Institution, *British Standard Method of Test for Soils for Civil Engineering Purposes* (BS 1377, London, 1990)
5. M.A. Hafez, M.J. Md. Noor, The relation between the strength of the remolded and field samples of cement clay column. *Electron. J. Geotech. Eng.* **13**, 1–14 (Bund. G, 2008)
6. K.M.M. Hossain, L. Mol, Some engineering properties of stabilized clayey soils incorporating natural pozzolans and industrial wastes. *J. Constr. Build. Mater.* 1–7 (2011)
7. Indiana Department of Transportation, *Guidelines Design Procedures for Soil Modification or Stabilization* (2008)
8. A.K. Khairul, K.C. Kok, Lime stabilized cohesive soils. *Jurnal Kejuruteraan Awam* **16**(1), 13–23 (2004)
9. S. Koliass, R.V. Kasselouri, A. Karahalios, Stabilisation of clayey soils with high calcium fly ash and cement. *Cement Concr. Compos.* **27**, 301–313 (2005)
10. S. Nontanandh, K. Amornfa, T. Jirathanathaworn, Engineering properties of remolded soft clayey soil mixed with cement, in *Proceedings of the 4th Regional Symposium on Infrastructure Development (4th RSID)*, Bangkok, Thailand, 3–5 April 2003
11. A. Senol, M.S. Bin-Shafique, T.B. Edil, C.H. Benson, Use of class-C fly ash for stabilization of soft subgrade, in *ACE proceedings*, pp. 963–972 (2002)
12. A. Senol, T.B. Edil, H.A. Acosta, C.H. Benson, Soft subgrades stabilization by using various fly ashes. *Resour. Conserv. Recycl.* **46**(2006), 365–376 (2005)
13. H.W. Xiao, F.H. Lee, Curing time effect on behaviour of cement treated marine clay, in *Proceedings of World Academy of Science, Engineering and Technology (PWASET)*, vol. 33, pp. 2070–3740 (2008)
14. I. Yilmiz, B. Civelekoglu, Gypsum: an additive for stabilization of swelling clay soils. *Appl. Clay Sci.* **44**(1–2), 166–172 (2009)

Plasticity Index of Soft Soil Modified with Fly Ash and Oil Palm Shell Activated Carbon

Siti Nur Aida Mario and Rudy Tawie

Abstract Soft soil is in the category of problematic soil because it has low bearing capacity, which is not suitable for construction of infrastructures. However, with suitable ground improvement such as soil modification, these grounds can be used as normal. Soil modification commonly uses cement as an additive to improve the characteristics of soft soils. In this study, soil modification with fly ash and oil palm shell activated carbon was proposed to evaluate the plastic characteristics of modified soft soil. These additives could be potential replacement of cement in order to cut down the usage of cement and hence promotes sustainable and green solution. Peat, a type of soft soil collected from Kuching, Malaysia was added with different types of additives in the laboratory. Laboratory tests were carried out to measure plastic characteristics of the modified soil samples. Plasticity of each sample was measured before and after the soil modification. It was observed that plastic characteristics of the modified soil showed improvement compared to the non-plastic peat soil. The test results were discussed with respect to liquid limit and plastic limit of the soil and effect of type of additives used.

Keywords Soft soil · Plasticity · Fly ash · Oil palm shell activated carbon

1 Introduction

Construction of infrastructures on a very soft soil is unsuitable due to problematic characteristics of soft soil such as high water content, high compression, and high organic content especially for peat soil, low shear strength and low bearing capacity [1]. Soil modification is sometimes required to improve properties of soil

S. N. A. Mario (✉) · R. Tawie
Faculty of Civil Engineering, Universiti Teknologi MARA, Kota Samarahan 94300,
Samarahan, Sarawak, Malaysia
e-mail: aidamario_87@yahoo.com

using various techniques including compaction, dewatering and by adding materials to the soil to enhance the strength and durability of soft soils.

The stability of structures constructed on soil will be affected by the stability of the soil. Certain soils due to their low bearing capacity pose problems in the construction of infrastructures. In Malaysia, types of soil are depending on various factors such as area, location and the surrounding [2]. Peat soil is well known for its good water retention compared to other types of soil. That is why peat contains very high in moisture up to more than 100 %. This condition leads to reduction of bearing capacity of peat.

The use of cementitious materials has been found to be effective in stabilizing and strengthening soft soil. The present study investigated the potential application of incorporating industrial wastes as alternative to cement with the aim to reduce the usage of cement and hence promotes sustainable and green solution using reusable wastes. This study also investigated the potential of using activated carbon to reduce the adverse effect of heavy metal contain in the fly ash to the environment and enhance engineering properties of peat. The results from this study showed that plastic characteristics of soft soil can be improved by adding fly ash and activated carbon into the soil.

2 Literature Review

Peat covers quite large areas in Malaysia and almost half of the peat land areas in this country are located in Sarawak state. Peat is a category of problematic soil because it consists of partially decayed plant materials such as leaves, branches and roots. It has very high moisture content and very low or non-plastic characteristic. It is a major construction problem when it comes to building infrastructures over peat due to the low bearing capacity of the soil and therefore unsafe to carry loads of the structures.

Soil stabilization refers to methods employed to stabilize soft soil in order to improve the soil workability [3]. Soil stabilization is very crucial at the early stage of the construction to enable infrastructures to be erected safely. There are several techniques that have been used to stabilize soft soil and the most commonly used techniques are chemical and mechanical stabilization. The first chemical stabilization was used by the Mesopotamians and the Romans. They realized that the load bearing capacity of soft soil can be improved by mixing it with stabilizer such as pulverized limestone and calcium [4]. Other stabilizers that have been used widely in chemical stabilization are cement, bentonite and lime.

Recently, there are many researches on stabilization of ground for construction of infrastructures but most of them focused on types of additives used. Not all additives are suitable for all types of soils. The additives are generally used as a binder, filled material that fills in the void of soil to increase density, moisture absorber, or to neutralize the harmful effects of a substance in the soil [5]. There are a number of researches that have studied the effectiveness of different types of

additives to improve the soil workability. For example, Huat et al. [6] investigated the effect of curing time and the increase in cement content on the unconfined compressive strength of modified peat soil samples with ordinary Portland cement. The authors found out that the strength of the modified peat soil increased gradually up to 28 days and higher strength can be achieved with higher amount of cement content. A study by Deboucha et al. [7] also showed similar improvement of peat soil properties by using cement, bentonite and sand to stabilize the soil. Wong et al. [8] determined that a minimum content of cement with slag and sand was required in order to stabilize the peat soil. According to them, peat soil has a very low amount of solid particles and therefore sufficient amount of cement is needed to form a reasonable load bearing capacity of the soil. Hashim and Islam [9] conducted a study to investigate a stabilization technique by soil columns, which has gained popularity for construction on soft soil. In their study, quality of stabilized peat soil columns was assessed by visual inspection and their strengths were confirmed from unconfined compressive strength tests. The above studies show that ordinary Portland cement is a good material for increasing the strength of peat because it binds the soil compared to other additives that only act as filled material to the soil. However, the use of ordinary Portland cement for soil stabilization is not only a costly approach but the manufacturing of cement leads to increase in carbon footprint and deterioration of environment.

The present study aimed to replace the use of ordinary Portland cement with fly ash and activated carbon. Fly ash was used as an alternative for cement replacement material in a study by Trivedi et al. [10]. The author investigated the effects of liquid limit, plastic limit and the optimum moisture content on soil stabilized with various amount of fly ash. Those soil parameters were found to influence the CBR values of soft soils. Large amount of fly ash used in soil is known to harm the environment especially the groundwater due to the heavy metal content in fly ash. Meanwhile, activated carbon has been proved to be excellent absorptive material and it is widely used as air purifier, filter media for water filtration, and soil conditioner. The effectiveness of activated carbon as heavy metal removal had been investigated by various researchers all over the globe. Zayat [11] studied the potential of removal of heavy metals in aqueous solution of activated carbon. The heavy metals removed by activated carbon in the study were lead, cadmium and copper. An experimental study by Asong [12] successfully showed removal of plumbum and zinc from chemical tests performed on various amount of activated carbon added to stock solution. In another study by Vasilyeva et al. [13], they found out that activated carbon could reduce toxicity in a highly contaminated soil. Activated carbon can act as a home to bacteria and neutralizes the contaminated soil. In the present study, the use of fly ash and activated carbon as additives are not only supposed to enhance the plastic characteristics of peat soil but also in line with sustainable approach to promote green environment for future generations.

3 Materials and Method

3.1 Soft Soil

The type of soft soil investigated in this study was peat. The soil was obtained from peat land at Petra Jaya, Kuching. Soil samples were excavated at a depth of 0.3–0.8 m below the ground surface. Physical observation of the peat soil at moist condition showed that the soil was dark brown in colour. The groundwater table was around 0.5–0.7 m from the surface based on the moisture content test.

3.2 Ordinary Portland Cement

Ordinary Portland cement is a common commercial product and is widely used in the construction industry. In this study, Portland cement produced by CMS Cement Sdn. Bhd., Kuching was used as a binder to stabilize the peat by hardening the soft soil over time.

3.3 Fly Ash

Fly ash is a by-product waste from combustion of coal in the electric power plant. In Kuching, fly ash produced by Sejangkat Power Corporation Sdn. Bhd. is sold commercially by Gobel Industry Sdn. Bhd. at a reasonable price. In this study, the fly ash was used as an alternative to cement in soil stabilization. The fly ash acted as moisture absorber to reduce excess moisture content in peat. Table 1 shows the chemical composition of the fly ash used in the present study.

3.4 Activated Carbon

Activated carbon used in this study was commercial oil palm shell activated carbon purchased from Bravo Green Sdn Bhd. It was produced by physical activation process with steam as the activating agent. There are two forms of activated carbon produced, namely, granular and powder. In this study, the powder form was used because of the larger pore and surface area. The key advantage of using activated carbon together with fly ash was to absorb the heavy metal content in fly ash.

Table 1 Chemical properties of fly ash

Element	Percentage
SiO ₂	58.0
Al ₂ O ₃	24.8
Fe ₂ O ₃	7.17
K ₂ O	3.14
CaO	2.40
MgO	1.95
TiO ₂	1.05
P ₂ O ₅	0.34
Na ₂ O	0.30
MnO	0.18
SO ₃	0.09
LOI	0.32

Source Sejngkat Power Corporation Sdn. Bhd

3.5 Method

Properties of peat soil collected from the field such as moisture content, Atterberg limit, degree of humification and specific gravity were determined in the laboratory. The physical tests were conducted before and after soil modification. Soil specimens were mixed with ordinary Portland cement, fly ash and activated carbon with varying amount from 0 to 60 % of the natural peat soil mass by using a blender. A total of 12 modified soil samples were prepared. For the three additives, the amount added were the same at 15, 30, 45 and 60 % of the peat mass. To make sure the additives were well blended into the peat soil, mixing was conducted for at least 10 min. All tests were performed as per American Society of Testing Materials (ASTM) standards. Chemical tests were also carried out to evaluate the removal of heavy metal content in fly ash after mixing with activated carbon. The tests took place in the Environmental Laboratory at Faculty of Civil Engineering, UiTM Shah Alam, Malaysia. Heavy metals which were found to be reduced as a result of addition of activated carbon were chromium, copper and lead.

4 Results and Discussion

Peat soil can be described as a complex type of soil. Its characteristics are dissimilar to other types of soil. Physical characteristics of peat have been tested as per ASTM standards [14–17]. Table 2 shows the physical characteristics of the peat soil.

Moisture content of peat samples were determined right after the soil sampling, which was taken from the range of 0 to 1.2 m. This procedure was carried out to determine the natural moisture content of peat as well as the groundwater table of

Table 2 Physical characteristics of peat

Moisture content by depth (%)	Surface to 0.3 m	0.3–0.6 m	0.6–0.9 m	0.9–1.2 m
	398.6	745.7	946.8	1097.3
Moisture content after sampling (%)	808.1			
Liquid limit (%)	167.13			
Plastic limit (%)	Non-plastic			
Degree of humification	H6			
Specific gravity	1.13			

the soil as indicated in Table 2. The test was carried out according to ASTM D2216-10.

4.1 Plasticity Index

Plastic limit and liquid limit are values determined to give an idea or indicate how soil will act under certain conditions. Plastic limit is a state of moisture in soil that separate plastic behaviour from solid behaviour or when the soil starts to behave in a plastic nature. Liquid limit is defined by a moisture content, which soil begins to act less as a viscous fluid and more like a plastic patty. Determination of plastic limit, liquid limit and plasticity index of soil in this study were determined in accordance with ASTM D4318-10. The measure of the range of moisture content between the plastic limit and liquid limit is known as the plasticity index (PI). PI is commonly used as an indication of soil shrink/swell properties and constructability. In soil modification, the purpose of measuring PI after soil modification is to indicate properties of the soil binder. As reported by Majeed and Taha [18], soft soil modified with very fine particles could result in the reduction of the PI value of the modified soft soil. From the values of plastic limit and liquid limit, plasticity index can be calculated as follows:

$$PI = LL - PL \quad (1)$$

where:

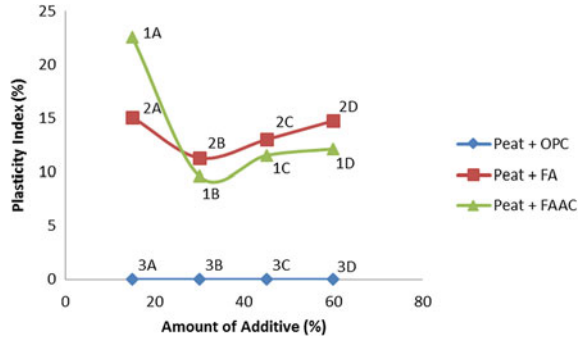
PI = Plasticity index

LL = Liquid limit (whole number)

PL = Plastic limit (whole number)

The plasticity indices for peat added with fly ash (FA) and peat added with fly ash combined with activated carbon (FAAC) are shown in Fig. 1. Peat added with ordinary portland cement (OPC) is classified as a non-plastic soil because the plastic limit could not be determined. This is because generally plastic limit test is difficult to be done on peat as no or little clay content is available. As for peat added with OPC, the plastic limit was also non-measurable. When cement reacts

Fig. 1 Variation of plasticity index with amount of additive



with natural water in peat, OPC will bind the soil particles and become hardened, thus reduced plasticity of the soil.

From Fig. 1, peat added with FAAC shows a greater reduction of plasticity index as compared with peat added with FA and the index increased slightly with respect to increasing in the dosage of FAAC added to peat. When added with FA alone, the plasticity index reduced at the first 15 and 30 % of FA dosage but increased gradually with the increasing FA dosage.

5 Conclusion

The peat soil investigated in this study was dark brown in colour where the groundwater table was about 0.5–0.7 m from the surface. The degree of humification can be classified as H6 (amorphous peat) or the soil is considered to be high in organic content and unsuitable for geotechnical application. The plastic limit and liquid limit of modified peat decreased with the increasing amount of additives. However, the reduction in liquid limit was more noticeable for peat added with FAAC than FA alone. Conversely, peat added with OPC was reported as non-plastic because plastic limit of the mixture was non-measurable.

Acknowledgments The authors gratefully acknowledge the financial support by Universiti Teknologi MARA (UiTM) Sarawak towards the conference fee for participation in the InCIEC 2013 International Civil and Infrastructure Engineering Conference. The authors also acknowledge with much appreciation the assistance by the technicians from Faculty of Civil Engineering, UiTM Shah Alam and UiTM Sarawak in preparing all the required equipment to conduct the laboratory tests.

References

1. A. Zainorabidin, I. Bakar, in *Engineering Properties of In-Situ and Modified Hemic Peat Soil in Western Johor*. Proceedings of 2nd International Conference on Advances in Soft Soil Engineering and Technology, (University Putra Malaysia Press, Malaysia 2003), pp. 173–182
2. J.M. Said, S.N.L. Taib, Peat stabilization with carbide lime. UNIMAS E- J. Civ. Eng. **1**(1), 1–6 (2009)
3. T. Abadjieva, in *Chemical Stabilisation For Low Cost Roads in Botswana*. First Road Transportation Technology Transfer Conference in Africa, 2001
4. T.E. Kowalski, D.W. Starry Jr, *Modern Soil Stabilization Techniques*, in *Annual Conference of the Transportation Association of Canada* (Saskatoon, Saskatchewan, 2007), pp. 14–17
5. S. Vitton, *Introduction to Soil Stabilization* (Michigan Technological University, Caterpillar, 2006)
6. B.M. Huat, M. Shukri, A.M. Thamer, Effect of chemical admixtures on the engineering properties of tropical peat soils. *Am. J. Appl. Sci.* **2**(7), 1113–1120 (2005)
7. S. Deboucha, R. Hashim, A. Alwi, Engineering properties of stabilized tropical peat soils. *Electron. J. Geotech. Eng.* **13**, Bund. E, 1–9 (2008)
8. L.S. Wong, R. Hashim, A. Alwi, Strength and permeability of stabilized peat soil. *J. Appl. Sci.* **8**(21), 3986–3990 (2008)
9. R. Hashim, M.S. Islam, A model study to determine engineering properties of peat soil and effect on strength after stabilization. *Eur. J. Sci. Res.* **22**(2), 205–215 (2008)
10. J.S. Trivedi, S. Nair, C. Iyyunni, Optimum utilization of fly ash for stabilization of sub-grade soil using genetic algorithm. *Procedia Eng.* **51**, 250–258 (2013)
11. M.E. Zayat, Removal of heavy metals by using activated carbon produced from cotton stalks. Thesis (M.Sc.), Department of Construction Engineering, American University in Cairo, 2009
12. A. Asong, The Removal of Plumbum and Zinc Using Activated Carbon. Thesis (B.Sc.), Faculty of Chemical and Natural Resource Engineering, UMP, 2008
13. G.K. Vasilyeva, E.R. Strijakova, P.J. Shea, Use of activated carbon for soil bioremediation, in soil and water pollution monitoring, protection and remediation, (Springer Netherlands, 2006), pp. 309–322
14. ASTM D2216-10 (2010) Standard Test Methods for Laboratory Determination of Water (Moisture) Content of Soil and Rock by Mass. Annual Book of ASTM Standards, Philadelphia, USA
15. ASTM D4318-10 (2010) Standard Test Methods for Liquid Limit, Plastic Limit, and Plasticity Index of Soils. Annual Book of ASTM Standards, Philadelphia, USA
16. ASTM D5715-00 (2006) Standard Test Method for Estimating the Degree of Humification of Peat and Other Organic Soils (Visual/Manual Method). Annual Book of ASTM Standards, Philadelphia, USA
17. ASTM D854-10 (2010) Standard Test Methods for Specific Gravity of Soil Solids by Water Pycnometer. Annual Book of ASTM Standards, Philadelphia, USA
18. Z.H. Majeed, M.R. Taha, Effect of nanomaterial treatment on geotechnical properties of a Penang soft soil. *J. Asian Sci. Res.* **2**(11), 587–592 (2012)

Rock Mass Classification System Used for Pahang-Selangor Raw Water Transfer Tunnel

Romziah Azit and Mohd Ashraf Mohamad Ismail

Abstract The recent Pahang-Selangor raw water transfer tunnel project had resulted in a large amount of rock mass classification data for the assessment of the rock mass class required for the design of tunnel support system. In this project, a rock mass classification by Japan Highway Public Corporation (JH) has been used to assess the rock mass class using geological mapping and geological documentation of the tunnel face and the side walls of the excavated tunnels. Although JH classification had been used for this project, other forms of classification using different criteria from Rock Mass Rating (RMR) and Q-System have also been widely used for tunnelling project all over the world. Since there have been few studies on the relationships among such different criteria of the classification systems, this study mainly focuses on the comparison between the JH and RMR classification systems for the water transfer tunnel. From the correlation analysis among the criteria used in both JH and RMR classification systems, there is higher correlation if the rock mass is in relatively good condition. It was also found that there is less consistency between JH and RMR classifications in the region of 'poor rock'. However, the correlation between both classification systems is still considered suitable to be used in this tunnelling project.

Keywords Rock mass classification · Japan Highway Public Corporation · Rock mass rating

1 Introduction

Rock masses are discontinuous and often have heterogeneous and anisotropic engineering properties. The heterogeneity of the intact rock and rock masses are influenced by a number of factors such as fracturing, bedding and weathering

R. Azit (✉) · M. A. M. Ismail
School of Civil Engineering, Universiti Sains Malaysia, Nibong Tebal, Penang, Malaysia
e-mail: romziah71@gmail.com

[1, 2]. After all, the mechanical behaviour of rock masses is dependent on the strength of the blocks created by random patterns of discontinuities and their strength. However, the classification of the rock mass is an indirect method and does not measure the mechanical properties like deformation modulus directly. Therefore, the classification system is necessary to take into account the factors that influence the stability of the rock masses. The result is an estimate of the stability quantified in subjective terms such as poor, acceptable, good and very good.

Rock mass classifications have played an important role in estimating the strength and deformability of rock masses for determining slope stability, support systems, as well as for considerations on items such as span of excavation, length of advance per round, and construction methods. The rock mass classification systems are used for various engineering designs and stability analyses. For example Liu and Chen [2] approached the application on the rock slope stability assessment for several rock slopes of the Southern Cross-Island Highway in Taiwan. Vardakos et al. [3] estimated the support system for Shimizu Tunnel in Japan and Khabbazi et al. [4] used to estimate the rock mass deformation modulus for tunnel and dam sites in western and northern Iran. The classification of rock masses encountered during tunnel excavation was made through evaluation of the mechanical and hydraulic properties of rock masses, as well as the thickness of overburden. In comparison to many other civil engineering situations, the uncertainties involved in underground rock engineering are high. Therefore, most of the tunnels constructed at present make use of various types of classification systems [5–8]. The rock mass classification system was developed for used at project feasibility and preliminary design stages. It is also used to provide initial empirical estimates of tunnel support requirements and practical engineering tools which forced the user to examine the properties of the rock mass.

1.1 Engineering Rock Mass Classifications

There are several established procedures for rock mass classifications such as Rock Mass Structure Rating (RSR), Rock Mass Rating (RMR), Rock Quality Index (Q System). The most common classification systems used are the RMR system published by Bieniawski in 1973 [9, 10] and Q system, first described in 1974 by Barton and Bieniawski [11]. Many researchers have studied the different rock mass classification systems either to compare or combine the systems. For example Choi and Park [7] made comparisons among different criteria of RMR and Q-system for rock tunnel in Korea and Sapigni et al. [8] used RMR-system to predict TBM performance. Meanwhile Palmström et al. [12] studied the limitations of Q-system. In year 2009, Palmström [13] combined the RMR, Q, and R_Mi Classification System into one set of tables. These enable the ground quality to be found directly and independently in the three systems from only one set of observations.

In this study, the rock mass condition at the Pahang-Selangor Raw Water Transfer Project (PSRWT) site will be classified using JH classification system. This classification is based on the RMR classification by Bieniawski 1973 [9] and Rock Mass Quality of Q system Barton and Bieniawski [11]. The classification system classified the rock with five parameters obtained. They are material strength, the rock quality designation (RQD), joint spacing, joint and ground water conditions.

1.2 Site Description

To compare the different criteria used in the rock mass classification systems between RMR and JH, PSRWT was selected as a study area. The purpose of the water transfer tunnel is to convey raw water from the Semantan River in Pahang State to a water treatment plant in Selangor State, Malaysia. The diameter of the main tunnel is 5.2 m with 44.6 km in length that crosses the Titiwangsa Main Ranges which mainly consists of granitic rock. The excavation methods for the tunnel used 3 numbers of Hard Rock Tunnel Boring Machine (TBM) and 4 New Austrian Tunnelling Method (NATM). NATM method was adapted for relatively less ground cover (overburden) zones and estimated low grade rock conditions. Figure 1 shows the NATM method at NATM 1 tunnel of the project.

Based on geological investigation and topography, NATM was designed mainly for relatively lower cover sections at the folded Paleozoic sedimentary rock zone. The sections were 5.9 km length at the Inlet and 2.9 km length at the outlet. Figure 2 shows the location of NATM 1 starting from Chainage (Ch.) 858 m to Ch. 2,785 m at the Inlet section.

1.3 Geological Condition

The tunnel alignment is mainly composed of Main Range granitic which forms the backbone of the Peninsular Malaysia and sedimentary rocks of Paleozoic and Mesozoic age. The geological map for the PSRWT tunnel is shown in Fig. 3.

The geology of the tunnel starts from the slightly metamorphosed Devonian sedimentary rocks from the inlet to Ch. 3.8 km while from Ch. 3.8 to Ch. 44.6 km, it consists of coarse to medium-grained granitic rocks forming the main range of Malaysia Peninsular. This rock is mainly black shale to schist, strongly folded by intrusion of granitic rocks in Triassic age. The rock near the boundary to granite is well silicified as hornfels by contacting with granitic rocks.

The estimated major faults crossing tunnel are 6 faults consisting of Karak Fault (Ch. 2.5 km), Krau Fault (Ch. 12.45 km), Bukit Tinggi Fault (Ch. 19.15 km), Lepoh Fault (Ch. 28.6 km), Kongkoi Fault (Ch. 31.35 km) and Tekali Fault (Ch. 39.0 km). Meanwhile the lineaments crossing tunnel alignment are 12, starting



Fig. 1 Excavation of NATM I at Pahang-Selangor raw water tunnel

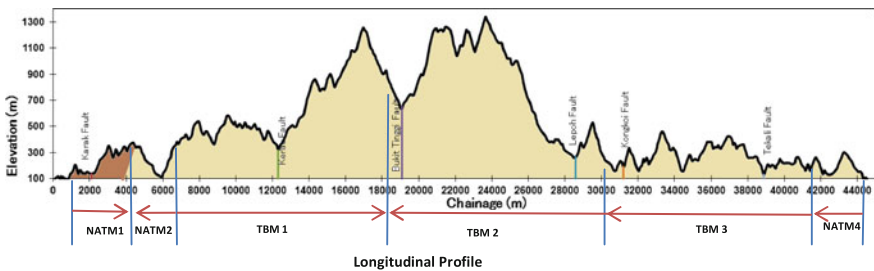


Fig. 2 Typical section of tunnel and arrangement for tunnel work (NATM & TBM)

from L-A to L-N as shown in Fig. 3. There are quartz dykes, which are extremely hard and accompanied by clay zones with less than 1 m thick average on both sides. Also a few quartz veins are developed in lower half downstream of tunnel.

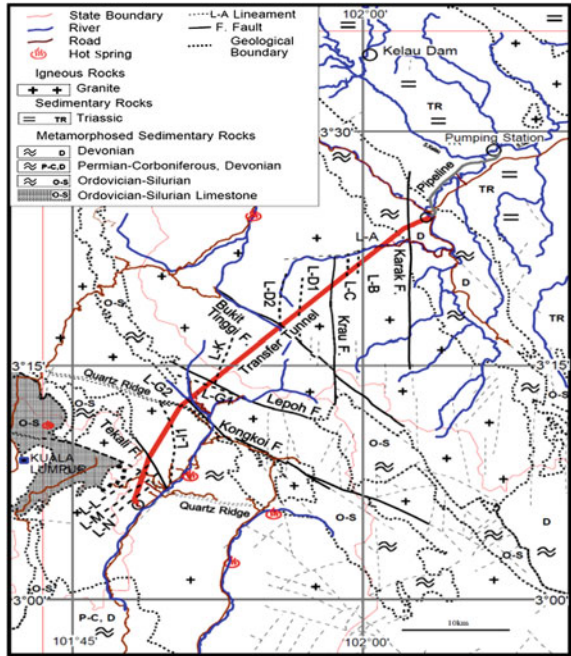
The study area, NATM 1 was composed of sedimentary rocks of Paleozoic and Mesozoic age. The minimum and maximum overburden range from 110 to 235 m, starting at Ch. 858 m to Ch. 2,785. This section has already experienced a folding and seepage in Devonian sedimentary rock zone and Karak Fault at Ch. 2.5 km.

2 Rock Mass Classifications

2.1 JH Classification

Rock classification for tunnel face and wall at this site are based on the standard in the JH classification. The compressive strength, weathering, spacing of joints,

Fig. 3 Geological map around the project site



conditions of joints, and the groundwater condition were estimated from the geological map of tunnel face data sheets. Rock mass was classified from the total points of tunnel face observation based on chart as presented in Fig. 4. The classification of the classes depended on rock categories from soft (layered) to hard rock (massive) conditions and all rock types.

The JH classification is rock mass rating system which relies primarily upon the following four general observation data related to the rock mass strength: compressive strength, weathering, spacing of joints and condition of joints. Overall rating of the rock mass is made by adding the ratings of the parameters, and the total rating (total point) is given a class representing the rock mass quality. Calculated RMR value used to find rock mass classes from very good rock to Faults and crushed rock zone or squeezing zones. General rock conditions corresponding to JH classification classes are listed in Table 1.

2.2 RMR Classification

Bieniawski in 1973 [9], published a detailed rock mass classification called the Geomechanics Classification or Rock Mass Rating (RMR) system for jointed rock masses. The system was originally developed for the calculation of rock load and tunnel support selection. Significant changes have been made over the years with

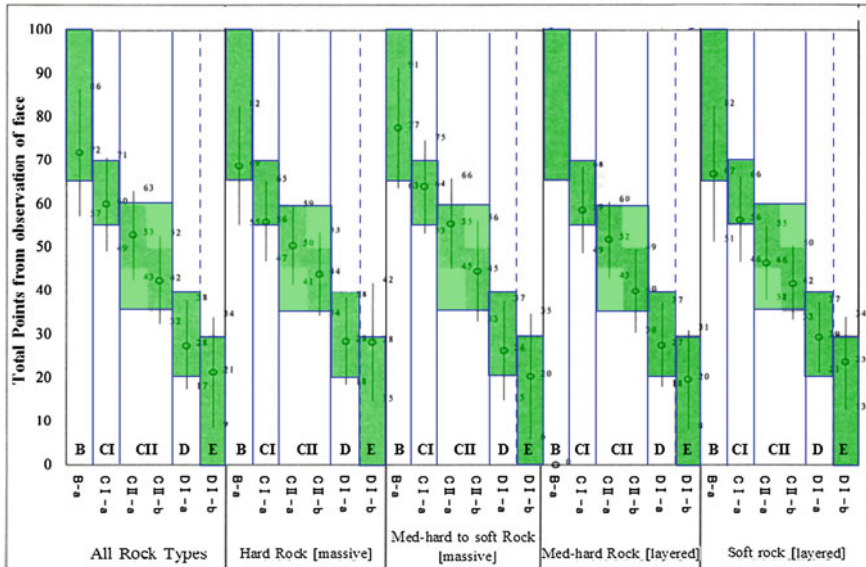


Fig. 4 JH classification rock mass classes

Table 1 JH rock mass classes ratings

Rock mass class	Description
A	Very good rock, hard and fresh
B	Good rock, hard and fresh but affected by weathering
CI	Fair rock, rock is weathered, some clay in joints
CII	Fair to poor rock weathered, loosed rock mass
DI	Very poor rock: considerably weathered rock mass, soft zones, partially soil properties
DII	Extremely poor rock: as above with potential rockfall
E	Faults and crushed rock zone, squeezing zones

Table 2 RMR rock mass classes ratings

RMR ratings	81–100	61–80	41–60	21–40	<20
Rock mass class	I	II	III	IV	V
Description	Very good rock	Good rock	Fair rock	Poor rock	Very poor rock

revisions in 1974, 1975, 1976 and 1989 [9–11]. RMR uses six parameters that are readily determined in the field; which are uniaxial compressive strength of the intact rock, Rock Quality Designation (RQD), spacing of discontinuities, condition of discontinuities, ground water conditions and orientation of discontinuities.

Table 3 Comparison of input parameters

Input parameters		Values or rating	
		RMR	JH
Compressive strength of intact rock	Very low strength (1–5 MPa)	1	0
	Low strength (5–25 MPa)	2	6
	Moderate strength (25–50 MPa)	4	12
	Medium strength (50–100 MPa)	7	18
	High strength (100–250 MPa)	12	25
	Very high strength (>250 MPa)	15	31
Rock quality designation (RQD)	Very good (90–100 %)	20	22
	Good (75–90 %)	17	22
	Fair (50–75 %)	13	16
	Poor (5–50 %)	8	11
	Very poor (<25 %)	5	5
Joint spacing	Very large spacing (Spacing >2 m)	20	22
	Large spacing (0.6–2 m)	15	16
	Moderate spacing (200–600 mm)	10	11
	Small spacing (60–200 mm)	8	5
	Very small spacing (<60 mm)	5	0
Joint condition	Very favour	30	26
	Slightly favour	25	19
	Moderately	20	13
	Unfavourable	10	6
Joint orientation	Very favourable	0	–
	Favourable	–2	–
	Fair	–5	–
	Unfavourable	–10	–
	Very unfavourable	–12	–
Ground water condition	Dry/Moist (<1 L/min)	15	0
	Wet (<10 L/min)	10	–5
	Dripping water (<25 L/min)	7	–7
	Flowing water (<125 L/min)	4	–10

The rating is an outcome of a supervised classification of each parameter. Calculated RMR value used to find rock mass classes from very good rock to very poor rock. The rating for the each parameter is summarized in Table 2.

3 Discussion

JH and RMR classification systems are based on a rating of three principal properties of a rock mass. These are the intact rock strength, the frictional properties of discontinuities and the geometry of intact rock defined by the discontinuities. In order to investigate the influence of these parameters, the approximate total range in values for JH and RMR are used as a basis of comparison. Table 3

Fig. 5 The correlation between the RMR and JH

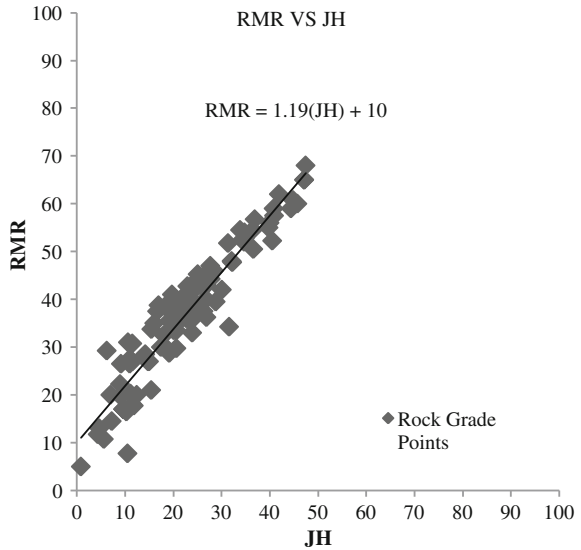
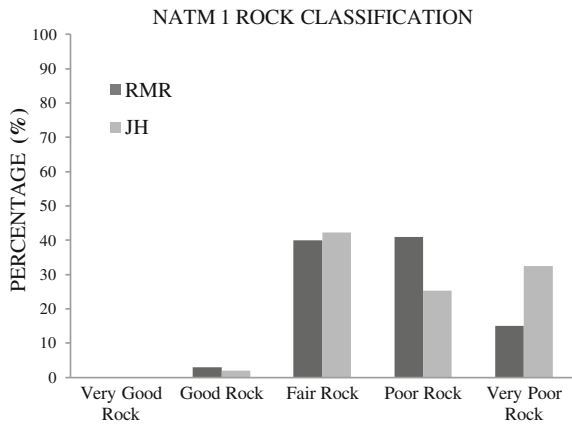


Fig. 6 The distribution of rock mass class for NATM 1



shows the comparison of common input parameters with the values or ratings used in RMR and JH classifications.

The excel spreadsheet is used to estimate the total values of RMR rating, based on the percentage of the differences in both classification systems. A scatter plot in Fig. 5 shows the correlation between RMR and JH. The linear relationship between RMR and JH classification systems is in the form of $RMR = 1.19(JH) + 10$.

The bar chart in Fig. 6 shows the rock classification in the percentage of the RMR and JH for NATM 1. According to the chart, less than 5 % for both classification systems is classified as a ‘good rock’ which is class B for JH and class I

Table 4 JH and RMR rock classifications

JH	Rock conditions	RMR	Rock conditions
A	Very good rock, hard and fresh	I	Very good rock
B	Good rock, hard and fresh but affected by weathering	I–II	Good rock
CI	Fair rock, rock is weathered	II	Fair rock
CII	Fair to poor rock weathered	III	
DI, DII	Very poor rock	IV–V	Poor rock
E	Fault and crushed rock zone	V	Very poor rock

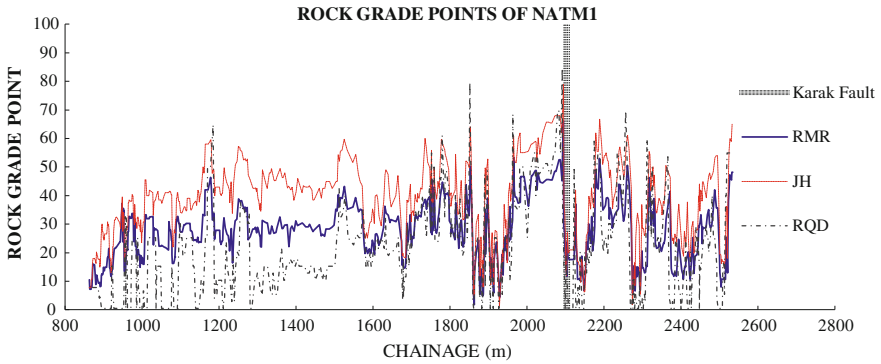


Fig. 7 Comparisons between the RMR, JH classification systems and RQD

or II for RMR. It can be classified that 95 % of the ground condition at NATM 1 classes from ‘fair rock’ to ‘very poor’ rock. The classes range from CI/CII, DI/DII to E for JH and III to V for RMR Classifications.

Comparison for both classification systems gives the percentage of ‘fair rock’ almost the same for both systems but it is slightly different for the ‘poor’ and ‘very poor’ rock classes’ condition. This happened because from total ratings of RMR, it gives the exact figure between rock classes, while JH gives a range of figures for rock masses classes.

General rock conditions corresponding to JH and RMR classifications are summarized in Table 4. The delineation of regions of the rock mass from ‘very good’ to ‘very poor’ between JH and RMR is based on comparison of rock mass classifications for both systems. The classes for ‘Good rock’ conditions range from B to A and II to I for JH and RMR classification systems respectively. For rock condition ‘Fair rock’ grade in RMR, it has been considered as the rock grade ranging from ‘Fair rock’ to ‘Fair to Poor rock’ in JH.

Comparison also had been made for the total grade point ratings between JH, RMR and RQD. The consistency between JH and RMR classifications indicates that RMR system has smaller ratings about 9–19 % compared to JH classification (Fig. 7). Basically, JH classification has higher ratings for the 3 parameters: strength of intact rock, weathering alteration and spacing of discontinuities, only

condition of discontinuities has lower rating than RMR system. From the correlation analysis among the criteria used in both JH and RMR classification systems, there is higher correlation if the rock mass is in relatively good condition.

4 Conclusion

The comparison of two or more classification systems will generally lead to better and more accurate results. It is important to know that the parameters give average values, and that it might be significant variation between the lowest and highest value and rating for most of them. The conclusion could be drawn from the current study that although total rating of RMR is lower than JH, the classes of rock conditions between both classification systems still remain the same. It was also found that there is less consistency between JH and RMR classifications in the region of 'poor rock' and 'very poor rock'. However, the correlation between both classification systems is considered suitable to be used in this tunnelling project.

Acknowledgments The authors would like to express their gratitude to Pahang-Selangor Raw Water Transfer Project Team and the consultants for providing their data.

References

1. C. Edelbro, *Rock Mass Strength: A Review* (Luleå tekniska universitet, Luleå, 2003), pp. 1402–1536
2. Y.-C. Liu, C.-S. Chen, A new approach for application of rock mass classification on rock slope stability assessment. *Eng. Geol.* **89**(1–2), 129–143 (2007)
3. S.S. Vardakos, M.S. Gutierrez, N.R. Barton, Back-analysis of Shimizu Tunnel No. 3 by distinct element modeling. *Tunn. Undergr. Space Technol.* **22**, 401–413 (2007)
4. A. Khabbazi, M. Ghafoori, G. R. Lashkaripour, A. Cheshomi, Estimation of the rock mass deformation modulus using a rock classification system. *Geomech. Geoeng.* **8**(1), 46–52 (2013)
5. G. Wang, Y. Shi, H. Liu, J. Kou, Z. Shan, C. Zhou, The Rock Mass Classification Methods for Deep Buried Tunnels, no. 574, pp. 1–9 (2006)
6. H. Stille, A. Palmström, Classification as a tool in rock engineering. *Tunn. Undergr. Space Technol.* **18**(4), 331–345 (2003)
7. S.Y. Choi, H.D. Park, Comparison among different criteria of RMR and Q-system for rock mass classification for tunnelling in Korea. *Tunn. Undergr. Space Technol.* **17**, 391–401 (2002)
8. M. Sapigni, M. Berti, E. Bethaz, A. Busillo, G. Cardone, TBM performance estimation using rock mass classifications. *Int. J. Rock Mech. Min. Sci.* **39**(6), 771–788 (2002)
9. Z.T. Bieniawski, Engineering classification of jointed rock masses. *Trans. S. Afr. Inst. Civil Eng.* **15**(12), 335–344 (1973)
10. Z.T. Bieniawski, *Engineering Rock Mass Classifications* (Wiley, New York, 1989), p. 251

11. N. Barton, Z.T. Bieniawski, RMR and Q: setting records straight. *Tunnels Tunn.* 26–29 (2008)
12. A. Palmström, N. As, Use and misuse of rock mass classification system with particular reference to the Q-System, **21**, 575–593 (2006)
13. A. Palmström, Combining the RMR, Q, AND RMi Classification System, <http://www.rockmass.net>, 25, (2009)

Electrokinetic Remediation to Remove Heavy Metal from Contaminated Soils Using Purging Solution

Sabariah Arbai, Zainab Mohamed, Kamaruzzaman Mohamed and AzinoorAzida Abu Bakar

Abstract This study was designed to determine the physical characteristic of soil from mining area, the level of heavy metal contamination on site, and performance of pH and concentration of heavy metal after electrokinetic. For each type of purging solution and soil sample, six days of treatment time were performed with low direct current of 1.076 V to each purging solution. Soil sample consists of sand and gravel. Changes on level of pH and concentration showed the movement of metal ions and electrons from anode to cathode. The removal efficiency for acetic acid is much higher with 78 % compare to deionized water of 53 %. The existing level of contaminant was also determined by using single factor index. This provides a better view on the existing level of metal contaminant at site.

Keywords Acetic acid · Deionized water · Heavy metal

1 Introduction

Electrokinetic remediation have been used for the remediation of soil for years and proven sufficient in situ process for remediation of contaminated soil containing organic contamination [1, 2]. The implementation of electrokinetic remediation involves inserting the anode and cathode electrode in the soil and applying an electric potential between them. The electric potential will then induce the movement of contaminant toward electrode well which generate acidic medium at anode and alkaline medium at cathode [3, 4]. The applications of a direct electric current to soils result in several changes such as pH and electrolyte concentration in the soil. These changes may impact the nature of the soil surface chemistry [5]

S. Arbai (✉) · Z. Mohamed · K. Mohamed · A. A. Bakar
Faculty of Civil Engineering, Universiti Teknologi MARA, 40450 Shah Alam, Selangor,
Malaysia
e-mail: sabariaharbai@salam.uitm.edu.my

and the success of electrokinetic itself. The key success of remediation holds by understanding the changes in transport process and the geochemical condition at various stages [6].

Recently, researchers developed numerous lab-scale studies to investigate the efficiency and feasibility of using electrokinetic. Their focus which was on the residual contamination distribution and the removal efficiency [7, 8], does not investigate the actual value of contaminant prior to collecting it from site area. These could provide a rough estimation on the level of contaminant. Furthermore researchers have found that some of technologies for remediation of soil unable to treat soil with low hydraulic permeability or those contaminated with mixed organic–inorganic wastes [9, 10]. The uses of thermal desorption and incinerators [11] are very costly and ineffective to remove these strongly absorbed contaminant. Electrokinetic is one alternative way to efficiently remediate soil containing organic contaminant however the development of electrokinetic as a way to treat contaminated soil in Malaysia is still in the early stage. The chemical phenomena of using purging solution [12] in electrokinetic remediation remains complex and few detailed studies are reported in literature [13]. Previously they use lactic acid, citric acid and propionic acid at concentration of 1 M as a purging solution [14] however no study was conducted by using acetic acid. Therefore, in this study a detailed assessment on electrokinetic by using acetic acid at concentration 0.02 M [15] and pH 3.29, to see the change of physical and chemical behaviour of contaminant in the soil.

This study involved the investigation of the physical and chemical properties of contaminated soil [16, 17]. The soil samples collected from site, might contained several heavy metals which could affect the life of human [18]. The major factors that contribute the movement of heavy metal in the soil are the type of soil, size of soil and pH distribution.

2 Materials and Method

2.1 Soil Samples

The soil was collected from Putra Perdana, Puchong from three different location namely location A, B and C. Physical properties of the soil sample were determined that are moisture content, particle size distribution, atterberg limit test and the particle density.

Electrokinetic process was run to remove the heavy metal contaminant (zinc) [19, 20]. The purging solution was acetic acid at concentration 0.02 M and pH 3.29 and deionized water pH 7. All the experimental step procedure is based on British Standards 1377: part 2, 1990 (BS standards) [21] and ASTM D 422-Standard Test method for particle size analysis of soils [22].

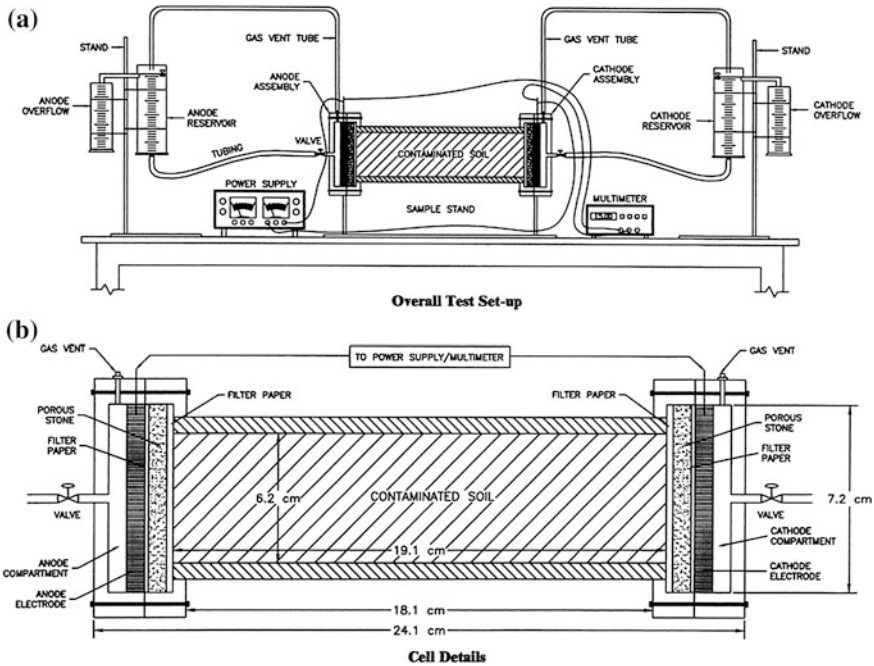


Fig. 1 Electrokinetic setup

2.2 Electrokinetic Set-up

Figure 1 shows the schematic diagram of the electrokinetic setup. This setup also incorporated two electrodes, two porous stones and tubing. This setup simulates one-dimensional transport of contaminants under an induced electrical potential [23, 24].

3 Results

The results of the moisture content, particle size distribution and average particle density are given in Table 1.

There are changes of pH from points P1 to P4 throughout six days. pH for soil using deionized water start with 7.1 at P1, located 6 cm from anode. The value gradually increased to 8.9 at P4 located 6 cm from cathode. pH in deionized water are in the range between 7 and 8, while pH for acetic acid purging is 3 and increase to 4 at P4.

These happen because low voltage DC current created from the electrokinetic will trigger the ion inside the purging solution to transport metal ion inside the soil

Table 1 Summary of physical properties of the soil

	MC (%)	Particle size distribution (%)				Avrg particle density
		Gravel	Sand			
			Coarse	Med	Fine	
A	13.3	17.8	32.2	41.1	8.7	2.60
B	16.5	23.9	38.7	29.0	8.3	2.69
C	13.0	31.5	36.8	27.6	4.0	2.57

sample toward the cathode. Inside deionized water, the solution dissociate to H^+ ion generate at anode migrate toward cathode, while OH^- will migrate to anode causing low value of pH at anode compare to that at cathode. Meanwhile for acetic acid, the solution will dissociate into ion H^+ and acetate ion CH_3COO^- . The H^+ decreases the pH and dissolves the metal ion. As a result, more heavy metal were deposited around point P4, which is located 6 cm from cathode reservoir. Based on the percentage difference, the movement of ions in acetic acid purging is much higher compared to that in the de-ionized water because acid contains more free ions which can easily rupture when there are force imposed to them.

The experimental results for the level of concentration determine the distribution of metal throughout the soil sample. Acetic acid is a weak acid with K_a equally to 1.8×10^{-5} with chemical formula of CH_3COOH . This means it can dissociate easily from their structure. Metal that is positively-charged attracts the electron pair from the purging solution. This allows electron density drawn to O-H bond to polarized release the H^+ at anode and formation of OH^- ions on the cathode. During reaction, water and acetic acid will oxidize and transport ions from point P1 to P4 and subsequently deposit the metal at cathode. These resulted in the decreases level of metal concentration at point P1. Overall removal of copper in deionized water is about 36–56 % while in acetic acid 66–93 %. While for zinc, the removal is about 55–60 % in deionized water and 64–86 % in acetic acid. It shows that in acetic acid with concentration 0.02 M it favour the removal of copper whereas zinc is much more favourable in deionized water. Both purging solutions acetic acid and deionized water are capable to remove contaminants as illustrated in Figs. 2 and 3. The removal efficiency for acetic acid is much higher with 78.35 % compared to that of deionized water of 52.89 %. The removal efficiency for acetic acid is much higher compare to deionized waters as acetic acid has higher conductivity value compare deionized water and much easier to transfer and migrate the electrons when there are source of electricity, illustrated in Figs. 4 and 5 respectively.

Tables 2 and 3 illustrate the level of contaminant for the distribution of heavy metal for zinc (Zn) and copper (Cu) respectively, within the soil samples site location. The range of level estimated that the level of copper are seriously polluted within the area. All three locations recorded level 5. However there are

Fig. 2 pH for soil using deionised water purging

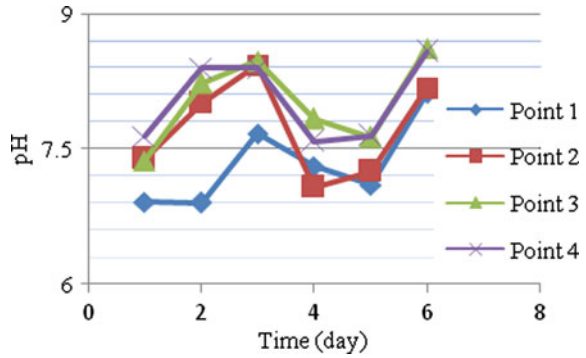


Fig. 3 pH for soil using acetic acid for purging

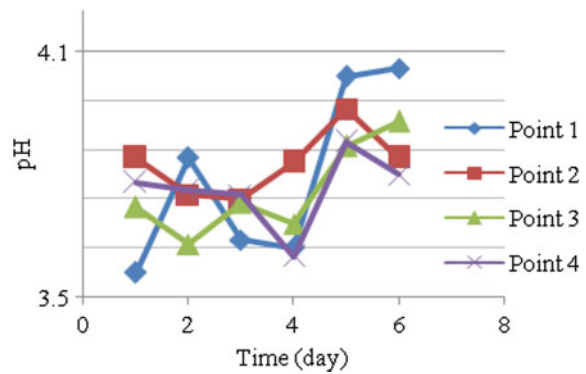
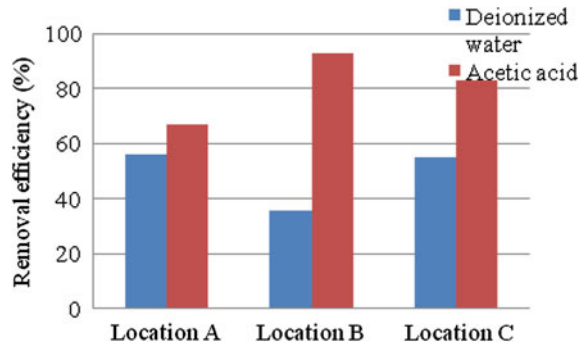


Fig. 4 Copper removal efficiency from each location



varied values recorded for zinc. For location A, it is slightly polluted with zinc and location B moderately polluted with zinc each in level 3 and 4. The worst level of contaminant for zinc is located at location C with level 5 where as for copper all locations are of highly polluted with copper.

Fig. 5 Zinc removal efficiency from each location

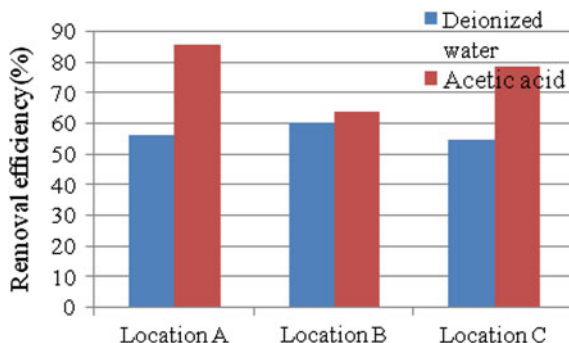


Table 2 Level of contaminant for copper (Cu)

Location/purging solution	Concentration of copper (mg/kg), Ci	ICRCL (Si)	Pi	Level of contaminant
Deionized water	A	2,845	423	6.72 5
	B	3,611	423	8.54 5
	C	5,010	423	11.84 5
Acetic acid	A	3,500	423	8.27 5
	B	3,050	423	7.09 5
	C	3,476	423	8.22 5

Table 3 Level of contaminant for zinc (Zn)

Location/purging solution	Concentration of Zinc (mg/kg), Ci	ICRCL (Si)	Pi	Level of contaminant
Deionized water	A	2,543.08	1,665	1.53 3
	B	3,811.24	1,665	2.20 4
	C	5,944	1,665	3.57 5
Acetic acid	A	4,500.17	1,665	2.70 4
	B	4,813.26	1,665	2.89 4
	C	6,546.13	1,665	3.93 5

4 Conclusion

The purpose of this study was to evaluate the effectiveness of electrokinetic in removing heavy metal from an ex-mining area. From the physical test that had been carried out, the soil collected contain low amount of moisture content and it consist of gravel and sand specifically silty sand. The soil samples were underwent a remediation by using electrokinetic. Two different purging solutions, deionized water and acetic acid were used to extract zinc from the soil. With a low direct current (DC) of electrokinetic of 1.076 V applied to measure the pH and concentration of copper and zinc, under the influence of low voltage and purging solution, the cation of zinc (Zn) and copper (Cu) migrates toward cathode.

The migrations of electron are dependent with physical and chemical before the electrokinetic process. The pH values are in the range of 7–8 for deionized water and 3–4 for acetic acid. Zinc exhibit reduction in the soil sample after the electrokinetic process by using both purging solution. Overall removal of copper in deionized water is about 36–56 % while in acetic acid 66–93 %. Zinc removal is 55–60 % in deionized water and 64–86 % in acetic acid. The removal efficiency for acetic acid is much higher with 78.35 % compare to deionized water 52.89 %. The existing site level of contaminant was also categorised using single factor index, the soil contaminated with zinc is at moderate level with grade 3 and 4 with exception of location C.

Acknowledgments This research was sponsored by Ministry of Higher Education (MOHE) under Fundamental Research Grant Scheme (FRGS).

References

1. N.C. Brady, R.R. Weil, *The Nature and Properties of Soils*, 11th edn. (Prentice Hall, New York, 1996)
2. K.R. Reddy, S. Chinthamreddy, Enhanced electrokinetic remediation of heavy metal in a glacial till soils using different electrolyte solution. *J. Environ. Eng.* **442**, 1–15 (2004)
3. A. Dube, R. Zbytniewski, T. Kowalkowski, B. Buszewski, Adsorption and migration of heavy metal in soil. *Pol. J. Environ. Stud.* **10**, 1–10 (2001)
4. V. Jurate, S. Mika, L. Petri, Electrokinetic soil remediation-critical review. *Sci. Total Environ.* **289**, 97–121 (2002)
5. S. Kim, K.W. Kim, D. Stubern, Evaluation of electrokinetic removal of heavy metal from tailing soils. *J. Environ. Eng.* **705**, 1–11 (2002)
6. K.R. Reddy, C.Y. Xu, S. Chinthamreddy, Assessment of electrokinetic removal of heavy metal from soils by sequential extraction analysis. *J. Hazard. Mater.* **B84**, 279–296 (2001)
7. K. Agnew, A.B. Cundy, L. Hopkinson, I.W. Croudace, P.E. Warwick, P. Purdie, Electrokinetic remediation of plutonium-contaminated nuclear site waste: result from a pilot scale on site trial. *J. Hazard. Mater.* **186**, 1405–1414 (2011)
8. A.P. Khodadoust, K.R. Reddy, K. Maturi, Effect of different agents on metal and organic contaminant removal from a field soil. *J. Hazard. Mater.* **B117**, 15–24 (2005)
9. K.R. Reddy, K. Maturi, Simultaneous removal of organic compound and heavy metal from soil by electrokinetic remediation with a modified cyclodextrin. *Chemosphere* **63**, 1022–1031 (2006)
10. K.R. Reddy, S. Chinthamreddy, Electrokinetic remediation of heavy metal contaminated soils under reducing agent. *Waste Manage. (Oxford)* **19**, 269–282 (1999)
11. D. Hallowes, V. Munnik, The ground work report 2008: wasting the nation, making trash of people and places, vol. 195(60) (groundWork, 2008), pp. 43–55
12. K.R. Reddy, C. Cameselle, Integrated electrokinetic soil flushing to remove mixed organic and metal contaminants. *J. Appl. Electrochem* **40**, 1269–1279 (2004)
13. E. Gidarakos, A. Giannis, Chelate agents enhanced electrokinetic remediation for removal cadmium and zinc by conditioning catholyteph. *Water Air Soil Pollut.* **172**, 295–312 (2006)
14. B. Kim, K. Baek, S. Ko, J. Yang, Research and field experiences on electrokinetic remediation in South Korea. *Sep. Purif. Technol.* **79**, 116–123 (2011)
15. Laboratory solution preparation, Flinnscientific, Inc, www.flinnsci.com, 2008, (1051–1065)

16. DR 5000 Spectrophotometer User manual, Hach Company, Catalog number DOC022.53.00654, 1st edn. (2005)
17. Laboratory Classification of Soil for engineering purpose, Texas Department of Transportation Construction division, TEX-142-E, (1999), 1–7
18. P. Lu, Q. Feng, Q. Meng, T. Yuan, Electrokinetic remediation of chromium and cadmium contaminated soil from abandoned industrial site. *Sep. Purif. Technol.* **98**, 216–220 (2011)
19. D. Kim, J. Cho, K. Baek, Pilot scale ex situ electrokinetic restoration of saline greenhouse soil. *J. Soil Sed.* **11**, 947–949 (2011)
20. R. Steimle, In situ remediation technology: electrokinetic, US environmental protection agency (USEPA), (1995)
21. BS 1377: 1990 *Soils for Civil Engineering Purposes*
22. ASTM D 422-Standard test method for particle size analysis of soils
23. A. Persat, R.D. Chambers, J.G. Santiago, *Basic Principle of Electrolyte Chemistry for Microfluidic Electrokinetic*, (Royal society of Chemistry, UK, 2009), 1–17
24. A.Z. Al-Hamdan, K.R. Reddy, Transient behavior of heavy metal in the soil during electrokinetic remediation. *Chemosphere* **71**, 860–871 (2008)

Part VII
Innovative Construction Materials and
Structures

Ultimate Load Carrying Capacity of Precast Lightweight Foamed Concrete Sandwich Panel (PLFP) with Double Shear Truss Connectors Under Axial Eccentric Loading

N. Mohamad, W. I. Goh, R. Abdullah, Ismail Ahmad, S. Samsuddin and M. H. A. Rahman

Abstract This paper studies the ultimate carrying capacity and structural behavior of precast lightweight foamed concrete sandwich panel (PLFP) with double shear truss connectors under axial and eccentric loading. Eight small scale PLFPs with various slenderness ratio were casted and tested. Ultimate load carrying capacity, load deflection profile, surface strains and crack pattern were recorded and analysed to compare the PLFP structural behaviour under two different loading conditions. Results obtained showed that PLFP was able to sustain higher axial loading compared to eccentric loading. PLFP with lower slenderness ratio achieved higher ultimate load carrying capacity compared to higher slenderness ratio. Comparison of deflection profiles also proved that PLFPs under axial loading achieved higher ultimate carrying capacity and compositeness reaction compare to PLFP under eccentric loading.

Keywords Sandwich panel · Lightweight · Foamed concrete · Double shear truss connectors · Axial loading · Eccentric loading

1 Introduction

As stated in [1], sandwich panel is similar to other conventional precast concrete members regarding to its design, detailing, manufacturing, handling, shipping and erection; however, because of the presence of a core layer of insulation, sandwich

N. Mohamad (✉) · W. I. Goh · I. Ahmad · S. Samsuddin · M. H. A. Rahman
Faculty of Civil and Environmental Engineering, Universiti Tun Hussein Onn Malaysia,
86400 Batu Pahat, Johor, Malaysia
e-mail: noridah@uthm.edu.my

R. Abdullah
Faculty of Civil Engineering, Universiti Teknologi Malaysia, 81310 Skudai, Johor, Malaysia

panels exhibit some unique characteristics and behaviors. Sandwich panel have all of the desirable characteristics of conventional precast concrete wall panel such as durability, economy, fire resistance, large vertical spaces between supports, and can be used as shear wall, bearing wall and retaining wall [1].

Various types of sandwich panel with different material and structural behavior had been developed by researchers for different usage and application. The application of lightweight foamed concrete was introduced by researchers either used in core layer or outer wythe [2–4]. Lightweight foamed concrete with density of 400–600 kg/m³ can be used in partition as insulation material and structural load bearing material in low load bearing system such as walls in low rise residential buildings [2, 5, 6]. Therefore, PLFP is one of the precast systems which uses lightweight foamed concrete as outer wythe layer. Mohamad et al. [7] investigated the structural performance of PLFP with single shear truss connectors as a load bearing wall using foamed concrete as outer wythes and polystyrene as the core. It was observed that PLFP can sustain the axial load applied in transferring the load from one wythe to another and slenderness ratio, H/t was found to have significant effect on the strength capacity of PLFP.

Although PLFPs were studied by previous researchers, they were focused more on axial load effect on the panel compared to the research work on PLFP under eccentric loading. Thus, this research focused and compared the axial and eccentric loading effect on PLFP with double shear truss connectors.

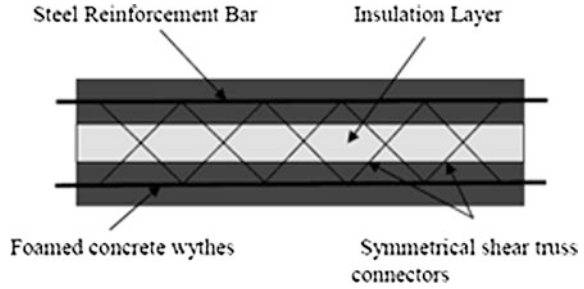
2 Design of PLFP with Double Shear Truss Connectors

A total of 8 small scale PLFPs were casted to study its structural behaviour and determine its ultimate load carrying capacity due to axial and eccentric loading effect by using Magnus frame until it failed. The slenderness ratio of PLFP is between 12 and 18.

The fabrication and the materials properties were referred to previous research conducted [8]. The concrete cover of 8 mm used and the thickness of each concrete wythe was fixed at 20 mm. Inner and outer wythe was made of lightweight foamed concrete with wet densities from 1,700 to 1,800 kg/m³ to achieve the target compressive strength of 10–15 MPa for all panels. Expanded polystyrene (EPS) was used as an insulation material in the core layer. The polystyrene sheet was cut into pieces and inserted in between the steel mesh.

A horizontal and vertical reinforcement with 4 mm diameter bars were tied to each other at 75 mm center to center as main reinforcement. Thus, it was strengthened by using 3 mm diameter steel bar as double shear truss connectors as illustrated in Fig. 1. Double shear truss connectors were bent to an angle of 45°

Fig. 1 Design of PLFP [3]



and tied to vertical reinforcement in the steel mesh. Five double shear truss connectors were used for each panel to transfer the load from one wythe to another. Every panel in this study was casted with 50 mm length with normal concrete capping at both ends to prevent from premature cracking around loading and supports areas as referred to [8].

3 Experimental Program

All PLFPs were casted using steel formwork. Space blocks used to maintain the concrete cover at 8 mm. A normal Grade 30 concrete was poured into the capping at both ends. After the capping hardened in about half an hour, the foamed concrete was poured into the specimen as inner layer and outer layers and trowel to obtain a smooth surface. Specimens were placed under ambient temperature and protected from direct sunlight with canvas. Formworks were dismantled after 28 days and panels were tested by using Magnus frame.

For axial loading, the load was applied at middle across the thickness of PLFP along top edge of the panel length. For eccentric loading, the loading was carried out by applying the load at an eccentricity $t/6$ along top edge of the panel length during the experimental programme. Load applied gradually until failure occurred, crack pattern and horizontal deflection were observed at each loading stage.

A total of six strain gauges were used for surface strain measurement and two Linear Voltage Displacement Transducers (LVDTs) were placed at the middle on each side of the panel as shown in Fig. 2.

PLFP specimens were tested using Magnus Frame with 1,000 kN loading capacity. Figure 3 shows the experimental set-up, where the PLFP was clamped to reaction frame correctly in the position to get the targeted end condition.

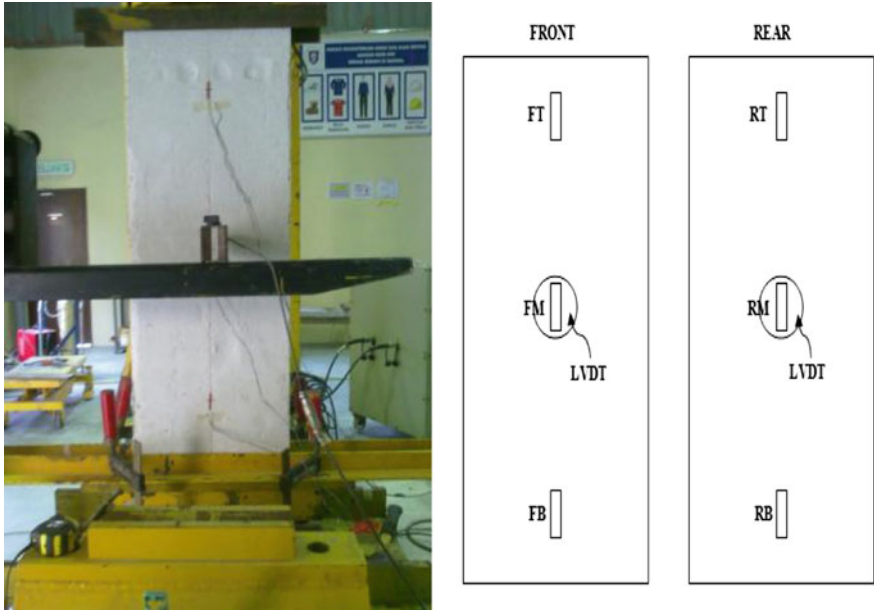


Fig. 2 LVDTs and strain gauges location

Fig. 3 Experiment set up



Table 1 Mixture ratio for casting of PLFPs

	Sand: Cement	Foam: Cement	Water: Cement
Ratio	2:1	0.65	0.55

Table 2 Dimensions and designation of PLFP

Panel	H × W × t (mm)	Slenderness ratio	t1 (mm)	t2 (mm)	C (mm)	Reinforcement (Vertical and horizontal) top and bottom	Diameter of shear connectors (mm)
PA-1	1,000 × 370 × 80	12.5	20	40	8	4 mmΦ@75 mm c/c	R3
PE-1	1,000 × 370 × 80	12.5	20	40	8	4 mmΦ@75 mm c/c	R3
PA-2	1,000 × 370 × 70	14	20	30	8	4 mmΦ@75 mm c/c	R3
PE-2	1,000 × 370 × 70	14	20	30	8	4 mmΦ@75 mm c/c	R3
PA-3	960 × 370 × 60	16	20	20	8	4 mmΦ@75 mm c/c	R3
PE-3	960 × 370 × 60	16	20	20	8	4 mmΦ@75 mm c/c	R3
PA-4	960 × 370 × 50	18	20	10	8	4 mmΦ@75 mm c/c	R3
PE-4	960 × 370 × 50	18	20	10	8	4 mmΦ@75 mm c/c	R3

PA Precast lightweight foamed concrete sandwich panel (PLFP) with double shear truss connectors under axial loading

PE Precast lightweight foamed concrete sandwich panel (PLFP) with double shear truss connectors under eccentric loading

4 Results and Analysis

4.1 Material Properties, Designation and Dimensions

PLFPs details with its designation, mechanical properties and slenderness ratio are tabulated in Tables 1, 2, and 3. The mixing ratio of specimen is referring to [8]. The foamed concrete mix ratio is given in Table 1; the wet density for foamed concrete is ±1,700 kg/m³ to achieve dry density at ±1,600 kg/m³. Nine cubes and 6 cylinders were prepared at the same time to determine the material properties of foamed concrete.

Table 3 Mechanical properties of PLFPs

Panel	Wet density (kg/m ³)	Dry density (kg/m ³)	Compressive strength, Fc (N/mm ²)	Split tensile strength, Ft (N/mm ²)	Modulus young, E (Mpa@ N/m ²)
PA-1& PE-1	1,760	1,751	12.00	1.56	12,500
PA-2 &PE-2	1,764	1,674	13.67	1.71	14,500
PA-3 & PE-3	1,725	1,445	7.10	0.99	7,800
PA-4 & PE-4	1,700	1,619	8.50	1.24	5,900

Table 4 Ultimate load carrying capacity of PLFPs

Panel	Ultimate load carrying capacity (kN)	Panel	Ultimate load carrying capacity (kN)	Percentage different in between PA and PE
PA-1	150	PE-1	133	11.33
PA-3	138.5	PE-2	119.5	13.70
PA-4	126	PE-3	81	35.71
PA-5	98.5	PE-4	82	16.76

4.2 Ultimate Load Carrying Capacity

Table 4 and Fig. 4 presents the ultimate load carrying capacity of PLFPs under axial and eccentric loading, from results, it was found that the ultimate load of PLFPs were decreased when the slenderness ratio increased. The loading condition also has significant effect on the ultimate load carrying capacity of PLFP, the ultimate carrying capacity of PLFPs decreased during eccentric loading compared to axial loading. The percentage different of ultimate loading under axial and eccentric loading were between 11 and 35 %.

4.3 Load Deflection Profile

As shown in Figs. 5 and 6, the relationship between load and horizontal deflection were well presented. All panels achieved certain degree of compositeness reaction; both wythes tend to move in the same direction until the panel reached ultimate load carrying capacity and failed.

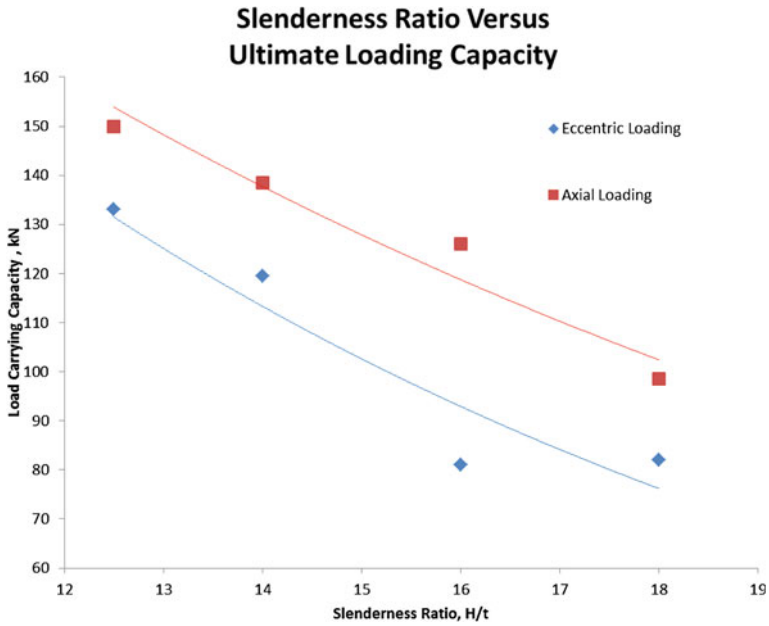


Fig. 4 Ultimate load carrying capacity of PLFP with various slenderness ratios under axial and eccentric loading

Fig. 5 Load versus horizontal deflection of PA-1

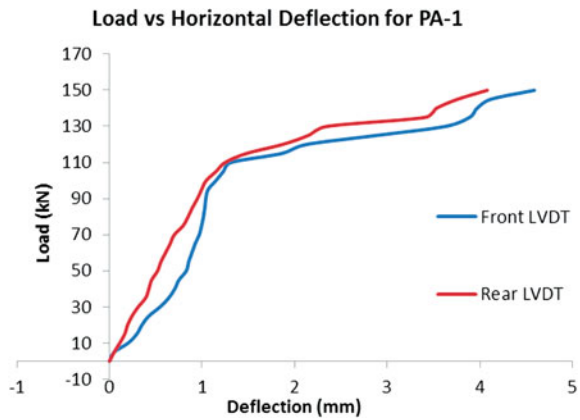


Fig. 6 Load versus horizontal deflection of PE-1

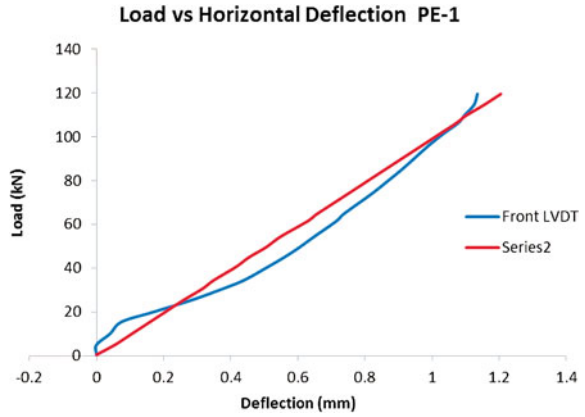
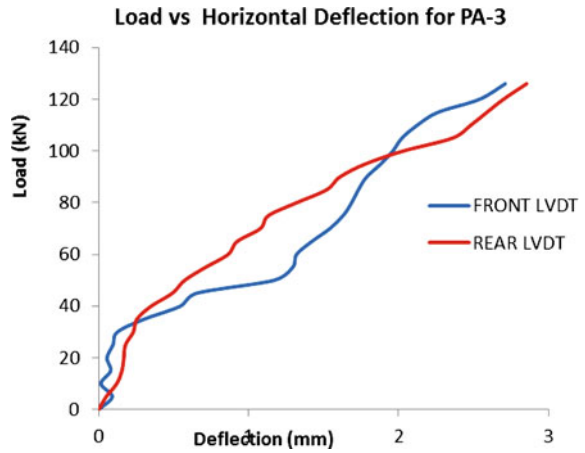
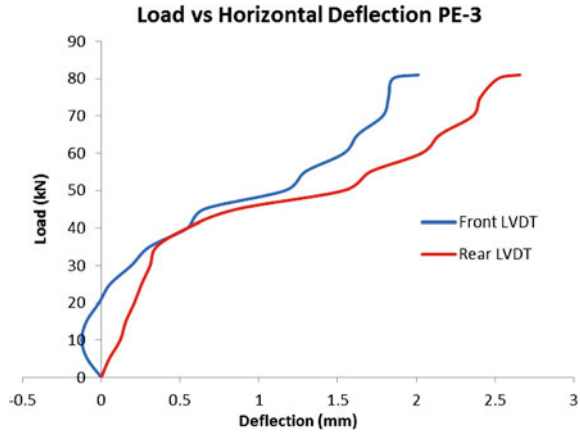


Fig. 7 Load versus horizontal deflection of PA-3



The trend of curves were similar to [9], at early stage of loading, deflection curves were nearly linear and behaved as elastic material. However, after first crack occurred, PLFPs behaved as nonlinear material. Deflections of PLFPs under axial loading were found to be more significant than PLFP under eccentric loading, higher deflection occurred when axial loading were applied.

Fig. 8 Load versus horizontal deflection of PE-3



PLFP with double shear truss connectors can be categorized as partially composite panel as referred to [1]. As stated in [1], the initial composite action (horizontal shear transfer) is attributed to the bond between the concrete and insulation layer with any contribution from the wythe connectors (Figs. 7, 8).

4.4 Surface Strain Distribution

Figures 9, 10 and 11 presents the surface distribution profile for PA-3 under axial loading. Figures 9, 10, and 11 indicate that the top and bottom parts of panel are under compression for front and rear wythes, where both wythes of the panel tend to move at same direction. However, at the middle part of panel as in Fig. 10, front wythe was under tension and rear wythe was under compression. This is due to bending during the loading until failure. For other PLFPs, the surface strain distribution was also under similar surface strain distribution and bending effects. From the trend of graphs the surface strain for both sides were moving along the same direction with unequal strain values. It proved that PLFPs with double shear truss connectors were achieved partially compositeness reaction.

Fig. 9 Strain distributions at top of PA-3

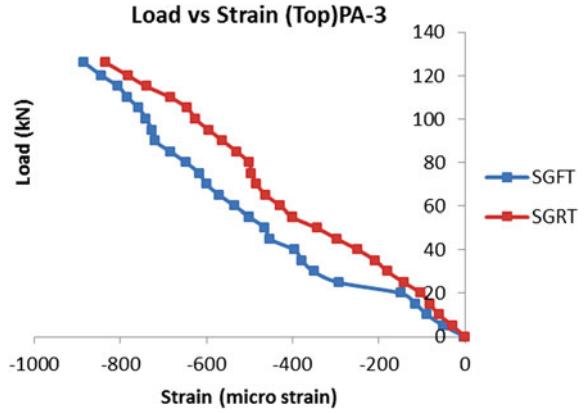


Fig. 10 Strain distributions at middle of PA-3

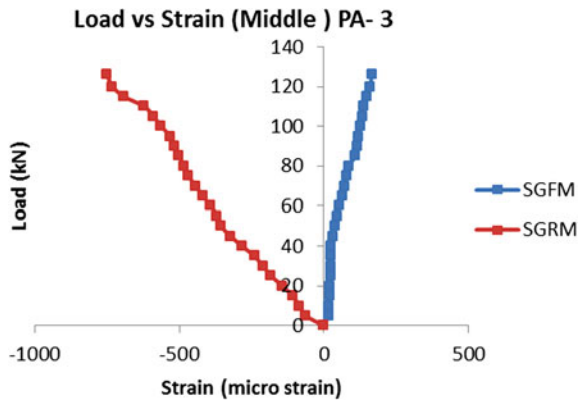


Fig. 11 Strain distributions at bottom of PA-3

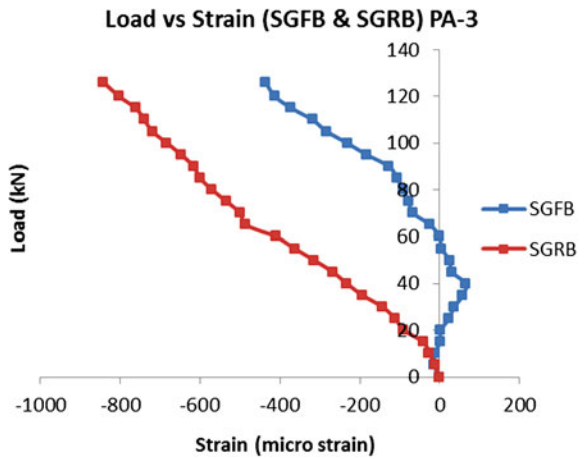


Fig. 12 Crushing at the bottom of PA-1



PA 1

4.5 Failure Pattern and Failure Mode

All PLFPs were loaded with axial and eccentric loading in a similar manner. It was observed that horizontal cracks occurred during loading. For PLFPs under axial

Fig. 13 Cracking at the middle of PA-3



PA 3

loading in Figs. 12 and 13, PLFPs cracked at the middle and bottom half, those cracks occurred because the loading were distributed evenly to both wythes.

As shown in Figs. 14 and 15, PLFPs under eccentric loading cracked at top half, those cracks may be attributed by the bending moment induced by eccentric loading.

Fig. 14 Crushing at the top part of PE-1



PE 1

One of the factor that attribute to the cracks at top part of panel may due to poor concrete quality and wired connections in between capping, main reinforcement and shear connectors.



PE 2

Fig. 15 Crushing at the top half of PE-2

5 Conclusion

Structural behavior and ultimate strength of PLFP with double shear truss connectors and slenderness ratio from 12.5 to 18 were studied under axial and eccentric loading. Test results were analyzed in terms of its ultimate load carrying capacity, load deflection profile, surface strain distribution, failure pattern and failure mode.

It was observed that, PLFP with double shear truss connectors was able to sustain both axial and eccentric loading with partially compositeness reaction. However, the ultimate load carrying capacity of PLFP decreased under eccentric loading compared to axial loading. The percentage difference of ultimate loading under axial loading and eccentric loading were between 11 and 35 %. This is due to the loading not applied at the neutral axis where one wythe will need to support higher load than the other. When the wythe with higher loading failed, the whole panel failed.

Therefore, the ultimate load achieved in PLFP was due to several factors which included its material strength, compressive strength, slenderness ratio, panel's height, reinforcement and loading conditions. For the load deflection profile, the similar trend of curves on both faces proved that both wythes in PLFP deflected together along the same direction and acted as partially composite panel.

Acknowledgments The author would like to thank Universiti Tun Hussein Onn Malaysia Ministry of Higher Education (FRGS Vot 0826) for its financial support.

References

1. PCI PCI Committee. State-of-the-art of precast/prestressed sandwich wall panels. PCI J. **42**(2) (1997)
2. M.A. Othuman Mydin, Y.C. Wang, Structural performance of lightweight steel-foamed concrete-steel composite walling system under compression. J. Thin-Walled Struct. **49**, 66–76 (2011)
3. N. Mohamad, M.H. Mahdi, Testing of precast lightweight foamed concrete sandwich panel with single and double symmetrical shear truss connectors under eccentric loading. Adv. Mater. Res. **335–336**, 1107–1116 (2011)
4. N. Mohamad, W. Omar, R. Abdullah, Precast lightweight foamed concrete sandwich panel (PLFP) tested under axial load: preliminary results. Adv. Mater. Res. **250–3253**, 1153–1162 (2011)
5. M.S. Hamidah, I. Azmi, M.R.A. Ruslan, K. Kartini, Optimisation of foamed concrete mix of different sand-cement ratio and curing conditions, in *Proceedings of the international conference on use of foamed concrete in construction*. University of Dundee, Scotland (Thomas Telford Publishing, London, 2005), pp. 37–44
6. D. Aldridge, Introduction to foamed concrete: What, Why, How? in *Proceedings of the international conference on use of foamed concrete in construction*, University of Dundee, Scotland (Thomas Telford Publishing, London, 2005), pp. 1–14
7. N. Mohamad, W. Omar, R. Abdullah, Structural behaviour of precast lightweight foamed concrete sandwich panel as a load bearing wall. OIDA Int. J. Sustain. Dev. **5**(03), 49–57 (2012)
8. N. Mohamad, The structural behaviour of PLFP as a load bearing wall. PhD Thesis. Universiti Teknologi Malaysia (2010)
9. A. Benayoune, A. Aziz, A. Samad, D.N. Trikha, A.A. Abang Ali, Structural Behaviour of eccentrically loaded precast sandwich panels. Constr. Build. Mater. **20**, 713–724 (2006)

Strain Behaviour of Exposed Steel Reinforcement Bars Using FBG Sensor

M. S. Hamidah, M. J. Faizal Mohd, M. S. Norhasri Muhd, I. Noorli and S. Vasagavijayan

Abstract Fiber Bragg grating (FBG) sensor system is being widely used as strain measurement system for civil structures. Nowadays, interest in using FBG sensor has been increased and widely used for health structural monitoring. In this paper, preliminary investigation on strain measurement for steel reinforcement bars due to different corrosion accelerated conditions is reported. The FBG sensors are used to measure the strain changes which the FBG sensor was glued to the surface of steel bars. Three (3) different corrosion accelerated conditions namely room temperature (RT), 5 % of sodium chloride (NaCl) solution and distilled water (DW) were used to develop the strain change in steel reinforcement. The results shows that the corrosion accelerated is significantly affect the overall strain change on the steel bars. FBG sensors are also able to capture the strain of steel bars due to corrosion accelerated variations. In addition, the results obtained from the FBG sensors reveal that the strain of steel rods immersed in 5 % NaCl solution was higher as compared to those immersed in distilled water and those exposed to room temperature.

Keywords Strain monitoring · Steel reinforcement bars · Fiber Bragg grating · Corrosion accelerated conditions

M. S. Hamidah (✉) · M. S. N. Muhd
Faculty of Civil Engineering, Universiti Teknologi MARA, Shah Alam, Malaysia
e-mail: hmohdsaman@yahoo.com

M. J. F. Mohd
Faculty of Civil Engineering and Earth Resources, Universiti Malaysia Pahang, Kuantan, Malaysia

I. Noorli
Faculty of Civil and Environmental Engineering, Universiti Tun Hussien Onn Malaysia, Batu Pahat, Malaysia

S. Vasagavijayan
Photronix Technologies (M) Sdn. Bhd., Puchong, Malaysia

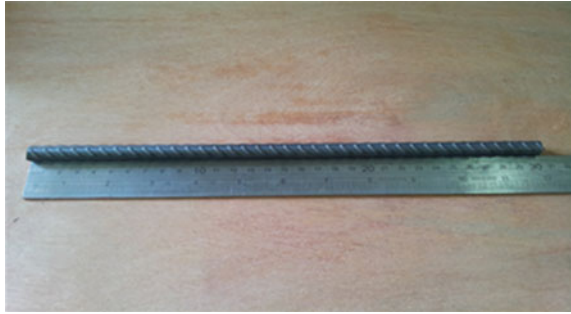
1 Introduction

A variety of strain measurement is commonly used such as electrical strain gauges, linear variable differential transformers and vibrating wire strain gauges [1]. Previous research has been investigated on corrosion of steel bar embedded in mortar with respect to change in strain measured by strain gauge [2]. However, it was indicated that corrosion potential measured by strain gauge is affected by changes of mortar volume not by corrosion product formation. It is revealed that several of conventional strain gauges offered some disadvantages in terms of size and electromagnetic interference, ease of embedment and potential for multiplexing if a number of sensors are used [3]. In the past years, interest in using fiber Bragg gratings (FBG) sensor in the development of structural health monitoring (SHM) have increased significantly due to its small size and the potential to provide a mean of remote detection with high precision and stability, immunization of light and insensitivity to environmental effects [4]. Interests in using kinds of novel FBG sensor in structure monitoring holds a great potential to allow strain measurement to be made in situations where the conventional strain gauge is unable to monitor the strain change. The use of FBG sensor enables direct strain measurement on reinforcement bars (steel rod) thus providing a more accurate data on initiation of corrosion [5]. Increasing demand in measuring strain of structures over long period of time as a monitoring technique has prompted the authors to explore further the strain change related to corrosion activity.

It shows that FBG has been recognized as one of the most significant enabling technologies for fiber monitoring system. According to Montanini and Pirrotta [6], FBG is spectral filters that present a resonance at the Bragg wavelength, whose value depends on the effective refractive index of the core and on the grating pitch. Previous papers on application of FBG sensors have been published and documented [4]. In this case, it is proved that the FBG based sensor able to monitor physical parameters such as temperature, strain or pressure and it is capable to measure physical parameters simultaneously [7]. Several literatures have pointed out that measurement of strain change in steel reinforcement is recorded when the reinforced concrete specimens subjected to loads [8–13]. It is demonstrated that different types of loading like static load, fatigue load, thermal load and dynamic load significantly affect the strain measurement.

In comparison with previous studies, in this present research the strain measurement of steel reinforcement will be measured without applied load. Ideally, this research will provide the quantitative data on strain change and how it governs the potential of steel reinforcement expose to various corrosion accelerated condition. Document written by Zhou and Ou [14] show that change in strain of steel reinforcement is an alternative parameter that can be used to describe deformation and crack opening in concrete. Numerous of successful studies performed on development of FBG-strain sensor for monitoring system in civil engineering application [15–21]. However, none of these researches relate to change in strain of steel bars due to corrosion accelerated.

Fig. 1 Length measurement of the steel bar



As summary, it is reveals that the capability of FBG sensor to measure the strain parameter with their flexibility makes an ideal option to be adopted as a technique in this study. The multiplexed FBG sensors were used to measure strain and temperature simultaneously by measuring the reflected wavelength using FBG Interrogation System. Eventually, by integrating the parameters through a multiplexed FBG sensor measurement, a simultaneous monitoring system to detect corrosion initiation would be established.

2 Methodology

2.1 Preparation of Steel Bars

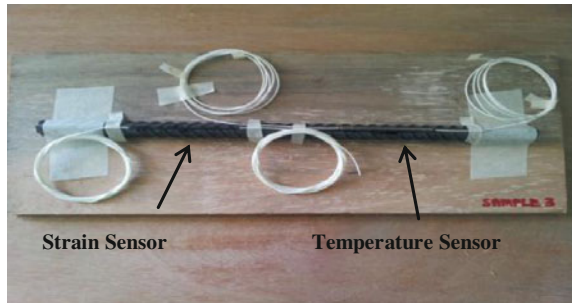
In this study, a high yield strength steel bar as the properties is according to ASTM-A36 with nominal size of 12 mm was used. Figure 1 shows the length of steel bar used is 300 ± 5 mm with no existing corrosion. Then, the steel bar was cleaned using sandpaper and immersed in nitric acid until the steel is silvery in color. Before the sensors are mounted on the steel bar, the weight of bar was weighed. Then, the sensors were secured on the bar by fixing firmly to surface of steel bar.

2.2 Preparation of FBG Sensor on the Surface of Steel Bars

The sensor can be divided into two parts which are FBG-strain sensor and FBG-temperature sensor. The FBG sensor that used in this study were fabricated and supplied by Photronix Technologies (M) Sdn. Bhd. The specification of fiber with Series 5147 single mode FBG fiber optic with $6 \mu\text{m}$ core diameter, $125 \mu\text{m}$ cladding diameter (NA, 0.2) and Bragg wavelength of 1554 nm (35 ± 0.5 mm grating length) was selected. Table 1 shows the central of Bragg wavelength for each sensor is used in this research.

Table 1 Central wavelength of Bragg at 25 °C

Sensor type/label	Center wavelength (nm)
Strain S1	1543.170
Strain S2	1559.450
Strain S3	1540.870
Temperature T1	1550.380
Temperature T2	1545.220
Temperature T3	1565.850

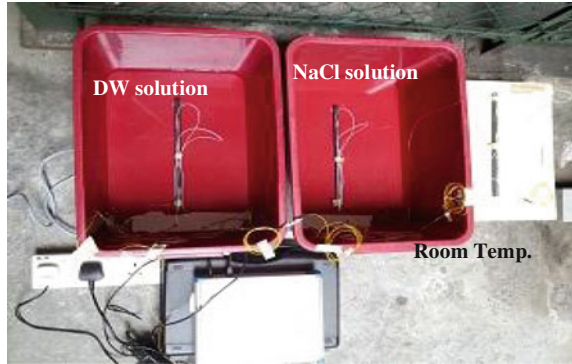
Fig. 2 Preparation of sensors fitted to the steel bar

Prior to fitting the sensor to steel bar, the FBG sensor was glued directly onto steel bar using special glue based polymer. Then, the sensor was protected using silicone gel. Meanwhile, the existing fiber optic (without Bragg grating and sensor) was encapsulated inside tubular plastic pipe of diameter 1 mm to protect it from aggressive alkaline environment. Figure 2 illustrates the arrangement of the sensor fitted to the steel bar.

2.3 Test Procedures

After fitting the sensors to steel bar and protected using silicone gel, the specimens will undergo to accelerated corrosion conditions comprise of (1) control condition at room temperature (RT); (2) immerse in distilled water (DW) and (3) immerse in 5 % of sodium chloride (NaCl) solution as shown in Fig. 3. The steel bars were exposed to corrosion conditions for two (2) months. To ensure the steel rod is completely submerged in solution, constant depth of 50 ± 5 mm from surface were maintained. The strain initiation and temperature changes are evaluated by FBG Interrogation system unit (FBG Scan 700).

Fig. 3 Steel bars exposed to accelerated corrosion



2.4 Principles of Fiber Bragg Grating Sensor

The transmitted optical wavelength corresponding to the strain and temperature changes are recorded. From these measurements, the fractional change in reflected wavelength over the strain and temperature will be calculated for all FBG sensor scanned. Figure 4 represents the principle setup for monitoring the changes in strain and temperature using FBG sensors.

In this experiment, a broadband light source is transmitted to the FBG through in-line single fiber optic. When the broadband light passes through the proposed FBG sensor, the narrowband spectra components corresponding to the FBG sensor wavelength is reflected. The shift Bragg wavelength consists of (1) Bragg wavelength due to strain change; and (2) Bragg wavelength due to temperature change. All the reflected signals were recorded and the spectra of reflected light were plotted using a FBG Interrogation System unit.

The principle of FBG is to measure the shift of reflected Bragg wavelength (λ_B), which is related to the effective refraction index (n_{eff}) and the periodicity (Λ) of the index variation of the grating area in fiber core. The strain can be determined using Eq. (1).

$$\varepsilon_m = \frac{1}{k} \left(\frac{\Delta\lambda_m}{\lambda_{om}} - \frac{\Delta\lambda_c}{\lambda_{oc}} \right) \tag{1}$$

where

- $\Delta\lambda_m$ wavelength shift of strain-measuring FBGs
- λ_{om} base wavelength of strain-measuring FBGs
- $\Delta\lambda_c$ wavelength shift of compensation FBGs
- λ_{oc} base wavelength of compensation FBGs.

Fig. 4 Test-setup for monitoring the strain and temperature on steel bar using FBG

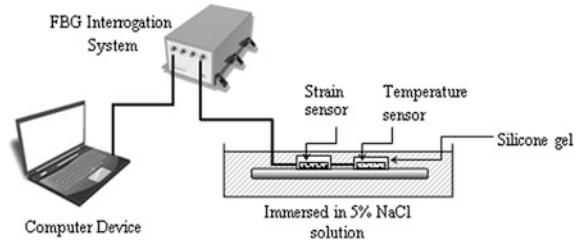
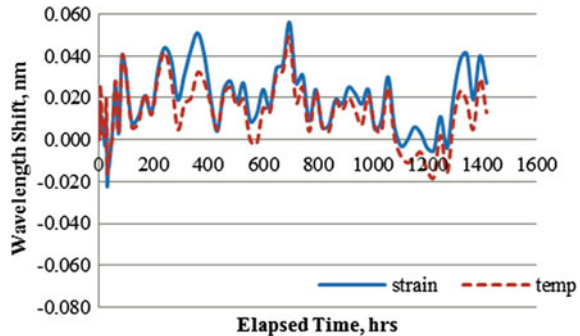


Fig. 5 Bragg wavelength shift of steel bar due to room temperature exposure



3 Results and Discussions

3.1 Simultaneous Measurement of Wavelength Shift of Strain and Temperature Using FBG Sensor

Responses to changes of simultaneously measured Bragg wavelength shift for strain and temperature of FBG sensors are demonstrated. Figure 5 shows the result on Bragg wavelength shift of strain and temperature when the steel bars exposed to room temperature (RT). The initial FBG sensor wavelength recorded are 1541.465 nm (S3) and 1566.138 (T3) having reflectivity of 91.39 and 85.12 %, respectively. Meanwhile, the initial wavelength measured by FBG was 1543.772 (S1) and 1545.537 nm (T1) for that steel bar immersed in distilled water (DW). Figure 6 displayed the wavelength shift results for strain and temperature of steel bar immersed in DW. The initial wavelengths of 1559.778 (S2) and 1545.537 nm (T2) with reflectivity of 93.60 and 86.16 % are recorded for sodium chloride (5 % NaCl). The results on wavelength shifts of strain and temperature are illustrated in Fig. 7.

The simultaneously measurement of FBG sensor changes with strain and temperature were discussed. It was found that both wavelength shift effects are only possible by different corrosion exposures. The graphs illustrates that the temperature recorded by FBG sensor has very strong impact on the FBG sensor signals for steel bars expose to distilled water and 5 % sodium chloride as compared to room temperature. It is can be seen that there is minimal changes to

Fig. 6 Bragg wavelength shift of steel bar due to distilled water exposures

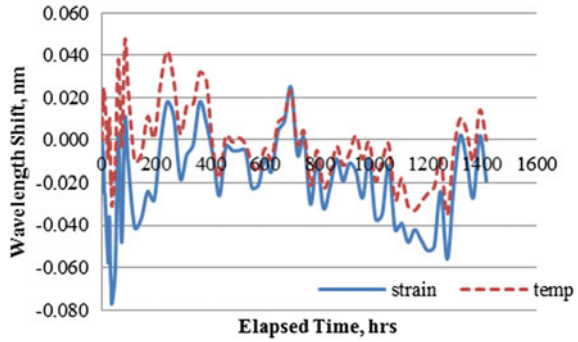
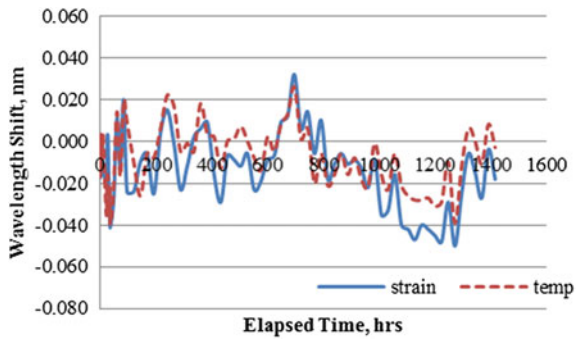


Fig. 7 Bragg wavelength shift of steel bar due to sodium chloride exposures



wavelength shift for strain and temperature of steel bar expose in control condition (room temperature) as there is no strain applied and the temperature is constant.

The graphs of wavelength shift for FBG-strain sensors and FBG-temperature sensors demonstrate consistent measurement of strain with the output values being independent of temperature values. The peak wavelength shift readings for FBG-strain sensor and FBG-temperature sensor are recorded at 29 days of exposure for all exposure conditions. The wavelength shifts increased uniformly after the light launched into the optical fiber at day-1. Then, the readings decrease significantly until day-53. It is noted that, the expose of distilled water and 5 % sodium chloride affect the Bragg wavelength shift readings considerably with respect to elapsed time. By measuring the Bragg wavelength shift, the aim of measuring the temperature and strain simultaneously with one fiber grating is realized. In the experiment, it can be seen that the change on wavelength shift for strain and temperature of sampled FBG change simultaneously.

3.2 Interaction Between Strain and Exposure Conditions

Figure 8 shows the typical reflection peaks of fiber Bragg grating (FBG) sensor. In order to measure strain changes of exposed steel bars, the wavelength recorded by

Fig. 8 Typical FBG sensor reflection peaks recorded by FBG sensor at 14th days of exposures

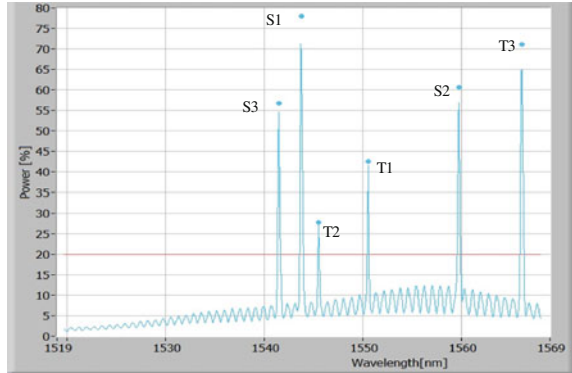
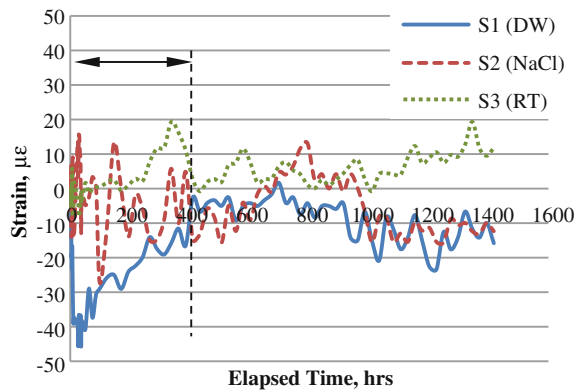


Fig. 9 Strain on steel bars due to different exposure conditions



FBG Interrogation unit were calculated using Eq. (1) taking into consideration the temperature effect. The strains on the steel bars due to different exposure conditions are displayed in Fig. 9. From the figure, it is observed that the performance of FBG could be by observing the increment of wavelength spectrum. At initial region, the readings obtained can be considered not measurable and hence strain was not measured. In this stage, the system is considered to be integrated with the surrounding environment before the FBG was performed and the reading is fully dependable to temperature effect. After 14 days of exposures, the strain readings are gradually increased due to mechanical deformation changing of the expose bars. The highest value of strain picked up by FBG is $11.6587 \mu\epsilon$ after exposed for 1-month to 5 % NaCl solution compared to other exposures. The difference in values between sensors may be explained by the small difference in the cross sectional area of the steel bars.

It is also shown that the strain readings for steel rods immersed in distilled water and 5 % sodium chloride have a highest strain compared to steel bar exposed to control condition (room temperature). This is meant that the expansion of cross sectional area of steel bars hosted by strain-FBG sensors is proportional to the

elapsed time of exposure. It can be observed that, the effect of exposure condition in room temperature is not much significant on the measurement of the changes in the strain as compared to other exposure conditions. By comparing the performance of the strain-FBG sensors, it is possible to draw the preliminary conclusion on the suitability of FBG sensor to measure the strains on cross sectional area of steel bars under different exposure conditions.

4 Conclusions

From this finding, the conclusions can be drawn as follows:

1. It is demonstrated that implementing the FBG sensor offers simultaneous strain and temperature of steel bars exposed to different exposure conditions.
2. FBG sensors are also able to capture the strain of steel bars with respect to corrosion accelerated variations.
3. Strain readings on steel bars exposed to distilled water and 5 % NaCl shows more effects as compared to control condition (room temperature).

References

1. C. Ayranci, A. Fahim, M. Munro, A novel strain sensor for reinforced concrete structures, A strain sensor for concrete structures. Journal compilation 2007, Blackwell Publishing Ltd. **44**, 191–200
2. G. Batis, Th Routoulas, Steel rebars corrosion investigation with strain gages. *Cement Concr. Compos.* **21**, 163–171 (1999)
3. M.B. Rao, M.R. Bhat, C.R.L. Murthy, K.V. Madhav, S. Asokan, Structural health monitoring (SHM) using strain gauges, PVDF film and fiber Bragg grating (FBG) sensors: A comparative study. *Proceeding of National Seminar on Non-Destructive Evaluation, Indian Society for Non-Destructive Testing, Hyderabad Chapter*, 2006
4. M. Majumder, T.K. Gangopadhyay, A.K. Chakraborty, K. Dasgupta, D.K. Bhattacharya, Fibre Bragg gratings in structural health monitoring-present status and applications. *Sens. Actuators A* **147**, 150–164 (2008)
5. K.T.V. Grattan, T. Sun, Fiber optic sensor technology: An overview. *Sens. Actuators A* **82**, 40–61 (2000)
6. R. Montanini, S. Pirrotta, A temperature-compensated rotational position sensor based on fibre Bragg gratings. *Sens. Actuators A* **132**, 533–540 (2006). doi:[10.1016/j.sna.2006.02.036](https://doi.org/10.1016/j.sna.2006.02.036)
7. T.L. Yeo, T. Sun, K.T.V. Grattan, Fibre-optic sensor technologies for humidity and moisture measurement. *Sens. Actuators A* **144**, 280–295 (2008). doi:[10.1016/j.sna.2008.01.017](https://doi.org/10.1016/j.sna.2008.01.017)
8. M.A. Davis, D.G. Bellemore, A.D. Kersey, Distributed fiber Bragg grating strain sensing in reinforced concrete structural components. *Cement Concr. Compos.* **19**, 45–57 (1997)
9. K.S. Kim, Dynamic strain measurement with fiber Bragg grating sensor system for smart structure. *Key Eng. Mater.* **270–273**, 2114–2119 (2004)
10. P. Moyo, J.M.W. Brownjohn, R. Suresh, S.C. Tjin, Development of fiber Bragg grating sensors for monitoring civil infrastructure. *Eng. Struct.* **27**, 1828–1834 (2005)

11. D.W. Jung, I.B. Kwon, N.S. Choi, Application of a temperature-compensating FBG sensor to strain measurement. *Adv. Mater. Res.* **26–28**, 1089–1092 (2007)
12. X. Tang, X. Tang, Y. Xu, W. Guo, Applications of fiber Bragg grating in strain measurement of concrete bridge. *Adv. Mater. Res.* **368–373**, 2286–2290 (2012)
13. C. Rodrigues, F. Cavadas, C. Félix, J. Figueiras, FBG based strain monitoring in the rehabilitation of a centenary metallic bridge. *Eng. Struct.* **44**, 281–290 (2012)
14. Z. Zhou, J. Ou, Development of FBG sensors for structural health monitoring in civil infrastructures. *Proceeding of North American Euro–Pacific Workshop ‘Sensing issues in civil structural health monitoring’*, Waikiki Beach, Oahu, Hawaii, 2004
15. K.S.C. Kuang, R. Kenny, M.P. Whenlan, W.J. Cantwell, P.R. Chalker, Embedded fibre Bragg grating sensors in advanced composite materials. *Compos. Sci. Technol.* **61**, 1379–1387 (2001)
16. C.F. Valdivielso, I.R. Matías, F.J. Arregui, Simultaneous measurement of strain and temperature using a fiber Bragg grating and a thermochromic material. *Sens. Actuators A* **101**, 107–116 (2002)
17. A.R.M. Kamil, T.M. Nasir, I. Azmi, Application of optical fiber Bragg grating sensor for structure monitoring. *Mater. Sci. Forum* **517**, 202–206 (2006)
18. Z. Dandan, W. Peng, Study of strain and temperature simultaneous measurement technology based on sampled grating. *Adv. Mater. Res.* **213**, 529–533 (2011)
19. H.C. Liang, J. Young, J.Y. Wu, K. Soo, L.H. Lin, K.S. Kyum, X.B. Peng, Y.Y. Wei, Material property research of high performance concrete on its early age by fiber Bragg grating sensor. *Adv. Mater. Res.* **452–453**, 618–622 (2012)
20. Z.Zhou, W. Liu, Y. Huang, H. Wang, J. Hea, M. Huang, J. Oua, Optical fiber Bragg grating sensor assembly for 3D strain monitoring and its case study in highway pavement. *Mech. Syst. Signal Process.* **28**, 36–49 (2012)
21. X. Tang, X. Tang, Y. Xu, W. Guo, Applications of fiber Bragg grating in strain measurement of concrete bridge. *Adv. Mater. Res.* **368–373**, 2286–2290 (2012)

Mechanical Properties of High-Strength Concrete Reinforced with PVA and Basalt Fibres

Tehmina Ayub, Nasir Shafiq, Muhd. Fadhil Nuruddin
and Sadaqat Ullah Khan

Abstract This chapter focuses on the mechanical properties of high-strength concrete (HSC) incorporating PVA and Basalt fibres. Total seven (07) mixes of HSC were prepared including one control mix (containing no fibre). Out of remaining six (06) mixes, three (03) mixes were containing PVA fibres as 1, 2 and 3 % by volume of the overall concrete, whereas in other three (03) mixes, Basalt fibres were added in the same range and dosage, as proposed for PVA fibres. The mechanical properties investigated in current study include compressive strength, splitting tensile strength and modulus of elasticity. Beside this, results of compressive strength of the cube and cylinder have also been compared in terms of cylinder/cube strength ratios. Experimental results showed that PVA fibres reinforced HSC attained higher mechanical properties in comparison to Basalt fibres reinforced HSC due better crack bridging ability and better concrete confinement.

Keywords PVA fibres · Basalt fibres · Compressive strength · Splitting tensile strength · Modulus of elasticity

1 Introduction

Since last century, high-strength concrete (HSC) of compressive strength ranging from 41 to 55 MPa or greater as per ACI 318-M08 [1], had been used for long span bridges and tall structures, as well as for earthquake-resistant structures due to its tremendous advantages in terms of reduced members' dimension to reduce self-weight, material consumption and seismic loads. In spite of such achievements and inherent advantages, application of high-strength concrete is obstructed due to lack

T. Ayub (✉) · N. Shafiq · Muhd. Fadhil Nuruddin · S. Ullah Khan
Civil Engineering Department, Universiti Teknologi PETRONAS (UTP), Bandar Seri
Iskandar 31750 Tronoh, Perak, Malaysia
e-mail: tehminal@neduet.edu.pk

of ductility and tensile strength; nevertheless, these disadvantages may be overcome by adding fibres, to make it suitable in structural applications; especially in seismic zones due to its ductile characteristics.

In literature, behaviour and characteristics of HSC containing fibres have not been discussed in detail [2]; however, considerable research has been carried out on High-Performance Fibre Reinforced Cementitious Composites (HPFRCCs) [3–6]. Literature on normal weight concrete containing fibres, especially steel fibres is also available in abundance [7–9]; therefore, ACI 318-M08 [1] has recognised it a “Construction Material” due to reported advantages and allowed the inclusion of deformed steel fibres in normal weight concrete only. However, use of deformed steel fibres in members reinforced with stainless steel or galvanized steel bars is not recommended due to unavailability of the data on corrosion problem or galvanized action of the fibres in concrete. This infers that the use of steel fibres may not be a recommended solution for tropical countries such as Malaysia, etc. Therefore, there is a need of investigating the potential use of other fibres, mainly non-metallic fibres, by determining their essential characteristics.

In the current study, mechanical properties of HSC reinforced with non-metallic fibres, particularly PVA and Basalt fibres, are determined. The reasons for selecting Basalt fibres are its recent use in concrete [8, 10–12], good tensile strength, similar characteristics to expensive carbon and glass fibres, and low cost than carbon fibres. However, PVA fibre is well studied in literature and more recently in engineering cementitious composites (ECC) [13–15] and this fibre also possesses good properties.

2 Experimental Program

This section describes the details of experimental program including material selection for the preparation of high-strength concrete (with and without fibres) and their testing of the mechanical properties.

2.1 Experimental Materials

Cement—Type I ordinary Portland cement (OPC) is used to produce high-strength concrete (HSC). The quantity of cement has been used as 450 kg/m^3 .

Fine aggregates—River sand with a fineness modulus of 3.55 is used as fine aggregate. The amount of fine aggregate is used as 670 kg/m^3 .

Coarse aggregates—Two sizes of coarse aggregates are used in the current study. First coarse aggregate was passed through a 20 mm (3/4") opening sieve and retained on 10 mm (3/8") opening sieve and the quantity used was 500 kg/m^3 . The quantity used for second coarse aggregate was 600 kg/m^3 and it was passed through a 10 mm (3/8") opening sieve. Selection of the aggregates was based on

the literature review which reveals that the crushed rock aggregates of 10–20 mm in size are not too angular and elongated; therefore, they should preferably be used in the manufacturing of HSC. Moreover, the bond strength between smaller size aggregates is greater than between larger size aggregates and for that reason smaller size aggregates (say 10–17 mm) tend to give better results [16].

Fibres—Two types of commonly available fibres: Polyvinyl Alcohol (PVA) and Basalt fibres are used in this study as two separate reinforcements for HSC. Fibres are selected by considering their reinforcing properties. As described in Table 1, both PVA and Basalt fibres possess good tensile strength and young modulus and these fibres have been added as 1, 2 and 3 % by volume of the overall concrete mix.

Water/Cement Ratio—To produce a highly workable concrete mix in the presence of fibres and to avoid honeycombing, a water/cement ratio of 0.4 is used in this experimental investigation; however for HSC, the recommended water/cement ratio ranges between 0.30 and 0.35 or lower for full compaction [16]. The reason of using a slightly higher water/cement ratio is the addition of fibres, which may increase water demand to avoid congestion during mixing, difficulty in full compaction and to avoid honeycombing.

Superplasticizer—Addition of fibres in the concrete mix reduces the workability of the fresh concrete; therefore, variable dosages of superplasticizer have been used, generally increasing with the increase in the fibre volume in order to increase the workability. The quantity of superplasticizer was mainly dependent on the target slump of 50 ± 10 mm. A summary of the high-strength concrete mix ingredient (with and without fibres) is described in Table 2.

2.2 *Mixing and Specimens Casting Details*

Careful attention was paid during the mixing of fibres into the concrete mix for even distribution; however, it was observed that with the increase of PVA and Basalt fibre volume, good mixing and handling became challenging which made difficulty to pour concrete mass in the moulds. This harsh behaviour of both fresh concretes significantly influenced the mechanical characteristics of hardened concrete and discussed in afterward sections. In order to maintain workability and to achieve desired slump of 50 ± 10 mm, increasing amount of superplasticizer was used with respect to the increasing fibre volume fraction of the fibres. Moreover, the use of small fibre volume fractions exhibited a relatively better distribution of fibres than higher fibre volume fractions. Kooiman [17] and Lambrechts [18] also confirmed this observation in their studies.

To obtain the strength results, three cylindrical specimens (100×200 mm) and three cubes of $100 \times 100 \times 100$ mm were cast. These specimens were used to determine the relationship between cylinder and cube strength. Moreover, three cylinders were additionally cast to determine the splitting tensile strengths for each HSC concrete type. During pouring of the moulds, it was observed that the major

Table 1 Properties of basalt and PVA fibres

Fibre details	Basalt fibres	PVA fibres
Fibre type	Filament type	Straw type
Diameter (μm)	18	660 (0.66 mm)
Cut length (mm)	25	30
Tensile strength (MPa)	4,100–4,840	900
Elastic Modulus (GPa)	93.1–110	23
Specific gravity	2.63–2.8	1.3
Elongation (%)	3.1	7

Table 2 Summary of the mix ingredients

Mix ingredients	Quantity (kg/m^3)
Portland cement	450
Fine aggregate (marine)	670
Coarse aggregates <10 mm	600
Coarse aggregate: 10–20 mm	500
Fibre volume content, V_f	PVA fibres = 13, 26 and 39 Basalt fibres = 26, 52 and 78
Water cement ratio	0.4
Superplasticizer	Variable dosage to maintain slump 50 ± 10 mm

concentration of the fibres was at the bottom of the moulds due to vibration. This observation is also reported in the literature by Robins et al. [19] who investigated the concentration of similar fibre volume (in terms of fibre distribution) in steel fibre reinforced sprayed concrete beams and traditionally cast fibre concrete beams and found that for the vibrated concrete at 1 % fibre volume fraction, the major concentration of fibres was at the bottom of the beams and this concentration was approximately four times greater than at the top.

2.3 Testing of the Specimens

After completion of the curing period, all specimens were air dried for a few hours then tested.

Compressive strength of three (03) concrete cubes of the size $100 \times 100 \times 100$ mm were determined according to B.S 1881-116: 1983 standard [20] whereas, splitting tensile strength testing of three (03) 100×200 mm cylinders had been carried out according to BS 1881-117:1973 [21], respectively using compression testing machine of 3,000 kN capacity. Compressive load was applied with loading pace of 0.3 kN/s. To determine the ratio of the cylinder to cube compressive strength, three 100×200 mm cylinders were also tested using compression testing machine of 1,000 kN capacity. To obtain the stress–strain behaviour of concrete, LVDT was also installed while testing cylinders.

Table 3 Compressive, split tensile test and elastic modulus results

Fibre Type	Fibre volume (%)	At 28 days			Avg. cylinder/cube strength ratio	
		Splitting strength (MPa)	Elastic modulus (MPa)	Compressive strength (MPa)		
				Cube	cylinder	
–	0	5.16	40.76	82.14	71.55	0.87
PVA	1	5.41	42.98	96.2	79.79	0.83
	2	6.51	38.69	94.43	77.29	0.82
	3	7.04	41.44	85.63	66.80	0.78
Basalt	1	5.16	42.01	89.66	76.58	0.85
	2	5.40	41.88	84.71	70.70	0.83
	3	5.68	42.54	78.6	64.56	0.82

3 Experimental Results and Discussion

Table 3 shows the 28 days test results of compressive strength (cube and cylinder), splitting tensile strength and modulus of elasticity for the specimens reinforced with different fibre content to observe the effect of the addition of various amounts of fibres on the splitting strength and modulus of elasticity. These test results are discussed in the succeeding sections.

3.1 Compressive Strength

Twenty-eight days compressive strength test results of the cubes and cylinders are presented in Table 3, whereas comparison of the compressive strength ratios with respect to the fibre volume increase is presented in Table 4. Looking at the strength ratios in Table 4, it is observed that PVA fibre volume fraction up to 1 % increased the compressive strength; however further increase in the volume fraction caused slight decrease in the compressive strength, although compressive strength remained higher than control except for the specimens reinforced with 3 % fibre volume. Similarly, in case of Basalt fibres, the maximum increase in compressive strength was observed with 1 % volume fraction. These results signify that with respect to compressive strength the maximum fibre volume fraction is 1 % for PVA and Basalt fibres.

Moreover, the comparison of the compressive strength of high-strength concrete reinforced with PVA and Basalt fibres shows that the addition of PVA fibres resulted in a slightly higher compressive strength as compared to the Basalt fibres (refer Table 4). The reason is that PVA fibres retain their shape in hardened concrete which offers bridging effect and better confinement of the concrete; however, during mixing, Basalt fibres amalgamate and vanish completely in the concrete mix due to their micro diameters which causes defragmentation into

Table 4 Ratio of cube compressive strength of HSC with and without fibres

Mix IDs	No fibre	1 % PVA	2 % PVA	3 % PVA	1 % Basalt	2 % Basalt	3 % Basalt
No fibre	1	–	–	–	–	–	–
1 % PVA	1.17	1	–	–	–	–	–
2 % PVA	1.15	0.98	1	–	–	–	–
3 % PVA	1.04	0.89	0.907	1	–	–	–
1 % Basalt	1.09	0.93	0.949	1.05	1	–	–
2 % Basalt	1.03	0.88	0.897	0.99	0.945	1	–
3 % Basalt	0.96	0.82	0.832	0.92	0.877	0.928	1

further small pieces. In the author's opinion, these small pieces of Basalt fibres intrude in the pores of the concrete instead of offering the fibre behaviour thus increase the brittleness of the concrete.

The relation between cylindrical and cube compressive strength ratios show that cylindrical strength is approximately 87 % of the cube strength for a control specimen; however this ratio decreases due to the addition of fibres. This slight reduction might be due to improper distribution and orientation of the fibres, concentration of the fibres at particular location(s) along the cylinder height and lack of end restraining effects.

3.2 Splitting Tensile Strength

As shown in Fig. 1, with respect to the control specimen, higher splitting tensile strength was obtained with PVA fibres reinforced HSC as compared to the Basalt fibres reinforced HSC, but still splitting tensile strength of Basalt fibre reinforced concrete improved with respect to the control specimen. It was also observed that irrespective of fibre type, increase in the fibre volume enhanced the splitting tensile strength of HSC. Using 1, 2 and 3 % PVA fibres, the increase in splitting tensile strength of high-strength concrete was observed as 4.8, 16.2 and 36.4 %, respectively. On the other hand, the addition of Basalt fibres caused a marginal increase in splitting tensile strength as compared to PVA fibres. Overall, using 1, 2 and 3 % fibre volume fractions of Basalt fibres, increase in the splitting tensile strength was found to be 0.12, 4.65 and 10.1 %, respectively. This shows that the addition of PVA fibres better improve the splitting tensile property of high-strength concrete in comparison to Basalt fibres. The reason is same as mentioned earlier that PVA fibres provide better lateral confinement in comparison to Basalt fibres.

Fig. 1 Variation in splitting tensile strength

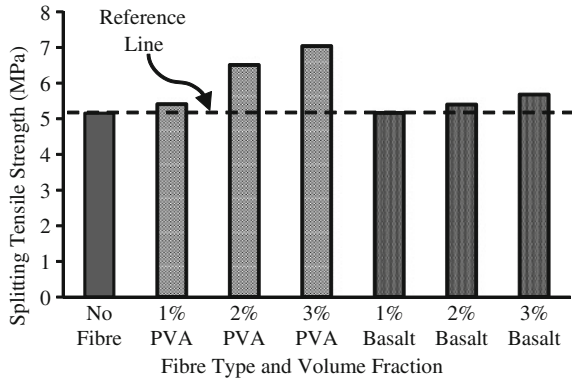
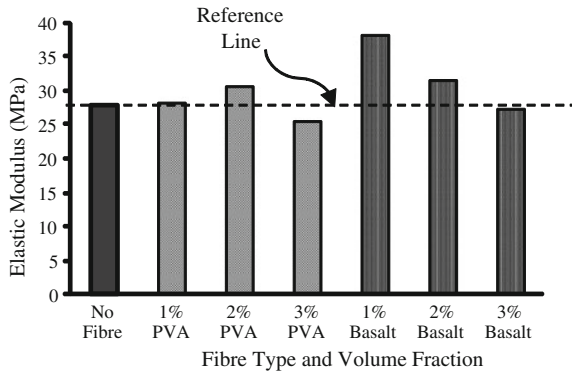


Fig. 2 Variation in elastic modulus



3.3 Elastic Modulus

Experimental results of elastic modulus are presented in Table 3, whereas the variation in the elastic modulus is plotted in Fig. 2.

The plotted values of elastic modulus in Fig. 2 shows an increasing trend due to the addition of PVA fibres up to 2 % volume fraction, whereas use of 3 % fibre volume fraction decreased the elastic modulus values in comparison to the control specimen. Similarly, use of Basalt fibres resulted in a higher elastic modulus with 1 % volume fraction and further increase in volume fraction decrease the elastic modulus; however, it remained higher than control (refer Fig. 2). The comparison of elastic modulus values (plotted in Fig. 2) for HSC reinforced with PVA and Basalt fibres shows that elastic modulus is improved for HSC reinforced with PVA fibres at all fibre volume fractions in comparison to that HSC in which Basalt fibres were used as reinforcement. These results endorse this conclusion that concrete confinement is better with PVA fibres, whereas Basalt fibres defragment into small pieces caused weak confinement consequently decreased the performance in comparison with PVA fibres.

4 Conclusions

The conclusions from this study are as follows:

1. For compressive strength, the optimal dosage for PVA and Basalt fibres was 1 %, which increased the compressive strength up to 17 and 9 %, respectively. Overall, compressive strength of high-strength concrete reinforced with PVA fibres was found to be higher than Basalt fibres (for the similar fibre volume fractions) due to hard and firm structure of PVA fibre, which retained fibre shape even after mixing in the concrete.
2. With respect to the control mixes, addition of PVA fibres improved the splitting tensile resistance. In addition, splitting tensile strength increased with the increasing PVA fibre volume, which was not observed in the case of Basalt fibre reinforced high-strength concrete.
3. Overall, modulus of elasticity of high-strength concrete is not influenced by the addition of 1–3 % fibre volume. In case of basalt fibre reinforced concrete, higher elastic modulus was obtained as compared to control as well as PVA fibre reinforced concrete.

Acknowledgments Financial support from Universiti Teknologi PETRONAS, Malaysia is highly acknowledged and thanks are extended to lab technicians during testing of the specimens and data acquisition.

References

1. American Concrete Institute and Portland Cement Association, ACI 318-08 & PCA notes on 318-08: building code requirements for structural concrete and commentary. ACI Committee 318, 2008
2. A. Sivakumar, M. Santhanam, Mechanical properties of high strength concrete reinforced with metallic and non-metallic fibres. *Cement Concr. Compos.* **29**, 603–608 (2007)
3. P. Richard, M. Cheyreyz, Reactive powder concretes with high ductility and 200–800 MPa compressive strength. *ACI Spec. Publ.* **144**, 507 (1994)
4. V.C. Li, On engineered cementitious composites (ECC). *J. Adv. Concr. Technol.* **1**, 215–230 (2003)
5. M. Lepech, V.C. Li, Long term durability performance of engineered cementitious composites. *Restor. Build. Monuments* **12**, 119–132 (2006)
6. Y.Y. Kim, G. Fischer, V.C. Li, Performance of bridge deck link slabs designed with ductile engineered cementitious composite. *ACI Struct. J.* **101**, 792–801 (2004)
7. J.A. Barros, J.A. Figueiras, Flexural behavior of SFRC: testing and modeling. *J. Mater. Civ. Eng.* **11**, 331–339 (1999)
8. L.J.Y.Y. Meng, Z. Yan, Experimental research on the mechanical behavior of chopped basalt fiber reinforced concrete. *Ind. Construct.* **6**, 002 (2007)
9. T. Ayub, S.F.A. Rafeeqi, in *Performance of Reinforced Concrete Beams Containing Steel Fibres*. Presented at the 5th International Specialty Conference on Fibre Reinforced Materials, Singapore, 2008

10. V. Ramakrishnan, N.S. Tolmare, V. Brik, Performance evaluation of 3-D basalt fiber reinforced concrete & basalt rod reinforced concrete, 1998
11. K. Huang, M. Deng, Stability of basalt fibers in alkaline solution and its effect on the mechanical property of concrete. *Act. Mater. Compos. Sin.* **1**, 027 (2010)
12. L.-J. Shen, J.-Y. Xu, W.-M. Li, F.-L. Fan, J.-Y. Yang, Experimental investigation on the static and dynamic behaviour of basalt fibers reinforced concrete. *Concrete* **4**, 026 (2008)
13. T. Horikoshi, A. Ogawa, T. Saito, H. Hoshiro, G. Fischer, V. Li, in *Properties of Polyvinylalcohol Fiber as Reinforcing Materials for Cementitious Composites*. International RILEM Workshop on HPRCC in Structural Applications, p. 147, 2006
14. V.C. Li, S. Wang, C. Wu, Tensile strain-hardening behavior of polyvinyl alcohol engineered cementitious composite (PVA-ECC). *ACI Mater. J. Am. Concr. Inst.* **98**, 483–492 (2001)
15. V.C. Li, C. Wu, S. Wang, A. Ogawa, T. Saito, Interface tailoring for strain-hardening polyvinyl alcohol-engineered cementitious composite (PVA-ECC). *ACI Mater. J. Am. Concr. Inst.* **99**, 463–472 (2002)
16. Design Guide of High Strength Concrete to Singapore Standard CP 65, Building and construction Authority, p. 93, 2007
17. A.G. Kooiman. Modelling steel fibre reinforced concrete for structural design. Dissertation for Faculty of Civil Engineering and Geosciences, Delft University of Technology. ISBN: 90-73235-60-X (2000)
18. A. Lambrechts, in *The Variation of Steel Fibre Concrete Characteristics. Study on Toughness Results 2002–2003*. International Workshop on Advances in Fiber Reinforced Concrete, Bergamo, Italy, pp. 135–148, 2004
19. P. Robins, S. Austin, P. Jones, Spatial distribution of steel fibres in sprayed and cast concrete. *Mag. Concr. Res.* **55**, 225–235 (2003)
20. BS 1881-116: 1983, Method for determination of compressive strength of concrete cubes. BSI, London, 1983
21. BS 1881-117: 1983, Method for determination of splitting tensile strength. BSI, London, 1983

Compressive Strength and Density of Unfired Lightweight Coal Ash Brick

Mohamad Ezad Hafez Mohd Pahroraji, Hamidah Mohd Saman,
Mohamad Nidzam Rahmat and Kartini Kamaruddin

Abstract Coal-fired thermal power plant produces million tons of coal ash which constitute of fly ash and bottom ash annually throughout the world. They were by-product and significant to be developed as brick to substitute the existing widely used traditional material such as clay and sand brick which were produced from depleting and dwindling natural resources. In the present study, the coal ash from coal-fired thermal power plant was used as the main raw material for the fabrication of unfired lightweight brick. The blended binder comprising of Hydrated Lime (HL)-Ground Granulated Blastfurnace Slag (GGBS) and Portland Cement (PC)-GGBS were used to stabilize the coal ash in the fabrication process. Foam was used to reduce the weight of the brick. The compressive strength in accordance to BS EN 772-1 and ambient density in accordance to AS/NZS 4456.8 were evaluated on the brick samples. The results indicated that the coal ash brick incorporating PC-GGBS system achieved higher compressive strength compare to the HL-GGBS system. However, as the quantity of foam increase, the strength and density for both brick systems decreased.

Keywords Fly ash · Bottom ash · Hydrated lime · Portland cement · Ground granulated blastfurnace slag (GGBS) · Foam · Masonry brick · Compressive strength · Density

M. E. H. M. Pahroraji (✉) · M. N. Rahmat
Faculty of Architecture, Planning and Surveying, Universiti Teknologi MARA, Shah Alam,
Malaysia
e-mail: ezadhafez@gmail.com

H. M. Saman · K. Kamaruddin
Faculty of Civil Engineering, Universiti Teknologi MARA, Shah Alam, Malaysia

1 Introduction

In Malaysia, traditional construction material such as clay and sand brick were currently being used as major building components in construction sector. These materials have been produced from the locally available natural resources that potentially will damage the environment due to their continuous exploitation and in its manufacturing process. Hence, the use of industrial by-product as raw material is significant for the development of construction material components as substitution for the traditional materials and this will provide an alternative or supplementary materials to the construction industry in a cost effective manner [1]. Therefore, it is a challenge to the researchers to recycle/reuse the potential available industrial by-products into useful construction materials.

There were many previous researchers who have reported interesting result in the use of industrial by-product to produce brick. However, among the industrial by-products that available worldwide in large amount and constantly produced is the coal ash which constitutes of fly ash and bottom ash. Ashes were produced from the coal-fired electric thermal power plant. The fly ash was obtained from the Electro Static Precipitator, while bottom ash was obtained from the bottom of the furnace due to heavier solid particles formed. Throughout the world, more than 65 % of fly ash produced from coal-fired power plant are disposed in landfills [2]. Due to the increase in landfill costs and current interest in sustainable development, the recycling of coal ash has become a great concern. In Malaysia, approximately 1,200 MW or 20 % of national electricity is supplied by the thermal power plant using coal as the fuel. The Sultan Abdul Aziz Shah electrical power generator in Kapar, Selangor alone uses 100 tons of coal per hour to generate electricity for the national grid. It produces about 15–20 tons Pulverized Fuel Ash (PFA) per hour [3]. While in Sarawak, the state government is planning to construct more coal-fired thermal power generation plants as back-up to the existing energy sources for the state. The Public Utilities Minister has mentioned that the state requires coal-fired power to complement its hydro power generation to meet high demand of energy intensive industries especially in the Sarawak Corridor of Renewable Energy (SCORE) due to the estimated total of one billion tons of coal reserve in Mukah-Balingian region [4]. Therefore, in general, Malaysia used about 11.2 million tons of coal per year and approximately over 2 million tons of coal ash is produced annually. However only small percentage was used or recycled with the remain of the ashes were sent for disposal to lagoons or ponds [5].

Many researchers have studied and reported on the use of fly ash as raw material for masonry brick [6–13], however, there is paucity of published work on the use of fly ash and bottom ash as the main raw material incorporating the combination of Hydrated lime (HL)-Ground Granulated Blastfurnace Slag (GGBS) and Portland Cement (PC)-GGBS as the binder. There is also little evidence on the research effort carried out in development of a lightweight bricks using industrial by-product [14]. Therefore, this paper focus on the utilization of coal ash from coal-fired electric thermal power plant as the main raw material and

stabilize using HL-GGBS and PC-GGBS system as the binder in the fabrication of unfired lightweight coal ash brick. The effect of HL-GGBS and PC-GGBS ratio to the compressive strength and the effect of addition of foam to the density of the brick were investigated.

2 Material and Methodology

2.1 Materials

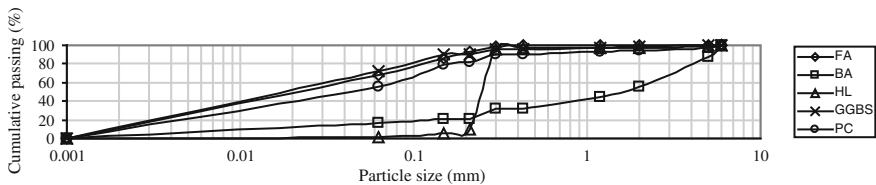
The main raw materials used in this study consisted of fly ash and bottom ash. The fly ash obtained is originally a by-product produced from Sejingkat, Sarawak coal-fired thermal power plant. The used of fly ash was larger than the bottom ash in amount because of the production ratio of fly ash is higher (80 %) compare to bottom ash (20 %) that produced from the total production of the coal ash at the power plant. In accordance to ASTM C618-08a [15], the fly ash is categorized as Class F base on its chemical composition (Table 1) in which the sum of silicon dioxide (SiO_2), aluminium oxide (Al_2O_3) and ferric oxide (Fe_2O_3) exceed 70 %. Class F fly ash is unstable in terms of the ability to bind because it contain less calcium oxide (CaO). Therefore, the fly ash requires stabilizer. The bottom ash was collected from Kapar Thermal Power Plant, Klang, Selangor and was dried at ambient temperature in the laboratory before used. The binders used in this study which aim to stabilize the brick unit comprising of HL-activated GGBS and PC-activated GGBS at various ratio. The function of HL and PC are as the activator to GGBS. Other materials used in this study were foaming agent synthetic type (MEYCO SLF-30) to produce foam and potable tap water in the mixing process. The chemical compositions of the main raw materials and binders are shown in Table 1. The results of particle size distributions of fly ash, bottom ash, HL, PC and GGBS were obtained by dry sieving method as per guideline provided by BS 1377-2:1990 [16] and are shown in Fig. 1. The specific gravity of fly ash, bottom ash, HL and GGBS was determined as per guideline provided by BS 1377-2:1990 [16]: Determination of particle density using small pycnometer method. The result is taken from the average of the mean of three tests. The specific gravity value was 2.41 for fly ash, 2.26 for bottom ash, 2.40 for HL and 2.90 for GGBS.

2.2 Mixing and Preparation of Brick Sample

Prior to commence of casting, the steel mould was cleaned for smooth surface by using air compressor and oiled. Thirty two (32) mix proportions were prepared and the percentage of material used is as shown in Table 2. The variations in the mixes were the stabilizer percentage content ratio of 30:70, 50:50, 70:30 and the

Table 1 Chemical composition of fly ash, bottom ash, hydrated lime, ground granulated blast-furnace slag and portland cement

Parameter	Percentage (%)				
	Fly ash	Bottom ash	HL	GGBS	PC
SiO ₂	48.56	59.04	0.18	29.99	18.66
Al ₂ O ₃	19.56	15.53	0.09	11.42	3.82
Fe ₂ O ₃	5.82	10.22	0.13	0.32	2.86
CaO	3.35	0.70	57.54	40.72	64.76
K ₂ O	2.93	1.34	0.03	0.35	0.23
MgO	1.84	0.22	1.99	5.13	1.79
Na ₂ O	0.88	0.09	0.02	0.20	–
TiO ₂	0.88	0.76	0.01	0.49	0.14
P ₂ O ₅	0.30	0.05	0.02	–	0.10
BaO	0.15	0.03	–	0.08	–
SO ₃	0.14	0.04	–	2.10	3.59
SrO	0.09	0.02	0.02	0.07	0.02
MnO	0.08	0.27	0.02	0.22	0.08
ZrO ₂	0.05	0.06	–	0.03	–
Cr ₂ O ₃	0.02	–	–	–	–
Rb ₂ O	0.01	–	–	–	–
Cl	–	–	0.02	–	0.01

**Fig. 1** Particle size distribution of fly ash (FA), bottom ash (BA), hydrated lime (HL), ground granulated blastfurnace slag (GGBS) and Portland cement (PC)

percentage content of foam used was 0, 25, 50, 75 and 100 %. The total number of masonry brick unit samples prepared in this study was two hundred and eighty eight (288) for the compressive strength test. All materials were used as received from the supplier without any prior treatment. Pan mixer was used in the process of mixing all of the materials. The mixture proportion series were prepared with 30 % constant amount of water by total weight of dry material. The masonry bricks were produce using soft mud method with foaming technique which require high amount of water and forming the shape using steel mould size of 215 × 102.5 × 65 mm. For all of the mixes series, the content of bottom ash and fly ash amount was fixed at 10 and 60 % respectively. The total percentage amount of binder content of HL-GGBS and PC-GGBS were fixed at 30 %. All materials were weighed using digital balance according to the series of mixture proportions to gain the exact amount as required for casting. During the mixing process, all

Table 2 Series of mixture proportions

Mix Code	Main raw material		Binder			Foam (%)	Water (%)
	Bottom ash (%)	Fly ash (%)	(HL-GGBS) or (PC-GGBS)				
			(%)				
			HL	PC	GGBS		
HL	10	60	30	–	–	0	30
PC	10	60	–	30	–	0	30
LG-1-0	10	60	10	–	20	0	30
LG-2-0	10	60	15	–	15	0	30
LG-3-0	10	60	20	–	10	0	30
PG-1-0	10	60	–	10	20	0	30
PG-2-0	10	60	–	15	15	0	30
PG-3-0	10	60	–	20	10	0	30
LG-1-25	10	60	10	–	20	25	30
LG-2-25	10	60	15	–	15	25	30
LG-3-25	10	60	20	–	10	25	30
PG-1-25	10	60	–	10	20	25	30
PG-2-25	10	60	–	15	15	25	30
PG-3-25	10	60	–	20	10	25	30
LG-1-50	10	60	10	–	20	50	30
LG-2-50	10	60	15	–	15	50	30
LG-3-50	10	60	20	–	10	50	30
PG-1-50	10	60	–	10	20	50	30
PG-2-50	10	60	–	15	15	50	30
PG-3-50	10	60	–	20	10	50	30
LG-1-75	10	60	10	–	20	75	30
LG-2-75	10	60	15	–	15	75	30
LG-3-75	10	60	20	–	10	75	30
PG-1-75	10	60	–	10	20	75	30
PG-2-75	10	60	–	15	15	75	30
PG-3-75	10	60	–	20	10	75	30
LG-1-100	10	60	10	–	20	100	30
LG-2-100	10	60	15	–	15	100	30
LG-3-100	10	60	20	–	10	100	30
PG-1-100	10	60	–	10	20	100	30
PG-2-100	10	60	–	15	15	100	30
PG-3-100	10	60	–	20	10	100	30

materials were placed in the mixer and mixed for one (1) minute until homogeneous. Water was poured in gradually until all the materials were uniformly mixed. Mixing continues for 10 min for the materials to properly blend before injecting foam that were generated using NCT Model foam generating machine into the mix slurry using lance. The ratio of foaming agent to water used was 1:30. The mixing continues for the foam to properly blend into the mix slurry. Then, the fresh slurry was poured into the steel mould. The samples were placed at drying area for 48 h before the mould can be removed. After removal of the brick samples

from the steel mould, the bricks were wrapped using several layers of cling film, kept at storage rack for air curing for 7, 28 and 56 days prior to the compressive strength test.

2.3 Test Methods

The compressive strength test was carried out in accordance to BS EN 772-1 [17] and ambient density according to AS/NZS 4456.8 [18]. The compressive strength of the brick sample was determined by using ELE compressive strength test machine with maximum load capacity of 1,500 kN running at a pace rate of 2.5 kN/s. The load is applied to the bed face of the masonry brick sample with the dimension of $215 \times 102.5 \text{ mm}^2$. This method has been done among other researchers [8, 19, 20]. The compressive strength is calculated by dividing the maximum load with the applied load area of the sample. The ambient density of the brick samples were determined by dividing the mass with volume.

3 Result and Discussion

Table 3 shows the result obtained from the tests. Two hundreds and eighty eight (288) brick samples from thirty two (32) mixes proportion were tested for compressive strength. Three samples were prepared for each curing days and the results were taken as average. The similar brick samples were used to determine the ambient density.

Class F fly and bottom ash contains high SiO_2 to promote strength, but with less contain of CaO in the composition, it requires stabilizer to aid in its binding process. Traditional binder such as HL and PC can be use as the stabilizer because both materials posses high content of CaO. However, HL and PC are among non-environmental friendly materials that eventually will damage the environment in its continuous exploitation and also in the manufacturing process. Therefore, hydraulic binder such as GGBS, a by-product from steel manufacturing process, is suitable to be used as stabilizer and substitution to HL and PC because of high contain of SiO_2 and CaO in its composition. However, GGBS on its own has only slow cementitious properties in which it requires an alkali to activate and accelerate these properties [21]. In the present study, HL and PC were used to provide the necessary alkalinity to activate the GGBS. The results show that brick using HL-activated GGBS system and PC-activated GGBS system as the binder have achieved higher compressive strength compare to the brick that using HL and PC on its own.

Table 3 Results of compressive strength test and density

Mix code	Compressive strength (N/mm ²)			Density (kg/m ³)
	7 days	28 days	56 days	
HL	3.61	13.98	19.71	1,713.3
PC	14.07	26.74	29.60	1,817.6
LG-1-0	9.13	20.84	26.18	1,767.7
LG-2-0	7.62	17.47	24.32	1,769.5
LG-3-0	5.29	15.89	22.25	1,763.5
PG-1-0	14.48	29.88	36.75	1,768.6
PG-2-0	17.69	33.61	39.18	1,755.1
PG-3-0	20.23	38.19	42.87	1,776.4
LG-1-25	7.71	19.43	22.29	1,748.2
LG-2-25	6.04	17.21	21.03	1,734.2
LG-3-25	4.93	15.78	18.70	1,739.2
PG-1-25	9.77	27.97	34.50	1,748.0
PG-2-25	11.90	30.28	36.69	1,759.8
PG-3-25	12.53	33.07	39.02	1,740.0
LG-1-50	6.33	15.19	17.62	1,691.5
LG-2-50	5.64	14.84	16.81	1,675.5
LG-3-50	4.53	13.88	15.02	1,675.2
PG-1-50	8.79	19.03	21.63	1,657.3
PG-2-50	9.20	19.55	24.34	1,650.5
PG-3-50	10.53	20.61	26.59	1,646.6
LG-1-75	3.32	10.56	13.26	1,451.7
LG-2-75	2.41	9.42	11.57	1,453.8
LG-3-75	1.53	8.41	10.78	1,462.4
PG-1-75	5.21	11.39	15.22	1,434.9
PG-2-75	6.17	12.87	16.16	1,454.1
PG-3-75	7.10	13.60	17.44	1,463.3
LG-1-100	0.93	2.90	3.85	1,096.1
LG-2-100	0.85	2.54	3.48	1,115.8
LG-3-100	0.72	2.16	3.19	1,116.3
PG-1-100	1.15	3.27	4.34	1,071.6
PG-2-100	1.38	3.49	4.85	1,085.4
PG-3-100	1.77	3.82	5.22	1,099.2

3.1 Compressive Strength

Mix code HL and PC serve as the controls which use 100 % hydrated lime and Portland cement respectively as the binder to stabilize the brick and without foam. The rest of the mixes were using combination of HL-GGBS and PC-GGBS as the binder. From the result observation of HL-GGBS system, the mix code LG-1-0 with binding ratio 30:70 indicates the highest compressive strength of 9.13 N/mm² at 7 days, 20.84 N/mm² at 28 days and 26.18 N/mm² at 56 days. When percentage of hydrated lime content in the HL-GGBS ratio was increased, it caused a

Fig. 2 Compressive strength of brick sample made of HL-GGBS system and PC-GGBS system without foam at 7, 28 and 56 days

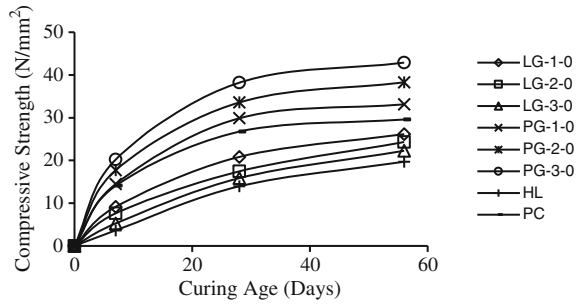
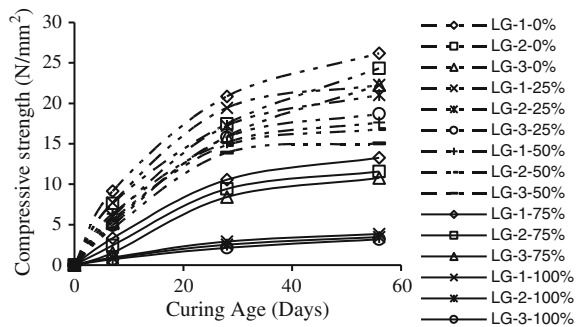


Fig. 3 Compressive strength of brick made of different percentage of foam for HL-GGBS system at 7, 28 and 56 days



decrease in the compressive strength. This is exhibited by samples mix code LG-2-0 with binding ratio 50:50 which recorded 7.62 N/mm^2 at 7 days, 17.47 N/mm^2 at 28 days, and 24.32 N/mm^2 at 56 days and also LG-3-0 with binding ratio 70:30 which recorded 5.29 N/mm^2 at 7 days, 15.89 N/mm^2 at 28 days, and 22.25 N/mm^2 at 56 days as shown in Fig. 2. This might be due to the lower total content of CaO and SiO₂ in the hydrated lime compare to GGBS. The higher total amount of CaO and SiO₂ content in GGBS might contribute in the increase of the compressive strength for the brick. The use of hydrated lime on its own as the binder as in the mix code HL recorded lower compressive strength of 3.61 N/mm^2 at 7 days, 13.98 N/mm^2 at 28 days and 19.71 N/mm^2 at 56 days compare to the mixes that were using HL-GGBS system at any ratio. Whereas for the PC-GGBS system, the mix code PG-3-0 with binding ratio 70:30 indicates the highest compressive strength of 20.23 N/mm^2 at 7 days, 38.19 N/mm^2 at 28 days and 42.87 N/mm^2 at 56 days. When percentage of Portland cement content in the PC-GGBS ratio was reduced, it caused a decrease in compressive strength. This is exhibited by samples mix code PG-1-0 with binding ratio 30:70 which recorded 14.48 N/mm^2 at 7 days, 29.88 N/mm^2 at 28 days and 36.75 N/mm^2 and also PG-2-0 with binding ratio 50:50 which recorded 17.69 N/mm^2 at 7 days, 33.61 N/mm^2 at 28 days and 39.18 N/mm^2 at 56 days as shown in Fig. 2. This might be due to the lower total content of CaO and SiO₂ in the GGBS compare to PC. The use of Portland cement on its own as the binder as in the mix code PC recorded lower compressive strength of 14.07 N/mm^2 at 7 days, 26.74 N/mm^2 at 28 days and 29.60 N/mm^2 at

Fig. 4 Compressive strength of brick made of different percentage of foam for PC-GGBS system at 7, 28 and 56 days

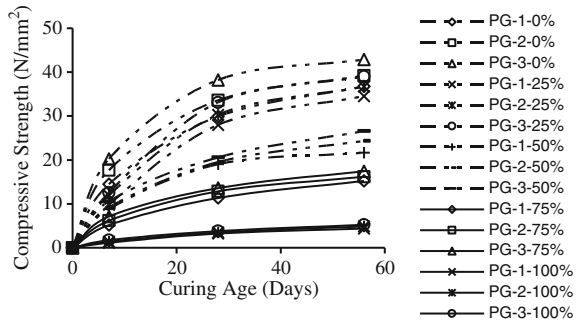
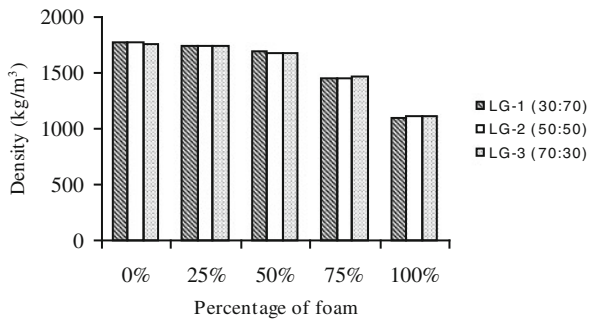


Fig. 5 Density of brick made of different percentage of foam for HL-GGBS system

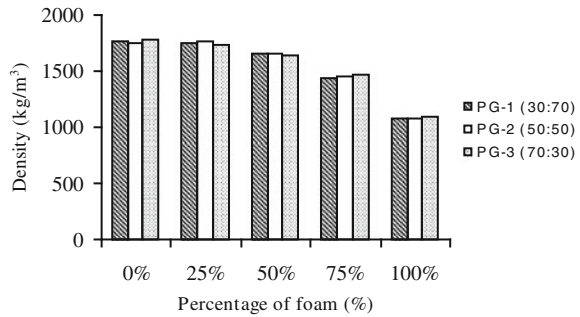


56 days compare to the mixes that were using PC-GGBS system at any ratio. However, when foam was used, the compressive strength shows reduction. The higher percentage of foam used, the more reduction was recorded. This indicate that the use of foam to lightweight the brick reduce the compressive strength. When 25 % of foam was added into the mixes for both system HL-GGBS and PC-GGBS, the compressive strength indicate only a slight decrease compare to mix without foam. When 50 and 75 % of foam was added, the reduction in compressive strength becomes more significant. At this percentage, even though the compressive strength reduces but the value at 28 days satisfies the minimum requirement of BS 6073 of 7.3 N/mm². However, when 100 % of foam was added, the compressive strength becomes very low and recorded below 4 N/mm² at 28 days. This is shown in Figs. 3 and 4.

3.2 Density

In this present study, foam was used to reduce the weight of the brick. The pre-formed foaming method was applied. The ratio of foaming agent to water used was 1:30 for the foam to be fully expanded [22]. The amount of foam injected into the

Fig. 6 Density of brick made of different percentage of foam for PC-GGBS system



mix slurry was control by using watch timer. The function of foam is to create pore structure by introducing air in the form of small bubbles within the bricks. As expected, the density of the brick decrease with the increase in the addition of foam in the mixes for both HL-GGBS and PC-GGBS system as shown in Figs. 5 and 6. However, a slight decrease in density can be seen for both mixes when only 25 % of foam content was used. This indicates that the 25 % amount of foam was not significantly sufficient to reduce the weight of the bricks. When the foam percentage was increased to 50 %, the density of the brick reduces by approximately 100 kg/m^3 . However, this is still considered heavy when the density was recorded approximately at $1,600 \text{ kg/m}^3$. The density of the brick reduces to approximately at $1,400 \text{ kg/m}^3$ when 75 % amount of foam was used. This can be considered balanced within the value of density and compressive strength achieved. By increasing the foam percentage to 100 %, the density of the brick reduces to approximately $1,100 \text{ kg/m}^3$. However, the compressive strength was extremely decreased and have not achieved the minimum requirement of BS 6073 [23].

4 Conclusion

This study was carried out to evaluate the significance of utilizing industrial by-products such as fly ash, bottom ash with the incorporation of HL-GGBS and PC-GGBS as binder with foam in developing the unfired lightweight coal ash brick. From the result of this study, conclusions can be drawn as the following:

1. The use of traditional binder such as hydrated lime and Portland cement can be reduced and replaced with GGBS, a by-product from steel manufacturing process.
2. Hydrated lime and Portland cement can be used to provide the necessary alkali for GGBS to activate and accelerate its slow cementitious properties.
3. The use of hydrated lime or Portland cement as an activator to GGBS as the stabilizer was able to increase the compressive strength of the brick compare to the use of hydrated lime or Portland cement on its own.

4. The use of PC-GGBS system has achieved higher compressive strength value compare to HL-GGBS system.
5. In the HL-GGBS system, the ratio of HL to GGBS at 30:70 has recorded higher compressive strength compare to the ratio 50:50 and 70:30.
6. In the PC-GGBS system, the ratio of PC to GGBS at 70:30 has recorded higher compressive strength compare to the ratio of 50:50 and 30:70.
7. The increase in the addition of foam in the mixes will decrease the compressive strength and density of the brick.
8. The addition of foam amount by 25 % was not significantly sufficient to reduce the density of the brick.
9. The amount of foam to 100 % was sufficient to reduce the density of the brick but achieved lowest compressive strength.
10. Compressive strength of masonry brick unit with 75 % of foam addition at 28 days satisfies the requirements in BS 6073 for the brick to be used as building material and the density reduces to approximately 1,400 kg/m³.

Further investigation on the durability aspects need to be carried out on the brick include flexural strength, water absorption, thermal conductivity and salt attack resistance.

Acknowledgments The authors wish to express thanks to Gobel Industry Sdn. Bhd. for providing fly ash, Kapar Energy Venture for bottom ash, YTL cement for GGBS and gratefully acknowledge Universiti Teknologi MARA for financial support [Excellence Fund Grant No. 600-RMI/ST/DANA5/3/Dst (411/2011)].

References

1. A. Pappu, M. Saxena, S.R. Asolekar, Solid wastes generation in India and their recycling potential in building materials. *Build. Environ.* **42**, 2311–2320 (2007)
2. R. Pradeep, Polymer fly ash-natural fiber composites for clutch facings. Presented at the International workshop on advances in asbestos-free friction composites-III (IWAAFC-III), ITMMEC, Indian Institute of Technology, Delhi, India, 2011
3. N.I. Khairul, H. Kamarudin, S.I. Mohd, Physical, chemical and mineralogical properties of fly ash. *J. Nucl. Relat. Technol.* **4**, 47–51 (2007)
4. Awang Tengah, Coal-fired power plants needed (2010), in <http://thestar.com.my/metro>, ed. by Kuching
5. P.K. Kolay, T. Kismoor, Geotechnical characterization of coal ashes from Sarawak for bulk utilization. *J. Solid Waste Technol. Manage.* **35**, 2009 (2009)
6. T. Cicek, M. Tanriverdi, Lime based steam autoclaved fly ash bricks. *Constr. Build. Mater.* **21**, 1295–1300 (2007)
7. P. Chindapasirt, K. Pimraksa, A study of fly ash-lime granule unfired brick. *Powder Technol.* **182**, 33–41 (2008)
8. O. Kayali, High performance bricks from fly ash. Presented at the World of Coal Ash (WOCA), Lexington, Kentucky, 2005
9. G. Cultrone, E. Sebastian, fly ash addition in clayey materials to improve the quality of solid bricks. *Construction and Building Materials* (2009), pp. 1178–1184

10. X. Lingling, G. Wei, W. Tao, Y. Nanru, Study on fired bricks with replacing clay by fly ash in high volume ratio. *Constr. Build. Mater.* **19**, 243–247 (2005)
11. C. Freidin, Stability of cementless building units on oil shale fly ash binder in various conditions. *Construction and Building Materials* (2002), pp. 23–28
12. C. Freidin, Cementless pressed blocks from waste products of coal-firing power station. *Construction and Building Materials* (2007), pp. 12–18
13. C. Freidin, W. Motzafi-Haller, Cementless building units based on oil shale and coal fly ash binder. *Construction and Building Materials* (1999), pp. 363–369
14. M.N. Rahmat, N. Ismail, J.M. Kinuthia, The potential of utilising industrial waste as lightweight building components—A preliminary investigation. *Modern Appl. Sci.* **4**, 35–46 (2010)
15. ASTM, “C618-08a,” in *standard specification for coal fly ash and raw or calcined natural pozzolan for use in concrete*, ed. by Pennsylvania, American Society for Testing and Materials (2008)
16. BSI, Methods of test for soils for civil engineering purposes. in BS 1377-2 Part 2: Classification tests, ed. by British Standard Institution (1990)
17. BSI, Methods of test for masonry units. in BS EN 772 Part 1: Determination of compressive strength, ed. by British Standard Institution (2011)
18. AS/NZS, Masonry units, segmental pavers and flags—Methods of test. in AS/NZS 4456 Method 8: Determining moisture content, dry density and ambient density, ed. by Australian/New Zealand Standard (2003)
19. J.E. Oti, J.M. Kinuthia, J. Bai, Engineering properties of unfired clay masonry bricks. *Eng. Geol.* **107**, 130–139 (2009)
20. H.M. Algin, P. Turgut, Cotton and limestone powder wastes as brick material. *Constr. Build. Mater.* **22**, 1074–1080 (2008)
21. D. D. Higgins, Soil stabilisation with ground granulated blast furnace slag. UK Cementitious Slag Makers Association (2005)
22. K. M. Ismail, M. S. Fathi, N. Manaf, Study of lightweight concrete behaviour. Universiti Teknologi Malaysia, 2004
23. BSI, Precast concrete masonry units. in BS 6073-1 Part 1: Specification for precast concrete masonry units, ed. by British Standard institution (2008)

Fibre Reinforced Modulus of Elasticity and Compressive Strength of Foamed Concrete

R. Suzila, M. S. Hamidah, A. Anizahyati and M. R. Ahmad Ruslan

Abstract The influence of fibres in various level of density of foamed concrete to improve the performance characteristics has been investigated. Fibres used are in two different types which are synthetic (polypropylene fibre) and natural (kenaf fibre). Those fibres were cut into same length which is 15 mm with proportion of 3 % by volume in the design mix. The effects on modulus of elasticity and compressive strength are reported. Compared to plain foamed concrete, specimens filled with polypropylene (PP) fibre at 1,800 kg/m³ density of foamed concrete, caused about 40 % increase in modulus of elasticity and a 18 % increase in the compressive strength. However, kenaf fibre specimens at 1,800 kg/m³ density of foamed concrete caused a decrease in modulus of elasticity by about 29 % and decrease in compressive strength by about 21 %. These indicate a vital gain in the ductility and strength when foamed concrete incorporating with polypropylene (PP) fibre as compared to kenaf fibre reinforced foamed concrete.

Keywords Compressive strength · Modulus of elasticity · Kenaf fibre · Polypropylene fibre · Foamed concrete

1 Introduction

Foamed concrete is an innovative approach of concrete technology that is inherent in term of cost and constructive over conventional concrete. It is produced using less material than regular concrete, thus making it a green alternative for typical heavy concrete. This surety less environment impact by using less cement, much less sand and eliminated function of gravel in conventional concrete, which all require large amount of energy to be produced. Owing to this noteworthy,

R. Suzila (✉) · M. S. Hamidah · A. Anizahyati · M. R. A. Ruslan
Faculty of Civil Engineering, Institute for Infrastructure Engineering and Sustainable Management (IIESM), Universiti Teknologi MARA, Selangor, Malaysia
e-mail: suzilarahmat@gmail.com

structural concrete has been widely manufactured by using foamed concrete in many applications such as insulating wall panels, thermally insulating foundation plates, precast and many more.

However, innovation has always been met with resistance. Foamed concrete, other than its lower strength, its mechanical characteristics also were lacking in some aspects [1] such as prone to low in elasticity, shrinkage and creep. This conundrum where influenced by the elimination of coarse aggregate function as a stronger matrix bond in the concrete.

One of the crucial characteristic of foamed concrete is the low elasticity and compressive strength due to its high porosity and the probability of high permeability [1, 2]. This could lead to increase in brittleness nature of foamed concrete and some disadvantage such as poor deformability [3]. The decisive problems of foamed concrete become the vital problems when these contribute to reduction of the strength and then affected performance and durability of the concrete.

Therefore, improving ductility and brittleness of foamed concrete is the key point to make them suitable as structural material with an endeavor to seek a superior mechanical property of foamed concrete. The vast attractions on the production of structural foamed concrete in many applications have become awareness for concrete industry to implement to greener environment and sustainable construction. These have renewed the interest in using fibres as a reinforcement that possess greater mechanical properties in term of elasticity and compressive strength.

There is now ample evidence that the application of discrete fibre has been proposed by many researchers in enhancement of foamed concrete mechanical properties such as Bagherzadeh et al. [3], Boghossian and Wedger [4] and Jones and McCarthy [5]. Conversely, review on the works of Libre et al. [6] and Rashdi et al. [7] has revealed that addition of fibre did not significantly affect the mechanical properties of foamed concrete.

Nevertheless, in spite of advantages that have been reported in this area [3–5], much more research is still needed. This is especially so because of the diversity of fibre types and various level of density may be obtained by foamed concrete.

The effect of two different types of fibre reinforcement on foamed concrete is reported in this paper. There are polypropylene (PP) and kenaf fibre. The paper reports and discusses the different effect from those sample incorporation with synthetic and natural fibre and the effect of various level of density on the modulus of elasticity and compressive strength of foamed concrete.

2 Experimental Work

2.1 Preparation of Foamed Concrete Specimens

Five series of foamed concrete with density ranging from 1,000 to 1,800 kg/m³ were cast. There were 90 number of specimens, which consist of 45 cylinders (100Ø × 200) mm and 45 cubes (100 × 100 × 100) mm for modulus of elasticity

test and compressive strength test respectively. For each series, the specimens were adopted with three batches of different fibre content. In this work, two types of fibre have been cut into 15 mm length to be incorporated at level of 3 % (by volume) of kenaf fibre and polypropylene fibre. For each series, 2.0: 1.0 sand cement ratio and 0.5 of water content were integrated. The polypropylene fibre used in this research is monofilament type whereas kenaf fibre used is bast type and was obtained from Lembaga Tembakau Negara (LTN). The Ordinary Portland Cement (OPC), river sand, tap water and foaming agent of synthetic type based (Finefoam 707) were used to generate foamed concrete mix.

The cylinder $100\text{Ø} \times 200$ mm and cubes $100 \times 100 \times 100$ mm were prepared for three replicate test specimens for both modulus of elasticity test and compressive strength test. The specimens were demoulded after 48 h casting in order to ensure a sufficient hardening for handling. Then, all the test specimens were subjected to water cured for 28 days.

2.2 Testing Method

2.2.1 Compressive Strength Test

Foamed concrete with density ranging from 1,000 to 1,800 kg/m³ were cast in $100 \times 100 \times 100$ mm cubes. The cubes were conducted by using the compressive machine at the pace rates of 3.00 kN/s as recommended by BS 1881: Part 4: 1997. The stress readings were recorded and analyzed to determine the effect of additional fibres to the compressive strength at the age of 28 days.

2.2.2 Modulus of Elasticity Test

The modulus of elasticity test was performed at the age of 28 days according to ASTM C469-02. Two linear variable differential transformers were connected to a digital transducer and the data were fed into a data logger. The load was applied at constant rate within the range 35 ± 5 psi per second. The data from both linear variable differential transformers (LVDTs) were averaged and plotted as stress–strain relationship graph. To obtain the elastic zone, the data were recorded when the data points starting at strain value of 50 million, up to 40 % of the ultimate load.

3 Results and Discussions

The results of 28-day modulus of elasticity and compressive strength of foamed concrete are presented in Table 1 with respect to the specimen level of densities and fibre type of each series. The series consist of plain foamed concrete (NLWC),

Table 1 Results of modulus of elasticity and compressive strength

Density (kg/m ³)	Modulus of elasticity (GPa)			Compressive strength (MPa)		
	NLWC	LWCK	LWCP	NLWC	LWCK	LWCP
1,000	3.88	3.21	5.87	1.91	1.23	1.82
1,200	5.18	4.59	7.78	2.37	1.44	7.01
1,400	7.95	7.10	11.54	3.69	4.68	13.44
1,600	10.69	9.54	16.35	13.25	10.87	16.93
1,800	16.36	11.59	22.96	16.16	12.84	19.04

PP reinforced foamed concrete (LWCP) and kenaf reinforced foamed concrete (LWCK).

3.1 Effects of Various Level of Density to Modulus of Elasticity and Compressive Strength

To study the effect of various level of density on elastic modulus and compressive strength of foamed concrete, five series of specimens were performed ranging between 1,000 to 1,800 kg/m³ for group addition of polypropylene fibre (LWCP), kenaf fibre (LWCK) and plain foamed concrete (NLWC). Figures 1 and 2 presents the modulus of elasticity and compressive strength of the series of unreinforced, reinforced with polypropylene fibre and kenaf fibre.

Obviously, the elastic modulus of foamed concrete incorporated with polypropylene fibre (LWCP) uptakes proportionally with increment of foamed concrete density. However, the compressive strength values shown abruptly increased between 1,200 and 1,600 kg/m³.

On the other hand, for both specimens with kenaf fibre (LWCK) and plain foamed concrete (NLWC) clearly shown a symmetrical trend or achieved almost the same values up to 1,600 kg/m³. But there is an overlapping results of compressive strength between kenaf reinforced foamed concrete (LWCK) and plain foamed concrete (NLWC) at the density ranging between 1,200 and 1,400 kg/m³. Nevertheless, at the end as of 1,800 kg/m³ lightweight concrete filled with PP fibre (LWCP) gives the highest value for both elastic modulus and compressive strength.

From Figs. 1 and 2, it shows that the value of elastic modulus and compressive strength increasing as the density level was increased for all foamed concrete specimens. It was observed that PP reinforced foamed concrete (LWCP) with the highest density of 1,800 kg/m³ gives the maximum elastic modulus value of 22.96 GPa as compared to kenaf reinforced foamed concrete (LWCK) and plain foamed concrete (NLWC) which are 11.59 and 16.36 GPa, respectively. Same goes to compressive strength, the highest strength of 19.035 MPa was given by PP reinforced foamed concrete (LWCP), whereas, 12.838 and 16.157 MPa for kenaf

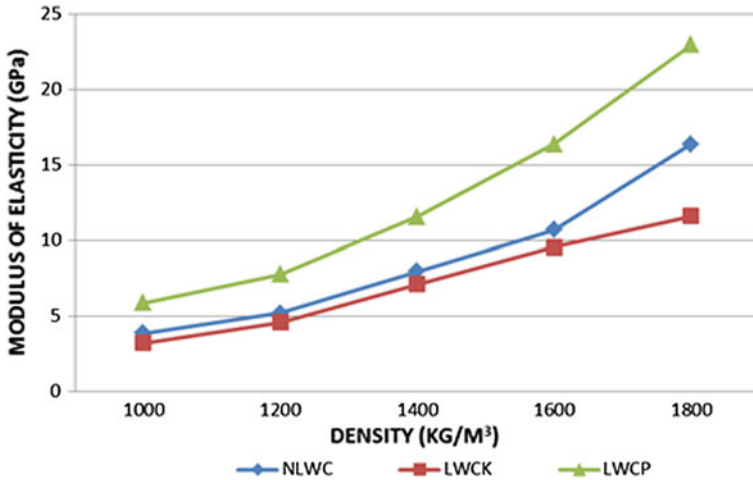


Fig. 1 Modulus of elasticity of lightweight concrete

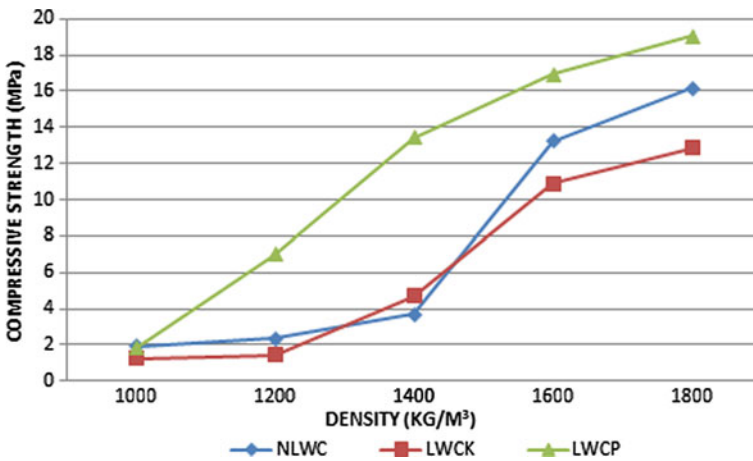


Fig. 2 Compressive strength of lightweight concrete

reinforced foamed concrete (LWCK) and plain foamed concrete (NLWC) respectively.

Owing to the high porosity, foamed concrete is more prone to deform. Apparently, the absence of coarse aggregate in foamed concrete leads to lower elasticity due to its lower density [5]. Consequently, this would affect the ductility of the foamed concrete and become more brittle [8]. Moreover, the size of voids in the foamed concrete will govern its compressive strength. The higher the compressive strength will indicate the lower void size. Foamed concrete which contain a lot of voids, the compressive strength will reduce according to the reduce of

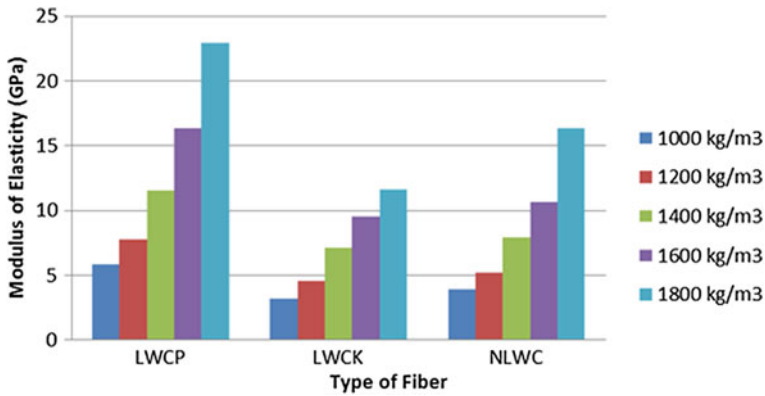


Fig. 3 Modulus of elasticity of lightweight concrete

density. This revealed that the elasticity and compressive strength of lightweight concrete is affected by the volumetric proportion of aggregate in the concrete in order to perform the stronger matrix bond [8].

3.2 Effects of Fiber Content

Foamed concrete is expected to manifest a low mechanical behaviour such as elastic modulus and compressive strength. In this work, two types of fibre were chosen which are polypropylene fibre (PP) and kenaf fibre to represent the enhancement in mechanical of different density of foamed concrete.

Results of elastic modulus and compressive strength of foamed concrete with different types of fibre were performed. The mean of elastic modulus and compressive strength from three identical specimens are expressed as depicted in Figs. 3 and 4 for group of five different levels of density of foamed concrete.

According to the results illustrated in Fig. 3, it can be seen that the modulus of elasticity for kenaf reinforced foamed concrete (LWCK) is lower than that of PP reinforced foamed concrete (LWCP) and plain foamed concrete (NLWC). This is predictable since the compressive strength as depicted in Fig. 4 also shows that kenaf reinforced foamed concrete (LWCK) records the lowest value as compared to the other two PP reinforced foamed concrete (LWCP) and plain foamed concrete (NLWC).

The elasticity and compressive strength increase as the density of foamed concrete increase. The foamed concrete specimens with addition of PP fibre (LWCP) attain the highest elasticity and compressive strength as compared to plain foamed concrete (NLWC). This proved that, inclusion of PP fibre in the foamed concrete mix improves the elastic modulus and compressive strength of the resulted foamed concrete. This finding is also in line with that reported by Jones and McCarthy [5].

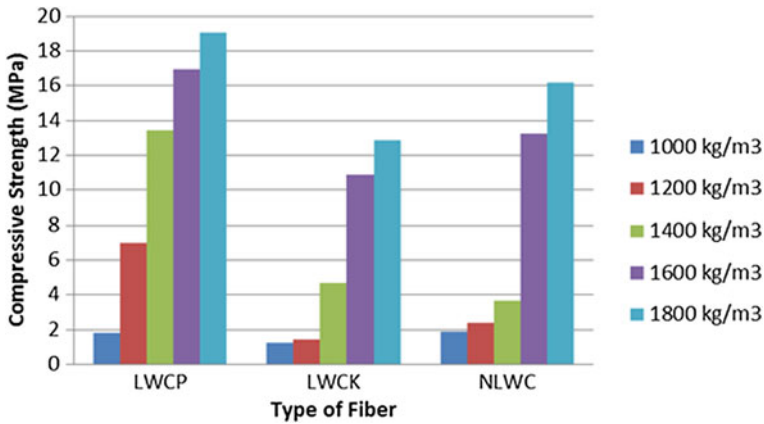


Fig. 4 Compressive strength of lightweight concrete

However, inclusion of kenaf fibre (LWCK) gives lesser impact to the modulus of elasticity and compressive strength of foamed concrete. In fact, the modulus of elasticity and compressive strength of kenaf reinforced foamed concrete (LWCK) is lower than those of plain foamed concrete (NLWC). This could be due to its high cellulose content that attribute to high absorption of moisture which negatively affects the mechanical properties of the resulted concrete [7]. High amount of absorbed water causes swelling of fibre. This could fill the gap between fibre and the matrix bond and eventually could lead to reduction in the elasticity and compressive strength [8].

These observations emphasize the importance of the matrix bond of foamed concrete to improve the performance of foamed concrete. The advantage that the polypropylene fibre contributes to the ductility of foamed concrete is obvious.

4 Conclusion

This study investigates the influence of incorporating fibre into the foamed concrete mix made of varies on the compressive strength and modulus of elasticity properties of the resulted foamed. The following conclusions can be drawn from the investigation:

1. Addition of polypropylene (PP) fibre appreciably increased the ductility and strength of foamed concrete. However, addition of kenaf fiber did not significantly enhance the modulus of elasticity and compressive strength. This could be due to kenaf high cellulose content that attribute to high absorption of moisture which affects these properties. Thus, polypropylene fibre (synthetic) contributes more to ductility and strength compared to kenaf fibre (natural) in this study.

2. Addition of polypropylene (PP) fibre (LWCP) to 1,800 kg/m³ density of foamed concrete caused a 40 % increase in modulus of elasticity and a 18 % increase in the compressive strength. However, kenaf reinforced foamed concrete (LWCK) at 1,800 kg/m³ density of foamed concrete caused a decrease in modulus of elasticity by about 29 % and decrease in compressive strength by about 21 %.
3. Modulus of elasticity and compressive strength of the foamed concrete increases as the density of foamed concrete increases. In other words, the elasticity and compressive strength of foamed concrete is affected by its density.

Acknowledgments This project was funded by Research Intensive Faculty grant [600-RMI/DANA5/3/RIF(889/2012)]. Special thanks to the Faculty of Civil Engineering UiTM Malaysia in providing the experimental facilities.

References

1. O. Kayali, M.N. Haque, B. Zhu, Drying shrinkage of fibre-reinforced lightweight aggregate concrete containing fly ash. *Cem. Concr. Res.* **29**, 1835–1840 (1999)
2. M. Gesoğlu, T. Özturan, E. Güneyisi, Effect cold-bonded fly ash aggregate properties on the shrinkage cracking of lightweight concretes. *Cem. Concr. Compos.* **28**, 598–605 (2006)
3. R. Bagherzadeh, H.R. Pakravan, A.-H. Sadeghi, M. Latifi, A.A. Merati, An investigation on adding polypropylene fibers to reinforce lightweight cement composites (LWC). *J. Eng. Fibers Fabrics* **7**(4), 13 (2012)
4. E. Boghossian, L.D. Wegner, Use of flax fibres to reduce plastic shrinkage in concrete. *Cem. Concr. Compos.* **30**, 929–937 (2008)
5. M.R. Jones, A. McCarthy, Preliminary views on the potential of foamed concrete as a structural material. *Mag. Concr. Res.* **57**(1), 21–31 (2005)
6. N.A. Libre, M. Shekarchi, M. Mahoutian, P. Soroushian, Mechanical properties of hybrid fiber reinforced lightweight aggregate concrete made with natural pumice. *Constr. Build. Mater.* **25**, 2458–2464 (2011)
7. A.A.A. Rashdi, S.M. Sapuan, M.M.H.M. Ahmad, A. Khalina, Combined effects of water absorption due to water immersion, soil buried and natural weather on mechanical properties of kenaf fibre unsaturated polyester composites (KFUPC). *Int. J. Mech. Mater. Eng. (IJMME)* **5**(1), 11–17 (2010)
8. A.M. Neville, *Properties of Concrete*, 4th edn. (Prentice Hall, Pearson, 1995)

Behavior of Reinforced Masonry Column Under Axial Loading Using Sand Quarry Dust Modular Unit

Zulhazmee Bakri, Zakiah Ahmad and Atikah Fatma Md Daud

Abstract Hollow sand cement block with quarry dust as sand replacement is an important addition to the types of masonry units available to the builder. Therefore this paper reports the investigation made on the column constructed using hollow quarry dust cement block (QUCB). The emphasis is given to study the crack patterns developed in the columns, the load carrying capacity of the block individually and when used in the masonry work. Two types of columns were prepared; short and tall column with and without reinforcement where tall column with size 260 mm (width) × 260 mm (length) × 3,190 mm (height) and 260 mm (width) × 260 mm (length) × 700 mm (height) for short column. The specimens were subjected to axial loads until failure. The results showed that the hollow quarry dust blocks have the potential to be used as construction structural elements.

Keywords Masonry · Hollow block · Reinforced column · Quarry dust · Compressive strength

1 Introduction

Masonry biggest application is in the main structures construction for a building like baffle wall, column, and so on. Masonry is widely used and started in the European countries and also some other developed countries [1]. In most cases the

Z. Bakri (✉) · Z. Ahmad

Faculty of Civil Engineering, Institute of Infrastructure Engineering and Sustainable Management (IIESM), Universiti Teknologi MARA, Shah Alam, Selangor, Malaysia

A. F. M. Daud

Department of Civil Engineering, Politeknik Sultan Salahuddin Abdul Aziz Shah, Shah Alam, Selangor, Malaysia

masonry is used purely as an infill wall. Although bricks belong to the conventional and traditional building materials, reinforced concrete frames are favored in construction industry nowadays.

Reinforced brick masonry consists of brick masonry which incorporates steel reinforcement embedded in mortar or grout. This masonry has greatly increased resistance to forces that produce tensile and shear stresses. The reinforcement provides additional tensile strength, allowing better use of brick masonry's inherent compressive strength. The two materials complement each other, resulting in an excellent structural material. The principles of reinforced brick masonry design are the same as those commonly accepted for reinforced concrete, and similar formulae are used.

The earliest method of placing reinforcement into brick masonry was simply to place iron or steel bars in mortar joints, as the bricks were laid. Later the reinforcement was placed in collar joints between two masonry wythes and surrounded by mortar or fine grout. Eventually the space between wythes was increased in width and filled with grout. The most recent means of constructing reinforced masonry incorporates hollow brick. These units are manufactured with large open cells which align vertically when the units are laid. Vertical reinforcement is placed in the cells by laying the brick over or around the bars, or by threading the bar in after the brick are laid.

There are various types of masonry unit on the market which are normally been used in some structural masonry construction. Those are stone, clay brick, concrete brick, concrete block, and calcium silicate brick [2]. Masonry hollow blocks are extremely versatile and durable. It offers cost effective and practical benefits for internal and external walls, column houses and industrial buildings. It is also has better substitute to work faster and faster to build a structure.

The current standard for designing masonry structure is for solid masonry. The Australian standard, AS 3700 Standards Australia 2001 [3] for structural masonry design, provides relatively simple unified design methodology for determining the design capacity of masonry elements based on empirical data and revisions of previous code provisions. The basic compression capacity of the section is determined from characteristic material strength and effective cross-sectional area. Member capacity is determined by applying a capacity reduction factor to the sectional resistance. Tabulated values of capacity reduction factor provided are a function of load eccentricities and member slenderness ratio. For other low strength compression materials, such as stone masonry, earth walls have historically been proportioned using simplified geometric rules of thumb. Therefore, Maniatidis and Walker [4] investigated the validity of using masonry design rules for the design of rammed earth structural elements under concentric and eccentric axial load. They found that the existing codes provided a good estimate on the structural capacity of rammed earth for small load eccentricities up to 10 %. Maroliya [5] compared the load carrying capacity of hollow concrete block masonry column and brick masonry column under axial load and found that the strength of column constructed with hollow concrete blocks gave less strength as compared to brick masonry. However the cost of column constructed with hollow

concrete blocks is very much less than that of brick masonry. Shah [6] studied the load carrying capacity, ductility and serviceability of unreinforced masonry columns with ferrocement by varying cement mortar thickness, gage-wire spacing and bond at the interface of ferrocement and brick columns and concluded that the reinforcement with ferrocement have very little benefit which is only on the reduction of cracks.

This study used new masonry product manufactured using quarry sand and supplied by ID Interlocking Brick Sdn Bhd. In order to use this block as a structural elements, there is a need to investigate the performance of the structural elements constructed using the quarry dust hollow block. Therefore, this study investigated the performance of reinforced masonry column when subjected to axial load.

2 Materials and Preparation of Samples

2.1 Quarry Dust Hollow Blocks

The quarry dust hollow blocks were supplied by ID Interlocking Bricks Sdn Bhd from Terengganu, Malaysia. The brick was manufactured using 1:5:5 (cement: sand: quarry dust). The size of hollow block is 190 mm (thick) \times 125 mm (length) \times 125 mm (width) as shown in Fig. 1.

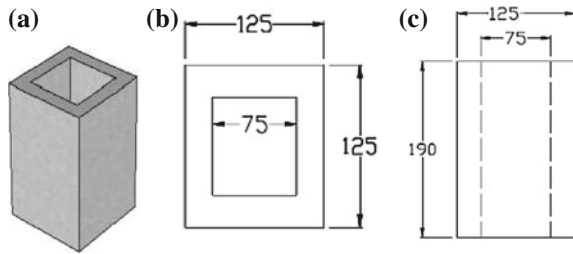
2.2 High Strength Mortar

The mortar is used for bonding blocks. This study used special high mortar strength called Emaco R1. The reason to use this special mortar is to expedite the curing process and also to achieve suggested strength of mortar (20 MPa) in 7 days. The mortar was prepared by adding the 0.2 L of water for 1 kg of EMACO R1. The mortar cubes of size 50 \times 50 \times 50 mm were prepared and subjected to compression test after 7 and 28 days.

2.3 Concrete

The concrete used to fill the hole was designed based on Grade 20 concrete. Concrete cubes of size 100 \times 100 \times 100 mm were casted and subjected to compression test after 7, 14 and 28 days.

Fig. 1 Hollow block; **a** schematic diagram, **b** top view and bottom view and **c** side view



2.4 Steel Reinforcement

The size of steel reinforcement used was estimated based on reinforced concrete design in accordance with BS5628 [7] for designing concrete column of cross-section 260×260 mm using formula as follows;

$$\frac{100A_s}{bd} \geq 0.4 \% \quad (1)$$

$$\frac{100A_s}{260 \times 260} \geq 0.4 \%$$

So, $A_s \geq 270 \text{ mm}^2$.

Hence provide 4T10 (314 mm^2) and hence A_s provided $\geq A_s$ required.

2.5 Columns Configurations with and Without Reinforcement

Two types of columns were constructed; short and tall columns.

1. Short column

The properties of masonry are influenced by the compressive strength and elastic modulus of bricks and mortar as well as other factors such as interfacial bond strength between brick and mortar, moisture in the brick at the time of laying, thickness of mortar joints, arrangement of bricks, workmanship etc. [8].

Compressive strength of masonry is an important characteristics used in the design of masonry structures. According to British standards (BS 5628: Part1: 1978) [7], the compressive strength of masonry can be determined from the unit strength method and prism test method. Therefore this study compared the compressive strength using unit strength method and prism method. The prisms or short columns were constructed with height (h) to thickness (t) ratio of 3.1 as recommended by the standard where height/thickness (h/t) ratio between 2 and 5 for determining the compressive strength of the masonry. Two types of short columns were prepared; with and without reinforcement.

Fig. 2 Detail cross section of a cluster of blocks

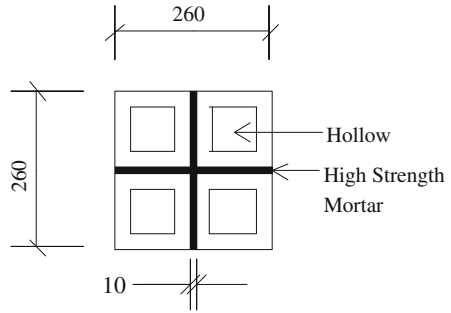


Fig. 3 Preparations from single to cluster four brick



Fig. 4 Construction of short column



The column was constructed using layers of a cluster of four blocks joined together using mortar of thickness 10 mm as shown in Figs. 2 and 3. Once the cluster was cured after 7 days, the cluster was stacked on top of each other using mortar as shown in Fig. 4. As for reinforced short column, the column was filled with concrete of Grade 20 and T10 reinforcement as shown in Fig. 5. Link was not used in this study to follow the similar conditions on site and as an Industrialised Building System (IBS). Three replicates were constructed for each column types.

Fig. 5 Detail cross section of brick column with reinforcement

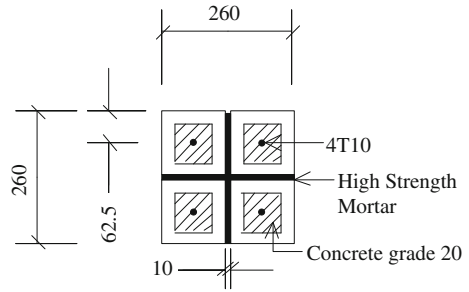


Fig. 6 Construction of tall column



2. Tall column

Two types of tall columns of size $260 \times 260 \times 3,190$ mm were constructed with and without reinforcement as shown in Fig. 6. Similar configuration as short column was used for the reinforcement and without reinforcement. Three replicates were constructed for each column types.

3 Test Methods

3.1 Compression Test

The compression test for mortar cubes, concrete cubes and columns were conducted based on BS5628-1:2005 [7].

The short and tall columns were tested using the Universal Testing Machine (UTM). For short column, Linear Variable Differential Transducers (LVDT) was placed at the mid-height as shown in Fig. 7 to measure the lateral displacement and for the vertical displacement; the measurement was recorded based on the in-built transducer.

Fig. 7 LVDT for short column



Fig. 8 LVDT for tall column



Figure 8 shows the test set-up for tall column. Six LVDTs were placed at the middle section of the column at two perpendicular faces to measure the lateral displacement in the x and y direction. One LVDT was placed at the top as shown in Fig. 9.

For tall columns, the displacements were also measured through three strain gauges placed at 1/3 height from top and bottom of the column and also at middle section of the column as shown in Fig. 9.

The preload was set manually at approximately 0.07 ton (0.7) kN. The samples were compresses until the point where the deflections increased dramatically with little or no increment in load.

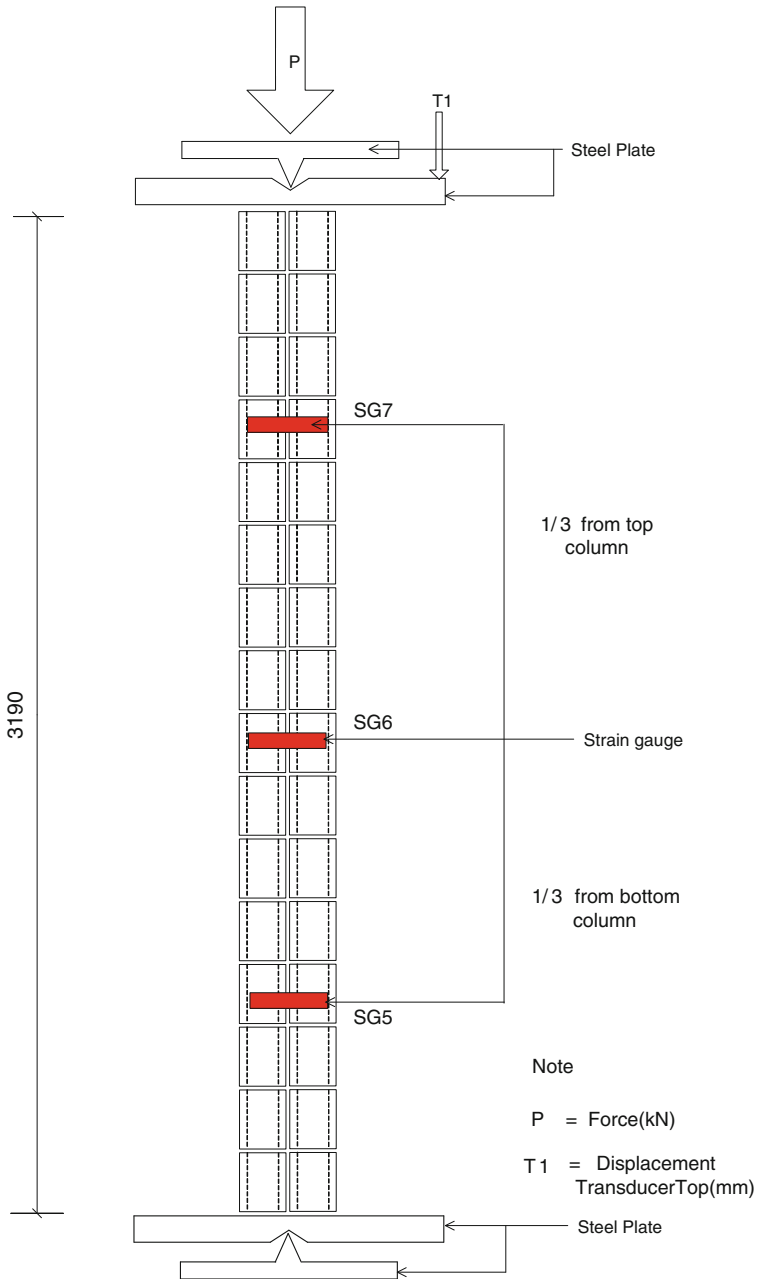


Fig. 9 Schematic drawing of the test set-up of tall column under compression

4 Results and Discussions

4.1 Compressive Strength of Mortar and Concrete

The compressive strength of mortar and blocks are tabulated in Table 1.

The compressive strength for mortar was found to be 30 N/mm^2 at 7 days and it is adequate for the minimum target which is 20 N/mm^2 at 28 days. Therefore, compression test for mortar was not conducted for 14 or 28 days because the required minimum strength has been achieved within 7 days.

From Table 1, it can be seen that the compressive strength of concrete at 28 days is about 20 N/mm^2 with averages density more than $2,400 \text{ kg/m}^3$ which is as per design.

The compressive strength of the hollow block is 4.9 N/mm^2 and is lower than the compressive strength of the mortar. This strength passed the minimum requirement for masonry (1.8 N/mm^2) in accordance with EN771-1-6 as well as specification given by Public Works Department, Malaysia which is 2.8 MPa for hollow blocks per 10 samples taken at random from the Contractor's stock pile of 1,000 or part thereof [9].

4.1.1 Short Column

The basic objective of present study is to know the load bearing capacity of the hollow blocks when used in the construction of columns and other such elements in any construction project. Beside this, the crack pattern at initial and final failure is also of importance.

Table 2 shows the compressive strength properties of short column under axial load. The compressive strength of reinforced column is 63 % higher than the compressive strength of column without reinforcement.

Figure 10 shows the load versus displacement curves for short column with and without reinforcement.

The curves display significant nonlinearity for both columns but the curve for reinforced column has bigger area under the curved compared to unreinforced column. This indicates that the reinforced column has the capability to absorb more energy before failure and able to sustain bigger load.

The significant contribution of the reinforcement can be seen after load reached about 100 kN. There is a sharp increase in strength for reinforced column but for unreinforced column, the strength was gradually reduced. From Table 2, it can also be seen that reinforced column failed at higher vertical and lateral displacement compared to displacement for unreinforced column. The presence of steel bar can be the mean reason for ductile behavior of this specimen.

Some of the failure patterns for unreinforced and reinforced columns are shown in Fig. 11a and b respectively.

Table 1 Compressive strength

Item	Days of curing	Density (kg/m ³)	Max load (kN)	Compressive strength (N/mm ²)
Mortar	7	1,814	74.8	29.9
Hollow block	>28 days	1,632.6	74.2	4.9
Concrete	7	2,431.3	89.6	19.9
	14	2,410.1	109.2	18.2
	28	2,425.6	115.0	20.1

Table 2 Compressive strength properties for short column with and without reinforcement

Column type	Maximum load (kN)	Max. lateral deflection (mm)	Max. axial displ. (mm)	Compr. strength (N/mm ²)
Without reinforcement	111	0.67	2.54	1.64
With reinforcement	300	1.05	11.38	4.44

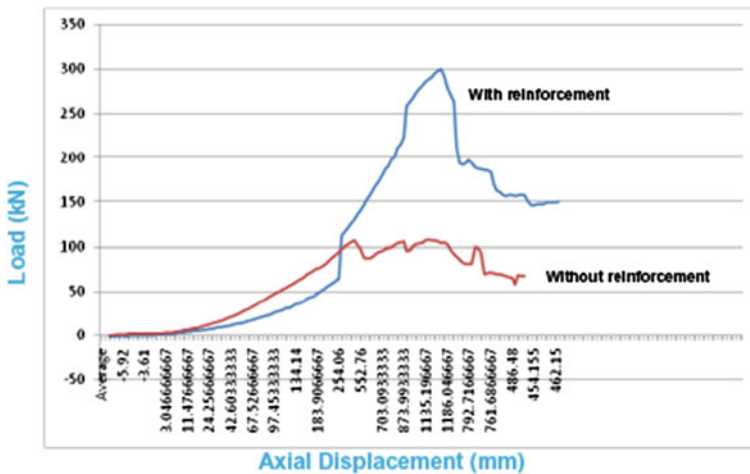


Fig. 10 Load versus displacement graphs for short columns

From Fig. 11, the unreinforced columns have more and bigger appearance of cracks and crushing modes compared to failed reinforced columns. This indicates that unreinforced column is more brittle than reinforced column. When observed closely on the failure modes, it can be seen that the failure in unreinforced column is initiated by the vertical crack in the block rather than splitting in the mortar which causing the masonry to fail together with the crushing of the blocks. This kind of failure mode is due to the block which is softer compared to mortar [10]. The block-mortar interface bond seems to remains intact. According to Matthana [11] when the brick is weaker than the mortar, the brick will be under triaxial compression and mortar will be under uniaxial compression and bilateral tension.

Fig. 11 Failure modes; **a** unreinforced column and **b** reinforced column

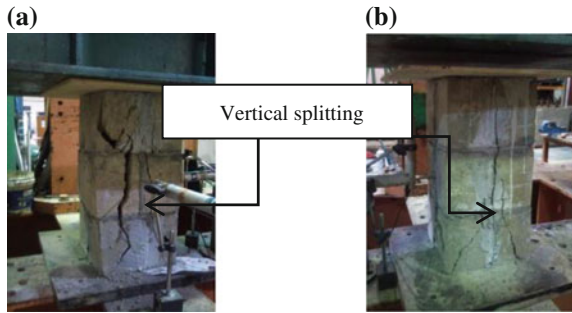
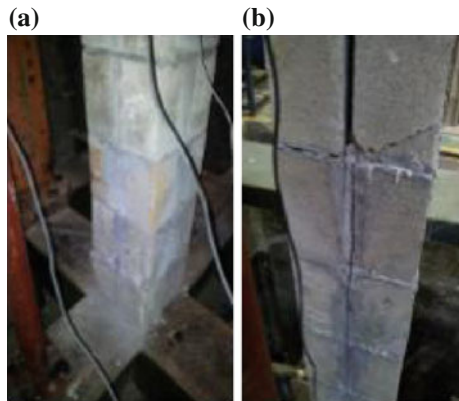


Fig. 12 Failure mode on C1; **a** at the *bottom* of the column and **b** at the *top* of the column



Under this scenario, the failure of masonry is initiated by tensile splitting. This stress will then extend to the brick below causing the masonry failure.

As for reinforced column, the failure mode is combination of vertical cracks in the blocks and shear cracks at the bottom block. As the bond strength is increased due to the infill concrete inside the hollow section failure of the masonry column takes place through the development of diagonal shear cracks [12].

4.1.2 Tall Column

Two columns denoted as C1 (reinforced column) and C2 (unreinforced column) were tested to failure. For C1, the failure started at the bottom of the column in the form of diagonal shear as shown in Fig. 12a and this is similar pattern as the failure mode on short reinforced column as seen in Fig. 12b. Later the partial disintegration of the block appeared at the top in the form of crushing and shearing in the block as well as splitting in the mortar joints which extended downward as shown Fig. 12b.



Fig. 13 Failure mode in column C2

Table 3 Compressive strength properties for short column with and without reinforcement

Column type	Maximum load (kN)	Max. lateral deflection (mm)	Max. axial displ. (mm)	Compr. strength (MPa)
Without reinforcement	3.86	5.7	370	0.60
With reinforcement	3.55	6.2	420	3.74

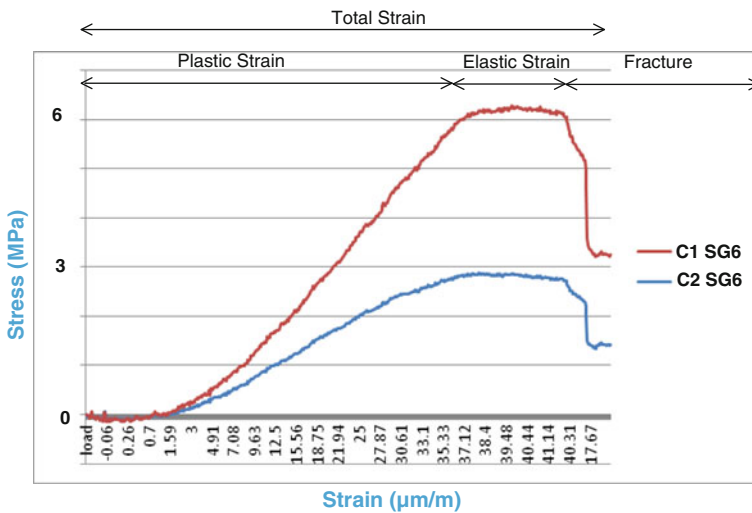


Fig. 14 Stress versus strain graphs for reinforced column (C1) and unreinforced column (C2) measured using strain gauges at the mid-height of tall column

In contrast, column C2, the failure started by crushing at the top of column accompanied by loud sound. Major splitting appeared in the block and extended down through the block and some parts of mortar joint as shown in Fig. 13.

Table 3 shows the compressive strength properties of tall column under axial load based on three replicates for each type of column. The compressive strength of reinforced column is 10 % higher than the compressive strength of column without reinforcement which is much lower differences than the short column.

Figure 14 shows the stress versus strain diagrams from one of the testes column for reinforced column C1 and unreinforced column C2 measured using strain gauges at the mid-height of the tall column. As shown in this diagram, the maximum stress for C1 is 6.2 MPa with a vertical shortening of 38 $\mu\text{m}/\text{m}$ and the maximum midpoint lateral displacement 3.74 mm measured by LVDT at the mid-height. The maximum compressive stress for C2 is 2.9 MPa which is 53.22 % lower than maximum compressive stress of C1. The vertical shortening for C2 is 25 $\mu\text{m}/\text{m}$ and midpoint lateral displacement of 0.60 mm and these values are lower than the values for C1.

The resulting stress–strain curve also provides a direct indication of the material properties. Both C1 and C2 columns are in elastic region until 33 $\mu\text{m}/\text{m}$ before entering on partially plastic and maintained in plastic region until 41 $\mu\text{m}/\text{m}$ before failure. Even though the elastic and plastic region of C1 and C2 is about the same, the compressive stress performance was different. The addition of reinforcement helps the column to be more ductile and achieve higher strength.

5 Conclusions and Recommendations

Two types of columns constructed using quarry dust blocks were investigated; unreinforced and reinforced column. The following conclusions were derived:

- (a) The compressive strength of hollow quarry dust block is 4.9 N/mm^2 and it passed the minimum requirement for masonry as specified by Public Works Department, Malaysia which is 2.8 MPa for hollow blocks.
- (b) The compressive strength of reinforced short column is 63 % higher than the compressive strength of unreinforced short column.
- (c) Unreinforced columns have more and bigger appearance of cracks and crushing modes compared to failed reinforced columns. This indicates that unreinforced column is more brittle than reinforced column.
- (d) The failure in unreinforced column is initiated by the vertical crack in the block rather than splitting in the mortar which causing the masonry to fail together with the crushing of the blocks. This kind of failure mode is due to the block which is softer compared to mortar.
- (e) The significant contribution of the reinforcement can be seen after load reached about 100 kN. There is a sharp increase in strength for reinforced column but for unreinforced column, the strength was gradually reduced.

- (f) The maximum stress for reinforced tall column is 6.2 MPa with a vertical shortening of 38 $\mu\text{m/m}$ and maximum midpoint lateral displacement of 3.74 mm.
- (g) The maximum compressive stress for unreinforced tall column is 2.9 MPa which is 53.22 % lower than maximum compressive stress of reinforced tall column. The vertical shortening for unreinforced column is 25 $\mu\text{m/m}$ and midpoint lateral displacement of 0.60 mm and these values are lower than the values for reinforced tall column.
- (h) The addition of reinforcement helps the column to be more ductile.

Acknowledgments The provision of quarry dust bricks by ID Interlocking Bricks Sdn Bhd is greatly acknowledged.

References

1. S. Somayaji, *Civil Engineering Materials*, 2nd edn. (Prentice Hall, Inc., Upper Saddle River, 2001)
2. D.F. Orchard, *Concrete Technology, Volume 2 Practice* (Wiley, New York, 1963)
3. Standards Australia. _2001_. "Masonry structures." Standard No. 3700, Sydney, Australia.
4. V. Maniatidis, P. Walker, Structural capacity of rammed earth in compression. *J. Mater. Civ. Eng.* **20**, 230–238 (2009)
5. M.K. Maroliya, Load carrying capacity of hollow concrete block masonry column. *IOSR J. Eng.* (IOSRJEN) **2**(10), 5–8 (2001)
6. A.A. Shah, Applications of ferrocement in strengthening of unreinforced masonry columns. *Int. J. Geol.* **5**, 21–27 (2011)
7. BS5628: 1 2005 - Code of Practice for Use of Masonry. Structural Use of Unreinforced Masonry.
8. A.W. Hendry, *Structural Masonry* (Macmillan Press, London, 1998)
9. MS 27:1971: Malaysian Standard: Specification of precast concrete block.
10. K.S. Gumaste, K.S. Nanjunda Rao, B.V. Venkatarama Reddy, K.S. Jagadish, Strength and elasticity of brick masonry prisms and wallettes under compression. *Mater. Struct.* **40**, 241–253 (2007)
11. M.H.S. Matthana, Strength of brick masonry and masonry walls with openings. PhD thesis, Department of Civil Engineering, Indian Institute of Science, Bangalore, India, 1996
12. G. Sarangapani, B.V. Venkatarama Reddy, K.S. Jagadish, Brick-mortar bond and masonry compressive strength. *J. Mater. Civil Eng. @ASCE*, **17**, 229–237 (2005)

Charpy's Impact Test on Co-cured In-line Joint Unidirectional Kenaf Fibre Reinforced Plastic Composite

Safarina Haslimawaty Hamdan, Anwar Zainal Abidin
and Zakiah Ahmad

Abstract Synthetic fibre reinforced polymer has gained popularity due to its good mechanical properties. Apart from synthetic fibre, natural fibre can also be used to reinforce polymer and should be encouraged due to its environment friendly nature, availability and biodegradability. Length of the natural fibre is based on the length of the plant itself and is limited (usually 5 ft) compared to synthetic fibre that can be manufactured to the desired length. Due to the limited length of natural fibre, overlapping joint can be an alternative method in order to produce a long natural fibre reinforced polymer composite. Unlike their synthetic reinforced plastic composite counterparts, the fracture behaviour of natural fiber reinforced plastic composite have hardly been investigated. Therefore this study investigated the effect of overlapping length on the impact toughness. A series of kenaf plastic composites were manufactured using treated and untreated fiber with different lengths of lap joints; 0, 10, 20, 30, 40 mm and a control specimen. Charp's impact tests were conducted on notched and unnotched samples. Based on the findings it can be concluded that the impact strength is proportionally increases with increasing length of the joint lapping of the kenaf. This indicates that joint lapping of kenaf fibre is stronger as the lapping length increases.

Keywords Kenaf • Fibre reinforced polymer • Impact • Strength • Charpy impact • Polymer • Epoxy

S. H. Hamdan (✉) • Z. Ahmad
Institute of Infrastructure Engineering and Sustainable Management, Universiti Teknologi
Mara, 40450 Shah Alam, Selangor, Malaysia
e-mail: rina_hamdan@yahoo.com; rina_hamdan@hotmail.com

A. Z. Abidin
Faculty of Civil Engineering, Universiti Teknologi Mara, 40450 Shah Alam, Selangor,
Malaysia

1 Introduction

Scientists and engineers in recent years have been attracted to natural fibre composite where preparation and evaluation of natural fibres have been made to identify any suitability for various applications [1]. This is due to their excellent specific mechanical properties, sustainability and low cost. Natural fibre composites are suitable for applications in the construction and automobile industry, for low cost sustainable housing and the interiors of automobiles [2]. The industrial use of plant fibres serves as an alternative source of income for farmers. In addition, natural fibres are an alternative to wood-based raw materials, reducing the depletion of rain forests.

The properties of natural fibres vary significantly depending on what part of a plant they are obtained from. Other factors such as age of plant [3] and growth conditions [4] also contribute to this variation in properties. Cellulosic fibres that are currently in use in the textile and composite manufacturing industry as raw materials can be classified into three main groups, related to the parts of the plants from which they are obtained. These are bast fibres (flax, hemp, jute and kenaf), leaf fibres (sisal, banana and palm), and seed fibres (cotton, coir and kapok). A lot of studies have been carried out on lignocellulosic composites using plant based natural fibres (from annual crops such as sisal, kenaf, hemp etc.) in combination with a resin matrix such as a thermosetting resin [5–7], thermoplastic resin [8], or biodegradable resin [9].

Composites containing unidirectional fibres are amongst the simplest form of composite materials and can have tensile strengths of up to 3 GPa [10] along the fibre axis. The suitability of natural fibres as reinforcement in polymeric matrix composites is highly dependent on their surface properties. The fibre surface is made up of a complex of diverse polymers consisting of cellulose, hemicellulose and lignin. Plant based natural fibres, have surfaces that contain impurities such as waxy residues [11] that affect their bonding with polymeric matrices. To enhance the bond strength, it is therefore necessary to apply some form of treatment to the surface to either change it physically or chemically. Bisanda [12], reported on the effect of treating sisal fibre bundles using 0.5 N NaOH on the wetting ability and coherence of sisal-epoxy composites. The composites were more rigid and denser due to their lower porosity. The compressive strength and water resistance of the composites was also improved following alkali treatment of the sisal fibre bundles. Towo and Ansell [13] investigated the effect of treatment of sisal fibre bundles with alkali solution on the mechanical properties of sisal fibre reinforced plastic composite using polyester and epoxy resin. He found that there is an increase in stiffness of composites with treated fibre but results in lower impact strength.

Application of natural fibre such as kenaf (*Hibiscus Cannabinus L*) in fibre-based composites no doubt will add some value towards the industrial applications [14] since kenaf fibre has tensile strength and modulus of 11.9 and 60 GPa, respectively [15]. Most of the studies on kenaf fibre composites have concentrated on static mechanical properties rather than impact. The composites also were made

of short distributed fibres rather than unidirectional fibres. For long unidirectional fibre composite, the fibres need to be jointed. For these materials to be effectively used in engineering applications, their behaviour in impact is of considerable interest.

Therefore this study investigated the impact strength of the unidirectional kenaf fibre composite with jointed fibres.

2 Sample Preparation and Test Methods

2.1 Preparation of Fibre

Kenaf fibres were obtained from Lembaga Kenaf dan Tembakau Malaysia located in Kelantan. The fibres were first undergone surface treatment. Two types of fibres were prepared; treated and untreated fibres. For treated fibre, the fibres were soaked in distilled water for approximately 3 h to clean and remove impurities on their surface and placed between tissue paper overnight to remove excess moisture followed by further drying in an air-circulating oven overnight at 80 °C. The fibres were immersed in a 0.06 M sodium hydroxide solution for 48 h and later rinsed in distilled water [6]. Excess NaOH was neutralized by soaking in dilute acetic acid (1 %) for 5 min followed by rinsing with distilled water three times. Litmus paper was used to verify that all the acid had been washed out of the fibres. The fibres were dried at room temperature between layers of tissue for 2 days, before further drying in an oven at 80 °C overnight.

2.2 Preparation of Kenaf Plastic Composite

The kenaf fibres were then cut to the desired lengths based on the joint lapping lengths required as shown in Fig. 1 where x varies for control, 0 mm (butt joint), 10, 20, 30 and 40 mm to fit the mould of length 250 mm.

These fibres were combed to remove residues and to align the fibres. Specific weights of the fibre bundles have been used for determining the amount of fibre required for each composite. To enable good penetration of resin, the fibres were divided into several bundles of approximately equal weight. The fibres were divided into equal proportion.

The resin used is epoxy resin which was supplied by ASACHEM (M) SDN BHD, Malaysia. Specimens of Kenaf fibre reinforced polymer (KFRP) were prepared by mixing kenaf fibres and epoxy resin in a 7:3 ratio.

The mix design of the composite is shown in Table 1. The resin came in two parts; the base resin and the hardener, Asasin 8505 A and Asahard 8505 B

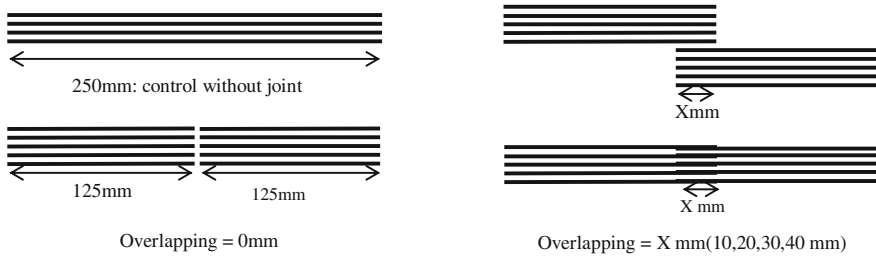


Fig. 1 Schematic diagram of joint and overlapping length of the joint

Table 1 Mix design of the composite

Item	Kenaf	Epoxy resin
Fraction (%)	70	30
Volume	250 mm × 20 mm × 4 mm = 20,000 mm ³	
Density (g/cm ³)	1.2	0.001067
Weight	70/100 × 20,000 mm ³ × 1.2 g/cm ³ = 16.8 g	30/100 × 20,000 mm ³ × 0.001067 g/cm ³ = 6.40 g

respectively. The designed proportion of part A and B was mixed together and stirred thoroughly until uniform mixture was obtained (about 5–6 min).

Figure 2 shows the mould used in the manufacturing and it was made from stainless steel. It is rigid enough to prevent distortion and constructed in such a manner as to facilitate the removal of the moulded specimens without damage. The mould was cleaned and coated with release agent, Freekote.

The first layer bundle was first placed inside the mould then the epoxy resin was poured in zig-zag patterns over the kenaf fibre bundle and then a second layer was placed inside the mould followed by the resin and the process was repeated until all the fibres have been placed. Zig-zag pattern ensures an even distribution of epoxy resin on the kenaf fibres [16]. A total of seven layers of kenaf fibres were applied for a single specimen having a total of fourteen bundles of kenaf fibres all together. To avoid loss of the resin, the mould was rested between the platens for about 5 min for the resin to pre-cure (harden a little bit). Then the mould was pressed at 60 bar for 24 h. Figure 2 shows the process flow in the manufacturing of the composite. The specimens prepared were plate of size 250 mm × 20 mm × 4 mm (length, width and thickness respectively). Figure 3 shows the close-up of the overlapping samples being prepared.

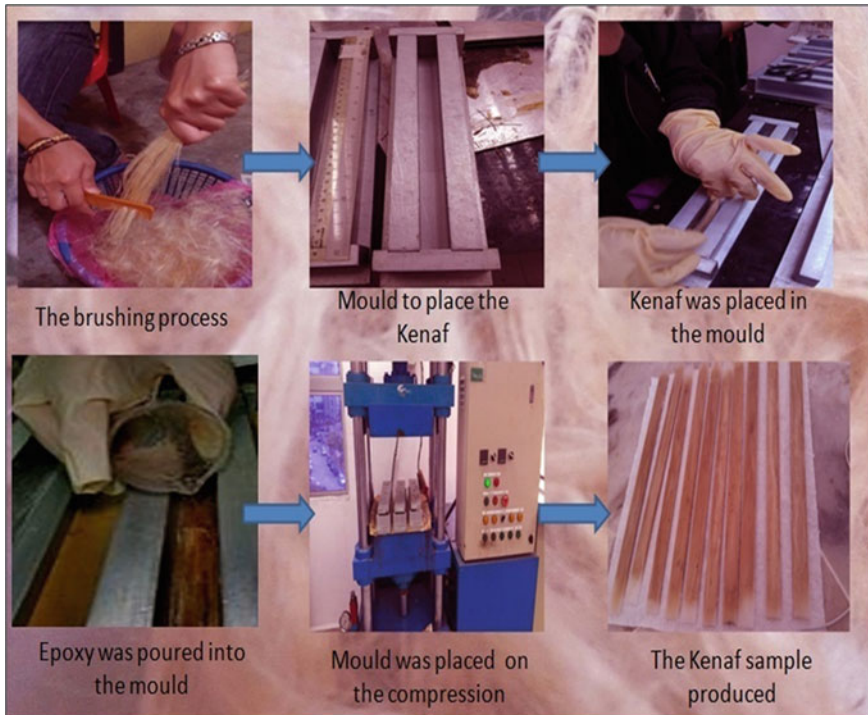


Fig. 2 Process flow of the manufacturing of the composite

2.3 Charpy's Impact test

The impact specimens were prepared with size 127 mm × 12.70 mm × 4 mm. Two types of specimens were prepared, notched and unnotched. The Charpy impact specimens were cut from the sheet in accordance with ASTM D6110. Figure 4a and b shows the dimensions of the specimens both for unnotched and notched specimens respectively. For notched specimens, the notch was machined using milling machine.

Impact energy is a measure of the work done to fracture a test specimen. The impact strength of the composites was determined using the edge-wise Charpy impact test according to ASTM D6110-10 (Fig. 5) using a 10.34 J pendulum. When the striker impacts the specimen, the specimen will absorb energy until it yields. At this point, the specimen will begin to undergo plastic deformation at the notch. The test specimen continues to absorb energy and work hardens at the plastic zone at the notch. When the specimen can absorb no more energy, fracture occurs.

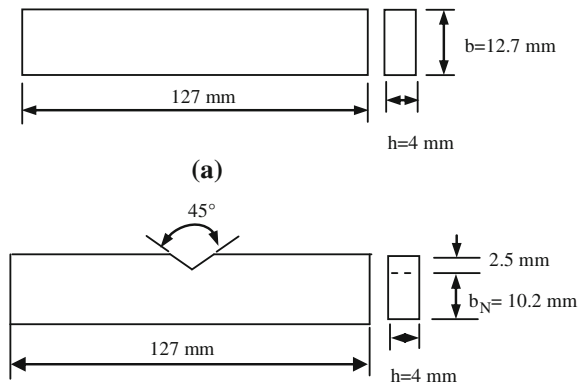
Specimens were manufactured according to method BS 3518-1, 1993 which is ideal for studying surface effects and materials exhibiting inter-laminar fractures.

The Charpy impact strength, for unnotched sample, a_{cU} , was determined using Eq. (1).



Fig. 3 Close-up view jointed fiber during manufacturing process

Fig. 4 Geometry and dimensions of the Charpy impact specimen, a unnotched specimen and b notched specimen



$$a_{cU} = \frac{w}{hb} \text{ (J/m}^2\text{)} \tag{1}$$

where W is the corrected energy, in Joules, absorbed by breaking the test specimen, h is the thickness, in millimetres, of the test specimen and b is the width, in millimetres, of the test specimen.

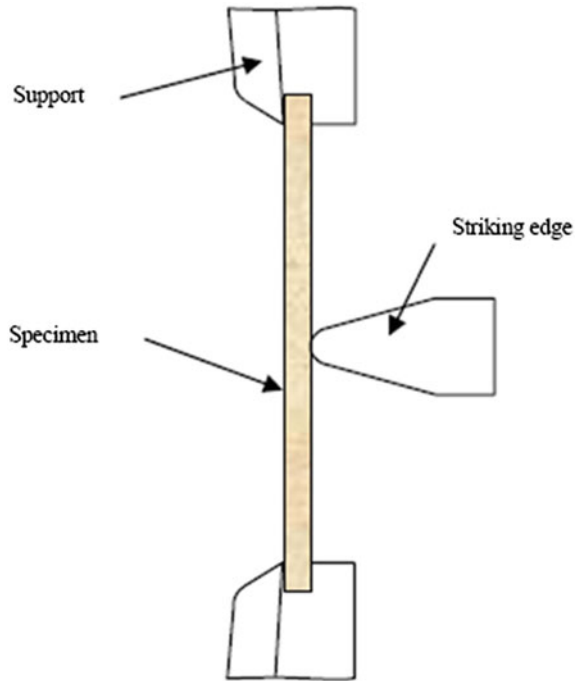
For the notched samples the a_{cN} was calculated using the following equation;

$$a_{cN} = \frac{W}{h \cdot b_N} \times 10^3 \text{ (J/m}^2\text{)} \tag{2}$$

where b_N is the remaining width (mm), at the notch base of the test specimen.

Five specimens were used for each composite type for determining the impact strength/toughness of the composites.

Fig. 5 Striking edge and support blocks for flatwise Charpy's impact test (plan view)



3 Results and Discussion

3.1 Toughness of Kenaf Fibre Reinforced Polymer

Figure 6 shows the summary of the impact strength of KFRP with different overlapping length, notched and unnotched as well as treated and untreated fibre.

In general, as the overlapping length increases the impact strength increases and the impact strength of KFRP with treated fibre is higher than composite with untreated fibre. The detail comparison is explained in next sections.

3.2 Toughness for Untreated Kenaf Fibre Reinforced Polymer

Table 2 tabulated the Charpy impact properties of the KFRP for the notched and unnotched samples together with standard deviation values. Five specimens were tested for each composite.

An analysis of variance (ANOVA) at 0.05 % probability was performed for the impact energy of composite. The ANOVA revealed that there is highly significant

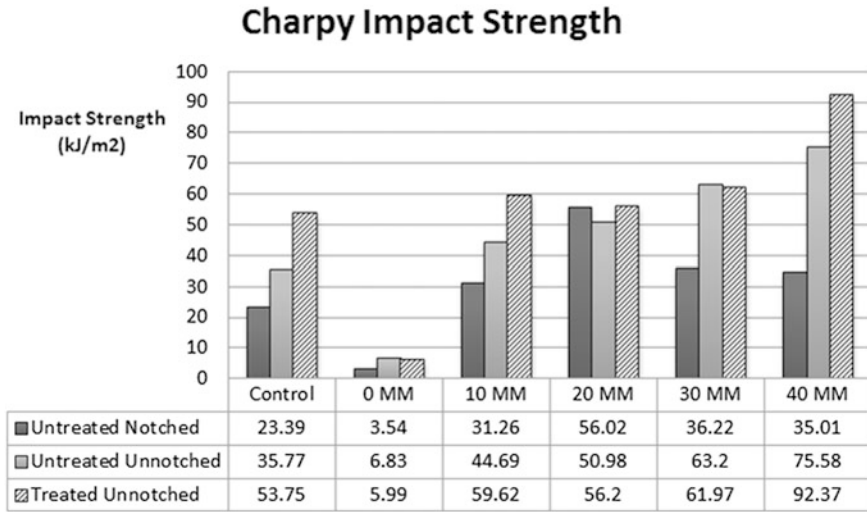


Fig. 6 Impact strength of all composites tested

Table 2 Impact energy of kenaf fibre reinforced composite with different overlapping length

Specimen	Untreated unnotched Impact strength (kJ/m ²)	Untreated notched Impact strength (kJ/m ²)	Treated unnotched Impact strength (kJ/m ²)
Control	35.77 (8.7) ^a	23.39 (9.64)	53.75 (4.3)
0 mm	6.83 (2.5)	3.54 (2.8)	5.99 (3.4)
10 mm	44.69 (21.4)	31.26 (13.5)	59.62 (12.7)
20 mm	50.98 (6.3)	56.02 (22.3)	56.20 (15.53)
30 mm	63.20 (8.7)	36.22 (7.7)	61.97 (22.4)
40 mm	75.58 (18.8)	35.01 (13.3)	92.37 (42.0)

^a Value in the bracket is the standard deviation

difference in the impact energy of unnotched specimens for all of the composites ($p = 0.000$).

For untreated and unnotched samples, the impact strength of KFRP composites increases as the overlapping length increases and the impact energy is higher than control specimens. At the overlapping section, the density is higher therefore more energy is required to initiate the cracks. At high strain rates, the crack initiation rate is faster than the surface crack opening rate, so the high volume fraction of fibre higher energy is required to initiate cracks and to subsequently propagate them and this accounts for the higher impact energy.

For notched specimens, there was significant difference in the impact energy for all overlapping lengths. The impact energy of butt joint (0 mm overlapping length) of notched specimens is the weakest as expected since at that section only resin that bonds the two sections together. A similar result was found for unnotched samples. The impact strength for notched samples were not in the same trend as

unnotched samples where the impact strength increases with overlapping length up to 20 mm length and as the overlapping length increases further the impact strength decreases. This may be due to weak fibre/matrix adhesion. According to Hojo et al. [17], for a given volume fraction of filler, the fracture strength composite was decreased as the average size of the filler increased. The impact strength of notched sample with 20 mm overlapping length is 10 % higher than control notched samples but this may be due to high variation in the samples since the standard deviation is highest, 22.3 % compared to other samples.

In general, the impact strength of notched samples is lower than the unnotched samples. The impact strength of control unnotched sample is 34.6 % higher than the impact strength of notched samples. This means that the composite specimens exhibit a ductile mode of failure and possess high impact strength when unnotched but undergo a transition to brittle fracture, accompanied by low impact energy, when notched. This behaviour arises from a locally high triaxial stress concentration at the notched tip which induces an increased rate of strain at the notched tip [18]. By applying the Vincent notch sensitivity criterion, the kenaf plastic polymer composite can be characterized as materials that are ductile in an unnotched state and brittle when a notch is introduced (notch brittle) [19].

3.3 Toughness for Treated Kenaf Fibre Reinforced Polymer

Table 2 also shows the summary statistics for experimental Charpy impact tests on unnotched and notched samples with treated and untreated kenaf fibre.

A paired *t*-test was performed to evaluate whether there is a significant difference in the impact energy of the unnotched KFRP with untreated and treated fibres. There were significant improvement in the impact energy for the KFRP and the impact energies for control samples increased by 33.5 %.

It can be clearly seen that KFRP using treated kenaf fibres yields the highest strength compared to KFRP with untreated fibres. This is due to surface treatment which provides better bonding between the matrix and kenaf fibres. This further reinforces the finding that treatment results in an increase in bond strength which creates stiffer composite. Results also indicate that as length of the lapping joint increases, the impact strength also increases. For the case of treated unnotched specimen, the 10 mm lapping joint recorded slightly higher impact strength compared to 20 mm lapping length. This is probably due to non-uniform specimen size during molding process.

The fibres for both untreated and treated fibre composites suffered tensile failure as shown in Fig. 7a and b respectively.

There is visible evidence of fibre pull-out from both untreated and treated fibre-epoxy resin composites but the pull-out fibres is more in untreated—epoxy resin composites (Fig. 7a). This presents further evidence of the improved bonding in sisal fibre bundle composites when epoxy resin is used. The increased bond strength is evident from the extent of damage observed on the fibre surfaces of

Fig. 7 Scanning electron microscopy of KFRP composite failed samples with; **a** untreated fibre, 70 \times and **b** treated fibre, 300 \times magnification

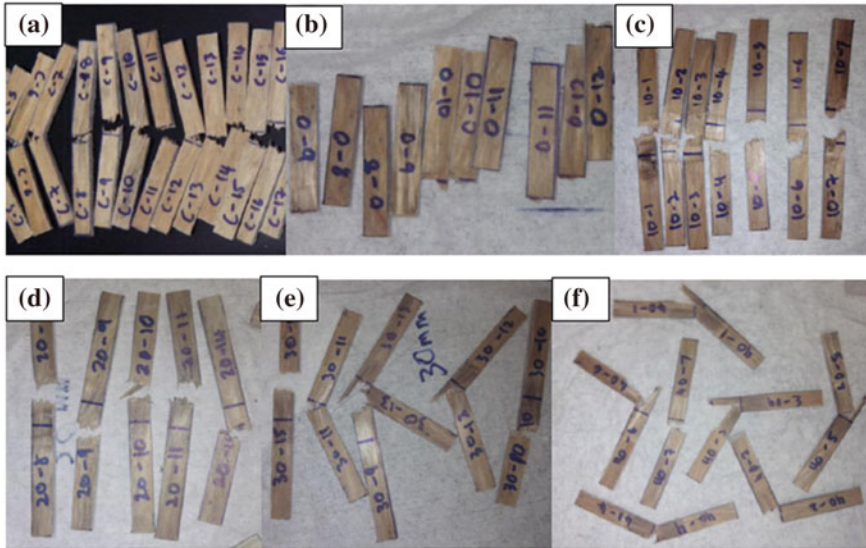
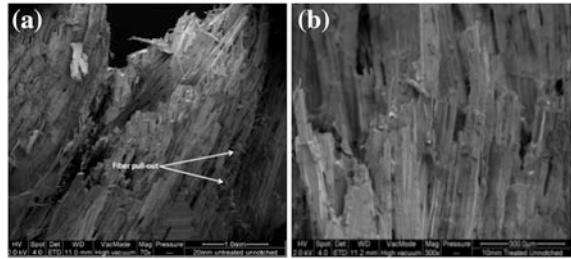


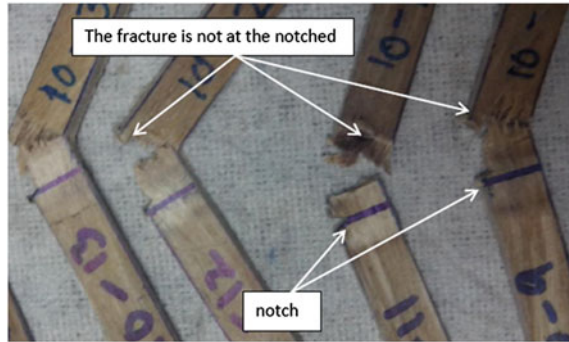
Fig. 8 Failure modes of KFRP's unnotched impact specimens with different overlapping length; **a** control, **b** 0 mm, **c** 10 mm, **d** 20 mm, **e** 30 mm and **f** 40 mm

both the untreated and treated fibre composites. Epoxy resin forms strong bonds with lignocellulosic fibres due to the formation of hydrogen bonds with hydroxyl groups on the fibre surface.

3.4 Failure Modes

Following Charpy impact the failure mode of the untreated unnotched KFRP composites (Fig. 8) were analysed. From Fig. 8a, b the failure mode of KFRP with 0 mm overlapping have smooth fracture surface compared to control with more zig-zags pattern which indicates very brittle failure and this is reflected by the low impact energy (Table 2). Similar characteristics were found for notched samples.

Fig. 9 Failure modes of KFRP's notched impact specimens showing the breaking not through the notched point



The weak internal bond allows debonding of fibres within the matrix resulting in shear movement between fibre and matrix. The frictional force resulting from the movement of fibres within the composite makes it behave less ductile material, hence the lower impact energy. As the overlapping length increases, the failure modes changes as seen in Fig. 8 from rather smooth fracture surface (Fig. 8b, c) to delamination and fibre pull out followed by tensile failure (Fig. 8d, e, f). The denser section of the longer overlapping length increase the resistance to fracture but the weak internal bond allows debonding of fibres within the matrix resulting in shear movement between fibre and matrix. The frictional force resulting from the movement of fibres within the composite makes it behave like a ductile material, hence the higher impact energy. A similar observation was made by Pavithran et al. [20] on untreated sisal-polyester composites.

Similar characteristics and behavior was found on notched untreated samples where the longer the overlapping length the less brittle modes can be seen. However the fracture was not through the notched but the samples failed outside the overlapping area as shown in Fig. 9 which is the less dense area and this may have caused the lower in the impact energy compared to unnotched samples as shown in Table 2.

4 Conclusion

The impact strength of kenaf fibre reinforced polymer composites was investigated and the conclusion is as follows;

- For untreated unnotched samples, the impact strength of KFRP composites increases as the overlapping length increases and the impact energy is higher than impact strength of control samples.
- In general, the impact strength of notched samples are lower than the unnotched samples. The impact strength of control unnotched sample is 34.6 % higher than the impact strength of control notched samples.

- For control treated unnotched samples, the impact strength of KFRP composites is 33.5 % higher than control untreated samples due to the improved bonding due to fibre surface treatment with alkali solution.

Acknowledgments This research was financially supported by the Fundamental Research Grant Scheme, Ministry of Higher Education Malaysia (600-RMI/ST/FRGS 5/3/Fst (6/2011) and Universiti Teknologi Mara is greatly acknowledged. The authors wish to thank the technical staff in the Composite Laboratory, Faculty of Mechanical Engineering and students from the Faculty of Civil Engineering for their assistance and support. Thanks are also extended to the Final Year Students who helped during the manufacturing of samples.

References

1. H. Anuar, N.A. Hassan, F. Mohd Fauzey, Compatibilized PP/EPDM-Kenaf fibre composite using melt blending method. *Adv. Mater. Res.* **264**, 743–747 (2011)
2. M.A. Hud, L.T. Drzal, A.K. Mohanty, M. Misra, Chopped glass and recycle newspaper as reinforcement fibers in injection moulded poly (lactic acid)(PLA) composite: a comparative study. *Compos. Sci. Technol.* **66**, 1813–1824 (2006)
3. N. Chand, S.A.R. Hashmi, Mechanical-properties of sisal fiber at elevated temperatures. *J. Mater. Sci.* **28**(24), 6724–6728 (1993)
4. B.C. Barkakaty, Some structural aspects of sisal fibers. *J. Appl. Polym. Sci.* **20**(11), 2921–2940 (1976)
5. E.T.N. Bisanda, M.P. Ansell, The effect of silane treatment on the mechanical and physical-properties of sisal-epoxy composites. *Compos. Sci. Technol.* **41**(2), 165–178 (1991)
6. L.Y. Mwaikambo, M.P. Ansell, Hemp fibre reinforced cashew nut shell liquid composites. *Compos. Sci. Technol.* **63**(9), 1297–1305 (2003)
7. S.H. Aziz, M.P. Ansell, The effect of alkalization and fibre alignment on the mechanical and thermal properties of kenaf and hemp bast fibre composites: part 1—polyester resin matrix. *Compos. Sci. Technol.* **64**(9), 1219–1230 (2004)
8. A.R. Sanadi, Renewable agricultural fibers as reinforcing fillers in plastics: mechanical properties of kenaf fiber-polypropylene composites. *Ind. Eng. Chem. Res.* **34**(5), 1889 (1995)
9. K. Oksman, M. Skrifvars, J.F. Selin, Natural fibres as reinforcement in polylactic acid (PLA) composites. *Compos. Sci. Technol.* **63**(9), 1317–1324 (2003)
10. P.T. Curtis, The fatigue behaviour of fibrous composite-materials. *J. Strain Anal. Eng. Des.* **24**(4), 235–244 (1989)
11. L. Mwaikambo, Plant-based resources for sustainable composites. Ph.D., University of Bath, 2002
12. E.T.N. Bisanda, The effect of alkali treatment on the adhesion characteristics of sisal fibres. *Appl. Compos. Mater.* **7**(5–6), 331–339 (2002)
13. A.N. Towo, M.P. Ansell, Weibull analysis of interfacial adhesion between thermosetting resin and sisal fibres using the droplet pull-out test, in *Proceedings of the Third International Workshop on Green Composites (IWGC-3)*, pp. 190–194, 16–17 March 2005, Kyoto, Japan
14. S.H. Aziz, M.P. Ansell, S.J. Clarke, S.R. Panteny, Modified polyester resins for natural fibre composites. *Compos. Sci. Technol.* **65**, 525–535 (2006)
15. R.M. Rowell, A. Sanadi, R. Jacobson, D. Caulfield, Properties of Kenaf/Polypropylene Composites. *Kenaf Properties, Processing and Products (Ag & Bio Engineering, Mississippi, 1999)*
16. S.H. Aziz, M.P. Ansell, S.J. Clarke, S.R. Panteny, Modified polyester resins for natural fibre composites. *Compos. Sci. Technol.* **65**, 525–535 (2006)

17. H. Hojo, W. Toyoshima, M. Tamura, N. Kawamura, Short and long-term strength characteristics of particulate-filled cast epoxy. *Polym. Eng. Sci.* **14**(9), 1604–1609 (1974)
18. A.J. Kinloch, R.J. Young, *Fracture behaviour of polymers*, Applied Science, London 421–471 (1983)
19. I.M. Ward, D.W. Hadley, *An Introduction to the Mechanical Properties of Solid Polymer* (Wiley, New York, 1993)
20. C. Pavithran, P.S. Mukherjee, M. Brahmakumar, A.D. Damodaran, Impact properties of natural fibre composites. *J. Mater. Sci. Lett.* **6**(8), 882–884 (1987)

Active Fatigue Crack Detection and Classification of Reinforced Concrete Beams Using Acoustic Emission

Noorsuhada Md Nor, Azmi Ibrahim, Norazura Muhamad Bunnori, Hamidah Mohd Saman, Soffian Noor Mat Saliah and Shahiron Shahidan

Abstract Active crack due to fatigue loading in reinforced concrete beams is a crucial phenomenon and need to be classified. Twelve beams were tested under three point loading with various fatigue loading in conjunction with acoustic emission monitoring. A total of six phases of fatigue maximum loading were performed on the reinforced concrete beams with frequency of 1 Hz, sinusoidal wave and 5,000 cycles for each phase. Two indices of qualitative analysis of acoustic emission signal such as RA value and average frequency were determined to classify the crack of the reinforced concrete beams subjected to the fatigue loading. The relationship of these two indices showed promising results corresponding to the development of active crack in the reinforced concrete beams as the maximum fatigue load increased.

Keywords Acoustic emission · RA value · Average frequency · Reinforced concrete · Fatigue loading

N. Md Nor (✉) · S. N. Mat Saliah
Faculty of Civil Engineering, Universiti Teknologi MARA, 13500 Permatang Pauh,
Pulau Pinang, Malaysia
e-mail: idanur211@gmail.com, idanur211@ppinang.uitm.edu.my

A. Ibrahim · H. Mohd Saman
Faculty of Civil Engineering, Universiti Teknologi MARA, 40450 Shah Alam, Selangor,
Malaysia

N. Muhamad Bunnori · S. Shahidan
School of Civil Engineering, Engineering Campus Universiti Sains Malaysia, Seri
Ampangan, Seberang Perai Selatan 14300 Nibong Tebal, Pulau Pinang, Malaysia

1 Introduction

Reinforced concrete (RC) structure has been used widely in civil engineering construction such as bridges, dams and buildings. These structures are exposed to fatigue loading during services. Fatigue is a process where the cracks developed slowly in the structures at initiation stage towards to the failure stage. Assessment of the fatigue crack progression in the RC structure is significantly important. The assessment is required in order to detect the incoming cracks in the structure before it is getting worse and becoming dangerous. Early assessment of the RC structure would be advantage as cost repair will be less and the service life of the structure could be prolonged. The cracks need to be classified therefore the behavior of the crack and the damage level can be identified. The crack can be assessed using acoustic emission (AE) technique. AE is defined as the class of phenomena whereby transient elastic waves are generated by rapid release of energy from localized sources within a material [1]. It is a useful technique to investigate local damage on RC structures in real time by using AE transducers. The cracks can be detected and monitored using transducer that coupled on the RC surface.

In crack classification a qualitative of AE parameter analysis is always utilised. Typical AE parameters are counts, amplitude, rise time and duration. Counts are the number of times of AE signal crossing a pre-set threshold level. Amplitude is the maximum positive or negative signal excursion during a hit. Rise time is a time interval between the first hit above threshold level and the peak amplitude. Duration is the time interval from the first signal threshold crossing to the end of threshold crossing. However, for crack classification of tensile crack and shear crack, relationship of two indices of RA value (rise time/amplitude) and average frequency (counts/duration) have been extensively applied by many researchers [2–8]. Figure 1 shows a typical relationship between average frequency and RA value and its association with tensile and shear crack modes. Tensile crack exhibits the opposing movement of the crack sides and produce short rise time and high frequency while shear crack produces lower frequency and longer rise time [4].

Relationship of average frequency and RA value has also been recommended by RILEM technical committee for classification of active cracks in concrete structures using relationship of these two indices [7]. The use of RA value and average frequency has been applied by many other researchers [2, 4, 5, 8–19]. For instance, crack classification of recycling concrete made of recycled aggregate under cyclic loading has been investigated by Watanabe et al. [8]. They found that the nucleation of tensile and shear cracks in recycling concrete is different from that of normal concrete. The changing of tensile crack and shear crack on RC beam under monotonic test has also been explored by Ohno and Ohtsu [20]. The discrimination of crack modes of cementitious material has been studied by Aggelis et al. [2–4] and found that these two indices exhibit strong sensitivity to the fracture mode. The classification of different crack types due to corrosion of prestressed concrete structure exposed to specific zones has been reported by Elfergani et al. [5]. Most of the researches are based on the analysis of AE signal at

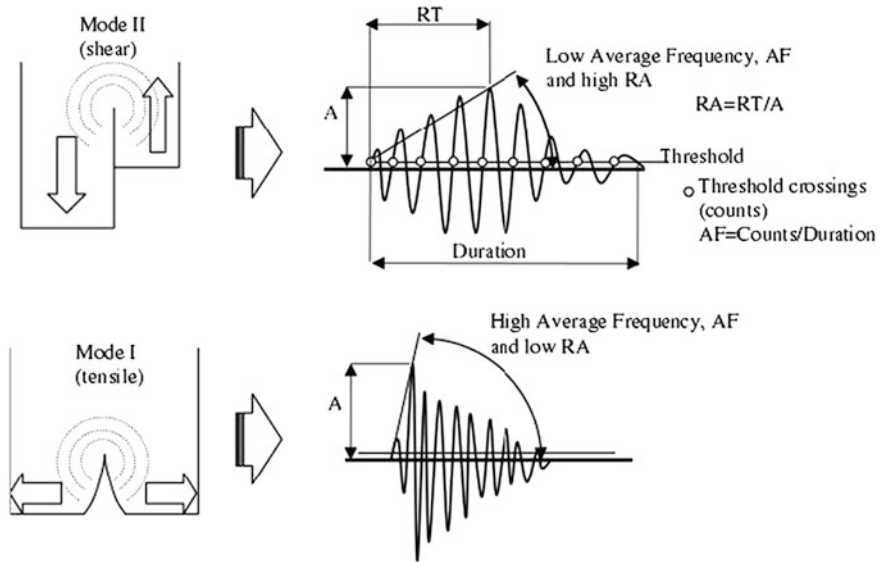


Fig. 1 AE source and typical corresponding waveform [6]

channel basis [2, 3]. However, the crack classification under dynamic loading as well as fatigue loading and its analysis based on located event is still limited.

In the present study, RC beams subjected to various fatigue load range concurrent with AE monitoring with four sensors were investigated. The classification of active cracks in the RC beam specimens is determined using the relationship between average frequency and RA value. The relationship is also compared between those obtained from the channel basis and those at the located event.

2 Experimental Programme

2.1 Preparation of Reinforced Concrete Beams

Twelve reinforced concrete (RC) beams with dimension of $150 \times 150 \times 750$ mm were prepared. The concrete was made up from cement, water, fine aggregate and coarse aggregate with proportion of 1:0.43:2.16:2.60, respectively. Then, 1 % of retarder of cement weight was added in the concrete mix to improve the workability of the fresh concrete. The maximum coarse aggregate of 20 mm was used. The beams were designed as a singly RC beam with two high yield steels of 16 mm to strengthen the tension part and two mild steels of 8 mm as hanger bars. In the stirrups, 12 mm diameter of mild steel with spacing of 100 mm centre to centre was used. The compressive strength at 28-day of the concrete mix was found to be 44.65 N/mm^2 .

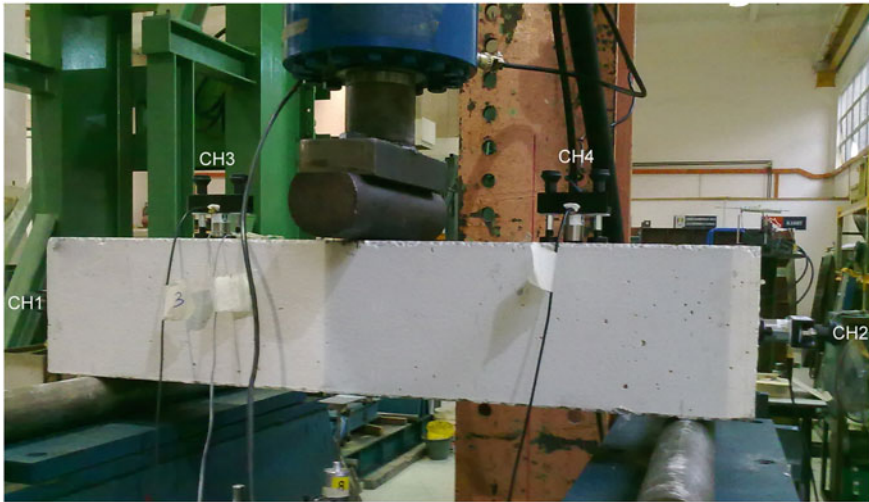


Fig. 2 Setup of the third point bending test for the RC beams

2.2 Fatigue Tests and AE Monitoring

All beams were tested under two different fatigue load range based two indices of first load crack (P_{cr}) and ultimate load (P_{ult}). The P_{ult} was determined from the static test for the same beam size with total of five RC beams which was conducted prior to the experimental work. The average P_{ult} from the static test was 158.85 kN. The P_{cr} was identified using theoretical calculation and based on the visual observation. Theoretical calculation shows that the P_{cr} was 23.94 kN and from observation, the P_{cr} was found to be 24 kN. Hence, the P_{cr} of 24 kN was used for the load ratio. The six load phases of the tests which are $0.5 P_{cr}$, $0.8 P_{cr}$, $1.0 P_{cr}$, $0.2 P_{ult}$, $0.5 P_{ult}$ and $0.6 P_{ult}$ with the constant minimum load, P_{min} of $0.1 P_{cr}$ were adopted. Hence, in Phase 1 to Phase 6, the maximum loads, P_{max} are 12, 19, 24, 32, 79 and 95 kN respectively. Minimum load, P_{min} of 2.4 kN was used throughout the test. A servo-hydraulic testing machine was employed for subjecting prismatic RC beams of $150 \times 150 \times 750$ mm to the required fatigue loading. The specimen set up is represented in Fig. 2. A sine wave load cycle was applied with frequency of 1 Hz. Each phase, the RC beams were loaded up to 5,000 fatigue cycles.

Four AE sensors (VS75-V) were applied on the beam as shown in Fig. 2. Two of them were coupled at the centre of the end section of the beam and the other two were coupled on the top side of the beam, 175 mm from the both edges. Both sensors were calibrated using Hsu–Nielson (H–N) technique [21]. The sensors were coupled on the beam surfaces using high performance grease. All sensors were considered coupled if the wave generated by at least three or more replicates of pencil lead fracture (PLF), produces high amplitude of above 95 dB or the sensitivity within +3 dB in different [21, 22]. A pencil with a Nielson shoe (Teflon

shoe) was used to break a 0.5 mm 2H lead to generate a simulated acoustic wave against the surface of the beam. This technique was used to ensure the sensor and the beam was in a good contact to provide a reliable result throughout the test.

AE threshold level was set at 45 dB to ensure a high signal above the noise level is recorded. The wave velocity of 4000 m/s was used throughout the test. The AE parameters fixed are reararm time of 1.62 ms, duration discrimination time of 400 μ s, pre-trigger samples of 200 and the sample rate of 10 MHz. The digital setting has been filtered for 25–850 kHz. The results were digitised, stored and visualised in AMSY-6 software.

For each load phase, the crack patterns were marked on the beam surface and designated as 1 to 6 (to represent Phase 1 to Phase 6).

2.3 AE Parameter Analysis

Qualitative AE parameter analysis was used to determine and classify the active fatigue crack of the RC beams subjected to loading of Phase 1 to Phase 6 either it is tensile or shear crack. The AE parameters used for analysis are count, duration, amplitude and rise time. The active fatigue crack for each phase is determined based on two indices of RA value and average frequency. The RA value is the rise time (μ s) over the maximum amplitude (μ v). The average frequency is the counts (number of threshold crossing) over the duration of the signal and noted as kHz. In the analysis of RA value and average frequency, two methods were utilised and compared. They are based on channel basis so called as conventional method and another one is based on the located event. In AMSY-6 listing, the located event is abbreviated as LE. The location was selected at where the shear crack (shear zone) occurred and designated as Section A (Sec A). Based on the graph of amplitude with respect to X-location shown in Fig. 2, Sec A is found representing highest amplitude up to 99 dB which shows high intensity of the crack. Higher amplitude events also increased as failure approaches [23]. In Sec A, the analysis is based on the located event from distance 0.1 m to 0.3 m and was calculated for each phase. The analysis also took into account the values obtained from Channels 1, 3 and 4 as shown in Fig. 3. However, the dominant value was from Channel 3. The analysis in Sec A was then compared with the analysis of the closest channel (sensor). The closest sensor to Sec A was Channel 3 (CH3) and data collected are based on the event value (EV).

3 Results and Discussion

3.1 Visual Observation of the Crack Patterns

Figure 4 shows the crack patterns of the RC beam under six different fatigue load range. Numbers 1 to 6 indicate the crack pattern corresponding to Phase 1 to Phase

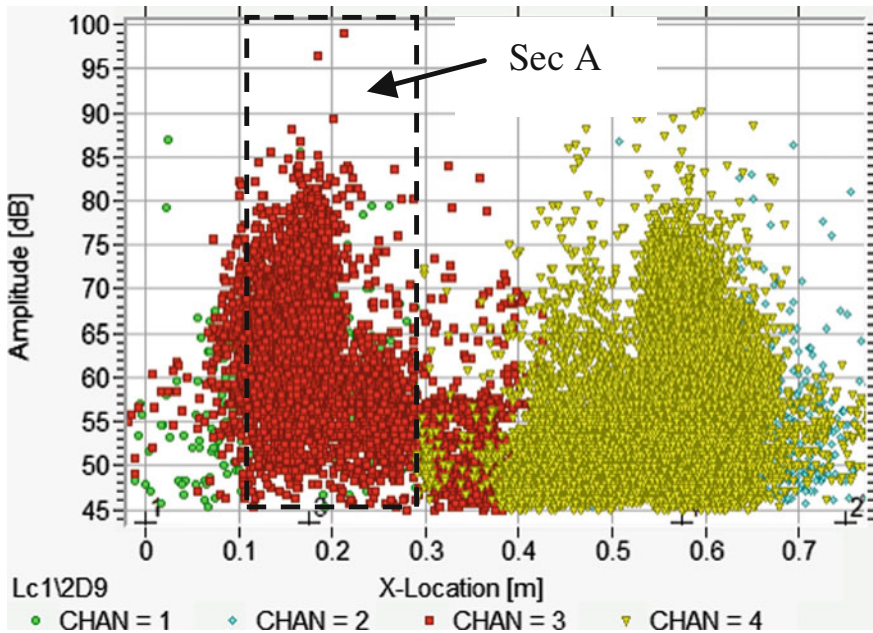
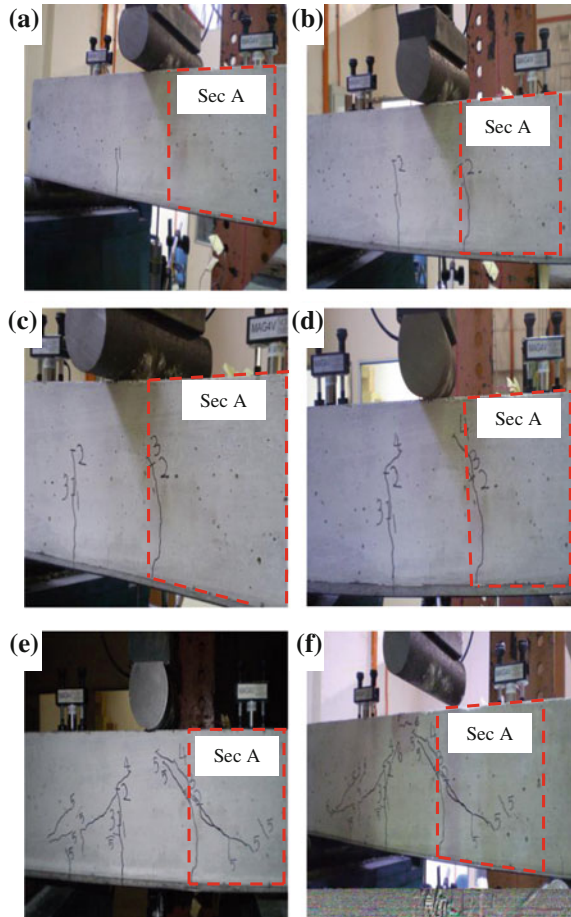


Fig. 3 Relationship between amplitude and X-location

6 of loading as shown in Fig. 4d, f. The cracks progressively increased as the load increased. Figure 4a shows no crack is developed on Sec A in Phase 1 when maximum loading (P_{max}) of 12 kN was applied. However, the first crack was developed at the centre of the beam and noted as 1. The first crack in Sec A was occurred as the loading of Phase 2 was applied or when the maximum load increased to 19 kN as shown in Fig. 4b. In this phase, the crack was almost vertically propagated over the mid height of the beam. Most of the cracks were started at the mid-span of the beam specimen. The third crack was then propagated just after from the crack tip happened in Phase 2. However, the occurrence of crack is not always from just a previous phase, but in some cases it continuous from that of earlier phase. For instance, crack in Phase 4 was propagated from tip of the crack appeared on Phase 2. From visual observation, all the crack patterns for the beam are almost the same, it can be considered that cracks in Phase 2 and Phase 3 at Sec A are tensile crack.

The shear cracks were progressively propagated when the maximum load applied is reached to the ultimate static load. When load of 79 kN was applied (Phase 5), the crack propagations were drastically increased and continuously propagates as maximum load increased to 95 kN. In Phase 5, a large shear crack is formed while the flexural crack becomes inactive [24]. In the relationship between average frequency and RA value, tensile crack was used to indicate the occurrence of flexural crack. The crack pattern appears on the beam when subjected to loading of all phases is represented in the crack pattern as shown in Fig. 4f.

Fig. 4 Crack pattern of RC beam subjected to increasing fatigue load range. **a** Phase 1 ($0.5 P_{cr}$); **b** Phase 2 ($0.8 P_{cr}$); **c** Phase 3 ($1.0 P_{cr}$); **d** Phase 4 ($0.2 P_{ult}$); **e** Phase 5 ($0.5 P_{ult}$); **f** Phase 6 ($0.6 P_{ult}$)



3.2 Relationship of Average Frequency and RA Value

Figures 5 and 6 show the relationship between average frequency and RA value for beam subjected to increasing fatigue load range. In left side of the figures show the graph for Section A (Sec A) and right side for channel basis. Sec A is the analysis of the results based on the located event. Meanwhile, channel basis is the analysis of the results based on the event of AE signal at Channel 3. In this case, Channel 3 is analysed due to close channel to Sec A. The diagonal line in the figures indicates the transition line between tensile crack and shear crack [8] and used as a reference line for crack classification. The plot in Figs. 5 and 6 are compared with those captured visually as shown in Fig. 4.

The plot in Fig. 5 was obtained from the specimen subjected to the fatigue loading with the maximum loading based on P_{cr} . It indicates a progression of crack

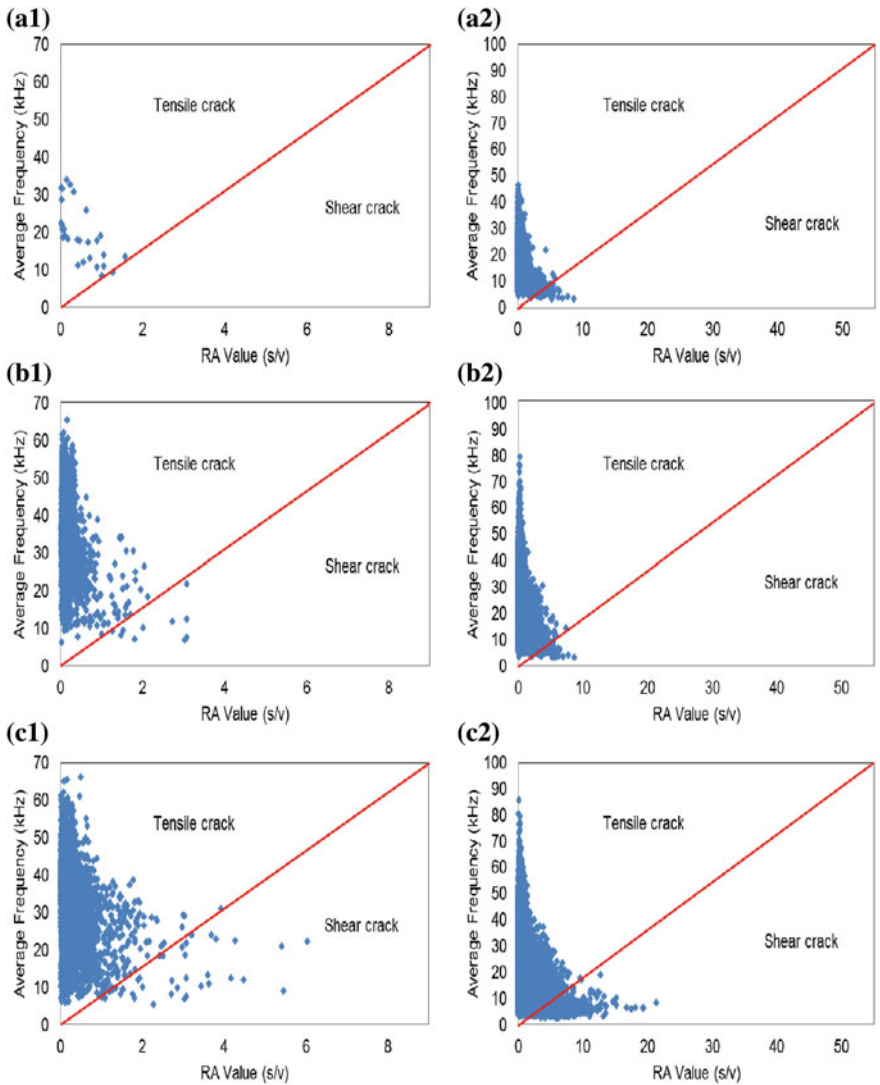


Fig. 5 Relationship between average frequency and RA value based on P_{cr} . **a** Phase 1; **b** Phase 2 and **c** Phase 3

since low load increment was applied on the beam for both Sec A and Channel 3. In Sec A, it started with tensile crack in Phase 1 while the shear crack started to develop in Phase 2 and it progressively increases when reached to Phase 3. However, it does not well corresponding to those of in Fig. 4b, c which the tensile cracks are observed.

In Channel 3, the relationship shows that the shear crack has occurred although the load of Phase 1 was adopted. In Channel 3, it indicates that the shear crack

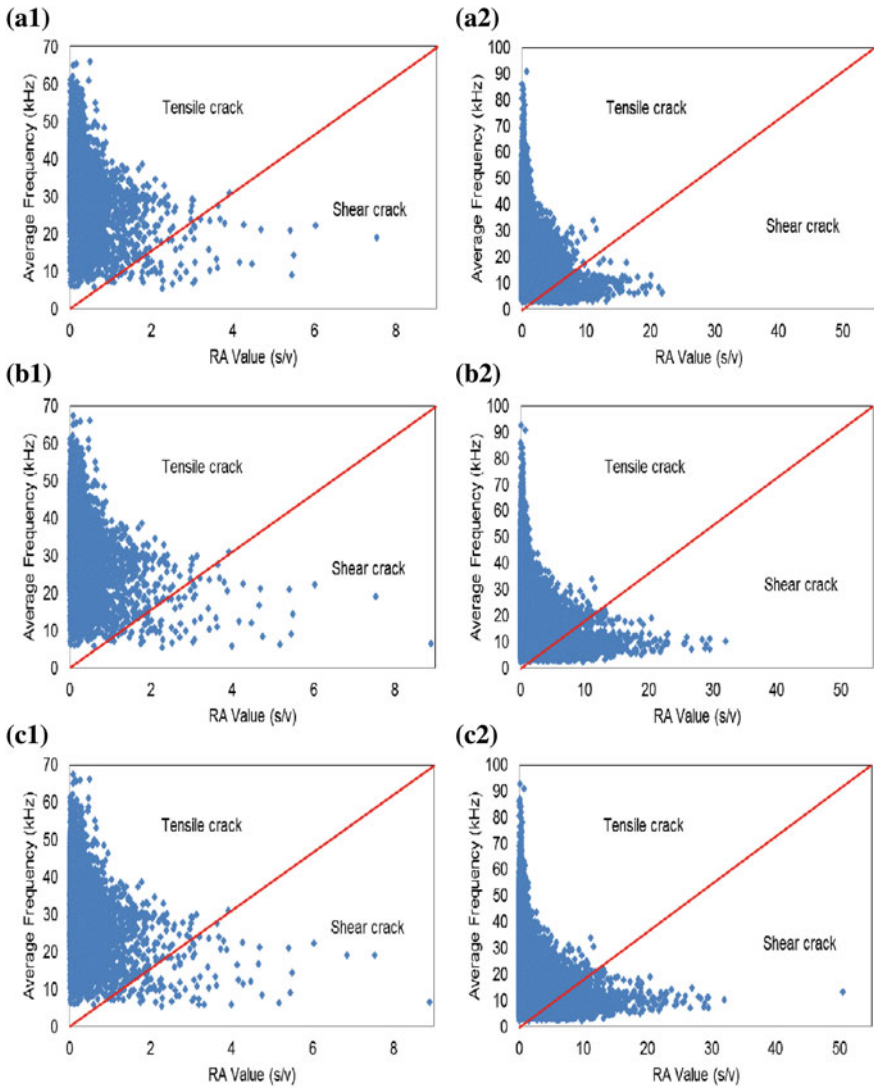


Fig. 6 Relationship between average frequency and RA value based on P_{ult} . **a** Phase 4; **b** Phase 5; **c** Phase 6

initiated in Phase 1 to Phase 3. From Fig. 3, the amplitude in Channel 3 is scattered anywhere along X-location based on time of arrival. The intensity at particular location for example Sec A (located event) represents a better explanation than Channel basis.

Figure 6 shows the relationship between average frequency and RA value for specimen when subjected to maximum loading based on P_{ult} (Phase 4 to Phase 6).

Fig. 7 Relationship between average frequency and RA value for beam subjected to all phases of fatigue loading based on AE signal of the located event in Sec A

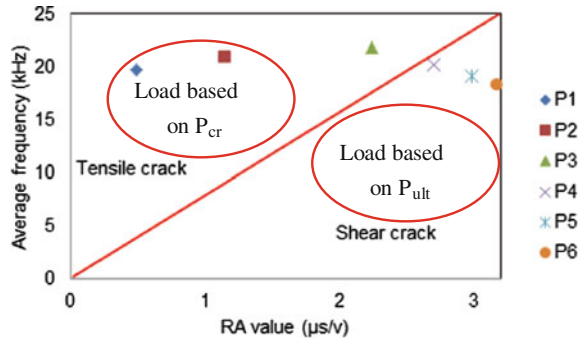
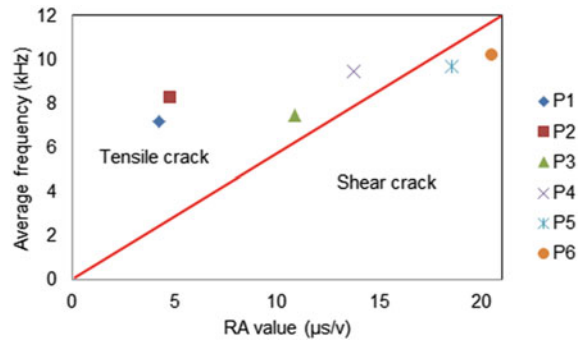


Fig. 8 Relationship of average frequency and RA value for beam subjected to fatigue loading of all phases based on AE signal in Channel 3



In Sec A (left figures), as continuation from previous phase, shear cracks progressively developed till Phase 6. However, based on Channel 3, high average frequency is produced as the maximum loading in Phase 4 ($0.2 P_{ult}$). It might be due to progression of high shear cracks in the beam as shown in Fig. 4d. In this case, results in Phase 5 and Phase 6 are almost the same due to no increment of cracks development in the beam when maximum load in Phase 6 ($0.6 P_{ult}$) has applied.

Figure 7 shows the fatigue crack classifications in the RC beams subjected to fatigue loading of all phases in Sec A which the analysis is based on the located event. This figure is based on the average of highest first 100 RA value. It is found that, when P_{cr} is applied, the cracks are in tensile and followed by shear when P_{ult} is applied. These plots of all phases are matched with the crack propagation captured as illustrated in Fig. 4. It can be used as an indication of the crack development in the beam on time as the AE signal captured by the sensors that relate with time of arrival.

When highest average of RA value in Channel 3 is used as shown in Fig. 8, there is no obvious trend for identification of cracks classification as those in the located event of Sec A. It is depicted that the crack was in tensile up to the load in Phase 4 range followed by shear crack when maximum load in Phase 5 and Phase 6 were applied.

4 Conclusions

This study addresses the classification of active fatigue cracks in the reinforced concrete beams subjected to various fatigue load range from 0.5 of first load crack up to 0.6 of ultimate strength. The AE analyses are performed in terms of the relationship between average frequency and RA value at Sec A. The relationships derived under each phase of loading are compared with physical crack pattern that marked on the beam surface.

It is deduced that the relationship based on located event are more representable and well corresponding to the physical crack pattern than those captured on channel basis. Hence, the classification of tensile crack and shear crack can be used as an early warning detection of the beam when subjected to fatigue.

Acknowledgments The financial support of this research by the Research Management Institute (RMI), Universiti Teknologi MARA (600-RMI/ST/DANA 5/3/Dst(37/2011)) and Universiti Sains Malaysia (ERGS (203/PAWAM/6730010) are gratefully acknowledged. The authors also thank Dr. Thomas Thenikl (Vallen Systeme) and Mr. Zulfahmy Awaldin (ZL Technologies Sdn. Bhd.) for supporting technical information on acoustic emission especially from Vallen Systeme. Special thanks to all technicians in heavy structural laboratory and concrete laboratory, Faculty of Civil Engineering, Universiti Teknologi MARA and Ministry of Higher Education, Malaysia.

References

1. ASTM E976-10 *Standard guide for determining the reproducibility of acoustic emission sensor response*. Non Destructive Testing Standard, 2005
2. D.G. Aggelis, A.C. Mpalaskas, D. Ntalakas, T.E. Matikas, Effect of wave distortion on acoustic emission characterization of cementitious materials. *Constr. Build. Mater.* **35**, 183–190 (2012)
3. D.G. Aggelis, A.C. Mpalaskas, T.E. Matikas, Investigation of different fracture modes in cement-based materials by acoustic emission. *Cem. Concr. Res.* **48**, 1–8 (2013)
4. D.G. Aggelis, Classification of cracking mode in concrete by acoustic emission parameters. *Mech. Res. Commun.* **38**(3), 153–157 (2011)
5. H.A. Elfergani, R. Pullin, K.M. Holford, Damage assessment of corrosion in prestressed concrete by acoustic emission. *Constr. Build. Mater.* **40**, 925–933 (2013)
6. K. Ohno, M. Ohtsu, Crack classification in concrete based on acoustic emission. *Constr. Build. Mater.* **24**(12), 2339–2346 (2010)
7. M. Ohtsu, Recommendation of RILEM TC 212-ACD: acoustic emission and related NDE techniques for crack detection and damage evaluation in concrete. *Mater. Struct.* **43**, 1187–1189 (2010). RILEM Technical Committee
8. T. Watanabe, S. Nishibata, C. Hashimoto, M. Ohtsu, Compressive failure in concrete of recycled aggregate by acoustic emission. *Constr. Build. Mater.* **21**(3), 470–476 (2007)
9. D.G. Aggelis, N.M. Barkoula, T.E. Matikas, A.S. Paipetis, Acoustic structural health monitoring of composite materials: damage identification and evaluation in cross ply laminates using acoustic emission and ultrasonics. *Compos. Sci. Technol.* **72**(10), 1127–1133 (2012)
10. D.G. Aggelis, D.V. Soulioti, N.M. Barkoula, A.S. Paipetis, T.E. Matikas, Influence of fiber chemical coating on the acoustic emission behavior of steel fiber reinforced concrete. *Cement Concr. Compos.* **34**(1), 62–67 (2012)

11. D.G. Aggelis, D.V. Soulioti, E.A. Gatselou, N.M. Barkoula, T.E. Matikas, Monitoring of the mechanical behavior of concrete with chemically treated steel fibers by acoustic emission. *Constr. Build. Mater.* **48**, 1255–1260 (2012)
12. D.G. Aggelis, T.E. Matikas, Effect of plate wave dispersion on the acoustic emission parameters in metals. *Comput. Struct.* **98–99**, 17–22 (2012)
13. D.G. Aggelis, E.Z. Kordatos, T.E. Matikas, Acoustic emission for fatigue damage characterization in metal plates. *Mech. Res. Commun.* **38**(2), 106–110 (2011)
14. D. Soulioti, N.M. Barkoula, A. Paipetis, T.E. Matikas, T. Shiotani, D.G. Aggelis, Acoustic emission behavior of steel fibre reinforced concrete under bending. *Constr. Build. Mater.* **23**(12), 3532–3536 (2009)
15. D.G. Aggelis, A.C. Mpalaskas, T.E. Matikas, Acoustic signature of different fracture modes in marble and cementitious materials under flexural load. *Mech. Res. Commun.* **47**, 39–43 (2013)
16. D.G. Aggelis, D.V. Soulioti, N. Sapouridis, N.M. Barkoula, A.S. Paipetis, T.E. Matikas, Acoustic emission characterization of the fracture process in fibre reinforced concrete. *Constr. Build. Mater.* **25**(11), 4126–4131 (2011)
17. C.U. Grosse, M. Ohtsu, Acoustic emission testing: basics for research—applications in civil engineering, in *Introduction* (Springer, Berlin, 2008)
18. M. Ohtsu, T. Isoda, Y. Tomoda, Acoustic emission techniques standardized for concrete structures. *J. Acoust. Emission* **25**, 21–32 (2007)
19. Y. Kawasaki, T. Wakuda, T. Kobara, M. Ohtsu, Corrosion mechanisms in reinforced concrete by acoustic emission. *Constr. Build. Mater.* **48**, 1240–1247 (2013)
20. K. Ohno, M. Ohtsu, Crack classification in concrete based on acoustic emission. *Constr. Build. Mater.* **24**(12), 2339–2346 (2010)
21. N. Md Nor, N. Muhamad Bunnori, A. Ibrahim, S. Shahidan, S.N. Mat Saliah, An observation of noise intervention into acoustic emission signal on concrete structure, in *Signal Processing and Its Applications (CSPA), 2011 IEEE 7th International Colloquium on*. 2011: IEEE
22. N. Muhamad Bunnori, Acoustic emission techniques for the damage assessment of reinforced concrete structures. PhD thesis, University of Cardiff, 2008
23. P.H. Ziehl, Development of a damage based design criterion for fiber reinforced vessels, in *Faculty of the Graduate School 2000*, The University of Texas at Austin, p. 307
24. A. Pimanmas, Behaviour and failure mode of reinforced concrete members damaged by pre-cracking. *Songklanakarin J. Sci. Technol.* **29**(4), 1039–1048 (2007)

Flexural Behavior of Reinforced Concrete (RC) Beams with Externally Bonded (EB) Carbon Fiber Reinforced Polymer (CFRP) Sheets

M. N. Nurbaiah, A. H. Hanizah and I. Nor Farhana

Abstract Strengthening is a way to lengthen the serviceability of building structures under increased loading requirements and severe conditions. Externally bonded (EB) is one of the strengthening techniques that is being practiced nowadays. The present investigation is studying on the enhancement in flexural performance and the effectiveness of un-cracked RC beams strengthened with Externally Bonded (EB) Carbon Fibre Reinforced Polymer (CFRP) sheet/s U-wrap anchorage systems with different locations and dimensions. A series of RC beams were fabricated with the dimensions of each beam as 170 mm width \times 270 mm depth \times 2,325 mm length. Five (5) variables were involved in this investigation. All beams were tested under four point bending. Test results show that the strengthened RC beams performed better than control beam with nominal increase in stiffness and higher ultimate load. The results show that the strengthened beams increase the flexural strength up to 35 % and decrease the deflection to about 40 % as compared to the control beam. Meanwhile, due to presence of U-wrap gave an effect in increasing load carrying capacity by 35 % than the control beam. The U-wraps at mid span has minimized the deflection by another 10 % compared to beams having U-wraps at the ends only.

Keywords Externally bonded · Strengthening · Flexural · Reinforced concrete beams · Stiffness

1 Introduction

Structural strengthening is the process of upgrading the structural system of an existing structure to improve the building's performance under existing loads or to increase the strength of the existing structure to carry additional loads. One of the

M. N. Nurbaiah (✉) · A. H. Hanizah · I. N. Farhana
Faculty of Civil Engineering, Universiti Teknologi MARA, Shah Alam, Malaysia
e-mail: nurbaiah@salam.uitm.edu.my

traditional methods of strengthening includes bonding the structural members with steel plates using epoxy. However, due to corrosion and heavy weight of the steel plate, difficulty of forming joint between steel plate and beam and intensive labour for surface preparation of the beam, therefore these create major setback of using steel plate as a strengthening material.

Extensive research has been carried out in this field to develop a new method that is reliable, cost effective and easy in handling as alternatives to steels and alloys [1, 2]. Besides, use of Fibre Reinforced Polymer (FRP) sheets as the material to strengthen structural members is becoming popular due to its high corrosive resistance and high strength-to-weight-ratio [3–5]. Hence, using Externally Bonded (EB) Fibre Reinforced Polymer (FRP) sheets to concrete structures has been widely accepted in the industries as a method of strengthening and retrofitting. This technique is done by bonding the CFRP sheets to the tension soffit of reinforced concrete beams using epoxy. However, this EB technique causes some reduction in ductility of the beam, but it results in a higher ultimate flexural strength and stiffness [5, 6]. Generally, concrete cover delamination is one of the failures of beam strengthened with Carbon Fibre Reinforced Polymer (CFRP) sheets. This failure may occur due to the peeling off of the bottom concrete cover along the level of the longitudinal steel reinforcement. Introducing an anchorage system on the ends of the FRP sheets is one solution to improve the performance of the EB FRP technique [7]. Meanwhile, Xiong et al. (2005), as in [8] identified that this problem can be delayed or even prevented by combining Carbon Fibre Reinforced Polymer (CFRP) sheets at the tension face of the beams and Glass Fibre Reinforced Polymer (GFRP) sheets by wrapping three sides of the beams continuously (U-wrap). The way of preventing debonding by introducing U-wraps is also in agreement with other researchers [9, 10]. Besides preventing delamination, the FRP U-wraps also could enhance the beams load carrying capacity [9, 11]. However, Ceroni et al. (2007), as in [7], reported that when the U-strips are concentrated at the ends, the strengthening material would experience local slip, cutting or debonding with a loss of effectiveness before they reached the tensile strength of FRP fibres. An efficient way to avoid debonding and allow tensile fracture of FRP fibers at the mid span of beam is by applying the strips as being distributed along the beam instead of concentrated at the ends.

Even though a lot of studies had been conducted, that performances and beneficial effect due to the arrangement of the U-wrap anchorage are still not yet quantified. Therefore, this research investigation aims to compare the flexural behaviour of strengthened RC beams with different locations and dimensions of U-wrap anchorage system in the same load condition.

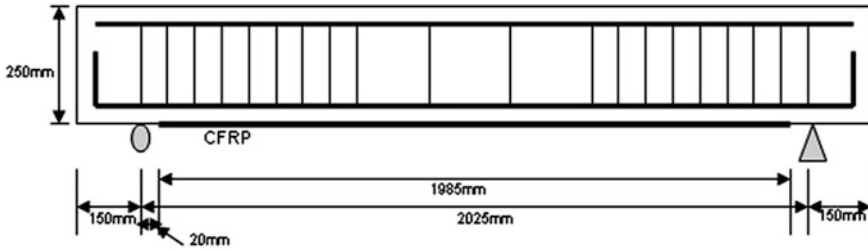


Fig. 1 CFRP sheets applied on the soffit

2 Experimental Programme

2.1 Test Series

There were two series of RC beam specimens prepared. In the first series, one (1) specimen of un-strengthened RC beam made of concrete grade 30 was prepared and were designated as CB (control beam).

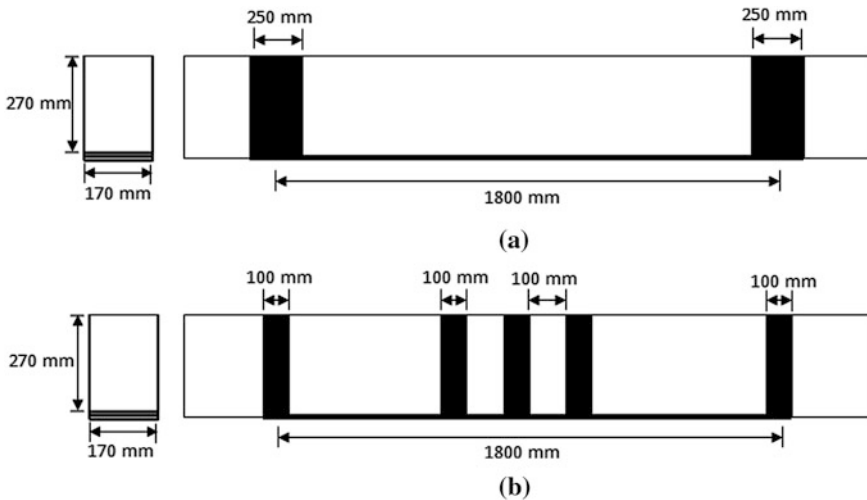
In the second series, a total of four (4) RC beams were prepared and strengthened using EB CFRP sheets. The RC beams strengthened with external CFRP sheets were designated as B-2C, B-1C-U, B-2C-U, and B-2C-UD where by letters B-1C or 2C are referring to the beam strengthened with one (1) or two (2) layers of CFRP sheets at the centre of the soffit of the beam. Each CFRP sheet used was 100 mm wide and 0.12 mm thick and it is bonded to the soffit of the beam. The letter U implies that the EB CFRP sheets are with U-wrap arrangement at the ends of the strengthening length. While, letters U and D represents the EB CFRP sheets covering the beam strengthened with U-wrap arrangement at both the end and the middle of the strengthening length. The cut-off point of each sheet to be applied on soffit face is 20 mm from each support as shown in Fig. 1. The details of the specimens prepared are shown in Table 1 and Fig. 2.

2.2 RC Beam Configuration

The RC beams are designed to be over reinforced in resisting internal shear force to ensure that the beams would fail in pure bending or flexure. All RC beams were prepared using the same configuration. Each beam is 2,325 mm length, 270 mm depth, 170 mm width, and 2,025 mm length between supports with 20 mm concrete cover thickness as shown in Fig. 3a and b. Each beam is reinforced longitudinally by two 12 mm diameter high yield strength steel bars positioned below the neutral axis of the beam to cater for the tension force, while two 10 mm diameter mild steel bars are used as tie bars located at the compression side of the beam. Eight (8) mm diameter stirrups are spaced at 75 and 225 mm

Table 1 Details of the RC beam specimens

Test series	RC beam designation	Strengthening method	Variable
1	CB	–	–
2	B-2C	EB	2 CFRP sheets
2	B-1C-U	EB	1 CFRP sheets with U-wrap at the end of the strengthening length
2	B-2C-U	EB	2 CFRP sheets with U-wrap at the both end of the strengthening length
2	B-2C-UD	EB	2 CFRP sheets with U-wrap at the both end and centre of the strengthening length

**Fig. 2** Strengthening scheme; **a** B-1C-U, B-2C-U; **b** B-2C-UD

centre-to-centre near the end and around the middle span respectively as shown in Fig. 3a. The RC beams were designed to have a span-to-effective depth ratio of 9.0, and therefore they are expected to fail in flexural. The shear reinforcement consists of two (2) 8 mm diameter plain mild steel bars closed stirrups, spaced at 225 mm spacing near mid span and ten (10) 6 mm diameter closed stirrups, spaced at 75 mm spacing positioned at each side of the beam. Figure 3a and b shows the beam configuration and its detail drawing.

2.3 Preparation of RC Beam Specimens

All RC beam specimens were cast using timber formwork and ready mix concrete designed for Grade 30. The formwork was dismantled from the RC beam specimens in the next day after concrete casting. After dismantling the formwork, the

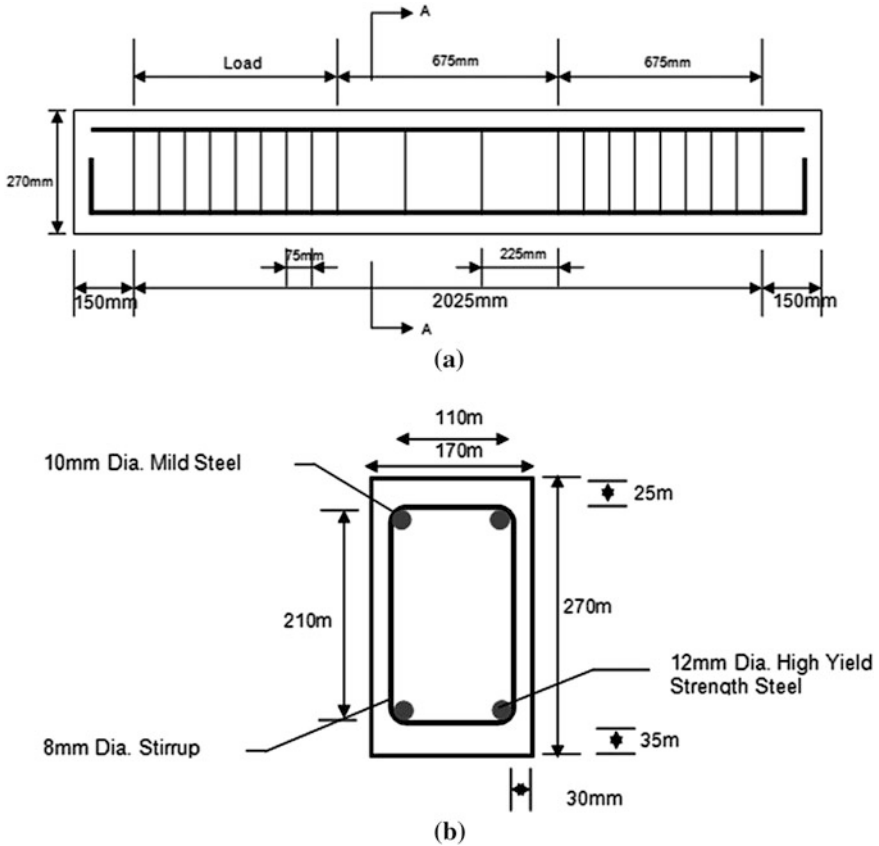


Fig. 3 The configuration details of RC beam specimens

RC beam specimens were wet cured by covering them with wet burlap for 28 days and cured for another two (2) weeks after installation of the EB with CFRP sheet/s.

2.4 RC Beam Specimens Strengthened with EB CFRP Sheets

In order to obtain good bonding between the concrete surface and CFRP sheet, the concrete surface was firstly roughened using a hand held diamond grinder. The surface was grinded about 1–2 mm thick. The surface of the specimen was also blown using compressed air to remove any excess particles. After cleaning process, the surface was applied with an adhesive. The CFRP sheet to be glued on the surface is 150 mm width and 0.12 mm thick in size and then was pressed into the surface with the adhesive. A paint roller was used to press the CFRP sheet to

Fig. 4 Experimental of strengthened beam set-up



ensure a uniform thickness of adhesive and expel any entrapped air. For two (2) sheets of CFRP, adhesive was applied onto each layer. Finally, a layer of adhesive was applied on the CFRP sheet for better adhesion. The thickness of adhesive applied was approximately 2 mm in thickness. To apply for the U-wrap anchorage system, a layer of U-shaped continuous CFRP sheet with specific dimension was glued to the bottom and lateral faces of the RC beam using adhesive.

2.5 Experimental Set-up

All RC beams were tested under four-point bending with a clear span 2,025 mm and internal span 675 mm. The RC beam EB CFRP sheet/s was fixed with strain gages and Linear Voltage Displacement Transducer (LVDT). One LVDT was placed at the mid span and the other two were placed under points of load applications to measure the vertical displacements. The flexural testing was performed by providing loading in load controlled mode at 0.02 kN/s until failure. The setting up of the flexural testing is shown in Fig. 4.

2.6 Four-Point Flexural Strength Test

All RC beam specimens were tested under flexural strength test (use four points bending). The four-point bending (flexure) static loading was performed using Universal Testing Machine with under displacement controlled at a constant head-loading rate of 0.015 mm/sec. Load increment, ultimate load, strain and deflection were recorded by data logger while the crack pattern was visualized manually.

3 Result and Discussion

The summary of experimental results for the two series of five (5) RC beams is illustrated in Table 2. The load versus deflection curves for EB CFRP sheets strengthened beams with and without U-wrap anchorage are shown in Fig. 5.

3.1 Load Displacement Curves

Figure 5 shows the evidence that applying EB CFRP sheets at the tension face of the RC beams enhances the ultimate flexural strength capacity, yield load and stiffness of the beam. Increasing a layer of CFRP sheet for strengthening significantly improves and provides stiffness of the RC beam. The strengthened beam with one (1) layer EB CFRP sheets (B-1C-U) recorded an increase by about 27 % compare to that control beam. The strengthened beam with two (2) layers EB CFRP sheets (B-2C-U) recorded about 36 % increase in strength capacity over the control beam and 12.9 % increase corresponding to one (1) layer EB CFRP sheet.

As shown in Fig. 5, the results reveal that by adding the U-wrap anchorage of CFRP sheets does not significantly enhance the strength capacity of the beam, but can expand the durability of the strengthened beam. Specimen B-2C-U has increased about 2.9 % over the strengthened beam without U-wrap (B-2C), while B-2C-UD has increased 34.56 % with respect to control beam but has no difference over the B-2C, respectively.

Figure 5 reveals that the RC beam strengthened with two (2) layers EB CFRP with U-wrap anchorage at its both ends (B02C-U) exhibits the higher ultimate load and stiffness than the other strengthened beam. The better performance of the beam could be attributed to the effect of U-wrap anchorage system and the number of layers applied at the bottom of the surface. However, these results cannot verify the experimental results conducted by Ceroni (2010), as in [12]. The investigation by Ceroni (2010), as in [12] revealed that by using distributed U-wrap anchorage the strengthened beam can exhibit higher ultimate load compare to the U-wrap at both ends of strengthening length. Nevertheless, this could be due to the locations of the U-distributed wrap anchorage. In this study, the distributed U-wrap anchorage was not wrapped along the beam, but only focused on the flexural area (between the load cells). Therefore, this would be one of the factors that affected the result.

3.2 Failure Mode and Crack Pattern

As shown in Table 2 and Fig. 6a, the control RC beam specimens were found to fail due to yielding of steel tension reinforcement followed by crushing of concrete at compression zone. There was no shear crack observed. The beam failed due to crushing of concrete in a ductile flexural mode.

Table 2 Summary of overall test result

Beam type	Yield point load, P_y (kN)	Deflection at yield point (mm)	Ultimate load P_u (kN)	Deflection at ultimate load (mm)	% increase of ultimate load	Failure mode
CB	89.13	11.18	97.02	28.21	—	Reinforcement yielding followed by concrete crushing
B-2C	117.82	12.73	148.26	23.89	34.56	Delamination of the CFRP strengthening near the support followed by concrete cover
B-1C-U	103.81	11.21	132.93	27.19	27.01	Delamination of the CFRP strengthening below the load points followed by concrete cover
B-2C-U	112.13	10.27	152.64	20.05	36.44	
B-2C-UD	107.09	9.95	148.26	18.98	34.56	Delamination of the CFRP strengthening near the support followed by concrete cover and rupture of CFRP sheet at U-wrap

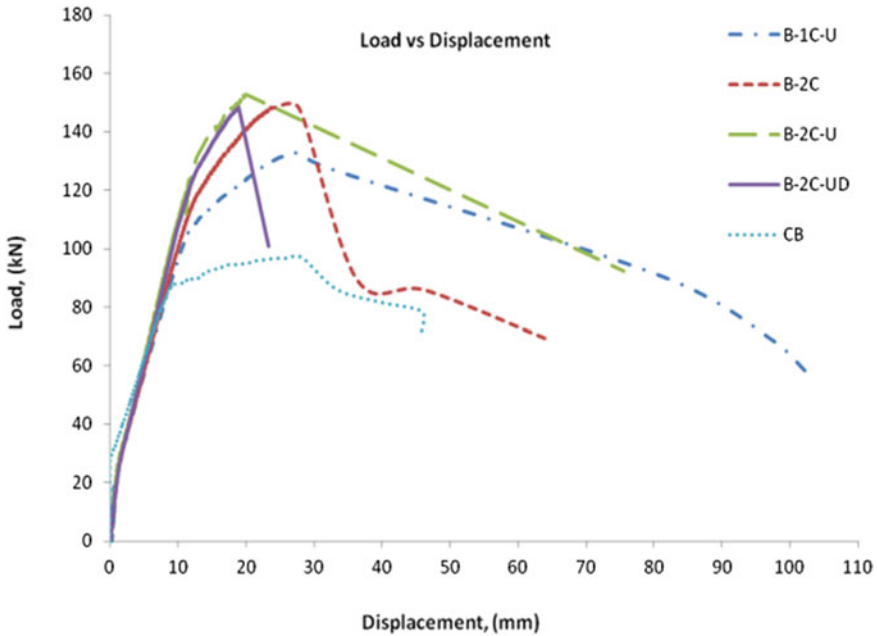
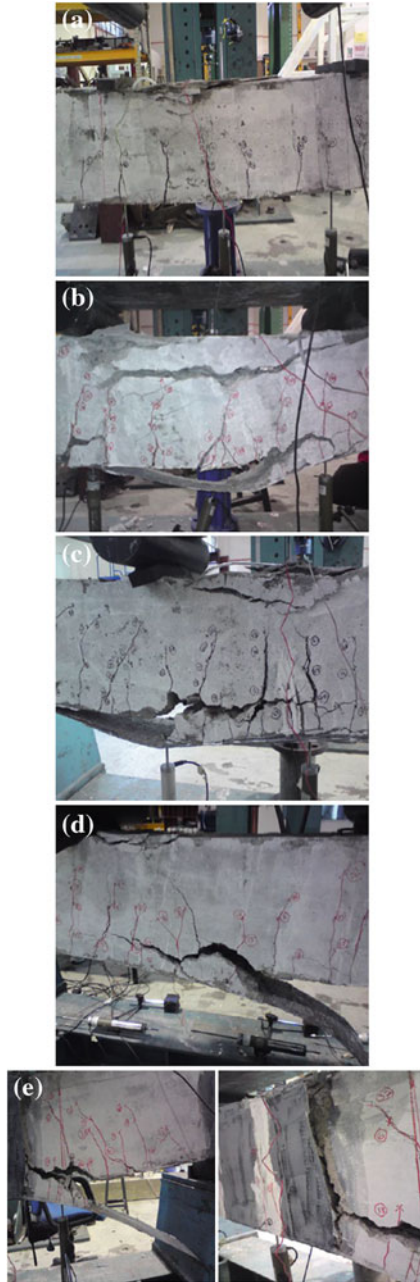


Fig. 5 Load deflection curve for the comparison of the beam performance between strengthened beam with and without anchorage system

For RC beam specimens strengthened with one (1) layer or (2) layers CFRP sheets with U-wrap failed by delamination of CFRP sheets at soffit of mid spans followed by concrete cover separation as shown in Fig. 6b and c. Concrete crushing at compression zone was also observed. Meanwhile, Fig. 6d and e show beams B-2C and B-2C-UD failed due to delamination of CFRP sheets near the supports after extensive cracking of the concrete covers below the load points. Rupture of U-wrap CFRP sheets at mid span was observed together with concrete crushing at compression zone [12].

The flexural cracks propagated from the bottom to vertically upwards as the load increased. However, the width of the cracks is small for strengthened RC beam specimens and this reflects the effect of the strengthening which makes the beams stiffer. The cracks continued to travel up along the depth of the beam until yielding of the steel reinforcement began. Unlike the control beam, the cracks were smaller in width and closely spaced. The number of cracks was increased but with shorter crack length especially around the mid-spans.

Fig. 6 Strengthened specimens after failure; **a** CB; **b** B-1C-U; **c** B-2C-U; **d** B-2C; **e** B-2C-UD



4 Conclusions

The following conclusions are drawn based on the experimental work of strengthened beams with Carbon Fiber Reinforced Polymer (CFRP) sheets.

1. The strengthened beams failed due to compression failure before and after yielding of steel bars, rupture of Fiber Reinforced Polymer (FRP) sheets, delamination of FRP sheets and concrete cover separation. In this research, the common failure mode is delamination of CFRP sheet, which leads to concrete cover separation. Concrete crushing at compression zone was observed during the experimental testing. Rupture of U-wrap at mid span also occurred in beams strengthened with distributed U-wraps.
2. The results reveal that adding the U-wrap anchorage of CFRP sheets does not significantly enhance the strength capacity of the beam, but by adding can expand the durability of the strengthened beam. In this study, the average flexural capacity was as high as 35.5 % for the beam strengthened using EB CFRP U-Wraps sheet anchorage. However, the flexural capacity for beams strengthened with EB CFRP sheets with no anchorage increases by 34.6 %.
3. Stiffness is enhanced for RC beams with strengthening system using CFRP sheets and U-Wrap anchorage. The stiffness has minimized the deflections at mid spans of the strengthened beams compared to the control beam. The beam strengthened with U-Wraps anchorage at the flexural area has reduced the deflection at mid span by 10.7 % compares to beam having only U-Wraps at the ends.
4. The different numbers of layers of CFRP sheet affect the flexural strength in such a way that the areas that contacted to the surfaces of the beams. The double area of CFRP sheet has increased the stiffness; hence the ultimate loads of beams also increase. Even though the percentage increase of ultimate load of beams strengthened with one layer of CFRP sheet and beams strengthened with two layers of CFRP sheets is relatively small, 12.9 %, the deflection at mid span was minimized by the beams strengthened with two layers of CFRP sheet.
5. The different locations of U-wraps anchorage of CFRP sheet have given an effect to the flexural strength and the deflection at mid span. The U-wraps anchorage can also delay or prevent the delamination or debonding failures of either concrete cover or FRP sheet. Delamination failures of CFRP sheet at the bottom were observed even though with the existing of U-wraps. The high stress concentration developed had caused the delamination failures.

Acknowledgments This research was financially supported by Fundamental Research Grant Scheme, Ministry of Higher Education (MOHE), Malaysia and Research Management Institute (RMI) of Universiti Teknologi MARA. The authors would like to thank the contribution of Daijobucon Sdn Bhd for supplying the CFRP sheets and to all technicians at heavy structures laboratory at UiTM.

References

1. G.C. Arya, J.L. Clarke, E.A. Kay, P.D. O'Regan, TR: Design guidance for strengthening concrete structures using fiber composite materials: A review. *Elsevier J. Eng. Struct.* **24**, 889–900 (2001)
2. B. Gao, J.K. Kim, C.K.Y. Leung, Experimental investigation of taper ended FRP strips in FRP strengthened RC beams, in *4th International Conference on Advanced Composite Materials in Bridges and Structures*, Calgary, Alberta, 20–23 July 2004
3. A. Khalifa, A. Nanni, Rehabilitation of rectangular simply supported RC beams with shear deficiencies using CFRP composites. *Elsevier Constr. Build. Mater.* **16**, 135–146 (2002)
4. N. Pestic, K. Pilakoutas, Concrete beams with externally bonded flexural FRP-reinforcement: Analytical investigation of debonding failure. *Compos. Part B: Eng.* **34**, 327–338 (2003)
5. N. Mohammad Noh, Effectiveness of RC beams strengthened with near surface mounted (NSM) fiber reinforced polymer (FRP) bars and externally bonded (EB) FRP sheets, MSc Thesis, Universiti Teknologi MARA, Malaysia (2008)
6. B. Gao, J.K. Kim, C.K.Y. Leung, Optimization of tapered end design for FRP strips bonded to RC beams. *Elsevier J. Compos. Sci. Technol.* **66**, 1266–1273 (2005)
7. F. Ceroni, M. Pecce, S. Mattys, L. Taerwe, Debonding strength and anchorage devices for reinforced concrete elements strengthened with FRP sheets. *Elsevier J. Compos. Part B: Eng.* **30**, 429–441 (2007)
8. G.J. Xiong, X. Jiang, J.W. Liu, L. Chen, A way for preventing tension delamination of concrete cover in midspan of FRP strengthened beams. *Elsevier J. Constr. Build. Mater.* **21**, 402–408 (2005)
9. A.H. Al-Saidy, A.S. Al-Harthy, K.S. Al-Jabri, M. Abdul-Halim, N.M. Al-Shidi, Structural performance of corroded RC beams repaired with CFRP sheets. *Elsevier J. Compos. Struct.* **92**, 1931–1938 (2010)
10. A.A. El-Ghandour, Experimental and analytical of CFRP flexural and shear strengthening efficiencies of RC beams. *Elsevier J. Constr. Build. Mater.* Article in press (2010)
11. F. Buyle-Bodin, Use of carbon fiber textile to control premature failure of reinforced concrete beams strengthened with bonded CFRP plates. *J. Ind. Text.* **33**, 145–157 (2004)
12. F. Ceroni, Experimental performances of RC beams strengthened with FRP material. *Elsevier J. Constr. Build. Mater.* **24**, 1547–1559 (2010)

Heat of Sorption and Moisture Buffering Properties of Building Insulation Materials

Neal Holcroft and Andy Shea

Abstract Latent heat of sorption exchanges in hygroscopic materials can affect thermal comfort, and potentially the heating requirements of buildings, while moisture buffering regulates humidity levels, allowing for a healthy indoor air quality. In this study experiments were conducted to compare the moisture buffering performance of three hygroscopic natural fibre insulation (NFI) materials (hemp-lime, hemp fibre, sheep's wool) alongside two more conventional materials (glass wool and gypsum plasterboard). Samples with a surface area of 200×200 mm were exposed to a cycle of step changes in relative humidity between 53 and 75 %, changing every 12 h in isothermal conditions. Their moisture buffering performance was then determined by their change in mass. Thermocouples were placed on the surface and 15 mm below the surface of each sample to record temperature changes. The hemp-lime sample showed the greatest moisture buffering capacity, around double that of the hemp fibre and sheep's wool, which had similar performances. In comparison, the mineral wool and gypsum plasterboard samples showed negligible moisture buffering. Temperature changes were greater at 15 mm than at the surface, with the overall balance of heating and cooling approximately equal at dynamic equilibrium. The sheep's wool saw the largest change in temperature, while the hemp-lime had a higher temperature difference over the whole cycle. These effects will clearly alter internal conditions and should be included in building simulations to determine their impact on energy use.

Keywords Moisture buffering · Heat of sorption · Natural fibre insulation

N. Holcroft (✉) · A. Shea

Building Research Establishment—CICM, University of Bath, Bath, UK

e-mail: N.Holcroft@Bath.ac.uk

1 Introduction

The operation of buildings accounts for around 30–40 % of global energy use [1], much coming from the burning of fossil fuels. The manufacture of building materials accounts for 40–50 % of total raw material flow, much of this with a high embodied carbon, such as steel and cement [2]. Therefore, as currently operating, buildings are a large source of greenhouse gases (GHG). With a population projected to peak at ≈ 10 billion by 2050 [3], (assuming a continuing convergence of fertility rates to replacement level) and the requirement for improvements in standards of living for the majority of these people, there will be a great demand for new housing and the improvement of existing housing in the coming years, resulting in increased use of limited resources and increases in GHG emissions.

Natural fibre insulation (NFI) materials sequester carbon taken up during photosynthesis within the building structure. Life cycle assessments based on UK production have shown that both hemp-lime [4] and sheep's wool [5] insulation have a negative embodied carbon on installation. These materials are also often by-products of food production, so do not take up extra land to produce.

All NFI materials are hygroscopic. Within their structure they have hydroxyl groups which will hydrogen bond with water molecules. The quantity of water adsorbed is related to the relative humidity of their environment, therefore they are able to stabilise the humidity of a room by adsorbing when the relative humidity increases and desorbing as it decreases [6]. This effect is particularly useful in cold or temperate regions with high humidity levels, where requirements for increased insulation and airtightness can have the unwanted effect of increasing the relative humidity to levels which induce mould growth [7], cause health issues [8], and potentially structural damage.

It has also been proposed that moisture buffering may reduce energy use through both direct and indirect effects on heating load [9]. An indirect saving would be to achieve a healthy level of humidity with a lower ventilation rate or greater airtightness [10], therefore losing less heated air to the outdoors, and using less power to run the ventilation system. A direct effect on heating load would be the effect of latent heat exchanges caused by the adsorption and desorption of water vapour.

Osanyintola and Simonson [9] examined the effects of the heat of sorption by comparing two simulations of a 12 m² bedroom in a Northern European climate, one with hygroscopic materials (wood fibreboard and cellulose insulation) and one without. Heating was set to maintain the room at 20–21 °C during the heating season, and moisture levels to that created by two people sleeping at night. The simulation was based on empirical data described in [11]. During occupation it was found that energy use was ≈ 10 % lower in the room insulated with hygroscopic materials, due to heat of sorption. However, over the whole heating season it was nearly equal because when the relative humidity was decreased (people left

the room) evaporative cooling increased energy use. Although, if heating controls were set to account for this it is possible that an energy saving could be achieved.

Qin et al. [12] also modelled the effect of moisture buffering on the cooling load of a building located in a tropical climate. It was estimated that energy use could be decreased by $\approx 16\%$ during occupied hours by reducing the indoor humidity and therefore indoor enthalpy.

The research presented in this paper forms part of preliminary laboratory testing for a project investigating the hygrothermal performance of insulation materials and their suitability for the retrofit of buildings. Moisture Buffering tests are being performed to assess the potential of a series of materials including hemp-lime, hemp fibre, sheep's wool, mineral wool and gypsum plasterboard. As a part of these tests the heat of sorption is also being measured.

2 Methods

2.1 Moisture Buffering Capacity

The ability of a material to adsorb and desorb water vapour was determined by exposing each sample to a cycle of step changes in relative humidity between 53 and 75 %, changing every 12 h, while kept in isothermal conditions of 23 °C in accordance with ISO 24353 [13]. The cycles were repeated until the amount of moisture adsorbed and desorbed was equal.

Each sample had an exposed surface area of 200 × 200 mm with a thickness representative of the product (Table 1). All other surfaces of the sample were covered in aluminium foil to prevent any moisture transfer (Fig. 3). The sample mass was recorded every minute to the nearest 0.1 g using an electronic balance. The conditions were created by placing the sample in a climate chamber with averaged vertical and horizontal air speeds of 0.38 and 0.88 m/s. A windscreen was used to prevent influence of airflow (Fig. 1). The temperature and relative humidity in the chamber were measured every 5 min using a Tiny Tag TV-4505 temperature and relative humidity probe.

The moisture buffering capacity ρ (g/m²) was then calculated using the formula:

$$\rho = \frac{m_a - m_d}{A} \quad (1)$$

where,

m_a Mass of the sample at completion of moisture adsorption process (g)

m_d Mass of the sample at completion of moisture desorption process (g)

A Surface area of sample (m²).

Table 1 Material properties

Material	Manufacturer	Thickness (mm)	Bulk density (kg/m ³ @ 23 °C, 60 % RH)	Thermal conductivity (W/mK)	Percentage of difference between plates
Hemp-lime	Lime technology	90	272 ± 14	0.073	8.41
Hemp fibre	Lime technology	75	42 ± 2	0.043	1.42
Sheep's wool	Black mountain	100	23 ± 4	0.045	1.22
Glass wool	Knauf	100	10 ± 1	0.041	2.23
Gypsum Pb	Knauf	12.5	640 ± 22	0.166	0.90

Fig. 1 Climate chamber with electronic balance and samples

The moisture sorption rate G_n (g/m²h) was also calculated at hourly intervals using the formula:

$$G_n = \frac{m_n - m_{n-1}}{\Delta t} \quad (2)$$

where,

- M_n Mass of the sample at time n
- M_{n-1} Mass of the sample at time $n-1$
- Δt Time elapse.

Fig. 2 LaserComp Fox 600 heat flow meter



2.2 Latent Heat of Sorption

The temperature at the adsorption/desorption surface, and at 15 mm below the surface (12.5 mm in the case of gypsum plasterboard) was measured using T-type Welded Tip Thermocouples. For the hemp-lime samples holes were drilled using a 3 mm drill bit from the base of the sample upwards. For the fibrous materials the insulation was slightly opened up with a probe and the thermocouple pushed in. For the gypsum plasterboard the thermocouples were secured to the top and underneath of the material using small strips of masking tape. Any small holes made for the thermocouples in the exterior of the sample were sealed up with aluminium tape. The calibration of the thermocouples had a standard deviation of between 0.08 and 0.14 °C, over a range of 0–30 °C.

2.3 Thermal Conductivity and Bulk Density

Thermal conductivity of the materials was measured using a Fox 600 heat flow meter (HFM) produced by LaserComp (Fig. 2). This consists of an upper and lower plate able to be maintained at different temperatures using Peltier elements and a water cooling system. Heat flux transducers (254 × 254 mm) are bonded to the centre of both plates, which measure temperature and heat flux every 0.7 s, and average them into blocks every 512 readings. The plates are closed around the sample and the HFM is run until the temperature gradient across the sample is measured to have reached steady-state as set by the equilibrium criteria. For these tests this was set so that heat flux must not vary more than 2 % for 10 successive blocks, with a minimum of 100 blocks for the denser hemp-lime and plasterboard samples, and for 5 successive blocks, with a minimum of 10 blocks for the other

lighter samples, while the temperature of each plate remained within 0.2 °C of the setpoint. The thermal conductivity is then calculated for both plates using the one-dimensional steady-state Fourier equation, and the percentage difference between each plate is given.

Samples of 600 × 600 mm were preconditioned at 60 % RH and 23 °C and weighed at regular intervals, to the nearest 1 g, to determine when they had reached hygric equilibrium. The final value was then used to calculate the sample density at those conditions. As the HFM is not in a conditioned laboratory, the samples were then wrapped in a thin plastic film to maintain this moisture content during testing. The upper and lower plates were set to 0 and 20 °C respectively as suggested for building applications in ISO 8990 [14]. The samples were weighed before and after the test to measure any change in moisture content.

3 Materials

3.1 NFI Materials

Both hemp based insulation materials are made from the stem of the hemp plant. The fibre is mechanically separated from the outside of the stem and the remaining central woody core (shiv) is used to make hemp-lime. The hemp fibre (95 %) is blended with a polyester binder (5 %) to keep the insulation to a specific density and treated with fire protectant. Sheep's wool insulation is produced by first cleaning (scouring) the wool and blending with a recycled polyester binder in the same proportions as with the hemp fibre insulation. The hemp shiv was mixed 1:1.5 parts with lime binder and formed into a 90 × 600 × 600 mm slab. It was conditioned at 23 °C and 60 % RH for 2 years, by which time it should have been fully carbonated. For the moisture buffering tests this slab was cut into 200 × 200 mm pieces using a wood saw.

3.2 Conventional Materials

Both glass wool and gypsum plasterboard are non-hygroscopic, although gypsum has been shown to have some moisture buffering properties [15]. Glass wool is made from recycled glass, which is heated to 1,500 °C and spun into fibre, then coated in a formaldehyde based resin as a binding agent. Plasterboard is made by making a gypsum slurry ($\text{CaSO}_4 \cdot 2\text{H}_2\text{O}$), which is formed into sheets, dried and cut into sections. The plasterboard sample was made by fixing the section of plasterboard above 100 mm of glass wool using four thin pieces of wood doweling so the sample was representative its configuration in an actual building (Figs. 3, 4).

Fig. 3 Test samples (*Back* Sheep’s wool, gypsum plasterboard, glass fibre; *Front* Hemp fibre, hemp-lime)

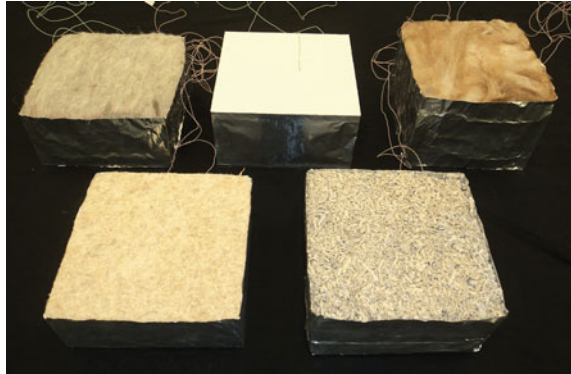
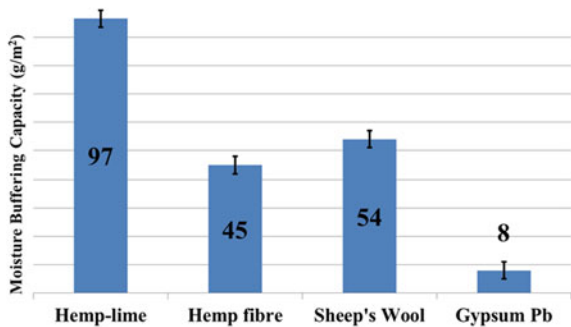


Fig. 4 Gypsum plasterboard sample



Fig. 5 Moisture buffering capacity of samples

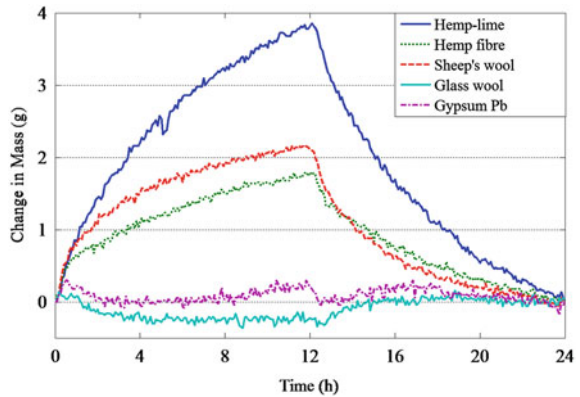


4 Results and Analysis

4.1 Moisture Buffering Capacity

Results of the moisture buffer capacity tests are given in Fig. 5. The hemp-lime sample showed the greatest capacity; roughly double that of the two natural open fibre materials, of which, the sheep’s wool sample performed slightly better than the hemp fibre. However, this may be related to the difference in thicknesses of the materials. The gypsum plasterboard sample only changed its mass by a small amount (0.2–0.3 g), which was difficult to clearly detect with the sensitivity of the

Fig. 6 Moisture adsorption and desorption at dynamic equilibrium



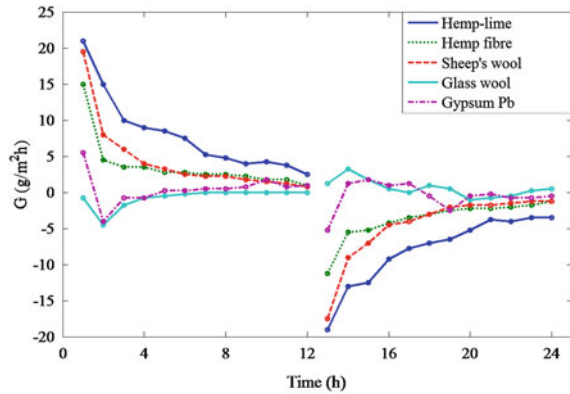
balance used. The glass wool and gypsum samples followed similar trends with slight changes in mass after a step change in relative humidity. Unexpectedly, the glass wool slightly decreased in mass by ≈ 0.3 g during the high relative humidity period (Fig. 6). Being inert and impervious to water it was expected there would be no change in mass. However, this result was a clear trend over all four cycles measured, although again the change in mass was very small and could potentially be due to the instrumentation.

Previous moisture buffering capacity tests have been conducted on hemp-lime and gypsum plasterboard, although they are not directly comparable to these tests as they were conducted under different conditions. The NordTest Project [15] used adsorption and desorption periods of 8 and 16 h respectively, and a change in relative humidity of 33–75 %. Under these conditions 12.5 mm of gypsum plasterboard buffered 27 g/m². Collet et al. [16] used the same protocol to test a hemp-lime sample that gave a value of 90 g/m², however, it was more dense (430 kg/m³) than the sample described in this paper.

Despite the differences in method between the NordTest Project and ISO 25343 the result for the hemp-lime sample matches well to Collet's measurements. This is because there is a relatively small change in water content of hemp-lime between 33 and 53 % RH, with larger changes happening at higher humidities [17]. Also, as can be seen in Fig. 7, between 8 and 12 h the moisture sorption rate had almost levelled off, and was much lower than the initial rate.

The moisture buffering capacity of gypsum plasterboard measured for the NordTest Project was higher than the result shown in this paper. Figure 6 shows that after 30 min the gypsum plasterboard sample had absorbed as much as was possible over this change in relative humidity, and so had reached hygric equilibrium. Therefore, the differences in time scheme had no effect on the results. However, as the change in relative humidity was greater in the NordTest Project the sample began absorption at a lower moisture content, so was able to absorb more moisture.

Fig. 7 Hourly moisture adsorption and desorption rates



4.2 Rates of Adsorption and Desorption

Over the first 20 min the sheep's wool and hemp fibre samples adsorbed moisture most rapidly (Fig. 6). However, after 30 min the hemp-lime had adsorbed more than the hemp fibre, and after 60 min, more than the sheep's wool. From then until the end of the adsorption period the hemp-lime continued to increase in mass at the fastest rate (Fig. 7). After 4 h the sheep's wool and hemp fibre samples converged on the same adsorption rate. After 12 h the hemp-lime sample was still adsorbing at $2.5 \text{ g/m}^2 \text{ h}$, while the hemp fibre was at $1 \text{ g/m}^2 \text{ h}$ and sheep's wool $0.75 \text{ g/m}^2 \text{ h}$. The desorption rates mirrored closely the adsorption rates as would be expected in a dynamic equilibrium.

Being a dynamic system the moisture buffering capacity test is a function of both the material's ability to store moisture and its permeability to water vapour. From these results it can therefore be inferred that, of the hygroscopic materials tested, the sheep's wool is the most permeable, as it has the fastest initial increase in mass, followed by hemp fibre then hemp-lime, which is in alignment with their measured densities (Table 1). However, as the rate of increase of the sheep's wool and hemp fibre slow while the hemp-lime continues at a higher rate it must have a greater storage capacity. Sorption isotherm and water vapour diffusion tests will be conducted to test this hypothesis.

4.3 Latent Heat Changes

When analysing this data it is important to consider that the thermocouples are only measuring a single point on the whole sample surface. There may be some variation across the surface, which is not detected by this method.

The temperature at 15 mm into the sample was higher than at the surface in all cases except the glass wool, for which both temperatures remain almost identical

Fig. 8 Surface temperature during adsorption and desorption

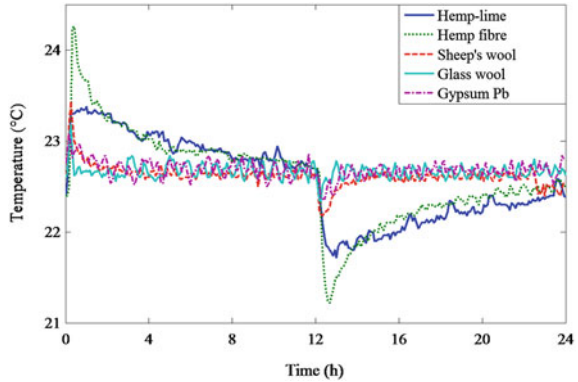
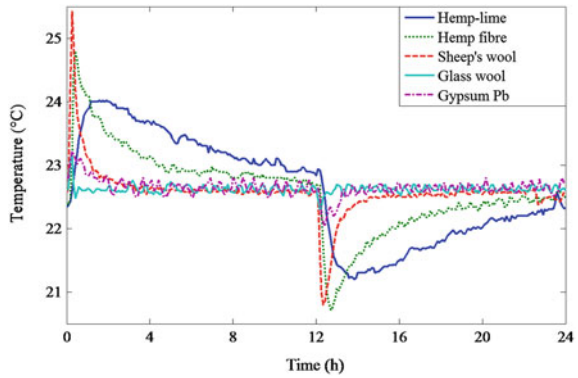


Fig. 9 Temperature at 15 mm below the surface



(Figs. 8, 9, y axes differ). Simulations of the hemp-lime sample conducted using the dynamic heat and moisture transfer software WUFI[®] predicted this result, showing that the maximum and minimum temperatures are likely to be 4–5 mm below the surface. This is due to air movement in the chamber quickly cooling the surface. This seems to have the largest effect on the sheep's wool sample, with its surface temperature being much cooler than at 15 mm.

At 15 mm (Fig. 9) the sheep's wool responded most rapidly to the step change in humidity, increasing 2.9 °C in 8 min, but then quickly returned to the ambient temperature. The hemp fibre increased 2.4 °C in 13 min but continued to give off heat, so cooling more slowly. The hemp-lime sample reacted more slowly taking 1 h to increase 1.7 °C, but then maintained a higher temperature than the other samples over the 12 h. The temperature underneath the gypsum plasterboard showed only a small increase of 0.5 °C.

These results correlate well with the rates of adsorption (Fig. 7). Indeed, the moisture sorption rate, G_n ($\text{g}/\text{m}^2 \text{ h}$), could be assumed to be directly proportional to the heat flux (W/m^2) produced by latent heat, which should be related to the change in temperature. This data will therefore be useful in validating future heat and moisture transfer models.

When comparing the temperatures during adsorption and desorption, the hemp-lime results are almost a mirror image, with the areas under (and above for desorption) the curve equal. For the sheep's wool and hemp fibre the temperature increase at the beginning of the adsorption period is greater than the decrease at the start of desorption. However, the temperature decrease is at a slower rate and stays cooler for a little longer so overall the difference is small. This effect may be due to a hysteresis between adsorption and desorption [18].

James et al. [19] also measured the effect of latent heat during moisture buffering tests. Again a different protocol was used using adsorption and desorption periods of 24 h each, and a change in relative humidity between 30 and 70 %. Three sections of 500 × 500 mm gypsum plasterboard were layered on top of each other and the temperature and relative humidity were monitored between the sheets. The step change in relative humidity induced a temperature increase of approximately 0.5 °C, the same as the temperature change recorded in this paper. However, it took 4–5 h rather than the 8 min shown here, which could be due to the layering of the plasterboard.

4.4 Thermal Conductivity and Bulk Density

The manufacturers of the hemp fibre and sheep's wool both gave thermal conductivities of 0.039 W/mK for dry samples. The measurements made at 60 % RH are both a little higher than this value, consistent with the adsorption of water vapour onto the fibres. The thermal conductivity of the glass wool was not affected by being at 60 % RH. However, if liquid water condensed within it then this would have a significant effect. The properties of hemp-lime are variable. Besides moisture content, the density is a significant factor in determining its thermal conductivity, but other factors may have an effect, such as: the types of lime and hemp used; the ratio of lime, hemp and water when mixed; the sample age, and therefore, extent of carbonation of the lime. However, the measured value is close to what would be expected for its density and moisture content [20].

During the test the hemp fibre sample increased its mass by 1 g (0.1 %), the sheep's wool by 2 g (0.3 %), and the hemp-lime by 2 g (0.02 %) showing that the technique of wrapping the samples in a thin plastic film was effective at maintaining the moisture content. For the hemp fibre and sheep's wool the percentage difference between the plates was less than 2 %, indicating good accuracy. For the hemp-lime sample it was 8 %. This is because moisture transfer is slower in hemp-lime, so a moisture gradient across the sample will not have had time to establish during the test period. The resulting moisture movement and latent heat exchanges make it more difficult to establish steady heat transfer.

5 Conclusions

The hemp-lime sample showed the largest moisture buffering capacity of the samples so far tested, adsorbing moisture at higher rate than the other materials except over the first hour after the step increase in humidity. The sheep's wool and hemp-fibre performed similarly, but with the sheep's wool adsorbing more rapidly over the first 4 h. The conventional materials had a negligible moisture buffering capacity. Hemp-lime should therefore be able to regulate indoor humidity the most effectively; however, the surface is usually finished with a lime plaster, which is likely to reduce its buffering capacity. The effect of this will be studied in future experiments.

The hemp-lime sample produced heat over the full adsorption period, but also cooled the most during the desorption period. The sheep's wool sample had an initial peak in temperature then quickly returned to ambient conditions, while the hemp fibre sample maintained temperatures between the two. Overall the heat produced was balanced out by the cooling effect, which should be expected at dynamic equilibrium. However, these heat flows should be included and building simulations as the heating load may be able to be adjusted to reduce energy use.

Acknowledgments The authors thank the EPSRC for funding this work (grant EP/J019917/1) and the following industrial partners for their support: Lime Technology, White Design Associates, Integrated Environmental Solutions, Arup, and Plant Fibre Technology. We also acknowledge the help and support of staff and students at BRE CICM, Department of Architecture and Civil Engineering at the University of Bath.

References

1. United Nations Environment Programme, *Buildings and Climate Change: Status, Challenges and Opportunities* (2007)
2. M. Jennings, N. Hirst, A. Gambhir, *Reduction of carbon dioxide emissions in the global building sector to 2050*, Report GR3, Grantham Institute for Climate Change, Imperial College London (2011)
3. United Nations, Department of Economic and Social Affairs, *World Population Prospects* (2011)
4. K. Ip, A. Miller, Life cycle greenhouse gas emissions of hemp-lime wall constructions in the UK. *Resour. Conserv. Recycl.* **69**, 1–9 (2012)
5. R.J. Murphy, A. Norton, *Life Cycle Assessments of Natural Fibre Insulation Materials*, National Non-Food Crops Centre, Imperial College London (2008)
6. A. Shea, M. Lawrence, P. Walker, Hygrothermal performance of an experimental hemp-lime building. *Constr. Build. Mater.* **36**, 270–275 (2012)
7. K. Sedlbauer, *Prediction of mould fungus formation on the surface of and inside building components*, Fraunhofer Institute for Building Physics (2001)
8. A. Arundel, E. Sterling, J. Biggin, T. Sterling, Indirect health effects of relative humidity in indoor environments. *Environ. Health Perspect.* **65**, 351–361 (1986)

9. O.F. Osanyintola, C.J. Simonson, Moisture buffering capacity of hygroscopic building materials: experimental facilities and energy impact. *Energy Buildings* **38**(10), 1270–1282 (2006)
10. C.J. Simonson, M. Salonvaara, T. Ojanen, Moderating indoor conditions with hygroscopic building materials and outdoor ventilation. *ASHRAE Trans.* **110**(2), 804 (2004)
11. C.J. Simonson, M. Salonvaara, T. Ojanen, Heat and mass transfer between indoor air and a permeable and hygroscopic building envelope: Part I—Field measurements. *J. Therm. Envelope Build. Sci.* **28**(1), 63–101 (2004)
12. M. Qin, G. Walton, R. Belarbi, F. Allard, Simulation of whole building coupled hygrothermal airflow transfer in different climates. *Energy Convers. Manage.* **52**, 1470–1478 (2011)
13. International Organization for Standardization, *Hygrothermal Performance of Building Materials and Products—Determination of Moisture Adsorption/Desorption Properties in Response to Humidity Variation*, ISO 24353 (2008)
14. International Organization for Standardization, *Thermal Insulation—Determination of Steady-state Thermal Transmission Properties—Calibrated and Guarded Hot Box*, ISO 8990 (1996)
15. C. Rode, R. Peuhkuri, L.H. Mortensen, K.K. Hansen, B. Time, A. Gustavsen, T. Ojanen, J. Ahonen, K. Svennberg, L.E. Harderup, J. Arfvidsson, *Moisture Buffering of Building Materials*, Department of Civil Engineering, Technical University of Denmark (2005)
16. F. Collet, J. Chamoin, S. Pretot, C. Lanos, Comparison of the hygric behaviour of three hemp concretes. *Energy Buildings* **62**, 294–303 (2013)
17. F. Collet, M. Bart, L. Serres, M. Jacques, Porous structure and water vapour sorption of hemp-based materials. *Constr. Build. Mater.* **22**(6), 1271–1280 (2008)
18. C.A.S. Hill, A.J. Norton, G. Newman, *Natural Fibre Insulation Materials—The Importance of Hygroscopicity in Providing Indoor Climate Control*, NOCMAT, Bath, UK, 6–9 Sept 2009
19. C. James, C.J. Simonson, P. Talukdar, S. Roels, Numerical and experimental data set for benchmarking hygroscopic buffering models. *Int. J. Heat Mass Transf.* **53**(19–20), 3638–3654 (2010)
20. L. Arnaud, *Comparative Study of Hygrothermal Performances of Building Materials*, NOCMAT, Bath, UK, 6–9 Sept 2009

Performance Based Design of Self-Compacting Concrete Incorporating Class F Fly Ash

Juli Asni Lamide and Roslli Noor Mohamed

Abstract The application of self-compacting concrete (SCC) in speeding the development of construction technology has become a growing trend due to its known advantages. It is now well established since it has three significant properties which are flowing or filling ability, passing ability and segregation resistance as the main self-compactability characteristics. As a result of all these capability, SCC has increased the workability in the fresh concrete properties while maintaining or even increase the strength in hardened concrete properties. This study presents an experimental study on the performance based design of self-compacting concrete incorporating Class F fly ash where a total of 6 cubes, 3 cylinders and 3 prisms were cast and tested to failure while another 6 cubes, 3 cylinders and 3 prisms were also prepared for the normal concrete (NC) as control specimens. The mix design of SCC was established based on limited water-powder ratio to meet the self-compactability characteristics. The performance of SCC was studied through the fresh concrete properties as well as the mechanical properties of hardened concrete. Experimental results on the fresh and hardened properties of SCC mix design indicated that both workability and strength of self-compacting concrete were found to be higher compared to the normal concrete.

Keywords Self-compacting concrete · Fly ash · Workability · Strength

1 Introduction

Self-compacting concrete (SCC) is known as an innovative concrete which flows under its own weight in fresh state without any agitation or mechanical consolidation to fill the formwork and encapsulate the reinforcement [1]. Because of its

J. A. Lamide (✉) · R. N. Mohamed

Faculty of Civil Engineering, University Technology of Malaysia, Johor Bahru, Malaysia
e-mail: juliasni88@yahoo.com

advantages compared to normal concrete (NC), SCC greatly improved the quality of concrete construction and thus it has been implemented extensively in bridge decks and piers, pavements, road surfaces, precast structural elements and also highrise building [2].

It is well known the design of SCC requires a careful combination of the various material components of the mixture. SCC must achieve high workability and flow into the formwork under its own weight without compaction and no segregation [3]. The plastic attributes of SCC is characterized by filling ability, passing ability and segregation resistance.

The mix design of concrete could be only considered as having self-compactability when all these three characteristic is achieved; namely filling ability, passing ability and segregation to resistance [4]. General experience has shown that the rheological study of concrete is important for the construction industry especially when dealing with SCC. The rheological properties of SCC is affected by the type and volume of superplasticizer, water to powder ratio, maximum size and proportion of coarse aggregate and mixing sequence and time as well [5].

2 Aims and Objectives

The aims and objectives of this study are:

1. To study the properties and performance of self-compacting concrete in fresh and hardened state.
2. To produce a concrete with high workability properties that can easily flows under its own weight in congested reinforcement zone in precast concrete connections.

3 Background of Problem

Self-compacting concrete is first developed by Professor Hajime Okamura in the early 1980s due to the problem of lacking of skilled workers to work in the construction [1]. By using SCC, the construction could be progressed with limited number of workers. Okamura introduced SCC technology based on using conventional superplasticizers so that highly flowable concrete could be created. In addition, viscosity-modifying agents (VMA) are also added to the mixture which is useful in increasing the plastic viscosity, thus prevents the occurrence of segregation [1].

In the 1990s, the technology starts to spread in Europe. They came with an approach which using powders such us cement, supplementary cementitious materials, and inert materials that are able to pass the 150 μm sieve to increase plastic viscosity. Later, the addition of polycarboxylate superplasticizers and

optimization of aggregates improved the quality of SCC and reducing the materials cost [1].

Generally, in any location of reinforcement congestion, placement of concrete and compaction of concrete, even with a mechanical vibrator, becomes very difficult [6]. Consequently, it will eventually lead to defects such as honey combing which affected the strength and durability of concrete. This undesirable phenomenon could be eliminated or minimised if congestion of reinforcement can be reduced through design optimization. However, another option is by using high workability concrete, which can flow easily around congested reinforcement, thus overcoming this problem.

As such, failure of precast concrete joint or connection always associated with the poor casting quality of concrete such as honeycombs, which, in most cases, resulted from the congestion of reinforcement [7]. Therefore, SCC could be applied in precast concrete industry because the use of self-compacting concrete (SCC) is expected to not only eliminating the vibration works, but perhaps more economical in performance compared to conventional concrete [6]. SCC also could reduce the construction time of concrete structure by eliminating the vibration works and reduction of noise problem especially in areas where vibration works are prohibited [8].

4 Experimental Set-Up

4.1 Materials

In order to produce for the concrete mix design, raw materials such as cement, fly ash, coarse aggregate, fine aggregate were prepared. The type of cement used in this study is Ordinary Portland Cement (OPC). Class F fly ash produced by coal-burning electric utilities obtained from Tanjung Bin Power Plant is used. Table 1 shows the chemical composition of Class F fly ash extracted from Tanjung Bin Power Plant. It has been decided that both coarse aggregates and fine aggregates used are crushed type. Sieve analysis was conducted according to BS 882: 1992 to find out the percentage of the fine aggregates that passes through 600 μm . The maximum size of aggregates used is 10 mm. Glenium ACE 389 RM was used as the superplasticizer.

4.2 Mix Design

The concrete mix is designed to achieve compressive strength of Grade 30. In this study, DOE method of mix design is used in order to design the concrete mix for normal concrete while for the SCC, the mix design is developed based on the

Table 1 Chemical composition of Class F fly ash [16]

Chemical contents	Formula	Concentrations (%)
Carbon dioxide	CO ₂	0.10
Silicon dioxide	SiO ₂	47.10
Aluminium oxide	Al ₂ O ₃	30.00
Iron oxide	Fe ₂ O ₃	7.34
Lime	CaO	7.21
Titanium dioxide	TiO ₂	1.83
Potassium oxide	K ₂ O	1.62
Magnesium oxide	MgO	1.52
Phosphorus pentoxide	P ₂ O ₅	1.37
Sodium oxide	Na ₂ O	0.72
Sulphur trioxide	SO ₃	0.49
Strontium oxide	SrO	0.32
Barium oxide	BaO	0.27

modification of previous research to meet the SCC requirements, as given by European Federation 2005 [9]. Table 2 shows the initial range of certain parameters as a guide to achieve self-compactability characteristics. During the mixing process, modification is made until a satisfactory mix is obtained, based on the results of fresh concrete properties. The mix design could be considered as SCC when satisfactory rheological properties of fresh concrete such as filling ability, passing ability and segregation resistances are achieved [10].

4.3 Experimental

Two types of experimental series were carried out after the mixing process is done. The first one is fresh concrete test, which consists of slump flow test, J-Ring test, L-Box ratio test, and V-funnel flow time. The second one is testing on the hardened concrete.

1. *Testing of fresh concrete:* Slump flow test was carried out to assess the flowability and the flow rate of self-compacting concrete in the absence of obstructions. The test was carried out based on the slump test described in EN 12350-2. The result obtained could be used as an indicator of the filling ability of self-compacting concrete. Based on Specification and Guidelines for SCC [11], the diameter ranging from 650 to 800 mm can be accepted for SCC. In the slump flow test, the flowrate can be measured through t_{500} and the segregation resistance can be observed [12].

Apart from slump flow test, J-Ring test, L-Box test and V-funnel test were also conducted in order to assess the flowability and passing ability, and also on the stability of SCC [13]. The L-Box ratio obtained from test should be in the range of 0.8–1.0 while for the J-Ring value, it should be within the range of 0–10 mm.

Table 2 Typical range of SCC mix composition [9]

Constituent	Typical range by mass (kg/m ³)	Typical range by volume (l/m ³)
Powder	380–600	
Paste		300–380
Water	150–210	150–210
Coarse aggregate	750–1000	270–360
Fine aggregate	Content balances the volume of the other constituents, typically 48–55 % of total aggregate weight	
Water/powder ratio by vol		0.85–1.10

Fig. 1 Dimensions of the J-ring and positions for measurement of height differences [10]

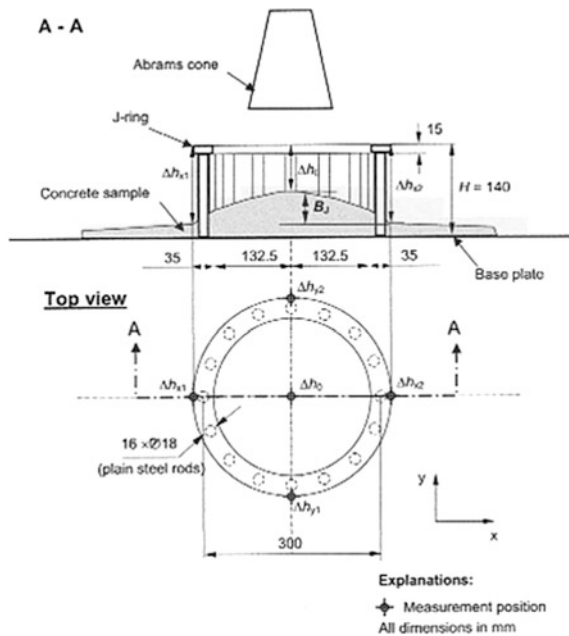


Figure 1 shows the dimensions of J-ring and positions for measurement of height differences in order to record the data for the need of calculating the blocking step value. The dimensions of L-box apparatus and the positions for measurement of H_1 and H_2 are shown in Fig. 2. H_1 and H_2 are used to calculate the value of L-box ratio. V-Funnel test is used to assess the viscosity, flowability and segregation resistance of self-compacting concrete. It indicates the period of a defined volume of SCC, needs to pass through a narrow opening. This test evaluates the flowing ability of SCC by measuring the time in seconds, taken for the mixture to completely empty out through the V-funnel. As stated by EFNARC [11], a concrete could only be qualified as SCC if the time taken ranging from 6 to 12 s.

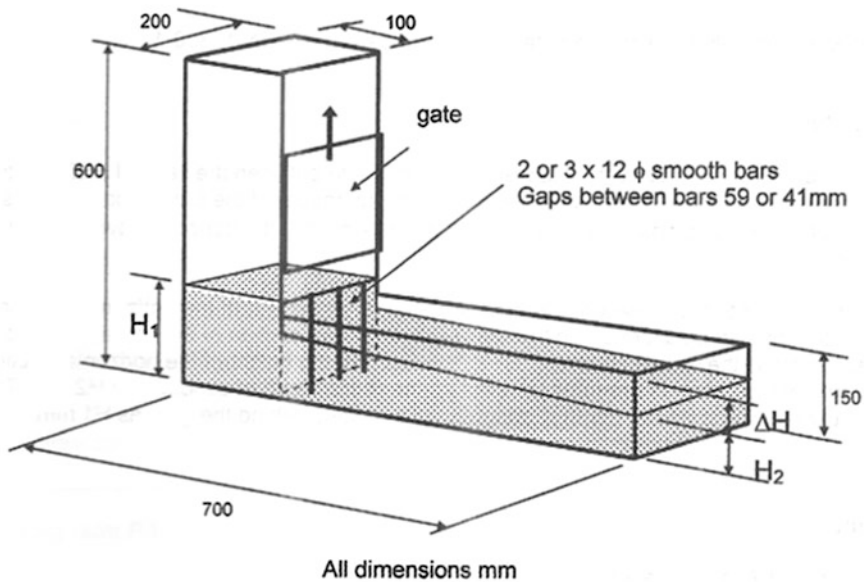


Fig. 2 Dimensions of L-box apparatus and positions for measurement of H_1 and H_2 [10]

2. *Testing of hardened concrete:* Testing on the hardened concrete was conducted to confirm the cube compressive strength, flexural tensile test and splitting tensile tests. The test compares the over mentioned properties between NC and SCC. The cube compressive test is carried out based on BS 1881: Part 108: 1983. A total of 12 concrete cubes with dimension of $100 \times 100 \times 100$ mm were prepared and tested at the age of 7 days and 28 days. The second test is splitting tensile strength of cylindrical concrete specimens. The test was carried out in accordance to BS 1881: Part 117: 1983. Total of 6 concrete cylinders with 150 mm in diameter and 300 mm height is to be tested after 28 days curing process. Another test was flexural test which is in accordance with (BS 1881: Part 118: 1983). The size of prism is $100 \times 100 \times 500$ mm. The flexural strength test was conducted at the age of 28 days under four points loading until the prisms fail and results of ultimate load was recorded.

5 Results and Discussion

5.1 Mix Design

In general, the mix design between the normal concrete and self-compacting concrete was different. The workability of SCC mix increased due to the approach of increasing the powder content while minimizing the content of coarse aggregate

Table 3 Mix proportions

Component	Content (kg/m ³)	
	NC	SCC
Characteristic strength (N/mm ²)	30	30
Cement	395.00	411.56
Fly ash	0	116.08
Coarse aggregate	967.50	629.10
Fine aggregate	824.20	752.82
Superplasticizer (1.5 % by powder weight)	5.93	7.91
Water	213.3	185.00
W/P Ratio	0.54	0.35

compared to the fine aggregate in the mixture. In contrast, the normal concrete showed a low workability due to the high portion of coarse aggregate compared to the fine aggregate. Therefore, NC mixture needs more energy in order to make the coarse aggregate flow with the cement paste easily and the passing ability is also affected by the content of coarse particles [14]. Table 3 presents mix proportions for NC and SCC used in this study. As shown in Table 3, the water-powder ratio was different between NC and SCC mixture. It was found that, the powder content in SCC mixture was increased with the addition of fly ash. Therefore, the SCC has a lower water-powder ratio compared to NC. Fly ash was added in the SCC mixture to ensure the water-powder ratio by volume is in the range of 0.85–1.10 thus, meets the requirement of self compacting concrete.

5.2 Fresh Concrete Testing

Figure 3 shows four testing that has been performed in the laboratory while Table 4 shows the results obtained from all these tests.

1. *Slump flow test*: For the slump flow test, the average diameter is 670 mm, while the t_{500} mm is 2.05 s. Based on Fig. 4, the circular spread of concrete makes the test result acceptable and it showed that the mixture flows homogeneously without any segregation. Therefore, the filling ability property for this mixture is achieved since all specified criteria have been fulfilled. According to Schutter [10], the higher the slump flow spread, the greater is the filling ability of the fresh mix. Meanwhile, the only test carried out to observe the workability properties of NC was the slump test and the result obtained from this test was 90 mm which is in the range of 60–180 mm.
2. *J-ring test*: The calculated J-ring value for this test is 9.25, which fall in the range of self-compactibility characteristics given by EFNARC [11]. In the J-Ring test, the presence of obstacles did not affect the flow of concrete. The observations indicated that the mixture flow homogeneously yet spread of



Fig. 3 Testing on fresh concrete properties for SCC

Table 4 Results of fresh properties of SCC

Name of test	Results	Range
Slump flow test	670	650–850 mm
t _{500 mm} Slump flow test	2.05	2–5 s
J-Ring test	9.75	0–10 mm
L-Box ratio	0.82	0.8–1.0
V-Funnel test	6	6–12 s

mixture was circular. The J-ring value will be higher if the mixture is obstructed by the bars, thus results to block the passing ability. The result obtained from this test is the blocking step B_j value which indicated the necessary level of passing ability of self-compacting concrete. This value actually indicates the passing ability by the size of the blocking step B_j between the levels of the concrete inside and outside of the ring at the end of its flow.

Fig. 4 Observation on segregation of mixture after filling the L-box



3. *V-funnel test*: As seen in Table 4, the V-funnel flow time, t_v is 6 s. Based on the range given by EFNARC [11], the result obtained is acceptable. The V-funnel flow time t_v measures the filling ability. The time is affected by the viscosity (water-powder ratio and the free water volume) itself. A substantial increase of t_v might occur which indicate a partial blocking caused by increased concentration of coarse aggregate at the bottom of the funnel. However, the filling ability of concrete is high enough to achieve satisfied result for this test because the smooth surface characteristic and spherical shape of fly ash improved the workability of concrete mixture [12].
4. *L-box test*: The L-Box ratio obtained from the L-Box test is 0.82 which was calculated by dividing the value of H_2 to H_1 . This test can be used to assess the passing ability and leveling ability of concrete. L-Box test was also used to detect the resistance segregation of the mixture. As shown in Fig. 4, the coarse aggregate still can be seen at the top of the L-box which means there are no segregation between the coarse aggregate and the cement paste.

5.3 Hardened Concrete Testing

Three different tests were performed in order to evaluate the hardened or mechanical properties of concrete whereby, every value that obtained from all testing was taken based on the average from the three tested specimens.

1. *Cube compressive strength*: Based on the results obtained, SCC achieved highest average compressive strength at the age of 7 days at 28.27 MPa, while the lowest compressive strength was the NC cube which is 25.36 MPa. The compressive strength results at the age 28 days are 37.65 and 42.18 MPa for NC and SCC respectively. It also showed the same pattern of result obtained as the compressive strength at the age of 7 days whereby, the compressive strength increase slightly for the SCC compared to NC. Figure 5 shows that the highest average compressive strength was at the age of 28 days. Therefore, it is

Fig. 5 Graph of compressive strength of normal concrete and self-compacting concrete

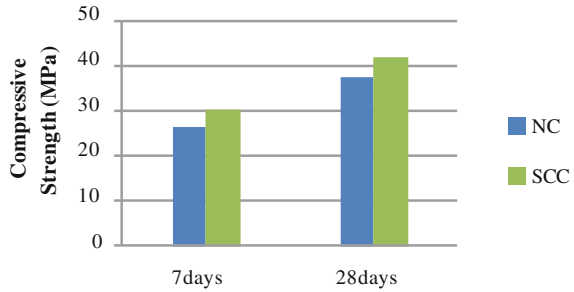


Fig. 6 Cylinder tensile splitting strength

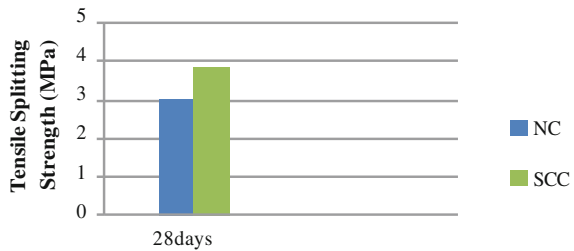
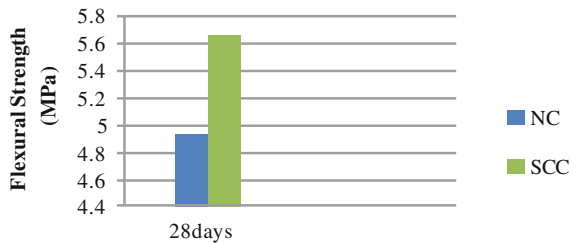


Fig. 7 Flexural strength



found that the compressive strength of SCC provides 10.74 % of increment compared to NC.

- Splitting tensile test:* As shown in Fig. 6, the tensile splitting strength of SCC specimens was slightly higher compared to NC cylinder. NC cylinder attained lower value due to a corresponding lower compressive strength as reported earlier in the compressive strength properties. The characteristic tensile splitting strength obtained through this test for SCC and NC is 3.84 and 2.98 MPa, respectively. According to previous researcher [15], the tensile strength of concrete is normally around 10 % from the compression strength of concrete. The mode of failure indicates that the cylinder has vertical crack at the centre of cylinder which means, with an extended load applied to the specimen the cylinder tend to split into two parts.
- Flexural tensile test:* As shown in Fig. 7, SCC shows high value of flexural strength compared to NC. The flexural strength recorded for SCC and NC from this test were 5.67 MPa and 4.93 MPa respectively and the percentage

difference for these two values is 13.05 %. Thus, it can be seen that, the uses of SCC in construction may benefit from the increment of flexural strength. In flexural test, there was no first crack found nearby the mid span of the prism when the load is increased. At about the peak loads, the stiffness of the segment started to decrease. A vertical crack quickly formed at the midspan of the segment as the peak load was reached and this led almost immediately to the segment being broken into two at the midspan. All specimens were failed without any earlier sign of cracks when the load was increased to the maximum level.

6 Conclusion

Based on the overall results, analysis and comparisons in term of the fresh concrete properties and hardened concrete properties between normal and self compacting concrete, the main conclusion that can be drawn are as follows:

- The addition of fly ash as part of powder content in the mixture does provide positive effects on the workability of SCC.
- The workability of SCC concrete is better than NC because its ability to flow under its own weight without any compaction efforts in order to fill the formwork.
- The increment in compressive and tensile strength of SCC can be explained by the lower water-powder ratio, as compared to NC. The use of SCC improved the mechanical properties such as compressive strength, tensile splitting strength and flexural behavior of the concrete compared to NC due to less of honeycombs and high quality concrete observed in SCC products.

A general conclusion that can be drawn is that the mixture was considered as SCC because the passing ability, filling ability and segregation resistance properties of SCC has been achieved and the most important thing when it is able to enhanced the mechanical properties of concrete. Thus, SCC mix design is greatly suggested to be used in precast concrete industry as it is able to overcome the problems in this industry.

Acknowledgments The authors wish to acknowledge the University Technology of Malaysia for the support that made this study possible, as well as all previous researchers who have supplied the information needed in preparing and writing of this paper.

References

1. Technical Committee, *An Introduction to Self-Consolidating Concrete (SCC)* (GRACE Construction Products, Cambridge, 2005)
2. S. Goel, S.P. Singh, P. Singh, Flexural fatigue strength and failure probability of Self Compacting Fibre Reinforced Concrete beams. *Eng. Struct.* **40**, 131–140 (2012)
3. V. Corinaldesi, Combined effect of expansive, shrinkage reducing and hydrophobic admixtures for durable self compacting concrete. *Constr. Build. Mater.* **36**, 758–764 (2012)
4. Technical Committee, *Mixture Proportioning Self-Consolidating Concrete (SCC)* (GRACE Construction Products, Cambridge, 2005)
5. A.S. El-Dieb, M.M. Reda Taha, Flow characteristics and acceptance criteria of fiber-reinforced self-compacted concrete (FR-SCC). *Constr. Build. Mater.* **27**(1), 585–596 (2012)
6. Y.W. Choi, H.K. Lee, S.B. Chu, S.H. Cheong, W.Y. Jung, Shear behavior and performance of deep beams made with self-compacting concrete. *Int. J. Concr. Struct. Mater.* **6**(2), 65–78 (2012)
7. H. Zardoum, Application of rigid bodies-spring model to precast structure reinforced with steel fibre. *J. Struct. Eng. JSCE* **45** (1999)
8. M.H.A. Beygi, J.V. Amiri, A.R. Moazen, N.R. Malidareh, M. Harajpoor, The investigation of effect of steel fiber on the shear behavior of self compacting concrete beams with normal and high strength, in *Our World In Concrete & Structures* (2008)
9. EPG (European Project Group). The European guidelines for self-compacting concrete. UK (2005)
10. G. De Schutter, P.J.M. Bartos, P. Domone, J. Gibbs, *Self-Compacting Concrete* (Whittles Publishing, Caithness, 2008)
11. EFNARC. Specification and guidelines for self-compacting concrete. **44** (2002)
12. B.K. Rao, Steel fibre reinforced self-compacting concrete incorporating class F fly ash. *Int. J. Eng. Sci. Technol.* **2**(9), 4936–4943 (2010)
13. P. Aggarwal, R. Siddique, Y. Aggarwal, S.M. Gupta, Self-compacting concrete-procedure for mix design. *Leonardo Electron. J. Practices Technol.* **12**, 15–24 (2008)
14. S. Grunewald, J.C. Walraven, Parameter-study on the influence of steel fibers and coarse aggregate content on the fresh properties of self-compacting concrete. *Cem. Concr. Res.* **31**, 1793–1798 (2001)
15. N. Arıoğlu, Z. C. Girgin, and E. Arıoğlu, Evaluation of ratio between splitting tensile strength and compressive strength for concretes up to 120 MPa and its application in strength criterion. *ACI Mater. J.* 103 (2006)
16. A.R. Awang, A. Marto, A.M. Makhtar, Geotechnical properties of tanjung bin coal ash mixtures for backfill materials in embankment construction. *EJGE* **16**, 1515–1531 (2011)

Mechanical Properties of Modular Cement Block Reinforced with Treated Oil Palm Trunk Fiber

Mazlina Mohamad and Zakiah Ahmad

Abstract As brick is not considered as Industrialised Building System (IBS) due to its size. Therefore, this study manufactured sand-cement block with modular dimension; 400 mm × 200 mm × 300 mm. However, sand-cement block is heavy and brittle especially with modular size. In-line with requirement for sustainable and environmentally friendly building materials, therefore this study is looking at the potential in using oil palm trunk fiber (OPTF) in the production of modular sand-cement block with high percentages fiber in order to reduce weight. The investigation on the mechanical properties of modular oil palm fiber sand-cement blocks have been carried out by varying process parameters, such as fiber condition (untreated and alkali treated) and fiber percentages (20, 30 and 50 % by volume). The treated and untreated fibers were characterised by tensile strength and scanning electron microscopy. The effects of fiber treatments on the physical and compressive strength properties of OPTF cement blocks were determined. The results showed that compressive strength of OPTF cement blocks increases with increasing in the fiber percentage due to the improvement of bonding between the matrix and fiber.

Keywords Oil palm trunk fiber · Treated fiber · Lightweight blocks · Modular unit

1 Introduction

In the construction of walling units, cement block is preferred due to bigger dimension as compared to bricks as well as reduction in the time of construction and manpower. However, cement block is heavy and the materials in cement block

M. Mohamad (✉) · Z. Ahmad
Institute of Infrastructure Engineering and Sustainable Management,
Universiti Teknologi Mara, 40450 Shah Alam, Selangor, Malaysia
e-mail: maz_3116@yahoo.com

becoming more expensive in the market, i.e. the price of sand and cement. One of the ways to reduce the weight of the block is to replace the sand with natural fiber at large quantity. The addition of the fibers not only reducing the weight but it improves a lot in terms of the block's mechanical properties. Such as non-abrasive, combustible, nontoxic, low cost, biodegradable properties, increase a flexural strength, bearing capacity, and also increased the impact toughness [1, 2].

From the previous research done by Stephens [3] on natural fiber reinforced concrete blocks, the addition of 1 % sugarcane bagasses fiber volume can improve the compressive and tensile strength of the concrete block slightly. He also had shown that the addition of 3 % fiber volume has enhanced the impact resistance. The reinforcement of the cement based composite with fiber has been seen since the Egyptian times where straws or horsehairs were added to mud bricks, as well as in early Japanese and Chinese housing construction where straw mats acting as reinforcements [4].

In order to provide a healthy ecosystem with low cost but high performance as demanded by industry, natural fiber is the best choice for environmentally product due to the biodegradability of plant fibers [5]. Some natural fibers have relatively high stiffness and strength without irritations to skin [4]. However, Abdul Khalil et al. [5] reported that natural fiber composite has low compatibility between cement matrix and fibers which form weak interface and leads to low mechanical properties. In obtaining strong bonding between matrix and fiber, modification is required either by matrix and fiber modification by using physical and chemical treatments or by adding interfacial additives such as chlorination, bleaching and delignition [6, 7]. Pretreatment of the fiber can modify the fiber's surface chemically by cleaning, prevent moisture absorption and enhance the roughness [6, 8] however, the effect of treatment affected by the types of chemical, concentration and processes involved [9].

In most lignocellulosic wastes, the chemical attack on the cellulose is retarded due to the presence of cellulose crystallinity, hence making treatment a necessity. Treatment using sodium hydroxide (NaOH) is found to be more effective compared to water in removing the oil, but this can result in a poorer fiber where the physical and mechanical properties will decrease with the increment of bulk density. Ray et al. [10] studied the alkali treatment of jute fibers and found that the treatment removed the lignin and hemicellulose, which later affects the tensile characteristics of the fibers. The removal of hemicellulose during treatment process has reduced the density and rigidity of the interfibrillar region. It has increased the capability of the fibrils in rearranging themselves along the direction of tensile deformation, resulted in better load sharing when the fiber is stretched. Hence, the stress development in the fiber will be higher. Other studies also reported on the effect of alkaline treatment on fibers such as sugarcane, coir and flax fibers which caused modification in the crystallinity [11] which indicates increment in the percentage of crystallinity index of treated fibers. This phenomenon is due to the better packing of cellulose chain caused by removing the cementing materials [11].

Based on the review work on the effect of treatment on fibers, therefore this research investigated on the physical and mechanical properties of cement modular block reinforced with treated oil palm trunk fiber.

2 Materials and Methods

2.1 Oil Palm Trunk Fiber

The oil palm trunk fibers (OPTF) were taken directly from the plantation. The fibers were kept for 2 days in order to easily remove the parenchyma which contains carbohydrates. This parenchyma can retard the concrete hardening process.

2.2 Determination of Physical Properties and Chemical Composition of OPTF

2.2.1 Density of Fiber

The apparent bulk density of the oil palm trunk fibers has been determined by using the Archimedes principle. Firstly the weight of the bundle of oil palm trunk fiber was taken and recorded as M_{fa} .

Secondly, the bundle was immersed in canola oil until wetted (Fig. 1) before the weight was recorded. Lastly, the apparent bulk density of OPTF bundle was then calculated by using the formula (1):

$$\rho_b = \rho_s \frac{M_{fa}}{M_{fa} - M_{fs}} \quad (1)$$

where

- ρ_b is the bulk density of oil palm trunk fiber
- ρ_s is the density of the solvent (canola oil = 920 kg/m³)
- M_{fa} is the weight of fiber in the air
- M_{fs} is the weight of fiber in the solvent.

Actually it is very difficult to properly determine the dimension of fibers as the natural fibers come in different texture and sizes. Therefore, eventhough Eichorn and Young [12], Devi et al. [13] and Mwaikambo and Ansell [14] agreed that fibers had a circular cross section, different methods have been used in determining the approximate values for the diameters of fibers. A calibrated FEG-SEM at an excitation voltage of 2 keV has been used to measure diameter of hemp fibers [12].

Fig. 1 Oil palm trunk fibers immersed in canola oil



While Devi et al. [13] and Mwaikambo and Ansell [14] used a stereo microscope, and SEM and image analysis techniques for pineapple and sisal fibers respectively. In this study, the diameter of the fiber was determined using SEM.

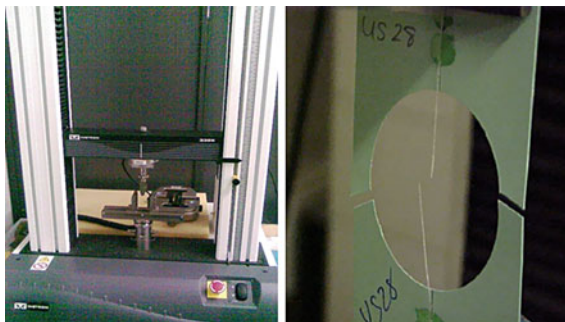
2.2.2 Determination of Tensile Strength of Oil Palm Fiber

Five (5) specimens of oil palm trunk fibers with approximately 70 mm of lengths were weight before mounted on manila-card coupons by using epoxy resin as shown in Fig. 2. The coupon has been gripped with hydraulic clamps of 5 kN load cell Instron machine. The tensile test has been conducted based on ASTM D885 (1995) [15] at a rate of 1 mm/min.

2.2.3 Determination of Chemical Composition of Oil Palm Trunk Fiber

The chemical composition was performed according to TAPPI standards (1985) [16]. Hollocellulose determination was carried out in the same manner as described by Wise et al. [17].

Fig. 2 Fiber tensile test set-up



2.3 Pre-treatment of Fiber

In the pre-treatment process, OPTF was treated with two types of solutions namely sodium hydroxide (NaOH) and water at room temperature. For water pretreatment, the fibers were soaked with water for at least for 2 h to remove impurities and large particles. For another treatment, the fibers were placed in a tanks filled with 0.2 M Sodium Hydroxide (NaOH) solution for 2 h. After two-hour treatments, the solution was drained and the treated OPTF fibers were washed with water. The density of fiber, thickness swelling, tensile properties were determined and analyzed.

2.4 Cement Composite

2.4.1 Binders

The cement binders constituents used were ordinary Portland cement, sand and OPTF. The fine aggregate used satisfied the sieved analysis grading in accordance with BS 882:1992.

2.4.2 Mixing and Casting

The ratio of cement to sand was set at 1.0 and 3.0 respectively. Length of OPTF used was 25 mm since from the previous studies by Jelani et al. [18], for grade 30 concrete the optimum length of OPTF is 25 mm. The detailed of mix proportion is shown in Table 1. The mixing method is critical to the properties of oil palm trunk fiber reinforced cement composite (OPTFC). The addition of fiber has to be uniformly dispersed in the mix in order to obtain homogenous OPTFC mixture. Therefore, the consistency of the matrix needs to be neither too stiff nor too wet to ensure that the mixture can have uniform distribution in the mould A very dry-zero

Table 1 Mix design (kg/m³)

% Vol. of OPTF	0	20	30	50
Vol. of OPTF (m ³)	0	4.8×10^{-3}	7.2×10^{-3}	1.2×10^{-2}
Weight of OPTF (Kg)	0	5.28	7.92	13.2
Vol. of cement (1 Part) (m ³)	6×10^{-3}	4.8×10^{-3}	4.2×10^{-3}	3.0×10^{-3}
Weight of cement (Kg)	18.9	15.12	12.23	9.45
Vol. of cement (3 parts) (m ³)	1.8×10^{-2}	1.44×10^{-2}	1.26×10^{-2}	9.0×10^{-3}
Weight of sand (Kg)	47.7	38.16	33.39	23.85
Water W/C = 0.5 (Kg)	9.45	7.56	6.62	4.73

Note ρ cement = 3,150 kg/m³ ; ρ sand = 2,650 kg/m³

Size block = 400 mm \times 200 mm \times 300 mm (total volume = 24×10^{-3} m³)

slump mix was used in manufacturing the cement block as it allow variation in OPT fibers volume fraction percentage without causing ‘balling’ which normally plague normal concrete mixture.

Slump test was carried out to find the water/cement ratio that produces zero slumps. It was found that the suitable zero slump water/cement ratio ranges between 0.45 and 0.65. Therefore, a ratio of 0.50 was used throughout the production. Before mixing process, fibers were dipped in water for 30 min to allow saturation in order to reduce water absorption during mixing process. Cement, fibers and sand were mixed by adding one-third of water at a time. The fresh mix was manually poured into the formwork of size 400 mm \times 200 mm \times 300 mm and vibrated for 2 min using portable vibration meter and compacted using vibration table. The block was demoulded after 24 h and covered with wet gunny sacks and sprinkled with water regularly.

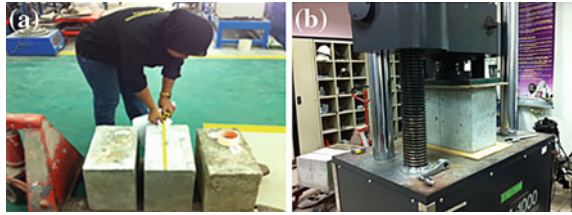
2.5 Compression Test

At least seven specimens were prepared for each parameters tested. The specimen size is 400 mm (length) \times 200 mm (width) \times 300 mm (thick) as shown in Fig. 3a. Compressive strength tests were performed in accordance with BS 1881: Part: 119: 1993 as shown in Fig. 3b at a rate of 2 mm/min. The Modulus of Elasticity was determined using method for determining the static modulus of elasticity in compression in accordance with BS 1881: Part 121: 1983.

2.6 Scanning Electron Microscopy

The OPTF and the fracture surfaces of concrete have been inspected using Scanning Electron Microscopy (SEM) at Metal Performance Technology Center, SIRIM Berhad. JEOL JSN6310 scanning electron microscope (SEM) equipped with a computer image analysis system was used, after gold coating.

Fig. 3 **a** Compression test specimens. **b** Test set-up for compression test



3 Results and Discussions

3.1 Properties of Control Oil Palm Trunk Fiber

The physical and mechanical properties and chemical composition of oil palm trunk fiber without pre-treatment are shown in Table 2.

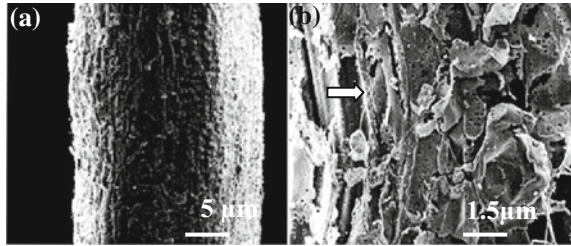
The fiber bundles are of varying cross section with cross-sections ranging from 0.3 to 0.6 mm in diameter. In terms of color, the vascular bundles of OPTF were light yellowish in fresh state and turned to dark grey when dried.

In this study the tensile strength of OPTF was found to be 300–600 N/mm² which is considered high when compared with other natural fiber such as sisal (280–568 N/mm²) and Jute (250–350 N/mm²) [19] but much lower than synthetic fibers namely E-glass fiber (2,000–2,500 N/mm²) and carbon fiber (4,000 N/mm²). Preferable synthetic fibers in composite material industry are glass (E = 70–80 GPa), aramid (E = 120 GPa) and carbon (E = 220–700 GPa) [20] but for natural fibers, hemp (69 GPa), sisal (E = 21 GPa) and kenaf (E = 53 GPa) are commonly used. However, due to low cost and better mechanical properties, glass fibers are preferable compared to others [21]. According to Fordos [22], thick wall is one of the criteria for a fiber to obtained greater tensile strength. Therefore, the high tensile strength value of the OPTF may be due to the thick wall and it was found that OPTF is not easily collapse even though the fiber has lost its moisture. By looking at the SEM photo on the fiber structure as shown in Fig. 4, the node like cell material indicated by the arrows holds adjacent ultimate fibers together which makes the fiber stiff and as compared to other fiber such as wood fiber [23].

The other advantage of OPTF is that it possesses high density (1,140 kg/m³). The high density also indicates that the fiber is strong. The high content of lignin in OPTF (23.03 %) also gives extra merit to the fiber because lignified cellulose fibers retain their strength better than delignified fibers when exposed to moisture [22]. With all these reasons, oil palm trunk fiber was found to have the potential as concrete reinforcement.

Table 2 Properties of oil palm trunk fiber

Properties	Values
Bulk density	1,140 kgm ⁻³
Tensile strength	300–600 N/mm ²
Modulus of elasticity	15–32 GPa
Hollocellulose	72.12
Lignin	23.03
Alpha-cellulose	46.58

Fig. 4 SEM micrograph showing the OPTF fiber at different magnification **a** 65× and **b** 1,500×

3.2 Effect of Treatment on Mechanical Properties of OPTF

Table 3 shows the summary of physical and mechanical properties of OPTF before and after treated with water and NaOH.

The moderately higher tensile strength properties for the OPTF treated with NaOH than OPTF treated with water is due condition of the characteristic of the fiber as explained in this section. According to Kolop et al. [2], low tensile strength will be obtained for fiber with water pretreatment as the fiber can be brittle and easily broken as a result on influenced by too much water content. It has been seen earlier that the alkali treatment reduces the fiber diameter and increases the strength of fiber. Some studies on the alkali treatment of jute-fibers reported [10] on the removal of lignin and hemicellulose, which affects the tensile characteristics of the fibers. The interfibrillar region was found to be less dense and rigid when the hemicelluloses was removed and thereby provide the fibrils capability to rearrange themselves along the direction of tensile deformation. When natural fibers are stretched, such rearrangements amongst the fibrils would result in enhancement on load sharing and hence result in higher stress development in the fiber.

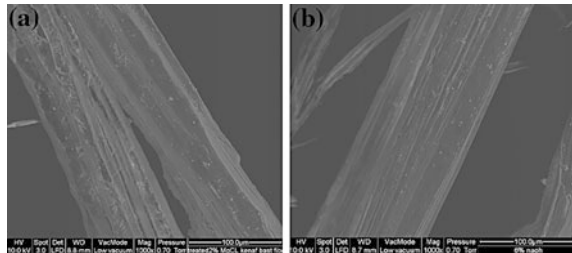
3.3 Effect of Treatment on Surface Morphology of OPTF

The surface morphology based on the level of smoothness and roughness of the OPTF before and after treatments were analysed using scanning electron microscopy (SEM). Significant changes have been observed after the treatments.

Table 3 Summary of physical and mechanical properties of OPTF

Treatment methods	Density (g/cm ³)	Thickness swelling (%)	Tensile strength (N/mm ²)	MOE (GPa)
Control	1.14	0	32.7	32
Water	1.24	0.12	28.5	31
NaOH	1.20	0.04	38.8	36

Fig. 5 OPTF fiber **a** after treated with water and **b** after treated with NaOH



Rougher surfaces were obtained which resulted from removal of non-cellulosic materials, surface impurities, waxes and organic substance. Figure 4a shows the SEM micrograph of untreated OPTF. The impurities can be clearly detected on the surface of untreated fiber. In Fig. 5a, fewer impurities have been removed from fiber surface after treated with water.

However, after treated with 0.2 M NaOH (Fig. 5b) the OPTF has smoother surfaces which indicate better removal of impurities and the diameter of the fiber also reduced. Alkali treatments change the accessibility, reactivity, structure and morphology in cellulosic fibers depending on factors such as degree of polymerization, physical state of the material, treatment temperature and alkali concentration [24, 25]. However, this study did not varies the NaOH concentration to see these effects on the fiber.

3.4 Effect of Treatment on Physical Properties of OPTF

The apparent bulk density is always less than the absolute density which includes all the pores and lumen due to the buoyancy effect cause by the trapped air. Based on Aziz and Ansell [26], high porosity of fiber will affect the density of material by reducing it which resulted in lower bulk density.

Natural fibers have lower density compared to glass fiber. The absolute density of natural fiber was found to be most probably between 1.2 and 1.6 g/cm³ [27]. From Table 3, it can be seen that the density of OPTF varied with the methods of treatments and the treatment shows positive changes in fiber densities. The density of OPTF treated with water is the highest followed by treated with NaOH and control OPTF. Nevertheless, both treatments did not show significant change in

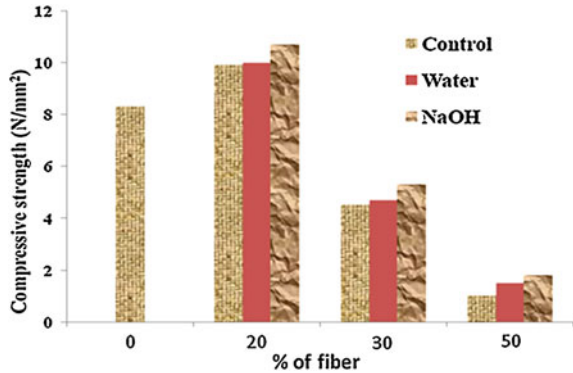
density. This happened as the dried fibers absorbed water during 2 h of pretreatment where the stress developed in the fiber increased due to interfibrillar swelling which explained the increase in the density of OPTF. The increase in water distribution in the fiber may result in stress and local weakness [28] and therefore under pressure a fiber can split into its fibrils as seen in Fig. 5a. Meanwhile, the treatments of NaOH at the same time have removed most of the impurities and chemically modify the surface of fiber [8] and swelled the fiber. The weight loss of the fibers was mainly due to loss of the carboxyl group containing fiber molecules fiber. Alkali penetrates more deeply inside the fiber because of interfibrillar swelling, resulting in fiber splitting (Fig. 5b) due to a less homogeneous distribution of alkali inside the fiber [29, 30]. The effect on thickness swelling of the fiber can be seen in Table 3. The results obtained show that fiber which was treated with NaOH display lower thickness swelling (0.04 %) than that of treated with water (0.12 %).

3.5 Compression Strength Properties of OPTF Cement Block

Figure 6 shows compressive strength of cement block reinforced with 0, 20, 30 and 50 % of OPT fiber. As the percentages of OPTF increases, the strength decreases. The composite cement reinforced with 20 % OPTF treated with NaOH gives the highest compressive strength which is 10.7 N/mm² and the lowest strength is seen for cement composite reinforced with 50 % untreated OPTF. This is due to lack of water for composites causes the mixing is not workable and difficult to mix homogeneously, then the packing of the fiber becomes difficult and voids are introduced into the product.

From the histogram, in general the compressive strength of the cement composites improved with 20 % OPTF for all types of cement composites and for this 20 % OPTF, the strength of cement composite with NaOH treated OPTF is higher than cement composite with water treated OPTF followed by cement composite with untreated OPTF. The increasing of compressive strength of pretreatment of fiber with NaOH is not surprising as in Table 3, it shows that tensile strength for OPTF treated with NaOH gives higher value compared to OPTF treated with water and untreated OPTF. NaOH pretreatment results in decreasing of spiral angle, such as increase in the molecular orientation and strength on a fiber surface, and closer to a fiber axis [8]. This indicates that the strength of cement composite depends on the strength of the fiber and this may not be the only reason since the bondability of the cement to fiber is also important. In general the NaOH treated fiber improves the compressive strength of the cement composite which can so be seen for cement composite with other percentages of OPTF (30 and 50 %). A similar trend was found from Augustine and Stephens [31] where the increments of sisal fiber volume lead to reduction of concrete compressive strength as the fiber fail to resist axial compressive load.

Fig. 6 Compressive strength of cement block with various percentage of OPTF



Addition of fibers into cement matrix will enhance tensile strength by reducing the rate of crack growth. However, the poor compatibility by natural fiber composites will form weak interface and leads to poor mechanical properties. To reduce this problem, pretreatment of fiber is important. According to Kalia et al. [32], by applying alkaline treatment has resulted in an improvement in strength of fibers which was also found in this study which lead to increase in strength of the cement composite. Alkaline pretreatment removed more lignin fractions from the biomass because of the solubilization of lignin in alkaline solution [33]. From this treatment, the fiber can improve the adhesion characteristics and strong fiber matrix interface bond as the treated surface allows for the absorption of the cement matrix.

4 Conclusion

Based on the experimental study, on the effect of pretreatment of OPTF on cement blocks, following conclusions are drawn:

- a. Pretreatment of NaOH contributes to higher value for tensile and MOE for OPTF compared with those having pretreatment with water and untreated fiber.
- b. OPTF treated with water gives higher value of thickness swelling and density of fiber which resulted in weak and brittle fiber as shown by the low tensile strength value.
- c. Cement blocks with NaOH treated fiber gives higher value in compressive strength compared with cement blocks with OPTF treated water and untreated fiber. The increasing of compressive strength of pretreatment NaOH fiber is not surprising because NaOH treated fiber has high tensile strength, providing good fiber matrix bonding, and able to interrupt the distribution of compressive stress that results in multi cracking in blocks.

Acknowledgments This study was funded by the Research Management Institute (RMI), Universiti Teknologi Mara, Malaysia.

References

1. K. Oksman, M. Skrifvars, J.F. Selin, Natural fibres as reinforcement in polylactic acid (PLA) composites. *Compos. Sci. Technol.* **63**, 1317–1324 (2003)
2. R. Kolop, W.I.M. Hazimam, J.W. Eng, Properties of cement blocks containing high content of oil palm empty fruit bunches (EFB) fibers, in *Proceedings of International Conference on Civil Engineering Practice*, 2008, pp. 1–7
3. D. Stephens, Natural fibre reinforced concrete blocks, in *Proceedings of 20th WEDC Conference: Affordable Water Supply and Sanitation*, Colombo, Sri Lanka, 1994
4. V.C. Li, Large volume, high-performance applications of fibers in civil engineering. *Inc. J Appl Polym Sci* **8**, 660–686 (2002)
5. H.P.S. Abdul Khalil, M. Siti Alwani, A.K. Mohd Omar, Chemical composition anatomy, lignin distribution, and cell wall structure of Malaysia plant waste fibers cell walls of tropical fibers. *BioResources* **1**, 220–232 (2006)
6. Y. Habibi, W.K. El-Zawawy, M.M. Ibrahim, A. Dufresne, Processing and characterization of reinforced polyethylene composites made with lignocellulosic fibers from Egyptian agro-industrial residues. *Compos. Sci. Technol.* **68**(7–9), 1877–1885 (2008)
7. N.A. Ibrahim, K.A. Haditon, K. Abdan, Effect of fiber treatment on mechanical properties of kenaf fiber-ecoflex composites. *J. Reinf. Plast. Compos.* **29**, 2192–2198 (2008)
8. S. Suradi, R.M. Yunus, A.K.Lovely, M.D.H Beg, in *Proceedings of World Engineering Congress on Advanced Processes and Materials*, Kuching, Sarawak, Malaysia, 2010, pp. 5–14
9. H. Ismail, N. Rosnah, H.D. Rozman, Effects of various bonding systems on mechanical properties of oil palm fibre reinforced rubber composites. *Eur. Polymer J.* **33**(8), 1231–1238 (1997)
10. D. Ray, B.K. Sarkar, A.K. Rana, N.R. Bose, The mechanical properties of vinyl ester resin matrix composites reinforced with alkali-treated jute fibres. *Compos. A* **32**, 119–127 (2001)
11. S.M. Luz, J. Del Tio, G.J.M. Rocha, A.R. Goncalves, Cellulose and cell lignin from sugarcane bagasse reinforced polypropylene composites: effect of acetylation on mechanical and thermal properties. *Compos. A*, **39**, 1362–1369
12. S.J. Eichhorn, R.J. Young, Composite micromechanics of hemp fibres and epoxy resin microdroplets. *Compos. Sci. Technol.* **64**(5), 767–772 (2004)
13. L.U. Devi, S.S. Bhagawan, S. Thomas, Mechanical properties of pineapple leaf fiber-reinforced polyester composites. *J. Appl. Polym. Sci.* **64**(9), 1739–1748 (1997)
14. L.Y. Mwaikambo, M.P. Ansell, Mechanical properties of alkali treated plant fibres and their potential as reinforcement materials II. Sisal fibres. *J. Mater. Sci.* **41**(8), 2497–2508 (2006)
15. ASTM D885 Standard Test Methods for Tire Cords, Tire cord fabrics, and industrial filament yarns made from manufactured organic-base fibers
16. Tappi Standard: Acid insoluble lignin in wood pulp. No. T 222 m 54 official standard 1 March 1954
17. L.E. Wise, M. Murphy, A.A. D' Addieco, Chlorite hollocellulose its fractionation and beating on summative wood analysis and on studies on the hemicellulose. *Paper Trade J* **122**(2), 35–46 (1996)
18. M.J. Jelani, Z. Ahmad, H.M. Saman, P.M. Tahir, The effect of length of fiber on concrete, in *Proceedings of Seminar Science and Technology and Science Social*, Kuantan Pahang, 27–29 May 2002
19. M.A. Aziz, P. Paramasivam, S.L. Lee, in *Concrete Reinforced with Natural Fibers*, ed. by R.N. Swamy. New Reinforced Concrete, vol. 2 (E&FN Spon, London, 1984)
20. P.T. Curtis, The fatigue behavior of fibrous composite-materials. *J. Strain Anal. Eng. Des.* **24**(4), 235–244 (1989)
21. P. Wambua, Natural fibres: can they replace glass in fibre reinforced plastics? *Compos. Sci. Technol.* **63**(9), 1259 (2006)

22. Z. Fordos, *Natural or Modified Cellulose Fibers as Reinforcement in Cement Composites*, ed. by R.N. Swamy. Natural Fiber Reinforced Cement and Concrete (E&FN Spon, London, 1988)
23. R.S.P. Coutts, Wood fiber reinforced composites, in *Natural fiber reinforced cement and concrete*, ed. by R.N. Swamy (Blackie and Sons Ltd, Glasow, 1988), pp. 1–62
24. X. Colom, F. Carillo, Crystallinity changes in lyocell and viscose-type fibres by caustic treatment. *Eur. Polymer J.* **38**(11), 2225–2230 (2002)
25. J. Crawshaw, W. Bras, G.R. Mant, R.E. Cameron, Simultaneous SAXS and WAXS investigations of changes in native cellulose fibre microstructure on swelling in aqueous sodium hydroxide. *J. Appl. Polym. Sci.* **83**(6), 1209–1218 (2002)
26. S.H. Aziz, M.P. Ansell, The effect of alkalization and fiber alignment on the mechanical and thermal properties of kenaf and hemp bast fiber composites. *Comp. Sci. Tech.* **64**, 1219–1230 (2004)
27. H.M. Akhil, M.F. Omar, A.A.M. Marzuki, S. Safiee, Z.A.M. Ishak, A. Abu Bakar, Kenaf fiber reinforced composites: a review. *Mater. Des.* **32**(8–9), 4107–4121 (2011)
28. H.B. Öztürk, S. Okubayashi, T. Bechtold, Splitting tendency of cellulosic fibres-Part 1: the effect of shear force on mechanical stability of swollen lyocell fibres. *Cellulose* **13**, 393–402 (2006)
29. H.B. Öztürk, T. Bechtold, Splitting tendency of cellulosic fibres-Part 3: splitting tendency of viscose and modal fibres. *Cellulose* **15**(1), 101–109 (2008)
30. H.B. Öztürk, S. Okubayashi, T. Bechtold, Splitting tendency of cellulosic fibres-Part 2: effects of fibre swelling in alkali solutions. *Cellulose* **13**, 403–409 (2009)
31. A.U. Elinwa, S.P. Ejeh, Characterization of sisal fiber reinforced concrete. *J. Civ. Eng. Res. Pract.* **2**(1), 1–14 (2005)
32. A. Kalia, B.S. Kaith, I. Kaur, Pretreatments of natural fibers and their application as reinforcing material in polymer composites—a review. *Polym. Eng. Sci.* **49**(7), 1253–1272 (2009)
33. M.J.Z. Chen, Comparison of four different chemical pretreatment of corn stover for enhancing enzymatic digestibility. *Biomass Bioenerg* **33**, 1381–1385 (2009)

Tensile and Interlaminar Shear Strength of Unidirectional Kenaf Fibre Reinforced Polymer with Overlapping Joint

Safarina Haslimawaty Hamdan, Anwar Zainal Abidin
and Zakiah Ahmad

Abstract Natural fiber has been chosen to replace the use of synthetic fiber because of its characteristics and the fact that it is environmentally friendly. Natural fiber has limited length which differs from synthetic fibers which can be fabricated with the desired length. Therefore, there is a need to join the length of natural fiber in the manufacturing of the plastic composite. Forming a longer length fiber plastic composite by using the method of jointing might results in lower strength compared to full length fibers. Therefore, this paper reported the investigation made on the tensile strength and interlaminar shear strength of kenaf fiber reinforced plastic composite by jointing the fibers through co-cured in-line joint by overlapping the fibers with different overlapping length (0, 10, 20, 30, and 40 mm). The effects of pre-treatment of the fibers with sodium hydroxide were also studied. The results shows that the composites can be manufactured by joint the fibers with maximum length of 20 mm overlapping length. Beyond that length, the specimens failed at outside the overlapping area.

Keywords Epoxy resin • Fiber • Interlaminar shear stress • Kenaf • Reinforced polymer • Tensile strength • Weight loss

S. H. Hamdan · Z. Ahmad (✉)
Institute of Infrastructure Engineering and Sustainable Management, Universiti Teknologi
MARA, 40450 Shah Alam, Selangor, Malaysia
e-mail: zakiahah@hotmail.com

A. Z. Abidin
Faculty of Civil Engineering, Universiti Teknologi MARA, 40450 Shah Alam, Selangor,
Malaysia

1 Introduction

Fiber such as glass, carbon, aramid, etc. has been used in the fiber reinforced polymer composites because of their favourable mechanical properties. However, these synthetic fibers are quite expensive. Therefore natural fibers such as jute, flax, hemp, kenaf etc. can be the alternative fibers in order to reduce the cost of the composites [1]. The emergence of these lignocellulosic fibres as a viable replacement for glass fibre in reinforcing polymeric matrices has attracted the interest of researchers over the past few decades [2, 3]. These fibres are known to deliver similar performance to glass fibres and can be 25–30 % stronger than glass fibres for the same weight [4]. The elastic moduli for natural fibres are comparable to those of E-glass, with flax having potentially the highest value compared to the other fibres. The main advantages of natural fibers include acceptable specific strength properties, low density, high toughness, good thermal properties, lightweight, non-corrosive, low cost and so on [5]. The low specific weight of natural fibers which resulted in a higher specific strength and stiffness compared to glass fiber and this is the characteristic that is important for designing the bending stiffness [6]. Kenaf is the crops that has been planted in Malaysia as alternative crops to replace tobacco for its fibers. Kenaf fiber has been shown to have good tensile strength and modulus of elasticity of 11.9 and 60 GPa respectively [7].

Besides having good mechanical properties, the properties of composites depend on the properties of the matrix and also their interfacial compatibility. However, adhesion between the hydrophilic fiber (such as jute fiber, sisal fiber) and hydrophobic matrix (such as polypropylene, polyester, epoxy) is poor [8]. Therefore, the bond between them needs to be improved. This may be improved by alkali treatment. It is believed that the alkali treatments results in an improvement in the interfacial bonding by giving rise to additional sites for mechanical interlocking, hence promoting more matrix/fiber interpenetration at the interface [3]. Alkali treatments may change the structure, accessibility, morphology and reactivity, in cellulosic fibres depending on factors such as treatment temperature, alkali concentration, its degree of polymerisation and the physical state of the material [9–11]. Silva and Al-Qureshi [12] analysed the mechanics of wetting systems of sisal fibre bundles in epoxy resin by comparing untreated fibres with those treated using 5 % NaOH solution. There was a decrease in the tensile strength of the fibres of approximately 14 % after treatment which may be due to the loss of hemicellulose and lignin.

The application of unidirectional fiber in the composites requires the fiber to be jointed in order to have a longer length composite. The strength of the composite will depend on the strength of the joint. Therefore an experimental investigation was performed to determine the tensile strength properties of unidirectional co-cured in-line joint of kenaf fiber reinforced plastic composites with different overlapping length (0, 10, 20, 30, 40 mm). The interlaminar shear stress plays a very important role in the damage of composite laminates. With higher interlaminar shear stress,

delamination can easily occur on the composite interface. Therefore this study also looked at the interlaminar shear strength of the composite.

2 Experimental

2.1 Materials

Kenaf fibers were collected from Lembaga Kenaf located in Kota Bahru, Kelantan. The supplied kenaf was processed by water retting in order to get the long fiber. The resin was two parts epoxy resin with based resin, Asasin 8505 and hardener, Asahard 8505 supplied by SIKA Malaysia. The mould release agent used was Frekote 700-NC.

Epoxy resin was prepared by mixing two components, based epoxy resin, Asasin 8505 and hardener, Asahard 8505 at ratio 70:30 respectively thoroughly at room temperature. The resin was placed in a vacuum oven to remove any bubbles formed during the mixing process.

2.2 Treatment of Fiber

Fibre samples were immersed in an aqueous alkaline solution of 0.06 M sodium hydroxide (NaOH) mixed with distilled water for about 24 h at room temperature. The fibre was washed with running tap water and then neutralised with an acetate buffer containing 0.01 mol/l of acetic acid and 0.01 mol/l of sodium acetate (pH 5.0). The fibre sample was sufficiently washed with distilled water until the pH value of the solution indicated 7.0. The fibers were dried at room temperature by placing them in between layers of tissue for 2 days, before further drying in an oven at 80 °C for 24 h.

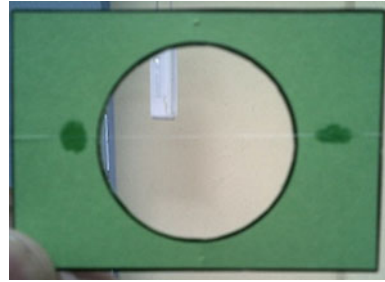
2.3 Moisture Content

In order to determine the weight loss of fibers during alkali treatment, the moisture content (MC) of the fibers was first calculated. The moisture content of the fibers was calculated according to Eq. (1). Firstly, the fibers were conditioned at room temperature for 24 h and weighed (w_1). Then they were dried at 105 °C for 4 h. The fibers were weighed again (w_2) after cooling down in a desiccator.

$$MC \% = \frac{w_1 - w_2}{w_2} \quad (1)$$

The measurement was performed three times for each sample to obtain a mean value.

Fig. 1 Single strand kenaf fiber mounted on coupon



2.4 Weight Loss in Percent

The weight loss of the fibers during alkali treatment was determined. The as received kenaf fibers of 0.25 g were conditioned at room temperature for 24 h and the weight was taken and denoted as w_m . The weight of the dried fibers (w_d) was calculated according to Eq. (2).

$$w_d = w_m - (w_m \times MC) \quad (2)$$

Then the fibers were treated with NaOH as explained in Sect. 2.2 and dried. The weight of the dried fibers after treated was measured and denoted as w_3 . The weight loss of the fibres was calculated according to Eq. (3).

$$\text{Weight loss} = \frac{(w_d - w_3)}{w_3} \quad (3)$$

The measurement was performed three times for each sample to obtain a mean value.

2.5 Tensile Strength of Fiber

The single strand of both treated and untreated kenaf was taken and attached on a manila-card coupon (Fig. 1) by using high performance glue. The tensile test was conducted according to ASTM D885 (1995) using Shimadzu Machine from Civil Engineering Fabrication Lab. The ends of the manila-card coupons were gripped by hydraulic clamps to align the fibre with the machine axis. The sides of the hole on the coupon were cut with a pair of scissors to allow load transfer to the fiber during tensile testing. The specimens were loaded with a crosshead speed of 1 mm/min. Ten (10) specimens, which were five treated and five untreated kenaf fibers were used in this test.

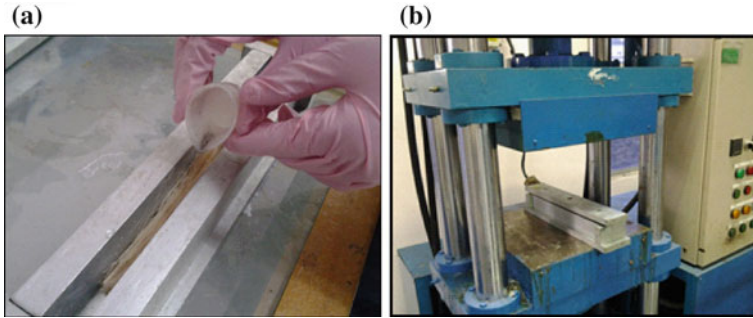


Fig. 2 Manufacturing the KFRP specimen; **a** Epoxy resin poured over layer of kenaf in a zig-zag pattern and **b** specimen allowed to rest before applying pressure

2.6 Preparation of Kenaf Fiber Reinforced Plastic Composite

The composites were manufactured using unidirectional kenaf fibre bundles with epoxy resins as the matrix materials. The untreated and treated fibers were combed to make them straight. All the combed kenaf fibers were cut to required length based on the different overlapping length (0, 10, 20, 30 and 40 mm) as well as control samples and to make samples of length 250 mm. The fibers were divided into several bundles with approximately equal weight.

The mould was cleaned using a soft scraper prior to clean off any residue left on the mould surface. A release agent, Frekote was applied to all surfaces exposed to the resin to make the process of releasing the composites easier, and prevent damage to the mould.

The composites were manufactured using a stainless steel mould as shown in Fig. 2a. The fibers were then inserted layer by layer into the mould, with a layer of epoxy matrix between the layers of the fiber bundles. At the bottom of the first fiber bundles and the top of last fiber bundle, no resin was introduced. The resin was allowed to rest for 3 min before the top cover was placed to avoid loose of resin in the mould. Once the top cover was placed onto the mould, the composite was rested for another 2 min before applying the full pressure of 60 bars (Fig. 2b) until the resin began to feel sticky. The samples were left for 24 h before demoulding. The samples prepared were of size 20 mm (width) \times 4 mm (thick) and 250 mm (length).

2.7 Tensile strength of KFRP

The static tensile strengths of the different KFRPs were measured using BS EN ISO 527-5 (1997) using straight edge specimens as shown in Fig. 3. The composites were fitted with 1.6 mm thick aluminium end tabs which were bonded with Sikadur resin to minimize damage to the outer fibers and matrix.

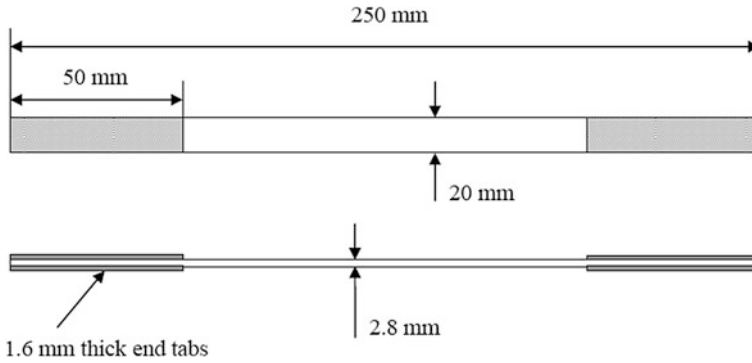


Fig. 3 Tensile test specimen

The tensile test was conducted using Universal Testing Machine Instron at a rate of loading of 1 mm/min.

2.8 Interlaminar Shear Strength

The apparent interlaminar shear strength is defined as the value of the apparent interlaminar shear stress at failure or when the load reaches a maximum value. Interlaminar shear test was carried out in accordance with BS EN ISO 14130. The specimens were cut from the prepared specimen in Part F to a size of 40 mm length \times 20 mm width \times 4 mm thick to give a bending specimen with span to depth ratio of 5:1 mm. The test was conducted on an INSTRON 100kN (3,382) with speed of the testing was 1 mm/min. All the samples' fracture surfaces before and after testing was examined by using Scanning Electron Microcopy (SEM). This value is determined using Eq. (4) as shown below.

$$\tau_M = \frac{3F_M}{4bh} \quad (4)$$

where F_M is the failure or maximum load, in Newtons, b is the width of the test specimen and h is the thickness of the test specimen.

3 Results and Discussions

3.1 Effect of Treatment on the Physical Properties of Kenaf Fiber

The weight loss of the kenaf fiber after treatment with NaOH was found to be 1.8 %. This reduction may be due to loss of the carboxyl group containing fiber molecules [13]. Figure 4 shows the surface morphology of the kenaf fiber bundle,

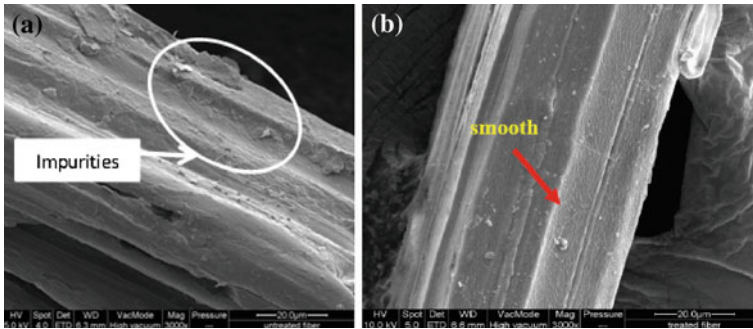


Fig. 4 SEM scans of kenaf fiber; **a** untreated fiber bundle and **b** treated fiber bundle showing the *impurities* and *smooth surface* respectively

untreated and treated with NaOH. A closer look of the treated fiber shows the effect of the NaOH on the surface. The smoothness and lack of debris on the surface due to attack by the alkali (Fig. 4b) as compared to the roughness of the untreated fiber (Fig. 4a) which can be associated with the weight loss and has been associated with better wetting of such fibers (Arnold 2008) can be clearly observed in Fig. 4b.

3.2 Effect of Treatment on the Tensile Strength of Kenaf Fiber

The tensile strengths of the treated and untreated kenaf fiber bundles were determined using the cross-sectional areas with the diameter of the fibers obtained using the microscopy methods. It can be observed that the average tensile strengths obtained for untreated fiber is 15.48 kN (140 MPa) which is 6.2 % higher than untreated fiber (14.57 kN, 132.5 MPa). This indicates that the treatment with NaOH decreased the tensile strength of the fiber. The density of the untreated and treated fiber is 1.19 and 0.75 g/cm³ respectively and this reflected in the value of tensile strength. The higher the density the higher the tensile strength.

3.3 Tensile Strength of KFRP Composite

The tensile test results for the treated and untreated KFRP have been plotted in Fig. 5 as a function of overlapping length. From this figure, it is clear that the KFRP with treated fiber are higher than KFRP with untreated fiber except for control samples which is quite surprising. For control specimens, KFRP with untreated fiber have tensile strength of 15.8 % higher than KFRP with treated

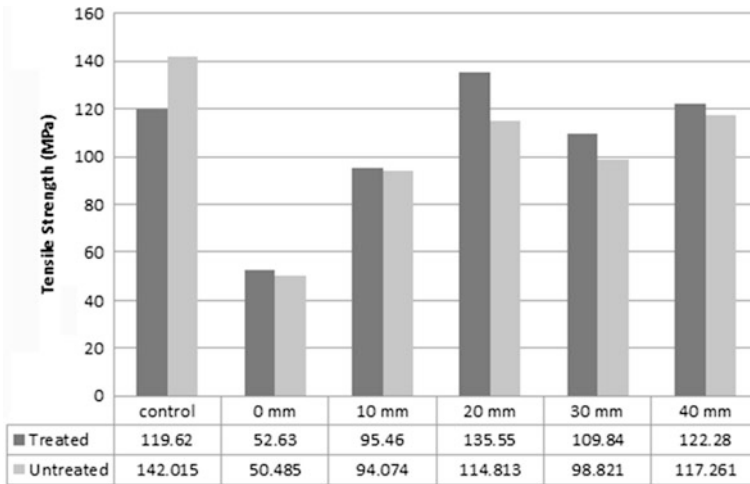


Fig. 5 Tensile strength of KFRP composite with treated and untreated fibers

fiber. This may be due to the tensile strength of untreated kenaf fiber is higher than treated fiber.

However as the overlapping length increases, for both KFRP composites, the tensile strength of the composites with treated and untreated fibers are increasing as the overlapping length increases up to 20 mm overlapping length excluding the control specimens.

When jointed with 20 mm overlapping length, the tensile strength of KFRP with treated fiber has no significant different in the tensile strength with that control KFRP with untreated fiber but higher than the control sample with treated fiber. The result also shows that fiber length has profound impact on the properties of the jointed composites. In small overlapping size, tensile strength is low due to the fact that length may be not sufficient enough for proper distribution of stress. As proper length is not available for stress distribution, failure occurs easily. But as the fiber length longer than 20 mm, the tensile strength decreases at the overlapping area as at that area, the density is high and the weak area will be outside the overlapping and induce weakness and the specimens mostly failed around those areas. Figure 6 shows the failure modes of the tensile specimens with different overlapping length. Both types of KFRP composites have similar failure patterns.

At the same time, the matrix resin need to hold the fibers together, therefore, the matrix has the important function of transferring applied load to the fibers. The efficiency of a fiber reinforced composite depends on the fiber–matrix interface and the ability to transfer stress from the matrix to the fiber [13]. The increase in tensile strength for the alkali treated kenaf fiber bundles in epoxy resin composites is linked to the improvement of surface properties. Treatment of kenaf fiber with low concentration of NaOH has been reported to improve the mechanical

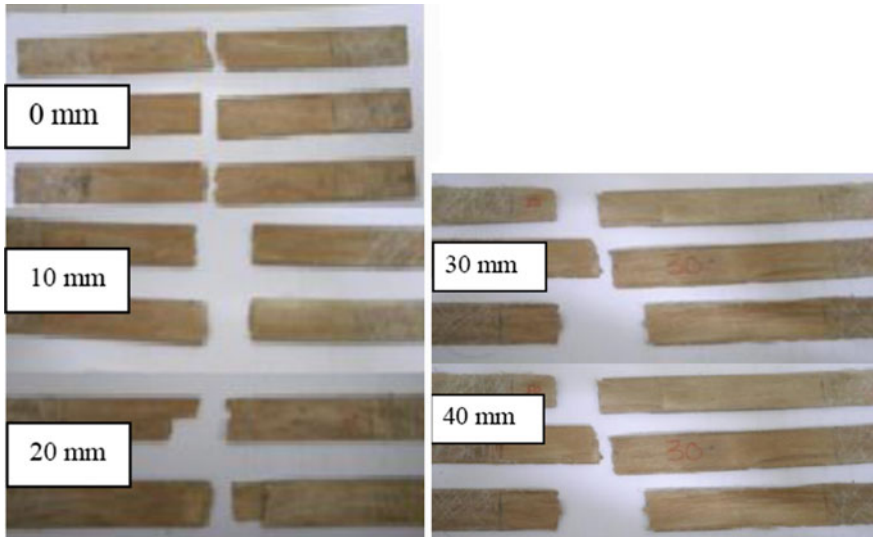


Fig. 6 Failure modes of tensile specimens

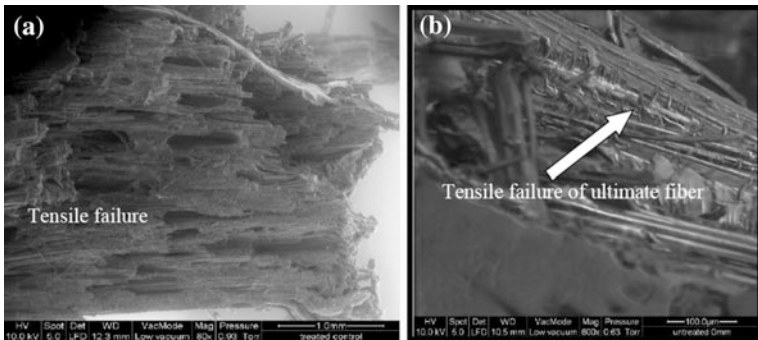


Fig. 7 Tensile failure of **a** treated kenaf fibre KFRP composite and **b** untreated kenaf fibre KFRP composite after tensile test

properties of natural fibers by improving their internal properties by facilitating rearranging of crystallites into well-ordered states [14, 15]. They suggested that the orderly rearrangement of crystallites reduces the number of weak points on the fiber surface resulting in better stress distribution along the fiber length.

The KFRP composite for both treated and untreated fiber suffered tensile failure as shown in Fig. 7a and b respectively. There is no visible evidence of single fiber pull-out from both untreated and treated fiber-epoxy resin composites which indicate good bonding between the fibers and the matrix. The good bond strength is evident from the extent of damage observed on the fiber surfaces of treated and

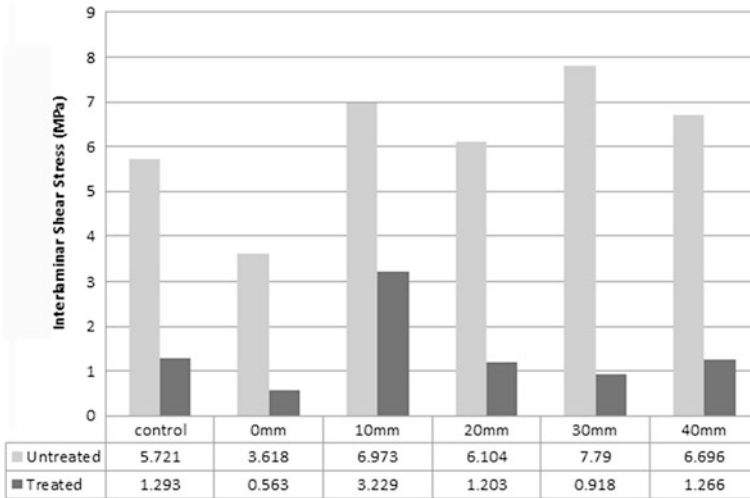


Fig. 8 Interlaminar shear stress for KFRP composite with different overlapping length

untreated KFRP composite. There is pull-out of ultimate fibers from the fiber bundles as shown in Fig. 7b coupled with tearing of fiber cell walls.

3.4 Interlaminar Shear Strength

The interlaminar shear stress plays a very important role in the damage of composite laminates. Figure 8 shows the result for interlaminar shear strength of KFRP composites with treated and untreated kenaf fiber as well as for different overlapping length.

From Fig. 8 it can be seen that the interlaminar shear strength of KFRP composite with untreated fiber is higher than KFRP composite with treated fibers. This provides evidence that the low in tensile strength of the composite since with high interlaminar shear stress, the delamination can easily occur on the composite interface. This also indicates the bonding of the treated KFRP composite is not as good as the KFRP composite with treated fiber.

4 Conclusions

The following conclusions can be drawn from this study:

1. The weight loss of the kenaf fiber after treatment with NaOH was found to be 1.8 % which can be seen from the smoothness and lack of debris on the surface due to attack by the alkali through SEM micrograph.
2. The average tensile strengths obtained for untreated fiber is 15.48 kN (140 MPa) which is 6.2 % higher than untreated fiber (14.57 kN, 132.5 MPa). This indicates that the treatment with NaOH decreased the tensile strength of the fiber. The density of the untreated and treated fiber is 1.19 and 0.75 g/cm³ respectively.
3. The tensile strength of kenaf fiber reinforced plastic composite without joint (control specimens) with untreated fiber has higher tensile strength than KFRP with treated fiber. However as the overlapping length increases, the tensile strength of the composites with treated and untreated fibers are increasing as the overlapping length increases up to 20 mm overlapping length excluding the control specimens.
4. The interlaminar shear strength of KFRP composites with untreated fiber is higher than KFRP composite with treated fibers. This provides evidence that the low in tensile strength of the composite. This also indicates the bonding of the treated KFRP composite is not as good as the KFRP composite with treated fiber.

Acknowledgments The work reported here was financially supported by the Ministry of Higher Education under Fundamental Research Grant Scheme (FRGS). We wish to acknowledge the support of the technical staff in the Composite Laboratory, Faculty of Mechanical Engineering. We also would like to extend our appreciation to the Civil Engineering Final Year students for the help in the manufacturing of samples.

References

1. S. Mohanty, S.K. Nayak, S.K. Verma, S.S. Tripathy, Effect of MAPP as a coupling agent on the performance of jute-PP composites. *J. Reinf. Plast. Compos.* **23**(6), 625–637 (2004)
2. S.H. Aziz, M.P. Ansell, S.J. Clarke, S.R. Panteny, Modified polyester resins for natural fibre composites. *Compos. Sci. Technol.* **65**, 525–535 (2006)
3. J. Gassan, A.K. Bledzki, Possibilities to improve the properties of natural fiber reinforced plastics by fiber modification—ute polypropylene composites. *Appl. Compos. Mater.* **7**(5–6), 373–385 (2000)
4. A.K. Mohanty, M. Misra, L.T. Drzal, Sustainable bio-composites from renewable resources: opportunities and challenges in the green materials world. *J. Polym. Environ.* **10**(1–2), 19–26 (2000)
5. H. Anuar, N.A. Hassan, F. Mohd Fauzey, Compatibilized PP/EPDM-kenaf fibre composite using melt blending method. *Adv. Mater. Res.* **264–264**, 743–747 (2011)
6. H.M.M.A. Rashed, M.A. Islam, F.B. Rizvi, Effects of process parameters on tensile strength. *J. Nav. Archit. Mar. Eng.* **3**, 1–6 (2006)
7. N.S. Abdul Rahman, External strengthening of reinforced concrete beams using kenaf fiber epoxy biocomposite plates. A report submitted in fulfilment of the requirements for the award of the degree of Bachelor of Civil Engineering, Faculty of Civil Engineering, Universiti Teknologi Malaysia, 2011

8. A.C. Karmaker, J.A. Youngquist, Injection molding of polypropylene reinforced with short jute fibers. *J. Appl. Polym. Sci.* **62**(8), 1147–1151 (1996)
9. X. Colom, F. Carillo, Crystallinity changes in lyocell and viscose-type fibres by caustic treatment. *Eur. Polymer J.* **38**(11), 2225–2230 (2002)
10. J. Crawshaw, W. Bras, G.R. Mant, R.E. Cameron, Simultaneous SAXS and WAXS investigations of changes in native cellulose fibre microstructure on swelling in aqueous sodium hydroxide. *J. Appl. Polym. Sci.* **83**(6), 1209–1218 (2002)
11. J. Borsa, T. Toth, E. Takacs, P. Hargittai, Radiation modification of swollen and chemically modified cellulose. *Radiat. Phys. Chem.* **67**, 509–512 (2003)
12. J.L.G. Silva, H.A. Al-Qureshi, Mechanics of wetting systems of natural fibres with polymeric resin. *J. Mater. Process. Technol.* **92–93**, 124–128 (1999)
13. H.B. Öztürk, T. Bechtold, Effect of NaOH treatment on the interfibrillar swelling and dyeing properties of lyocell (TENCEL) fibres. *Fibres Text. East. Eur.* **15**(5–6), 64–65 (2007)
14. R. Karnani, M. Krishnan, R. Narayan, Biofiber-reinforced polypropylene composites. *Polym. Eng. Sci.* **37**(2), 476–483 (1997)
15. L.Y. Mwaikambo, M.P. Ansell, Mechanical properties of alkali treated plant fibres and their potential as reinforcement materials II. Sisal fibres. *J. Mater. Sci.* **41**(8), 2497–2508 (2006)

Compressive Strength of Laminated Rubber Bearing Due to Different Temperature Exposure

Norliyati Mohd Amin, Anizahyati Alisibramulisi
and Norhayati Kadir

Abstract In Malaysia, the usage of laminated rubber bearing (LRB) is lacking due to low seismic intensity. Nevertheless, it is still used as precaution to public safety. The determination of the suitable rubber according to temperature is very important since Malaysia is one of the hot climate countries. Thus, temperature is one of important parameters to be taken into account. Commonly, rubber will melt and change their strength properties immediately if highly exposed to high temperature, and the situation is the same for LRB. The LRB is a combination of rubber and steel which is good to isolate earthquake energy. The objectives of this study is to determine the compressive strength performance of LRB using three different temperatures; room temperature (26–28 °C), 30 °C and 50 °C. The result shows that the maximum loads under compression test were between 373.2 and 793.3 kN for the three variable temperatures studied.

Keywords Laminated rubber bearing (LRB) · Temperature · Compression test

1 Introduction

Laminated Rubber Bearing (LRB) is one of base isolation systems. LRB is commonly used to absorb seismic loading produced by earthquakes energy. The bearings are generally placed at bottom of the building to make sure the overall building structural elements are not affected due to earthquake loading. In structural earthquake engineering, natural rubber and steel are used as base isolator for energy removal systems to reduce earthquake effect on structures. Laminated

N. M. Amin (✉) · A. Alisibramulisi
Faculty of Civil Engineering, IIESM, Universiti Teknologi MARA, Shah Alam, Malaysia
e-mail: norliyati_ma@yahoo.com.my

N. Kadir
Faculty of Civil Engineering, Universiti Teknologi MARA, Shah Alam, Malaysia

natural rubber and steel, as a bearing can provide high vertical stiffness and flexibility in horizontal direction to ensure that they can support the loading from the structure and prevent excessive sideways from any horizontal loading especially when earthquakes occur. The determination of suitable rubber according to temperature is very important since Malaysia itself is one of the hot climate countries. The temperature is one of important parameters to be taken into account. Rubber can shift their properties due to changes of temperature caused by surrounding environments.

1.1 Objective

The aim of this study is to measure the effectiveness of LRB subjected to compression load with variable temperatures and can be subdivided into:

1. To evaluate the mechanical properties of LRB when compressively loaded and different temperatures were imposed on it.
2. To determine the load of maximum breaking point of LRB due to vertical loads with the different temperatures.

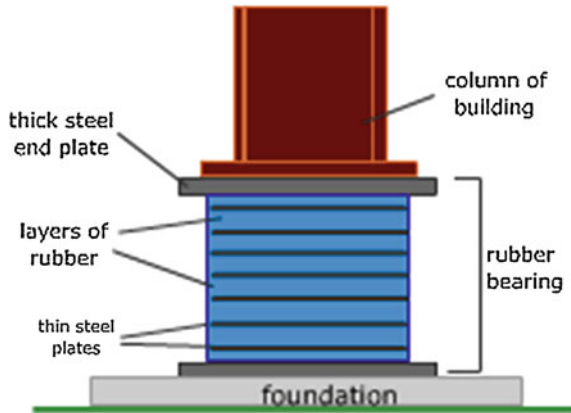
1.2 Significance of Study

Rubber can be categorized into two types, which are synthetic rubber and natural rubber. The synthetic rubber is not highly suggested in Malaysia because of its higher cost compared to the natural rubbers. Laminated Rubber Bearing is a combination of steel and natural rubber in which the interval layers contribute in preventing seismic loading. Natural rubber is also very suitable to be used for strengthening application and it is also environmental—friendly. Therefore, this research is conducted to evaluate the mechanical properties of LRB due to different temperatures.

1.3 Scope of Work

To investigate the mechanical properties of LRB, natural rubber with different value of temperatures was tested under compression. There is steel plate between rubber and it forms several layers. Three values of temperature were decided based on tropical climate range, where the samples were heated in oven for room temperature (26–28 °C), 30 °C and 50 °C. Then, the samples were imposed with vertical loads.

Fig. 1 Component of laminated rubber bearing [2] (IDEERS Resistant Building 2000)



2 Laminated Rubber Bearing as Base Isolation System

Base Isolation systems reduce building vibrations during earthquakes. This means that the building is less shaking, thus, the chance of damage can be reduced. To have a fixed-base, normally a building is supported directly on this system. When base isolation is used, special structural bearings are inserted between the bottom of the building and its base foundation. A bearing is a device to allow constrained relative motion between two or more parts, typically rotation or linear movement. Bearings may be classified as large space according to the motions it allows and according to its principle of operation as well as by the directions of applied loads it can handle. The most recent and interesting application in seismic isolation for building is Laminated Rubber Bearing (LRB).

Laminated Rubber Bearings components are shown in Fig. 1. The bearings are designed to be very stiff and strong for vertical loads so that it can carry the weight of the building. However, it is designed to be much weaker for horizontal loads, so that it can move sideways during an earthquake [1].

2.1 Application of Laminated Rubber Bearing

LRB have been used to isolate substructure so that the super structure do not collapse easily during an earthquake where the superstructure may follow the movement of building gently. More recently, elastomeric bearings have been increasingly employed in buildings and bridges as a means of decoupling the structure from seismic ground motions. Since most buildings and bridges have service lives of at least 30–60 years, questions about the long-term behavior of base-isolation bearings arise. The dynamic response of building and lifeline structures subjected to earthquakes ground motion is dependent upon a number of factors, including structural configuration, mass, stiffness, damping and ductility [3].

Fig. 2 Difference of two types of building with and without bearing [2] (IDEERS Resistant Building 2000).
a Building with fix base.
b Building with base isolation bearing

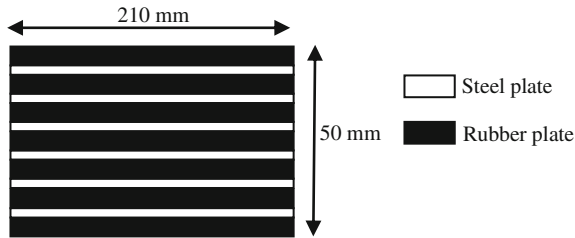
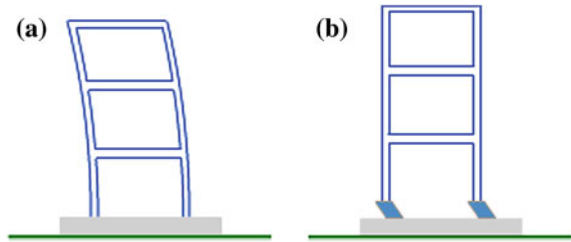


Fig. 3 LRB dimensions

Buildings with small damping ratios and natural period in the same range as the influence of strong motion are likely to have significantly amplified responses, and hence suffer damage in earthquake. Historically, the philosophy behind most design standard has been to provide sufficient strength to resist dynamically-induced lateral forces, while limiting damage to an acceptable level. Newer design methodologies have maintained this philosophy, but have explicitly incorporated more advance concept such as ductility, stability, and energy dissipation under cycling loading. The behaviors of building with and without isolation bearing are shown in Fig. 2.

2.2 Effects of LRB Subjected to Different Temperatures

LRB does not perform well at high temperature which is (greater than 70 °C) and low temperature but do perform quite well at temperature between these extremes [3]. At temperature above 70 °C, many elastomers degrade via a mechanism of cross linking or by a mechanism of reversion; breakage of crosslink creating free radicals which reform into cyclic structures [4]. Both mechanisms increase the hardness and modulus of the elastomers, resulting in embrittlement. For example [4] observed an 80 % reduction in the elongation at break in 170 days, and a doubling of the modulus in 50 days for vulcanized natural elastomers heated at 70 °C. Another significant property is the behavior of an LRB at a low temperature. The temperatures of interest are the cold crystallization temperature and the



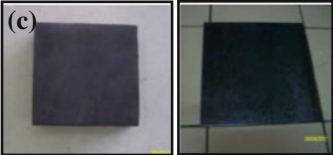
Figure	Remarks
 <p>(a)</p>	<p>Firstly, the 2.5 mm steel plates were cut into small sizes by using hydraulic swing beam shearing machine as shown in Fig.4 (a).</p>
 <p>(b)</p>	<p>After that, the steel plate was loaded on the machine and the machine cut those plates into the dimensions required.</p>
 <p>(c)</p>	<p>The rubber and steel plate have been ensured to be of the same sizes before continuing to the next stage.</p>

Fig. 4 **a** Machine that was used to cut the steel plate. *Remarks* Firstly, the 2.5 mm steel plates were cut into small sizes by using hydraulic swing beam shearing machine as shown in Fig. 4a. **b** Steel plate was loaded on the machine to be cut. *Remarks* After that, the steel plate was loaded on the machine and the machine cut those plates into the dimensions required. **c** Materials used. *Remarks* The rubber and steel plate have been ensured to be of the same sizes before continuing to the next stage. **d** Epoxy on rubber sheet. *Remarks* Next, rubber sheet surface has been applied with epoxy. Two minutes were allowed before joining it together with steel plates. **e** Joining the steel and rubber. *Remarks* Some pressure has been applied to the surface after joining the material so that it can stick perfectly. The same steps were repeated until finish. **f** Completed samples. *Remarks* The completed samples have been cured for 2 weeks in room temperature so that the strength required is achieved

glass transition. Many properties change when cold crystallization occurs, including increases in the hardness and shear stiffness and a decrease in maximum elongation at break [1].



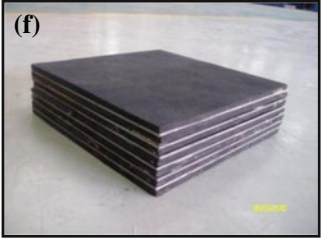
Figure	Remarks
 <p>(d)</p>	<p>Next, rubber sheet surface has been applied with epoxy. Two minutes were allowed before joining it together with steel plates</p>
 <p>(e)</p>	<p>Some pressure has been applied to the surface after joining the material so that it can stick perfectly. The same steps were repeated until finish.</p>
 <p>(f)</p>	<p>The completed samples have been cured for two weeks in room temperature so that the strength required is achieved.</p>

Fig. 4 continued

3 Experimental Investigation

3.1 Experimental Set-Up

The LRB are produced with 210 mm × 50 mm dimensions, whereby, the rubbers are 5 mm × 7 pieces and steel plates are 2.5 mm × 6 pieces. The sizes were chosen from previous experiment which was conducted by Japanese researchers [3]. The dimensions were proposed by them and they investigated the aging effect on damping ratio of LRB. In their experiment, rubber properties of degradation

Fig. 5 Sample of LRB in the microwave oven



Fig. 6 Experimental set-up

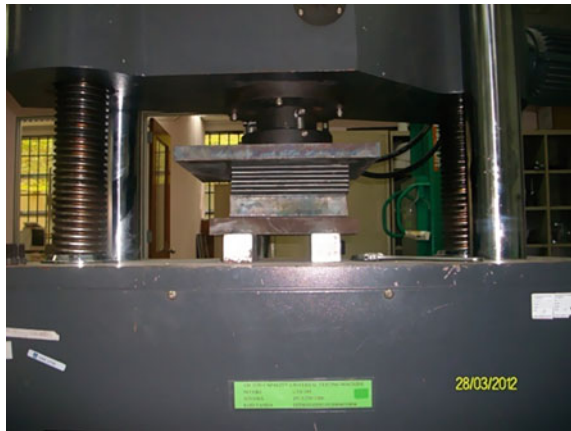
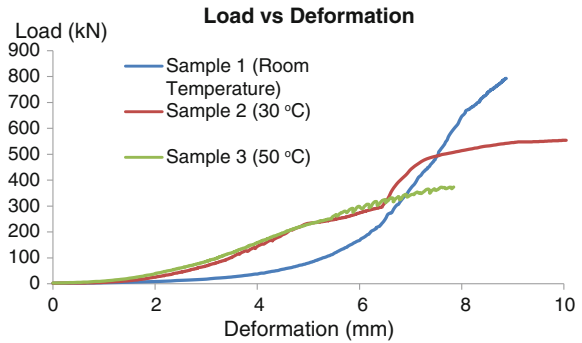


Table 1 Result of LRB subjected to compressive loads and different temperatures

Temperature	Sample 1 room temperature (26–28 °C)	Sample 2 30 °C	Sample 3 50 °C
Maximum breaking point (kN)	793.3	556.4	373.2
Stress (N/mm ²)	62.9	44.1	29.6
Deformation (mm)	8.9	10.6	7.8
Strain (%)	4.44	5.2	3.9

process were mainly focused compared to this study, where LRB was exposed to different temperatures to determine its mechanical properties. Figure 3 shows the dimension of Laminated Rubber Bearing used in this study.

Fig. 7 Load versus deformation



3.2 Manufacturing of Laminated Rubber Bearing Samples

Laminated rubber bearing was fabricated using steel plate and rubber sheet with epoxy. The procedures of manufacturing laminated rubber bearing polymer are shown in Fig. 4a–f.

3.3 Heating the Samples

The equipment that has been used for heating the samples is microwave oven as shown in Fig. 5. The microwave oven was set to the according temperature and the samples were put into it for about fifteen (15) minutes. Note that, the three temperatures applied were: room temperature, 30 and 50 °C.

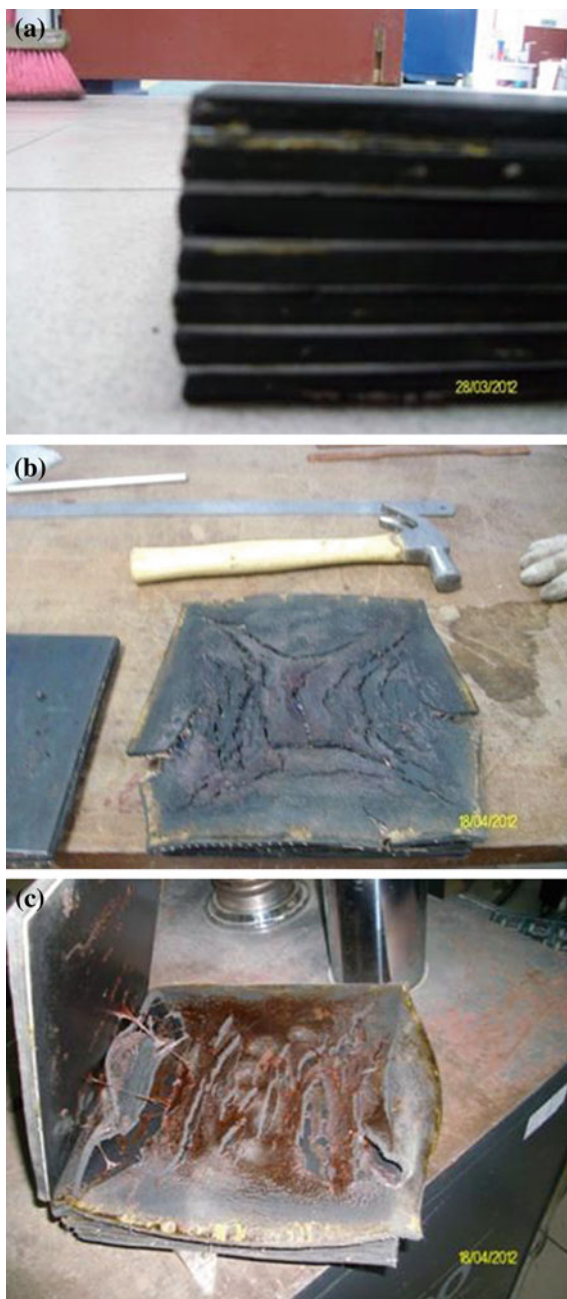
3.4 Vertical Load of Laminated Rubber Bearing

Universal Testing Machine (UTM) is the equipment that has been used for vertical load test. The equipment consisted of a 100 kN capacity actuator with a mini controller. The actuator was mechanically connected to the specimen through a reaction loading frame. The LRB was placed between these two plates as shown in Fig. 6. The test was carried out under displacement control condition.

4 Results and Discussions

This section discussed the obtained results in accordance to the objectives of this study.

Fig. 8 LRB mode of failures. **a** Sample 1 (room temperature). **b** Sample 2 (30 °C). **c** Sample 3 (50 °C)



4.1 Deformation of LRB

Table 1 shows the result of the compression test on three LRB samples with three different temperatures. The highest maximum break point was 793.3 kN at room temperature, while the lowest for maximum break point was 373.2 kN at 50 °C. For the stress, the maximum stress was 62.9 N/mm² at room temperature and the lowest stress was 29.6 N/mm² at 50 °C. The highest deformation was 30 °C sample with 10.6 mm deformation, while, the minimum deformation was 7.8 mm from 50 °C sample. Maximum and minimum strain were 5.2 % (30 °C sample) and 3.9 % (50 °C sample) respectively.

From Fig. 7, it is observed that during the testing, the 30 °C sample goes smoothly until it reaches 300 kN load. After it reaches 300 kN, the sample starts to fail slowly but deformation remains constant until it totally breaks at 556.4 kN. For the 50 °C sample, after the load reach around 250 kN, the sample starts to break and fails drastically at 373.2 kN which is believed due to the high temperature exposure. Nevertheless, maximum breaking point load 793.3 kN is obtained from room temperature sample.

4.2 Failure Mode of Laminated Rubber Bearing

From Fig. 8, Sample 2 and 3 shows that the rubber looks fissure and it is caused by the heat that is trapped in the rubber. The excessive damage can be seen with the rubber is burning inside.

5 Conclusion

From this study, it can be concluded that, LRB exposed to different temperatures and subjected to compressive load, its mechanical properties are affected as follows:

1. LRB exposed to high temperature (50 °C) leads to higher failure rate due to its melting behavior.
2. The highest maximum breaking point load is 793.3 kN from room temperature sample, whereas the lowest maximum breaking point load is 373.2 kN from 50 °C sample.
3. The maximum stress, 62.9 N/mm² is obtained from room temperature sample and the lowest stress 29.6 N/mm² is obtained from the 50 °C sample.
4. Maximum and minimum strain are 5.2 and 3.9 %, obtained from 30 °C sample and 50 °C sample respectively.

Acknowledgments This project was funded by Research Intensive Faculty Grant [600-RMI/DANA. 5/3/RIF(225/2012)], University of Technology MARA (UiTM), Malaysia. Special thanks to the faculty of Civil Engineering UiTM Malaysia in providing the test facilities.

References

1. K. Morita, S. Yamagami, M. Takayama, Long-term performance test of laminated rubber bearing for seismic isolation system. 3rd international conference on advances in experimental structural engineering, Berkeley, (2009)
2. S.K. Jain, S.K. Thakkar, Quasi-static testing of laminated rubber bearings. J. Inst. Eng. India Civ. Eng. Div. **84**, 110–115 (2003)
3. E. Takaoka, Y. Takaneka, A. Kondo, M. Hikita, H. Kitamura, Heat mechanic interaction behavior of laminated rubber bearing under large and cyclic lateral deformation, in *Proceedings of the 14th Conference on Earthquake Engineering*, Beijing, China, 12–17 October 2008
4. Paramashanti, Y. Kitane, Y. Itoh, S. Kito, K. Muratani, Experimental investigation of aging effect on damping ratio Laminated Rubber Bearing

Effect of Superplasticizers on Workability of Fly Ash Based Geopolymer

Behzad Nematollahi and Jay Sanjayan

Abstract This paper evaluates the effect of different commercial superplasticizers (SPs) usually used for ordinary Portland cement concrete production such as naphthalene, melamine (second generation of products) and modified Polycarboxylate based (latest generation) on the workability of a class F fly ash paste activated by 8 M NaOH solution (28.6 %) + Na₂SiO₃ (71.4 %) with a SiO₂/Na₂O ratio of 2.0. These SPs at a dosage of 1 % by mass of fly ash were added to the fresh paste and flowability of the activated fly ash paste was measured by mini slump test and compared with that of the paste without using any SP. The experimental results indicated that each SP affected the workability of the fly ash geopolymer differently. When the NaOH + Na₂SiO₃ used as the activator the modified Polycarboxylate based SPs (latest generation) was the most efficient type which increased the relative slump of the paste up to 45 % with reference to the paste without using any SP.

Keywords Fly ash based geopolymer · Superplasticizer · Activator · Workability · Mini-slump test

1 Introduction

Geopolymer in the contrary to ordinary Portland cement (OPC) is a novel engineering cement-less binder with environmentally sustainable characteristics [1]. Reference [2] coined the term geopolymer to describe the inorganic aluminosilicate polymers produced by synthesizing natural materials such as kaolinite clay or industrial by-products such as fly ash and slag with highly alkaline activators. In

B. Nematollahi (✉) · J. Sanjayan
Faculty of Engineering and Industrial Sciences, Swinburne University of Technology,
Melbourne, VIC, Australia
e-mail: bnematollahi@swin.edu.au

this study geopolymer is produced by mixing Class F (low calcium) fly ash which is an industrial by-product of coal-fired power stations [3] containing high amounts of silicon and aluminum as the source material with a multi-compound activator composed of NaOH and Na_2SiO_3 solutions. The production of fly ash based geopolymer requires approximately 60 % less energy than that required for manufacture of OPC resulted in low carbon emission [4].

High range water reducing admixtures commonly known as superplasticizers (SPs) are added to OPC concrete to reduce its water content while maintaining a constant workability resulting in higher strength and durability of concrete. However, SPs can be used to “plasticize” or fluidize the concrete by maintaining a constant water content resulting the concrete to flow better with no change in the compressive strength. There are several types of SPs such as lignosulphonates (Lig), naphthalene (N) and melamine-based (M), and modified Polycarboxylates (PC) [5].

The effect of SPs in OPC paste, mortar and concrete has been widely evaluated by several authors such as [6–9] and many others. Recently, some studies have been conducted on the effect of the SPs on slag based geopolymers [10–14].

On the contrary, effect of the SPs on fly ash based geopolymer has been received less attention. Reference [15], for instance, studied the effect of latest generation of SPs based upon vinyl copolymer and polyacrylate copolymer on the workability of fly ash based geopolymer pastes activated by only 8 M NaOH solution. They concluded that addition of these SPs does not increase the workability of the activated fly ash pastes. Reference [16] studied the effect of a N based SPs on workability of the fly ash based geopolymer concrete activated by 8 M NaOH solution (28.6 %) + Na_2SiO_3 (71.4 %) with a $\text{SiO}_2/\text{Na}_2\text{O}$ ratio of 2.0. It was concluded that addition of N based SP improved the workability of fresh concrete. Reference [17] evaluated the effect of Lig, M and PC based SPs on paste rheology (i.e. yield stress and plastic viscosity) of alkali activated fly ash. They concluded that when 12.5 M NaOH solution (85 %) + Na_2SiO_3 (15 %) with a $\text{SiO}_2/\text{Na}_2\text{O}$ ratio of 3.3 used as the activator the PC based SPs (with a dosage of 0.8 %) seems to be the most effective type, however, these researchers have not studied the effect of N based SP in their study. Reference [18] studied the effect of two different SPs (N based and PC based) in the workability of the fly ash based geopolymer concrete. They concluded that N and PC based SPs did not greatly improve the workability of the concrete activated by 7 M KOH solution (28.6 %) + Na_2SiO_3 (71.4 %) with a $\text{SiO}_2/\text{Na}_2\text{O}$ ratio of 2.0. Reference [19] studied the effect of a PC based SP on workability of self compacting geopolymer concrete. They concluded that addition of PC based SP with the dosages of 3–7 % by mass of fly ash resulted in increase in the workability of the fly ash based geopolymer concrete activated by 12 M NaOH solution (28.6 %) + Na_2SiO_3 (71.4 %) with a $\text{SiO}_2/\text{Na}_2\text{O}$ ratio of 2.06 with respect to the concrete containing 3 % SPs. However, these researchers did not report the effect of the SP (i.e. increase/decrease in the workability of the concrete) with respect to the original concrete without using any SP.

Table 1 Chemical composition of fly ash determined by XRF

Chemical	Component (wt. %)
Al ₂ O ₃	27.0
SiO ₂	48.8
Fe ₂ O ₃	10.2
CaO	6.2
MgO	1.4
TiO ₂	1.3
P ₂ O ₅	1.2
K ₂ O	0.85
Na ₂ O	0.37
SO ₃	0.22
BaO	0.19
SrO	0.16
MnO	0.15
ZrO ₂	–
LOI ^a	1.7

^a Loss on ignition

As demonstrated in the above, the inconsistency in the research results reported is due to diversities in the conditions in which fly ash based geopolymer pastes, mortars and concrete were prepared such as composition of the fly ash, nature and concentration of the activators used, type and dosage of SPs, etc. Hence, the objective of this study is to evaluate the effect of different SPs on the workability of the fly ash based geopolymer pastes.

2 Material

2.1 Fly Ash

The low calcium fly ash (class F) used in this study was supplied from Gladstone power station in Queensland, Australia. Table 1 present the chemical composition and loss on ignition (LOI) of the fly ash determined by X-ray Fluorescence (XRF).

2.2 Activator

The investigated activator was a multi-compound activator composed of sodium hydroxide and sodium silicate solutions. The sodium hydroxide solution was prepared with a concentration of 8.0 M using sodium hydroxide (NaOH) beads of 97 % purity supplied by Sigma-Aldrich and tap water. The Grade D sodium silicate solution (Na₂SiO₃) was supplied by PQ Australia with a specific gravity of 1.53 and a modulus ratio (Ms) equal to 2.0 (where Ms = SiO₂/Na₂O,

$\text{Na}_2\text{O} = 14.7 \%$ and $\text{SiO}_2 = 29.4 \%$). Sodium silicate and sodium hydroxide solutions were mixed together with $\text{Na}_2\text{SiO}_3/\text{NaOH}$ ratio of 2.5 to prepare the multi-compound activator.

2.3 Superp Lasticizers

Six types of superplasticizers (SPs) investigated in this study were as follows: one melamine-based powder (M), two naphthalene-based (N1, N2), and three modified Polycarboxylate admixtures (PC1, PC2, PC3). According to [20], melamine-based and naphthalene based SPs are classified as the second generation of SPs which their fluidization mechanism is based on electrostatic inter-particle repulsion; whereas, modified Polycarboxylate SPs are considered as the third generation (latest generation) of SPs which in addition to electrostatic repulsion benefits from steric repulsion produced by lateral ether chains on the SP's molecule. All these SPs are commercial products supplied by SIKA and BASF, Australia commonly used in conventional ordinary Portland cement (OPC) concrete. The characteristics of the SPs used in this study are summarized in Table 2.

3 Experimental Procedure

To prepare the activated fly ash paste, the ratio of activator to fly ash was held constant equal to 0.30 and activator and fly ash were mixed together in a mixer for 4 min. Subsequently different SPs with the dosage of 1 % by mass of fly ash was added to the fresh paste and mixed for another 4 min. Table 3 lists the various mixes prepared using different activators and SPs in this study. Following [13], mini slump tests also known as spread-flow tests were conducted to determine the flowability of the fly ash based geopolymer pastes. According to [21], a layer of the fresh paste about 25 mm in thickness was poured into the truncated conical mould (top diameter = 70 mm, bottom diameter = 100 mm, height = 50 mm) and tamped 20 times with tamper. Subsequently the conical mould was filled with the paste and tamped as specified for the first layer. The top surface of the mould was leveled and the extra paste was removed. After 1 min the conical mould was lifted vertically and diameter of the paste spread was measured along two perpendicular directions. The relative slump value was derived from the following equation:

$$\Gamma_p = (d/d_0)^2 - 1 \quad (1)$$

where Γ_p is relative slump, d is the average of two measured diameters of the paste spread and d_0 is bottom diameter of the conical cone, equals to 100 mm in this study [22]. The flowability of each mix was tested twice and compared with that of the paste without using any SP.

Table 2 Physical and chemical properties of the SPs

SP	Chemical base	Appearance/ color	pH (20 °C)	Density (g/ cm ³)
PC1	Modified polycarboxylate	Light brown liquid	6.5	1.05
PC2	Modified polycarboxylate	Clear brown liquid	5.0 ± 1.0	1.07
PC3	Modified polycarboxylate	Light brown liquid	4.3 ± 0.5	1.06
N1	Sodium naphthalene formaldehyde sulphonate	Dark brown liquid	7.0 ± 0.5	1.2
N2	Sodium naphthalene formaldehyde sulphonate	Dark brown liquid	7.0	1.21
M	Sulphonated melamine methanol condensate	Gray powder	8.0–10.0	0.80

Table 3 List of various mixes prepared using different activators and superplasticizers

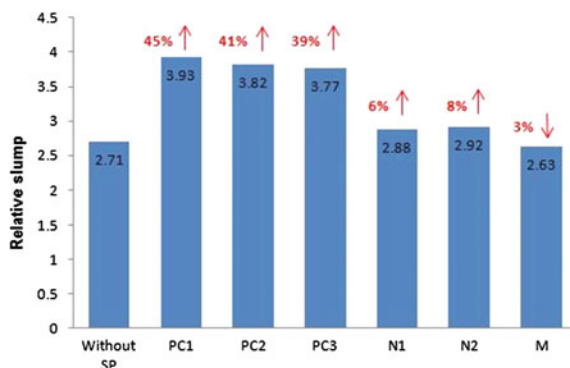
Mix number	Type of superplasticizer
1	–
2	N1
3	PC1
4	PC2
5	PC3
6	N1
7	N2
8	M

3.1 Results and Discussions

The relative slump of the paste with and without using different SPs is presented in Fig. 1. As can be seen in this figure, relative slump of the pastes with using modified Polycarboxylate-based SPs (PC1, PC2 and PC3) and naphthalene- based SPs (N1 and N2) were increased with respect to that of the paste without using any SP; however, the relative slump of the paste with using melamine-based powder (M) was decreased with respect to that of the paste without using any SP. The increase in relative slump was 45, 41, 39, 6, 8 % for the pastes with using PC1, PC2, PC3, N1 and N2 respectively with reference to the paste without using any SP and the decrease in relative slump was 3 % for the paste with using M based SP with reference to the paste without using any SP. Similar results have been reported by [17] for flow table spread in fly ash based geopolymer mortar with using M and PC based SPs. However, the effect of N based SP on the workability of activated fly ash mortar has not been investigated in their study.

From the mini slump test results it can be concluded that each type of SPs influenced the fly ash based geopolymer paste differently. This could be due to the instability of these commercial SPs designed for use with OPC in high basic media

Fig. 1 Effect of different SPs on relative slump of the fly ash based geopolymer paste with using multi-compound activator ($\text{Na}_2\text{SiO}_3/\text{NaOH} = 2.5$)



such as $\text{NaOH} + \text{Na}_2\text{SiO}_3$ [17, 23]. In other words according to [23], all of the SPs used in this study were chemically unstable in multi-compound activator ($\text{Na}_2\text{SiO}_3/\text{NaOH} = 2.5$) with pH equals to 13.36 at 23 °C and all of them experienced structural changes which resulted in loss of their fluidifying characteristics. In summary, in the case of fly ash based geopolymer activated by multi-compound activator ($\text{Na}_2\text{SiO}_3/\text{NaOH} = 2.5$), PC based SPs (latest generation) would be the most effective type of SPs resulted in 39–45 % increase in relative slump with reference to the paste without using any SP. It could be due to the fact that although PC based SPs were also chemically unstable in multi-compound activator ($\text{Na}_2\text{SiO}_3/\text{NaOH} = 2.5$); however, existence of several lateral chains in its structure results in steric repulsion that compensates the tendency of particles to form complexes, therefore their plasticizing (fluidifying) ability would be greater than N based SPs [17].

4 Conclusions

In this study the effects of six different SPs (three modified Polycarboxylate (PC) based, two naphthalene (N) based and one melamine (M) based SP) on workability of fly ash based geopolymer paste has been evaluated. Based on the experimental results, it is concluded that the effect of different SPs on the workability of fly ash based geopolymer directly depends on the type of SPs. In the case of fly ash based geopolymer activated by multi-compound activator ($\text{Na}_2\text{SiO}_3/\text{NaOH} = 2.5$), modified Polycarboxylate (PC) based SPs (latest generation) would be the most effective type resulted in 39–45 % increase in relative slump with reference to the paste without using any SP.

Acknowledgments The authors gratefully acknowledge SIKA Australia and BASF Australia for supplying the commercial superplasticizer products used in this study.

References

1. P. Duxson et al., Geopolymer technology: the current state of the art. *J. Mater. Sci.* **42**, 2917–2933 (2007)
2. J. Davisovits, Geopolymers: inorganic polymeric new materials. *J. Therm. Anal.* **37**, 1633–1656 (1991)
3. T. Bakharev, Geopolymeric materials prepared using Class F fly ash and elevated temperature curing. *Cem. Concr. Res.* **35**, 1224–1232 (2005)
4. Z. Li, Z. Ding, Y. Zhang, Development of sustainable cementitious materials, in *Proceedings of the International Workshop on Sustainable Development and Concrete Technology* (2004) pp. 55–76
5. A.M. Neville, *Properties of Concrete* (Pearson Education Limited, Essex, 1995)
6. S. Hanehara, K. Yamada, Interaction between cement and chemical admixture from the point of cement hydration, absorption behaviour of admixture, and paste rheology. *Cem. Concr. Res.* **29**, 1159–1165 (1999)
7. J. Brooks et al., Effect of admixtures on the setting times of high-strength concrete. *Cem. Concr. Compos.* **22**, 293–301 (2000)
8. F. Puertas, T. Vázquez, Early hydration cement. Effect of admixtures superplasticizers. *Materiales de Construcción* **51**, 53–61 (2001)
9. S. Chandra, J. Björnström, Influence of cement and superplasticizers type and dosage on the fluidity of cement mortars—Part I. *Cem. Concr. Res.* **32**, 1605–1611 (2002)
10. T. Bakharev, J. Sanjayan, Y.-B. Cheng, Effect of admixtures on properties of alkali-activated slag concrete. *Cem. Concr. Res.* **30**, 1367–1374 (2000)
11. M. Palacios, F. Puertas, Effect of superplasticizer and shrinkage-reducing admixtures on alkali-activated slag pastes and mortars. *Cem. Concr. Res.* **35**, 1358–1367 (2005)
12. M. Palacios, P.F. Banfill, F. Puertas, Rheology and setting of alkali-activated slag pastes and mortars: effect of organic admixture. *ACI Mater. J.* **105**, 258–264 (2008)
13. Q. Wang, L. Li, C.P. Wu, Z.T. Sui, Research on adaptability of slag-based geopolymer with superplasticizer. *Key Eng. Mater.* **405**, 129–134 (2009)
14. M. Palacios, Y.F. Houst, P. Bowen, F.M. Puertas, Adsorption of superplasticizer admixtures on alkali-activated slag pastes. *Cem. Concr. Res.* **39**, 670–677 (2009)
15. F. Puertas, A. Palomo, A. Fernández-Jiménez, J. Izquierdo, M. Granizo, Effect of superplasticisers on the behaviour and properties of alkaline cements. *Adv. Cem. Res.* **15**, 23–28 (2003)
16. D. Hardjito, S.E. Wallah, D.M. Sumajouw, B.V.D. Rangan, On the development of fly ash-based geopolymer concrete. *ACI Mater. J. Am. Concr. Inst.* **101**, 467–472 (2004)
17. M. Criado, A. Palomo, A. Fernández-Jiménez, P. Banfill, Alkali activated fly ash: effect of admixtures on paste rheology. *Rheol. Acta* **48**, 447–455 (2009)
18. D.L. Kong, J.G. Sanjayan, Effect of elevated temperatures on geopolymer paste, mortar and concrete. *Cem. Concr. Res.* **40**, 334–339 (2010)
19. F.A. Memon, F. Nuruddin, S. Demie, N.F. Shafiq, Effect of superplasticizer and extra water on workability and compressive strength of self-compacting geopolymer concrete. *Res. J. Appl. Sci. Eng. Technol.* **4**, 407–414 (2012)
20. M.R. Rixom, N.P. Mailvaganam, *Chemical Admixtures for Concrete* (Taylor & Francis, London, 1999)
21. American Society of Testing and Material, ASTM C1437, *Standard Test Method for Flow of Hydraulic Cement Mortar* (2007)
22. H. Okamura, K. Ozawa, Mix design for self-compacting concrete. *Con. Libr. JSCE* **25**, 107–120 (1995)
23. M. Palacios, F. Puertas, Stability of superplasticizers and shrinkage reducing admixtures in highly basic media. *Mater. Constr.* **54**, 65–86 (2004)

The Effect of Steel Fibre on Flexural Strength of Fibre Reinforced Concrete at High Temperature

Clotilda Petrus, Ruqayyah Ismail, Fariz Aswan Ahmad Zakwa, Nur Ashikin Marzuki, Nor Hafida Hashim and Khairil Imran Fadillah

Abstract Good infrastructure is needed to facilitate the economic functioning of one country. Infrastructure can be defined as structural elements which provide framework and supporting the entire development of a nation. Typical Civil infrastructures are referring to the technical structure that support the needs of a society such as roads, bridges, water supply, tunnel and so forth and it is essential to sustain comfortable living conditions. In tunnel structure, it is very important to use material that can sustain high temperature so that catastrophe accidents can be avoided by preventing sudden collapse from occurring in case of fire. This research is investigating the effect of steel fiber on flexural strength of fiber reinforced concrete at high temperature. Inclusion of fiber in concrete has proven to improve the mechanical properties of concrete and delay failure of structures. The flexural and compression strength of concrete with 0.5 % volume fraction of steel fiber when subjected to high temperature was investigated. The concrete is design with compression strength of 50 MPa and the type of steel fiber used is hooked end steel fiber. From the experimental results obtained from 30 samples of $500 \times 100 \times 100$ mm beams, it is concluded that incorporating steel fiber can increase the flexural stress of concrete as compared to the normal concrete as high as 74.42 % at temperature 600 °C. The ductility of the concrete with steel fiber also observed to improve about 15.7 %.

Keywords Steel fibre · High temperature · Flexural · Strength · Steel fibre ratio

C. Petrus (✉) · R. Ismail · F. A. A. Zakwa · N. A. Marzuki · N. H. Hashim · K. I. Fadillah
Faculty of Civil Engineering, Universiti Teknologi MARA, Permatang Pauh, Pulau Pinang,
Malaysia
e-mail: clotilda166@ppinang.uitm.edu.my

1 Introduction

A dysfunctional infrastructure can cause many problems to the society around it especially at the time it is needed the most such as when the time of flash flood, monsoon flood or fire. The problem can cost tremendously from properties, health to life. From [1] SMART tunnel structures in Kuala Lumpur for example, in case of flash flood occur in Kuala Lumpur and the drainage system is stuck with trash due to lack of maintenance, it may sink the whole city Apart from a dysfunctional due to natural disaster, a man made problem such as accidents and fire can also causing a problem or even worse a catastrophe that can be written in a history book. As an example, on 26 October 2001 a historic day for Switzerland as the day a mass tragic happens at Gotthard tunnel's southern entrance. Eleven death had been confirmed by Swiss official after two trucks, one carrying tires collided, sparking a fire that raised temperature in part of the 17 km tunnel to 1,000 °C and brought down large chunks of the roof. Up to 40 cars and vans been fused to a molten mass were reported to be at the heart of the disaster zone which blaze throughout the night. Rescue workers were unable to approach within 100 m of the accident area. The effect of even small fires in a confined space like a tunnel is extremely serious because of inability of gasses and heat to disperse. For instance, carbon monoxide is highly toxic at very low concentration, having this trapped in a confined space allows concentration to build well beyond fatal. Ironically, the Gotthard tunnel is assumed as the safest tunnel in Europe with a security cell at every 250 m and can accommodate 70 people each, equipped with state of the art fire detection system and a ventilation system that allows air inside the tunnel that will be fresh and smoke transferred in 15 min. None of that was enough to prevent the tragedy and this incident had triggered safety issues on other infrastructures construction.

From [2] and [3] in Gotthard tragedy, the theory behind the falling roof of the tunnel when an explosion happen is, the temperature on the scene at the moment is too high that it pushes water content in the concrete to upper part. When it comes to void in the concrete, the vapors will trap in it and make the pressure in the void itself high and causing an explosion or spalling. In addition, the concrete can't cater the load that applied from the tunnel structure and makes it collapse. This research work, investigates the effect of inclusion of steel fibre in concrete to improve its flexural strength and the ductility. High strength concrete and improved ductility should be beneficial to prevent drastic reduction of concrete flexural strength and sudden collapse of structures. There are two main objectives outlines in this study, namely to determine the flexural strength of concrete incorporated with 0.5 % hooked end steel fibers and to evaluate the flexural reduction rate when the samples are exposed to high temperatures.

2 Literature Review

High temperature is one of the disastrous factors that causes a failures and collapse of structures. From [2] and [3], Gotthard tunnel is only one example in many of it, the most famous tragedy would be world trade center, where both of the twin towers had easily fallen to the ground when it been hit by aircraft which produce thousands of degree Celsius rapidly in a confine space. The reason on world trade collapse is due to the building which made by steel structure have a deleterious effect where the structure is melting and losing its strength by the increase of temperature. Same pattern happen to Gotthard, when the temperature increase, the strength of the concrete structure failed and fall to the ground. Theoretically, when the temperature is increase, the water content in the concrete will vaporize and if the heat is applied under the sample, the moisture content will disperse to the upper side of the structure. When there is a void in the structure, those moistures will be trapped in the void and increases the pressure inside it which eventually will produced spalling of concrete. However, these effects can be overcome by inclusion of fibers in the concrete.

Fibers in concrete will provide crack arrestment mechanism as well as to filled the void when the heat is applied. When the heat is applied, the fiber will melt and filled the void which will prevent the vapor increased the pressure and avoid spalling. Structurally, fiber reinforced concrete possesses higher flexural strength as compared to plain concrete. Therefore, it is very important to understand the behavior of structures and its flexural strength when subjected to high temperature. Flexural strength is a parameter to define the ability of the concrete to resist deformation when load is applied to it. Higher flexural strength means it will take a bigger load to make the structure deform before it failed. In engineer point of view, it is always desirable to have a structural member with sufficient flexural strength to ensure safety and functionality of the intended designed structures. Plain concrete is a normal concrete consist of gravel, sand, and cement. Plain concrete usually tend to have low flexural strength compared to steel fiber reinforced concrete. The inability of concrete to resist crack on itself deteriorate its flexural strength. The inclusion of fibers such as, steel fibres in the concrete mix is one of the solutions to overcome the problem of cracking. Lau and Anson [4] studied the effect of high performance steel fiber reinforced concrete on high temperature by using high performance cement and normal strength cement and reported that steel fiber reinforced concrete have a better flexural strength than concrete without steel fiber. However, Purkiss (1984) [5] in his study on steel fiber reinforced concrete at elevated temperature showed that, the sample start to reduced its flexural strength at a temperature of 4,000–5,000 °C and at 8,000 °C, 80 % of the flexural is already loss. The author then concluded that the volume fraction and type of fiber only to have secondary effect in flexural strength reduction and there is a correlation between loss in cube strength and loss in flexural strength.

The flexural strength of plain concrete and steel fiber reinforcement concrete is obtained via two different methods. Flexural strength for plain concrete is the

stress capacity which is determined by a third point test. This test is conducted to find the stress at maximum load that can be sustained by a prismatic beam. For steel reinforced concrete, the term flexural strength itself is divided into three different results. By conducting this test, one should know that there is a big difference between first crack strength. Ultimate flexural strength is the stress at the point of maximum load that can be sustained during the third point test. Equivalent flexural strength is the stress capacity at a point of specific deflection in a third point test.

3 Experimental Set Up

In this study, Portland cement was being used since it is the most common cement that has been used in steel fibre reinforced concrete with a compressive strength f_{cu} 50 MPa according to BS 5328:1997. Crushed gravel aggregate with maximum size of 10 mm was chosen to prevent undue interference between aggregate and fibre at mixing stage. The fine aggregates are oven dried prior to mixing to reduce water content in concrete sample which may produce spalling. The concrete mix was designed with aggregate, sand, cement ratio as 2:1.8:1 and water cement ratio of 0.45. Hooked end type steel fibre with size 20 mm and diameter of 0.25 mm were used to minimize the tendency for the fibre to cluster in the mixer. The ultimate tensile strength of the fibre was found to be 1,815 N/mm². Two concrete mixtures were prepared and labelled as M1 for concrete mixture with no fibre and as M2 for concrete mixture with 0.5 % steel fibre. The quantity of steel fibres used must not be less than 40 kg/m³ as it is the average amount required to improve concrete toughness and must not exceed 60 kg/m³ as upper limit for economic purpose. Hooked end type steel fibres were chosen in this experiment as it represents the most typical shape of steel fibre in construction industry. A total of 30 samples of 500 × 100 × 100 mm beams were prepared with concrete mix designed of grade 50 which consists of fifteen samples with plain concrete and fifteen samples of steel fibre reinforced concrete. All samples were left to harden for approximately 24 h before they were cured for 28 days in curing tank. All samples are tested and exposed to high temperature after 28 days. Details on the samples are tabulated in Table 1. The specimens are labeled according to their concrete mix type M1 for plain concrete and M2 for fibre reinforced concrete, followed by the temperature which is ranging from 200 to 800 °C. A total number of 30 specimens of 150 × 150 × 150 mm concrete cube for compression test (Fig. 1) and also 30 specimens of 500 × 100 × 100 mm concrete beam for flexural test (Fig. 2) were also prepared.

4 Experimental Set Up

The experimental results were tabulated in Table 2, the data shows that the maximum force of the sample is decreasing proportionally with increasing

Table 1 Sample details

Specimen	Nos.	Size	Concrete grade
<i>Cube</i>			
M1	3	150 × 150 × 150 mm	50
M1-200	3	150 × 150 × 150 mm	50
M1-400	3	150 × 150 × 150 mm	50
M1-600	3	150 × 150 × 150 mm	50
M1-800	3	150 × 150 × 150 mm	50
M2	3	150 × 150 × 150 mm	50
M2-200	3	150 × 150 × 150 mm	50
M2-400	3	150 × 150 × 150 mm	50
M2-600	3	150 × 150 × 150 mm	50
M2-800	3	150 × 150 × 150 mm	50
<i>Beam</i>			
M1	3	500 × 100 × 100 mm	50
M1-200	3	500 × 100 × 100 mm	50
M1-400	3	500 × 100 × 100 mm	50
M1-600	3	500 × 100 × 100 mm	50
M1-800	3	500 × 100 × 100 mm	50
M2	3	500 × 100 × 100 mm	50
M2-200	3	500 × 100 × 100 mm	50
M2-400	3	500 × 100 × 100 mm	50
M2-600	3	500 × 100 × 100 mm	50
M2-800	3	500 × 100 × 100 mm	50

Fig. 1 Compression test

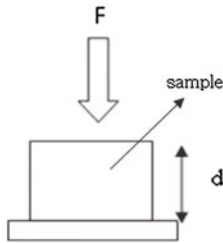


Fig. 2 Flexural test

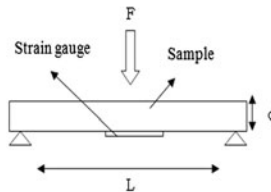


Table 2 Result analysis

Sample	Maximum force (kN)	Maximum stress (kN/m ²)	Strain (μ)	Displacement (mm)
<i>Beam</i>				
M1	8.09	83.77	42,670	1.11
M1-200	7.06	62.54	32,401	1.00
M1-400	3.21	45.97	32,978	0.70
M1-600	2.35	43.63	28,382	0.40
M1-800	1.85	30.62	21,358	0.16
M2	9.26	118.66	49,371	1.33
M2-200	8.86	97.40	36,003	1.01
M2-400	4.28	76.89	35,995	0.83
M2-600	3.58	76.10	31,971	0.64
M2-800	2.57	38.63	24,487	0.17

temperature. As the temperature increases the maximum force decreases. Similar pattern were observed in the flexural strength for beam samples. It was also noticed that there was a significant drop of flexural strength at the lower temperature, namely at 200–400 °C. However, the drop of flexural strength became less drastic as the temperature increases further. Observation on the displacement and strain showed that the ductility of fiber reinforced concrete is improved as compared to the ductility of plain concrete. The ductility of the concrete with steel fiber improved about 15.7 %. A detail analysis and comparison of the experimental results between mixture M1 and M2 are presented in Table 3. From the data analysis, it is obvious that the flexural strength of steel fiber reinforced concrete is higher than that of plain concrete by 41.65 % at normal temperature and as high as 74.42 % for specimens at 600 °C.

It is also observed that the flexural strength of fiber reinforced concrete is increasing with increasing temperature. However, the difference of flexural strength for plain concrete and fiber reinforced concrete become insignificant at temperature of 800 °C.

Figure 3 describe the difference level by comparing mixture sample without fiber (M1) and mixture sample with fiber (M2). It is clearly shows that by adding in steel fiber, the flexural strength indicate an increase in any temperature. Initial stress of M2 is 118 kN/m² and initial stress for M1 is 83 kN/m². Significant drop happen at temperature 400 °C for both mixture which is around 35 % of flexural strength loss from initial flexural strength. At 800 °C, the residual flexural strength for both mixtures is almost the same. Figures 4 and 5 shows the force displacement curve. Both Figures shows that as temperature go high, the force will proportionally decreasing. For initial force on no fiber sample is 8 kN with displacement of 1.1 mm and when the mixture added with steel fiber, the force increase to 9 kN and displacement of 1.3 mm. At highest temperature, maximum force of mixture with no fiber is 1.8 kN and mixture for steel fiber is 2.5 kN.

Table 3 Improvement on the sample

Beam	Flexural strength (kN/m ²)	Average flexural strength (kN/m ²)	Percentage increase	Moment (kNm)
M1	83.73	83.77	41.65	1.01
	83.80			
	83.78			
M2	118.75	118.66	41.65	1.16
	118.65			
	118.59			
M1-200	62.66	62.54	55.7	0.88
	62.48			
	62.49			
M2-200	97.36	97.40	55.7	1.11
	97.48			
	97.36			
M1-400	45.98	45.97	67.26	0.40
	46.01			
	45.92			
M2-400	76.93	76.89	67.26	0.54
	76.88			
	76.86			
M1-600	43.68	43.63	74.42	0.29
	43.54			
	43.67			
M2-600	76.32	76.10	74.42	0.45
	76.11			
	75.87			
M1-800	30.66	30.62	26.16	0.23
	30.66			
	30.54			
M2-800	38.66	38.63	26.16	0.32
	38.54			
	38.69			

5 Conclusion and Recommendation

It can be concluded that the flexural strength of concrete can be improved by adding steel fibers to the concrete. The strain data between normal mixture and steel fiber mixture shows that steel fiber also can increase the ductility and also the serviceability of the concrete around 15.7 % at room temperature. However, both samples become less ductile as the temperatures are increases. The performance of

Fig. 3 Comparison on steel fiber mix with none steel fiber mix

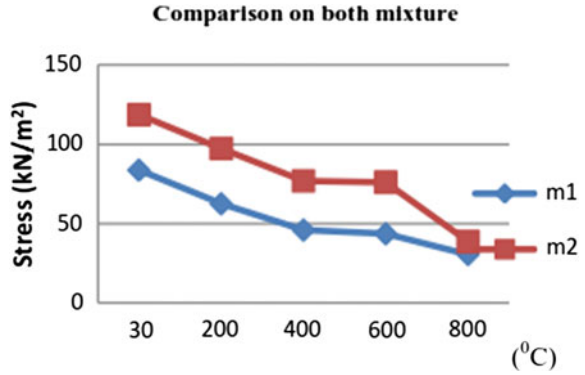


Fig. 4 Force displacements for no fiber mixture

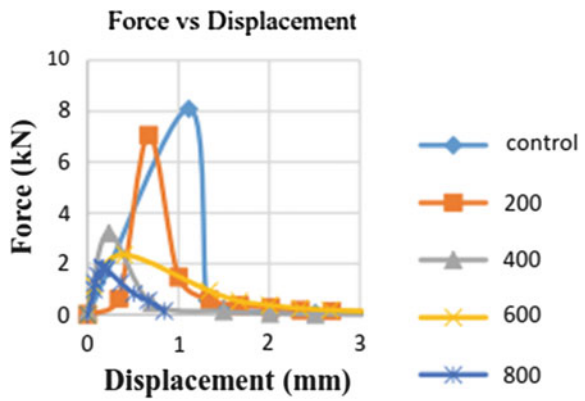
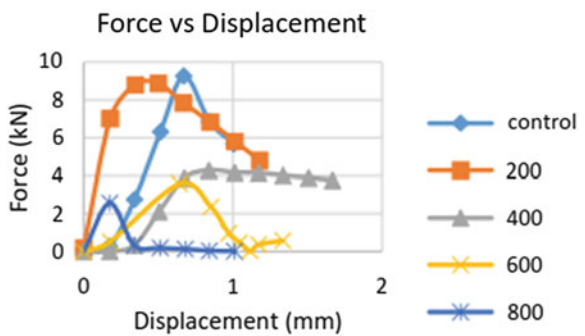


Fig. 5 Force displacements for steel fiber mixture



the fiber reinforced concrete is optimum up to the temperature of 600 °C however, the effect of steel fiber to the flexural strength become less significant at temperature more than 600 °C. It was observed that adding steel fiber can increase the residual flexural strength of the concrete around 74.42 % at temperature 600 °C as

one of the example. The results of obtained in this study agree well with the previous finding by other researchers.

The inclusion of fiber in concrete has proven to increase the flexural strength of beam and improve its ductility. Nevertheless, more study should be conducted to understand the behavior of fiber reinforced concrete when subjected to high temperature by varying more parameters such as the steel fiber ratio, the type of concrete and the range of temperatures, volume of void inside the sample and its effect on spalling.

Acknowledgments This research is part of our main research of the Basic Study of High Temperature Resistance on Hybrid Fibre Reinforced Concrete funded by Fundamental Grant Research Scheme (FRGS), Ministry of Higher Education of Malaysia (Ref. No. 600-RMI/FRGS 5/3 (42/2012)). We thank Research Management Institute (RMI), Universiti Teknologi MARA (UiTM) Malaysia and all academic staff of Faculty of Civil Engineering, UiTM Pulau Pinang for their full support of this research.

References

1. http://en.wikipedia.org/wiki/SMART_Tunnel
2. The Times, Tragedy of Gotthard, 2001
3. <http://en.wikipedia.org/wiki/GotthardRoadTunnel>
4. A. Lau, M. Anson, Effect of high temperature on high performance steel fiber reinforced concrete, 2006
5. J.A. Purkiss, Steel Fibre reinforced concrete at elevated temperatures. Int J Cement Comp Lightweight Concrete, **6**(3), (1984)

Compressive Behavior of Steel Fiber Reinforced Concrete After Exposed to High Temperatures

Ruqayyah Ismail, Fariz Aswan Ahmad Zakwan, Clotilda Petrus,
Nur Ashikin Marzuki, Nor Hafida Hashim
and Muhammad Fahmi Mustafa

Abstract This study focus on the compressive properties of Steel Fiber Reinforced Concrete after being exposed to temperature between 20 and 800 °C. The effect of elevated temperatures on the compressive strength and elastic modulus (stiffness) of concrete are presented. High Strength Concrete (HSC) samples for this study were prepared with and without steel fibers. The volume dosage of steel fibers is 0.5 % out of total volume of concrete. The results indicate that the compressive strength and elastic modulus of HSC is increasing at the early phase but then decreasing with the increasing temperature, and the loss of elastic modulus is quicker than the compressive strength. Based on experimental result, the HSC mixes retained about 45 % of their compressive strength, on average, after exposure to 600 °C, and this was further reduced to only 8.7 % of High Strength Concrete C50-with steel fiber (HSCWF50SF) and 20 % of High Strength Concrete C50-without steel fiber (HSCNF50SF).

Keywords High strength concrete · Steel fibers · Elevated temperatures · Compressive behavior · Elastic modulus

1 Introduction

Compressive performance of concrete is important for the evaluation and repair of concrete structures at high temperature [1]. There were many relevant studies have been carried out on the high-strength concrete (HSC) and normal-strength concrete (NSC) [2]. The results showed that the mechanical properties of NSC and HSC

R. Ismail (✉) · F. A. A. Zakwan · C. Petrus · N. A. Marzuki · N. H. Hashim · M. F. Mustafa
Faculty of Civil Engineering, Universiti Teknologi MARA, Permatang Pau,
Pulau Pinang, Malaysia
e-mail: ruqayyah812@ppinang.uitm.edu.my

were declining slowly with the increasing of temperature. There were also observed that explosive spalling will occurred during the heating process [3, 4].

Steel fiber mixed in HSC can effectively prevent spalling and improve the residual mechanical properties of HSC at high temperature [5]. HSC is able to achieve higher strengths and better durability compared to normal strength concrete (NSC) [6]. Moreover, HSC behaves differently than NSC when exposed to elevated temperatures because it tends to lose more strength and spall more [1, 7].

Fire is one of the most severe risks to any buildings and structures. The importance of enhancing concrete performance at high temperature is definitely crucial. Many relevant studies have been carried out on high performance concrete and concretes incorporating steel fibers [8]. This study investigates the compressive behavior of the concrete subjected to different maximum temperatures with steel fiber and without steel fiber. The addition of steel fiber in concrete is able to modify micro and macro cracking. The steel fibers inhibit crack growth and cracks at their origin.

This study is conducted to investigate the compressive behavior of steel fiber reinforced concrete mixed with and without steel fibers after being exposed to high temperature (20, 200, 400, 600, 800 °C). The high temperature test and compression test were carried out with specimens of $150 \times 150 \times 150 \text{ mm}^3$.

2 Experimental Details

2.1 Materials

The cement materials used in this study were Portland cement (PC) equivalent to ASTM Type I. The chemical compositions of the cement are shown in Table 1.

The coarse aggregate used was crushed limestone with nominal sizes of 20 mm. The specific gravity of the aggregate was 2.58 g/cm^3 . Natural river sand, with a fineness modulus of 2.79, was used as fine aggregate. The steel fibers used were hooked fibers with a length of 50 mm and an aspect ratio of 71.

2.2 Mix Proportioning

A total of 15 concrete mixes were prepared in two series with and without steel fibers. Series I mixes were prepared without steel fiber (HSCNF50SF) and Series II mixes were prepared with 0.5 % steel fiber (by volume). The details of the mix proportions are shown in Table 2.

Table 1 Chemical compounds cement

Compounds	% by mass
Silica (SiO ₂)	20.20
Lime (CaO)	63.60
Alumina (Al ₂ O ₃)	5.40
Iron Oxide (Fe ₂ O ₃)	4.30
Magnesia (MgO)	0.94
Sulfur Trioxide (SO ₃)	3.00
Loss on Ignition (LOI)	1.35
Insoluble Residue	0.30
Alkalies (Na ₂ O + 0.658 K ₂ O)	0.56
Tricalcium Aluminate (C ₃ A)	7.20
Tricalcium Silicate (C ₃ S)	54.00

Table 2 Mix proportions

Ingredients	Unit	Quantities	
		High strength concrete C50-without steel fiber (HSCNF50SF)	High strength concrete C50-with steel fiber (HSCWF50SF) + 0.5 % steel fiber
Cement	kg	23.95	23.95
Water	kg	11.42	11.42
Coarse aggregate	kg	50.69	50.69
Fine aggregate	kg	46.79	46.79
Steel fiber	kg	–	1.26
Astop admix PC30	ml	220	210

2.3 Specimen Preparation and Test

The concrete mixtures were prepared in a pan mixer. For each mix, a total of 15 specimens, including $150 \times 150 \times 150 \text{ mm}^3$, were cast in steel moulds. To prevent the steel fibers from breakage, tamping rods were not used while pouring High Strength Concrete C50-with steel fiber (HSCWF50SF) into the concrete moulds. The moulds were then placed on a vibrating table for about 30 s and the top surfaces were finished off with the help of trowel. Then the specimens were kept in the moist curing room at $23 \pm 2 \text{ }^\circ\text{C}$ for up to 24 h. The concrete specimens were cured according to ASTM standard C192 [9].

Specimens were cured under water in a custom designed temperature controlled curing tank at $35 \text{ }^\circ\text{C}$.

After curing process is completed, the 12 concrete specimens were heated with electrical furnace as shown in Fig. 1 at four different temperatures. Every three samples were heated up to 200, 400, 600, and $800 \text{ }^\circ\text{C}$ subsequently. The furnaces

Fig. 1 Electric furnace

were programmed to reach the target temperatures at a rate of $5\text{ }^{\circ}\text{C}/\text{min}$. The maximum temperatures were maintained for 1 h to ensure the temperature is in stable condition.

Compression strength test were carried out using Denison compression machine with a 3,000 kN capacity [10]. The average results from the compression test are taken from three concrete specimens. The test was conducted according to the method standard [11]. A pace rate of the testing machine is equal to 6.8 kN/sec was used to test the specimens. The results of the compression tests are summarized in Table 3 for the unheated and in Table 4 for the heated specimens.

3 Behavior of Unheated Concrete

3.1 Compressive Strength

All cubes were tested at the age of 28 days. High Strength Concrete C50 without steel fiber (HSCNF50SF) showed lower compressive strength compared to High Strength Concrete C50 with steel fiber (HSCWF50SF). The compressive strength of High Strength Concrete C50 without steel fiber (HSCNF50SF) is 50.31 MPa showed a decrease (2.59 %) from High Strength Concrete C50 with steel fiber

Table 3 Test results for unheated concrete

Concrete specimen	Addition of fibers	Compressive strength (MPa)	Strain at peak stress
HSCNF50SF	No	50.31	0.011
HSCWF50SF	0.5 % steel	51.65	0.015

Table 4 Test results of concrete cubes after exposure to elevated temperature

Temperature (°C)	Type	Compressive strength, f (MPa)	Strain at peak stress
200	HSCNF50SF	41.61	0.042
	HSCWF50SF	48.98	0.020
400	HSCNF50SF	43.04	0.020
	HSCWF50SF	50.35	0.022
600	HSCNF50SF	27.16	0.026
	HSCWF50SF	41.58	0.026
800	HSCNF50SF	14.98	0.031
	HSCWF50SF	38.32	0.017

(HSCWF50SF) which is 51.65 MPa. When the steel fibers are added, the compressive strength is increased.

3.2 Stress Strain Curve

A stress–strain curves of unheated concrete specimens were obtained from the compression tests cubes with a controlled of displacement rate as shown in Fig. 2. For the concrete prepared with steel fiber a higher strain at the peak stresses was observed, but steeper descending paths in the stress–strain curves. The addition of 0.5 % steel fibers has result a higher stress value with changed in the shape of the stress–strain curves can be observed.

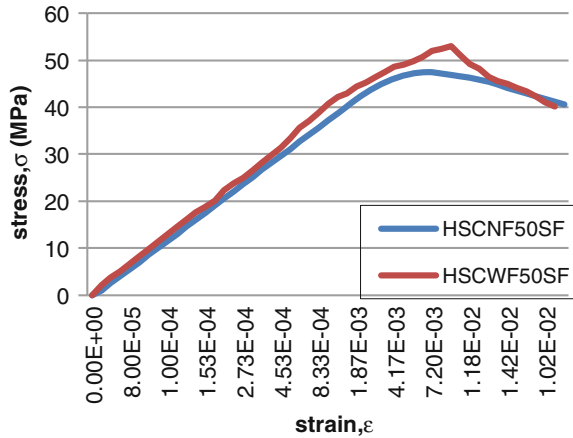
4 Behavior of Concrete After Exposed to High Temperature

4.1 Compressive Strength

The average values of compressive strength, for High Strength Concrete C50 without steel fiber (HSCNF50SF) and High Strength Concrete C50 with steel fiber (HSCWF50SF) are reported in Table 4, respectively.

From Table 4 it shows that for High Strength Concrete C50 without steel fiber (HSCNF50SF), compressive strength at 400 °C (43.04 MPa) is greater than at 200 °C (41.61 MPa), 600 °C (27.16 MPa), and 800 °C (14.98 MPa). Similarly,

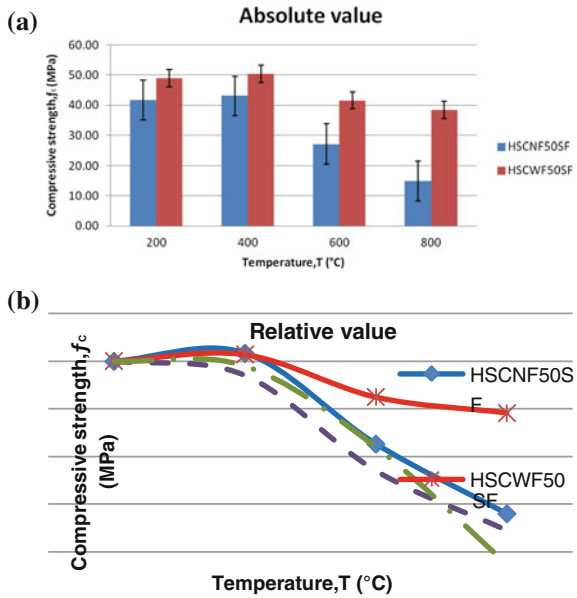
Fig. 2 Stress–strain curve of unheated concrete cube



for HSCWF50SF, compressive strength at 400 °C (50.35 MPa) is greater than that at 200 °C (48.98 MPa), 600 °C (41.58 MPa), and 800 °C (38.32 MPa). It implies that at temperature 400 °C, the compressive strength is higher for both high strength concrete with or without steel fiber. It also can be observed that at 800 °C, the compressive strength for high strength concrete with steel fibre has increased more than 50 %.

The absolute and relative compressive strength of High Strength Concrete C50 without steel fiber (HSCNF50SF) and High Strength Concrete C50 with steel fiber (HSCWF50SF) exposed at different temperatures are given in Fig. 3. In order to discuss the scattered of test data, the standard deviation are calculated and displayed as error bars in Fig. 3a. All the relative standard deviations (ratio of standard deviation to arithmetic mean of test data) are lower than 10 %, which means the data scattered is smaller and the reliability of test results are higher. As seen from Fig. 3a, after the same heat exposure, the compressive strength of High Strength Concrete C50-with steel fiber (HSCWF50SF) is higher than of High Strength Concrete C50-without steel fiber (HSCNF50SF). The compressive strength of HSCNF50SF and HSCWF50SF has the same trend with the temperature increases. As seen from Fig. 3a, the critical temperature is at 400 °C. After the exposure of 600–800 °C, the internal damage on HSC increases gradually with the increasing temperature, which reduced the compressive strength. The strength losses of HSCNF50SF and HSCWF50SF after 600 °C are 27.16 and 41.58 MPa. After being exposed to 800 °C, the steel fiber oxidizing decarbonization and High Strength concrete (HSC) lead to the restoring of compressive strength. The relationship between the relative compressive strength, f and the temperature, T for HSCNF50SF and HSCWF50SF was compared with results taken from Hu and Dong [12] and Guo [13]. As shown in Fig. 3b, the curve proposed by Hu and Dong [12] fits the test data well. Figure 3b also shows the curves of the relative compressive strength of Guo [13] after elevated temperatures. Comparative analysis shows that, the critical temperatures of Guo [13] and Hu and Dong [12] are 400

Fig. 3 **a** Absolute value.
b Relative value of relationship compressive strength for HSCNF50SF and HSCWF50SF with heating temperature



and 200 °C respectively, indicating that the compressive strength decreases significantly beyond the corresponding critical temperatures. The critical temperature of High Strength Concrete C50-with steel fiber (HSCWF50SF) is 400 °C, and the decline rate of Guo [13] strength curve is higher than Hu and Dong [12].

Furthermore, the HSCWF50SF curve has an increasing trend when the temperature is not higher than 400 °C. This is due to HSCWF50SF is undergoing the “high temperature curing” when the exposure temperature is not higher than 400 °C, which makes the cement hydration reaction and the pozzolanic reaction is fully utilized and the strength is slightly improves compared with the High Strength Concrete C50-without steel fiber (HSCNF50SF).

4.2 Stress Strain Curve

Figures 4 and 5 shows the compressive stress–strain curves of High Strength Concrete C50-without steel fiber (HSCNF50SF) and High Strength Concrete C50-with steel fiber (HSCWF50SF) after exposure to different temperatures. After exposure to 200–400 °C, the heat damage of specimen increases gradually, thus the stress–strain curves become flatter with the temperature increases. The compressive strength and deformation modulus decrease constantly, meanwhile the corresponding peak strain and ultimate strain increase rapidly. After exposure to 600–800 °C, the steel fiber oxidizing decarbonization and the HSC sintering result in the increase of HSC brittleness, and the peak points of stress–strain curves move

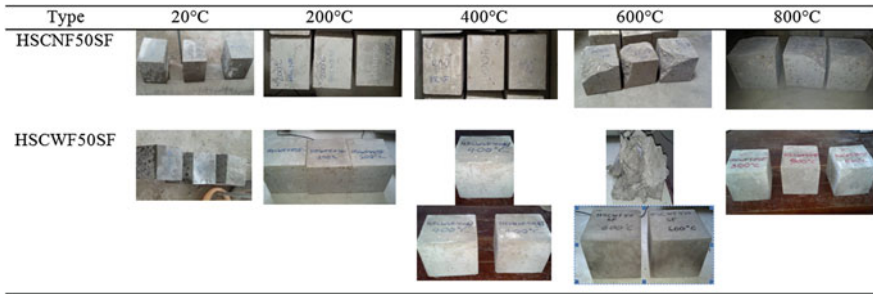
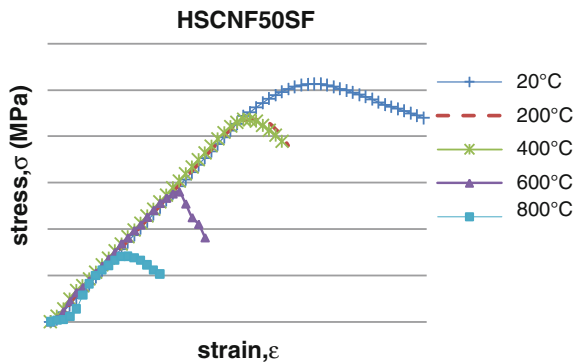


Fig. 4 Occurrence of explosive spalling

Fig. 5 Stress–strain curves of HSCNF50SF



left and upwards. Therefore, the peak strain decreases, and the compressive strength restores.

4.3 Explosive Spalling

From Fig. 6, it shows the result of explosive spalling. After exposed to temperature of 600 and 800 °C, HSCNF50SF suffered a significant spalling. While concretes specimen using steel fiber (HSCWF50SF) performed well until 800 °C. One of sample exposed to temperature of 600 °C is exhibit severe explosive spalling. The sample experienced explosive spalling because thermal expansion of the aggregate and splitting of pieces of aggregate close to the surface because of physical or chemical changes. Explosive spalling is caused by a vapor-pressure mechanism and physical or chemical changes. The addition of steel fiber in the high strength concrete can improved it performance against explosive spalling at high temperature.

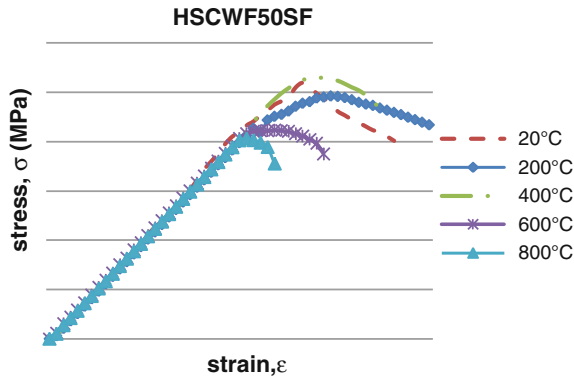


Fig. 6 Stress–strain curves of HSCWF50SF

5 Conclusion

Through this research work, the compressive behavior and the effect of temperature on high strength concrete with steel fiber were investigated. The incorporation of steel fiber was found effectively improve the compressive strength of High strength concrete at high temperature. The critical temperature for High Strength Concrete C50-without steel fiber (HSCNF50SF) and High Strength Concrete C50-with steel fiber (HSCWF50SF) are found to be 400 °C.

The results of compressive strength stress–strain relationship at elevated temperatures were presented. High strength concrete (HSC) were prepared in two series with and without the use of steel fibers. The following conclusions can be drawn from the results:

1. The compressive behavior of steel fiber reinforced concrete mixed with and without steel fibers after exposed to high temperature (20, 200, 400, 600, and 800 °C) is determined by compressive strength, strain–stress curve and explosive spalling. It can be concluded that the steel fiber reinforced concrete mixed is highly recommended to be used in construction industry especially for structure that exposed to higher risk of fire explosion.
2. High Strength Concrete C50-with steel fiber (HSCWF50SF) is found more durable than High Strength Concrete C50-without steel fiber (HSCNF50SF) after exposed to high temperature.
3. The used of steel fibers are found effective in reducing the degradation of compressive strength of the concrete after exposure to the elevated temperatures.

Acknowledgments This research is part of our main research of the Basic Study of High Temperature Resistance on Hybrid Fibre Reinforced Concrete funded by Fundamental Grant Research Scheme (FRGS), Ministry of Higher Education of Malaysia [Ref. No. 600-RMI/FRGS

5/3 (42/2012)]. We thank Research Management Institute (RMI), Universiti Teknologi MARA (UiTM) Malaysia and all academic staff of Faculty of Civil Engineering, UiTM Pulau Pinang for their full support of this research.

References

1. R. Manish, *Development and Evaluation of High Performance Fiber Reinforced Concrete as a Repairing Material*, Master's thesis, West Virginia University, WV, 2012
2. M. Husem, The effects of high temperature on compressive and flexural strengths of ordinary and high-performance concrete. *Fire Saf. J.* **41**, 155–163 (2006)
3. P. Kalifa, F.-D. Menneteau, D. Quenard, Spalling and pore pressure in HPC at high temperatures. *Cem. Concr. Res.* **30**, 1915–1927 (2000)
4. Kodur VKR, Spalling in High Strength Concrete Exposed to Fire-Concerns, Causes, Critical Parameters and Cures, in *Proceedings, ASCE Structures Congress*, Philadelphia, PA, American Society of Civil Engineers, 2000, pp. 1–9
5. P. Pliya, A.-L. Beaucour, A. Noumowe, Contribution of cocktail of polypropylene and steel fibres in improving the behaviour of high strength concrete subjected to high temperature. *Constr. Build. Mater.* **25**, 1926–1934 (2011)
6. ACI 544.1R, Report on Fiber Reinforced Concrete (Reapproved 2009), American Concrete Institute, Farmington Hills, MI, 1996
7. C.S. Poon, Z.H. Shui, L. Lam, Compressive behavior of fiber reinforced high performance concrete subjected to elevated temperature. *Cem. Concr. Res.* **34**(12), 2215–2222 (2004)
8. K. Nishioka, N. Kakimi, S. Yamakawa, K. Shirakawa, Effective applications of steel fibre reinforced concrete, *Fibre-Reinforced Cement and Concrete. RILEM Symposium*, 1975, pp. 425–433
9. ASTM C192, *Standard Practice for Making and Curing Concrete Test Specimens in the Laboratory* (ASTM International, West Conshohocken, PA, 2007)
10. J.-C. Lee, W.-J. Kim et al., Compressive properties of amorphous metal fiber reinforced concrete exposed to high temperature. *J. Korea Inst. Build. Constr.* **12**(2), 183–193 (2012)
11. ASTM C39, *Standard Test Method for Compressive Strength of Cylindrical Concrete Specimens* (ASTM International, West Conshohocken, PA, 2011)
12. H. Hu ,Y. Dong, Experimental research on strength and deformation of high-strength concrete at elevated temperature. *China Civ. Eng. J.* **35**, 44–47 (2002)
13. Z. Guo, X. Shi, *Behaviour of Reinforced Concrete Atelevated Temperature and its Calculation* (Tsinghua University Press, Beijing, 2002)

Part VIII
Bioremediation and Engineering

An Assessment of Water Demand in Malaysia Using Water Evaluation and Planning System

M. F. Ali, A. Saadon, N. F. Abd Rahman and K. Khalid

Abstract Water supply and demand is one of the hot topics discussed in the community today. Higher growth rate of the population has drawn heavily on the natural resource base in Malaysia. Trend of supply and demand in the Langat catchment, water availability assessment and water storage capacity to supply and demand were investigated using a new accounting concept and analytical approach, Water Evaluation and Planning (WEAP) system. The assessment model is computed based on three scenarios—Scenario 1: Higher Population Growth, Scenario 2: Water Year Method and Scenario 3: Extended Dry Climate Sequence. The study found that Langat catchment is relatively sensitive to the growth of demands, suggesting that slight changes in population growth will alter the present water availability. Furthermore, the populations increase to 7 % with the increment of climate variation of the current condition, thus exposing the study area with water scarcity problem.

Keywords Langat catchment · Water evaluation and planning · Water demand and water supply

1 Introduction

Infrastructure development is a key factor for the socioeconomic development in Malaysia, where water resources and water supply are available. Lately, water supply situation in the country has changed from a relative abundance to one of scarcity. Over the years, population growth and urbanization are arresting rapidly increasing in demands and pressure on the water resources, besides contributing to the rising of water pollution [1]. It is critically vital to develop the knowledge and

M. F. Ali (✉) · A. Saadon · N. F. Abd Rahman · K. Khalid
Fakulti Kejuruteraan Awam, Universiti Teknologi Mara, Shah Alam, Malaysia
e-mail: mohdfozi@salam.uitm.edu.my

skills that are necessary to safeguard our catchments and river basins without altering the socioeconomic development, in order to manage the water resources available in a sustainable way [2].

Malaysia has experienced extensive economic development since the 1980s, resulting in increasing water demands in the commercial and industrial development centers. Being prepared to be a developed nation by 2020, the effort to develop and manage this vital resource have to be guided by national perspectives with an integrated and environmentally sound basis. The main concern of the Malaysian government to lay within the availability and sustainability of water resources especially in Selangor, where a precious water resource is decreasing [3]. The Klang Valley experiences a serious water crisis during the first eight months of 1998. A severe water shortage caused due to a low observed rainfall and runoff during the period of March to September 1998. This led to the widespread water rationing in many parts of Selangor and Wilayah Persekutuan, affected over one million consumers and hundreds of industries. Department of Water Supply, Selangor claimed that the cost of handling the crisis by the Government ran into about RM56 million. The high cost was incurred for the rental and maintenance of mobile trucks from private companies and Government agencies, the operational costs, emolument of workers and purchase of mobile treatment facilities for treatment of water such as the one used at the lake in Mines Wonderland. The lessons from the crisis illustrated the needs for sensible management of water resources and distribution to avoid the recurrence of the experiences.

Astonishingly, as an alternative, future water management will shift from building new water supply systems to a better operating system [4]. The variation of water values in time and space will increasingly motivate efforts to address water scarcity and reduce water conflicts. In dealing with this condition, many integrated tools have been developed purposely to help manage water resources [5]. For instance, hydro-economic models represent spatially distributed water resource systems, infrastructure, management options and economic values in an integrated manner. In this particular tool, water allocations and management are either driven by the economic value of water or economically evaluated to provide policy insights and reveal opportunities for better management [6].

Considering all the above issues, this study utilizes the integrated hydrology and water allocation model, Water Evaluation and Planning (WEAP) to evaluate the impact of demand and supply on water resource availability [7] particularly within Langat catchment. Therefore, the investigation consisted in the use of water consumption for human needs, for agricultural and others in the study area due to their position along the Langat basin. The goals of the study are (1) to investigate the trend of supply and demand in Langat catchment (2) to assess the water availability in Langat Catchment using the Water Evaluation and Planning (WEAP) and (3) to investigate the water storage capacity and the factors of fluctuation on supply and demand in Langat catchment.

2 Materials and Method

2.1 Study Area

The Langat river basin has a total catchment area of approximately of 1,815 km². It lies within latitudes of 2°40'152"N to 3°16'15"N and longitudes of 101°19'20'E to 102°1'10'E. The length of the main river is 141 km and mostly situated 40 km east of Kuala Lumpur. The catchment is drained by three major tributaries; Langat River, Semenyih River and Labu River. However, the research undertaken the upper part of the Langat catchment [8]. The main tributary, Langat river flows about 182 km from the main range (Banjaran Titiwangsa) at the Northeast of Hulu Langat District in south-southwest direction, and draining into the Straits of Malacca. The main reach of Semenyih River is flowing south-southwest direction through the town of Semenyih, Bangi Lama and finally merges with Langat River at about 4 km to the east of Bangi Lama town. There are two reservoirs in the study area including Langat dam and Semenyih dam. Currently about eight water treatment plants are operating in the Langat basin [9].

The upper part of the Langat basin selected as a study area. The demand sites are lies in the Hulu Langat District. The majority of the land use in the study area is a forest reserve, followed by agriculture and built-up area for housing and other developments. The industrial sector is also minimal in the study area.

2.2 Input Data

Data sets for the year 2000–2010 were used in this study, the period which naturalized flow data are available. Data of meteorological and hydrological such as rainfall, ground water and evaporation gained from the Department of Irrigation and Drainage Malaysia (DID) which are the stations are scattered in the upper part of the catchment area. The Federal Department of Town and Country Planning supplied Land use map for Peninsular Malaysia and the population data were obtained from local authorities. Catchment map and survey map were attained from Department of Survey and mapping Malaysia (JUPEM). All the data used as input in WEAP, Water Evaluation And Planning model.

2.2.1 Overview of Model

The Stockholm Environment Institute (SEI) developed water Evaluation and Planning (WEAP). It is a unique water resources and planning software where it stimulates hydrologic pattern based on climatic input. WEAP allows user to build scenarios with scenarios, for instance, increase in temperature or heavier rainfall, along with assumptions towards water demand, infrastructure and regulation [10].

All human activities can incorporate in WEAP in order to predict water shortage and water quality based on a model scenario.

2.2.2 Building the Model

Water in WEAP, the model is called “areas”. Building the areas by adding GIS based Raster and Vector maps in the projected areas. The map is used to orient and construct the system and refine the necessary area boundaries. The background vector data can be added from a SHAPEFILE format. This format can be created by most GIS software [7].

Once the area is open, the Years, Time Steps and Units are set. In this study, the Current Account is set to be year 2000 with the Last Year Scenarios to the year 2010. The Year 1990 will serve as the “Current Accounts” year for this study. The Current Accounts year is chosen to serve as the base of the model, and all system information (for instance, demand and supply data) is the input into the Current Accounts. The Current Accounts is the dataset from which the scenarios are built. A default scenario, the “Reference Scenario” carries forward the Current Accounts data into the entire project specified (2000–2010).

River path is drawn in WEAP by clicking on the “River” symbol in the Element window. The direction of the flowing river is built from the headwaters (upper stream) of the main river (Fig. 1). The whole process is continued by building the entire network of the Upper Langat Catchment.

Hydrological processes occurring in the catchment were modelled and stream flow, simulated on a monthly time-step, was compared to the naturalized flow series available. Once the proposed model was simulating the naturalized flow series satisfactorily, water demand sites were added and WEAP was run in its water allocation mode using the rainfall-runoff parameters determined from the first phase. This was done in order to assess WEAP’s ability to simulate water resources and water uses in the catchment. Simulated stream flow was compared to the measured flow from four different gauging stations located on the Langat main stream. The model as it used in this study operates at the WEAP sub-catchment scale and on a monthly time-step.

2.2.3 Demand Sites

The water demand is the total of water required to meet domestic, commercial, agriculture, institutional and industrial uses. The current domestic water demand for the basin is estimated at about 300–350 MLD [11]. The Sungai Langat river basin has an estimated total population of 951,800 (2000). Over the last decade from 1991 to 2000, the population growth rate of the study area has been increasing at 7.64 % per annum. There are four major districts under the Sungai Langat catchment namely Hulu Langat (upper basin), Kuala Langat, Sepang and Seremban.

Table 2 Breakdown of major land use categories by district, 2000, sg langat catchment

District	Land use categories			
	Built-up areas (ha) (%)	Agriculture (ha) (%)	Reserved forest (ha) (%)	Others (ha) (%)
Hulu Langat	18,020 (22.4)	18,020 (22.4)	18,020 (22.4)	18,020 (22.4)
K. Langat	8,660 (12.7)	8,660 (12.7)	8,660 (12.7)	8,660 (12.7)
Sepang	7,980 (23.3)	7,980 (23.3)	7,980 (23.3)	7,980 (23.3)
Klang	2,580 (35.6)	2,580 (35.6)	2,580 (35.6)	2,580 (35.6)
Seremban	8,520 (18.9)	8,520 (18.9)	8,520 (18.9)	8,520 (18.9)

Connecting the Demand with Supply and Creating the Return Flow Links

To ensure demand is satisfied in WEAP, the user needs to connect the supply system, which identified previously for each demand site. These can be accomplished in the schematic view where the transmission link is added. The link needs to be first positioned on the river, then pointing to the demand node. This includes all six demand site nodes and agriculture node. Next, the user needs to connect the return flow from the demand sites. The return flow links connected back to the rivers. Next, the Return Flow Routing is set. If multiple Return Flow links are created for a demand node, then Routing factors for all of the links must be summed to 100 %.

3 Results and Discussion

The computation of the model was done by computing the entire model for the Reference Scenario—the default scenario that was generated using Current Account information for the period specified for the project (2000–2010). The results will be appearing once the computation is completed. In WEAP, the typical scenario modeling effort consists of three steps; Current Accounts year is chosen to serve as the base year of the model. In this study, the year 2000 was selected to be the base; the Reference scenario is established from the Current Accounts to simulate the likely evolution of the system without intervention; and What-if scenarios can be created to alter the “Reference” scenario and evaluate the effects of changes in policies and/or technologies. The following results for Upper Langat river were made based on three scenarios; Scenario 1: High Population Growth (7 %), Scenario 2: Using Water Yield Method to evaluate Climatic Variation and Scenario 3: Extended Dry Climate Sequence.

3.1 Current Account (Year 2000)

Under this condition, the demand site data were identified based on Annual Water Use Rate of 110 million m³ for all populations. The total of agricultural areas that will take into account where the total area is 23,030 ha with 1,000 m³ of

Table 3 Overall water demand for year 2000

District	Land use categories	
	Population or area	Water demand (million m ³)
Hulu Langat	46,766	5.1
Cheras	163,550	18.0
Kajang	229,655	25.3
Semenyih	49,076	5.1
Hulu Semenyih	3,408	0.4
Beranang	14,071	1.5
Agriculture	23,030 ha	23.0
Total		78.1

consumption per hectare. Table 3 shows the water consumption for the year of 2000 for the seven demand sites which are the main target of the study. All the data were acting as the base input to the model in order to project the water demand in the next 10 years in the Reference Scenario.

3.2 Reference Scenario

The basic principle in WEAP is that the Reference Scenario is always exists where the changes in its description in the Area/Manage Scenario will reflect its actual role. In this model, the Reference Scenario is “Base Scenario with Population Growth of 2.2 % and Increased of Irrigation Water Needs”. The population rate increased about 2.2 % from year 1990 to 2000, based on the growth rate of the Hulu Langat District.

Figure 2 shows the result derived from the Reference Scenario with the projected water demand for the year of 2000–2010. The graph shows that the Unmet Demand is a zero value. These indicate that the water availability under the Reference Scenario, which based from previous population growth rate of 2.2 % is relatively sufficient. A detailed projected total water demand for the duration of study up to year 2010 is 1,101.1 million m³.

3.3 Scenario 1: Higher Population Rate (7 %)

In order to foresee the impact of possible condition of the model, a new scenario is created. The new scenario is to evaluate the impact of a population growth rate for Langat area higher than 2.2 % for the period of 2001–2010. Using the Manage Scenario tool, a new scenario named “High Population Growth” is added where under this scenario the increasing population growth rate is from 2.2 to 7 % and the agriculture area increase linearly at a rate of 3,000 ha per year. Fig. 3 shows

Fig. 2 Result of Reference Scenario

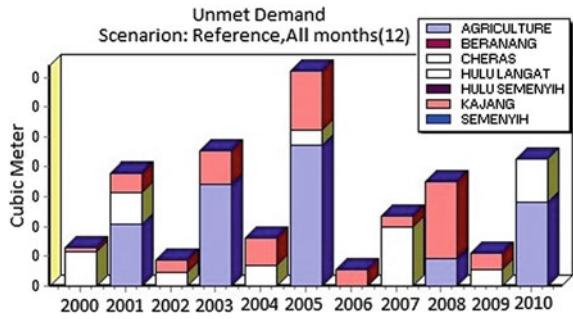
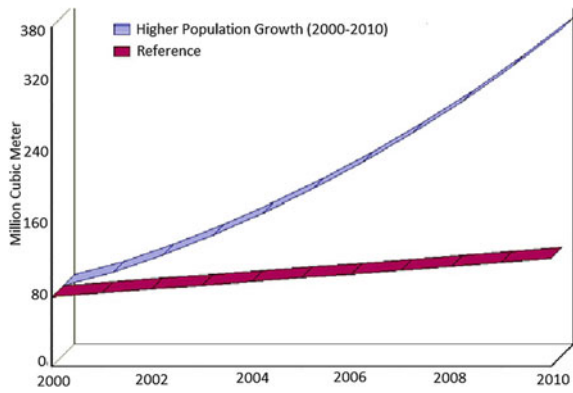


Fig. 3 Water demand projection under Reference Scenario and Scenario 1



the projection of water demand based on both scenarios, Reference Scenario and Scenario 1: Higher Population Growth (7 %) for Langat Catchment. The results show that the water demand in 2010 for the case of the high population growth rate was almost three times higher compared to 2000.

The projected total water demand for both conditions are total water demand for Scenario 1 is 2,213.2 million m³ compared to the year 2000 with total amount of 1,101.1 million m³. For Reference Scenario and Scenario 1: Higher Population Growth (7 %) for Langat Catchment, the Unmet Demand value in the year 2010 is 30.7 million m³. This finding shows that there will be a shortage of water supply in 2010 if the population is increasing at a rate of 7 %. The reservoir storage volume is reduced and a significant drop of reservoir volume as in Fig. 4 in year 2009 and 2010.

3.4 Scenario 2: Water Year Method

The Water Year Method is used to exercise the variety of supply and resources of water. This method is a simple tool to represent the variation in climate data. The year sequence is created to consist of the sequence of climatic variation in the scenario period. Each year of the period is assigned one of the climate categories.

Fig. 4 Reservoir storage volume under Reference Scenario

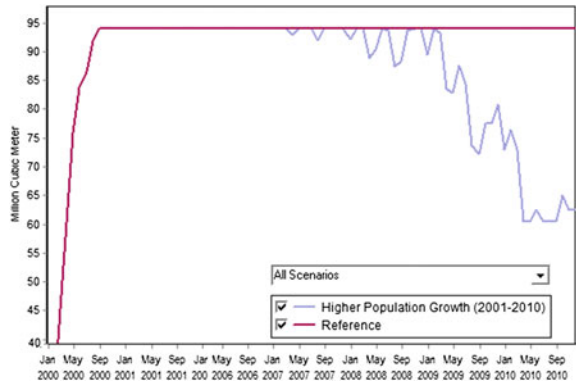
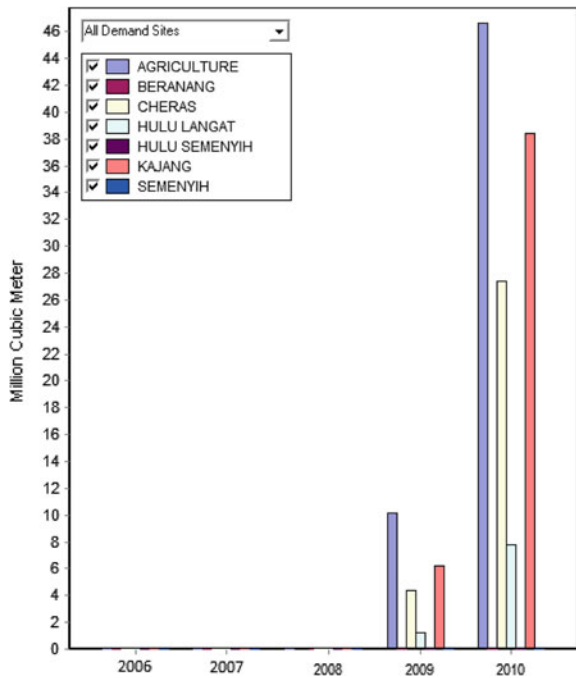


Fig. 5 Unmet demand for water year method under Scenario 1



There are four categories of climate regimes, namely very dry, dry, wet and very wet which is compared relative to a normal year. While the value of a normal year is given as 1, the dry years have a value less than 1 and very wet years have a value of larger than 1. Each year of the period is assigned one of the climate categories.

Figure 5 shows the result of Unmet Demand for Water Year Method under the Scenario 1 (Higher Population Growth (7 %)). The graph shows that the water supply only can accommodate up to year 2008. The agriculture demand is insufficient of 10.1 million m³ and 46.6 million m³ for the year 2009 and 2010, respectively.

Fig. 6 Result of unmet demand for Scenario 3 in comparison with the Reference Scenario

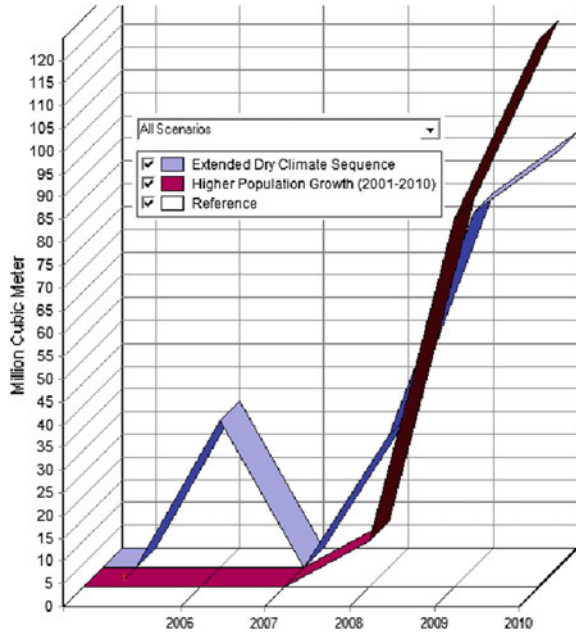
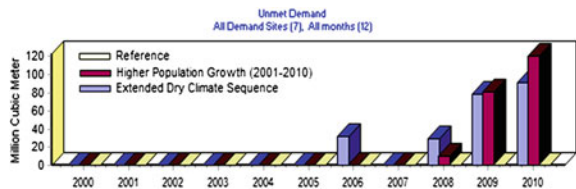


Fig. 7 Overall result of Scenario 3 in comparison with the Reference Scenario



About 38.4 million m³ insufficient water demand is also observed at the Kajang demand site in 2010.

3.5 Scenario 3: Extended Dry Climate Sequence

This scenario creates in order to evaluate the model towards the Extended Dry Climate Sequence in Langat Catchment. A new scenario is created from the Reference Scenario named the “Extended Dry Climate Sequence” and the climate variation is adjusted to evaluate the impact of water supply.

The climatic variation for Scenario 3: Extended Dry Climate Sequence is then assigned to Scenario 1 and Reference Scenario in order to foresee the impact towards the water demand and supply. Figures 6 and 7 show the results for Scenario 3: Extended Dry Climate Sequence in comparison to the Reference Scenario.

Table 4 Unmet Demand projection data

Scenario/year	Unmet water demand (million m ³)	
	Reference Scenario	Scenario 3
2000–2005	0	0
2006	0	32.4
2007	0	0
2008	0	28.9
2009	0	77.9
2010	0	91.3
Total	0	230.5

Fig. 8 Result of Unmet Demand for Scenario 3 in comparison with the Scenario 1

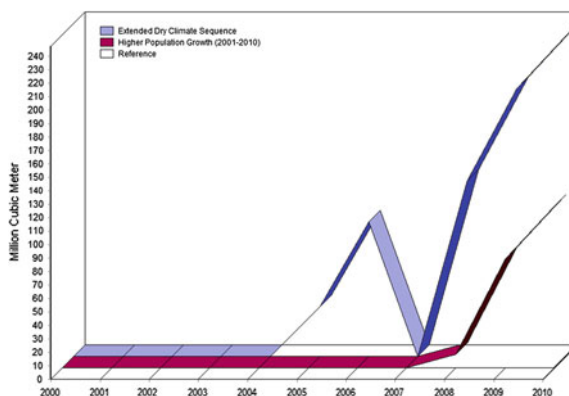
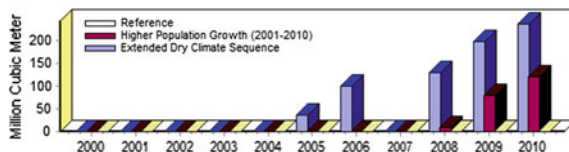


Fig. 9 Overall result for Scenario 3 in comparison with the Scenario 1



It is clearly shown from the graph a significant value of Unmet Demand for Scenario 3.

The details Unmet Demand Projections data for Scenario 3 is summarized in Table 4 and observed that the Unmet Demand was started in the year 2006 with a value of 32.4 million m³.

The same results are examined for the for Scenario 3: Extended Dry Climate Sequence in comparison to Scenario 1 where there is significant value of Unmet Demand as highlighted in Figs. 8 and 9.

Table 5 indicates the details result of Unmet Demand for Extended Dry Climate Sequence in comparison with Scenario 1. Under this scenario, the Unmet Demand is started as early as the year 2005. This clearly showed that with the highest population growth rate and dryer climate, Unmet Demand increases substantially.

Table 5 Unmet Demand projection data

Scenario/year	Unmet water demand (million m ³)	
	Scenario 1	Scenario 3
2005	0	37.0
2006	0	101.1
2007	0	0
2008	10	130.2
2009	80.8	198.8
2010	120.2	273.9
Total	211.1	704.1

4 Conclusion

Based on the reference data for the year 2000, the results of the Reference Scenario at the population growth at 2.2 % shows the availability of water resources is adequate up to the year 2010 with zero value of Unmet Demand analysis. However, when the assessment model is evaluated based on Scenario 1 reflected by a significant value of Unmet Demand in the year 2010 by the amount of 30.7 million m³. This indicate shortages of water in the study in 2010 and a significant drop to a reservoir storage volume in the year 2009 and 2010.

The Scenario 2 results indicated that the water supply only can accommodate up to year 2008. The agriculture demand is insufficient of 10.1 million m³ and 46.6 million m³ for the year 2009 and 2010, respectively. About 38.4 million m³ insufficient water demand is also observed at the Kajang demand site in 2010.

Finally, the climatic variation for Scenario 3 is then assigned to Scenario 1 and Reference Scenario in order to foresee the impact towards the water demand and supply, results the highest population growth rate and dryer climate, Unmet Demand increases substantially.

Acknowledgments The Exploratory Research Grant Scheme (ERGS), Ministry of Higher Education, and Universiti Teknologi MARA (UiTM), Malaysia, funded the project.

References

1. Global Water Partnership (GWP), Integrated water resources management, Global Water Partnership Technical Advisory Committee Background Paper no. 4. Sweden, 2000. Available at <http://www.gwp.org/Global/The%20Challenge/Resource%20material/IWRM%20at%20a%20glance.pdf>. Accessed 10 Sept 2012
2. A.G. Bobba, T.D. Prowse, J.Y. Diiwu, D. Milburn, Sensitivity of hydrological variables in the arctic watershed, Coppermine River, NWT, Canada due to hypothetical climate change. *J. Environ. Hydrol.* **13**, 22 (2005)
3. R.Z. Abidin, in *Buletin Ingenieur*, Economic Planning Unit (EPU), Water resources management in Malaysia, vol. 22 (2004), pp. 8–10

4. E. Le Roy, *A Study of the Development of Water Resources in the Officiants Catchment, South Africa; Application of the WEAP Models*, Unpublished M.Sc. thesis, Imperial College, London, 2005
5. J.J. Harou, P.V. Manuel, D.E. Rosenberg, J.M. Azuara, J.R. Lund, R.E. Howitt, Hydro-economics models: concepts, design, applications and future prospects. *J. Hydrol.* **375**, 627–643 (2009)
6. D. Conway, A. Persechino, S. Ardoin-Bardin, H. Hamandawana, C. Dieulin, G. Mahe, Rainfall and water resources variability in sub-saharan Africa during the twentieth century. *J. Hydrometeorology* **10**, 41–59 (2009)
7. H. Sarah, *Beyond building model: using WEAP to inform climate change adaptation policy in Guatemala*, Stockholm Environmental Institute, 2007. Available online at http://www.weap21.org/downloads/Beyond_Building_Models_Using_WEAP_to_inform_climate_change_adaptation.pdf. Accessed 20 Sept 2012
8. A. Suki, M. Kemil, T.P. Mok, Water quality profile of Sungai Langat. *J. Pertanika* **11**(2), 273–281 (1998)
9. K.R. Ayub, S.H. Lai, H.A. Aziz, SWAT application for hydrologic and water quality modelling for suspended sediments: a case study of Sungai Langat’s catchment in Selangor, in *Proceedings of International Conference on Water Resources*, Langkawi, May 2009
10. D. Purkey, A. Huber-Lee, A DSS for long-term water utility planning, southwest. *J. Hydrol.* **4**, 18–31 (2006)
11. KTA, *Sungai Langat integrated river basin management study, final report, vol. 3, technical studies part 1 of 4, CS-SG119.KTA* (Tenaga Sdn. Bhd, Kuala Lumpur, 2005)
12. Malaysian Centre for Remote Sensing Satellite Images (Ministry of Science, Technology and Innovation (MOSTI), Malaysia, 2001)

Water Quality Measures Using QUAL2E: A Study on RoL Project at Upper Klang River

M. F. Ali, M. H. Ahmad, K. Khalid and N. F. Abd Rahman

Abstract The degradation of the water quality and ecosystem are vulnerable to urbanization processes and activities. Increase numbers of population and industrial activities continue to increase a consumption of water and followed by the increasing of waste discharges to the natural waterways. These issues are very critical mostly in the developing countries and not excluded to the upper part of the Klang River basin. The current Water Quality Index (WQI) at both inlet and outlet of the study area is falling under Class III. The mitigation processes are needed to improve the index value before further degradation of the river downstream. Furthermore the stream flows that passage the city centre of Kuala Lumpur needed to be maintained in order to boost economic sector growth like tourism and other business activities. The Department of Irrigation and Drainage, Government of Malaysia is currently initiating the River of Life (RoL) rehabilitation program to mitigate the water quality and quantity of Klang River. This paper presents the current water quality study of the upper part of Klang River, which consists of six water quality parameter. This study involved an in situ works and followed by a laboratory investigation. Data analysis was carried out using QUAL2E software and proposes mitigation measures which to satisfy the objective of the RoL program. The study area was exposed to a high concentration of Biochemical Oxygen Demand (BOD), Chemical Oxygen Demand (COD) and Ammoniacal Nitrogen (AN) which contributed to the pollution of the river. At high numbers of total coliform also redound to the unsafe and unhealthy for portable water. In QUAL2E, a total maximum daily load (TMDL) analysis was calculated from a stream outfall and Indah Water Konsortium (IWK) outlet and finally the prediction load was carried out in order to be conformed for Class II. The study shows that the QUAL2E software was performed well in simulating the water quality parameter and able to incorporate in the rehabilitation program at the study area in order to conserve the natural qualities of the environment.

M. F. Ali (✉) · M. H. Ahmad · K. Khalid · N. F. A. Rahman
Fakulti Kejuruteraan Awam, Universiti Teknologi MARA, Shah Alam, Malaysia
e-mail: mohdfozi@salam.uitm.edu.my

Keywords Klang River · River of Life · QUAL2E · Water quality parameter

1 Introduction

Having a good water quality is important for a healthy river and ecosystem. Thus, various water quality parameters need to be measured in order to determine the health of the river water so that it is safe to use for any purpose. In Malaysia, the water quality index introduced by the Department of Environment (DOE) is being practiced for almost 25 years [1]. Most of the pollutants are generated due to human activities including urbanization processes, while the rest is due to natural degradation of soil and other components of the urban environment. The Non-Point Source (NPS) pollutants are normally carried to surface water bodies by storm runoff and typical sources of urban NPS pollutants are summarized in urban stormwater management manual for Malaysia [2].

The upper part of Klang River is included as one of the river rehabilitation program which conducted by the government of Malaysia. Besides improving the water quality, the program will transform the Klang River into a vibrant and liveable waterfront with high economic value. The transformation is divided into three components: river cleaning, river master planning and beautification and river development. With full implementations of the program, WQI of the river basin is expected to improve from current Class III–V to Class IIB by the year 2020 [3]. A monitoring study to evaluate an effectiveness of the project on the water quality assessment is required. An investigation was utilized a QUAL2E software for the measurement, analyse and predict of a future data in the basin. As water quality of the stream flows is affected during low-flow periods, a water quality model, QUAL2E uses a low flow analysis for creating a worst condition scenario [4]. A steady state model such as QUAL2E is appropriate to be used in a system that has steady state inputs. The models would be able to interface of river and their tributary and it will easily point out the source of pollutant. Models can simulate more than 15 water quality parameters [5]. A few studies of water quality were successfully conducted on Malaysian climate including in Langat River Basin [6], Tebrau River, Segget River [7], Johor River [8] and Selangor River [9].

The study area lies in between $3^{\circ} 14.11' N$, $101^{\circ} 44.55' E$ and $3^{\circ} 11.45' N$, $101^{\circ} 45.41' E$, about 7 km long and covers three major tributaries, namely Gisir River, Sering River, and Kemensah River. Klang River originates from Klang Gate Dam, Hulu Kelang (Fig. 1). The upstream of Klang River flows through a major residential and commercial area. Sering River originates from the northern parts of Hulu Kelang and flows through major areas of the Hulu Kelang area. A Gisir River originates from the Wangsa Maju area and flows through a major commercial area before it reaching the confluence of Klang River. The upstream of Kemensah River flows through a major residential area at the Kemensah Height which is situated near the National Zoo.

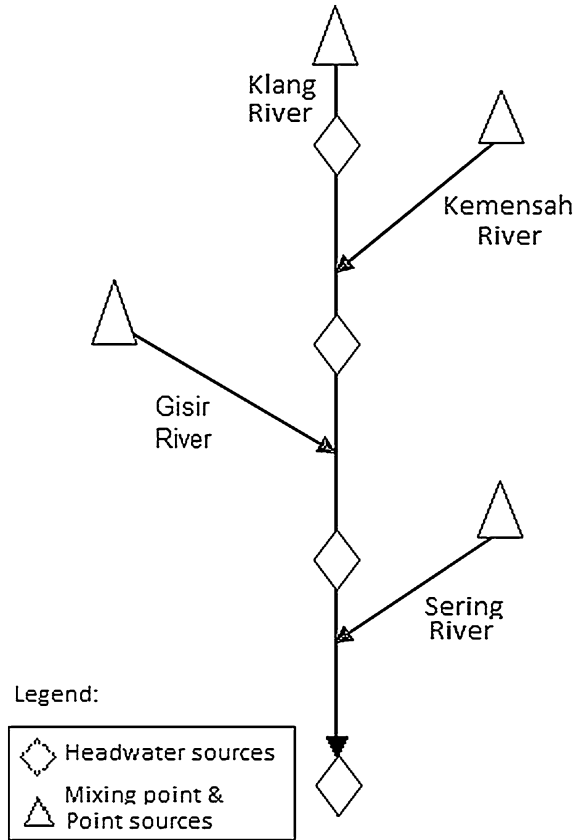
Fig. 1 The study area

2 Materials and Method

A water sampling was conducted in October 2012. A water samples were collected from 41 locations along the mainstream of Klang River and tributaries. On-site surveys were conducted on September 2012 at several locations to assess the impact of the proposed project towards current in-stream water quality. Figure 2 shows detailed sampling locations along the river basin. Every sample was collected at the end of reach and at the mixing point. Besides the point source, other samples were also collected along 7 km of the study area for modelling of water quality. An in situ measurement was carried out for pH, dissolved oxygen (DO), conductivity and temperature using YSI Model 85, a handheld water quality instrument. A hydraulics data such as depth and width were also recorded.

Samples for laboratory analysis were collected at each location and the pollutant sources, which contributed to the water pollution, were identified. Analysis of BOD, COD, TSS, AN, SS and E-coli was conducted using a standard method for the examination of water and wastewater methods within the recommended holding time. The QUAL2E able to represent each reach as in Table 1 distinguished the headwaters of the Klang River basin at upper stream. These data then will be compared from the previous study conducted in April 2011 which represents data before the mitigation takes place. The QUAL2E program then calibrates water quality data at all points of interest. The following section will discuss the comparing output of each parameter before and after mitigating.

Fig. 2 Sampling locations



3 Results and Discussion

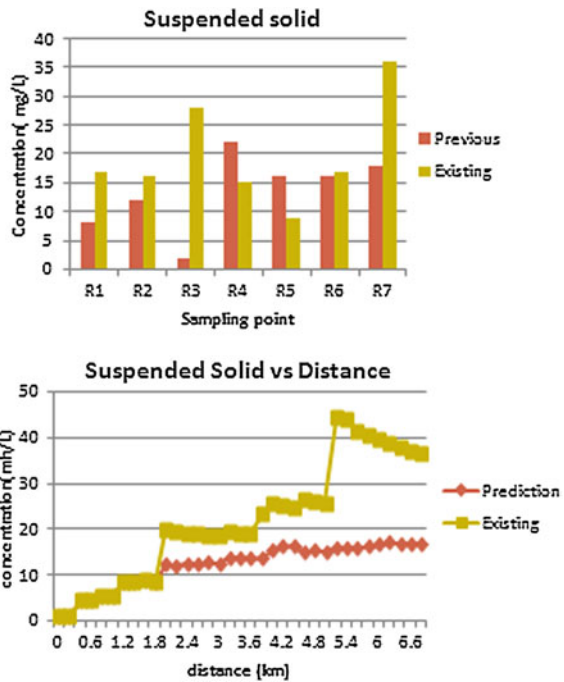
3.1 Suspended Solid

Suspended solid (SS) concentration is an important parameter used as an indicator of pollution in municipal and industrial water supply. These values are also used to determine organic, inorganic particles and immiscible liquids. The SS values were between 1 and 44 mg/L for all the water sampling points (Fig. 3). The concentrations of the SS were fluctuated due to the difference of point sources entering the river and originate from residential, industrial, and commercial areas. The level of SS at R1, R3 and R7 were exceedingly higher compared from the previous data due to the incomplete current construction works along Klang River. The deepening river depth can cause the sediment flow with the water to the downstream. A movement of water and the kinds of sediment load will be affected by the depth and width of a channel [10]. The concentration of SS became lower at point R5 due to a mixing of Klang River with other tributary. Mixing with the increasing

Table 1 QUAL2E reach representation

Reach number	Reach representation		
	Reach name	Begin river (km)	End river (km)
R1	Klang River 1	0.0	3.8
R2	Kemensah River	0.0	3.0
R3	Klang River 2	3.8	4.6
R4	Gisir River	0.0	3.0
R5	Klang River 3	4.6	5.6
R6	Sering River	0.0	1.2
R7	Klang River 4	5.6	7.0

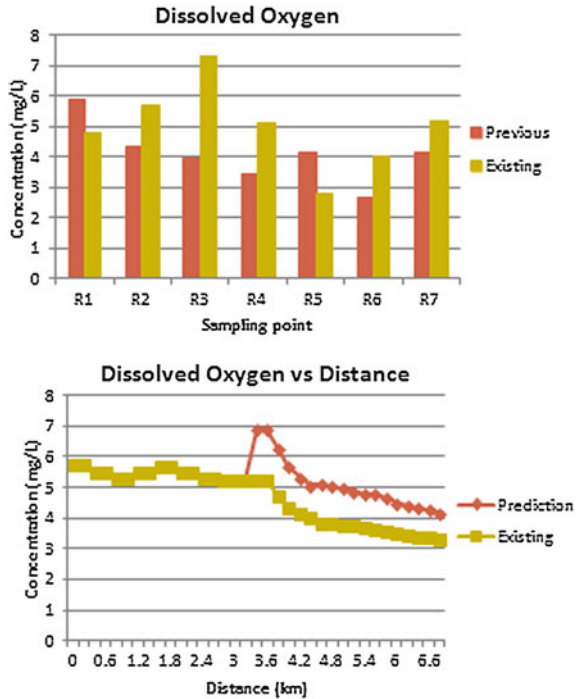
Fig. 3 Concentration of SS and analysis by QUAL2E



water volumes gave higher dilution of water and decreased the concentration of suspended solid in the water.

Concentrations of SS at sampling points along Klang River indicate that the content could be partly contributed by effluent discharges and soil erosion along the river. It can be seen from the water quality measured in terms of sewage and suspended solids from soil erosion and sedimentation, all registered negative trend for the period 1988–1994 on the use and threats to the Malaysian rivers and worsened for all 116 rivers over the same period [11]. Interim National Water Quality Standards (INWQS) recommended that threshold level of suspended solid

Fig. 4 Comparison of the DO and analysis by QUAL2E



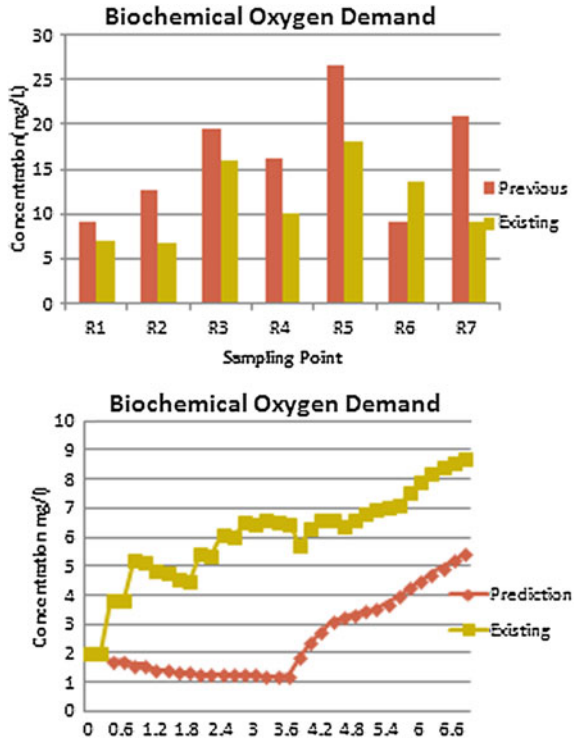
for Malaysia River is 50 mg/L for Class IIA. A water quality modelling of suspended solid was modelled following the standard required by INWQS. Both of the results of existing and prediction value by QUAL2E were observed within INWQS requirement which is not exceeded 50 mg/l for class IIA.

3.2 Dissolved Oxygen

The process uses measurement of DO levels in the basin is useful to provide a full scale control of the activity level in the aeration basin [12]. This will meet the objective for the river of life project to increase the quality of water along Klang River. Most of the DO values observed improved comparing before implementation of the mitigation processes as shown in Fig. 4. The improvement is expected since the rehabilitation of the rivers at the upstream almost heading to complete. The deepening of river depth and the improvement of the riverbank will cause an increasing in velocity of the stream flows and it helps the river water re-aeration.

DO readings measured were within the range of 3.3–5.77 mg/L, which indicates the river water is at an acceptable limit. The DO levels in the river observed were high at the upstream of Klang River indicates that minimum pollution occurred in the river. Then DO level were fluctuated until the distance 3.4 km,

Fig. 5 Concentration of BOD and analyse by QUAL2E



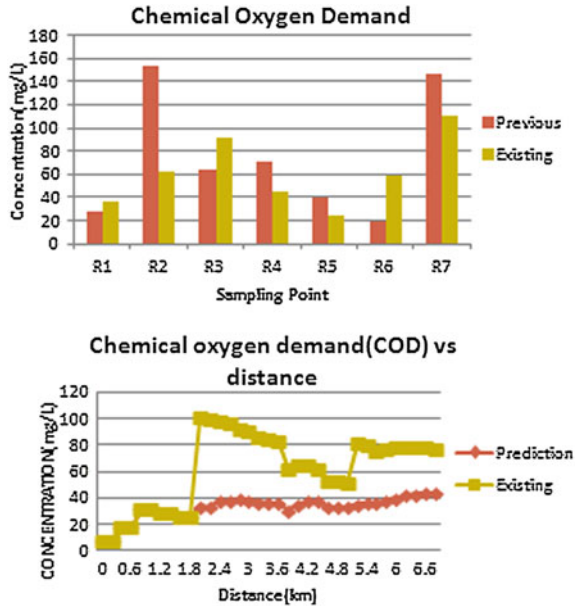
then the concentration for modelling of dissolved oxygen was extremely increase due to the implementation of the mitigation measure at that point.

3.3 Biochemical Oxygen Demand

Figure 5 shows that the BOD value was highest at the point R5 where the pollutants contributed from Sering River and the industrial area at the Klang River bank before mixing at point R6. The effluent discharge from the factories and raw food processing industries such as meat, fish and vegetables is detected as one of the major contributors of BOD pollutions at the point. The microorganism and bacteria start to harm the dissolved oxygen and the process of decreasing of the BOD.

The Biochemical Oxygen Demand (BOD5) measured was in a range of 2–8.7 mg/L. This indicates that the stream has gone into the polluted level and the stream can be categorized as severe impact towards organic loading. Since BOD value is within the Class IV of the NWQS, any residual waste or other permissible organic loading should be prohibited from entering the water bodies neither to maintain the water quality nor rehabilitate the existing water quality. A Gisir River

Fig. 6 Concentration of COD and analysis by QUAL2E



is contributed severe BOD level into the Klang River comparing to Sering River. BOD concentrations remained this high during peak storm runoff because of increasing in dilution [13]. In the modelling, all the point sources were predicted to treat at 90 % the output shows the BOD concentration was decreased to range from 2.00 to 5.45 mg/L which under Class II on INWQS.

3.4 Chemical Oxygen Demand

COD concentration level observed was varied among the sampling points and the COD values were extremely high at point R2 and R7, as in Fig. 6. The organic material from squatters at point R2 contributed the highest concentration of COD 153 mg/L where a direct point source from the man-made sanitation without any proper treatment was observed. After the rehabilitation along Klang River, the concentration of COD reduced to 63 mg/L which is below standard A of INWQS classification. However, at point R7, the COD concentration increased most probably due to the high discharge of wastewater from the two-sewage treatment plant unit that are located nearby the streams.

The QUAL2E analysed the COD values and found that it varies from 8.0 to 101 mg/L. The pollutants probably produced by the discharges from sewage treatment plant and nearby industrial. A previous study was reported a high value of COD in the study area due to industrial discharge of Industrial Area of Varanasi which discharged a large quantity of organic waste effluent into the streams [14].

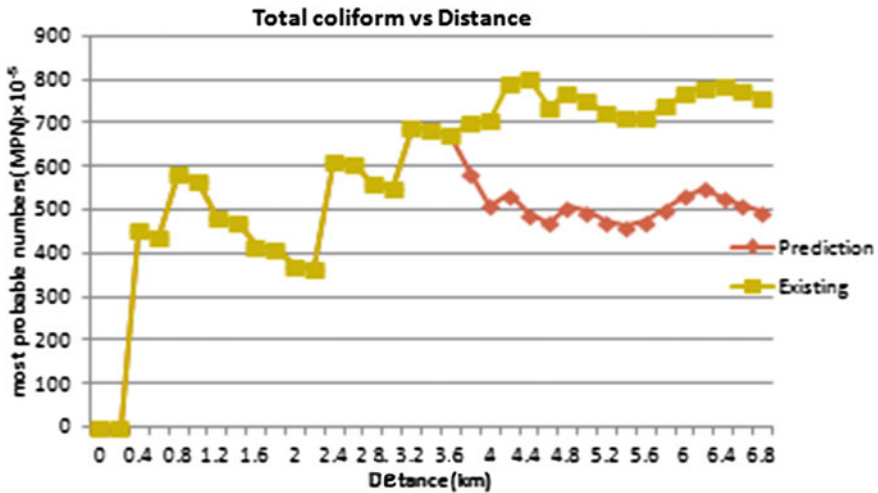


Fig. 7 Total coliform analysis by QUAL2E

The simulation of QUAL2E concerning predictions on the concentration of effluent discharge shown that all the point source concentration must below than 120 mg/l in order to achieve the standard requirement for DOE.

3.5 Ammoniacal Nitrogen

The analyses show all sampling points were decreased in term of AN concentration if compared from the previous 2011 data. The highest concentration was recorded on the sample R3. The location of R3 is near to residential and commercial area. Moreover, along the point R3 reach there is a point source discharge effluent from the printing factory into the river.

3.6 Total Coliform

The microbial quality of wastewater is usually measured by the concentration of the two primary sources of water-borne infection faecal coliforms and nematode eggs [15]. The increased existence of E-Coli in the streams is directly reflected in a significant drop in BOD value. The results shown in Fig. 7 show that a Total Coliform at Klang River exceeding 2,400 MPN/100 mL. The highest values for total coliform recorded at the Klang River with the reading of 792.48×10^5 MPN/100 mL and the lowest value at upstream is 0 MPN/100 mL. The comparison shows limited changes at the beginning of river distance due to a

very high number of bacteria exist in the river. With the mitigation measure taken Chainage 3.2 km, a number of total coliform is predicted drop to less than 500 MPN/100 mL.

4 Conclusion

A monitoring of water pollution sources seems very important in managing the river water quality in the country and all parties should actively involve in order to minimize the environmental issues. An analysis of current samples taken from a various locations proved that the current water quality of the Klang River improved from Class IV in 2011 to Class III. The study showed the QUAL2E software was performed well in simulating the water quality parameter and able to incorporate in the rehabilitation program in the study area in order to conserve the natural qualities of the environment. The simulations show that the expected mitigation measures will improve the water quality of the streams to Class II based on INWQS Classification. A continuous monitoring of the river basin is suggested in order to make sure the successful of the RoL.

Acknowledgments The project was supported by the Exploratory Research Grant Scheme (ERGS), Ministry of Higher Education, and Universiti Teknologi MARA (UiTM), Malaysia.

References

1. G. Department of Environment Malaysia, Interim National Water Quality Standards for Malaysia, Retrieved on March 17, 2013 from <http://www.doe.gov.my/index.php?option=comcontent&task=view&id=244&Itemid=615&lang=en>. (2005)
2. Department of Irrigation and Drainage, Urban stormwater management manual for Malaysia. Department of Irrigation and Drainage, Ministry of Agriculture, Malaysia, (2000)
3. Official Website of Greater Kuala Lumpur/Klang Valley Ministry of Federal Territories and Urban Wellbeing, 20 April 2013. <http://app.kwpcb.gov.my/greaterklkv/entrypoint-project-river>
4. M. Mohamed, in *Proceedings of the 1st Technical Meeting of Muslim Water Researchers Cooperation (MUWAREC) 2008*. Water Quality Models in river management. December, Malaysia, pp. 14–26
5. H.A.S. Ali, Using HEC-RAS and QUAL2E to assess Johor River water quality. Civil-Hydraulics and Hydrology, UTM, pp. 34–38. Unpublished, (2010)
6. N.B. Hashim, R. Ismail, K.A. Nasir, M. Ismail, A.R. Malek, Baseline study of water quality in Langat River Estuary, UTM, 2004. Unpublished
7. IPASA, Institute of Environmental and Water Resource Management (IPASA), The study of pollution prevention and water quality improvement of Sungai Tebrau and Sungai Segget. Volume II, Final Report, UTM. 2002. Unpublished
8. A.H. Ahmed Suliman, Using HEC-RAS and QUAL2E to assess Johor River water quality. Master thesis, Universiti Teknologi Malaysia, Johor, 2010. Unpublished

9. M. Mohamed, J.D. Stednick, F. Smith, Comparison of field measurements to predicted reaeration coefficients, k_2 , in the application of a water quality model, QUAL2E, to a tropical river. *Water Sci. Technol.* **46**(9), 47–54 (2002)
10. I. Matsuda, River Morphology and Channel Processes, in Fresh Surface Water, in *Encyclopedia of Life Support Systems, Developed under the Auspices of the UNESCO*, ed. by J.C.I. Dooge (EOLSS Publishers, Oxford, 2004)
11. K.R. Ayub, F.A.H. Asaari, R. Abdullah, T.L. Lau, N. A. Zakaria, Ab. A. Ghani, C.K. Chang, in *3rd National Civil Engineering Conference. Water Quality Assessment at Perai Industrial Park*. Penang, (2004), pp. 127–138
12. F. Fang, K.W. Easter, P.L. Brezonik, Point nonpoint source water quality trading: a case study in the Minnesota River Basin. *J. Am. Water Resour. Assoc.* **41**, 645–658 (2005)
13. D.R. Dudley, J.R. Karr, Concentration and sources of fecal and organic pollution in an agricultural watershed. American Water Resources Association, (1979)
14. S. Kumar, P.K. Mishra, N.L. Singh, K.K. Singh, P. Srivastava, Water quality of river varuna in Varanasi City, Uttarpradesh, India. *Asian J. Biochem. Pharm. Res.* **2**(2), 231–240 (2012)
15. C.A. Scott, N.I. Faruqui, L. Raschid-Sally, *Wastewater Use in Irrigated Agriculture Coordinating the Livelihood and Environmental Realities* (CAB International Publishing, Wallingford, 2004), pp. 1–197

Performance of Aquatic Macrophytes on Removal and Accumulation of Sulfate and Potassium from Domestic Wastewater

Zul Hilmi Saidin, Ramlah Mohd Tajuddin, Dzaraini Kamarun
and Norazah Abdul Rahman

Abstract Phytoremediation had been well accepted worldwide as one of the most successful green technologies for domestic wastewater treatment. This technology utilizes aquatic macrophytes to remove and extract macronutrients from the domestic wastewater and accumulate them in their plant tissues. However, most of the previous studies only focused on the use of aquatic macrophytes for removing and extracting nitrogen and phosphorous components. Thus, they overlook on sulfate (SO_4^{2-}) and potassium (K^+) as one of crucial macronutrient contaminants in domestic wastewater. Moreover, studies on removal and uptake of SO_4^{2-} and K^+ from domestic wastewater and their detail distribution and storage in macrophyte tissues are very limited. Therefore this study focused on performance of aquatic macrophytes in removing SO_4^{2-} and K^+ from domestic wastewater. The accumulation and translocation of SO_4^{2-} and K^+ throughout macrophyte bodies were also determined. The phytoremediation system was designed and fabricated in the Hydrology Laboratory in Universiti Teknologi MARA (UiTM), Shah Alam. Water Hyacinth (*Eichhornia crassipes*), Caladium (*Colocasia esculenta*) and Water Lettuce (*Pistia stratiotes*) were used in our study to demonstrate that local macrophytes may also have higher nutrients removal or uptake than other macrophytes. The performance of macrophytes in removing and accumulating SO_4^{2-}

Z. H. Saidin (✉) · R. M. Tajuddin

Faculty of Civil Engineering, Universiti Teknologi MARA, Shah Alam, Selangor, Malaysia
e-mail: zhsaidin@gmail.com

D. Kamarun

Faculty of Applied Science, Universiti Teknologi MARA, Shah Alam, Selangor, Malaysia

N. A. Rahman

Faculty of Chemical Engineering, Universiti Teknologi MARA, Shah Alam, Selangor,
Malaysia

and K^+ and their relationship were determined and reported. The results of this study are significant for sustainable approach for domestic wastewater which would satisfy towards wholly aspect of macronutrient criteria. Hence phyto-remediation process becomes alternative to compete with the other green technologies for national development.

Keywords Aquatic macrophytes · Phytoremediation system · Potassium · Sulfate · Wastewater treatment

1 Introduction

Phytoremediation had been well accepted worldwide as one of the most successful green technologies for domestic wastewater treatment. This technology utilizes aquatic macrophytes to remove and extract macronutrients from the domestic wastewater and accumulate them in their plant tissues. Thus, the phytoremediation currently becomes popular as an alternative technology in wastewater management. This is due to its ability to protect both the environment and public health in an economical way at a lower cost compared to conventional wastewater treatment [1, 2].

In recent years, there were extensive studies on phytoremediation of macronutrients using aquatic macrophytes. These include the phyto-treatments of golf courses surface water [3, 4], anthropogenic retention ponds, lakes and wetlands [5–8], groundwater [9], swine wastewater [10, 11], dairy manure wastewater [12, 13], municipal wastewater [14] and industrial wastewater [15].

Previous studies mainly focused on the ability and efficiency of the aquatic macrophytes to remove and extract nitrogen (N) and phosphorous (P) components which were regarded as contaminants in the domestic wastewater [3, 4, 6, 11]. Although the phytoremediation system has the ability to remove N and P components effectively from wastewater, but the removal mechanisms of the other macronutrients such as SO_4^{2-} and K^+ are poorly understood. Thus, they overlook on these macronutrients as a portion of crucial contaminants in the domestic wastewater. Moreover, studies on removal and uptake of SO_4^{2-} and K^+ from domestic wastewater and their detail distribution and storage in macrophyte tissues are very limited.

In domestic wastewater, SO_4^{2-} and K^+ are regarded as abundant elements. The concentrations of SO_4^{2-} and K^+ are ranged between 20–500 mg/L [16] and 13–20 mg/L [17], respectively. SO_4^{2-} is often associated with heavy metals that affect disturbance of microbial process and nutrient imbalance in wastewater [18, 19]. Meanwhile, availability of K^+ affect the salinity and pH in wastewater [17]. These macronutrients enrichment if not well treated would cause adverse impact to the sources of water supply, biodiversity of aquatic life and contributes to water borne diseases [7, 9, 20, 21].

Therefore, this study focused on performance of aquatic macrophytes in removing SO_4^{2-} and K^+ from domestic wastewater. The accumulation and translocation of SO_4^{2-} and K^+ throughout macrophyte bodies (leaves, stems and roots) were also determined. The relationship between macrophyte species and their removal; and accumulation capacity were also determined and reported. The results of this study are significant for sustainable approach for domestic wastewater which would satisfy towards wholly aspect of macronutrient criteria. Hence phytoremediation process becomes alternative to compete with the other green technologies for national development.

2 Materials and Methods

This study was conducted in 3 stages: (a) Design and fabrication of the phyto-remediation system, (b) Phytoremediation process of SO_4^{2-} and K^+ , and (c) Analysis of SO_4^{2-} and K^+ in domestic wastewater and macrophyte tissues.

2.1 Design and Fabrication of the Phytoremediation System

The phytoremediation system was designed and fabricated in the Hydrology Laboratory of the Faculty of Civil Engineering in Universiti Teknologi MARA (UiTM), Shah Alam. Figure 1 shows the setup of phyto-system in the laboratory, whilst Fig. 2 is a schematic diagram of the phytoremediation system. Table 1 described details of the phyto-system as labeled in Fig. 2.

This system was designed as a batch system to integrate with the conventional wastewater treatment system when applied at site. The wastewater samples were collected from Mawar Residential Sewage Treatment Plant within the Universiti Teknologi MARA (UiTM), Shah Alam. The wastewater was sampled using grab sampling method [22]. Plastic containers for sampling were thoroughly rinsed with 10 % of nitric acid and distilled water to remove contaminants. After that the wastewater was fully filled up and tightly closed in order to prevent any aeration or oxidation process [22].

Aquatic macrophytes were chosen as they were low-priced and easily available locally. They consisted of the water hyacinth (*Eichhornia crassipes*) (WH), caladium (*Colocasia esculenta*) (CD) and water lettuce (*Pistia stratiotes*) (WL). They were collected from the section 8 Lake in Shah Alam. Each of the macrophytes was cleaned thoroughly with distilled water [23], softly trashing the soft tissues, before placing them in separated containers.

Fig. 1 Schematic diagram of the phytoremediation system

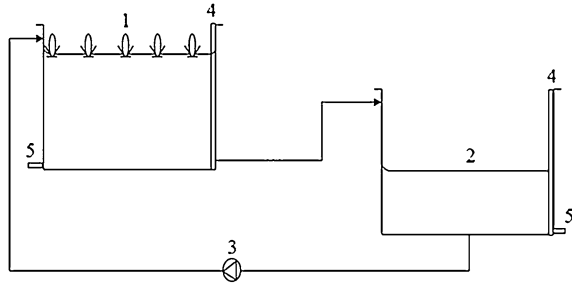
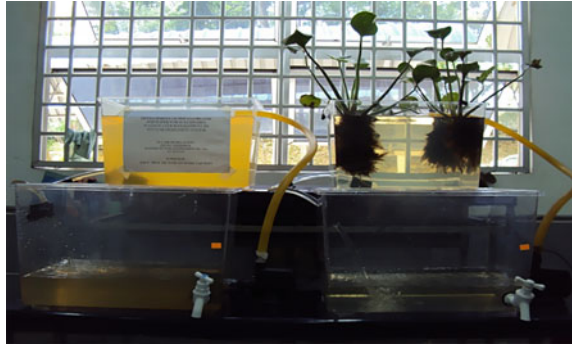


Fig. 2 Setup of phytoremediation system and control system in laboratory



2.2 Phytoremediation Process of SO_4^{2-} and K^+

The phytoremediation process was carried out immediately after the collection of wastewater samples. The wastewater samples were poured in the phyto and control systems and measured for initial level (0 day). The measurements of pH, turbidity, SO_4^{2-} and K^+ concentrations were carried out immediately within a day.

The macrophytes were introduced into the phytoremediation system. A similar system was also setup without any macrophytes to act as the control. The wastewater was initially filtered using a cotton sieve to trap suspended solids. Volume losses during the treatment due to water sampling and/or evaporation were replaced by adding distilled water [11]. The phytoremediation process was allowed to proceed until the macrophytes showed symptoms of death (survival capacity) or the nutrient concentrations in the wastewater became significantly consistent.

2.3 Analysis of SO_4^{2-} and K^+ on Domestic Wastewater and Macrophyte Tissues

The pH level of the wastewater was measured with a pH meter and the turbidity level with a turbidity meter using the procedures described by Hach Company [24]. The SO_4^{2-} and K^+ concentrations of both the phyto and control systems were

Table 1 Detail description of the phytoremediation system

No.	Apparatus/equipment	Description
1	Phytoremediation tank	Dimension: 0.66 × 0.44 × 0.35 m Material: polyvinyl chloride (PVC) Depth of wastewater: 0.22 m
2	Reservoir tank	Dimension: 0.66 × 0.44 × 0.35 m Material: polyvinyl chloride (PVC) Depth of wastewater: 0.09 m
3	Total volume of wastewater (both tanks) Water pump	24 L Type: super 300 multi-use pump Head of pressure: 2.2 m Flow of wastewater: 6 L/min
4	Level meter	–
5	Discharge valve	–

determined by using a Spectrophotometer DR5000 according to the Sulfaver 4 Method (8031) and Tetraphenylborate Method (8049) [24], respectively.

As for macrophyte tissues analysis, phytoremediated aquatic macrophytes were transferred into different containers, according to their species before being cleaned with saline water (2 M NaCl), aqueous ethylenediaminetetraacetic acid (EDTA) (2 g/L), tap water and deionized water [25], softly trashing with tissues. They were then sorted into leaf, stem and root parts. Each separated macrophyte bodies of roots, stems and leaves were dried at ambient temperature (27 °C) before oven dried at 80 °C for 48 h. The dried tissues were weighed and grounded to powder form [11]. The dried tissues (1.0 g dry weight) were digested using Milestone Ethos Plus according to acid sulfuric digestion method with 8 ml of HNO₃ 65 % and 2 ml of H₂O₂ 30 % via published procedure [26]. The samples after digestion were cooled to room temperature. Next, they were filtered through the Whatman No. 1 filter paper and then 0.45 μm membrane filters in order to reject the suspended substances. Later, they were analyzed for SO₄²⁻ and K⁺ using Inductively Coupled Plasma-Optical Emission Spectrometry (ICP-OES) (Perkin Elmer Optima 7300 DV).

3 Data Analysis

Removal rate (%) of SO₄²⁻ and K⁺ were determined using the following formula:

$$R (\%) = (C_0 - C_t) / C_0 \times 100 \% \quad (1)$$

where C₀ is the initial concentration of SO₄²⁻ and K⁺ (mg/l) and C_t is the concentration of SO₄²⁻ and K⁺ (mg/l) at time t (days). The data were analyzed for mean, standard deviation (n = 3) and error bar with 5 % of value using the statistical package within Microsoft® Excel Version 2010.

4 Results and Discussion

Table 2 presents initial and final concentrations and removal rate of pH, turbidity, SO_4^{2-} and K^+ for phyto and control systems.

4.1 Performance of Aquatic Macrophytes in Changing pH and Turbidity Levels from Domestic Wastewater

The pH level in WH system was at alkaline range for 1-day to 4-day (highest 8.44) and change to acidic state after 5-day (lowest 5.83) until end of treatment. The pH level in CD system was at alkaline state started from 1-day to 15-day (highest 7.91) and the pH level was reduce towards acidic state for 16-day to 24-day (lowest 6.31) and remain alkaline state until end of treatment. The pH level was kept within an alkaline range (highest 7.78) in water lettuce system. The pH level in control system differs within a day, where at alkaline state from 1-day to 4-day, reduce to acidic state from 5-day to 15-day and back to alkaline state from 16-day to 30-day (Fig. 3).

The turbidity of the phyto-systems in the WH, CD and WL reduced from 43.97 NTU to 0.86 NTU, 57.50 NTU to 0.64 NTU and 58.40 NTU to 0.83 NTU, respectively compared to control systems which reduced from the level of 57.93 NTU to 1.31 NTU (Table 2). While the removal rate of the phyto- systems in the WH, CD and WL were 98.04, 98.89 and 98.58 %, respectively compared to removal rate of the control system was 97.74 % (Table 2).

The changes of pH level in phyto-systems were moved toward stability or consistency, compared to control system. This is due to the utilization of the carbonate compounds during the algal photosynthesis [6], where macrophytes enhanced this process via root system. The pH values were decrease to acidic state for both WH (at the end of treatment) and CD systems (day-16 to day-24) could be explained by the oxidation of wastewater organic matters, the nitrification of N containing compounds [27] and CO_2 is dissolved from the atmosphere and produced by decomposition of organic matter. It is readily soluble in water, combining with the water to form carbonic matters [28].

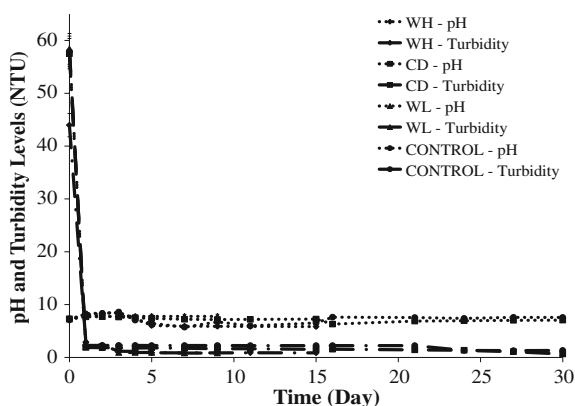
Turbidity levels in the phyto and control systems were significantly declined at beginning of treatment (1-day) where CD system was able to reduce more turbidity level higher than the other systems. The results also prove that the sole system itself able to reduce the turbidity level with evidence of the reduction in the control system. Besides, the turbidity level was more enhanced with the presence of macrophytes in the phyto-system. The reason behind this fact is that the roots of the macrophytes were proficient to trap particulate matters during the phyto-treatment [11]. It also has been reported that abundant root system in the phyto-treatment could secretes large amount of root exudates. They are polymeric in nature and assists in the coagulation and sedimentation processes of the suspended particles by destabilizing the colloidal suspensions [29].

Table 2 Initial and final concentrations and removal rate of pH, turbidity, SO_4^{2-} and K

Parameters	Phytoremediation systems			Control systems	
	WH	CD	WL		
Initial concentration	pH	6.99 ± 0.00	7.31 ± 0.08	7.24 ± 0.00	7.31 ± 0.08
	Turbidity	43.97 ± 0.15	57.50 ± 3.27	58.40 ± 4.11	57.93 ± 3.29
	SO_4^{2-}	15.67 ± 2.08	15.67 ± 0.58	8.00 ± 0.00	14.00 ± 3.61
	K^+	8.23 ± 0.06	6.03 ± 0.06	6.23 ± 0.06	6.03 ± 0.06
Final concentration	pH	5.83 ± 0.17	7.05 ± 0.06	7.77 ± 0.04	7.57 ± 0.05
	Turbidity	0.86 ± 0.57	0.64 ± 0.08	0.83 ± 0.05	1.31 ± 0.04
	SO_4^{2-}	12.67 ± 0.58	6.00 ± 0.00	5.00 ± 0.00	13.00 ± 1.00
	K^+	37.10 ± 0.35	0.60 ± 0.02	14.45 ± 0.00	16.50 ± 0.04
Removal rate (%)	Turbidity	98.04	98.89	98.58	97.74
	SO_4^{2-}	19.15	61.71	37.50	7.14
	K^+	-77.82	90.05	-56.89	-63.46

Mean ± standard deviation (n = 3)

Fig. 3 Changes of pH and turbidity levels during phytoremediation process

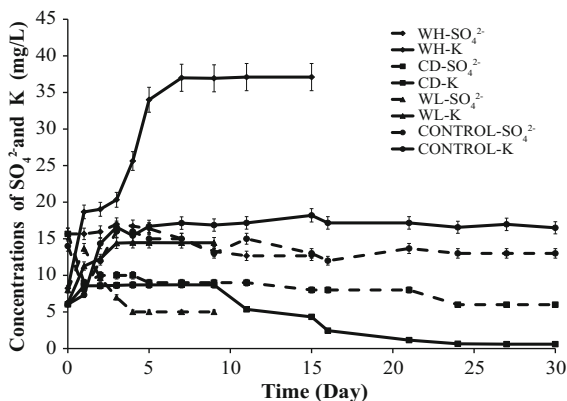


4.2 Performance of Aquatic Macrophytes in Removing SO_4^{2-} and K from Domestic Wastewater

After the period of treatment, WH, CD and WL effectively remove 61.71, 37.50 and 19.15 % of SO_4^{2-} in the phyto-systems, respectively, whilst control system removes 7.14 % at the end of treatment period (Table 2). Besides, WH and WL in the phyto-systems and control system showed increments of 77.82, 56.89 and 63.46 % of K^+ , respectively. Somehow, in CD system, the level of K reduced to 90.05 % at the end of phyto-treatment (Table 2).

Although macrophytes in the phyto-systems had a limited effect on SO_4^{2-} , but they could perform as stabilizer for transformation of SO_4^{2-} in wastewater process. This was verified by the trend of SO_4^{2-} in phyto-systems were more stable than the control system, which values of SO_4^{2-} in the control system was fluctuate

Fig. 4 Changes of SO_4^{2-} and K^+ concentrations during phytoremediation process



within a day (Fig. 4). The fate of S in the wastewater is mainly governed by the redox state dynamic in the root system, with the availability of organic carbon and O_2 [30, 31] and sulfate-reducing bacteria [32].

Under aerobic condition in the phyto-systems and control system, the losses of SO_4^{2-} caused by oxidation of sulfide (S^{2-}) to SO_4^{2-} and dissociation reactions of S^{2-} to hydrogen sulfide (H_2S) which is largely volatile and emitted to atmosphere [33]. Increase of pH (to alkaline state) in the initial stage of the experiments (Fig. 3) indicated that H_2S emitted to the atmosphere [34]. Losses of SO_4^{2-} was also due to heavy metal precipitation to form insoluble metal sulphates (such as FeSO_4 , ZnSO_4) and mineral precipitation to form mineral sulphates (such as CaSO_4), when SO_4^{2-} was more favorable than S^{2-} in wastewater [33]. Furthermore, with the presence of the macrophytes could enhance the sulphates precipitation process.

In addition, phyto-systems demonstrated higher reduction of SO_4^{2-} than control system since macrophytes provide a suitable roots zone for biological assimilation into macrophyte tissues or microorganism biomass as organic S [33]. They also released O_2 via root zone for direct re-oxidation of S^{2-} to SO_4^{2-} [32] and stimulate microorganism growth and activity [35]. The uptake of SO_4^{2-} also is more favored compare to S^{2-} since it is highly toxic to macrophytes and microorganisms. S^{2-} is also competitor for O_2 consumption [33, 36], hence it mainly present in anaerobic condition.

Nevertheless, there are no consistencies of K^+ concentration in the both phyto and control systems. However, CD system shows positive trends of K^+ removal (Fig. 4). It have been stated that the K^+ concentration rose as natural wetland communities tended to export K^+ [3, 37]. Somehow, they did not mention the factors of K^+ rises. Thus, in the present study, K^+ level rising most probably resulted from degradation of macrophytes tissues during phyto-treatment process. This was in line when the macrophytes were reached at aging phase (mostly degraded).

The availability of K^+ in the wastewater also was affected by salinity and pH in wastewater [17]. This is because of the K^+ in the wastewater is related to hardness

by proportion of CaCO_3 . However, the present results revealed that there were no significant relationship between pH and K^+ since pH levels for both phyto and control systems moved towards stability.

4.3 Accumulation and Translocation of S and K Throughout Macrophyte Bodies

At the end of the experiment, CD exhibited higher accumulation capacity for S and K of 157.03 and 1,937.69 mg/L, respectively, compared to S and K in WH of 200.93 and 1,530.95 mg/L; and WL of 75.76 and 83.67 mg/L, respectively (Fig. 5).

Although Wu et al. [32] reported that S is essential for macrophytes growth which supposed to be equal or larger than P, somehow in this study the contents of K in the all of examined macrophytes tissues were higher than the S (Fig. 5). This heading towards that the K was not limiting growth of the macrophytes compared to S.

As S^{2-} may lead to phytotoxic effects, macrophytes in the phyto-system more favor SO_4^{2-} . Hence the uptake of S was mainly by SO_4^{2-} . Thus, S was detected in the macrophyte tissues in this study leading to verify the above statement. Somehow, some of macrophytes show deterioration effect, such as WH and WL, as they may uptake of metal sulphates (such as FeSO_4 , ZnSO_4). These metal sulphates especially FeSO_4 have toxic effects on the macrophytes since Fe^{2+} is also phytotoxin [33]. As a result, it reflected that macrophytes capable to prevent phytotoxin by accumulated most of S in below-ground mass before distribute to above-ground mass (Fig. 5).

It has been reported that K^+ was important macronutrients for macrophyte growth, especially for biomass yield and foliar area [14], thus K^+ was translocated higher in above-ground mass compared to below-ground mass (Fig. 5). This case was contradict with the statement that macrophytes has a problems in uptake base cations such as K^+ when they are normally occur in rich anion environment (e.g. NO_3^-) as their main macronutrient source [38]. Besides, K^+ has excellent water solubility thereby it is easy to mobile throughout macrophytes tissues but very difficult to precipitate.

4.4 Relationship Between Macrophytes Species and Their Performance Against Removal and Accumulation of S and K

Relationship between removal and accumulation rates for S and K^+ of WH and WL were inversely proportional. Both of WH and WL performed well in removing SO_4^{2-} and accumulating K^+ . But then, negative rate were noticed for removal of

Fig. 5 Distribution of S and K throughout macrophytes bodies

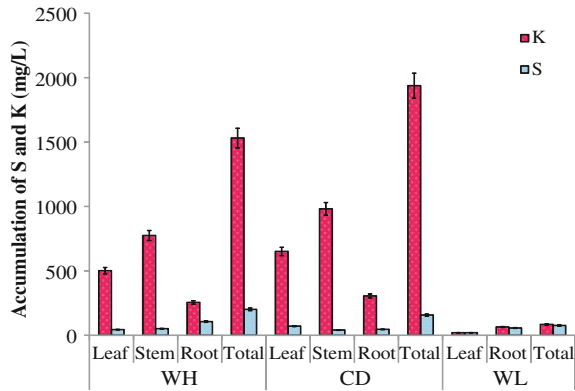
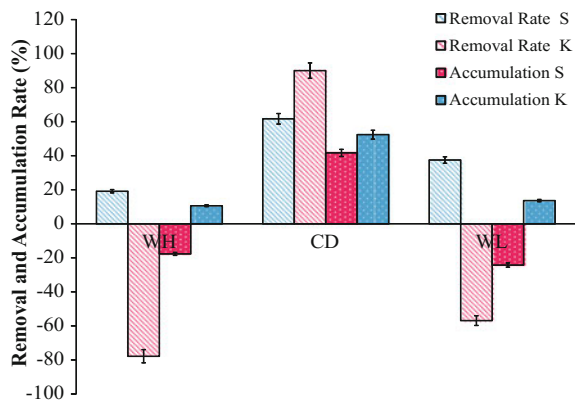


Fig. 6 Performances of macrophytes based on removal and accumulation rate of S and K



K^+ and accumulation of S. Conversely, CD performed better in removing and accumulating of both S and K^+ (Fig. 6). Thus, make CD was the best removal and accumulator species of S and K^+ rather than others species. Performance of macrophytes on SO_4^{2-} and K^+ removal was also in relation with their physical and biomass characteristics.

It has been stated that macrophytes with higher potential capacity for biomass production could perform better macronutrients removal [39]. It appears that S was difficult to mobile throughout macrophyte bodies compared with K^+ . On the other hand, SO_4^{2-} was constantly removed in domestic wastewater by phyto-systems.

5 Conclusions

In conclusion, the performances of the three aquatic macrophytes in removing and accumulating the SO_4^{2-} and K^+ from domestic wastewater using phytoremediation system were evaluated. CD displayed more capacity to reduce and accumulate SO_4^{2-} and K^+ compared to the other macrophytes. Thus, the results have indicated

that the selection of aquatic macrophytes is a crucial stage in determining the performance in phytoremediation system. Subsequently, this proves that different macrophyte species have variation abilities for macronutrients removal and uptake.

The authors also recommend that the relationship between macrophyte survival and growth in the phytoremediation system need to be established. This is an important measurement criterion since the growth of plants influence the removal and uptake mechanisms of the plants.

Acknowledgments This research work was supported by a grant from the Research Management Institute (RMI) [No.: 600-RMI/ST/DANA 5/3/Dst (284/2009)] and [No.: 600-RMI/DANA 5/3/RIF (691/2012)], Universiti Teknologi Mara (UiTM). The authors would like to acknowledge the valuable technical support given by Noorul Hilmi Md Salleh and Muhamad Hazli Shariei. They also thank UiTM for its laboratory facilities.

References

1. R.M. Tajuddin, B. Abdullah, A.M. Baki, N. Zaharudin, The potential of aquatic plants as phytoremediator for treatment of industrial wastewater. *Malays. Water Resour.* **21**, 352–353 (2007)
2. A.R. Raju, C.T. Anitha, P.D. Sidhimol, K.J. Rosna, Phytoremediation of domestic wastewater by using a free floating aquatic angiosperm, *Lemna minor*. *Nat. Environ. Pollut. Technol.* **9**, 83–88 (2010)
3. E.A. Kohler, V.L. Poole, Z.J. Reicher, R.F. Turco, Nutrient, metal, and pesticide removal during storm and nonstorm events by a constructed wetland on an urban golf course. *Ecol. Eng.* **23**, 285–298 (2004)
4. S. Zul Hilmi, M.T. Ramlah, K. Dzaraini, and A.R. Norazah, Phytoremediation of nutrient contaminants from golf courses surface water, in *Proceeding Universiti Malaysia Terengganu International Annual Symposium (UMTAS)*, Kuala Terengganu, Malaysia, 2011
5. H. Brix, Do macrophytes play a role in constructed treatment wetlands? *Water Sci. Technol.* **35**(5), 11–17 (1997)
6. H.Q. Chang, X.E. Yang, Y.Y. Fang, P.M. Pu, Z.K. Li, Z. Rengel, In-situ nitrogen removal from the eutrophic water by microbial-plant integrated system. *J. Zhejiang Univ. Sci. B* **7**(7), 521–531 (2006)
7. C.H. Sim, Y. Mohd Kamil, B. Shutes, S.C. Ho, M. Mashhor, Nutrient removal in a pilot and full scale constructed wetland, Putrajaya City, Malaysia. *J. Environ. Manage.* **88**, 307–317 (2008)
8. K. Chunkao, C. Nimpee, K. Duangmal, The King's initiatives using water hyacinth to remove heavy metals and plant nutrients from wastewater through Bueng Makkasan in Bangkok, Thailand. *Ecol. Eng.* **39**, 40–52 (2012)
9. P.M. Ayyasamy, S. Rajakumar, M. Sathishkumar, K. Swaminathan, K. Shanti, P. Lakshmanaperumalsamy, S. Lee, Nitrate removal from synthetic medium and groundwater with aquatic macrophytes. *Desalination* **242**(1), 286–296 (2009)
10. J. Cheng, B.A. Bergmann, J.J. Classen, A.M. Stomp, J.W. Howard, Nutrient recovery from swine lagoon water by *Spirodela punctata*. *Bioresour. Technol.* **81**(1), 81–85 (2002)
11. Q. Xian, L. Hu, H. Chen, Z. Chang, H. Zou, Removal of nutrients and veterinary antibiotic from swine wastewater by a constructed macrophyte floating bed system. *J. Environ. Manage.* **91**, 2657–2661 (2010)

12. T.A. DeBusk, J.E. Peterson, K.R. Reddy, Use of aquatic and terrestrial plants for removing phosphorus from dairy wastewaters. *Bioresour. Technol.* **5**, 371–390 (1995)
13. R.D. Sooknah, A.C. Wilkie, Nutrient removal by floating aquatic macrophytes cultured in anaerobically digested flushed dairy manure wastewater. *Ecol. Eng.* **22**, 27–42 (2004)
14. M.A.O. Bustamante, M.V. Mier, J.A.E. Estrada, C.D. Domínguez, Nitrogen and potassium variation on contaminant removal for a vertical subsurface flow lab scale constructed wetland. *Bioresour. Technol.* **102**, 7745–7754 (2011)
15. F.W. Ntengwe, An overview of industrial wastewater treatment and analysis as means of preventing pollution of surface and underground water bodies-the case of Nkana Mine in Zambia. *Phys. Chem. Earth* **30**(11–16), 726–734 (2005)
16. A. Wiessner, P. Kuschik, M. Jechorek, H. Seidel, M. Kästner, Sulphur transformation and deposition in the rhizosphere of *Juncus effusus* in a laboratory-scale constructed wetland. *Environ. Pollut.* **155**, 125–131 (2007)
17. M. Arienzo, E.W. Christen, W. Quayle, A. Kumar, A review of fate of potassium in the soil-plant system after land application of wastewater. *J. Hazard. Mater.* **164**, 415–422 (2009)
18. J. Derome, T. Nieminen, Metal and macronutrient fluxes in heavy-metal polluted scots pine ecosystem in SW Finland. *Environ. Pollut.* **117**, 287–293 (1998)
19. E. Ruth-Balaganskaya, O. Kudrjavitseva, Sulphur mitigation in the soil-plant system contaminated by deposits from nickel industry: a field manipulation. *Environ. Pollut.* **117**, 287–293 (2002)
20. V.H. Smith, Eutrophication of freshwater and coastal marine ecosystems: a global problem. *Environ. Sci. Pollut. Res.* **10**(2), 126–139 (2003)
21. M. Munn, J. Frey, A. Tesoriero, The influence of nutrients and physical habitat in regulating algal biomass in agricultural streams. *Environ. Manage.* **45**(3), 603–615 (2010)
22. United State Environmental Protection Agency (USEPA), *Operating Procedure: Wastewater Sampling, Science and Ecosystem* (Support Division, Athens, 2013)
23. V.K. Mishra, A.R. Upadhyay, V. Pathak, B.D. Tripathi, Phytoremediation of mercury and arsenic from tropical opencast coalmine effluent through naturally occurring aquatic macrophytes. *Water Air Soil Pollut.* **192**, 303–314 (2008)
24. Hach Company, *Standard Manual Procedure* (Hach Company World Headquarters, USA, 2007)
25. S. Gajalakshmi, E.V. Ramasamy, S.A. Abbasi, High-rate composting-vermicomposting of water hyacinth (*Eichhornia crassipes*, Mart. Solms). *Bioresour. Technol.* **83**, 235–239 (2002)
26. Milestone, Application Note for Closed Vessel Microwave Digestion, Dried Plant Tissue, Milestone Inc.: United State, 2000
27. C. Münch, P. Kuschik, I. Röske, Root stimulated nitrogen removal—does for limited areas or all of a constructed wetland?, in *Proceedings of ninth International Conference on Wetland Systems for Water Pollution Control*, (Avignon, 2004), p. 395–402
28. C. Neal, M. Harrow, R.J. Williams, Dissolved carbon dioxide and oxygen in the river thames: spring-summer 1997. *Sci. Total Environ.* **210**(211), 205–217 (1998)
29. P. Chiranjeevi, R. Chandra, S.V. Mohan, Ecologically engineered submerged and emergent macrophyte based system: an integrated eco-electrogenic design for harnessing power with simultaneous wastewater treatment. *Ecol. Eng.* **51**, 181–190 (2013)
30. P. Sturman, O. Stein, J. Vymazal, L. Kröpfelova, Sulphur cycling in constructed wetlands, in *Wastewater Treatment, Plant Dynamics and Management in Constructed and Natural Wetlands*, ed. by J. Vymazal (Springer Science + Business Media B.V, Dordrecht, 2008), pp. 329–344
31. A. Wiessner, K.Z. Rahman, P. Kuschik, M. Kastner, M. Jechorek, Dynamics of sulphur compounds in horizontal sub-surface flow laboratory-scale constructed wetlands treating artificial sewage. *Water Resour.* **44**, 6175–6185 (2010)
32. S. Wu, C. Jeschke, R. Dong, H. Paschke, P. Kuschik, K. Knöller, Sulfur transformations in pilot-scale constructed wetland treating high sulfate-containing contaminated groundwater: a stable isotope assessment. *Water Res.* **45**, 6688–6698 (2011)

33. S. Wu, P. Kuschik, A. Wiessner, J. Müller, R.A.B. Saad, R. Dong, Sulphur transformations in constructed wetlands for wastewater treatment: a review. *Ecol. Eng.* **52**, 278–289 (2013)
34. S.D. Machemer, J.S. Reynolds, L.S. Laudon, T.R. Wildeman, Balance of S in a constructed wetland built to treat acid mine drainage, Idaho Springs, Colorado, USA. *Appl. Geochem.* **8**, 587–603 (1993)
35. S. Wu, Z. Chen, M. Braeckevelt, E.M. Seeger, R. Dong, M. Kästner, H. Paschke, A. Hahn, G. Kayser, P. Kuschik, Dynamics of Fe(II), sulphur and phosphate in pilot-scale constructed wetlands treating a sulphate-rich chlorinated hydrocarbon contaminated groundwater. *Water Res.* **46**, 1923–1932 (2012)
36. O. Pedersen, T. Binzer, J. Borum, Sulphide intrusion in eelgrass (*Zostera marina* L.). *Plant, Cell Environ.* **27**, 595–602 (2004)
37. J.H. Peverly, Stream transport of nutrients through a wetland. *J. Environ. Qual.* **11**, 38–42 (1982)
38. J.G.M. Roelofs, Impact of acidification and eutrophication on macrophyte communities in soft water in the Netherlands. *Aquat. Bot.* **17**, 139–155 (1983)
39. Z.C. Zheng, T.X. Li, F.F. Zeng, X.Z. Zhang, H.Y. Yu, Y.D. Wang, T. Liu, Accumulation characteristics and removal of nitrogen and phosphorous from livestock wastewater by *Polygonum hydropiper*. *Agric. Water Manag.* **117**, 19–25 (2013)

Greywater Reclamation Using Recycled Vertical Subsurface-Flow Constructed Wetland (RVFCW) for Non Potable Usage

Azianabiha A. Halip @ Khalid, Siti Nurulhuda Mohd Imran
and Shahrul Azwan Shakrani

Abstract Nowadays, the usage of a greywater as additional water resources options is increasing due to decline of water quantity available worldwide. The growing of recycled greywater for non potable purpose have been widely used around the world not only by water-scarce and dry regions countries such as in the Middle East and North Africa but also intensively applied by densely populated European countries such as England and Germany. Typically, about 100–200 L of greywater are being produced per person each day which represent the largest portion of domestic wastewater. Due to this soaring volume of greywater generated, it provides high potential for water conservation in household source. Nevertheless, greywater is always contaminated and required pre-treatment. The aim of this study was to study the potential and removal pollutant of RVFCW in greywater treatment. Four samples of greywater from two different sources were treated using RVFCW and the water quality parameters were tested after 4, 24 and 48 h. The results show that RVFCW has a potential in greywater treatment and able to remove more than 80 % of water parameters such as TSS, COD and turbidity. Thus, this study concluded that the RVFCW is capable as alternative treatment system for non-potable greywater reuse.

Keywords Greywater · Vertical flow constructed wetland · Wastewater reuse · Wastewater recycling · Alternative water source

A. A. Halip @ Khalid (✉) · S. N. M. Imran · S. A. Shakrani
Faculty of Civil Engineering, Universiti Teknologi Mara (UiTM), Shah Alam, Selangor,
Malaysia
e-mail: azianabiha@gmail.com

1 Introduction

In Malaysia, the water shortage and water scarcity is not a major the problem. With high number of rainfall distribution, the quantity of water resources available is enough for the long term period usage and the water crisis is rarely occurs. However, uncontrolled water usage can leads to wastage and could affect the sustainability of water supply in the future. In order to ensure that the water is used efficiently, the recycling of greywater for non potable purpose is one of the options. Greywater is usually defined as all of the wastewater produced in a household except toilets waste which known as a blackwater [1]. Yet, the raw greywater is often contaminated and possible presence of harmful microorganism. Moreover, without careful handling it will cause water logging, smell, and released of chemicals and anthropogenic elements [2, 3]. Pollutants such as metals that originated from rusty pipes and other chemicals content in household products such as detergents and preservatives can cause environmental harm when accumulated in the soil thus affecting plants and other microorganisms in the soil. It might also pose various health problem occurred primarily through direct contact with human body. In most countries, regulations or specific guidelines for greywater reuse are not available or are insufficient, hence used without any significant pre-treatment and a practice mistakenly considered safe [4]. The aim of this study were to assess the potential of RVFCW in greywater treatment based on removal capacity of selected pollutants.

2 Materials and Methods

2.1 Materials

The RVFCW method proposed is a modification technique that was described in [4]. Figure 1 presents schematic layout of RVFCW. The RVFCW consists of upper tank (wetland plant and media) ($76 \times 18 \times 45$ cm) and lower tank (treated sample) ($76 \times 18 \times 45$ cm). In this study, the media used consists of a 10 cm layer of sand, followed by a 10 cm layer of gravel with 5–10 mm diameter and a 10 cm layer of limestone pebbles with 5–10 mm diameter at the surface. For the purpose of this greywater treatment, a species of wetland plant called *Eichhornia Crassipes* (water hyacinth) has been chosen due to its high nutrient assimilative capacity and ability to filter suspended materials.

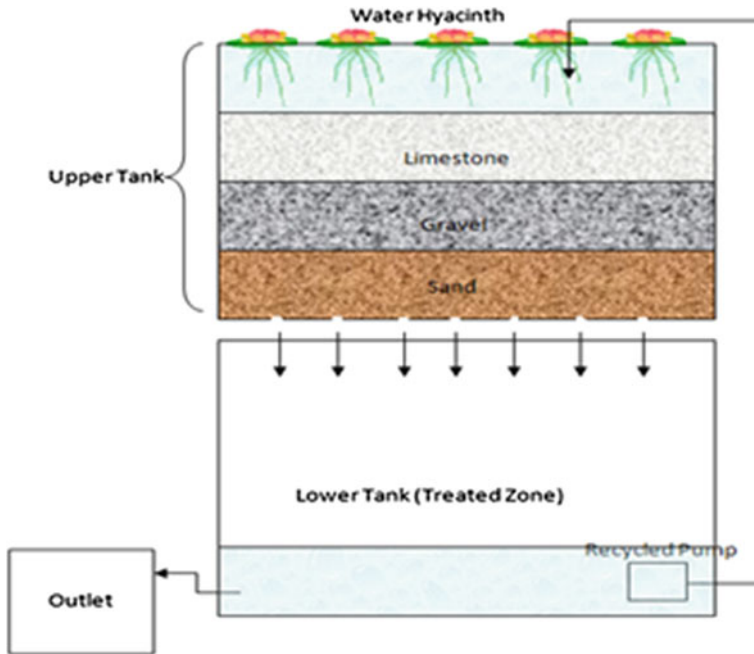


Fig. 1 Schematic diagram for RVFCW layout

2.2 Methods

The RVFCW system was constructed using two plastic aquarium tank with an upper tank was placed over a lower container. Holes were punctured at even intervals in the bottom of the upper tank. This was to allow water from the top to flow into the bottom tank. There is a plumbing pipes design to support an upper tank together with bottom tank.

When the greywater was introduced to the system, the greywater was percolated through the upper layer which consists of wetland plant; *E. crassipes* (water hyacinth) and three types of media. Then, it infiltrated from bottom layer of upper tank through the holes to the lower tank which acts as treated tank. The water pump was introduced to recycle the water back to upper tank through the perforated pipe. The process was continued until the time required for study the treated samples.

At the beginning of the study, the pore volume of the filter section and treated water reservoir was emptied and 20 L of raw greywater was introduced. For this study, raw greywater samples were collected from effluent in two different locations in UiTM Shah Alam. There were at Dataran Cendekia Cafeteria sump and Teratai College sump. A subsample of raw water was collected for analysis (time zero) of water quality parameters. Then, the samples of treated greywater were taken immediately after passed bed on period of 4, 24 and 48 h. It then was

Table 1 Removal percentage for different water parameters using RVFCW system

Parameters	Average removal (%)
pH	±10
Conductivity	0
TSS	100
Turbidity	93–99
Color	86–96
Nitrite	0
Phosphorus	0–47
Iron	87–98
COD	84–98
BOD	0–50

analysed for water quality parameters namely pH, conductivity, total suspended solid (TSS), turbidity, colour, nitrite, phosphorus, iron, chemical oxygen demand (COD) and biochemical oxygen demand (COD).

3 Result

In this study the concentration of the pollutants for each water sample were recorded during different time interval and presented in a table and figure for analysis. The summary of the overall performance in the form of average removal percentage is as stated in Table 1.

At the end of the experiment time, the RVFCW were effective in removing virtually all the TSS and about 99 % of turbidity. For colour, the removal was about 96 %. For iron and COD, the removal was about 98 % each. However, only partial of phosphorus and BOD were removed (47 and 50 % respectively). No nitrite removal was found in RVFCW treatment. For pH, the result indicates that it slightly approaches to neutral condition while conductivity always increases within time frame.

Table 2 shows in details the greywater parameter's value over the course of 48 h treatment.

For clearer comparison, the concentration of individual parameter is graphically generated as in Fig. 2.

For pH and conductivity, the chart shows the concentration recorded during the time interval instead of the removal percentage as per other parameter. Based on data in Fig. 2, each sample developed a same decreasing pattern except for nitrite, phosphorus and BOD concentration.

Table 2 Greywater quality using RVFCW within zero time until 48 h

Parameter	Sample 1			Sample 2			Sample 3			Sample 4						
	Raw	4 h	24 h	48 h	Raw	4 h	24 h	48 h	Raw	4 h	24 h	48 h				
pH	5.11	7.29	7.34	7.48	5.87	6.78	7.14	7.40	7.82	7.17	7.25	6.99	8.17	7.79	7.66	7.04
Conductivity (µs/cm)	233	391	400	430	126	247	263	265	272	321	340	351	267	275	314	303
TSS (mg/L)	0.10	0.06	0.04	0	0.12	0.08	0.04	0	0.06	0.04	0.02	0	0.04	0.03	0.02	0
Turbidity (NTU)	50	18	4.47	1.47	46.5	15.5	0.92	0.69	17.2	8.79	2.25	1.21	26.2	11.8	1.08	0.93
Colour (PtCo)	435	170	93	60	428	155	17	16	263	139	29	26	282	155	32	23
Nitrite (mg/L)	0.029	0.075	0.014	0.001	0.012	0.006	0.050	0.022	0.049	0.093	0.259	0.400	0.024	0.085	0.250	0.450
Phosphorus (mg/L)	0.34	0.29	0.09	0.18	0.44	0.25	1.76	0.30	3.00	8.50	23.00	5.00	1.53	3.89	11.5	3.51
Iron (mg/L)	0.82	0.73	0.06	0.05	0.15	0.11	0.03	0.02	1.52	0.79	0.20	0.16	3.84	1.43	0.10	0.06
COD (mg/L)	230	140	60	38	200	120	46	32	118	54	33	18	96	41	13	2
BOD (mg/L)	36	162	108	96	144	114	36	96	30	12	6	24	12	54	30	6

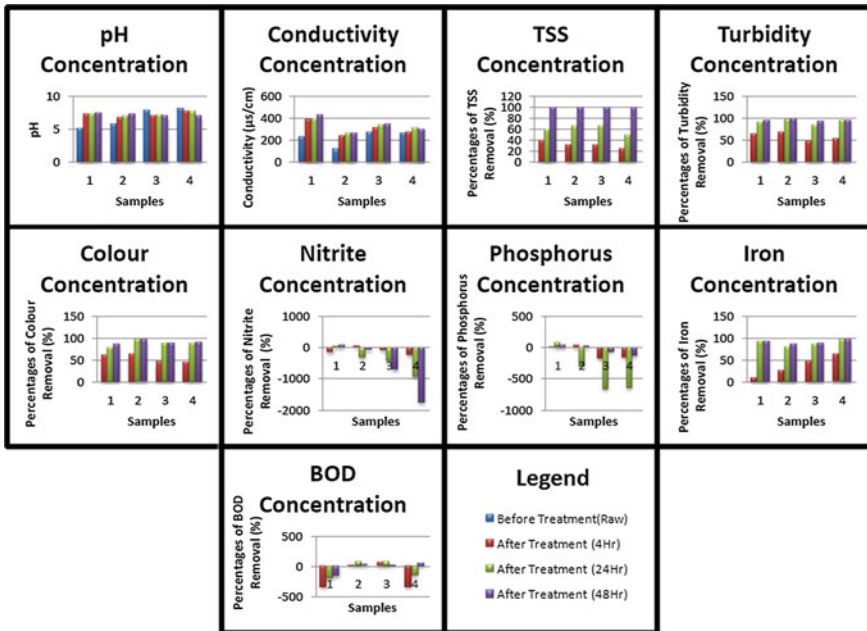


Fig. 2 Comparison of pollutants removal in different time scale

4 Discussion

After all the data has been obtained, analysis on the result was conducted in order to assess the effectiveness of RVFCW in treating greywater. As stated in previous chapter, the result has been encouraging by reflecting on the percentage of removal achieved at the end of treatment process. Details analysis of each parameter is as follows.

4.1 pH

The result shown that the pH value slightly approached to neutral. The reason was due to the uses of the limestone media in RVFCW. The previous research on limestone application in treatment of wastewater is founded effective in neutralize the pH. Koenig and Liu [5] stated that limestone supplies effective buffering capacity for pH control if the alkalinity in the influent wastewater is insufficient for complete autotrophic denitrification. Alkalinity supplied through limestone dissolution is a function of pH, which in turn depends on the initial alkalinity of the wastewater and progress of denitrification. The specific limestone dissolution rate, in gram limestone dissolved per unit gram of limestone is inversely proportional to

pH for pH values lower than 7.1. Research by Aziz et al. [6] revealed that limestone able to increase the pH from the input value of pH 7. Moreover, the dissolution of limestone by acidic waters releases alkalinity, which in turn increases pH. As a result, the used of limestone media has major impact in neutralize pH of greywater.

4.2 Conductivity

In term conductivity, the result indicates the increment within hours. All samples have shown an augmentation or expansion in term of conductivity. From review of related literature it can be concluded that the higher value of conductivity was due to the higher ionic value. Yalcuk and Ugurlu [7] reported that the effluent conductivity values were higher than the influence conductivity values in all systems of wetland. The high value obtained due to high ion concentration in the effluent. Soltan and Rashed [8] further stated that the different media solutions exhibited increasing conductivity with increasing metal concentrations and duration of exposure to plants.

4.3 TSS and Turbidity

For TSS, the 100 % of removal was achieved. The reason was the amount of TSS was quite low in greywater sources compared if the sources taken from blackwater. Based on the finding from literature review, the removal of TSS was due to the sedimentation and filtration process in RVFCW. Stowell et al. [9] reported that the sedimentation process in wetland occurs due to gravitational settling of solids in wetland settings while filtration was occurs due to particulates filtered mechanically as water passes through substrate, and root masses. In case of sedimentation and filtration in RVFCW, the greywater passing through water hyacinth plant to filtration media which consists of limestone, gravel and sand due to gravitational settlings. Most of suspended solids were filtrated out and settled beyond the substrate of constructed wetlands. As a proved to the result of Stowell et al. [9], report by Yalcuk and Ugurlu as in [7] stated that more than 90 % removal of BOD₅, COD and TSS can be achieved in vertical surface flow (VSF) system, which make the result has become more obvious.

As TSS, similar trend was observed in turbidity removal. Reduction of turbidity as depicted in Fig. 2 due to sedimentation and filtration as well as removal of TSS. On the other hand, Gopal [10] reported that the water hyacinth were used for floc removal or settling in water treatment. The result is a significant decrease in turbidity due to the removal of flocs and also slight reduction in organic matter in the water. Sklarz et al. [11] further reported that 80 % of the turbidity and 75 % of

the COD were removed within the first hour. As a result, the combination of RVFCW and water hyacinth were effective in terms of turbidity removal.

4.4 Color

As TSS and turbidity were decreased, the value of colour was as well decreased. Normally, the colour of wastewater increased with higher turbidity due to high amount suspended solid. This caused the water becomes more turbid and cloudy. The sedimentation and filtration process that occurred was able to remove TSS and turbidity effectively which directly impact on colour removal in RVFCW. As a result, the colour was removed nearly to 98 % of removal. So, it can be further concluded that the RVFCW was effective in terms of colour removal.

4.5 Nitrite and Phosphorus Removal

In terms of nitrite, very minimal and neglectable removal value was obtained in sample 1 and for other samples the result shows an increment within hours instead. The increment of nitrite was proved by Kantawanichkul et al. as in [12]. In vertical flow systems process, greater oxygen transport ability than the horizontal sub-surface flow beds and they are more effective for the mineralization of biodegradable organic matter and for nitrification through the activity of ammonia-oxidizing bacteria. Moreover, in vertical flow bed, a passive air pump (removing oxygen depleted air and introducing fresh air) supplies the oxygen required for the nitrification process. Green et al. as in [13] further discuss about nitrification process. In the study it was stated that, in nitrification process, ammonia is oxidized mainly to nitrate and nitrite. As long as the value of nitrate is high, the same thing goes to the value of nitrite. The nitrification process may add the value of nitrate and nitrite. This finding was supported by Seidel as in [14] through a statement that the higher nitrification efficiency was noted in vertical flow beds based on the Seidel model. So, as long as nitrification process occurs, the value of nitrite would increase.

Basically, as stated by Zurita et al. as in [15], the vertical flow constructed wetland (VFCW) were more effective for phosphorus removal. But the result indicates an increment of total phosphorus available in greywater. The reason was supported by Brix and Arias as in [16] through a statement of the phosphorus removal in vertical flow constructed wetland is very limited, and it is not possible to obtain a sand bed medium that has a sufficient high capacity to bind phosphorus for a prolonged period. The report further stated that the removal of phosphorus in the vertical flow constructed wetland system will be fairly low, typically 20–30 %. In the present study, the result showed plants also affected phosphorus

removal. The reason was phosphorus removal in wetlands may take place due to plant uptake [12].

4.6 Iron

For iron, the result showed that after 24 h treatment, the removal was nearer to 98 % of removal. The high iron removal was founded due to water hyacinth uptake the iron. Water hyacinth were effective in removing excess nutrient, heavy metals, toxic metal, minerals and organic chemicals, and herbicides from polluted water. The report further stated that the deprotonation reaction of water hyacinth during the uptake of metal ions from aqueous solution, as shown by decrease in pH [8]. Furthermore, Jayaweera et al. as in [17] founded that water hyacinth were most efficient in phytoremediating iron as these plants showed a highest removal efficiency of 47 % during period of optimum growth at the 6th week. In heavy metal removal, Aziz et al. as in [6] founded that limestone was capable to remove more than 90 % of heavy metal from a solution of 2 mg/L.

4.7 COD and BOD

After 24 h, the results shown the COD removal was about 90 % removal. This result can be supported by Yalcuk and Ugurlu as in [7] which founded that more than 90 % removal of BOD₅, COD and TSS can be achieved in vertical surface flow systems. Sklarz et al. as in [11] also reported that 80 % of the turbidity and 75 % of the COD were removed within first hour in recirculating vertical flow constructed wetland. The use of water hyacinth in wastewater was founded effective by Jianbo et al. as in [18] with 64.4 % of COD removal rate. Finally, it shown that, the combination of RVFCW with water hyacinth was effective in COD removal.

Initially, RVFCW was effective to remove the BOD in greywater [18]. But, BOD was required for decomposition of organic matter by microorganism. However, at the same time oxygen were required for process of nitrification of nitrite and nitrate by ammonia. So, the amount of the BOD was increase within the time and unable to achieve optimum removal efficiency.

5 Conclusion and Recommendation

From the study, the RVFCW system was proven to have a potential in greywater treatment. Most of water quality parameters showed high removal efficiency except for nitrite, phosphorus and BOD. A less efficiency of nitrite removal was

due to nitrification process in RVFCW. Therefore, it could be concluded that higher greywater concentration was more efficient in removing pollutants from greywater due to the sedimentation and filtration besides the presences of microorganism for biodegradation.

Besides, the study showed uptake of heavy metal by plants increased with increasing metal concentrations. *E. crassipes* had higher capacity to accumulate iron. However, if the heavy metals concentration exceeded the ability of the plant to adsorb, it will resulted in plant wilting due to the toxic impact thus increased the metal and organic content of greywater. On the other hand, the use of Limestone was also founded effective in removal iron as heavy metal and also to neutralize pH of greywater. Finally, combination of RVFCW with *E. crassipes* as wetland plant and limestone media were gives better performance on removal pollutant in greywater.

From this study, there are many possibilities of further research scopes to be investigated. For future work, following recommendations were suggested to improve efficiency of RVFCW:

- To study greywater efficiency when different number of plant is introduced in the constructed wetland. The uses of water hyacinth in greywater treatment only limited to certain parameter. Some of the parameter such as nitrite and phosphorus not totally removed. Process combination of wetland plant must be studies to determine the performance of wetland plant. Some of the wetland plant not able to perform in combination.
- To introduced activated sludge to provide additional microorganism and better aeration method to be implemented in the experimental setup. This is to cater the removal of BOD as this study was only able to achieved not more than 50 % efficiency.
- To use soil media with emergent macrophyte based. The uses of soil with combination of emergent plant may be effective on removal pollutant. Not only plant uptakes the pollutant in a root and leaves but may be soil uptake some of pollutant.
- To use different media for filtration to treat greywater. The use of other media may be effectives in removal certain parameter. Combination of good media will effect the efficiency of RVFCW.

References

1. Capital Regional District, *Greywater Reuse Study Report*. (NovaTec Consultants Inc, 2004), pp. 1027–1042
2. P. Ridderstolpe, *Introduction to Greywater Management*. EconSan Publication Series, Econsanres Programme and Stockholm Environment Institute (SEI), Report 2004-4, WRS Uppsala AB (2004)

3. P.P. Paulo, Greywater Treatment in Constructed Wetland at Household Level, Final Report at Ecological Alternatives in Sanitation-Advanced International Training Programme, Sweden 2005 and Mexico 2006 (2005)
4. A. Gross, M.Y. Sklarz, A. Yakirevich, M.I.M. Soares, A recirculating vertical flow constructed wetland for the treatment of domestic wastewater. *Desalination* **246**, 617–624 (2006)
5. A. Koenig, L.H. Liu, Use of limestone for pH control in autotrophic denitrification: continuous flow experiments in pilot-scale packed bed reactors. *Biotechnology* **99**, 161–171 (2002)
6. H.A. Aziz, N. Othman, M.S. Yusuff, D.R.H. Basri, F.A.H. Asaari, M.N. Adlan, F. Othman, M. Johari, M. Perwira, Removal of copper from water using limestone filtration technique-determination of mechanism of removal. *Environ. Int.* **26**, 395–399 (2001)
7. A. Yalcuk, A. Ugurlu, Comparison of horizontal and vertical constructed wetland systems for landfill leachate treatment. *Bioresour. Technol.* **100**, 2521–2526 (2009)
8. M.E. Soltan, M.N. Rashed, Laboratory study on the survival of water hyacinth under several conditions of heavy metal concentrations. *Adv. Environ. Res.* **7**, 321–334 (2003)
9. R. Stowell, R. Ludwig, J. Colt, G. Tchobanoglous, Concepts in aquatic treatment design. *J. Environ. Eng. Div.* **107**, 919–940 (1981)
10. B. Gopal, *Water Hyacinth: Aquatic Plant Studies Series* (Elsevier, Amsterdam, 1987)
11. M.Y. Sklarz, A. Gross, A. Yakirevich, M.I.M. Soares, A recirculating vertical flow constructed wetland for the treatment of domestic wastewater. *Desalination* **246**, 617–624 (2009)
12. S. Kantawanichkul, S. Kladprasert, H. Brix, Treatment of high-strength wastewater in tropical vertical flow constructed wetland planted with *Typha angustifolia* and *Cyperus involucratus*. *Ecol. Eng.* **35**, 238–247 (2009)
13. M. Green, E. Friedler, Y. Ruskol, I. Safrai, Investigation of alternative method for nitrification in constructed wetlands. *Water Sci. Technol.* **35**(5), 63–70 (1997)
14. K. Seidel, *Macrophytes and Water Purification, Biological Control of Water Pollution* (Pennsylvania University Press, Philadelphia, 1996)
15. F. Zurita, J.D. Anda, M.A. Belmont, Treatment of domestic wastewater and production of commercial flowers in vertical subsurface-flow constructed wetlands. *Ecol. Eng.* **35**, 861–869 (2009)
16. H. Brix, C.A. Arias, The use of vertical flow constructed wetlands for on-site treatment of domestic wastewater: new danish guidelines. *Ecol. Eng.* **25**, 491–500 (2005)
17. M.W. Jayaweera, J.C. Kasturiarachchi, R.K.A. Kularatne, L.J. Wijeyekoon, Contribution of water hyacinth (*Eichhornia crassipes* (Mart.) Solms) grown under different nutrient condition to Fe-removal mechanisms in constructed wetlands. *Environ. Manage.* **87**, 450–460 (2008)
18. L.U. Jianbo, F.U. Zhihui, Y. Zhaozheng, Performance of a water hyacinth (*Eichhornia crassipes*) system in the treatment of wastewater from a duck farm and the effects of using water hyacinth as duck feed. *Environ. Sci.* **30**, 513–519 (2008)

Effect of Water Pressure to Water Loss in Water Distribution Network

Irma Noorazurah Mohamad, Nur Syahiza Zainuddin, Azianabiha A. Halip @ Khalid and Mohamad Radhwan Abd Karim

Abstract Water loss control is a very crucial part in practicing good water management. However, not all losses can be avoided and became a matter especially when the lost water has no value. Water loss through leakage can be minimized by a proper pressure management. This study discusses possibility of water loss due to pressure effect at Universiti Teknologi MARA, Shah Alam, Selangor. It explores the amount of water loss by comparing between current bills with the theoretical calculation based on number of consumer in the specified area. EPA-NET 2.0 was used to illustrate the analysis of water flow within pressurized pipe network. The programme analyses the pressure at each nodes, track the flow of water in each pipes and elevation of the water in each tanks during simulation period. After the whole system is simulated, results are presented in pressure distribution and velocity distribution. Water loss result shows slightly no significant because of the small differences between actual and theoretical values. Even though the pressure distribution quite high but with small water loss shows that water distribution network is in stable operating condition.

Keywords Water loss · Pressure distribution · Water distribution network · Pressurized pipe networks · Hydraulic simulation

1 Introduction

Water supply in Malaysia mainly comes from river and stream. In 1980s, the demand for water supply is grown rapidly especially in residential and industrial sector. This water is distributed to consumer by proper design reticulation system. Water distribution network involves interconnection between pipes, sources and

I. N. Mohamad (✉) · N. S. Zainuddin · A. A. Halip @ Khalid · M. R. A. Karim
Faculty of Civil Engineering, Universiti Teknologi MARA, Shah Alam, Selangor, Malaysia
e-mail: irma1095@salam.uitm.edu.my

hydraulic control element such as pumps, valves, regulators and tanks. A normal concept of water distribution network is to deliver water to consumers based on demand quantities and desired pressures. The major problem faced by the water utility provider worldwide is non-revenue water. Non revenue water is the difference between net production of water into the water distribution network and the amount of water that is billed. Non revenue water also interpreted as a water loss from public water utilities due to poor water distribution network facilities and management, the losses may caused by corrosive environments, soil movement, poor construction standards, fluctuation of water pressure, and excessive traffic loads and vibration. Due to these causes, water losses could occur at different components such as transmission pipes, distribution pipes, service connection pipes, joints, valves, fire hydrants, storage tanks and reservoirs [1].

Water loss through leakage can be minimized by a proper pressure management. Previous study showed pressure management is an important measure for the long term reduction of real losses which happen through pipe burst due to high pressure [2]. Pressure management in water distribution network can be illustrated if there is a leaking garden hose that has a pressure of 414 kPa and then the pressure being reduced to 207 kPa, there will be less water loss through that leak [3]. The same principle holds true in a water utility's distribution system. It is a well-known fact that with decrement of pressure within the system, it also will reduce water loss. The principle behind pressure management is simple—lower system pressures during periods of lower demands (when system pressures normally rise) and reduce the flow rate from existing background leakage (those small weeping leaks from fittings and joints). An additional benefit of pressure management is the related reduction in water main break frequencies which in turn help to extend the life of the underground infrastructure. The economic effect through losses of water is not only the concern of the water provider but also the customers who have to pay more than what is actually being utilised. Hence, a strategic water management to improve water losses through proper pressure management can be adopted since it will not only provide a financial gain but also help in saving precious water for a sustainable environment.

2 Study Area

This study outlines the importance of proactive pressure management as part of a strategy for effective real losses solution. Water supply in Universiti Teknologi MARA (UiTM), Shah Alam campus is feed by three major water tanks with the total capacity reach to 3.9 million gallons (MG). This study only covers for the water distribution network within Water Tank 3 with the capacity 800,000 gallons (G). This water tank distributes treated water to students' college which are Melati College and Mawar College. The reason of choosing this area is the capabilities in higher water demand from the college area especially during semester. Based on the population of consumer, these two colleges are identified having highest

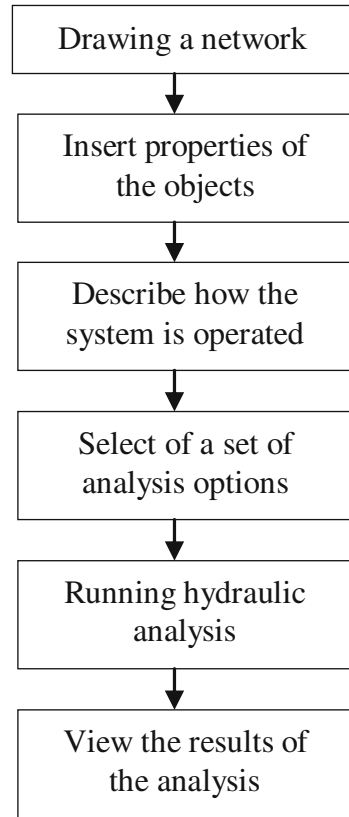
number of resident compare with other colleges in UiTM Shah Alam campus which is about 3,500 capacity of residents each. Comparison between actual water bills and theoretical water demand was carried out to identify on existing of water losses amount. The main parameters being used to identify the stabilisation of water piping systems in this selected study areas which are water flow, pressure and velocity.

3 Hydraulic Simulation Model

Hydraulic simulation models are becoming of common use among planners, water utility personnel, consultants and many others which involved in analysis, design, operation or maintenance of water distribution systems [4]. EPANET 2.0 software was selected for this study where this model can perform steady-state and extended period simulations for networks of junctions, pipes, pumps, valves, and storage structures, calculating flow of water, pressures, tank elevations, concentration of chemical species, water age, and source tracing. EPANET 2.0 is a computer program that performs extended period simulation of hydraulic and water quality behavior within pressurized pipe networks. It is designed to be a research tool which it can be used for many different kinds of applications in distribution network analysis such as sampling program design and hydraulic model calibration. EPANET 2.0 models a water distribution network as a collection of links connected to nodes. The links represent pipes, pumps, and control valves while the nodes represent junctions, tanks, and reservoirs. EPANET 2.0 tracks the flow of water in each pipe, the pressure at each node and the height of water in each tank throughout the network during a simulation period comprised of multiple time steps [5].

EPANET 2.0 was used to analyze the piping system where the trend of flow velocity and pressure can be predicted based on the parameter setting over an extended period of time. In addition, pressure analysis was identified to see whether it is enough to supply water to consumer. Figure 1 shows the overview step taken in EPANET simulation process. System required to install and run EPANET 2.0 is Windows 95/98/NT with IBM/Intel-compatible personal computer [6]. Once the new project in EPANET 2.0 created, network or water distribution network was drawn as representing the actual water distribution network. The basic description of the network placed in text file format also can be imported into EPANET 2.0. This network must contain nodes and links objects such as reservoir, junction, tank, pipes and pumps. Then, the properties for each objects assigned in the EPANET 2.0 must be allocated accordingly. Parameter needed for the nodes such as demand, head and pressure. While for the links, parameters required such as length, pipe friction factor, size of diameter, roughness, flow, velocity and head loss. Then, the flow of the systems should be described in the system by knowing the direction of the network.

Fig. 1 Illustration of step in simulation process



Next, the analysis options of the simulation can be in single period analysis and an extended period analysis. Time pattern chosen in this study is an extended period analysis. This is important to make the network more realistic by making demands at the nodes vary in a periodic way. Normally, a 1 h pattern time step is more typical number and it is the default assigned to new project. But, pattern time step of 3 h was selected thus making demands change at eight different times of the day with the total duration set to 24 h which means the network analysis run for one-day period. With enough information needed, the simulation was run. Lastly, the results for an extended period analysis were viewed in a various form.

4 Results and Analysis

This study analyse the trend of water pressure within pressurized pipe network using EPANET 2.0 software. Velocity distribution also being discussed too. Locations with high or inadequate pressure, velocity and flow have been obtained through the

extended period simulation analysis. The results are directly viewed on the network map during the simulation process. The output results have been carried out against by time. This study focused on the simulation process at peak hour duration which are at 7 a.m. and 5 p.m. respectively. Analyses are focused more on pressure distribution and velocity distribution on the pressurized pipe network.

4.1 Network Simulation

Simulation is carried out during the peak hours which are at 7 a.m. and 5 p.m. respectively. Total of 30 nodes and 30 links are identified in this simulation process. Those nodes and links represent the actual water distribution network system in the selected study area. Highest pressure showed during the simulation at 7 a.m. was 232.77 kPa which happen at nodes 2. Then, follow by nodes number 12 and 11 with 231.46 and 230.59 kPa respectively. This high pressure occurred because of the velocity of water at this time is slightly high due to the high water demand from consumer preparing themselves going to class in the morning.

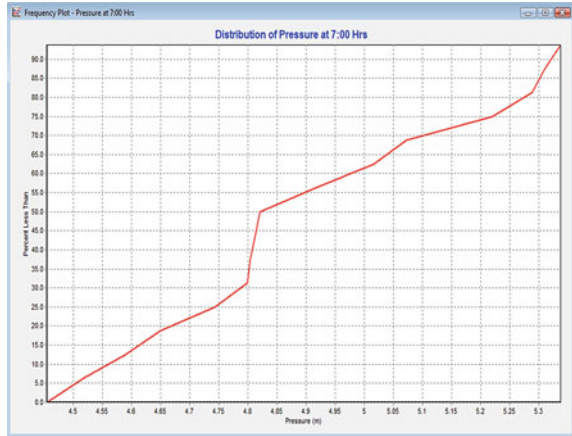
Velocity of water at 7 a.m. shows to be high compare with velocity distribution at 5 p.m. The highest velocities are recorded at pipe link 8 which is 3.69 m/s. While, there are another links considered with high velocity values at link 13 and link 9 with 2.51 and 2.41 m/s respectively. All this pipes supplies water to water tank above Mawar College building.

On the other hand, simulation result at 5 p.m. shows slightly similar with the result obtained at 7 a.m., where at this time water consumption is high due to high water demand. Highest pressure are recorded at node 2 followed by node 11, 12 and 13 with 331.72, 329.98, 238.23 and 178.72 kPa, respectively. Others nodes recorded lower pressure value. However, by comparing with pressure level at 7 a.m., pressure values at 5 p.m. were much higher and this phenomenon is because total water demand including consumer needs is much concern. Intension for having heavy activity such as washing clothes were done during this hour compare in the morning.

Scenario for velocity result at 5 p.m. is also similar with previous analysis. However, highest value still recorded at Mawar College pipes which labelled as link 8, 13, 9 and 14 with a value of 4.38, 3.01, 2.87 and 2.30 m/s, respectively. Both cases gave the same trend velocity. Highest values was recorded at the same College which known as Mawar College. This is because Mawar College has their own pump that contains capacity of 30 m³/h at 57 m head which the flow of water distribution can be high and same goes for velocity.

At normal water consumption condition, higher pressure will cause greater flow through any given pipe size. However, increasing of flow will cause pressure to be decreased downstream due to friction loss factor. This happen because of the water velocity is increasing as well. High quality of water supply system is when capacity of pressure is adequate with type and diameter of the pipes. In this study, most of the pipes have a diameter of 200 mm. According to the standard, the

Fig. 2 Distribution of pressure at 7 a.m.



actual capacity of pressure in the pipe is between 150 to 300 kPa. Therefore, the simulated pressure at the selected study area considered having high pressure comparing with the standard regulation.

4.2 Pressure Distribution

The details explanation on pressure distribution at 7 a.m. and 5 p.m. are illustrated in Figs. 2 and 3 respectively. Highest pressure achieved in the simulation process during 7 a.m. is 5.34 m which equal to 232.77 kPa. The trend can be seen in Fig. 2 are slightly proportional to the percentage. There are about 32 % or 10 nodes from the whole total nodes having pressure less than 4.8 m or 209.23 kPa. Nodes having pressure in the range of 4.8 m (209.23 kPa) to 4.825 m (210.32 kPa) is about 1.9 % which equal to only 1 node and the rest of the nodes (19 nodes or 93.3 %) were having a pressure between 5.34 m or 232.77 kPa to 4.825 m or 210.32 kPa.

While as shown in Fig. 3, the distribution of pressure at 5 p.m. is not directly proportional to the percentage. Most of the nodes are having a pressure between 2 to 7.61 m or between 87.18 to 331.72 kPa. There is about 62 % or 19 nodes from the whole nodes having pressure below than 3.53 m or 153.87 kPa. The rest of the nodes (11 nodes) were having a pressure greater or equal to 6.26 m or 272.87 kPa.

4.3 Velocity Distribution

Distribution of velocity at 7 a.m. shows about 70 % or 21 links including pipes and pump are having a velocity below than 1 m/s. While, another 17 % or 5 links having a velocity between 1 to 2 m/s. There are about 7.5 % or 2 links having a

Fig. 3 Distribution of pressure at 5 p.m.

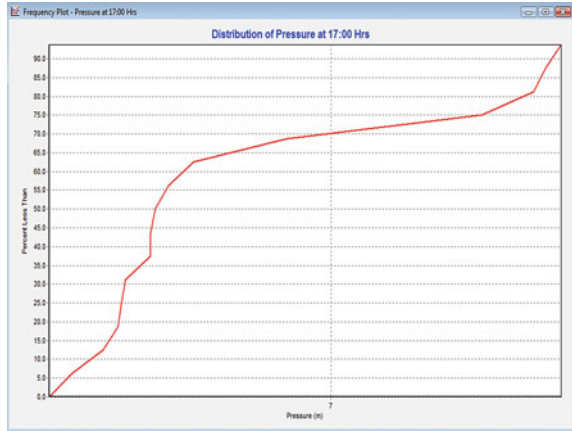
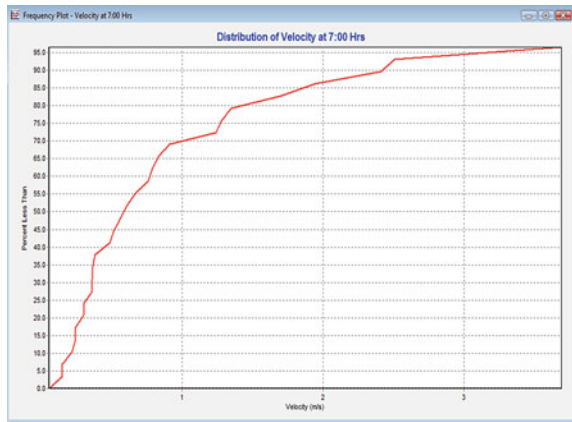
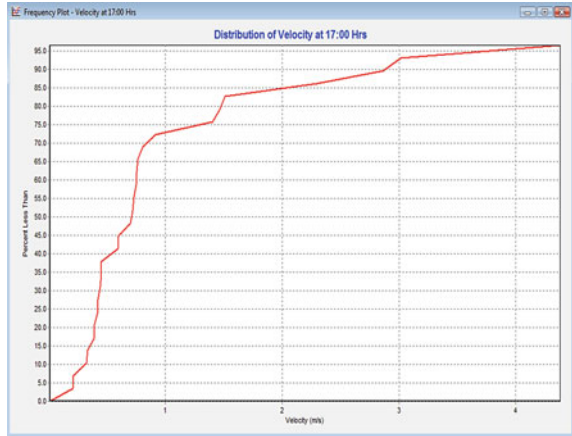


Fig. 4 Distribution of velocity at 7 a.m.



velocity between 2 to 3 m/s and the rest of the links (2 links) are having a velocity greater than 3 m/s but below 4 m/s. While, for velocity distribution at 5 p.m. allocated 73 % from the whole system is having a velocity below than 1 m/s. This percentage is equal to 22 links out of the total of 30 links. Another 4 links or 12 % are having a velocity in the range of 1 to 2 m/s respectively. And the rest of the links which equal to 4 links having a velocity greater than 2 m/s until the maximum velocity in this network is 4.38 m/s. These velocity distributions are shown in Figs. 4 and 5 respectively.

Fig. 5 Distribution of velocity at 5 p.m.



4.4 Water Losses

Water loss analysis are determined through the comparison between the actual and calculation of water demand. Actual water demand for Water Tank 3 which supplies water to Mawar College and Melati College is recorded up to 519,908.25 m³/year or 1,424.46 m³/day. While the theoretical total rate of water demand for both colleges is 1,400 m³/day. There are only 1.7 % differences and with this very minimal different values represents that the water distribution network is stable without any leakage or losses.

5 Conclusion

The current water supply infrastructure is still adequate to meet the water needs for both Mawar College and Melati College respectively. This can be seen from comparison of both actual and calculation of water demand. The actual water demand is slightly high compare with calculation amount with different of 24 m³/day or 1.7 % only. This difference can be ignored because of the small amount. The occurrence of water loss also can be detected through the pressure level. The EPANET 2.0 simulation shows Mawar College record highest pressure level at 7 a.m. and 5 p.m. with 232.77 and 331.72 kPa respectively. Both values were recorded at the same nodes labeled as node 2 and considered slightly higher than the standard.

This can be concluded that most of the pipes in the area not having too high pressure and still under good condition. Study also found that water distribution network in the study area is in stable operating system. However, there have some locations that need to be control in the future. Availability for the infrastructure supplying water is influence by the proper pressure management. Therefore, high pressure must be controlled with efficiently.

Acknowledgments The authors would like to thank Research Management Institute (RMI), Universiti Teknologi MARA for providing financial support through excellence fund. The authors would like to acknowledge the contribution of Jalur Cahaya Sdn. Bhd., for training courses and to all persons involved that have been cooperative and supportive in making this study successful.

References

1. K.R. Ku-Mahamud, W.H. Wan Ishak, and M.S. Abu Bakar, Managing Water Loss for Sustainability of Rural Water Supply. in *Proceedings of the Rural ICT Development Conference (RICTDC 2007)*, Sintok, Kedah, Malaysia, 20–21 Nov 2007
2. A.M. Lalonde, C. Au, P. Fanner, J. Lei, City of Toronto Water Loss Study and Pressure Management Pilot, Miya Arison Group, unpublished
3. B.V. Clarke, *Water Loss Reduction through Pressure Management* (Singer Valve Inc, Surrey, 2005)
4. T.M. Walski, Technique for calibrating network models. *J. Water Resour. Plan. Manage.* **109**(4), 360–372 (1983)
5. M.A. Haytham, Water Supply Network Simulation using EPAnet, unpublished
6. L.A. Rossman, *EPANET 2 Users Manual* (Environmental Protection Agency, USA, 2000)

Monitoring and Preserving Water Quality Using GIS Tools and Statistical Approach

GIS in Water Quality

Mohd Adhar Abd Samad and Mohd Khairy Kamarudin

Abstract Agricultural chemical like nitrate (NO_3) in the river surfaces may constitute to human health risk, e.g. a cancer disease. The consumers need water in most daily activities, especially in drinking water, clean foods, etc. The emerging of the Geographical Information Science's (GIS) and statistical approach help in analyzing and monitoring these chemicals. This study was conducted using Quantum GIS (QGIS) and integrating statistical approach for estimating agricultural chemical's concentration of rivers in Klang Valley basin. The spatial data of Klang Valley Basin, water quality stations, land use, and selected agriculture chemical in 6 months (January 2008 to July 2008) were used by using the combination of QGIS software and statistical approach in estimating these chemical's concentration of rivers. The study found that nitrate located within the areas that covered by agricultural activities and urban activities. The Kruskal–Wallis method was used to find the influence of water level toward the quantity of nitrate. The proper study toward the water-quality standards is necessary for preserving and monitoring water resource from being polluted.

Keywords GIS · Open source software · Kruskal–Wallis method · Nitrate · Monitoring

1 Introduction

River pollution in Malaysia is common issues and it is critical in states of Selangor and W. P. Kuala Lumpur (both are located in Klang Valley Basin). Although Malaysia as a Tropical country with high annual rains that capable of meeting a

M. A. A. Samad (✉) · M. K. Kamarudin
Department of Science Survey and Geomatics, Universiti Teknologi Mara (UiTM),
Arau, Perlis, Malaysia
e-mail: adhar260@perlis.uitm.edu.my

domestic consumption and industrial need, the water pollution restricted the full utilization of the water and unsuitable for human consumption [1]. A study to estimate agricultural chemicals, e.g. Nitrate concentration in rivers by using open source GIS i.e. QGIS software are necessary as a mechanism for problem solving, to make decision support, analyze, determination, and estimation. The conventional approach in handling environmental pollution is by using statistical method [2]. The GIS approach is the latest method in solving the water pollution problems. Common GIS software like ESRI's ArcInfo is available in the market and is useful in solving real phenomenon [3, 4]. The issue in implementing GIS's commercial (ArcInfo) in the environment analysis is the price and cost of the software. Since the open-source GIS software is available, the opportunity in utilizing the GIS science and technology in solving the environmental issue e.g. water pollution can be done by individual or organization [5, 6, 7]. The GIS technology is a powerful tool in solving the phenomena [8]. This study tries to utilize QGIS software and statistical analysis of selected agricultural chemical's data in a regional surface-water of Klang Valley basin for evaluating the chemical's concentration. Data collected for this study were used in conjunction with digital spatial data on agricultural chemical use, and land use to model the probability of agricultural chemical concentrations being within a particular concentration range. This method may be useful to water managers and suppliers attempting to meet the current drinking water standards.

2 Study Area

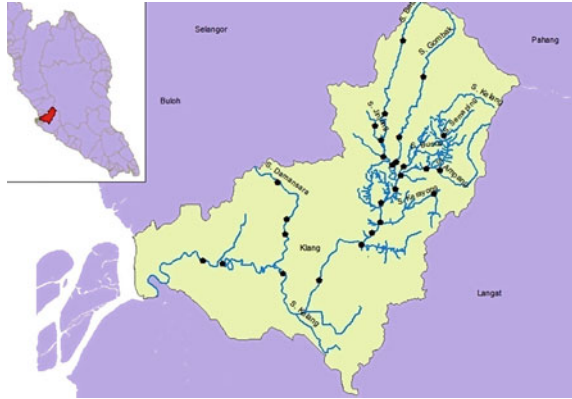
The Klang Valley Basin area has been selected in this study. Figure 1 illustrates the Klang Valley Basin. It is located as part of W. P. Kuala Lumpur, and part of Selangor state. The characteristic of this basin is consist of rivers from W. P. Kuala Lumpur through Selangor state and ends at Port Klang. It also has 28 water quality stations located along the river network. The Klang Valley Basin located between the Banjaran Titiwangsa and Straits of Malacca with a steep geographical area. The land is covered by agricultural and urban activities.

3 Data and Methodology

3.1 Variable and Spatial Analysis

The characteristic of this basin is consist of rivers from W. P. Kuala Lumpur through Selangor state and ends at Port Klang. It also has twenty eight (28) water quality stations located along the river network. The current investigation involved a data sampling of agricultural chemicals (i.e. nitrate) over 6 months (January

Fig. 1 Study area in Klang river



2008 to July 2008) and spatial data of Klang Valley Basin, water quality stations, and land use to estimate these chemical by combination of GIS application i.e. QGIS and analysis with supported by statistical analysis help in clear information analysis tools, to shows the relationship between nitrate data in the river.

3.2 Kruskal–Wallis and Linear Regression Analysis Method

The chemical data and spatial data were analyzed using statistical approaches, i.e. linear regression [9, 10] and the Kruskal–Wallis method. This method used to determine and identify the relationship between the chemical quantities and tidal phenomena.

4 Results

The first discussion is towards spatial data, e.g. river's data, land used cover data, and basin station that attribute of agricultural chemical. The output is a map which showed the chemical concentration of rivers in Klang Valley Basin. The quality is displayed in five classifications, starting from 'very low' (0.0–0.19 mg/l) labeled in blue color, 'low' (0.2–0.39 mg/l) labeled in green color, 'moderate' (0.4–0.59 mg/l) labeled in yellow color, 'high' (0.6–0.79 mg/l) labeled in red color, and 'very high' (0.8–1 mg/l) labeled in black color. The output from QGIS can be seen through the rational of agricultural chemicals flow in river. The condition of chemicals is shown in various outputs depending on chemical quantity that is measured by water quality stations. The spatial data of land use is useful in understanding the activities (development and agricultural) that contribute toward chemicals in river. The statistical approach used to strengthen the analysis of spatial data and its attributes, i.e. chemicals data. The water level analysis on chemicals

can strengthen the output whereby to see the influence from water level affects the chemical quantity in rivers. Lastly, the linear regression is used in this study to see the reliability of data in agricultural chemical in the river by using SPSS's software.

4.1 Result of Nitrate in River from January 2008 to July 2008

Referring to Figs. 2 and 3 shows the result of the nitrate concentration in the river of Klang Valley Basin. The 28 basin stations represent the quality of the river in the January 2008. The highest nitrate was found in the basin station of IK03, IK06, IK16, and IK23, are covered by urban area that is shown in Fig. 3. It seems that not only agricultural activities contributes nitrate into the river. Theoretically, urban area with high density population is producing to nitrate into rivers by the sewage-treatment plants [11]. The low and very low nitrate quantity (IK2, IK16, IK17, IK20, IK21, and IK22) are found at the area has no agricultural activities. The amount of nitrate in the river depends upon the distance travelled by the water. The nitrate quantity decreases as the distance increases. This phenomenon can be described in Fig. 3; the IK03 station shows the very high nitrate quantity, but once it flows to another location (IK02), the nitrate quantity decreases.

Figures 4 and 5 show the nitrate reading for March 2008. The highest nitrate readings were collected from IK11, IK12, IK13 and IK17. It seems the urban activities, and agricultural activities have an important role in supplying nitrate into river. In Fig. 5, the river located at station IK04 is surrounded by the agricultural land where the nitrate quantity is only in moderate scale. It can be assumed that the agricultural activity in this area uses less agricultural chemical in their plantations.

The nitrate quantity for May 2008 are shown in Figs. 6 and 7 shows the highest nitrate quantities are at IK13, IK17, IK20, and IK24. The nitrates in the river were contributed by agricultural and urban activities. Although agronomic land area is less, the contribution from agricultural chemicals also produces high nitrate quantity. It can be proven by analyzes the chemical quantity in river IK13 which it surrounded by agricultural land. The nitrate quantity varies from month to month.

Figures 8 and 9 shows the nitrate quantity for July 2008 collected from stations IK17, IK18, IK20 and IK25 with the highest value recorded. However, the IK11 to IK13 stations have the lower amount of nitrate. Meanwhile the IK13 and IK17 stations recorded high chemical quantity.

4.2 Statistical Analysis on Nitrate in January to July 2008

Figure 10 shows the summary of nitrate in four data sample that has been taken in January 2008 to July 2008. The graph shows the station IK17 has the most consistencies in highest nitrate quantity. This analysis shows the occurrence and

Fig. 2 Nitrate reading of Klang Valley basin in January 2008

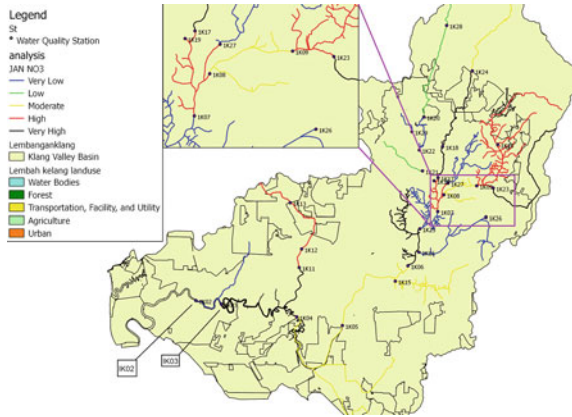
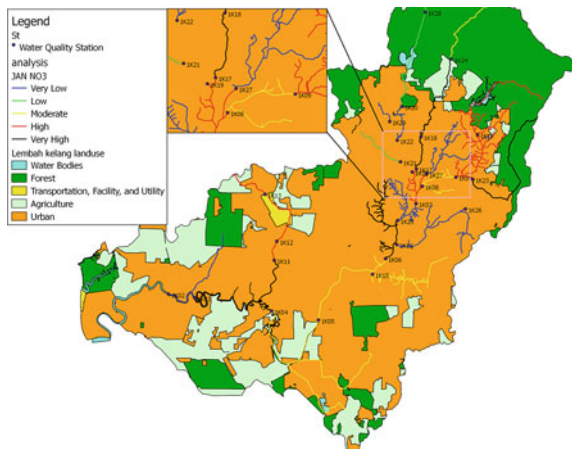


Fig. 3 Nitrate reading and land use cover of Klang Valley basin in January 2008



similarities between nitrate quantities within four data samples. This shows that IK17 is the most polluted river that needs to be monitor and action taken by the authorities to reduce the quantity of chemicals. Other rivers are in moderate condition where the nitrate quantity is in a tolerable level. Based on land used data, IK17 is located in urban area where it can be concluded that both agricultural and urban activities contribute to the nitrate found in the river.

4.3 Analysis Relationship of Water Level and Agricultural Chemicals Using Kruskal–Wallis Test Statistical Method

This test has been used to see the relationship between water level and agricultural chemicals toward water pollution. This test creates a hypothesis (High = Normal = Low) by processing in the SPSS software. At 95 % of the confidence interval,

Fig. 4 Nitrate reading of Klang Valley basin in March 2008

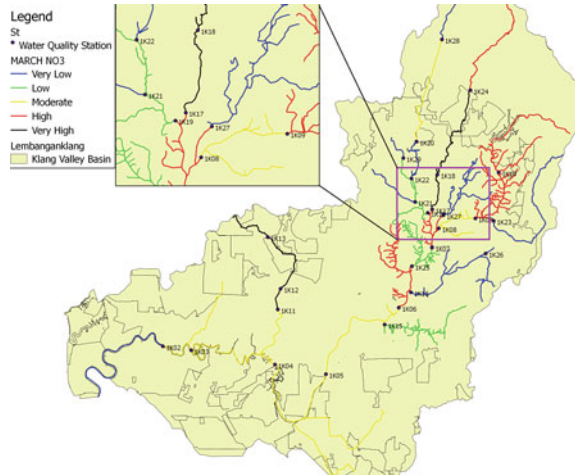
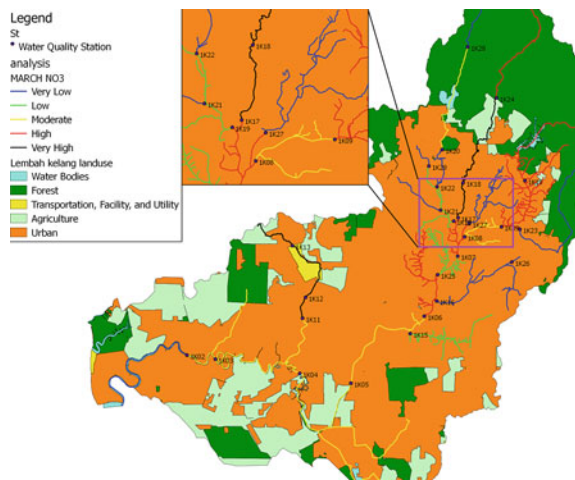


Fig. 5 Nitrate reading and land use cover of Klang Valley basin in March 2008



the hypothesis test will be passed if alpha value ($\alpha = 0.05$) less than the p value. Tables 1, 2 and 3 are the results of Kruskal–Wallis where the test is passed in 95 % confident interval. The pass conditions, is the alpha (α) values = 0.05 and must not exceed from the p -value = 0.360 (Asymp. Sig in SPSS). Since the alpha is less than the p -value, there is no relationship between water level and agricultural were affected to river. The water level of river seems not affected the quantity of chemical.

Fig. 6 Nitrate reading of Klang Valley basin in May 2008

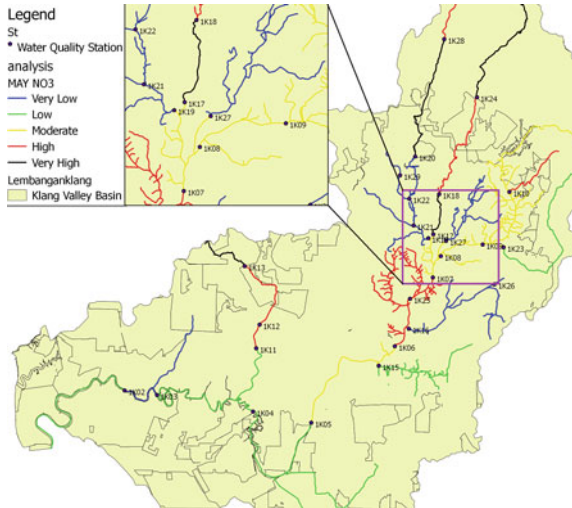
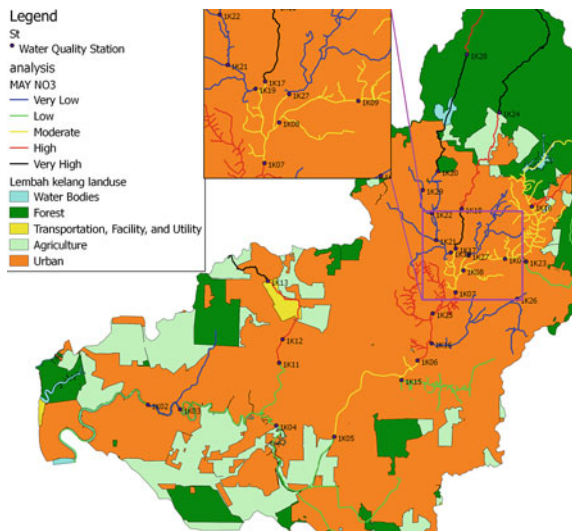


Fig. 7 Nitrate reading land use cover of Klang Valley basin in May 2008



4.4 Linear Regression Analysis in Determine the Influence of Rivers Length Toward NO₃ Quantity

This Linear Regression analysis is performed to find the influence of river length toward quantities of NO₃ and PO₄ in water. The river length is measured using QGIS tools, i.e. geometry calculation from the attribute table. Figure 11 is the attribute table of river where in the column 'River_Leng', as a river length. Based on Fig. 12, illustrates the influence of river length toward quantities of nitrate in

Fig. 8 Nitrate reading of Klang Valley basin in July 2008

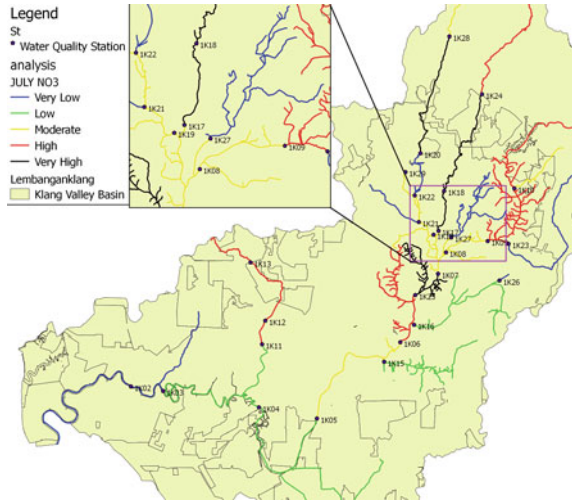


Fig. 9 Nitrate reading and land use cover of Klang Valley basing in July 2008

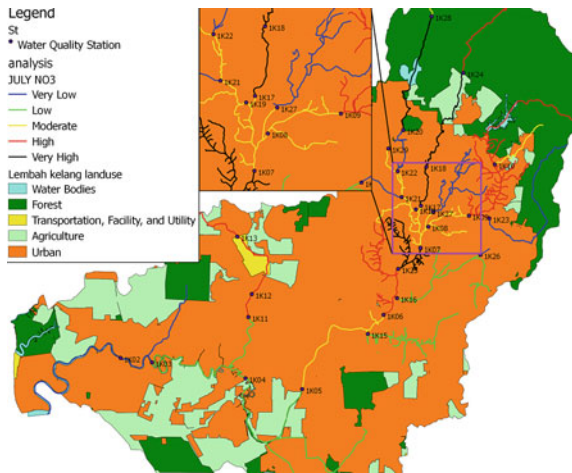


Table 1 Descriptive statistics of water level and nitrate quantity

	N	Mean	Std. Deviation	Minimum	Maximum	Percentiles		
						25th	50th (Median)	75th
NO ₃	111	0.3018	0.26929	0.01	1.00	0.0200	0.2600	0.5100
Water level	111	1.86	0.457	1	3	2.00	2.00	2.00

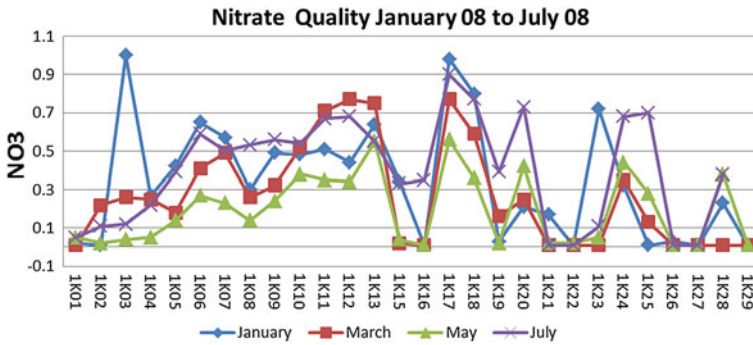


Fig. 10 Summary of nitrate reading in Klang Valley basin for January 2008 to July 2008

Table 2 Ranks NO₃

	Water level	N	Mean rank
NO ₃	High	20	52.12
	Normal	86	58.00
	Low	5	37.10
	Total	111	

Table 3 Test statistics^{a,b}

	NO ₃
Chi Square	2.368
df	2
Asymp. Sig.	0.306

^a Kruskal–Wallis Test

^b Grouping Variable: Water Level

river where river length is independent variable and NO₃ quantity is depending to river length. The relationship between river length and NO₃ quantity is shown in negative relationship. It means any increasing of river length will produce low nitrate quantity in river. Besides, the short river length is to produce higher nitrate quantity in river. This test was performed by using SPSS software to find the slope of the regression line. Table 2 shows the result of linear regression where it found the slope equation of NO₃ quantity and river length is ($Y = -9.351E - 7(X) + 0.314$). This slope is showing the relationship of NO₃ quantity (Y) with river length (X). The analysis found that the river’s length is the influence to NO₃ quantity. The slope equation is used to determine the NO₃ quantity in river that based on any input of river length (short or long).

Attribute table - River calculate2

	NAME	STN_NAME /	River_Leng
0	S. Kelang	1K01	18086.52
1	S. Kelang	1K02	12792.68
2	S. Kelang	1K03	25860.61
3	S. Kelang	1K04	38373.98
4	S. Kelang	1K05	14440.43
5	S. Kelang	1K06	30022.19
6	S. Kelang	1K07	11831.92
7	S. Kelang	1K08	10802.79
8	S. Kelang	1K09	63996.18
9	S. Semaping	1K10	7027.67
10	S. Damansara	1K11	2305.03
11	S. Damansara	1K12	8106.93
12	S. Damansara	1K13	5408.01
13	NULL	1K15	25769.35
14	S. Kerayong	1K16	24391.68
15	S. Gombak	1K17	4315.49
16	S. Gombak	1K18	12974.98
17	NULL	1K19	14958.24
18	NULL	1K20	12341.77
19	NULL	1K21	6215.57
20	NULL	1K22	7133.5
21	S. Ampang	1K23	17828.7
22	S. Gombak	1K24	13897.43
23	S. Kelang	1K25	24528.04
24	NULL	1K26	961.64
25	S. Bunas	1K27	22474.07
26	S. Batu	1K28	6906.7
27	S. Jinjang	1K29	2883.6

Look for in NAME Search

Show selected records only Search selected records only

Advanced search Help

Fig. 11 Attribute table of river

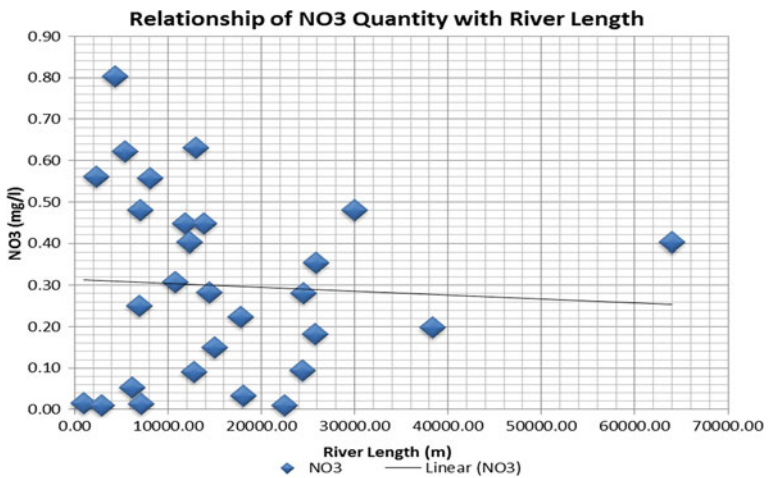
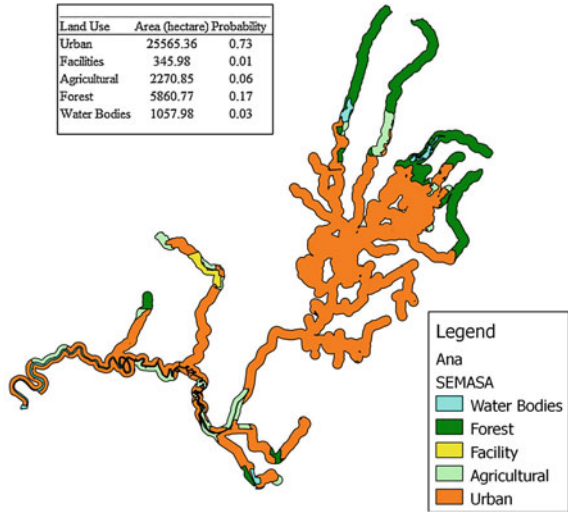


Fig. 12 Relationship of NO₃ quantity with river length

Fig. 13 Analysis of buffering river and intersect with land use



4.5 Determining the Probability of Agricultural Chemical Using Buffering River in One Kilometer (km)

This analysis is to see the possibility of land cover in producing nitrate by buffering river in one (1) km. Using QGIS software to process buffering the river in one km and capture any land cover within the buffer coverage. Figure 13 illustrates the output of buffer where it was found the urban area is the largest area surrounded along the river. The second is forest, and agricultural in third place. This analysis intends to see the probability of land use influence to chemical quantity in the river of Klang Valley basin. Urban area is the most probably contributing to chemical in the river. Since the agricultural area is smaller than urban land, the contribution toward chemical concentration in river is minor compared to urban area.

4.6 Conclusion

The above results found the agricultural chemicals in the river of Klang Valley Basin are contributed from land use activities. The agricultural activities and urban activities are the major contribution of chemicals in the rivers. Agricultural used the agro-chemical on crop or plantation to increase their productivity. The highest quantity of the chemical in the agriculture can reduce the water quality and a risk to human’s health. This study found not all agricultural land produce pollution to rivers. It depends upon the quantity of chemical is used in agricultural.

The phenomena of water level in range high level, normal level, and low level in Klang Valley basin is not influenced the quantity of nitrate. It has been proven using analysis by a graph bar, and Kruskal–Wallis Test. The quantity of nitrate in river depends on the usage of agricultural chemical on plantation and urban activities. The result shows two stations (IK17 and IK26) have highest quantity of chemical's concentration in river. The actions to protect and preserve these rivers are necessary to protect our generation.

Acknowledgments The authors would like to thank the Department of Environment Malaysia for give the author opportunity to do this research. The author likes to thank the anonymous referees for their comments and observations on draft of this paper.

References

1. Y.B.E. Wong, The need for a water demand management plan for Selangor. (2009)
2. S. Shrestha, F. Kazama, Assessment of surface water quality using multivariate statistical techniques: a case study of the Fuji river basin. *Jpn. Environ. Model. Softw.* **22**(4), 464–475 (2007)
3. M. Di Luzio, R. Srinivasan, J.G. Arnold, A GIS-coupled hydrological model system for the watershed assessment of agricultural nonpoint and point sources of pollution. *Trans. GIS* **8**(1), 113–136 (2003)
4. C. DiBona, S. Ockman, *Open Sources: Voices from the Open Source Revolution*. (O'Reilly Media, Incorporated, USA, 1999)
5. C. DiBona, S. Ockman, *Open sources: Voices from the Open Source Revolution*, (O'Reilly Media, Incorporated, USA, 1999)
6. A. Yaakup, F. Johar, A. Bakar, S. Zalina, S. Sulaiman, M. Baharuddin, Integrated land use assessment: the case of Klang Valley Region, Malaysia, (2005)
7. A. Yaakup, M. Ludin, A. Nazri, A. Bakar, S. Zalina, S. Sulaiman, Spatial planning and decision support system for urban metropolitan planning and monitoring: a case of Klang Valley, Malaysia, (2005)
8. G. Cdmara, H. Onsrud, *Open-Source Geographic Information Systems Software: Myths and Realities*, (2004)
9. W.A. Battaglin, D.A. Goolsby, Using GIS and logistic regression to estimate agricultural chemical concentrations in rivers of the midwestern USA, in *IAHS Publications-Series of Proceedings and Reports-Intern Assoc Hydrological Sciences*, vol. 235, (1996), pp. 253–260
10. T. Kazi, M. Arain, M. Jamali, N. Jalbani, H. Afridi, R. Sarfraz, A.Q. Shah, Assessment of water quality of polluted lake using multivariate statistical techniques: a case study. *Ecotoxicol. Environ. Saf.* **72**(2), 301–309 (2009)
11. W. Körner, U. Bolz, W. Süßmuth, G. Hiller, W. Schuller, V. Hanf, H. Hagenmaier, Input/output balance of estrogenic active compounds in a major municipal sewage plant in Germany. *Chemosphere* **40**(9), 1131–1142 (2000)

The Effectiveness of *Pseudomonas putida* Atcc 49128 as Biodegradable Agent in Biodiesel Soil Contamination

N. M. Sunar, Q. A. Emparan, A. T. A. Karim, S. F. M. Noor, M. Maslan, F. Mustafa and N. Khaled

Abstract Soil contamination has become a major problem because of the large amounts of manmade pollutants and chemicals that have been put into the environment. This study aims to determine the growth rate of *Pseudomonas putida* to treat soil that has been contaminated with pure biodiesel, B100. The effectiveness on bioremediation have been conducted by examined several physico-chemical tests for biodiesel-contaminated soil before and after seeding with *Pseudomonas putida*. The physico-chemical tests involved were pH, nitrogen, phosphorus, sulfate and organic carbon. The experimental results show that after 20 days pure culture *Pseudomonas putida* able to remove approximately 69 % of nitrogen, 27 % of sulphate, however, no removal for phosphate and organic carbon. The results indicated that the application of this bacterium is suitable for the degradation of nitrogen and sulfate in biodiesel-contaminated soil. The *Pseudomonas putida* growth has slightly increased from Day 2 (3.0×10^7 CFU/ml) to Day 8 (4.1×10^7 CFU/ml). After Day 8, the amount of *Pseudomonas putida* slightly starts to deplete until Day 20 (4×10^6 CFU/ml). The available nutrient in the sample is low once the bacterium has used them as source of carbon and energy before Day 8. Overall, this study proved that *Pseudomonas putida* is the effective microorganism and potentially exploit as useful oil-soil biodegradable agent.

N. M. Sunar (✉) · M. Maslan

Department of Chemical Engineering Technology, Faculty of Engineering Technology (FTK), University Tun Hussein Onn Malaysia (UTHM), 86400 Parit Raja, Batu Pahat, Johor, Malaysia
e-mail: shuhaila@uthm.edu.my

Q. A. Emparan · A. T. A. Karim · F. Mustafa · N. Khaled

Department of Water And Environmental Engineering (DWEE), Faculty of Civil And Environmental Engineering (FKAAS), University Tun Hussein Onn Malaysia (UTHM), 86400 Parit Raja, Batu Pahat, Johor, Malaysia

S. F. M. Noor

Department of Science and Mathematics, Centre For Diploma Studies, University Tun Hussein Onn Malaysia (UTHM), 86400 Parit Raja, Batu Pahat, Johor, Malaysia

Keywords Biodiesel · Biodiesel-contaminated soil · Biodegradability · Bioremediation · *Pseudomonas putida*

1 Introduction

Demand for renewable fuel especially biodiesel is increasing worldwide due to the new legislation seek to reduce our dependence on oil from foreign countries, to achieve the goals of the Kyoto protocol and to support agriculture. The EU-directive 2009/28/EC has target for renewable in the transport fuel mix of 10 % by 2020, subject to the sustainability of production [1]. Biodiesel usage has also increased due to factors such as the rising cost of petroleum based-fuel, the emission from such fuels and the realization that our oil will not last forever. In addition, using pure biodiesel or biodiesel diesel blends instead of pure diesel fuel in diesel engine can emit less air pollution due to its higher oxygen concentration and lack of aromatic compounds and sulphur [2]. Due to the current fuel standards and also warranty limitation from car manufacturer, the near-future oil composition in Europe and the United States (US) is the blending of low proportion of bio-ethanol (5–5 %) with petroleum or biodiesel (up to 20 %) with diesel. Since the early 21th century onwards, other states such as Australia, Brazil, Canada, Germany, China, South Korea and also Malaysia are also beginning to mandate that all diesel fuel sold at the petrol stations should at least contain 2 % of biodiesel. However, the commercialization of biodiesel or biodiesel/diesel blends on the markets of many countries may cause environmental damages due to spill. The contaminated area can be cleaned-up by biodegradation technology, bioremediation method, a technique based on the action of microorganisms, in which hazardous contaminants will be turned into non substances such as carbon dioxide (CO₂), water (H₂O) and biomass [3]. Due to the high cost of classical remediation processes, for example soil excavation and incineration, bioremediation is a promising and cost effective technological development for cleaning up soil contaminated by biodiesel. Biodegradation technologies first proved practical on a wider scale during the Exxon Valdez oil spill took place in Alaska. Since then, they have been used more frequently in many countries [4].

Many microorganisms are capable of using oil products as energy source in aqueous environment. They are ubiquitous in the environment and are able to metabolize the different types of hydrocarbon, as contained in oil products [5]. In fact, the degradation of hydrocarbon by microorganisms depends to their molecular weight, metabolism of microorganisms and also environmental conditions. Several factors such as amount of nutrient supply and oxygen content have influenced the degradation rate of hydrocarbons [6]. Most of the hydrocarbon degradation studies reported in literature have been carried with single or mixed bacterial strains isolated because of their stability to grow in media with hydrocarbon as only carbon source.

Pseudomonas putida is not pathogenic to environment and human health due to lack of certain genes including those for enzymes that digest cell membranes and well of human and plants. It is gram negative [7], chemoorganotrophic, aerobic obligate and aerobically respiratory metabolisms. It is straight or curved rods with dimensions range between 0.5 and 1.0 μm in diameter and 1.5 to 4.0 μm in length respectively. It is arranged commonly individually or in small clusters or chains and grown under aerobic conditions in common substrates. They formed irregularly large colonies producing water-soluble exopigment, which diffuse into atmosphere and dyes it yellow or blue-green. The optimum temperature of its growth is 35 $^{\circ}\text{C}$ [4].

Pseudomonas putida is tolerant to a xenobiotics especially polyaromatic hydrocarbons (PAHs) and play a vital role in the treatment of petroleum contaminated soil [8]. It occurs in various environmental niches because of its metabolic versatility and low nutritional requirement [9]. Recently, many studies on degradation of hydrocarbon by bacterium consortia, including *Pseudomonas putida* have been carried out because of its high capability to degrade recalcitrant substances and inhibiting xenobiotics. In this sensed, it can adapt to diverse substrates and posses some catabolic pathways capable of acting on recalcitrant substances [7].

In one study by Pasqualino [10] after 28 days pure biodiesel fuel was 98 % biodegraded in comparison to 50 and 56 % by diesel fuel and gasoline, respectively. The researchers found that biodiesel degraded faster than petrodiesel. In studies by Walker et al. [11] shown that heavy fuel oil had a low biodegradation of 11 % due to its higher proportion of high molecular weight aromatics whereas gasoline was only 28 % biodegraded. Besides that, Hamed et al. [12] previously studied the biodegradation of soil that has been exposed to crude petroleum oil by means of bacterial consortium (*Pseudomonas stutzeri* AT3, *Bacillus thuringiensis* AT5, *Bacillus pumilus* AT11 and *Bacillus cereus* AT15). The removal of hydrocarbon is highest by *Pseudomonas stutzeri* AT3 (90 %), followed by *Bacillus thuringiensis* AT5 (56.67 %), *Bacillus cereus* AT15 (52.33 %) and *Bacillus pumilus* (50.60 %).

Microbial growth is one of the consequences of the biodegradability of pure biodiesel, diesel and their blends. The aim of this study therefore, to investigate the growth rate of *Pseudomonas putida* to treat soil that has been contaminated with biodiesel. The effectiveness on bioremediation for biodiesel contaminated-soil was also evaluated in this study.

2 Materials and Method

2.1 Biodiesel

The biodiesel is palm-based biodiesel which produced by transesterification with methanol were obtained from Biodiesel Pilot Plant, Faculty of Engineering Technology (FTK), University Tun Hussein Onn Malaysia (UTHM). The collected

biodiesel were filled in clean dark bottles made of plastics with a volume of 1,500 ml for further experimentations.

2.2 Soil

The soil samples were taken at campus area. The soil samples were collected in the range of 7–8 kg from the surface of 5–10 cm deep layer of soil. The collected soil samples were then put into the clean dark plastic containers with a volume of 5,000 ml for further experimentations.

2.3 *Pseudomonas putida* Broth Culture

Pure *Pseudomonas putida* ATCC 49128 were purchased from United States of America (USA) in dry culti-loop form. This *Pseudomonas putida* samples were stored in chiller at 4 °C prior to cultivation procedure. Approximately 16 g of medium (nutrient broth) was filled into the 2,000 ml Erlenmeyer flask containing 2,000 ml of distilled water. The mixtures were stirred gently and then dissolved by heating on hot plate at 100 °C for about 2 h until complete dissolution. After that, the medium was sterilized in autoclave at 121 °C for about 15 min. It was then allowed to cool down for a few minutes until its temperature drop in between 35 and 37 °C. One loops shaft was removed from the handle straight into the medium according to the manufacturer's instruction. The mixtures were then stirred until homogeneous and keep in the chiller at 4 °C for 48 h.

2.4 Soil-Biodiesel Mixture

Spill simulations with biodiesel in soil were carried out in accordance with Taylor and Jones [13], with modification. In brief, pure fuels biodiesel, B100 was added into the clean plastic containers with a volume of 5,000 ml containing 1,000 g of dried soil. The soil-biodiesel mixture samples were then inoculated with approximately 200 ml of 1.0×10^6 CFU/ml of *Pseudomonas putida* broth culture and placed in dark condition.

2.5 Enumeration of *Pseudomonas putida*

Approximately 25 g of inoculated soil samples were dissolved in 250 ml Erlenmeyer flask that containing 225 ml of sterilized distilled water. The flask was then shaken on orbital digital shaker with shaking speed of 200 rpm for approximately

Table 1 Summarized of physico-chemical results

Parameter	Sample			Standard	Reference
	Soil + <i>P. putida</i> (control)	Soil + B100 + <i>P. putida</i> (day 0)	Soil + B100 + <i>P. putida</i> (day 20)		
pH	7.99	7.71	7.30	6–7.5	USDA [14]
Total organic carbon (%)	0.060	0.048	0.045	0–0.05 %	Bohm et al. [15]
Total nitrogen (ppm)	18.34	16.75	5.23	5–15 ppm	
Sulfate (ppm)	28.32	25.85	18.69	5–20 ppm	
Phosphate (ppm)	0.377	0.324	0.085	0.5–0.9 ppm	
Moisture content, (%)	20.82 %	26.74 %	36.58 %	40–60 %	Bell [16]

30 min. After leave for sedimentation time approximately for 2 h, then 1 ml of supernatant from each flask was placed into sterile dilution bottles containing 9 ml of sterile distilled water in triplicate. Approximately 1,000 μ l of the dilutions series were carried out through membrane filtration procedure. The filter papers were placed onto warm Chromagar *Pseudomonas* media agar. The Chromagar *Pseudomonas* media agar was prepared according to manufacturer's instruction. Inoculated media agar has been incubated at temperature of 37 °C. After 24 h after incubation the colonies of *Pseudomonas putida* were counted.

3 Results and Discussion

Table 1 summarizes some of the physico-chemical results. In Day 0, some values of tested parameters obtained such as total nitrogen, sulfate, and phosphate are not in the range of the soil standard [14, 15]. However, the tested parameters obtained are in the range of soil standard guidelines, after treated with *Pseudomonas putida*. The study found that after 20 days of bioremediation, the removal were up to 69 and 27 % for nitrogen and sulphate, respectively. The nitrogen and sulfate was used by *Pseudomonas putida* to survive and perform its microbiological process and result in reduction of these parameters in the sample of B100. The pH of soil sample was changed from more alkaline (pH 7.71) to almost neutral (pH 7.3) after seeding with *Pseudomonas putida*. The moisture content of sample B100 was increased from 26.74 % (Day 0) to 36.58 % (Day 20) possibly due to the degradation of contaminants in the sample of B100 produced carbon dioxide (CO₂), water (H₂O) and biomass as a by-product of bioremediation [3]. Figure 1 shows that the bacteria colony has slightly increased from Day 2 (3.0×10^7 CFU/ml) to Day 8 (4.1×10^7 CFU/ml). Additional carbon source offered from biodiesel may lead to increase of *Pseudomonas putida* growth. However, after Day 8, the amount

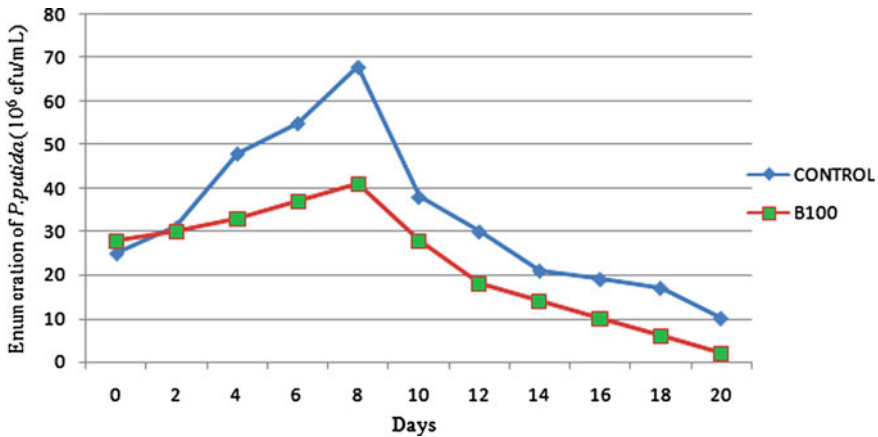


Fig. 1 The survival of *Pseudomonas putida* (10^6 CFU/ml) for sample of B100 and control

of colony *P. putida* starts to deplete up to 1 Log until Day 20 (4.0×10^6 CFU/ml). The depletion colony *Pseudomonas putida* might be due to the availability of nutrient in the sample that become low once the bacteria has used them as source of carbon and energy. Nevertheless, the amount of *Pseudomonas putida* is still high which is at 10^6 CFU/ml even until up to Day 20. This result indicated that the *P. putida* survival is high. The growth of bacteria was elevated high in control sample than B100 sample until Day 20.

4 Conclusion

Based on the obtained data it is concluded that *Pseudomonas putida* was effective microorganism and suitable as oil-soil biodegradable agent. Physico-chemical tests proved there is indication of nutrient consumed in soil-biodiesel mixture after 20 days of bioremediation. The bioremediation treated level of nutrients content which is initially comes from biodiesel contamination. The *Pseudomonas putida* was suitable for the bioremediation of biodiesel-soil contamination based on these survival results. Future study was recommended by prolonged time length of bioremediation for necessary optimum survival rate of *Pseudomonas putida* in biodiesel-soil contamination.

Acknowledgments We are grateful to the Incentive Research Grant (Vote 1192) and Research Acculturation Grant Scheme (Vote R002) from Research & Innovation Centre UTHM for financial supports of this work.

References

1. A. Elazhari-Ali, A.K. Singh, R.J. Davenport, I.M. Head, D. Werner, Biofuel components change the ecology of bacterial volatile petroleum hydrocarbon degradation in aerobic sandy soil. *Env. Pollut.* **173**, 125–132 (2013)
2. G. Purcella, Do it yourself guide to biodiesel: your alternative fuel solution for saving money, reducing soil oil dependency, helping the planet (Ulysses Press, Berkeley, 2008), pp. 33–34
3. A. Pinto Mariano, R. Clayton Tomasella, L. Marcondes de Oliveira, J. Contiero, D.F de Angelis, Biodegradation of biodiesel/diesel blends. *Afr. J. Biotechnol.* **7**(9), 1323–1328 (2008)
4. R. Kucerova, Application of *Pseudomonas putida* and *Rhodococcus* spp. by biodegradation of PAHs, PCBs and NEL soil samples from the hazardous waste dump in Pozdatky. *Min. Geol. Pet. Eng. Bull.* **18**, 97–101 (2006)
5. E.Z. Ron, E. Rosenberg, Biosurfactants and oil bioremediation. *Biotechnology* **13**(3), 249–252 (2002)
6. M.T. Balba, Bioremediation of oil- contaminated soil: microbiological methods for feasibility assessment and field evaluation. *J. Microbiol. Methods* **32**(2), 155–164 (1998)
7. P.C Ignacio, B. Judith, D. Katrin, M.D.S Vitor, W. Christoph, Industrial biotechnology of *Pseudomonas putida* and related species. *Appl. Micro. Biotechnol.* **93**, 2279–2290 (2012)
8. A.K. Haritash, C.P. Kaushik, Biodegradation aspects of polycyclic aromatic hydrocarbons (PAHs): a review. *J. Hazard. Matter* **169**, 1–15 (2009)
9. K. Timmis, *Pseudomonas putida*: a cosmopolitan opportunist par excellence. *Environ. Microbiol.* **4**, 779–781 (2002)
10. J.C. Pasqualino, D. Montane, J.S Salvado, Effects of biodiesel in the biodegradability of fossil-derived fuels. *Biomass Bioenergy* **30**, 874–879 (2006)
11. D. Walker, L. Petrakis, R. Colwell, Comparison of biodegradability of crude oil and fuel oils. *Can. J. Microbiol* **22**, 598–602 (1976)
12. S.B. Hamed, A. Maaroufi, A. Ghram, B.A.G. Zouhaier, M. Labat, *Afr. J. Biotechnol.* **12**(14), 1636–1643 (2013)
13. L.T Taylor, D.M. Jones, Bioremediation of coal tar PAH in soil using biodiesel. *Chemosphere* **44**, 1131–1136 (2001)
14. H.L. Bohm, B.L. McNeal, G.A. O'Connor, *Soil Chemistry*, 3rd edn. (Wiley, USA, 2001), p. 307
15. N. Bell (2003). Improving garden soils with organic matter. Extension service, Oregon State University (OSU), pp. 7–8
16. The United States Department of Agriculture Natural Resources Conservation Service (USDA), *Soil survey staff*, *keys to soil taxonomy*, 8th edn. (Natural Resources, Washington DC, 1998)

The Quality of Kenaf Retting Water After Retting Using *Bacillus cereus* for Fiber Extraction

Mohd Nazrin Othman, Ramlah Mohd Tajuddin, Zakiah Ahmad and Mohd Fozi Ali

Abstract The aim of this study was to compare the water quality of wastewater from kenaf retting process with and without the use of *Bacillus cereus*. The retting process duration was 1 week. The reading on temperature, pH, turbidity, dissolved oxygen (DO), Biochemical Oxygen Demand (BOD), Chemical Oxygen Demand (COD), suspended solid (SS) and ammonical nitrogen (NH₃-N) was taken daily during the retting period. The end result of the wastewater quality was then compared.

Keywords Kenaf · Water retting · Water quality · *Bacillus cereus*

1 Introduction

For over 6000 years kenaf (*Hibiscus cannabinus* L., Malvaceae) was primarily used as a cordage crop and secondarily as a livestock feed [1]. Retting process is a method use in order to loosen up the fiber so that it can be extract from the stalk. In the retting process, the long stalk of the plant were cut at ground level before being tied up in the bundle and immersed in slow moving water, ponds or tanks. Once

Universiti Teknologi MARA (UiTM) and under grant Lembaga Kenaf dan Tembakau Negara (LKTN) with reference number 100-RMI/GOV 16/6/2 (5/2012) (sponsor).

M. N. Othman (✉) · R. M. Tajuddin · M. F. Ali
Department of Water Resources and Environmental System, UiTM, Shah Alam, Malaysia
e-mail: nazrinoth88@yahoo.com

Z. Ahmad
Institute of Infrastructure and Sustainable Engineering Management, Faculty of Civil Engineering, UiTM, Shah Alam, Malaysia

the retting process is complete, the fiber was pulled out from the stalk and allowed to dry under the sun.

The length of retting period, as reported in the literature, varies considerably from 5 to 22 days [2, 3] before the fiber was ready for extraction. In order to shorten the retting time a bacteria from *Bacillus* sp. which is *Bacillus cereus* ATCC2 was added into the retting water. From previous studies, large numbers of Firmicutean bacteria of the genus *Bacillus*, viz., *B. subtilis*, *B. polymyxa*, *B. mesentericus*, *B. cereus* and *B. macerans*, and anaerobic bacteria of genus *Clostridium*, viz., *C. tertium*, *C. aurantibutyricum*, and *C. felsineum* have been isolated from retting water, along with large numbers of Gram-negative genera such as *Erwinia* and *Pseudomonas* [4]. *Bacillus* sp. was known to produce pectinolytic enzyme, an enzyme which produce by plant-pathogenic bacteria and fungi. These enzymes are essential in the decay of dead plant material by nonpathogenic microorganism thus assist in recycling carbon compounds in biosphere [5]. Previous study shows that activities of polygalacturonase (PG) produced by *Bacillus* sp. strains were higher than those produce by *Aspergillus niger* [6], *Aspergillus* sp. and *A. niger* ATCC 20107 [7], *Aureobasidium pullulans* [8] and *Tubercularia vulgaris* [9].

B. cereus is a spore-forming bacteria, Gram positive, aerobic or facultatively anaerobic [10]. *B. cereus* are closely related to *B. thuringiensis* and *B. mycoides* and known to cause food poisoning or spoilage because they can survive mild heat treatment [11, 12]. Its pathogenicity is linked to the production of two toxins; a thermostable emetic enterotoxin [13] and a thermosensitive diarrhoegenic enterotoxin [14]. It is generally admitted that a population of more than 10^5 bacteria per gramme is required for intoxication to occur [13]. Its ability to sporulate makes it quite resistant to heat treatment [10].

Water quality of the retting water was change due to the retting process. The degradation process produces smell and also change in color of the water use for retting. The use of *B. cereus* in the retting process do shorten the time but may cause the water to be more polluted than using tap water. In this paper, the quality of retting water with and without bacteria was compared.

2 Method

Bacillus cereus ATCC2 was bought from Next Gene. The *B. cereus* was activated for 24 h before starting the lab works. 500 ml of Luria–Bertani (LB) broth, Miller (AMRESCO) was prepared. The *B. cereus* was aseptically transferred into the LB nutrient broth. The LB broth containing *B. cereus* was put in the incubator with shaker. The shaker was set at 120 rpm and the *B. cereus* was incubated for a week at room temperature. Two retting tank measured $42 \times 24.5 \times 30$ cm was used in the retting process. The fresh kenaf plant was obtained from National Kenaf and Tobacco Board (LKTN). The stalk of kenaf was measured up to 40 cm before it were cut. The kenaf weight for each tank was ± 1.250 kg. 24.5 L and 500 ml of

nutrient broth containing *B. cereus* was added on one tank and 25 L of tap water was added into the other tank. The kenaf stalk was immersed and retted for a week. The temperature, pH, and turbidity was checked by using HORIBA Water Checker U-10, Type 440-220, HORIBA Ltd while DO, BOD₅, COD, SS and NH₃-N was taken daily using Hach Standard method. All the parameter was taken daily for 1 week retting duration.

3 Result and Discussion

Tables 1 and 2 shows the result of the retting process in 1 week duration. From the observation, the color of water changed from clear to murky for both tap water and water seeded with *B. cereus*. The waters started to emit little smell on the second days of retting. However, the smell started to build up at day 4 in retting tank containing tap water and foul-smell was emitted from retting tank containing *B. cereus* seeded water on day 5. Both waters get murkier as the days goes by. From the tables, the demand of oxygen for Day 0 was higher in the *B. cereus* seeded water which was 21.33 mg/l compared to tap water which was 0.58 mg/l. These can be explained by the need of oxygen for biochemical process for carbohydrate and protein breakdown by *B. cereus*. The low reading of BOD₅ for tap water could possibly cause by the low concentration of microorganism that came from the air or maybe from the kenaf stalks itself. Also the reading of COD from tap water also shows the lowest reading which was 109 mg/l compare to *B. cereus* seeded water which was 475 mg/l. The concentration of NH₃-N for tap water for Day 0 was lower than *B. cereus* seeded water which read 15.4 mg/l. As for suspended solid the reading was 0.6 and 14.3 mg/l respectively for tap water and *B. cereus* seeded water for Day 0. The turbidity of tap water was 0 NTU. This could possibly mean that the water was clean that the amount of suspended solid in the water too low that the turbidity is unmeasurable. For *B. cereus* seeded water however, the reading was 1.0 NTU. This could be possibly cause by the broth and the concentration of *B. cereus* in the water. As for pH, for day 0, both readings were above 7.0 which 7.4 for tap water and 7.6 for the seeded water. Both type of water were cleared for Day 0. As days went by from Day 0 to Day 7, the concentration of DO start to dropped On Day 7, the concentration of DO for tap water was reduced from 7.56 to 6.02 mg/l while for *B. cereus* seeded water, the concentration of DO was reduced from 7.13 to 4.95 mg/l. The trend of BOD₅ tap water was that the reading escalated from 0.58 to 21.57 mg/l before slowly decreased steadily to 17.79 mg/l on Day 7. As for *B. cereus* seeded water the trend of BOD₅ was that it decreased sharply from 21.33 to 18.57 mg/l before it gradually decreased and have a sudden increased on Day 5 before started to decrease again. Possible explanations for this trend were that the consumptions of oxygen for breaking down nutrients compound was not high enough to in tap water. As for *B. cereus* which is facultative anaerobic, it was able to breakdown nutrient when the concentration of dissolved oxygen reached where it no longer able to use oxygen as energy to generate ATP for nutrient breakdown. COD for tap water increased gradually over time. For *B. cereus*

Table 1 Data of water quality for tap water during retting period

Water type	Water quality parameter	D ₀	D ₁	D ₂	D ₃	D ₄	D ₅	D ₆	D ₇
Tap water	DO ₀ (mg/l)	7.56	7.21	6.97	6.93	6.67	6.40	6.24	6.02
	DO ₅ (mg/l)	6.98	0.02	0.03	0.03	0.07	0.02	0.02	0.09
	BOD ₅ (mg/l)	0.58	21.57	20.82	20.70	19.80	19.14	18.66	17.79
	COD (mg/l)	109	174	303	462	685	1,110	1,260	2,150
	NH ₃ -N (mg/l)	0.21	1.32	2.33	3.00	5.55	5.13	5.60	6.60
	SS (mg/l)	0.6	13.3	17.3	21.3	39.6	40	80	63.3
	Turbidity (NTU)	0	1.0	2.0	2.0	2.0	3.0	4.0	6.0
	pH	7.4	5.9	5.7	5.7	5.5	5.3	5.1	5.3
	Temp (°C)	28	27	27	27	28	28	27	28
	Water observation	Clear	Murky	Murky with little smell	Murky with little smell	Murky with little smell	Murky with smell	Murky with smell	Murky with smell

Table 2 Data of water quality for *B. cereus* seeded water during retting period

Water type	Water quality parameter	D ₀	D ₁	D ₂	D ₃	D ₄	D ₅	D ₆	D ₇
<i>Bacillus cereus</i>	DO ₀ (mg/l)	7.13	6.23	6.10	6.00	5.97	6.15	6.12	4.95
	DO ₅ (mg/l)	0.02	0.04	0.01	0.02	0.02	0.02	0.01	0.04
	BOD ₅ (mg/l)	21.33	18.57	18.27	17.94	17.85	18.39	18.33	14.73
	COD (mg/l)	475	320	660	1,226	886	1,336	1,233	1,633
	NH ₃ -N (mg/l)	15.4	19.3	22.1	23.8	27.7	27.9	26.9	26.0
	SS (mg/l)	14.3	23.3	60	60	153.3	133.3	180	186.6
	Turbidity (NTU)	1.0	1.5	4.0	8.3	8.0	12.0	16.0	28.0
	pH	7.6	6.3	6.0	5.9	5.6	5.5	5.2	5.7
	Temp (°C)	28	27	27	27	28	28	27	28
	Water observation	Clear with light gold color	Murky	Murky with little smell	Murky with little smell	Murky with little smell	Murky with little smell	Murky with foul-smell	Murky with foul-smell

Fig. 1 Trend of BOD for tap water and *B. cereus* seeded water during retting period

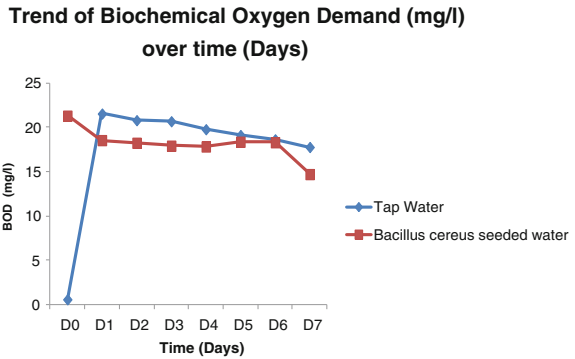


Fig. 2 Trend of COD for tap water and *B. cereus* seeded water during retting period

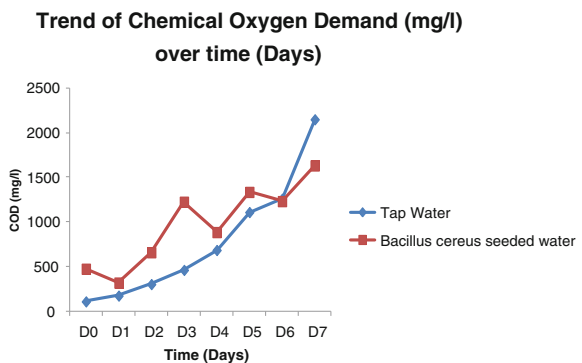
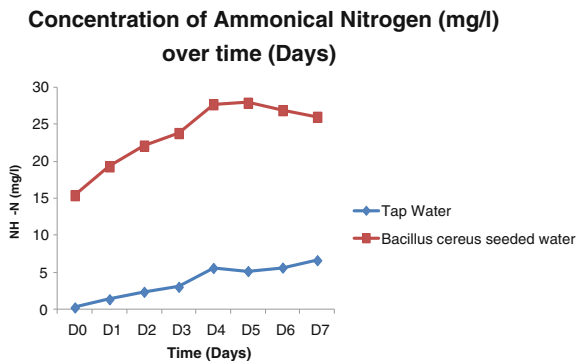


Fig. 3 The concentration of ammonical nitrogen for tap water and *B. cereus* seeded water during retting period



seeded water the reading of COD was much more random. The production of $\text{NH}_3\text{-N}$ by *B. cereus* seeded water was higher than tap water as expected. Also the turbidity and suspended solid reading from *B. cereus* seeded water also higher than tap water. This can be seen that the amount of discarded barks that suspended at the bottom of the tank with *B. cereus* is higher than the tank with tap water only. As for pH, both of

Fig. 4 The concentration of suspended solid for tap water and *B. cereus* seeded water during retting period

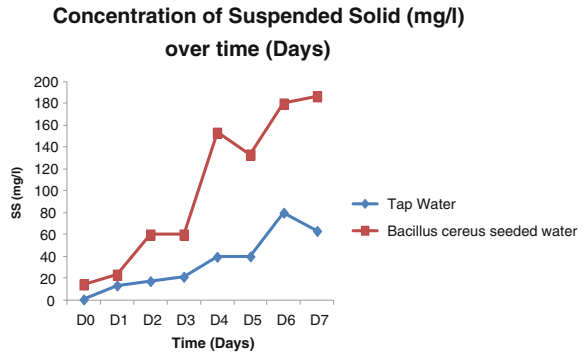


Fig. 5 Turbidity of tap water and *B. cereus* seeded water during retting period

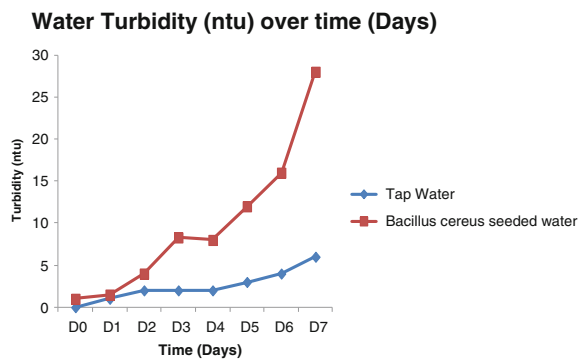
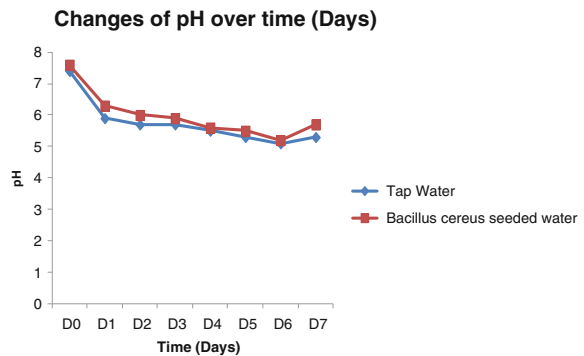


Fig. 6 Changes of pH for tap water and *B. cereus* seeded water during retting period



water type shows decreasing in the reading but have slightly increased on Day 7. These can be explained by the activity of pectinolytic enzyme known as Exo-PGases which produce digalacturonic acid as the main end product [15, 16]. The temperature of water in both tank, however, have the same reading throughout the experiment. Figures 1, 2, 3, 4, 5, and 6 showed more clear comparison of each parameter for both

types of water. According to Interim National Water Quality Standards for Malaysia, both waters can be classified as Class V as most of the parameter meets the Class V classification.

4 Conclusion

As the conclusion, it is clear that from the results obtained and observation the quality of wastewater from retting process using the *B. cereus* was worse than the quality of wastewater from using only tap water. From the comparison the BOD₅, COD, NH₃-N, SS, Turbidity of *B. cereus* seeded water was the highest compared to tap water. Also the DO and pH for *B. cereus* seeded water was lower compare to tap water. The wastewater generated from retting process can be classified as Class V. Thus, it was recommended that the wastewater to be treated first priority to the water which contained the bacteria which were pathogenic.

Acknowledgments The financial support and kenaf supply from National Kenaf and Tobacco Board (LKTN) and Universiti Teknologi MARA, Malaysia is thankfully acknowledged.

References

1. J.M. Dempsey, Fiber Crops (The Univ. Presses of Florida, Gainesville, 1975)
2. I.B. Pole-Evans, South African fibre plants I. Ambari or Deccan hemp: *Hibiscus cannabinus* L. So. Afr. Jour. Ind. **1**, 198–208 (1917)
3. S.A.G. Caldwell, Sunn and Bombay hemps. Text. Mfr **62**, 455–466 (1936)
4. Z. Ahmed, F. Akther, Jute retting: an overview. Online J Biol Sci **1**, 685–688 (2001)
5. P. Albershiem, Pectin lyase from fungi. Meth. Enzymol **8**, 628–631 (1966)
6. S.S. Pereira, E.F. Torres, G.V. Gonzales, M.G. Rojas, Effect of different carbon sources on synthesis of pectinase by *Aspergillus niger* in submerged and solid fermentations. Appl. Microbiol. Biotechnol. **39**, 36–41 (1993)
7. G. Larios, J.M. Garcia, C. Huiton, Endopolygalacturonase production from untreated lemon peel by *Aspergillus* sp. CH-Y-1043. Biotechnol. Lett. **11**, 729–734 (1989)
8. F. Federici, M. Petruccioli, Growth and polygalacturonase production by *Aureobasidium pullulans* on orange peel waste. Microb. Alim. Nutri **3**, 39–46 (1885)
9. M.J.V. Fonseca, S. Said, The pectinase produced by *Tubercularia vulgaris* in submerged culture using pectin or orange-pulp pellets as inductor. Appl. Microbiol. Biotechnol. **42**, 32–35 (1995)
10. E. Chorin, D. Thuault, J. Cleret, C. Bourgeois, Modelling *Bacillus cereus* growth. Int. J. Food Microbiol. **38**, 229–234 (1997)
11. K. Koo, P.M.N. Foegeding, H.E. Swaisgood, Development of a streptavidin-conjugated single-chain antibody that binds *Bacillus cereus* spore. Appl. Environ. Microbiol. **64**(7), 2497–2502 (1998)
12. K.P. Francis, R. Mayr, F. von Stetten, G.S.A.B. Stewart, S. Scherer, Discrimination of psychotrophic and mesophilic strains of the *Bacillus cereus* group by PCR targeting major cold shock protein genes. Appl. Environ. Microbiol. **64**(9), 3525–3529 (1998)

13. K.M. Johnson, *Bacillus cereus* foodborne illness-an update. *J. Food. Protect* **47**, 145–153 (1984)
14. J.M. Goepfert, W.M. Spira, H.U. Kim, *Bacillus cereus*: food poisoning organism. A review. *J. Milk Food* **35**, 213–227 (1972)
15. R.S. Jayani, S. Saxena, R. Gupta, Microbial pectinolytic enzyme: a review. *Process Biochem.* **40**, 2931–2944 (2005)
16. T. Sakai, T. Sakamoto, J. Hallaert, E.J. Vandamme, Pectin, pectinase and protopectinase: production, properties and applications. *Adv. Appl. Microbiol.* **39**, 231–294 (1993)

Part IX
Synergistic Innovative Management

Sustainable Considerations in the Operation of Onsite Construction Equipments and Vehicles: A Malaysian Perspective

M. Waris, Mohd. Faris Khamidi and Arazi Idrus

Abstract Construction industry is mainly accountable for high energy consumption, greenhouse gas emissions, waste generation and land consumption. The emerging notion of sustainability in construction has led towards the acceptance of practices which endure human well being, energy conservation, efficiency and economics of the system. Precedent research has shown that the focus of sustainable literature was mostly on selection of construction materials and their impacts, along with the operational phase. However, during the construction phase, emissions from the onsite equipment and machineries are also the main contributor of environmental risk and hazards. Thus, mitigating these impacts is one of the important aspects of sustainable planning for onsite construction activities. This paper reports on the findings of a study for consideration of sustainable practices in the operation of onsite construction equipments in Malaysia. A questionnaire survey was conducted among a classified group of Class G7 contractors of Construction Industry Development board (CIDB). The result shows that the respondents are well aware with the understanding of sustainable construction. Nevertheless, the environmental friendly practices for the utilization of onsite heavy construction equipment and vehicles are not highly adopted by the contractors. The research findings will also help to explore a number of specific activities that could be practiced for showing commitment to sustainable acquisition and use of construction equipments.

M. Waris (✉)

PhD. Student, Department of Civil Engineering, Universiti Teknologi PETRONAS,
31750 Tronoh, Malaysia
e-mail: alwaris2002@yahoo.com

Mohd. F. Khamidi

Senior Lecturer, Department of Civil Engineering, Universiti Teknologi PETRONAS,
31750 Tronoh, Malaysia

A. Idrus

Professor, Department of Civil Engineering, National Defence University of Malaysia,
57000 Kuala Lumpur, Malaysia

Keywords Managing sustainable construction · Onsite equipment usage · Sustainability

1 Introduction

The emerging concept of sustainable construction in recent years has led to the need of innovative techniques to align construction activities with the dimensions of sustainable development. Construction organizations are accountable for the impacts of an implemented project on the society, environment and economy long after the project has been completed. Therefore, construction and sustainable development issues are closely related because this sector is a principal contributor to global resource depletion [1]. As an example, in the European Union, buildings are accountable for more than 40 % of the total energy consumption and construction sector is estimated to generate approximately 40 % of all man-made waste [2]. Sustainable development has now become a significant subject discussed and debated at various levels e.g. national, international, governmental, non-governmental and as well within the academic circles as an agenda of socio-economic and environmental development. A fair amount of diversity is existed among the definitions of sustainability and sustainable development. However, most of them agree that the concept is based on the three pillars i.e. social, environmental and economy [3]. The most common and famous definition for sustainable development is defined as “Satisfaction of present needs without compromising the ability of future generations to meet their own needs” [4]. Sustainability is, therefore, considered as an ultimate objective where balance in socio-economic activities and environmental concerns are appropriately addressed. The concept of sustainability in construction is reviewed by many researchers and its focus keeps on shifting in past several years. Sustainable construction is a broad term and it includes the whole process from the basic and detailed design, engineering, planning and procurement, construction towards the approved deliverable to the client and then the different stages over the product’s lifetime which consisted of operation, maintenance, refurbishment, re-construction, demolition and recycling [5]. International Council for Research and Innovation in Building and Construction (CIB) in the agenda 21 emphasized on the notion of sustainable construction through environmental, socio-economic and cultural aspects. This agenda has identified many vital issues and challenges such as, management and organization; product and building issues and resource consumption in construction [2]. Thus, this paper particularly aims to address sustainability concerns due to the operation of onsite mechanized construction equipments.

2 Sustainable Views in Construction Industry

The concept of sustainability is about considering the full life-cycle of a project. It not only consists of project life cycle, but also the asset and product life cycle that must be taken in account from the conception phase till the completion and disposal [3]. The concept of sustainability in construction industry is reviewed by many researchers and its focus keeps on shifting in past several years. Table 1 shows a summary that how the concept of sustainability evolves in the construction industry. It is apparent from the above table that the views and concepts varies on sustainability according to the focal points of precedent researchers. However, the differences have somehow the same meaning in order to address the future well-being of the ecology and its inhabitants [6]. Sustainable construction is a broad term and it includes the whole process from the basic and detailed design, engineering, planning and procurement, construction towards the approved deliverable to the client and then the different stages over the product's lifetime which consisted of operation, maintenance, refurbishment, re-construction, demolition and recycling [5].

3 Onsite Mechanized Practices in Construction

After the World War II, the growing need of infrastructure and industrialization has changed the manual methods with the mechanized and equipment based in order to meet the shorter timelines and complexities of designs. During this era, construction equipment capacities were also increased with the innovation of torque convertor and power shift transmission system. The old concrete batch and mixing facilities were replaced from manually controlled to hydraulically and electronically controlled systems [16]. As a results of this incremental development in construction technology, today's construction projects are highly mechanized and becoming more so every day [17]. The role of construction machineries are being increasing to improve the performance, productivity, working standards and efficiency of contractors [18]. These require innovative and modern machineries to cater the needs of the clients and contractors and achieved project objectives [19]. Furthermore, the growing industrialization in construction leads to offsite prefabrication of concrete, structural and finish elements that are then installed or assembled rather than produced on site. Consequently, production equipment is being replaced on the construction site by earth moving, transportation and other material handling equipments [20]. The typical construction site will employ several or all of the following equipment types: such as earthmoving equipments, transporting equipments, material handlers, concrete pumps, hoists and lifts cranes etc. [21]. Researchers have suggested that the adoption of mechanized practices speed up the execution of site works, thus shorten the project completion time and cost. Many manual methods are getting obsolete and

Table 1 Summary of sustainable views in construction industry

Study	Year	Focus
Boostra and Tossavainen [7]	1998	Minimize energy demands during construction and operation and use of renewable energy
Cole and Larsson [8]	1998	Green building, environmental issues and CO ₂ emissions
Hakkinen, Huovila, Bordeau and Nibel [9]	2002	Construction process and indicators of sustainable construction
Brophy and Lewis [10]	2005	Procurement procedure, management issues, valuating of assessment methods
Nair et al. [11, 12]	2005	Socio-cultural, economic technologic and environmental factors including strategies
Kibert [13]	2005	Green building design and delivery
Persson et al. [14]	2008	Cultural and social context of society
Cheng, Pouffary, Svenningsen, and Callaway [15]	2008	Sustainable building and construction initiative

redundant in industrialized countries due to expansive and shortage of skilled labour [19, 22, 23]. The construction projects are usually classified in to residential, commercial, industrial and heavy works [24]. Therefore, each of these categories has its own level of equipment usage. For example residential projects have a light level of equipment use. It requires simple and traditional machines like fork-lifters, backhoe, hauling and hoisting equipments, material handling along with pneumatic tools. Commercial projects have moderate use of equipments and machineries. Industrial and heavy construction projects required intense and high utilization of machinery for carrying out mass excavation, stabilizing, compacting, asphalt paving and finishing, pipelines, railroads and many other special activities [25]. In the last 50 years, architects and civil engineers have delivered gigantic and huge infrastructure around the globe. It can be stated without any doubt that such enormous achievements in modern civilization cannot be possible without the aid of mechanized construction practices.

4 Environmental, Health and Safety Implications of Mechanization

In the construction industry, various efforts have been exerted to evaluate environmental impacts associated with raw materials to recycling or disposal. Most of these studies have been concerned with energy inventories—“the phase of life cycle assessment involving the compilation and quantification of input and output (ISO 1998)”—and Greenhouse Gas Emissions (GHG) emissions across various stages of the structure’s life cycle [26]. However, GHG emissions from onsite equipment usage during the construction phase have not been fully investigated in

the precedent literature. It is not clear which work type, equipment, or activity is the main source of emissions from onsite equipment during construction [27]. All non-road construction equipments, machineries and vehicles which are power-driven by diesel engine have a high impact on environment. The emissions from these equipments are considered as source of air pollution. The United States Environmental Protection Agency (EPA) stated that the US construction industry is comprised of approximately 2 million equipments, machineries and vehicles which are powered by diesel engine. These engines are operated by fossil fuel, hence discharge significant amount of carbon dioxide, hydrocarbons and particulate matter. EPA report further exemplifies that a road bulldozer with an engine capacity of 175 hp releases particulate matter which is equal to the emissions produced by 500 new auto mobiles [28]. In United States, 5,839.3 million metric tons (MTs) of CO₂ is produced by the usage of fossil fuels to operate heavy construction equipments in 2008 [29]. According to the Korean National Institute of Environmental Research (2009), air pollutant emissions from onsite construction equipment account for 6.8 % (253, 058 MTs/year) of the overall emissions produced in Korea. The main component in such emissions is carbon dioxide, which affects climate change [30]. The average rate of production of emissions is much greater for construction equipments as compared to passenger vehicles because of differences in the fuel type i.e. diesel versus gasoline, engine technology and horse power [31]. Equipment categorization, age and horsepower and as well as type of fuel used, can greatly affect rates of emissions [32]. The former studies have focused on other categories such as material selection, structure design, and materials recycling [27]. Furthermore, previous efforts to reach sustainability have primarily focused on the environmental performance of facilities in the “use” phase, and such efforts are lately being expanded to mitigate environmental impacts from the “construction” phase [33]. Among the environmental impacts from construction processes (e.g., waste generation, energy consumption, resource depletion, etc.), emissions from construction equipment account for the largest share (more than 50 %) of the total impacts [34]. Based on the previous study, it was determined that during construction phase, earthwork produces highest percentage of GHG emissions [27]. Controlling these emissions is therefore a critical step in the environmental management of construction processes. Mechanized practices are also associated with the accidents and injuries of workers at the site. Past studies have established that construction equipments, plant and machineries are major causes of site accidents and injuries [17, 35]. In many developed countries, accidents and mishaps rates are higher in construction as compared to other industries. For example, in United States construction industry is also prone to fatal accidents. It accounts more than 22 % of injuries [36]. UK construction industry is also recorded as most hazardous and risky in terms of health and safety of workers. During the last 25 years, more than 2,800 deaths have been traced in construction related activities [37]. In contrast to this, the fatality rate in developing countries like Nigeria, Thailand, and Tanzania are much higher than many European countries. This is due to the fact that health and safety considerations are kept at the lowest priorities in executing construction activities [38]. The increased level of awareness and the application of mechanized equipments and machineries are considered as a

positive thrust for the advancement of construction industry. Despite the fact that it has abundant benefits for the stake holders. Nevertheless, its adoption has certain drawbacks for the environment and the people working in its vicinity. Therefore, it is very much important for the designers, planners, clients and contractors to rethink their policies and practices in order to reduce the environmental impacts and also save their fuel and money.

5 Sustainable Usage of Onsite Equipments and Vehicles

The growing need of environmental concerns and legislations has led to adoption of emissions reduction techniques and safe operation of construction equipments and vehicles. Usually, it has been considered that sustainable practices are much expensive and require sufficient amount of budget for practicing effectively. Therefore, United States Environmental Protection Agency (EPA) has emphasized the adoption of emission reduction practices by offering certain incentives to the operators [32]. In this context, Voluntary Diesel Retrofit Program, Carl Moyer Program and Texas Emissions Reduction Plan are noteworthy efforts that were initiated as incentive programs in order to reduce the greenhouse gas emissions. Under these programs, operators of the construction equipments are encouraged and offered incentives to adopt environmental friendly practices for achieving low carbon emissions. These incentives were offered for those operators who promote the use of exhaust treatment devices, reduce idling time, upgrade their engines, use ultra low sulphur, bio-degradable fuel and keep their equipments in good working condition [39]. The precedent research shows that the proper selection of construction equipment and machineries can also be helpful to reduce GHG emissions. As, GHG emissions are directly related to the operation of equipment. The more the operating hour of machinery, the higher the energy consumption and hence more will be the rate of emissions [27]. The Dutch Government has introduced sustainable criteria for the procurement of heavy duty equipments and vehicles. This criterion embarks procedures and guidelines for ensuring green practices in hiring, operation and maintenance of non-road vehicles and equipments [40].

6 Research Objective

In Malaysia, the Green Technology Programme (GTP) was initiated by Construction Industry Development Board (CIDB) in 1999. It is an environmental development program for achieving good environmental practices in the construction industry [41]. Keeping this in view, the main objective of this research paper is to determine the level of awareness and adoption of sustainable practices by the Malaysian contractors in the acquisition and use of onsite construction equipments and machines.

7 Methodology

The primary data required for this study was collected through questionnaire survey. This methodology is considered as a cost effective and time saving in order to achieve better results in shorter duration. The traditionally techniques for collecting responses from the targeted respondents are postal mails, fax and electronic mails. However, for this research work a web survey tool was used effectively for getting feedbacks from the respondents. This has helped us a lot in achieving momentum and a good data base of the survey participants. For the purpose of achieving the desired research objectives, a structured or close-ended questionnaire was designed to gain the views from the industry practitioners. A total number of 400 Class A, Grade G7 civil contractors (Kuala Lumpur and Selangor based) were randomly selected from CIDB database. Grade G7 are large contractors and usually engaged in heavy and complex construction activities with no limit. Hence, they are more familiar with the phenomenon of sustainable practices for onsite construction activities. Before sending the questionnaire, it was dully confirmed and assured that all the targeted respondents are doing construction business and engage in civil and infrastructure works. According to the MBAM survey that despite a high percentage of contractors in Malaysia, only 12 % are actually running construction business [42].

8 Results and Analysis

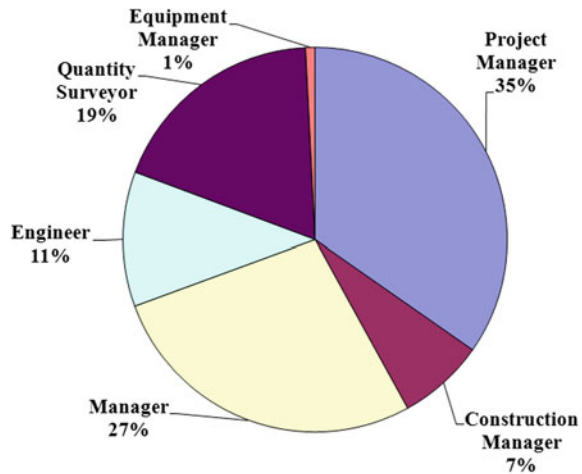
A total of 86 completed questionnaires were received out of 400 giving an overall response rate of 21.5 %. The findings of the survey are as follows;

8.1 Background and Experience of the Respondents

The data analysis indicates that most of the responses are from project managers. It accounts 35 % of the feedbacks as compared to the other categories of respondents. Figure 1 shows their pie-chart distributions of respondents.

Figure 2 shows the involvement of construction firms in different infrastructure projects. It has been observed that majority of the respondents i.e. 60.5 % are participating in roads and highways projects (It is to be noted that respondents are provided more than one options to select in this question of the survey). The result of the survey shows that 88 % of the respondents have completed their bachelor's education. Some of the respondents have also acquired additional postgraduate qualifications i.e. Master of Science or Master of Engineering degree with a percentage of 3.25 and 4.8 % respectively. This reveals that the respondents have a

Fig. 1 Distribution of respondents primary job function



good academic background and satisfactory knowledge for providing sufficient details and inputs for the outcome of this research work.

Analysis of the feedbacks also shows that 31.5 % of the respondents have working experience within the range of 11–20 years, while 22.6 % have more than 20 years of field experience. The respondents whose working experience is between 6 and 10 years are 21 %. Rest of the 25 % respondents has less than 5 years experience in construction projects. These statistics represent that questionnaires are mostly filled by the experienced and senior professionals having vast experience in construction projects. Their opinions and views are quite important and reliable in order to establish the findings.

8.2 Knowledge of Sustainable Construction

In order to implement the sustainability in construction projects, the understanding and knowledge of professionals is mandatory. The response of the questionnaire survey indicates a good understanding of Malaysian contractors towards sustainable construction practices. The current level of knowledge with the sustainable construction practices is shown in Fig. 3 as pie-chart distribution. It shows that 85 % of the respondents claimed that they have sufficient knowledge of sustainable concepts, where as 14 % have insufficient with this phenomenon. Apart from that, 1 % of the respondents are undecided and not aware with the notion of sustainability.

In Malaysia, going green in construction is being very much emphasized by the Government. Under the 10th Malaysian Plan, the Government has started many initiatives for achieving sustainable socio-economic and environmental development [24]. However, the successful implementation of green practices will be the

Fig. 2 Respondents participation in infrastructure projects

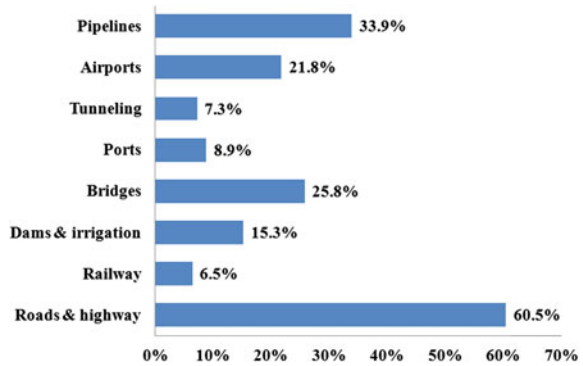
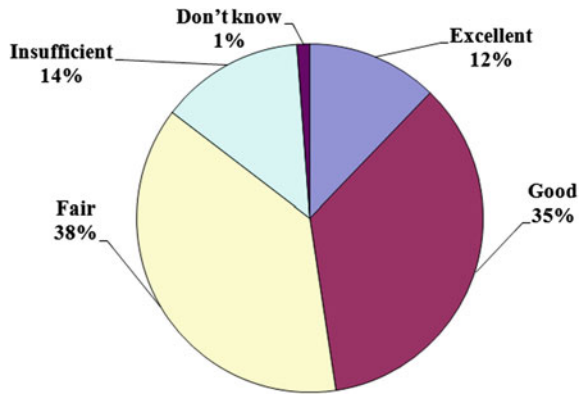


Fig. 3 Knowledge in sustainable construction



joint responsibility of private sector as well. All these efforts will not be fruitful, until the Government and the private sector does not collaborate and participate for showing their concern towards sustainable agenda. The respondents feedbacks show that both the Government and private sector are considered equally responsible for achieving sustainability in construction industry. Figure 4 shows percentage of responses as pie chart distribution.

The research survey further examines the respondents view about the importance of sustainability practices in the acquisition and use of mechanized construction equipments. The respondents were asked that whether the considerations of sustainability aspects are important issue in mechanized construction.

The result reveals that importance related to sustainability was high, as 83 % are in agreement that sustainable considerations are important issue and to be considered in the procurement and operation of construction equipment and vehicles. Table 2 shows the agreement of respondents to sustainably considerations.

Fig. 4 Percentage distribution of responsibility towards sustainability

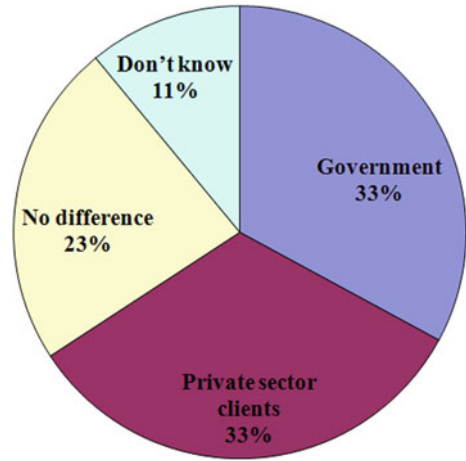


Table 2 Sustainable considerations in mechanized construction

S.No.	Level of importance	Percentage (%)
1	Yes	83
2	No	7
3	Don't know	10
Total		100

8.3 Sustainable Practices for Onsite Construction Equipments and Vehicles

A number of sustainable practices for the operation of onsite construction equipments have been suggested in the precedent literature (Table 3). Hence, their level of adoption in the Malaysian construction industry is evaluated via this research survey. This study has used 5-point Likert scale (with 1 = never, 2 = seldom, 3 = sometimes, 4 = regularly and 5 = highly) to measure the commitment of respondents towards sustainable practices. The purpose of Likert ranking is to facilitate respondents to express the direction and strength of opinion on the statements in the questionnaire. The use of 5-point Likert scale was considered appropriate because it increases the reliability of the measure, reduce social desirability and biasness among respondents. It also helps them to be aware with the phenomenon under study and given the option to typically skip the scale in the case of ambiguity, and has been used by previous researchers. The reliability of 5-point Likert scale was determined by using Cronbach's alpha coefficients. Ideally, the Cronbach alpha coefficient of a reliable scale should be greater than 0.70 [43]. A reliability test for the fourteen sustainable practices as shown in Table III was conducted by using the SPSS software. The Cronbach alpha for the used Likert scale is 0.908. This indicates that the data collected for the analysis is interrelated and consistent. The mean score for the adoption of sustainable

Table 3 Mean score, rank and average index

Sustainable practices factors	Overall mean score	Rank	Average index indicator
Efficient use of equipment/machineries (such as reducing idling time, planning of travelling routes etc)	3.6744	1	High
Opt equipments/machineries that best fit the intended purpose by size and capacity	3.6512	2	High
Opt for the best engine power for machineries	3.4070	3	Average
Implementation of timely and preventive maintenance plan	3.4070	3	Average
Efforts to minimize vibration impact on workers and surroundings	3.3372	4	Average
Procure energy efficient machinery/equipment	3.2907	5	Average
Limit the level of dust pollution by construction equipments	3.2558	6	Average
Periodic assessment of operator health and safety	3.2558	6	Average
Implementing noise controlling plan	3.0814	7	Average
Implementing energy saving plan	2.4651	8	Low
Investing technological controls that will reduce air pollution and emissions	2.4535	9	Low
Reduced diesel emissions by using new engine technologies and post combustion controls	2.4186	10	Low
Implementing green house gas emission (CO _x and NO _x , SO _x etc) control plan	1.7907	11	Low
Use of biodegradable fuel and lubricants	1.2558	12	Very low

practices for the data under observation was 2.910 which indicate that respondents are committed in a moderate manner. The minimum and maximum scores were 1.256 and 3.674 respectively. Table III shows the mean score, rank and average index assessment indicator for the corresponding sustainable factor [44]. It is apparent from the Table 3 that a number of sustainable practices have already been adopted by the Malaysian contractors in order to show their commitment towards green construction. However, it is still moderately adopted in all its manifestations. The mean score and the corresponding average index values indicate that respondents have show low concern in controlling greenhouse gas emissions from the onsite heavy equipments and vehicles.

9 Conclusion

This research paper has investigated the current level of sustainability considerations in the acquisition and usage of onsite mechanized construction equipments. The respondents feedbacks indicate that they are aware and have a good knowledge of sustainable construction. Nevertheless, the implementations of sustainable practices are still at moderate level. It has been further determined that greenhouse gas emission (GHG) is a low priority concern for the practitioners. The outcome of

this research effort has established that the Malaysian construction industry must raise its level of adoption towards green practices, particularly with respect to the control of air pollution from heavy construction equipments and non-road vehicles.

References

1. W.E. Rees, The built environment and the ecosphere: a global perspective. *J. Build. Res. Inf.* **27**(4–5), 206–220 (1999)
2. International Council for Building (CIB), *Agenda 21 on sustainable construction*, Rotterdam, 1999
3. C. Labuschagne, A.C. Brent, Sustainable project life cycle management: the need to integrate life cycles in the manufacturing sector. *Int. J. Proj. Manage.* **23**(2), 159–168 (2005)
4. World Commission on Environment and Development, *Brundtland report: Our common future*, United Nations, New York, 1987
5. U. Persson, Management of Sustainability in Construction Works, Ph.D. Dissertation, Division of Construction Manage, Lund University, Sweden, 2009
6. G. Atkinson, Sustainability, the capital approach and the built environment. *J. Build. Res. Inf.* **36**(3), 241–247 (2008)
7. C. Boostra, P. Tossavainen, R. Hurril, J. Parviainen, N. Schaffroth, Testing and evaluation of LCA and LCC tools for buildings, in *International Conference Performance Assessment of Buildings*, Canada, 1998
8. R.J. Cole, N. Larsson, Primary analysis of the GBC assessment process, in *International Conference Performance Assessment of Buildings*, Canada, 1998
9. T. Hakkinen, P. Huovila, L. Bordeau, S. Nibel, CRISP network on construction and city related sustainability indicators: structuring of indicators and status of work, in *International Conference Sustainable Building*, Norway, 2002
10. V. Brophy, J.O. Lewis, Current building procurement procedures—a potential barrier to sustainable design and construction, in *World Sustainable Building Conference*, Tokyo, 2005
11. D.G. Nair et al., A conceptual framework for sustainable affordable housing for the rural poor in less developed economies, in *World Sustainable Building Conference*, Tokyo, 2005
12. R. Yin, V. Cheng, Policy option for sustainable construction, in *World Sustainable Building Conference*, Tokyo, 2005
13. C.J. Kibert, *Sustainable Construction: Green Building Design and Delivery* (Wiley, New York, 2005)
14. U. Persson et al., Ten years of sustainable construction—perspective from a north construction manager and a south architect point of view, in *World Sustainable Building Conference*, Australia, 2008
15. C. Cheng, S. Pouffary, N. Svenningsen, M. Callaway, The Kyoto protocol, the clean development mechanism and the building and construction sector, A report for the UNEP sustainable buildings and construction initiative, united nations environment programme, Paris, France, 2008
16. R.L. Peurifoy, C.J. Schexanyder, A. Shapira, *Construction Planning, Equipment, and Methods*, 7th edn. (McGraw-Hill, New York, 2006)
17. G.I. Idro, Effect of mechanisation on occupational health and safety performance in the Nigerian construction industry. *J. Constr. Developing Countries* **16**, 27–45 (2011)
18. D.A. Day, N.B.H. Benjamin, *Construction Equipment Guide*, 2nd edn. (Wiley, New York, 1991)
19. R.P. Indoria, Mechanization in roads sector, in *Indian Highways*, 2009
20. A. Shapira, G. Lucko, C. Schexnayder, Cranes for building construction projects. *J. Constr. Eng. Manage.* **133**, 690–700 (2007)

21. D. Arditi, S. Kale, M. Tangkar, Innovation in construction equipment and its flow into the construction industry. *J. Constr. Eng. Manage.* **123**(4), 371–378 (1997)
22. T. Prasertrunguang, B.H.W. Hadikusumo, Heavy equipment management practices and problems in Thai highway contractors. *J. Eng. Constr. Architectural Manage.* **14**, 228–241 (2007)
23. L.H. Seeley, *Building Economics*, 4th edn. (Macmillan Press Limited, London, 1996)
24. Economic Planning Unit, *Tenth Malaysian plan* (Prime Minister Department, Putrajaya, Malaysia, 2010)
25. K.A.M. Kamar, Z.A. Hamid, Z. Ismail, Modernising the Malaysian construction industry through the adoption of industrialised building system, in *6th International Conference Multinational Joint Ventures for Construction Works*, Kyoto, Japan, 2010
26. International Standards Organization, *ISO 14041*, Geneva, 1998
27. B. Kim, H. Lee, H. Park, H. Kim, Green house gas emissions from onsite equipment usage in road construction. *J. Constr. Eng. Manage.* 982–990 (2012)
28. P. Lewis, W. Rasdorf, H. Frey, S. Pang, K. Kim, Requirements and incentives for reducing construction vehicle emissions and comparison of nonroad diesel engine emissions data sources. *J. Constr. Eng. Manage.* **135**, 341–351 (2009)
29. U.S. Energy Information Administration (EIA), *Emissions of greenhouse gases in the United States*, Washington, DC, 2009
30. Korea Institute of Construction Technology, *Civil engineering cost data*, Gyeonggi-do, Republic of Korea, 2010
31. Northeast States for Coordinated Air Use Management, *Heavy-duty engine emissions in the Northeast*, Boston, 1997
32. H. Avetisyan, E.M. Hooks, S. Melanta, Decision models to support greenhouse gas emissions reduction from transportation construction projects. *J. Constr. Eng. Manage.* **138**, 631–641 (2011)
33. F.A. Peña-Mora et al., A framework for managing emissions during construction. Presented at the National science foundation international workshop on green buildings and sustainable construction, Cairo, Egypt, 2009
34. A.A. Guggemos, A. Horvath, Decision-support tool for assessing the environmental effects of constructing commercial buildings. *J. Architectural Eng.* 87–195 (2006)
35. N. Kartam, Integrating safety and health performance into construction CPM. *J. Constr. Eng. Manage.* **123**, 121–126 (1997)
36. T.W. Loushine, P.L.T. Hoonakker, P. Carayon, M.J. Smith, Safety and quality management systems in construction: some insight from contractors, in *IJIE Conference*, Las Vegas, USA, 2003
37. Health and Safety Executive, *The health and safety executive statistics*, UK, 2009
38. E. Mbuya, N.M. Lema, Towards development of a framework for integration of safety and quality management techniques in construction project delivery process. *Int. J. Qual.* **14**, 1–15 (1996)
39. K. Bailey, *Emission Reduction Incentives for Off-Road Diesel Equipment Used in the Port and Construction Sectors* (ICF Consulting, Virginia, 2005)
40. Dutch Ministry of Infrastructure and the Environment, *Criteria for the sustainable procurement of heavy-duty motor vehicles and mobile equipment including maintenance services*, The Hague, 2011
41. W.N. Osman, Z.M. Udin, D. Salleh, Green technologies and their application in Malaysian construction industry, in *3rd International Conference Technology and Operations Management*, Bandung, Indonesia, 2012
42. A.T.S. Bahaman, *The Key Issues in the Malaysian Construction Industry: Public and Private Sector Engagement* (Master Builders Association of Malaysia, Penang, 2011)
43. G. Iarossi, *The Power of Survey Design: A User's Guide for Managing Surveys, Interpreting Results, and Influencing Respondents* (World Bank, Washington, DC, 2006)
44. A. Majid, Assessment of Work Performance, Ph.D. Dissertation, Loughborough University, UK, 1997

Factors Contributing to Building Maintenance Performance of Heritage Buildings

Syed Burhanuddin Hilmi Syed Mohamad, Zainal Abidin Akasah
and Mohammad Ashraf Abdul Rahman

Abstract An assessment of the building maintenance performance for heritage building is critical to determine whether the routine procedure of work meet the prescribed requirements. Malaysia has been initiating the conservation works for old and heritage building approximately 4 decades ago. The awareness of maintenance managers of heritage buildings are slowly increasing but still need to improve their understanding on what shall be done in order to obtain the best practice approach in heritage building maintenance management. The lack of maintenance also makes the starting point of structural deterioration problem and will require millions of ringgits to repair, rehabilitate and conserve the effected buildings and structures. The study will evaluate the significant factors that contribute to maintenance performance of heritage building in Malaysia. Research data will be collected through questionnaire form, interview and site observation. The collected data will be analyzed by using Statistical Package for the Social Sciences (SPSS) and Partial Least Squares Structural Equation Modelling (PLS-SEM) software to examine the structure of interrelationships among constructs (the dependent and independent variables). Expected outcome is to recommend the most critical factors that will influence the maintenance management system and give significant correlation between the building deterioration variables in heritage building maintenance. Thus, be able to use the significant variables in developing the building maintenance model to support the management maintenance system for heritage building in Malaysia.

Keywords Contributing factors · Building maintenance · Building performance · Heritage building

S. B. H. S. Mohamad (✉) · Z. A. Akasah · M. A. A. Rahman
Faculty of Civil and Environmental Engineering, Universiti Tun Hussein Onn Malaysia
(UTHM), Parit Raja, Batu Pahat, Johor, Malaysia
e-mail: burhan@uthm.edu.my

1 Introduction

On Monday, July 2008, Melaka and George Town, historic cities of the Straits of Malacca have been added as new cultural sites to UNESCO's World Heritage List. These two cities have developed over 500 years of trading and cultural exchanges between East and West in the Straits of Malacca [1].

Currently, Malaysia has four World Heritage Sites recognised by the United Nations Educational, Scientific and Cultural Organization's (UNESCO) World Heritage List. There are the historic cities of Melaka and George Town along the Straits of Malacca, the Archaeological Heritage of the Lenggong Valley (AHLV) in Perak, Gunung Mulu National Park in Sarawak and Kinabalu Park in Sabah [2]. With this title, it will give advantages to Malaysian government in bringing more efforts to preserve the historical architecture, restore and refurbish old houses and prevent them from being demolished and replaced with new buildings.

The Ministry of Information, Communications and Culture under the Department of National Heritage The Department began as the Heritage Division under the Ministry of Culture, Arts and Heritage. It was upgraded to a Department on 1st March 2006. It is a vital progress and a great responsibilities in reviving, conserving and maintaining the nation's heritage as established in the National Heritage Act 2005.

Heritage conservation in Malaysia also been considered as a new practice compared to the more developed countries in the world [4]. Malaysia has inherited 91 heritage buildings including the indigenous traditional buildings from the Malays, Indians, Chinese and Colonials era.

The conservation of historical buildings is a method on preserving structures which are historically and culturally important to the nation [5]. Conservation involves works undertaken to preserve the condition of the building to its original state and this also includes the subsequent maintenance works. Maintenance is identified as a means on prolonging the lifespan of the historical structures. Without proper and systematic maintenance works, without doubt, the historical buildings will deteriorate and becoming dysfunctional as well as unfit to be used. The importance of the maintenance plays in protecting historic buildings during the formation of Society of Protected Ancient Buildings (SPAB) [6].

The relevant factors causing building deterioration need to be identified and analyzed in order to sustain the original condition of the heritage building. Furthermore, the significant factors can also be justified and a better maintenance system for heritage building can be developed to improve the current practice in building maintenance management. Acknowledging the significant of maintenance for historical buildings, this research therefore is seen as the vital to highlight on the maintenance performance influence factors for historical buildings within the Malaysia context.

2 Background and Problem Statement

The historical rehabilitation and maintenance works can be considered as a popular method use in Malaysia. On the other hand, heritage building has been an essential factor in town developing which plays an important role in generating income to Malaysia tourism sector as well as the country's great and beautiful landmark [7].

The fifth Malaysia's Prime Minister, Datuk Seri Abdullah Ahmad Badawi during his speech in NAFAM Conference in Kuala Lumpur, billion of ringgit has been spent and wasted in repairing public buildings due to Malaysia's poor maintenance culture. This is such a waste because if the defects were spotted earlier and rectified, it will not develop into big problems and cost more money. In another event, the critical issues concerning the absence of systematic maintenance works became one of the key topics discussed by the Prime Minister during his opening speech for Development of Maintenance Culture, a national seminar conducted on 23rd September 2003. He expressed his concern on the need to cultivate the culture of prioritizing and protecting the structural quality of a building amongst the Malaysian. In addition, the Prime Minister also highlighted that the understanding on the importance of maintaining the buildings should not be limited to new buildings only as the historical buildings also have their own significant value [8].

The growth of the environmental and conservation concerns has paralleled the increasing emphasis on maintenance and refurbishment of buildings as an alternative to redevelopment in recent years. Good maintenance management will able to maximize a building's effective lifespan, minimize energy and materials resource consumption and preserving old buildings by keeping them fit for modern use as an alternative to redevelopment. From previous reviews, many countries have stated that the lack of maintenance is the starting point of structural deterioration which resulted in the structures falling into disrepair very quickly [9].

There is ambiguity at the relationship between building conservation and building maintenance management. Four major focuses framework is needed to resolve this ambiguity as the following [9]:

- the specific reasons for conserving all or part of a building or monument (conservation philosophy);
- how and in what ways this will then affects its value and utility (concurrence and conflicts of interest);
- how we may evaluate the conflicts and benefits of the conservation process on the use and management of the building as a whole (a framework for evaluating conservation);
- what means we carry out the conservation (sourcing skills and expertise).

Malaysia had initiated the effort of conserving heritage buildings just approximately 30–40 years ago. The awareness is slowly increasing [10]. Maintenance managers of heritage buildings have little guidance on what best practice approach to the maintenance management of heritage buildings [11].

The research finding by Abdul Rashid and Ahmad suggested that it is not so much an issue of negligence, but one of a failure to give maintenance the requisite priority. There is another more profound problem relating to the issue of maintenance; whilst most people would agree that a regime of regular maintenance is the ideal, providing good value for money and a better investment performance. Maintenance is always wrongly perceived as a low status professional activity [5].

On the other hand, Mohd Isa et al. suggested that maintenance is most significant in order to conform to the conservation good practice. The theory and practice of maintenance needs for historic building in Malaysian are still not duly addressed. Good maintenance practice is one of the important perspectives that still leave a gap in effective management strategies [3].

Therefore, if related government agencies fail to develop a comprehensive maintenance performance assessment approach, the potential of expenses for existing heritage buildings rehabilitation and repair work will increase. The heritage building value also will decrease within a period of time. Failure to detect the causes of building deterioration will also give a significant impact to the durability and strength of heritage building.

However, in Malaysia there is always a need to evaluate the significant factors that contribute to building maintenance performance of heritage buildings in Malaysia, especially using the multivariate statistical application software like Partial Least Square Structural Equation Modelling (PLS-SEM). Many of the researchers focus on the heritage building maintenance management system and conserved heritage building best maintenance practice guidelines.

3 Research Aim and Objectives

The aim of this research is to develop a model in assessing the performance of building maintenance for heritage buildings in Malaysian heritage buildings. Thus, the objectives of this research are as follows:

1. identify the factors contributing to the building maintenance performance of heritage building.
2. determine the most significant factors of building maintenance performance in Malaysian heritage building.
3. develop building maintenance performance model for heritage buildings in Malaysia.

4 Scope of Research

The research will be focusing the heritage buildings in Malaysia and emphasize on building maintenance performance criteria. The expected respondents are from management level and the technical staffs: consultants, heritage conservation

professionals, building maintenance professionals, building maintainers, and specialist contractors involving with the maintenance management of historical buildings in Malaysia.

5 Literature Review

The life of building elements and components can be extended considerably by adopting a planned maintenance approach so that problems can be identified in their early stages and preventive maintenance carried out to avoid early failure [9].

Historic preservation technology plays an important role from initial project investigations through final construction. The historic preservation technology combines investigation methods, materials, and construction methods used to preserve, rehabilitate, restore or reconstruct a building. Therefore, understanding how preservation technology choices made in a project can affect the success of the project outcome is critically important [12].

5.1 Building Maintenance Management

Management is the control and organization of something. Maintenance Management is the organization of maintenance within an agreed policy (BS3811) [13]. Building maintenance management has been implemented decades ago to overcome the building services problems. Building services are crucial in most high buildings or skyscrapers. Budget will be the major issues in fulfilling all the requirements and to give comfort to the building occupants.

British Standard Glossary of terms (3811:1993) stated maintenance as the combination of all technical and associated administrative actions intended to retain an item in, or restore it to, a state in which it can perform its required function [14].

Management of maintenance can comprise more than the control of activities and can be addressed broadly under the headings of 'technical' and 'control' [14]. The technical content includes determining what plant or equipment is to be maintained, how and when; identifying problems and diagnosing causes; monitoring effects; preparing and analysing records and technical information; initiating procedures to cope with situations before they arise; and ensuring that the chosen techniques are achieving the required results.

The control element is aimed at providing that required technical service at minimum expense, and can involve management of labour, spares and equipment to match the workload; locating where work is required; organising transport; setting priorities; and coordinating action. It can extend to setting budgets,

monitoring expenditures, identifying high maintenance cost plant and collecting information to form a basis for decision making.

5.2 Heritage Building

Section 2(1) Act 645 of National Heritage Act (2005) and UNESCO (1972) has stated “building” as a building or groups of separate or connected buildings which, because of their architecture, their homogeneity or their place in the landscape, are of outstanding universal value from the point of view of history, art or science.

Historic buildings require special maintenance to sustain its aesthetic value in terms of building materials, unique architecture and historical heritage values [15].

5.3 Factors Contributing to Building Maintenance Performance

Some of the factors that contribute to the building maintenance performance for heritage buildings from literature review are as in Table 1.

6 Research Methodology

The identification, selection and implementation of methodology are very important criteria in all fields of research. It needs to be well planned and displayed in a comprehensive research methodology flow chart. Research methodology is a crucial part in research ensuring that the research can be conducted correctly with specific and organized methods. Figure 1 shows the proposed research methodology flow chart of the proposed research: *Factors Contributing to Building Maintenance Performance of Heritage Building*.

6.1 Data Collection

The data collection process is based on the problem statement and the title of the research. The aims and objectives are then set. A literature review of building deterioration mechanisms and current building maintenance management especially for the heritage building will be reviewed from all sources of references such as journals, thesis, books, articles and etc. The summary of relevant literature review will be briefly given in tabulation form. Methods of data collection involves design questionnaire, conducting pilot study and surveys.

Table 1 Summary of contributing factors to building maintenance performance of heritage building

Contributing factors to building maintenance performance for heritage buildings	References
1 The importance of historical buildings	[5]
2 Human behaviour/Attitudes	[5, 11, 16–18]
3 Maintenance policy and organization	[3, 5, 9, 11, 14, 15, 19–22]
4 Maintenance effectiveness	[5, 11, 16, 18–23]
5 Task planning and scheduling	[19, 22]
6 Maintenance approach—current practice	[3, 5, 9, 11, 19–22]
7 Financial factor/Aspect/Problems	[5, 11, 15, 16, 18, 20–22, 24, 25]
8 Risk management	[14, 20, 23]
9 Customer perspective	[22, 25]
10 Information management and CMMS	[11, 14, 19, 20, 22]
11 Environment/Surrounding	[9, 11, 23]
12 Technical aspects	[3, 5, 9, 12, 14, 15, 17, 20, 22, 26]
14 Institutional and training facilities	[14, 16, 18, 25]
15 Continuous improvement	[14, 16, 18, 19, 20, 22, 23]
16 Human resources management/Internal process	[5, 11, 15, 17–19, 22, 24, 25]
17 Spare part management	[16, 19]
18 Regulations and guidelines	[3, 5, 15, 16, 24]
19 Contracting out maintenance	[5, 14, 16, 19, 21, 22]

Source Summary from literature

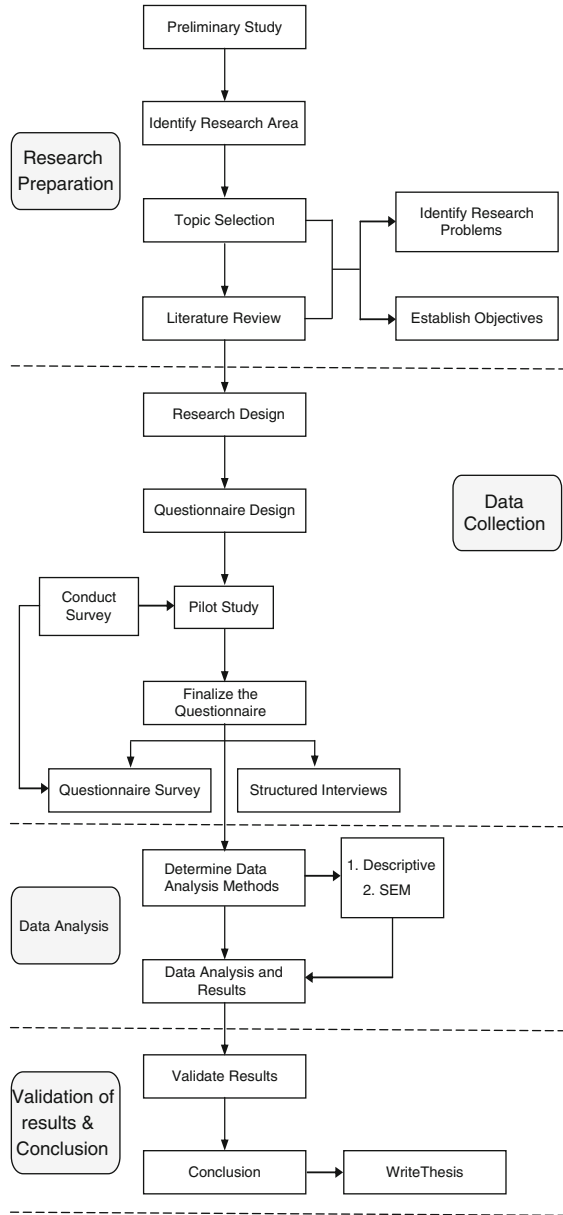
6.2 Data Analysis

The collected data will be analyzed by using Partial Least Square-Structural Equations Modelling (PLS-SEM) software. SmartPLS 2.0 software is able to measure the significant of covariance by testing and estimating the causal relationship between independent variable and dependent variable. The results will interpret the level of significance for each items/variables to the deterioration factors that would be influencing the effectiveness of maintenance management system.

7 Research Significant

This research will contributes to the growing body of knowledge in maintenance performance criteria specifically on the improvement of Malaysian heritage building maintenance performance criteria. It is becoming increasingly difficult to ignore the importance of heritage building to our current and future social-economy impacts. In maintenance work, the phrase like “maintain as it is” is always kept in building maintainer minds to sustain the original functions of building structures, building services system and building appearance.

Fig. 1 Research methodology flow chart



This research is might be extends of work on finding the possible major issues contributing to the lagging of a proper maintenance programme [5]. The case study result indicated that maintenance undertaken for historical building in Malaysia is still on a loose based. The research are intended to highlight the establishment of maintenance management, the responses on the importance of maintenance works

to be undertaken for historical buildings, factors governing the effectiveness of maintenance works on historical buildings and maintenance approaches, inclusive of maintenance programmed undertaken maintenance approaches, inclusive of maintenance programmed undertaken on the structural, non-structural elements as well as the services systems.

It has been supported by Sodangi et al. [11] mentioned that the maintenance of heritage building takes a cautious approach in order not to unnecessarily disturb or destroy the historic fabric; damage the character of the building and alter the features which give the building historic, architectural and cultural significance. Therefore, a specific framework is required for managing the maintenance of heritage buildings.

Motivated from their work, this research proposes to study further on the significant maintenance performance criteria which can be indicators in supporting the loose based in historical building maintenance programme and framework.

8 Expected Outcomes

The study perhaps will identify the critical factors that influence the maintenance system and closing some missing link in terms of building maintenance criteria. The results from significant inter-relationship between the building performance variables in heritage building maintenance will be used to improve the heritage building maintenance approach.

In the end, recommendations and the improvement solution will be discussed in detail in order to produce a useful reference and guidance to the Department of National Heritage. The research results hopefully, can be a main source to improve the existing policy and procedure, prior to the heritage building maintenance performance factors.

Acknowledgments The authors would like to express gratitude to Universiti Tun Hussein Onn Malaysia and all colleagues for the valuable support and advice in conducting the research.

References

1. UNESCO, Eight new sites, from the Straits of Malacca, to Papua New Guinea and San Marino, added to UNESCO's World Heritage List (2008), <http://whc.unesco.org/en/news/450>. 03 Dec 2012
2. BERNAMA, Malaysia now has four world heritage sites, New Straits Times, 2012
3. A.F. Mohd-Isa, Z. Zainal-Abidin, A.E. Hashim, Built heritage maintenance: a Malaysian perspectives. *Procedia Eng.* **20**, 213–221 (2011)
4. A.Z.A. Akasah, B.M. Alias, Analysis and development of the generic maintenance management process modeling for the preservation of heritage school buildings. *Int. J. Integr. Eng. (Issue Civ. Environ. Eng.)* **1**(2), 43–53 (2009)

5. R. Abdul-Rashid, A.G. Ahmad, The implementation of maintenance works for historical buildings: a review on the current scenario. *Procedia Eng.* **20**, 415–424 (2011)
6. W. Morris, *The SPAB Manifesto* (Society for Protection of Ancient Building (SPAB), London, 1877)
7. S.A.H.S. Mustapa, K.S. Kamal, M.Z. Zainul, Rehabilitation of heritage buildings in Malaysia, in *International Seminar on Modern Urban and Architectural Heritage*, Museum Bank Mandiri, pp. 126–133, 2005
8. R.A. Rashid, A.G. Ahmad, Overview of maintenance approaches of historical buildings in Kuala Lumpur: a current practice. *Procedia Eng.* **20**, 425–434 (2011)
9. P. Wordsworth, *Lee's Building Maintenance Management*, 4th edn. (Blackwell Science Ltd., Oxford, 2001)
10. N.F.N. Azhari, E. Mohamed, Public perception: heritage building conservation in Kuala Lumpur. *Procedia-Soc. Behav. Sci.* **50**, 271–279 (2012)
11. M. Sodangi, A. Bin Idrus, F.M. Khamidi, Examining the maintenance management practices for conservation of heritage buildings in Malaysia, National Postgraduate Conference (NPC), 19–20 Sept, pp. 1–7, 2011
12. Y. Robert A, *Historic Preservation Technology* (Wiley, USA, New Jersey, 2008)
13. P. Procter, *Cambridge International Dictionary of English*, Cambridge University Press, 1995
14. CIBSE Guide M, *Maintenance engineering and management: a guide for designers, maintainers, building owners and operators, and facilities managers*. The Chartered Institution of Building Services Engineers London, 2008
15. N.I. Hashim, M.A.O. Mydin, Maintenance management system of administration heritage buildings in Malaysia. *Ann. Fac. Eng. Hunedoara Int. J. Eng.* **10**(3), 475–478 (2012)
16. M.A.A. Rahman, Z.A. Akasah, M.S. Abdullah et al., Issues and problems affecting the implementation and effectiveness of heritage buildings maintenance, in *The International Conferences on Civil and Environmental Engineering Sustainability*, Johor Bahru, Malaysia, 2012
17. C. Briffett, *Building Maintenance Technology in Tropical Climates* (Singapore University Press, Singapore, 1995)
18. M.A.A. Rahman, Z.A. Akasah, S.F. Zuraidi, Maintenance management success factors for heritage building: a framework, in *12th International Conference on Structural Repairs and Maintenance of Heritage Architecture* (Chianciano, Italy, 2011), pp. 653–658
19. C. Cholasuke, R. Bhardwa, J. Antony, The status of maintenance management in UK manufacturing organisations: results from a pilot survey. *J. Qual. Maintenance Eng.* **10**(1), 5–15 (2004)
20. D. Worthing, S. Bond, *Managing Built Heritage: The Role of Cultural Significance*, Oxford (Blackwell Publishing Ltd., UK, 2008)
21. B. Wood, *Building Maintenance*, Oxford (Blackwell Publishing Ltd., UK, 2009)
22. B. Chanter, P. Swallow, *Building Maintenance Management*, 2nd edn. (Blackwell Publishing Ltd., Oxford, 2007)
23. C.W. Kuen, S. Zailani, Y. Fernando, Critical factors influencing the project success amongst manufacturing companies in Malaysia. *Afr. J. Bus. Manage.* **3**(1), 16–27 (2009)
24. S.N. Kamaruzzaman, E.A. Zawawi, A. Omar, Preliminary evaluation of problems involved in maintaining heritage buildings in Malaysia. *Prof. J. Inst. Surveyors, Malays.* **46**(1), 30–38 (2011)
25. S.H. Zulkarnain, E.M.A. Zawawi, M.Y.A. Rahman et al., A review of critical success factor in building maintenance management practice for university sector. *World Acad. Sci. Eng. Technol.* **59**, 195–199 (2011)
26. Act 645, National Heritage Act 2005, 2006

Strength, Weakness, Opportunity and Threat Attributes of Malaysian Construction Firms in International Market

Che Maznah Mat Isa, Hamidah Mohd Saman, Siti Rashidah Mohd Nasir and Aini Jaapar

Abstract Competitive and saturated construction markets has led many domestic firms to expand internationally. Hence, the firms must adopt a superior and an effective strategy in order to endure the increasing dynamics and uncertainties in the foreign markets. In the early stage of strategic planning, one of the basic but important steps is to identify the strength, weakness, opportunity and threat (SWOT) attributes of the firms before they expand internationally. This process is very crucial to help the firms to manage and ease the inherent complexities and difficulties within international market domain. In this study, survey questionnaires were sent to 109 Malaysian construction firms listed under Construction Industry Development Board Malaysia (CIDB) with 21 % response rate. Relative importance index (RII) was used to rank the SWOT attributes. The findings revealed the following ranked attributes: Strengths—project management skill, financial strength and specialist expertise; Weaknesses—shortage of financial resources, shortage of labor and material resources and lack of research and development; Opportunities—increased in profitability, opening up new market and accessibility to new service areas; Threats—inflation and currency fluctuations, policy, law and regulations of host country and increase of interest rate. This study illustrates the identification of the most important SWOTs that exist in international construction operations. Hence, the findings would offer valuable information and practical guidance to construction firms in their preparatory works to internationalize.

Keywords Strength · Weakness · Opportunity · Threat · SWOT attributes · Malaysian construction firms · International market

C. M. M. Isa (✉) · H. M. Saman · S. R. M. Nasir · A. Jaapar
Institute of Infrastructure Engineering and Sustainability Management, Faculty of Civil Engineering, UiTM, Shah Alam, Malaysia
e-mail: chema982@salam.uitm.edu.my

1 Introduction

An international business domain is saturated with complex variables that may affect the firm's performance if they are not well identified and effectively managed. This scenario warrants the firms to correctly identify and carefully examine their strengths, weaknesses, opportunities and threats associated with international operations. SWOT analysis is a common method used by organizations to identify and utilize their strengths to exploit opportunities, to recognize and reduce their weaknesses and to minimize the known threats and challenges.

In his study, Ref. [1] examined the firms' strengths and weaknesses by utilizing the factors related to management and organization, operations, and finance, while economic, social, political, markets, and competition factors were used to examine the opportunities and the threats to the firms' business. Various studies have been carried out related to SWOTs for other foreign competitors such as the Vietnamese, Chinese, Singaporean and Korean in the international market [1–7].

Despite, their fast internationalization, Malaysian construction firms are not well studied and this has resulted in lack of information on the international construction conditions. Thus, the firms must be informed and understand the internal and external risks and threats and at the same time acquire and strengthen their capabilities to seize the opportunities abundantly available in the emerging markets.

Hence, this study aims to gain insights of the Malaysian firms in the international construction market, through identification of the SWOTs and finally producing a clear essence based on relative importance of the SWOT attributes.

2 Literature Review

Numerous studies have been carried out in relation to the opportunities, threats, risks and challenges in international market [8–10]. According to Ref. [2], determination of the firm's strengths and weaknesses and matching them with the opportunities and threats is a critical strategic decision that requires extensive environmental scanning. Following to that, Ref. [3] investigated some of the critical issues and successful strategies obtained by global contractors to sustain and growth in international market, concluding that the uncertainties and aggressive changes of global construction can cause serious threats to the international players. Thus, Ref. [3] suggested that the firms must acquire complementary capabilities and skills, and improve their strengths to encounter the challenges in the rapidly changing market environment.

Based on the study by Ref. [4], SWOT analysis was used to assess the Chinese contractors' dynamic capabilities in the international market environment. Some of the SWOT attributes used by Ref. [4] in their study were related to market competition, economic, social and political environment, management, financial

and technological abilities and, cost and resources differences. The findings show that Chinese government played an important role by holding a strong support and promotion to the contractors.

The study revealed that the strengths of Chinese contractors were from the low costs of workforce, materials, machinery and equipment, and specialty expertise. They were also found having lack of capabilities and commitment in research and development, inadequate design capacity, lack of highly skilled labor and low productivity, weak financing capacity, lack of familiarity with the local system, and language disadvantage.

Therefore, Ref. [5], recommended for the foreign contractors to grab the opportunities in Chinese market by offering their dynamic capabilities in distinguished products and services thus complementing the local Chinese contractors those were behind in design and technical capability, project management skills and financial capacity together with lack of experience in international projects.

Nonetheless, the nature and complexity of international business environment are very uncertain and different from one country to another. A study by Ref. [6] on Vietnamese firms shows that they lagged behind other foreign firms in financial capacity, experience in complex projects, knowledge in advanced design and construction technology, and management ability.

Another study carried out by Ref. [7] on Chinese contractors in Africa revealed that the needs for good infrastructure, availability of financing sources and availability of natural resources are among the top opportunities.

Therefore, various complex variables that can affect the performance of construction firms need to be considered in managing and reducing the risks associated with international market [8]. Thus, the companies must have the strengths required to endure the increasing and changing threats and uncertainties in international construction industry.

Figure 1 depicts the intention of this paper which is to identify and analyze the relative importance of SWOT factors of Malaysian firms in the international construction market.

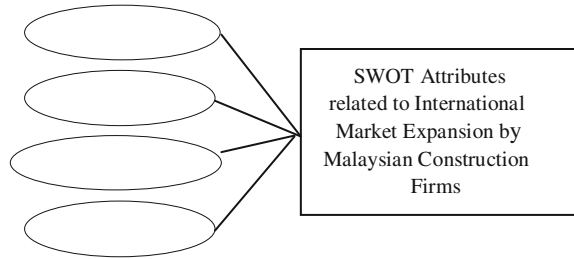
The input variables to SWOT attributes of the construction firms were identified from the previous studies [3–8], which some of them were discussed in the literature section is shown in Table 1.

This paper builds on these earlier contributions by examining the relative contribution of a more comprehensive range of the SWOT attributes identified by the firms with international experience. All four categories of the SWOT attributes were jointly considered across the previous studies.

3 Methodology

The target population is from the cross-section of Malaysian construction firms those undertaken and completed projects in the international market. The selection is based on Ref. [11] record with 109 firms registered as global players operating

Fig. 1 SWOTs attributes related to international market expansion



in 49 countries. Their involvements in international projects includes various sectors such as buildings, infrastructures, branches of engineering, mechanical and electrical, power transmission and plant, and oil and gas.

The survey questionnaires with cover letter were sent with self-addressed and prepaid enveloped to the respondents. They were requested to return the questionnaires within 3 weeks-time from the date of the letter posted. The cover letter explained the objectives and the relevancy of the study, and assured the respondents' confidentiality. A contact number was also provided in case clarifications are needed.

The questionnaires analyzed in this paper are selected based on three sections. [Section 4.1](#) enquires on the respondents' background, international contracting experience and the specific countries of operation. Part B solicits their opinions to evaluate the SWOT attributes based on the level of agreement. Each opinion was measured using a 5-point Likert scale (1: Disagree; 2: Disagree; 3: Agree; 4: Much Agree; and 5: Strongly Agree).

Several statistical analysis techniques namely normality test, reliability test and ranking of relative importance index (RII) were used in this study. The purpose of each method and its results are explained in the following section.

4 Analysis of Results and Discussion

The following results are critically analysed and discussed based on opinions and views from the respondents and supported by the literature reviews done earlier.

4.1 Respondents

The respondents were the chief executives, general managers, senior managers, project managers, contract managers and other executives holding managerial posts and in charge of international projects in the selected firms. In total, twenty-three (23) respondents returned the completed questionnaires giving a response rate of 21 %. In order to increase the rate of response, various strategies were

Table 1 SWOT attributes related to international market expansion

SWOT attributes	
Strengths	<i>Project Management Skill</i> : Ability to complete projects on time, within budget and quality set
	<i>Financial Strength</i> : Ability to increase the needed financing for purposes of bidding projects
	<i>Specialist Expertise</i> : Comprehensive technical and management skills compared to competitors
	<i>Track Record</i> : Successfully completed local and oversea projects in the past
	<i>International Network</i> : Strong relationship with foreign partners in foreign countries
	<i>Technology Capability</i> : Strong knowledge and experience to handle technically complex projects
	<i>Resources Availability</i> : Ability to support and manage equipment, material and labors
Weaknesses	<i>Quality</i> : Ability to produce good quality products/services
	<i>Shortage of Financial Resources</i> : Lack of ability to offer attractive financial resources
	<i>Shortage of Labor Resources</i> : Difficulty in obtaining labors
	<i>Shortage of Material Resources</i> : Difficulty in obtaining material and equipment
	<i>Loss of Experience and Key Employees</i>
Opportunities	<i>Lack of Research</i> : Lack of information and up-to-date data regarding the host country
	<i>Increased Profitability</i> : Improved and enhanced profit of the company for long term run
	<i>Technological Innovation</i> : Establish new and improved technologies for construction activities
	<i>Opening up New Markets</i> : Internationalization leading to new business opportunities
	<i>Accessibility to New Service Areas</i> : Explore new types of construction markets
	<i>Beneficiary International Agreements</i> : New prospects of construction market
Threats	<i>Maintain and maximize shareholder's return</i>
	<i>Mergers</i> : Establish international relationship by joint venture or strategic alliances
	<i>Interest Rate Increase</i> : Unstable cost of capital
	<i>Inflation and Currency Fluctuation</i>
	<i>Policy, Law and Regulations</i> : Different interpretation especially on FDI in the host country
	<i>Bribery in the Host Country</i> : Difficulty in dealing with the moral problems
	<i>Foreign Competitors in the Host Country</i> : Competition from different foreign firms
	<i>Cultural Differences</i> : Difficulty in dealing with people/organizations in different environment
<i>Price war with competitors</i>	

carried out to follow up, such as phone calls, personal distribution, reminders by letter and emails and through personal contacts. Hence, the response rate is reasonable since most of the survey done in Malaysia generated a rate that falls between 10 and 20 % [12].

4.2 Normality Test

Normality tests were conducted to assess whether the data on the variables collected are normally distributed. In this study, the normality of the variables was established by evaluating the data distributions for skewness and kurtosis as shown in Table 2. The standard error is the range of possible error occurs in data (Good standard error value <1.0).

The results show the values of the standard error for skewness and kurtosis of 0.481 and 0.935, respectively. Both values indicate that the standard errors are good values (<1.0). Hence, the normality assumption for each variable was met, which indicates that the all SWOT attributes are normally distributed.

4.3 Reliability Test

Reliability test using Cronbach's coefficient was conducted to measure the internal consistency of the SWOT attributes as shown in Table 3.

The results reveal Cronbach's values for all SWOT attributes are greater than 0.7 which is the minimum level recommended by [13]. It is also supported by [14] that the widely-accepted social science cut-off of alpha should be 0.70 or higher.

4.4 Measurement of SWOT Attributes Related to International Market Expansion

The mean of responses were translated into Relative Importance Index (RII) reflecting the SWOTs attributes agreed by the respondents and were ranked accordingly. The discussion viewed is based on the first three SWOT attributes that reached the highest ranking.

Nevertheless, other attributes also have some influence critical to the success of the Malaysian firms in international market. Table 4 shows the ranking of each attributes based on the RII.

The following discussion are based on the first three ranked agreed statement under each attributes shown in Table 4.

4.4.1 Strength Attributes

The first three strength attributes that reached the highest ranking are the "project management skill", "financial strength" and "specialist expertise" with RII values of 0.957, 0.896 and 0.843, respectively. These strengths are required by the companies to endure the increasing threats and uncertainties in the rapid changing

Table 2 Normality tests on SWOT attributes

Variables	Skewness		Kurtosis	
	Statistic	Standard error	Statistic	Standard error
Strength	-0.119	0.481	0.997	0.935
Weakness	-0.464	0.481	-0.460	0.935
Opportunity	-0.712	0.481	0.188	0.935
Threat	-0.891	0.481	-0.579	0.935

Table 3 Cronbach's coefficient for SWOT attributes

Attributes	Cronbach's alpha
Strength	0.876
Weakness	0.899
Opportunity	0.777
Threat	0.895

international market environment [3, 8]. Reference [2] recommended that the international contractors offer their strengths in distinguished products and services, thus complementing the local contractors those were behind in design and technical capability, project management skills and financial capacity together with lack of experience in international projects. In return, the operation costs were lowered and at the same time they adapted comfortably with the local cultures and industry practices [2].

4.4.2 Weakness Attributes

The first three weakness attributes with the highest ranking are “shortage of labour and shortage of material”, “shortage of financial” resources and lack of research and development, with RII values of 0.861, 0.852 and 0.722, respectively. A study carried out by Ref. [7] on Chinese contractors in Africa revealed the needs for availability of natural resources, availability of financing and good infrastructures to ensure smooth operations. Previous studies have revealed that international firms such as Vietnamese and Chinese lagged behind other firms in financial capacity, lack of capabilities and commitment in research and development, inadequate design capacity, lack of highly skilled labour and low productivity, lack of familiarity with the local system, have language disadvantage, unfamiliar with modern project management technique, inferior in design and technical ability and lack of experience in international projects [2, 6].

Table 4 Ranking of SWOT attributes based on RI value

SWOT attributes	RII	Ranking
<i>Strengths</i>		
Project management skill	0.957	1
Financial strength	0.896	2
Specialist expertise	0.843	3
Track record	0.809	4
International network	0.839	5
Technology capability	0.809	4
Resources	0.800	6
Quality	0.765	7
<i>Weaknesses</i>		
Shortage of labour resources	0.861	1
Shortage of material resources	0.861	1
Shortage of financial resources	0.852	2
Lack of research and development	0.722	3
Loss of key employees	0.696	4
<i>Opportunities</i>		
Increase firm profitability	0.817	1
Accessibility to new service areas	0.757	2
Opening up new markets	0.739	3
Technological innovation	0.722	4
Beneficiary international agreements	0.722	4
Maintain and maximize shareholder's return	0.678	5
Mergers	0.670	6
<i>Threats</i>		
Inflation and currency fluctuations	0.826	1
Policy, law and regulations of host country	0.809	2
Increase of interest rate	0.800	3
Bribery in the host country	0.757	4
Foreign competitors in the host country	0.748	5
Price war with competitors	0.696	6
Cultural differences	0.643	7

4.4.3 Opportunity Attributes

The first three opportunity attributes that reached the highest ranking are “increase in firm profitability”, “accessibility to new service areas” and “opening up new markets” with RII values of 0.817, 0.757 and 0.739, respectively. The finding reveals that profitability is the most important goals related to the firms in international construction. The reason may be due to the fact that firms need higher profitability to counterbalance the greater risks and efforts in setting up their international operations. This is supported by a previous study where the decision to enter a new foreign market is of critical importance for the company's profit making ability and sustainable growth [7]. Reference [2] emphasized on the

availability of the export opportunities for the firms to increase their construction revenues, learn from competitors by improving their service standards.

4.4.4 Threat Attributes

The first three threat attributes agreed by the respondents and reflected in the highest ranking are “inflation and currency fluctuations”, “policy, law and regulations of host country” and “increase of interest rate” with RII values of 0.826, 0.809 and 0.800, respectively. The inflation, currency and interest rate fluctuations are some of the common economic risks which had high influence over the project cost [15]. As identified by Ref. [16], threats represent external aspects such as competitive environments resulting from changes in governmental policies and society of the host country, as well as the international environment. These aspects were identified from previous studies which these threats are evidenced on the basis of significant events in terms of the political and economic environments [7, 10]. Hence, the identification of the important threats allows the firms to manage them effectively.

5 Conclusions

The main objective of this study is to provide information for the firms to examine and leverage their strengths to seize the abundant opportunities and at the same time to identify and overcome their weaknesses which intensify the threats in international market. Through identification of SWOT attributes, the internal and external conditions of international scenario become evident. The findings fortify that the strengths of Malaysian construction firms are largely attributed by their project management skill and specialist expertise and supported by strong financial. While operating in the international construction market, the firms present some weaknesses, which include shortage of labour, material, financial resources and lack of research and development. The ever changing international market also offers opportunities by accessing the new service areas and opening up new markets to increase the firms’ profitability. However, the imposed threats due to inflation, interest and currency fluctuations, the policy, law and regulations of host country are well balanced by the benefits gained from the opportunities and the firms’ project management skill and specialization. The limitations in this study include a small sample size from a limited number of construction firms and the method of analysis used. Hence, the findings are confined to opinions obtained from these contractors and cannot be generalised to the rest of the population. However, it provides insights for the construction firms on the SWOT attributes related to the international market scenario that may affect the firms’ performance. Further empirical study will be conducted on a bigger sample focusing on the correlation between the attributes by using SWOT analysis to evaluate the cross

over and intertwined attributes. It is hoped that this study contribute to an international strategic management body of knowledge.

Acknowledgments The authors would like to thank the Faculty of Civil Engineering, UiTM and Research Management Institute, UiTM (Project Code: 100-RMI/SF 16/6/2 (33/2012) and MOSTI (Science Fund: Project No.: 06-01-01-SF0516) for providing the financial support for this research. We are also grateful to the professionals and managers from Malaysian construction firms, Malaysian Construction Industry Development Board (CIDB) and other institutions that have participated in this research.

References

1. H. Wehrich, The TOWS matrix: a tool for situational analysis. *Long Range Plan. J.* **15**(2), 54–66 (1982)
2. I. Dikmen, M.T. Birgonul, Neural network model to support international market entry decisions. *J. Constr. Eng. Manage. ASCE* **130**(1), 59–66 (2004)
3. S.H. Han, D.Y. Kim, H.S. Jang, S. Choi, Strategies for contractors to sustain growth in the global construction market. *Habitat Int.* **34**(1), 1–10 (2010)
4. Z.Y. Zhao, L.Y. Shen, J. Zuo, Performance and strategy of Chinese contractors in the international market. *J. Constr. Eng. Manage.* **135**(2), 108–118 (2009)
5. F. Yean, Y. Ling, Y. Gui, Strengths, weaknesses, opportunities, and threats: case study of consulting firms in Shenzhen, China. *J. Constr. Eng. Manage.* pp. 628–636 (2009)
6. F. Yean, Y. Ling, V. Min, C. Pham, T.P. Hoang, Strengths, weaknesses, opportunities, and threats for architectural, engineering, and construction firms: case study of Vietnam. *J. Constr. Eng. Manage.* **135**(10), 1105–1113 (2009)
7. C. Chen, R.J. Orr, Chinese contractors in Africa: home government support, coordination mechanisms, and market entry strategies. *J. Constr. Eng. Manage.* **135**(11), 1201–1210 (2009)
8. S. Gunhan, D. Arditi, Factors affecting international construction. *J. Constr. Eng. Manage.* **131**(3), 273–282 (2005)
9. M.K. di Marco, J.E. Taylor, A.M. Asce, P. Alin, Emergence and role of cultural boundary spanners in global engineering project networks. *J. Manage. Eng.*, 123–132 (2010)
10. S. Lee, R. Jeon, J. Kim, J. Kim, Strategies for developing countries to expand their shares in the global construction market: phase-based SWOT and AAA analyses of Korea. *Engineering* pp. 460–470 (2011)
11. Construction Industry Development Board Malaysia, Report 2010, www.cidb.gov.my
12. T. Ramayah, L.C. Yan, M. Sulaiman, SME e-readiness in Malaysia: implications for planning and implementation. *Sci. J. Manage.* **11**(1), 103–120
13. J. Nunally, *Psychometric theory*, 2nd edn. (McGraw-Hill, New York 1978)
14. G.D. Garson, *Generalized linear models and generalized estimating equations*, statnotes: Topics in multivariate analysis. Retrieved from <http://faculty.chass.ncsu.edu/garson/pa765/statnote.htm> (2011)
15. R. Al-sabab, in *Evaluating significant risks in the middle east north Africa (MENA) construction projects from perspective of multinational firms.*, Proceedings of the CIB W78 2012: 29th International Conference, Beirut, Lebanon
16. M.E. Porter, Industry structure and competitive strategy: keys to profitability. *Financ. Anal. J.* **36**(4), 30–41 (1980)

Application of Automation Technology in Malaysian Construction Industry

Siti Rashidah Mohd Nasir, Che Maznah Mat Isa and Kamilah Ali

Abstract Automation Technology has been widely used in the construction by developed country such as Japan and South Korea because of its good performance and beyond satisfactory in project workmanship. However, in Malaysian construction industry, Automation Technology is poorly accepted by the construction players. Implementation of Automation Technology may assist in reducing problems such as labor shortage, high fatalities in accidents and low quality which are among the major factors lead to project delay. Thus, this paper studies the acceptance of Automation Technology among the contractors and the limitations and barriers of the Automation Technology implementation. Questionnaires were distributed to Class A contractor in Kuala Lumpur area. The results of this study will shed some lights to the construction players in implementing Automation Technology in Malaysian construction industry, thus strategies to move forward can be recommended.

Keywords Automation technology · Contractor · Acceptance · Limitation · Barrier

1 Introduction

Automation Technology is an application of mechanical electronics (mechatronics) and computers for production of goods and services. Automation Technology is synonym and related closely with robotic. Nowadays, robots are widely used in construction and admitted by many construction companies especially in the developed countries such as Japan and South Korea that the quality of the works

S. R. M. Nasir (✉) · C. M. M. Isa · K. Ali
Faculty of Civil Engineering, UiTM, Shah Alam, Malaysia
e-mail: sitir015@salam.uitm.edu.my

done in the present of Automation Technology in their construction is beyond the satisfactory [1]. However the implementation of Automation Technology in construction is still not been fully practiced in Malaysian construction industries even there are many advantages that can be found based on the achievements by the countries that already applied Automation Technology in their construction [2]. Malaysian construction industries still practicing the traditional method in their construction project even though among of them, there are people with the knowledge of the advantages of Automation Technology implementation. The construction industry sector is also an important engine of growth for development of the country, thus this paper study the awareness of automation technology among the contractors; identify the advantages; and limitations and barriers faced by the contractor in implementing Automation Technology in Malaysian construction industry.

2 Literature Review

Automation Technology in construction can be defined as the using a device (robots or machines) in other to do the tasks automatically that originally done by human in other to achieve the objectives of the construction project that are reduce in cost, high in quality, complete in time and zero accidents and fatalities at the construction site [2]. The device is programmed in order to adapt with the construction site environment and be able to carry out the job smoothly [1, 2].

2.1 Automation Technology in Malaysian Construction Industry

In the growth of construction industry in Malaysia, there are crucial problems that being faced by the entire individual that involved in the construction works. One of the problem is the high accident rate occurred in the construction industry due to the traditional method practiced by most of construction companies [3]. Accidents in the construction industry have the highest number of death case compared to other sector on death category [4]. According to the Malaysian Occupational Accidents Statistics in 2012, the statistic of accidents involves death in Malaysian construction industry recorded 48 numbers which is the highest rate in comparison to the other sectors [5]. Apart from the highest rate of accident, other problems faced in Malaysian construction industry are shortage in labor and poor quality in the construction industry. The shortage of labor has become an issue because of the selective attitude of local labor. This is due to expansion of education, improvement in living condition and access to upward mobility [6]. Foreign workers comprised of 69 % from the total 800,000 of registered workers.

When they first arrived in Malaysia, the foreign workers are usually unskilled and this gives an impact on the productivity as well as the quality of the construction industry [6].

In the early 90s, applications and activities of robotics and automation in the industry had started. The aims of the applications are to optimize equipment operations, improve safety, and enhance perception of workspace and also to ensure quality of environment for occupants [7]. Over the past few decades, improvements to productivity in the construction industry have been insignificant compared with other industries. Productivity improvements in other industries, especially manufacturing, have stemmed to a large extent from the effective implementation of new technologies [8]. However, the introduction of new technologies in the construction industry to fully automate the building process has been limited [8]. This is due to the insufficient attention to process improvement which became a major barrier to automation and other technological progress of construction [1].

2.2 Advantages of Automation Technology Application in Construction Industry

Application of automation and robotics in construction is addressed from perspective of raising building projects performance to serve the client and the environment. The robotics and automation systems in construction industry can achieve the following advantages [7]:

- Higher safety for both workers and the public through developing and deploying machines for dangerous jobs;
- Uniform quality with higher accuracy than that provided by skilled worker;
- Improving work environmental as conventional manual work is reduced to a minimum, so the workers are relieved from uncomfortable work positions;
- Eliminating complains about noise and dust concerning works such as removal, cleaning or preparation of surfaces; and
- Increasing productivity and work efficiency with reduced costs.

Apart from that, contractors utilize automated technologies on projects as a means of saving cost, reducing project durations, improving quality and consistency and gaining other related project benefits [8]. In addition, automation construction opened up possibilities for all-weather construction, unaffected by the outdoor climatic conditions [3]. Furthermore, factory automation has been adopted to cope with the issue of an individual automated robot's movement in order to increase its productivity. This gives a result in the dramatic decline of construction material dissipation [3].

2.3 Limitation and Barrier in Implementing Automation Technology in Construction Industry

In Japan, there is a great deal of demand for automation and robotics. This is due to the “3K” image of construction is perceived by the workers “Kitsui” hard, “Kitanai” dirty, “Kiken” dangerous environments and strongly generally felt by the industry, the government and the public [9]. Due to the effect of the negative image of construction lead to the crucial shortage of skilled workers, increasing wages and increasing the cost of construction in Japan [9].

Japanese policy of not allowing workers from other countries into Japan exacerbates the problem. Skilled labor shortages are limited to certain geographical areas and trades and the problem is more skill shortage than labor shortages. Unlike in the United States, training the abundant supply of unemployed or unskilled workers may be more practical than building expensive machines that may only put more people out of work [9]. Providing job opportunities is far more valuable politically than investing in technology that may be perceived as a threat to constituents’ job [9].

Apart from that in automated construction site one of the barriers of its implementation is the technological barriers which the robot must cope with the complexity of the construction process involving a dynamic and evolving site beside the need to perform multiple tasks with differing characteristics [10]. Other than technological barriers, the economical barriers also affect the implementation of a robotic system in construction [10].

One of the hurdles to automating the construction process is the design of a project. The design that had been stated is the design of a facility inhibits both the use of available automated equipment during construction and the successful development of new automated equipment [8]. Furthermore, the capabilities of automated equipment are constrained in the aspect of physical of the design [8].

3 Methodology

The questionnaire were designed with reference to previous research [2, 3, 7]. In this study, Likert scale was used in order to produce a highly reliable scale and easy to be understood by the respondents. Two sets of Likert scale were used in the questionnaire. In measuring the Awareness on AT in Malaysian Construction industry, the suitable Likert scale based on the frequency [11] were used as follows: 1—never; 2—rarely; 3—sometimes; 4—often; and 5—always. While for question for Factors and Limitation in implementing AT, the suitable Likert scale based on the level of agreements [11] were used as follows: 1—strongly disagree; 2—disagree; 3—neutral (undecided); 4—agree; and 5—strongly agree.

The respondents are Class A contractor where the list of contractor was obtained from Pusat Khidmat Kontraktor. They were selected based on their vast experience in construction industry. The research area is within the Kuala Lumpur. This area were chosen due to its rapid development in construction and in addition, most of the Class A contractor companies were located in this area.

From the list obtained, the total number of contractor companies in Kuala Lumpur is 352 companies [12]. The number of sample requires for this study is 184 with 95 % of confidence level using interpolation respondents with margin of error are 5 % [13].

The pilot study was conducted with the subject matter experts to discuss and validate the questionnaire. For that purpose, the experts were randomly chosen which consists of Class A contractor, engineers and consultants from private and government companies. The selection were made for their vast experience in construction industry. Subsequent to the pilot study, the questionnaire was amended according to the comments and suggestion from expert.

Following to that, the questionnaire survey was initially distributed via email in February 4, 2013. Due to the poor respond rate, the questionnaire was redistributed by hand and by postal. The collection of questionnaire was extended to May 15, 2013. In order to obtain the number of sample of 184 respondents, 300 questionnaires had been distributed. Simple Random Sampling was selected as a sampling method. By using this technique, the differences that do occur are result of chance, not of the conscious or unconscious of researcher bias in selection [14].

4 Results and Analysis

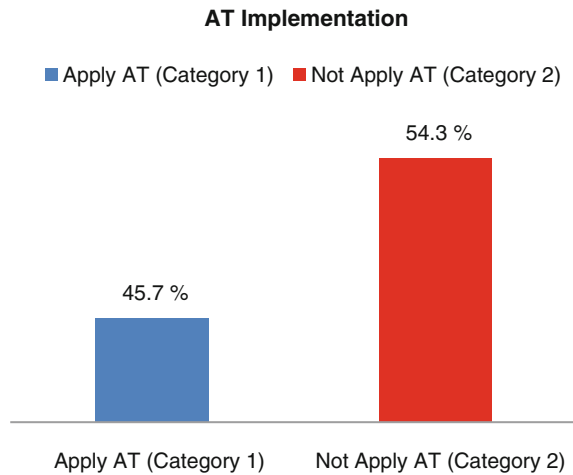
From the reliability test performed, the value of Cronbach's Alpha is 0.865. The value is in the range of 0.8–0.9 which is considered as good [15]. Thus, none of the question in the questionnaire survey should be excluded and this means that the questionnaire is relevant to the topic researched.

The number of successfully collected questionnaire is 184 with respond rate is 61.3 %. Although the number of collected sample is less than 300, the respond rate of 61.3 % has achieved the required sample size of 95 % confidence level and 5 % margin error [13].

In this study, this analysis evaluates 2 different types of respondents and categorized as Category 1—Respondents who had applied Automation Technology in the projects; and Category 2—Respondents who has not applied Automation Technology in the projects. Figure 1 shows the percentage of respondents for both categories.

From 184 numbers of successfully collected samples, Fig. 1 shows the Category 1 consists of 45.7 % respondents while 54.3 % consists of Category 2.

Fig. 1 Distribution of respondents apply automation technology in projects



4.1 Analysis of Category 1: Respondents Applied Automation Technology

Figure 2 shows that 43.2 % of the respondents involved in roads and bridges; followed by 30.6 % of buildings; 17.1 % of drainage; and 0.9 % of marine and coastal. The highest percentage of area of expertise for Category 1 are roads and bridges; and buildings as compared to others. This shows that Category 1 respondents have significantly applied Automation Technology in the roads and bridges projects. This is supported by Elattar [7] where road paving robots have shown a high level of automation through various functions.

Figure 3 shows 29 % of company in Category 1 has established 6–10 years while 71 % of the company has established more than 10 years.

The respondents of Category 1 were asked in the questionnaire to indicate their opinion on the factors that lead them to consider application of Automation Technology in their projects. The factors are as follows: Prevent the hazardous to the workers; Reduced the fatalities in accident rate; Reduced the construction cost; Solved the skilled labor shortage problem; Increase the quality with high accuracy of the project; Increase productivity in the construction; Complete the project within contract time; Improve work environment; Increase the efficiency of works; Eliminate complains about noise and dust; Dangerous works can be done by robots; and Design of the project involving robots to produce accurate measurement and to handle the dangerous and difficult situation at the construction site.

From the analysis conducted using mean value, Fig. 4 shows that among the factors, respondents in Category 1 has agreed that the major factors led to the application of Automation Technology are prevent hazardous, labor shortage, increase quality and improve environment which received mean value of 4.58, 4.39, 4.36 and 4.35 respectively as shown in Fig. 4. Previous study has also agreed

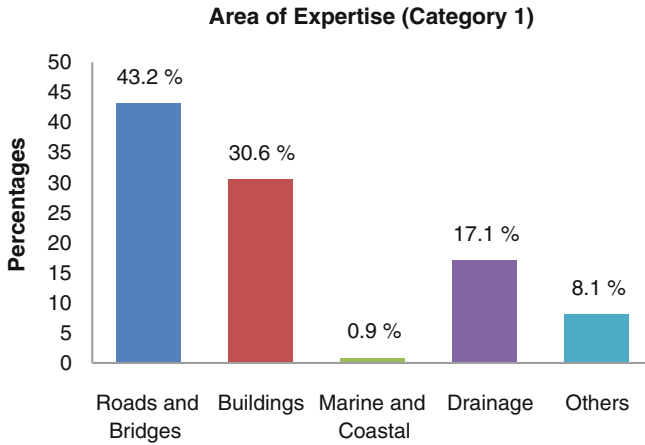
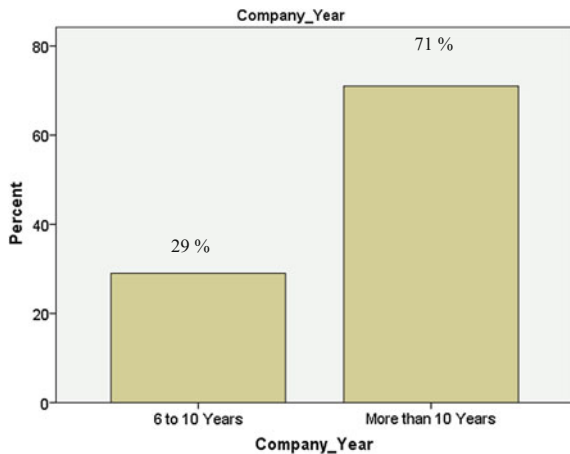


Fig. 2 Respondents expertise (Category 1)

Fig. 3 Year of company establishment (Category 1)



that the Automation Technology can achieve advantages such as higher safety for both workers and public; obtain uniform quality; improving work environmental and labor shortage [7, 8, 16].

The Automation Technology implementation in construction can increase the safety at the construction site because Japan already adopted construction automation systems experienced definite improvement in their construction work environment as well as safety [3]. The quality of the works done is also high when Automation Technology in construction is implemented by applying Robotics and automation systems in construction industry, the main advantages that will be achieved is the uniform quality with higher accuracy than that provided by the skilled worker [7].

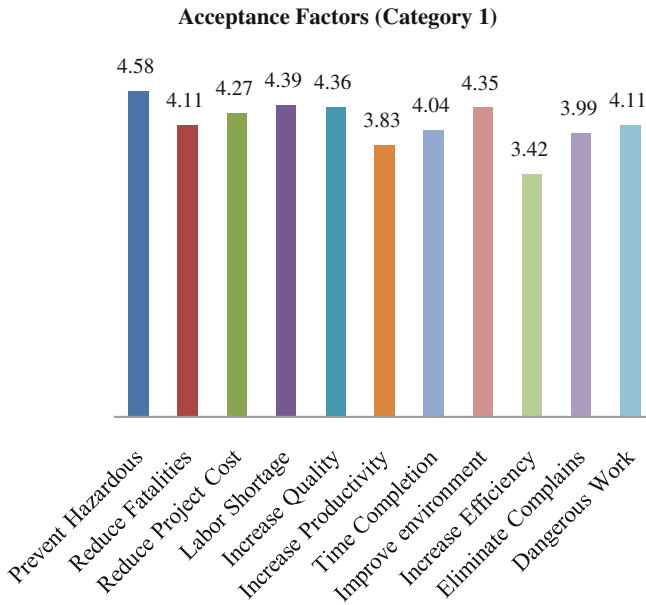


Fig. 4 Acceptance factors of AT by Category 1

The benefits of Automation Technology application in Malaysian construction industry is important to be realized due to the problems that being faced by contractors as well as the persons who are directly in charged at the construction site.

The advantage of Automation Technology can reduce the rate of accident at construction site. According to the statistic by the Malaysian Department of Occupational Safety and Health, the construction industry has the highest number of fatalities accidents of 48 number of victims as compared to the others sectors [5].

Apart from that, labor shortage and poor quality of the works done by unskilled and foreign workers in Malaysian construction industry has been an issue and has been reported to contribute to low productivity [17]. Although the unskilled workers are normally cheap, however, their inefficiently works has resulted in a high construction wastage which leads to high construction cost [17].

Low quality of work were also an issue to Malaysian construction industry, where numerous indications and complaints of low quality of work in construction have been made by consumers through media and authorities and this has contributed to decrease in quality of life, uncomfortable and unfriendly environments [17].

Furthermore, Malaysian construction industry also facing with delay in project completion where 17.3 % of construction projects has reported to experience more than three (3) months delay and some of the projects were abandoned [18].

Table 1 Correlation table of Spearman test

Correlations			Company year	Application
Spearman's rho	Company year	Correlation coefficient	1.000	0.332 ^a
		Significant (2-tailed)	–	0.002
		N	84	84
	Application	Correlation coefficient	0.332 ^a	1.000
		Significant (2-tailed)	0.002	–
		N	84	84

^a Correlation is significant at the 0.01 level (2-tailed)

Having the application of Automation Technology may assist Malaysian construction industry to overcome these problems.

A correlation analysis using Spearman's test was conducted to establish the relationship between year of company establishment and application. Table 1 shows that there are no significant difference between year of Company Establishment and AT Application with $p = 0.002$. This indicates that year of company establishment does not influence the decision in AT application. The correlation coefficient is 0.332, indicates that company with less than 10 years experience may also has the consideration of Automation Technology application in their projects.

4.2 Analysis Category 2: Respondents Have Not Applied Automation Technology

Figure 5 shows 50 % of the respondents in Category 2 involved in building projects while roads and bridges; drainage; and marine coastal received 26.7, 15.3 and 1.3 % respectively.

Figure 6 shows 84 % of the company in Category 2 has established more than 10 years and 16 % established in 6–10 years.

The respondents were also been asked to indicate their opinion of barrier factors of Automation Technology which are as follows: High cost to start using implements the Automation Technology in the construction; Reduced the job opportunities, hence the unemployed people will increase; Robots function only for limited programmed works; Lack support from the government, social and individual that involved in the construction industry; Automation Technology and robotics are costly to be updated and maintained; Technological barriers (complexity at site location must be cope by the robots); Lack of interest to implement Automation Technology in construction due to lack of information; Most of robots are not versatile for different site locations; Design of the project involving robots; Automation Technology do not give plausible (significant) image in the construction industry; Design of the project involving robots will increase in project

Fig. 5 Respondents expertise (Category 2)

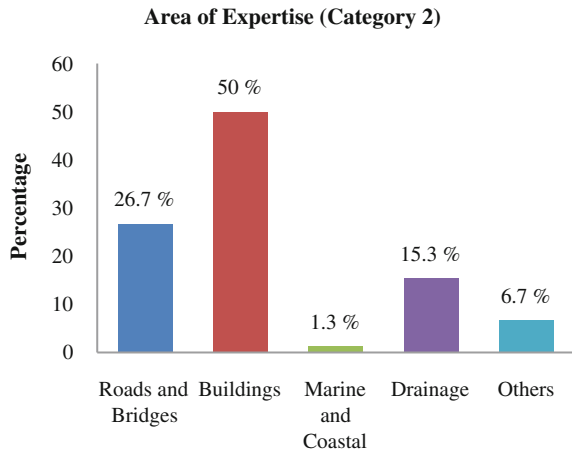
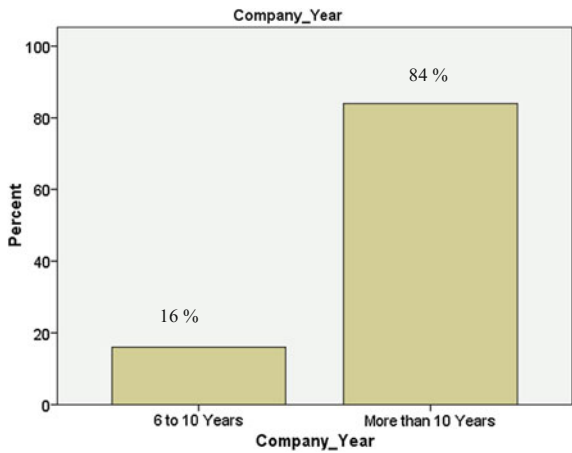


Fig. 6 Year of company establishment (Category 2)



cost; and Automation Technology that had been damaged and cannot be repaired may gives an impact to environment such as radioactive substances.

Figure 7 shows the barrier factors of Automation Technology application indicate by respondent by Category 2. The main factors are high cost, limited function and high cost to maintain which received mean value of 4.57, 4.4 and 4.24.

The major barrier for automation and robotics in construction is because of the high costs and shortage of public money for research and development. This problem was faced in European construction industry where the development to a higher degree of automation in the construction industry has been going at a slow pace [16].

Robots and automated systems are subject to severe scrutiny for their cost effectiveness. However, in adopting Automation Technology in construction, the development of a comprehensive, multidimensional analysis of costs and benefits

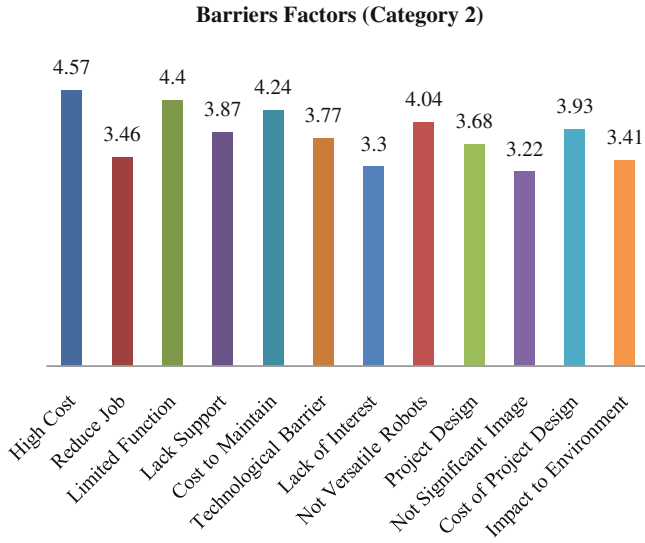


Fig. 7 Barrier factors of AT by category

associated with specific robotic application must be taken into consideration. It is quite important to analyze success through the technical and economic feasibility [7]. This economic feasibility is determined by the analysis of the costs and benefits associated with their development and field implementation [7].

The capabilities of automated equipment are constrained in the aspect of physical of the design [8]. In automated construction site one of the barriers of its implementation is the technological barriers which the robot must cope with the complexity of the construction process involving a dynamic and evolving site beside the need to perform multiple tasks with differing characteristics [10].

5 Conclusion

Major acceptance factors on Automation Technology application in construction industry based on contractors’ perspective which are highly agreed are as follows: Prevent the hazardous to the workers; Solved the skilled labor shortage problem; Increase the quality with high accuracy of the project; and Improve work environment.

On the other hand, the barrier factors of Automation Technology application are as follows: High cost to start using implements the Automation Technology in the construction; Robots function only for limited programmed works; Automation Technology and robotics are costly to be updated and maintained; and Most of robots are not versatile for different site locations.

In view to the results and analysis, the contractors have to change the attitude to have opportunity-oriented personality and openness to change besides always be updating with the growth of the technology in the construction industries around the world.

In addition, the government should support the application of Automation Technology in construction industry by providing facilities or financial fund for construction companies that interested to implement the Automation Technology. This is to ensure that contractors will give cooperation that lead to mutually beneficial for both sides. Malaysian government need to give special attention to the construction industries because the construction industry is critical to national wealth creation and enables others industries such as manufacturing, services and education.

The government should also conduct research on technology exchange with other country that already implement the Automation Technology, so that the knowledge can always be updating with the rapid growth and change in technology nowadays. Thus, assist the Malaysian construction industry to move forward with the new technology in construction.

References

1. S.B. Mohammad, in *Engineering Approach System to Assess Defect and Deterioration of Building Structures*, International Seminar on Application of Science and Mathematics (2011)
2. R. Mahbub, in *An Investigation into the Barriers to the Implementation of Automation and Robotics Technologies in the Construction Industry*, Ph.D. thesis, School of Urban Development, Faculty of Built Environment and Engineering, Queensland University of Technology, 2008
3. C. Han, *Human–Robot Cooperation Technology: an Ideal Midway Solution Heading Towards the Future of Robotics and Automation in Construction* (Hanyang University, Korea, 2011), pp. 13–18
4. V.G.C.H. Hui, in *Risk Assessment on Safety in Construction*, Master thesis, Universiti Teknologi Malaysia, 2011
5. Department of Occupational Safety and Health Official Website, *Occupational accidents statistics 2012*, <http://www.dosh.gov.my/index>. May, 2013
6. Z.A. Hamid, A.M. Kamar, Modernising the Malaysian construction industry, 2010 CIB World Congress (2010)
7. S.M.S. Elattar, Automation and robotics in construction: opportunities and challenge. *Emirates J. Eng. Res.* **13**(2), 21–26 (2008)
8. M.M. Hewitt, J.A. Gambatese, in *Automation Consideration During Project Design*, International Symposium on Automation and Robotics in Construction (ISARC), Washington D, 2002
9. J.G. Everett, H. Saito, Automation and robotics in construction: social and cultural differences between Japan and the United States, in *Automation and Robotics in Construction XI*, ed. by A. Chamberlain (Springer, Berlin, 1994), pp. 223–229
10. J. Neelamkavil, in *Automation in the Prefab and Modular Construction Industry*, Automation and Robotics: 26th International Symposium on Autoamation and Robotics in Construction (2009)

11. W.M. Vagias, *Likert-Type Scale Response Anchors*. Clemson University, 2006
12. Ministry of Works Malaysia, Contractor Service Centre (PKK) Official Website, <http://pkk.kkr.gov.my/home>. March 2013
13. R.V. Krejcie, D.W. Morgan, Determining samples size for research activities. *J. Educ. Psychol. Measur.* **30**, 607–610 (1970)
14. P. Singh, C.Y. Fook, G.K. Sidhu, *A Comprehensive Guide to Writing a Research Proposal* (United Kingdom, 2006)
15. J.A. Gliem, R.R. Gliem, in *Croanbach Alpha Reliability Coefficient for Likert-Type Scales*, Midwest Research to Practice Conference in Adult, Continuing, and Community Education Calculating, Interpreting, and Reporting, 2003
16. Shinko Research Co., in *Autoamtion of Building Construction and Building Products Industry—state of Art in Japan*. Shinko Research Co., Ltd, 2007
17. S.N.H. Salahuddin, *Factors Affecting Construction Time Performance for IBS in Malaysian Construction Industry*. Universiti Teknologi Malaysia, 2010
18. A.S. Ali, A. Smith, M. Pitt, C.H. Choon, Contractors' perception of factors contributing to project delay: Case studies of commercial project in Klang Valley Malaysia. *J. Des. Built Environ.* University of Malaysia, Malaysia **7**, 43–57 (2010)

Part X
Nano-Materials for Engineering

Alteration of Nano Metakaolin for Ultra High Performance Concrete

A. Mohd Fadzil, M. S. Muhd Norhasri, M. S. Hamidah, M. R. Zaidi and J. Mohd Faizal

Abstract The utilization of Ultra High Performance Concrete (UHPC) in the construction industry is growing towards in the new millennium. UHPC produce a very high strength and durable concrete to withstand aggressive attack from nature such as sulphate, chloride and others. The production of UHPC depends on several factors for instance high consumption of cement, very fine aggregates, utilizing pozzolanic material such as silica fume and additions of hyper plasticizers. Now days with the recent development of nanotechnology, nano materials has been produced and utilize in the concrete. Due to the effects of ultrafine particles, nano material will helps to enhance strength and durability of conventional UHPC mix. In this research, nano metakaolin has been developed by using high energy milling from raw kaolin. Zirconia oxide of jar and ball were used and the duration of milling is 24 h. The mix proportion of this research also includes metakaolin as cement replacement material to 10 % and nano metakaolin as additives from 1, 3, 5, 7 and 9 %. Nano metakaolin inclusion in UHPC mix will be evaluated for cementitious properties in terms of standard consistency and setting time whereas for mechanical properties compressive strength test will be performed. For setting time shows that the addition of nano metakaolin at every replacement level will increase setting of cement paste and the optimum retardation effect were recorded by NKA1. The addition of nano metakaolin at 7 % records the highest strength compare to other specimens. The action of nano metakaolin at 1 % acts as ultra-filler and refines the microstructure of concrete. Furthermore, nano metakaolin also produces a secondary hydration product by optimizing the remaining calcium hydroxide which was not fully removed during the hydration period.

A. M. Fadzil (✉)

Institute of Infrastructure and Sustainability Management, Universiti Teknologi MARA,
Shah Alam, Malaysia
e-mail: fadiil2013@yahoo.com

M. S. Muhd Norhasri · M. S. Hamidah · M. R. Zaidi · J. Mohd Faizal
Faculty of Civil Engineering, Universiti Teknologi MARA, Shah Alam, Malaysia

Keywords UHPC · Nano material · Metakaolin · Nano kaolin · Setting time · Compressive strength

1 Introduction

Now days, the application of Ultra High Performance Concrete (UHPC) is commonly used in the construction industry. Due to the rigid and unique design that needs structures that can resist very high load, UHPC becomes the solution. Determination of UHPC is concrete that can carries load that is more than 100 MPa [1, 2]. Despite of high strength, UHPC mix is also very durable due to aggressive attack such as sulphate and chloride. UHPC mix can reduce the size of structures such as beam and column and this will contribute in cost saving and time [3]. However, there is many factors that to be governed in the production of UHPC. The main criteria in UHPC mix are to produce a very dense concrete and that includes a very fine microstructure which less void and compact. Selective materials especially the selection of fine aggregates and minimizing the size of coarse aggregates portion was the main factor in the contribution to a very dense UHPC mix. Selection of binder materials which is cement and also the addition of micro fine materials are needed. In the conventional UHPC mix, the inclusion of silica fume as additive in the mix is required to ensure a very high strength is achieve [4, 5]. Pozzolanic materials also been added as additive such as silica fume, metakaolin, fly ash and rice husk.

The usage of pozzolanic materials in the UHPC mix is needed due to effect of filler, promotes the formation of Calcium Silica Hydrate (CSH) by reacting with Calcium Hydroxide and finally the pozzolanic reaction that influence in promoting additional strength [6]. The terms pozzolanic materials is any materials that consists silica or alumina or silica and alumina when react with water during the hydration process will creates the binding effect and promoting CSH gel [7, 8]. As been mentioned earlier, silica fume was the main material in conventional UHPC mix because of the high silica content that will helps in the strength development. The application of other pozzolan such as metakaolin, fly ash and rice husk also been implemented recently by researchers to see the potential of creating pozzolanic reaction in UHPC mix [9, 10].

Since the new millennium, the study and application of nano materials in concrete has growing an interest to researcher all over the world. The utilisation of nano silica, nano alumina and titanium oxide were common nano materials applied as strength enhancement agent and producing a very durable concrete [11, 12]. However due to cost and the availability of nano materials, the application of those materials is not been implemented widely in the UHPC mix.

The process of producing nano materials can be divided into two. First is top to bottom approach that involves milling technique and second bottom to top approach which using chemical synthesis method [11–14]. Those processes can

produce nano size materials only the end product is different. Milling can be considered as low cost process for producing nano materials only the disadvantages was the size of particle is not uniform and the quality of end product depends on milling speed, ball, jar type and duration of milling. Another approach by using chemical synthesis involves high end instrument which expensive but produce uniform size of nano product.

Nano kaolin was a product based from kaolin or white clay. Kaolin needs treatment which involves calcination process to make it reactive and change to metakaolin [7, 15]. Metakaolin was one of pozzolanic materials which are proven to enhance strength and durability of concrete [16–18]. Metakaolin size which in micro size around 1–2 μm performs as micro filler in concrete microstructure and promoting hydration product. Nano metakaolin addition as additives will increase the effect as nano filler that will helps to refines the microstructure of UHPC. In addition, nano metakaolin promotes hydration product by acting as secondary hydration process to concrete. Furthermore by implementing milling process which is inexpensive while producing nano metakaolin will gives alternative to the concrete industry on the utilisation of nano materials in UHPC mixes.

2 Methodology

2.1 Production of Metakaolin and Nano Metakaolin

Kaolin was procured from AKI Kaolin (M) Sdn Bhd at Puchong Malaysia. Metakaolin was produced by calcining process from 700 °C for 3 h. This treatment was needed in order for kaolin to chemically reactive to metakaolin. For nano kaolin, high energy milling was the technique approach to refine the particles of kaolin from micron to nano size. Fritsch Pulverisette Analyzer was the machine used and the speed of milling was fixed to 400 rpm. To perform the milling process, 3 mm diameter ball and jar type were fixed to Zirconia Oxide (ZrO_2). The selection of those properties was important in milling process to optimize the end product of milling. Duration of milling for nano kaolin was fixed to 24 h. Finally to perform nano metakaolin, nano kaolin will undergo calcination process for 3 h and the temperature was fixed to 700 °C.

2.2 Cementitious Properties

Cementitious properties of nano metakaolin paste for standard consistency and setting time were determined using the Vicat apparatus in accordance with BS EN 196-3:2005 + A1:2008. The flow of the test was done on seven specimens which OPC, MK10, NK1, NK3, NK5, NK7 and NK9. In this experiment, OPC was the

Table 1 Mix proportion for cementitious properties

Specimen	Binder (g)	Metakaolin (g)	Nano Metakaolin (g)
OPC	500	–	–
MK10	450	50	–
NKA1	450	50	5
NKA3	450	50	15
NKA5	450	50	25
NKA7	450	50	35
NKA9	450	50	45

control specimen and MK will react as cement replacement method for every specimen and also as a mix (MK10). Finally NK will acts as additives based on percentage from 1 to 9 %. All specimens were test on the standard consistency, initial and final setting time. Table 1 shows the mix proportion to determine cementitious properties.

2.3 Strength Properties

To determine the strength properties of nano metakaolin paste, specimen will prepare by using 50 mm cube mould. Metakaolin will act as cement replacement materials and fixed to 10 % of cement weight. Washed sand were used and sieved at 3 mm. The size of granite coarse aggregate is fixed to 10 mm. Glenium suretec 389 were used as superplasticizers and the dosage is fixed to 2 %. Nano metakaolin as an additive was added to the paste from 1, 3, 5, 7 and 9 %. All specimens will be water cured until age of testing from 3, 7 and 28 days. Table 2 shows the mix proportion for this research.

3 Result and Discussion

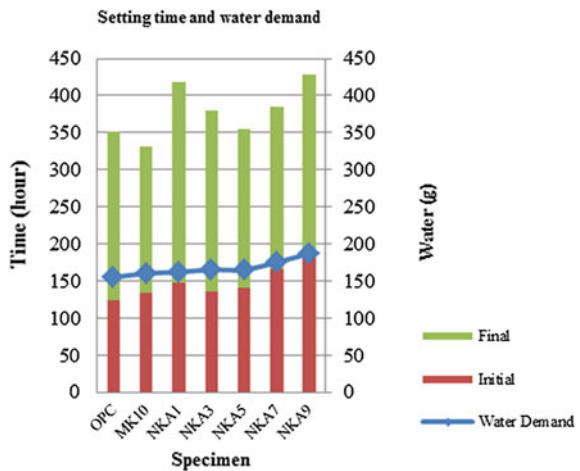
3.1 Cementitious Properties

The findings for cementitious properties were portrayed by Fig. 1. For standard consistency, the addition of nano metakaolin at every level of replacement increase the water demand of cement paste compare to OPC. NKA9 which contains of 9 % of nano metakaolin records the highest increase in water which 187 g. From this figure confirms that the influence of larger surface area of nano metakaolin compare to OPC creates more spaces in the paste and resulting for nano metakaolin paste needs more water to fully reach the level of consistency. For setting time, the evaluation was evaluated for initial and final set. Again the same pattern

Table 2 Mix proportion for UHPC

Mix	OPC (kg/m ³)	Water (kg/m ³)	Fine (kg/m ³)	Coarse (kg/m ³)	HRWR (kg/m ³)	MK (kg/m ³)	NK (kg/m ³)
OPC	800	160	800	433	16	0	0
MK10	720	160	800	433	16	80	0
NKA1	720	160	800	433	16	80	8
NKA3	720	160	800	433	16	80	24
NKA5	720	160	800	433	16	80	40
NKA7	720	160	800	433	16	80	56
NKA9	720	160	800	433	16	80	72

Fig. 1 Standard consistency and setting time for nano metakaolin paste



were recorded where increase in nano metakaolin percentage will retard and delayed the setting time for both initial and final set. For initial set NKA9 recorded the longest time of setting compare to other mix. However for final set, two mixes shows almost the same result which is NKA1 and NKA9. This happen due to the alumina content in the mix especially for NKA1 optimally blends with MK and OPC and creates more spaces for water to be hydrated [7, 19, 20].

3.2 Compressive Strength

Result for compressive strength was presented by Figs. 2 and 3. Compressive strength data was given by Figs. 2 and 3 shows the relative strength of UHPC mix containing nano metakaolin. From Fig. 2, the addition of nano metakaolin at early age which 3 day curing does not influence strength compare to OPC due to high cement content. The inclusion of nano metakaolin as additives at every level of

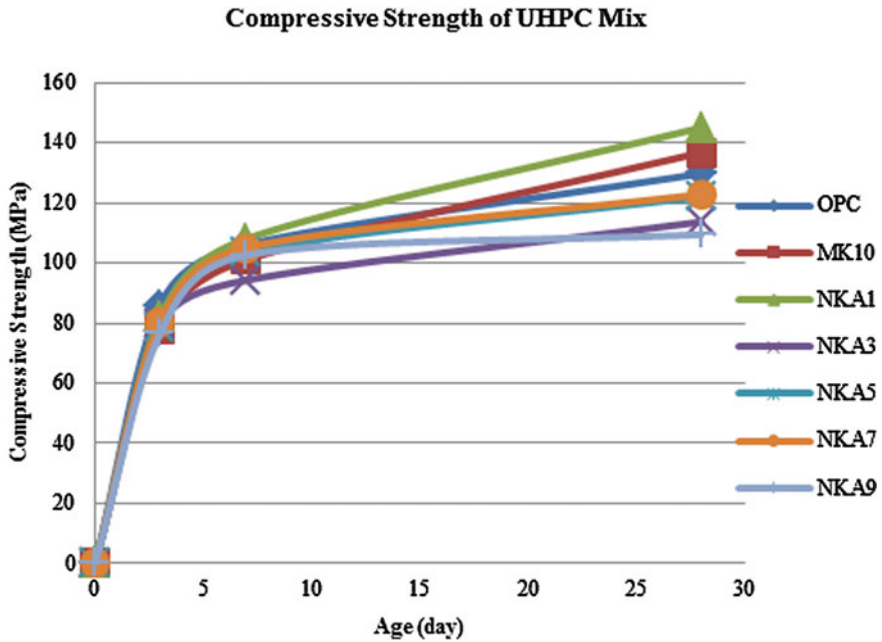


Fig. 2 Compressive strength for UHPC mix

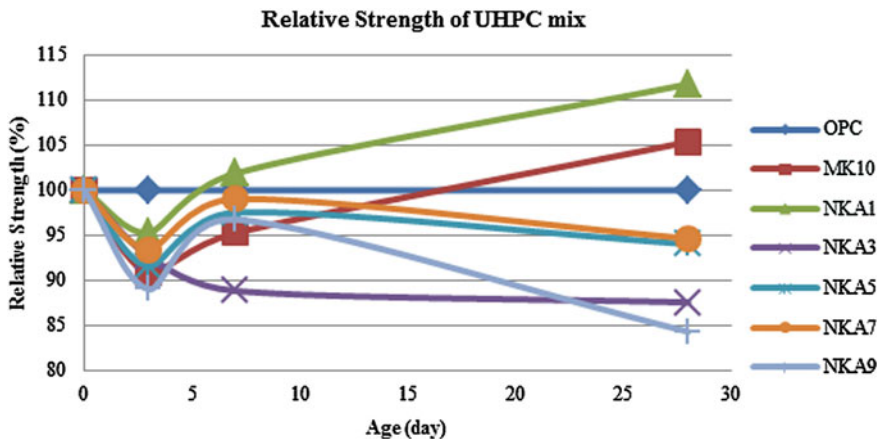


Fig. 3 Relative strength for UHPC mix

percentage didn't merge uniformly with cement matrix and causing unhydrated nano metakaolin paste to form with calcium silica hydrate. Although size of nano metakolin is finer than OPC, due to dilution effect causing delaying the strength. However, starting at day 7 nano metakaolin concrete starts to develop strength and

records higher than OPC. The highest strength were recorded by NKA1 which 1 % additives of nano metakaolin. From this, shows that the effect of nano particles of nano metakaolin influence strength enhancement due to high content of silica in nano metakaolin compare to OPC. The strength development of NKA1 is cause by a complete dilution effect and resulting in a uniform and homogenous structure of concrete. Furthermore nano metakaolin acts as ultrafiller by replacing and filling the micro voids also supports the phenomena. Eventually, at 28 day curing NKA1 records the highest strength compare to other mix and this is where complete action of nano metakaolin which is ultra filler, promoting calcium silica hydrate gel by reducing the formation of calcium hydroxide and finally ultra pozzolanic reaction of nano metakaolin that's promoting additional calcium silica hydrate gel to performs a dense structure concrete by reinforcing bonding of cement matrix structure. Influence of nanometakaolin creates a secondary hydration product also known as formation of crystal nucleus role or nucleation effect. Nucleus role effect means the addition of nano metakaolin creates additional hydration product in the surface of existing C-S-H gel [19]. These secondary gels create a penetration wall in the gel so the formation of C-S-H gel is uniform and effecting in the early strength of concrete.

Results for relative strength were shows by Fig. 3. For relative strength the trend supports the findings for compressive strength. At 3 day curing, nano metakolin mix does not improve the strength compare to OPC because the relative percentage was less than 100 % for OPC. However at 7 day curing, NKA1 mix improves the strength relative compare to OPC and other mix. Almost 2 % improvement was recorded by NKA1 compare to OPC. Finally at 28 curing, NKA1 mix consistently recorded the optimum relative strength by increment around 12 % compare to OPC. Surprisingly another mix which MK10 consists of metakaolin at 10 % gives 6 % increment of strength relatively better than OPC. This shows that the addition of nano metakaolin proves to influence strength and 1 % addition of nano metakaolin helps to optimize the UHPC mix compare to OPC.

4 Conclusions

From this research the conclusions can be offered are:

1. Nano metakaolin increase the water requirement of cement paste at every level of additives to reach its consistency.
2. The addition of nano metakaolin as additive will delayed in setting time initially and final set due to finer particles size and increase in surface area.
3. Nano metakaolin shows slow effect of strength at early age due to dilution effect. Eventually, starting from day 7 strength development of nano metakaolin will develop and the optimum strength performed by NKA1 mix consists of 1 % additives of nano metakaolin.

References

1. P.K. Mehta, P.J.M. Monteiro, *Concrete: Microstructure, Properties and Materials* (Taylor & Francis, London, 1993)
2. V.M. Maholtra, P.K. Mehta, *Pozzolan and Cementitious Materials* (Taylor & Francis, London, 1996)
3. C. Wang et al., Preparation of ultra-high performance concrete with common technology and materials. *Cement Concr. Compos.* **34**, 538–544 (2012)
4. E. Güneysi et al., Strength, permeability and shrinkage cracking of silica fume and metakaolin concretes. *Constr. Build. Mater.* **34**, 120–130 (2012)
5. R. Hamid, K.M. Yusof, M.F.M. Zain, A combined ultrasound method applied to high performance concrete with silica fume. *Constr. Build. Mater.* **24**(1), 94–98 (2010)
6. A.M. Neville, *Properties of Concrete* (Prentice Hall, Englewood Cliffs, 2005)
7. B.B. Sabir, S. Wild, J. Bai, Metakaolin and calcined clays as pozzolans for concrete: a review. *Cement Concr. Compos.* **23**(6), 441–454 (2001)
8. J. Bai, S. Wild, B.B. Sabir, Chloride ingress and strength loss in concrete with different PC–PFA–MK binder compositions exposed to synthetic seawater. *Cement Concr. Res.* **33**(3), 353–362 (2003)
9. A. Tfraoui et al., Metakaolin in the formulation of UHPC. *Constr. Build. Mater.* **23**(2), 669–674 (2009)
10. N.Y. Mostafa et al., High replacements of reactive pozzolan in blended cements: microstructure and mechanical properties. *Cement Concr. Compos.* **32**(5), 386–391 (2010)
11. K. Sobolev, F.I.R. Hermsillo, L.M. Torres-Martinez, in *Nanomaterials and Nanotechnology for High-Composites. SP-254-8*, ed. by K. Sobolev and S.P. Shah. Nanotechnology of Concrete: Recent Developments and Future Perspectives. ACI. (2008), pp. 93–120
12. F. Sanchez, K. Sobolev, Nanotechnology in concrete: a review. *Constr. Build. Mater.* **24**, 2060–2071 (2010)
13. K. Sobolev, The development of a new method for the proportioning of high-performance concrete mixtures. *Cement Concr. Compos.* **26**(7), 901–907 (2004)
14. F. Pacheco-Torgal, S. Jalali, Nanotechnology: advantages and drawback in the field construction and building materials. *Constr. Build. Mater.* **25**, 582–590 (2011)
15. S. Wild, J.M. Khatib, Portlandite consumption in metakaolin cement pastes and mortars. *Cem. Concr. Res.* **27**(1), 137–146 (1997)
16. A.Y. Atta et al., Preparation of analcime from local kaolin and rice husk ash. *Appl. Clay Sci.* **61**, 8–13 (2012)
17. S.K. Babanajad, Y. Farnam, M. Shekarchi, Failure criteria and triaxial behaviour of HPFRC containing high reactivity metakaolin and silica fume. *Constr. Build. Mater.* **29**, 215–229 (2012)
18. P. Duan et al., Influence of metakaolin on pore structure-related properties and thermodynamic stability of hydrate phases of concrete in seawater environment. *Constr. Build. Mater.* **36**, 947–953 (2012)
19. X. Li, H. Chen, The influence of Nano-kaolin to cement performance. *Appl. Mech. Mater.* **174–177**, 1208–1213 (2012)
20. M.F. Arshad, in *School of Civil Engineering 2010*, Influence of Multiple Blended Binders on Properties and Performance of Concrete, Universiti Sains Malaysia, Malaysia

Hybrid Nanoparticle-Based XLPE/SiO₂/TiO₂ and XLPE/SiO₂ Nanocomposites: Nanoscale Hybrid Assembling, Mechanics and Thermal properties

Josmin P. Jose, Zakiah Ahmad and Sabu Thomas

Abstract This report demonstrates the successful use of hybrid nanoparticles of SiO₂ and TiO₂ in cross-linked polyethylene (XLPE) and reports the comparison of mechanical properties and thermal stability of XLPE/SiO₂/TiO₂ nanocomposites compared to XLPE/SiO₂, at different filler concentrations and with neat XLPE. In the present system of XLPE/SiO₂ nanocomposites, tensile strength and thermal stability show an increasing trend with nanoparticles, followed by a decaying trend at higher filler loading, whereas in XLPE/SiO₂/TiO₂ composites the property improvement is directly proportional to the filler concentration by avoiding the possibility for aggregation. It is found that the hybrid nanoparticles are efficiently dispersed in XLPE matrix, have the potential to reduce the tendency of aggregation by the combined effect of surface treatment on the nanoparticles and difference in surface characteristics of two kinds of nanoparticles. This results a direct correlation in property improvement with nanofiller concentration. This structure–property correlation is established using TEM images.

Keywords Hybrid nanoparticle · XLPE nano composites · Polymer mechanics

1 Introduction

Recent and ongoing research on organic/inorganic hybrid polymer nanocomposites has shown significant improvements in mechanical and thermal properties, without compromising other properties and processability. It is very important to

J. P. Jose (✉) · S. Thomas
School of Chemical Sciences, Mahatma Gandhi University, Kottayam,
Kerala 686 560, India
e-mail: josminroselite@gmail.com

Z. Ahmad
Institute of Infrastructure Engineering and Sustainable Management, UiTM, Shah Alam,
Selangor, Malaysia

have better mechanics and thermal stability for XLPE nanocomposites for insulation applications. The major challenge faced by these hybrid nanocomposites is the incompatibility between the organic polymer and inorganic filler and the strong tendency of aggregation of nanoparticles [1, 2]. Surface treatment on nanoparticles can reduce the degree of aggregation to some extent by two ways: (1) by reducing the surface free energy of nanoparticles, (2) by increasing the compatibility between the polymer and inorganic metal oxide nanofillers [3]. Even the surface treatment has not fully succeeded in avoiding the strong aggregation tendency of nanoparticles and thus there is negative effects on properties at higher filler loadings due to the dominant filler–filler interaction over filler–matrix interaction. Changing the surface energetics of the filler is the alternative way of breaking the filler aggregates [4]. Very recently, hybrid system of two or more nanoparticles has found promising in enhancing the dispersion of nanoparticles and thus by increasing the mechanical and thermal properties [5, 6]. Uddin and Sun have reported that silica nanoparticles reduced the agglomeration of alumina nanoparticles in the epoxy matrix dispersed by sonication method [7]. In the present study, it is tried to introduce the synergistic effect of SiO₂ and TiO₂ nanoparticles in effective dispersion in XLPE matrix by eliminating the tendency of aggregation by the combined effect of surface treatment on nanoparticles and the difference in surface characteristics of two kinds of nanoparticles. This is evidenced by the TEM, tensile measurements and thermogravimetric analysis, especially the results at higher filler loading. In XLPE/SiO₂ nanocomposites, tensile strength and thermal stability show an increasing trend with nanoparticles, followed by a decaying trend at higher filler loading, whereas in XLPE/SiO₂/TiO₂ composites the property improvement is directly proportional to the filler concentration by avoiding the possibility for aggregation. This experiment was designed to avoid nanoparticle coalescence, which is one of the most severe obstacles to the attainment of reliable results.

2 Materials and Methods

Low-density polyethylene (PETROTHENE NA951080), density 0.94 g/cm³ was obtained from Equistar, USA. Polyethylene with 0.1 % maleic anhydride was obtained from Dupont, United States. The cross-linking agent dicumyl peroxide (DCP) and antioxidant Irganox were used. The nano-SiO₂ and SiO₂/TiO₂ with 100 % silane, trimethoxyoctyl-reaction product was obtained from Evonik Industries, United States.

Silane-modified nano-SiO₂/XLPE and SiO₂·TiO₂/XLPE composites were prepared by melt mixing using dicumyl peroxide as the curing agent. The nanocomposites with 2, 5 and 10 wt. % nanoparticles were prepared. The PE-g-MAH 5 wt. %, cross-linking agent, DCP 1.5 wt. % and antioxidant 0.5 wt. % were used. The mixing was done in a Haake mixer at 160 °C and 60 rpm for 12 min. The temperature, rotation speed, time of mixing and the amount of PE-g-MAH, DCP

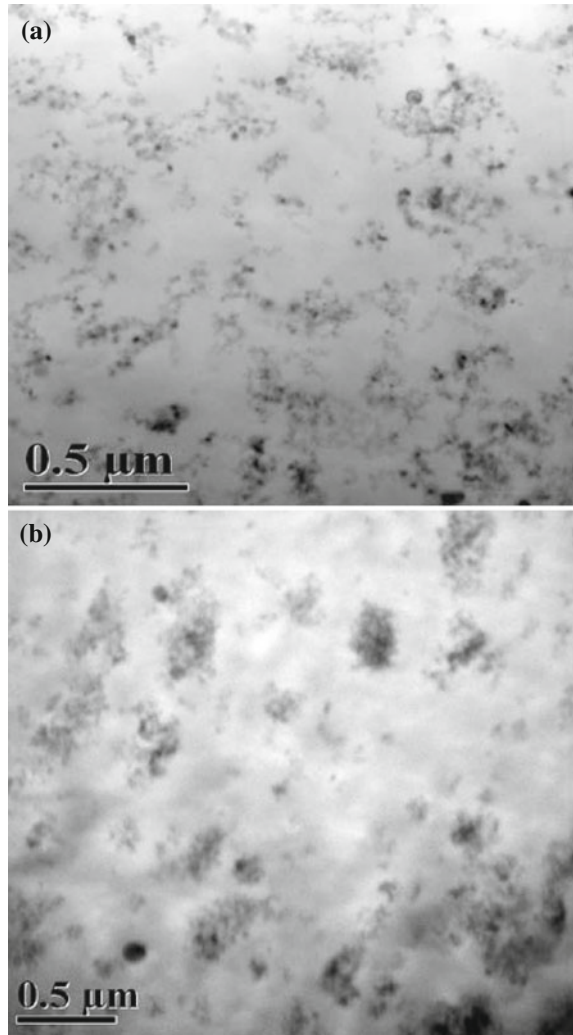
and Irganox were kept constant for all mixes. The mixed nanocomposites were compression moulded in a hydraulic press at 180 °C for 5 min. The nanocomposites with 2, 5 and 10 wt. % SiO₂ content were designated as S2, S5 and S10 and nanocomposites with SiO₂/TiO₂ were designated as ST2, ST5 and ST10. Composite of XLPE with other ingredients without nanofiller designated as X was also prepared for comparison. Samples were characterized by TEM, tensile measurements and TGA.

The Transmission Electron Microscopy images of the nanocomposites were taken in JEOL JEM transmission electron microscope with an accelerating voltage of 200 keV. Ultrathin sections of bulk specimens (about 100 nm thickness) were obtained at -120 °C using an ultramicrotome fitted with a diamond knife. Tensile tests were performed at room temperature using Tinius Olsen H50KT universal testing machine. The rectangular shaped samples of ASTM standard D638 with dimensions 10 × 1 × 0.05 cm were used. The span length and cross-head speed used for the testing were 70 and 10 mm/min respectively. The thermal stability and decomposition characteristics of nanocomposites were tested using a Schimadzu, DTG 60, Simultaneous DTA-TG instrument with thermal controller TA-60 WS at N₂ atmosphere. The heating rate was 10 °C/min from 25 to 800 °C.

3 Morphological Analysis

Transmission Electron Microscopy images of ST5 and S5 are shown in Fig. 1. Homogeneous distribution of inorganic fillers has been found in nanocomposite of XLPE/SiO₂/TiO₂ at 5 wt. % of filler loading. In contrast, a poor distribution of nanoparticles is observed in XLPE/SiO₂ with same concentration of nanofiller, since agglomerates were found in that system. These data provide evidence that significant dispersion level is achieved in ST5 compared to S5. The two reasons for nanoparticle aggregation are (1) its inherent tendency to reduce the surface free energy, (2) the formation of hydrogen bonding due to the presence of OH groups. In this case the surface treatment on nanoparticles decreases the surface free energy as well as prevents the formation of hydrogen bonds between the nanoparticles during the preparation of the composite samples [8, 9]. In order to overcome the tendency for aggregation surface treatment is playing role in the XLPE/SiO₂ nanocomposite, while the synergistic effect of surface treatment and difference in surface characteristics of two kinds of nanoparticles contribute towards XLPE/SiO₂/TiO₂ nanocomposite and this leads to more efficient dispersion of inorganic, polar, hydrophilic filler in an organic, non-polar and hydrophobic polymeric matrix.

Fig. 1 TEM micrographs of XLPE/SiO₂/TiO₂ (a) and XLPE/SiO₂ (b) at 5 wt. % of filler loading



4 Mechanics

Table 1 collects the mechanical properties of neat XLPE and nanocomposites. The highlights of the results can be summarized as follows. (1) Both XLPE/SiO₂ and XLPE/SiO₂/TiO₂ nanocomposites show better values compared to neat XLPE. (2) While comparing the two groups of nanocomposites hybrid nanoparticle filled composites (XLPE/SiO₂/TiO₂) show enhanced properties for all mechanical characteristics, tensile strength and modulus than silica filled composites. (3) Even at low concentration (2 wt. %) higher value for tensile strength and modulus is obtained for hybrid nanoparticle filled composites, i.e. lower filler concentration is

Table 1 Tensile strength and Young's modulus of neat XLPE and nanocomposites

Sample	Tensile strength (MPa)	Young's modulus (MPa)
X	7.8 ± 1.0	132 ± 7
S2	9.6 ± 1.0	149 ± 6
S5	10.3 ± 1.0	178 ± 9
S10	9.3 ± 1.0	210 ± 11
ST2	10.5 ± 1.0	176 ± 7
ST5	11.8 ± 1.0	185 ± 5
ST10	12.1 ± 1.0	218 ± 13

enough to achieve maximum efficiency by proper dispersion of nanofillers. (4) Tensile strength of XLPE/SiO₂ nanocomposites shows an increasing trend with increasing concentration of nanoparticles, followed by a decaying trend at higher filler loading, whereas in XLPE/SiO₂/TiO₂ composite the property improvement is directly proportional to the filler concentration by avoiding the chance for aggregation.

The mechanical performance depends on several factors like: filler loading, extent of interaction between matrix and filler, change in morphology in polymeric matrix by introducing the nanoparticles, enhanced interface between filler and polymer, particle surface characteristics like specific area, roughness, surface free energy etc. [8]. As the interaction between the filler and matrix is improved by increased compatibility and decreased aggregation tendency, the stress is much more efficiently transferred from the polymer matrix to the inorganic filler, resulting improved tensile properties [10]. However, particle aggregation tends to reduce the strength of the material. Aggregates can act as strong stress concentrators [1]. The superior mechanical properties of hybrid nanoparticle filled composites even at higher concentration can be further explained as the limited tendency of aggregation of two kinds of nanoparticles due to the difference in surface characteristics and thereby reduction in prevailed filler–filler interaction over filler–matrix interaction.

It is understood that, an attractive interface will decrease the mobility of the polymer chains and a repulsive interface will increase the mobility [11]. The alkyl chain on surface treatment can act as a link between the polymer and filler, which makes an attractive interface and thus the reduced polymer chain mobility.

Modulus enhancement depends on intrinsic properties of matrix as well as interactions between matrix and filler. The reinforcing capability of nanofillers is caused by an immobilization of the polymer chains [12]. The high modulus value is the direct result of reduction in mobility of polymer chains. The polymer filler interaction can contribute towards physical network density. For the present system, polymer chain immobilization could be attained by transformation of normal polymer chain to the constraint polymer in the vicinity of nanofillers [13]. The immobilized polymer layer (constraint polymer) around the filler surface, is the direct result of the effective interaction between filler and polymer. This immobilized phase can contribute to the total network density of the polymer and thus the effective stress transfer in mechanical stretching.

Fig. 2 The TGA graphs of XLPE(X), XLPE/SiO₂ 2 wt. % (S2), XLPE/SiO₂ 5 wt. % (S5), and XLPE/SiO₂ 10 wt. % (S10)

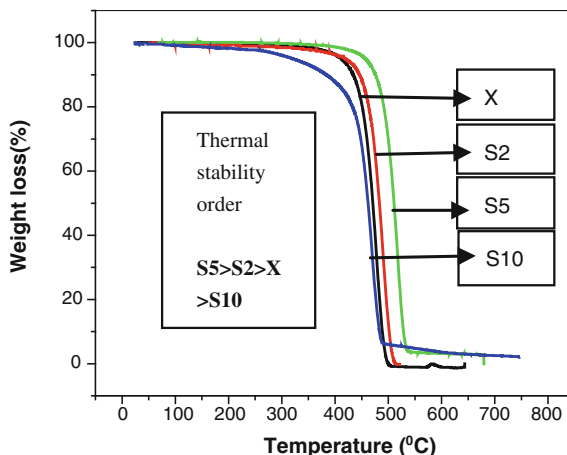
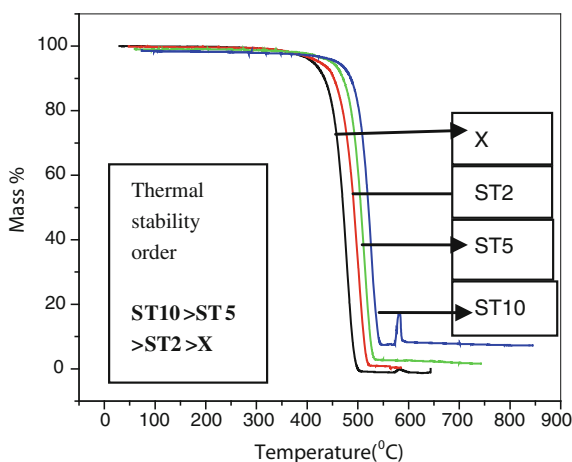


Fig. 3 The TGA graphs of XLPE(X), XLPE/SiO₂/TiO₂ 2 wt. % (ST2), XLPE/SiO₂/TiO₂ 5 wt. % (ST5), and XLPE/SiO₂/TiO₂ 10 wt. % (ST10)



The contributing factors to the improved mechanics of hybrid nanocomposites can be summarized as (a) efficient reinforcement (b) proper dispersion of nanofillers in XLPE matrix by evading the self aggregation tendency in the neighbourhood of another filler, leading to a uniform microstructure (c) formation of immobilized polymer phase in the vicinity of nano materials.

5 Thermal Analysis

The thermal stability was investigated by TGA in N₂ atmosphere. Figures 2 and 3 present the TGA curves of XLPE/SiO₂ and XLPE/SiO₂/TiO₂ nanocomposites respectively. The presence of fillers shifts the degradation temperature towards

higher value, indicating higher thermal stability of the composites with respect to the neat XLPE. As the filler content increases the thermal stability also increases proportionally, except for XLPE/SiO₂ at 10 wt. % concentration. At this higher filler concentration, filler–filler interaction dominates over filler–polymer interaction and the property shows a decaying trend. But for hybrid system of composites, thermal stability shows increasing trend up to 10 wt. % nanofiller concentration. Enhancement in the thermal stability can be justified by taking into account several factors like [8, 14] (1) inorganic nanoparticles possess higher heat capacity and thermal conductivity than XLPE, which means that the nanoparticles preferably absorbs heat, resulting in XLPE chains starting to degrade at higher temperatures. (2) qualitative explanation observed in many studies involves the formation of a stable carbon/nanoparticle surface. This surface exhibit analogous characteristics that the resultant char provides protection to the interior of the specimen [15]. The TGA values are in good agreement with the mechanical data regarding the reduced aggregation tendency in hybrid nanoparticle composites.

6 Conclusions

The present work is concentrated on the effect of hybrid SiO₂/TiO₂ nanoparticles and SiO₂ nanoparticles on mechanical and thermal characteristics of XLPE matrix, at different filler loadings. The results can be summarized as follows:

1. Hybrid nanoparticles-filled composites show better mechanical and thermal properties compared to the XLPE/SiO₂ nanocomposite.
2. The XLPE/SiO₂ nanocomposite shows a decaying trend of properties at higher filler loading, whereas XLPE/SiO₂/TiO₂ composite shows an increasing trend even at higher filler loading.
3. The TEM images prove the reduced tendency of aggregation in hybrid nanoparticle filled composite and this confirm the enhancement in mechanics and thermal stability.

References

1. S.P. Thomas, S. Thomas, S. Bandyopadhyay, Polystyrene/calcium phosphate nanocomposites: preparation, morphology and mechanical behaviour. *J. Phys. Chem. C* **113**, 97–104 (2009)
2. W. Cheng, W. Miao, L. Zhang, J. Peng, Covalently bonded PE/SiO₂ nanocomposites synthesized by reactive extrusion. *Iran. Polym. J.* **20**(8), 681–687 (2011)
3. X. Huang, F. Liu, P. Jiang, Dielectrics and electrical insulation. *IEEE Trans. Dielectr. Electr. Insul.* **17**, 1697–1704 (2010)
4. N. Nugay, B. Erman, Property optimization in Nitrile rubber composites via hybrid filler systems. *J. Appl. Polym. Sci.* **79**, 366–374 (2001)

5. A. Das, K.W. Stockelhuber, S. Rooj, D.Y. Wang, G. Heinrich, Synergistic effects of expanded nanoclay and carbon black on natural rubber compounds. *Raw Mater. Appl.* **63**(7/8), 296–302 (2010)
6. J. Li, P.S. Wong, J.K. Kim, Hybrid nanocomposites containing carbon nanotubes and graphite nanoplatelets. *Mater. Sci. Eng. A* **483**, 660–663 (2008)
7. M.F. Uddin, C.T. Sun, Improved dispersion and mechanical properties of hybrid nanocomposites. *Compos. Sci. Technol.* **70**, 223 (2010)
8. G. Malucelli, P. Palmero, S. Ronchetti, A. Delmastro, L. Montanaro, Effect of alumina nano fillers on the thermal and mechanical behaviour of low density polyethylene—Al₂O₃ composites. *Polym. Int.* **59**, 1084–1089 (2010)
9. X. Zhang, L.C. Simon, In situ polymerization of hybrid polyethylene-alumina nanocomposites. *Macromol. Mater. Eng.* **290**, 573–583 (2005)
10. L. Cui, H.Y. Cho, J.W. Shin, N.H. Tarte, S.I. Woo, Polyethylene—montmorillonite nanocomposites: preparation, characterization and properties. *Macromol. Symp.* **260**, 49–57 (2007)
11. H. Yu, J. Liu, Z. Wang, Z. Jiang, T. Tang, Combination of carbon nanotubes with Ni₂O₃ for simultaneously improving the flame retardancy and mechanical properties. *J. Phys. Chem. C* **113**, 13092–13097 (2009)
12. V.M. Liyinov, R.A. Orza, M. Kluppel, M. Duin, Rubber–filler interactions and network structure in relation to stress–strain behavior of vulcanized, carbon black filled EPDM. *Macromolecules* **44**, 4887–4900 (2011)
13. Y. Rao, J.M. Pochan, Mechanics of polymer-clay nanocomposites. *Macromolecules* **40**, 290–296 (2007)
14. H. Zhai, W. Xu, H. Guo, Z. Zhou, S. Shen, Q. Song, Preparation and characterization of PE and PE-g-MAH/monmorillonite nanocomposites. *Eur. Polymer J.* **40**, 2539–2545 (2004)
15. C. Calebrese, L. Hui, L.S. Schadler, J.K. Nelson, A review on the importance of nanocomposites processing to enhance electrical insulation. *IEEE Trans. Dielectr. Electr. Insul.* **18**, 938–945 (2011)

About the Author

Dr. Rohana Hassan is the Deputy Director of Institute for Infrastructure Engineering and Sustainable Management, Universiti Teknologi MARA (UiTM). She is also a Senior Lecturer and actively doing research in the field of timber engineering, engineered wood product, timber design and composites materials and also a regular invited speaker in the same field. She is also actively being invited as a speaker on research methodology and analysis using SPSS for the post graduate studies in the Faculty of Civil Engineering, UiTM. She also sits as an advisory committee in product system certifier for Malaysian Timber Industrial Board, Malaysia. Her timber engineering research papers and journals have been published locally and internationally.

Dr. Zulhabri Ismail is the Head of Legal Aspects in Built Environment/Sustainable Development Research Initiative Group Universiti Teknologi MARA (UiTM), active researcher in Construction Law and Construction Management, to-date he has published more than 40 papers in which most of them are indexed publications. He is a regular speaker on research methodology, research writing strategies and one of the research methodology experts for research postgraduate studies of UiTM. He sits as one of the Judging Panel of Society of Construction Law Essay Writing Competition for Vincent Powell Smith Prize (Malaysia), Chairman/Technical Program Chair for various IEEE conferences.

Dr. Mohd Fadzil Arshad is a fellow researcher of Institute for Infrastructure Engineering and Sustainable Management (IIESM). He is also a senior lecturer for Faculty of Civil Engineering, Universiti Teknologi MARA, Malaysia. He obtained his PhD from University Sains Malaysia in Civil Engineering and holds a Masters degree in structural Engineering. Previously he has been working as site engineer and site manager with KADA Development before joining UiTM as a lecturer. His interest area is on construction materials and structure engineering. He has been winning research awards in many competitions and exhibitions, has been publishing papers in many journals and presenting his research work in many conferences nationally and internationally.

Dr. Norliyati Mohd Amin has been working as a lecturer at Universiti Teknologi MARA (UiTM), Shah Alam Malaysia for 12 years. She completed her Ph.D. from Kyushu University Japan in 2011. She received her Master of Science in Civil Engineering (Structure) from Universiti Teknologi MARA (UiTM), Shah Alam, Malaysia in 2007 and obtained her BEng (Civil Engineering) from Kyushu University in 1999. Her research interests include computational mechanics, model analysis, dynamic analysis, model order reduction and seismic isolation system. Currently she has been appointed as Fellow at Institute for Infrastructure Engineering and Sustainable Management (IIESM), UiTM, Shah Alam, Malaysia.

Dr. Marina Yusoff is the fellow researcher and coordinator of Quality and Standard of Institute for Infrastructure Engineering and Sustainability Management, Faculty of Civil Engineering and Senior Lecturer of Faculty of Computer and Mathematical Sciences, Universiti Teknologi MARA. She holds a Ph.D. in Information Technology and Quantitative Sciences (Intelligent Systems) from Universiti Teknologi MARA. She previously worked as a senior executive of Information Technology in SIRIM Berhad, Malaysia. She also holds a Bachelor Degree in Computer Science from the University of Science Malaysia and Master of Science in Information Technology from Universiti Teknologi MARA. She is currently an active researcher in flood management, graphology, image processing and has developed many intelligent systems. She has published journals and presented her research in many conferences locally and internationally.

Author Index

A

Abbasi, Bushra, 377
Abd Rahman, Nor Faiza, 757
Abdul Awal, Abu Sufian Muhammad, 51
Abdullah, Redzuan, 541
Abidin, Anwar Zainal, 611, 689
Adnan, Azlan, 201
Ahmad, Ismail, 541
Ahmad, Juraidah, 389
Ahmad, Zakiah, 27, 61, 85, 97, 141, 597, 611, 675, 689, 825, 895
Akasah, Zainal Abidin, 851
Ali, Kamilah, 871
Ali, Mohd Fozi, 743, 757, 825
Ali, Mohd Hafiz Md, 191
Alisibramulisi, Anizahyati, 589, 701
Al-Khatib, Issam, 331
Amaruddin, Haslin Idayu, 3
Amin, Norliyati Mohd, 3, 177, 701
Amini, Nity Mohammad, 75
Ansell, Martin, 37
Arbai, Sabariah, 531
Arshad, Ahmad Kamil, 355, 369, 389
Arshad, Fadzil, 887
Arshad, Mohd Fadzil, 169, 191, 501
Ashaari, Yasmin, 423
Awang, Haryati, 437
Ayub, Tehmina, 567
Azit, Romziat, 519

B

Bahari, Noor Iza, 355
Baharudin, Fauzi, 303
Bakar, Afidah Abu, 97
Bakar, Azinoor Azida Abu, 531
Bakri, Zulhazmee, 597
Berhan, Mohamad Nor, 477
Bhkari, Norshariza Mohamad, 97

Brandon, Daniel, 37
Bregulla, Julie, 37
Buhari, Rosnawati, 399
Bunnori, Norazura Muhamad, 625

C

Chiang, Jeffrey, 225

D

Daneshpour, Seyed Abdolhadi, 377
Derahman, Adnan, 437
Desai, Dhawal, 215

E

Emparan, Quin, 817

F

Fadhil Nuruddin, Muhd, 567
Fadillah, Khairil Imran, 721
Farhana, Ismail Nor, 637
Fauzi, M. A. M., 169

G

Goh, Wan Inn, 541

H

Hafez, M. A., 449
Halip Khalid, Azianabiha A, 783, 795
Hamdan, Safarina Haslimawaty, 611, 689
Hamid, Hanizah Ab., 237, 637
Hamid, Shahrin, 75
Haniff, Ahmad Muhammad, 757
Harris, Richard, 37

Hashim, Nor Hafida, 721, 731
 Hassan, Rohana, 3, 27, 61, 75, 107, 117
 Holcroft, Neal, 649
 Hussin, Tengku Anita Raja, 75

I

Ibrahim, Azmi, 27, 61, 201, 237, 625
 Idrus, Arazi, 837
 Imran, Siti Nurulhuda Mohd, 783
 Isa, Che Maznah Mat, 861, 871
 Iskak, Asma Nabilla, 303
 Ismail, Mohd Ashraf Mohamad, 519
 Ismail, Rozaina, 201, 237
 Ismail, Ruqayyah, 721, 731

J

Jaafar, Mohd Faizal Md, 887
 Jaapar, Aini, 861
 Jais, Ismacahyadi Bagus Mohd, 369
 Jose, Josmin, 895
 Jumaat, Mohd Zamin, 15

K

Kadir, Norhayati, 701
 Kamaruddin, Kartini, 389, 577
 Kamarudin, Faizah, 5011
 Kamarudin, Mohd Khairy, 805
 Kamarun, Dzaraini, 389, 769
 Kanadasan, Jegathish, 249
 Karim, Abdul Razak Abdul, 461
 Karim, Mohamad Radhwan Abd, 795
 Khaidzir, Mohamad Omar Mohamad, 15
 Khaidzir, Mohamad Shakri Mohamad, 449
 Khairulniza, Ahmad Anuar, 169
 Khalid, Khairi, 743, 757
 Khamidi, Mohd Faris, 837
 Khin Maung, Win, 287
 Ku, Bee Fang, 153

L

Lamide, Juli Asni, 663
 Lau, Tze Liang, 129
 Lee, Wei-Koon, 263, 275

M

Mah, Darrien Yau Seng, 315
 Mahmoudi, Mohadeseh, 377
 Mario, Siti Nur Aida, 511
 Marzuki, Nur Ashikin, 721, 731

Maslan, M., 817
 Mazlan, Dianah, 51
 Md Daud, Atikah Fatma, 141, 597
 Mohamad Shariff, Mohamad Shakr, 449
 Mohamad, Irma Noorazurah, 263, 343, 795
 Mohamad, Mazlina, 107, 675
 Mohamad, Noridah, 541
 Mohamad, Syed Burhanuddin Hilmi Syed, 851
 Mohamed, Kamaruzaman, 531
 Mohamed, Roslli Noor, 663
 Mohamed, Zainab, 477, 489, 531
 Mohd, Md Jaafar Faizal, 557
 Mohd-Nordin, Mohd Mustaqim, 489
 Muhamad Azlan, Hafizah, 85
 Mukri, Mazidah, 501
 Mustafa, F., 817
 Mustafa, Masria, 369, 423
 Mustafa, Muhammad Fahmi, 731
 Mutalib, Khairul Effendy Ab, 107

N

Najid, Mohamad Noor Faiz Mohamad, 423
 Nanthagopalan, Prakash, 215
 Nasir, Siti Rashidah Mohd, 861, 871
 Nazrin, Fadzli Mohamed, 153
 Nematollahi, Behzad, 713
 Nizam Shakimon, Mohd, 61
 Noor, Normikmah Mohammad, 369
 Noor, S. F. M., 817
 Noorli, I., 557
 Nor Jihan, Abd Malek, 3
 Nor, Noorsuhada Md, 625
 Norazlan Khalid, 501, 817
 Norbaya, S., 449
 Nurbaiah, Mohammad Noh, 637
 Nurliza, Jasmi, 169, 191
 Nuryazmeen, Farhan Haron, 343
 Osman, Nur Masyitah, 437
 Othman, Mohd Nazrin, 825

P

Pahroraji, Mohamad Ezad Hafez Mohd, 577
 Paridah Md, Tahir, 97
 Pender, Michael, 461
 Petrus, Clotilda, 721, 731
 Puaad, Muhammad Bazli Faliq Mohd, 85
 Putuhena, Frederik, 315

R

Rahman, Faiza, 743
 Rahman, M. Hadi A, 541

Rahman, Mohammad Ashraf Abdul, 851
 Rahman, Norazah Abdul, 769
 Rahman, Zanariah Abd, 423
 Rahmat, Mohamad Nidzam, 577
 Razak, Hashim Abdul, 249
 Resdi, Tuan Asmaa Tuan, 275
 Ridzuan, Ahmad Ruslan Mohd, 169, 191, 589
 Rohani, Munzilah Md., 399

S

Saadon, Azlinda, 743
 Sabahiah, Nur, 413
 Sa'don, Norazzlina M., 461
 Saidin, Zul Hilmi, 769
 Salehe, Afdal Haziq Mohamad, 315
 Saliyah, Soffian Noor Mat, 625
 Salim, Nurul Ainain Mohd, 477
 Samad, Mohd Adhar Abd, 805
 Saman, Hamidah Mohd, 557, 577, 589, 625,
 861, 887
 Samsuddin, Suryani, 541
 Sana, Ahmad, 323
 Sanjayan, Jay, 713
 Shaffie, Ekarizan, 389
 Shafiee, Amirudean, 303, 389
 Shafiq, Nasir, 567
 Shahidan, Shahiron, 625
 Shakrani, Shahrul Azwan, 783
 Shalji, Muhammad Shahril Mohd, 117
 Shea, Andy, 649
 Sidek, Muhd Norhasri Muhd, 501, 557, 887
 Sukor, Abdul, 413
 Sulaiman, Wan Noor Azhar Wan, 177
 Sunar, N. M., 817
 Suzila, Rahmat, 589

T

Tajuddin, Ramlah Mohd, 769, 825
 Tawie, Rudy, 511
 Thomas, Sabu, 895
 Thomson, Andrew, 37

U

Ullah Khan, Sadaqat, 567

V

Van, Tze Che, 129
 Vasagavijayan, S., 557

W

Wahab, Mohd Jamil Abdul, 15
 Walker, Peter, 37
 Wardah, Tahir, 343
 Waris Khan, Muhammad, 837
 Win, Ni Lar, 287
 Wong, Meng, 225

Y

Yahya, Zahrullaili, 355
 Yusoff, Marina, 27, 117
 Yusoff, W. M. F. W., 169

Z

Zaidi, Mat Rifin, 887
 Zainuddin, Nur Syahiza, 795
 Zakwan, Fariz Aswan Ahmad, 721, 731